Wireless Communications and Mobile Computing

Scalable Network Infrastructures and Technologies for Internet of Things in Media Computing

Lead Guest Editor: Jun Ye
Guest Editors: Marwan Al-Akaidi and Jemal H. Abawajy

Scalable Network Infrastructures and Technologies for Internet of Things in Media Computing

Wireless Communications and Mobile Computing

Scalable Network Infrastructures and Technologies for Internet of Things in Media Computing

Lead Guest Editor: Jun Ye
Guest Editors: Marwan Al-Akaidi and Jemal H. Abawajy

Chief Editor

Associate Editors

Academic Editors

Contents

Contents

Contents

Contents

Hindawi
Wireless Communications and Mobile Computing
Volume 2023, Article ID 9871392, 1 page
https://doi.org/10.1155/2023/9871392

Retraction

Retracted: A Comprehensive Review of Lightweight Authenticated Encryption for IoT Devices

Wireless Communications and Mobile Computing

Received 12 December 2023; Accepted 12 December 2023; Published 13 December 2023

This article has been retracted by Hindawi, as publisher, following an investigation undertaken by the publisher [1]. This investigation has uncovered evidence of systematic manipulation of the publication and peer-review process. We cannot, therefore, vouch for the reliability or integrity of this article.

Please note that this notice is intended solely to alert readers that the peer-review process of this article has been compromised.

Wiley and Hindawi regret that the usual quality checks did not identify these issues before publication and have since put additional measures in place to safeguard research integrity.

We wish to credit our Research Integrity and Research Publishing teams and anonymous and named external researchers and research integrity experts for contributing to this investigation.

The corresponding author, as the representative of all authors, has been given the opportunity to register their agreement or disagreement to this retraction. We have kept a record of any response received.

References

[1] Z. AlJabri, J. Abawajy, and S. Huda, "A Comprehensive Review of Lightweight Authenticated Encryption for IoT Devices," *Wireless Communications and Mobile Computing*, vol. 2023, Article ID 9071969, 31 pages, 2023.

Hindawi
Wireless Communications and Mobile Computing
Volume 2023, Article ID 9783176, 1 page
https://doi.org/10.1155/2023/9783176

Retraction

Retracted: Design and Application of Land Resource Management System Based on Internet of Things

Wireless Communications and Mobile Computing

Received 17 October 2023; Accepted 17 October 2023; Published 18 October 2023

This article has been retracted by Hindawi following an investigation undertaken by the publisher [1]. This investigation has uncovered evidence of one or more of the following indicators of systematic manipulation of the publication process:

(1) Discrepancies in scope
(2) Discrepancies in the description of the research reported
(3) Discrepancies between the availability of data and the research described
(4) Inappropriate citations
(5) Incoherent, meaningless and/or irrelevant content included in the article
(6) Peer-review manipulation

The presence of these indicators undermines our confidence in the integrity of the article's content and we cannot, therefore, vouch for its reliability. Please note that this notice is intended solely to alert readers that the content of this article is unreliable. We have not investigated whether authors were aware of or involved in the systematic manipulation of the publication process.

Wiley and Hindawi regrets that the usual quality checks did not identify these issues before publication and have since put additional measures in place to safeguard research integrity.

We wish to credit our own Research Integrity and Research Publishing teams and anonymous and named external researchers and research integrity experts for contributing to this investigation.

The corresponding author, as the representative of all authors, has been given the opportunity to register their agreement or disagreement to this retraction. We have kept a record of any response received.

References

[1] Q. Song, "Design and Application of Land Resource Management System Based on Internet of Things," *Wireless Communications and Mobile Computing*, vol. 2022, Article ID 2726673, 14 pages, 2022.

Hindawi
Wireless Communications and Mobile Computing
Volume 2023, Article ID 9754794, 1 page
https://doi.org/10.1155/2023/9754794

Retraction

Retracted: Application of Rotationally Symmetrical Triangulation Stereo Vision Sensor in National Dance Movement Detection and Recognition

Wireless Communications and Mobile Computing

Received 17 October 2023; Accepted 17 October 2023; Published 18 October 2023

This article has been retracted by Hindawi following an investigation undertaken by the publisher [1]. This investigation has uncovered evidence of one or more of the following indicators of systematic manipulation of the publication process:

(1) Discrepancies in scope
(2) Discrepancies in the description of the research reported
(3) Discrepancies between the availability of data and the research described
(4) Inappropriate citations
(5) Incoherent, meaningless and/or irrelevant content included in the article
(6) Peer-review manipulation

The presence of these indicators undermines our confidence in the integrity of the article's content and we cannot, therefore, vouch for its reliability. Please note that this notice is intended solely to alert readers that the content of this article is unreliable. We have not investigated whether authors were aware of or involved in the systematic manipulation of the publication process.

Wiley and Hindawi regrets that the usual quality checks did not identify these issues before publication and have since put additional measures in place to safeguard research integrity.

We wish to credit our own Research Integrity and Research Publishing teams and anonymous and named external researchers and research integrity experts for contributing to this investigation.

The corresponding author, as the representative of all authors, has been given the opportunity to register their agreement or disagreement to this retraction. We have kept a record of any response received.

References

[1] D. Jiang, "Application of Rotationally Symmetrical Triangulation Stereo Vision Sensor in National Dance Movement Detection and Recognition," *Wireless Communications and Mobile Computing*, vol. 2022, Article ID 9032400, 12 pages, 2022.

Hindawi
Wireless Communications and Mobile Computing
Volume 2023, Article ID 9867804, 1 page
https://doi.org/10.1155/2023/9867804

Retraction

Retracted: Design and Implementation of Online Japanese Examination System Based on Genetic Algorithm

Wireless Communications and Mobile Computing

Received 17 October 2023; Accepted 17 October 2023; Published 18 October 2023

This article has been retracted by Hindawi following an investigation undertaken by the publisher [1]. This investigation has uncovered evidence of one or more of the following indicators of systematic manipulation of the publication process:

(1) Discrepancies in scope
(2) Discrepancies in the description of the research reported
(3) Discrepancies between the availability of data and the research described
(4) Inappropriate citations
(5) Incoherent, meaningless and/or irrelevant content included in the article
(6) Peer-review manipulation

The presence of these indicators undermines our confidence in the integrity of the article's content and we cannot, therefore, vouch for its reliability. Please note that this notice is intended solely to alert readers that the content of this article is unreliable. We have not investigated whether authors were aware of or involved in the systematic manipulation of the publication process.

Wiley and Hindawi regrets that the usual quality checks did not identify these issues before publication and have since put additional measures in place to safeguard research integrity.

We wish to credit our own Research Integrity and Research Publishing teams and anonymous and named external researchers and research integrity experts for contributing to this investigation.

The corresponding author, as the representative of all authors, has been given the opportunity to register their agreement or disagreement to this retraction. We have kept a record of any response received.

References

[1] Z. Dengqing and Y. Zhangwei, "Design and Implementation of Online Japanese Examination System Based on Genetic Algorithm," *Wireless Communications and Mobile Computing*, vol. 2022, Article ID 3678607, 11 pages, 2022.

Hindawi
Wireless Communications and Mobile Computing
Volume 2023, Article ID 9813136, 1 page
https://doi.org/10.1155/2023/9813136

Retraction

Retracted: Building English Audio-Visual and Oral Mobile Teaching System Based on Virtual Augmented Reality Technology

Wireless Communications and Mobile Computing

Received 17 October 2023; Accepted 17 October 2023; Published 18 October 2023

This article has been retracted by Hindawi following an investigation undertaken by the publisher [1]. This investigation has uncovered evidence of one or more of the following indicators of systematic manipulation of the publication process:

(1) Discrepancies in scope
(2) Discrepancies in the description of the research reported
(3) Discrepancies between the availability of data and the research described
(4) Inappropriate citations
(5) Incoherent, meaningless and/or irrelevant content included in the article
(6) Peer-review manipulation

The presence of these indicators undermines our confidence in the integrity of the article's content and we cannot, therefore, vouch for its reliability. Please note that this notice is intended solely to alert readers that the content of this article is unreliable. We have not investigated whether authors were aware of or involved in the systematic manipulation of the publication process.

Wiley and Hindawi regrets that the usual quality checks did not identify these issues before publication and have since put additional measures in place to safeguard research integrity.

We wish to credit our own Research Integrity and Research Publishing teams and anonymous and named external researchers and research integrity experts for contributing to this investigation.

The corresponding author, as the representative of all authors, has been given the opportunity to register their agreement or disagreement to this retraction. We have kept a record of any response received.

References

[1] D. Xinzhen and R. Zhifen, "Building English Audio-Visual and Oral Mobile Teaching System Based on Virtual Augmented Reality Technology," *Wireless Communications and Mobile Computing*, vol. 2023, Article ID 1387219, 13 pages, 2023.

Hindawi
Wireless Communications and Mobile Computing
Volume 2023, Article ID 9805273, 1 page
https://doi.org/10.1155/2023/9805273

Retraction

Retracted: Enterprise Management Resource Protection System Based on Digital Information Technology

Wireless Communications and Mobile Computing

Received 17 October 2023; Accepted 17 October 2023; Published 18 October 2023

This article has been retracted by Hindawi following an investigation undertaken by the publisher [1]. This investigation has uncovered evidence of one or more of the following indicators of systematic manipulation of the publication process:

(1) Discrepancies in scope
(2) Discrepancies in the description of the research reported
(3) Discrepancies between the availability of data and the research described
(4) Inappropriate citations
(5) Incoherent, meaningless and/or irrelevant content included in the article
(6) Peer-review manipulation

The presence of these indicators undermines our confidence in the integrity of the article's content and we cannot, therefore, vouch for its reliability. Please note that this notice is intended solely to alert readers that the content of this article is unreliable. We have not investigated whether authors were aware of or involved in the systematic manipulation of the publication process.

Wiley and Hindawi regrets that the usual quality checks did not identify these issues before publication and have since put additional measures in place to safeguard research integrity.

We wish to credit our own Research Integrity and Research Publishing teams and anonymous and named external researchers and research integrity experts for contributing to this investigation.

The corresponding author, as the representative of all authors, has been given the opportunity to register their agreement or disagreement to this retraction. We have kept a record of any response received.

References

[1] W. Zhou, "Enterprise Management Resource Protection System Based on Digital Information Technology," *Wireless Communications and Mobile Computing*, vol. 2022, Article ID 3277750, 13 pages, 2022.

Hindawi
Wireless Communications and Mobile Computing
Volume 2023, Article ID 9801082, 1 page
https://doi.org/10.1155/2023/9801082

Retraction

Retracted: Visual Communication-Based Virtual Reality Design of Imaging Information Collection and Display System

Wireless Communications and Mobile Computing

Received 17 October 2023; Accepted 17 October 2023; Published 18 October 2023

This article has been retracted by Hindawi following an investigation undertaken by the publisher [1]. This investigation has uncovered evidence of one or more of the following indicators of systematic manipulation of the publication process:

(1) Discrepancies in scope
(2) Discrepancies in the description of the research reported
(3) Discrepancies between the availability of data and the research described
(4) Inappropriate citations
(5) Incoherent, meaningless and/or irrelevant content included in the article
(6) Peer-review manipulation

The presence of these indicators undermines our confidence in the integrity of the article's content and we cannot, therefore, vouch for its reliability. Please note that this notice is intended solely to alert readers that the content of this article is unreliable. We have not investigated whether authors were aware of or involved in the systematic manipulation of the publication process.

Wiley and Hindawi regrets that the usual quality checks did not identify these issues before publication and have since put additional measures in place to safeguard research integrity.

We wish to credit our own Research Integrity and Research Publishing teams and anonymous and named external researchers and research integrity experts for contributing to this investigation.

The corresponding author, as the representative of all authors, has been given the opportunity to register their agreement or disagreement to this retraction. We have kept a record of any response received.

References

[1] Y. Qi, T. Sun, and Y. Li, "Visual Communication-Based Virtual Reality Design of Imaging Information Collection and Display System," *Wireless Communications and Mobile Computing*, vol. 2022, Article ID 1929596, 12 pages, 2022.

Hindawi
Wireless Communications and Mobile Computing
Volume 2023, Article ID 9789176, 1 page
https://doi.org/10.1155/2023/9789176

Retraction

Retracted: Construction of Accounting Internal Control Management Platform Based on IoT Cloud Computing

Wireless Communications and Mobile Computing

Received 17 October 2023; Accepted 17 October 2023; Published 18 October 2023

This article has been retracted by Hindawi following an investigation undertaken by the publisher [1]. This investigation has uncovered evidence of one or more of the following indicators of systematic manipulation of the publication process:

(1) Discrepancies in scope
(2) Discrepancies in the description of the research reported
(3) Discrepancies between the availability of data and the research described
(4) Inappropriate citations
(5) Incoherent, meaningless and/or irrelevant content included in the article
(6) Peer-review manipulation

The presence of these indicators undermines our confidence in the integrity of the article's content and we cannot, therefore, vouch for its reliability. Please note that this notice is intended solely to alert readers that the content of this article is unreliable. We have not investigated whether authors were aware of or involved in the systematic manipulation of the publication process.

Wiley and Hindawi regrets that the usual quality checks did not identify these issues before publication and have since put additional measures in place to safeguard research integrity.

We wish to credit our own Research Integrity and Research Publishing teams and anonymous and named external researchers and research integrity experts for contributing to this investigation.

The corresponding author, as the representative of all authors, has been given the opportunity to register their agreement or disagreement to this retraction. We have kept a record of any response received.

References

[1] L. Song, "Construction of Accounting Internal Control Management Platform Based on IoT Cloud Computing," *Wireless Communications and Mobile Computing*, vol. 2022, Article ID 9552118, 13 pages, 2022.

Hindawi
Wireless Communications and Mobile Computing
Volume 2023, Article ID 9787542, 1 page
https://doi.org/10.1155/2023/9787542

Retraction

Retracted: Construction of User Behavior Web Data Mining Model for Internet Marketing

Wireless Communications and Mobile Computing

Received 17 October 2023; Accepted 17 October 2023; Published 18 October 2023

This article has been retracted by Hindawi following an investigation undertaken by the publisher [1]. This investigation has uncovered evidence of one or more of the following indicators of systematic manipulation of the publication process:

(1) Discrepancies in scope
(2) Discrepancies in the description of the research reported
(3) Discrepancies between the availability of data and the research described
(4) Inappropriate citations
(5) Incoherent, meaningless and/or irrelevant content included in the article
(6) Peer-review manipulation

The presence of these indicators undermines our confidence in the integrity of the article's content and we cannot, therefore, vouch for its reliability. Please note that this notice is intended solely to alert readers that the content of this article is unreliable. We have not investigated whether authors were aware of or involved in the systematic manipulation of the publication process.

Wiley and Hindawi regrets that the usual quality checks did not identify these issues before publication and have since put additional measures in place to safeguard research integrity.

We wish to credit our own Research Integrity and Research Publishing teams and anonymous and named external researchers and research integrity experts for contributing to this investigation.

The corresponding author, as the representative of all authors, has been given the opportunity to register their agreement or disagreement to this retraction. We have kept a record of any response received.

References

[1] M. Wei, "Construction of User Behavior Web Data Mining Model for Internet Marketing," *Wireless Communications and Mobile Computing*, vol. 2022, Article ID 2813718, 10 pages, 2022.

Hindawi
Wireless Communications and Mobile Computing
Volume 2023, Article ID 9839571, 1 page
https://doi.org/10.1155/2023/9839571

Retraction

Retracted: Analysis of Language Characteristics of Multimedia English Based on Internet of Things

Wireless Communications and Mobile Computing

Received 8 August 2023; Accepted 8 August 2023; Published 9 August 2023

This article has been retracted by Hindawi following an investigation undertaken by the publisher [1]. This investigation has uncovered evidence of one or more of the following indicators of systematic manipulation of the publication process:

(1) Discrepancies in scope
(2) Discrepancies in the description of the research reported
(3) Discrepancies between the availability of data and the research described
(4) Inappropriate citations
(5) Incoherent, meaningless and/or irrelevant content included in the article
(6) Peer-review manipulation

The presence of these indicators undermines our confidence in the integrity of the article's content and we cannot, therefore, vouch for its reliability. Please note that this notice is intended solely to alert readers that the content of this article is unreliable. We have not investigated whether authors were aware of or involved in the systematic manipulation of the publication process.

Wiley and Hindawi regrets that the usual quality checks did not identify these issues before publication and have since put additional measures in place to safeguard research integrity.

We wish to credit our own Research Integrity and Research Publishing teams and anonymous and named external researchers and research integrity experts for contributing to this investigation.

The corresponding author, as the representative of all authors, has been given the opportunity to register their agreement or disagreement to this retraction. We have kept a record of any response received.

References

[1] Y. Zhu, "Analysis of Language Characteristics of Multimedia English Based on Internet of Things," *Wireless Communications and Mobile Computing*, vol. 2022, Article ID 7257265, 9 pages, 2022.

Hindawi
Wireless Communications and Mobile Computing
Volume 2023, Article ID 7136290, 10 pages
https://doi.org/10.1155/2023/7136290

Research Article

Combat Response Training Tester Based on Intelligent Force-Measuring Sensor and Digital Circuit

Chen Liu

Heze University Sport and Health University, Heze, 274015 Shandong, China

Correspondence should be addressed to Chen Liu; liuchen@hezeu.edu.cn

Received 10 August 2022; Revised 28 September 2022; Accepted 6 October 2022; Published 2 May 2023

Academic Editor: Jun Ye

In combat sports, the team members take attack and defense as the core of sports, and the technical movements are not periodic and the application process is irregular. During the competition, observe the opponent's neutral position, judge timely, and react quickly. At the same time, athletes are required not only to master skilled technical movements but also to have rapid and accurate adaptability. In order to improve athletes' rapid response ability, according to the rapid response training scheme, a combat response training tester based on a force-measuring intelligent sensor and digital circuit is designed to improve the athletes' response ability. Firstly, a comprehensive test system of combat trainer is designed based on the intelligent force-measuring sensor and MSP430, which can measure the response time, speed, and strength of boxing. Secondly, a wavelet filtering algorithm is used to filter the sensor measurement data. Finally, the striking force and striking time of each action are recorded by sensors and data acquisition devices to reflect the striking effect and reflect the "accurate" objectives of the project characteristics. Based on the noninterference and anti-interference of e-touch piezoelectric film, it can be made into universal force-measuring sensors of different specifications for fight competitions according to needs. After being connected into a module network in parallel, it can be connected with the microcontroller to determine the hit area. In addition, the team reaction training test device has laid a foundation for the scientific evaluation of improving the team members' reaction ability and attack defense conversion ability. The launch of the comprehensive ability tester for combat athletes introduces the previous fuzzy evaluation of athletes' comprehensive ability into a new way of scientific quantitative measurement and evaluation, which will provide a scientific basis for the selection of combat vibration items, the regulation of training process, the inspection of training effect, and the formulation of enrollment and examination standards for sports colleges and universities. The results show that the instrument can obtain the parameters of hitting strength, strength endurance, hitting speed, speed endurance, hitting impulse, and hitting power of sports biomechanics on the group of fighting events, which provides a reliable basis for coaches to implement teaching and training for athletes.

1. Introduction

Since the reform and opening up, people's living standards have been continuously improved [1]. After solving the problem of food and clothing, health has become a major concern of the society [2]. With the successful holding of the 2008 Beijing Olympic Games, China has officially entered the ranks of sports powers and realized the dream of becoming a sports power. Nowadays, national fitness has become a topic of increasing concern. In fact, after elite sports, there must be a vigorous national fitness movement [3]. Due to the accelerated pace of modern people's life, the shortage of urban land, and the large population of our country, the places for citizens' sports and fitness in cities are becoming more and more limited [4]. Therefore, gyms have become more and more people's fitness choices. In addition, the changes in people's living conditions today also give fitness equipment a space for considerable development. In the past, most people were engaged in physical labor, so they did not have much interest in fitness after work; more and more people engaged in mental work [5]. Because they spend a long time in the office, they take the bus even when they go to and from work. Therefore, these people lack necessary exercise, and their bodies are generally in a subhealth

state. Many people catch a cold when they encounter the wind. For these people, sports and fitness have become extremely important. After all, the body is the capital of the revolution. Due to the limitations of space and time, many mental workers choose to go to the gym for fitness [6].

Wushu is the quintessence of the Chinese nation. Chinese people have always had a yearning and love for boxing Wushu [7]. It can be said that almost every Chinese has a Kung Fu dream when they are young. Therefore, the fight training device in the gym is bound to be welcomed by many people [8]. This device integrating testing and fitness can not only help those who like boxing to do fight training but also let people release the pressure in work and life in the process of boxing [9]. Modern fight training equipment is no longer a wooden stake in ancient times [10]. It is a comprehensive training system integrating fitness and testing. The target surface of the fight training device is no longer a hard material like a wooden pile, but is connected to a cylinder [11]. When boxing, the air is squeezed and the target will move back. In this way, a buffer of a certain distance is formed to protect the fist. The change of air pressure in the cylinder can also just reflect the fist force [12]. The signal of the change of air pressure is collected by the air pressure sensor and then sent to the a/d converter of the single-chip microcomputer to obtain the fist force [13]. The speed measurement principle of the system is to use the hc-sr04 ultrasonic sensor installed above the target surface to continuously emit ultrasonic waves at equal time intervals, detect the distance of the fist in the process of punching through the reflected wave, and obtain a speed through the ratio of the distance difference measured every two adjacent times to the time used. In this way, multiple speed values can be obtained in the process of punching, and the maximum value can be calculated in the program and defined as the fist speed. The reaction time of human boxing is completed by the timer of MSP430 single-chip microcomputer. Therefore, the combat trainer can be used as a continuous boxing exercise and can also be used to test the reaction time, boxing speed, and boxing strength of a boxing [14]. Literature [15] takes judo competition as the object and puts forward a time-motion performance evaluation method. In the following years, the literature [16] used the time-dynamic performance evaluation method in the research of comprehensive fighting movement, which was quite effective and was followed by other scholars. Literature [17] published papers to look for ways to distinguish the physiological characteristics of high-level and low-level comprehensive wrestlers and the physiological differences between ground skills and standing skills. He found that the level of comprehensive wrestlers largely depends on the anaerobic ability of the athletes [18]. The requirements for anaerobic ability of ground skills are higher, and the ratio of motion to stop is significantly higher than that of standing skills. Standing skills require higher dynamic strength and explosive power. Literature [19] proposed that the movement stop ratio of comprehensive fighting was 1 : 2 to 1 : 4, which was between the typical ratios of judo, wrestling, karate, and Taekwondo, regardless of a round interval, reflecting the combination of ground technology and standing technology; most competitions end in the third round, and the high-intensity movements mainly belong to the ground entanglement part [20].

The rest of this paper is organized as follows. Section 2 discusses the overall design of the combat response tester, including the system structure design for the combat response training tester and the hardware circuit design of the system. In Section 3, research on a pressure-testing algorithm based on wavelet filtering algorithm is studied. Section 4 presents the test results. Finally, the full text is summarized in Section 5.

2. The Overall Design of Combat Response Tester

2.1. System Structure Design for Combat Response Training Tester. The reaction training tester is mainly composed of a hitting model, hardware, control and data acquisition, and human-computer interaction. The striking model is the basis of the whole equipment, and the characteristics of "fast, accurate, and very" of fighting sports are fully considered. The model is mainly composed of a strike module, base post, and indicator light. The installation position of the indicator light is convenient for athletes to observe. The indicator lights of different colors at different positions are on, which requires athletes to respond quickly according to the training plan arranged by the coaches and complete the corresponding technical and tactical actions to improve the reaction ability of the team members. The striking target in the striking module is the target for professional training. The striking position is marked, and the sensor is located directly below the striking position. The striking force and striking time of each action are recorded by sensors and data acquisition devices to reflect the striking effect and reflect the "very" and "accurate" objectives of the project characteristics. A sliding groove is designed in the base column to facilitate the adjustment of the height of the striking module, so as to adapt to athletes of different heights. The chassis can not only simulate the swing range of the sandbag but also prevent the injury of team members by adjusting the tightness of the 8 springs. The overall structure of the combat response test instrument system is shown in Figure 1. The design of the system includes an upper computer terminal and a lower computer. The lower computer is connected to MCU through WiFi. The system adopts the modular design concept, which divides the system into a microprocessor, signal acquisition module, WiFi communication module, and system power module. This design is based on an MSP430F149 single-chip microcomputer produced by TI Company of the United States as the application foundation and effectively combines with various hardware systems to complete the overall design of the system. MSP430F149 is the core control module of the system and the central processing module. It realizes the main interaction of man-machine information through the combination of independent keys and a 12864LCD liquid crystal display. The user can operate according to the current operation level displayed on the screen by pressing the key. After the user selects a gear as the flexibility training intensity, the controller will select the corresponding gear channel through a certain logic operation; then, the user selects the ascending or

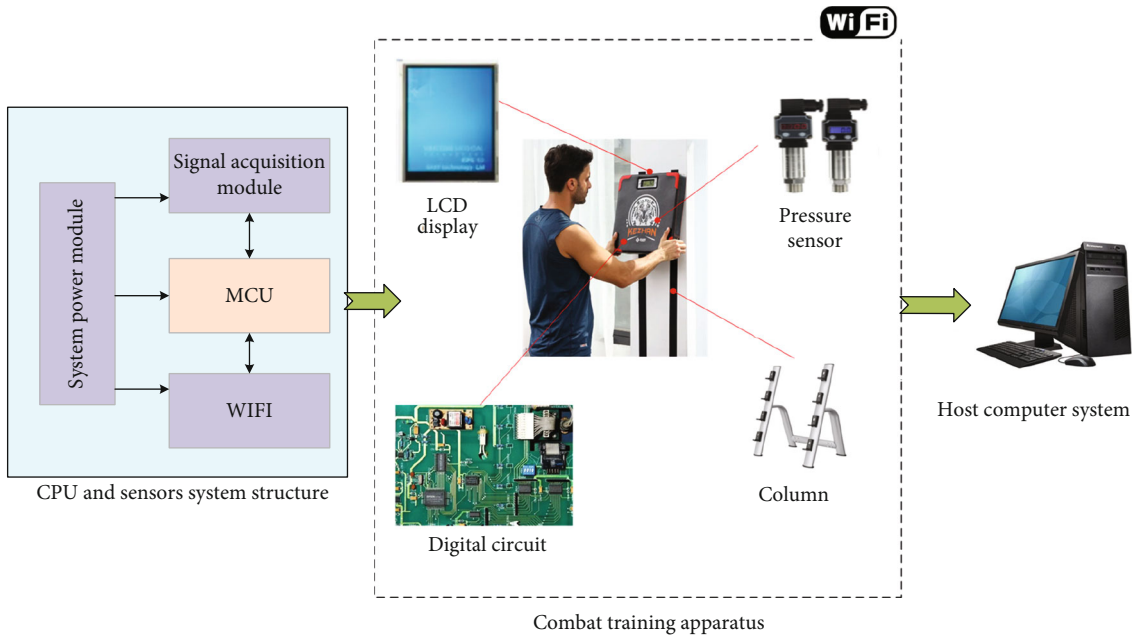

Figure 1: The structure of the multiple physiological parameter measurement systems.

descending according to the screen prompt, and the controller controls the forward or reverse rotation of the motor through certain logic operation to realize the ascending or descending of the trainer. At the same time, the user's selection will be displayed on the LCD screen.

2.2. Hardware Circuit Design of the System. The hardware circuit diagram of the fight training instrument is shown in Figure 2. The instrument is composed of a single-chip microcomputer with a display screen and a function control keyboard on the periphery and a target mold (a reaction mold and a gravity sensor mold that randomly displays the strike points). There are decoding, coding and sensor signal acquisition, and holding circuits in the target mold. When working, the indicating signals of each hitting point are generated by the single-chip microcomputer program. When the athlete hits the target mold, the mold circuit will return the athlete's action signal to the single-chip microcomputer, which will display the test results on the display screen or transmit the data to the advanced computer.

The tester has five operating modes. When in use, the user can select the working mode and set the test parameters through the keyboard on the host control panel and select the target mold at the same time. (1) Reaction ability test: the main machine is equipped with a standard mold with random luminous dots. Set the random times: the light on prompt time, record the time gap between the light on and the target hit, and display the cumulative result of the effective response time. (2) Hit rate test: set the number of random lights on N, record the athlete's effective hitting times m, and then, the ratio of m to n is the hit rate. (3) Striking force test: the main machine is equipped with a gravity-sensing mold. Set the function key "force" to measure the striking force of the athlete. This status is a dynamic test. (4) Weighing: set the function key "weigh," at this time, the tester is a 500 kg scale, which can be used to divide the weight level of athletes. This status is a static test. (5) Hitting frequency test: set the function key "n/min" to evaluate the effective hitting times of athletes in unit time (meaning that the strength must be greater than a given value). Features of the tester: it can be used by a single machine, small and flexible, and can also be connected to the computer for statistical management; the interface between the target mold and the host adopts the plug-in connection mode, which can be flexibly replaced according to the test object and test item; the software is portable and easy to upgrade the erasability of a single-chip computer program. Parameter indicators can be set according to user requirements.

Furthermore, the core processor of the system is MSP430F149, which needs to provide a +5 V power supply. The OP07 used in the system design differential amplifier circuit needs to provide ±5 V power supply. Therefore, a 220 V general AC power supply cannot meet the design requirements. It must be processed by the peripheral power circuit to obtain the required voltage to supply power to the system. The spoke pressure sensor is adopted, which has high sensitivity, good linearity, stable performance, a large pressure range of 0-1000 kg, an output voltage of 0-10 V, and a response frequency of 1000 Hz; the data acquisition system uses the shelf product USB-2852a of Beijing Altai Technology. The acquisition card is a data acquisition card based on a USB bus, which can be directly connected to the USB interface of the computer to form a data acquisition, waveform analysis, and processing system in various fields such as laboratories and product quality inspection centers.

3. Research on Pressure-Testing Algorithm Based on Wavelet Filtering Algorithm

3.1. Design of Force Sensor Based on e-Touch. The e-touch piezoelectric film contains many flat hole structures, in

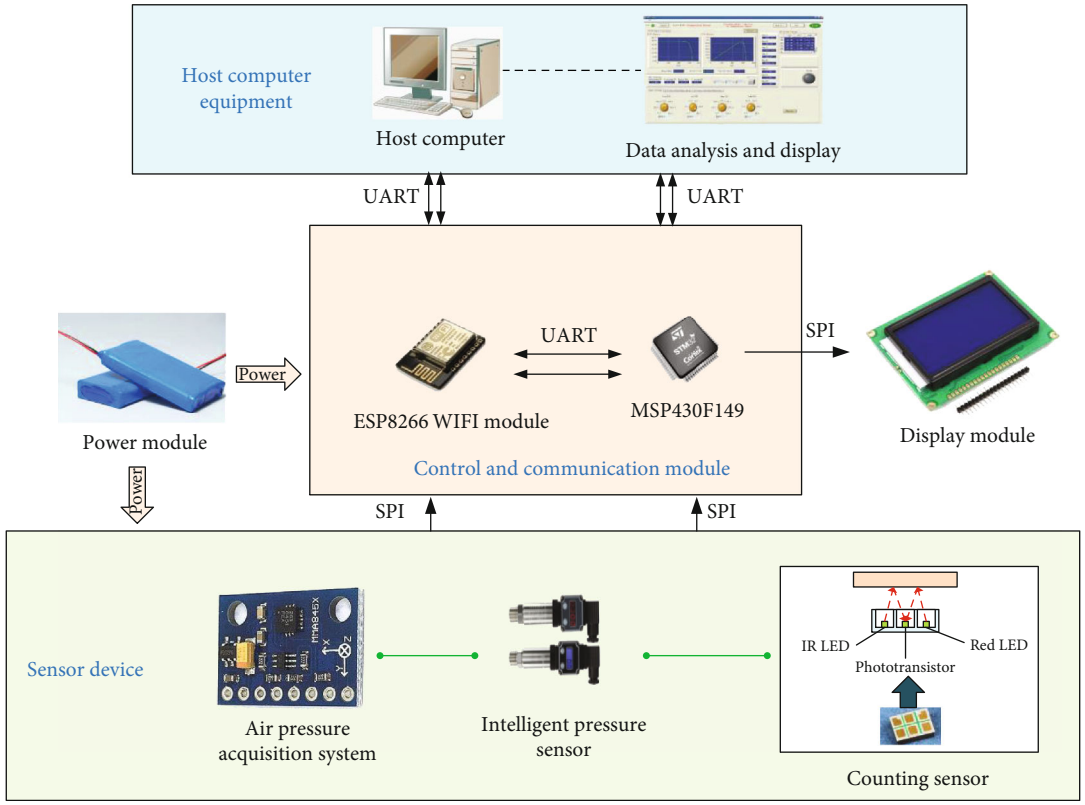

Figure 2: The hardware structure of the health bracelet terminal.

which permanent positive and negative charges are stored. When the piezoelectric film is subjected to dynamic stress, the thickness changes and corresponding charges are generated. These charges accumulate on the upper and lower electrodes of the film, resulting in charges corresponding to the force. The e-touch piezoelectric film produced by Beixin Electronic Technology was selected in the test. Its main parameters are piezoelectric charge coefficient 10 pc/n, piezoelectric frequency range 1 khz~100 khz, capacitance 17 pf/cm^2, impedance 10 mΩ/cm^2, and pressure range 0.1 kPa~1000 kPa.

After learning from many mature advantages of Taekwondo electronic protector and studying its induction recognition stability, signal acquisition, collision misjudgment, and so on, in this paper, a kind of force-measuring sensor for an electronic protective device is made and realized by sticking buffer material on the front and back sides of the ordinary e-touch piezoelectric film. The overall structure of the sensor system is designed in Figure 3. It is embedded in the protective device for use and choose piezoelectric films of different shapes according to the shape and thickness of the protective device, adjust the material and thickness of buffer materials on both sides to meet the needs of different gender and level competitions, and eliminate their own and external disturbances. Flexible shielding materials and shielding wires are used to shield power frequency and electromagnetic interference, and finally, the sensor is embedded in the protective device.

A group of force-measuring sensor modules with the same shape, thickness, and impact resistance value is connected in parallel through the bus and embedded in the used protective gear or corresponding equipment, and the distribution position is adjusted to ensure that at least one sensor module can be effectively hit during use. The positive output end of each sensor module is connected to the bus after connecting the diode to avoid mutual influence.

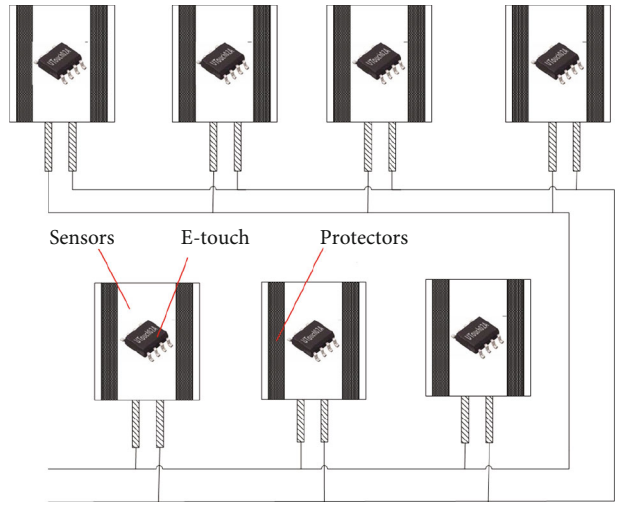

Figure 3: Structure diagram of pressure sensor based on e-touch.

3.2. Wavelet Filtering Processing of Pressure Measurement Data. The function (or mathematical principle) of continuous

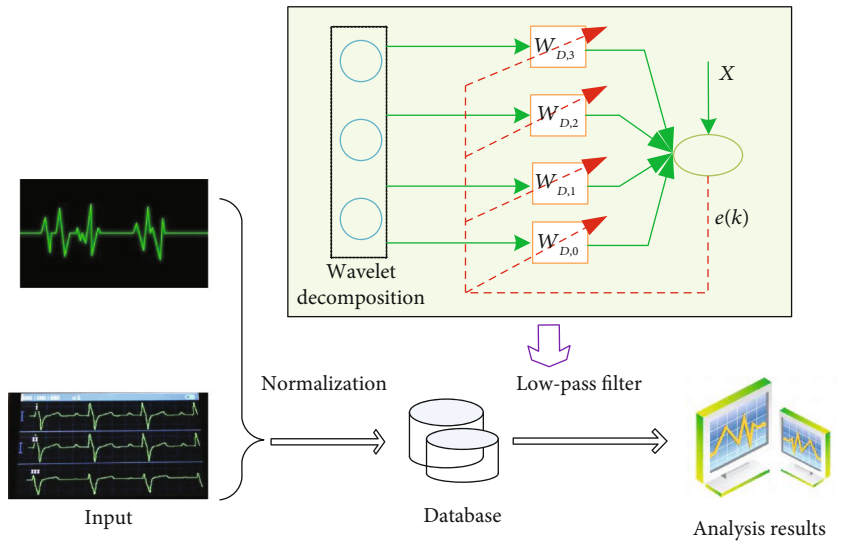

Figure 4: Structure diagram of pressure sensor based on e-touch.

wavelet filter is the same as that of a digital filter. The difference between the two is that the former is a continuous function and the latter is a finite discrete sequence. This difference directly leads to the difference in the implementation of filtering between the two. That is, after a basic continuous function filter is given, people can arbitrarily adjust its filtering scale and adapt to the data with any sampling rate, even to the data with unequal interval sampling. As for digital filtering, when the scale or sampling rate changes, people often need to reconstruct the corresponding digital filter. At the same time, the filters applied to pressure instrument data and aerodynamic data are different (low-pass and derivative, respectively), but the two types of filters must be strictly consistent in terms of filtering scale. In this regard, compared with digital filters, the continuous function filter is easy to realize the scale matching in the filtering process because it is easy to adjust the scale. This paper attempts to use the low-pass parent wavelet and the first-order derivative and second-order derivative mother wavelet to replace the digital filter to filter the pressure measurement data.

The implementation block diagram of the wavelet filtering algorithm is shown in Figure 4.

As shown in Figure 4, the low-pass filter is the core of the whole algorithm. Next, the wavelet filtering algorithm will be used to process the sensor data. Given the function $f(t)$, define the following transformation [21]:

$$\begin{aligned} W_0^\tau f(t) &= f * \theta^\tau(t), \\ W_2^\tau f(t) &= \frac{1}{\tau^2} f * \psi^\tau(t). \end{aligned} \tag{1}$$

Traditionally, $\theta^\tau(t)$ is called the smooth function (or sampling function). In wavelet theory, $\psi^\tau(t)$ is called parent wavelet (or scaling function). People can construct innumerable parent wavelets that satisfy Equation (3), such as the Shannon function, Hnr function, and B.spline function. τ is the time scale where $*$ represents the convolution operator, which is easy to obtain

$$W_2^\tau f(t) = \frac{1}{\tau^2} f * \left(\tau^2 \frac{d^2\theta^\tau}{dt^2}\right)(t) = \frac{d^2}{dt^2}(f * \theta^\tau)(t) = \frac{d^2}{dt^2} W_0^\tau f(t). \tag{2}$$

$W_0^\tau f(t)$ is the result of low-pass filtering of $f(t)$ on a time scale τ. Formula (2) shows that $W_2^\tau f(t)$ is actually the second derivative of $W_0^\tau f(t)$, that is, the second derivative of the low-pass filtering result of $f(t)$ on τ, so $\psi^\tau(t)$ can be considered as the second derivative filter on τ. As long as the speed of punching remains stable, the time scale and space scale of pressure measurement are equivalent.

Therefore,

$$\Delta g^\tau(t) = W_0^v \Delta g(t) = \Delta g * \theta^v(t), \tag{3}$$

where v is the speed of punching. Construct parent wavelet and parent wavelet as

$$\begin{aligned} \theta(t) &= G(t)S(t) = e^{-\left(t^2/2\delta^2\right)} \cdot \frac{\sin \pi t}{\pi t}, \\ \psi(t) &= \ddot{\theta}(t) = e^{-\left(t^2/2\delta^2\right)} \left(\frac{t \sin \pi t}{\pi \delta^4} + \frac{(\sin \pi t/\pi t) - 2\cos \pi t}{\delta^2} + \frac{2(\sin \pi t/\pi t) - \pi t \sin \pi t - 2\cos \pi t}{t^2}\right), \end{aligned} \tag{4}$$

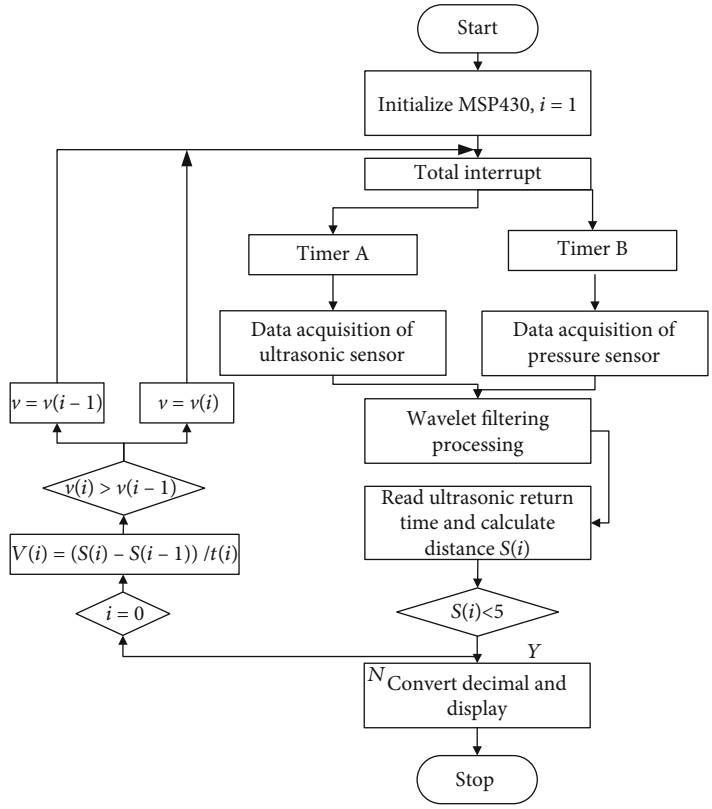

Figure 5: The algorithm flowchart of prediction sampling frequency.

$G(t)$ and $S(t)$ are Gauss function and Shannon function, respectively, and δ is the constant that controls the length of the filter window. $S(t)$ is the best low-pass filter in theory, since its frequency response is the most ideal Harr function. If the filtering scale (cut-off half wavelength) of $\theta(t)$ and $\psi(t)$ is dimensionless 1, the parent wavelet $\theta^{\tau}(t)$ and parent wavelet $\psi^{\tau}(t)$ after time scale calibration can be obtained by Equation (1).

However, $S(t)$ decay rate $O(1/t)$ is too slow to be directly used for filtering. In Equation (4), $G(t)$ is introduced so that $\theta(t)$ has a faster decay rate, which is nearly a compactly supported (finite length). When δ is large enough, $\theta(t)$ decibel defined by Equation (3) is close to the low-pass requirements in Equation (3). And $\theta(t)$ frequency response is very close to the Harr function; $\theta(t)$ constructed from Equation (4) is very close to the bandpass requirements. $\theta(t)$ and $\psi(t)$ can be regarded as parent wavelets and parent wavelets, respectively, and their basic filtering scales (cut-off half wavelength) are both 1 (dimensionless). When the scales of both are calibrated and adjusted, the same filtering scales can be ensured as long as the scale parameters s of both are kept equal. On the basis of multiresolution analysis of signals, Mallet and Meyer proposed a fast algorithm for computing discrete orthogonal wavelet transform, namely, Mallet algorithm. By orthogonally projecting the signal $x(t)$ into the spaces Vj and Wj, the discrete approximation signal $cj(t)$ and discrete detail signal $dj(t)$ of $x(t)$ under resolution j can be obtained. The whole flowchart is designed as shown in Figure 5.

As is shown in Figure 5, the fight trainer system measures the reaction time of the boxer by timer B. First, set the counting mode of timer B to continuous counting. Since the system clock is set to 8 MHz and the count value CCR0 is 8000, it takes 1 ms to count each time, and the millisecond count value is saved in register m_second, when the value of second m_second reaches 1000, the second register carries one bit, and m_second is cleared. Since the maximum reaction time is set to be no more than 10 ms, it is unnecessary to consider the carry problem of seconds and minutes. The cut-off condition for timer B timing is the fist target spacing $s > 5$ cm, so when this condition is met, the m_second is merged and stored in time t. The timer interrupt is used in the program design. When the count value reaches 8000, it enters the interrupt function, performs time conversion, sets the count value, and then returns to the main function cycle for the next count until the cut-off condition is met. Furthermore, the ultrasonic speed measurement program is mainly completed by timer A; that is, timer a records the echo high-level time. Setting P1.2 to CCIOA, timer A captures input. When the high level at the capture input comes, it starts counting, that is, the rising edge capture; when the capture input low level arrives, the counting ends, that is, the falling edge capture. Take the timer count value as the timing time. The distance of the fist is calculated from the timing time and the ultrasonic speed. After the program delays for 4 ms, the next measurement is carried out. The speed can be calculated from the time difference and distance difference of continuous measurement. The purpose of dynamic

speed measurement can be achieved by continuous measurement in the cycle program until the speed measurement cut-off condition $s > 5$ cm is met.

4. Analysis of Test Results

The test process of the beat tester is as follows: connect CH1 and CH2 channels of the oscilloscope to the output end of the force-measuring sensor module and the output end of the conditioning circuit, respectively. Apply different levels of dynamic impact force to the sensor module through the dynamic impact force calibrator and observe the corresponding output peak value by the oscilloscope. The experimental results are shown in Table 1.

When the sensor module of the same specification is replaced for measurement, its output voltage changes slightly with the output voltage of the conditioning circuit, but the output is proportional, within a difference of ±0.3. In the test, when the output voltage of the sensor module is 115 V, it does not change, obviously reaching the upper limit of the generated charge. In order to meet the use requirements, replace the buffer material with a higher damping coefficient and calibrate again. The calibration results of a group of sensor modules with the same specification can also be noted. The output results before the output voltage no longer changes have a certain deviation, but they all change with the change of the force application height and the proportion is basically the same, ranging from 0 to 0.5.

Watchdog timer (WDT) is a common component in the design of MCU. In practical application, due to the existence of interference noise such as power supply and other electromagnetic interference, it is easy to cause the MSP430 program to run away. At this time, it is necessary to effectively handle the program to make it run normally so that the machine can return to the normal working state. A watchdog timer is designed to solve this problem, and its function is particularly important in the loop program. In general, WDT is used by setting a timing time, which is just a little longer than the total time for program execution. When the timing time is up, the device will reset automatically. In the process of program execution, the watchdog timer will be reset automatically to start counting again; that is, the watchdog timer will not work under the normal operation of the program. However, when the program runs away due to interference, it cannot clear the WDT before the scheduled time is reached. At this time, the WDT will overflow, causing the system to reset, and the program will restart to run normally.

4.1. Prediction Results of Sampling Frequency Based on BP Neural Network. In order to accurately measure the impact force, each force-measuring sensor is calibrated by a dynamic impact force calibrator. Pull up the impact rod of the calibrator to different heights to generate different impact forces. The dynamic impact is connected to the sensor module of the oscilloscope. A number of force-measuring sensor modules with the same shape and thickness are manufactured, and 1 mm rubber buffer materials are used up and down.

Table 1: Output of force-measuring sensor module and conditioning circuit.

Height	Force sensor module output/V	Conditioning circuit output/V
0.01	9.5	2.3
0.02	19.7	3.2
0.03	32.5	5.6
0.04	66.2	11.0

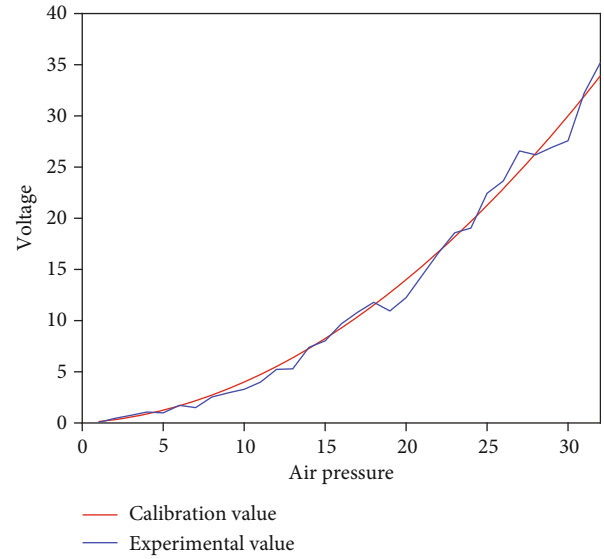

Figure 6: Pulse waves filtered by second-order Butterworth filter.

Connect the output signals vout+ and vout- of the air pressure sensor to P6.0 after differential amplification. The P6.0 port is set as its second function. The analog input channel 0 of the A/D converter performs A/D conversion. The reference voltage of the A/D converter selects the internal reference voltage as the reference. After the speed measurement program is completed, open the ADC, use the sampling timer, and convert the mode multiple times in a single channel. In the ad interrupt program, take the sampling value from ADC12MEM0, that is, the measured voltage. The relationship between voltage and punch force is obtained by experiment; place the fight trainer vertically with the target facing up. The measured output voltage values of weights with different weights are shown in Figure 6.

Figure 6 shows that the output voltage varies with the applied force; the output voltage of the sensor module of the same specification also exists because of the slight difference between the sensor itself and the buffer material -1.6 V~ +2 V difference. The relationship between the output voltage and force is similar to a linear function. Two load cell modules with the same shape and thickness and 1 mm plastic plate as buffer material are made for calibration. Change the thickness of the buffer material and the output voltage of the material, so as to distinguish the force-measuring sensors applicable to different levels and shapes of protective devices. Through programming, the collected voltage value

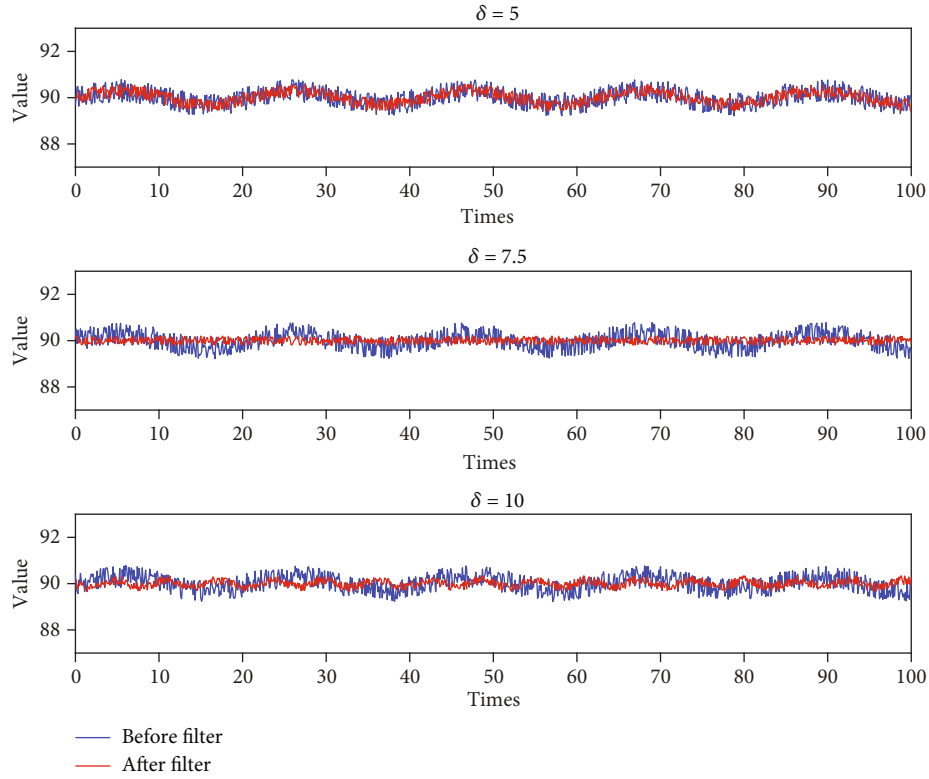

Figure 7: Analysis of filtering effect of low pass filter.

can be converted into the corresponding impact force during subsequent processing.

4.2. Result Analysis of Wavelet Filtering Algorithm. The selection of the window width parameter δ is the key. Theoretically, the larger the δ is, the better. In practical calculation, if δ is too large, it will bring a greater edge effect and increase the correlation of filtered data. Therefore, an appropriate compromise should be made between window width and edge effect (and data correlation), which is also a problem that must be considered by any filtering method. In this paper, the method of experimental debugging is used to take a value, that is, filter δ segment of analog data, and then adjust the size of δ so that the relative accuracy of filtering results can reach 0.5%.

The low-pass filter and second-order derivative filter are performed for $f(t)$, respectively. The scale parameters δ are taken take 5, 7.5, and 10, respectively. The filtering statistical results are shown in Figure 7.

It can be found that when s is between 6 and 8 km, the 10 km term can be easily extracted with good accuracy. For $\delta = 10$, the filter has the best accuracy. However, considering that the relative accuracy has reached 0.5% when taking 7.5 and the large 8 value causes a large edge effect and data correlation, it can be considered that $\delta = 7.5$ is enough to meet the requirements. Since the filter must be of finite length, for the parent wavelet $\theta(t)$ and the parent wavelet $\psi(t)$. We only intercept $y \in [-20, 20]$, and more than 99.99% of the energy in the calculation table is concentrated in this interval.

The scale parameter s is adjustable. The above filtering experiments only take four scales. In fact, after the basic parent wavelet and mother wavelet are constructed, people can filter on the desired scale by adjusting s. According to the data characteristics of the airborne gravimeter, it can be given that the scale range of s is 1~100 km, which can meet the requirements of the airborne gravimeter for various resolutions.

4.3. Validation of Combat Response Training Tester. Aerobic boxing is a kind of aerobics that integrates boxing, taekwondo, and other fighting sports on the basis of traditional aerobics. With the accompaniment of music with a clear rhythm, the exercisers show their health, power, and pride between their cool fists and feet. Therefore, it is widely welcomed by college students, especially boys. This paper makes an experimental study on the introduction of aerobic fight gymnastics into college aerobic classes, aiming to improve the interest of college boys in taking part in fight sports, further improve the quality of fight teaching, and provide a basis for fight teaching. This paper makes an experimental study on the introduction of aerobics into aerobic classes in colleges and universities, aiming to improve the interest of college boys in participating in aerobics, further improve the quality of aerobic teaching, and provide a basis for aerobic teaching. The subjects were trained in aerobics once a week for up to 17 weeks, each time lasting for 90 minutes. The experimental group used an aerobic intervention method for teaching, and the control group used the three-

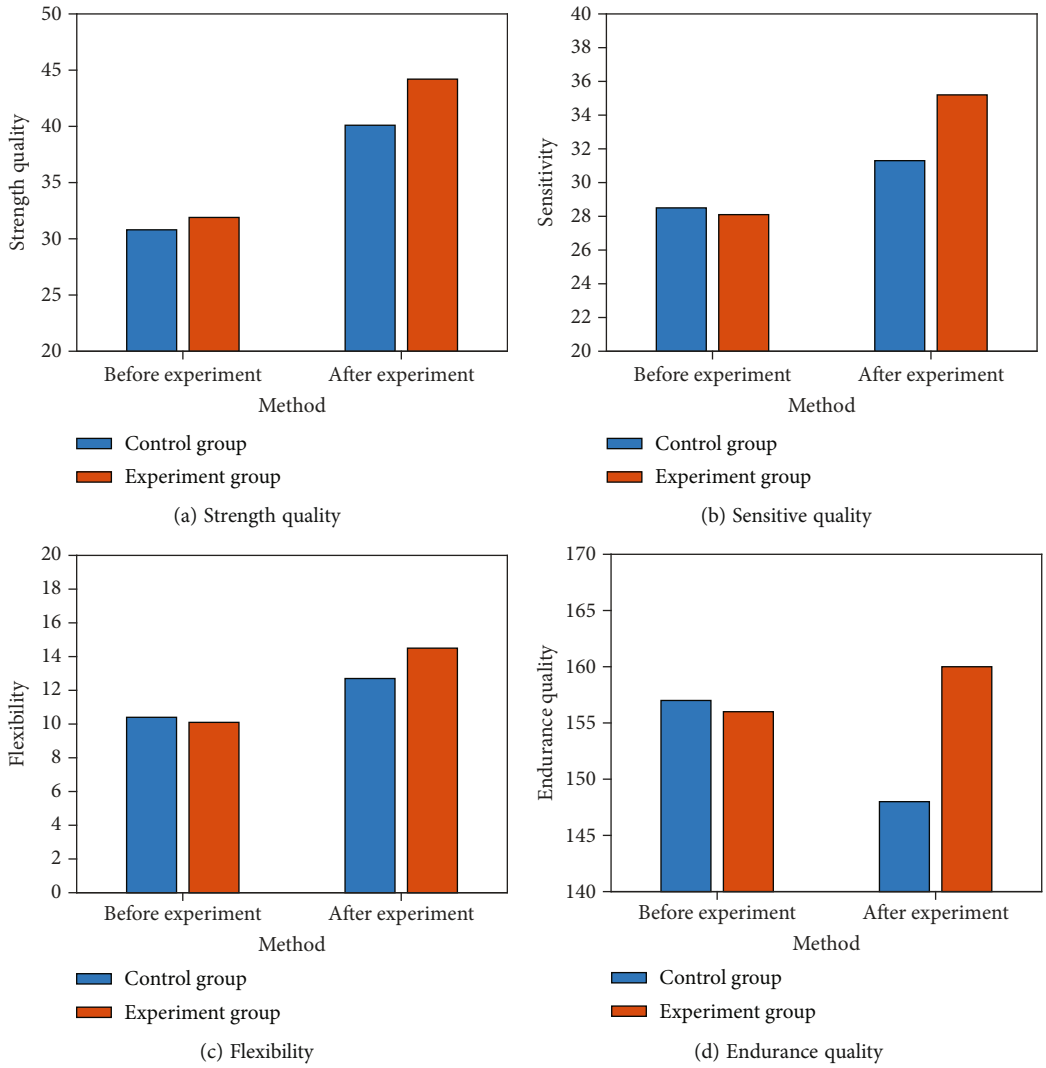

Figure 8: Comparison of physical test results between the control group and the experimental group.

level routine action of the "public aerobic grade exercise standard" [22]. During the experiment, the subjects generally did not participate in other forms of exercise. The experimental results are shown in Figure 8.

Before the experiment, there was no significant difference in physical fitness between the control group and the experimental group ($p > 0.05$); that is, the physical fitness level of the two groups of students was the same. After 17 weeks of aerobic intervention exercise, there were significant differences in four indicators of physical fitness between the two groups ($p < 0.05$), and the experimental group was significantly better than the control group in three indicators of strength, agility, and flexibility, and there was no significant difference in endurance quality between the two groups. It can be seen that aerobic exercise can significantly improve the physical quality of college boys, and the exercise effect is better than the standard routine exercise of mass aerobics. The experimental results show that the fighting instrument can effectively improve strength and sensitivity, and also improve flexibility and patience. Aerobic boxing can improve the interest of college boys in learning aerobics and improve the imbalance between men and women in the teaching of boxing. Aerobic boxing exercises can significantly improve the strength, flexibility, agility, and endurance of students. From the final special skill examination results of aerobics in the experimental group and the control group, boys have higher enthusiasm and initiative in learning aerobics and better learning effect.

5. Conclusion

Based on the basic principle and theory of embedded design, combined with the design practice of traditional fight training device, this paper analyzes and studies the design of other related fitness equipment, including hardware simulation and software simulation, and basically grasps the design theory and design principle of comprehensive fight training system. In the design process, the sp430 single-chip microcomputer is used to store and calculate the data collected by the ultrasonic sensor and the air pressure sensor. At the same time, a force-measuring sensor for combat competition based on the e-touch piezoelectric film is proposed. The

voltage follower with convenient conversion, high sensitivity, and good output voltage ratio is used as its conditioning circuit for the subsequent AD conversion. The output voltage is corresponding to the impact force through calibration, so as to prepare for the accurate calculation of the force, duration, and frequency. In addition, this paper mainly uses the wavelet filtering algorithm to process the data collected by the data sensor and obtains relatively high accuracy. The experiment shows that the introduction of a combat-testing instrument based on an intelligent sensor can help to improve the interest of training, improve the training effect, and promote the popularity of combat sports in the world. The wireless communication technology is used to connect all the fight trainer systems with the upper computer, and a database system is established, which contains the personal test records of each user. As a result, all test equipment in the same gym can be connected with the upper computer to establish a comprehensive user database system.

Data Availability

The datasets used and/or analyzed during the current study are available from the corresponding author upon reasonable request.

Conflicts of Interest

The authors declare that they have no conflicts of interest regarding the publication of this paper.

References

[1] U. Fidan, M. Yildiz, and İ. Çalikuşu, "Design and development of an upper extremity performance analysis system for combat sports," *Sigma Journal of Engineering and Natural Sciences*, vol. 39, no. 1, pp. 97–109, 2021.

[2] M. S. Khan, M. O. Tariq, M. Nawaz, and J. Ahmed, "MEMS sensors for diagnostics and treatment in the fight against COVID-19 and other pandemics," *IEEE Access*, vol. 9, pp. 61123–61149, 2021.

[3] J. Henderson, J. Condell, J. Connolly, D. Kelly, and K. Curran, "Review of wearable sensor-based health monitoring glove devices for rheumatoid arthritis," *Sensors*, vol. 21, no. 5, p. 1576, 2021.

[4] R. Palanivelu and P. S. S. Srinivasan, "Safety and security measurement in industrial environment based on smart IoT technology based augmented data recognizing scheme," *Computer Communications*, vol. 150, pp. 777–787, 2020.

[5] Y. Ma, J. Ouyang, T. Raza et al., "Flexible all-textile dual tactile-tension sensors for monitoring athletic motion during taekwondo," *Nano Energy*, vol. 85, article 105941, 2021.

[6] D. Li, S. Hu, Q. Fan et al., "Phage display screening of TIGIT-specific antibody for antitumor immunotherapy," *Bioscience, Biotechnology, and Biochemistry*, vol. 83, no. 9, pp. 1683–1696, 2019.

[7] J. M. Hughes, E. Gaffney-Stomberg, K. I. Guerriere et al., "Changes in tibial bone microarchitecture in female recruits in response to 8 weeks of U.S. Army Basic Combat Training," *Bone*, vol. 113, pp. 9–16, 2018.

[8] M. Tabben, M. Ihsan, N. Ghoul et al., "Cold water immersion enhanced athletes' wellness and 10-m short sprint performance 24-h after a simulated mixed martial arts combat," *Frontiers in Physiology*, vol. 9, p. 1542, 2018.

[9] T. Ambroży, W. Wąsacz, A. Koteja et al., "Special fitness level of combat sports athletes: mixed martial arts (MMA) and Thai boxing (Muay Thai) in the aspect of training experience," *Journal of Kinesiology and Exercise Sciences*, vol. 31, no. 95, pp. 25–37, 2021.

[10] M. L. Everitt, A. Tillery, M. G. David, N. Singh, A. Borison, and I. M. White, "A critical review of point-of-care diagnostic technologies to combat viral pandemics," *Analytica Chimica Acta*, vol. 1146, pp. 184–199, 2021.

[11] Y. Ruan, X. Yu, H. Wang et al., "Sleep quality and military training injury during basic combat training: a prospective cohort study of Chinese male recruits," *Occupational and Environmental Medicine*, vol. 78, no. 6, pp. 433–437, 2021.

[12] L. Feng, W. Chen, T. Wu et al., "An improved sensor system for wheel force detection with motion-force decoupling technique," *Measurement*, vol. 119, pp. 205–217, 2018.

[13] W. L. Liu, L. Zhu, Y. Y. Qi et al., "Effects of injection pressure variation on mixing in a cold supersonic combustor with kerosene fuel," *Acta Astronautica*, vol. 139, pp. 67–76, 2017.

[14] S. J. Chuang, Y. C. Sung, C. Y. Chen, Y. H. Liao, and C. C. Chou, "Can match-mimicking intermittent practice be used as a simulatory training mode of competition using Olympic time frame in elite taekwondo athletes?," *Frontiers in Physiology*, vol. 10, p. 244, 2019.

[15] E. Franchini, "High-intensity interval training prescription for combat-sport athletes," *International Journal of Sports Physiology and Performance*, vol. 15, no. 6, pp. 767–776, 2020.

[16] R. Reale, L. M. Burke, G. R. Cox, and G. Slater, "Body composition of elite Olympic combat sport athletes," *European Journal of Sport Science*, vol. 20, no. 2, pp. 147–156, 2020.

[17] J. Chycki, A. Kurylas, A. Maszczyk, A. Golas, and A. Zajac, "Alkaline water improves exercise-induced metabolic acidosis and enhances anaerobic exercise performance in combat sport athletes," *PLoS One*, vol. 13, no. 11, article e0205708, 2018.

[18] N. Hammami, S. Hattabi, A. Salhi, T. Rezgui, M. Oueslati, and A. Bouassida, "Profil des blessures en sports de combat : revue de la litterature," *Science & Sports*, vol. 33, no. 2, pp. 73–79, 2018.

[19] D. Zubac, R. Reale, H. Karnincic, A. Sivric, and I. Jelaska, "Urine specific gravity as an indicator of dehydration in Olympic combat sport athletes; considerations for research and practice," *European Journal of Sport Science*, vol. 18, no. 7, pp. 920–929, 2018.

[20] R. Reale, G. Slater, and L. M. Burke, "Weight management practices of Australian Olympic combat sport athletes," *International Journal of Sports Physiology and Performance*, vol. 13, no. 4, pp. 459–466, 2018.

[21] X. Wang, W. Song, Y. Ruan et al., "Core muscle functional strength training for reducing the risk of low back pain in military recruits: an open-label randomized controlled trial," *Journal of Integrative Medicine*, vol. 20, no. 2, pp. 145–152, 2022.

[22] J. Wąsik, D. Bajkowski, G. Shan, R. Podstawski, and W. J. Cynarski, "The influence of the practiced karate style on the dexterity and strength of the hand," *Applied Sciences*, vol. 12, no. 8, p. 3811, 2022.

Hindawi
Wireless Communications and Mobile Computing
Volume 2023, Article ID 9871392, 1 page
https://doi.org/10.1155/2023/9871392

Retraction

Retracted: A Comprehensive Review of Lightweight Authenticated Encryption for IoT Devices

Wireless Communications and Mobile Computing

Received 12 December 2023; Accepted 12 December 2023; Published 13 December 2023

This article has been retracted by Hindawi, as publisher, following an investigation undertaken by the publisher [1]. This investigation has uncovered evidence of systematic manipulation of the publication and peer-review process. We cannot, therefore, vouch for the reliability or integrity of this article.

Please note that this notice is intended solely to alert readers that the peer-review process of this article has been compromised.

Wiley and Hindawi regret that the usual quality checks did not identify these issues before publication and have since put additional measures in place to safeguard research integrity.

We wish to credit our Research Integrity and Research Publishing teams and anonymous and named external researchers and research integrity experts for contributing to this investigation.

The corresponding author, as the representative of all authors, has been given the opportunity to register their agreement or disagreement to this retraction. We have kept a record of any response received.

References

[1] Z. AlJabri, J. Abawajy, and S. Huda, "A Comprehensive Review of Lightweight Authenticated Encryption for IoT Devices," *Wireless Communications and Mobile Computing*, vol. 2023, Article ID 9071969, 31 pages, 2023.

Hindawi
Wireless Communications and Mobile Computing
Volume 2023, Article ID 9071969, 31 pages
https://doi.org/10.1155/2023/9071969

Review Article

A Comprehensive Review of Lightweight Authenticated Encryption for IoT Devices

Zainab AlJabri, Jemal Abawajy, and Shamsul Huda

School of Information Technology, Deakin University, Geelong, Victoria 3217, Australia

Correspondence should be addressed to Jemal Abawajy; jemal.abawajy@deakin.edu.au

Received 20 March 2022; Accepted 23 August 2022; Published 21 February 2023

Academic Editor: Chin-Ling Chen

Internet of Things (IoT) is a promising technology for creating smart environments, smart systems, and smart services. Since security is a fundamental requirement of IoT platforms, solutions that can provide both encryption and authenticity simultaneously have recently attracted much attention from academia and industry. This article analyses in detail state-of-the-art lightweight authenticated encryption (LAE) targeted to IoT systems. This work provides a thorough description of the algorithms, and the study systematically classifies them to facilitate understanding of relevant intricacies of the schemes. Among reviewed algorithms, there is a trade-off to retain design security, resources cost, and efficient performance. ACORN is the effective scheme on various platforms in terms of utilization of resources and power consumption, while MORUS and AES-CLOC are the fastest in hardware platforms. However, they are susceptible to misuse despite their resistance to side channel attacks. In contrast, JOLTICK, PRIMATESs, COLM, DeoxysII, OCB, and AES-JAMBU are provably resistant to nonce misuse. The challenges for possible future research are summarized. Overall, the article provides researchers and developers with practical guidance on various design aspects and limitations as well as open research challenges in the current lightweight authenticated encryption for IoT.

1. Introduction

The Internet of Things (IoT) refers to a paradigm in which physical objects (IoT devices) autonomously communicate with each other and connect to the Internet via embedded devices such as sensors and actuators [1]. It is estimated that there will be approximately 75.44 billion IoT connected devices in 2025 [2]. These IoT devices enable automation, monitoring and controlling, remote processes, data collection and analytics to drive insights, generate workflows, optimize processes, and more. With these capabilities, IoT is transforming a wide range of industries including healthcare, agriculture, transportation, and the energy sector [3, 4] with massive potential improvement in sustainable social and economic development. For example, an IoT-enabled smart transportation network will improve productivity, reduce costs, and enhance public safety and security [5, 6]. IoT is revolutionizing many aspects of healthcare, such as enabling remote patient care, which benefits patients, their families, healthcare providers, and insurance companies [7]. Similarly, IoT is deployed in the energy industry to modernize infrastructure, improve operational efficiency and reliability, provide consumers with affordable energy, and enable industry to monitor and access energy sources [8]. Table 1 lists the acronyms and abbreviations throughout the paper.

While IoT provides ample opportunities for digital transformation, it poses significant security threats [9–11]. These threats include distributed denial of service attacks [10], botnets [12], privacy and confidentiality breaches [11], and IoT-targeted malware [13]. IoT data flows through the network and requires data encryption and authenticity to ensure confidentiality (C) and integrity (I). For example, ensuring C of vital signs observation from a remote patient monitoring system is crucial. Although it is important for medical practitioners to trust the signs observation they receive as an authentic data, IoT devices have very minimal security settings in place. Consequently, there is hardly any encryption facility for securing sensitive and critical information. Furthermore, there is no built-in mechanism to ensure data authenticity. Since tampering with IoT data

Table 1: List of acronyms and abbreviations.

Acronyms	Abbreviation	Page
IoT	Internet of Things	1
LAE	Lightweight authenticated encryption	1
C	Confidentiality	1
I	Integrity	1
AE	Authenticated encryption	2
ASIC	Application service integrated circuit	2
FPGA	Field programmable logic array	2
PKI	Public key infrastructure	2
SSL	Secure socket layer	2
TLS	Transport layer security	2
ECC	Elliptic curve cryptography	2
MAC	Message authentication code	2
SSO	Single sign on	2
ECDH	Elliptic curve Diffie Hellman	2
CoAP	Constrained application protocol	2
NIST	National Institute of Standards and Technology	2
CASEAR	Authenticated encryption security applicability and robustness competition	2
AVR	Atmel microcontroller	3
MSP	Mixed signal microcontroller	3
ARM	Advanced reduced instruction set computer	3
AMD	x86 instruction set	3
LoRaWan	Low range wide area networks	5
AMQP	Advanced message queuing protocol	5
MQTT	Message queue telemetry transport	5
IND	Indistinguishability	6
NM	Non-malleability	6
IND-CPA	Indistinguishability-chosen plaintext attack	6
IND-CCA	Indistinguishability-chosen ciphertext attack	6
NM-CPA	Non-malleability-chosen plaintext attack	6
INT-PTXT	Integrity-plaintext attack	6
INT-CTXT	Integrity-ciphertext attack	6
E	Encryption oracle	6
D	Decryption oracle	6
K	Key	6
KM	Known message	6
KC	Known ciphertext	6
CM	Chosen message	6
CC	Chosen ciphertext	6
AD	Associated data	8
AEAD	Authenticated encryption with associated data	8
EaM	Encrypt-and-MAC	9
EtM	Encrypt-then-MAC	9
MtE	MAC-then-encrypt	9
CTR	Counter mode	9
GCM	Galois counter mode	9
CWC	Carter Wegman counter mode	9
HTTP	Hypertext transfer protocol	9
UDP	User datagram protocol	9

Table 1: Continued.

Acronyms	Abbreviation	Page
DTLS	Transport layer security	9
IPsec	Internet protocol security	9
IAPM	Encryption modes with almost free message integrity	10
OCB	Block cipher mode of operation for efficient authenticated encryption	10
EPBC	Efficient error-propagating block chaining	10
CLOC	Low overhead counter feedback mode	10
CCM	CBC-MAC	10
XOR	Exclusive-OR gate	10
ROM	Read only memory	11
RAM	Random access memory	11
LUTs	Lookup tables	11
GE	Logic equivalent	11
NAND	Not-AND	12
Bps	Bits per second	12
V	Variable	15

could have a profound impact, it is a practical necessity to minimize the manipulations and the exposure of sensitive information to malicious parties.

With the growing number of IoT-born attacks, the need for securing the IoT and data has recently received a significant attention from the industry and research community [13]. Generally, the dominant basis for security is the application of cryptographic algorithms to ensure C and I of information. IoT devices are constrained by the area footprint, power consumption, energy, and throughput [14]. Therefore, the conventional cryptographic algorithms are computationally expensive, which is potentially unreasonable for conveying restricted device requirements. The study in [15] highlighted the importance of lightweight cryptography for IoT devices and particularly LAE for improving IoT device security. This has generated a substantial amount of literature with promising cryptography schemes as security solutions for the IoT. However, these published studies are commonplace and researchers and developers should focus on collating them for use.

LAE promises better efficiency and security compared to conventional cryptography, and is suitable for IoT applications restricted by resources, power consumption, and energy. Explicitly, it combines data C and authenticity services in one algorithm. Less prerequisite than separated encryption composition. It encrypts and authenticates the messages in order to protect users and secure data network communication. Typically, it can be integrated between sensing layer and network layer, within various connections of network layer, between network and service layers, and between service and interface layers.

Existing reviews on authenticated encryption (AE) have been published [15–20]. These studies are proposed for industrial IoT, smart cards, sensors, smart low-resource devices, smartphones, and power grid systems. However, these studies are fragmented in terms of security, not comprehensive enough to enhance understanding of relevant aspects, and focusing on general high-level performance issues. The security threats and parameter specification were not considered in [17]. Data authenticity that occurs in transit or at storage cannot be detected because data integrity countermeasure is not considered among the reviewed schemes. Schemes' functionality criteria and their security requirements were not discussed in [15]. The study in [18] did not include compelling security justification and instead discussed cryptographic schemes, which are proved to be no longer safe for use [16, 21]. One recent review [22] has studied lightweight cryptography, considering two separate schemes as lightweight block cipher primitive for encryption, and lightweight hash function for authenticity.

The work of [17] focused on block cipher algorithm performance in application service integrated circuit (ASIC). Similarly, the focus of [18] is lightweight block cipher implementation in ASIC and field programmable logic array (FPGA). Block cipher algorithms were reviewed in [19], but did not consider the resources cost of the schemes by imposing computationally expensive schemes for IoTs such as Twofish [23]. The study by [24] evaluated the performance metrics of lightweight cryptography. However, the LAE scheme was not considered in these reviews as a built-in solution. The review [25] determined the performance of CASEAR algorithms for IoT but did not consider security threats imposed due to IoTs are being placed in uncontrolled environment. The survey in [20] explored Dexoys, MORUS and POET studied in FPGA, Intel Core i7-4770 and Intel Core i5-3210M platforms, but MORUS and POET are prone to nonce misuse and provable forgery attacks, respectively, [26]. In [20], the scheme Dexoys has two forms with diverse nonce misuse feature, but this work surveyed the version threaten to nonce manipulation attack. Overall, LAE were surveyed for efficiency performance metrics and eliminating security threats and resources cost [15, 20].

Targeting IoT applications or resource-constrained devices is usually seen from performance perspectives either for low power, low area metrics, or high throughput, disregarding the security of the algorithms. Most existing reviewed schemes are based on lightweight symmetric algorithms (cryptographic scheme where two parties share the same key) [27, 28], while LAE should be further studied for IoT. In [27] and [28], lightweight symmetric encryptions were designated for restricted IoT; however, a communication header can be manipulated without detection. Thus, they require additional hashing scheme to validate data I, which adds to the computational expenditure. To ensure C and I objectives, we need to validate data and provide security controls for protection against different types of IoT attacks. Nonetheless, it is very challenging to deploy endpoints security controls such as malware guards and conventional security. Conventional endpoints security controls cannot be applied as the IoT gateway network, and local endpoint networks have different protocols [29]. Constrained devices also restricted the ability to use a public key infrastructure (PKI) based authentication scheme such as Secure Socket Layer (SSL) and Transport Layer Security (TLS). This is due to the expenditure imposed by the PKI hardware implementation, the SSL certificate maintenance, and key management for a large number of IoT devices [30].

Lightweight identity approach was introduced by eliminating PKI certificate requirement [31]. However, the algorithm is based on certificateless elliptic curve cryptography (ECC), hash-based message authentication code (MAC), and secure hashing algorithm, which are conventional mechanisms requiring computational resources. Authenticating a large number IoT nodes in a hostile environment that stores secret keys imposes physical security loss, which in turn will affect the entire network and jeopardize the IoT system [32]. Manual installation of common symmetric keys is very difficult for numerous numbers of devices. To reduce the workload of key management, single-sign-on (SSO) based approaches can be applied that require user interaction, and numerous devices require self-authentication. The application of SSO-based protocols is limited since it requires a user response [33]. Self-authentication can be combined with elliptic curve Diffie Hellman (ECDH), and the initialized key, yet this approach requires high computation compared to lightweight cryptography [34].

The cloud-assisted IoT system includes an IoT gateway, cloud, and service server falls under the TCP/IP protocol [35]. However, the IoT nodes and the IoT gateways have different protocols, for instance the constrained application protocol (CoAP). Although CoAP is a popular lightweight IoT protocol, it is susceptible to many well-known attacks [36, 37]. Unfortunately, IoT nodes are constrained by resources and due to their heterogeneous nature, deploying conventional mechanisms may not be practical. Recently, the research community has shown interest in AE due to National Institute of Standards and Technology (NIST) calling for lightweight ciphers and the finished AE security applicability and robustness competition (CASEAR). NIST has been conducting the lightweight cryptography project to select one or more LAE and hashing schemes suitable for constrained environments including IoTs. In 2019, fifty-seven candidates have been submitted to the project which fifty-six schemes are accepted as a first round. Many schemes eliminated for the second round due to their limitation on providing security criteria and implementation characteristics including performance and cost. In the second round, thirty-two schemes were qualified. Recommended schemes are expected to resist side channel attack to provide additional security level against physical attacks. Such criteria are significant for IoT devices because they are deployed in hostile environment and unattended places. Thus, devices are protected from replication and manipulation [38].

Internal reviewers as well as the wider community conduct analysis and evaluation of candidates. After rounds of candidates' elimination, ten become finalist recently. These are ASCON, Elephant, GIFT-COFB, Grain-128AEAD, ISAP, PHOTON-Beetle, Romulus, SPARKLE, TinyJAMBU, and Xoodyak. NIST encourages public evaluation and publication of schemes security, implementation, and performance. According to [39], TinyJAMBU employs minimum resources compared to ASCON, Romulus, GIFT-COFB, and Xoodyak, but supports a low throughput. Xoodyak, in contrast, achieves the highest throughput to facilitate low-latency application requirement but resources are expensive. Of these schemes, ASCON, GIFT-COFB, and Romulus have shown a reasonable trade-off between resources and performance. ASCON was a winner in the CASEAR competition besides ACORN. Both schemes have been targeting constrained devices in terms of security, applicability, and robustness. However, schemes are yet to be evaluated for IoT platforms. As well, the standardization process is ongoing, with calls to investigate LAE preferences for IoTs. Subsequently, LAE is a promising option for IoT devices and motivates future research into lightweight cryptography.

In this paper, we present a review of state-of-the-art LAE for IoT taking into account various aspects of the algorithms including potential attacks. The cipher design parameters such as block size, and key size are crucial parameters for providing security, in addition to other attacks targeting AE such as nonce misuse attacks and side-channel attacks. This study proceeds based on the existing approaches to address the challenges of providing secure and effective AE solutions for IoT applications. The review provides a thorough description of the algorithms and systematically they are classified to facilitate an understanding of the related intricacies and relevant aspects. It discusses how these ciphers resist various design attacks by considering the design characteristics and underlying primitives. We also introduce a system model and threat model for AE applicability in IoT.

Our study comprehensively reviews a benchmark of LAE and promises the security based on the literature. It also reviews the effective performance of IoT based on several platform-related metrics, with an observation of the relevant challenges. The contributions of this review are as follows:

(i) We present a generalized IoT system model that is suitable for explaining AE within different model layers. We highlight various IoT challenges based on

the system model, system requirements, and introduce threat model with applicable IoT applications

(ii) We present a comprehensive state-of-the-art LAE method for IoT platforms. We review the construction of AE design classifications and underlying primitives. We reviewed and examined the schemes based on their design security including C and I security, nonce misuse property, and side channel attacks

(iii) We compare discuss the challenges of LAE performance benchmarks and introduce functionality criteria, platform awareness, and resource limitations as factors for comparison fairness. Moreover, we comparatively reviewed the most prominent performance in different platforms including FPGA, ASIC, 8 bits Atmel microcontroller (AVR), 16 bits mixed signal microcontroller (MSP), 32 bits advanced reduced instruction set computer (ARM), and x86 instruction set (64 bits AMD).

(iv) We discuss the challenges and key issues in LAE for IoT, which will be useful for future research

The remainder of this paper is organized as follows. Section 2 introduces the IoT system model and Section 3 IoT system requirements. Section 4 models schemes' threats. Section 5 introduces the state-of-art LAE algorithms and their limitations, with reference to the existing literature on the design, classification, and basis primitives. Section 6 comprehensively discusses the algorithms' functionality, while Section 7 comparatively discusses the security vulnerability, functionality, and performance aspects. Section 8 discusses open problems and finally Section 9 concludes this review.

2. System Model

To illustrate this work's system requirements, we have modelled a four-layer IoT architecture compiled from the International Telecommunication Union IoT architecture [40]. The model includes sensing layer, network layer, service layer, and interface layer, where they interact according to the use-case. Each layer illustrated in Figure 1 should provide sufficient data for I and C in transmission besides other securities such as access control and availability. The IoT data are transmitted between the layers composed of a data header and a payload depending on the technology. For example, low range wide area networks (LoRaWAN) constitute the most applied technology for transmitting sensor data with a maximum packet size of 255 bytes includes 13 bytes header [41].

The system architecture must deliver functional guarantees and security requirements for the IoT to bridge the gaps between physical devices and virtual world. Interconnection of IoT devices enables information collection, aggregation, exchange, processing, and proper data interpretation. At the sensing layer, existing embedded devices are enabled to collect information and exchange them with each other. For instance, low-power sensors attached to a patient facilitate remote monitoring of medical devices (i.e., wearable devices and smart sensors), and send the stored record to the network layer. The encapsulated record in this example includes alerts, medication dosage, condition status, and risky private information [42].

The main concerns in IoT sensing layer determination include things size, cost, resources, energy consumption, hybrid network, and communication [43]. Devices are equipped with sensing capability such as radio frequency identity tags, sensors, and actuators. These devices should be designed with the aim to minimize resources as well as deployment costs. Heterogenous issues involve communication via hybrid networks to enable information exchange between things. IoT is expected to interconnect with industrial networks to facilitate smart services. At the sensing layer, the devices have limited power consumption and restricted resources.

The network layer plays a vital role in connecting the things together and exchange sensed data with surrounding awareness. Data aggregation, encapsulation, and routing with regard to the network protocol are processed in the network layer. Various networks are connected and several protocol types serve to connect low-power nodes together, such as IEEE802.15.4, IEEE 802.15.1, and LoRaWAN. Reliable communication facilitates the encapsulation and routing, such as CoAP, advanced message queuing protocol (AMQP), and message queue telemetry transport (MQTT). The network varieties cause security issues, deployment difficulties, and communication issues. Of these concerns, data C and user privacy are critical due to mobility, complexity, and deployment [43]. Since some IoT devices are physically placed in untrusted environments, they risk user identification and threaten to device manipulation. Attackers can create faulty messages, which disturb the network's functionality and isolate devices from the network.

The service layer consists of middleware devices to provide collaborative IoT services related to identification, authorization, aggregation, decision support, and reactions. These technologies cooperate with services and IoT applications to provide a cost-effective product. Several types of hardware and software utilized with supported service protocols help to achieve user objectives. In this layer, the IoT demonstrates middle service activities. Service organization and providers develop various standards to undertake these activities. The service layer facilities the activities based on common application, service protocols, and application programming interfaces. The services include processing, analysis, integration, management, security, and user interface. These services input processed information, collaborate, and provide results to the user application layer. Security of this layer should be able to protect the operations from privacy leakage of location tracking, information manipulation, spoofed information, faulty routing path, and more.

The interface layer overcomes various technology vendor interconnections, where the searching service is integrated. This layer helps to identify and match application requirements. Application maintenance demands secure remote configuration of I and C transmission between the

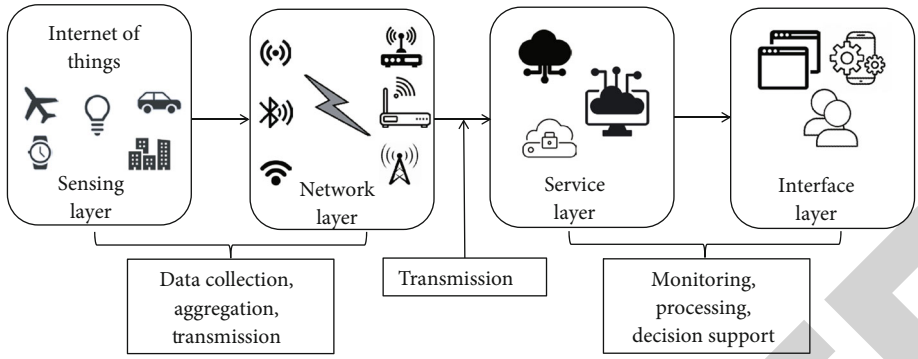

Figure 1: Typical IoT system architecture.

layers, secure software update and download, and administrator authentication. Users then view results and decisions employing an application on their smartphones, and personal computers [42, 44]. Most IoT devices are constrained and designated security solutions should consider resources, energy efficiency, and performance. The light computation security schemes at constrained devices are in high demand; however, proposing a secure solution with these aspects prior to deployment is critical [45].

3. System Requirements

The aim of the AE is to ensure C of message (i.e., the contents of transmitted message will not be read by unauthorized recipient) and I (i.e., the message have not been modified during transmission by any means) of the messages exchanged between the genuine sender and receiver [46]. IoT application collects, exchanges data, and transmits the data to remote servers such as cloud computing for further processing and critical decision-making. The data is critical and personal and for example in health-related information, it requires stringent C against data disclosure [47]. Maintaining data I provides a means of detecting unauthorized data manipulation [48]. Such assurance is important for IoTs because they are prone to receiving forge data. Forged data is applicable since devices can be accessed, managed, and connected to several things from various places [49].

C prevents the disclosure of messages to parties not authorized to view the message or the decision [50]. To satisfy the C requirement, AE defines data C by three notions: it must be capable of Indistinguishability (IND) and Non-malleability (NM). IND and NM prevent against Indistinguishability-chosen plaintext attack (IND-CPA), Indistinguishability-chosen ciphertext attack (IND-CCA), and Non-malleability-chosen plaintext attack (NM-CPA) [51, 52]. Furthermore, I detects the forge message and/or tampered data. It also thwarts IoT functionality from false response that disturbs the IoT operation [53]. To enable I detection requirement, the check must be guaranteed from the time data has been created, transmitted or stored by illegitimate users. It must also be able to defend against Integrity-plaintext (INT-PTXT) and Integrity-ciphertext (INT-CTX) attacks [54].

4. Threat Modeling

Threat models for AE as stated in CASEAR as well as NIST target conventional confidentiality and integrity proofs, and leave nonce robustness and side channel attacks as optional threats [55]. Definitions of AE security assume that received encrypted data will go through the decryption oracle and the whole plaintext is recomputed [56]. Using a conventional algorithm, data recovering, recovering keys, manipulation of encrypted data constitute threats. These threats are examined using properties of IND and NM besides different integrity violations against INT-PTXT and INT-CTX. However, using these models, it has been identified that real world threats including information leak via side channel attacks cannot be captured [57]. In practice, nonces also have been breached via repetition or manipulation [58]. To address these risks, we expand our model to include two more threats. First, nonce is controlled by adversary and nonce randomness is not guaranteed. Second, the packet header will not be encrypted for routing purposes but can be manipulated by the adversary. Thus, our model threat can be seen a practical way to assess data cryptography violations.

The system shown in Figure 2 describes a communication channel from an authorized sender A to intended receivers B and F, and the adversary H, where the ability of the adverse situation is characterized by the link capabilities. The message is transmitted from nodes through a gateway to the Internet in order to be accessed by users. The transmitted message is composed of a payload, packet header, and a tag. In this analysis, the focus is on how the attacker successfully breaches the message encryption and gains knowledge, which in turn lead to content or/and successful verification of a faulty payload or/and a faulty header tag [59].

The adversarial model is defined by IND-CPA, IND-CCA, INT-PTXT, INT-CTXT, and NM-CPA, fault attack, and forgery attack. The adversary targets message C and I by launching these attacks on LAE. The threats of breaching schemes lead to access transmitted message, key recovery, message manipulation, and packet header manipulation. These threats are achievable with prior knowledge related to the scheme as summarized in Table 2. These include the knowledge of encryption oracle (E), decryption oracle (D),

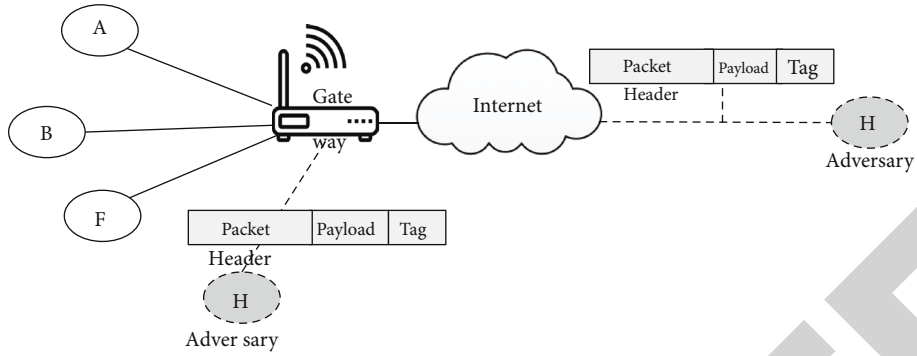

Figure 2: Adversaries source of threats as *H* while *A*, *B*, and *F* are honest participants.

Table 2: Attacks of algorithms with confidentiality or integrity breach and adversaries knowledge.

Attacks	Type				Knowledge					Threat[a]
	C	I	EO	DO	K	KM	KC	CM	CC	
IND-CPA	√	×	√	×	×	√	×	√	×	(a)
IND-CCA	√	×	×	√	×	×	√	×	√	
NM-CPA	√	×	√	×	×	√	×	√	×	(b)
INT-PTXT	×	√	√	×	×	√	×	√	√	
INT-CTXT	×	√	×	√	×	×	×	√	√	
Fault	√	×	√	√	×	×	×	×	×	(a), (b)
Forgery	×	√	×	√	×	×	×	√	√	(c), (d)

[a] Threats are (a) recover the secret key, (b) recover the message, (c) manipulate packet header, (d) manipulate message.

key (K), known message (KM), known ciphertext (KC), the chosen message (CM), or the chosen ciphertext (CC).

Breaches of C occur when any of IND-CPA, IND-CCA, NM-CPA, and fault attacks is violated. These lead to data disclosure, where eavesdropper reveals data without permission and infers some useful information that consequently helps to establish a series of attacks [60]. It can also be used to compromise the device and obtain privileges. For example, an adversary who can intercept and exploit a smart home locker can access house controls and result in multiple thefts by taking the owner benefits for future theft [61]. In home utilities, users share habits, lifestyles, browsing interests, and activities that can be revealed by the attacker. IND has been extensively studied in [62–64]. It ensures that an adversary who chooses two messages—Ma and Mb, has a ciphertext of one of them—cannot distinguish which message corresponds to the ciphertext.

IND-CPA is breached when the adversary has access to encryption oracle and one CC results from two KM. The adversary has to distinguish CC corresponding to KM in order to breach the message C. The vulnerability of this attack allows the attacker to recover the messages underlaying a selected ciphertext or the secret key and then disclose the message. For example, *H* node is impersonating *A* node intended to send a message to *B*, and the message includes a content related only to A node. He/she can manipulate the packet header to present *A* node if he/she breaches IND-CPA. Furthermore, IND-CCA is subverted by an adversary using the machine decryption to answer his/her own requests and break into the underlying system that chose the ciphertext. This was queried according to a previously known message and ciphertext pairs [65, 66]. Maintaining this knowledge, he/she obtains a bilateral proof of knowledge from a user that allows him/her to generate the same proof of knowledge to another user. For example, *H* node has the decryption machine oracle of *B* node and receives a message from F node, and then is able to playback some of the previously known pairs that were received by *B* node earlier. An NM-CPA violation implies the non-malleability and a C threat. Attacker H node reconstructs a ciphertext that is differentiated from a known message to compromise NM-CPA [51, 67]. The attacker has the same knowledge of the chosen plaintext attack and manipulates the packet header to present himself as honest *A*, *B*, or *F*.

Fault attack is a technique to inject or modify errors using voltage, power, glitching clock, and laser fault injection, which threatens C [68]. An interesting consequence leads to an error output that can be analyzed to reveal secret information, such as recovering cryptographic secret keys [69]. To be effective, it is implemented through several approaches such as timing attack, differential and simple power analysis, statistical fault attack, differential fault analysis, and collision fault analysis [70, 71].

The schemes data I is breached when INT-PTXT, INT-CTXT, or Forgery attacks are violated. Breaking the I of the message achieved by adversary *H*, who generates a ciphertext that is mapped to a meaningful message that has never been generated previously by the honest user *A* and present himself as *A*. This attack requires knowledge of the encryption oracle, chosen message, and its corresponding

ciphertext. In this scenario, if the algorithm does not protect the security of INT-PTXT, *H* changes the packet header to be the same as A by sending this encrypted message to *B* or *F* without detection.

For the attacker perpetrating INT-CTXT, the I of the message requires the production of a ciphertext that is never generated previously, irrespective of whether the plaintext is new or meaningful. In this scenario, the adversary enquires about the ciphertext by accessing the decryption oracle. If the algorithm is not secure against ciphertext I, the adverse *H* manipulates the ciphertext sent by *B* to a different ciphertext that has never been transmitted before to the honest *A*, and *A* accepts. An example is an attacker modifying the alert in a smart healthcare system to a fault alert stating that the patient is in danger, or alters patient medicine configuration to increase the dosage. It is thereby accepted as a lawful alert and causes complications or even death [72]. In a smart city, the risk of manipulation can switch off the device causing an interruption [73].

Forgery attacks infringe on I assurance. It occurs when the mechanism is prone to causing message payload manipulation but the message tag is accepted as valid [46]. The attack exploits the algorithm leaked state information to improve the differential success [74, 75] and modify message payload and its packet header [76]. The adverse *H* launches a chosen plaintext forgery by obtaining the corresponding ciphertext of different consecutive blocks of the last algorithm block. Then, forges messages occur. This can be achieved by deleting one ciphertext block and duplicating another block or substituting the blocks. The forgery in this scenario is then not detected where the decryption results in the same I tag as the original legitimate message payload.

Fault attack is a technique devised to inject or modify erroneous using voltage, power, glitching clock, and laser faults injection threatens the confidentiality and leads to key recovery [68]. An interesting consequence is error output, which can be analyzed to reveal secret information like recovering cryptographic secret keys [69]. To be an effective attack it is implemented through several approaches, for example timing attack, differential and simple power analysis, Statistical Fault Attack, Differential Fault Analysis and Collision Fault Analysis [70, 71].

4.1. Other AE-Related Threats. Extracting cryptographic key is a vital threat resulting from several attacks including fault attack, forgery attack, and node impersonation attack [77, 78]. Physical access to the IoT devices increases the chance of inducing faults so a device operates in abnormal configuration, which results in a leakage. An example for this is leaking a secret key in the power source while the device operates [79].

Since the key can be stored in the IoT node, it is prone to clone attack that mimics the legitimate key materials and other information [80]. It makes it possible for a replica node to participate in the network with similar capabilities to an authorized node showing knowledge of the key. Key agreements without a secure connection is also pose a threat if there is not well-established asymmetric algorithm or secure pairing methods authenticating IoTs and preventing nodes impersonation and other node threats [77, 78]. If a message is encrypted by the key stored in an impersonated node and sent to the destination, the latter will validate the authenticity of the sender and retrieve the information successfully since it contains the knowledge of the key [81].

The IoT connectivity problem highlights the agreements problem such that different network technologies for mobile communication (2G, 3G, 4G, and 5G) and wireless network (Bluetooth low energy, WiMax, and LoRaWAN) used to communicate sensors data to users applications [81]. There are various key agreement schemes studied in the literature: ElGamal [82] and ECC [83], Lattice based asymmetric cryptosystem [84] and Password based authentication [78]. Nonce plays a significant role in protecting modern LAE schemes against the threat of two identical messages being encrypted into two related ciphertexts [85]. When schemes are unsecure against nonce misuse, the attacker manipulates the nonce or repeats them. In other algorithms, designers assume specific nonce configuration upon implementation, which does not withstand attacks [86]. The vulnerability of these threats is message patterns leak; the messages become inevitable, and hence recovered by the attacker. In some algorithms, the damage is worse [87].

5. State-of-the-art Lightweight Authenticated Encryption and Their Limitations

LAE was designated to consume less computation compared to conventional algorithms in current communication protocols. It tolerates a small footprint, minimum power consumption, and low energy. Additionally, it provides a desirable security level and can be easily integrated with existing protocol algorithms and restricted embedded devices. The encryption and decryption engines with interfaces are shown in Figure 3. The encryption oracle takes the message, key, and a nonce as inputs to produce a ciphertext and an I tag. The decryption oracle is used to verify the tag I and decrypt the ciphertext. It uses the shared secret key, and the same nonce to return either the message as plaintext or a special symbol to indicate counterfeit ciphertext.

AE schemes were constructed to encrypt and authenticate the message only; however, as they emerged in application, there was a need for additional data to be authenticated but not encrypted. Routing headers in the TLS protocol, for example, should be kept clear so that the packet is routed to the destination. If the header is encrypted, the routers cannot read the routing details and hence it is difficult to forward the packet to the final destination [88]. For this reason, there is a need to provide AE protection and authenticity to secret data and the authenticity of other associated data (AD). This leads to the existence of AE with associated data (AEAD), where the headers or nonsecret data are called AD [89–91].

The AE design schemes attractive to researchers and many schemes have been devised. Today, these schemes are targeted by designers and standardization authorities for their capabilities and design computation lightness. The widely paradigm "generic composition" combines the

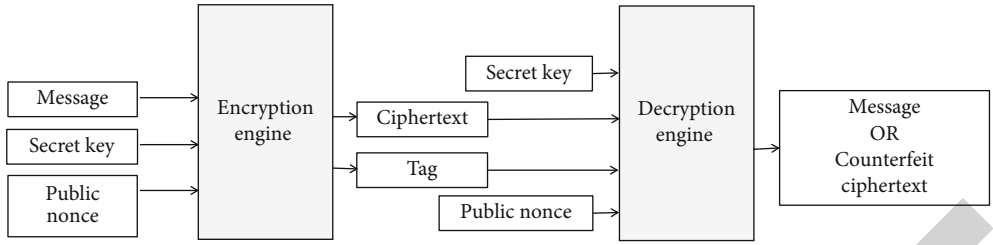

Figure 3: Authenticated encryption and decryption engine interfaces.

encryption algorithm with MAC [92]. However, many studies demonstrate that AE schemes can be more efficient than the generic composition [93]. As a result, various schemes are in demand for desirable features like robustness against nonce misuse, plaintext leakage, performance, and resistance to side channel attacks.

Among various AE schemes, the treatment of the public nonce should be properly protected to ensure I. The treatment of nonces can be clarified by using compositions such as MAC-then-Encrypt (MtE), Encrypt-then-MAC (EtM), and Encrypt-and-MAC (EaM) [56]. In the case of EaM and Encrypt-then-Mac (EtM), the nonces have to be encapsulated for I verification [94]. This is mainly because an attacker can manipulate a tag without being detected, where the MAC can still be verified. However, MtE does not require the nonce's inclusion since any change in it is detected by generating an invalid MAC. Accordingly, threats of inadequate implementation are increasingly higher in EaM and EtM [95].

Efficiency of scheme can be enhanced by implementing them in parallel. However, selecting the mode of operation, algorithm different computations, and the properties of an algorithm affects the resources cost. For example, in the same hardware platform fully parallelizable AES in Counter Mode (CTR) requires an estimation of 90 K gates, whereas the Galois Counter Mode (GCM) mode needs an additional 30 K gates and Carter Wegman Counter Mode (CWC) requires an additional 100 K gates for I [96, 97]. These key criteria have to be considered when industrial engineers require the best possible specifications for an IoT platform.

The popular IoT protocol CoAP is deployed as a lightweight protocol but it is insecure. It employs a hypertext transfer protocol (HTTP) translation based on the packet loss of the user datagram protocol (UDP). Several security studies on CoAP reviewed in [36, 37, 98] reported attacks including, but not limited to, DoS, spoofing attack, sniffing, hijacking, cross-protocol attacks, parsing attacks, amplification attacks, replay attacks, and relay attacks. To address these attacks, encryption is deployed using Datagram Transport Layer Security (DTLS) and Internet Protocol Security (IPsec). However, binding CoAP with DTLS or IPsec is deploying conventional cryptographic, which increase the computation expenditure, and does not address the scarce resource problem. Furthermore, it is revealed the handshake messages cause fragmentation. These drawbacks highlight the importance of protection using lightweight solutions.

5.1. Authenticated Encryption Algorithm Taxonomy. We present an AE taxonomy that is divided into two-pass and single-pass based on the number of runs for data processing [99]. The taxonomy constructs a single-key and two-keys category based on the number of secret keys required to provide C and I components, which are either one identical key or two different keys. This classification is shown in Figure 4, where each category is then further constructed according to the scheme primitive as block cipher scheme, generic composition, tweakable block cipher, or permutation-based scheme. The algorithms, which are constructed based on these schemes, are listed under the group.

The single-pass scheme involves processing one run to compute the encryption and tag using one key, or two separate keys for each run. This scheme is a single pass-through on data to obtain the ciphertext and the tag. A typical approach uses a single key for the encryption/MAC engine or two keys: one to generate a ciphertext and the other for the authentication tag. This strategy reduces the computation overhead compared to the two-pass approach by approximately half of the required efficiency. IAPM (Encryption Modes with Almost Free Message Integrity) [100] and COFB [101] are under the one-key group while OCB (Block Cipher Mode of Operation for Efficient Authenticated Encryption) [102], and EPBC (Efficient Error-Propagating Block Chaining) [103] operate under the two-key scheme. IAPM and OCB are parallelizable, in contrast to EPBC and COFB, which are unparallelizable. OTR [104], OCB3 [105], TAE [106], PFB [89], AEZ, Dexoys, and Joltik are classified as tweakable one-key which are parallelizable except PFB.

The two-pass scheme is grouped into a generic composition of existing algorithms using two distinct keys and the AE mode of operation, which employs a single key. Generic composition is a technique combining conventional encryption and MAC algorithms to provide C and I service. It is classified based on how the integration functions in three modes MtE, EtM, and EaM. MtE calculates the integrity tag (MAC) of the message using the sender's first key (K1) by the sender. The MAC is concatenated with the message and then encrypted under a different key (K2). On his behalf, the receiver decrypts the ciphertext to recover the plaintext and MAC. Message MAC is calculated and verified against the acknowledged MAC tag. The message is accepted only if the tag is verified. In EtM, the sender encrypts the message, computes the MAC and appends it for exchange. At the receiver's end, the received MAC is verified against the calculated

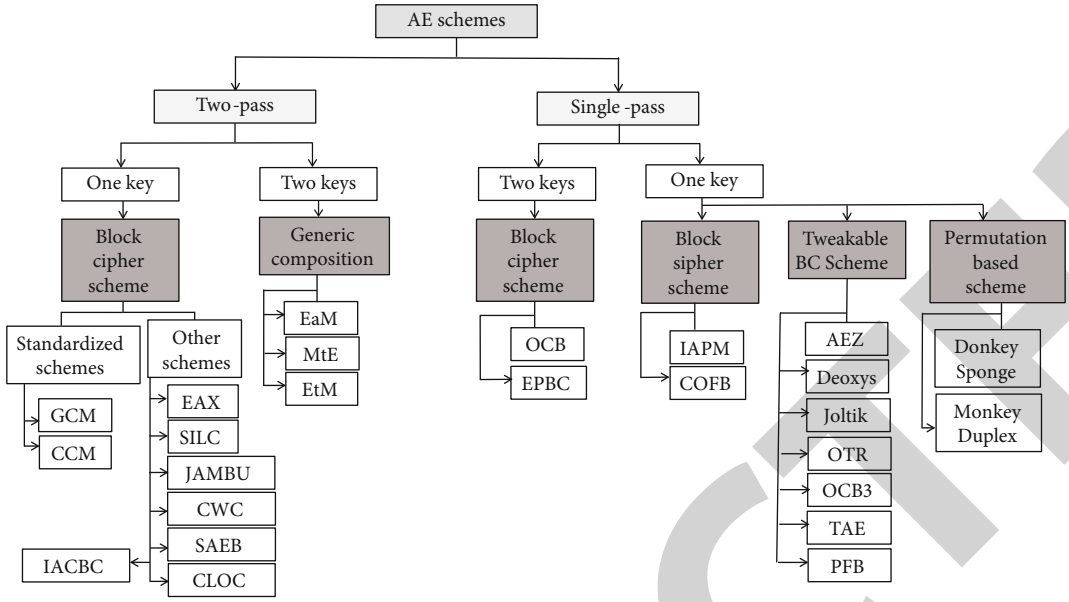

Figure 4: Taxonomy of authenticated encryption schemes.

MAC and then decrypts the ciphertext for the message. Referring to the EaM mode, the MAC tag and ciphertext are deduced simultaneously. The receiver decrypts the ciphertext and verifies the computed message MAC with the received MAC for I assurance. The EtM composition is commonly adopted since it is standardized by NIST and strongly unforgeable in terms of C and I. It is adopted in network protocols such as IPsec, SSH, and TLS. However, its construction can potentially create expensive overhead, as it requires two runs of high computations [56, 69].

The one-key category uses the same key for encryption and MAC modules. These modules are based on the cryptographic mode of operations applied to existing algorithms [100, 107]. Four modes are in this category, namely, counter with CBC-MAC (CCM) [108], EAX [109], GCM [96], and CWC [110], which are standardized by NIST as methods for block cipher on AE (ISO/IEC 19772 : 2009) except CWC. SAEB [111], Compact Low overhead Counter Feedback Mode (CLOC) [112], and JAMBU [113] are online, they use only exclusive-OR gate (XOR) operations, and not parallelizable. Various categories of AE schemes are shown in Figure 5. They are classified based on the underlying modules (i.e., C and I provided by separate components), number of secret keys (i.e., can be more than one), and number of data runs (i.e., how many data runs are essential to provide C and authenticity).

5.2. Criteria for Comparing LAE'S. In this section, the criteria involved in the algorithm comparison are specified. They were chosen based on algorithm design properties, functionalities, security vulnerabilities, performance, and resource requirements.

(1) *Design parameters*. There are four parameters of each algorithm including the size of the Message or Plaintext M, Key K, Nonce or Initialization Vector N, AD, and Authentication tag T. When the key size is small, the key space is small and exhaustive key search becomes feasible and easy to perform. If the algorithm key is 128 bits then, key space is approximately 3.4×1038 [114]. This large number protect against brute force attack vulnerability, regardless of the algorithm's sophistication [115]

(2) *Online*. The algorithms is online if there is no dependency relation between the ciphertext generated from a block and an earlier input block to the encryption oracle or a post input block to the encryption oracle. Such feature allows the sender to encrypt plaintext blocks before subsequent plaintexts or the plaintext lengths are known. Similarly, the receiver decrypts ciphertext blocks online in the order they were computed during encryption. It reduces the waiting time required to start a computation and enhances the algorithm's efficacy rate [116]

(3) *Parallelizable*. The encryption or decryption of an algorithm is parallelizable if the i^{th} block operates independently of the remaining j^{th} block such that $i \neq j$. The feature enhances design efficiency and improves its throughput. It is indicated as either encryption E being parallel or decryption D or both. Parallelized designs have an advantage particularly when it comes to providing a range of transmission rates [117]

(4) *Intermediate Tag*. The tag that enables the receiver to detect a mismatch of authenticity during the earlier stage after initial block decryption will considerably enhance time-efficiency for discarding un

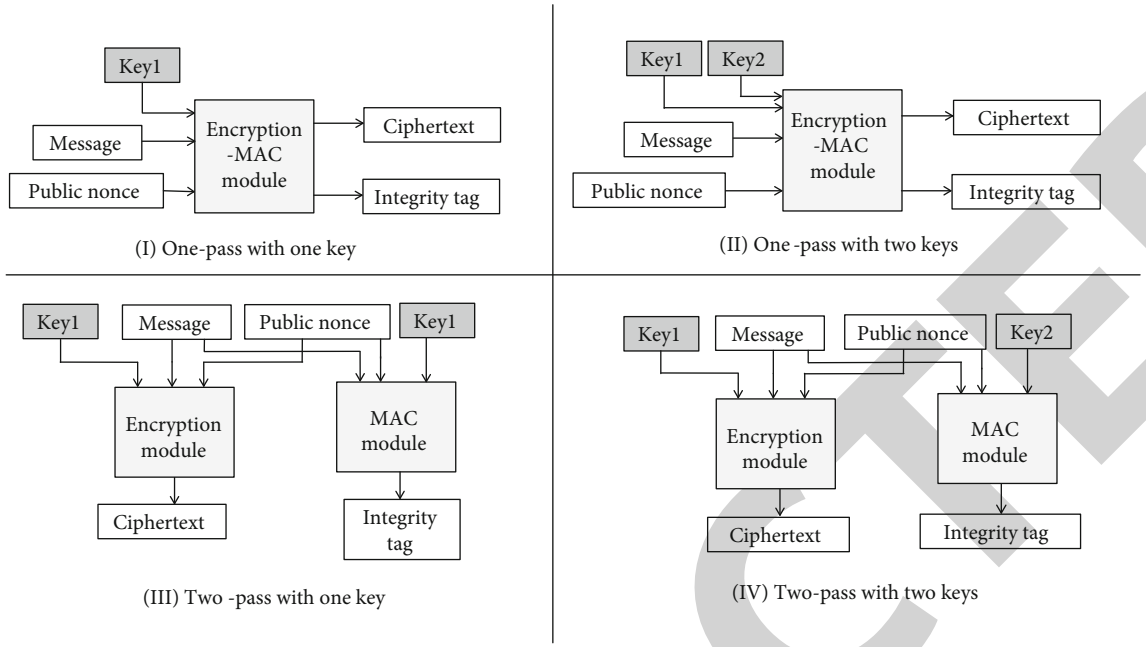

Figure 5: AE schemes modules with interfaces (I) one-pass with one key, (II) one-pass with two keys, (III) two-pass with one key, and (IV) two-pass with two key.

authenticated data without the need to decrypt all the message block [99]

(5) *Inverse-Free*. This feature exists when an inverse operation of the encryption namely a decryption is not necessary to decrypt the ciphertext. In other words, the algorithm uses the same encryption engine for decryption, which significantly determines the amount of dedicated size for the implementation on chips [99]

(6) *Area and Memory*. Number of registers in Read Only Memory (ROM) and Random Access Memory (RAM) are sufficient metrics for memory cost indicating the utilized area of the algorithm where intermediate values are stored. In contrast, lookup tables (LUTs), Slices (consist of LUTs and flip-flop gate), and fundamental figure logic equivalent (GE) give measurements of benchmark size for FPGA and ASIC. However, GEs imprecisely map into platform-specific metrics. For instance the GE for ASIC is equivalent to two-input not-AND (NAND) gates, while the FPGAs LUT is equivalent to six two-input NAND gates. The issue of mapping gap has been discussed in the literature [117, 118]

(7) *Power Consumption*. Power consumed plays a key role in performance measurement for restricted devices since battery shortage in IoT devices is still challenging [42]. A security algorithm with low computation consumes less power, hence, the battery discharges slowly. On the other hand, energy consumption signifies power being consumed on a periodic basis, which increases proportionally to the power. Therefore, power dissipation in a light-weight device ensures its capability for sufficiently operating the algorithm

(8) *Throughput*. This specifies the number of processing bits per second (bps) of input data within the algorithm. Higher throughput while preserving power consumption and utilized area is still questionable in IoT devices [119]. The acceptance of the throughput against area-power trade-off is based on the use case and the device restrictions

(9) *Code Size*. This denotes the code storage memory implied on ROM. Restricted devices limit the memory storage and any access between ROM and RAM while being executed [120]. Hence, the high access between memories lead to significantly increased device overheads

(10) *Execution Time*. This is indicated using the waiting time from the start process of the encryption and until the authentication tag is output. There is a correlation between AE design type and execution time. For example, a two-pass scheme doubles the execution time of a one-pass scheme using the EtM approach. As a result, execution time is affected by the algorithm design, such that some two-pass schemes require more computations and dependencies

(11) *Algorithm Size and IoT Device Resource*. The algorithm's computation required adequate metrics from the perspective of available resources. Such figures correlated to how small is the algorithm to fit into devices, which indicated in terms of utilized

area, power, code size, and execution time with reasonable throughput rate and number of cycles [60]. A small amount of resources left for security algorithms is evident in many IoT devices. Despite security protocols inherits in network layer for example TCP/DTLS1.2 within CoAP or Internet Protocol security IPsec encapsulated as MQTT, they are inadequate for IoT constrained storage (i.e., Radio Frequency Identification, Wireless Sensor Network, Microcontroller, and Near Field Communication), low power devices with limited battery capacity (i.e., smart cards and sensors) and computing power [121, 122]. Therefore, the range of encryption and authenticity algorithms supplied for an application are limited in view of device capability [123, 124]

6. Algorithms in the Review

In this section, we introduce the reviewed algorithms, which are grouped into block cipher-based, stream cipher-based, permutation-based and encrypt, and MAC algorithm. Details of the algorithm and their functionality features are discussed briefly.

6.1. Block Cipher-Based Lightweight Authenticated Encryption (BCAE). AES-GCM is an AEAD in GCM. It is a current NIST standard for AE which is an inherit feature of TLS [125], SSH [126] and IPsec [127]. Algorithm C is achieved using an incremental counter based (CTR). This incremental counter is encrypted, then XORed with the block message. The size of initial IV for the message is 96 bits, which is padded with an additional 31 bits of zero values. Despite being practically deployed, it does not withstand against nonce misuse and other attacks. To overcome this weakness, a modified version defined as AES-GCM-SIV [128], although never been considered before for IoT, is a proper recommendation when resources are limited.

AES-CLOC is an AES-128-based AEAD that facilitates CLOC. It takes 128 bits key, 96 bits nonce, 240 bits plaintext, 112 bits AD, and 128 bits tag to generate 240 bits ciphertext. Specifically, CLOC was designed to overcome NIST methods for AE, which were only combined with block cipher primitive. Additionally, it reduces the precomputation overhead, which improve the performance for short input data compared to the standardized modes, where less calls are required for the encryption/MAC engine. For example, if a message consists of a one block nonce, one block AD input data, and one block plaintext, CLOC requires 4 calls to the cipher engine, instead of 7 calls in EAX and 5 or 6 in CCM.

JOLTIK is a LAE scheme based on AES block cipher designed especially for hardware applications. It is tweakable to 64 bits cipher, and distinct keys are suggested with four sets of parameters to achieve a 64 bits security for C and authenticity. The sets' sizes were formatted as <key size-tag size> to be 64-64, 80-112, 96-96, and 128-64. The algorithm is composed of two parts, these are encryption and verification where the encryption takes a variable length message, variable AD, fixed length nonce, and a K bits key to generate m bits cipher and an authentication tag. All sets have been mathematically proved to provide security even when a nonce is reused. As the scheme is designed for hardware, it is efficient in hardware platforms and utilizes a small area.

SCREAM is a tweakable block cipher that work on 128 bits data processed using 128 bits key with AD. SCREAM is simple in design and encourages good performance on different architecture. The designers introduced a masking countermeasure against side channel attacks. The security level achieved by design is 128 bits. Low overheads are another feature so that no additional cipher calls were used for the masking generation against side channel attack. Besides, compact design allows a fully parallelization with minimum ciphertext size. There are two recommended parameters for SCREAM that are computationally secure with the provided security level, either 10 steps with single key security, or 12 steps with related key security.

SILC-AES is an authenticated block cipher based with two versions SILC-AES and SILC-LED. SILC-AES encrypts 64 or 128 bits message with 128 bits key length, 96 bit or 64 bits nonce, and 64 I tag. With provable security, it is optimized and evaluated on standard hardware, and generated a small footprint with low transmission rate suitable for low-rate applications especially when throughput is not essential. Similarly, SILC-LED, which operates on 64 bits message, 80 bits key, 48 bits nonce, and 32 bits I tag is recommended for a low data transmission and limited battery device.

AEGIS is an AEAD that is suitable for protecting protocol packets. AEGIS-128 is constructed as five AES rounds to process 128 bits message, while AES-256 is constructed as six AES rounds. Both versions are argued by the designer to function at a high security level but this has not been proven, and besides they are not robustness against nonce reuse.

COLM is a block cipher based on AEAD features. It is designed to achieve online misuse resistance and fully parallelizable. COLM uses an AES-128 with a key and state of 128 bits length. C and I of the design achieve a security level of 64 bits even when the nonce repeated, which withstand against different attacks.

Deoxys-v1.41operates using a key length of either 128 bits or 256 bits to construct two modes: DeoxysI and DeoxysII. DeoxysI requires nonce respecting where nonce never repeat, while DeoxysII resists nonce misuse and nonce can repeat without affecting the algorithm's security. The tag size is 128 bits and a 64 bits for the first version, while it is 120 bits for the second version. However, security degrades for C and authenticity with respect to nonce repetitions on the second version. Deoxys perform well with reference to software implementation.

AEZ is an AEAD block cipher mode of operation. It is constructed as two versions with respect to the number of rounds; these are 4 and 10 rounds. The designers argue it is the easiest to use, however it is complex in implementation. The difficulty comes from the mode complexity of connecting two unrelated mechanisms. The scheme security has been attacked using side channel attacks as analyzed in [129].

AES-JAMBU is an AE based on AES-128 block cipher that operates on 128 bits key constructed on the JAMBU mode of operation. The designers compared JAMBU to

other existing modes of operation and claimed that its resistance to nonce misuse is similar to CFB mode, which maintains a strong level of security. In contrast, JAMBU is the most lightness mode in terms of computation and provides bijective n-bit authentication security to the 2n bits block size.

Tiaoxin is a family of nonce resistance scheme and it operates on 128 bits message, 128 bits key, 128 bits nonce, AD of 128 bits, and a 128 bits tag. The security level of is claimed to be 128 bits for C and authenticity. However, it is not resistant with respect to nonce repeating and can be used to recover state bytes and to compromise the C. Besides, if an adversary knows a key, he can easily generate a tag collision.

6.2. Stream Cipher-Based Lightweight Authenticated Encryption (SCAE). ACORN is constructed based on stream cipher that processes bit-by-bit; however, it processes 32 steps in parallel, which makes it faster in hardware and software platforms [130]. The encryption and authentication shares 293 bits state encrypted via 128 bits key, 128 bits nonce to generate a 128 bits tag. The authentication deploys a concatenation of six linear feedback shift registers. The major characteristics of ACORN v1, v2, and v3 are online, parallelizable, inverse-free, and robust. The first two versions are mathematically are proven to be insecure. The work in [131] revealed that ACORN_v1 is not resistant to state collision, where two distinct input messages produce the same ciphertext. The [131] attack was deployed on a standard PC. The fault attack in [132] fully recovers two initial states of ACORN_v2 with time complexity, then establishes key recovery and forgery attack. Thus, ACORN_v2 is insecure because of the nonlinear feedback function that has been replaced by the filtering function in ACORN_v3 and provides a larger security margin against guess-and-determine attacks. A side-channel attack has been established on ACORN_v2 by [133] to recover the full key, which is then addressed by an additional masking countermeasure. It is practically tested on an ARM processor and proved its resistance to [133] attack.

The MORUS family has two internal sizes, 640 bits and 1280 bits, and two different key sizes, 128 bits and 256 bits that construct three recommended parameters, MORUS-640-128, MORUS-1280-128, and MORUS-1280-256. The tag size reaches a maximum of 128 bits and can be shorter. However, the designers recommend using a 128 bits tag so that the I will be 128 bits, and the C reaches the number of key bits. The three parameter sets, however, are not resistant to nonce misuse and the security withstands it only if a reused nonce is encrypted with a changing key. However, this algorithm has not been mathematically proven against the designers' claimed security strength.

6.3. Permutation-Based Lightweight Authenticated Encryption (PBAE). ASCON_v1.2 is constructed as a sponge-based scheme operating on a variable length input to produce a fixed length output. The operation state of 320 bits includes 128 bit key, 128 bit nonce, 128 bit tag, 64 bit data block, and 12 and 6 rounds for two intermediate permutations. It is been the winner of CASEAR competition and a candidate for ongoing NIST standardization. There is much research community interest in the efficiency metric for various platforms, given that ASCON is oriented for hardware platform. These include unprotected versions against differential power attacks as reported in [134], and protected versions in [130, 135].

PRIMATEs-80 and PRIMATEs-120 are two variants of AEAD and consist of three modes of operation namely APE, HANUMAN, and GIBBON. It takes an input a key generated by key generator, AD, message, and nonce to generate a ciphertext and I tag. All algorithms can resist attacks with security levels of 80bits and 120bits, which has been mathematically proved by designers. PRMATE permutations are defined by different round constants, which are generated by 5 bit LFSR and various round numbers.

NORX is a family of authenticated ciphers with scalable architectures so that the extent of parallelism and tag size are arbitrary. NORX operates on 128 bits or 256 bits with 128 bits or 256 bits key, where the same security level holds. However, it cannot resist nonce reuse although it performs well on both software and hardware platforms.

Ketje is a family of the AEAD scheme based on sponge. It takes as input a secret key and a nonce, then some AD that are authenticated but not encrypted and a plaintext. A ciphertext and authenticating tag are produced to ensure the data and the packet headers security. The design aimed to serve memory constrained devices and assume the nonce is unique for each communication to achieve security. Thus, it is unsecure to implement if an adversary repeats the nonce and recovers the data.

The Keyak family is another version of the Ketje with similar intermediate operations. The similarity is that it takes a unique secret input but with its AD that are not encrypted and a plaintext. It then produces a ciphertext and a tag that authenticates both the AD and the plaintext. The recipient party who has the same-shared secret key can decrypt and authenticate the ciphertext. The designers claim it resists to nonce misuse if an adversary reuses the nonce that cannot retrieve the key or any internal state.

6.4. Encrypt and MAC Scheme. OCB is an authenticated mode of operation that is fully parallelizable. This mode is standardized by NIST for lightweight methods based on block cipher. Due to OCB characteristics to encrypt an arbitrary message length into a ciphertext with minimal length, this means using cheap offset computations and key setup. It also resists nonce misuse. These features are suitable for restricted resources devices and low cost IoT applications.

7. LAE Comparisons and Discussions

We present a comparison of various LAE using criteria noted in Section 6 part B criteria. These features affect an algorithm's design efficacy, security, and resource measures. Algorithms were eliminated from the review due to vulnerability threats or insufficient studies done on them. For example, AES-COPA and ElmD are mathematically proven to be insecure in [35] and [36], respectively. SliScp [136] has not

received sufficient attention in the literature, although it was published for a while. WAGE [137], ACE [138], and Elephent [139] were recently designed and excluded due to insufficient analysis on them. COMET [140] and MixFeed have been threatened by weak keys as demonstrated in [141].

7.1. Security Vulnerabilities Comparison. Table 3 compares algorithms based on their security strength. The security strength is evaluated based on the availability of mathematical proof of their C and I, nonce misuse robustness, and side channel attacks. Algorithms, which are proven to maintain message C and I, are resistant to nonce misuse and resistant to side channel attacks beside other security attacks, are desirable. If IoT nodes are captured and altered to repeat the nonces the data will be revealed. Many protocols are compromised due to nonce misuse such as Wi-Fi Protected Access 2 (WPA) and Wired Equivalent Privacy (WEP). Thus, in terms of security, algorithms, which can resist nonce misuse are highly desirable.

The study shows that AES-JAMBU, Tiaoxin, AEGIS, and MORUS_v2 are not mathematically proven to be secure against C and I attacks. An interesting observation is that ASCON_v1.2, JOLTIK, PRIMATEs, COLM, DeoxysII, OCB, and Keyak maintain their message C and authenticity. However, ASCON_v1.2 is not robustness against nonce misuse because nonce repetition for two varying messages can reveal their differences. Furthermore, excess reuse of the nonces releases the algorithm internal state, which can be identified using structural attacks.

From the perspective of nonce resistance, whereby the nonce can be modified or altered without affecting the security of the algorithm, JOLTICK, PRIMATESs, COLM, DeoxysII, OCB, and AES-JAMBU are secure. Selecting these is more powerful in terms of security for uncontrolled environment. However, the nonce should be unique for every encryption query to prevent message leakage in ACORN_v3 ASCON_v1.2 AES-CLOC, SCREAM, SILC-AES, SILC-LED, AEGIS, NORX, AEZ, Ketje_v2, and Keyak. These schemes fail to deliver the C when the adversary manipulates the nonce. Thus, they are suitable for controlled environments where nonce randomness is preserved to ensure data C and authenticity.

JOLTIK has two versions, and one of them is nonce-misuse resistance. In this version, a birthday bound security is proven for reused nonce for 64 bits for plaintext C, I of plaintext, I of nonce, and I of AD. This provides the 64bits security with only one query to the block cipher. Similarly, OCB3, AES-GCM, and PRIMATEs in APE mode are proven for reused nonce. As far as we know, AES-GCM, ACORN_v3, AES-CLOC, Tiaoxin, and AEZ have been studied and found to be insecure against fault attacks. A key problem of these algorithms is that fault attack recovers the key and reveals the message information. Hence, they are not recommended for IoT devices because they can be cloned when they are placed in untrusted environment.

COLM and DeoxysII have the same 64 bits size for birthday bound security. COLM security bound is supported with ELmD and COPA security proofs. In contrast, AES-JAMBU was analyzed with repeated nonces for two identical messages, and the first two blocks can be revealed. Although, both ELmD and COPA are threatened by forgery attacks based on tag guessing, such that the attack does not violate their birthday bound security.

7.2. Functionality Comparisons. Table 4 summarizes the algorithms' functionalities in bits, namely, message block size, key length, nonce length, tag size, online, parallelism, required inverse for decryption, intermediate tags, and if its support AEAD. DeoxysI, DeoxysII, NORX, AEZ, and Keyak take variable plaintext length and variable AD. Unlike others, these algorithms have the potential to be deployed on various protocols with different data communication size. The IPv6 and IEEE 802.15.4, for instance, differ on the payload size that has to be protected and the associated header length.

More concretely, the frame size in IEEE802.15.4 is 127 bytes such that the maximum header length is 25 bytes, which leaves 102 bytes for the payload. It supports a scenario for AE where only 86 bytes of payload encrypted, 25 bytes for header authenticity, and 16 bytes reserved for the integrity tag [162]. In contrast, IPv6 frames defined in RFC 2640 use AE to support the encryption of 1224 bytes payload and 40 bytes of AD.

It is observed that AES-GCM, JOLTIK, DeoxysI, DeoxysII, and OCB support the need for encryption and decryption engines for the processing, in contrast to other algorithms, which do not. This functionality affects the resources required for implementation so that algorithms can have one engine for encryption and decryption or two separate oracle engines. Despite the shortcomings of the need to inverse algorithms, JOLTIK, DeoxysI, DeoxysII, and OCB encryption and decryption engines are parallelable.

7.3. Performance Comparisons. Table 5 compares the algorithms' features with corresponding hardware performance metrics. In the literature there seems to be some confusion when comparing algorithms' implementation. To overcome this problem, we explain two factors when reviewing the performance of the algorithms.

(1) *Platform-Awareness*. The variation of the benchmarked platform is the basis for comparison. Different technologies have their own device mappings, leading to technology-specific performance. For example, the metrics of implementing SILC in ASIC are differentiated from FPGA. Building units based on the FPGA approach are mostly done on LUTs rather than logic gates, the most fundamental hardware metric, while the ASIC area is measured in mm^2. An algorithm built on the same technology is analyzed for a specific platform type [163]

(2) *Resources Limitation*. Targeting restricted devices, small area, low power consumption, and throughput have to be considered. For example, the approach, which achieves low power requires shortage battery, withstands longer until a battery replacement is essential, simultaneously the algorithm footprint has to be minimum

Table 3: Authenticated encryption algorithms security comparison.

Algorithm	Provable confidentiality	Provable authenticity	Nonce misuse resistance	Side channel attacks
AES-GCM [142]	√	×	×	Cache attack [143], Fault attack [70]
ACORN_v3 [144]	√	√	×	Fault attack [132]
ASCON_v1.2 [145]	√	√	×	×
AES-CLOC [112]	√	√	×	Fault attack [146]
JOLTIK [147]	√	√	√	×
PRIMATEs [148]	√	√	√	×
SCREAM [149]	√	√	×	√
SILC-AES [150]	√	√	×	×
SILC-LED [150]	√	√	×	×
AEGIS [151]	×	×	×	×
COLM [152]	√	√	√	×
DeoxysI [153]	√	√	×	×
DeoxysII [153]	√	√	√	×
OCB [102]	√	√	√	×
NORX [154]	√	√	×	×
AES-JAMBU [155]	×	×	√	×
Tiaoxin [156]	×	×	×	Fault attack [157]
AEZ [158]	√	√	×	Fault attack [129]
Ketje_v2 [159]	√	√	×	×
Keyak [160]	√	√	×	×
MORUS_v2 [161]	×	×	×	×

We observe that BCAE algorithms receive much more interest on performance testing when targeting Field Programmable Gate Array (FPGA) and Application Specific Integrated Circuit (AISC). Similarly, rather than ASIC, FPGAs were mostly targeted by performance developers. The hardware built as ASIC technology is relatively more expensive than the FPGA platform and ASIC usually is a production platform while FPGA serves as a validation platform. On the other hand, BCAE algorithms are easy to design and deploy compared to permutation-based and stream cipher-based algorithms.

From the metric perspective, area, power, and throughput are reported for various performance levels while TimexArea and its efficiency are not considered. The area computation is mapped differently based on the platform so that LUTs represented FPGA while mm^2 stands for ASIC. Such differences ensure area fraction within a device is differentiated from other platforms because the selected device featured the accessible resources. Furthermore, a wide range of algorithms with several schemes are investigated, yet tested platforms vary and consequently so do the available resources. Benchmarking the algorithm potentially is affected by testing platform, hardware or software design architecture, algorithm arithmetic, algorithm characteristics (i.e., parallelizable, inverse-free, online), and attacks countermeasure (i.e., side channel masking). Thus, a comparison should be aware of the differences between various platforms.

Table 6 compares algorithms for software performance in 8 bit AVR, 16 bit MSP, 32 bit ARM, and amd-64 bit. It includes the family, mode of operation, speed for encryption E, and decryption D in cycles/bytes, ROM, and RAM in bytes, cycle count in cycles, type of implementation and platform, and the name of the protocol if it is validated to work within the protocol.

The ROM and RAM memories besides cycle count were not reported in many of implementations, while the speed of the algorithm was done to assess software performance. A key reason is the capabilities that software devices have where 8bits platforms are of less interest for practical applications. We observe from Table 6 that speed computation varies, where some developers indicate their implementation include encryption only engines some include encryption and decryption, others have not indicate the number of engines. This variation leads to unfair conclusions that an algorithm is performing well by implementing the encryption engine only. The encryption processing time is also affected and can be doubled for a full encryption and decryption engines. For practical IoT, where the algorithm is implemented in IEEE 802.5.4 or IPv6, a few algorithms, namely AES_GCM, ACORN_v2, ASCON_v1.2, NORX, and Ketje are validated on both protocols. Other algorithms are not validated for the maximum payload and I tag length and nonetheless supported by these protocols.

7.4. BCAE Performance Comparison. AES-CLOC, SCREAM, AES-JAMBU, AES-SILC, Aegis, AEZ, JOLTIK, Tiaoxin, COLM, DeoxysII, and LED-SILC were benchmarked on ASIC and FPGA with performance shown in Figure 6 and Figure 7, respectively. Based on area utilization, AES-CLOC [20], Scream-10 [149], and AES-JAMBU [48] are

Table 4: Characteristics of authenticated encryption candidates, v means variable.

Algorithm	Message	Key	Nonce	Tag	Online	Parallel (E/D)	Inverse free	Intermediate tag	AEAD
AES-GCM	128	128	96	128	√	√/×	×	×	√
ACORN	128	128	128	128	√	√/√	√	×	√
ASCON	128	128	128	128	√	×/×	√	×	√
CLOC	128	128	96	64	√	×/×	√	×	√
JOLTIK	128	128	32	64	√	√/√	×	×	√
PRIMATEs	80	80	80	80	√	×/×	√	×	√
	120	120	120	120	√	×/×	√	×	√
SCREAM	128	128	96	128	√	√/√	√	×	√
SILC-AES	128	128	64 96 112	128	√	×/√	√	×	√
Aegis	128	128	128	128	√	√/×	√	×	√
	256	256	256	128	√	√/×	√	×	√
COLM	128	128	64	128	√	√/√	√	√	√
DeoxysI	V	128	64	128	√	√/√	×	×	√
DeoxysII	V	128	120	128	√	√/√	×	×	√
OCB	128	128	128	64	√	√/√	×	×	√
NORX	V	96	32	96	√	√/√	√	×	√
SILC-LED	64	80	48	32	√	×/√	√	×	√
AES-JAMBU	128	128	64	64	√	×/×	√	×	√
Tiaoxin	128	128	128	128	√	√/√	√	×	√
AEZ	V	384	128	128	×	√/√	√	×	√
Ketje	128	128	128	128	√	×/×	√	√	√
Keyak	V	288	V	128	√	√/×	√	√	√
MORUS	128	128	128	128	√	×/×	√	×	√

the lightest in ASIC while AES-JAMBU, AES-SILC, and LED-SILC in [164] utilized the smallest footprints in FPGA. AES-SILC in [25] consumed as little as 5.98 mWatt utilizing 3004 LUTs, while in [164] dissipated higher power of 9200 mWatt and substantiality less area of 1160 LUTs were computed. The major variations in the benchmarks are the platform type of FPGA where Spartan-6 dissipated an extremely high amount of power to process the ciphers.

Due to design simplicity and a few interfaces of AES-CLOC and Scream-10 in ASIC, they achieve higher throughput compared to the other of 6840 and 4577 Mbps, respectively. AES-JAMBU [48] reported 0.058 mm^2 and 3.39 mWatt, which is enormously less than consumption of AES-CLOC, which was reported as 18.79 mWatt. Scream [25] and JOLTIK [25] utilized 0.114 mm^2, 0.842 mWatt and 0.178 mm^2 and 0.96 mWatt, for area and power, respectively. For throughput, in contrast Scream approached a higher bandwidth of 128 Mb per seconds while JOLTIK sent 20 Mbps. Thus, Scream can be used for high bandwidth applications like Wi-Fi-based wireless sensor network, whereas JOLTIK is recommended for low throughput applications like smart Bluetooth [165].

AES-GCM dissipated 1666 mWatt, however in terms of area, GCM mapped into smaller FPGA LUTs. AES in GCM is a two-pass scheme-facilitating headers AD authentication, which is inherent in IPsec and TLS. It is, however, vulnerable to forgery attacks on the I tag [166], where certain cyclic keys can be repeated. Using AES-GCM-SIV [128], instead of AES-GCM, accelerates the instructions and is predicated to perform faster.

Aegis [60], AES-CLOC [20], and AES-SILC [60] were the highest throughput with 8650 Mbps, 6840 Mbps, and 6400 Mbps, respectively, whereas DexoysII [60], JOLTIK [25], and COLM [60] had 18.63 Mbps, 20 Mbps, and 23.75 Mbps, respectively, as the lowest throughputs in Figure 5(b). Of these, AES-SILC and Aegis consumed 4.36 and 7.52 mWatt while maintaining a low area of 0.0677 mm^2 and 0.1661 mm^2. In contrast, DexoysII and COLM consumed significantly less, i.e., 0.0988 and 0.0177 mWatt, respectively, but inefficient area footprint being 531.91 mm^2 and 505.05 mm^2, also, respectively.

AES-CLOC and SCREAM tested on 8bit AVR as illustrated in Figure 8. Based on the resources, ROM memory assessments AES-CLOC [112] used less bytes compared to SCREAM-10 [149], i.e., 2980 bytes and 3221 bytes, respectively. In contrast, the bytes utilized as RAM memory number much less for SCREAM with 80 bytes measured while AES-CLOC required 362 bytes. Variations come from the experiment measurements so that CLOC was measured for encryption and decryption engines while SCREAM was not.

The algorithms' performance in 64 bit ARCH were measured in terms of the speed, meaning that Aegis, AEZ and AES-SILC are the fastest algorithms and required only

Table 5: Authenticated encryption hardware performance metrics.

Algorithm	Family	Mode	Area	Power (mWatt)	Throughput (mbps)	Implementation
AES_GCM [167]	BCAE	GCM	9167 LUTs	1666	×	Zynq-7000 PYNQ
ACORN_v2 [25]	SCAE	×	0.035 mm^2	0.163	8	CMOS UMC 130
ACORN32 [60]	SCAE	×	0.0169 mm^2	3.130	34040	TSMC 65 nm
ACORN_v2 [25]	SCAE	×	476 LUTs	0.582	8	Zynq-7000 XC7Z020
ACORN32 [167]	SCAE	×	7342 LUTs	1646	×	Zynq-7000 PYNQ
ACORN [164]	SCAE	×	418 LUTs	9200	1225.5	Spartan-6
ASCON GMU [60]	PBAE	Monkey duplex	1408.4 mm^2	0.0235	3.310	TSMC 65 nm
ASCON [25]	PBAE	Monkey duplex	0.083 mm^2	0.655	106.67	CMOS UMC 130
ASCON [25]	PBAE	Monkey duplex	1312 LUTs	2.160	106.67	Zynq-7000 XC7Z020
ASCON [167]	PBAE	Monkey duplex	7726 LUTs	1648	×	Zynq-7000 PYNQ
ASCON [164]	PBAE	Monkey duplex	684 LUTs	×	60.1	Spartan-6
AES-CLOC [112]	BCAE	CLOC	5628 LE	×	400.7	FPGA cyclone IV
AES-CLOC [25]	BCAE	CLOC	0.544 mm^2	2.858	128	CMOS UMC 130
AES-CLOC [25]	BCAE	CLOC	2767 LUTs	3.766	128	Zynq-7000 XC7Z020
AES-CLOC-GMU [20]	BCAE	CLOC	0.0140 mm^2	18.79	6840	TSMC 65 nm
JOLTIK [25]	BCAE	TAE	1325 LUTs	1.380	20	Zynq-7000 XC7Z020
JOLTIK [25]	BCAE	TAE	0.178 mm^2	0.96	20	CMOS UMC 130
PRIMATEs [25]	PBAE	GIBBON	1187 LUTs	3.547	66.67	Zynq-7000 XC7Z020
PRIMATEs [25]	PBAE	GIBBON	0.106 mm^2	1.064	66.67	CMOS UMC 130
Scream-10 [149]	BCAE	TAE	17292 um^2	×	4577	65 NM CMOS
SCREAM [25]	BCAE	TAE	0.114 mm^2	0.842	128	CMOS UMC 130
Scream [25]	BCAE	TAE	2235 LUTs	4.106	128	Zynq7000 XC7Z020
AES-SILC [150]	BCAE	SILC	15675.5 GE	×	764.12	90 nm ASIC
AES-SILC [25]	BCAE	SILC	0.187 mm^2	2.345	128	CMOS UMC 130
AES-SILC [48]	BCAE	SILC	0.1031 mm^2	7.000	640	CMOS UMC 130
SILC-GMU[60]	BCAE	SILC	0.0677 mm^2	4.360	6400	TSMC 65 nm
AES-SILC [25]	BCAE	SILC	3004 mm^2	5.980	128	Zynq7000 XC7Z020
AES-SILC [164]	BCAE	SILC	1052 LUTs	9200	76.6	Spartan-6
AES-SILC [164]	BCAE	SILC	1198 LUTs	×	48.1	Zynq7000XC7VX485T
AES-SILC [164]	BCAE	SILC	1160 LUTs	×	59.13	Zynq-7000 XC6VLX760
LED-SILC [164]	BCAE	SILC	872 LUTs	8400	15.1	Spartan-6
AES-CLOC [164]	BCAE	CLOC	1604 LUTs	1089	68.7	Spartan-6
AES-CLOC [164]	BCAE	CLOC	1306 LUTs	×	45.72	Zynq-7000 XC7VX485T
AES-CLOC [164]	BCAE	CLOC	1282 LUTs	×	52.03	Zynq7000XC6VLX760
Aegis_128 [167]	BCAE	×	17323 LUTs	2139	×	Zynq7000 PYNQ
Aegis_265[167]	BCAE	×	19716 LUTs	2039	×	Zynq7000 PYNQ
Aegis-GMU [60]	BCAE	×	0.1661 mm^2	7.520	8650	TSMC 65 nm
DeoxysII [167]	BCAE	XEX	10681 LUTs	1738	×	Zynq7000 PYNQ
DeoxysII [60]	BCAE	XEX	531.91 mm^2	0.0988	18.63	TSMC 65 nm
DeoxysII	BCAE	TAE	14107 GE	×	×	×
AES-OCB [167]	BCAE	OCB	10432 LUTs	1683	×	Zynq7000 PYNQ
OCB-GMU [60]	BCAE	OCB	0.1442 mm^2	27.42	4920	TSMC 65 nm
NORX [60]	PBAE	Monkey duplex	0.1231 mm^2	19.51	57400	TSMC 65 nm
NORX [48]	PBAE	Monkey duplex	0.1039 mm^2	4.370	2400	CMOS UMC 130
NORX [164]	PBAE	Monkey duplex	1424 LUTs	1280	2989.0	Spartan-6
AES-JAMBU [164]	BCAE	JAMBU	191 LUTs	737	×	Zynq7000XC7VX485T
AES-JAMBU [164]	BCAE	JAMBU	244 LUTs	713	×	Zynq7000XC6VLX760
AES-JAMBU [60]	BCAE	JAMBU	0.3887 mm^2	3.110	3170	TSMC 65 nm

Table 5: Continued.

Algorithm	Family	Mode	Area	Power (mWatt)	Throughput (mbps)	Implementation
AES-JAMBU [48]	BCAE	JAMBU	0.0580 mm^2	3.390	128	CMOS UMC 130
Tiaoxin [60]	BCAE	×	0.0140 mm^2	9.360	1115320	TSMC 65 nm
Tiaoxin [48]	BCAE	×	0.2282 mm^2	11.68	4270	CMOS UMC 130
AEZ-GMU	BCAE	XEX	0.1186 mm^2	22.07	2980	TSMC 65 nm
Ketje_jr [60]	PBAE	Monkey wrap	0.0172 mm^2	3.270	14550	TSMC 65 nm
Ketje_sr [60]	PBAE	Monkey wrap	0.0276 mm^2	4.710	29090	TSMC 65 nm
MORUS [25]	SCAE	×	0.27 mm^2	2.830	256	CMOS UMC 130
MORUS [60]	SCAE	×	50965 um^2	×	114.8 Gbps	TSMC 65 nm
MORUS [161]	SCAE	×	179 slices 4122 LUTs	×	94117	FPGA Vertix-7
MORUS [25]	SCAE	×	4286 LUTs	4.899	256	Zynq7000 XC7Z020
COLM [60]	BCAE	Encrypt-linear Mix-encrypt mode	505.05 mm^2	0.0177	23.75	TSMC 65 nm
COLM [48]	BCAE	Encrypt-linear Mix-encrypt mode	0.3274 mm^2	12.08	580	CMOS UMC 130
COLM [164]	BCAE	Encrypt-linear Mix-encrypt mode	2521 LUTs	×	37.1	Zynq7000XC7VX485T
COLM [164]	BCAE	Encrypt-linear Mix-encrypt mode	2511 LUTs	×	38.9	Zynq7000XC6VLX760
COLM [167]	BCAE	Encrypt-linear Mix-encrypt mode	13861 LUTs	1796	×	Zynq7000 PYNQ

2.15 cycle/bytes, 4.57 cycle/bytes and 4.9 cycle/bytes, respectively, to process a message while operating on different modes. Conversely, JOLTIK, consumed an extremely large number of cycles of 1590.87 cycle/bytes which affected memory utilization.

Taking side channel attacks resistance into account, SCREAM design integrated a masking countermeasure that protects against manipulation and faults injection to recover the encryption key. This is recommended for 8 bits and 64 bits. Dexoys, however, is vulnerable to nonce-misuse and deemed to be unsecure algorithm in untrusted environment IoT.

7.5. SCAE Comparisons. ACORN_v2 [25, 60] and MORUS [25, 60] are stream cipher-based authenticated algorithms benchmarked on ASIC as illustrated in Figure 9. ACORN is the most area and power efficient algorithm, which is designed for resource-constrained environments and it incorporates three functions: the keystream generator, feedback bits function and state update function. However, these three functions are based on two Boolean functions of basic AND and XOR gates and are faster on FPGA and ASIC.

ACORN performance on ASIC reported by [25] is effective in terms of area and power metrics utilizing 0.035 mm^2 and 0.9 mWatt compared to [60] being 0.0169 mm^2 and 3.13 mWatt. The reason for the performance variations is the design that target efficient throughput in [60] as it was extremely higher than [25] who reported 34040 Mbps compared to only 8 Mbps. However, targeting FPGA PYNQ [167], it was the worst in terms of battery dissipation since it consumed 8200 mWatt, which was extremely higher than Spartan6 [164] and Zynq-7000 [25]. For this reason, it is not recommended for small IoT application with limited battery like medical devices that are attached to the human body.

MORUS on the other hand, utilized a smaller ASIC footprint of 0509 mm^2 [60] compared to 0.27 mm^2 [25], while higher power ranging from 35.39 mWatt [60] to 2.83 mWatt [25] was consumed. For FPGA, it utilized approximately 4122 LUTs on Zynq-7000 [25] and 4286 LUTs on Virtex [161] while transmission rate reached 256 Mbps [25] compared to ACORN which transmitted 8 Mbps [25]. Hence, MORUS achieved higher throughput performance compared to ACORN.

ACORN performance was measured on 8 bits AVR, 16 bits MSP, and 32 bits ARM. The same RAM memory of 184 bytes required for the algorithms, yet the dissipation varied. As Figure 10 shows, 32 bits ARM employed the smallest number of 267168 cycles to encrypt a message; 8 bits AVR required 464381 cycles and 16 bits ARM needed 626192 cycles. Such metrics were affected by the ACORN number of rounds to generate a cipher keystream and the construction of a nonlinear feedback function.

Tiaoxin and MORUS reported the higher speed of 3.53 cycles/bytes and 4.87 cycles/bytes, respectively. ACORN of v2 and v3 processed a message as relatively the same speed such that v3 was faster by 0.31 cycles/bytes. Although Tiaoxin has been mathematically proved for its nonresistance feature against fault attack, it is recommended to add a proper masking protection layer to resist against side channel attack. MORUS on the other hand can be broken using nonce-repetition and should not be implemented unless nonce resistance is ensured.

Table 6: Authenticated encryption software performance metrics.

Algorithm	Family	Mode	Speed E/D (cycles/bytes)	ROM (bytes)	RAM (bytes)	Cycle count (cycles)	Implementation	Protocol
AES_GCM [167]	BCAE	GCM	E/D: ×	×	367	975184	8 bits AVR	IEEE 802.15.4
AES_GCM [167]	BCAE	GCM	E/D: ×	×	367	2369572	16 bits MSP	IEEE 802.15.4
AES_GCM [167]	BCAE	GCM	E/D: ×	×	367	1197073	32 bits ARM	IEEE 802.15.4
AES-CLOC [112]	BCAE	CLOC	×:750 Per 16 bytes	2980	362	1999	8 bits AVR	×
Scream-10 [149]	BCAE	TAE	×	3221 Words	80 Words	E: 7646 D: 7672	8 bits AVR	×
AES-SILC [150]	BCAE	SILC	×: 4.9	×	×	×	Intel 64 bits	×
LED-SILC [150]	BCAE	SILC	×: 40	×	×	×	Intel 64 bits	×
ACORN_v2 [168]	SCAE	×	E: 6.38 D: 6.52	×	×	×	amd64 bits	×
ACORN_v2 [162]	SCAE	×	E/D: ×	×	184	464381	8 bits AVR	IEEE 802.15.4
ACORN_v2 [162]	SCAE	×	E/D: ×	×	184	626192	16 bits MSP	IEEE 802.15.4
ACORN_v2 [162]	SCAE	×	E/D: ×	×	184	267168	32 bits ARM	IEEE 802.15.4
ACORN_v3 [168]	SCAE	×	E: 6.23 D: 6.36	×	×	×	amd64 bits	IEEE 802.15.4
ACORN [120]	SCAE	×	E: 54.13	×	×	×	amd64 bits	IEEE 802.15.4
ASCON_v1.2 [162]	PBAE	Monkey duplex	E/D: ×	×	183	534908	8 bits AVR	IEEE 802.15.4
ASCON_v1.2 [162]	PBAE	Monkey duplex	E/D: ×	×	183	619523	16 bits MSP	IEEE 802.15.4
ASCON_v1.2 [162]	PBAE	Monkey duplex	E/D: ×	×	183	83118	32 bits ARM	IEEE 802.15.4
ASCON_v1.2 [120]	PBAE	Monkey duplex	E: 16.41	×	×	×	amd64 bits	×
ASCON [168]	PBAE	Monkey duplex	E: 7.32 D: 7.38	×	×	×	amd64 bits	×
AES-CLOC [120]	BCAE	CLOC	E: 81.76	×	×	×	amd64 bits	×
JOLTIK [120]	BCAE	TAE	E: 1590.87	×	×	×	amd64 bits	×
PRIMATEs [120]	PBAE	GIBBON	E 6611.66	×	×	×	amd64 bits	×
SCREAM [120]	BCAE	TAE	E: 54.58	×	×	×	amd64 bits	×
Aegis [120]	BCAE	×	E: 2.15	×	×	×	amd64 bits	×
AEZ [120]	BCAE	XEX	E: 4.57	×	×	×	amd64 bits	×
Deoxys [120]	BCAE	XEX	E: 16.41	×	×	×	amd64 bits	×
AES-OCB [120]	BCAE	XEX	E: 20.35	×	×	×	amd64 bits	×
NORX [162]	PBAE	Monkey duplex	E/D: ×	×	207	124062	8 bits AVR	IEEE 802.15.4
NORX [162]	PBAE	Monkey duplex	E/D: ×	×	207	75727	16 bits MSP	IEEE 802.15.4
NORX [162]	PBAE	Monkey duplex	E/D: ×	×	207	16685	32 bits ARM	IEEE 802.15.4
NORX_v3 [168]	PBAE	Monkey duplex	E: 6.9 D: 6.92	×	×	×	amd64 bits	×
NORX [120]	PBAE	Monkey duplex	E:11.9	×	×	×	amd64 bits	×
LED-SILC [120]	BCAE	SILC	E: 9.9	×	×	×	amd64 bits	×
Tiaoxin [120]	SCAE	×	E: 3.53	×	×	×	amd64 bits	×
AEZ [120]	BCAE	XEX	E: 4.57	×	×	×	amd64 bits	×
Ketje [162]	PBAE	Monkey wrap	E/D: ×	×	158	311949	8 bits AVR	IEEE 802.15.4
Ketje [162]	PBAE	Monkey wrap	E/D: ×	×	158	372720	16 bits MSP	IEEE 802.15.4
Ketje [162]	PBAE	Monkey wrap	E/D: ×	×	158	148381	32bits ARM	IEEE 802.15.4
Ketje [168]	PBAE	Monkey wrap	E: 5.35 D: 5.34	×	×	×	amd64 bits	×
Ketje [120]	PBAE	Monkey wrap	E: 173.52	×	×	×	amd64 bits	×

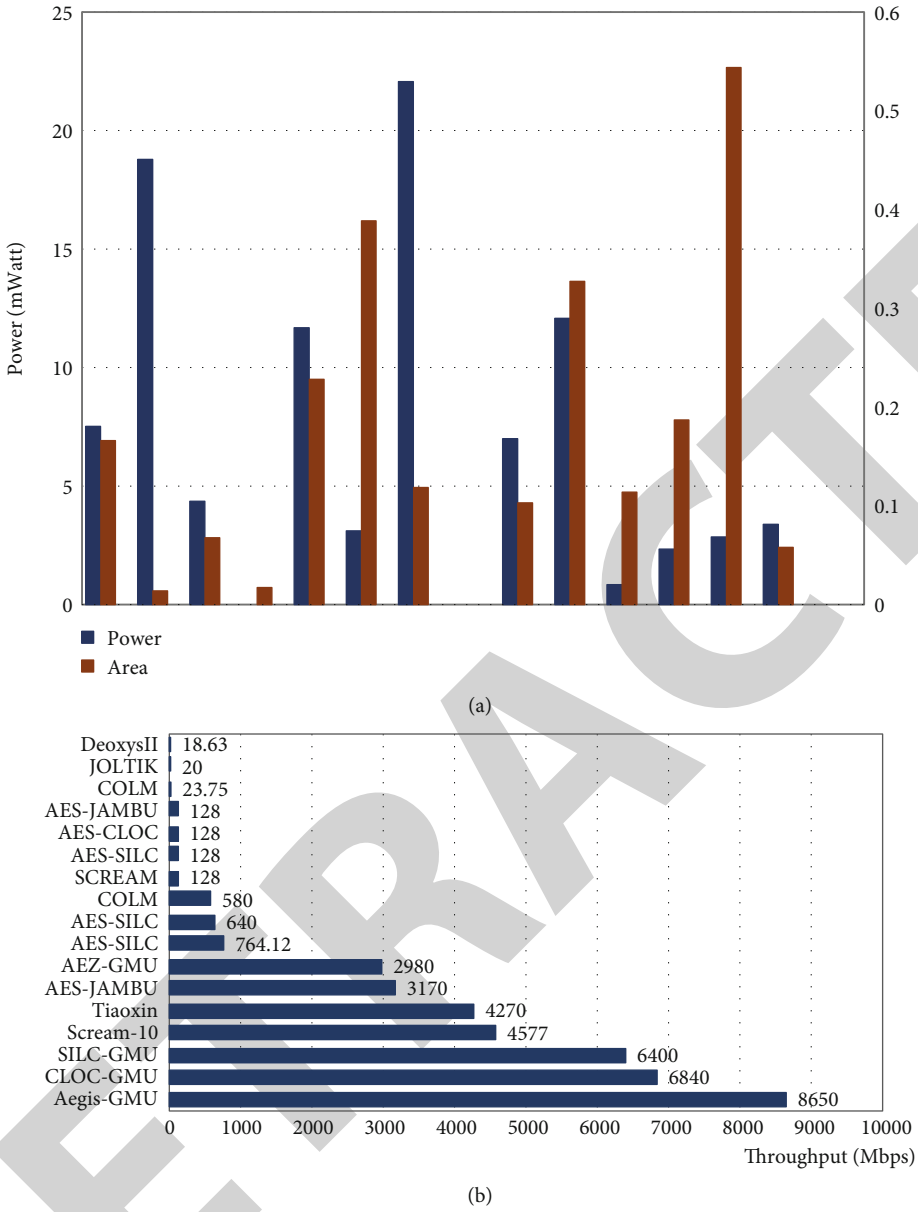

Figure 6: Metric performance of BCAE-based targeted ASIC, (a) power and area for BCAE-based targeting ASIC, (b) throughput for BCAE-based targeting ASIC.

7.6. PBAE Comparisons. NORX, Ketje_sr, Ketje_jr ASCON, and PIRMATEs performance in ASIC is shown in Figure 11(a) and 11(b). ASCON [25] outperforms other ciphers with efficient power and small implementation area. It utilizes 0.083 mm^2, consumes 0.655 mWatt in ASIC while consuming 684 LUTs [164] and 2.16 mWatt [25] in FPGA.

PRIMATE [25] is the second most efficient cipher targeting area footprint and power consumption that utilized 0.106 mm^2, 1.064 mWatt, and 66.67 Mbps in ASIC while also consuming 3.547 mWatt, 1187 LUTs, and 66.67 Mbps in FPGA. However, PRIMATE is not nonce-resistance that if nonce misuse occurs then an adversary can reveal the plaintext, unlike ASCON, which is nonce misuse resistance. Similarly, both algorithms cannot resist side channel attacks.

Ketje_jr [60] is also recommended cipher under PBAE-based category. It employs small area of 0.0172 mm^2, consumes a power of 3.27 mWatt, with high transmission of 14550 Mbps. From the optimization perspective, NORX [60] is not recommended for resource-constrained devices in ASIC or FPGA because it consumes the most of the platforms resources. The resources were reported of 0.1231 mm^2 area and 19.51 mWatt of dissipated power in ASIC while consuming 100 mWatt and area of 1424 LUTs in FPGA.

ASCON, NORX, and Ketje were benchmarked on 8 bits AVR, 16 bits MSP, and 32 bits ARM. The area utilization computed in terms of RAM were 183 bytes, 207 bytes, and 158 bytes, respectively. However, there was some fluctuation on the cycle, whereby 32bits ARM was reported with the lowest cycle count for the three ciphers as shown in

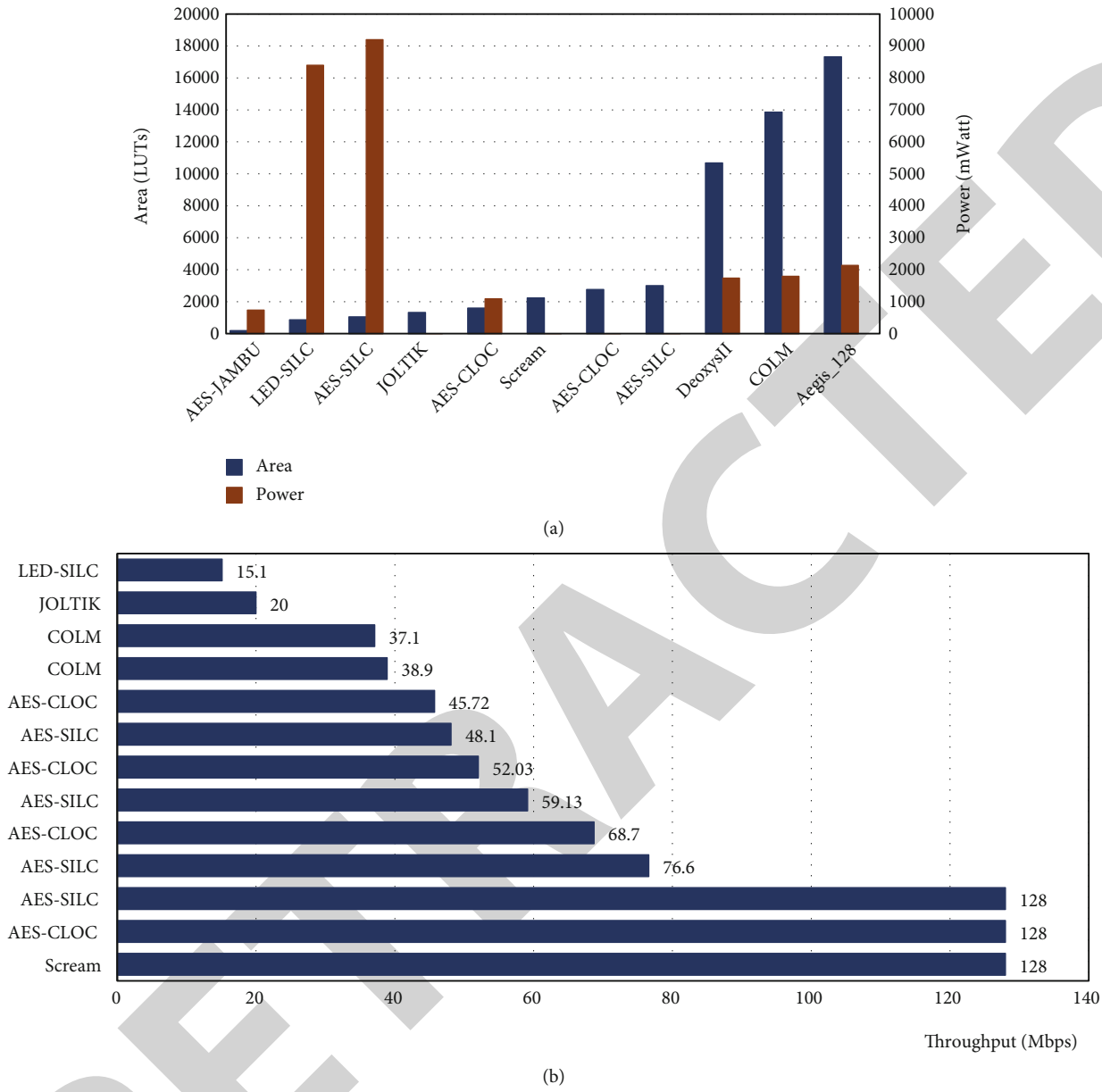

Figure 7: Metric performance of BCAE-based targeted FPGA, (a) power and area metrics for BCAE-based targeting FPGA, (b) throughput for BCAE-based targeting FPGA.

Figures 12(a)–12(c) to be 83118 cycles, 16685 cycles, and 148381 cycles, respectively, and these outcomes are part of IEEE802.15.4. This is due to the high processing speed of 32bits ARM compared to the AVR and MSP.

Ketje, NORX, and Ascon were the fastest algorithm in 64 bits ARM which required 10.69 cycles, 11.9 cycles, 14.7 cycles for processing AE. NORX is not resistant to nonce misuse unlike Ketje and ASCON, so consequently it is not recommended for untrusted environments even if it is reported the best performance on 64bits AMD. PRIMATEs operating in the GIBBON mode of operation were measured as having an extremely high number of cycles for processing, which reached up to 6611.66 cycles/bytes and could not resist nonce misuse nor fault attacks.

7.7. J. Encrypt and MAC Methods. OCB is an EaM scheme. The algorithm was designed as parallelizable with efficient offset calculation and low intermediate dependency that require a few cycles. The scheme overcomes the Galois Field GF(2^n) which adds an overhead to hardware implementation via modular addition, yet this requires more chip area than XOR gates. The work in [60] optimized the algorithm AES-OCB in TSMC 65 nm ASIC and utilized 0.1442 mm^2, 27.42 mWatt, and 4920 Mbps. It generated a small footprint area with high power consumption and high throughput.

On 64 bits AMD, the speed reported is 20.35 cycles/bytes. This kind of measurement derives from the fact that the algorithm required an inverted decryption, which simply adds to the cost of resources. In spite of this, it is faster on

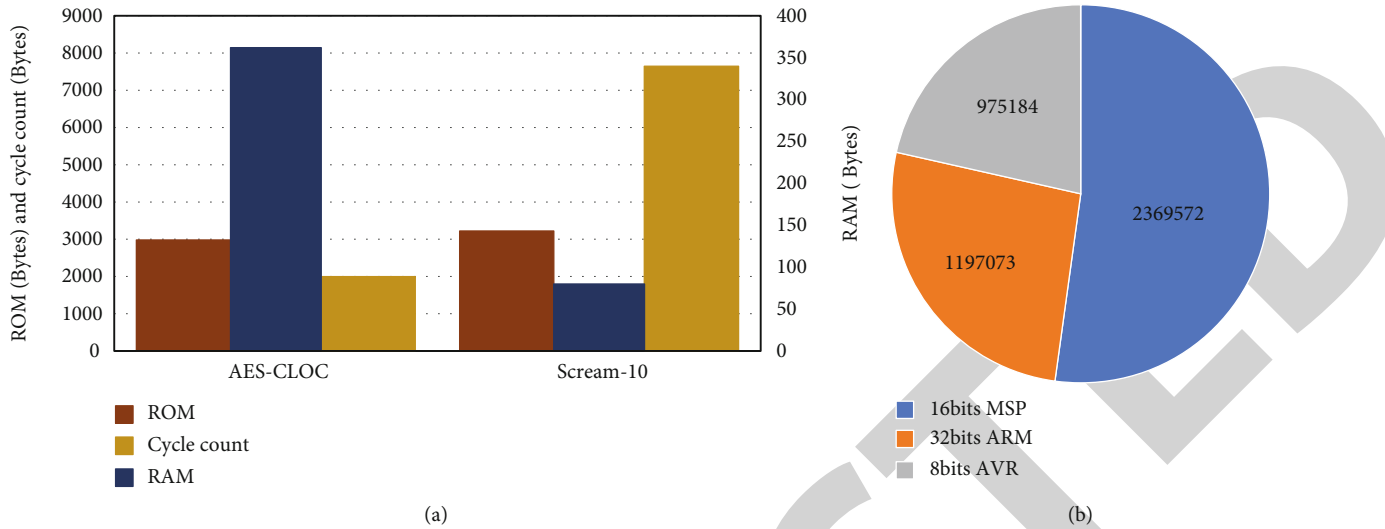

Figure 8: BCAE-based algorithms memory utilization and cycle count (a) BCAE-based algorithms memory utilization and cycle count, (b) cycle count of AES-GCM in software platforms.

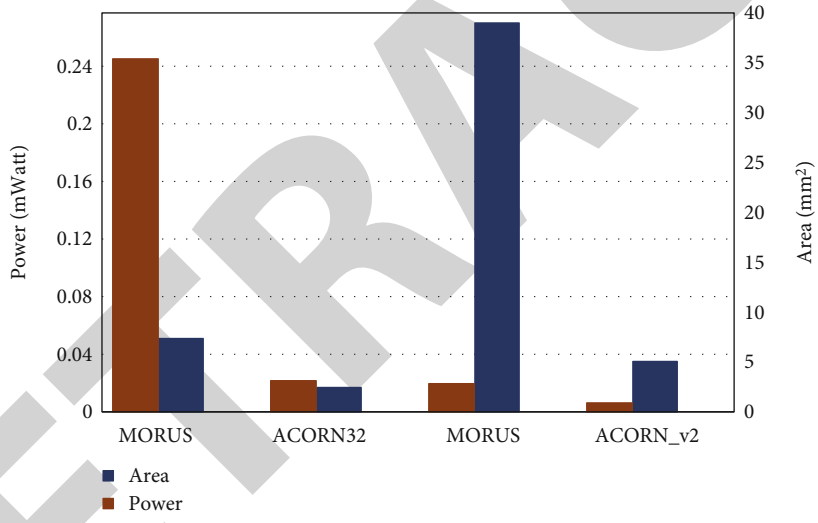

Figure 9: Power and area metrics performance for SCAE-based targeting ASIC.

hardware platforms since the encryption and decryption engines can be parallelized.

8. Open Problems

Deploying LAE to provide C and I of data on a single scheme is a future direction for smart IoT devices to follow. Data should be protected and authenticated simultaneously on transit and storage in order to protect them against unauthorized disclosure or misuse. However, there are major problems, which are explained in more detail.

8.1. Communication Limitations

(1) *Diverse Communication*. Connection to IoT devices is facilitated via a variety of wireless communications [169]. These protocols' links range from short to wide area that affects the selection of connection protocol. Establishing a cryptographic security solution should consider many properties of these protocols to ensure a practical and flexible usability. A proper LAE solution that comprehensively takes into account different wireless communication protocols and their limitations is a major research problem. For example, we can evaluate the specification of LoRaWAN, IEEE 802.15.4, and IPv6 and propose an LAE scheme based on their specification requirements. Then, benchmarking the solution for IoT devices is a future work that will address the scalable resilient requirement, which ease IoT devices' connectability to the network

(2) *Multiple Protocols*. IoT devices use different protocols to communicate. Although many protocol

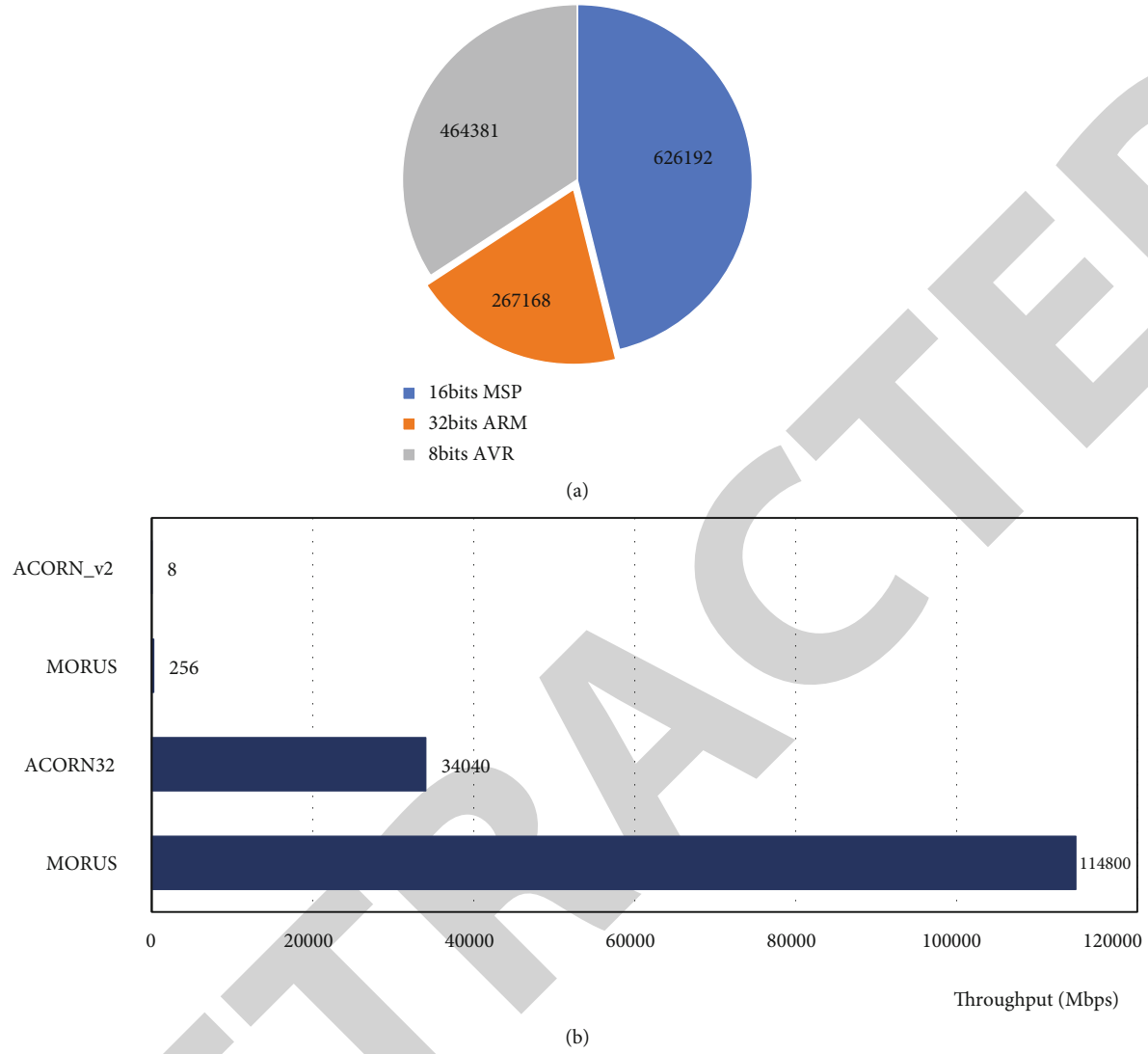

Figure 10: Metrics performance of SCAE-based targeting ASIC (a) power and area for SCAE-based targeting ASIC, (b) throughput for SCAE-based targeting ASIC.

standards exist for various IoT applications, there is no unified protocol yet [170]. As a result, the protection of data should be properly assured against unauthorized access to devices, when data is stored within them, and when data is exchanged between different devices. In these scenarios, users' data should not be manipulated nor accessed which requires multiple layers of data protection to ensure security features. A lightweight protection scheme is a significant way to curtail expenditure. However, exposure of long term keys threat is to be addressed through a lightweight protocol similar to [171]. This protocol delivers a validated perfect forward secrecy such that an adversary cannot access any previous negotiated session keys if the long-term keys are exposed. Furthermore, the protocol demonstrates a strong protection against replay attacks. Adversary capturing the communicated message and resending it again will be detected immediately

(3) *Multinetwork Approach*. IoT networks differ in their architecture [172]. A framework can include a cloud service provider with IoT edge computing node while another could not. Thus, proposing a solution, which examines a specific architecture will restrict the usability but a solution investigated for an ubiquitous framework will provide the necessary network heterogeneity

8.2. Algorithms' Design Security

(1) *Security Characteristics*. LAE schemes should consistently be examined against recent attacks [173, 174]. These could be design attack for example a quantum forgery attack or implementation attack like a fault

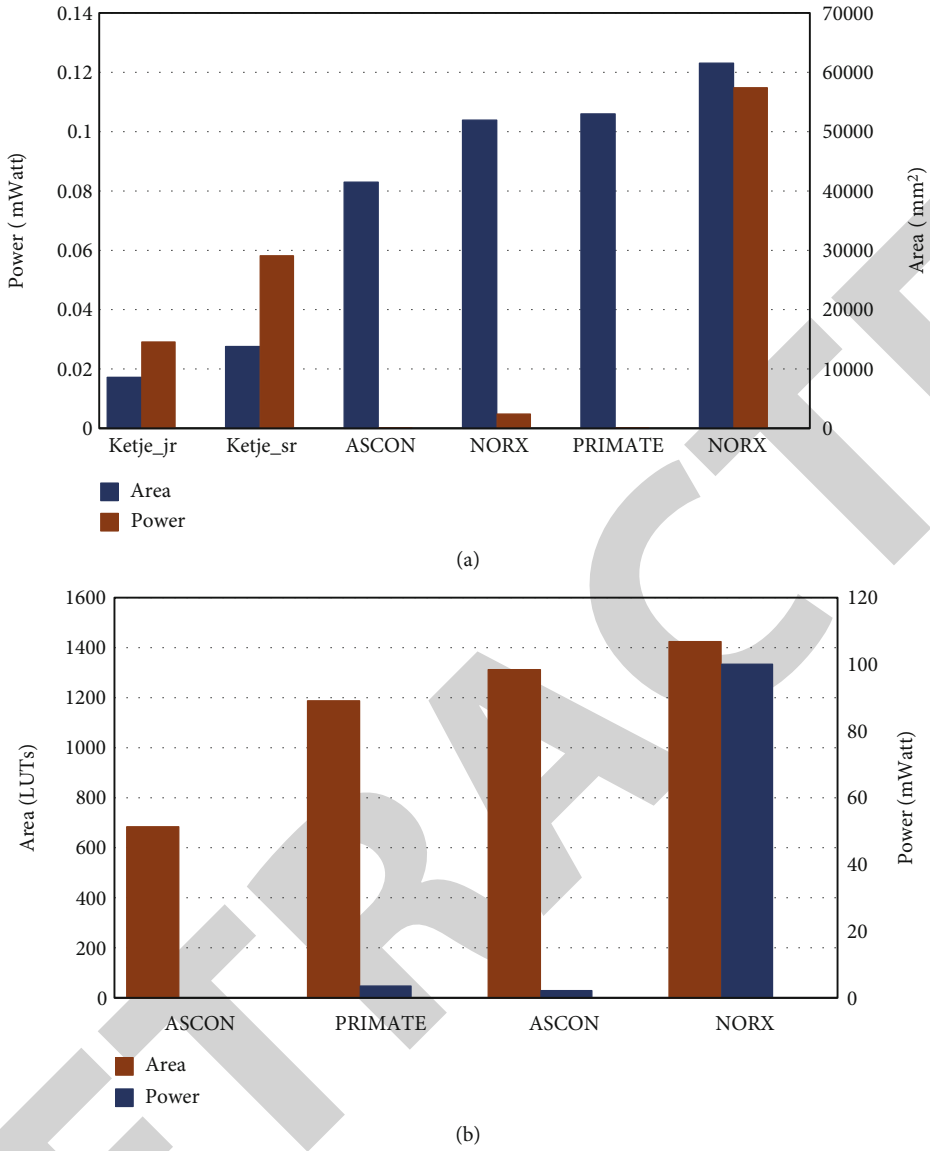

Figure 11: Power and area for PBAE-based targeting: (a) ASIC, (b) FPGA.

attack. However, there are many attacks to be considered in the literature and a detailed security analysis will address designers' claims. An automatic application that assesses design security characteristics and extracts cryptographic mean parameters that provide up-to-date security would be a powerful tool

(2) *Attack Assessment*. Variety of security attacks tool is a useful pre-decision assessment for developers to consider [175]. Proper cryptographic attacks can be converted to an automatic tool-based strategy to assess and validate a scheme's strength. Such a tool is useful prior to implementing the algorithm into an IoT system. Furthermore, LAE algorithms with AD are more practical for examining IoT networks. Hence, researching how to convert LAE schemes into AEAD for IoT framework is required

(3) *NIST AE*. As NIST standardizes AE under the lightweight cryptography project [55], there are 32 candidates announced in round 2. Recently, the finalists were announced and these were ASCON, Elephant, GIFT-COFB, Grain-128 AEAD, ISAP, PHOTON-Beetle, Romulus, SPARKLE, TinyJAMBU, and Xoodyak. Security analysis, attacks assessment, and platform performance comparisons are still being researched, which contributes directly to the standardization process. Comparisons of new schemes done in this paper lead the way to more research on this topic

8.3. Platforms Limitations. Proposing an encryption and authenticity solution scheme should consider devices'

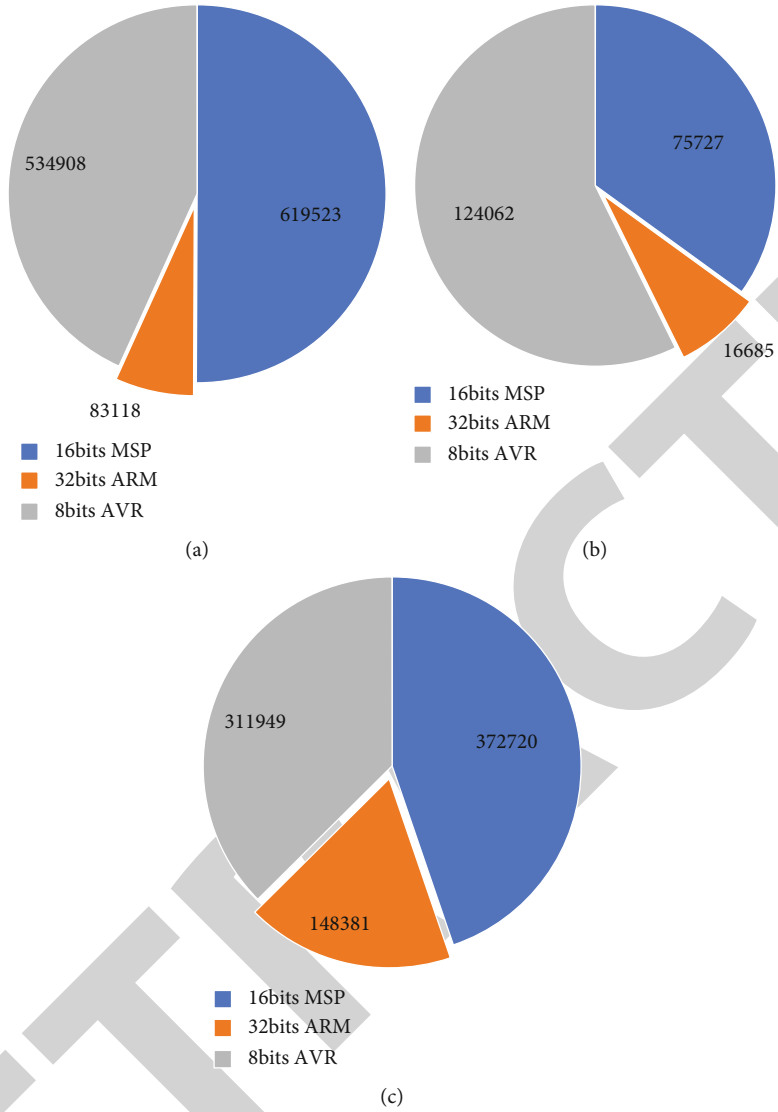

Figure 12: PBAE-based algorithms cycle count on 8 bits AVR, 16 bits MSP, and 32 bits ARM, (a) cycle count of ASCON_v1.2 in software platform, (b) cycle count of NORX in software platforms, and (c) cycle count of Ketje in software platforms.

diverse features, constraints, limitations, as well as providing efficient performance [176]. However, to ensure these characteristics while maintaining design security constitute a trade-off challenge. A scheme is able to resist attacks threatening IoT devices when placed in an uncontrolled environment (e.g., nonce misuse, quantum attacks, and side channel attacks) and still having to retain reasonable cost and performance efficiency, continues to be a problem.

9. Conclusion

The growth of IoT devices exposes data confidentiality and integrity breaches. IoT data encryption and checking its integrity are prerequisites for preventing information disclosure and detecting adversary data manipulation. As a result, there is a demand for a light computation scheme that can maintain a trade-off with up-to-date design security level, performance efficiency, and reasonable cost. LAE is an effective scheme compared to other lightweight cryptography primitives. It encrypts and authenticates the information as well the packet header and proposes a future direction that addresses limited device requirements. Recent studies have shown a lack of algorithm design being taken into account, leading to weak algorithms being discussed in the IoT literature or conventional cryptographic solutions that are not suitable for limited resource platforms. We presented a state-of-the-art LAE with security, design characteristics, and performance comparisons. Major problems regarding the establishment of LAE for IoT devices are highlighted here. Future research on this topic should propose a lightweight scheme for IoT devices as long as the main focus is kept on up-to-date security against attacks, with a trade-off between performance efficiency and cost of resources.

Conflicts of Interest

The authors declare that there are no conflicts of interest regarding the publication of this paper.

Acknowledgments

The first author would like to acknowledge financial support from the Sultanate of Oman Government. We appreciate Maliha Omar for her assistance. Finally, we thank the anonymous referees whose suggestions improved the presentation of the paper.

References

[1] S. Ghanavati, J. H. Abawajy, D. Izadi, and A. A. Alelaiwi, "Cloud-assisted IoT-based health status monitoring framework," *Cluster Computing*, vol. 20, no. 2, pp. 1843–1853, 2017.

[2] Statista, "IoT: number of connected devices worldwide 2012-2025," 2019, https://www.statista.com/statistics/471264/iot-number-of-connected-devices-worldwide/files/172/iot-number-of-connected-devices-worldwide.html.

[3] M. Lombardi, F. Pascale, and D. Santaniello, "Internet of things: a general overview between architectures, protocols and applications," *Information*, vol. 12, no. 2, p. 87, 2021.

[4] L. D. Xu, W. He, and S. Li, "Internet of Things in industries: a Survey," *IEEE Transactions on Industrial Informatics*, vol. 10, no. 4, pp. 2233–2243, 2014.

[5] J. Lin, W. Yu, N. Zhang, X. Yang, H. Zhang, and W. Zhao, "A survey on internet of things: architecture, enabling technologies, security and privacy, and applications," *IEEE Internet of Things Journal*, vol. 4, no. 5, pp. 1125–1142, 2017.

[6] D. Izadi, J. Abawajy, and S. Ghanavati, "An alternative node deployment scheme for WSNs," *IEEE Sensors Journal*, vol. 15, no. 2, pp. 667–675, 2015.

[7] J. H. Abawajy and M. M. Hassan, "Federated Internet of Things and cloud computing pervasive patient health monitoring system," *IEEE Communications Magazine*, vol. 55, no. 1, pp. 48–53, 2017.

[8] M. Maryska, P. Doucek, P. Sladek, and L. Nedomova, "Economic efficiency of the Internet of Things solution in the energy industry: a very high voltage frosting case study," *Energies*, vol. 12, no. 4, p. 585, 2019.

[9] M. Michael, "Attack landscape H1 2019: IoT, SMB traffic abound," *Threats and Research*, vol. 1, 2019https://blog.f-secure.com/attack-landscape-h1-2019-iot-smb-traffic-abound/.

[10] B. R. Ray, M. U. Chowdhury, and J. H. Abawajy, "Secure object tracking protocol for the Internet of Things," *IEEE Internet of Things Journal*, vol. 3, no. 4, pp. 544–553, 2016.

[11] D. Mauro, W. Rodrigues, K. Gama, J. A. Suruagy, and P. A. D. S. Gonçalves, "Towards a multilayer strategy against attacks on IoT environments," in *2019 IEEE/ACM 1st International Workshop on Software Engineering Research & Practices for the Internet of Things (SERP4IoT)*, pp. 17–20, Montreal, QC, Canada, May 2019.

[12] E. Bertino and N. Islam, "Botnets and Internet of Things security," *Computer*, vol. 50, no. 2, pp. 76–79, 2017.

[13] N. Neshenko, E. Bou-Harb, J. Crichigno, G. Kaddoum, and N. Ghani, "Demystifying IoT security: an exhaustive survey on IoT vulnerabilities and a first empirical look on internet-scale IoT exploitations," *IEEE Communication Surveys and Tutorials*, vol. 21, no. 3, pp. 2702–2733, 2019.

[14] R. Chetan and R. Shahabadkar, "A comprehensive survey on exiting solution approaches towards security and privacy requirements of IoT," *International Journal of Electrical and Computer Engineering*, vol. 8, no. 4, p. 2319, 2018.

[15] M. Agrawal, J. Zhou, and D. Chang, "A survey on lightweight authenticated encryption and challenges for securing industrial IoT," in *Security and Privacy Trends in the Industrial Internet of Things*, C. Alcaraz, Ed., pp. 71–94, Springer International Publishing, Cham, 2019.

[16] J. Kaur, A. Kumar, and M. Bansal, "Lightweight cipher algorithms for smart cards security: a survey and open challenges," in *2017 4th International Conference on Signal Processing, Computing and Control (ISPCC)*, pp. 541–546, Solan, India, September 2017.

[17] S. Ghosh, R. Misoczki, L. Zhao, and M. R. Sastry, "Lightweight block cipher circuits for automotive and IoT sensor devices," in *Proceedings of the Hardware and Architectural Support for Security and Privacy*, Toronto, ON, Canada, 2017.

[18] B. J. Mohd, T. Hayajneh, and A. V. Vasilakos, "A survey on lightweight block ciphers for low-resource devices: comparative study and open issues," *Journal of Network and Computer Applications*, vol. 58, pp. 73–93, 2015.

[19] D. A. Saraiva, V. R. Q. Leithardt, D. de Paula, A. Sales Mendes, G. V. González, and P. Crocker, "PRISEC: comparison of symmetric key algorithms for IoT devices," *Sensors*, vol. 19, no. 19, p. 4312, 2019.

[20] S. Koteshwara and A. Das, "Comparative study of authenticated encryption targeting lightweight IoT applications," *IEEE Design & Test*, vol. 34, no. 4, pp. 26–33, 2017.

[21] O. G. Abood, M. A. Elsadd, and S. K. Guirguis, "Investigation of cryptography algorithms used for security and privacy protection in smart grid," in *2017 Nineteenth International Middle East Power Systems Conference (MEPCON)*, pp. 644–649, Cairo, Egypt, December 2017.

[22] M. Rana, Q. Mamun, and R. Islam, "Lightweight cryptography in IoT networks: a survey," *Future Generation Computer Systems*, vol. 129, pp. 77–89, 2022.

[23] E. Jintcharadze and M. Iavich, "Hybrid implementation of Twofish, AES, ElGamal and RSA cryptosystems," in *2020 IEEE East-West Design & Test Symposium (EWDTS)*, pp. 1–5, Varna, Bulgaria, September 2020.

[24] L. M. Shamala, G. Zayaraz, K. Vivekanandan, and V. Vijayalakshmi, "Lightweight cryptography algorithms for Internet of Things enabled networks: an overview," *Journal of Physics: Conference Series*, vol. 1717, no. 1, p. 012072, 2021.

[25] N. Samir, A. S. Hussein, M. Khaled et al., "ASIC and FPGA comparative study for IoT lightweight hardware security algorithms," *Journal of Circuits, Systems and Computers*, vol. 28, no. 12, p. 1930009, 2019.

[26] M. Nandi, "Forging attacks on two authenticated encryptions COBRA and POET," *IACR Cryptology ePrint Archive*, vol. 8873, p. 363, 2014.

[27] S. Roy, U. Rawat, and J. Karjee, "A lightweight cellular automata based encryption technique for IoT applications," *IEEE Access*, vol. 7, pp. 39782–39793, 2019.

[28] Y. M. Khattabi, M. M. Matalgah, and M. M. Olama, "Revisiting lightweight encryption for IoT applications: error performance and throughput in wireless fading channels with and without coding," *IEEE Access*, vol. 8, pp. 13429–13443, 2020.

[29] R. Yugha and S. Chithra, "A survey on technologies and security protocols: reference for future generation IoT," *Journal of Network and Computer Applications*, vol. 169, p. 102763, 2020.

[30] I. Ali and F. Li, "An efficient conditional privacy-preserving authentication scheme for vehicle-to-infrastructure communication in VANETs," *Vehicular Communications*, vol. 22, p. 100228, 2020.

[31] S.-Y. Tan, K.-W. Yeow, and S. O. Hwang, "Enhancement of a lightweight attribute-based encryption scheme for the Internet of Things," *IEEE Internet of Things Journal*, vol. 6, no. 4, pp. 6384–6395, 2019.

[32] U. Chatterjee, R. S. Chakraborty, and D. Mukhopadhyay, "A PUF-based secure communication protocol for IoT," *ACM Transactions on Embedded Computing Systems*, vol. 16, no. 3, p. 67, 2017.

[33] L. Guo, M. Dong, K. Ota et al., "A secure mechanism for big data collection in large scale Internet of vehicle," *IEEE Internet of Things Journal*, vol. 4, no. 2, pp. 601–610, 2017.

[34] A. A. Alamr, F. Kausar, J. Kim, and C. Seo, "A secure ECC-based RFID mutual authentication protocol for Internet of Things," *The Journal of Supercomputing*, vol. 74, no. 9, pp. 4281–4294, 2018.

[35] S. Huda, S. Miah, J. Yearwood, S. Alyahya, H. Al-Dossari, and R. Doss, "A malicious threat detection model for cloud assisted internet of things (CoT) based industrial control system (ICS) networks using deep belief network," *Journal of Parallel and Distributed Computing*, vol. 120, pp. 23–31, 2018.

[36] R. H. Randhawa, A. Hameed, and A. N. Mian, "Energy efficient cross-layer approach for object security of CoAP for IoT devices," *Ad Hoc Networks*, vol. 92, p. 101761, 2019.

[37] R. A. Rahman and B. Shah, "Security analysis of IoT protocols: a focus in CoAP," in *2016 3rd MEC International Conference on Big Data and Smart City (ICBDSC)*, pp. 1–7, Muscat, Oman, March 2016.

[38] Y. Meng, W. Zhang, H. Zhu, and X. S. Shen, "Securing consumer IoT in the smart home: architecture, challenges, and countermeasures," *IEEE Wireless Communications*, vol. 25, no. 6, pp. 53–59, 2018.

[39] K. Mohajerani, R. Haeussler, R. Nagpal et al., "Hardware benchmarking of round 2 candidates in the NIST lightweight cryptography standardization process," in *2021 Design, Automation & Test in Europe Conference & Exhibition (DATE)*, pp. 164–169, Grenoble, France, February 2021.

[40] T. S. Sector, "Overview of the Internet of Things," *International Telecomunication Union*, vol. 1, 2020https://www.itu.int/rec/T-REC-Y.2060/en.

[41] A. M. Yousuf, E. M. Rochester, and M. Ghaderi, "A low-cost LoRaWAN testbed for IoT: implementation and measurements," in *2018 IEEE 4th World Forum on Internet of Things (WF-IoT)*, pp. 361–366, Singapore, February 2018.

[42] L. Catarinucci, D. De Donno, L. Mainetti et al., "An IoT-aware architecture for smart healthcare systems," *IEEE Internet of Things Journal*, vol. 2, no. 6, pp. 515–526, 2015.

[43] S. Li, "Chapter 1 - introduction: securing the Internet of Things," in *Securing the Internet of Things*, S. Li and L. D. Xu, Eds., pp. 1–25, Syngress, Boston, 2017.

[44] P. V. Paul and R. Saraswathi, "The Internet of Things — a comprehensive survey," in *2017 International Conference on Computation of Power, Energy Information and Commuincation (ICCPEIC)*, pp. 421–426, Melmaruvathur, India, 2017.

[45] S. Li, "Chapter 3 - security and vulnerability in the Internet of Things," in *Securing the Internet of Things*, S. Li and L. D. Xu, Eds., pp. 49–68, Syngress, Boston, 2017.

[46] H. Q. A. Mahri, L. Simpson, H. Bartlett, E. Dawson, and K. K.-H. Wong, "Forgery attacks on ++AE authenticated encryption mode," in *presented at the Proceedings of the Australasian Computer Science Week Multiconference*, Canberra, Australia, 2016.

[47] M. Wazid, A. K. Das, S. Shetty, J. J. P. C. Rodrigues, and Y. Park, "LDAKM-EIoT: lightweight device authentication and key management mechanism for edge-based IoT deployment," *Sensors*, vol. 19, no. 24, p. 5539, 2019.

[48] F. Dalipi and S. Y. Yayilgan, "Security and privacy considerations for IoT application on smart grids: survey and research challenges," in *2016 IEEE 4th International Conference on Future Internet of Things and Cloud Workshops (FiCloudW)*, pp. 63–68, Vienna, Austria, 2016.

[49] A. Mosenia and N. K. Jha, "A comprehensive study of security of Internet-of-Things," *IEEE Transactions on Emerging Topics in Computing*, vol. 5, no. 4, pp. 586–602, 2017.

[50] D. N. Le, C. Bhatt, and M. Madhukar, *Security Designs for the Cloud, IoT, and Social Networking*, Wiley, 2019.

[51] D. Dolev, C. Dwork, and M. Naor, "Nonmalleable cryptography," *SIAM Review*, vol. 45, no. 4, pp. 727–784, 2003.

[52] Z. Huang, S. Liu, X. Mao, K. Chen, and J. Li, "Insight of the protection for data security under selective opening attacks," *Information Sciences*, vol. 412, pp. 223–241, 2017.

[53] X. Li, M. Wang, H. Wang, Y. Yu, and C. Qian, "Toward secure and efficient communication for the Internet of Things," *IEEE/ACM Transactions on Networking*, vol. 27, no. 2, pp. 621–634, 2019.

[54] S. Dziembowski, K. Pietrzak, and D. Wichs, "Non-malleable codes," *Journal of the ACM*, vol. 65, no. 4, pp. 1–32, 2018.

[55] M. S. Turan, K. McKay, D. Chang et al., "Status report on the second round of the NIST lightweight cryptography standardization process," *National Institute of Standards and Technology Internal Report*, vol. 8369, no. 10, p. 6028, 2021.

[56] M. Bellare and C. Namprempre, "Authenticated encryption: relations among notions and analysis of the generic composition paradigm," *Journal of Cryptology*, vol. 21, no. 4, pp. 469–491, 2008.

[57] S. Vaudenay, "Security flaws induced by CBC padding—applications to SSL, IPSEC, WTLS," in *Advances in Cryptology — EUROCRYPT 2002. EUROCRYPT 2002. Lecture Notes in Computer Science*, vol. 2332, Springer, Berlin, Heidelberg.

[58] P. Rogaway and T. Shrimpton, "A provable-security treatment of the key-wrap problem," in *Advances in Cryptology - EUROCRYPT 2006. EUROCRYPT 2006. Lecture Notes in Computer Science*, vol. 4004, Springer, Berlin, Heidelberg.

[59] A. W. Atamli and A. Martin, "Threat-based security analysis for the Internet of Things," in *2014 International Workshop on Secure Internet of Things (SIoT)*, pp. 35–43, Wroclaw, Poland, 2014.

[60] S. Kumar, J. Haj-Yahya, M. Khairallah, M. A. Elmohr, and A. Chattopadhyay, "A comprehensive performance analysis of hardware implementations of CAESAR candidates," *Cryptology ePrint Archive*, vol. 2017, p. 1261, 2017, 2019/12/16/03 : 27 : 58. http://eprint.iacr.org/2017/1261.

[61] "Inside the smart home: IoT device threats and attack scenarios - security news - trend micro AU," 2019, https://www.trendmicro.com/vinfo/au/security/news/internet-of-things/

inside-the-smart-home-iot-device-threats-and-attack-scenarios.

[62] N. A. Moldovyan, A. A.-M. Nashwan, D. T. Nguyen, N. H. Nguyen, and H. M. Nguyen, "Deniability of symmetric encryption based on computational indistinguishability from probabilistic ciphering," in *Information Systems Design and Intelligent Applications*, pp. 209–218, Springer, 2018.

[63] R. Cheng, J. Yan, C. Guan, F. Zhang, and K. Ren, "Verifiable searchable symmetric encryption from indistinguishability obfuscation," in *Proceedings of the 10th ACM symposium on information, computer and communications security*, pp. 621–626, Singapore Republic of Singapore, 2015.

[64] C. Guo, X. Fu, Y. Mao, G. Wu, F. Li, and T. Wu, "Multi-user searchable symmetric encryption with dynamic updates for cloud computing," *Information*, vol. 9, no. 10, p. 242, 2018.

[65] V. Koppula and B. Waters, "Realizing chosen ciphertext security generically in attribute-based encryption and predicate encryption," in *Advances in Cryptology – CRYPTO 2019. CRYPTO 2019. Lecture Notes in Computer Science*, vol. 11693, Springer, Cham.

[66] D. Boneh, E. Boyle, H. Corrigan-Gibbs, N. Gilboa, and Y. Ishai, "Zero-knowledge proofs on secret-shared data via fully linear PCPs," in *Advances in Cryptology – CRYPTO 2019. CRYPTO 2019. Lecture Notes in Computer Science*, vol. 11694, Springer, Cham.

[67] J. Katz and M. Yung, "Unforgeable encryption and chosen ciphertext secure modes of operation," in *Fast Software Encryption*, G. Goos, J. Hartmanis, J. Leeuwen, and B. Schneier, Eds., vol. 1978, pp. 284–299, Springer Berlin Heidelberg, Berlin, Heidelberg, 2001.

[68] K. Manandhar, X. Cao, F. Hu, and Y. Liu, "Detection of faults and attacks including false data injection attack in smart grid using Kalman filter," *IEEE Transactions on Control of Network Systems*, vol. 1, no. 4, pp. 370–379, 2014.

[69] C. Dobraunig, *On the Security and Design of Authenticated Encryption, [Ph.D. thesis]*, Graz University of Technology, 2017.

[70] C. Dobraunig, M. Eichlseder, T. Korak, V. Lomné, and F. Mendel, "Statistical fault attacks on nonce-based authenticated encryption schemes," in *Advances in Cryptology – ASIACRYPT 2016*, J. H. Cheon and T. Takagi, Eds., vol. 10031, pp. 369–395, Springer Berlin Heidelberg, Berlin, Heidelberg, 2016.

[71] J. Balasch, B. Gierlichs, and I. Verbauwhede, "An in-depth and black-box characterization of the effects of clock glitches on 8-bit MCUs," in *2011 Workshop on Fault Diagnosis and Tolerance in Cryptography*, pp. 105–114, Nara, Japan, 2011.

[72] "CMS responds to data breach affecting 75,000 in federal ACA portal | Healthcare Finance News," 2018, https://www.healthcarefinancenews.com/news/cms-responds-data-breach-affecting-75000-federal-aca-portal.

[73] A. Zanella, N. Bui, A. Castellani, L. Vangelista, and M. Zorzi, "Internet of Things for smart cities," *IEEE Internet of Things Journal*, vol. 1, no. 1, pp. 22–32, 2014.

[74] S. Wu, H. Wu, T. Huang, M. Wang, and W. Wu, "Leaked-state-forgery attack against the authenticated encryption algorithm ALE," in *Advances in Cryptology - ASIACRYPT 2013. ASIACRYPT 2013. Lecture Notes in Computer Science*, vol. 8269, Springer, Berlin, Heidelberg.

[75] Y. Liu, Y. Sasaki, L. Song, and G. Wang, "Cryptanalysis of reduced sliscp permutation in sponge-hash and duplex-AE modes," in *Selected Areas in Cryptography – SAC 2018. SAC 2018. Lecture Notes in Computer Science*, vol. 11349, Springer, Cham.

[76] J. Lu, "Almost universal forgery attacks on the COPA and marble authenticated encryption algorithms," in *ASIA CCS '17: Proceedings of the 2017 ACM on Asia Conference on Computer and Communications Security*, pp. 789–799, Abu Dhabi, United Arab Emirates, 2017.

[77] S. Raza, L. Wallgren, and T. Voigt, "SVELTE: real-time intrusion detection in the Internet of Things," *Ad Hoc Networks*, vol. 11, no. 8, pp. 2661–2674, 2013.

[78] N. Saxena, S. Grijalva, and N. S. Chaudhari, "Authentication protocol for an IoT-Enabled LTE network," *ACM Transactions on Internet Technology*, vol. 16, no. 4, pp. 1–20, 2016.

[79] W. Diehl, A. Abdulgadir, F. Farahmand, J.-P. Kaps, and K. Gaj, "Comparison of cost of protection against differential power analysis of selected authenticated ciphers," *Cryptography*, vol. 2, no. 3, p. 26, 2018.

[80] L. Li, G. Xu, L. Jiao et al., "A secure random key distribution scheme against node replication attacks in industrial wireless sensor systems," *IEEE Transactions on Industrial Informatics*, vol. 16, no. 3, pp. 2091–2101, 2020.

[81] F. Meneghello, M. Calore, D. Zucchetto, M. Polese, and A. Zanella, "IoT: Internet of threats? A survey of practical security vulnerabilities in real IoT devices," *IEEE Internet of Things Journal*, vol. 6, no. 5, pp. 8182–8201, 2019.

[82] T. Maitra, M. S. Obaidat, D. Giri, S. Dutta, and K. Dahal, "ElGamal cryptosystem-based secure authentication system for cloud-based IoT applications," *IET Networks*, vol. 8, no. 5, pp. 289–298, 2019.

[83] J. Hermans, R. Peeters, and B. Preneel, "Proper RFID privacy: model and protocols," *IEEE Transactions on Mobile Computing*, vol. 13, no. 12, pp. 2888–2902, 2014.

[84] J. Zhang, Y. Yu, S. Fan, Z. Zhang, and K. Yang, "Tweaking the asymmetry of asymmetric-key cryptography on lattices: KEMs and signatures of smaller sizes," in *Public-Key Cryptography – PKC 2020. PKC 2020. Lecture Notes in Computer Science*, vol. 12111, Springer, Cham.

[85] E. Andreeva, G. Barwell, R. Bhaumik, M. Nandi, D. Page, and M. Stam, "Turning online ciphers off," *IACR Transactions on Symmetric Cryptology*, vol. 2017, no. 2, pp. 105–142, 2017.

[86] V. T. Hoang, T. Krovetz, and P. Rogaway, "Robust authenticated-encryption AEZ and the problem that it solves," in *Advances in Cryptology – EUROCRYPT 2015. EUROCRYPT 2015. Lecture Notes in Computer Science*, vol. 9056, Springer, Berlin, Heidelberg.

[87] J. Mattsson and M. Westerlund, "Authentication key recovery on Galois/counter mode (GCM)," in *Progress in Cryptology – AFRICACRYPT 2016. AFRICACRYPT 2016. Lecture Notes in Computer Science*, vol. 9646, Springer, Cham.

[88] M. Bellare and B. Tackmann, "The multi-user security of authenticated encryption: AES-GCM in TLS 1.3," in *Advances in Cryptology – CRYPTO 2016. CRYPTO 2016. Lecture Notes in Computer Science*, vol. 9814, Springer, Berlin, Heidelberg.

[89] Y. Naito and T. Sugawara, "Lightweight authenticated encryption mode of operation for tweakable block ciphers," *IACR Transactions on Cryptographic Hardware and Embedded Systems*, vol. 2020, pp. 66–94, 2019.

[90] P. Grubbs, J. Lu, and T. Ristenpart, "Message franking via committing authenticated encryption," in *Advances in*

Cryptology – CRYPTO 2017. CRYPTO 2017. Lecture Notes in Computer Science, vol. 10403, Springer, Cham.

[91] P. Rogaway, "Authenticated-encryption with associated-data," in *Proceedings of the 9th ACM conference on Computer and communications security*, pp. 98–107, Washington, DC USA, 2002.

[92] D. Chang, A. K. Chauhan, N. Gupta, A. Jati, and S. K. Sanadhya, "Exploiting the leakage: analysis of some authenticated encryption schemes," in *Security, Privacy, and Applied Cryptography Engineering. SPACE 2016. Lecture Notes in Computer Science*, vol. 10076, Springer, Cham.

[93] E. Andreeva, V. Lallemand, A. Purnal, R. Reyhanitabar, A. Roy, and D. Vizár, "Forkcipher: a new primitive for authenticated encryption of very short messages," in *Advances in Cryptology – ASIACRYPT 2019. ASIACRYPT 2019. Lecture Notes in Computer Science*, vol. 11922, Springer, Cham.

[94] T. Kohno, A. Palacio, and J. Black, "Building secure cryptographic transforms, or how to encrypt and MAC," Cryptology ePrint Archive, 2003.

[95] M. Bellare and P. Rogaway, "Encode-then-encipher encryption: how to exploit nonces or redundancy in plaintexts for efficient cryptography," in *Advances in Cryptology — ASIACRYPT 2000. ASIACRYPT 2000. Lecture Notes in Computer Science*, vol. 1976, Springer, Berlin, Heidelberg.

[96] D. McGrew and J. Viega, "The Galois/counter mode of operation (GCM)," *submission to NIST Modes of Operation Process*, vol. 20, 2004.

[97] T. Kohno, J. Viega, and D. Whiting, "The CWC-AES dual-use mode," *Submission to NIST Modes of Operation Process*, vol. 1, 2003.

[98] S. Arvind and V. A. Narayanan, "An overview of security in CoAP: attack and analysis," in *2019 5th International Conference on Advanced Computing & Communication Systems (ICACCS)*, pp. 655–660, Coimbatore, India, 2019.

[99] H. Almahri, "Analysis of selected block cipher modes for authenticated encryption, [Ph.D. thesis]," Queensland University of Technology, Australia, 2018.

[100] C. S. Jutla, "Encryption modes with almost free message integrity," in *Advances in Cryptology — EUROCRYPT 2001. EUROCRYPT 2001. Lecture Notes in Computer Science*, vol. 2045, Springer, Berlin, Heidelberg.

[101] A. Chakraborti, T. Iwata, K. Minematsu, and M. Nandi, "Blockcipher-based authenticated encryption: how small can we go?," *Journal of Cryptology*, vol. 33, no. 3, pp. 703–741, 2020.

[102] P. Rogaway, M. Bellare, and J. Black, "OCB: a block-cipher mode of operation for efficient authenticated encryption," *ACM Transactions on Information and System Security (TISSEC)*, vol. 6, no. 3, pp. 365–403, 2003.

[103] A. Zúquete and P. Guedes, "Efficient error-propagating block chaining," in *Crytography and Coding. Cryptography and Coding 1997. Lecture Notes in Computer Science*, vol. 1355, Springer, Berlin, Heidelberg.

[104] K. Minematsu, "Parallelizable rate-1 authenticated encryption from pseudorandom functions," in *Advances in Cryptology – EUROCRYPT 2014. EUROCRYPT 2014. Lecture Notes in Computer Science*, vol. 8441, Springer, Berlin, Heidelberg.

[105] T. Krovetz and P. Rogaway, "The software performance of authenticated-encryption modes," in *Fast Software Encryption. FSE 2011. Lecture Notes in Computer Science*, vol. 6733, Springer, Berlin, Heidelberg.

[106] M. Liskov, R. L. Rivest, and D. Wagner, "Tweakable block ciphers," in *Advances in Cryptology — CRYPTO 2002. CRYPTO 2002. Lecture Notes in Computer Science*, vol. 2442, Springer, Berlin, Heidelberg.

[107] H. Delfs, H. Knebl, and H. Knebl, *Introduction to Cryptography*, Springer, 2002.

[108] D. Whiting, R. Housley, and N. Ferguson, *Counter with cbc-mac (ccm)*, RFC3610, 2003.

[109] M. Bellare, P. Rogaway, and D. Wagner, "The EAX mode of operation," in *Fast Software Encryption. FSE 2004. Lecture Notes in Computer Science*, vol. 3017, Springer, Berlin, Heidelberg.

[110] T. Kohno, J. Viega, and D. Whiting, "CWC: A high-performance conventional authenticated encryption mode," in *Fast Software Encryption. FSE 2004. Lecture Notes in Computer Science*, vol. 3017, Springer, Berlin, Heidelberg.

[111] Y. Naito, M. Matsui, T. Sugawara, and D. Suzuki, "SAEB: a lightweight blockcipher-based AEAD mode of operation," Cryptology ePrint Archive, 2019.

[112] T. Iwata, K. Minematsu, J. Guo, and S. Morioka, "CLOC: authenticated encryption for short input," in *Fast Software Encryption. FSE 2014. Lecture Notes in Computer Science*, vol. 8540, Springer, Berlin, Heidelberg.

[113] T. H. Hongjun Wu, "The JAMBU lightweight authentication encryption mode (v2. 1)," *CAESAR Competition Proposal*, vol. 1, 2016.

[114] S. R. Nagpaul and S. K. Jain, *Topics in Applied Abstract Algebra*, Thomson Brooks/Cole, 2005.

[115] M. R. Adhikari and A. Adhikari, *Basic Modern Algebra with Applications*, Springer India, 2013.

[116] G. Bertoni, J. Daemen, M. Peeters, and G. Van Assche, "Permutation-based encryption, authentication and authenticated encryption," Directions in Authenticated Ciphers, 2012.

[117] I. Kuon and J. Rose, "Measuring the gap between FPGAs and ASICs," *IEEE Transactions on Computer-Aided Design of Integrated Circuits and Systems*, vol. 26, no. 2, pp. 203–215, 2007.

[118] A. Ehliar and D. Liu, "An ASIC perspective on FPGA optimizations," in *2009 International Conference on Field Programmable Logic and Applications (FPL)*, pp. 218–223, Prague, Czech Republic, 2009.

[119] M. D. Aagaard, M. Sattarov, and N. Zidaric, "Hardware design and analysis of the ACE and WAGE ciphers," 2019, http://arxiv.org/abs/1909.12338.

[120] R. Ankele and R. Ankele, "Software benchmarking of the 2nd round CAESAR candidates," *IACR Cryptology ePrint Archive*, vol. 2016, p. 740, 2016, https://api.semanticscholar.org/db00fe6cffa7ab78e80e9a61fc4ec15fb2481c16?_ga=2.231023199.1524844265.1576644624-134252252.1576552945.

[121] W. Trappe, R. Howard, and R. S. Moore, "Low-energy security: limits and opportunities in the Internet of Things," *IEEE Security and Privacy*, vol. 13, no. 1, pp. 14–21, 2015.

[122] D.-D. Dinu, A. Biryukov, J. Groszschaedl, D. Khovratovich, Y. L. Corre, and L. Perrin, "FELICS - fair evaluation of lightweight cryptographic systems," p. 2015, 2015, https://api.semanticscholar.org/980fef72a502338685c6b4ad2aedf424b7560691.

[123] X. Jia, Q. Feng, T. Fan, and Q. Lei, "RFID technology and its applications in Internet of Things (IoT)," in *2012 2nd*

International Conference on Consumer Electronics, Communications and Networks (CECNet), pp. 1282–1285, Yichang, China, 2012.

[124] J. Zhou, Z. Cao, X. Dong, and A. V. Vasilakos, "Security and privacy for cloud-based IoT: challenges," *IEEE Communications Magazine*, vol. 55, no. 1, pp. 26–33, 2017.

[125] J. Salowey, A. Choudhury, and D. McGrew, "AES Galois counter mode (GCM) cipher suites for TLS," *Request for Comments*, vol. 5288, 2008.

[126] K. Igoe and J. Solinas, "AES Galois counter mode for the secure shell transport layer protocol," *IETF Request for Comments*, vol. 5647, 2009.

[127] L. Law and J. Solinas, "Suite B cryptographic suites for IPsec," *IETF Request for Comments*, vol. 4869, 2007.

[128] S. Gueron, A. Langley, and Y. Lindell, "AES-GCM-SIV: specification and analysis," *IACR Cryptology ePrint Archive*, vol. 2017, p. 168, 2017.

[129] H. Q. Al Mahri, L. Simpson, H. Bartlett, E. Dawson, and K. K.-H. Wong, "A fault-based attack on AEZ v4.2," in *2017 IEEE Trustcom/BigDataSE/ICESS*, pp. 634–641, Sydney, NSW, Australia, 2017.

[130] W. Diehl, F. Farahmand, A. Abdulgadir, J.-P. Kaps, and K. Gaj, "Face-off between the CAESAR lightweight finalists: ACORN vs. Ascon," in *2018 International Conference on Field-Programmable Technology (FPT)*, p. 184, Naha, Japan, December 2018.

[131] M. Liu and D. Lin, "Cryptanalysis of lightweight authenticated cipher ACORN," in *Posed on the Crypto-Competition Mailing List*, Crypto Competition, 2014.

[132] X. Zhang, X. Feng, and D. Lin, "Fault attack on ACORN v3," *The Computer Journal*, vol. 61, no. 8, pp. 1166–1179, 2018.

[133] A. Adomnicai, J. J. Fournier, and L. Masson, "Masking the lightweight authenticated ciphers ACORN and Ascon in software," *IACR Cryptology ePrint Archive*, vol. 2018, p. 708, 2018.

[134] H. Groß, E. Wenger, C. Dobraunig, and C. Ehrenhöfer, "Suit up!–made-to-measure hardware implementations of ASCON," in *2015 Euromicro Conference on Digital System Design*, pp. 645–652, Madeira, Portugal, 2015.

[135] H. Gross and S. Mangard, "Reconciling $d+1$ masking in hardware and software," in *Cryptographic Hardware and Embedded Systems – CHES 2017. CHES 2017. Lecture Notes in Computer Science*, W. Fischer and N. Homma, Eds., vol. 10529, Springer, Cham, 2017.

[136] R. AlTawy, R. Rohit, M. He, K. Mandal, G. Yang, and G. Gong, "sLiSCP: Simeck-based permutations for lightweight sponge cryptographic primitives," in *Selected Areas in Cryptography – SAC 2017. SAC 2017. Lecture Notes in Computer Science*, vol. 10719, Springer, Cham.

[137] M. Aagaard, R. AlTawy, G. Gong, K. Mandal, R. Rohit, and N. Zidaric, "WAGE: An Authenticated Cipher," *IACR Transactions on Symmetric Cryptology*, pp. 132–159, 2020.

[138] M. Aagaard, R. AlTawy, G. Gong, K. Mandal, and R. Rohit, *ACE: An Authenticated Encryption and Hash Algorithm*, Submission to NIST-LWC, 2019.

[139] C. Dobraunig and B. Mennink, *Elephant v1*, NIST, 2019.

[140] S. Gueron, A. Jha, and M. Nandi, *COMET: counter mode encryption with authentication tag*, NIST, 2019.

[141] M. Khairallah, "Weak keys in the rekeying paradigm: application to COMET and mixFeed," *IACR Transactions on Symmetric Cryptology*, vol. 2019, pp. 272–289, 2020.

[142] D. A. McGrew and J. Viega, "The security and performance of the Galois/counter mode (GCM) of operation," in *Progress in Cryptology - INDOCRYPT 2004. INDOCRYPT 2004. Lecture Notes in Computer Science*, vol. 3348, Springer, Berlin, Heidelberg.

[143] B. Lapid and A. Wool, "Cache-attacks on the ARM TrustZone implementations of AES-256 and AES-256-GCM via GPU-based analysis," in *Selected Areas in Cryptography – SAC 2018. SAC 2018. Lecture Notes in Computer Science*, vol. 11349, Springer, Cham.

[144] H. Wu, "ACORN: a lightweight authenticated cipher (v3)," *Candidate for the CAESAR Competition*, vol. 2016, 2016https://competitions.cr.yp.to/round3/acornv3.pdf.

[145] C. Dobraunig, M. Eichlseder, F. Mendel, and M. Schläffer, "Ascon v1. 2: Lightweight authenticated encryption and hashing," *Journal of Cryptology*, vol. 34, no. 3, pp. 1–42, 2021.

[146] D. B. Roy, A. Chakraborti, D. Chang, S. D. Kumar, D. Mukhopadhyay, and M. Nandi, "Fault based almost universal forgeries on CLOC and SILC," in *Security, Privacy, and Applied Cryptography Engineering. SPACE 2016. Lecture Notes in Computer Science*, vol. 10076, Springer, Cham.

[147] J. Jean, I. Nikolić, and T. Peyrin, "Joltik v1. 3," *CAESAR Round*, vol. 2, 2015.

[148] E. Andreeva, B. Bilgin, A. Bogdanov et al., "PRIMATEs v1," Submission to CAESAR, 2014.

[149] V. Grosso, G. Leurent, F. X. Standaert et al., "SCREAM & iSCREAM side-channel resistant authenticated encryption with masking," Submission to CAESAR, 2014.

[150] T. Iwata, K. Minematsu, J. Guo, S. Morioka, and E. Kobayashi, "SILC: simple lightweight CFB," CAESAR submission, 2014.

[151] H. Wu and B. Preneel, "AEGIS: a fast authenticated encryption algorithm," in *Selected Areas in Cryptography – SAC 2013. SAC 2013. Lecture Notes in Computer Science*, vol. 8282, Springer, Berlin, Heidelberg.

[152] E. Andreeva, A. Bogdanov, N. Datta et al., *COLM v1*, Submission to the CAESAR Competition, CASEAR, 2016.

[153] J. Jean, I. Nikolic, T. Peyrin, and Y. Seurin, *Deoxys v1. 41*, Submitted to CAESAR, 2016.

[154] J.-P. Aumasson, P. Jovanovic, and S. Neves, "NORX: parallel and scalable AEAD," in *Computer Security - ESORICS 2014. ESORICS 2014. Lecture Notes in Computer Science*, vol. 8713, Springer, Cham.

[155] H. Wu and T. Huang, "JAMBU lightweight authenticated encryption mode and AES-JAMBU," *CAESAR Competition Proposal*, vol. 1, 2014.

[156] I. Nikolic, "Tiaoxin-346," *Submission to the CAESAR Competition*, vol. 1, 2014.

[157] I. Salam, H. Q. A. Mahri, L. Simpson, H. Bartlett, E. Dawson, and K. K.-H. Wong, "Fault attacks on Tiaoxin-346," in *Proceedings of the Australasian Computer Science Week Multiconference*, pp. 1–9, Brisband Queensland Australia, 2018.

[158] V. T. Hoang, T. Krovetz, and P. Rogaway, "AEZ v1: authenticated-encryption by enciphering," CAESAR 1st Round, Competitions, 2014, cr. yp. to/round1/aezv1.pdfl.

[159] G. Bertoni, J. Daemen, M. Peeters, G. Van Assche, and R. Van Keer, "CAESAR submission: Ketje v2," CAESAR First Round Submission, 2014.

[160] G. Bertoni, J. Daemen, M. Peeters, G. Van Assche, and R. Van Keer, *Keyak v2*, CAESAR Submission, 2015.

Hindawi
Wireless Communications and Mobile Computing
Volume 2023, Article ID 9813136, 1 page
https://doi.org/10.1155/2023/9813136

Retraction

Retracted: Building English Audio-Visual and Oral Mobile Teaching System Based on Virtual Augmented Reality Technology

Wireless Communications and Mobile Computing

Received 17 October 2023; Accepted 17 October 2023; Published 18 October 2023

This article has been retracted by Hindawi following an investigation undertaken by the publisher [1]. This investigation has uncovered evidence of one or more of the following indicators of systematic manipulation of the publication process:

(1) Discrepancies in scope
(2) Discrepancies in the description of the research reported
(3) Discrepancies between the availability of data and the research described
(4) Inappropriate citations
(5) Incoherent, meaningless and/or irrelevant content included in the article
(6) Peer-review manipulation

The presence of these indicators undermines our confidence in the integrity of the article's content and we cannot, therefore, vouch for its reliability. Please note that this notice is intended solely to alert readers that the content of this article is unreliable. We have not investigated whether authors were aware of or involved in the systematic manipulation of the publication process.

Wiley and Hindawi regrets that the usual quality checks did not identify these issues before publication and have since put additional measures in place to safeguard research integrity.

We wish to credit our own Research Integrity and Research Publishing teams and anonymous and named external researchers and research integrity experts for contributing to this investigation.

The corresponding author, as the representative of all authors, has been given the opportunity to register their agreement or disagreement to this retraction. We have kept a record of any response received.

References

[1] D. Xinzhen and R. Zhifen, "Building English Audio-Visual and Oral Mobile Teaching System Based on Virtual Augmented Reality Technology," *Wireless Communications and Mobile Computing*, vol. 2023, Article ID 1387219, 13 pages, 2023.

Hindawi
Wireless Communications and Mobile Computing
Volume 2023, Article ID 1387219, 13 pages
https://doi.org/10.1155/2023/1387219

Research Article

Building English Audio-Visual and Oral Mobile Teaching System Based on Virtual Augmented Reality Technology

Deng Xinzhen[1] and Ren Zhifen[2]

[1]*Faculty of Education, Henan University, Kaifeng, China*
[2]*Anyang University, Anyang, China*

Correspondence should be addressed to Ren Zhifen; 2016122574@jou.edu.cn

Received 30 May 2022; Revised 29 August 2022; Accepted 8 September 2022; Published 20 February 2023

Academic Editor: Jun Ye

Aiming at the problem that the current English textbooks still provide video materials in the form of CD-ROMs, which affects the learning effect, a research method of English audio-visual mobile teaching system based on virtual and augmented reality technology is proposed. The system first builds a recognition map database and stores it in the cloud and names the corresponding video files according to the name of the recognition map, then uses Unity3D to design and render the scene, design the virtual video playback button of the ImageTarget object, and write script code to realize the recognition map database and its corresponding video, access, and finally, generate a user-friendly mobile application. Users only need to point the lens at the book illustration to present the visual effect of superposition of virtual and real and realize the playback of English teaching videos on mobile devices. The results show that compared with the original image grayscale distribution map, the pixels near the 0 value of the pixel distribution map after twice filtering are significantly reduced, which reduces the hole noise of the image, and the original image and the image after twice filtering are not 0. The peak value of the pixel is close, maintaining the detailed characteristics of the image. The application of augmented reality technology to English video teaching enables users to enjoy novel learning methods and an interactive experience combining virtual and real.

1. Introduction

In the information age, many universities still do not use advanced information technology in the process of teaching English listening and speaking in the classroom, but rely solely on offline teaching and do not know how to change from the traditional teaching method to the mobile micro-learning method. This teaching method has great drawbacks. On the one hand, the classroom time is limited, and students have no time to digest the new knowledge they have learned. On the other hand, the spare time is not fully utilized, resulting in the waste of a lot of learning resources. English audio-visual teaching mainly trains the ability of listening, speaking, reading, and writing, and the cultivation of this ability requires a lot of repetitive practice; obviously, there is not such sufficient time in the classroom. If the students simply listen to the teacher's teaching and do not practice by themselves, it is difficult for them to master the skills of college English audio-visual skills. There is another problem; some students are diligent in thinking; they will have many problems, but the class time is limited, and many problems cannot be solved. Faced with this situation, we need our teachers to actively seek solutions. This problem can be effectively solved by the combination of real classroom and online classroom, and the mobile teaching system is created based on this solution. With the development of network technology and the widespread popularization of mobile smart devices, mobile learning has gradually become popular in school teaching. Combining the convenience, practicability, and efficiency of mobile devices with college English audio-visual teaching, the construction of a mobile audio-visual teaching mode of big English is the main direction of modern college English audio-visual teaching reform.

The application of virtual and augmented reality technology in college English audio-visual teaching is becoming more and more extensive, especially the function of English

network platform is becoming more and more powerful. Reform the traditional classroom-style college English teaching mode, establish a new model of English audio-visual mobile teaching based on virtual and augmented reality technology, and integrate virtual and augmented reality technology into college English audio-visual teaching, to achieve the goal of college English audio-visual teaching.

Augmented reality is also called hybrid reality technology. The technical principle is to simulate the physical information that is difficult for people in a certain range of time and space, such as visual information, sound information, taste information, and tactile information, with the help of scientific technology. The technical principle is the project risk prevention mechanism, which is the law or standard based on in the implementation of the project, usually based on the experience of past failures. Then, it is superimposed into the real world through certain technical transformation, so that it can be felt by our organs and can make people feel or even surpass the sensory experience of reality. Through the sensory organs, we can know the colorful world. Compared with traditional virtual reality technology, augmented reality technology achieves more different immersive effects. It can organically combine the information generated by computer with the scenes in the real world, to provide more accurate and efficient auxiliary operation interface for users in medical and engineering fields [1]. The combination with mobile teaching system can reflect the cloud data, including text, video, and other information in real time in mobile devices with the help of mobile network, present a more real visual effect with the help of virtual augmented reality technology, and give users a more novel English audio-visual and oral learning method.

2. Literature Review

Many universities in the United States use virtual reality equipment to publicize campus culture. They will record a panoramic introduction of the campus and send it to students preparing for admission, to help freshmen adapt to campus life in advance and better understand campus culture [2]. Despite Google's efforts to promote, virtual reality technology still cannot be popularized on a large scale in colleges and universities in various countries [3]. Leading universities in various countries have not widely applied VR technology in the classroom, and some of them believe that VR technology is not the core of teaching, and it is difficult to apply VR to all courses due to the factors of teaching methods and situations; they believe that, for example, language and literature courses are different from professional courses such as architecture, physics, medicine, and biology, and there is no demand for VR technology. The high-tech industries vigorously developed by the country listed in the outline of the 13th five-year plan for national economic and social development of the People's Republic of China issued by the national two sessions in 2016, including innovation and industrialization in emerging frontier fields such as robots, aviation equipment, intelligent transportation, virtual reality, and interactive film and television; as a new technical field, virtual reality is developing at a very fast speed [4]. The guidance of national policies and practical needs has stimulated a virtual reality entrepreneurial boom, and the relevant entrepreneurial teams have increased explosively. The research report released by the National Advertising Research Institute and several institutions shows that the virtual reality user group has a trend of spreading from the first tier cities to the whole country. China joined the research ranks of virtual reality technology only in the 1990s, but with the rapid development of computer field in China in recent years, it also drives the development of virtual reality technology [5].

In recent years, the large-scale attempts in commercial projects have made virtual reality stand out. With the continuous maturity of technology, the space art of virtual reality is a new form of artistic language combining sculpture, painting, image, and other media. Virtual reality has a wide range of applications, but it is still in the exploratory stage. Virtual reality technology involves electronic technology. At the same time, it needs to apply the knowledge of visual perception, physiology, psychology, ergonomics, and other disciplines. Virtual reality should be promoted from the technical level to the artistic level. Its research and practical application in the field of art is an urgent need to explore. In recent years, virtual reality research boom broke out in China, and many related research companies appeared, but few developed in the field of Education [6]. As a concept stock on the tuyere, virtual reality is still expected to make huge profits in games and film and television. The application of virtual reality in education has been thunderous, but the rain is small. The intention of "immersive education" and "virtual education" of LETV China is reached. At the product launch site of LETV, the CEO of New Oriental said that the panoramic teaching environment created by virtual reality technology can enable students to "immerse learning" and improve learning efficiency in English classroom. From the virtual reality video launched by LETV, it can be seen that wearing the head mounted virtual reality display, learners will have the feeling of being in it. They can watch the virtual classroom 360° and enhance students' understanding of the classroom learning environment and experience effect [7].

3. Virtual Augmented Reality Technology

3.1. Augmented Reality Technology

3.1.1. Working Framework of Augmented Reality System. A complete augmented reality system framework should include six main functional modules, namely, scene acquisition, target recognition and tracking, target registration, virtual real fusion, virtual real interaction, and image display. Its workflow is shown in Figure 1.

3.1.2. Target Recognition, Tracking, and Registration Technology. The tracking registration technology based on computer vision uses algorithms such as image recognition to obtain the position of the target in the real scene in real time, so as to realize the function of target tracking. The tracking registration technology combining computer vision

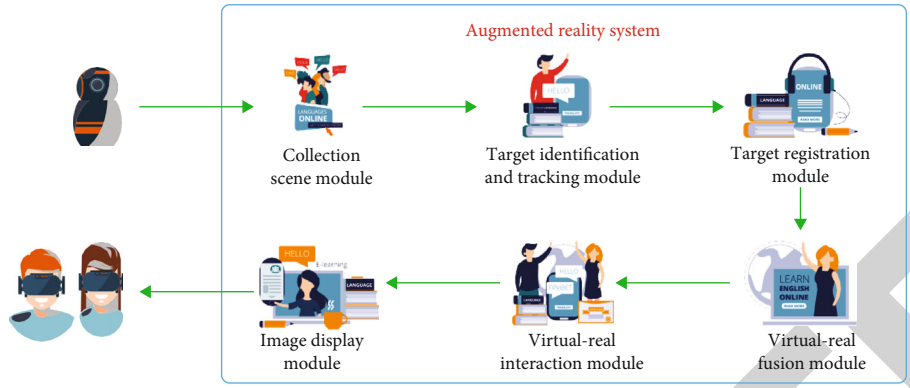

Figure 1: Framework of augmented reality system.

and tracking sensor combines the advantages of both, which not only has the advantages of sensor in outdoor environment but also includes the dynamic tracking function of real scene. In the technology of target tracking and recognition, many researchers outside China are constantly improving the efficiency of target recognition and tracking.

3.1.3. Display Technology. The development direction of augmented reality is mostly concentrated in the field of vision. Common display terminals include PC screen display, mobile screen display, and projection display equipment. Among wearable devices, there are mainly helmet-mounted display and spectacle display devices; wearable devices are represented by smart watches and wireless headphones. The rapid development of wireless technology has driven the maturity of wearable ecology, making wearable devices enter the rising stage. There will be various forms of products derived from the market, such as smart glasses, AR, and VR technology, and helmet-mounted display can be subdivided into projection helmet-mounted display, free-form surface helmet-mounted display, and so on.

3.1.4. Augmented Reality Interactive Technology. Augmented reality interaction technology has changed the traditional way of human-computer interaction. Users can send instructions and obtain responses to the computer without the help of hardware equipment and realize the communication between human and computer through the interaction and control of virtual objects. If there is no ready hardware device, it can be simulated by downloading the network debugging assistant. The realization of augmented reality interaction technology is based on target recognition, tracking, and registration [8, 9]. According to the dependence on hardware, augmented reality interaction technology can be roughly divided into two types. The first is to obtain video stream or image only by using image input device and identify and register the target according to the system design, so as to obtain the target in the natural scene, and it is mainly used for rapid target detection, especially in some edge devices, such as autonomous driving. Unmanned vehicles, etc., need to quickly identify and feedback the obtained images and videos for the control system to respond quickly. The second is to assist the detection and recognition of targets with the help of data gloves and wearable sensing devices. At the same time, the user's instructions can be detected by hardware sensing.

According to the position relationship between virtual objects and real objects in space, multichannel augmented reality interaction technology can be divided into interaction modes with depth consistency and interaction modes without depth consistency [10, 11]. Augmented reality interaction based on depth consistency can present the correct position relationship (depth information) between real objects and virtual objects in the same scene; augmented reality uses various techniques for presentation, including optical projection systems and monitors and realizes the mutual occlusion between virtual objects and real objects. This interaction technology is commonly used on configurable binocular cameras, depth cameras, and other devices that can obtain the depth of the scene. Virtual objects have depth data and can achieve perspective effects in real scenes. With the help of 3D reconstruction and collision detection technology, it can block each other with the targets in the real scene, to realize the interaction based on depth consistency, make the interaction mode closer to nature, and make the interaction effect between virtual objects and real scenes more realistic. According to the instruction mode, the instruction-based augmented reality interaction technology can be divided into static instruction interaction and dynamic instruction interaction [12, 13]. Static instruction interaction is to transfer the information such as manual identification code, human hand, or human body static action to the system, obtain the static instruction through the identification and detection algorithm, and feed back the instruction information to the system, so as to make the system respond. Dynamic instruction interaction is to take the image recognition instruction in consecutive frames with timing information as information and feed back the result to the system. The difference between static instruction interaction and static instruction interaction is that static instruction interaction can obtain one frame information in a scene film or video as data, while dynamic instruction system needs to obtain images of continuous frames, such as somatosensory action recognition.

3.2. Calibration Technology of Augmented Reality. When the virtual object is registered in the real scene, it needs to maintain an accurate alignment relationship with the real scene in real time. Therefore, it is necessary to calibrate the camera. Camera calibration is the process of solving camera internal parameters, external parameters, and distortion parameters. Camera internal parameters include camera focal length (f_x, f_y), principal point coordinates (c_x, c_y), and distortion factor λ. External parameter matrix includes rotation matrix R and translation vector T, and distortion parameters include $[k_1, k_2, p_1, p_1]$, as shown in Table 1 [14, 15].

3.2.1. Coordinate System and Camera Model. In augmented reality system, four coordinate systems are involved, which are world coordinate system, pixel coordinate system, camera coordinate system, and image coordinate system. The objects in the real scene are transformed from the world coordinate system to the camera coordinate system in the form of optical signals and finally presented to the pixel coordinate system. The relationship between the three coordinate systems is shown in Figure 2.

The scene entering the camera in the real scene can be described as the conversion relationship between the world coordinate system and the camera coordinate system. In order to determine the location of the camera in the real scene and describe the attitude and orientation of objects in space, it is necessary to set a coordinate system in space. Cameras and space objects are different. Space object determination is based on the direction of an absolute coordinate system and three axes relative to the inertial system, but the camera is more complex because the camera needs to determine the position and the direction of the line of sight. The conversion relationship between camera coordinate system and world coordinate system is shown in

$$\begin{bmatrix} x_c \\ y_c \\ z_c \end{bmatrix} = R \begin{bmatrix} x_w \\ y_w \\ z_w \end{bmatrix} + T. \tag{1}$$

The projection relationship formula between the image coordinate system and the camera coordinate system is shown in

$$Z_c \begin{bmatrix} x \\ y \\ 1 \end{bmatrix} = \begin{bmatrix} f\,0\,0\,0 \\ 0\,f\,0\,0 \\ 0\,0\,1\,0 \end{bmatrix} \begin{bmatrix} X_c \\ Y_c \\ Z_c \\ 1 \end{bmatrix}. \tag{2}$$

After the camera obtains the image data in the real scene, it needs to present the image on the display terminal to form a digital image. Let the physical size of the unit pixel be Δx and Δy in the x-axis direction and y-axis direction, respectively, and the conversion formula from pixel coordinate system to image coordinate system is shown

Table 1: Camera parameters.

Parameter	Parameter formula	Number of parameters
Internal parameters	$K = \begin{bmatrix} f_x\,\lambda\,u \\ 0\,f_y\,v \\ 0\,0\,1 \end{bmatrix}$	6
External parameters	$R = \begin{bmatrix} r_1\,r_2\,r_3 \\ r_4\,r_5\,r_6 \\ r_7\,r_8\,r_9 \end{bmatrix}\ T = \begin{bmatrix} t_1 \\ t_2 \\ t_3 \end{bmatrix}$	7
Distortion parameters	$[K_1, K_2, P_1, P_2]$	3

$$u = \frac{x}{\Delta x} + u_0, \tag{3}$$

$$v = \frac{x}{\Delta y} + v_0. \tag{4}$$

The relationship between pixel coordinate system and image coordinate system is shown in Figure 3.

3.2.2. Camera Calibration. The calculation process is as follows: firstly, a homography matrix H can be calculated for each calibration board image collected by the camera, in which the parameter λ is constant and not 0, and the parameters $r1$ and $r2$ are two unit vectors of the image plane in the world coordinate system, which are orthogonal to each other, in which the parameter k is the internal parameter matrix of the camera, and the relationship is shown in

$$H = [h_1\,h_2\,h_3] = \lambda K[r_1\,r_2\,t]. \tag{5}$$

The parameter matrix K in the camera can be written in the form of

$$h_1^T K^{-T} K^{-1} h_2 = 0, \tag{6}$$

$$h_1^T K^{-T} K^{-1} h_2 = h_2^T K^{-T} K^{-1} h_2. \tag{7}$$

Set:

$$A = K^{-T} K^{-1}. \tag{8}$$

Write the matrix as shown in

$$A = K^{-T} K^{-1} = \begin{bmatrix} A_{11} & A_{12} & A_{13} \\ A_{21} & A_{22} & A_{23} \\ A_{31} & A_{32} & A_{33} \end{bmatrix}. \tag{9}$$

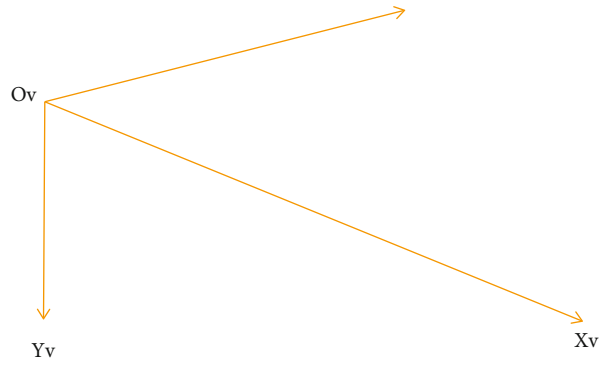

Figure 2: Relationship between three coordinate systems.

Formula (10) can be obtained by solving the formula.

$$A = \begin{bmatrix} \frac{1}{f_x^2} & 0 & \frac{-u}{f_x^2} \\ 0 & \frac{1}{f_x^2} & \frac{-v}{f_x^2} \\ \frac{-u}{f_x^2} & \frac{-v}{f_x^2} & \frac{u^2}{f_x^2} + \frac{v^2}{f_x^2} + 1 \end{bmatrix}. \tag{10}$$

Finally, the internal parameters of the camera are obtained, as shown in the formula below.

$$f_x = \sqrt{\frac{\lambda}{A_{11}}}, \tag{11}$$

$$f_y = \sqrt{\frac{\lambda}{A_{11}\left(A_{11}A_{22} - A_{12}^2\right)}}, \tag{12}$$

$$u = \frac{-A_{13}f_x^2}{\lambda}, \tag{13}$$

$$v = \frac{\left(A_{12}A_{13} - A_{11}A_{23}\right)}{\left(A_{11}A_{22} - A_{12}^2\right)}, \tag{14}$$

$$\lambda = \frac{A_{33} - \left[A_{13}^2 + v\left(A_{12}A_{13} - A_{11}A_{23}\right)\right]}{A_{11}}. \tag{15}$$

The parameters of the camera rotation matrix are expressed in vector form:

$$R = [r_1, r_2, r_3]. \tag{16}$$

According to the homography matrix H described in formula (5), the translation matrix T and rotation matrix R of the external parameters of the camera can be calculated, as shown in the formula:

$$r_1 = \lambda K^{-1}h_1, \tag{17}$$

$$r_2 = \lambda K^{-1}h_2, \tag{18}$$

$$r_3 = r_1 \times r_2, \tag{19}$$

$$T = \lambda K^{-1}h_3. \tag{20}$$

3.2.3. Real-Time Filtering Processing of Depth Image. In some cases, due to the strong reflected light on the surface of the irradiated object, the depth camera is overexposed, and the chip inside the camera cannot calculate the phase deviation, resulting in cavity noise [16, 17]. In order to remove the noise of hole and pixel jitter in depth image and ensure the quality of gesture image and real-time recognition efficiency, this study improves the traditional filtering algorithm and proposes a twice filtering algorithm to remove the noise in depth image. Image sensor CCD and CMOS introduce image acquisition due to the sensor material properties, working environment, electronic components, and circuit structure. After the weighted window filtering process, the division by zero mean filtering process is used. The distribution diagram of the original depth image and the pixel gray value processed by the twice filtering algorithm is shown in Figures 4(a) and 4(b). Figure 4(a) is the pixel gray value distribution diagram of the original image, and Figure 4(b) is the pixel gray value distribution diagram processed by the algorithm [4, 18].

Compared with the gray distribution map of the original image, the pixels near the zero value of the pixel distribution map after twice filtering are significantly reduced, which reduces the cavity noise of the image, and the peak value of the nonzero value pixels of the original image and the image after twice filtering is close to each other, maintaining the detailed characteristics of the image.

4. Design of English Audio-Visual and Oral Mobile Teaching System Based on Virtual Augmented Reality Technology

In the teaching objectives of English, special emphasis is placed on audio-visual ability, and the teaching goal of English audio-visual is to cultivate students' practical language ability, so that students can effectively conduct English audio-visual communication in future work and communication, so that work or communication can be successfully completed to meet the needs of economic development and international exchanges, to be able to understand English lectures, daily English conversations, and lectures on general topics and basically understand slow English programs in English-speaking countries, with a speaking rate of about 130 words per minute and be able to grasp the main idea and grasp the main points, can use basic listening skills to aid comprehension, be able to communicate in English during the learning process and be able to discuss a topic, have the ability to converse with people from English-speaking countries on everyday topics, be able to make brief speeches on familiar topics after preparation, with relatively clear expression and basically correct pronunciation and intonation, and be able to use basic conversational strategies in conversation. The ancients said: "If you want to do well, you must first sharpen your tools." Augmented reality requires development platforms and tools as "sharp tools"

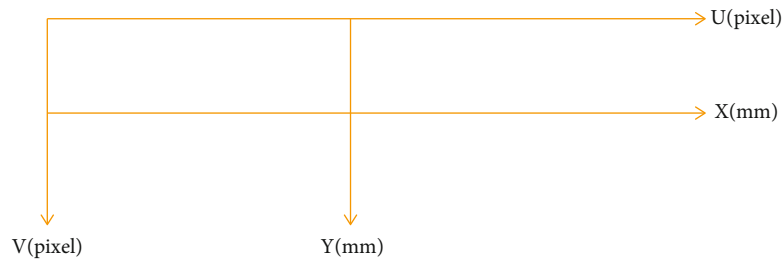

Figure 3: Pixel coordinate system and image coordinate system.

for research and development, so that software can be transformed from design blueprints into entities. In order to reduce the complexity and difficulty of augmented reality application development, many optimizations have been made for augmented reality development platforms, design platforms, and interactive platforms and have successively provided basic toolkits for designing and developing augmented reality, such as Unity 3D and Qualcomm SDK, Android SDK, 3D modeling software, and audio and video processing software. These tools include the most basic functions involved in augmented reality design and development, providing stable and convenient technical support for research and development. The core of augmented reality is to construct a "real" scene composed of virtual scenes on real objects and to achieve interaction.

4.1. Introduction to Relevant Technologies

4.1.1. Unity3D. Unity3D is an augmented reality design engine developed by Unity Technologies with interactive graphics as the development environment. It provides the creation and rendering of scene models, supports the import of Vuforia SDK extension toolkit and tracking and detection under its corresponding interface, and realizes the AR application of virtual reality superposition and human-computer interaction. Unity3D can import 3D models in FBX obj format into the scene and environment and can add physical materials such as fog effect, wind, rain, ground, sky, sunlight and water, environmental sound effect, and video animation to the virtual scene. At the same time, it supports real-time browsing, testing, and editing of 3D application scenes [19, 20]. It is a cross platform development tool, which can release products directly to the required platforms, such as Android, IOS, and Windows.

4.1.2. Vuforia SDK. Vuforia augmented reality SDK is a software development kit launched by Qualcomm for augmented reality applications for mobile devices. It uses computer vision technology to identify and capture planar images or simple three-dimensional objects in real time, allowing developers to place virtual objects through the camera viewfinder and adjust the position of objects on the solid background in front of the lens [21, 22]. The data flow of Vuforia SDK includes four modules:

(1) Input conversion module. The camera obtains the image of each frame of the current real scene and converts it to the converted image format through the image converter

(2) Database module. Refers to the form of data storage, including local device databases and cloud databases

(3) Tracking detection module. It mainly realizes target tracking, which is composed of track Er, user defined targets, and word targets

(4) Rendering input module. Including video background renderer and application code

These four modules are closely combined to transmit data and feedback problems to each other, which makes the Vuforia SDK play a good adaptation role in Unity3D. Combined with the powerful engine function of Unity3D, developers can develop excellent augmented reality interactive applications through simple design.

4.2. Overall Design of VBook

4.2.1. Design Objectives. In "College English audio-visual speaking," there will be three models (scene dialogue) in the speaking out part of each unit, each model corresponds to an illustration, and each illustration corresponds to a scene dialogue video [23]. The goal of vbook design is to scan the pictures in teaching materials through mobile devices, track them in real time, and match them with the identification pictures of cloud database. If the matching is successful, the video corresponding to the illustration will be seamlessly superimposed on the illustration of the teaching material, and the video playback, pause, full screen display, and other functions will be realized through the script code, so that users can experience augmented reality interaction and meet the characteristics of software ease of use.

4.2.2. Design Idea. Traditional augmented reality technology uses ARToolKit tool or 3D registration technology based on tracker and vision to realize marker recognition and virtual real superposition. The disadvantage is that the recognition degree is low and limited to the recognition of pure black or pure white two-dimensional images. The development of tools based on Unity3D and Vuforia SDK makes augmented reality technology have a broader application stage. Its markers adopt the method of feature point detection, which can recognize not only two-dimensional color images but also three-dimensional models, with strong real-time tracking effect. The illustrations of English audio-visual

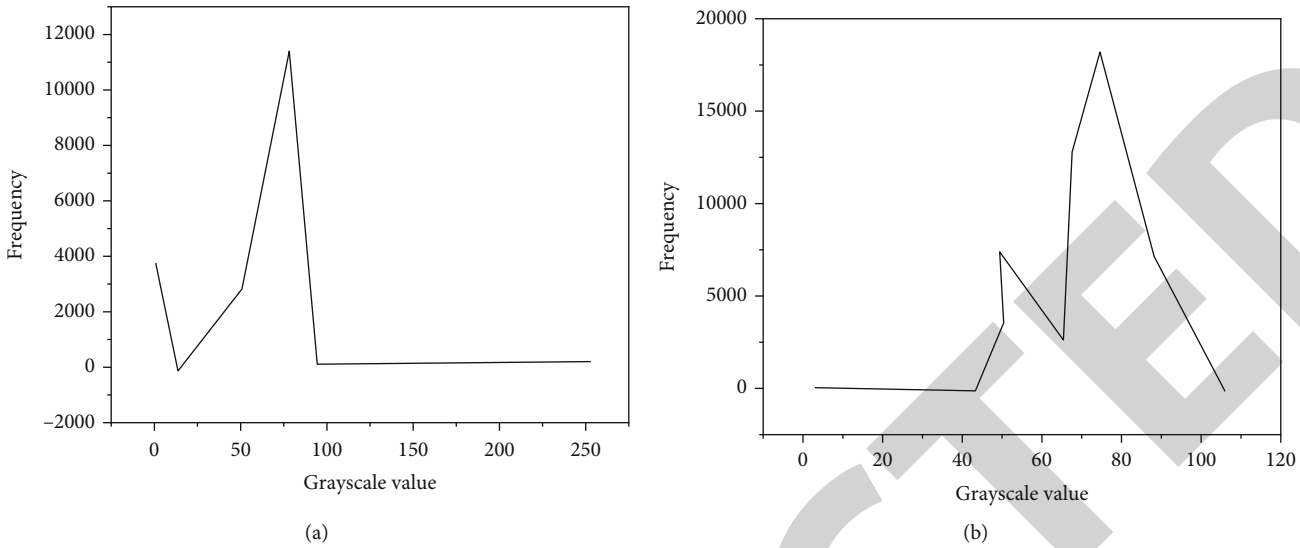

Figure 4: (a) Pixel gray value distribution: original image. (b) Distribution of pixel gray value: image after twice filtering.

and oral teaching materials are mainly color images, which are suitable for development with the Unity3D integrated Vuforia SDK toolkit, and the Unity3D engine can automatically generate terminal applications suitable for mobile devices, which is convenient for users.

4.2.3. Technical Scheme. The overall technical development route of the application is shown in Figure 5. Preliminary setting: including the whole application development process and the setting of docking points between software and hardware.

3D construction: from the perspective of role and model, it is divided into two parts. Maya is now the mainstream 3D animation software. The field of 3D visual art creation outside China is generally in Maya. Due to the huge Maya software system, comprehensive functions, and free combination of tools, Maya software can be applied to various 3D animation production processes. This time, Maya software is selected not only because of its convenience and strength but also because of its convenient connection between motionbuilder and motion capture software.

Motion capture: this part consists of two parts: limb motion capture and expression capture. Ipistudio and faceshift software and Microsoft Kinect somatosensory device are used to form two systems.

VR/AR: Unity3D is a game development tool developed by unity technologies. It is a professional game engine integrated across platforms. IPhone 8, MAC, WebGL, etc. can be released to Windows platform. This research also makes use of Unity3D's cross platform output and good creative interface. This part of Vuforia is an extension of Unity3D and serves as an important software toolkit for AR development (Vuforia augmented reality SDK). Upload the image that needs to be used as an identification image to Qualcomm's server, and then, turn the image into a black-and-white image; strengthen and extract image feature points; load feature points into package; Unity3D decompresses the package identification package and matches it in the program. When the program runs, it will continuously compare the feature point data package with the camera view content and search the spatial position of the identification map in real time. It uses graphics recognition technology to detect and track images in real time, reverse the motion trajectory of the camera through the processor, and then, perfectly superimpose the developer's virtual object on the real scene picture to realize AR effect output.

4.3. Detailed Design. Detail design: the focus of this part is to break through the nonstandard part of some technical applications. It needs to make some special customization or significantly improve the efficiency through design skills.

(1) Adjust Kinect dual position to record action information, and select the two opposite directions to obtain the best acquisition effect

(2) Change the proofreading apparatus to make the motion capture data more accurate. Replace the square proofreading board in IPI studio with a cross wooden frame, which improves the alignment efficiency of the two Kinect devices in the proofreading process and quickly generates the camera position relationship file

(3) Use the identification mechanism of Vuforia extension to make an appropriate identification diagram to improve the identification efficiency

(i) The color block with similar lightness should be avoided in the recognition map; otherwise, when it becomes a black-and-white map, only the lightness relationship is left, and the shape characteristics of the picture are not obvious. For seemingly complex pictures, it is difficult to generate recognition points because of the similar lightness. The Hough transformation is a way to connect the edge pixels by using the global characteristics of the images. The basic idea is the duality of the point-line

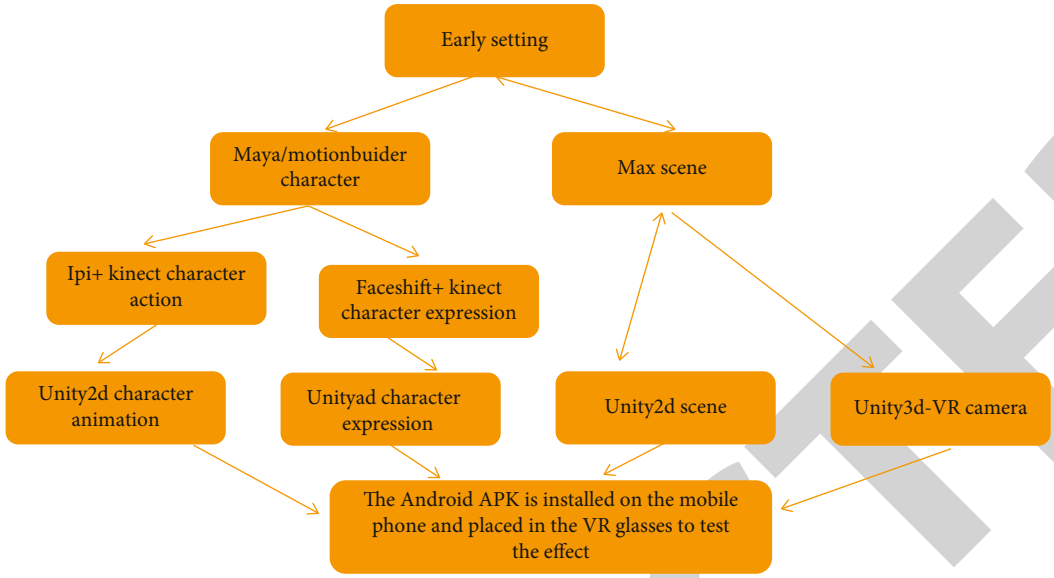

Figure 5: Application development technical scheme.

(ii) The dividing line between color blocks is an important indicator of recognition efficiency. The design of color colliding picture can still keep a clear dividing line in the recognition picture after gray processing. These boundaries of strong contrast between color and lightness are an important position for program automatic recognition of information in computer graphics and imaging

(iii) The uneven distribution of recognition information on the way may also lead to very low recognition rate. For example, the image boundaries appear at one end or in a small range of the recognition map

(iv) If the three-dimensional object to be displayed by fusion is not placed in the middle of the recognition map, the error of limit optical and computing power will be maximized. Therefore, the virtual object needs to be in the central area of the recognition map as far as possible; compared with electronic computing, it has the advantages of high speed, high broadband, and low power consumption. Otherwise, the imaging result will have imperfect vibration

4.4. System Functions

4.4.1. Functional Structure. The overall goal of web-based virtual teaching system is to provide students with a good online learning platform by providing online video, online browsing teaching courseware, online real-time interaction between teachers and students, online experiment, and downloading all kinds of teaching resources. The overall function of the virtual teaching system is shown in Figure 6.

The web-based virtual teaching system mainly includes two parts: virtual course platform and online experiment subsystem. The virtual course platform mainly includes personnel management, virtual classroom, online video playback, online message, in station email, electronic whiteboard, and teaching resource display functions. The goal of the virtual course platform is to provide students with a good online learning platform. The online experiment subsystem mainly includes online experiment, experiment management, and virtual teaching scene module.

4.4.2. Use Case Analysis. This paper abstractly analyzes the system from the perspective of entity objects and object behavior involved in web-based virtual teaching system and obtains the use case diagram of web-based virtual teaching system, as shown in Figure 7.

Virtual teaching system includes three types of users: administrators, teachers, and students. Administrator users are automatically established after system initialization, and teachers and student users need to be established through system registration. The user registration case description is shown in Table 2.

After the teacher users register and improve their personal information through the user registration module, the administrator needs to review the teacher information before entering the teacher platform of the virtual teaching system. The use case description of teacher audit is shown in Table 3.

When teachers need to open an online course, they can apply for an open course through the application course module. The use case description of teachers applying for courses is shown in Table 4.

After the teacher's application for the course is completed, the course becomes to be approved. The teacher can open the corresponding course only after it is approved by the administrator. The use case description of the audit course is shown in Table 5.

After entering the online experiment module, students can program the experimental items provided by teachers online, save the experimental status, and download the experimental items. The online experiment case description is shown in Table 6.

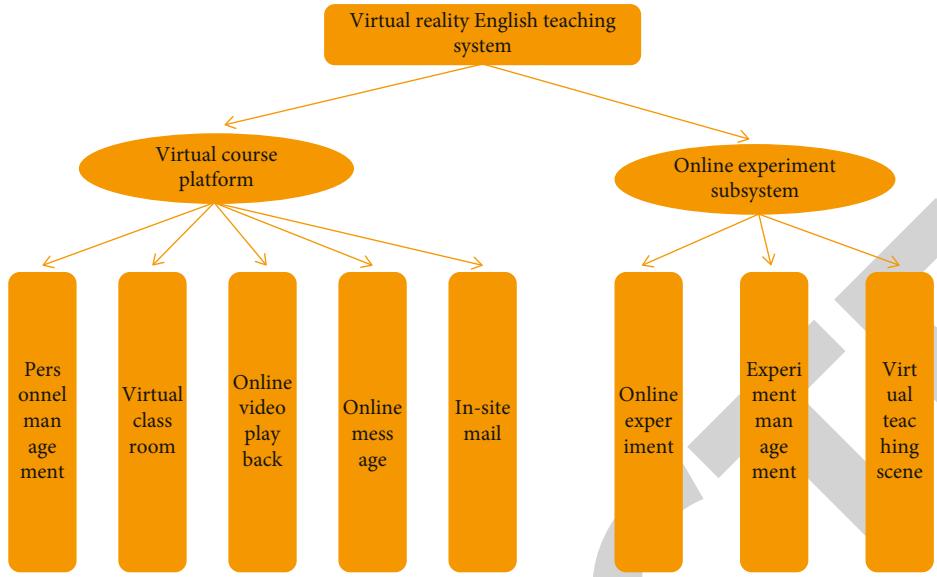

Figure 6: Overall functional structure of the system.

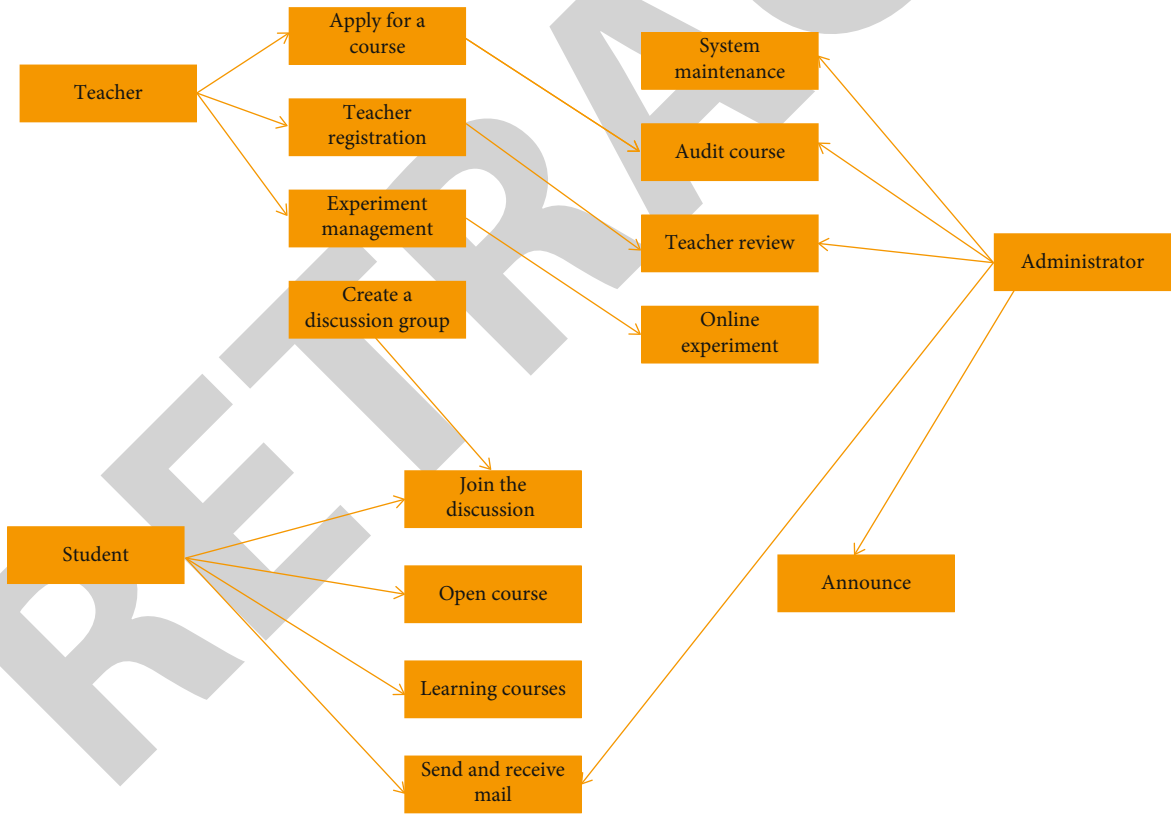

Figure 7: Use case diagram of web virtual teaching system.

According to the design objectives and requirements, based on the design principles of simplicity, efficiency, and convenience for users, the design of VBook is divided into three core modules.

(1) Image preprocessing and storage. Cut the captured textbook illustrations to the same size and name them according to certain rules, preprocess them with Vuforia SDK tool, process the pictures into recognizable pictures, and save them to the cloud

(2) Video preprocessing and storage. Obtain the video data from the CD, name it according to the corresponding picture name, and then, save it to the local server

Table 2: User registration case description.

Use case name	User registration
Range	User registration module usage
Level	User purpose
Major participants	Students and teachers
	Focus
Relevant personnel and concerns	Teachers want users to enter the registration information correctly
	Students want users to enter their registration information correctly
Preconditions	Log in to the user registration system correctly

Table 3: Description of teacher audit cases.

Use case name	Administrator audit teacher
Range	Application of teacher audit module
Level	User purpose
Major participants	Administrators
	Focus
Relevant personnel and concerns	Hope can get the login permission correctly.
	It is hoped that the relevant data of all approved teachers will be correctly stored in the database
Preconditions	The user has registered a user as a teacher, and the teacher is waiting for approval

Table 4: Use case description of teachers applying for courses.

Use case name	Teachers apply for courses
Range	Use of teacher application course module
Level	User purpose
Major participants	Teacher
Relevant personnel and concerns	Concerns of relevant personnel
	Teachers hope to correctly submit their applied courses and apply for open courses
Preconditions	Teachers can log in to the system correctly and legally
Guarantee of success	All correct data can be saved in the database.

Table 5: Use case description of audit course.

Use case name	Audit course
Range	Use of course review module
Level	User purpose
Major participants	Administrators
Relevant personnel and concerns	Concerns of relevant personnel
	The administrator wants all the data stored in the database to pass the audit correctly
Preconditions	The teacher has passed the identity authentication and applied for the course. The course is waiting for approval
Guarantee of success	Teachers can correctly apply for corresponding courses, the approved courses can be viewed by students, and teachers cannot modify the approved courses. All correct data can be saved in the database.

(3) Data matching and processing. Including AR design and user use. Among them, the rectangular box part of the dotted line is AR design, and the data matching of the user's use process is outside the dotted line box: the user scans the illustration, matches the identification diagram saved in the cloud, uses the script code to access and obtain the corresponding video, and displays the video to the user

The system design is based on Unity3D development tool and Vuforia SDK augmented reality software development kit. Designed with the MVC framework of Unity3D,

Table 6: Online experiment case description.

Use case name	Online experiment
Range	Use of online experiment module
Level	User purpose
Major participants	Student
Relevant personnel and concerns	Concerns of relevant personnel Students hope to experiment through the online experiment function
Preconditions	Students pass identity authentication and enter the online experiment function
Guarantee of success	Teachers have successfully opened online experiments and set experimental data

model M includes access to components, data files, renderers, cameras, and other objects; view v presents the model and manages the engine rendering of Unity3D; controller C receives user input and invokes the event method of the model object. It mainly realizes data matching and AR scene design.

(1) Identification map creation and feature point recognition

(i) Identification diagram creation. Select the illustrations in the textbook for shooting, cut the pictures and name them regularly, use Vuforia SDK to process and generate the identification map, build the identification map database and save it to the cloud, and generate two secret keys for accessing cloud data: access key and secret key. When the user uses the camera scan of the mobile device, he accesses the cloud database through the secret key

(ii) Feature point recognition. The recognition image generated after the processing of the original image is a gray image, which is matched by feature points. Vuforia provides the star rating standard of matching degree. The more the number of stars, the higher the success rate of scanning matching and the shorter the scanning recognition time. Therefore, when preprocessing the image, try to make the image star reach a higher star level as much as possible

(2) Unity3D scene construction

Download Vuforia SDK toolkit vuforia-unity.unitypack and integrate it into Unity3D. Create a new Unity3D project scene and add arcamera, ImageTarget, and video objects of Vuforia SDK to the scene, respectively. The bottom ImageTarget object is the recognition map carrier, which is used to match the picture obtained by arcamera with the recognition map. When the matching is successful, the upper video object will be displayed. The video object is the video carrier and displayed in the form of customized virtual play button picture. The video playback can be controlled through the button.

In the actual design, the video object is overlaid on the ImageTarget object as a subobject of ImageTarget, so that the video can be displayed with illustrations all the time.

(3) Video preprocessing and storage

Copy out all the scene dialogue videos in the CD-ROM given by the textbook and name them according to the corresponding illustration name, and then, upload the named video files to the locally accessible server to ensure that any mobile terminal can access these video materials, but the visiting user cannot change the video materials to ensure the integrity and consistency of the data.

(4) Script for video playback

The function of video object controlling video playback is realized by writing script code. The Vuforia SDK provides the TargetFinder class to judge whether the pictures obtained by arcamera match the database data of identification pictures. The picture information after successful matching is saved to Target-Finder. TargetSearchResult.

First, get the video path according to the picture name:

Video. m_path = "Video storage server URL directory path" +target SearchResult. Target Name + ". 3g2"; the core code of the script to realize video loading, playback, pause, and full screen functions is as follows:

(i) Video loading and playback

Video. Video Player. Load (video. m _ path, video. MediaType, false, 0); video. Video Player. Play(true, 0);

(ii) Video pause

If (video. Current State = = Video Player Helper. MediaState.PLAYING){video. Video Player. Pause(); }

(iii) Video full screen

Play Fullscreen Video At End Of Frame (Video Playback Behaviourvideo)

(5) Implementation and release of mobile applications

Unity3D can directly publish applications to different platforms. Here, select Android platform to generate VBook.apk installation package file, and send this installation

package file to Android mobile phone to install and run directly.

5. Conclusion

The English audio-visual and oral mobile teaching system can realize the connection between the real classroom and the online classroom, expand the complete large-scale learning mode to the fragmented learning mode, stimulate students' enthusiasm for audio-visual learning, and greatly improve the learning efficiency. The mobile teaching mode of English audio-visual can significantly improve the teaching of English audio-visual. Augmented reality technology, as an extension of virtual reality technology, has brought unprecedented visual experience to people, making people sigh the infinite charm of modern technology. As a fast-developing new form of software, it is constantly infiltrating into the field of learning, gradually promoting the development of the field of learning and research. Experience and restore the reality of knowledge by building a ubiquitous learning space that seamlessly integrates virtual space and physical space and further meets the needs of knowledge seekers for interactivity, immediacy, and personalization. This article relies on Unity3D's powerful rendering engine and visual operation interface, coupled with Vuforia toolkit and its powerful augmented reality effect; developers can get started in a very short time. VBook mainly uses augmented reality technology to vividly present the learning video in front of users, so that users can feel the interactive experience different from traditional learning methods, that is, it solves the problem of students' difficulty in obtaining textbook video and also stimulates students' interest in learning. Of course, the application of augmented reality is not only that but also a considerable number of places need to be used. In the future, we will further study augmented reality technology, and augmented reality will be popularized in China.

Data Availability

The data used to support the findings of this study are available from the corresponding author upon request.

Conflicts of Interest

The authors declare that there are no conflicts of interest regarding the publication of this paper.

References

[1] C. Duan, "Design of online volleyball remote teaching system based on AR technology," *Alexandria Engineering Journal*, vol. 60, no. 5, pp. 4299–4306, 2021.

[2] P. H. Lin and S. Y. Chen, "Design and evaluation of a deep learning recommendation based augmented reality system for teaching programming and computational thinking," *Access*, vol. 8, pp. 45689–45699, 2020.

[3] X. Wu, "Research on English online education platform based on genetic algorithm and blockchain technology," *Wireless Communications and Mobile Computing*, vol. 2020, Article ID 8827084, 7 pages, 2020.

[4] R. Dutta, A. Mantri, and G. Singh, "Evaluating system usability of mobile augmented reality application for teaching Karnaugh-maps," *Smart Learning Environments*, vol. 9, no. 1, pp. 1–27, 2022.

[5] Y. Y. Dyulicheva, "The use of augmented reality technology to improve the efficiency of teaching," *Informatics in School*, vol. 3, pp. 37–46, 2020.

[6] C. S. Chan, J. Bogdanovic, and V. Kalivarapu, "Applying immersive virtual reality for remote teaching architectural history," *Education and Information Technologies*, vol. 27, no. 3, pp. 4365–4397, 2022.

[7] X. Shan, "Research on content design of media facade and augmented reality for preschool education," *Region - Educational Research and Reviews*, vol. 3, no. 1, pp. 41–46, 2021.

[8] J. Jang, Y. Ko, W. S. Shin, and I. Han, "Augmented reality and virtual reality for learning: an examination using an extended technology acceptance model," *Access*, vol. 9, pp. 6798–6809, 2021.

[9] M. Romano, P. Díaz, and I. Aedo, "Empowering teachers to create augmented reality experiences: the effects on the educational experience," *Interactive Learning Environments*, vol. 6, pp. 1–18, 2020.

[10] A. F. Batista, M. Thiry, R. Q. Gonalves, and A. Fernandes, "Using technologies as virtual environments for computer teaching: a systematic review," *Informatics in Education*, vol. 19, no. 2, pp. 201–221, 2020.

[11] J. Li, T. Luo, and J. Lu, "Research on inquiry teaching method supported by virtual reality technology," *Creative Education Studies*, vol. 9, no. 1, pp. 247–253, 2021.

[12] J. Duan and R. Gao, "Research on college English teaching based on data mining technology," *EURASIP Journal on Wireless Communications and Networking*, vol. 2021, Article ID 192, 2021.

[13] P. Wang and S. Qiao, "Emerging applications of blockchain technology on a virtual platform for English teaching and learning," *Wireless Communications and Mobile Computing*, vol. 2020, Article ID 6623466, 10 pages, 2020.

[14] Z. Xu, M. M. Kamruzzaman, and J. Shi, "Method of generating face image based on text description of generating adversarial network," *Journal of Electronic Imaging*, vol. 31, no. 5, 2022.

[15] R. Xie, "Intangible cultural heritage high-definition digital mobile display technology based on VR virtual visualization," *Mobile Information Systems*, vol. 2021, Article ID 4034729, 11 pages, 2021.

[16] P. F. Torres, A. F. P. Costa, V. L. C. Junior et al., "A mobile educational tool designed for teaching and dissemination of grid connected photovoltaic systems," *Computers and Electrical Engineering*, vol. 76, pp. 168–182, 2019.

[17] K. Sharma and B. K. Chaurasia, "Trust based location finding mechanism in VANET using DST," in *Fifth International Conference on Communication Systems & Network Technologies*, pp. 763–766, IEEE, Gwalior, India, 2015.

[18] T. Jiang, "Digital media application technology of mobile terminals based on edge computing and virtual reality," *Mobile Information Systems*, vol. 2021, Article ID 3940693, 10 pages, 2021.

[19] S. Ghareeb, A. J. Hussain, D. Al-Jumeily et al., "Evaluating student levelling based on machine learning model's performance," *Discover Internet of Things*, vol. 2, no. 1, 2022.

Hindawi
Wireless Communications and Mobile Computing
Volume 2023, Article ID 9867804, 1 page
https://doi.org/10.1155/2023/9867804

Retraction

Retracted: Design and Implementation of Online Japanese Examination System Based on Genetic Algorithm

Wireless Communications and Mobile Computing

Received 17 October 2023; Accepted 17 October 2023; Published 18 October 2023

This article has been retracted by Hindawi following an investigation undertaken by the publisher [1]. This investigation has uncovered evidence of one or more of the following indicators of systematic manipulation of the publication process:

(1) Discrepancies in scope
(2) Discrepancies in the description of the research reported
(3) Discrepancies between the availability of data and the research described
(4) Inappropriate citations
(5) Incoherent, meaningless and/or irrelevant content included in the article
(6) Peer-review manipulation

The presence of these indicators undermines our confidence in the integrity of the article's content and we cannot, therefore, vouch for its reliability. Please note that this notice is intended solely to alert readers that the content of this article is unreliable. We have not investigated whether authors were aware of or involved in the systematic manipulation of the publication process.

Wiley and Hindawi regrets that the usual quality checks did not identify these issues before publication and have since put additional measures in place to safeguard research integrity.

We wish to credit our own Research Integrity and Research Publishing teams and anonymous and named external researchers and research integrity experts for contributing to this investigation.

The corresponding author, as the representative of all authors, has been given the opportunity to register their agreement or disagreement to this retraction. We have kept a record of any response received.

References

[1] Z. Dengqing and Y. Zhangwei, "Design and Implementation of Online Japanese Examination System Based on Genetic Algorithm," *Wireless Communications and Mobile Computing*, vol. 2022, Article ID 3678607, 11 pages, 2022.

Hindawi
Wireless Communications and Mobile Computing
Volume 2022, Article ID 3678607, 11 pages
https://doi.org/10.1155/2022/3678607

Research Article

Design and Implementation of Online Japanese Examination System Based on Genetic Algorithm

Zeng Dengqing[1] **and Yang Zhangwei**[2]

[1]*School of Foreign Languages, Ping Xiang University, Ping Xiang 337055, China*
[2]*Center for Network and Technology Education, Ping Xiang University, Ping Xiang 337055, China*

Correspondence should be addressed to Yang Zhangwei; yzw@pxu.edu.cn

Received 1 June 2022; Revised 1 September 2022; Accepted 16 September 2022; Published 26 November 2022

Academic Editor: Jun Ye

In order to solve the problem of online inspection of students' theoretical knowledge of Japanese, this paper further optimizes and adjusts the design of the online Japanese examination system and presents an online Japanese examination system based on genetic algorithm. Taking the Japanese test as the research object, on the basis of comprehensively analyzing the problems of slow test paper composition, low success rate, and low quality of traditional online test systems, an intelligent test composition model based on genetic algorithm is proposed, and the implementation process of genetic algorithm and the key steps are described in detail. The results show that the online Japanese examination system based on genetic algorithm can meet the needs of test paper generation in more complex situations. After a long time of operation and continuous improvement, the online Japanese examination system has obtained the adaptability of the best solution. The value of the fitness is 99.666667; when the fitness is at this value, the error of the question type score of the test paper is 0, the average difficulty error on the test paper is 0, and the error of the section test point distribution is 0.666667. This fully illustrates the stability and effectiveness of the Japanese online examination system, which can meet the needs of daily Japanese majors and improve the efficiency of Japanese teaching.

1. Introduction

Since the beginning of the new century, with the rapid development of science and technology, computer network technology has been gradually applied to all walks of life. At the same time, the continuous progress of computer network technology has brought many conveniences to many fields and provided technical support for the development of education industry. For example, a large number of computers are used in the classroom and laboratory to deal with various tasks in the teaching process, which is more convenient, fast, and safe. Among them, we can use the intelligent computing advantages of genetic algorithms to develop and improve the online examination system. Based on the advantages and principles of genetic algorithm, this paper analyzes the advantages and disadvantages of online examination system. At the same time, taking the Japanese examination as the research object, based on the comprehensive analysis of the problems of slow speed, low success rate, and low quality of the traditional online examination system, an intelligent paper generation model based on genetic algorithm is constructed to further improve and optimize the Japanese online examination system. Through an efficient and stable Japanese online examination system, we can effectively detect the problems existing in students' daily Japanese learning, improve the quality of Japanese teaching, and stimulate students' enthusiasm and initiative.

2. Related Works

Liu and others said that China started late in the research of online examination system. In 1998, China began to rise the online education platform and introduced the online examination system into the online education platform. The introduction of the online examination system improved the efficiency of examination management, reduced the

work pressure of teaching staff, and solved the difficult problem of examinee's remote examination [1]. Sugisawa and others said that soon, major universities in China have successively developed online examination systems, among which the development of Shanghai Jiaotong University and Beijing University of Posts and telecommunications is more prominent [2]. Alaqbi and others said that after the twenty-first century, China's science and technology has entered an era of rapid development [3]. In addition to colleges and universities, social training institutions have gradually introduced online examination systems, such as computer grade examination and driving school examination involving a wide range of people. Clivaz and others said that with the progress of China's science and technology, China's online examination system technology has also made progress and effectively develop various online examination software to make the online examination system more comprehensive [4]. In recent years, Chinese experts have invested a lot of energy in the research of automatic online examination system and have also made breakthroughs in this field and achieved fruitful results. The Dragon Online Examination System developed in recent years has a more complete functional system and can also be optimized for various test questions, ensuring that various operating interfaces are more convenient during the optimization process.

Mizuma and others say that the first test developed algorithm in online testing was book test generation. Test paper generation is very inefficient, which makes it more efficient for teaching staff [5]. In addition, the quality of the papers varies, largely depending on the competence of the examiners. To address these issues, automated tests can be performed. Makino and others stated that these tests are not automatically computerized to select the required questions from the education test questions to conduct the test. The accuracy and quality of testing remains difficult to maintain. Therefore, experts have introduced technical testing on this basis, and the main research is the study of nontechnical testing concepts automatic [6]. Lie and others stated that "intelligent test paper generation" has become the core technology of the online test system. For example, by adding complex intelligent algorithms to the automatic online examination system, the efficiency of online examination paper generation has been significantly improved [7]. Tian, Z and others said that the online examination system developed in recent years has become more and more complete, with a convenient and fast test paper generation function [8]. Acosta and others said that the system is mainly applicable to enterprise level examination, has perfect functions and advantages, and can fundamentally solve users' problems from reality [9]. For example, the operation steps are scientific and convenient, the test paper is convenient and fast, multiple people are supported online, and the confidentiality of the answer process is guaranteed. However, it has not developed more basic functions in the research of examination system technology, mainly expanding, reforming, and perfecting the original functions.

The analysis of domestic and foreign research by Cao et al. shows that the online examination system has a high reputation and is relatively developed [10]. At present, the research of online examination system mainly focuses on the production of intelligent examination papers and the automatic scoring technology. With the technical support of genetic algorithm, intelligent technology can effectively improve the efficiency and accuracy of the online examination system, as shown in Figure 1.

3. Method

Genetic algorithms start with a potential population, which is a combination of multiple individuals with different codes. Chromosomes act as the main carrier, which determines the external shape of an individual. In the initial population, according to the principle of natural evolution, a better approximate solution is gradually generated, individuals are selected according to their fitness, and then crossover and mutation are combined to generate a new population. This process enables the new population to be better than the initial population, and the optimal individual in the latest population can be used as an approximate optimal solution to the problem. The flowchart of the genetic algorithm is shown in Figure 2.

The genetic algorithm starts from the population and evaluates the individuals in the population, instead of searching from the individual, which is conducive to the global selection, so the genetic algorithm is easier to achieve optimization; on the contrary, the traditional optimization algorithm is to search for the individual, so it is extremely easy to achieve optimization. It is very likely to fall into a local optimal solution, which is the advantage of genetic algorithm different from traditional optimization algorithm. Genetic algorithms search based on probability, rather than performing deterministic orientation, so the search is larger, and the population is generated and the individuals in the population are evaluated. The genetic algorithm will organize the search by itself according to the fitness function and select individuals with large fitness to form a new group, so it has strong organization and adaptability [11].

The initial population is composed of n individuals by using random function. The first step is to measure the number of populations. A common approach is to record the population as 50 or multiples of 50 as the default. Past research has shown that population size is directly related to the success and quality of test paper production. If the population is unreasonably determined, the problem of local optima arises [12].

Coding method is the basis of genetic algorithm. The level of coding directly determines the quality of problem-solving. Since genetic algorithm was proposed, after years of development, many different coding methods have been formed, among which the most widely used are as follows: hybrid coding, binary coding, and real coding. In particular, genetic algorithms play a great role in the fields of function optimization, production scheduling, pattern recognition, neural networks, and adaptive control.

The selection of fitness function must meet two conditions: There is no "premature" phenomenon in the early stage, and there will be no "recession" in the later stage. Only

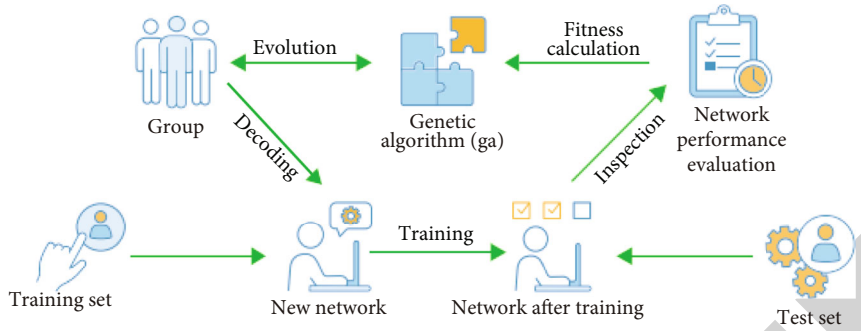

Figure 1: Design and implementation of online Japanese examination system based on genetic algorithm.

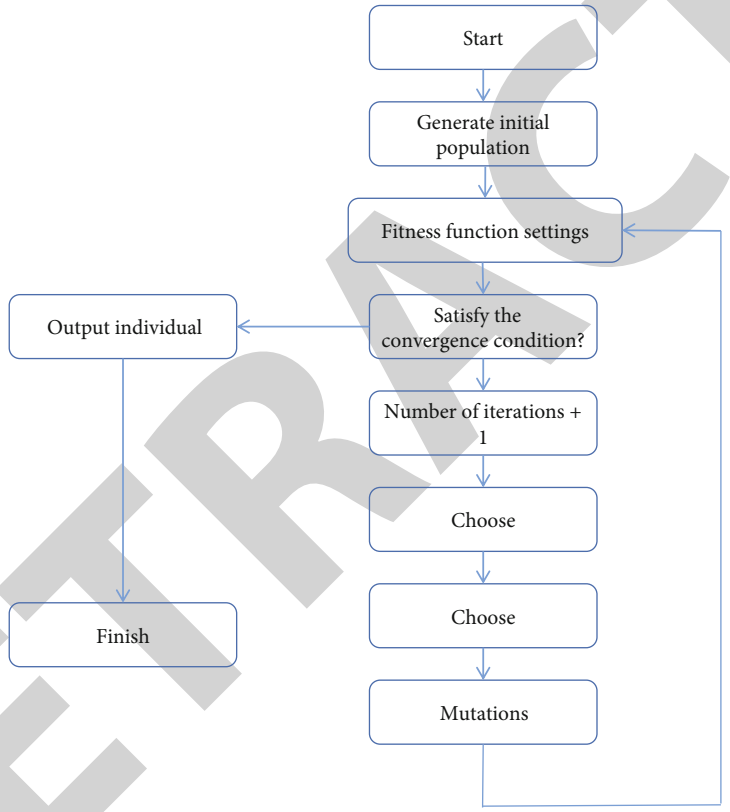

Figure 2: Flow chart of genetic algorithm.

the fitness function that meets these conditions can improve the fitness between individuals, reduce differentiation, and obtain the optimal results as a whole [13, 14]. In practice, this transformation process is relatively simple, as shown in the following formula:

$$\min f(x) = \max(-f(x)). \tag{1}$$

When the total value of the desired optimization result is positive, it shows that the desired optimization result is basically consistent with the problem of individual fitness, as shown in the following formula:

$$F(X) = f(x). \tag{2}$$

Through the adjustment of the overall fitness function, objective function and constraints, the optimization between corresponding individuals is realized to ensure that the optimal solution can be obtained at present, as shown in the following formula:

$$F(X) = \alpha f(x) + \beta. \tag{3}$$

Above, $F(X)$ is the fitness function, α is the normal number, $f(x)$ is the objective function, and β is the constant coefficient. The objective function can be scaled and translated. There are many methods to determine the coefficient,

as shown in the following formula (5):

$$\alpha = \frac{(C_{mult} - 1) f_{avg}}{f_{\max} - f_{avg}}, \tag{4}$$

$$\beta = \frac{\left(f_{\max} - C_{mult} f_{avg}\right) f_{avg}}{f_{\max} - f_{avg}}. \tag{5}$$

Or as shown in the following formula (7):

$$\alpha = \frac{f_{avg}}{f_{avg} - f_{\max}}, \tag{6}$$

$$\beta = \frac{-f_{\min} f_{avg}}{f_{avg} - f_{\min}}. \tag{7}$$

The selection operator is based on the different fitness of different individuals. The state of its chromosomes in the next stage depends on the optimization degree and limit performance of the chromosomes. Individuals with high fitness will continue to be replicated in the next stage, while those with low fitness Individuals will be eliminated directly in the next stage. Its operation strategy is to retain the best individual, prevent the emergence of local optimal solution, and adhere to the elite retention strategy. The function of selecting operators in the genetic algorithm is to avoid the destruction of the Geshan gene and to improve the computational efficiency as a whole [15]. The main selection methods of the selection operator include the wheel selection method and the random selection method. This document mainly selects the selection method of the roulette, as shown in Figure 3.

The crossover operator is mainly calculated according to specific principles and methods. In the process of random selection of the whole population, it is necessary to ensure that the chromosomes meet the requirements of relevant exchange and groups were randomly paired and selected for crossover operation, which can make the overall optimization effect the best [16].

When using a genetic algorithm, certain control parameters must first be established in order for the algorithm to achieve its intended purpose. The control parameters include crossover rate, mutation rate, and termination iteration. In order to optimize the performance, the following parameter design methods are usually selected.

The operation process of the trial method is to first arrange and combine all the main parameters, then operate the parameters obtained by these combinations, and finally compare and comprehensively analyze the results obtained by the operation, and select the optimal control list. The empirical method is based on the judgment of professional teachers or scholars and past research experience to determine the analysis value of specific parameters [3].

The above introduction shows in detail the application process and operation principle of genetic algorithm in intelligent test paper generation. It also simply points out the problems and avoidance methods of genetic algorithm in

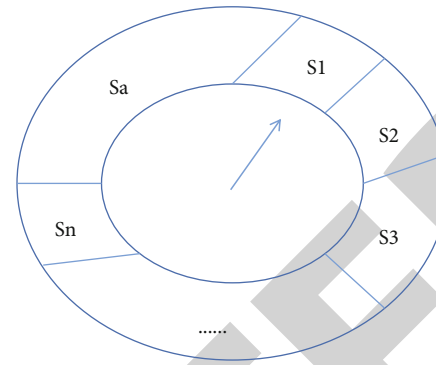

Figure 3: Schematic diagram of wheel disc selection.

each use stage. Through analysis, we can know that the basic strategy of genetic algorithm is "segment coding and survival of the fittest", and the solution process is the simulation of the survival process of the "chromosome" fittest. To improve operational efficiency and optimize results. It acts as a smart module during the special process of making the test paper. With various combinations of variants and intersections, designs can be considered in a repetitive way of thinking so that the individual situation can be played from the population, so as to ensure that the whole variation is only controlled within the mother for observation. The operation flow chart of the test paper generation system is shown in Figure 4.

In the overall operation, each participating functional module will be coded to facilitate the real-time search of constraint groups during actual operation. The design of coding should be distinguished according to different question types. Class structure design mainly designs the main module classes and the relationship between classes and uses the way of class diagram to express. According to the question types, a fixed corresponding function module can be directly established. An example of designing a partition code is shown in Table 1.

In addition to encoding a large number of individuals with question numbers, there are M questions in the whole question bank, which need to be distinguished by binary string description documents, as shown in the following formula:

$$A1A2 \cdots \mathrm{An}1B1B2 \cdots Bn2C1C2 \cdots Cn3. \tag{8}$$

If the total score of the test paper is set to *Total_Mark*, the following calculation formula can be obtained, as shown in the following formula:

$$\sum_{i=1}^{p} \partial_i = Total\_Mark, \tag{9}$$

In this formula, set the frequency of each number in the weighted average of each component. The formula is shown

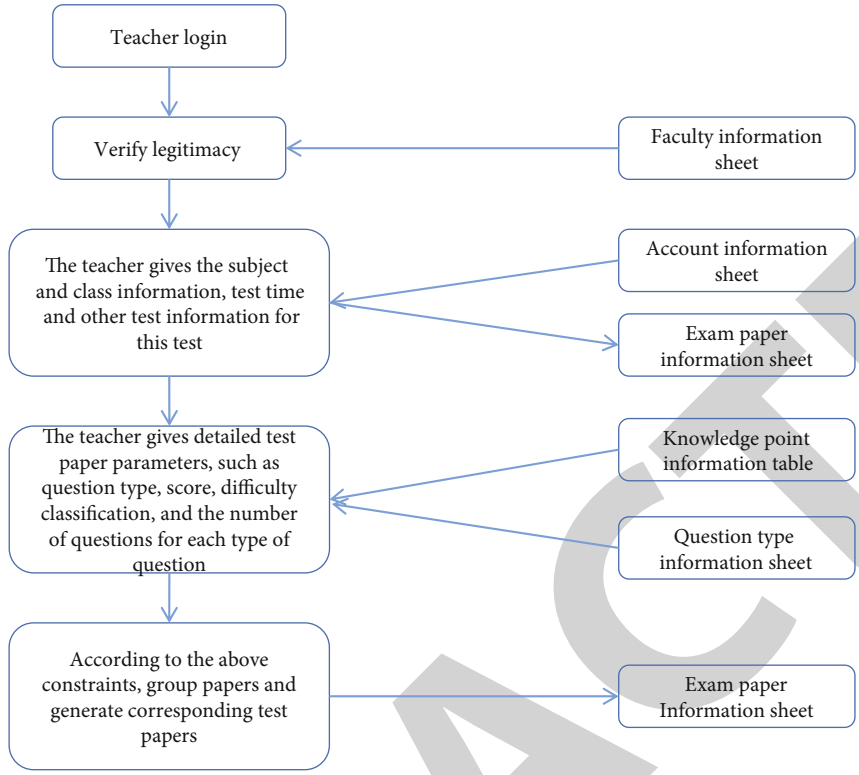

Figure 4: Operation flow chart of test paper generation system.

Table 1: Example of designing a partition code.

Single choice questions						Multiple choice questions						Completion				Noun interpretation		Short answer questions		Case
3	6	...	38	27	19	6	...	41	29	71	75	...	59	67	78	89	99	87	75	

in the following formula:

$$\text{Minimize } f = r_1 * \left[\left(\sum_{i=1}^{p} da_i\right)/p\right] + r_2 * \left[\left(\sum_{i=1}^{p} db_i\right)/q\right] + \cdots \tag{10}$$

When using a special algorithm, the problem is solved in terms of the minimum value of the motion function so that the corresponding motion function is included as follows:

$$F = C - f. \tag{11}$$

The basic requirements of fitness function are as follows: One is to ensure that all variables are positive in the case of input. The second is to ensure consistent progress throughout the optimization process. The fitness function can construct various benefit parameters, and the fitness function can also be used to represent various individual spaces (S). The corresponding function (F) is shown as follows:

$$f : S \longrightarrow R^{+}. \tag{12}$$

The three elements constituting the total fitness function are summed to obtain the value of the total fitness function. The formula is shown in the following formula:

$$f(x) = T(x) + R(x) + E(x). \tag{13}$$

After long-term of hard work and continuous improvement of Japanese online testing, the genetic algorithm has gained the strength of the best solution after long-term development and growth. The physical value is 99.666667. When this value is output, the error of the test result query type is 0, the error of the average difficulty of the test is 0, and the error of the distribution of some test points is 0.666667. The process of obtaining the fitness of this optimal solution is shown in Figure 5.

In Figure 5, the horizontal axis represents the evolutionary algebra, and the vertical axis represents the power of the previous genetic algorithm.

The test indicator system must be composed of many practical parameters in order to be optimal. A reasonable test index system directly determines the quality of the test paper. The main indicators are as follows:

(1) Basic knowledge of Japanese. It refers to the basic knowledge and skills that students must master in Japanese learning. These Japanese knowledge and skills are tested in the test paper

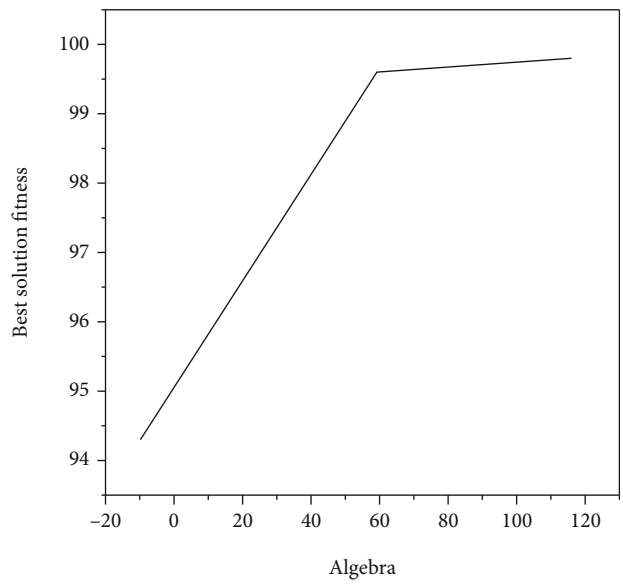

Figure 5: Fitness curve of optimal solution.

(2) Japanese examination outline. Reflect the main direction of the Japanese test to the examinee, and prompt the key knowledge points

(3) The difficulty of Japanese test. It mainly refers to the difficulty and ease of the examinee to correctly answer the test question. The difficulty of objective questions can be calculated by the following formula, as shown in the following formula:

$$P - \frac{R}{N}. \tag{14}$$

The complexity of the subjective test questions can be calculated using the following formula, as shown in the following formula:

$$P_i = \frac{X_i}{K_i}. \tag{15}$$

Combined with the actual needs, we can set up a set of mathematical model, and then set some constraint variables for this mathematical model. Controlling the complexity of the overall question types on the Japanese electronic test paper, it is necessary to set up a set of standard test paper mechanism. The NP complete problem is a subclass of the NP class problems, a subclass with special properties and special meaning. Before generating the test paper, we should first determine the question type distribution, test site range, difficulty coefficient, score distribution, etc., of the whole set of test paper. Combined with the actual situation, we can ensure the scientificity and reference value of test paper generation, as shown in Tables 2–3.

Table 2: Information of objective questions such as single choice questions.

Listing	Data type	Allow null
Question number	bi gint	—
Question type number	int	—
Test score	int	—
Answer time	float	—
Test question stem	varchar(1 000)	—
Option A	varchar(1 000)	—
Option B	varchar(1000)	—
Option C	varchar(1 000)	—
Option D	varchar(1 000)	—

4. Experiment and Analysis

Establish an examination database named in and complete the creation of the required data table. After the database is created, the connection between the foreground interface of the system and the background database needs to be established. The connection operation to the database is used repeatedly in the program. Therefore, the functions of database connection, query object creation, and result set creation are encapsulated in a name. The database connection of the system adopts data connection pool technology. As a detection means, the examination should be serious and have special high requirements for security. Therefore, users are divided into two categories: administrators and candidates [17]. They have different levels. When entering the system, they need authentication and need to enter the authentication code. The administrator account is specifically set up for people who can make whole-system changes to the computer, install programs, and access all the files on the computer. Only users who have the administrator have full access to other user accounts on the computer. The authentication identification code here is the unique random number directly generated by the system for each server connection. Users must enter the identification code when logging in; otherwise, they will not be able to log in. Especially in the student Japanese examination, once the candidate opens the browser and enters the login interface, the corresponding unique ID code will be generated. At this time, the system will automatically track the user. Before the end of the examination, the user is not allowed to log in again, so the candidate cannot log in from multiple windows and places at the same time, so as to effectively avoid the students cheated in the Japanese online exam, as shown in Figure 6.

After passing the authentication, students enter the online examination home page, select the specific content of the Japanese test, and call out the test paper for examination, and the candidates' answers are saved on the server in the form of documents. During the Japanese online examination, you can click to submit the answer after completing each page of the examination questions and then do the examination questions on the next page. If you want to quit the exam halfway, you can click quit halfway. The system

Table 3: Information table of subjective questions such as question and answer questions.

Listing	Data type	Allow null
Question number	bigint	—
Question type number	int	—
Test score	1nt	—
Answer time	float	—
Test question stem	varchar(1 000)	—
Standard answer	varchar(1 000)	—
Coding discrimination	int	—
Difficulty coding	1nt	—
Course number	int	—

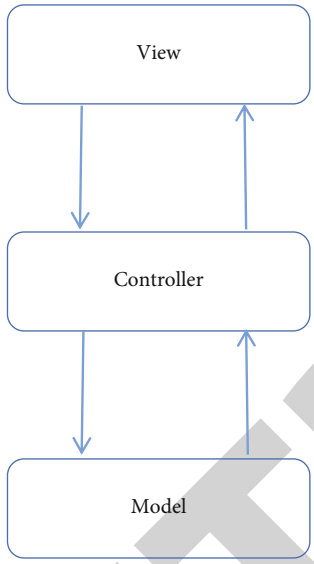

Figure 6: System login interface.

will automatically display the test questions and correct answers that you have taken before you quit and make a comparison to get the score. If all the test questions are completed or the test time is over, the system will display all the test questions and their standard answers and compare them with the answers made by the user and give scores. The test question upload interface can use the function of batch upload in the process of uploading test questions, which can effectively reduce the burden of database [18, 19]. Testing the question bank adjustment interface in the test question information management module, the administrator can view, delete, and modify the content of the test question bank. After using the online Japanese examination system, the whole examination process is as follows: The examinee enters the entrance page of the online Japanese examination system through the browser, enters the Japanese examination system after entering the correct user information, and randomly selects the test questions. After clicking "start," the system will automatically generate the test paper and display it on the client through the browser; The system starts timing and begins the exam. After the examinee submits the test paper, the computer automatically marks the objective questions, obtains the score, and counts the score into the database. Subjective questions such as short answer questions can be marked by a combination of computer and manual. Therefore, the online Japanese examination system should consider the following functions: (1) realize the management of examination question bank, such as the establishment of question bank, the entry, and modification and deletion of questions. The types of questions in the question bank are mainly objective questions such as single choice, blank filling, and judgment. (2) Students log in to the system on the Internet and randomly select test questions for examination. During the examination, it can automatically count the time and display the students' remaining time. At the end of the examination, it can automatically take up the paper and change the paper [20]. (3) Students' test scores can be queried online, and their own test papers can be rechecked. (4) Realize the seamless link with the college educational administration management system, and students' scores can be automatically imported into the educational administration management system to facilitate students' query. (5) Japanese teachers can set the test parameters before the test, such as test subjects, test time, and test scope. (6) After the examination, the Japanese teacher can analyze the results of the examination, such as the score of each chapter and question type, and the score statistics of each class. (7) Users logging into the system, including system administrators, teachers, and students, should have different permissions [21].

Different login identities can be selected for system login: super administrator, administrator, teacher, and student. Log in to different function interfaces according to permissions. The process of administrator login management module is shown in Figure 7.

The administrator login management module function is used to verify the administrator's identity when entering the examination management system. When logging in the examination management system, the system allows the administrator to express his identity. Different administrators have different permissions. The system verifies whether the administrator is a legal user. When the user name and password entered by the administrator are correct, he can enter the management system. Open corresponding management functions for administrators according to different permissions. A complete software testing management tool should be able to manage all aspects of the testing process. The flow of teacher login management module is shown in Figure 8.

The function of the teacher login management module is mainly to complete the test paper generation, and submission after the teacher is authorized. The system stores the test paper in the database test paper table to generate the form of question bank for students to extract the test and view the results. Teachers can also query student users, enter scores, and publish examination arrangements and other news information. The teacher can review the students' homework. The process of student user login examination module is shown in Figure 9.

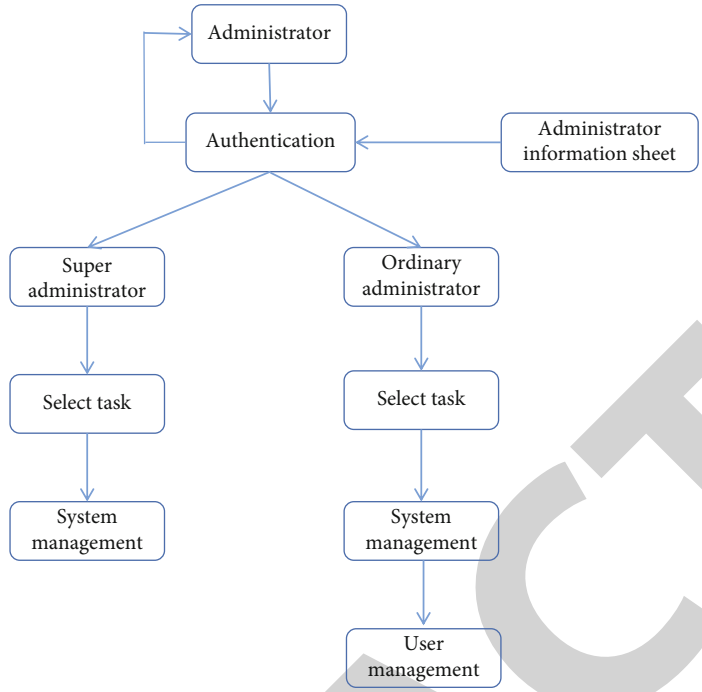

Figure 7: System flow chart of administrator login management function.

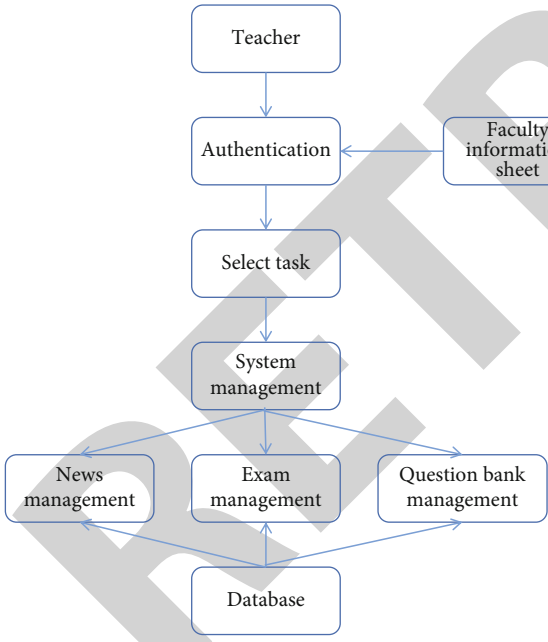

Figure 8: Teacher login management module process.

Student user authentication means that during the Japanese online exam, the examinee can log in to the system to take the exam only after he/she has passed face recognition or ID card recognition [23]. Identity authentication is very important in the process of Japanese online examination. It is related to the seriousness of the examination. The online Japanese examination system supports the exemption of the invigilation link, and all the examination room requirements can be achieved through the examination setting. Therefore, the main thing in the Japanese examination system is the various functions of the examination room environment, such as the test time, the list of candidates, the topic selection group papers, and the scoring criteria. After logging in, students can choose subjects and take tests. After the exam, they can see the correct answers and scores of the questions they have done.

The general input and output stream classes in Java language use the single byte reading method for data I/O operation. That is, only one byte of data is read or written at a time. This method is obviously cumbersome and inefficient. The reading and writing process is shown in Figure 10.

Because the Java language provides a buffer class specially used to improve the I/O efficiency of the system, it is like providing a temporary buffer when reading and writing data. A data block of buffer size can be read at a time. It can reduce the number of read and write data. If you transmit only a little data each time, you need to be transmitted many times, which will waste a lot of time. And then this data block can be written to the target device at one time [24]. Setting up a data buffer to read one data block at a time to improve system performance is particularly important in network data transmission. The flow chart of reading and writing using data buffer class is shown in Figure 11.

For the verification of the existence and legitimacy of the input information from the client, it is realized by client-based programming. For example, the student and teacher administrators must pass the verification of the existence and legitimacy of the input from the client when registering or logging in. Specifically, if the information that must be filled in is not filled in, the system will give an existential warning. For example, for those systems that do not meet the requirements in terms of type composition, length

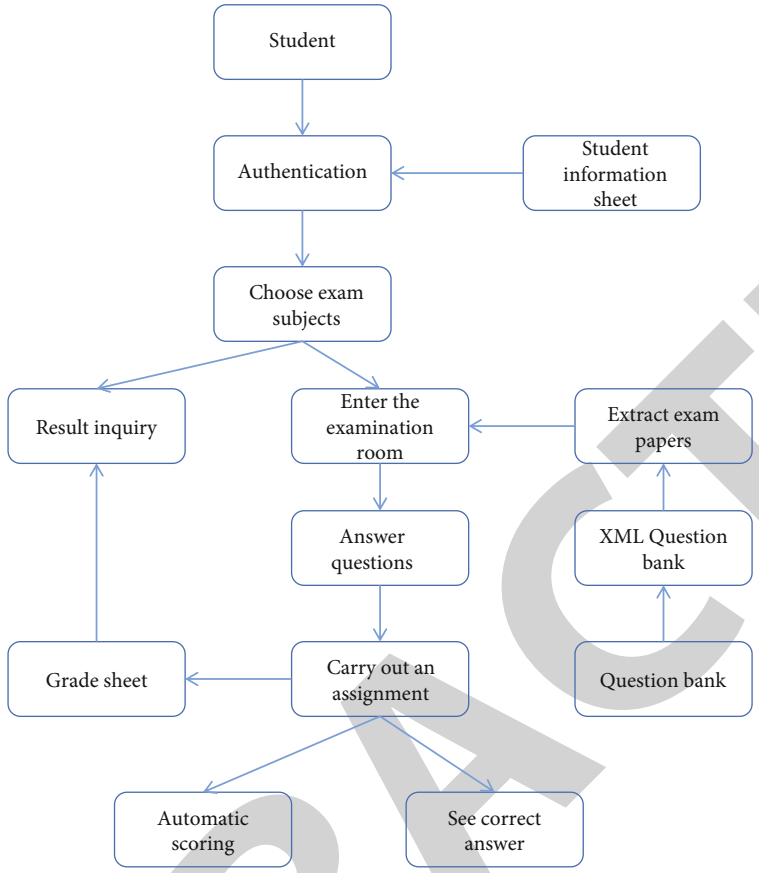

Figure 9: Student user login examination module process.

Figure 10: Single byte read and write.

Figure 11: Reading and writing process using data buffer class.

extreme value, and so on, the system will also give a warning on the client. This can greatly reduce the burden of the server and improve the reliability of the program and the running speed of the system.

Aiming at server-side user exceptions in the server-side database, the server-side programming is used to correct the user's misbehavior to ensure the normal operation of the system. For example, when the data content, data type, data format, and data scheduled processing process are obtained by the system from the client conflict with the database in the server, the system can give a warning in time and guide the correct processing method. In this system, this abnormal message processing mechanism runs through the processing of all data and shows good fault-tolerant performance in the practice of remote test run of the Japanese examination system [25].

And the system has very strict identity authentication procedures. Student administrators must be authenticated to log in, and their permissions are different for different users. For example, different administrators can only operate with their own permissions. Through strict identity authentication and different authority settings, the security of online examination system and data security are guaranteed. In addition, we also optimize the source code by writing modular functions and encapsulating process code in an object-oriented way to improve the reusability and execution efficiency of the source program.

In order to complete the test of all the learning contents of the Japanese course, each database has a data table according to the type of questions (single-choice, fill-in-the-blank, true-false, and short-answer questions) [26]. When the administrator sets the test parameters, he can select the test subjects. The following tables are established in the question bank: multiple-choice question sheet, fill-in-the-blank question sheet, judgment question sheet, and short-answer question sheet, which are used to store questions of various types.

Add difficulty, bias, and other attributes to each question to improve test quality. The student information table is used to store important student information, usually including student number, ID number, name, department chair, and other items. Information can be sent through the University's Academic Administration. The user table is used

to store management information, including number, user name, password, authorization, and other equipment. The teacher table is used to store teacher information, including account number, password, name, office, and other items. The quiz table is used to store quizzes created by the quiz algorithm. Answers are used to store answers to student tests. We can also establish a score table to make statistics and analysis of students' scores.

In this way, the online Japanese examination system can be realized both functionally and safely, which improves the convenience of Japanese examination.

5. Conclusion

The genetic algorithm is based on the theory of evolution and can complete the intelligent questionnaire very well. In this paper, a mathematical model of the genetic algorithm is established for the test-setting part of the online Japanese examination system, and then the model is realized by editing the code. Genetic algorithm can solve many deficiencies in the traditional way of setting test papers, such as low efficiency and poor quality of test papers, which greatly optimizes the fairness and poor reference of traditional test papers. After a period of testing and analysis of the system, the functional modules of the online Japanese examination system can stably carry out various tasks such as grouping papers, but there are still many imperfections, and various drawbacks are still unavoidable. There are still many undiscovered problems, and various problems must be gradually discovered in the long-term operation and use. By constantly finding problems and solving problems, the system can be made more perfect and more practical.

Data Availability

The data used to support the findings of this study are included within the article.

Conflicts of Interest

The authors declare that they have no conflicts of interest or personal relationships that could have appeared to influence the work reported in this paper.

Acknowledgments

This study is supported by the Scientific Research Fund of the Jiangxi Provincial Education Department: Design and implementation of online examination system for college Japanese in post-epidemic era (GJJ212712).

References

[1] Z. Liu, J. Liu, and Z. Liu, "Analysis, design, and implementation of impulse-injection-based online grid impedance identification with grid-tied converters," *IEEE Transactions on Power Electronics*, vol. 35, no. 12, pp. 12959–12976, 2020.

[2] H. Sugisawa, T. Shinoda, Y. Shimizu, and T. Kumagai, "Cognition and implementation of disaster preparedness among Japanese dialysis facilities," *International Journal of Nephrology*, vol. 2021, Article ID 6691350, 9 pages, 2021.

[3] A. Al-Aqbi, R. Al-Taie, and S. K. Ibrahim, "Design and implementation of online examination system based on msvs and SQL for university students in Iraq," *Webology*, vol. 18, no. 1, pp. 416–430, 2021.

[4] S. Clivaz and T. Miyakawa, "The effects of culture on mathematics lessons: an international comparative study of a collaboratively designed lesson," *Educational Studies in Mathematics*, vol. 105, no. 1, pp. 53–70, 2020.

[5] M. Mizuma, H. Yamamoto, H. Miyata et al., "Impact of a board certification system and implementation of clinical practice guidelines for pancreatic cancer on mortality of pancreaticoduodenectomy," *Surgery Today*, vol. 50, no. 10, pp. 1297–1307, 2020.

[6] S. Makino and D. Lehmberg, "The past and future contributions of research on Japanese management," *Asian Business & Management*, vol. 19, no. 1, pp. 1–7, 2020.

[7] Z. W. Lie, Q. L. Zheng, S. Zhou, and H. L. Rauf, "Virtual energy-saving environmental protection building design and implementation," *International Journal of System Assurance Engineering and Management*, vol. 13, Supplement 1, pp. 263–272, 2022.

[8] Z. Tian, S. Tian, T. Wang, Z. Gong, and Z. Jiang, "Design and implementation of open source online evaluation system based on cloud platform," *Journal on Big Data*, vol. 2, no. 3, pp. 117–123, 2020.

[9] J. Acosta, F. Amórtegui, A. Escobar, L. M. Leon, and S. Rivera, "Design and implementation of prototype for XLPE cable aging test," *Revista Internacional de Métodos Numéricos para Cálculo y Diseño en Ingeniería*, vol. 36, no. 3, pp. 36–44, 2020.

[10] M. Cao, "Design and implementation of multidimensional interaction in online English course under the assistance of Omnimedia," *Scientific Programming*, vol. 2021, Article ID 3713161, 10 pages, 2021.

[11] N. Choudhary, "Design and implementation of wildfire monitoring system," *International Journal for Modern Trends in Science and Technology*, vol. 7, no. 5, pp. 139–143, 2021.

[12] K. Sharma and B. K. Chaurasia, "*Trust based location finding mechanism in VANET using DST*," in *Fifth International Conference on Communication Systems & Network Technologies*, pp. 763–766, IEEE, Gwalior, India, 2015.

[13] A. Muneer and D. Zhan, "Design and implementation of automatic painting mobile robot," *IAES International Journal of Robotics and Automation (IJRA)*, vol. 10, no. 1, pp. 68–74, 2021.

[14] P. Elechi and C. O. Ahiakwo, "Design and implementation of an automated security gate system using global system for mobile communication network," *Journal of Network and Computer Applications*, vol. 7, no. 1, pp. 1–10, 2021.

[15] S. Kaddoura, D. E. Popescu, and J. D. Hemanth, "A systematic review on machine learning models for online learning and examination systems," *PeerJ Computer Science*, vol. 8, no. e986, 2022.

[16] L. Hu, "Design and implementation of a component-based intelligent clothing style cad system," *Computer-Aided Design and Applications*, vol. 18, no. S1, pp. 22–32, 2020.

[17] J. Li and W. Li, "On-line pid parameters optimization control for wind power generation system based on genetic algorithm," *IEEE Access*, vol. 8, pp. 137094–137100, 2020.

Hindawi
Wireless Communications and Mobile Computing
Volume 2022, Article ID 5340517, 11 pages
https://doi.org/10.1155/2022/5340517

Research Article

Performance Evaluation of Multiagent Reinforcement Learning Based Training Methods for Swarm Fighting

Huanli Gao, Yahui Cai, He Cai, Haolin Lu, and Jiahui Lu

School of Automation Science and Engineering, South China University of Technology, Guangzhou 510641, China

Correspondence should be addressed to He Cai; caihe@scut.edu.cn

Received 13 August 2022; Accepted 24 September 2022; Published 11 October 2022

Academic Editor: Jun Ye

In this paper, we conducted a performance evaluation of two multiagent reinforcement learning based training methods for swarm fighting, namely, the multiagent reinforcement learning (MARL) training method, and the combined multiagent reinforcement learning and behavior cloning (MARL-BC) training method. The behavior cloning expert is taken from some well-trained model in the final steady phase by the MARL training method. From the perspective of winning rate, the performances of these two different training methods can be divided into three phases. In the first phase, learning progresses slowly for both these two training methods. As the model trained by the MARL training method grows stronger, the experience of the behavior cloning expert gradually becomes useful, and the second phase kicks off where the MARL-BC training method takes obvious advantage. Surprisingly, the advantage of the MARL-BC training method will disappear as the learning progress goes on because in this final phase the expert of the behavior cloning training method can no longer offer the right strategy in presence of the ever changing environment and opponent.

1. Introduction

The core mechanism of reinforcement learning (RL) is feedback. In the process of RL, agents perceive the environment, take actions based on observation, and receive feedback from the environment to adjust their actions. By extensive trial and error, agents tend to exhibit the desired behavior expected by the trainer. RL has also inspired many other learning methods, such as Q learning [1], Neuro-Dynamic Programming [2], Policy Gradient Learning [3], and so on. These novel RL related learning methods have drastically improved the ability of RL from the perspective of perception and expression, thus facilitating the application of RL in many scenarios, such as robotics, computer vision, health, transportation, finance, games, autonomous driving, natural language processing, and other aspects [4–13].

Multiagent reinforcement learning (MARL) is an important research direction of RL because the problem that can be solved by a single agent is very limited. In the scenario of swarm fighting, multiagent systems should make timely judgment according to the change of the environment and take action in the next move, such as attacking, avoiding, encircling, and cheating. In order the win the fighting, the multiagent system need to learn how to collaborate in the process of reinforcement learning, and strive to maximize the benefits in the changing environment. For example, for unmanned aerial vehicle air combat, the environment is evolving with high dynamic subject to complex conditions, such as intermittent signal interference and dense fire threat. Thus, it would be impossible to obtain a feasible fighting strategy by a single and centralized learning method. Instead, distributed and collaborative decision-making by multiple agents would be necessary. However, the behaviors of multiagent systems are essentially unstable Markov decision-making process, which makes it extremely difficult, if possible, to obtain any affirmatively effective solution by rule-based methods. On the contrary, it is the very property of RL to effectively deal with complex and dynamic environment. Recently, the MARL method proves to be a promising way to solve the swarm fighting problem [14]. The players on both sides in the swarm fighting constantly interact with the environment, learn the reward value of each behavior through RL, and combine these reward values to find the optimal strategy. The multiagent deep deterministic policy

gradient was proposed in [15], which established a framework featuring centralized training and decentralized execution. Reference [16] proposed the Deep Reinforcement Opponent Network algorithm with two neural networks, where one neural network is designed to evaluate its own Q value, while the other neural network is designed to learn policy representations for other agents. In this way, the intentions of other agents can be understood which helps to improve algorithm performance. In [17], a novel cooperative multiagent reinforcement learning method was conceived for both discrete and continuous action spaces, called FACtored Multiagent Centralised policy gradients (FACMCA). Like the Multiagent Deep Deterministic Policy Gradient method, FACMCA also uses depth determination policy gradients to learn policies. However, FACMCA learns a centralized but decomposed critic that combines the application of each agent into a joint action-value function via a nonlinear monotonic function. The authors of [18] utilized additional state information in MARL and proposed a new actor-critic framework, namely value-decomposition actor-critic (VDAC). This framework achieves a reasonable balance between training efficiency and algorithm performance. As the number of agents increases, the input of centralized reviewers under the centralized training distribution execution framework increases linearly, increasing the difficulty of training. To address this issue, [19] introduced an attention mechanism to solve the issues of dataset and training. Efficient communication is crucial for effective cooperation of agents. [20] explored the communication among agents and proposed the Multiagent Bidirectionally-Coordinated Network. A communication channel through a two-way recurrent neural network was built, and the agents could store local information while communicating continuously. RL may encounter the problem of sparse rewards during training, i.e., the agent does not get any reward after many decision-making steps, which makes the learning process of the agent difficult [21]. In such cases, the researchers thought of using behavior cloning to speed up the learning progress, i.e., the agent imitates the behavior of the expert, making its own behavior close to the expert. Behavior cloning was invoked in [22] for autonomous driving. By collecting action-observation pairs in advance, the model was trained to control the steering wheel, accelerate, and brake by imitating experts. The DeepMind team also used behavior cloning to initialize the policy network when training AlphaGo [23]. They encoded each chessboard state as a tensor through an encoder, and trained the policy network through supervised learning. This method greatly improves the accuracy of the model placing chess pieces and speeds up the training speed. Some other works related to behavior cloning can be found in [24, 25].

In this paper, we build a 3 V3 swarm fighting simulation environment based on the Unity platform, and conducted performance evaluation of two MARL based training methods for swarm fighting. In particular, for the first method, we directly employ the MARL training method, and for the second method, we combine the MARL training method and the behavior cloning training method by appropriately weighting between these two methods, leading to the combined MARL and behavior cloning (MARL-BC) training method. The behavior cloning expert adopted in this paper is taken from some well-trained model in the final steady phase by the MARL training method. From the perspective of winning rate, the performances of these two different training methods can be divided into three phases. In the first phase, learning progresses slowly for both these two training methods. The reason is obvious for MARL training method. While, for the MARL-BC training method, since the data available for learning is mainly for opponents of comparable ability, for the scenarios where the opponent is weak, these data could not bring any extra benefits. As the model by the MARL training method grows stronger, the experience of the behavior cloning expert gradually becomes useful, and the second phase kicks off where the MARL-BC training method takes obvious advantage. Surprisingly, the advantage of the MARL-BC training method will disappear as the learning progress goes on. The reason behind this is that in the final phase, the model trained by the MARL training method still keeps learning from the environment and its opponent, while the model trained by the MARL-BC training method has to follow the rules of the expert to some extent. Therefore, the resulted strategy cannot effectively adapt to the ever changing environment and opponent.

2. Environment and Agent Setting

In this paper, we build the 3 V3 swarm fighting simulation environment based on the Unity platform. Unity is a platform for real-time 3D interactive content creation and operation, which has been widely used in game development, art, architecture, automobile design, and other fields. Also, Unity has a powerful physics engine based on NVIDIAphysX or Havok and an AAA-grade image rendering engine. Based on the above engines, Unity can simulate rigid bodies, particles, and other realistic physical environments with high accuracy. Most importantly, Unity enables fast distributed simulation. When tasks require fast simulation speed other than the frame rate of the rendering process, Unity can simulate from the code level and significantly improve the learning efficiency of RL.

2.1. Environment Setting. Based on the Unity platform, the simulation environment can support a large number of agents to train in a single environment. Figure 1 shows the top and side views of the specific environment. The environment is bounded by boundaries 200 meters long and 160 meters wide, including six intelligent tanks, three in the red teams and three in the green teams. These intelligent tanks have the same attributes and will be referred to as agents later. The agents in both teams have certain endurance and fire limits. The goal of each team is to annihilate the other with maximal efficiency and minimal loss.

The winning condition for each team is to annihilate all agents of the other team. A time limit is added to avoid endless battles. If the time limit is exceeded, the game will be tied. The specific rules are given by Algorithm 1, where Red.num and Green.num represent the number of surviving agents in red team and green team, respectively, and

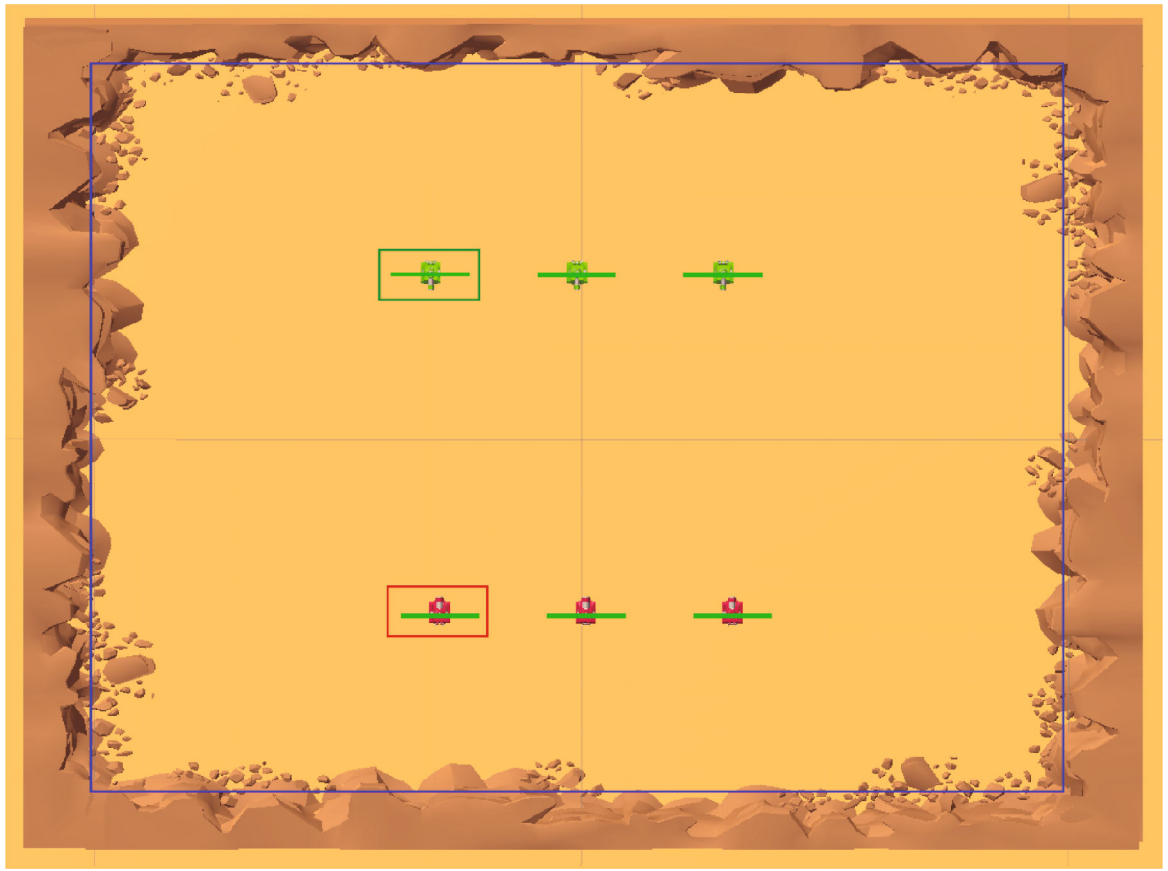

(a) Top view of the simulation environment

(b) Side view of the simulation environment

Figure 1: Top and side views of the swarm fighting simulation environment.

```
Input: Begin//bool value, initialize the environment,
whether to start round.
Output: Winner of this round.
  Execute this program each frame.
  MaxEnviormentStep =8000//Defines the maximum.
  number of steps in the environment.
  for i≤ MaxEnviormentStep && Begin do.
      ++i.
      if Red.num ==0 && Green.num ==0 then
          return tie
      else if Red.num ==0 then
          return Green.win
      else
          return Red.win
return null
```

Algorithm 1: Global Rules

Green.win (Red.win) means green team (red team) wins the fighting. An independent script acts as a judge throughout the environment, which analyzes each frame in the environment to ensure that the execution of global rules is correct.

2.2. Agent Setting. Each agent has two continuous actions: forward, turn, and a discrete action: fire or not. The agent obtains environmental information by communicating with the surrounding agents through sensors. Now we introduce the basic configuration information of the agent.

2.2.1. Motion. According to the task requirements, the agent can only move in the XOZ plane in the global coordinate system, and the motion control of the agent follows the second-order unicycle model, which is given by

$$\begin{bmatrix} \phi(k+1) \\ x(k+1) \\ y(k+1) \end{bmatrix} = \begin{bmatrix} x(k) + v(k) \cdot \cos(\phi(k)) \cdot T_s \\ y(k) + v(k) \cdot \sin(\phi(k)) \cdot T_s \\ \phi(k) + \omega(k) \cdot T_s \end{bmatrix}, \quad (1)$$

where $(x(k), y(k))$ denote the Cartesian coordinate of the agent; $\phi(k)$ denotes the anticlockwise angle of the agent with respect to the x-axis; $v(k)$ and $\omega(k)$ denote the linear and angular velocities of the agent, respectively; T_s denotes the sampling time. Moreover, we impose limits for linear and angular velocities for each agent. In particular, $v(k) \in [-10m/s, (20m/s)]$, and $\omega(k) \in [-10^\circ/s, (10^\circ/s)]$.

2.2.2. Perception. The agent has three ways to perceive the surrounding environment, i.e., by Raycast Observations, by communication with teammates, and by self-observation. As shown in Figure 2(a), an omnidirectional laser detector is employed by each agent to detect the surrounding obstacles, where 14 rays with a length of 35 m are emitted from the agent to the surroundings to form an omnidirectional laser detector. Each ray returns an n-dimensional vector, where n is the number of detected tags. In this paper, we set the tags to be Wall, Enemy, and Teammate. In Figure 2(b), we can see that the 5th ray detects the enemy, the 8th ray detects the teammate, and the 10th-12th rays detect the wall.

In the simulation environment, we suppose there is regular communication between agents of the same team. By communication, the agents can share information with each other, including HP, velocity, and position, as shown in Table 1.

The agent can obtain the information of the opponents within a certain range that are not blocked by obstacles through observation. If the opponent is behind the agent, there is a 20% chance that the opponent's information can be obtained. The opponent's speed and HP information are summarized in Table 2.

2.2.3. Attack Capability. The agent can attack the opponent by firing projectiles. When the agent chooses to shoot, the projectile acquires an initial angle and an initial velocity relative to the agent's coordinate system. In the simulation environment, the air resistance is ignored, and thus the projectile's trajectory in the air is parabolic subject to gravity. When the projectile hits any object, it will explode, causing damage to all the agents within the blast radius. Let D_i represent the distance between agent i and the projectile, ζ represent the maximum damage of the projectile, η represents the blast radius. Then the damage H_i caused by the projectile to agent i is described as follows:

$$H_i = \begin{cases} \zeta^* \left(\dfrac{\eta - D_i}{\eta} \right) & D_i \le \eta \\ 0 & D_i > \eta \end{cases}. \quad (2)$$

The initial velocity at which an agent fires a projectile is controllable. If an agent fires a shell when the opponent is close to it, the shell may injure itself.

2.3. Reward Setting. In the process of RL training, by setting appropriate positive and negative rewards, the agent can be guided to learn the correct behavior. In the simulation environment, there are two kinds of rewards, agent-wise and group-wise. Agent rewards are used to optimize individual behaviors, so that agents can learn basic behaviors such as attack or retreat. Group rewards are used to encourage cooperative behaviors of group members. The specific positive and negative rewards are given in Tables 3 and 4. The terminologies in the tables are explained as follows:

(i) *HP* represents the remaining blood volume of the agent, and *FullHP* represents the full blood volume of the agent. *HP_Sum* represents the total *HP* of a team

(ii) *ResetTimer* denotes the current number of steps, and *MaxEnvironmentSteps* denotes the longest number of steps in a round. If the number of steps is exceeded, the fight will be forced to end

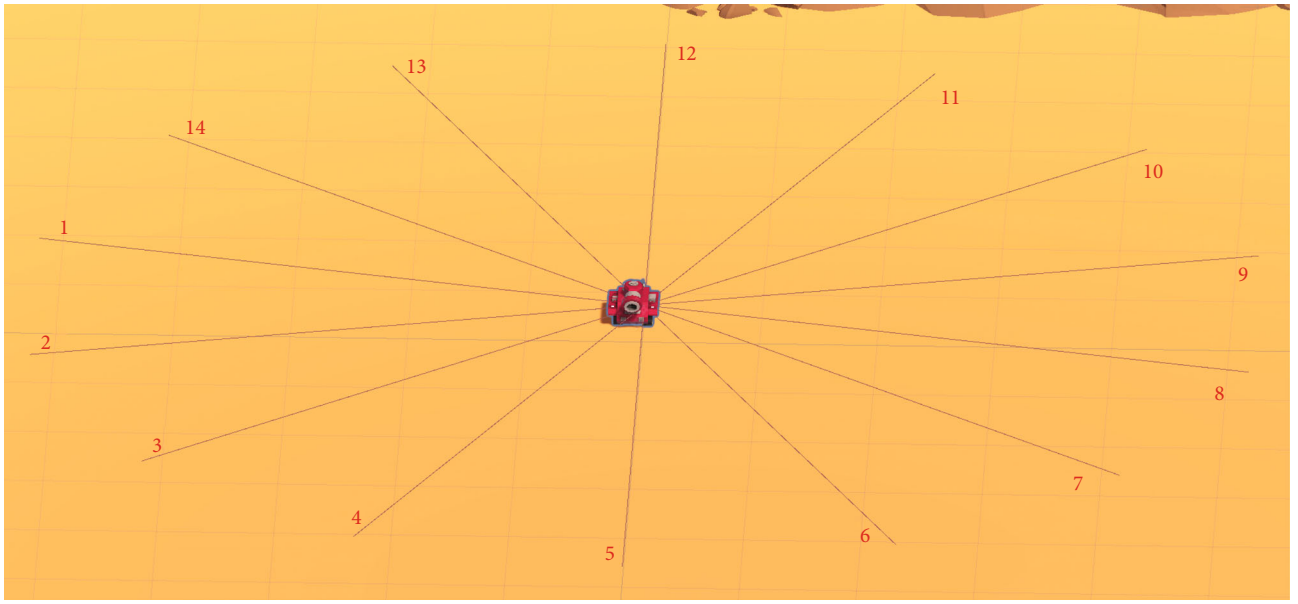

(a) The sensor of the agent

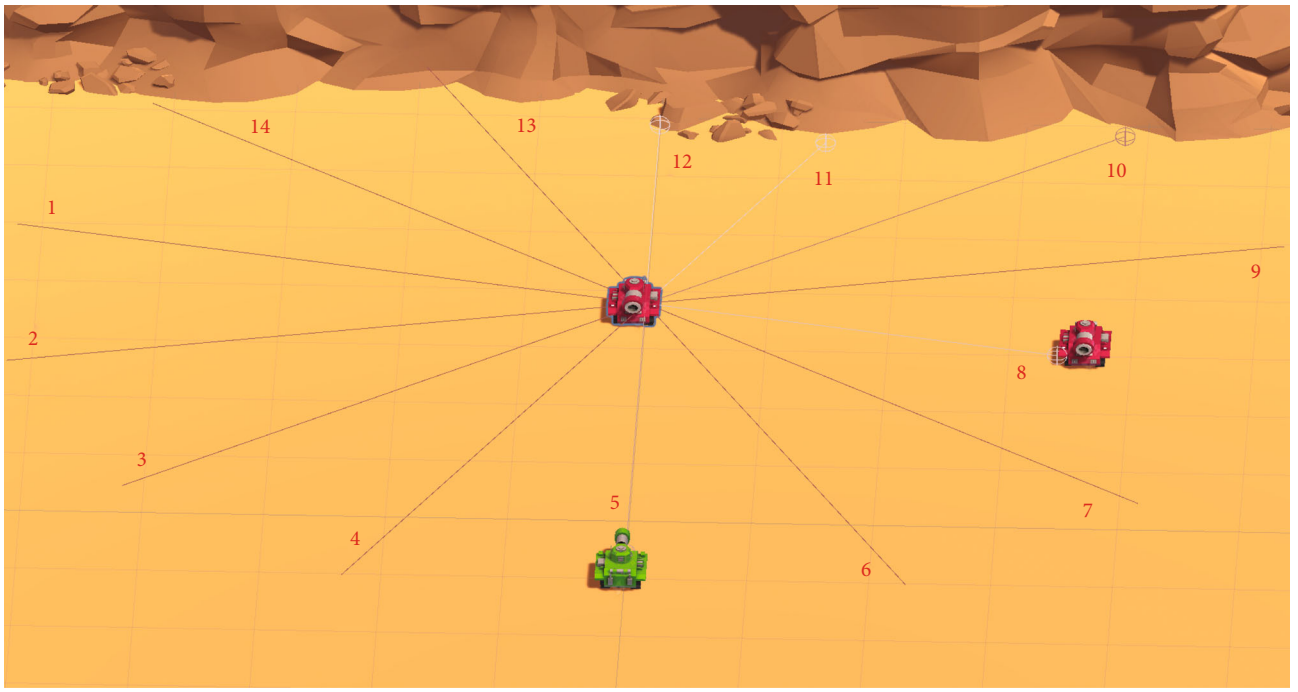

(b) Detection by the sensor

Figure 2: The working principle of the sensor.

Table 1: Information obtained by communication.

Number of feature	Meaning of feature
1	The remaining HP of the agent
2	The X-coordinate of the agent
3	The Z-coordinate of the agent
4	The X-direction velocity of the agent
5	The Z-direction velocity of the agent

Table 2: Information obtained by self-observation.

Number of feature	Meaning of features
1	The remaining HP of the opponent
2	The X-direction velocity of the agent
3	The Z-direction velocity of the agent

Table 3: Positive reward setting.

Type	Situation	Reward
Agent	Projectile hits opponent	$0.1 * \left(\frac{H_i}{\zeta}\right) + 0.15 * \left(\frac{\text{HP}}{\text{FullHP}}\right)$
	Group wins	$0.6 + \left(\frac{\text{HP}}{\text{FullHP}}\right) * \left(1 - \left(\frac{\text{ResetTimer}}{\text{MaxEnvironmentSteps}}\right)\right) * 0.6$
	Opponent is killed	$0.15 * \left(\frac{H_i}{\zeta}\right) + 0.2 * \left(\frac{\text{HP}}{\text{FullHP}}\right)$
Group	Opponent is killed	0.1
	Group wins	$0.9 - 0.5 * \left(\left(\frac{\text{ResetTimer}}{\text{MaxEnvironmentSteps}}\right) + 0.2 * (HP_{\text{Sum}})\right)$

Table 4: Negative reward setting.

Type	Situation	Reward
Agent	Agent is killed	$-0.2 + \left(\frac{\text{ResetTimer}}{\text{MaxEnvironmentSteps}}\right) * 0.1$
	Group failed	-0.1
	Injure teammates	$\left(-0.2 * \left(\frac{H_i}{\zeta}\right)\right)$
Group	Group ties	$-0.2 + \left(\frac{\text{ResetTimer}}{\text{MaxEnvironmentSteps}}\right) * 0.12$
	Group fails	$-0.8 + \left(\frac{\text{ResetTimer}}{\text{MaxEnvironmentSteps}}\right) * 0.5$

3. Algorithm

RL is a trial-and-error-based machine learning method. During the learning process, the agent is not told what actions to take, but must try to discover which action may produce more benefits. Let s_t represent the state of the agent at step t, a_t represent the action taken by the agent at step t, and r_{t+1} represent the reward obtained by the agent performing action a_t in state s_t. The agent uses the reward of each step as feedback to adjust the weighted parameters of the reinforcement learning network to maximize the reward, and the agent also learns the optimal strategy at each step. In the process of MARL, in order to strengthen the cooperation between agents, the rewards of the environment are mostly shared rewards. We want the agent's behavior to maximize the group's future reward. However, during the training process, the agent may terminate early and be removed from the environment. The removed agent cannot learn the success or failure of the group from subsequent phase. This problem is known as the postmortem credit allocation problem. The MA-POCA algorithm proposed by the Unity team solves this problem very well [26]. The algorithm introduces an attention mechanism at the input of RL, so that the network has the ability to deal with a variable number of agents, which is convenient for us to add or delete agents during the training process. In this experiment, we choose this algorithm to train the agent.

Table 5: Hyperparameters used for this experiment.

Type		MARL	MARL-BC
Hyperparameters	Batch size	1024	1024
	Buffer size	20480	20480
	Learning rate	0.0001	0.0001
	Entropy bonus	0.005	0.005
	Num epoch	3	3
Network settings	Hidden units	512	512
	Num layers	3	3
Reward signals	Discount factor	0.99	0.99
	Strength	1.0	1.0
Behavior cloning	Steps	/	100 M
	Strength	0.5	0.5

In the experiment, we set up two groups of experiments. One group of experiments only use MA-POCA algorithm, and the other group of experiments use MA-POCA and behavioral cloning. In behavioral cloning, the most important factor is the demo model. The demo of this experiment comes from the agent with the highest winning rate obtained from many experiments. We train 100 M times to get the agent model through MARL by self-play. At this far, the capability of the agent reaches a bottleneck. We set the

(a) Swarm fighting starts

(b) Green team is attacking

(c) Three agents are killed

(d) Three agents remain

(e) The green team surrounds the red team

(f) The green team wins

Figure 3: The whole process of a single round of swarm fighting.

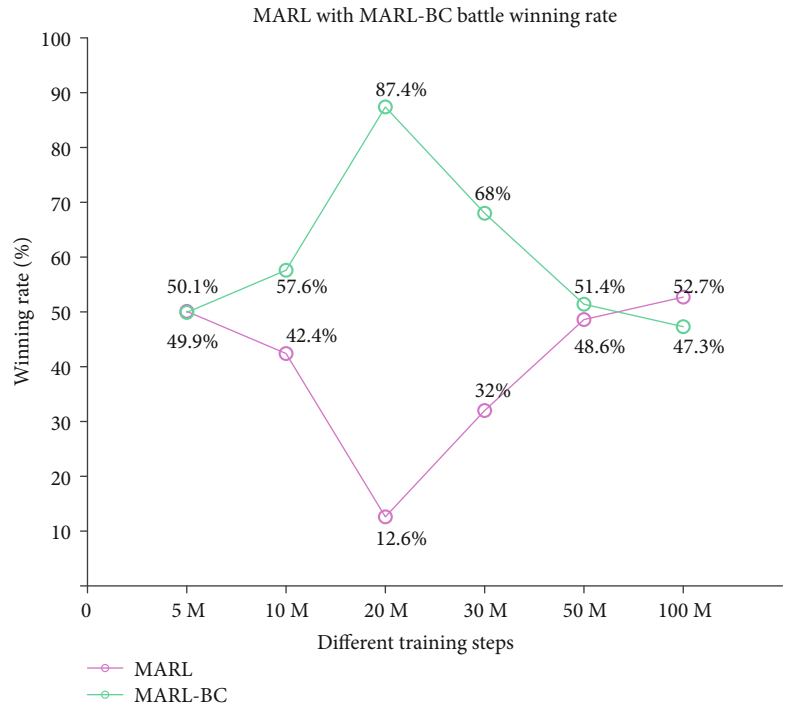

Figure 4: Winning rate of different training methods.

adversary with stronger attributes in terms of speed, HP, angular velocity, and field of view. By gradually strengthening the properties of the adversary, the ability of the agent is gradually improved. Finally, we obtain an agent model with a higher winning rate. By recording the behavior of the agent during testing, we obtain the demo files used for behavioral cloning training. In the initial stage for the MARL-BC method, the agent's decision is made equally based on the knowledge from RL and from the demo files of the expert by the behavioral cloning training method. This training process will continue for 100 M steps.

The experiment is conducted in the ML-Agent development environment of Unity, where the version number is 0.28.0. The hyperparameters used in this experiment are listed in Table 5, and those parameters not listed in the table just take default values. The terminologies of Table 5 are explained as follows:

(i) Hyperparameters

Batch Size Setting Batch Size to 1024 means collecting 1024 data samples at one time for training. Generally speaking, small batch size will increase the randomness of the gradient descent, thus making the algorithm difficult to converge. On the other hand, increasing batch size can reduce sample randomness, improve learning efficiency, and make the direction of the gradient descent more stable.

Buffer Size refers to the amount of experience to collect before updating the policy model. For the swarm fighting of three agents, setting Buffer Size to be 20480 can help the agents learn quickly.

Learning rate corresponds to the magnitude of each gradient descent update step. Excessive learning rate will violate the stability of the training process. Extensive experiments show that the model considered in this paper has better performance when the learning rate is set to be 0.0001.

Entropy Bonus encourages agent to take unpredictable actions. Setting Entropy Bonus to be 0.005 can help the agent improve the generalization ability in the training process.

Num Epoch denotes the number of times to pass through the experience buffer when performing gradient descent optimization. Decreasing Num epoch will make the updates more stable, but in the meantime slows down the training speed. To balance stability and training efficiency, we set Num epoch to be 3.

(ii) Network Settings

Hidden Units represent the neural network units of the hidden layer, ranging from 32 to 512 as recommended by the official document. In this paper, the number of hidden units is set to be 512 to maximize the ability of the agents.

Num layers refers to the number of hidden layers of the neural network. Taken into account the complex situation of swarm fighting, we set Num layers to be 3.

(iii) Reward Signals

Discount Factor denotes the discount factor for future rewards coming from the environment. It reflects how far into the future the agent should care about the possible rewards. Since the swarm fighting problem is a long sequence process, we set Discount Factor to be 0.99.

Strength represents the multiplication coefficient of the original reward. It is set to be 1 by the official recommendation.

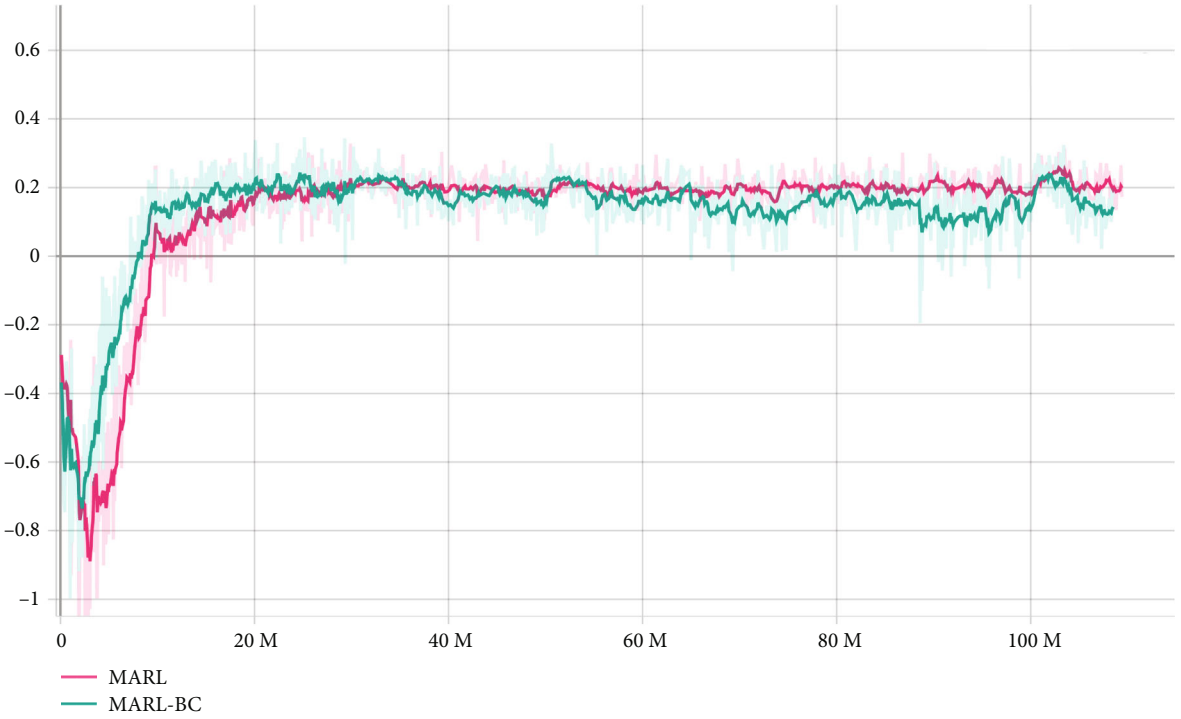

(a) Cumulative agent reward throughout the training process

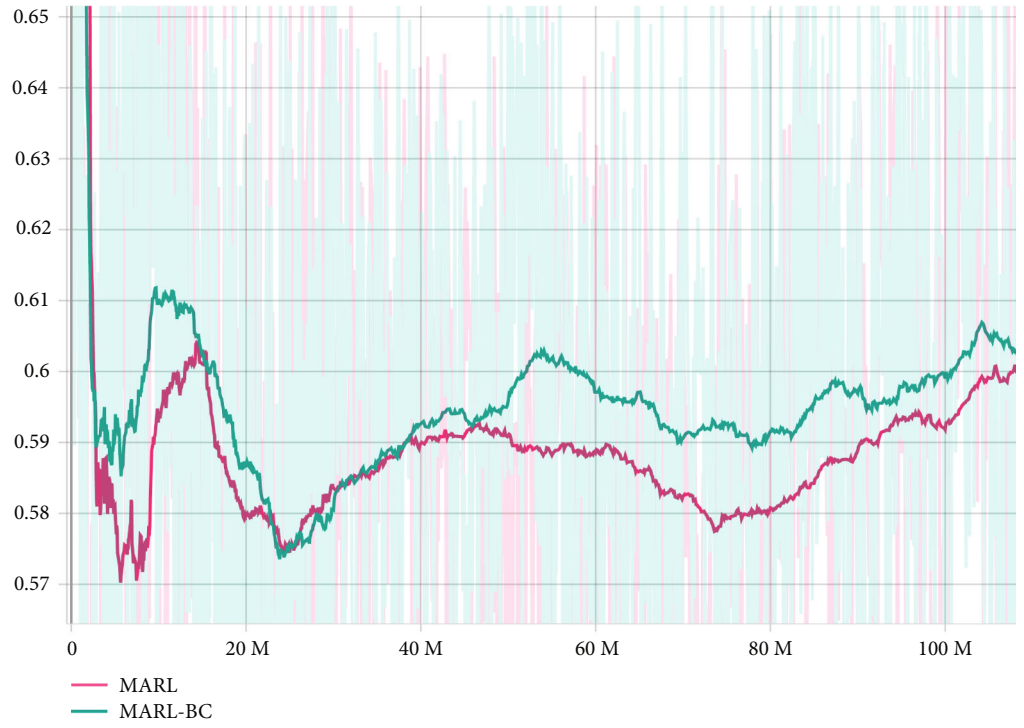

(b) Cumulative group reward throughout the training process

Figure 5: Cumulative reward of agent and group.

(iv) Behavior Cloning

Steps represent the training steps of behavior cloning, which are set to be 100 M. After 100 M steps, the model will no longer be trained by the behavior cloning method.

Strength represents the proportion of behavior cloning training in the training process. In this paper, it is set to be 0.5, i.e., the agents will be trained equally by the MARL and the behavior cloning training method.

Two indicators are adopted to evaluate the performance of the algorithm, namely, the winning rate and the cumulative reward. We conduct ten sets of parallel tests of the same environment to speed up the test efficiency. To make the experimental results fair, we set up two identical competitions in each set of test where the two sides of competitors shall switch their initial status. In order to make the experimental results more convincible, we measure the winning rate of the model through at least 2000 rounds of tests. As mentioned above, the agent takes different actions in different states. The system gives different rewards according to the quality of the action. If the average reward value of the agent is large, it means that the agent makes more correct decisions, and the training effect of the agent is better. Figure 3 shows the whole process of a single round of swarm fighting.

4. Results

The results are shown by Figures 4 and 5. Figure 4 shows the winning rate of MARL and MARL-BC based training method at different training steps. MARL refers to the training method by MA-POCA, which is represented by the pink line. MARL-BC refers to the training method by MA-POCA plus behavior cloning, which is represented by the green line.

At 5 M steps, the winning rates of both sides are similar. Starting from 5 M steps, the winning rate of MARL-BC gradually increases until it reaches 87.4% at 20 M steps. After that, the winning rate of MARL-BC starts to decline. At 50 M steps, the winning rates of the two training methods are close to each other again, where the winning rate of MARL-BC is only 2.8% better than that of MARL. When the training continues up to 100 M steps, the winning rate of MARL is 52.7%, which has exceeded the winning rate of MARL-BC.

Figure 5(a) shows the profile of the cumulative reward throughout the whole training process. In the early training phase, the cumulative reward of MARL-BC is almost the same as that of MARL, and both of which show a downward trend. As the experiment continues, the cumulative reward of MARL-BC first reaches the inflection point and starts to increase, ahead of the cumulative reward of MARL. The cumulative reward of MARL reaches its inflection point at 3 M and also starts to increase, but it is slower than MARL-BC. The cumulative reward of MARL-BC keeps being higher than that of MARL until the experiment reaches 22 M steps, at which the two cumulative rewards of the two training method are equal. In the next period, the cumulative rewards of MARL-BC and MARL are comparable. When the experiment reaches 54 M steps, the cumulative reward of MARL begins to lead MARL-BC, which continues until the end of the experiment. Figure 5(b) shows the profile of the group reward throughout the whole training process. Similar to Figure 5(a), MARL-BC reaches the inflection point first, but the difference is that as the training progresses, the group reward of the MARL-BC method is larger than that of MARL.

As described above, behavior cloning helps agents learn quickly to fight against opponents. While, behavior cloning helps the agent beat the agent trained with a certain number of steps. When faced with an agent with low intelligence which is insufficiently trained, behavior cloning cannot help much. Therefore, at 50 M steps, the number of training steps of the agent of MARL is not enough, and MARL-BC cannot provide useful experience. At this phase, MARL-BC and MARL have almost the same winning rate. As the experiments proceeded, the model using the MARL method became more sophisticated. Prior knowledge of behavioral cloning comes into play, helping agents using MARL-BC progress rapidly and maintain a high winning rate. In the final phase of the experiment, the agent using the MARL method learns from wrong decisions and keeps updating the model, and thus the ability of the agent is still growing. However, for the behavior cloning method, due to the limited scenarios covered by prior knowledge, the strategies provided by prior knowledge are not necessarily optimal, hindering the model's progress to some certain extent. The winning rate gap between the two method starts to narrow down, and finally the winning rate of the agent using the MARL method surpassed that of the agent using MARL-BC. If the training continues, the results are not difficult to predict that the advantage of the agent trained using the MARL method will become larger, and the winning rates of the two will converge with a steady difference.

5. Conclusion

In this paper, we evaluate the performance of two multiagent reinforcement learning based training methods, namely, MARL and MARL-BC. Two performance evaluation indicators are adopted, i.e., the winning rate and the cumulative reward. By comprehensive experiments, the following results are revealed.

(i) To some extent, behavior cloning can help agents learn strategies quickly to deal with specific opponents, which enables agents to defeat their opponents before and during training with extra knowledge and experience. However, as the number of the training steps keeps growing, the knowledge and experience from the behavior cloning may prevent the modeling from improving compared with the MARL training method which, for all the training process, keeps learning from its opponent and the environment

(ii) Because of the limitations of behavioral cloning training method in the later phase of training, it should be considered as an auxiliary training method in the prephase of the training process, rather than a training method for the whole training process

Data Availability

The data used to support the findings of this study are available from the corresponding author upon request.

Conflicts of Interest

The authors declare that they have no conflicts of interest.

Acknowledgments

This research was funded in part by the National Natural Science Foundation of China under grant number 62173149, 62276104, and in part by the Guangdong Natural Science Foundation under grant number 2021A1515012584, 2022A1515011262.

References

[1] C. J. C. H. Watkins, *Learning from delayed rewards*, King's College, Cambridge United Kingdom, 1989.

[2] D. P. Bertsekas and J. N. Tsitsiklis, "Neurodynamic programming: an overview," in *Proceedings of 1995 34th IEEE conference on decision and control*, vol. 1, pp. 560–564, New Orleans, LA, USA, 1995.

[3] D. Silver, G. Lever, N. Heess, T. Degris, D. Wierstra, and M. Riedmiller, "Deterministic policy gradient algorithms," in *International conference on machine learning. PMLR*, vol. 32, no. 1, pp. 387–395, Beijing, China, 2014.

[4] C. Huang, S. Lucey, and D. Ramanan, "Learning policies for adaptive tracking with deep feature cascades," in *Proceedings of the IEEE international conference on computer vision*, pp. 105–114, Venice, Italy, 2017.

[5] K. Yu, C. Dong, L. Lin, and C. C. Loy, "Crafting a toolchain for image restoration by deep reinforcement learning," in *Proceedings of the IEEE conference on computer vision and pattern recognition*, pp. 2443–2452, Salt Lake City, UT, USA, 2018.

[6] H. Xu, S. Feng, Y. Zhang, and L. Li, "A grouping-based cooperative driving strategy for cavs merging problems," *IEEE Transactions on Vehicular Technology*, vol. 68, no. 6, pp. 6125–6136, 2019.

[7] M. Tan, "Multi-agent reinforcement learning: independent vs. cooperative agents," in *Proceedings of the tenth international conference on machine learning*, pp. 330–337, Amherst, MA, USA, 1993.

[8] S. Bajpai, "Application of deep reinforcement learning for Indian stock trading automation," 2021, https://arxiv.org/abs/2106.16088.

[9] K.-F. Tang, H.-C. Kao, C.-N. Chou, and E. Y. Chang, "Inquire and diagnose: neural symptom checking ensemble using deep reinforcement learning," *NIPS Workshop on Deep Reinforcement Learning*, 2016.

[10] J. Wang, T. Shi, Y. Wu, L. Miranda-Moreno, and L. Sun, "Multi-agent graph reinforcement learning for connected automated driving," in *Proceedings of the 37th International Conference on Machine Learning (ICML)*, pp. 1–6, Vienna, Austria, 2020.

[11] J. Wu, Z. Huang, W. Huang, and C. Lv, "Prioritized experience-based reinforcement learning with human guidance: methdology and application to autonomous driving," 2021, https://arxiv.org/abs/2109.12516.

[12] J. Luketina, N. Nardelli, G. Farquhar et al., "A survey of reinforcement learning informed by natural language," 2019, https://arxiv.org/abs/1906.03926.

[13] O. Vinyals, I. Babuschkin, W. M. Czarnecki et al., "Grandmaster level in StarCraft II using multi-agent reinforcement learning," *Nature*, vol. 575, no. 7782, pp. 350–354, 2019.

[14] M. L. Littman, "Markov games as a framework for multi-agent reinforcement learning," in *Machine learning proceedings 1994*, pp. 157–163, New Brunswick, New Jersey, USA, 1994.

[15] R. Lowe, Y. I. Wu, A. Tamar, J. Harb, O. Pieter Abbeel, and I. Mordatch, "Multi-agent actor-critic for mixed cooperative-competitive environments," *Advances in neural information processing systems*, vol. 30, 2017.

[16] H. He, J. Boyd-Graber, K. Kwok, and H. Daume, "Opponent modeling in deep reinforcement learning," in *International conference on machine learning PMLR*, vol. 48, pp. 1804–1813, New York City, NY, USA, 2016.

[17] B. Peng, T. Rashid, C. Schroeder de Witt et al., "Facmac: factored multi-agent centralised policy gradients," *Advances in Neural Information Processing Systems*, vol. 34, pp. 12 208–12 221, 2021.

[18] J. Su, S. Adams, and P. Beling, "Valuedecomposition multi-agent actor-critics," in *Proceedings of the AAAI Conference on Artificial Intelligence*, vol. 35no. 13, pp. 11 352–11 360, 2021.

[19] S. Iqbal and F. Sha, "Actor-attention-critic for multi-agent reinforcement learning," in *International conference on machine learning. PMLR*, pp. 2961–2970, Los Angeles, USA, 2019.

[20] P. Peng, Y. Wen, Y. Yang et al., "Multiagent bidirectionally-coordinated nets: emergence of human-level coordination in learning to play starcraft combat games," 2017, https://arxiv.org/abs/1703.10069.

[21] D. Rengarajan, G. Vaidya, A. Sarvesh, D. Kalathil, and S. Shakkottai, "Reinforcement learning with sparse rewards using guidance from offline demonstration," 2022, https://arxiv.org/abs/2202.04628.

[22] F. Codevilla, M. Muller, A. Lopez, V. Koltun, and A. Dosovitskiy, "End-to-end driving via conditional imitation learning," in *2018 IEEE international conference on robotics and automation (ICRA)*, pp. 4693–4700, Brisbane, QLD, Australia, 2018.

[23] D. Silver, A. Huang, C. J. Maddison et al., "Mastering the game of Go with deep neural networks and tree search," *Nature*, vol. 529, no. 7587, pp. 484–489, 2016.

[24] F. Codevilla, E. Santana, A. M. Lopez, and A. Gaidon, "Exploring the limitations of behavior cloning for autonomous driving," in *Proceedings of the IEEE/CVF International Conference on Computer Vision*, pp. 9329–9338, Seoul, Korea, 2019.

[25] Y. Chen, J. Su, and W. Wei, "Multi-granularity textual adversarial attack with behavior cloning," 2021, https://arxiv.org/abs/2109.04367.

[26] A. Cohen, E. Teng, V.-P. Berges et al., "On the use and misuse of absorbing states in multi-agent reinforcement learning," 2021, https://arxiv.org/abs/2111.05992.

Hindawi
Wireless Communications and Mobile Computing
Volume 2022, Article ID 4708496, 16 pages
https://doi.org/10.1155/2022/4708496

Research Article

Cooperative Driven Algorithm for Couzin Model Based Fish School by Multiple Predators

He Cai, Taiyuan Zhang, Huanli Gao, Jiahao Long, and Jiali Wen

School of Automation Science and Engineering, South China University of Technology, Guangzhou 510641, China

Correspondence should be addressed to Huanli Gao; hlgao@scut.edu.cn

Received 13 August 2022; Accepted 23 September 2022; Published 3 October 2022

Academic Editor: Jun Ye

The predation of large school of fish by the cooperation of multiple predators of different species is one of the most marvelous scene in the sea. In this paper, we study how to drive the fish school to the surface of the sea by the cooperation of multiple predators. In particular, we have first proposed a modified Couzin model for the fish school, which, on top of the classic Couzin model, also takes into consideration the effect imposed passively by the predators. The basic idea for the driven algorithm is to drive behind the fish school to some delicate extent so that, on one hand, the fish school shall move towards the target region, and on the other hand, the fish school will not disperse and spread away. Moreover, if some fish strays away from the fish school, the predator will take actions to force it back which can greatly reduce the possibility for the fish school to split into multiple subgroups. Comprehensive simulation results are provided to validate the proposed algorithm.

1. Introduction

Collective motions of swarm systems have been widely seen in nature, such as birds migrating in formation in the sky [1, 2], fish marching in the sea [3, 4], locusts moving in swarms [5], bacteria forming colonies [6], and human gathering [7]. A common feature behind these phenomena is that the swarm of individuals exhibits a high degree of order when facing external influences, and many scientists believe that the individuals in these biological clusters might just follow simple rules based solely on neighboring information which surprisingly leads to the emergence of the global intriguing and complex swarm behaviors. These swarm behaviors show desired and inspiring properties from many aspects, such as the strong robustness in the distribution of organizational structure and the strong flexibility and adaptability to the changes of the environment with high efficiency. Over the past two decades, with the rapid development of information technology, researchers have acquired the ability to track and analyze biological clusters [8]. By collecting and analyzing the movement process of individuals in the swarm with high quality data and advanced statistical techniques, some mathematical models for the swarm movement have been established. By mimicking the behaviors of the swarm systems in nature, these mathematical models have been adopted by engineers to solve real world problems involved mostly with unmanned swarm systems [9, 10].

The pioneer works modeling swarm system behaviors can be found in Aoki [11], Huth and Wissel [12, 13], and Reynolds [14] which focus on computer simulations of the collective movement of fish schools and birds. Although the flocking motion models in these works have different implementation forms, the individuals in the swarm follow similar behavior rules, which is referred to as the "SAC" rules. Here, SAC is short for separation, alignment, and cohesion. The separation and cohesion rules require the individual spatially to avoid collision with neighboring individuals, yet stay closer to its neighbors, and the alignment rule requires the individual's motion direction to be consistent with the directions of its neighbors. The SAC rule is of fundamental significance to the study of swarm motion, which has given rise to fruitful model variants explaining

the fascinating swarming behaviors of living creatures. An important way to realize the alignment rule is called "velocity average," which requires the individual of a swarm to adjust its own speed (direction) by referring to the average speed (direction) of its surrounding neighbors so that the clusters can achieve consistent convergence of all individual motion directions. There are three classic models based on the philosophy of velocity average, namely, the Vicsek model, the social force model, and the Couzin model. The Vicsek model [15] is also known as the self-propelled particle model. The basic concepts and methods are borrowed from physics, where the individuals are treated as particles. These particles are supposed to run at a constant speed rate in a square area with periodic boundaries. Various clustering phenomena have been revealed subject to different particle densities and noise levels. In the case of high density of particles and low noise, it was found that all the particle directions of motion will synchronize from random initial state. In the social force model [16], the interaction relationship between individuals is viewed as external force from the perspective of Newtonian mechanics. The total force imposed on an individual from its surrounding neighbors is called social force, which makes the individual accelerate, decelerate, or steer, thus forming the swarm behaviors of the entire group. The Couzin model [17] takes a discrete-time form for individual kinematics, and the individuals move at a constant speed rate subject to random perturbations. In this model, the individual's perceptual area is divided into three nonoverlapping domains: the repulsive domain, the formation domain, and the attractive domain, which correspond straightforwardly to the separation rule, alignment rule, and cohesion rule, respectively. The Couzin model shows how differences between individuals affect the structure of groups, and how individuals can accurately change their spatial position within a group using simple local rules of thumb without knowing where they are. Later, in [18], Couzin defined the informed individuals, depicting those individuals that are able to perceive danger, find foraging place, or know migration routes in real-life swarms. It was shown that if there are a few number of informed individuals with clear directions of movement in the model, they can guide the movement of the entire cluster even if other individuals are unaware of their existence. Surprisingly, the larger the group is, the smaller the proportion of informed individuals is needed to lead the group. In addition, if there are two expected directions, the entire cluster will move in one or the average direction of the two while maintaining cohesive, i.e., the entire cluster can still make a unified decision even if the information transmitted by the informed individuals conflicts. In 2011, the Couzin team further reported in [19] that under a wide range of conditions, a strongly stubborn minority can determine group selection, but the presence of noninformed individuals spontaneously inhibits this process, thus giving back control to the majority, i.e., noninformed individuals can promote democratic decision-making. Besides the work done by the Couzin team, the Couzin model has been also adopted by many other researchers. For example, Dong et al. proposed a speed-adaptive Couzin cluster model based on fuzzy rules [20]. Jung et al. adopted mediation as a new shared control approach to control the influence of human groups and used mediators to shape a Couzin model-like ring domain [21].

The predation of large school of fish by the cooperation of multiple predators of different species is one of the most marvelous scene in the sea. In real life, the predators will drive the fish school to the surface of the sea before predation. As is often the case, the number of the predators is far more less than that of the fish school. Thus, it is interesting to study how to drive the fish school to the surface of the sea by the cooperation of the predators, which is the main concern of this paper. In particular, we have first proposed a modified Couzin model for the fish school, which, on top of the classic Couzin model, also takes into consideration the effect imposed passively by the predators. The basic idea for the driven algorithm is to drive behind the fish school to some delicate extent so that, on the one hand, the fish school shall move towards the target region, and on the other hand, the fish school will not disperse and spread away. Moreover, if some fish strays away from the fish school, the predator will take actions to force it back which can greatly reduce the possibility for the fish school to split into multiple subgroups. Compared with the cooperative driven problem for 2-dimensional sheep herd considered in [22], the technical difficulties are much more challenging for the cooperative driven problem considered in this paper since the fish school are moving in 3-dimensional space. In contrast to [22], the main technical contributions of this paper are as follows. First, to achieve cooperation between predators and avoid mutual interference, by projecting the fish school to the xoy plane, the fish school is divided into several groups and each predator is responsible for one group of fish. Second, to drive fish school to move towards the destination, the tail of the fish school is defined as some projection point associated with both the centers of the destination and the fish school. Third, to force the stray fish back to the fish school, an arcuate trajectory is conceived for the predator by appropriately designing a novel 3-dimensional arcuate mapping.

2. Notations

Let $\mathbb{R}$ and $\mathbb{N}$ denote the sets of real numbers and positive integers, respectively. Given $x \in \mathbb{N}$, $\underline{x} \triangleq \{y | y \in \mathbb{N}, y \leq x\}$. Given a set $\mathbb{P}$ with finite number of elements, let $\mathbf{C}(\mathbb{P})$ denotes the cardinality of the set $\mathbb{P}$. Given a point $x \in \mathbb{R}^3$ and a region $\mathbb{X} \subseteq \mathbb{R}^3$, the distance between x and $\mathbb{X}$ is defined by

$$\mathbf{d}(x, \mathbb{X}) = \inf_{y \in \mathbb{X}} ||x - y||. \tag{1}$$

In 3D space, given angle θ and rotation axis $n = (n_x, n_y, n_z)^T$, the rotation matrix $\mathbf{T}(\theta, n)$ is defined as

$$\mathbf{I}_1 = \begin{pmatrix} n_x^2(1 - \cos\theta) + \cos\theta \\ n_x n_y(1 - \cos\theta) + n_z \sin\theta \\ n_x n_z(1 - \cos\theta) - n_y \sin\theta \end{pmatrix}, \tag{2}$$

$$\mathbf{I}_2 = \begin{pmatrix} n_x n_y(1-\cos\theta) - n_z \sin\theta \\ n_y^2(1-\cos\theta) + \cos\theta \\ n_y n_z(1-\cos\theta) + n_x \sin\theta \end{pmatrix}, \quad (3)$$

$$\mathbf{I}_3 = \begin{pmatrix} n_x n_z(1-\cos\theta) + n_y \sin\theta \\ n_y n_z(1-\cos\theta) - n_x \sin\theta \\ n_z^2(1-\cos\theta) + \cos\theta \end{pmatrix}, \quad (4)$$

$$\mathbf{T}(\theta, n) = [\mathbf{I}_1, \mathbf{I}_2, \mathbf{I}_3]. \quad (5)$$

For a nonzero vector $x \in \mathbb{R}^3$, let $\mathbf{o}(x) = x/||x||$ denote the unit vector which has the same direction as x. For two nonzero vectors $x, y \in \mathbb{R}^3$, let

$$\Theta(x, y) = \arccos\left(\frac{\langle x, y\rangle}{||x|| \cdot ||y||}\right). \quad (6)$$

For nonzero vectors $x, y \in \mathbb{R}^3$, the steering angle limit function is defined by

$$\Gamma(x, y, \xi) = \begin{cases} x, & \Theta(x, y) < \xi, \\ \mathbf{T}\left(\xi, \dfrac{x \times y}{||x \times y||}\right) y, & \Theta(x, y) \geq \xi, \end{cases} \quad (7)$$

where $\xi > 0$ denotes the maximum steering angle per unit time.

For $x, y \in \mathbb{R}^3$, $||y|| \neq 0$, the projection function is defined by

$$K(x, y) = \frac{\langle x, y\rangle}{||y||}\mathbf{o}(y). \quad (8)$$

For $x, y \in \mathbb{R}^3$, $||x|| \neq 0$, $||y|| \neq 0$, the plane projection function is defined by

$$M(x, y) = x - ||x|| \cos(\Theta(x, y))y. \quad (9)$$

3. Modified Couzin Model

As shown in Figure 1, in this paper, we will study how to use two predators to drive a school of fish to a target area in 3D space. In what follows, we suppose the position and velocity vectors of all fish and predators are expressed in a common coordinate system.

Suppose the number of fish in the school is N. For $i \in \underline{N}$, the motion of fish i is described by

$$p_i(k+1) = p_i(k) + Tv_i(k), \quad (10)$$

where T denotes the sampling period, and $p_i(k), v_i(k) \in \mathbb{R}^3$ denote the position and velocity of the ith fish at the kth step, respectively.

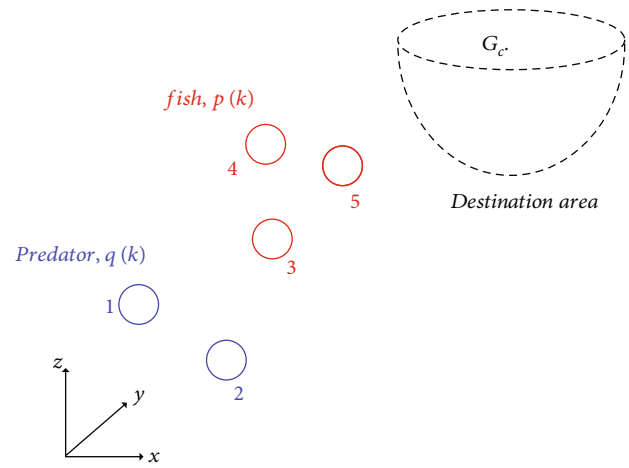

Figure 1: Task description.

Let the number N_p of predators be 2. For $i \in \underline{N_p}$, the motion of predator i is described by

$$q_i(k+1) = q_i(k) + Tu_i(k), \quad (11)$$

where $q_i(k), u_i(k) \in \mathbb{R}^3$ denote the position and velocity of the ith predator at the kth step, respectively.

To describe the relative position between different fish, for $i, j \in \underline{N}$, $i \neq j$, define

$$p_{ij}(k) = p_i(k) - p_j(k), \quad (12)$$

and between fish and predator, for $i \in \underline{N}$, $j \in \underline{N_p}$, define

$$p_{ij}^q(k) = p_i(k) - q_j(k). \quad (13)$$

For $i \in \underline{N}$, the velocity of the ith fish is given as follows

$$v_i(k+1) = \begin{cases} v\mathbf{o}\left(\Gamma\left(\mathbf{T}(\sigma_i(k), n_i(k))v_{pi}(k), v_i(k), \xi\right) + v_{qi}(k)\right), & \mathbf{o}(n_i(k)) \neq \mathbf{o}(v_{pi}(k)), \\ v\mathbf{o}\left(\Gamma\left(v_{pi}(k), v_i(k), \xi\right) + v_{qi}(k)\right), & \mathbf{o}(n_i(k)) = \mathbf{o}(v_{pi}(k)), \end{cases} \quad (14)$$

where $v > 0$ denote the speed rate for fish. $v_{pi}(k), v_{qi}(k) \in \mathbb{R}^3$ denote the effects from other fish and from predator at the kth step, respectively, which will be detailed later. $\mathbf{T}(\sigma_i(k), n_i(k))$ defined the way how the noise is imposed on the fish school. In real life, animal decision-making is affected by external disturbances, and we model this effect by rotating $v_{pi}(k)$ by an angle $\sigma_i(k)$, which satisfies $\sigma_i(k) \sim N(0, \sigma)$ and varies with time along the rotation axis $n_i(k) = (n_{ix}(k), n_{iy}(k), n_{iz}(k))^T$, which is given by

$$n_i(k) = \mathbf{o}\left(\begin{bmatrix} -1 + 2 \cdot \text{rand}\ (1) \\ -1 + 2 \cdot \text{rand}\ (1) \\ -1 + 2 \cdot \text{rand}\ (1) \end{bmatrix}\right), \quad (15)$$

with rand (1) denoting a random noise signal that is

uniformly distributed between 0 and 1. By left multiplying $v_{pi}(k)$ by $\mathbf{T}(\sigma_i(k), n_i(k))$, it means that at the kth step, $v_{pi}(k)$ takes $n_i(k)$ as the rotation axis and rotates $\sigma_i(k)$ radium counterclockwise. When a fish needs to change its direction of motion, it is usually impossible to turn 180° immediately. Therefore, we need to add a limit to the magnitude of the fish's steering angle in the model, which is realized by the function Γ in the law of (14).

For $i, j \in \underline{N}, i \neq j$, if $\Theta(v_i(k), p_{ji}(k)) > \alpha/2$, then, the jth fish is invisible to the ith fish. Otherwise, it is visible to the ith fish. Here, α determines the size of the blind area. Fish in the blind area of fish i do not have any impact on fish i. Figure 2(a) is an example used to show the definition of the blind area of fish i. Fish k (point c_k) is in the blind area of fish i, while fish j (point c_j) is outside the blind area of the fish i.

As shown in Figure 2(b), fish has blind area (blue) and three zones: the repulsive zone (zor), the directional alignment zone (zoo), and the attractive zone (zoa). We use three positive constants R_r, R_o, R_a to fine the three zones for zor, zoo, and zoa, respectively. For $i, j \in \underline{N}, i \neq j$, when fish j is outside the blind area and located at the zor zone of fish i at the kth step, fish j satisfies $j \in N_{ri}(k)$, where

$$N_{ri}(k) \triangleq \left\{ j : \left\| p_{ij}(k) \right\| < R_r, \Theta\left(v_i(k), p_{ji}(k)\right) \leq \frac{\alpha}{2}, j \in \underline{N}, j \neq i \right\}. \tag{16}$$

When fish j is outside the blind area and located at the zoo zone of fish i at the kth step, fish j satisfies $j \in N_{oi}(k)$, where

$$N_{oi}(k) \triangleq \left\{ j : R_r \leq \left\| p_{ij}(k) \right\| < R_o, \Theta\left(v_i(k), p_{ji}(k)\right) \leq \frac{\alpha}{2}, j \in \underline{N}, j \neq i \right\}. \tag{17}$$

When fish j is outside the blind area and located at the zoa zone of fish i at the kth step, fish j satisfies $j \in N_{ai}(k)s$, where

$$N_{ai}(k) \triangleq \left\{ j : R_o \leq \left\| p_{ij}(k) \right\| < R_a, \Theta\left(v_i(k), p_{ji}(k)\right) \leq \frac{\alpha}{2}, j \in \underline{N}, j \neq i \right\}. \tag{18}$$

Now, we are ready to present $v_{pi}(k)$ as follows

$$v_{pi}(k) = \begin{cases} d_{ri}(k), & N_{ri}(k) \neq \varnothing, \\ d_{oi}(k), & N_{ri}(k) = \varnothing \& N_{oi}(k) \neq \varnothing \& N_{ai}(k) = \varnothing, \\ d_{ai}(k), & N_{ri}(k) = \varnothing \& N_{oi}(k) = \varnothing \& N_{ai}(k) \neq \varnothing, \\ \frac{1}{2}(d_{oi}(k) + d_{ai}(k)), & N_{ri}(k) = \varnothing \& N_{oi}(k) \neq \varnothing \& N_{ai}(k) \neq \varnothing, \\ v_i(k), & N_{ri}(k) = \varnothing \& N_{oi}(k) = \varnothing \& N_{ai}(k) = \varnothing, \end{cases} \tag{19}$$

where $d_{ri}(k), d_{oi}(k), d_{ai}(k)$ are the influences of other neighbors located in zor, zoo, zoa on fish i at the kth step, respectively. Their corresponding mathematical expressions are as follows

$$d_{ri}(k) = -\sum_{j \in N_{ri}(k)} \mathbf{o}\left(p_{ij}(k)\right), \tag{20}$$

$$d_{oi}(k) = \sum_{j \in N_{oi}(k)} \mathbf{o}\left(v_j(k)\right), \tag{21}$$

$$d_{ai}(k) = \sum_{j \in N_{ai}(k)} \mathbf{o}\left(p_{ij}(k)\right). \tag{22}$$

The physical meanings of the cases in Equation (19) are explained as follows. Case $N_{ri}(k) \neq \varnothing$ means that a part of the fish in the fish school are too close to fish i, which will make fish i stay away from this part of the fish. Case $N_{ri}(k) = \varnothing \& N_{oi}(k) \neq \varnothing \& N_{ai}(k) = \varnothing$ means that fish i is only affected by the fish located in the zoo area, and in this case, it will adjust its speed direction to be consistent with the average speed direction of the fish in its zoo area. Case $N_{ri}(k) = \varnothing \& N_{oi}(k) = \varnothing \& N_{ai}(k) \neq \varnothing$ means that fish i is only attracted by the fish located in the zoa area, moving towards them. Case $N_{ri}(k) = \varnothing \& N_{oi}(k) \neq \varnothing \& N_{ai}(k) \neq \varnothing$ means that fish i will move towards the fish located in the zoa area while aligning as much as possible with the average speed direction of the fish located in the zoo area. Case $N_{ri}(k) = \varnothing \& N_{oi}(k) = \varnothing \& N_{ai}(k) = \varnothing$ means that there is no fish visible to fish i. At this point, fish i will keep the current state of motion. It is noteworthy that under the motion mechanism of Equation (20), fish tend not to collide with each other.

For $i \in \underline{N}, j \in \underline{N_p}$, $v_{qi}(k)$ takes the following form

$$v_{qi}(k) = \gamma \sum_{j=1}^{N_p} f_{ij}(k), \tag{23}$$

where $\gamma > 0$ denotes the strength of the effect from the predator, and $f_{ij}(k)$ denotes the repulsive force imposed by the jth predator on the ith fish at the kth step. $f_{ij}(k)$ has the following form

$$\mathrm{f}_{ij}(k) = \alpha\left(\left\| p_{ij}^q(k) \right\|\right) \mathbf{o}\left(p_{ij}^q(k)\right), \tag{24}$$

where

$$\alpha(x) = \begin{cases} 10^4, x \leq l_r, \\ \dfrac{1}{x - l_r} - \dfrac{1}{l_e - l_r}, l_r < x \leq l_e, \\ 0, l_e < x, \end{cases} \tag{25}$$

with $l_r > 0$ denoting the distance below which predators repel fish greatly between fish and predator, and l_e denoting the distance a predator starts to affect a fish. The profile of $\alpha(x)$ is shown by Figure 3 with $l_r = 5$, $l_e = 25$.

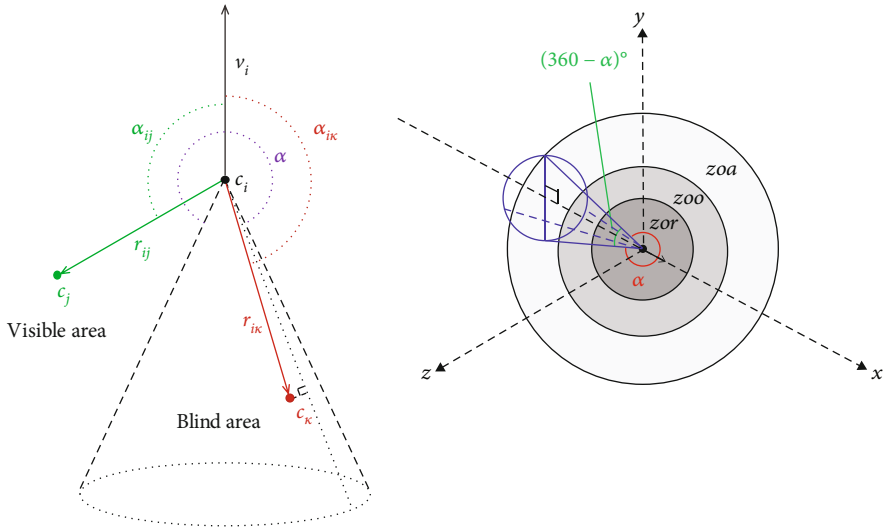

(a) The blind area of the fish (b) The blind area and three zones of the fish

FIGURE 2: The blind area and three zones of the fish.

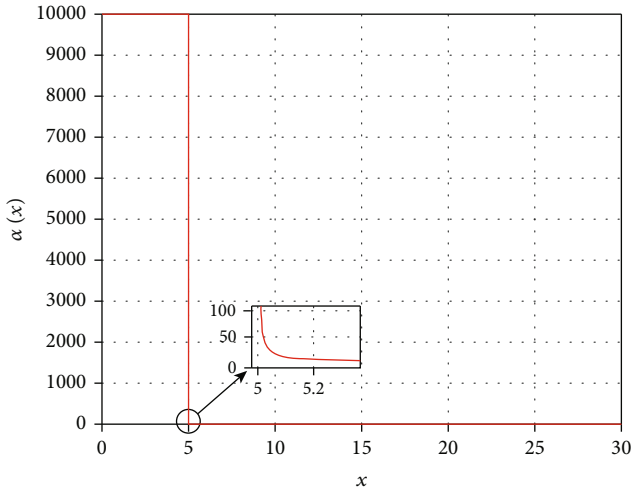

FIGURE 3: Profile of $\alpha(x)$ with $l_r = 5$, $l_e = 25$.

4. Algorithm

Given $p_{dc} \in \mathbb{R}^3$, the destination area for the fish school is defined by

$$\mathbb{P}_{dc} = \left\{ p : p \in \mathbb{R}^3, \|p - p_{dc}\| \le r_d, 0 \le \Theta\left(p - p_{dc}, [0,0,-1]^T\right) \le \frac{\pi}{2} \right\}, \tag{26}$$

where $r_d > 0$ denotes the radius of the hemisphere of the destination. It should be chosen such that the following two requirements can be simultaneously satisfied:

$$p_i \in \mathbb{P}_{dc}, \forall i \in \underline{N}, \tag{27}$$

and

$$\left\| p_i - p_j \right\| \ge R_r, \forall i, j \in \underline{N}, i \ne j. \tag{28}$$

Mathematically, the control task considered in this paper is to design $u_i(k)$ for predators such that, under the initial condition

$$\mathbf{d}(q_i(0), \mathbb{P}_{dc}) > 0, \forall i \in \underline{N_p}, \tag{29}$$

and

$$\mathbf{d}(p_i(0), \mathbb{P}_{dc}) > 0, \forall i \in \underline{N}, \tag{30}$$

for all $i \in \underline{N}$,

$$\lim_{k \longrightarrow \infty} \mathbf{d}(p_i(k), \mathbb{P}_{dc}) = 0. \tag{31}$$

Inspired by the predatory behavior of the real-world predators on fish school, we realize the spatial driving algorithm in the following way.

(1) The predator moves towards the destination at the tail of the school of fish

(2) When a fish is found out of the group, the predator drives it back to the school

Now, we will introduce the driving algorithm as follows.

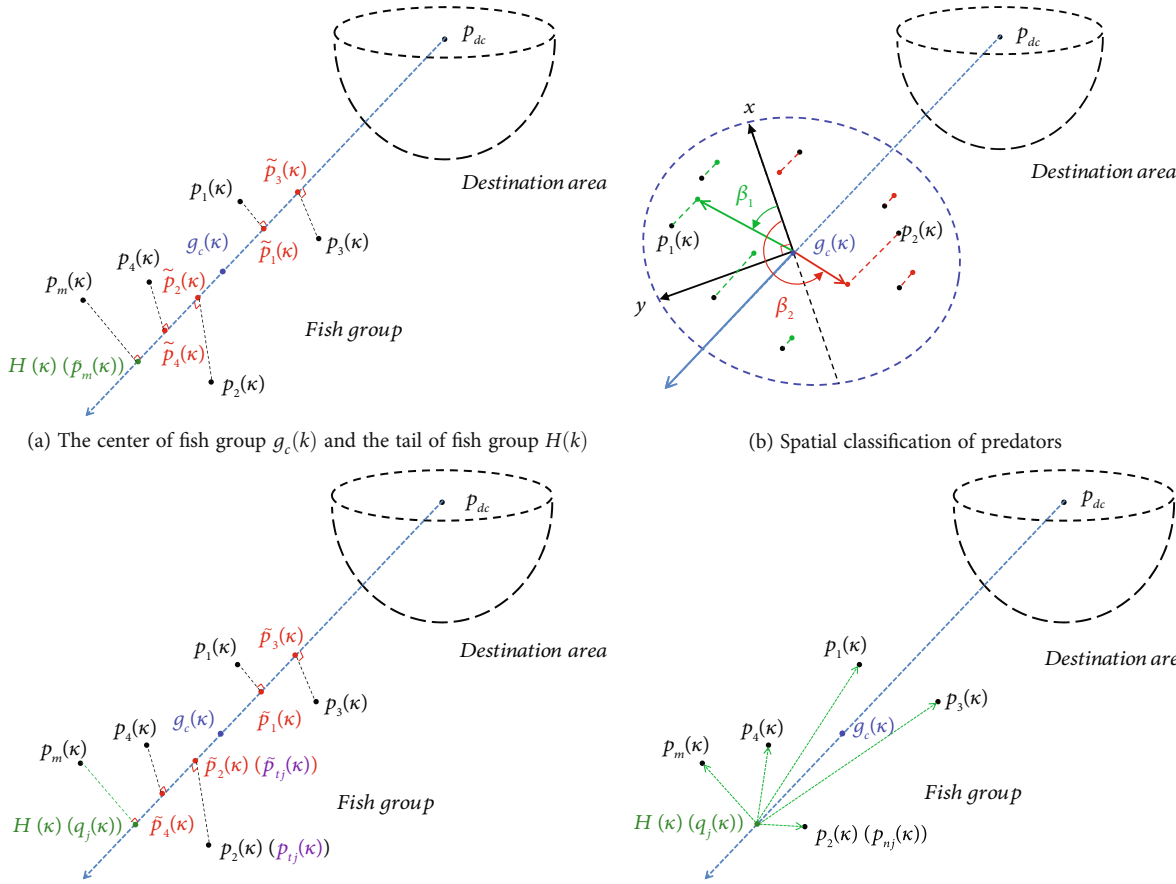

(a) The center of fish group $g_c(k)$ and the tail of fish group $H(k)$

(b) Spatial classification of predators

(c) The stray fish $p_{tj}(k)$

(d) The fish $p_{nj}(k)$ closest to predator j

FIGURE 4: Graph illustrations of the definitions.

First, we define two important points.

$$g_c(k) = \frac{1}{N}\sum_{i=1}^{N} p_i(k), \tag{32}$$

and

$$H(k) = K(p_m(k) - p_{dc}, g_c(k) - p_{dc}), \tag{33}$$

where $p_m(k)$ satisfies

$$p_m(k) = \left\{p_i(k)\colon \forall j \neq i, \text{it follows } \langle p_i(k) - p_{dc}, g_c(k) - p_{dc}\rangle \geq \left\langle p_j(k) - p_{dc}, g_c(k) - p_{dc}\right\rangle\right\}. \tag{34}$$

The points defined by (32) and (33) are called the center of fish group and the tail of fish group, respectively, which is illustrated by Figure 4(a).

Since $N_p > 1$, we will assign the task for the predators and let them cooperate to fulfill the task. Based on a common coordinate system, the fish school will be classified into several groups by the predators, and each predator will be in charge of one group in a cooperative way so that the whole fish school is under control by all the predators. Compared with the case of a single predator, the merits for the cooperation of multiple predators are fourfold. First, the workload for each predator will be reduced. Second, multiple predators can deal with larger fish school. Third, the control efficiency will be raised by multiple predators. Fourth, the success rate to fulfill the driving task is higher for the case of multiple predators.

We divide the fish school into N_p groups, and each predator is responsible for one group. For $i \in \underline{N}, j \in N_p$, the fish i for which predator j is responsible satisfies $i \in \overline{N_j}(k)$, where

$$N_j(k) \triangleq \left\{i : (j-1)\frac{2\pi}{N_p} < \Theta(M(p_i(k), p_{dc} - g_c(k)), \mathbf{o}((p_{dc} - g_c(k)) \times l(k))) \leq j\frac{2\pi}{N_p}\right\}, \tag{35}$$

where $l(k)$ denotes a vector which satisfies $\mathbf{o}(l(k)) \neq \mathbf{o}(p_{dc} - g_c(k))$, $\|l(k)\| \neq 0$ at the kth step.

As shown in Figure 4(b), the direction vector of the x-axis is $\mathbf{o}((p_{dc} - g_c(k)) \times l(k)))$. The predator decides whether to be responsible for fish i through the angle β_i between the projection of fish i on the $x - g_c(k) - y$ plane and the x-axis.

Input: $p_1(k), \cdots, p_N(k)$, $q_1(k), \cdots, q_{N_p}(k)$,
$\delta_i(k), \cdots, \delta_{N_p}(k)$.
Output: $u_1(k+1), \cdots, u_{N_p}(k+1)$,
$\delta_i(k+1), \cdots, \delta_{N_p}(k+1)$

for $(i = 1, i \le N_p, i = i + 1)$ **do**
  if $\delta_i(k) = 0 \& \|q_i(k) - K(q_i(k) - p_{dc}, g_c(k) - p_{dc})\| \le D_p$ **then**
    $\delta_i(k) = 2$.
  else
if $(\delta_i(k) = 1 \& \Theta(q_i(k) - g_c(k), p_{dc} - g_c(k)) \le \Theta_{\min}) | (\delta_i(k) = 1 \& (\Theta(p_{ti}(k) - g_c(k), p_{dc} - g_c(k)) - \Theta(q_i(k) - g_c(k), p_{dc} - g_c(k))) > \theta_{tmin})$ **then**
    $\delta_i(k) = 0$.
  else if $\delta_i(k) = 2 \& \|q_i(k) - K(q_i(k) - p_{dc}, g_c(k) - p_{dc})\| > D_p$ **then**
    $\delta_i(k) = 1$.
  if $\delta_i(k) = 0$
    $\delta_i(k+1) = 0$
    $u_i(k+1) = v_{arc}(g_c(k) - q_i(k), H(k) - q_i(k), \theta)$.
  if $\delta_i(k) = 1$ **then**
    $\delta_i(k+1) = 1$
    $u_i(k+1) = v_{arc}(g_c(k) - q_i(k), p_{ti}(k) - q_i(k), \theta)$
  if $\delta_i(k) = 2$ **then**
    $\delta_i(k+1) = 2$
    if $\|q_i(k) - p_{ni}(k)\| \le D_{np}$ **then**
      $u_i(k+1) = 0$.
  else
      $u_i(k+1) = o(p_{dc} - g_c(k))$.
return result

Algorithm 1: Predator space driven algorithm.

For $i \in \underline{N}, j \in \underline{N_p}$, the position vector $p_{tj}(k)$ of the fish that deviates most from the fish school for which predator j is responsible satisfies

$$p_{tj}(k) = \{p_i(k): i, l \in N_j(k), \forall l \neq i, \text{it follows } \|p_i(k) - K(p_i(k) - p_{dc}, g_c(k) - p_{dc})\| \ge \|p_l(k) - K(p_l(k) - p_{dc}, g_c(k) - p_{dc})\|\}. \quad (36)$$

As shown in Figure 4(c), the distance between $p_2(k)$ and its projection $\tilde{p}_2(k)$ on line $g_c(k)p_{dc}$ is the largest, and thus, $p_2(k)$ is recorded as $p_{tj}(k)$.

For $i \in \underline{N}, j \in \underline{N_p}$, the position vector $p_{nj}(k)$ of the fish that is closest to predator j satisfies

$$p_{nj}(k) = \{p_i(k): i, l \in \underline{N}, \forall l \neq i, \text{it follows} \|q_i(k) - p_i(k)\| \le \|q_i(k) - p_l(k)\|\}. \quad (37)$$

As shown in Figure 4(d), the distance between predator $q_j(k)$ and fish $p_2(k)$ is the smallest, so $p_2(k)$ is recorded as $p_{nj}(k)$.

In order for the predator to drive the stray fish back into the school, the predator needs to move towards the stray fish following an arcuate trajectory. To this end, we need to define the following velocity update function, for $x, y \in \mathbb{R}^3$, $\|x\| \neq 0$,

$$v_{arc}(x, y, \theta) = v_d \mathbf{o}(-\mathbf{o}(y - K(y, x)) \sin\theta + \mathbf{o}(x) \cos\theta), \quad (38)$$

where $v_d > 0$ is a constant.

In what follows, we let $D_p > 0$ denote the judgment condition for predator state switching, and let $D_{np} > 0$ denote the judgment condition for predator velocity updating. Moreover, for $i \in \underline{N_p}$, let $\delta_i(k)$ denote the flag bit of the state of predator i. The space driven algorithm consists of two phases as follows.

(1) Initialization

Select design parameters $r_d, \theta, v_d, D_p, D_{np}$.
Let $\delta_i(0) = 2, i \in \underline{N_p}$.
Set up upper step limit $T_{\max} > 0$.

(2) Iteration: run Algorithm 1 until k reaches $T_{\max}$ or the task objective (31) is achieved

The explanation of Algorithm 1 is as follows.

The predator has three states, where each state corresponds to a special speed update strategy. In this paper, we use $\delta_i(k), i \in \underline{N_p}$ as the status flag of the predator i at the k th step, and different values of $\delta_i(k)$ correspond to different

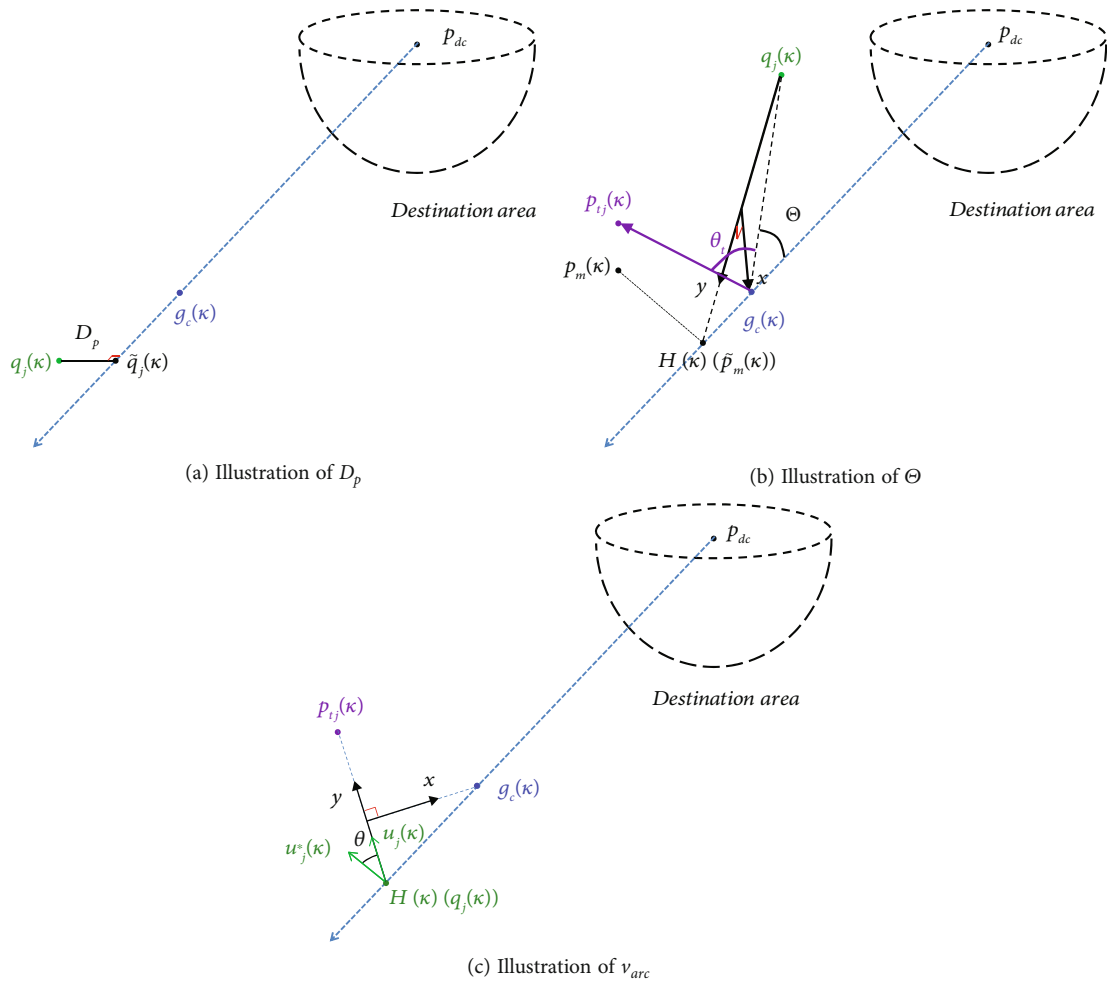

FIGURE 5: Illustration of D_p, Θ and v_{arc}.

states of the predators. $\delta_i(k)$ takes value in $0, 1, 2$. At the starting moment, that is, when $k = 0$, we set by default that $\delta_i(k) = 2$.

$\delta_i(k) = 2$ means that the predator i is near the tail $H(k)$ of the fish school and chooses to follow the fish school while keeping a certain distance D_{np} away from the fish school. In this way, the predator imposes repulsive force on the fish school to drive it to the destination area. In this state, predator i needs to first detect whether there is a fish deviating from the fish school that it is responsible for at the current moment. The detection is realized by comparing the distance of predator i to the line $g_c(k) - p_{dc}$ with a threshold $D_p > 0$. If the distance of predator i to the line $g_c(k) - p_{dc}$ is greater than D_p, the predator i should change $\delta_i(k)$ to 1. Otherwise, it maintains its current state. For example, as shown in Figure 5(a), the distance of predator j to the line $g_c(k) - p_{dc}$ is equal to D_p.

If $\delta_i(k)$ remains to be 2 after detection, predator i will update its motion as follows. Let $p_{ni}(k)$ denote the distance between the predator i and the school of fish at the kth step. If $p_{ni}(k) \le D_{np}$, in order to keep a certain distance away from the fish school, the predator i should stop moving, that is, set $u_i(k+1) = 0$. Otherwise, it should drive the fish group to the destination while moving towards the fish group, that is, set $u(k+1) = o(p_{dc} - g_c(k))$.

$\delta_i(k) = 1$ means that predator i is driving the stray fish back into the school. Before we update the velocity of the predator i, we need to determine whether the state of the predator i needs to be switched at the current moment. We judge the positional relationship between the predator and the fish school by the angle $\Theta(q_i(k) - g_c(k), p_{dc} - g_c(k))$ or the angle $\Theta(p_{ti}(k) - g_c(k), p_{dc} - g_c(k)) - \Theta(q_i(k) - g_c(k), p_{dc} - g_c(k))$. When the former is acute, it means that the predator i has moved to the front of the fish school. At this time, the predator i should set $\delta_i(k) = 0$. When the latter is greater than the threshold $\theta_{t\,\min} > 0$, it means that the predator has moved to a position where it cannot drive the stray fish back to the school. In such circumstance, the predator i also need to set $\delta_i(k) = 0$. If none of the above occurs, it maintains its current state. For example, as shown in Figure 5(b), $\Theta = \Theta(q_i(k) - g_c(k), p_{dc} - g_c(k))$ is an acute angle. It is obvious that the predator $q_j(k)$ is in front of the fish group. θ_t is $\Theta(p_{ti}(k) - g_c(k), p_{dc} - g_c(k)) - \Theta(q_i(k) - g_c(k), p_{dc} - g_c(k))$, which can be used to measure the relative position of predator j with respect to the stray fish $p_{tj}(k)$. Obviously, when Θ is too small

Table 1: The value of parameters setting for simulation experiments.

Parameter	Symbol	Unit	Value
Prey num	N	—	100
Exclusion domain	R_r	Unit length	1
Formation domain	$\Delta R_o(R_o - R_r)$	Unit length	3.6
Attraction domain	$\Delta R_a(R_a - R_o)$	Unit length	35.6
Visible area	α	Rad	$\frac{3}{2}\pi$
Maximum steering rate	ξ	Rad/s	$\frac{2}{9}\pi$
Speed of fish	v	Unit length/s	2
Speed of predator	v_d	Unit length/s	25
Turning angle	θ	Rad	$\frac{\pi}{3}$
Error angle	σ	Rad	0.05
Time increment	ΔT	s	0.1
Destination's radius	r_d	Unit length	30
Repulsive force coefficient	γ	—	0.1
Predator num	N_p	—	2
Minimum rotation angle	$\theta_{t\ \min}$	Rad	$\frac{\pi}{18}$
Minimum return angle	$\Theta_{\min}$	Rad	$\frac{\pi}{4}$

or θ_t is too large, the predator's repulsive force on the stray fish will keep it away from the school.

If $\delta_i(k)$ remains to be 1 after the above judgment, predator i updates its motion as follows. In order to drive the stray fish back into the school, we need to make the predator i move along a suitable trajectory so that the stray fish can move towards the school. To this end, we update the velocity of the predator i through the function v_{arc}, which is illustrated by Figure 3. As shown in Figure 5(c), predator j moves towards the target fish $p_{tj}(k)$. To be able to approach the fish in an arcuate trajectory, at each moment the predator j needs to turn $u_j(k) = \mathbf{o}(p_{tj}(k) - q_i(k))$ counterclockwise by θ, i.e., from $u_j(k)$ to $u_j^*(k)$. Here, $u_j^*(k)$ denotes the actual velocity of the predator j calculated by v_{arc}, which can be calculated by the following equation

$$u_j^*(k) = v_{arc}\left(g_c(k) - q_j(k), u_j(k), \theta\right). \tag{39}$$

$\delta_i(k) = 0$ means that predator i should return to the tail $H(k)$ of the fish school. Like the other two states, we need to first decide whether $\delta_i(k)$ needs to be changed. If the distance of predator i to the line $g_c(k) - p_{dc}$ is less than or equal to D_p, which means the predator i has returned to the tail of the fish school, the predator i should change $\delta_i(k)$ to 2. Otherwise, it maintains its current state. If $\delta_i(k)$ remains to 1 after the above judgment, predator i updates its motion as follows. In order not to collide with the fish and cause the fish to disperse when returning to the tail of the fish, the predator needs to move along a trajectory bypassing the fish. To do so, we update the velocity of the predator i by the function v_{arc}. We use $u_j^*(k)$ to denote the actual velocity of the predator j, which can be calculated by the following equation

$$u_j^*(k) = v_{arc}\left(g_c(k) - q_j(k), H(k) - q_j(k), \theta\right). \tag{40}$$

5. Simulation Results and Analysis

In this section, we conduct comprehensive simulation experiments to verify the algorithm and analyze the effect of different parameters value on the simulation results. The parameters γ, $\Theta_{\min}$, N_p, and $\theta_{t\ \min}$ are taken into consideration. A total of 100 tests are performed for one set of parameters. Suppose M of 100 tests are successful, i.e., the predators push the fish to the target area within the time limit.

(i) Success rate evaluation indicator is defined by

$$\Xi = \frac{M}{100}. \tag{41}$$

(ii) Consider the M successful tests. Suppose the number of task completion steps for the ith test is k_{fi}. Then,

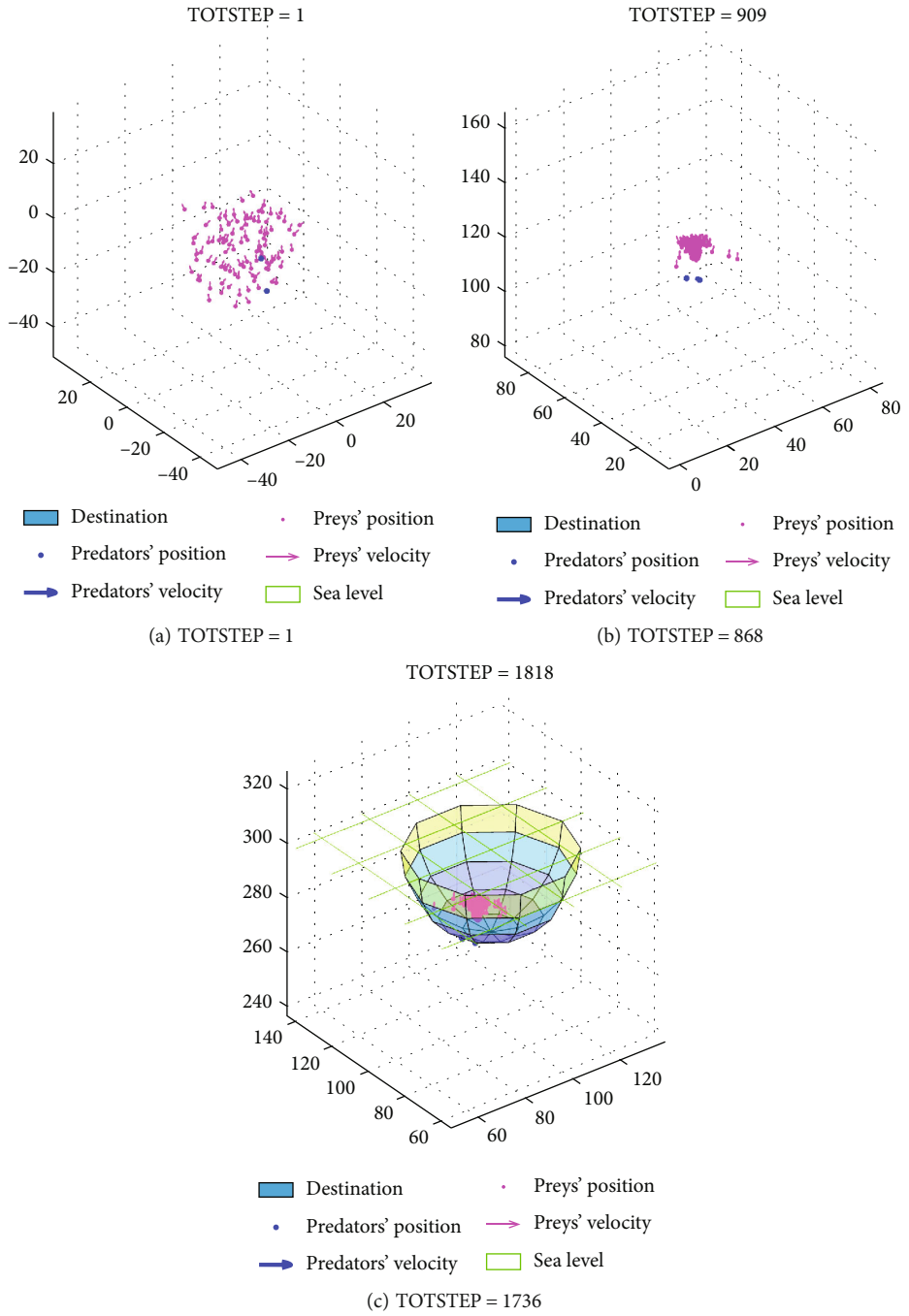

Figure 6: Three different moments showing the predators succeed in driving the fish to the target area.

the average step evaluating indicator for control efficiency is defined by

$$\Phi = \frac{\sum_{i=1}^{M} k_{fi}}{M}. \tag{42}$$

The algorithm parameters are given in Table 1, which can be classified into model parameters and control algorithm parameters. First, the model parameters are determined in the way that the fish school shall exhibit typical swarm behaviors as in nature, which in our case is the vortex movement. Once the model parameters are obtained, we will determine the control algorithm parameters by trial and error. The control algorithm parameters are finally settled down by a weighted evaluation of both the indicators of success rate and control efficiency. A whole driving process under the proposed driven algorithm is shown by Figure 6, where the fish school has been driven to the target area by the predators successfully.

In what follows, we will examine how the control parameters shall affect the performance of the algorithm. To this

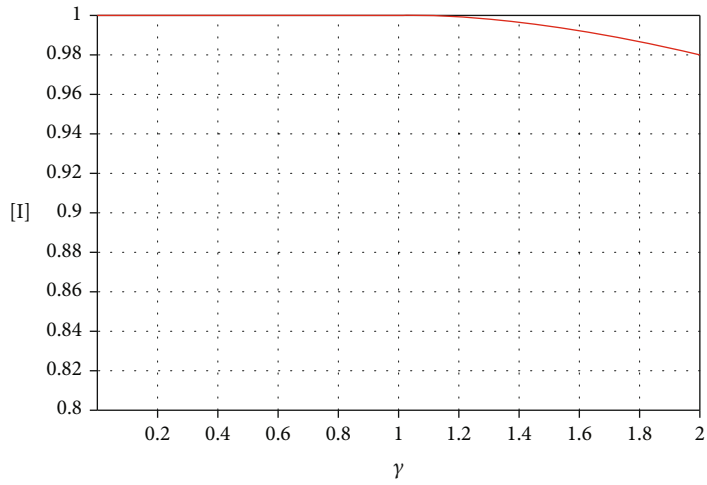

(a) The changes of Ξ with respect to γ

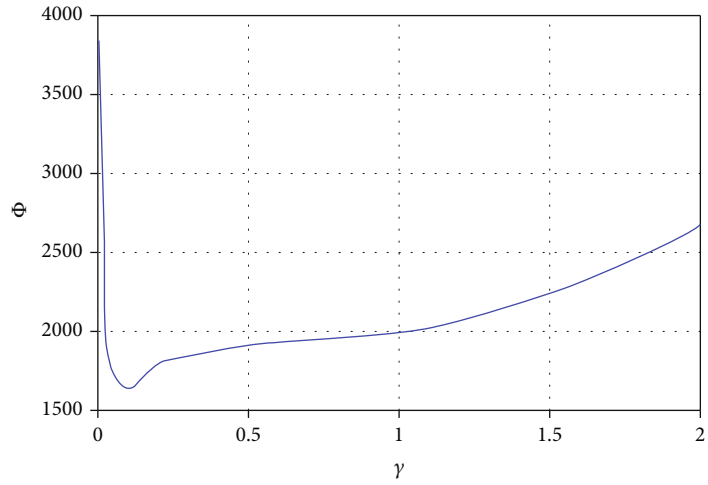

(b) The changes of Φ with respect to γ

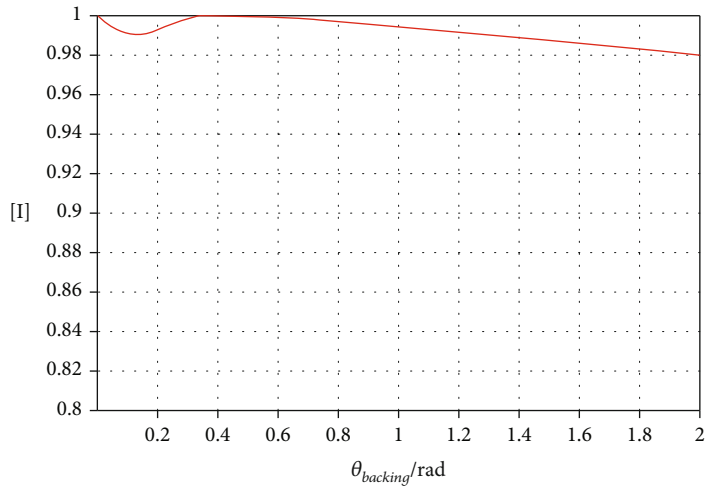

(c) The changes of Ξ with respect to $\Theta_{\min}$

Figure 7: Continued.

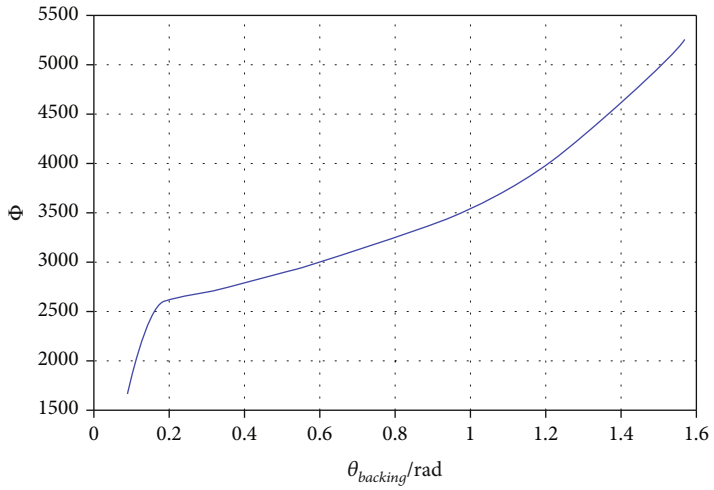

(d) The changes of Φ with respect to $\Theta_{\min}$

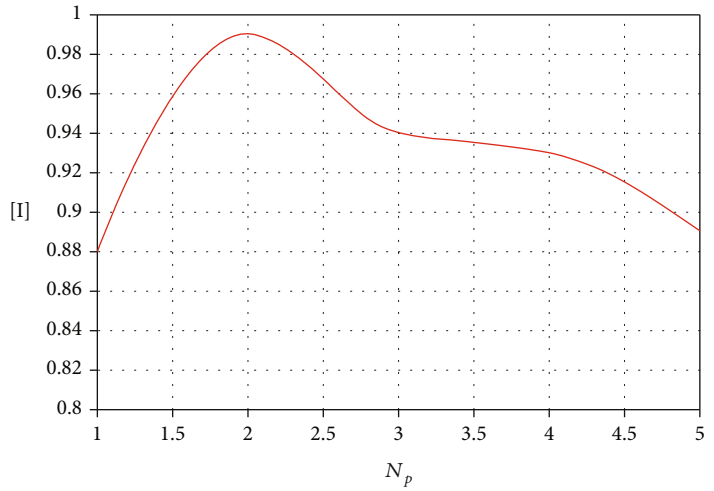

(e) The changes of Ξ with respect to N_p

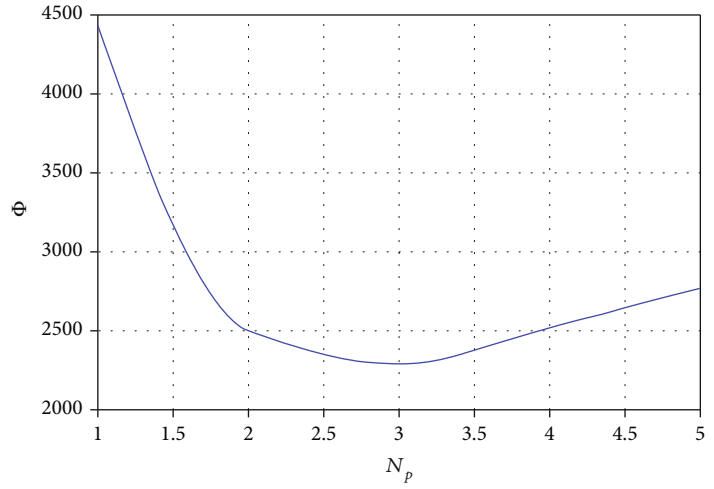

(f) The changes of Φ with respect to N_p

Figure 7: Continued.

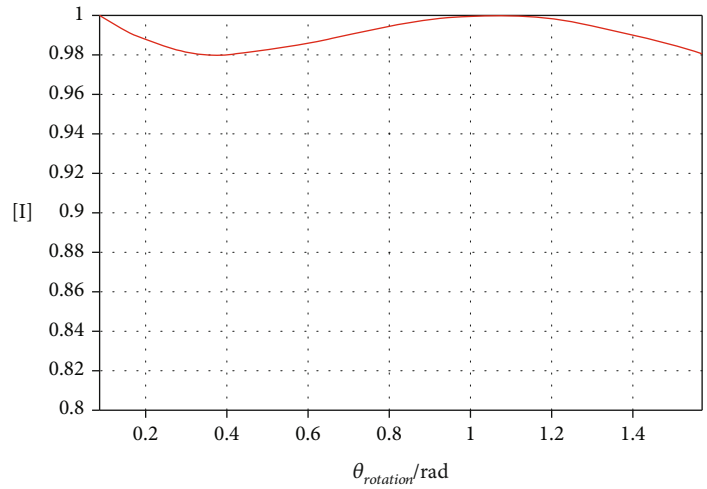

(g) The changes of Ξ with respect to $\theta_{t\ \min}$

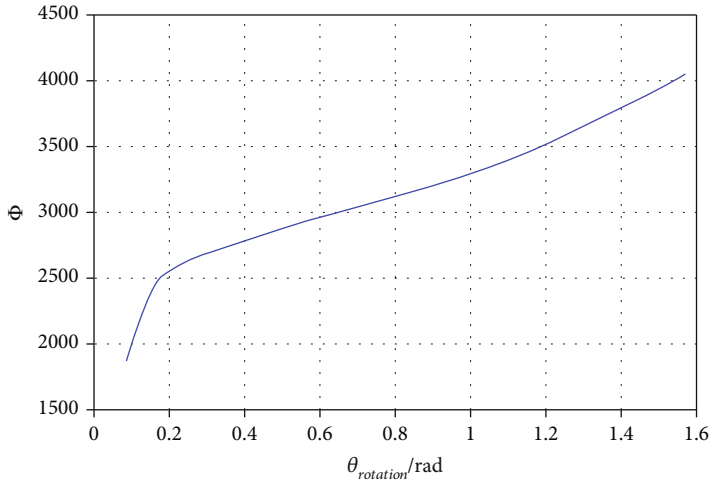

(h) The changes of Φ with respect to $\theta_{t\ \min}$

FIGURE 7: The changes of Ξ and Φ with respect to design parameters.

end, key parameters should be determined first which have significant impact on control performance. To do so, experiments are conducted in the way that for each time, and the tested control parameter varies in its allowable range with other control parameters being fixed. If the two indicators vary significantly with respect to the variation of the tested control parameter, then, the tested control parameter will be treated as a key control parameter. In this way, four key control parameters are determined by extensive experiment results in this paper, namely, γ, $\Theta_{\min}$, N_p, and $\theta_{t\ \min}$.

Figure 7 shows the profiles of the two evaluation indicators Ξ, Φ changing with respect to γ, $\Theta_{\min}$, N_p, and $\theta_{t\ \min}$, respectively. The parameter we change in Figures 7(a) and 7(b) is the repulsive force coefficient γ. When it is increased from 0.005 to 2, the success rate remains above 90%. While, when the value of the coefficient is around 0.1, there is a minimum value for the average step. On one hand, if the coefficient is too small, the fish is not sensitive to predators' repulsion force, thus resulting in a longer time to complete the task. On the other hand, if the coefficient is too large, the predators' repulsion will override the original expected velocity direction, causing some small fish to escape from the group.

As shown in Figures 7(c) and 7(d), we let the minimum return angle $\Theta_{\min}$ change from $\pi/36$ to $\pi/2$. The geometric meaning of Θ is shown in Figure 7(b). According to Figures 7(c) and 7(d), the success rate remains stable more than 98% regardless of the change of $\Theta_{\min}$. But the change of $\Theta_{\min}$ will lead to the change of average step. The larger the minimum return angle, the quicker the predator can return to the tail of the fish group. Thus, there is less time for the predator's repulsive force acting on the stray fish, making it difficult for the stray fish to return to the school, which in turn requires the predator to spend more time to drive the stray fish back to the fish school. The predator tends to force back the stray fish. However, when the angle exceeds $\Theta_{\min}$, the predator is expected to return to the tail of the fish group, causing the predator to go back and forth. This movement will change the direction of the velocity of the fish group, which will also increase the average step. It

will not end until the stray fish returns to the group. Because the area of attraction is wide enough, the stray fish may return to the group by the cohesion rule. That is why the algorithm can still have high success rates when $\Theta_{\min}$ gets larger.

As shown in Figures 7(e) and 7(f), we let predator num N_p change from 1 to 5. Note that when the number of predators is changed from 1 to 2, the success rate can reach up to more than 90%, and yet the average step is greatly reduced. In comparison with the case of a single predator, multiple predators can effectively prevent individual fish from leaving the group. In the case of a hundred fish, a suitable value for the number of predators is two or three. Note that when the number of predators reaches four or five, the average time step increases and the success rate decreases. The reason is that as the number of predators increases, the repulsive force of the predators imposed on the fish increases. Thus, the fish are more likely to spread out, and the stable motion of the fish school is violated.

As shown in Figures 7(g) and 7(h), we let the minimum rotation angle $\theta_{t\ \min}$ change from $\pi/36$ to $\pi/2$. The geometric meaning of θ_t is shown in Figure 5(b). This parameter can greatly affect the efficiency of the algorithm. The purpose of this parameter is to make the relative position between the predator and the stray fish being appropriate. When $\theta_t > \theta_{t\ \min}$, it means that the predator's repulsive force on the stray fish will drive the fish out of the group. Note that the success rate remains steady above 98% regardless of the change of $\theta_{t\ \min}$. But as the value of rotation angle gets larger, the average step increases. The underlying reason is when $\theta_{t\ \min}$ becomes larger, there will be more undesirable points on the predator's trajectory. When the predator is located at these undesirable points, the predator's repulsive force will drive the stray fish out of the group, which results in predators spending more time driving stray fish back into the school.

The proposed control algorithm is involved with many design parameters, and naturally, it is interesting to seek the best parameter combination so that the proposed control algorithm can achieve certain optimal control index. Here, we introduce a brief sketch to conduct parameter optimization. The allowable ranges for the parameters should be determined first. For each parameter, we take a few values from its allowable range, and all values of all the parameters together constitute the set of parameter combination candidates. Next, we conduct experiments with the parameters taken from this candidate set and select a few promising parameter combinations that perform well. Finally, by choosing certain parameter optimization algorithm, such as genetic algorithm or simulated annealing algorithm, we take the selected parameter combinations as the input of the parameter optimization algorithm and then get the final parameter combination that makes the best control index.

6. Conclusion

In this paper, we have studied how to drive a fish school to the destination area by the cooperation of multiple predators. First, a modified Couzin model is proposed for modeling the fish school, which, on top of the classic Couzin model, also takes into consideration the force imposed by the predators. A cooperative driven algorithm is proposed, which accomplishes the driving task through the cooperation among multiple predators. Predators first classify the fish into N_p groups, each of which is managed by a predator. Then, the predators determine their motion by detecting whether there are outliers in the school. When a stray fish is detected, the predator moves towards the fish following an arcuate trajectory. When the predator approaches some certain point, it is able to drive the stray fish back into the school. When there is no fish out of the group, the predator will move towards the destination at the tail of the fish school. Extensive simulations have been performed, which have verified the effectiveness of the algorithm. Moreover, a detailed analysis has been given discussing how the control parameters shall affect the performance of the algorithm. Since there are multiple predators, during the movement of the predators, they may impose overly large repulsion force on a small portion of the fish, which may accidentally make them deviate from the main body of the fish school to such an extent that it would be rather difficult, if possible, to drive them back to the fish school. The reason behind this phenomenon is of course complicated, involving swarm model validation, algorithm parameter selection, and algorithm mechanism design. We will further consider in our future work how to seek desired balancing between the effectiveness and efficiency of the driven algorithm.

Nomenclature

$p_i(k)$: The position of the ith fish at step k
$v_i(k)$: The velocity of the ith fish at step k
$q_i(k)$: The position of the ith predator at step k
$u_i(k)$: The velocity of the ith predator at step k
$p_{ij}(k)$: The relative position of the jth fish towards the ith fish
$p_{ij}^q(k)$: The relative position of the jth predator towards the ith fish
$v_{pi}(k)$: The effect from other fish to the ith fish at step k
$v_{qi}(k)$: The effect from predator to the ith fish at step k
$\sigma_i(k)$: The angle for introducing noise to the velocity of the ith fish
$n_i(k)$: The rotation axis in 3D space for introducing noise to the ith fish
ξ: The maximum steering rate of fish
R_r: The positive constant used to fine zor
R_o: The positive constant used to fine zoo
R_a: The positive constant used to fine zoa
α: The angle used to determine the size of the blind area of fish
$N_{ri}(k)$: The set of labels of all the fish visible to the ith fish and in zor of the ith fish at step k
$N_{oi}(k)$: The set of labels of all the fish visible to the ith fish and in zoo of the ith fish at step k
$N_{ai}(k)$: The set of labels of all the fish visible to the ith fish and in zoa of the ith fish at step k

$d_{ri}(k)$: The influence of other neighbors located in zor on fish i at the kth step
$d_{oi}(k)$: The influence of other neighbors located in zoo on fish i at the kth step
$d_{ai}(k)$: The influence of other neighbors located in zoa on fish i at the kth step
γ: The coefficient used to represent the strength of the effect from the predator
$f_{ij}(k)$: The repulsive force imposed by the jth predator on the ith fish at the kth step
l_r: The distance below which predators repel fish greatly between fish and predator
l_e: The distance a predator starts to affect a fish
p_{dc}: The center of the fish group's destination
r_d: The radius of the fish group's destination
$\mathbb{P}_{dc}$: The destination of the fish group
$g_c(k)$: The center of the fish group at step k
$H(k)$: The tail of the fish group at step k
$p_m(k)$: The position of the fish furthest from the destination in the direction from the center of the fish school to the center of the destination at step k
$N_j(k)$: The set of the labels of all the fish subject to predator j at step k
$p_{tj}(k)$: The position of the fish that deviates most from the fish school for which predator j is responsible at step k
$p_{nj}(k)$: The position of the fish that is closest to predator j at step k
D_p: The judgment condition for predator state switching
D_{np}: The judgment condition for predator velocity updating
$\delta_i(k)$: The status flag of the predator i at the kth step
θ_{tmin}: The positive constant used to compare with the angle $\Theta(p_{ti}(k) - g_c(k), p_{dc} - g_c(k)) - \Theta(q_i(k) - g_c(k), p_{dc} - g_c(k))$ to determine the state of the predator i
$\Theta_{\min}$: The positive constant used to compare with the angle $\Theta(q_i(k) - g_c(k), p_{dc} - g_c(k))$ to determine the state of the predator i.

Data Availability

The data used to support the findings of this study are available from the corresponding author upon request.

Conflicts of Interest

The authors declare that they have no conflicts of interest.

Acknowledgments

This research was funded in part by the National Natural Science Foundation of China under grant number 62173149 and 62276104 and in part by the Guangdong Natural Science Foundation under grant number 2021A1515012584 and 2022A1515011262.

References

[1] I. L. Bajec and F. H. Heppner, "Organized flight in birds," *Animal Behaviour*, vol. 78, no. 4, pp. 777–789, 2009.

[2] M. Nagy, Z. Akos, D. Biro, and T. Vicsek, "Hierarchical group dynamics in pigeon flocks," *Nature*, vol. 464, no. 7290, pp. 890–893, 2010.

[3] U. Lopez, J. Gautrais, I. D. Couzin, and G. Theraulaz, "From behavioural analyses to models of collective motion in fish schools," *Interface Focus*, vol. 2, no. 6, pp. 693–707, 2012.

[4] N. C. Makris, P. Ratilal, S. Jagannathan et al., "Critical population density triggers rapid formation of vast oceanic fish shoals," *Science*, vol. 323, no. 5922, pp. 1734–1737, 2009.

[5] J. Buhl, D. J. Sumpter, I. D. Couzin et al., "From disorder to order in marching locusts," *Science*, vol. 312, no. 5778, pp. 1402–1406, 2006.

[6] A. Sokolov, I. S. Aranson, J. O. Kessler, and R. E. Goldstein, "Concentration dependence of the collective dynamics of swimming bacteria," *Physical Review Letters*, vol. 98, no. 15, article 158102, 2007.

[7] M. Moussaid, D. Helbing, and G. Theraulaz, "How simple rules determine pedestrian behavior and crowd disasters," *Proceedings of the National Academy of Sciences*, vol. 108, no. 17, pp. 6884–6888, 2011.

[8] M. Ballerini, N. Cabibbo, R. Candelier et al., "Empirical investigation of starling flocks: a benchmark study in collective animal behaviour," *Animal Behaviour*, vol. 76, no. 1, pp. 201–215, 2008.

[9] R. Azoulay and S. Reches, "UAV flocks forming for crowded flight environments," in *Proceedings of the 11th International Conference on Agents and Artificial Intelligence - Volume 2*, pp. 154–163, Prague, Czech Republic, 2019.

[10] X. Cao, H. Sun, and G. E. Jan, "Multi-AUV cooperative target search and tracking in unknown underwater environment," *Ocean Engineering*, vol. 150, pp. 1–11, 2018.

[11] I. Aoki, "A simulation study on the schooling mechanism in fish," *Nippon Suisan Gakkaishi*, vol. 48, no. 8, pp. 1081–1088, 1982.

[12] A. Huth and C. Wissel, "The simulation of the movement of fish schools," *Journal of Theoretical Biology*, vol. 156, no. 3, pp. 365–385, 1992.

[13] A. Huth and C. Wissel, "The simulation of fish schools in comparison with experimental data," *Ecological Modelling*, vol. 75, pp. 135–146, 1994.

[14] C. W. Reynolds, "Flocks, herds and schools: a distributed behavioral model," in *Proceedings of the 14th annual conference on Computer graphics and interactive techniques*, pp. 25–34, New York, United States, 1987.

[15] T. Vicsek, A. Czirok, E. Ben-Jacob, I. Cohen, and O. Shochet, "Novel type of phase transition in a system of self-driven particles," *Physical Review Letters*, vol. 75, no. 6, pp. 1226–1229, 1995.

[16] P. Romanczuk, M. Bar, W. Ebeling, B. Lindner, and L. Schimansky-Geier, "Active Brownian particles," *The European Physical Journal Special Topics*, vol. 202, no. 1, pp. 1–162, 2012.

[17] I. D. Couzin, J. Krause, R. James, G. D. Ruxton, and N. R. Franks, "Collective memory and spatial sorting in animal groups," *Journal of Theoretical Biology*, vol. 218, no. 1, pp. 1–11, 2002.

[18] I. D. Couzin, J. Krause, N. R. Franks, and S. A. Levin, "Effective leadership and decision-making in animal groups on the move," *Nature*, vol. 433, no. 7025, pp. 513–516, 2005.

[19] I. D. Couzin, C. C. Ioannou, G. Demirel et al., "Uninformed individuals promote democratic consensus in animal groups," *Science*, vol. 334, no. 6062, pp. 1578–1580, 2011.

[20] H. Dong, Y. Zhao, and S. Gao, "A fuzzy-rule-based Couzin model," *Journal of Control Theory and Applications*, vol. 11, no. 2, pp. 311–315, 2013.

[21] S.-Y. Jung, D. S. Brown, and M. A. Goodrich, "Shaping Couzin-like torus swarms through coordinated mediation," in *2013 IEEE International Conference on Systems, Man, and Cybernetics*, pp. 1834–1839, Manchester, UK, 2013.

[22] Q. Dong, M. Jiang, X. Xu et al., "Cooperative driven algorithm for sheep herd trajectory tracking by two sheepdogs," in *2021 40th Chinese Control Conference (CCC)*, pp. 5478–5483, Shanghai, China, 2021.

Hindawi
Wireless Communications and Mobile Computing
Volume 2023, Article ID 9754794, 1 page
https://doi.org/10.1155/2023/9754794

Retraction

Retracted: Application of Rotationally Symmetrical Triangulation Stereo Vision Sensor in National Dance Movement Detection and Recognition

Wireless Communications and Mobile Computing

Received 17 October 2023; Accepted 17 October 2023; Published 18 October 2023

This article has been retracted by Hindawi following an investigation undertaken by the publisher [1]. This investigation has uncovered evidence of one or more of the following indicators of systematic manipulation of the publication process:

(1) Discrepancies in scope
(2) Discrepancies in the description of the research reported
(3) Discrepancies between the availability of data and the research described
(4) Inappropriate citations
(5) Incoherent, meaningless and/or irrelevant content included in the article
(6) Peer-review manipulation

The presence of these indicators undermines our confidence in the integrity of the article's content and we cannot, therefore, vouch for its reliability. Please note that this notice is intended solely to alert readers that the content of this article is unreliable. We have not investigated whether authors were aware of or involved in the systematic manipulation of the publication process.

Wiley and Hindawi regrets that the usual quality checks did not identify these issues before publication and have since put additional measures in place to safeguard research integrity.

We wish to credit our own Research Integrity and Research Publishing teams and anonymous and named external researchers and research integrity experts for contributing to this investigation.

The corresponding author, as the representative of all authors, has been given the opportunity to register their agreement or disagreement to this retraction. We have kept a record of any response received.

References

[1] D. Jiang, "Application of Rotationally Symmetrical Triangulation Stereo Vision Sensor in National Dance Movement Detection and Recognition," *Wireless Communications and Mobile Computing*, vol. 2022, Article ID 9032400, 12 pages, 2022.

Hindawi
Wireless Communications and Mobile Computing
Volume 2022, Article ID 9032400, 12 pages
https://doi.org/10.1155/2022/9032400

Research Article

Application of Rotationally Symmetrical Triangulation Stereo Vision Sensor in National Dance Movement Detection and Recognition

DaiLi Jiang

Academy of Music and Dance, Yulin Normal University, Yulin, Guangxi 537000, China

Correspondence should be addressed to DaiLi Jiang; xjiangdailix@ylu.edu.cn

Received 22 July 2022; Revised 30 August 2022; Accepted 3 September 2022; Published 25 September 2022

Academic Editor: Jun Ye

Information acquisition is an important branch of information science. It is the product of the development and cross-integration of traditional sensing technology and other multidisciplines. It is characterized by the high precision, high speed, integration, and intelligence of information acquisition. An important part of information acquisition, it studies how to acquire the geometric structure and scale information of objects in three-dimensional space. With the continuous development of the level, the acquisition of 3D information has become more and more important in scientific research and industrial production. This paper takes 3D information acquisition technology as the main line. From the perspectives of fusion, effectiveness, physical limit, and measurement efficiency, high-resolution 3D information acquisition techniques are studied. In this paper, the upper and lower limb movements of each behavioral segment are segmented according to the difference. An omnidirectional stereo vision sensor composed of a single camera and two secondary conical mirrors is designed, which solves the problems of large size, narrow field of view, and asynchronous image acquisition of traditional binocular vision sensors, effectively ensuring image perspective. The invariance of projection avoids image distortion caused by curved mirror imaging and reduces the difficulty of subsequent work. The three-dimensional Delaunay triangulation algorithm is used to replace the traditional Poisson reconstruction algorithm to generate the triangular mesh model. The triangular mesh model obtained by the multiview stereo reconstruction algorithm is relatively rough. This article uses Zbrush's ZRemesher and geometric-divide functions to smooth and simplify the model. The results show that the accuracy of the algorithm proposed in this paper is as high as 89.25% in the motion recognition of body elements. The dynamic mapping method is used to map the texture of the triangular mesh model, so that the realism of the model reaches 91.23%.

1. Introduction

In recent decades, with the booming of computer vision, machine learning, and artificial intelligence, machine vision-based perception and human-computer interaction technologies have been developed significantly [1]. Camera-based vision sensors, supplemented by infrared depth sensors (IR-ToF), inertial sensors (IMU), and other composite sensors have provided us with massive, multidimensional image and video data resources; the widespread use of Internet technology, especially the popularity of smart mobile devices, has further simplified the way people access visual resources [2]. In the face of massive data, how to quickly process, accurately identify, and analyze the image and video information content has become an important issue in the field of computer vision. Further, the goal of human-computer interaction technology based on computer vision is to study how to simulate human vision and the human brain's external perception, so that "machines can adapt to humans" and computers can understand human behavioral expressions. The vision-based interaction technology is aimed at using computer vision as an effective input modality in human-computer interaction to detect, locate, track, and recognize valuable behavioral visual cues in user interaction and then predict, understand, and respond to user interaction intentions, especially through the recognition of postures, gestures, and activities, to assist humans in their work

and even surpass human cognitive speed and accuracy [3]. In particular, the recognition of postures, gestures, and activities can assist human work and even surpass human cognitive speed and accuracy to achieve more efficient human-machine behavioral interaction. Among the above aspects, human pose estimation has long been an important topic in the field of intelligent human-machine interaction. Pose recognition is the basis for action and behavior recognition, and 3D human pose estimation is more complex than 2D pose estimation tasks because it introduces spatial parameter information such as depth. The 3D human pose estimation task estimates the position, rotation, and pose parameters of the human body in a camera coordinate system or world coordinate system from the input single frame or continuous image sequence; among them, the monocular camera view and RGB image input are the most urgent and valuable directions with the least constraints and the widest application scenarios.

Panoramic stereo sensing 3D measurement and 3D reconstruction is an emerging technology with great development potential and practical value, which can be widely used in many fields such as aerospace, medical treatment, robot vision, industrial inspection, intelligent transportation, mold rapid prototyping, virtual reality, geographic survey, animation film and television, and game production. Vision-based 3D reconstruction methods are divided into binocular (multivision) stereo vision method and monocular stereo vision method [4]. As an important branch of computer vision technology, vision-based 3D reconstruction technology is based on Marr's vision theoretical framework and has formed a variety of theoretical methods. For example, according to the number of cameras, it can be divided into monocular vision method, binocular vision method, and multivision method; according to the different principles, it can be divided into area-based vision method, feature-based vision method, model-based vision method, and rule-based vision method. At present, most panoramic stereo perception technologies use multivision or binocular methods (multiple cameras) to shoot the subject-object or scene from different viewpoints simultaneously or use monocular methods (single camera) to shoot the subject-object or scene from different viewpoints separately. Monocular vision-based 3D reconstruction refers to the use of a single camera to capture images for 3D reconstruction [5]. The images can use single or multiple images from a single viewpoint or multiple images from multiple viewpoints. Single point-of-view imaging can be used to obtain object depth information by analyzing two-dimensional features of the image, i.e., the X-recovery shape method. This type of method has a simple equipment structure and can achieve 3D geometric model reconstruction using a single image or a few images but requires idealized imaging and reconstruction conditions. Multiview imaging matches feature points in different images according to the relevant constraints and derives the 3D spatial coordinates according to the matching constraints to achieve 3D model reconstruction. This type of method can realize the reconstruction process camera self-calibration, suitable for large 3D scene reconstruction, when the image information is more adequate reconstruction effect is better, but the operation is complex, and the reconstruction time is longer. Use the camera shooting position and lens angle to reduce shooting errors, so as to obtain better imaging results.

China is a multiethnic country with a long history and a vast territory, and the long years have created a profound cultural accumulation, resulting in colorful and colorful folk dances, operas, and martial arts. However, some folk dances and operas are in danger of being lost due to unstable transmission methods and longevity [6]. These performing arts are valuable treasures of the Chinese nation and an important part of intangible cultural heritage, which needs to be recorded, protected, and passed down intact. The transmission of human culture relies on symbolic systems, such as words for recording language, pentameter for recording music, and dance scores for recording movements [7]. Without symbol systems, the transmission and development of culture would be constrained. With the development of artificial intelligence technology, computers can now convert a speech into words and music of a single instrument into a pentatonic score, but it is difficult for computers to convert a human movement into a dance score. The research in this paper tries to fill this technical gap by using 3D human motion capture data to generate a folk dance score, which solves the problem of computer difficulty in converting 3D human motion into a movement score, fills the absence of a movement recording method from the computer technology level, and improves the recording and transmission system of human movement.

2. Related Works

With the development of science and technology nowadays, image recording has become the most direct and common way to record. With the help of cameras, the dance movements of actors are recorded in the form of photos or videos. However, it is difficult to record the actors' dance movements in an all-around way, even with multiple cameras, and the recorded data can only be recorded from a limited angle [8]. The involvement of dance artists and performers is also required in the reproduction. The acquired data is difficult to be exploited further. If one wishes to modify the acquired data, it requires the performers to reperform it all over again, generating a large amount of work. With the application of digitalization in the field of folk dance, a technical solution for digital preservation and display of folk dance has emerged, which uses skeletal mask animation for virtual dance display based on the acquired movement data [9]. Folk dances from different regions vary greatly, with different costumes and dance forms, and even for minority dances from the same region, each dance is similar in style but also has its characteristics. However, it is difficult to show the unique flavor of folk dances through stick models or manually drawn models, which requires a three-dimensional display to describe the movements of folk dancers in sufficient detail and restore the original dance posture. According to the model analysis, the calculation method of the relevant size is given, and the structural design steps of the single-camera omnidirectional stereo vision sensor are given in combination with the influence of parameters on the accuracy.

The algorithm process for single-person pose recognition usually consists of inferring the human body detection region from the input image through the target detection network, cropping the human body region, and then finding the coordinates of the key points of the human body within the detection

region. Such problems are often based on powerful deep convolution neural networks, which use iterative convolution, pooling, or residual networks to extract two-dimensional features such as heatmap, and obtain the key point coordinates and confidence level by taking the maximum autocorrelation coordinates [10]. Single target recognition is the basis of all human pose recognition, and the method of convolutional networks regressing two-dimensional key point locations through supervised learning forms the basis of most subsequent algorithms for human pose recognition based on depth methods. The early motion segmentation methods mainly studied one or several kinematic features and used them to determine the segmentation position. Trivedi et al. proposed a segmentation algorithm based on joint space when they studied human arm motion simulation and data analysis [11]. Wang et al. proposed a method to segment motion data by detecting motion velocity changes when they studied content-based multimedia information retrieval [12].

With the rapid development of computer intelligent vision technology, the correction of wrong movements realized by image recognition can not only correct the dancer's dance posture and assist the dancer's training but also produce important value for dance technique analysis and promote the development of sports dance [13]. However, due to the complex movements of sports dance, there are many kinds of movements, and the difficulty of image recognition is high, so the image signal-to-noise ratio obtained by traditional image processing methods is low, and the visual effect is poor, which cannot meet the user's requirements for the accuracy of wrong movement recognition and make it difficult to realize comprehensive correction of dance movements. To eliminate the influence of factors such as movement speed, light intensity, and occlusion, Li et al. proposed a feature extraction-based approach to study the problem of adaptive recognition of erroneous action images [14]. Oparina et al. proposed a semidirect method of image linearity tracking matching algorithm [15]. Firstly, the important regions of the image are selected for feature point feature and linear feature matching; secondly, the motion recovery structure method is used to reconstruct the feature points; next, the linear feature point tracking and camera pose estimation are realized by using the inverse synthesis image; finally, the tracking and matching of linear feature points are completed by combining the tracking feature points, so that the points with the low matching degree can be obtained as the basis for wrong action correction.

3. Folk Dance Temporal Segmentation Algorithm for Limb Movement

Action recognition methods commonly include probabilistic statistics-based methods, model-based methods, and syntax-based methods. There are three main traditional action recognition feature extraction methods: one is based on human joint point features; the other is based on optical flow, and the third is based on spatiotemporal interest points. In addition to traditional action recognition feature extraction methods, there are also deep learning-based feature extraction methods that can be effectively applied to human action recognition. The model-based action recognition method refers to the reference model of some predefined standard actions, then compares the actions to be recognized with the standard actions, and finally realizes the classification and recognition of the actions to be recognized [16]. Based on the cooperation, we propose to first divide the limb movements into different behavior segments and then divide and conquer the upper and lower limb movements in each behavior segment based on the differences. Template matching, dynamic programing, and dynamic time warping are all specific methods of model-based action recognition. The method based on the human joint point feature is based on the principle that the skeletal structure determines the human motion, and the motion is tracked and analyzed by the change of joint point, which is not disturbed by environmental factors but ignores some flexible changes of muscle or shape will make the motion recognition produce a great error, as shown in Figure 1.

The current recognition of human action is currently divided into two main technologies based on computer vision images and based on wearable devices according to the way the recognition system works. Action recognition based on sequential data can be divided into offline action recognition and online action recognition according to the output method of action tags. Online action recognition has sequential and real-time nature compared to offline action recognition. Most of the motion recognition used nowadays in the fields of animation, gait analysis, biomechanics, ergonomics, etc. can be extended to motion capture technology or dynamic capture technology. Motion capture can be subdivided into real-time and non-real-time capture from the perspective of real-time.

$$\begin{aligned} \left\| E^{t+1} - 2XC^t + X^2 \right\| &\le \delta_1, \\ u^{t+1} &= \max\left(\alpha_{\min}, \delta \mathrm{u}^t\right). \end{aligned} \tag{1}$$

After obtaining the upper and lower limb element movements through motion segmentation, the focus of analysis and recognition is to judge their Laban symbols, i.e., to determine the time, corresponding body part, and direction of the movements. The action time can be determined by the number of frames of motion capture data, the corresponding body parts can be determined by the corresponding nodes in the human skeleton model, and the action direction needs to be judged separately for the different nature of upper and lower limb actions in terms of Laban direction category. The goal of human-computer interaction technology based on computer vision is to study how to simulate human vision and the external perception of the human brain, so that "machines can adapt to humans" and computers can understand human behavioral expressions. For the same human action, after motion capture device acquisition, different human skeleton scale information and different human orientation angle information will cause the difference in motion data, so the normalized node 3D coordinates and Li group features based on human skeleton topology are used to represent the motion data to eliminate the influence of different scales and angles on the data.

For the upper limb movements, its analysis and recognition need to focus on the characteristics of the final gesture, from the rule-based perspective, we propose to use normalized coordinates to calculate the limb vector features to recognize

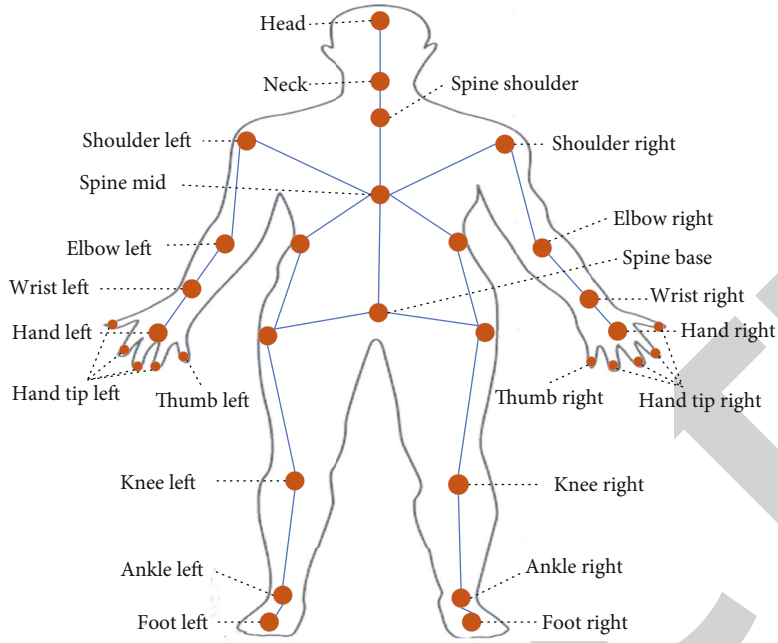

Figure 1: Action recognition method based on human joint point features.

the movements through the folk dance space division method, and from the neural network-based perspective, we propose to use the Li group features to recognize the movements through the subsample aggregation limit learning network and then get the recognition results of the upper limb movements through the strategy fusion to generate the upper limb dance spectrum [17]. For the lower limb movements, since their analysis and recognition need to focus on the moving process, to make full use of the temporal and spatial information in the motion sequences, we propose to recognize the movements with skeletal features through a two-way gated recurrent unit neural network, to recognize the movements with Li group features through a Li group network, and then to combine the advantages of the two neural networks to obtain the recognition results of the lower limb movements through network fusion and generate the lower limb dance score.

$$p(x|\theta) = \sum_{k=1}^{n} \frac{\beta k}{\alpha \phi(x|\theta k)}. \quad (2)$$

To validate the proposed method, the datasets used in this chapter include three self-collected datasets (datasets X, Y, and Z) and the Mocap dataset, each of which is briefly described below.

Dataset X: upper limb elemental action dataset. It contains 462 elemental actions, 228 for the left arm and 234 for the right arm, which is manually segmented and labeled with categories. The number of frames per elemental action is about 200, and each of the left arm and right arm contains 10 common categories.

Dataset Y: lower limb elemental action dataset. It contains 21085 elemental movements, which are manually segmented and labeled with categories. Both the left and right legs contain 48 categories, including 8 horizontal and 6 vertical categories. Each category contains 400 elemental actions, and the number of frames of elemental actions ranges from 95 to 200 frames.

Dataset Z: Continuous limb movement dataset. It includes 122 continuous movements of walking gait (vertical and horizontal change of center of gravity), jumping gait, and arm swing, covering most of the basic limb movements.

Mocap dataset: a behavioral (continuous limb movement) motion capture dataset. It contains a variety of behaviors such as walking up steps, moving from sitting to standing, cleaning windows, and throwing punches. The data was recorded with the cooperation of 152 volunteers. The signal is processed by a computer to obtain the spatial position information of different objects (trackers) on different time measurement units.

A motion capture system is a device used to accurately measure the motion of a moving object in a three-dimensional space. It records the motion of a moving object (tracker) in the form of a signal utilizing capture devices arranged in space and then uses a computer to process the signal to obtain information about the spatial position of different objects (trackers) on different units of time measurement. A complete motion capture system consists of roughly the following components: sensors, signal capture equipment, data transmission equipment, data processing equipment, etc. In this paper, the equipment used to capture dynamic arts such as folk dance, opera, and martial arts belongs to the optical motion capture OptiTrack-marked motion capture system. The operation flow of the OptiTrack motion capture system is shown in Figure 2. The motion capture system requires camera calibration first, using dynamic and static calibration rods to determine the camera's internal (focal length, optical center) and external (position and orientation in 3D physical space) parameters [18]. Then

comes the model initialization, OptiTrack optical motion capture pastes passive reflective marker points on key parts of the human body, detects and tracks the marker points using multiple cameras, and solves the spatial position of the marker points by stereo vision technology, to obtain the motion data of human joints in physical space. Then the motion capture process starts, and the system records the complete human motion trajectory. Finally, the motion capture data in BVH (Biovision Hierarchy) format is output.

In a segment of 3D human motion capture data, a series of continuous folk dance element movements are included. The main task of this chapter is to slice and dice the human body motion to get the limb element movements and prepare for the subsequent element movement recognition. Since the upper and lower limb movements are synergistic, and the upper and lower limb movements are different in the folk dance analysis due to their relationship with the center of gravity of the human body, we propose to segment the limb movements into different behavioral segments and then divide and conquer the upper and lower limb movements in each behavioral segment based on the differences [19]. In the behavior segmentation, this chapter adopts the subspace clustering algorithm based on the regular constraint of the elastic net to segment the limb behavior segments by using the association between adjacent frames of temporal data. In the action segmentation of folk dance elements, the difference between upper and lower limb actions is that the analysis of upper limbs generally does not consider the body's center of gravity, while the analysis of lower limbs focuses on the center of gravity movement process. Therefore, a segmentation method based on a combination of rate threshold and region division without considering the center of gravity is proposed for the upper limb movements, and a segmentation method based on the directional cut of the center of gravity movement and Gaussian mixture model is proposed for the lower limb movements.

4. Folk Dance Movement Recognition Based on Single-Camera Omnidirectional Stereo Vision

The single-camera omnidirectional stereo vision sensor measurement system mainly consists of a computer, image acquisition card, camera, and quadratic cone reflector optical system. The quadrilateral reflector optical system is two quadrilateral reflectors placed on the top and bottom, coaxially, the upper quadrilateral eliminates the top, covered with a rectangular plane mirror, the lower quadrilateral hollows without a top, and the center of the camera and the optical axis are perpendicular to the upper and lower planes [20]. Center camera O forms virtual camera A by oblique imaging of upper prism, virtual camera B by plane imaging of upper prism, and virtual camera C by secondary imaging of lower prism One shot can get a pair of images with parallax, which is equivalent to virtual cameras A and C shooting from different directions. Like the traditional binocular vision principle, the use of space points in a pair of virtual camera image plane imaging coordinates can be derived from the three-dimensional coordinates of space points to achieve the function of binocular vision measurement. Since the quadrilateral prism reflector optical system is completely symmetrical in four horizontal directions, it can constitute four pairs of virtual cameras, thus realizing binocular measurement in each horizontal direction. Pose recognition is the basis of action and behavior recognition, and 3D human pose estimation is more complicated than 2D pose estimation because it introduces spatial parameter information such as depth.

Four prismatic reflectors optical system imaging is more complex; the upper and lower prism size, bevel angle, relative distance, and camera installation position directly affect the sensor field of view range, working distance, measurement accuracy, size, and other key indicators. The upper and lower prism size and bevel angle and the scope of the public field of view, shape, and measurement distance are closely related, and inappropriate parameter settings may lead to an insufficient field of view or no public field of view; upper and lower prism relative distance directly affects the baseline distance and sensor volume, inappropriate distance will lead to reduced accuracy, and the sensor structure is large and redundant; camera installation position affects the proportion of the imaging area reasonably [21]. The reasonable placement of the camera can make the field of view increased and the measurement accuracy improved. The size of each structure of the quadrilateral cone reflector optical system is the key to the sensor design. At the same time, the measurement accuracy as an important performance index of the sensor design plays a key role in influencing the parameter configuration. The calculation method of relevant dimensions is given according to the model analysis, and the structural design steps of the single-camera omnidirectional stereo vision sensor are given in combination with the influence of parameters on the accuracy.

The method of recovering depth information by using monocular images, i.e., taking various cues in a single or multiple images using only a single camera in a fixed position, is called the monocular image method. This method is often referred to as "getting shape from X" or "recovering shape from X," where X can represent light changes, light and dark, contours, and textures. The method of using light variations is called photometric stereology. The orientation of the target surface in a scene can be recovered using images acquired under a range of different lighting conditions. The images with different illumination can be obtained by shifting the light source, which is the light shift to recover the surface orientation. The method is characterized by its simplicity of implementation but requires controlled illumination. The orientation of the target surface corresponding to the given pixel can be determined by creating a lookup table using a correction target of a known shape. The method of using light and dark is called the recovering shape from light and dark method. When an object in a scene is illuminated by light, it will appear to have different luminance due to the different orientations of various parts of the surface. This spatial variation in luminance is manifested in the image after imaging as changes in brightness and darkness on the image, which are closely related to the orientation of various parts of the object's surface. By establishing the image brightness constraint equation, the grayscale of the pixel can be associated with the orientation, so it is possible to

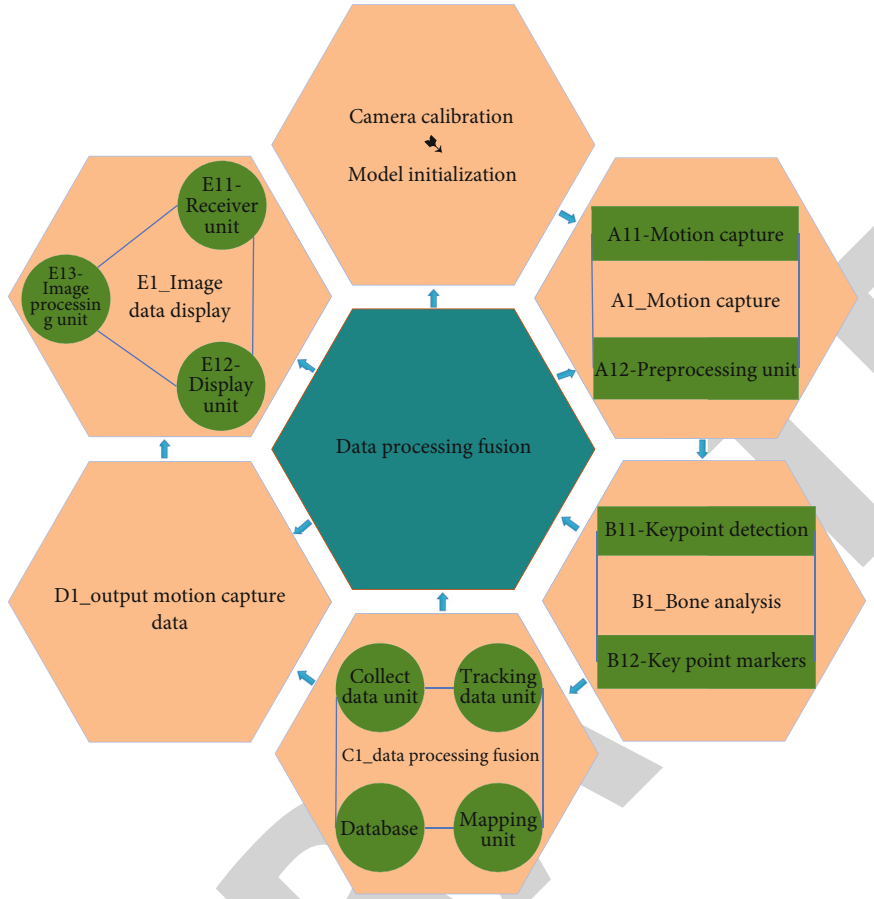

Figure 2: Motion capture system operation flow.

solve the image brightness constraint equation to obtain the orientation of the target surface.

$$p = \begin{Bmatrix} 0 & 1 & 0 \\ 0 & 0 & \lambda \\ 1 & \frac{1}{\lambda} & 0 \end{Bmatrix}. \tag{3}$$

According to the number of cameras, it can be divided into monocular vision method, binocular vision method, polycule vision method, rule-based visual methods, and more. With the advancement of technology, image sequences and video images have been widely used. The addition of temporal coordinates allows one to obtain information about motion from them, and the depth of the stereoscopic scene is further obtained by the motion information of the target. In recent years, optical flow has also been used in techniques for image processing and navigation control, including motion detection, image segmentation, calculation of focus, luminance, motion-compensated coding, and stereo parallax measurement. Motion estimation is a major aspect of optical flow research. Although optical flow fields are superficially like the dense motion fields derived from motion estimation, optical flow not only is a study of optical flow field determination but also can be applied to estimate three-dimensional properties and scene structure. In deriving the scene structure, the changes in the image are first represented by optical flow, and then the optical flow is used to derive the three-dimensional structure and motion of the object. However, the optical flow method has some drawbacks, for example, sometimes optical flow may be observed even if no motion occurs because of changes in illumination conditions, and in regions lacking changes in gray levels, actual motion is often not observed.

$$\begin{Bmatrix} u \\ 1 \\ v \end{Bmatrix} = \begin{bmatrix} x & 1 \\ y & 1 \end{bmatrix} \begin{bmatrix} s_x & 0 & C_x \\ 1 & s_y & 0 \\ C_x & 0 & 1 \end{bmatrix}, \tag{4}$$

where s_x is the distance between adjacent pixels in the horizontal direction of the image sensor, s_y is the distance between adjacent pixels in the vertical direction of the image sensor, and (c_x, c_y) is the coordinates of the principal point of the image.

$$\begin{bmatrix} x_c \\ y_c \\ z_c \\ 1 \end{bmatrix} = \begin{bmatrix} R & T \\ 0^T & 1 \end{bmatrix} \begin{bmatrix} x_w \\ y_w \\ z_w \\ 1 \end{bmatrix}. \tag{5}$$

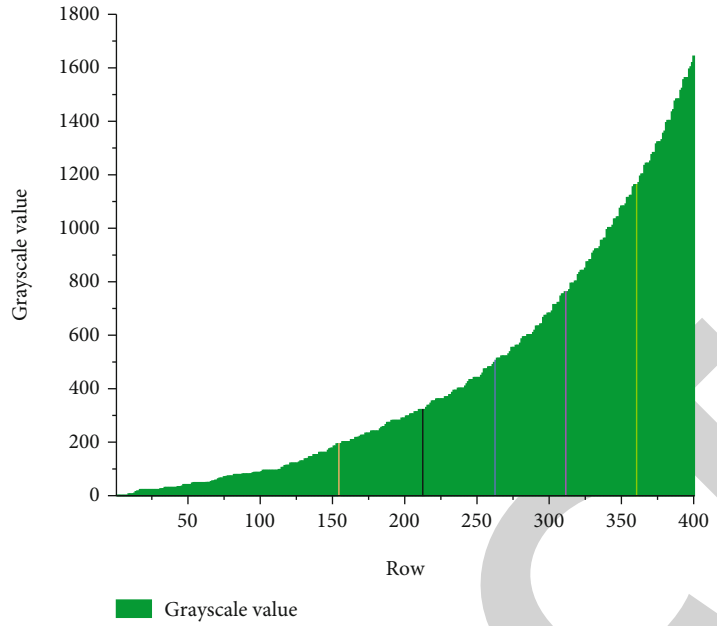

Figure 3: Schematic diagram of the grayscale distribution of the image.

The core part of the laser vision sensor is the camera, and according to the different chip types, there are CCD cameras and CMOS cameras; CCD cameras use the photoelectric effect to convert optical signals into analog current signals and get digital images through signal amplification and analog-to-digital conversion processing; CMOS cameras are based on the complementary effect to get analog current signals and get digital images through signal amplification and analog-to-digital conversion processing. The CMOS camera is based on the complementary effect to obtain the analog current signal, and the digital image is obtained through signal amplification and analog-to-digital conversion. The size of a frame acquired by the camera in real-time in the laser vision sensor is 640×480, and it is known from the image acquired without a filter that the image acquired without a filter often contains a lot of noise information; the filter filters out the noise and the gray value of some pixel points in the image acquired with a filter is less than 255. It is necessary to use an image preprocessing algorithm to enhance the contrast of the image so that the gray value of the pixel points in the stripe area and the background area in the image is less than 255. The difference between the gray value of the pixels in the stripe area and the background area is more obvious as shown in Figure 3. The commonly used image enhancement algorithms include histogram equalization, gamma transform, Laplace transform, and gray stretching algorithms.

Pixel points of each region are counted, the overlapping and nonoverlapping regions between the projection map and the original segmentation map of each view are compared, and the error rate is calculated according to max {pixel points of the region present in the original map only, pixel points of the region present in the projection only}/common region pixel points, and the error test method 2 is to compare the intercept lengths in each direction of the projection and the original view. Using the original segmentation and projection listed in the data, the intercept length through the center point on each angle of the projection is calculated using the center as the reference, and the intercept length through the center point on each angle of the original segmentation is also calculated. Conditions requiring imaging and reconstruction are ideal. Multiview imaging matches feature points in different images according to relevant constraints and derives three-dimensional space coordinates according to the matching constraints. For each angle of the projection and original segmentation in each view direction, the error rate is calculated at $(|W_S - W_0|)/W_0$, W_S is the intercept length of the current projection at the current angle, and W_0 is the intercept length of the current original segmentation at the current angle. The average of the errors over the 180 directions is used as the average error in the final view direction. Calculate the intercept length in each direction through the center point. Iterate over the pixel points, and calculate the angle $t = \text{arccot}\,(y/x)$ based on the pixel point (x, y) relative to the center point. The angular errors are collated to obtain the angular error data for each view, as shown in Figure 4.

In the analysis of the data obtained from the above experiments, the test error with both methods shows that the rear-view error is relatively large. Ideally, the main- and rear-view contours should be vertically symmetrical according to the mirror, so the error can be reduced by adjusting the placement angle of the object under test, the camera shooting position, and the lens angle to reduce the shooting error, to get a better imaging effect. During the experiment, we also found that due to the reflection of light from the surface of the object, sometimes the noise generated in the binarization of the initial image is larger, and for this influencing factor, we obtained a better reconstruction effect by adjusting the light source and the threshold value. The subsequent need to further improve

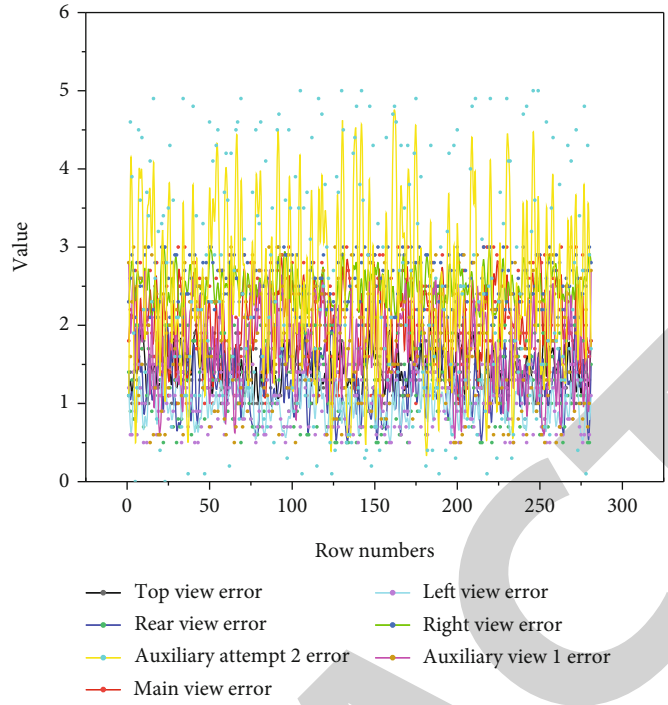

Figure 4: Statistical results of error data for each viewpoint.

the accuracy of the device, while reducing environmental interference, is to improve the accuracy of foreground extraction and reduce reconstruction errors.

5. Simulation Experimental Data Analysis and Results

This paper takes the Dai peacock dance as an example. In the process of 3D dance digitization, the dancers' peacock movements such as running down the hill, walking in the forest, drinking water, chasing, playing, dragging wings, sunning wings, spreading wings, shaking wings, shining wings, pointing water, stomping branches, resting branches, opening screen, and flying are captured. Through the modeling software, the character model is created in 3D Studio Max according to the actual body proportions of the dancers, while the data of the task model is restored according to the Dai dance costume, and then the 3D data is bound to the data of the character model so that the dance can be restored. Compare the action to be recognized with the standard action, and finally realize the classification and recognition of the action to be recognized. Model matching, dynamic programming, and dynamic spatiotemporal warping are all specific methods for model-based action recognition.

For the validity of partial hierarchical semantic segmentation, when there is a limb self-obscuring situation, the semantic segmentation based only on the whole body contour or only on the 2D key point annotation cannot escape from the multivalue ambiguity dilemma; because the self-obscuring relationship between limbs is shown, this part of depth information can be used to guide the geometric model to produce correct parameter results during segmentation supervision or optimization, and the geometric model can correctly distinguish the arm. The geometric model can correctly distinguish the anterior-posterior relationship and thus obtain the correct 3D pose parameters. Considering that the EllipBody model has fewer triangular facets compared to the SMPL model, it also has the advantage of faster forward time. In the test results of the LSP dataset, the EllipBody model with surface subdivision from 0 to 4 times has a 4×4 growth in the number of facets, and the forward time eventually exceeds that of the SMPL model; the EllipBody model already has a higher prediction accuracy of human semantic segmentation than the SMPL model with a smaller number of facets; as the number of surface subdivision increases, the accuracy converges. The reason for this convergence is that when the projection resolution of individual slices in the rendering pipeline is lower than the minimum pixel size of 256×256 required as input to the network, the additional surface subdivision will no longer have a positive effect on improving segmentation prediction accuracy, as shown in Figure 5, i.e., a diminishing marginal effect.

Compared with offline action recognition, online action recognition is sequential and real-time. Most of the motion recognition currently used can be extended to motion capture technology or motion capture technology in the fields of animation, gait analysis, biomechanics, and ergonomics. The premise of extracting the centerline of the ROI region is to extract the ROI region from the image. The commonly used algorithms for extracting ROI region are threshold method, watershed segmentation method, K-means clustering method, and edge detection method. In this subsection, the edge detection algorithm is used to extract the ROI region from the acquired image after grayscale stretching and to reject the pixel points with a grayscale value less than K in the image, $f(\mathrm{m}, \mathrm{n})$. The gradient operators are Laplacian, Roberts, Sobel, and Scharr. This subsection uses the

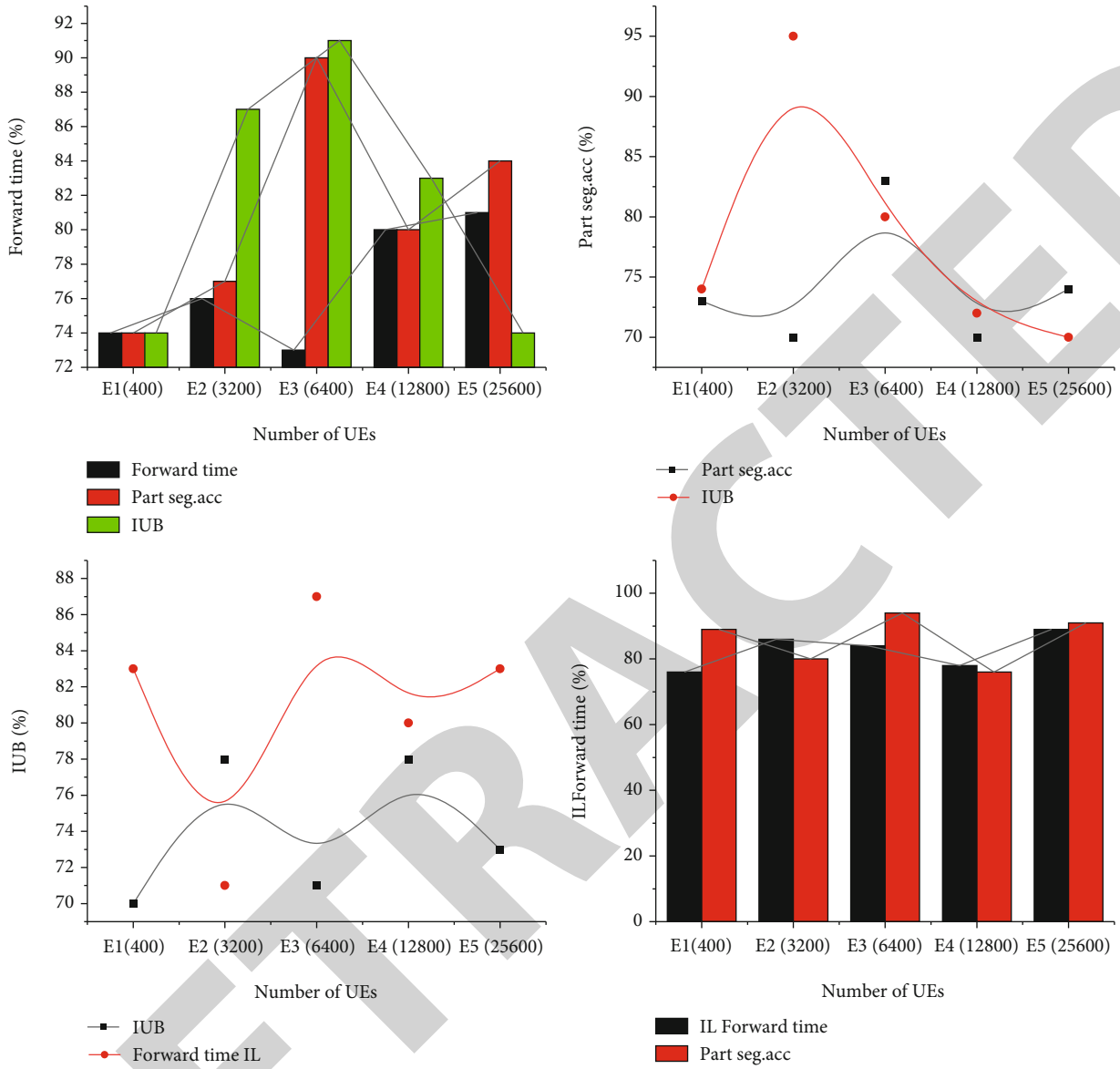

Figure 5: Model performance comparison results.

Scharr operator to obtain the horizontal and vertical derivatives of the acquired image after grayscale stretching. From the gradient magnitude and column distribution images of the grayscale stretched acquisition image, it is known that there is more noise in the gradient magnitude image. The noise in the gradient magnitude image needs to be removed using the filtering algorithm. This subsection uses the Gaussian filtering algorithm to deal with the noise in the gradient amplitude image and sets the template window size to 7×7 and the standard deviation to 3. The Gaussian filtering algorithm can effectively remove the noise in the gradient amplitude image, but the edge of the stripes in the gradient amplitude image is relatively coarse after Gaussian filtering. Then the nonmaximum suppression algorithm is used to refine the streak edges in the Gaussian filtered gradient magnitude image, and the refined edge image is shown in Figure 6.

From Figure 6, there are pixel points with relatively small gradient amplitude in column 202 of the refined stripe edge image, which is not conducive to the selection of stripe edges. Then the threshold method is used to suppress the pixel points with small gradient amplitude in the refined stripe edge image to obtain the actual stripe edge image. Since there are more than two extreme points of gradient amplitude in each column of the actual stripe edge image, we obtain the location of extreme points in each column of the actual stripe edge image by using the extreme value search algorithm, taking the location of the first extreme point in each column of the actual stripe edge image as the upper boundary value of each column, take the location of the last extreme point in each column of the actual stripe edge image as the lower boundary value of each column, and calculate the width value of each column of the actual stripe. The width of each column is calculated. The movement direction needs to be judged according to the different nature of the upper and lower limb movements. For the same human action, different human skeleton scale information and different human body orientation angle

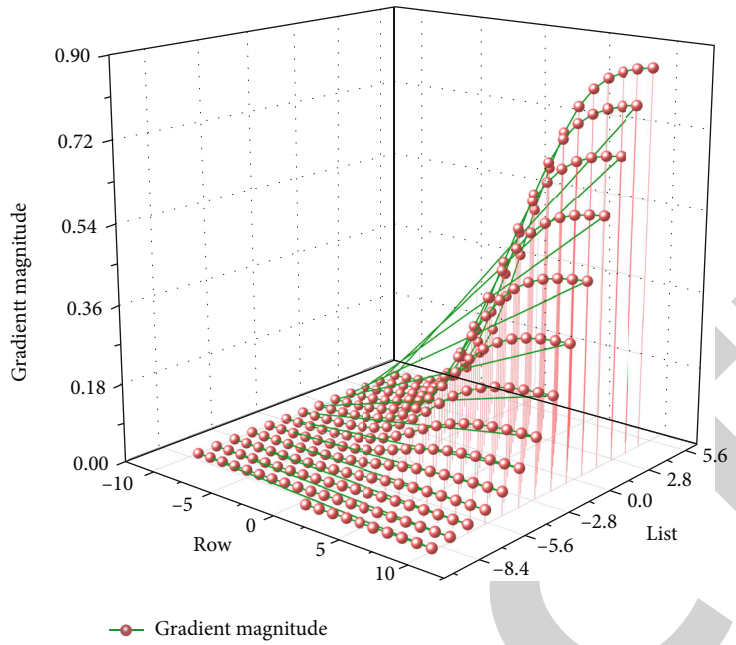

Figure 6: Distribution of gradient amplitude.

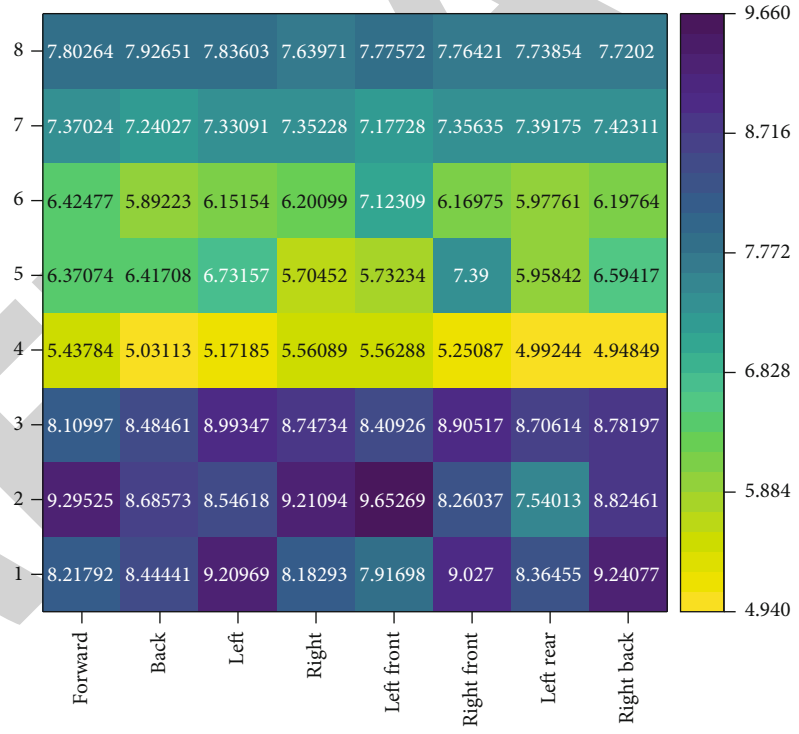

Figure 7: Confusion matrix of 8 horizontal and 3 vertical levels in support action recognition.

information will cause differences in motion data after being collected by motion capture equipment.

The results were based on data set B. The recognition accuracy of 8 types of actions and 3 types of actions in the vertical direction "low," "medium," and "high" was calculated separately, considering that the number of each type of action in the data set Y. The number of actions in the horizontal direction is 3,200, and the number of actions in the vertical direction is 6,400, so we further counted the wrong score in case of recognition errors, and the corresponding confusion matrix is shown in Figure 7. The accuracy rate of action recognition in the vertical direction is higher than that in the horizontal direction. The reason is that the number of categories in the vertical direction is smaller and the

distance between classes is larger, which is easier to distinguish; while the number of categories in the horizontal direction is larger and the distance between classes is smaller, the actions are easy to appear at the category boundaries confusing. In the horizontal direction, for the action categories that are easy to make accurate judgments and easy to correct by eye, such as "front," "left," and "right," people are less likely to be confused when doing such actions. The probability of confusion is low, the movement data are mostly clear, and the recognition accuracy is higher in the horizontal direction; while the clarity of the movements in the categories of "left front" and "right front" is slightly lower, and the probability of deviation is higher than that of "front" and "left," "left" and "right," and the recognition accuracy decreases; for "back," "left-back for the back," "left-back," and "right back" directions, the eyes have little correction effect, which makes the probability of deviations in the movements increase and makes them more likely to be ambiguous and unclear, so the recognition accuracy rate is lower in the horizontal direction. In the vertical direction, the movements are easier to distinguish, and the error tolerance rate is relatively high, so the overall recognition effect is better than that in the horizontal direction.

The frame rate of the raw motion capture data used in the lower extremity support motion recognition was 150 frames per second (fps). The higher frame rate was chosen for the raw data at the time of recording to ensure accuracy and thus to be able to distinguish small differences in motion. However, the high frame rate data may have some redundancy. Therefore, we downsample the raw data in dataset B to reduce data redundancy and speed up the model training process. To investigate the effect of different sampling parameters on recognition results, we conduct comparison experiments for different frame rates of 5, 10, 50, and 150 fps, which are obtained by uniform downsampling. The different downsampling parameters correspond to the recognition accuracy and training time (averaged over the results of the two legs). A lower frame rate can significantly reduce the training time but has a smaller impact on the recognition accuracy. When the frame rate of the data is reduced from 150 fps to 5 fps, the training time is reduced by about 30%, while the recognition accuracy decreases only by less than 0.2%. Therefore, in practice, a compromise between frame rate and computation time can be chosen.

6. Conclusion

Considering that human upper and lower limb movements are cooperative, and there are differences in the Laban analysis due to the different relationship between the upper and lower limb movements and the center of gravity of the human body, this paper divides the limb movements into different behavioral segments according to the collaboration. The upper and lower limb movements of each segment are divided and processed. The integration of rotationally symmetric triangular displacement sensor and vision measurement system is studied. The principle and design of the sensor are given, and the fusion of multiple sensors in the physical layer is realized. The system error and compensation technology introduced by the RST sensor during installation and adjustment are studied, and the geometrical optical measurement model of the sensor is proposed. Aiming at the loss of the ring when the rotational symmetry decreases, an error compensation method based on neural network is proposed, and the uncertainty of the displacement measurement of the experimental prototype of the sensor is given. In this paper, we choose to use Delaunay triangulation to form a triangular mesh model, which effectively reduces the running time of model postprocessing. In behavior segment segmentation, a subspace clustering algorithm based on elastic net rule constraints is adopted, and the association between adjacent frames of temporal data is used to segment limb behavior segments. In this paper, the recognition of folk dance movements based on rotationally symmetric triangulation vision sensor camera has achieved good results. However, due to the lack of depth information and some invisible information in the specular 2D imaging, the specular imaging of 3D objects with different geometric properties may be the same, or an object is projected into different 2D images from different angles, making 3D reconstruction more difficult. Based on this, we plan to continue to explore in the field of mirror imaging technology in the future to further improve the research work of ethnic dance movement recognition.

Data Availability

The data used to support the findings of this study are available from the corresponding author upon request.

Conflicts of Interest

The author is unaware of competing financial interests or personal relationships that may influence the work published in this article.

Acknowledgments

This article was financially supported by the 2020 Key Project of "Research Center for Cultural Construction and Social Governance in Ethnic Areas," Key Research Base of Humanities and Social Sciences in Colleges and Universities in Guangxi (project number: 2020YJJD0007).

References

[1] A. Z. Md Faridee, S. R. Ramamurthy, and N. Roy, "HappyFeet: Challenges in building an automated dance recognition and assessment tool," *GetMobile: Mobile Computing and Communications*, vol. 22, no. 3, pp. 10–16, 2019.

[2] C. Chen, F. S. Alotaibi, and R. E. E. Omer, "3D mathematical modelling technology in visual rehearsal system of sports dance," *Applied Mathematics and Nonlinear Sciences*, vol. 7, no. 1, pp. 113–122, 2022.

[3] S. Xiao, H. Gritton, H. Tseng, D. Zemel, X. Han, and J. Mertz, "High-contrast multifocus microscopy with a single camera and z-splitter prism," *Optica*, vol. 7, no. 11, pp. 1477–1486, 2020.

[4] R. J. Lloyd, "The power of interactive flow in salsa dance: a motion-sensing phenomenological inquiry featuring two-time world champion, Anya Katsevman," *Qualitative Research in Sport, Exercise and Health*, vol. 13, no. 6, pp. 955–971, 2021.

Hindawi
Wireless Communications and Mobile Computing
Volume 2023, Article ID 9801082, 1 page
https://doi.org/10.1155/2023/9801082

Retraction

Retracted: Visual Communication-Based Virtual Reality Design of Imaging Information Collection and Display System

Wireless Communications and Mobile Computing

Received 17 October 2023; Accepted 17 October 2023; Published 18 October 2023

This article has been retracted by Hindawi following an investigation undertaken by the publisher [1]. This investigation has uncovered evidence of one or more of the following indicators of systematic manipulation of the publication process:

(1) Discrepancies in scope
(2) Discrepancies in the description of the research reported
(3) Discrepancies between the availability of data and the research described
(4) Inappropriate citations
(5) Incoherent, meaningless and/or irrelevant content included in the article
(6) Peer-review manipulation

The presence of these indicators undermines our confidence in the integrity of the article's content and we cannot, therefore, vouch for its reliability. Please note that this notice is intended solely to alert readers that the content of this article is unreliable. We have not investigated whether authors were aware of or involved in the systematic manipulation of the publication process.

Wiley and Hindawi regrets that the usual quality checks did not identify these issues before publication and have since put additional measures in place to safeguard research integrity.

We wish to credit our own Research Integrity and Research Publishing teams and anonymous and named external researchers and research integrity experts for contributing to this investigation.

The corresponding author, as the representative of all authors, has been given the opportunity to register their agreement or disagreement to this retraction. We have kept a record of any response received.

References

[1] Y. Qi, T. Sun, and Y. Li, "Visual Communication-Based Virtual Reality Design of Imaging Information Collection and Display System," *Wireless Communications and Mobile Computing*, vol. 2022, Article ID 1929596, 12 pages, 2022.

Hindawi
Wireless Communications and Mobile Computing
Volume 2022, Article ID 1929596, 12 pages
https://doi.org/10.1155/2022/1929596

Research Article

Visual Communication-Based Virtual Reality Design of Imaging Information Collection and Display System

Yichen Qi,[1,2] **Tong Sun**,[3] **and Yan Li**[4]

[1]*Visual Communication Design, PhD Program in Design, Faculty of Decorative Arts, Silpakorn University, Bangkok 10200, Thailand*
[2]*Shandong Youth University of Political Science, Jinan 250103, Shandong, China*
[3]*Visual Communication Design, Shandong Youth University of Political Science, Jinan 250103, Shandong, China*
[4]*Big Data and Artificial Intelligence, Weifang Vocational College, Weifang 262737, Shandong, China*

Correspondence should be addressed to Yichen Qi; 160108@sdyu.edu.cn

Received 26 July 2022; Revised 24 August 2022; Accepted 1 September 2022; Published 25 September 2022

Academic Editor: Jun Ye

Imaging image acquisition and display has always been an important application field of visual communication art. A good imaging acquisition and display system can give the audience an excellent visual experience. However, conventional imaging image acquisition equipment is too bulky and expensive. At the same time, the existing imaging acquisition technology is generally only suitable for two-dimensional plane design. It is difficult to construct the three-dimensional and realistic sense of actual objects, which makes the development of the entire imaging system slow. Existing imaging acquisition technologies have difficulty keeping pace with the technological age. In this paper, according to the actual needs, a three-dimensional imaging technology was proposed to improve the efficiency of imaging image acquisition. And the principle of imaging information display was used to enhance the visual communication effect. Then, at the algorithm level, virtual reality technology was combined with convolutional neural network-related algorithms to improve the overall accuracy of the algorithm and control the error well. The experimental results showed that the optimized VR technology leads the whole stage in terms of mean square error. Among them, after testing 400 samples in the two experiments, the error performance is controlled below 0.32, and the best error control performance is 0.07; the unoptimized virtual reality technology error control is not ideal. The minimum error failed to break below 0.2, and the optimized algorithm had a high accuracy of 99.3%, which greatly improved the feasibility of the imaging information acquisition and display system.

1. Introduction

Visual communication is an aesthetic design that is presented to the audience after beautifying and modifying the original objects through intermediate media such as visual media. A good visual communication design can reflect the graphic depiction with the characteristics of the times and stunning visual effects. In the entire complex visual communication design process, the quality of imaging image acquisition plays an important role in the visual effect presented by the final visual communication design, because the acquisition of imaging images has a great impact on the material preparation of visual communication design,and the image presented in the final visual communication design is also based on the display results of imaging image acquisition. Therefore, how to design an excellent imaging information acquisition and display system is the key to produce the best visual communication effect. Although the traditional image acquisition equipment and technology are relatively complete in function, they have been gradually unable to adapt to the high demand in this field in the Internet era due to the disadvantages of high price and heavy equipment. How to choose the imaging image acquisition equipment and related implementation methods suitable for the Internet era has become a problem that has attracted much attention in this field. In addition, the final displayed image of the entire imaging information acquisition and display system is limited by the performance of traditional methods, and

its imaging accuracy and resolution are not ideal. A good simulation environment is lacking to better display the imaging images. In order to solve the above problems, it is necessary to optimize the original image acquisition device and acquisition method and to improve the overall restoration effect of the imaging image. At the same time, in order to reflect the scientific and professional nature of the constructed system, science and professionalism are important factors in building a system, and this paper will adopt virtual reality related technologies for system design and research.

In this paper, the virtual reality technology is improved, and the convolutional neural network model related algorithm is introduced to improve the performance of the whole system. The practical application is combined to provide scientific support for the imaging information acquisition and display system constructed in this paper to make the whole system more efficient. The innovations of this paper are as follows: (1) the three-dimensional imaging technology is used to realize the three-dimensional design of the information acquisition process of the imaging image, and the operation of imaging information acquisition is simplified. (2) The virtual reality technology is optimized in combination with the convolutional neural network-related algorithms, so that the main performances such as the accuracy and control error of the optimized algorithm are significantly improved.

2. Related Work

Imaging image acquisition and display has always been a hot research topic in the field of visual communication design, and many scholars have done a lot of research to improve a more efficient imaging system. Among them, scholar Ding et al. analyzed the current situation and exposed problems of existing imaging image acquisition equipment and technology. A strategy to optimize the field of view problem in the acquisition device was proposed. Then, by starting from the control condition of minimum resolution, the quality of the whole imaging image was optimized, and finally, the feasibility of this strategy in real environment operation was discussed [1]. Gupta and Choi proposed a novel design strategy for imaging information acquisition and display systems. The acquisition of imaging images was simplified. At the same time, the efficiency of the acquisition process was guaranteed. Compressed sensing techniques were then used to optimize image accuracy after imaging image acquisition [2]. Lockwood and his team described the zebrafish imaging image acquisition process in detail and discussed how to ensure the smooth progress of the image acquisition process without affecting the survivability of the target object in practical situations. Finally, the commonly used imaging techniques were combined and optimized accordingly to solve the above problems [3]. Aiming at the problems encountered in the process of image acquisition of human body structure imaging, Koga et al. proposed an inverse kinematics method to reconstruct human body posture and shape. Finally, the effectiveness of the improved imaging image acquisition was verified by the driving experiment of the car [4]. Lee and his team reviewed and analyzed the existing real-time imaging image information acquisition methods. Imaging image evaluation modes were constructed to optimize the acquisition process. Then, the improved imaging image acquisition method was applied to the thermal imaging field to better acquire NIR images. Finally, the precision and accuracy level of the method were verified by experiments [5]. The above studies on imaging image acquisition and display provided a lot of theoretical knowledge for the development of related systems. The algorithm framework of image acquisition technology was greatly enriched. However, the above research did not adopt a scientific and reliable technology to construct the system and lacked sufficient real data support.

In view of the lack of scientific and reliable technology to build the entire imaging image acquisition and display system, the virtual reality technology can be used to solve the problem. Virtual reality technology is a booming frontier technology, which has also attracted many scholars to study this technology. Among them, the scholar Maples-Keller and his team briefly explained the development process of virtual reality technology. The related research of virtual reality technology in the field of psychotherapy was deeply reviewed and discussed. The achievements of virtual reality technology in this field were listed. Finally, the future work of virtual reality technology in psychotherapy was prospected [6]. Hyun and Lee analyzed the difficulties faced in fire prevention and control and research in the past combined with practical problems. The feasibility of virtual reality technology application in this field was analyzed. Finally, through relevant experiments, the reliability of the designed fire research model was proved [7]. Zhang et al. applied virtual reality technology to the university asset management system and analyzed in detail the role of the technology in optimizing the visualization capability of the system. Finally, the designed system was simulated by a real case to verify the overall performance [8]. Mai et al. combined somatosensory equipment with virtual reality technology to explore the impact of the implementation of this technology on the lives of cerebrovascular patients. The experimental results demonstrated the effectiveness of the method [9]. Ding et al. expounded the current situation of physical education in colleges and universities in actual teaching. The reasons for the unsatisfactory effect of the teaching process were summarized. A specific plan to implement virtual reality technology to construct a physical education system was proposed. Finally, the actual effect of the system was tested through an example [10]. The above-related researches on virtual reality technology have well demonstrated the comprehensiveness and good development prospects of the technology, which played an important role in expanding the application field of the technology. However, the experimental accuracy of the above studies is not ideal, which is difficult to meet the high-precision requirements of imaging images.

3. Construction Method of Visual Communication Art Imaging Information Collection and Display System

3.1. Construction of Imaging Information Acquisition and Display System. Under the background of the rapid development of Internet technology, it is difficult for traditional

image imaging information acquisition equipment to meet the high standards and technical requirements of imaging images. Therefore, this paper adopts the thriving virtual reality technology to optimize the whole imaging process. At the same time, when constructing an imaging information acquisition and display system, the traditional method is based on two-dimensional plane design, which makes the proportion and visual effects of the acquired imaging images not close to reality and the visual communication is too simple. Based on this, this paper proposes a three-dimensional imaging technology to improve the information acquisition process of imaging images, so that viewers can perceive the acquired imaging images more intuitively and clearly. This is an attempt to embody realism. The information acquisition process under the 3D imaging technology is shown in Figure 1.

It can be seen from Figure 1 that the information acquisition structure under the three-dimensional imaging technology abandons the shortcomings of the traditional method, which have low utilization of each component of the target object and insufficient acquisition angles. At the same time, the imaging image acquisition device not only collects visual information in the vertical direction of the optical axis but also covers the central area of the optical axis with an acquisition camera. In the specific operation process, the acquisition device moves unidirectionally along the optimal direction with a fixed angle from the optical axis, which makes the entire acquisition process simpler than the traditional method and improves the acquisition efficiency [11].

After the acquisition of imaging image information is completed, data processing and structural reconstruction of the acquired 3D imaging information are also required, which is an important step in expressing virtual reality of 3D actual objects in reality. There are two main application methods for 3D reconstruction, namely, 3D reconstruction based on RGB-D depth camera and depth estimation and structure reconstruction based on deep learning. Since the imaging image operation process proposed in this paper mainly uses the technology in the field of deep-level information processing, this paper adopts the computer three-dimensional reconstruction method for processing, and the specific process is shown in Figure 2.

In the three-dimensional reconstruction process shown in Figure 2, there are a total of n acquired element imaging images. The imaging image captured by the acquisition device with the farthest relative distance from the target object is used as the comparison image. Then, all the imaging images are mapped from the unreal aperture to the 3D virtual space by back-projection, and finally, the final 3D reconstructed imaging image is obtained by scaling, translation, and overlapping.

Finally, the reconstructed imaging images are visualized, and the corresponding 3D stereo images are displayed in real time. In the process of image display, it mainly performs operations such as retouching, cropping, line optimization, light and shadow effect processing, and zooming on the image. The scaling operation is one of the most important operation links. In this paper, the zoom function of the imaging image display part combines the principle of image zoom to optimize the overall visual effect of the image display. The specific principle is shown in Figure 3.

Figure 3 shows that the optimization method for the zoom operation in the imaging information display theory proposed in this paper based on the principle of image zoom is intuitive, simple, and effective. The reduced image based on the original imaging image is only reduced as a whole, and the proportion of three-dimensional objects in the entire image will not be changed. At the same time, the higher precision of the imaging image can also be guaranteed, and the operation principle of magnification is similar. The size is changed, but the scale will not change. Although the precision is relatively small, the visual communication effect will also be enhanced [12]. The two operations satisfy different needs, respectively, but the final display effect is obviously enhanced compared with the traditional display method.

3.2. Virtual Reality Technology. Virtual reality technology is an important research direction of emerging simulation technology in recent years. It is a comprehensive and efficient practical technology that combines a variety of technologies. The specific structure is shown in Figure 4.

As can be seen from Figure 4, the virtual reality technology is formed by the combination of seven technologies. Among them, three-dimensional computer graphics technology and wide-angle stereoscopic display technology are very suitable for the imaging image processing system of this paper. The following is a specific introduction to the virtual reality technology algorithm [13, 14]. In the design of 5G network virtual reality technology, Formula (1) specifies the direction setting of the action space. C_1 indicates that there are closely associated conversion types in all objects in the specified declaration. The weights of directed action sequences reflect the enormous diversity of data products in the statement:

$$N_{tn} = 1 - \sum \frac{(2\gamma_m\gamma_t + C_1)(2\varphi_{mt} + C_2)}{(\gamma_m^2 + \gamma_t^2 + C_1)(\varphi_m^2 + \varphi_t^2 + C_2)}. \tag{1}$$

The impact of g_i performance is described by introducing artificial intelligence modeling techniques. The relevant code elements are shown in the following formulas:

$$K(g_i, l_h) = K(g_i)K\left(\frac{l_h}{g_i}\right),$$

$$K\left(\frac{l_h}{g_i}\right) = \sum_{p=1}^{p} K\left(\frac{l_h}{w_p}\right)K\left(\frac{w_p}{g_i}\right), \tag{2}$$

$$k_p = \sum \frac{2p}{p+1} + \left[\frac{1}{2} + \frac{1}{2p}\right]\left[\frac{c_2 - c_1}{3}\right]^2 + \frac{2(c_2 - c_1)}{3}. \tag{3}$$

In order to achieve the effect of $c_2 - c_1$ evolution from rule formulation to actual implementation of specific virtual reality technology [15], the static analyzer method can be used for specific analysis and processes:

$$C_{ha} = \int_0^{\infty} gF_h(t)\int_0^t (t-m)gF_a(m). \tag{4}$$

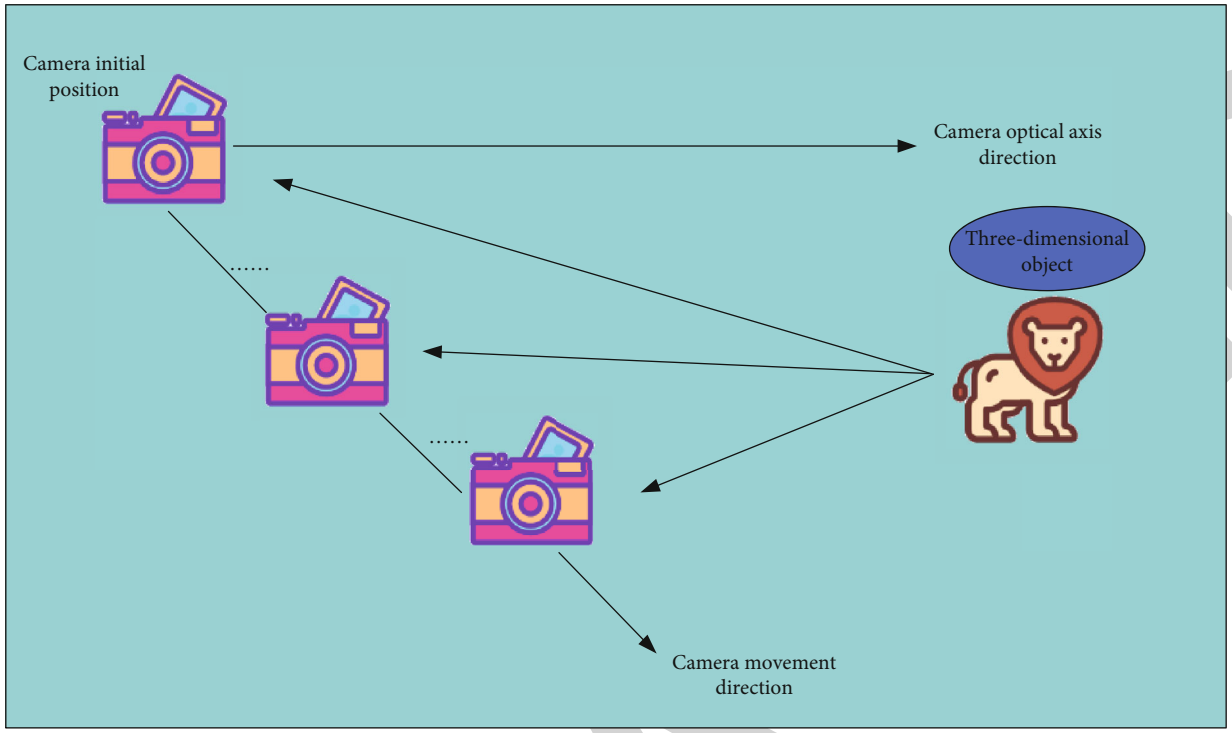

Figure 1: Imaging information acquisition structure under 3D imaging technology.

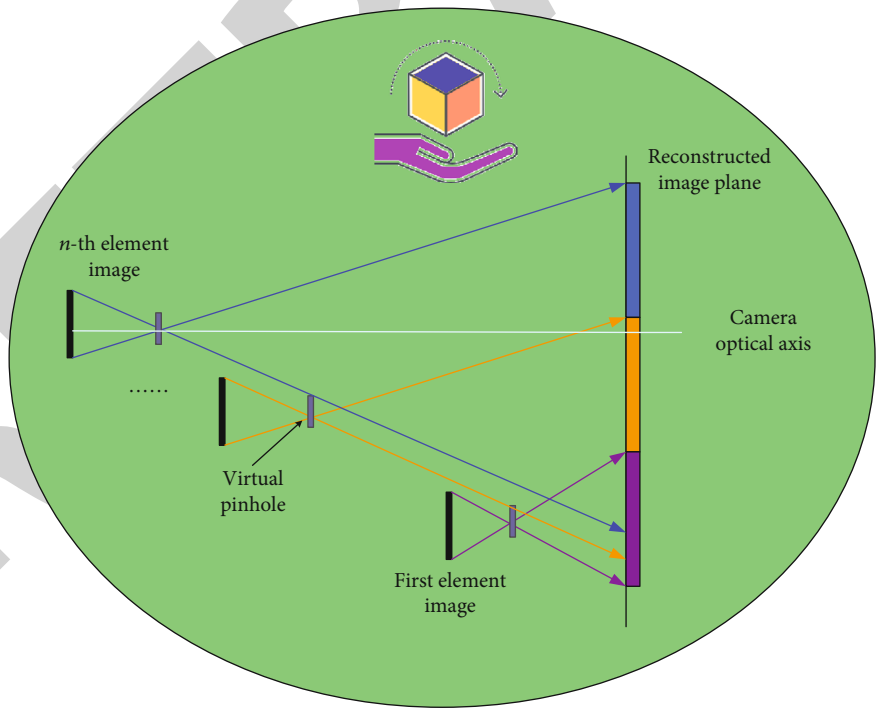

Figure 2: 3D reconstruction process of imaging information acquisition.

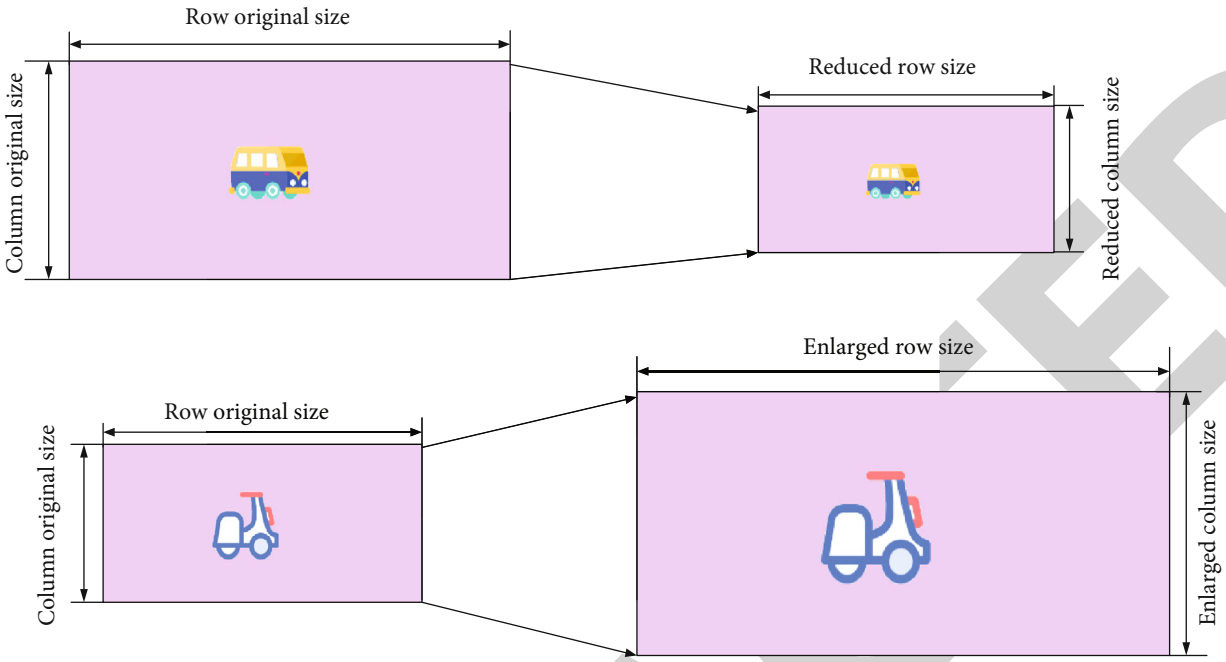

Figure 3: Principle of imaging information display.

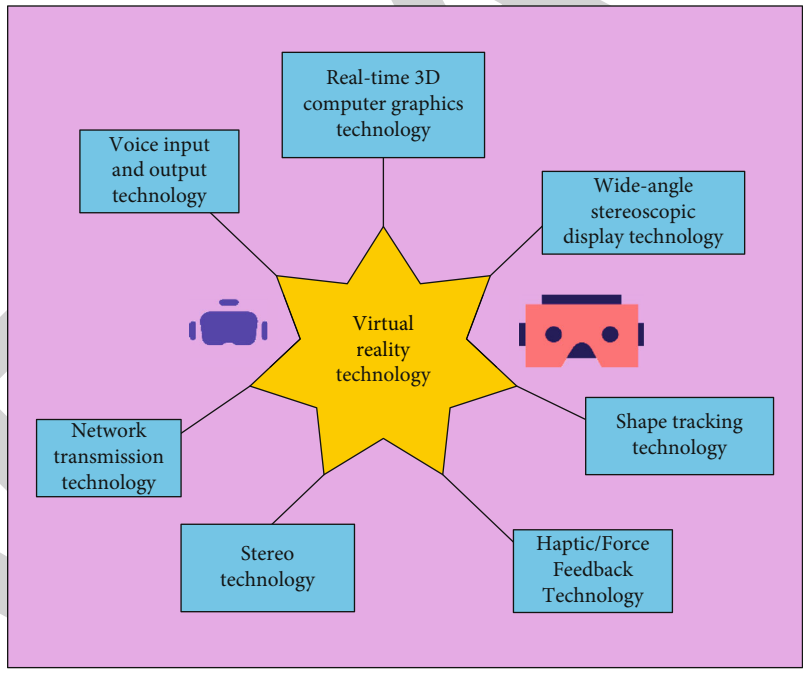

Figure 4: Composition of virtual reality technology.

As can be seen from Formula (4), in this process, the $t - m$ single-program report generates a set of data attributes used in the input process for its own behavior gF_h. This collection has been digested and processed accordingly. Finally, a digital signal object $C_{ha}s$ is formed:

$$\ln\left(\frac{N_{iv}}{N_{iv}-1}\right) = \beta + \chi \ln N_{iv} - 1, \tag{5}$$

$$\sum_{m=1}^{\varepsilon} Xm \times k = \frac{\sum_{m=1}^{\varepsilon}\left(\left(L + Z_I/\sum_1^y L_\theta\right)/C + Z + Zc\right)}{\chi + \beta \ln N_{iv} + (K/C)}. \tag{6}$$

The technical information in Formula (6) is denoted by N_{iv}, the same set of audio data items $\beta + \chi$ is denoted by ε, and the series of digital signal objects is also denoted by L_θ. $Xm \times k$ is the claim granted by the input object k, which conforms to the process Z information and data objects. And according to the formula, the statement is expanded

even if the data item u is equal to the process $\sum_{m=1}^{\varepsilon} Xm \times k$ output data object.

3.3. Convolutional Neural Network Optimization Virtual Reality Technology. In order to improve the accuracy and error control of the entire imaging information acquisition and display system, this paper introduces a convolutional neural network-related algorithm to optimize virtual reality technology [16, 17]. The specific derivation process of the algorithm is as follows. When the imaged image is input, the image data is input to the central area of the optical axis node. Therefore, the output value in the connection point in the input process is set to the same value as the input value. At the same time, the base station, which is an intermediate hub, plays an important role in the connection point in the output process. Only one of all base stations is selected as the active base station. And the transmission values of all the connection points of the base station of the intermediate hub will be sent to the base station and outputted by it.

The connection point in the input process is represented as $n_i, i = \{1, 2, \cdots, y\}$, and there are y experimental samples in total. Equation Formula (7) represents the input representation of the connection point G in the model:

$$G_h = \sum_{h=1}^{y} \eta_{ih} n_i. \tag{7}$$

The imaging image information obtained from the base station to the connection point is shown in Formula (8):

$$S_h = \sum_{h=1}^{y} \frac{1}{\left\{1 + \left[\left(\sum_{i=1}^{y} \eta_h S_h\right)^{-1} - 1\right]^2\right\}'} = \sum_{h=1}^{y} \frac{1}{\left[\left(G_h^{-1} - 1\right)^2\right]}. \tag{8}$$

Among them, η_h is used to represent the power required from the ground base station G_h^{-1} of the connection point with image information to the center position h of the connection point, and S_h represents the element information in the image.

The activation function also needs to be configured in the whole process, as shown in Formula (9):

$$T = \sum_{h=1}^{y} \frac{1}{\left\{1 + \left[\left(\sum_{i=1}^{y} \eta_h S_h\right)^{-1} - 1\right]^2\right\}^{2'}}. \tag{9}$$

In Formula (9), the cell in the output process contains S connection points. The optimal governing formula [18] for the image can be expressed as the mean of the squared error of the error, as shown in Formula (10):

$$R = \left(\frac{1}{N}\right) \sum_{n=1}^{y} \left[\bar{t} - t\right]^2 = \left(\frac{1}{N}\right) \sum_{n=1}^{y} R_h. \tag{10}$$

The introduction of convolutional neural networks into virtual reality technology will correspondingly change the σR framework. However, the relevant properties of the neural network can be modified to obtain the minimum value of ϕ. The function of σd_{ih} is to adjust the decoupling. Equation Formula (11) is the specific expression:

$$R_{ih} = \sum \begin{cases} \eta_{ih} = -\phi\left(\dfrac{\sigma R}{\sigma d_{ih}}\right), \\ \eta_h = -\phi\left(\dfrac{\sigma R}{\sigma \eta_{ih}}\right). \end{cases} \tag{11}$$

In addition, in the rate optimization of the imaging information acquisition and display process, the total number of $a_i \eta_h S_h^2$ optimization parameters between the neural network and the access points in the outer layer of the factor is shown by Formula (12):

$$\eta_{ih} = a_i \eta_h S_h^2 \left[1 - \sum_{i=1}^{y} \eta_{ih} a_h\right] \varepsilon_h. \tag{12}$$

Formula (13) represents the calculation method of the total number of connection optimization parameters [19]:

$$\eta_h = \sum_{h=1}^{s} t^2 S_h \left[1 - \sum_{h=1}^{s} \eta_h S_h\right] \left[\bar{t} - t\right]^2. \tag{13}$$

Among them, $\bar{t}$ and t belong to the variables of η_1, which are used to specify the maximum and minimum values of the variation range, respectively. Then, the optimized algorithm framework can be put into practical application. By selecting the $\sum_{h=1}^{s} \eta_h S_h$ improvement strategy of the neural network that meets the conditions of the system, the purpose of assigning the interactive weight of the algorithm framework is achieved. This process can also effectively improve the accuracy of the overall system. After combining the convolutional neural network technology with the algorithm, the system will get higher performance. The specific strategies are as follows:

$$\min\left(R\right) = \sum_{h=1}^{s} \int \left(\eta_{1,} \cdots, \eta_y\right). \tag{14}$$

In Formula (14), $\min(R)$ represents the relative deviation value of the system, and $(\eta_{1,} \cdots, \eta_y)$ is the fixed weight after the strong joint numbering. It contains the connection points that store data during the input process and the weights of the endpoints that are affected. The connection points located in the central area of the model and the associated evaluation test model of the connection point module during export are also included. m is used to count the sum of the quantities of various parameters of the system [20].

The optimization algorithm is used to explore and solve the problem of insufficient storage capacity of the whole system. Since the coverage area of the algorithm model is approximately at the level of $\int(\eta_{1,} \cdots, \eta_y)$, it will be of great

help to the whole system if the algorithm can be perfectly integrated into the system. Due to the strong correlation between the steps and methods when $W - R$ performs the optimization operation, Formula (15) can be used to express the training method with an intensity of $R < W$:

$$\int_i = \sum_{i=1} \begin{cases} W - R, R < W, \\ 0, R \geq W. \end{cases} \tag{15}$$

In Formula (15), R represents the accumulated value of all $R \geq U$ at this stage. In order to distinguish the parameter N_s in the optimization process to achieve the effect of satisfying the integration efficiency of $\int_1 (W - R)/W \in [0, 0.5]$, and at the same time, the reduction of the integration efficiency caused by the decryption operation can be minimized as much as possible, and this paper uses the following formula for further derivation:

$$N_s = \left\{ 2\left(\frac{\int_1 W - RR < W}{W} \right), \frac{\int_1 (W - R)}{W} \in [0, 0.5]. \right. \tag{16}$$

In order to transform into a dimensionless expression through the correlation operation pair $\int_1 (W - R)/W \in [0.5, 1]$, this paper will use a max-minimization technique that can efficiently process information. The advantage is that it can keep the original state of the target object unchanged. At the same time, the occurrence of data duplication can be effectively avoided. In this regard, the normalization formula of the data in the input process proposed in this paper is

$$N_s = \left[1 - 2\left(1 - \left(\frac{\int_1 W - RR < W}{W} \right)^2 \right], \frac{\int_1 (W - R)}{W} \in [0.5, 1]. \right. \tag{17}$$

By reducing all the key information in the algorithm model to a representation range of only $[0, 1]$, the method is defined as normalization $\int_1 (W - R)/W \in [0.5, 1]s$, and its solution is expressed as follows:

$$a' = \sum_{i=1}^{y} \frac{a - a_{\min}}{a_{\max} - a_{\min}} + \frac{\int_1 (W - R)}{W} \in [0.5, 1]. \tag{18}$$

The function of the normalization process λ is to convert the information with specification errors in the target data set into random values between $[0, 1]$. Formula (19) is an elaboration of the specific conversion process:

$$a' = \sum_{i=1}^{y} \frac{a - \overline{a_{\min}}}{\lambda} + a_{\max} - a_{\min}. \tag{19}$$

Each site is composed of three layers: a connection layer that represents the operation of the input process, a connection layer that stores hidden information, and a connection layer that is used for convolution operations. The weights of the three layers are defined as χ, μ, and β, respectively, and the relational expression is shown in Formula (20):

$$\chi_z^k = \sum_{i=1}^{N} \eta_{iz} a_i^k + \sum_{z'}^{N} \eta_{z'z} p_{z'}. \tag{20}$$

If the transmission task is completed for each data, $\eta_{z'z}$ $p_{z'}^{k-1}$ work will continue to be performed in the receiver of the entire system. Then, only by entering 111, the next nerve cell can continue to operate as a new transmission information system. This will also affect the parameter values of the subsequent input process as follows:

$$\beta_{z'}^{k-1} = \sum_{k \longrightarrow 1}^{z} \eta_z \left(p_{z'}^{k-1} \right) + \eta_{z'z} p_{z'}^{k-1}. \tag{21}$$

For all neurons existing in the input process, the original information of the connection layer unit that stores the hidden information and the output variable of the unit existing in the output process at time step k are shown in Formula (22):

$$\mu_{z'}^{k-1} = \sum_{z=1}^{N} \eta_{z0} p_z^k + \eta_z \left(p_{z'}^{k-1} \right). \tag{22}$$

Virtual reality technology is accelerating its penetration into production and life. In the production field, it is mainly used in the R&D and design of new products to reduce R&D costs and shorten the R&D cycle. Therefore, it is necessary to study the optimized virtual reality technology.

4. Application of Virtual Reality Technology to Imaging Information Collection and Display System

4.1. Application of Imaging Information Acquisition and Display System. In order to verify the visual communication effect of the proposed imaging information acquisition and display system, this paper will take two methods of questionnaire survey and simulation experiment to comprehensively investigate the feasibility and professionalism of the system. This paper interviews four professionals in the field of visual communication technology design. The structure and composition of each part of the imaging information acquisition and display system and the specific realization results are shown. After that, a corresponding questionnaire survey is conducted to explore the construction effect of the system proposed in this paper from the perspective of professional designers. The survey results are shown in Table 1.

In Table 1, each professional scored each section on a scale of 0 to 5. It can be seen that the four professionals have a good overall impression of the imaging information acquisition and display system in this paper. The highest score is the design of the system information collection part and the system algorithm design, with an average score of 4.75 points. The lowest score was in the imaging information

Table 1: Comprehensive evaluation of the system by professionals.

Evaluation angle	Evaluator				Mean
	P1	P2	P3	P4	
Design effect of information collection part	5	4	5	5	4.75
Information display part of the design effect	4	5	4	4	4.25
System algorithm design	5	5	5	4	4.75
System overall structure design	5	5	4	4	4.5

display section, with an average score of 4.25. Although the score is acceptable, compared with other designs, there are still some details in this part that need to be refined.

In addition, this paper also selects 50 experimental volunteers who are quite interested in visual communication design or take it as a hobby. The 50 people spend a month familiarizing themselves with and using the system in their daily lives. The purpose is to contrast with the views of professionals. The feasibility and practicability of the imaging information acquisition and display system designed in this paper are investigated from the perspective of ordinary people. One month later, the 50 people are given a satisfaction survey. The questions in the questionnaire are all related to the design of the system in this paper. Each person can evaluate the question. The scoring interval is $0 - 10$ points. The higher the score, the higher the satisfaction with the question. The final questionnaire results are shown in Table 2.

It can be seen from the results in Table 2 that the overall satisfaction of the 50 volunteers in the study is good with the imaging information acquisition and display system proposed in this paper. The average satisfaction score of the 5 questions is above 8.7 points, of which the highest average score is 9 points and the lowest is 8.76 points. And none of the 50 volunteers scored below 6 on each of the 5 questions. This shows that the overall performance of the system is excellent in all angles.

In addition, this paper compares and analyzes the performance of the original designed imaging information acquisition and display system and the currently widely used traditional system. The advantages and disadvantages of the system in the simulation environment compared to the traditional system are explored. The simulation test is carried out for the important imaging image stitching effect in the whole imaging process. Imaging image stitching is the intermediate stage of information acquisition and imaging display. The implementation effect of this stage can determine the degree of absorption of the results of the previous stage and the degree of completion of the final presentation results. In this paper, a group of data that has gone through the imaging information acquisition stage is selected as the experimental sample. The above two methods are used to test the time-consuming condition of this sample 8 times, respectively. The test results are shown in Table 3.

It can be seen from Table 3 that the two methods are not ideal in the processing speed of the imaging image stitching stage, and the time required to complete the entire stage is more than 5800 ms. However, the information acquisition and display system proposed in this paper is significantly better than the traditional system in a total of 8 test time consumption. The time consumption of each test is reduced by more than 28% in comparison, with an average reduction rate of 30.8%.

In view of the relatively slow processing speed in the image stage, this paper appropriately reduces the testing range of the entire imaging image. Whether the time required for stitching of imaged images can be reduced under such optimized conditions is explored. Table 4 shows the specific data enumeration.

From the data in Table 4, it can be seen that after the range of the image to be tested is appropriately reduced, the time consumption of the two systems in the imaging image stitching stage is greatly shortened. The average consumption time of the traditional system is reduced from 8534.45 ms to 1926.88 ms. The average consumption time of the system proposed in this paper also has an optimization difference of 4606.42 ms, and in terms of the average reduction rate, the time consumption of the system designed in this paper is reduced by 32.1% compared with the traditional system after using the above improved method. This also proves the time-consuming advantage of the imaging data acquisition and display system designed in this paper.

In order to detect the final imaging effect of the imaging information acquisition and display system, this paper selects the human body structure as the experimental object. The image rendering level of the human body under the system environment of this paper is explored, as shown in Figure 5.

It can be seen from Figure 5 that in the final display effect, the display completion of the entire human body is close to perfect. At the same time, the imaging image is clear. The light and shadow handling is also done just right. The presented portrait is very close to the actual collection scene, and the degree of restoration is very high.

4.2. Application of Virtual Reality Technology. In order to verify the overall performance optimization effect of the system using virtual reality technology, this paper compares the relative error performance of the system with the real operating environment without virtual reality technology. In this paper, a total of 1000 imaging image information samples are selected as experimental objects, and the samples are applied in these two environments, respectively. At the same time, in order to improve the accuracy of the data, this paper will conduct two comparative experiments under the same experimental conditions, and the final results are shown in Figure 6.

It can be seen from Figure 6 that in the two comparisons of relative errors under the same conditions, the relative error control performance in the environment using virtual

Table 2: System satisfaction survey results.

Question	Score						Mean
	10	9	8	7	6	<6	
Q1	18	13	12	5	2	0	8.8
Q2	21	11	14	2	2	0	8.94
Q3	17	16	10	6	1	0	8.84
Q4	18	14	8	8	2	0	8.76
Q5	23	12	7	8	0	0	9

Table 3: Time consumption comparison of the two systems.

Number of tests	Time consuming		Reduction rate
	Legacy system (ms)	Optimized system (ms)	
1	8699.5	5820.6	33.1%
2	8455.3	5962	29.5%
3	8416.9	5643.1	33.0%
4	8523.6	5933.6	30.4%
5	8551.7	6121.4	28.4%
6	8449.3	6002.9	30.0%
7	8632.9	5952.4	31.0%
8	8546.4	5883.4	31.2%
Mean	8534.45	5914.93	30.8%

Table 4: Time consumption comparison of the two systems after the improved strategy.

Number of tests	Time consuming		Reduction rate
	Legacy system (ms)	Optimized system (ms)	
1	1865.9	1362.5	27.0%
2	1882.4	1259.6	33.1%
3	1933.6	1296.3	33.0%
4	1946.5	1299.3	33.2%
5	1889.1	1316.5	30.3%
6	1886.3	1278.2	32.2%
7	2013.6	1377.3	31.6%
8	1997.6	1278.4	36.0%
Mean	1926.88	1308.51	32.1%

reality technology is significantly better. The highest relative error is only 1.44, and the lowest is an excellent error control level of 0.18.

4.3. Optimized Application of Virtual Reality Technology. This paper tests the main performance of virtual reality technology optimized by convolutional neural network-related technologies. This paper compares the performance of this algorithm with three commonly used algorithms applied to the imaging image processing systems under the same experimental conditions. High precision has always been the key standard of imaging image processing, so this paper first selects relevant samples to test the accuracy of imaging

Figure 5: Human body imaging display effect.

image processing. In order to ensure the feasibility of the experiment, this paper divides the samples into test samples and training samples on average. Among them, the requirements of various indicators in the experimental environment of the training samples are more stringent. The final accuracy data of the two samples are shown in Figure 7.

It can be clearly seen from Figure 7 that the optimized virtual reality technology proposed in this paper has absolute advantages in both sample accuracies. Among them, the training accuracy is reached an extremely high-precision level of 99.3%, and the test sample accuracy is also reached the level of 97.9%; in contrast, the other three algorithms do not achieve a very good level of accuracy on the imaged images. The highest accuracy values of the random forest algorithm, KNN, and NNGA algorithms are 84%, 87.5%, and 77.3%, respectively.

After testing the precision comparison, this paper also selects another important analysis indicator for testing, that is, the recall rate. The processed imaging image samples are also divided into test and training samples. Other factors in the experimental environment are also unchanged. The specific recall performance of the four algorithms is shown as follows.

Figure 8 shows the different recall performance of two experimental samples of the four algorithms. The recall rates of the optimized virtual reality technology training samples and test samples proposed in this paper are 0.85% and 0.83%, respectively. Compared with the average recall rate of the KNN algorithm of two samples of 1.93% and the average recall rate of NNGA of 2.33%, the algorithm in this paper is in a backward position in terms of recall rate. Although this is a normal phenomenon in the pursuit of higher accuracy, it also reflects the improvement space of the algorithm in this paper in terms of recall optimization.

In addition, in order to make an intuitive comparison between the virtual reality technology optimized by the convolutional neural network algorithm and the unoptimized technology, this paper selects 2000 imaging image samples and also conducts two comparison experiments under the same conditions. The actual performance of the two VR technologies is tested, and the performance of the two technologies is compared according to the tested error data. The experimental data is shown in Figure 9.

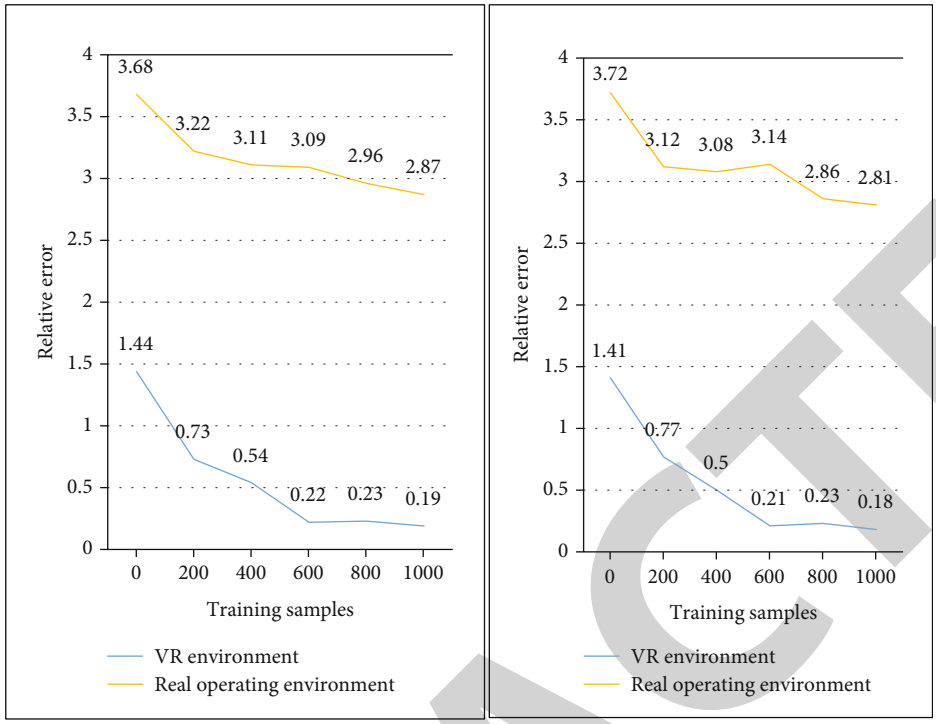

Figure 6: Comparison of relative errors in two operating environments.

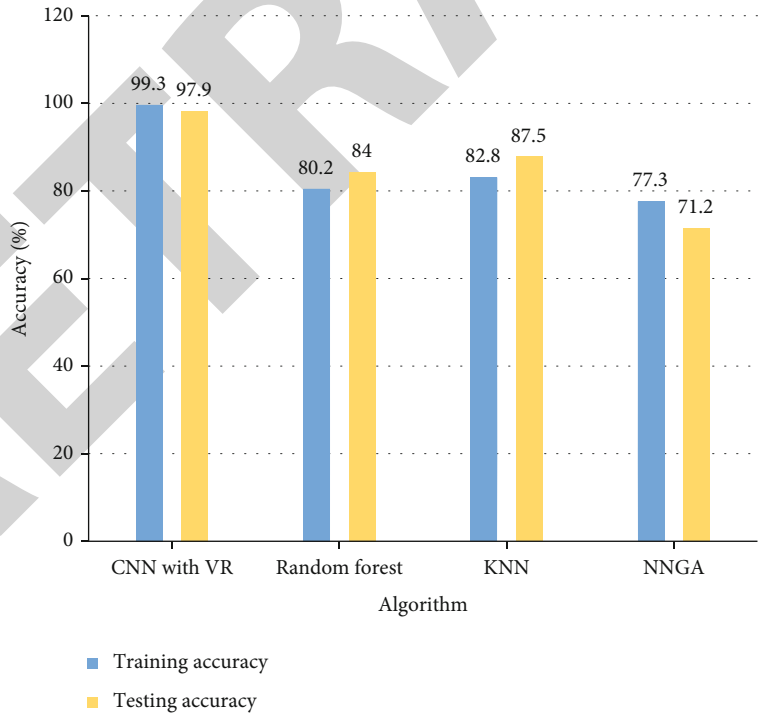

Figure 7: Accuracy comparison of the four algorithms.

In the error performance of the two experiments in Figure 9, the optimized VR technology leads the whole stage in terms of mean square error. Among them, after testing 400 samples in the two experiments, the error performance is controlled below 0.32, and the best error control performance is 0.07; the unoptimized virtual reality technology error control is not ideal. The minimum error failed to break below 0.2.

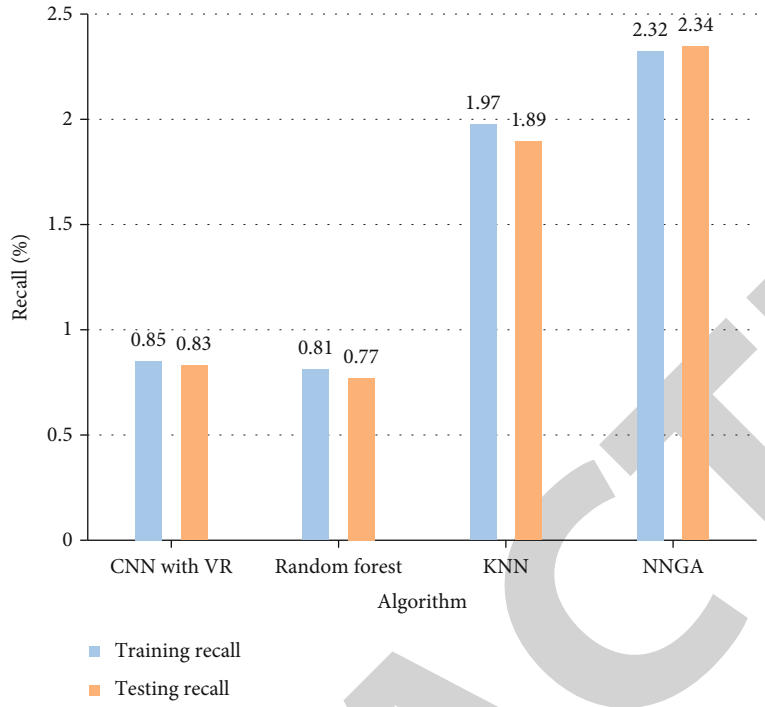

Figure 8: Comparison of recall rates of the four algorithms.

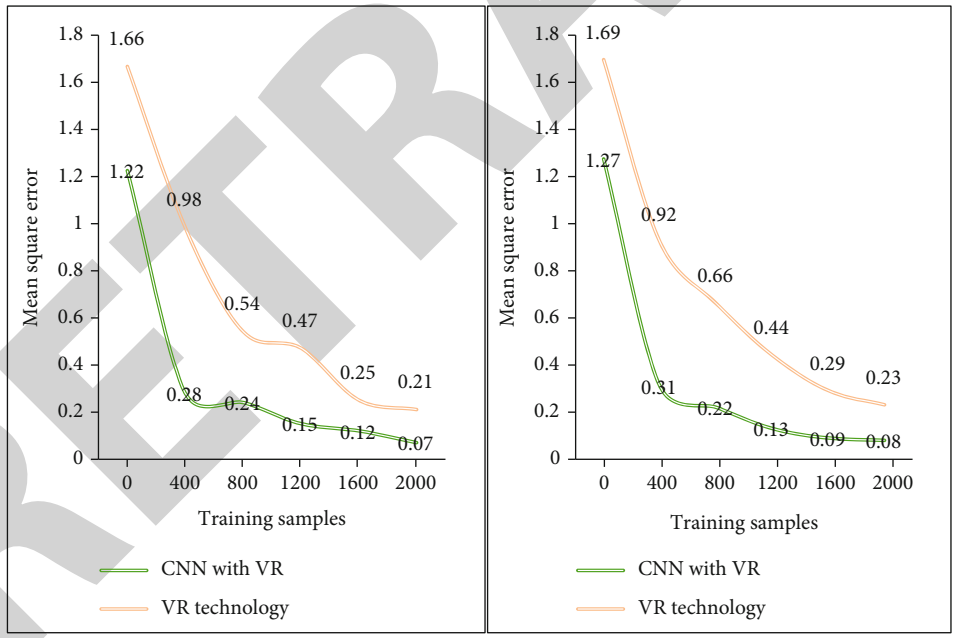

Figure 9: Two comparisons of the error performance of the two algorithms.

5. Conclusions

The advantages of digital image processing are high processing accuracy, rich processing content, complex nonlinear processing, and flexible adaptability. Generally speaking, the content can be processed only by changing the software; so, it is widely used. How to design an imaging image processing system to show stunning visual communication effects on the three-dimensional appearance of actual objects and at the same time expand the extension of contemporary visual communication design, this has always been a problem that relevant designers are eagerly concerned about and researched. This paper provided a critical review of traditional imaging image acquisition devices and techniques. The use of 3D imaging technology to construct a very efficient acquisition process was proposed. Computer 3D reconstruction methods were used to perform key reconstruction operations on the acquired imaging images.

Hindawi
Wireless Communications and Mobile Computing
Volume 2022, Article ID 6898098, 10 pages
https://doi.org/10.1155/2022/6898098

Research Article

Design and Implementation of Financial Management System Based on Computer Network Technology

Jianwei Yan

Finance Department, Kunming Medical University, Kunming, 650500 Yunnan, China

Correspondence should be addressed to Jianwei Yan; yanjianwei@kmmu.edu.cn

Received 13 July 2022; Revised 3 September 2022; Accepted 8 September 2022; Published 22 September 2022

Academic Editor: Jun Ye

At present, financial management systems have been applied in many universities. University's usage of the financial management system to achieve ideal results in formulating financial plans, strengthening financial control, and improving the efficiency of financial management. The healthy and long-term development of a university is inseparable from scientific financial management methods. With the rapid development of computer technology, the use of financial management tools is an effective way to improve the quality of financial management. The article applies computer network technology to the financial management system. The main functions of the financial management part and the accounting management part of the system are set as data recording and data statistics display. The financial management system combines the financial management of the university with the informatization of the industry, which realizes the computerization of accounting, and replaces the traditional manual financial mode. The results show that the average response time, data throughput per second, and number of requests per second of the transformed system are higher than those of the untransformed traditional system, and the ratio is about 5% higher. This shows that the financial management system constructed by the computer network technology can play a certain role in the operation of the university.

1. Introduction

Data management system is a comprehensive information management system that uses information technology to manage modern university. Data management systems are widely used in enterprises, government units, schools, and other fields. By utilizing IT and network technologies, it can support the most advanced university management solutions, integrate all internal and external information sources, and provide systematic management for decision-making, management, and evaluation of business development. Among them, the financial management system is an important unit, which can predict, make decisions, and manage the development of the university based on the distribution and statistical data analysis of students and teachers, funds, and information. With the advent of the "Internet Plus" era, all kinds of university are facing the challenge of the information tide, and the competition among university is becoming increasingly fierce. Internet plus has had a significant impact on industry, education, medical care, and other fields. The university adopts advanced financial management system, which can realize the efficient management and control of financial information. Therefore, it is necessary to improve the efficiency of financial management, reduce management costs, and improve the accuracy and consistency of financial information.

For the financial management system, domestic and foreign experts have a lot of research. Based on the balance between the interests of the shareholders, Sherquzieva discussed the role of dividend policy in the financial management system of joint-stock companies, which are aimed at improving the investment attractiveness of joint-stock companies. Scientific advice and practical advice on the effective dividend policy of joint-stock companies were provided [1]. Qian analyzed the construction and implementation of financial management system in e-commerce. It mainly introduced database technology, B/S structure, and the main content of MVC model. At the same time, the main content and business research methods of the financial management system were explained [2]. Malikov proposed an algorithm

to construct a university management system, which determined the financial goals of the university, configured the financial management subsystem, and supported the information of the financial management system. Besides, the financial management rules were formulated and implemented to present the financial goals of the university as a next-level three-tier model [3]. Although his research is relatively comprehensive, the accuracy rate needs to be improved. Kondratenko et al. discussed some features of developing adaptive financial management systems in domestic firms. A multivariate model was proposed that allowed a detailed study of the interdependence of features, the closeness of the relationship between variables, and so on. It was concluded that developing an adaptive financial management system in a university can help improve the financial performance of the university [4]. The limitation of their research is that it is theoretically strong and lacks practical operation methods. These studies provide some reference for this paper, but the financial management system used is too backward and cannot reflect the latest advanced technology. Therefore, computer technology is introduced to improve the relevant system.

For the use of computer technology in the system, based on the big data Internet technology and research on the related technologies of agricultural product brand e-commerce recommendation system, Tong proposed a hybrid collaborative filtering method for agricultural product brand strategy recommendation combining explicit and implicit. The research results found that the system cannot only help users to quickly recommend agricultural products that meet their needs in the massive information but also provide more similar information for users to identify [5]. Xiaojuan studied the integrated management system of mobile data network security and discussed in detail the research and implementation of the security event management mechanism. The proposed event management can be regarded as an extension of the concept of network management, enriching the content of network management functions [6]. Mammadov et al. proposed the structure of a computer-aided design management system (CADMS). The system provided high performance, flexibility, versatility, and project program accuracy. Algorithm support was developed to manage the computer-aided design process of the FMS to enable an integrated computer-aided design process [7]. But the shortcoming of his research is that the scope of application is too narrow. These algorithms connect the computer and the system very well and provide support for the experimental computer network transformation of the financial system in this paper.

This paper combines the computer system with the financial management system of the university. On the basis of expanding and unifying the existing system, combined with the existing technology, the overall framework and module functions of the financial management system are analyzed and designed in detail, and the specific implementation process and interface are given. The experimental results show that the average response time of the system after the improvement of the computer network is about 4.3 s, and the data throughput per second is about 8150, which is about 5.7, which is higher than that of the system before the transformation.

2. Construction Method of Financial Management System

As an important part of the university's development, the finance department must budget, manage, and analyze all aspects of the university's operations [8, 9]. In addition, the financial department also needs to be responsible for fund management and appropriation cashier work. In order to improve the level and efficiency of financial management, it is an urgent problem to use the latest popular computer technology and efficient resources to build a comprehensive university financial management system that serves users [10, 11].

After the university uses the financial management system, the timely exchange of financial data is realized, the cooperation between departments is deepened, the financial management of the university is strengthened, and the operation of the university is more smooth and efficient. At the same time, it has financial loopholes and the risk of being hacked. This is the main role of the financial management system. Therefore, when designing the reformed system, first of all, the purpose of system development should be clarified according to the actual needs of the university. Then, the main functions of the system are determined around the system development purpose, and then, the main function modules are divided with the function realization as the center, and then, each function module is designed [12]. Each module of this system is independent at first, and the coupling is low. Therefore, in order to speed up the development progress, the synchronous development mode can be adopted [13].

By considering the code redundancy and system adaptability and stability in the system development process, the system architecture is designed in the sense of scalability, with three elements: presentation layer, logic layer, and data. The multilevel design allows each logic level to be independent of itself, which makes the system more flexible and easier to maintain [14]. The main users of the program are the university's financial personnel. Combined with actual accounting and needs, the program is divided into five parts, including financial management topics. The system modules are shown in Figure 1.

In this system, different system functions have corresponding module designs. Each part of the module is connected through the database to realize the whole process of data exchange. Each module has its own special structural characteristics to deal with corresponding different business [15]. The interception of data information by each module corresponds to the entire business processing process, and the acquisition of surrounding notifications is the result of analysis and processing in the IOC container and proxy class. During this process, the system performs permission detection on it to complete the corresponding log management function. The system usage diagram shows the corresponding functions of the roles in the system and plays a direct role in the system development process. The roles in

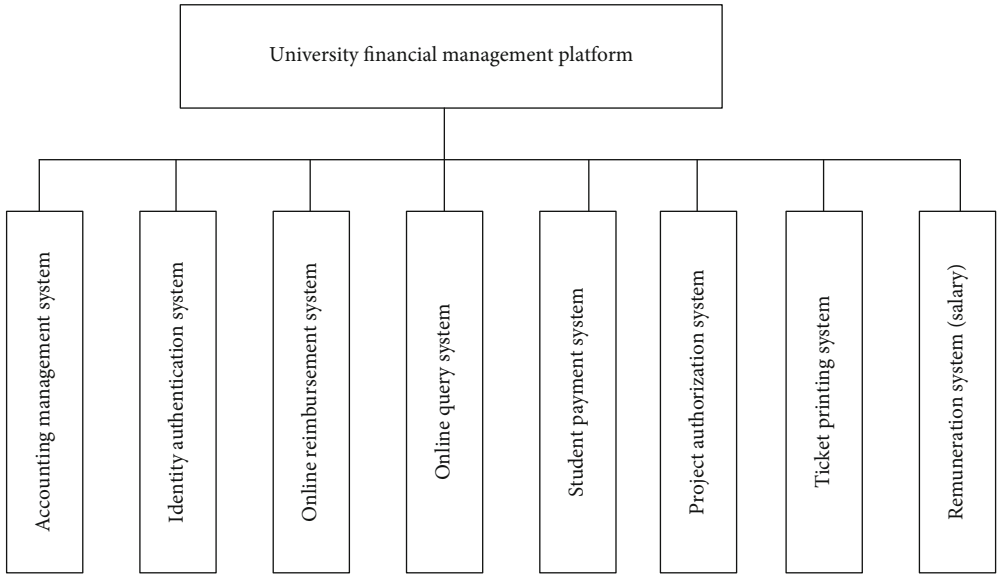

Figure 1: Financial management system module.

the program, the definition of permissions for each role, and the reasons for their assignment are described in detail [16]. The main roles involved in the financial management system are administrators, accountants, and cashiers [17]. As the university grows, the financial management system also needs to integrate operations. Examples used by system administrators are shown in Figure 2.

The operating system designed in this paper cannot only realize the management of financial work but also meet the aesthetic needs and usage habits of most people. The functional modules of the system are also designed to be very clear, and users can quickly grasp the operating functions of the system with the help of the instruction manual [18]. The system also suffers from occasional bugs that do not affect use. In addition, the system does not require high computer configuration. A normal work computer can run the system. Therefore, this paper believes that the system can meet the user's operational needs [19].

System design quality metrics include system security performance, response speed, system operation efficiency, and ease of use [20, 21]. When designing this system, the security of financial data is considered, which is the key to reflect the security performance of the entire system. Therefore, the system sets the corresponding operation authority for different users and also designs a strict examination and approval rules for the management of various assets. In addition, in order to facilitate the staff to quickly search for the required data, when designing the system, special attention is paid to the design of the system search function. The system can realize fuzzy search function by an adopting multifield method.

According to the functional requirements of the university financial system and the characteristics of personnel use, the network topology diagram of the following system is designed [22, 23]. Through this network architecture idea, each application server can be connected to the core switch quickly and effectively, and then, the secondary switches on each floor can distribute data to The physical location of each financial department is then connected to each specific business computer client; considering the security of the network, a firewall is finally set between the core switch and the school router to achieve the security policy on the hardware, outside the router and the public network. Direct connection is convenient for data exchange and remote access. This networking method is simple, fast, efficient, and safe. It cannot only meet the daily work of financial personnel but also facilitate system administrators to solve network failure problems in a timely manner. It is a mature network program, as shown in Figure 3.

3. Platform Implementation

(1) In financial management, payroll accounting is an important module. Payroll accounting is important because it involves the financial income and expenses of an entire unit. There are many factors involved in labor, and employee wages are directly included in the financial budget, so the requirements for accuracy are high. By designing the salary management module, monthly salary reports can be generated for employees to view and use, which is conducive to improving the efficiency of salary management and maximizing cost savings. From the overall function point of view, the salary management module needs to have the following functions: (1) staff management—enter, modify, and delete the basic information and salary data of employees; (2) payroll management—adjust the basic salary and variable salary, and generate the final payroll report; (3) salary adjustment—adjust the working years, positions, and other information, and confirm the amount of relevant subsidies; and (4) salary inquiry—provide salary information inquiries

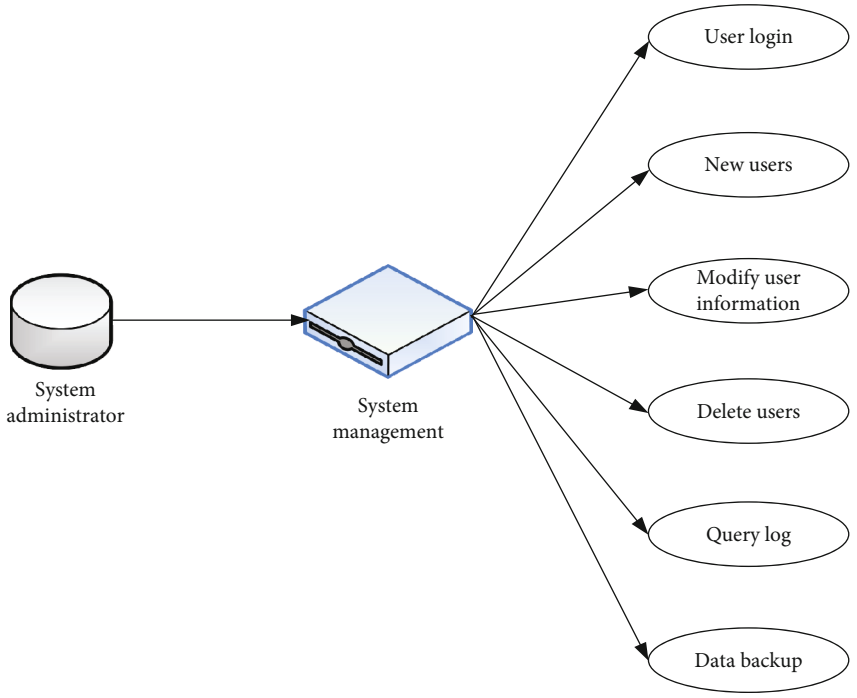

Figure 2: Example diagram of system administrator.

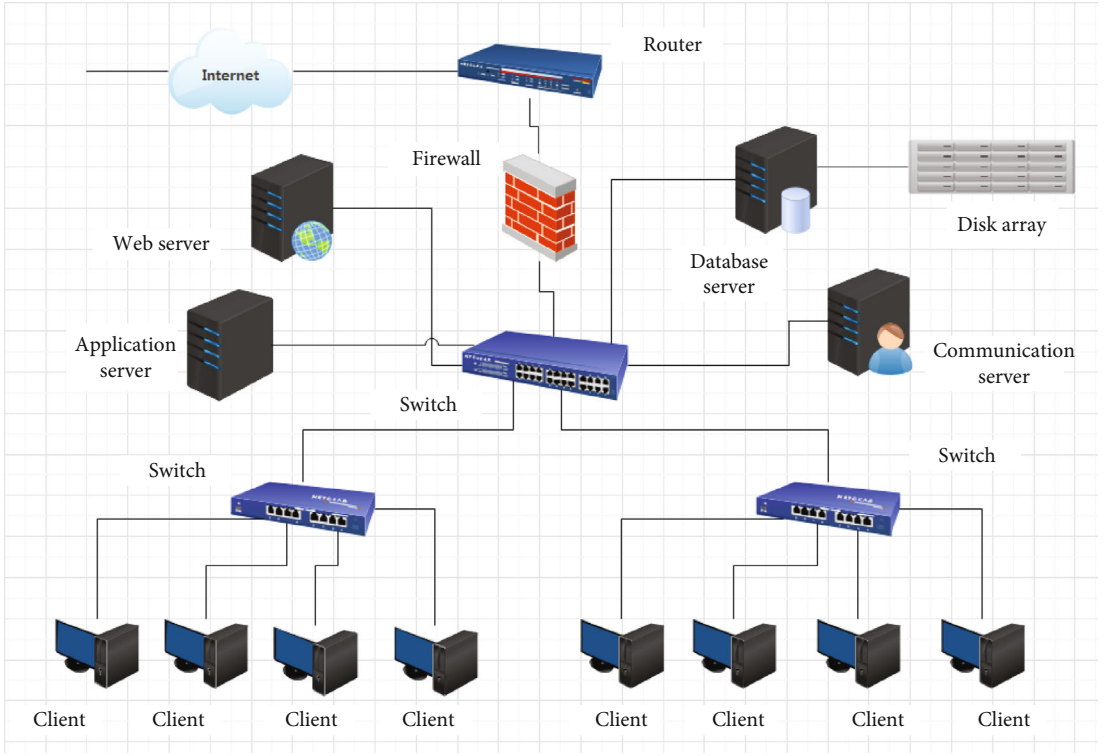

Figure 3: Network topology of financial management system in colleges and universities.

(2) Fixed assets are an important part of asset management, which will directly affect the efficiency of production and operation. The designed asset management module should include the following functions: (1) asset class—categorize, aggregate, and query asset classes; (2) the way of increase and decrease—add, modify, and delete fixed asset information; (3) usage status—record the usage status,

and mainly accrue depreciation; (4) card management—evaluate usage; and (5) provision management—depreciation is accrued according to the specified accounting period

(3) There are accounting processing system, accounting subjects, voucher entry, modification, review, and query (see Figure 4)

(4) In the identity authentication system, the design of the identity authentication system adopts a hierarchical structure, which is mainly divided into a data layer, authentication channel layer, and authentication interface layer and is divided into multiple functional modules, the most important of which are identity authentication module and authority management module. Include the kinds of roles defined for the user (e.g., normal user, advanced user, and admin user). Because the identity authentication system involves user privacy, the security design should be strengthened

(5) The online reimbursement system enables the reimbursement person to fill in the "reimbursement form" online and print it

(6) An online inquiry system can realize project inquiry, salary inquiry, etc.

(7) There are student payment system, import, maintenance, modification of student information, and docking with WeChat payment data (see Figure 5)

(8) In the project authorization system, the project leader can authorize and manage various projects

(9) In the payment platform system, manage charging items; you can view, reverse, import lists, view details, and restart items (see Figure 6)

The financial management system can combine the actual financial management needs of university to achieve efficient financial management. The financial management system has the characteristics of planning, control, and information consistency and has played an irreplaceable role in finance and operation and financial supervision. At present, many universities have used modern financial management systems, and only some small and university or private university use the manual management mode. In addition, most government units, enterprises, and institutions also use modern financial management systems. The traditional manual financial management method has a huge workload, and the efficiency of data record search is low, and it cannot provide statistical and analysis functions for financial management.

This paper believes that the financial management system of such university should have the function of enhancing the decision-making ability of the university leadership. University financial data can provide data support for university leaders to make correct decisions, and the system should have a good expansion function.

The system environment in the design and testing of this system has chosen the Microsoft operating system. This is because compared with the Linux operating system, it is easier to build a running environment in the Microsoft operating system, but if the Microsoft operating system is used directly, there are also many problems. For example, system security performance is not as good as Linux, and there is lack of some functional options. Therefore, this paper uses the Microsoft operating system and the inherited software package together to complete the construction of the operating environment of the system. In most cases, the system testing and operational requirements can be met. The specific hardware environment is shown in Table 1.

In the aspect of improving system reliability, the first is to carry out redundant design of network equipment and adopt the mode of multidevice and multichannel to ensure that after a single device fails, the user's request can still be transmitted to the service system. At least, it is necessary to ensure that the key network links have backup links, so as to ensure that the failure of one network device does not affect the normal operation and access of the entire system. The application server adopts a cluster mechanism, which also ensures load balancing and avoids a single point of failure. Moreover, it provides customers with a capacity expansion mechanism that can grow linearly according to the capacity growth and can achieve the goal of increasing the user capacity of the linear system by increasing the number of application servers.

The system development software environment requires Microsoft Windows 7 operating system to deploy the PC, SQL SERVER2008 is used as the background database for development, IE8 is used as the browser for testing, RAM is 8GB, and Microsoft Visual Studio 2010 is used as the development platform. The specific software development environment is shown in Table 2.

The software system is also designed for redundancy. The authentication, authorization, and billing modules of the system service platform support cluster deployment from the model and use the Cluster mechanism of WebLogic to realize the concurrent operation of the system. By using JNDI technology to achieve information synchronization between multiple systems, even if a single system fails to work normally, another system can still handle the user's request. Moreover, the synchronization of this information is real time, and the user does not feel the abnormality caused by the local fault during the use.

The financial management system of this paper is realized based on B/S mode. In the implementation process, the local client is developed through the browser, the tool used for browser development is Internet Explorer 7, and the plug-in install-IEtester is installed to test the compatibility of different versions.

Through careful analysis of the system requirements, it is determined that the incremental model is used to develop the system. Because the incremental model can be developed in units of incremental packages of a requirement, even at

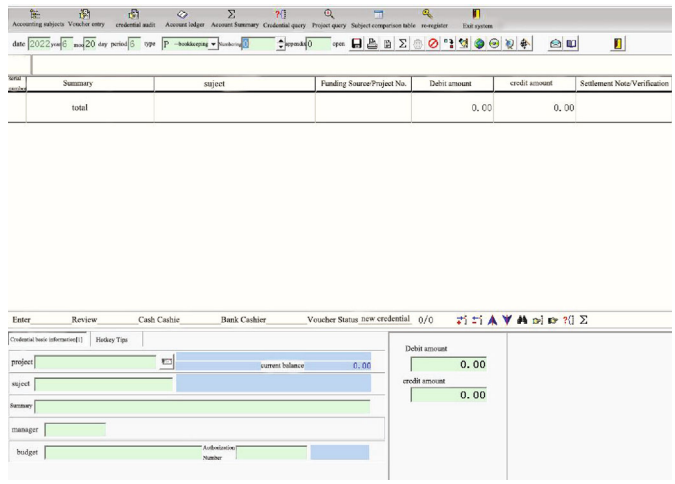

Figure 4: Accounting processing system.

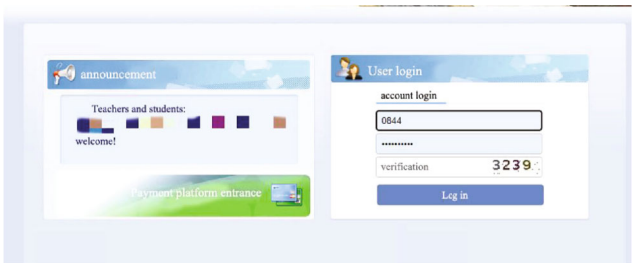

Figure 5: Student payment system.

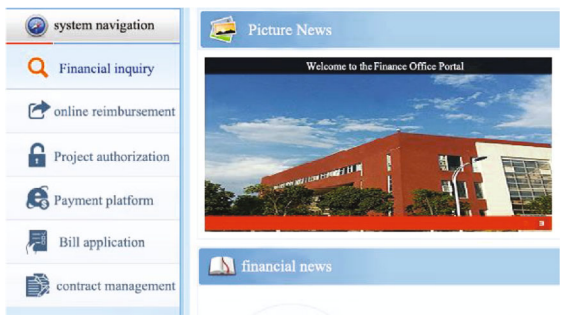

Figure 6: Payment platform system.

the beginning of the design, as long as a requirement incremental package is clarified, development can be started without waiting for all requirements to be constructed. Here, "a requirement incremental package" refers to the specific demand of a customer. As long as this incremental package is small enough, a certain incremental package may need to be further adapted to customer needs and changes. The impact is tolerable for the entire project development process. As a user, in the process of system development, there are many opportunities to modify the requirements, so that the final system can meet the actual needs of users to the greatest extent. Figure 7 shows a screenshot of the user login module implementation interface.

After completing the interface design of the form, the system further designs the business processing layer. Further analysis is carried out by taking the business layer of the credential management module as an example. First, a business type Voucher class for the module is created in the system, which realizes the proxy and interception of information processing more conveniently and quickly. Then, an interface class IVoucher class is created. In this process, the business that needs to be processed needs to declare the business processing method. Specifically, the main declaration methods include save, delete, and audit methods. These declarations implement their processing functions in the Voucher class, which facilitates data exchange in the database.

On the one hand, an IOC container can be used to form a target object that can inherit the IVoucher interface, which can act as a proxy IOC container in the future system work, and then complete the business class Voucher. On the other hand, it can also be used to add relevant information to intercept the associated operations. Only in this way, while exchanging information on the form interface, it is possible to carry out certain surrounding notification operations for the corresponding specific business. Once the operation of the form interface is completed, the button on the toolbar can be clicked to perform the corresponding functional operation and achieve the response of the related business at the same time.

Usually, the form of the table design in the database is mainly determined by the corresponding attributes of the data entity to be designed, and the specific setting of each attribute is also determined according to the corresponding field. At the same time, each field can also have its own attribute characteristics. The conceptual structure of the database refers to the logical structure form that can be automatically recognized by the system during the background movement of the system. This structure is different from the client's display database. It is the key point to connect the client and the background system. The rationality of its setting directly affects the stability of the system operation.

In the detailed design process of the system, it is necessary to decompose the entity classes into data classes and

Table 1: Hardware environment for system development.

Hardware name	Model and configuration	Usage time	Quantity
Host	Lenovo	The whole experimental process	1
Memory	8G	The whole experimental process	1
Hard disk	1TB	The whole experimental process	1
Network card	10/100 Mbps	The whole experimental process	1

Table 2: System software configuration.

Serial number	Name of software	Version	Use
1	Microsoft Windows	11	Operating system
2	SQL SERVER	2019	Database development
3	IE	8	Software support
4	Microsoft Visual Studio	2019	System development

Figure 7: Screenshot of the login interface.

then abstract the concrete data structure. The following takes the credential management module as an example to illustrate the data structure of the system. The university's projects may be distributed in different regions, and the rules for financial statements or auditing are different in each region, so template settings can be made according to specific financial formulations to meet the needs of different businesses.

According to the actual needs of the financial management system, this paper designs the system as a whole, puts forward the overall design goal of the system, and designs the system logic architecture. It includes the specific design of data access layer, business logic layer, and user presentation layer. The network structure of the system is shown through the network topology diagram, the functional structure of the system is described and displayed graphically, and the design of the system data table is shown.

4. System Performance

4.1. Response Time. The financial system before and after the system improvement is tested, and the number of tests is 50 times. The response time of the system before and after the improvement is compared, and the results are shown in Figure 8.

As can be seen from Figure 8, the average response time of the traditional financial management system is about 7 s, and the response time is not stable. In the 50 test time, there are 5 fluctuations, accounting for 10% of the total test time, and the fluctuation of the fluctuation is more than 50%. The average response time of the system after the transformation of the computer network is about 4.3 s. And during the test, the response time is basically stable, and the fluctuation is basically stable at about 15%. It can be seen that the financial management system designed in this paper is better than the traditional system.

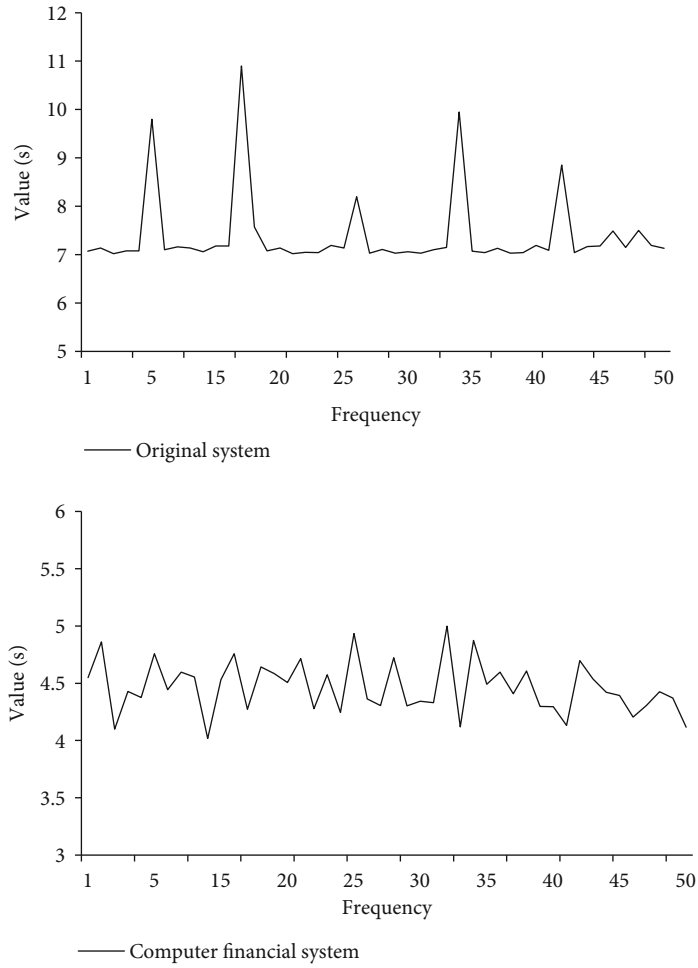

Figure 8: Response time.

4.2. Throughput per Second. Throughput is a limit indicator, that is, an indicator when network devices are fully configured on all ports and work at the highest wire speed of the ports. If the highway traffic system connecting different cities is used as an analogy, the throughput of a switch is equivalent to the sum of the traffic flow in and out of all cities in the system, that is, the sum of the bidirectional packet forwarding rates of all ports of the switch. The size of the throughput is mainly determined by the internal and external network port hardware of the network device and the efficiency of the program algorithm, especially the program algorithm. For a device that needs to perform a large number of operations, the low efficiency of the algorithm greatly reduces the communication volume.

Throughput is a metric when network devices are fully configured on all ports and operating at maximum speed. By taking highway links in different cities as an example, the modified result is equivalent to the sum of the inbound and outbound traffic of all cities in the system, that is, the sum of the bidirectional packet forwarding rates of all switch ports. The output size mainly depends on the application of the internal and external network ports of the network device and the performance of the system algorithm, especially the system algorithm. For devices that need to perform a large number of tasks, the poor performance of the algorithm can greatly reduce the amount of communication. This paper makes statistics on the throughput per second before and after the system improvement, and the results are shown in Figure 9.

As can be seen from the comparison in the figure, the data throughput per second of the traditional university financial system is about 7900, and the ups and downs are about 10%. After the transformation, the data throughput of the system per second is about 8150, and the ups and downs are about 8%. It can be seen that the stability of the system transformed by the computer network is better than that of the original system, and the throughput per second is about 3% higher than that of the traditional system.

4.3. Number of Requests per Second. The performance of the system is mainly tested for response time, throughput per second, and number of requests per second, and the corresponding time and throughput have been tested. Here, the number of requests per second of the financial management system is also tested, and the results are shown in Figure 10.

As can be seen from the figure, the average data request per second of the original financial management system is around 5, and the highest is 7.6. The average number of

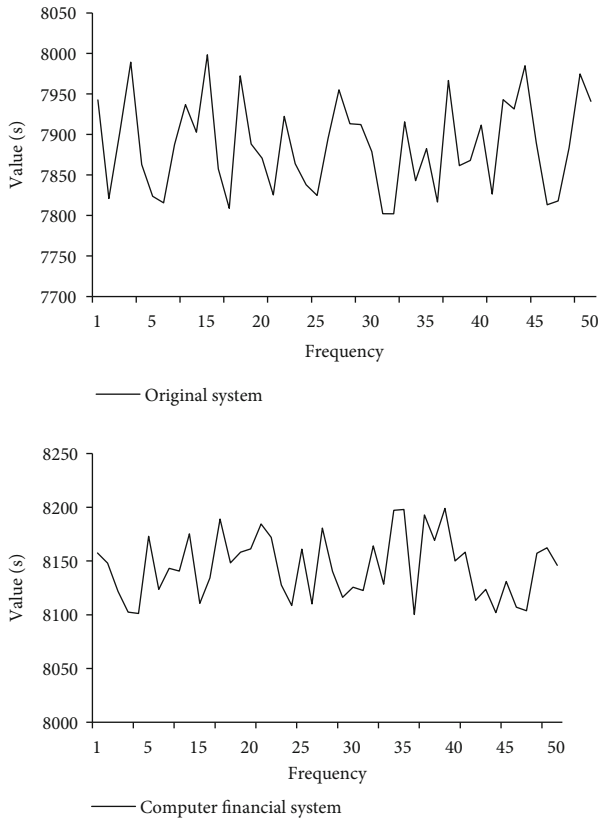

Figure 9: Throughput per second.

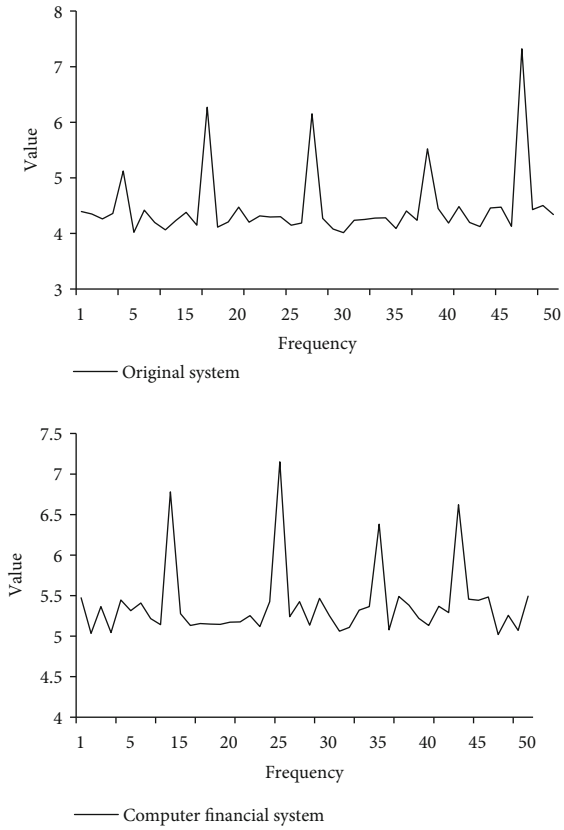

Figure 10: Number of requests per second.

requests per second for the financial management system constructed by computer network technology is around 5.7, with a maximum of 7.4. It can be seen that the average request volume of the system constructed in this paper is higher than that of the traditional financial system, while the highest request volume is slightly lower than that of the traditional financial system. Therefore, when universities choose a financial system, they need to choose different methods to build a financial management system according to their own needs, so as to achieve better results.

5. Conclusion

In the current era of information technology leading the industrial economy, Chinese university must make great efforts in informatization. By sorting, analyzing, and processing information, the useful content for the university can be obtained quickly. And the financial management system designed and implemented in this paper is to solve this kind of problem. This paper starts from the background of software engineering and system analysis and discusses the design and implementation of the system from the aspects of related theoretical technology, system requirement analysis, system design, and system test implementation. Aiming at the current overall development of the financial management system of university, the operation requirements that conform to the actual situation and follow the basic principles of developing cognition and combining with income are put forward. According to the process management and characteristics of university, the functional modules of the system are shared in detail. Of course, there are some downsides. The built financial management system does not have the functions of a complete system, and some functions cannot be clearly defined, which leads to the system design not using more advanced design techniques. After that, by analyzing different business conditions and financial management system information, comparing the compatibility and integration of different programs, improving the system service department, and making the system play a greater role.

Data Availability

The data of this paper can be obtained through email to the authors.

Conflicts of Interest

The author declares that there is no conflict of interest regarding the publication of this work.

References

[1] I. Sherquzieva, "The role of dividend policy in the financial management system of joint-stock companies," *International Finance and Accounting*, vol. 2019, no. 3, pp. 22–22, 2019.

[2] J. Qian, "The construction and implementation of financial management system in electronic commerce," *Agro Food Industry Hi Tech*, vol. 28, no. 1, pp. 1415–1419, 2017.

[3] V. V. Malikov, "The algorithm for building a financial management system at the enterprise," *Business Inform*, vol. 3, no. 506, pp. 344–348, 2020.

[4] N. O. Kondratenko, M. M. Novikova, and N. Y. Spasv, "Developing an adaptive financial management system at an enterprise," *The Problems of Economy*, vol. 1, no. 47, pp. 78–84, 2021.

[5] Z. Tong, "Application of information system and computer internet technology in integration of geographical indication agricultural products," *Journal of Physics Conference Series*, vol. 1982, no. 1, pp. 012144–012146, 2021.

[6] X. Ma, "Research and implementation of computer data security management system," *Procedia Engineering*, vol. 174, pp. 1371–1379, 2017.

[7] J. Mammadov, I. Aliyev, G. Huseynova, and G. Orujova, "Algorithmic support for the management of the computer-aided design of flexible manufacture system and its equipment," *Cybernetics and Systems Analysis*, vol. 57, no. 6, pp. 950–958, 2021.

[8] V. Tkachenko, "Financial cycle controlling in the anti-crisis financial management system of the enterprise," *Modern Economics*, vol. 20, no. 1, pp. 296–301, 2020.

[9] X. T. Li, J. Wang, and C. Y. Yang, "Risk prediction in financial management of listed companies based on optimized BP neural network under digital economy," *Journal of Manufacturing Processes*, 2022.

[10] P. Handayati and M. Palil, "The village financial management system: a policy towards independent villages," *Jurnal Ekonomi dan Studi Pembangunan*, vol. 12, no. 1, pp. 1–9, 2020.

[11] M. Lai, "Smart financial management system based on data ming and man-machine management," *Wireless Communications and Mobile Computing*, vol. 2022, Article ID 2717982, 10 pages, 2022.

[12] S. Lin, "Financial performance management system and wireless sharing network optimization of listed university under BPNN," *Mobile Information Systems*, vol. 2021, no. 4, Article ID 3443189, 11 pages, 2021.

[13] B. V. Nabijonov, "Methodological foundations for the development of the financial management system," *Theoretical & Applied Science*, vol. 93, no. 1, pp. 246–250, 2021.

[14] H. Zhang, "A deep learning model for ERP enterprise financial management system," *Advances in Multimedia*, vol. 2022, Article ID 5783139, 11 pages, 2022.

[15] S. Samad, "Theory of planned behavior and knowledge sharing among nurses in patient computer management system: the role of distributive justice," *Management Science Letters*, vol. 8, no. 5, pp. 427–436, 2018.

[16] Y. Lu, Y. Wang, and R. Chen, "Design of enterprise financial information management system based on blockchain technology," *Security and Communication Networks*, vol. 2022, Article ID 2566615, 8 pages, 2022.

[17] X. Xu, "Optimal control method of power system based on computer aided technology," *Computer-Aided Design and Applications*, vol. 19, no. S4, pp. 102–112, 2021.

[18] X. Wang, "Mathematical model of quantitative evaluation of financial investment risk management system," *Mathematical Problems in Engineering*, vol. 2022, Article ID 2439549, 14 pages, 2022.

[19] Z. Xu, M. M. Kamruzzaman, and J. Shi, "Method of generating face image based on text description of generating adversarial network," *Journal of Electronic Imaging*, vol. 31, no. 5, article 051411, 2022.

[20] Z. Xu, G. Zhu, N. Metawa, and Q. Zhou, "Machine learning based customer meta-combination brand equity analysis for marketing behavior evaluation," *Information Processing & Management*, vol. 59, no. 1, p. 102800, 2022.

[21] Y. Yang, "Design and implementation of an accounting risk identification system for the financial industry based on computer technology," *Revista de la Facultad de Ingenieria*, vol. 32, no. 6, pp. 1–8, 2017.

[22] H. Li, C. Huang, and L. Gu, "Image pattern recognition in identification of financial bills risk management," *Neural Computing and Applications*, vol. 33, no. 3, pp. 867–876, 2021.

[23] X. Wang, Z. Ting, X. Wang, and F. Yili, "Harshness-aware sentiment mining framework for product review," *Expert Systems with Applications*, vol. 187, p. 115887, 2022.

Hindawi
Wireless Communications and Mobile Computing
Volume 2023, Article ID 9787542, 1 page
https://doi.org/10.1155/2023/9787542

Retraction

Retracted: Construction of User Behavior Web Data Mining Model for Internet Marketing

Wireless Communications and Mobile Computing

Received 17 October 2023; Accepted 17 October 2023; Published 18 October 2023

This article has been retracted by Hindawi following an investigation undertaken by the publisher [1]. This investigation has uncovered evidence of one or more of the following indicators of systematic manipulation of the publication process:

(1) Discrepancies in scope
(2) Discrepancies in the description of the research reported
(3) Discrepancies between the availability of data and the research described
(4) Inappropriate citations
(5) Incoherent, meaningless and/or irrelevant content included in the article
(6) Peer-review manipulation

The presence of these indicators undermines our confidence in the integrity of the article's content and we cannot, therefore, vouch for its reliability. Please note that this notice is intended solely to alert readers that the content of this article is unreliable. We have not investigated whether authors were aware of or involved in the systematic manipulation of the publication process.

Wiley and Hindawi regrets that the usual quality checks did not identify these issues before publication and have since put additional measures in place to safeguard research integrity.

We wish to credit our own Research Integrity and Research Publishing teams and anonymous and named external researchers and research integrity experts for contributing to this investigation.

The corresponding author, as the representative of all authors, has been given the opportunity to register their agreement or disagreement to this retraction. We have kept a record of any response received.

References

[1] M. Wei, "Construction of User Behavior Web Data Mining Model for Internet Marketing," *Wireless Communications and Mobile Computing*, vol. 2022, Article ID 2813718, 10 pages, 2022.

Hindawi
Wireless Communications and Mobile Computing
Volume 2022, Article ID 2813718, 10 pages
https://doi.org/10.1155/2022/2813718

Research Article

Construction of User Behavior Web Data Mining Model for Internet Marketing

Ming Wei

Guanghua School of Management, Beijing 100000, China

Correspondence should be addressed to Ming Wei; 2101220932@stu.pku.edu.cn

Received 28 July 2022; Revised 24 August 2022; Accepted 8 September 2022; Published 22 September 2022

Academic Editor: Jun Ye

With the rapid development of the Internet and the rapid change of the era of big data, data mining has played a great role in exploring and discovering potential valuable information from the vast sea of data and has become one of the most popular research and practice fields. At the same time, the emerging marketing model of network marketing is sweeping the market, and network marketing is increasingly replacing the traditional marketing model with its unique advantages, such as wide coverage, fast dissemination, and being more flexible and targeted. Preserving, researching, and analyzing the behavior of network marketing users are the difficulties of current network marketing. It is the focus of this paper to explore how to use Web data mining technology to model the user behavior of Internet marketing. For the above problems, this paper used the weight calculation algorithm of users' daily behavior feature items and the sequential pattern discovery algorithm based on multiple factor constraints to scientifically construct the online marketing user behavior model. The experimental results have shown that the sequential pattern discovery algorithm based on multiple factor constraints could save 30%-40% of the running cost when building a user behavior model. At the same time, the user behavior model constructed by this algorithm has improved the simulation and prediction accuracy of user behavior by 37%, which showed that the use of Web data mining to build network marketing user behavior model could provide an objective basis for the strategic development of network marketing.

1. Introduction

In recent years, the data in the web has been increasing at a rate of 1 million web pages per day. The widespread popularity of computer networks has made the Internet develop into a huge distributed information space with hidden potential value knowledge and immeasurable data. The reason is that people's lives are inseparable from the Internet. Various shopping software, entertainment software, takeaway software, and travel software are flooded in people's daily lives, and everyone's clothing, food, housing, and transportation have left traces on the Internet. Today, with the rapid development of the Internet, the mass production and collection of various forms of information have caused an explosion of information. For ordinary network users, how to quickly and accurately obtain valuable network information, find out what is useful to them, and find out more valuable knowledge has become an important topic currently faced. On the other hand, as the Internet is becoming more and more popular today, because of its low cost, convenience and speed, and not being limited by time and space, e-commerce has developed extremely rapidly since its inception and has become popular all over the world.

At the same time, the advantages of network marketing, a marketing model that combines the Internet with modern digital electronic methods, are gradually emerging. Based on the above discussion, it is necessary to build a user behavior model for network marketing with the help of web data mining today when network marketing is popular. It obtains useful information from a large amount of data, finds out customer purchasing preferences, and provides personalized services to increase customer retention time. It taps potential users to expand market share, which is of great strategic significance to help e-commerce take off.

This paper uses Web data mining technology to study the construction of online marketing user behavior model.

It uses the weight calculation algorithm of users' daily behavior feature items and the sequential pattern discovery algorithm based on multiple factor constraints, which is aimed at providing a more accurate and rich database for user behavior research in the face of Internet marketing, so as to better improve the construction of behavior models. Constructing a scientific and accurate user behavior model can better promote the implementation of network marketing strategy and the selection of marketing methods and objects and then have a more profound impact on the development of e-commerce. In this paper, the experiment and result analysis of sequential pattern discovery algorithm based on multiple factor constraints show that the user behavior model constructed by this algorithm can save about 40% of the running cost. The innovation of this paper are as follows: (1) a sequential pattern discovery algorithm constrained by multiple factors is used for the construction of the user behavior model, which makes the research of this model more scientific and accurate. (2) Based on Web data mining technology and the construction of user behavior model, it provides more scientific algorithm support for network marketing and even e-commerce.

2. Literature Review

On the booming and ubiquitous Internet, a large amount of online user behavior data is generated every day, so the analysis of network user behavior has developed rapidly from scratch. Sarker et al. proved that user behavior has certain regularity through a large number of experiments, but did not find a suitable method to mine the features [1]. After analyzing various algorithms and software, Qian et al. found that the behavior of Internet users has its unique regular characteristics, and this behavioral characteristics play an important role in predicting the future behavior of most Internet users [2]. Many scholars in China and other countries have done a lot of work on how to improve the efficiency of data mining. However, most of the current methods have certain defects, such as high algorithm complexity and being easy to fall into the local optimal solution or large amount of calculation. Shin believed that the behavior of network users is a process with a certain subjective initiative. Due to the concealment of network users themselves, it is difficult for network users to obtain their real identities [3]. Singh et al. proposed a new PPSA scheme to protect users' sensitive data from being acquired or leaked by external analysts or aggregation service providers [4]. Esdar et al. found in their research that user behavior has a significant guiding effect on e-commerce websites, which can help e-commerce websites improve web page interaction design and enhance user experience [5]. Although the current academic analysis of user behavior is varied, most of the existing analysis only emphasizes strong privacy protection. User behavior analysis for online marketing only protects its privacy is very limited, which is difficult to meet the need of behavior analysis.

With the rapid development of science and technology and the continuous improvement of people's living standards, network terms such as the Internet and web have also begun to appear in thousands of households. In order to have a deeper understanding of consumers' purchasing preferences and consumption habits in the Internet age, web-based data mining is proposed. Gang was the first to explain web data mining. Web data mining is to start from the large-scale raw data stored in the web background information database, mining the information that is helpful to marketers and can be used directly, and finally display it to marketers in a concise and intuitive way [6]. Agirre believed that data mining also known as database knowledge discovery is mainly composed of seven parts: data cleaning, data integration, data selection, data transformation, pattern discovery, pattern evaluation, and knowledge representation [7]. The main purpose of Web data mining is to convert these data into useful information to help companies make better marketing strategies. Most of the current research focused on text mining, but there was no report on image data mining. When Lixia et al. researched algorithms in data mining, they found that the decision tree algorithm is currently the most widely used and adaptable data mining algorithm. The decision tree algorithm belongs to the inductive reasoning algorithm, which can use the approximate discrete value function to process the noisy data and then analyze to obtain the expression [8]. On the other hand, Kazanidis et al. pointed out that there are many methods of data mining, including classification, regression analysis, cluster analysis, feature analysis, and web data mining. Different methods are applied in different occasions, and they have different characteristics [9]. Jeffery et al. suggested predicting user access requests. Based on the user's previous access situation, the content of the page that the user will visit next was dynamically generated [10]. Due to its low accuracy, traditional data mining requires users to make multiple operation attempts. However, the task of Web data mining would rely on the self-operation and operation of the Internet, which can improve the intelligence of interactive learning and coordination. Therefore, its addition not only improved the efficiency of data mining but also saved valuable time for users.

3. Construction Method of User Behavior Web Data Mining Model for Internet Marketing

3.1. Internet Marketing User Behavior

3.1.1. e-commerce. e-commerce is a new economic and commercial activity in the information environment, and it is also the main carrier and platform for the development of the information economy. Since its birth in 1997, e-commerce has gone through more than 20 years of exploration and development. China's Internet construction and e-commerce development have played a pivotal role in the world [11]. Since 2013, China's e-commerce transaction volume has been rising steadily, from 1 billion in 2013 to 7 billion in 2020 with a rapid development, as shown in Figure 1.

As shown in Figure 2, the average annual growth rate of China's e-commerce transaction volume was also generally on the rise, reaching its peak in 2018 and up to 57.8%. The e-commerce market has broad development space and huge

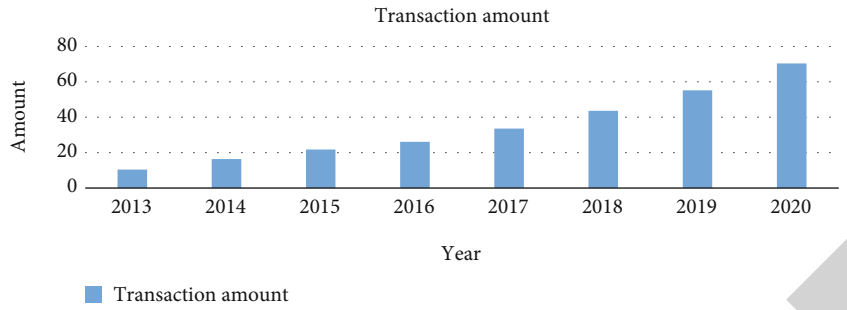

Figure 1: China's e-commerce transaction scale from 2013 to 2020 (trillion yuan).

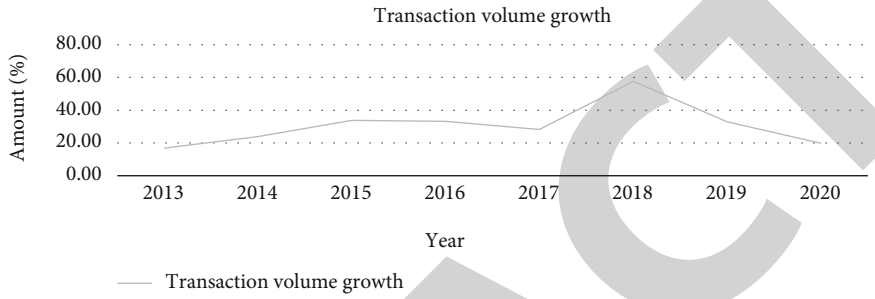

Figure 2: Growth rate of e-commerce transactions in China from 2013 to 2020.

Table 1: Scale and growth rate of e-commerce employment in China from 2015 to 2017.

	Employment scale (10,000 people)	Year-on-year growth rate
2015	2698	16.54%
2016	3255.74	21.78%
2017	3790.43	15.74%

potential, and is becoming a new engine for the rapid and sustainable development of China's national economy.

At present, e-commerce has been shining brightly in economic life, and it is playing an increasingly important role in manufacturing, commerce and trade and financial industry. e-commerce urges people to make rational use of "fragmented time," cultivate people's new consumption habits, and promote the rapid growth of consumer demand. For example, thanks to the development of e-commerce, people can easily realize the freedom of shopping by simply moving their fingers on their mobile phones without having to squeeze out a large chunk of time for shopping. By the end of 2016, the number of online shopping users in China reached 467 million, and the transaction size of the online retail market was 5,155.6 billion yuan, a year-on-year increase of 26.2%. The development of e-commerce has created a large number of jobs, as shown in Table 1. By the end of 2016, China's e-commerce services directly or indirectly created 37.6043 million jobs, and e-commerce has also become the preferred field for mass entrepreneurship and innovation.

3.1.2. Internet Marketing. The development of e-commerce gave birth to network marketing. This is due to the development of e-commerce, which enables people to shop easily. The traditional marketing combined with traditional commerce has lost its rooted soil, and new marketing models will naturally appear to replace it. Network marketing was born in the 1990s. It is a new type of marketing method based on the Internet and effectively using the network medium to spread a large amount of data information [12]. It can effectively use the social media and digital information that has been popularized at present, so that marketing goals can be achieved faster and better. Network marketing is the result of three combined forces of marketing, technology, and economy. At present, the most common understanding of network marketing is a series of activities that realize the purpose of enterprise marketing by focusing on the customer and using the network as the medium. Its specific principle is that enterprises carry out network marketing around customers and use the network as a medium to spread marketing to promote the realization of network marketing purposes, as shown in Figure 3.

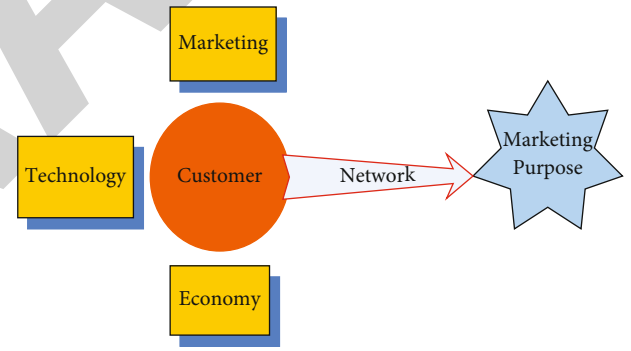

Figure 3: Basic structure of network marketing.

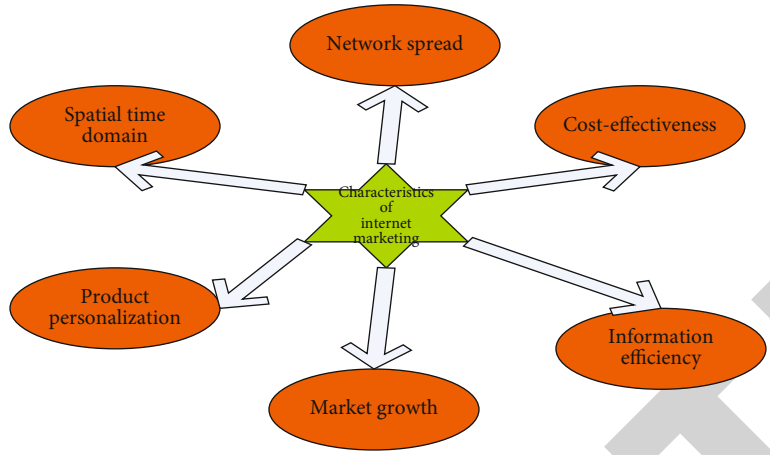

Figure 4: Characteristics of Internet marketing.

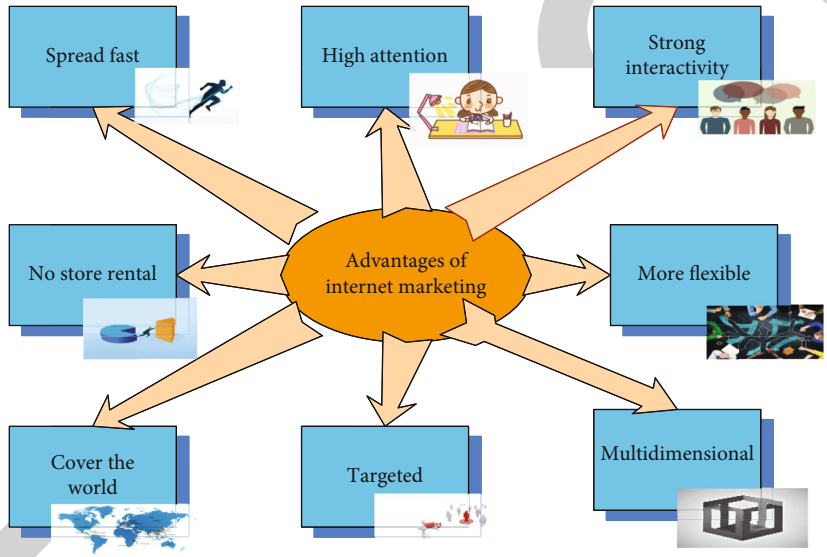

Figure 5: Advantages of Internet marketing.

It should be pointed out that "Internet marketing" does not equal "e-commerce." Internet marketing is a means to achieve the purpose of e-commerce, and e-commerce is the ultimate purpose of Internet marketing. Network marketing occupies an important position in the whole process of e-commerce, and e-commerce is an advanced stage pursued by the development of network marketing [13]. Compared with the traditional marketing model, network marketing has the following characteristics, as shown in Figure 4.

Network marketing does not necessarily mean that the purpose of e-commerce can be achieved. However, in order to achieve e-commerce, Internet marketing must be a prerequisite. For the development of enterprises, network marketing will play an irreplaceable and important role in traditional marketing. In the long run, network marketing has the following eight advantages, as shown in Figure 5.

3.1.3. Types of Internet Marketing Users. For network marketing, the most important foundation is the user [14–16]. User behavior is the various behaviors that users do during the process of entering the e-commerce platform until exiting, usually including browsing clicks, decision-making, and evaluation. Capturing user behavior and adjusting the network marketing strategy is the key to the success of network marketing. As a very important part of network marketing, customer analysis is based on customer classification to carry out marketing activities, which is more targeted and has better marketing effects.

Through research and analysis, this paper divided the types of users of network marketing into three categories.

(1) For homeless users, the number of types of homeless users and all the values are relatively low. From this trend, it can be seen that homeless users are not very interested in online marketing activities. They are only in a wait-and-see state, so the marketing focus of this user is to stimulate the user's interest in shopping

Table 2: Differences between different user behaviors.

	Nomadic user	Follow other users	Active user
Clicks	0 ~ 20	21~200	201~500
Browsing dwell time(s)	≤20	22~50	51~60
The number of purchases	≤5	6~100	≥200

(2) Follow other users. As the name implies, it is to pay attention to the behavior of other users. This type of user is generally less proactive, and most of them pay more attention to the consumption of others. Therefore, in the face of such users, the focus of online marketing is to expand the marketing scale for the consumption points that they are concerned about to consolidate such users

(3) Active users are more active on the e-commerce platform, which is commonly known as the "hand-picking party." They are keen on consumption and cannot resist the means of online marketing. In the face of this type of users, new online marketing methods should be constantly created to attract their attention, while consolidating and developing new active users

Different types of users have different user behaviors, and the types of users can be analyzed from the user's click behavior, browsing time, purchase records, and other behaviors. For example, active users are keen to see now and buy now, so their traffic data is high. However, on the other hand, because they skip the shopping cart step, they have relatively low data on adding to the cart, as shown in Table 2.

Users' browsing behaviors can be classified into four categories, such as click, add to cart, favorite, and purchase [17]. In fact, by calculating the number of times in each period and making a line graph, the user's browsing behavior can be further observed, as shown in Figure 6. Among them, Figure 6(a) shows that the number of times the user clicks on the item changes with time. Figure 6(b) shows the change in the number of users adding to the shopping cart over time.

According to the above chart, Table 3 gives the clustering results divided into 8 segments, which comes from the ordered clustering analysis of the Q language. Q language is a special language for cluster analysis, which is characterized by the ability to analyze time-sorted data and more intuitively show the hidden laws behind the data.

3.2. Construction of User Behavior Feature Model Based on Internet Marketing

3.2.1. Extraction of User's Daily Behavior Feature Items. In order to better describe the behavioral characteristics of users, the various behaviors of users can be regarded as a set. Here, the user behaviors are defined as actitem = $\{act_{id}, sem\}$, act_{id} is the ID of the user behavior to which they belong, and sem is the behavior represented by the behavior feature item.

In view of the above settings, this paper obtains the formula for calculating the behavior degree as follows:

$$\mathrm{ActItem}_{act_i} = \left(\frac{\sum_{\forall act \in act_i} c_{act}}{\sum_{\forall act} c_{act}} + \frac{\sum_{\forall act \in act_i} d_{act}}{\sum_{\forall act} d_{act}}\right). \quad (1)$$

Among them, $\sum_{\forall act \in act_i} c_{act}$ represents the number of times that the behavior occurs in the face of online marketing, $\sum_{\forall act} c_{act}$ represents the number of times the user's behavior occurs in the entire complete trajectory, $\sum_{\forall act \in act_i} d_{act}$ represents the duration of the current behavior, and $\sum_{\forall act} d_{act}$ represents the total time of the user's behavior in the entire complete trajectory.

The weight of a feature item is calculated according to the entire calculation formula. If it is greater than a certain threshold, it means that this behavior is more important to the user. If it is greater than this threshold, it indicates that this behavior of customers is relatively frequent, and it is an important data source for researching customer behavior and building customer behavior models. Thus, it is included in the user's behavior set, and its corresponding behavior feature items are collected into the behavior feature item set.

3.2.2. Calculation of the Weight of the User's Daily Behavior Feature Item. Through the above research, the behavior feature items of the user's daily behaviors can be obtained. However, in the process of modeling, the extracted behavior feature items need to be calculated with a certain weight. The weight value indicates the influence of the feature item on the user trajectory data model. There are many ways to calculate the degree and weight:

(1) Word frequency: the word frequency is defined as the comparison value between the number of documents D containing the feature item and the number of all documents, which can be expressed as the following formula:

$$DF = \frac{D}{D_{\mathrm{total}}}. \quad (2)$$

(2) Mutual information (MI): mutual information is used to measure the amount of information that an event contributes to other events. In the selection process of feature items, mutual information can be used to measure the degree of correlation between keyword k and category L_i, as shown in

$$\mathrm{MI}(K, D_i) = \frac{p((K, D_i))}{P(T) * P(D_i)}. \quad (3)$$

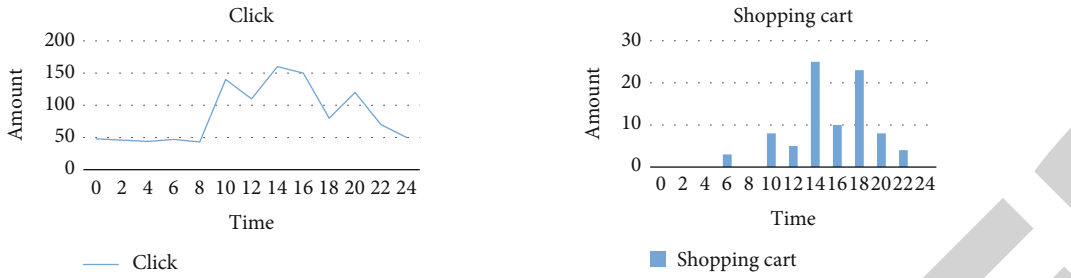

(a) Graph of user clicks on items over time (b) Graph of the times of the user adding to the shopping cart over time

Figure 6: Line chart of the number of times users clicked items and added to carts.

Table 3: Time series clustering results of user clicks.

8	Q1 = {1, 2, 3, 4, 5, 6, 7, 8, 9, 10}
	Q2 = {11, 12, 13, 14, 15, 16, 17, 18}
	Q3 = {19, 20, 21, 22, 23}
	Q4 = {24, 25, 26, 27, 28, 29, 30}
	Q5 = {31, 32, 33, 34, 35}
	Q6 = {36, 37, 38}
	Q7 = {39, 40, 41, 42, 43, 44, 45, 46}
	Q8 = {47, 48}

Among them, K represents the keyword, D represents the document D containing the feature item, and P represents the contribution information of an event.

(3) TF-IDF method: TF-IDF is a weighting technique often used in user information retrieval and data mining to evaluate the importance of a word to a certain document set or a certain corpus. Through TF-IDF, the user's daily behavior and activity types can be counted, as well as the representativeness and discrimination of each word to the user. Its calculation formula is as follows:

$$tf_{i,j} = \frac{m_{i,j}}{\sum_k m_{k,j}}. \tag{4}$$

Reverse document frequency measures the general importance of words, which is of great significance in the field of natural language processing, especially for language models and text classification. The IBF of a specific word can be calculated by dividing the total number of documents by the number of documents containing the word and then taking the logarithm of the quotient. The calculation formula is as follows:

$$ibf_i = \log \frac{|B|}{|\{j : s_i \in b_j\}|}. \tag{5}$$

(4) Analytic hierarchy process: it solves problems by decomposing, by dividing a large problem into different levels. The highest level is the target level, the lowest level is the specific solution, and the rest are various indicators that affect decision-making [18]. The type of model that this paper needs to build is a hierarchical vector model. In the initial stage of model creation, AHP is used. Through AHP, the model is divided into three layers. The first layer is users, the second layer is behavior, and the third layer is feature items.

The main flow chart of AHP is shown in Figure 7.

When calculating the importance of a word, it simply counts the number of occurrences of the word. However, in actual situations, it is necessary to consider not only the number of occurrences of the user's behavioral feature items but also the weight of each user's behavioral feature items. So $m_{i,j}$ in Formula (4) is calculated as

$$m_{i,j} = \sum_{k=1}^{n} \text{item}_{k,i} * w_{k,i}. \tag{6}$$

Then, the same can be obtained, and Formula (4) can be changed to

$$tf_{i,j} = \frac{\sum_q \text{item}_q * w_q}{\sum_k \sum_q \text{item}_k q * w_{k,q}}. \tag{7}$$

$tf_{i,j}$ represents the importance of user j's behavioral feature i, and the expression for reverse behavioral frequency ibf_i becomes

$$ibf_i = \log \frac{|B|}{1 + \sum_j |\{j : t_i \in b_j\}| * w}. \tag{8}$$

Based on the above operations, the weight calculation formula of the behavior feature item of user j can be finally obtained as follows:

$$w_{i,j} = tf_{i,j} \times ibf = \frac{\sum_q \text{item}_q * w_q}{\sum_k \sum_q \text{item}_k q * w_{k,q}} \times \log \frac{|B|}{1 + \sum_j |\{j : t_i \in b_j\}| * w}. \tag{9}$$

3.2.3. Representation of User Trajectory Data Model. The user model reflects the characteristics of the user's daily behavior to a certain extent and also reflects the user's point

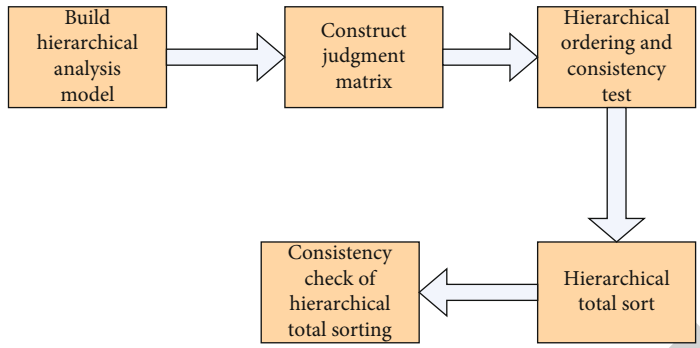

Figure 7: Main flow chart of AHP.

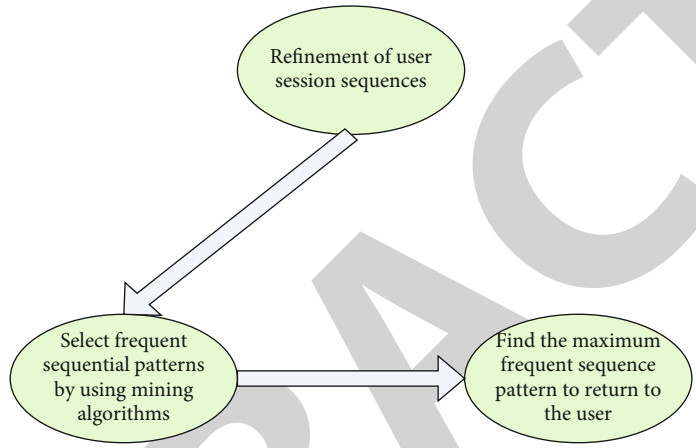

Figure 8: Sequence pattern mining process diagram.

of interest. According to the feature extraction algorithm mentioned above, an improved hierarchical vector model is used to describe the user's daily behavior and activity characteristics [19].

If the user has U with m characteristic behaviors and n different main behaviors, then, the user's trajectory data model can be expressed by the following formula:

$$\text{Model}_u = \{(S_1, W_1, M_1), (S_1, W_1, M_1), (S_n, W_n, M_n)\}. \tag{10}$$

3.3. Sequential Pattern Discovery Algorithm Based on Multiple Factor Constraints

3.3.1. Sequential Pattern Mining Algorithm. The so-called sequence refers to the combination of elements arranged in a certain order. In everyday life, there are examples of this everywhere, such as the steps of the user's account opening procedures in the bank, the sequence of the consumer's consumption behavior in the store, and the pages that the user visits the website and browses in turn.

The so-called sequential pattern mining is the process of finding all frequent sequences with support greater than or equal to the threshold for a data set and a performance index, that is, the minimum support threshold [20]. The sequence pattern mining process is shown in Figure 8.

3.3.2. Inadequacies of Traditional Apriori-Like Algorithms. As a classic algorithm for sequential pattern mining, the Apriori-like algorithm is one of the most commonly used algorithms in log mining and occupies an important position in the research and application process. However, due to some limitations of its own, the actual effect of this algorithm is not very good, which is mainly reflected in two aspects including the efficiency of the algorithm and the effectiveness of the mining results [21].

First, the space-time overhead of this algorithm is very large, and the algorithm efficiency is not high. The basic idea and implementation steps of the Apriori-like algorithm for sequential pattern discovery are based on the traditional Apriori algorithm. In practical applications, the scale of this database is often very large, which brings huge time overhead. This kind of algorithm is an iterative method, which will repeatedly execute the above process, so the huge space-time overhead often becomes a heavy burden for mining work and affects the efficiency of mining.

Secondly, in terms of the validity of the mining results, although the coverage of frequent sequence pattern mining is relatively high, it cannot distinguish the sequence patterns with high meaningful value from the useless patterns very well. It cannot really distinguish the difference between sequences, cannot really reflect the user's interest, and cannot filter the results carefully and effectively.

Facing the problem of low validity of mining results, an intuitive solution is to introduce other evaluation mechanisms. Based on this idea, this paper introduced a new constraint factor to improve the original method.

3.3.3. Algorithm Improvement Based on Multiple Factor Constraints

(1) Page Interest Factor. Page interest is a measure, which is a measure of the user's interest in a page. For the measurement of page interest, there are generally two methods of composition, one is based on the number of user visits, and the other is based on the time of user visits [22].

First of all, this paper defines the user's page interest in page r_i as B_i. If the total number of user visits to this page is n and the total number of visits to all internal pages is N, there are

$$B_i = \frac{n}{N}. \tag{11}$$

Assuming that for any page $r_i \in R$ and any user $U_j \in U$ who has visited the page, if the total time is t_i^j when U_j stays on r_i, the number of visits is m_i^j, and the average visit time of U_j on the page is $\text{ave}_j(r_i) = t/m_i^j$, then there are

$$\text{ave}_j(r_i) = \frac{t_i^j}{m_i^j}. \tag{12}$$

For any page $r_i \in R$, the number of users who have visited the page is M_i, and the average access time of page r_i is AVE(r_i); then,

$$\text{AVE}(r_i) = \frac{\sum_{j=1}^{M_i} \text{ave}_j(r_i)}{M_i}. \tag{13}$$

Next, the page interest degree factor is defined which is used in this article: for any $r_i \in R$, its page interest degree is recorded as A_i; then there are

$$A_i = \frac{\text{AVE}(r_i)}{\text{max\_AVE}(R)}. \tag{14}$$

In actual use, it would be found that the page interest factor calculated by different pages may vary greatly. Therefore, the optimization formula in this paper is

$$A_i = 0.3, \frac{\text{AVE}(r_i)}{\text{max\_AVE}(R)} \le 0.3. \tag{15}$$

When the page interest degree is between 0.3 and 1, there is the following formula:

$$A_i = \frac{\text{AVE}(r_i)}{\text{max\_AVE}(R)}, 0.3 \le \frac{\text{AVE}(r_i)}{\text{max\_AVE}(R)} \le 1. \tag{16}$$

After introducing the page interest factor, another important factor is considered that affects the user's visit behavior, that is, page importance.

Table 4: Data table of sequential patterns based on multiple factors.

Page sequence	Weighted support	Page sequence	Weighted support
A	75	EG	16
B	150	AG	0
C	56	BG	0
G	27	CA	0
AB	6.75	CEG	15.4
BE	0	BCE	17.1
CG	0	BCEG	6.5

Table 5: Sequence pattern data table based on traditional Apriori-like algorithm.

Page sequence	Weighted support	Page sequence	Weighted support
A	50	ACE	10
CE	50	BCEG	20
AB	30	ABCE	10
BEG	20	ABCEG	10

(2) Page Importance Factor. The importance of a page also affects the degree of user interest in the page to a large extent. There are many ways to measure the importance of a page. This article adopts a method to measure the importance of a page, which is the content link ratio. This paper defines that for any page $r_i \in R$, its content link ratio CLR_i is a ratio. If the number of links contained on page r_i is L_i and the amount of information contained on the page is G_i, then there are

$$\text{CLR}_i = \frac{G_i}{L_i}. \tag{17}$$

In order to facilitate the calculation, CLR_i need to be mapped to the (0, 1] interval. For any page $r_i \in R$, its page importance is recorded as V_i; then there are

$$V_i = \frac{\text{CLR}_i}{\text{max\_CLR}_R}. \tag{18}$$

With the user interest factor and page importance factor, the improved Apriori-like algorithm is be further improved, so that the frequent sequence patterns mined by it can better reflect the user's browsing interest.

For the algorithm proposed above, the core criterion for frequent sequence determination is the support degree. Next, a new support degree calculation method proposed for the improvement of the above algorithm, as shown in the formula:

$$W\_\text{Support}(q) = \text{Support}(q) \frac{\sum_{i=1}^{m} A_i V_i}{m}. \tag{19}$$

Among them, the weighting factor for revising the traditional support degree is the arithmetic mean value of the

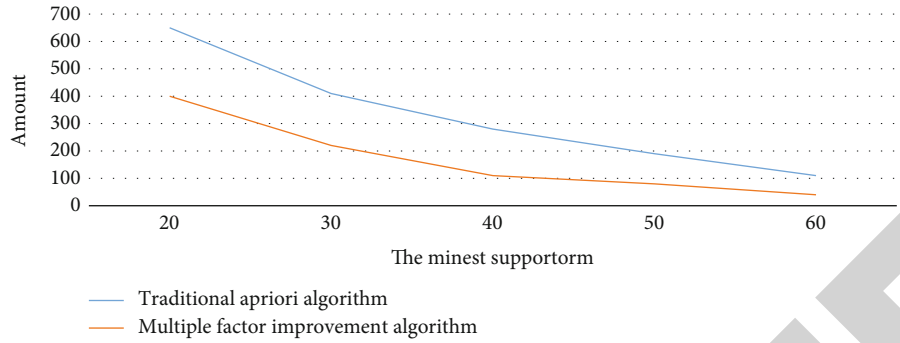

Figure 9: Comparison of experimental results between traditional Apriori-like algorithm and multifactor sequential pattern discovery algorithm.

products of all page interest degree factors and page importance factors in the sequence.

4. Experiment of User Behavior Modeling Based on Web Data Mining

To facilitate observation of the results, two experiments are employed to test the improved frequent sequence mining algorithm. One is a simulation experiment using fictitious data. The data comes from a simulation experiment collected by a simulated network. Compared with the real data, the amount of data is less and the calculation effect is more intuitive in order to illustrate the process of algorithm execution, and the other is an experiment using real data to show the effect of the algorithm.

4.1. Simulation Experiment of Fictitious Data. For the first experiment, assuming that each record in Table 3 occurs 10 times in the database. The total number of database transactions is 100, and the minimum support threshold is given as 10. The details are shown in Table 4.

After processing by this algorithm, 5 frequent sequences were got, the maximum frequent sequences are <B, C, E> and <C, E, G>. In contrast, if the traditional Apriori-like algorithm is used to mine and analyze the same data, the execution data table is shown in Table 5. It can be seen that the improved algorithm has a very obvious filtering effect on frequent sequence patterns. It can be seen from the table that the multifactor-based sequence pattern discovery algorithm filters the experimental data from (A, 75) to (BCEG, 6.5). Obviously, the screening effect of this method is very good.

4.2. Real Data Experiment. The experimental data used in this paper comes from the session identification and path supplement of user behavior web data for network marketing. For the information related to the weighting factor, it is obtained through additional program statistics and saved in the form of auxiliary table files for the algorithm to directly call used to avoid excessive overhead during algorithm execution.

Using the traditional Apriori-like algorithm as a comparison, 20, 30, 40, 50, and 60 are chosen as the minimum support thresholds. After the mining work of the two methods, the following results can be obtained, as shown in Figure 9.

The first thing to point out here is that the number in the graph refers to all the frequent sequences mined, not the maximum frequent sequence. It can be seen from the above results that with the increase of the minimum support, fewer and fewer sequences are screened. However, it is obvious that the sequential pattern discovery algorithm based on multiple factor constraints has better screening effect than the traditional Apriori-like algorithm from the beginning. In fact, many sequences like <A, B> and <A, C> in Experiment 1 were filtered out very early, and the newly added weight factor has played a good filter effect on low-value sequences.

4.3. Experimental Results. The experimental results have shown that the sequential pattern discovery algorithm based on multiple factor constraints can greatly save the model runtime cost when building a user behavior model, which is roughly 30%-40%. At the same time, the user behavior model constructed by the algorithm has a 37% increase in the accuracy of user behavior simulation and prediction. Of course, there is still no good evaluation method and standard for how to accurately measure the value of a frequent sequence pattern, which does not mean that the fewer the number of sequences mined, the better the results. This should be evaluated and revised according to the actual situation. For example, the number of sequences obtained in the study of the purchase demand of Internet marketing users is too large, but the reason for too many is that the sample of such demand data sources is complex. Too many of them are objective situations, so at this time, it is not possible to over-screen the experimental data to avoid destroying the authenticity and objectivity of the data. However, it is certain that the improved algorithm proposed in this paper can indeed play a good role in correcting the mining process, filter out a large number of useless patterns, and reduce the redundancy of mining results to a certain extent.

5. Conclusions

Web data mining is a young technology and a promising discipline. With the continuous rapid development of the Internet, various network-based services and e-commerce

Hindawi
Wireless Communications and Mobile Computing
Volume 2022, Article ID 2882964, 11 pages
https://doi.org/10.1155/2022/2882964

Research Article

Research on English Vocabulary and Speech Corpus Recognition Based on Deep Learning

Wang Zhen

Department of Public Education, Inner Mongola Techical College Of Construction, Hohhot 010070, China

Correspondence should be addressed to Wang Zhen; b20160904105@stu.ccsu.edu.cn

Received 8 June 2022; Revised 14 August 2022; Accepted 22 August 2022; Published 19 September 2022

Academic Editor: Jun Ye

In order to investigate how to recognize English words and speech corpus, an English vocabulary and English speech recognition model based on deep learning algorithm was proposed. Through recommending key technical problems and solutions based on deep learning algorithm, how to realize the recognition of English vocabulary and speech corpus was investigated. In the research, the accuracy of the method on the English vocabulary and speech corpus recognition based on the deep learning algorithm increased 79% over the previous methods. Combined with the principle of the deep automatic encoder and deep learning algorithm, the research emphasis was on the effects of speech recognition framework for speech corpus. The speech recognition research based on the theory of deep learning not only had a theoretical guidance meaning but also had the use value in the practical application.

1. Introduction

Due to the complex changes in speech pronunciation, the large amount of data of speech signals, the high dimension of speech feature parameters, and the large amount of computation for speech recognition and evaluation, high-demand software and hardware resources and algorithms are required for large-scale speech signal processing. However, the traditional speech recognition algorithm dynamic time warping algorithm, hidden Markov model, and artificial neural network have their own advantages and disadvantages, they have encountered unprecedented bottlenecks, and it is difficult to further improve their accuracy and speed. In recent years, with the development of deep learning research in the field of machine learning and the accumulation of big data corpus, speech recognition and evaluation technology has developed rapidly. Language is an essential element in people's daily communication. Speech is also an essential means of information exchange in people's daily life and work. Clear speech expression can further clarify the expression of information and further simplify the main idea that people want to express. In addition, a large piece of relatively complex information can be decomposed into different parts to help people better communicate and analyze [1]. But with the development of information technology and Internet technology, the emergence and development of speech recognition has gradually changed the people's living habits. By using intelligent terminal, computer, intelligent wear equipment, speech recognition can be realized. Speech recognition technology has become one of the technical means of language communication in today's society. How to better apply this technology to assist people's communication is the focus of research [2]. Therefore, combining the principle of deep autoencoder and deep learning algorithm, an English vocabulary and English speech recognition model based on deep learning algorithm is proposed, which focuses on the influence of speech recognition framework on speech corpus.

Speech recognition technology was mainly divided into the following stages. In 1950s, Audrey in AT&T Bell Laboratory was the prototype of speech recognition. In late 1960s and early 1970s, it has a significant progress [3]. In late 1980s, it has a breakthrough. In early 1990s, many large companies launched their own speech recognition apps. The Audrey system, first developed at AT&T Bell Labs in the 1950s, was the first speech recognition system capable of

recognizing 10 English digits. However, substantial progress was made in the late 1960s and early 1970s [4]. The main reason was the introduction of linear predictive coding plane (LPC) technology and dynamic time warping (DTW) technology, which could effectively solve the problem of feature extraction and unequal length matching of speech signal. Speaking skills at that time were generally based on the principle of template matching. And the name is limited to identifying the difference between special people and small words. The identification of specific population segregation based on cepstral prediction and DTW techniques has been observed. At the same time, vector quantization (VQ) and hidden Markov model (HMM) theory were proposed [5].

In the late 1980s, lab speech recognition research finally had a breakthrough. For the first time in the lab, the barriers of large vocabulary, continuous speech, and nonspecific people were by combining all three characteristics in one system, typically Carnegie Mellon University's Sphinx system. It was the first high-performance nonspecific large vocabulary continuous speech recognition system. During this period, speech cognition research was further understood, characterized by the use of HMM models and neural network devices in speech cognition [6]. Zhang et al. at AT&T Bell Labs evaluated the HMM model for a wide range of applications. They engineered the original difficult HMM pure mathematical model, so that more researchers could understand it and make statistical methods that will become the mainstream of speech recognition technology. Statistical methods shifted researchers' attention from micro to macro. They no longer deliberately pursued refinement of speech features but constructed the best speech recognition system more from the overall average (statistical) perspective [7]. The research on speech recognition in China started in the 1950s. The Institute of Acoustics of Chinese Academy of Sciences began to conduct speech research. The real beginning of speech recognition in China should be the generation of RTSRS(01), a speech recognition system which used bandpass filter bank parameters and realized by Institute of Acoustics of Chinese Academy of Sciences in 1978. In the 1980s, professors from Tsinghua University proposed an implicit Markov model based on segment state distribution, which effectively solved the pruning problem of language identification in multilingual continuous recognition system [8]. In 2004, some scholars used HMM and GMM to score Chinese pronunciation and tone, respectively. Downhill Simplex Search optimized subsystem parameters in order to achieve the same scoring standard consistent with Chinese experts. Fluent application systems included FLUENCY of Language Technology Research Institute of Carnegie Mellon University and School of Information of Kyoto University in Japan. Some institutions in China, such as PLASER at Hong Kong University of Science and Technology, Department of Electronic Engineering at Tsinghua University, Department of Computer Science of Harbin Institute of Technology, and the Department of Computer Science of Harbin Institute of Technology, have also made some significant progress in these researches. However, most researches in China were to assist the learning of Chinese pronunciation [9].

2. Methods

2.1. Key Technologies of Deep Learning

2.1.1. Energy Probability Model. Introducing RBM into network modeling is a breakthrough with theoretical guiding significance for deep neural networks [10]. Using RBM as an energy model, it is possible to model arbitrarily distributed data. The Boltzmann machine is a large class of neural network models, but the most commonly used one in practice is the RBM. The RBM itself is simple, just a two-layer neural network, so it is not strictly considered as a category of deep learning. When the minimum energy of the overall network is calculated iteratively, it means that the system is in steady state at this time and the network parameters we require are also the network parameters at this time.

2.1.2. Pretraining Layer by Layer. In the past, neural networks determined the initial value through random initialization, at which time the random option value was required. It was often inconsistent with the actual situation, so the final effect was not ideal [11]. With RBM, the model is built in the middle of the two adjacent layers, and the training is carried out layer by layer from bottom to top. After several iterations, RBM enters a relatively stable state. Each neuron in the visible layer is connected to all the neurons in the hidden layer, but there is no connection between the neurons in the same layer, and all the neurons have only two output states. In this case, the hidden layer and the visible layer are equivalent to the same features in more than one space in different expressions, so as to determine the initial value consistent with the weight of the actual situation [12].

2.1.3. Network Parallel Training. Considering that there are several hidden layers in the deep neural network, each of which has more than 1000 nodes, the number of relevant parameters is likely to exceed 1 million. In such a large-scale network, the time of data training will be greatly extended without parallel processing. The BP neural network is mainly composed of the input layer, the hidden layer, and the output layer. The number of nodes in the input and output layer is fixed. Whether it is a regression or a classification task, choosing the appropriate number of layers and the number of hidden layer nodes will affect the performance of the neural network to a large extent. Parallel processing can be completed by hardware or software. The hardware method requires the support of GPU or distributed computing cluster. The software method means that the parameters of data subset are updated by multithreading and the updated results are unified at an appropriate time to complete the parallel training of the network [13].

2.2. Encoder Category Based on Depth Theory

2.2.1. Deep Autoencoder. The input required by the deep autoencoder is the original data feature. And the middle

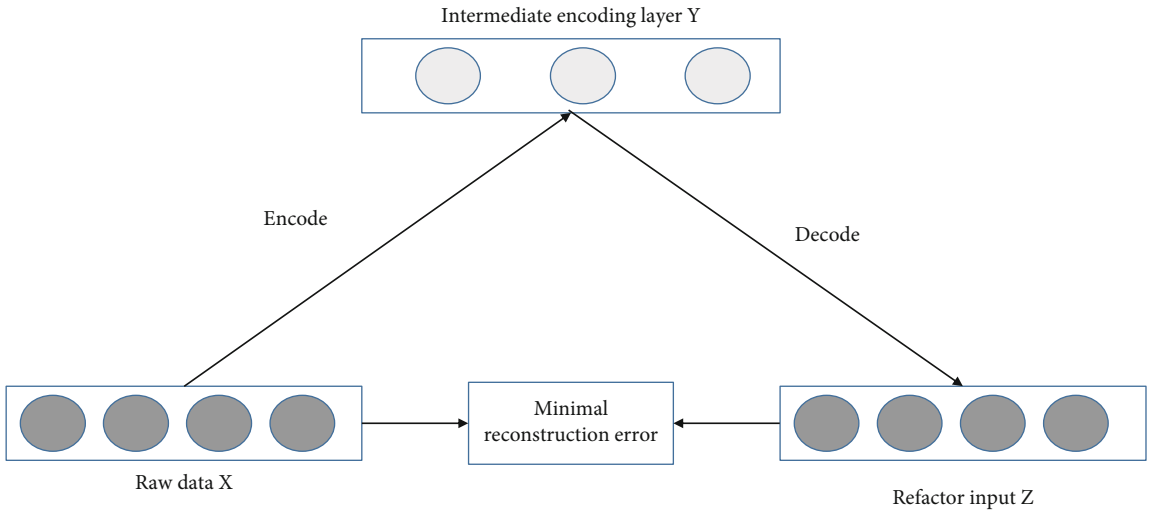

Figure 1: Autoencoder model.

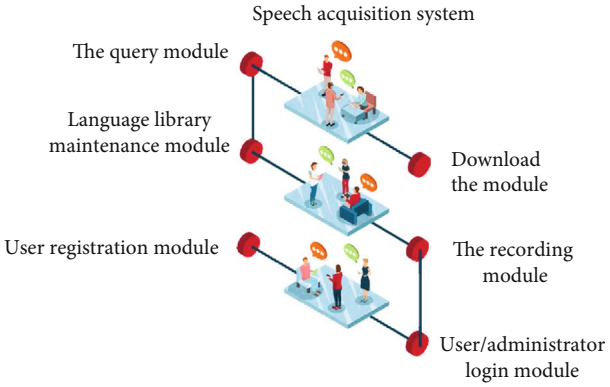

Figure 2: Speech acquisition system module.

layer encoding feature is obtained by different hidden layer encoding and the original input is reconstructed according to the decoding. Autoencoder is a kind of neural network, whose basic idea is to directly use one layer or more layer of neural network to map the input data and get the output vector. The model is shown in Figure 1. Network parameter adjustment is mainly aimed at minimizing the mean square error between original input and reconstructed input. The calculation method of loss function is shown in

$$J(W,b)=\left[\frac{1}{m}\sum_{i=1}^{m}J\left(W,b,x^{(i)},y^{(i)}\right)\right]+\frac{\lambda}{2}\sum_{l=1}^{n_i-1}\sum_{i=1}^{s_l}\sum_{j=1}^{s_{l+1}}\left(W_{ji}^{(l)}\right)^2, \tag{1}$$

$$J(W,b)=\left[\frac{1}{m}\sum_{1}^{m}\left(\frac{1}{2}\left\|x^{(i)}-h_{W,b}x^{(i)}\right\|^2\right)\right]+\frac{\lambda}{2}\sum_{l=1}^{n_i-1}\sum_{i=1}^{s_l}\sum_{j=1}^{s_{l+1}}\left(W_{ji}^{(l)}\right)^2. \tag{2}$$

In formula (1) and formula (2), the first term represents average reconstruction error. The second term represents regularization constraint term, aiming to prevent overfitting [14]. m represents the amount of training data. W and b are parameters of the encoder. $x^{(i)}$ and $y^{(i)}$ represent the original input and reconstruction input in turn, and their relationship is shown in

$$y^{(i)}=h_{W,b}\left(x^{(i)}\right). \tag{3}$$

2.2.2. Denoising Autoencoder. The training data required for this encoder is random noise that is superimposed on the raw data before providing it to the network (adding random noise to input layer nodes or according to some probability to make some input layer nodes 0). After the coding module is used to obtain the coding representation of the middle layer, the original data is reconstructed on the output layer to obtain more prominent features in robustness. The original data layer (the data in it is the raw data, without any processing) is the original json format data, because the original data has two kinds of data: start log and event log.

2.2.3. Sparse Autoencoder. Sparse autoencoder, another important extension model of autoencoder, also has good feature extraction performance. Sparse means that the hidden layer node has a high probability of 0 and sparse autoencoder is an unsupervised machine learning algorithm that constantly adjusts the parameters of the autoencoder by calculating the error between the autoencoding output and the original input to finally train the model. Autoencoders can be used to compress the input information and extract useful input features, and its non-0 time is relatively short (there is a long distance between it and 0; that is, it is in active state) [15]. Research on the visual perception system of human brain shows that the distribution of visual cortex cells in V1 region is sparse after the human brain receives natural image signals, even though only a few of them are activated at the same time. The output state of the hidden layer of the network is limited, so that the nodes of the hidden layer enter the sparse state, and the average output of the nodes of the hidden layer is equal to 0. In this way, the proportion of active nodes is relatively small, and the homogeneity of

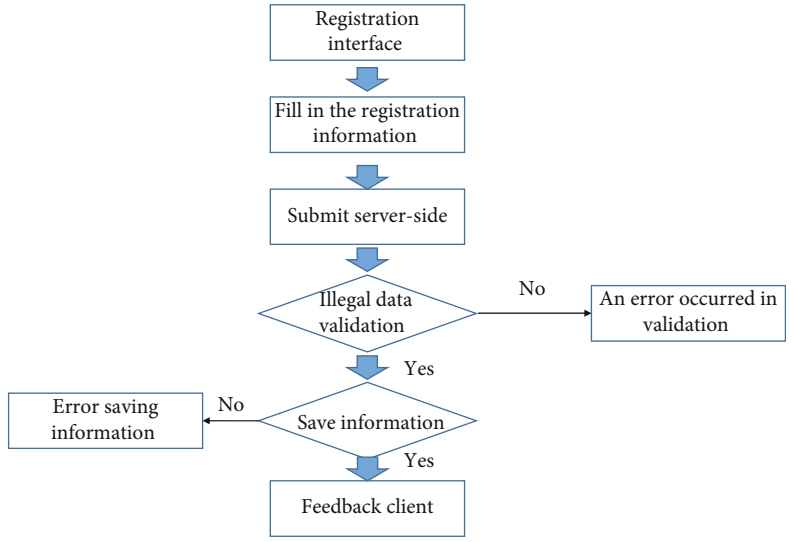

Figure 3: User registration process.

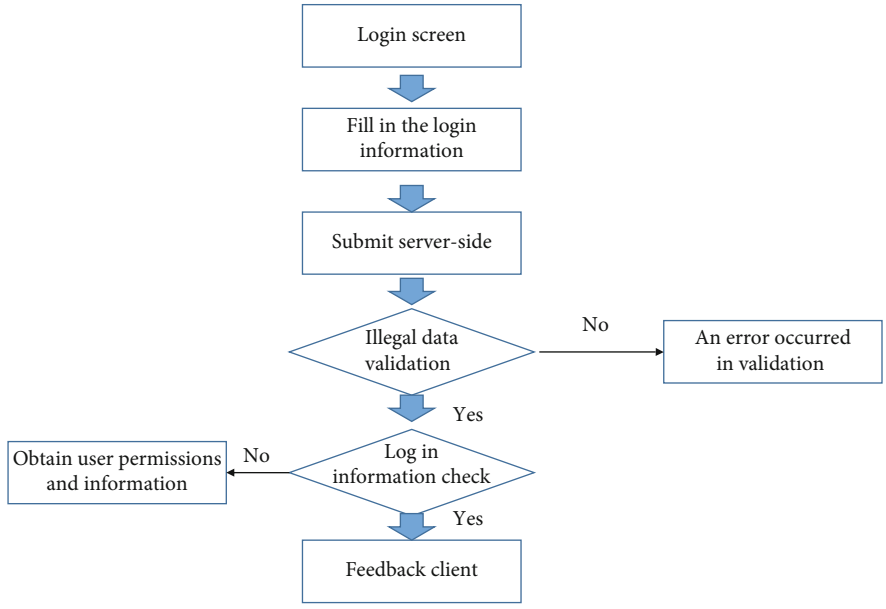

Figure 4: Login module process.

the characteristics of the nodes of the hidden layer will not occur [16]. The loss function of sparse autoencoder is shown in

$$J_{\text{sparse}}(W,b) = J(W,b) + \beta \sum_{j=1}^{s_2} \text{KL}\left(\rho \| \bar{\rho}_j\right). \tag{4}$$

The first term of formula (4), which is the same as formula (1), represents the size of reconstruction error. The second term is KL distance, representing the gap between the expected sparsity and the actual value, which can be calculated by the following expression, as shown in

$$\text{KL}\left(\rho \| \bar{\rho}_j\right) = \rho \log \frac{\rho}{\bar{\rho}_j} + (1-\rho) \log \frac{1-\rho}{1-\bar{\rho}_j}. \tag{5}$$

$\bar{\rho}_j$ represents the average output value of nodes at the hidden layer, which satisfies

$$\bar{\rho}_j = \frac{1}{m} \sum_{i=1}^{m} \left[a_j^{(2)}\left(x^{(i)}\right)\right]. \tag{6}$$

2.3. System Framework Based on Deep Autoencoder

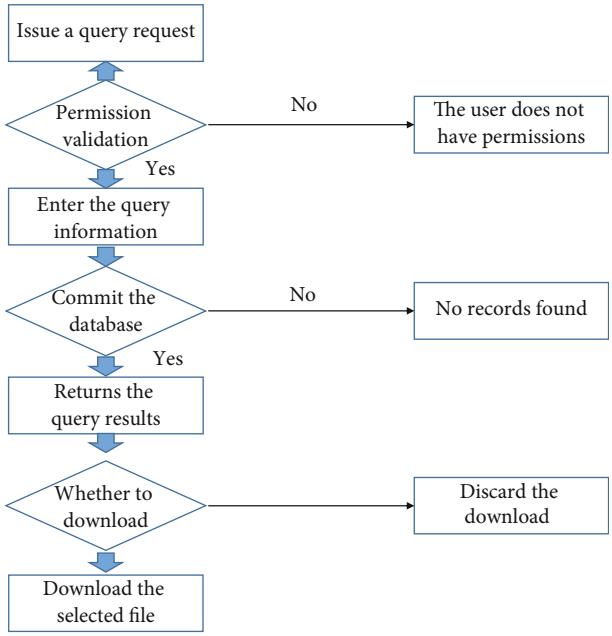

Figure 5: Query and download module flow.

2.3.1. Experimental Corpus. The original data required in the experiment are all from TIMIT speech data set. The full name of TIMIT is The DARPA TIMIT Acoustic-Speech Continuous Speech Corpus, which is collected and constructed by Texas Instruments, Massachusetts Institute of Technology, and Stanford Research Institute. There are 6,300 sentences sampled at 16 kHz from eight different locations in the United States, and all sentences are manually segmented and labeled.

2.3.2. Feature Preprocessing. In the process of extracting high-level features, deep neural networks generally need to receive acoustic features such as MFCC and Fbank. Because of the copronunciation phenomenon, it is necessary to extract digital features from images (or texts) for use by various models. Sometimes, you need to extract numerical features from images (or text) for use by various models. Deep learning models can be used not only for classification regression but also for extract features. The trained model is usually used to input pictures and output as extracted feature vectors. It is generally necessary to expand the short-term features to obtain the superframe features carrying context information. Original feature extraction is as follows: according to the parameters of frame length 20 ms and frame shift 10 ms, the 39-dimensional MFCC features (12-dimensional output + 1-dimensional logarithmic energy and their first- and second-order differences) are extracted from the original speech through the HCopy file provided by HTK. A voice sample in the data for detailed description is selected. First, two text files should be created in the same root directory, named YL. conf and YL. scp, respectively. The former mainly writes parameters for MFCC extraction, and the latter is the path of sample files and generated files. The yangli.mfc file can be obtained in the same directory after the extraction is successful. Since the file format cannot be directly viewed, the HList tool can be used to convert it to a txt file.

Data preprocessing is as follows: 5 frames are added before and after the features obtained in the previous step to obtain 11 consecutive superframe features. Then, the cepstrum mean variance is normalized. The processed features are input through the visibility layer as training samples of the network model [17]. In the process of normalization of each dimension of superframe feature, the two points cannot be ignored. First, normalization can reduce the influence caused by feature difference between channel and individual. Second, Gauss-Bernoulli RBM model is selected in the process of modeling the input layer and the first hidden layer whose node states conform to Gaussian distribution. At this time, the energy function is shown in

$$E(v,h)=\sum_{i\in V}\frac{(v_i-a_i)^2}{2\sigma_i^2}+b^Th-\sum_{i\in V,j\in H}\frac{v_i}{\sigma_i}h_iw_{ij}. \quad (7)$$

After CMVN processing, input data distribution in formula (7) satisfies

$$\begin{cases} a_i=0, \\ \sigma_i=1. \end{cases} \quad (8)$$

The energy function is equivalent to

$$E(v,h)=\sum_{i\in V}\frac{v_i^2}{2}-b^Th-\sum_{i\in V,j\in H}v_ih_iw_{ij}. \quad (9)$$

2.3.3. Autoencoder Structure. The structure of the encoder includes the number of hidden layers, the number of nodes contained in each hidden layer, and the node type of each hidden layer [18]. After many experiments, the deep autoencoder used in the study consists of seven layers, including an input layer, an output layer, and five hidden layers, and the number of nodes in each layer is $490\times720\times720\times50\times720\times720\times490$ [19].

2.3.4. Network Training Algorithm

(1) Gauss-Bernoulli RBM Training. Because the network input has the speech cepstrum feature, the value is between $[-\infty, +\infty]$, which is obviously different from the black and white image signal. Gauss-Bernoulli RBM is often selected as the input layer and the first hidden layer to build the model. In practice, data preprocessing is needed to normalize the input feature mean and variance. The first several layers of the model are mainly divided into visible layer (490 Gauss nodes) and hidden layer (720 Bernoulli nodes). Here is the training algorithm.

(1) Given a sample v of training data, the activation probability of hidden layer node hj can be expressed as shown in

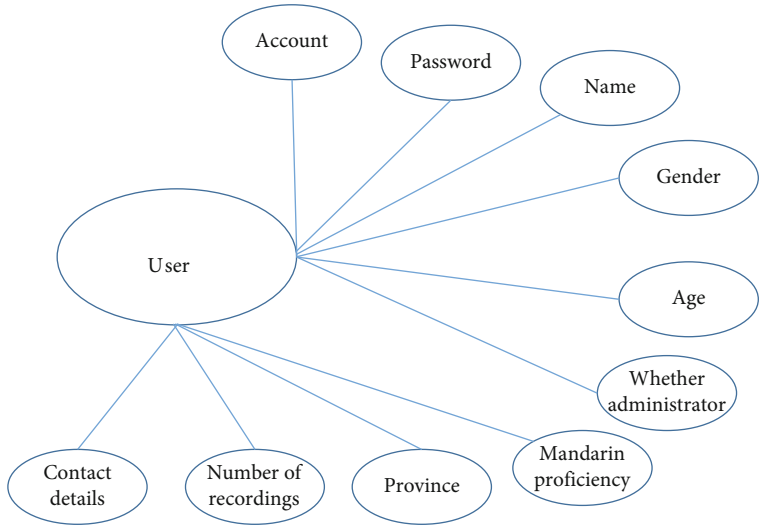

Figure 6: User entity attribute diagram.

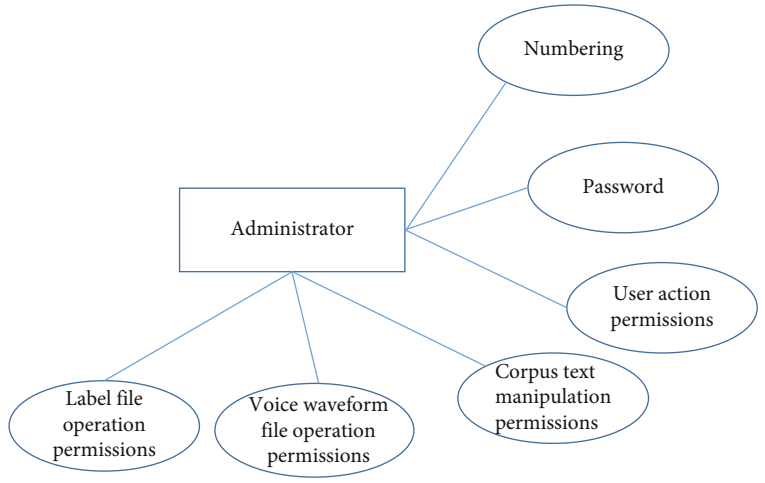

Figure 7: Administrator entity diagram.

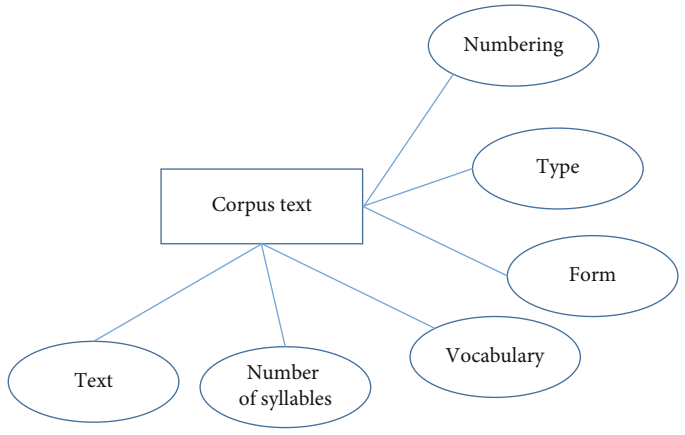

Figure 8: Corpus text entity diagram.

$$p(h_j = 1|v) = \sigma\left(b_j + \sum_{i\in \text{vis}} v_i w_{ij}\right) \tag{10}$$

(2) Randomize the hidden layer node values obtained in (1) to generate 0 and 1 activation states, and deduce the visible layer input v' according to the hidden layer node states. For the linear visible layer element, its reconstruction formula is expressed as

$$v' = N\left(b_i + \sum_{j\in hid} h_j w_{ij}, 1\right) \tag{11}$$

(3) The reconstructed visible layer state value v is used as the input of RBM structure. The hidden layer probability h is calculated again according to step (1)

(4) Update weight parameters according to formula (12), where <. > is the average value of all samples in each small batch and ε is the learning rate, as shown in

$$\Delta w_{ij} = \varepsilon\left(<v_i h_j> - <v_i' h_j'>\right) \tag{12}$$

The initialization parameters of the model are as follows: the weight of the connection is set to a small value and the node bias is set to 0. When each size is done, there are 256 minibatch models. Degrees are 0.01. The activation probability value of each node of the last training hidden layer h1 is retained as the input data of visible layer of RBM in the upper-middle layer of superposition structure [20].

(2) Bernoulli-Bernoulli RBM Training. The output value of the hidden layer of the first Bernoulli-Bernoulli RBM model is directly defined as the input value of the visible layer of the next RBM, and then, the connection weight between $h1$ and $h2$ of the hidden layer is continued to be trained. Compared with Gauss-Bernoulli RBM, the training method is basically similar, but the visible layer nodes obey Bernoulli distribution. Here, the hidden layer state is used to reconstruct the visible layer, and the basic formula is shown in

$$p\left(v_i' = 1|h\right) = \sigma\left(b_i + \sum_{i\in \text{hid}} h_i w_{ij}\right). \tag{13}$$

(3) Network Parameter Tuning. After the initial model is pretrained, network parameters need to be adjusted, usually through backpropagation (BP) [21]. The sample overall loss function can be written as shown in

$$J(W, b) = \left[\frac{1}{m}\sum_{i=1}^{m} J\left(W, b, x^{(i)}, y^{(i)}\right)\right] + \frac{\lambda}{2}\sum_{l=1}^{n_i-1}\sum_{i=1}^{s_l}\sum_{j=1}^{s_{l+1}}\left(W_{ji}^{(l)}\right)^2, \tag{14}$$

$$J(W, b) = \left[\frac{1}{m}\sum_{i=1}^{m}\left(\frac{1}{2}\left\|h_{W,b}\left(x^{(i)}\right) - y^{(i)}\right\|^2\right)\right] + \frac{\lambda}{2}\sum_{l=1}^{n_i-1}\sum_{i=1}^{s_l}\sum_{j=1}^{s_{l+1}}\left(W_{ji}^{(l)}\right)^2. \tag{15}$$

The first term of formula (14) is the mean square deviation term, which reflects the degree of difference between reconstruction and original input features. The second term is added to avoid the overfitting problem, which is the so-called regularization term. The contribution of the first and second terms to the loss function can be balanced by increasing the weight attenuation parameter λ. $h_{W,b}(x^{(i)})$ represents the reconstruction result obtained through the process of coding and decoding the sample $x^{(i)}$ through the network. The present invention provides a research on the recognition of English vocabulary and speech corpus based on a deep learning algorithm, which comprehensively evaluates the English pronunciation quality of the preset object through the two different aspects of the English pronunciation and the English vocabulary, so that it can comprehensively evaluate the English pronunciation quality of the preset object. It can accurately evaluate the actual English pronunciation accuracy and standard degree of the preset object and give an objective and reliable pronunciation quality evaluation score accordingly, so as to effectively improve the English pronunciation quality and improve the experience of learning English.

3. Results and Analysis

The design of the overall structure of the system is to reasonably divide the whole system into various functional modules, so as to correctly handle the relationship between and within modules, as well as the data connection between them, and then to define the internal structure of each module [22].

3.1. Structural Design of the System. In the system, C/S system architecture is used, including five function modules, namely, user registration module, user administrator login module, recording module, database maintenance module, and query and download module (see Figure 2).

3.2. Detailed Design

3.2.1. System Module

(1) User Registration Module. The registration module realizes the user registration function and corresponds the recording information with the account, which is convenient for users to query and use in the future. Account number, password, age, gender, Mandarin proficiency, and native place will be written into the user information form as

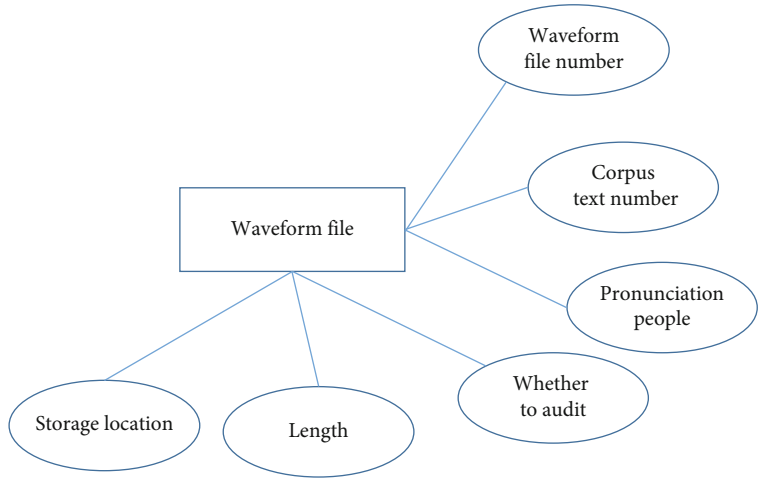

Figure 9: Pronunciation waveform file entity diagram.

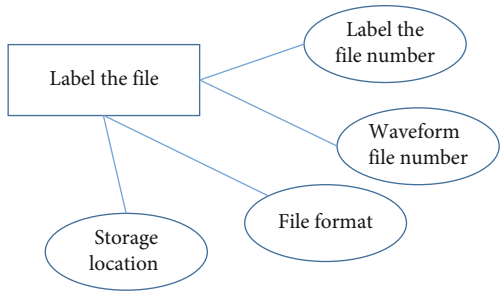

Figure 10: Labeling the file entity diagram.

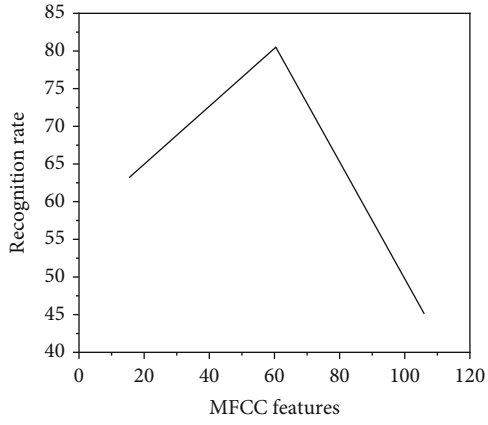

Figure 11: Comparison of recognition rates between MFCC features and DAE midlayer features (broken lines).

required. If the registration fails, the system prompts you to review the registration information and returns to the registration page. Its functional flow chart is shown in Figure 3.

(2) User Administrator Login Module. The login module ensures that users can log in to the system with legitimate identities and obtain the recording information for easy query and modification. First, the user fills in the account number and password as parameters and passes them to the server, which is compared with the information in the user information table [23]. If the authentication fails, an error message is displayed and the registration page is displayed. If the authentication succeeds, the user information and permission are displayed. Its function flow chart is shown in Figure 4.

(3) Recording Module. Recording module includes a recording program. After the program receives the user's request, according to the user's choice, the corresponding recording text is selected. The second step is to initialize the recording device on the machine and start recording. After the recording is complete, the user information, recording files, and text information are sent back to the server as parameters, and the save program is invoked for further processing.

(4) Database Maintenance Module. Database maintenance module is used to operate the database for administrators. The client provides an exchange interface, which is convenient for administrators to log in so as to manage and audit the user, corpus text, waveform files, and annotated files. The first step is to identity verification to see whether they have the authority to manage the database. After passing the verification, they can operate and manage the database and save the process of modifying information.

(5) Query and Download Module. The user sends a query request to confirm the user permission. Then, the query information input by users (articulator attributes, corpus text keywords, waveform file numbers, etc.) is transferred to the server as parameters. And the server returns the query result, and the user can select the corresponding file according to the returned result for download. Its function flow chart is shown in Figure 5.

3.2.2. The Conceptual Design of Database. The goal of the conceptual design is to accurately describe the information schema of the application domain and support the various applications of the user, so that it is easy to transform into database logic schema and easy to understand by the user. The typical method of conceptual model design is E-R

method. A diagram is composed of three parts, including entity, attribute, and connection. According to the requirement analysis of the system function and database described above, the E-R diagram of the system can be obtained, as shown in Figures 6–10.

3.2.3. System Implementation

(1) Implementation of Landing Module. In the process of system design, no matter if it is divided into several modules and different modules, its operators are different. The foundation of any successful application's security policy is a robust means of authentication and permission control and secure communications that provide data integrity and confidentiality. The design of login module is mainly to verify the correctness of user account and password.

(2) Implementation of Registration Module. It is mainly used for the personal information of registered users. Each user can view and modify their own information, as well as refer to previous personal recording records.

(3) Implementation of Recording Module. The first step is to initialize the recording device on the local device, and then, start recording after the user selects the corresponding text. After recording, the recording file is saved to the server.

(4) Implementation of Language Library Maintenance Module. It is mainly to achieve the management of the database, including the management of users, corpus text, waveform file management, and labeling file management.

(5) Implementation of Query and Download Module. Through the search function, users can find the corresponding text corpus, waveform files, and annotated files and download the required files.

Taking the tagging of speech corpus as an example, a complete speech corpus should not only contain original speech data and corresponding pronunciation text but also corresponding label files. In order to improve the utilization value of speech corpus, the key is to label the speech corpus completely. Corpus refers to a large-scale electronic text library scientifically sampled and processed. With the help of computer analysis tools, researchers can carry out relevant language theory and applied research. The label process of speech corpus is a process of language knowledge formalization. The label quality and depth of the speech corpus directly affect the accuracy and richness of information mined from the speech corpus and determine the availability and value of the speech corpus to a great extent. Based on statistical principles, we can find the habitual collocation of language, and the corpus can help us to better master the language. Is the tool for our research and collocation. A complete label system is a very important part of corpus construction, and the complete label includes segmenting and prosodic label. The so-called English phonetic segment annotation is to segment each phonetic unit (sentence, word, character, syllable, consonant, and vowels) in a continuous speech stream and describe their timbre characteristics, mainly including vowels, consonants, and combinations of vowels and vowels, vowels and consonants, and consonants and consonants.

A GMM-HMM acoustic model is simultaneously trained on HTK platform for the two features (unsupervised and supervised) and MFCC features obtained through deep autoencoder model training. The recognition accuracy of words and sentences is used as the experimental comparison results, as shown in Figure 11.

4. Conclusions

As one of the hottest research fields at present and in the future, deep learning has achieved good results in the field of speech recognition. The performance of speech recognition system often directly affects the effect experience of most intelligent systems, so the future development direction must be to combine the two technologies to promote mutual progress. Based on the theory of deep learning, the research comprehensively discusses the application value and effect of deep learning model in the field of speech recognition, starting from speech feature extraction and acoustic modeling.

(1) Taking acoustic feature extraction as the research object, the research work was carried out based on the deep autoencoder model. Deep autoencoders belonged to multilayer network model and were widely used in data dimension reduction and feature extraction based on unsupervised training. The research focused on the analysis of the deep learning model from the perspectives of feature data preprocessing, model structure, and network training parameters. The automatic encoder was established based on the speech features in MATLAB platform to extract the new speech features from the original MFCC features. Finally, HTK recognition tool was used to test and verify the TIMIT English speech corpus. Compared with the original situation, the new features extracted from the unsupervised and supervised training improved the English word recognition rate by 1.64% and 2.86% and the English sentence recognition rate by 2.55% and 6.53%, respectively

(2) Taking acoustic modeling as the research object, the research work was carried out based on DNN-HMM. As a discriminative model, deep neural network was applied in the field of acoustic modeling. It relied on the output layer to represent the HMM state output probability. And with the help of its own network structure, it could meet the requirements of complex feature modeling. It replaced the original GMM model and combined with HMM to obtain the acoustic model based on DNN-HMM. The acoustic models based on the GMM-HMM and DNN-HMM were modeled by Kaldi speech recognition system platform. Finally, experiments on TIMIT speech corpus prove that compared with

the GMM-HMM model, the English word recognition error rate and sentence recognition error rate of DNN-HMM model were reduced by 30.3% and 17.2%, respectively

Currently, with the rapid development of computer technology, English vocabulary and speech corpus recognition technology have also obtained the rapid development. And there are more and more technologies applied to the actual products, such as speech input system and computer assisted language learning system. Products are constantly emerging, which provides superior service for the people. For an excellent speech synthesis and recognition system, a speech corpus with high information content and low redundancy is essential. It can be seen that speech corpus plays an important role in speech recognition, speech synthesis, and other areas of speech research.

In the research, an English vocabulary and speech corpus was proposed and built to expand the sources of speech corpus and improve the efficiency of English vocabulary and speech corpus recognition and synthesis system construction. The following work were mainly completed.

(1) For English vocabulary and speech corpus selection, the original corpus text was automatically downloaded from the Internet firstly, and then, the greedy algorithm was used to screen the original corpus (based on high frequency words and three-tone words), and the final recorded corpus text was obtained

(2) For speech recording and corpus management system, the recording module working process and the design idea were described in detail. And the speech database management system was implemented, which was convenient for user to operate text, audio files, and tagging corpus query and download files. The recording work was tested, and the English vocabulary and speech corpus was established

(3) For speech file label, the speech corpus label standards and guidelines for corpus label in the United States were introduced. And then, preliminary speech label files were automatically generated by the program without alignment, which could effectively reduce the workload. And then through the software, the manual alignment work was performed and the final label files were obtained

Data Availability

The data used to support the findings of this study are available from the corresponding author upon request.

Conflicts of Interest

The author declares that there are no conflicts of interest.

References

[1] V. H. Vu, Q. P. Nguyen, K. H. Nguyen, J. C. Shin, and C. Y. Ock, "Korean-Vietnamese neural machine translation with named entity recognition and part-of-speech tags," *IEICE Transactions on Information and Systems*, vol. 103, pp. 866–873, 2020.

[2] D. Lemmenmeier-Batinić, "Converting raw transcripts into an annotated and turn-aligned TEI-XML corpus: the example of the corpus of Serbian forms of address," *Slovenščina 2 0 Empirical Applied and Interdisciplinary Research*, vol. 9, no. 1, pp. 123–144, 2021.

[3] K. Zvarevashe and O. O. Olugbara, "Recognition of speech emotion using custom 2d-convolution neural network deep learning algorithm," *Intelligent Data Analysis*, vol. 24, no. 5, pp. 1065–1086, 2020.

[4] L. R. Kishline, S. W. Colburn, and P. W. Robinson, "A multimedia speech corpus for audio visual research in virtual reality (l)," *The Journal of the Acoustical Society of America*, vol. 148, no. 2, pp. 492–495, 2020.

[5] Y. Ahn, S. J. Lee, and J. W. Shin, "Cross-corpus speech emotion recognition based on few-shot learning and domain adaptation," *IEEE Signal Processing Letters*, vol. 28, pp. 1190–1194, 2021.

[6] J. Liu, W. Zheng, Y. Zong, L. U. Cheng, and C. Tang, "Cross-corpus speech emotion recognition based on deep domain-adaptive convolutional neural network," *IEICE Transactions on Information and Systems*, vol. E103.D, no. 2, pp. 459–463, 2020.

[7] W. Zhang, P. Song, D. Chen, C. Sheng, and W. Zhang, "Cross-corpus speech emotion recognition based on joint transfer subspace learning and regression," *IEEE Transactions on Cognitive and Developmental Systems*, vol. 14, pp. 588–598, 2021.

[8] W. Zheng, W. Zheng, and Y. Zong, "Multi-scale discrepancy adversarial network for crosscorpus speech emotion recognition," *Virtual Reality & Intelligent Hardware*, vol. 3, no. 1, pp. 65–75, 2021.

[9] L. Li and L. Cao, "Semantic analysis of literary vocabulary based on microsystem and computer aided deep research," *Mobile Information Systems*, vol. 2021, Article ID 8624147, 13 pages, 2021.

[10] S. P. Yadav, S. Zaidi, A. Mishra, and V. Yadav, "Survey on machine learning in speech emotion recognition and vision systems using a recurrent neural network (RNN)," *Archives of Computational Methods in Engineering*, vol. 29, no. 3, pp. 1753–1770, 2022.

[11] K. Chouhan, A. Shrivastava, C. Gangadhar, V. Shukla, and S. K. Jain, "Speech recognition classification with ANN implementation using machine learning algorithm," *Linguistica Antverpiensia*, vol. 2021, no. 1, pp. 2785–2796, 2021.

[12] M. Rojc and I. Mlakar, "An LSTM-based model for the compression of acoustic inventories for corpus- based text-to-speech synthesis systems," *Computers and Electrical Engineering*, vol. 100, article 107942, 2022.

[13] X. Ren, "Research on a software architecture of speech recognition and detection based on interactive reconstruction model," *International Journal of Speech Technology*, vol. 24, no. 1, pp. 87–95, 2021.

[14] O. Ivanova, J. J. Meilán, F. Martínez-Sánchez, I. Martínez-Nicolás, T. E. Llorente, and N. C. González, "Discriminating speech traits of Alzheimer's disease assessed through a corpus

of reading task for Spanish language," *Computer Speech & Language*, vol. 73, article 101341, 2022.

[15] I. Lefter, A. Baird, L. Stappen, and B. W. Schuller, "A cross-corpus speech-based analysis of escalating negative interactions," *Frontiers in Computer Science*, vol. 4, article 749804, 2022.

[16] S. Kibria, A. M. Samin, M. H. Kobir, M. S. Rahman, M. R. Selim, and M. Z. Iqbal, "Bangladeshi Bangla speech corpus for automatic speech recognition research," *Speech Communication*, vol. 136, pp. 84–97, 2022.

[17] A. Pandey and D. L. Wang, "Self-attending RNN for speech enhancement to improve cross-corpus generalization," *IEEE/ACM Transactions on Audio, Speech, and Language Processing*, vol. 30, pp. 1374–1385, 2022.

[18] L. Xia, G. Chen, X. Xu, J. Cui, and Y. Gao, "Audiovisual speech recognition: a review and forecast," *International Journal of Advanced Robotic Systems*, vol. 17, no. 6, 2020.

[19] C. M. Chen, M. C. Li, and M. F. Lin, "The effects of video-annotated learning and reviewing system with vocabulary learning mechanism on English listening comprehension and technology acceptance," *Computer Assisted Language Learning*, vol. 35, pp. 1557–1593, 2020.

[20] R. Baumann, K. M. Malik, A. Javed, A. Ball, B. Kujawa, and H. Malik, "Voice spoofing detection corpus for single and multi-order audio replays," *Computer Speech & Language*, vol. 65, article 101132, 2021.

[21] J. Basu, S. Khan, R. Roy, T. K. Basu, and S. Majumder, "Multilingual speech corpus in low-resource eastern and northeastern Indian languages for speaker and language identification," *Signal Processing*, vol. 40, no. 10, pp. 4986–5013, 2021.

[22] J. Gideon, M. G. McInnis, and E. M. Provost, "Improving cross-corpus speech emotion recognition with adversarial discriminative domain generalization (ADDoG)," *IEEE Transactions on Affective Computing*, vol. 12, no. 4, pp. 1055–1068, 2021.

[23] A. Vempala and E. Blanco, "Extracting biographical spatial timelines: corpus and experiments," *IEEE/ACM Transactions on Audio, Speech, and Language Processing*, vol. 28, pp. 1395–1403, 2020.

Hindawi
Wireless Communications and Mobile Computing
Volume 2023, Article ID 9839571, 1 page
https://doi.org/10.1155/2023/9839571

Retraction

Retracted: Analysis of Language Characteristics of Multimedia English Based on Internet of Things

Wireless Communications and Mobile Computing

Received 8 August 2023; Accepted 8 August 2023; Published 9 August 2023

This article has been retracted by Hindawi following an investigation undertaken by the publisher [1]. This investigation has uncovered evidence of one or more of the following indicators of systematic manipulation of the publication process:

(1) Discrepancies in scope
(2) Discrepancies in the description of the research reported
(3) Discrepancies between the availability of data and the research described
(4) Inappropriate citations
(5) Incoherent, meaningless and/or irrelevant content included in the article
(6) Peer-review manipulation

The presence of these indicators undermines our confidence in the integrity of the article's content and we cannot, therefore, vouch for its reliability. Please note that this notice is intended solely to alert readers that the content of this article is unreliable. We have not investigated whether authors were aware of or involved in the systematic manipulation of the publication process.

Wiley and Hindawi regrets that the usual quality checks did not identify these issues before publication and have since put additional measures in place to safeguard research integrity.

We wish to credit our own Research Integrity and Research Publishing teams and anonymous and named external researchers and research integrity experts for contributing to this investigation.

The corresponding author, as the representative of all authors, has been given the opportunity to register their agreement or disagreement to this retraction. We have kept a record of any response received.

References

[1] Y. Zhu, "Analysis of Language Characteristics of Multimedia English Based on Internet of Things," *Wireless Communications and Mobile Computing*, vol. 2022, Article ID 7257265, 9 pages, 2022.

Hindawi
Wireless Communications and Mobile Computing
Volume 2022, Article ID 7257265, 9 pages
https://doi.org/10.1155/2022/7257265

Research Article

Analysis of Language Characteristics of Multimedia English Based on Internet of Things

Yu Zhu

Foreign Language Department, Lanzhou University of Arts and Science, Lanzhou, Gansu 730000, China

Correspondence should be addressed to Yu Zhu; 1000439@luas.edu.cn

Received 28 May 2022; Revised 15 August 2022; Accepted 18 August 2022; Published 16 September 2022

Academic Editor: Jun Ye

The emergence of the Internet of Things is the inevitable trend of the development of science and technology. There are great differences between Multimedia English based on the Internet of Things and conventional English. Only by deeply analyzing it in combination with the language characteristics of Multimedia English can Multimedia English based on the Internet of Things play its due role. This paper analyzes the language characteristics of Multimedia English under the Internet of Things and finds that from the perspective of vocabulary, the pure professional vocabulary in Multimedia English accounts for 25% of all English vocabulary, and the pure professional vocabulary and semiprofessional vocabulary account for 58% of the total vocabulary. This represents that Multimedia English has an extremely obvious professionalism, so we need to focus on the meaning of professional and semiprofessional words when using English; otherwise, it is easy to affect the actual use effect of Multimedia English with the Internet of Things as the core because of the polysemy of one word.

1. Introduction

The development speed of Internet of Things technology is very fast. By analyzing the language characteristics of Multimedia English under the background of Internet of Things, we can effectively understand various factors that need to be paid attention to during the use of Multimedia English and avoid affecting the future development of Multimedia English due to improper use of English [1]. From the perspective of language, Internet of Things English can be regarded as an expression of scientific and technological English terms. In use, it has the advantages of strong language professionalism and semantic rigor. As long as we can identify the industry field in advance and understand the English translation corresponding to the industry before using English, we can make Multimedia English play its due value. Therefore, it is necessary to study the language characteristics of Multimedia English based on Internet of Things.

2. Method

2.1. Analysis of Multimedia Internet of Things. Multimedia cyberphysical system refers to a network that connects any object with telecommunication network, radio and television network, Internet, and satellite positioning network through audio, video, GIS, and other information sensing equipment according to the agreed protocol for information exchange and communication, to realize intelligent identification, positioning, tracking, monitoring, and management [2]. It is not only a branch of the application of the Internet of Things but also a network extended and expanded on the basis of telecom network, radio and television network, Internet, and satellite positioning network. Compared with traditional MSNs (multimedia sensor networks), which are designated by traditional multimedia sensors independently in an unattended environment, MCPS can perceive more comprehensive multimedia information such as audio, video, and image, geographic location information, and event information and can realize environmental monitoring of fine-grained and accurate information. It can be widely used in battlefield visual monitoring, environmental monitoring, safety monitoring, traffic monitoring, smart home, medical and health, and other fields. MCPS organically combines the advantages of MSNs such as self-organization and unattended with the advantages of multimedia technology in sensing rich media. On the one hand,

MCPS has the common characteristics of traditional MSNs such as self-organization, multihop routing, and resource constraints. On the other hand, MCPS has significant personalized characteristics in energy consumption distribution, QoS requirements, and sensing model (see Table 1) [3, 4].

2.2. Internet of Things in Multimedia English. The concept of the Internet of Things was first proposed by Bill Gates. The technology used by the Internet of Things also comes from abroad. Therefore, most of the professional terms about the Internet of Things are foreign words, which need to be translated. Therefore, from the perspective of Chinese people, English terms and vocabulary under the Internet of Things often sound strange. For example, "cloud computing" is a literal translation of cloud computing. Such a name is very abstract. It is difficult to directly see the mechanism behind the technology through the translation. However, from the perspective of readers, when readers read the technology starting with "cloud," they do not need to understand the complex technology and structural system behind it. As long as "cloud" is regarded as a common name, they can further consult more materials for in-depth understanding. Just like the Java technology, we are familiar with now, we may not write the Java language, but we all know that the Java language can realize many applications. Cloud technology is also an important support for the development of Internet of Things technology. Figure 1 shows the key technologies of the Internet of Things [5].

Internet of Things is an emerging technology field. The professional texts in this field have typical scientific and technological stylistic characteristics, such as scientific and technological English. The vocabulary used is highly professional, and the professional vocabulary and terms tend to be complex. Long length, difficult memory, and inconvenient reading and writing are a major feature of science and technology terms. Therefore, there are many abbreviations in Internet of Things English terms, such as loT, 5G, NFC, and QoE. The acronyms usually have polysemy. For example, NFC can be translated into both near field communication and not from concentration, which is a way of producing fruit juice. It may also refer to the National Football Conference. The translator needs to pay special attention to correctly identify the acronyms and give the correct translation. In addition to professional vocabulary, there are some interdisciplinary semitechnical words that appear more frequently. Such semitechnical words have polysemy and flexible collocation. Even in the same major, different meanings may appear. Speck, for example, means "speck" and "speck" in the Internet of Things. Bus is no longer the meaning of "bus" in the English terminology of the Internet of Things, but should be translated into "bus." English for science and technology often involves various mathematical formulas. From the perspective of English language, there are obvious differences between the expression of these formulas and Chinese expression. For example, when leading out a single formula, we need to use the passive form of verbs. "Be + - ed word segmentation + (by/as) + mathematical formula" is a common form [6, 7].

Example 1.

$$\text{In this} \cdots \cdots \text{can be given} + w(y) = \begin{cases} 0 \le y \le M - 1, \\ \text{others.} \end{cases} \quad (1)$$

Example 2.

$$\text{The} \cdots \cdots \text{is given} + H(x) = 1 - \mu s^{-1}, 0.9 \le \mu \le 1.0. \quad (2)$$

Combined with the actual needs of Internet of Things Multimedia English, Internet of Things English terms can be roughly divided into existing standard translation English and nonstandard translation English. There are three kinds of Internet of Things English terms with standardized translations, namely, abbreviations, compounds, and semitechnical words. The translation of such terms has been determined and is commonly observed and used within the industry. The focus of the translation of such terms is not the accuracy of translation, but to summarize the translation methods from the standardized translation, so as to provide reference for the translation of terms without standardized translation [8]. For example, when translating abbreviations, according to the popularity of abbreviations in China, the full translation name of abbreviations can be used, or abbreviations can be used directly. Due to the different ways of word formation of Chinese and English compound words, the translation of compound words can be divided into word-to-word literal translation and flashback translation. The translation of Internet of Things English terms without standardized translation, such as the name of new technology, new compounds, and abbreviations, will be more complex. Although the terms translated by the author are not authoritative at this time, the accuracy and readability of Internet of Things English terms without standardized translation can be ensured by combining the professional knowledge of Internet of Things stored by the author, the translation methods of standardized terms, and the discussion of academic circles on the methods of translating nonstandard terms. Table 2 shows the number of terms corresponding to different translation methods and examples [9].

2.3. Principles of Using Multimedia English Language Based on Internet of Things

2.3.1. Accuracy Principle. The principle of accuracy means that the translation of professional English should faithfully and accurately express the information of the source language in the target language and try to keep the information transmitted by the translation consistent with the information transmitted by the original text, that is, information equivalence [10, 11]. The content of professional English is often more serious. Unlike literary works with gorgeous rhetoric and rich modifiers, it pursues not the artistic beauty of language, but the accuracy and clarity of expression. Accuracy is first reflected in the choice of word meaning. Professional English translation is not simply to choose a translation method from an entry in the English Chinese dictionary, but to accurately select the word meaning and

Table 1: Traditional MSNs and MCPS.

	MSNs	MCPS
Same point	Self-organizing, multihop routing, resource constrained, energy sensitive, and easy to arrange	
Difference	Single-image coding and single-information fusion mechanism	Content-based image coding and on-demand information fusion mechanism
	The energy consumption of information in the process of receiving and transmitting is relatively high	The energy consumption of information in the process of receiving and transmitting is relatively low
	The perceived information is rich but not comprehensive, so it is impossible to make accurate judgment	The perception scene is comprehensive and convenient for accurate and intelligent judgment
	Geographic information is difficult to calibrate	Easy to perceive current geographic information

Figure 1: Key technologies of Internet of Things.

Table 2: Number of terms and examples corresponding to different translation methods.

Classification	Translation category	Quantity	Examples	Translation
Standard English	Abbreviations	61	IoT	Internet of Things
	Compound words	40	Star-topology	Star topology
	Semi technical words	7	Repeater	Repeater
No standardized English	Literal translation	46	Occupancy sensors	Occupancy sensor
	Disassembly and translation combination method	7	Smart metering solutions	Intelligent metering solution
	Untranslatable method	18	Weightless	Weightless

faithfully convey the meaning of the original text on the basis of a correct understanding of the original text. For example: average is of two kinds, general average and particular average. There are two kinds of average, one is general average and the other is particular average. "Average" in this sentence does not mean "average price," but should be translated into "average." If it is translated into "average price," it will not faithfully convey the meaning of the original text. "Agreement" means "consent" in general English and "terms" in professional English. It can be seen that when the same word appears in different professional fields, the concepts expressed are often different.

2.3.2. Normative Principle. Normative principle means that the language and writing style used should comply with the language and writing norms of professional English, that is, the English translation given by the translator must ensure that it should read like an article written by an expert, and the professional terms and expressions should meet the requirements of the document. For example, in international trade sales contracts, price terms are often used. Different price terms represent the responsibilities, expenses, determination of delivery place, risks, and boundaries of the buyer and the seller. These words or terms are conventional and cannot be replaced. For example, "insurance policy" should be translated into "insurance policy," which does not mean "insurance policy." Therefore, when using English, you should be familiar with the professional terms that often appear in various fields. When encountering professional terms that you do not understand, you must not interpret them literally. The safest way is to consult the dictionaries in relevant business fields or consult relevant professionals. Figure 2 shows the structure of the Internet of Things [12].

2.3.3. Principle of Unity. The principle of unity means that the "translated names, concepts, and terms" used in the process of professional English translation should be unified at any time, and it is not allowed to change the same concept or term at will. In the process of professional English translation, we should maintain the accuracy, preciseness, and

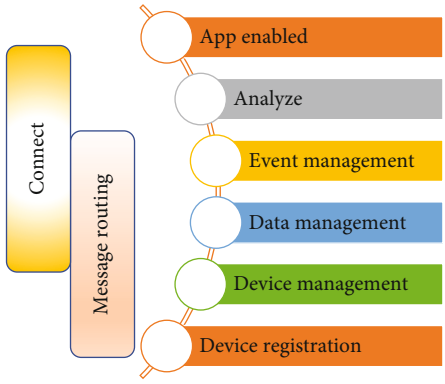

Figure 2: Structure of Internet of Things.

consistency of the translation of professional terms. For example, when using English, we cannot translate "down payment" into "deposit" and "down payment" for a while, because these professional terms have relatively fixed meaning and translation after long-term use, and their arbitrary use will cause unnecessary misunderstanding and disputes. For the translation of professional general terms, the translator should search the relevant professional English literature and dictionaries and choose the correct translation usage to ensure the stability and unity of English use [13, 14].

3. Multimedia English Language Features with Internet of Things as the Core

The language features of Internet of Things Multimedia English can be reflected in vocabulary, syntax, and rhetoric. The importance of vocabulary, syntax, and rhetoric is different.

3.1. English Vocabulary Analysis

3.1.1. Pure Professional Vocabulary. Pure professional vocabulary consists of those special words or terms only used in a certain specialty or discipline, such as hydroxide and diode. With the development of science and technology, as well as the emergence of new disciplines and new specialties, such words emerge in endlessly. From the perspective of language features, this pure professional vocabulary has precise and narrow meaning and strong pertinence. When reading a highly professional article, you must understand the pure professional vocabulary in this field in advance. Only in this way can you master the specific content of the article. On the contrary, it will lead to a significant increase in dyslexia. Figure 3 shows the proportion of pure professional vocabulary [15].

3.1.2. General Professional Vocabulary. General professional vocabulary consists of those words often used by different majors; there are a large number of such words. Because this kind of words have a wider range of use and higher frequency than pure scientific and technological words, they appear in articles of different majors, and there are relatively stable word meanings in different majors. For example, the word power has the meanings of "force," "electricity," and "power" in mechanical mechanics and "power" in mathematics [16, 17].

3.1.3. Derived Vocabulary. Derivative vocabulary is a kind of vocabulary generated by Internet of Things English vocabulary by means of synthesis, transformation, and derivative word formation. This kind of vocabulary often occupies a very large proportion in scientific English literature. For example, there are more than 3000 entries composed of prefixes such as hydro-, hyper-, and hypo- in the literature of English for science and technology majors before 2021. The number of suffixes indicating disciplines, such as -log, is as large as that indicating behavior, nature, state, etc. It should be noted that abbreviations are also an important part of EST vocabulary. Abbreviations have the advantages of economy and simplicity. Figure 4 shows the structure of derived words [18].

3.2. English Syntactic Analysis. In the Internet of Things multimedia vocabulary, you can find a certain number of passive voice. Passive voice can see the remarkable characteristics of crop Internet English. Passive voice has objectivity and authenticity, and there will be no subjective and speculative expression. At the same time, nonfinite verb structure can also be used in Multimedia English. Through this syntactic structure, we can better and more accurately describe the relationship between professional things, as well as the actual situation of the change of the position and state of things. Starting from the syntactic features of English, Multimedia English under the Internet of Things will also use noun phrases and phrases (mainly nouns + of + modifiers with action meaning) to express the meaning of a sentence, which is a form of nominalization structure. Generally speaking, nominalized syntactic structures are often widely used in EST, because nominalized syntactic structures have the advantages of simplicity, accuracy, strictness, objectivity, and large amount of information. In addition, according to the statistics of 1.07 million words computer corpus of Shanghai Jiaotong University, the average length of professional English sentences is 21.4 English words, English short sentences with less than 7 words (including 7 words) account for only 19% of all sentences, and long sentences with more than 40 words account for 7%. Professional English can use long sentences to describe the complex and changeable objective world and maximize the meaning behind English sentences. Figure 5 shows the proportion of English word length.

Language style is based on the common core. The common core of language is the "Convention" used by all kinds of styles, and the different language characteristics of different styles are "variation" on the basis of convention. Scientific activity is a record activity, which must express its content in written form. The characteristics of "variation" and "expression habit" of EST syntax on the basis of "Convention" are mainly reflected in the following points: first, the extensive use of long sentences and sentence sets. From the perspective of stylistics, sentence length and compound sentence are two factors that constitute the stylistic

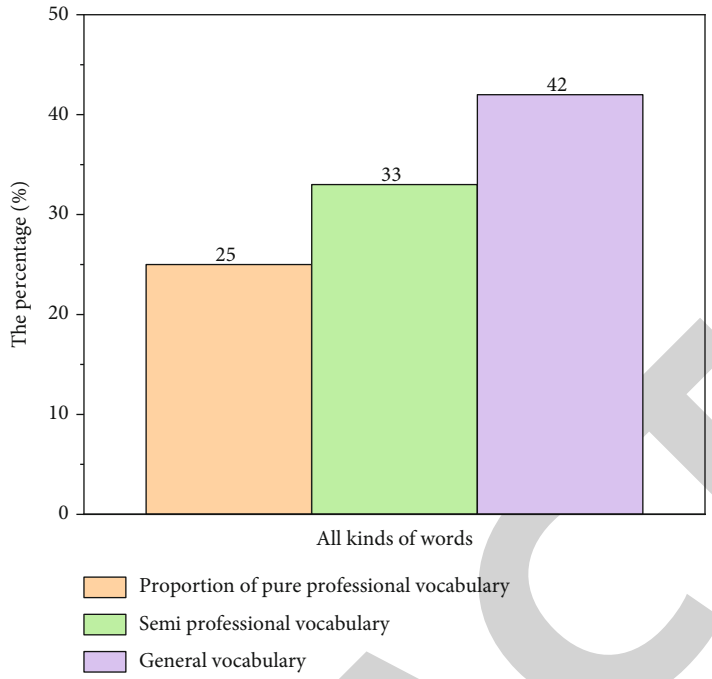

Figure 3: Proportion of pure professional vocabulary. Note: the proportion of pure professional vocabulary in professional journals is 25%; 33% of semiprofessional vocabulary; regular vocabulary 42%.

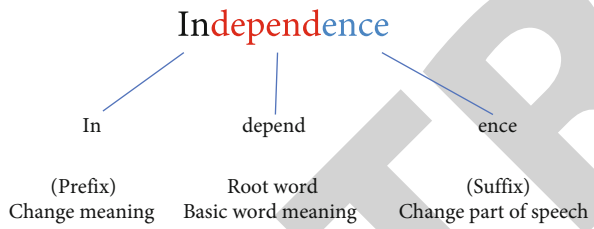

Figure 4: Derived vocabulary structure.

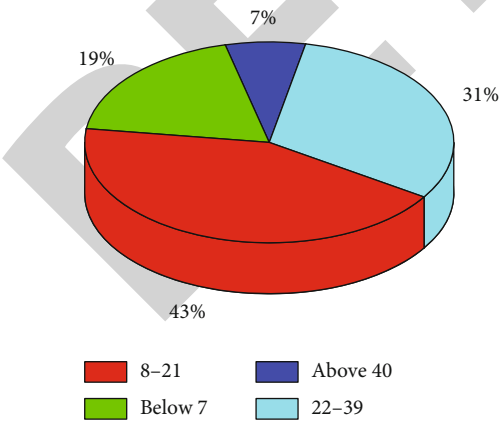

Figure 5: Proportion of English word length.

characteristics of a text. Long sentences and compound sentences have the characteristics of complex structure and large information capacity and can express English under complex concepts. In EST, long sentences and compound sentences are often used to express complex concepts, internal relations between things, and complex ideological content. The choice of sentence pattern should obey the ideological content. Scientific and technological style requires a comprehensive, accurate, complete, rigorous, and logical description of objective things. Therefore, there will be a large number of long sentences and compound sentences in EST. Second, passive sentences are widely used. One of the characteristics of scientific and technological style is the objectivity of description, which reduces the subjective factors and subjective colors in English sentences. Passive sentences are one of the means of objectifying literal expression. Passive sentences are widely used in scientific and technological articles, especially when describing situations. Its advantage is that it cannot mention unnecessary objects, produce concise and objective stylistic effects, and highlight the important information and facts to be expressed. From the perspective of textual function, when choosing the voice, the speaker focuses on the intermediary and goal, making it the theme of the clause. The whole clause takes it as the starting point of the conversation, to highlight the key points and make the stylistic structure more reasonable and the context more coherent. Figure 6 shows the syntactic structure.

3.3. English Rhetoric Analysis

3.3.1. Sentence Patterns and Tenses. Sentence patterns and tenses are generally used in professional English to objectively state facts and problems, describe processes and states, and explain characteristics and functions. Most of the reasons are general, frequent, and characteristic. Therefore, in this style, declarative sentence patterns are widely used, and the predicate verbs are mainly in the general tense, such as the general present tense, the past tense, and the future tense.

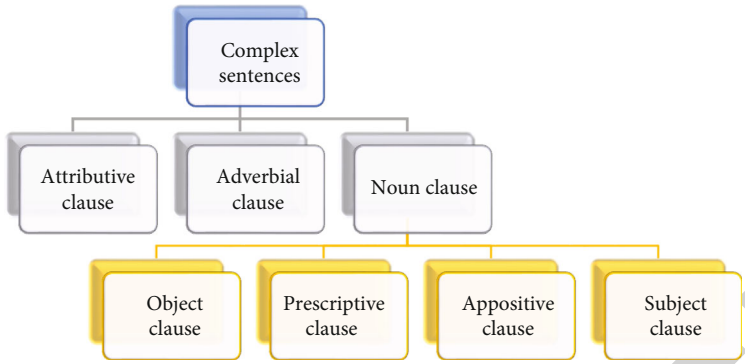

Figure 6: Syntax structure.

3.3.2. Tone. Professional authors often involve various preconditions, conditions, and occasions when explaining things, putting forward ideas, discussing problems, and deriving formulas. In order to avoid the conclusion being too arbitrary, we always start from the perspective of assumption, guess, suggestion, and doubt, which often requires the use of subjunctive mood. On the other hand, many writers are willing to use subjunctive mood to make their tone euphemistic and smooth in order to express their humility, caution, and leeway. In order to make the expression clearer, the derived formula is sometimes described.

For example:

$$\text{For a}\cdots\cdots\text{choose} + H(F) = -\sum_{y=1}^{K}\frac{|c_y|}{|D|}\log_2\frac{|c_y|}{|D|}. \quad (3)$$

When the active voice of lead to, write and other verbs or verb phrases leads to a mathematical formula, its basic format is "subject + verb + mathematical formula." The subject here, according to the different verbs selected, can be served by the subject pronoun this, the formula itself, a variable or condition in the formula, or a noun phrase with action meaning.

For example:

$$\text{Subtracting}\cdots\cdots\text{leads to} + g_R(E,B) = \frac{g(E,B)}{H_B(E)}. \quad (4)$$

3.3.3. Imperative Sentence. Imperative sentences generally appear in the instructions, operating procedures, operation instructions, precautions, and other positions of professional articles. Usually, because imperative sentences are serious, they are mostly used in the way of admonishing, advising, advising, and commanding users or operators.

For example:

$$\text{The period}\cdots\cdots\text{is} + \phi(u) = \text{eup}\left(-\frac{(u-b)^2}{\sigma^2}\right). \quad (5)$$

3.3.4. Other Rhetorical Features. Due to the objectivity and informativeness of multimedia professional English articles under the Internet of Things, they show some obvious characteristics in sentence structure and other language characteristics, such as the use of separation structure, nonverbal symbols, inversion, and ellipsis. Professional English is used to convey objective truth and facts, reject subjectivity and conjecture, eliminate ambiguity, and strive to be concise, concise, standardized, and logical. The above language features are formed according to the requirements of professional English itself. Figure 7 shows the rhetorical structure of English emphasis sentences.

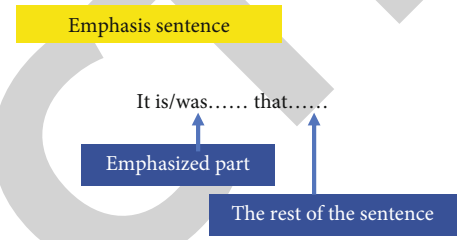

Figure 7: Rhetorical structure of emphasis sentence.

3.4. Multimedia English Language Translation Based on Internet of Things

3.4.1. Sequential Method. Some English long sentences describe a series of actions, either in logical relation or in chronological order, which is basically similar to the expression of Chinese. The sentence order of the original English text can be maintained during translation. In general, most of the object clauses, appositions, and paratactic sentences in English can be translated by sequential method. In fact, using the sequential method is to convey the deep meaning of the original text with the expression habits of Chinese rather than the surface meaning of words, words, and sentences. Sometimes, using the sequential method, the original text must be cut in the appropriate place. By using colons to segment the long sentences of the original text, the Chinese sentences can be shortened, which can make the level of English translation clear at a glance and more in line with the expression habits of Chinese.

3.4.2. Reverse Order Method. Due to the different ways of thinking between Chinese and English, the two languages

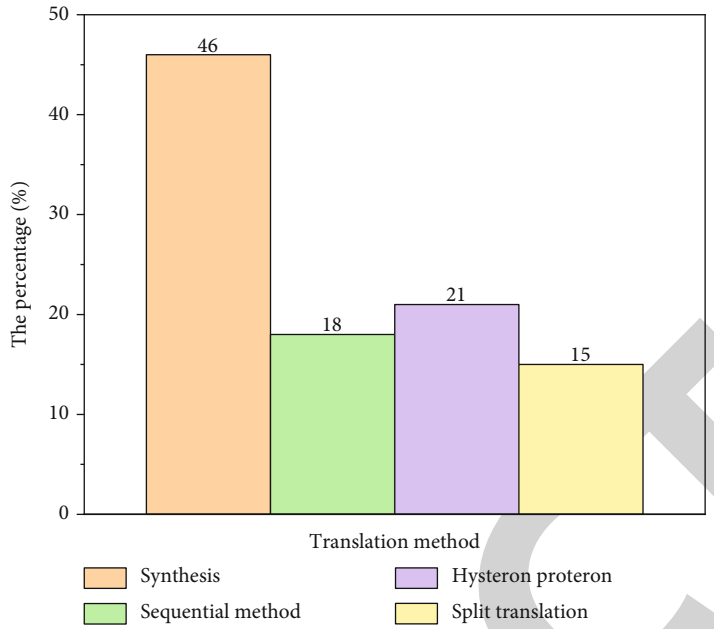

Figure 8: Frequency of four translation methods in articles. Note: 15% for split translation method; the reverse order method is 21%; sequential method 18%; the comprehensive method is 46%.

are also very different in the order of expression. Chinese is generally "first cause and consequence," "first order and then subject," and "what happens first is said first, and what happens later is said later." However, most of the time, English and Chinese are just the opposite, putting the main sentence at the beginning of the sentence and the analysis or explanation part at the back. Therefore, when the narrative level of English long sentences is opposite to the logical order of Chinese, we should pay attention to the use of Chinese customary expression in translation. From the later translation of the original text, we should adjust the order of the original language in order to improve the quality of translation.

3.4.3. Variable Order Method. If the structure of English middle and long sentences is complex and the order of some components is different from Chinese habits, the expression order can be changed locally. When translating this sentence, we should pay attention to the word order change of the attributive. For example, when translating the attributive clause, the postattributive phrase and attributive clause in English are often placed in front of the central word when they are translated into Chinese. Therefore, in the process of translation, we can deal with the English attributive clause in advance, to make the translation meet the habits of Chinese.

3.4.4. Split Translation. Because postmodifiers or various phrases often appear in professional English, some English sentences are very long. In order to conform to Chinese expression habits, we can usually translate a series of postmodifiers in long sentences and their modifying components, that is, we can disassemble phrases or clauses into short sentences, to reflect the unique rhythm of Chinese. If the number of words in the sentence is large, it can be combined with the expression of commonly used short sentences in Chinese to separate long sentence patterns, so as to avoid affecting people's reading quality because English sentences are too long.

3.4.5. Comprehensive Method. When dealing with individual Internet of Things Multimedia English long sentences, sometimes, simply using any of the translation methods of sequence method, reverse order method, variable order method, and split translation method cannot work. This requires us to comprehensively consider the actual needs of sentences, so as to select the appropriate sentence processing methods. Through careful deliberation and taking into account the relationship between contexts, we can comprehensively process the whole sentence according to the logical order and expression habits of Chinese. A scholar once analyzed the frequency of the use of the four translation methods. The frequency of the use of the four methods is shown in Figure 8.

3.5. Internet of Things Multimedia English Translation Skills

3.5.1. Technical Terms. Scientific and technological terms should properly reflect the conceptual connotation of the things referred to and the content of specific things in some disciplines. Such as medical terminology haemoglobin (hemoglobin). In addition, the same word has different meanings in general English and professional English. For example, taxi in aviation refers to aircraft taxiing on water (ground), average in insurance refers to average, and different words with the same conceptual connotation are used in different majors. For example, "brain" is expressed by brain and encephalon in general English and medical English, respectively. Finally, EST has different meanings in different disciplines. For example, bit is "drill bit" in

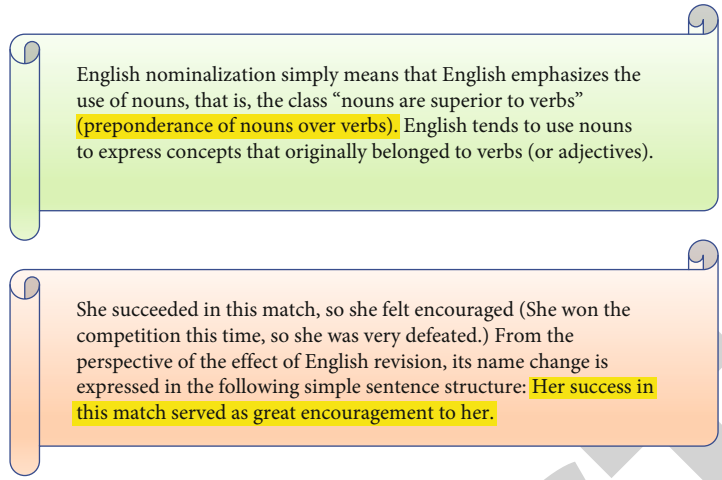

Figure 9: Nominalized verbs.

petroleum specialty, "military knife and cutting knife" in machining industry, "binary number" in mathematics, and "byte" and "function" in computer specialty. For machinery and equipment, it refers to the meaning of "function," and if it appears in articles on mathematics or computer language, it is the meaning of "function." Various disciplines and specialties of modern science and technology permeate, influence, and contact each other. This leads to the flexibility of word meaning and the cross use of words. A word can not only have different professional colors but also be integrated in the same major or set in one article.

For example:

Electrode potential depends on the concentration of the ions.

The determination of trace concentrations of mercury in mineral materials is described.

In the above two examples, the same word has different meanings. The first sentence is "concentration," which is a chemical concept, and the second sentence is "quantity," which is a way to calculate the size of matter physically.

3.5.2. Nominalized Action Noun. Due to the differences in sentence structure and expression between English and Chinese, nominalization is common in scientific and technological style. When translating these nominalized action nouns, in order to better convey the ideological content of the original text and make the translation more in line with the expression habits of Chinese and more smooth and natural, it is often necessary to carry out part of speech conversion, that is, a part of speech in English is not necessarily translated into the corresponding part of speech in Chinese, but to make appropriate conversion to translate the nominalized action nouns in English into verbs in Chinese. In order to make the narration concise and clear, nonfinite verbs are widely used in EST, including past participle, present participle, gerund, and verb infinitive. Nonfinite verbs not only make the sentence structure rigorous and logical, but also deepen the difficulty of understanding and translation. When encountering such sentences, we must clarify the context and analyze their components, to accurately understand the meaning of the sentence and translate correctly. Figure 9 shows nominalized verbs.

3.5.3. Nonfinite Verbs and Passive Voice. In order to make the narration concise and clear, professional English often uses a large number of nonfinite verbs, including past participle, present participle, gerund, and verb infinitive. Nonfinite verbs not only make the sentence structure rigorous and logical, but also deepen the difficulty of understanding and translation. When encountering such sentences, we must clarify the context and analyze their components. Only in this way can we accurately understand the meaning of the sentence and translate correctly.

The passive voice is much more used in English than in Chinese. Since the main purpose of professional English is to express scientific discoveries, scientific facts, experimental reports, and various explanations, it makes it necessary to add a large number of objective statements in English to output more views, use more passive voice, and reflect scientificity and objectivity.

4. Conclusion

To sum up, this paper analyzes the Multimedia English language based on the Internet of Things. Through the comprehensive analysis of language structure and language characteristics in language analysis, this paper finds out various elements that can affect the use effect of Multimedia English. For example, language translation methods and professional terms in different industries will have an impact on the normal use of multimedia language. Therefore, in order to improve the use effect of Multimedia English language based on the Internet of Things, it is necessary to actively analyze the characteristics of English language and sort out the vocabulary, syntax, rhetoric, and other elements in the language guided by phonetic features, so as to optimize the multimedia language and avoid affecting the normal use of English due to improper language. It should be noted that although the multimedia language under the Internet of Things is more serious than conventional

Hindawi
Wireless Communications and Mobile Computing
Volume 2022, Article ID 9097029, 11 pages
https://doi.org/10.1155/2022/9097029

Research Article

Swimming Movement Guidance Training System Based on OpenCL Technology

Xiaopeng Tian

Sports & Military Training Department, Zhejiang A&F University, Hangzhou 311300, China

Correspondence should be addressed to Xiaopeng Tian; tianxiaopeng@zafu.edu.cn

Received 1 June 2022; Revised 8 August 2022; Accepted 18 August 2022; Published 14 September 2022

Academic Editor: Jun Ye

In order to improve the physical quality and even ability of swimmers, this study built OpenCL technology for the swimming movement design system of swimmers, so as to design a series of movements. Combined with the capture system, this paper captures and processes the athletes' movements, obtains the key position information, and calculates the accurate data. It can provide effective guidance for accurately positioning athletes' swimming movements, enable users to have a clearer understanding of their own movements, improve users' movements, and enhance the system operation effect. According to the technology and application requirements of virtual swimming training simulator, the overall design scheme of the device is determined. From the point of view of ensuring the comfort and safety of simulated virtual swimming, the design, installation, and strength verification of the supporting structure are carried out. Hardware design and selection shall be carried out according to the requirements of head position detection and virtual environment presentation, including the design of positioning ball set, camera selection, and VR head display selection. The software functions of head position detection program and virtual scene program are designed according to the requirements of natural human-computer interaction. The designed swimming guidance training system has complete functions and stable operation and can be used as an auxiliary tool for swimming training.

1. Introduction

Swimming is valued by the state, and swimmers in the swimming field have higher requirements for posture. But in the actual swimming process, it is difficult to achieve their own positioning. In this paper, a guidance system is built for the swimming movements of swimmers to cover the swimming movements and monitor the movements of swimmers [1]. Through real-time motion capture, the motion is transmitted to the computer through the sensor to process the data and give correct instructions to the athlete, as shown in Figure 1. In this paper, the system adopts OpenCL technology to accelerate the system and optimizes the algorithm in the image processing technology to ensure the image processing quality and improve the application effect of the system [2]. And carry out experiments to ensure the effective coverage of the system for swimmers, provide accurate positioning guarantee for their movement rhythm and amplitude, and provide effective guidance for accurately locating swimming movement problems of athletes, so that users can have a clearer understanding of their movements and improve user actions to improve system performance. According to the technical and application requirements of the virtual swimming training simulation device, the overall design scheme of the device is determined. At present, human motion analysis based on vision is still a challenging subject in computer vision. The core problem in motion analysis is human posture estimation. The task of human posture estimation is to identify the human body and locate the joint points of human parts through computer image processing algorithm. Its applications include human behavior understanding, human re recognition, human-computer interaction, health monitoring, and motion capture [3]. Artificial intelligence technology has gone deep into sports training projects. Professional guidance and artificial intelligence-assisted training make the training process of athletes more scientific. By collecting a large number of athletes' training data and using computer technology for visual

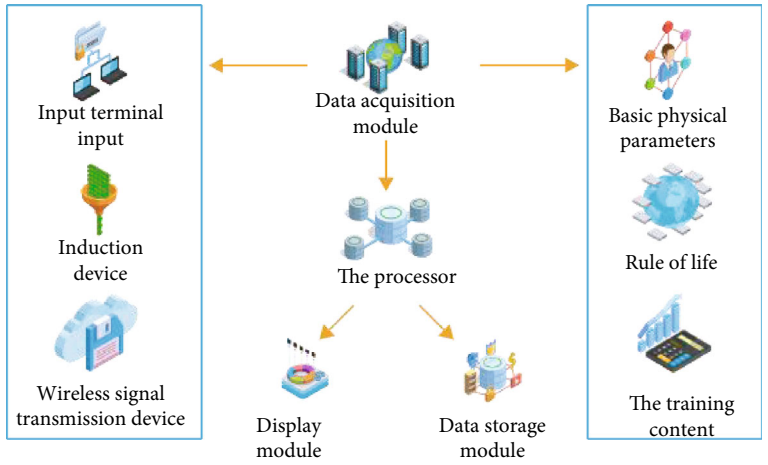

Figure 1: Swimming movement guidance training system.

analysis, athletes can comprehensively master their own growth process. The rapid development of the new generation of information technology represented by Internet technology, big data technology, cloud storage technology, virtual reality technology, etc., and the cross integration between different disciplines have led to the continuous development and innovation of a new round of scientific and technological revolution and industrial revolution. The emergence of a series of scientific and technological products and new models has made human life more convenient and intelligent in the new era [4].

2. Research on Pose Detection Method

In the virtual swimming training simulation device, accurate and real-time detection of the position and posture of the set pieces can make the virtual swimming scene change according to the user's movement and head rotation, which is the key step to realize natural human-computer interaction [5]. The essence of pose detection is to obtain the corresponding relationship between the spatial coordinates of feature points and the image coordinates and then solve the conversion matrix between the object coordinate system and the camera coordinate system [6]. Among them, the acquisition of the image coordinates of feature points and the determination of the corresponding relationship are the focus of this research. The main content of this chapter is to introduce the basic principle of pose solution and camera calibration method and introduce in detail the positioning ball image recognition method and feature point image coordinate calculation method used in this topic.

2.1. Principle of Pose Solution

2.1.1. Camera Model. The most basic pinhole model in the camera model includes four coordinate systems:

(1) Object coordinate system *Ow* is a user-defined three-dimensional coordinate system

(2) The camera coordinate system *Oe* is a rectangular coordinate system established with the camera optical center as the origin and the optical axis as the *Z* axis

(3) The image physical coordinate system *o* is a planar two-dimensional coordinate system established with the principal point (the intersection of the optical axis and the imaging plane) as the origin, and its *x* and *y* axes are parallel to the *x* and *y* axes of the camera coordinate system, respectively

(4) The image pixel coordinate system *o* is a planar two-dimensional coordinate system established with the upper left corner of the image as the origin. Its *u* and *v* axes are parallel to the *x* and *y* axes of the image physical coordinate system [7]. Different from the other three coordinate systems, the coordinates in the image pixel coordinate system are in pixels

The conversion relationship between the four coordinate systems based on the camera pinhole model is described as follows:

(1) *From Object Coordinate System ow to Camera Coordinate System o.* According to the coordinate conversion principle, the conversion from the object system (x_w, y_w, z_w) to the camera system coordinates (x_c, y_c, z_c) can be completed through the rotation matrix R and the translation vector t, as shown in the following formula:

$$\begin{bmatrix} x_c \\ y_c \\ z_c \end{bmatrix} = \begin{bmatrix} r_{11} & r_{12} & r_{13} \\ r_{21} & r_{22} & r_{23} \\ r_{31} & r_{32} & r_{33} \end{bmatrix} \begin{bmatrix} x_w \\ y_w \\ z_w \end{bmatrix} + \begin{bmatrix} t_1 \\ t_2 \\ t_3 \end{bmatrix} = R \begin{bmatrix} x_w \\ y_w \\ z_w \end{bmatrix} + t. \tag{1}$$

Secondly, the coordinates and matrix form are shown in the following formula:

$$\begin{bmatrix} x_c \\ y_c \\ z_c \\ 1 \end{bmatrix} = \begin{bmatrix} R & \mathrm{t} \\ 0^T & 1 \end{bmatrix} \begin{bmatrix} x_w \\ y_w \\ z_w \\ 1 \end{bmatrix}. \tag{2}$$

(2) *Coordinate Conversion from Camera Coordinate System Oc to Image Physical Coordinate System 0*. The projection of any point p in the 3D scene on the camera imaging plane is p [8]. According to the similar triangle principle, it can be seen that there is a relationship between the camera system coordinates (x_c, y_c, z_c) of point p and the image physical system coordinates (x, y) of point P as shown in the following formula:

$$\begin{cases} x = \dfrac{f x_c}{z_c}, \\ y = \dfrac{f y_c}{z_c}. \end{cases} \tag{3}$$

Secondly, the coordinates and matrix form are shown in the following formula:

$$z_c \begin{bmatrix} x \\ y \\ 1 \end{bmatrix} = \begin{bmatrix} f & 0 & 0 & 0 \\ 0 & f & 0 & 0 \\ 0 & 0 & 1 & 0 \end{bmatrix} \begin{bmatrix} x_c \\ y_c \\ z_c \\ 1 \end{bmatrix}. \tag{4}$$

(3) *Coordinate Conversion from Image Physical Coordinate System 0 to Image Pixel Coordinate System O_i*. The main point is theoretically located at the center of the image, but due to the defects of camera manufacturing technology, the main point often deviates from the center of the image [9]. Similarly, due to the manufacturing process deviation, the actual pixels are often not square, and there are scale differences in the u and v directions. Assuming that the coordinates of the main point in the image pixel coordinate system O_i are (c_x, c_y), and the physical lengths of each pixel in the u, v directions are k, l, respectively, the conversion relationship between the image physical coordinates (x, y) and the image pixel coordinates (u, v) is shown in the following equation:

$$\begin{cases} u = \dfrac{x}{k} + c_x, \\ v = \dfrac{y}{l} + c_y. \end{cases} \tag{5}$$

Its homogeneous coordinates and matrix form are shown in the following formula:

$$\begin{bmatrix} u \\ v \\ 1 \end{bmatrix} = \begin{bmatrix} \dfrac{1}{k} & 0 & c_x \\ 0 & \dfrac{1}{l} & c_y \\ 0 & 0 & 1 \end{bmatrix} \begin{bmatrix} x \\ y \\ 1 \end{bmatrix}. \tag{6}$$

Combining the above equations (2), (4) ,and (6), the conversion relationship between the object system coordinates (x_w, y_w, z_w) of point P and the image pixel coordinates (u, v) of its image point is obtained as follows:

$$z_c \begin{bmatrix} u \\ v \\ 1 \end{bmatrix} = \begin{bmatrix} f_x & 0 & c_x & 0 \\ 0 & f_y & c_y & 0 \\ 0 & 0 & 1 & 0 \end{bmatrix} \begin{bmatrix} R & t \\ 0^T & 1 \end{bmatrix} \begin{bmatrix} x_w \\ y_w \\ z_w \\ 1 \end{bmatrix}, \tag{7}$$

where f_x and f_y are the focal length in pixels, and c_x and c_y are used as internal parameters of the camera.

2.1.2. PnP Problems. PnP is a classical problem in the field of computer vision, the calibration of camera external parameters. Assuming that there are n different P points, according to the internal parameter matrix and distortion parameters obtained from camera calibration, as well as the object system coordinates (x_w, y_w, z_w) and image coordinates (u, v) of N groups of P points, n groups of conversion formulas can be listed [10]. To solve the PnP problem, the relative pose of the object coordinate system ow and the camera coordinate system OE is determined from the conversion formula of $n\,(2 < n < 6)$, that is, the external parameter matrices R and t. Solving the PnP problem can effectively solve the pose of objects based on a single image, avoiding the problem of determining the corresponding relationship between image points in the pose solution method based on multiple images [11]. PnP (Perspective-n-Point) is a method for solving 3D to 2D point-to-point motion. The purpose is to solve the pose of the camera coordinate system relative to the world coordinate system. It describes how to estimate the pose of the camera when the coordinates of a 3D point (relative to the world coordinate system) and the pixel coordinates of these points are known (that is, to solve the rotation matrix and translation vector from the world coordinate system to the camera coordinate system). It is quite a wide range of vision-based pose solving methods. This subject plans to adopt the re projection algorithm realized by OpenCV, obtain the coordinates of the feature point object system through the positioning ball group measurement, obtain the camera internal parameters and distortion

parameter matrix through the camera calibration, and obtain the feature point image coordinates through the image processing method. Finally, combined with the above known information, the relative position and orientation ph2c of the positioning ball group in the camera coordinate system in each moving image is solved [12].

2.2. Camera Calibration Method. Camera calibration is the process of obtaining camera internal parameters and distortion parameters. The commonly used calibration methods can be divided into traditional camera calibration methods and camera self-calibration methods. Among them, the traditional camera calibration method uses the known scene structure information for calibration. Usually, the high-precision known structure information is provided by the precision calibration block, which is often difficult to achieve in practical applications. Therefore, although the traditional method has high calibration accuracy, it is difficult to apply [13]. The camera self-calibration method is calibrated by the corresponding relationship between image points. Because it does not need calibration blocks, it has the advantages of flexibility and convenience compared with the traditional methods; however, its calibration process is complex, and the nonlinear method is used for calibration, which has low accuracy and insufficient robustness. After the camera calibration is completed, the re projection error is often used as the evaluation standard of the final calibration effect. The re projection error considers not only the calculation error of homography matrix, but also the measurement error of image points. In the homography transformation from the object plane to the image plane as shown in Figure 2, x is a point in the object plane, x' is the corresponding point of x in the image plane, and the relationship between them should meets the relationship shown in the following equation [14].

$$x' = Hx, \tag{8}$$

where H is a plane homography matrix.

Then, the form of re projection error is shown in the formula:

$$\varepsilon = d^2(x\boxtimes\hat{x}) + d^2\left(x'\boxtimes\hat{x}'\right) \text{subject to } \hat{x}' = \hat{H}\hat{x}, \tag{9}$$

where $\hat{x}$ is the estimated value of x, $\hat{x}$ is the estimated value of x', and $\hat{H}$ is the estimated value of H. In the process of camera calibration, since the mark points on the chessboard calibration board are standard points formulated strictly according to the size, it can be considered that x is absolutely accurate, and the estimation $\hat{x}$ of x is itself, so the re projection error degenerates into a unilateral transformation error under the strong constraint condition $x = \hat{x}$, as shown in the following equation.

$$\varepsilon = d^2\left(x', \hat{x}'\right) = d^2\left(x', \hat{H}x\right). \tag{10}$$

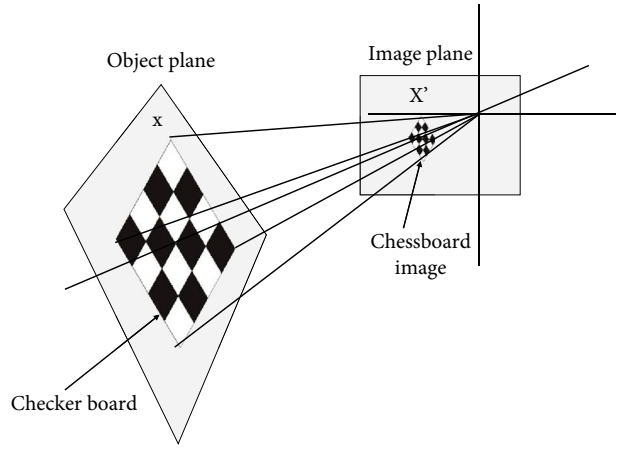

Figure 2: Plane homography transformation.

3. Swimming Image Processing Application

The extraction and synthesis of key technology action pictures are aimed at analyzing the technical advantages and disadvantages of the observation object from the perspective of key actions. For the 3D modeling of the observed object, aiming at the swimming posture information, the image processing method is studied to lay the foundation for the next chapter [15].

3.1. Analysis of Key Information during Turning. A certain distance should be reserved before swimming turns to facilitate adjustment of movements. The deceleration caused by nonstandard actions and other factors will greatly affect the turning effect, so it is also important to analyze the breaststroke action before turning [16], through the angle between knee joint, hip joint, trunk body, and horizontal plane. From these three angles, we can determine the rhythm of the swimmers' turning process and whether the body position at each stage is correct and then give targeted optimization opinions. For the region image, it is necessary to determine the hue value range according to the color model, as shown in Table 1.

After positioning the color, calculate the coordinate system according to its spherical center point, as shown in Table 2.

3.2. Analysis and Research of Image Processing in the Field of Swimming. In order to obtain the swimmer's posture information, it is necessary to process the image. Image processing is a technology for analyzing, processing, and processing images to meet the needs of key information extraction and positioning [17]. From the origin, image processing is actually an application of signal processing in the field of digital images, because most of the images at this stage are stored in digital form. After studying the main flow of image processing, the main flow of image processing in this system is determined: first, the image gray is removed, then the noise is removed, and finally the edge is detected. After the processing of component method, the image with R matrix, G matrix, and B matrix as gray value is obtained [18]. Gaussian filtering is also a typical linear smoothing filtering method,

Table 1: Range of color hue values.

Color	Hue value H range
Yellow	30-50
Green	70-90
Blue	100-122
Purple	150-170

Table 2: Object coordinate system of feature points.

Color	X coordinate/mm	Y coordinate/mm	Z coordinate/mm
Green	0	-38	0
Yellow	35.83	12.66	0
Purple	-17.91	12.66	-31.03
Blue	-17.91	12.66	-31.03

which has good performance in eliminating Gaussian noise. Therefore, Gaussian filtering is also widely used in all kinds of image processing to remove noise. Gaussian filtering is a kind of linear smoothing filtering, which is suitable for eliminating Gaussian noise and is widely used in the noise reduction process of image processing. In layman's terms, Gaussian filtering is a process of weighted averaging of the entire image. The value of each pixel is obtained by weighted averaging of itself and other pixel values in its neighborhood. Gaussian filtering is actually a weighted average of each pixel in the field. The filtered value of each pixel is jointly determined by the points in the field with it as the central point, that is, each point is weighted and averaged to obtain the value of the point [19]. The Gaussian kernel for image convolution by Gaussian filter is usually a $3 * 3$ or $5 * 5$ Gaussian template. The commonly used Gaussian template is shown in Figure 3.

According to the content of Figure 3, the position parameters in each template are calculated by Gaussian function, and the calculation formula is as follows:

$$G(x, y) = \frac{1}{2\pi\sigma^2} e^{x^2+y^2/2\sigma^2}. \tag{11}$$

x^2 and y^2 in the formula represent the distance, that is, the distance between a pixel and the center point in the field. In the formula, O represents the standard deviation [20]. It can be seen from the formula that the smoothing effect changes with the size of the standard deviation. The larger the standard deviation, the better the smoothing effect. The smaller the standard deviation, the more general the smoothing effect.

4. Analysis and Evaluation of Swimming Movements

This chapter captures the swimming before turning. In this process, the information of key positions includes knee joint, hip joint, and the angle between the trunk and the horizontal plane. Through the observation of these three angles, we can determine whether the swimmer's movement before turning is standard and then determine whether the speed decreases. The original intention of the system design proposed in this paper is to improve the standard of athletes' turning movements. In order to achieve this goal, it is necessary to compare the movements of the observed with the standard movements. Therefore, it is necessary to compare both the standard data and the comparison algorithm [21]. Then, combined with their own understanding of swimming, a comparison algorithm is designed to let the observed clearly understand the problems and standard degree of their own actions. At the end of this chapter, the algorithm is implemented by an example.

4.1. Application of Image Processing Algorithm in Swimming Detection

4.1.1. Sobel Operator. Sobel operator belongs to discrete difference operator. As a common method of edge detection, Sobel operator convolutes all pixels of the image through the kernel of the operator. The cores here are mainly two templates of $3 * 3$. Two sets of values can be obtained by plane convolution between the horizontal and vertical matrix templates and the points in the image, which are the horizontal and vertical brightness difference values, respectively. For the processed image, select the appropriate threshold to extract the edge. The implementation in this example is as follows: the image before processing is represented by C. The transverse test results are represented by G_x, and the longitudinal test results are represented by G_y. Formula (12) and formula (13) represent G_x and G_y, respectively.

$$G_x = \begin{bmatrix} -1 & 0 & +1 \\ -2 & 0 & +2 \\ -1 & 0 & +1 \end{bmatrix} * C(4-1), \tag{12}$$

$$G_y = \begin{bmatrix} +1 & +2 & +1 \\ 0 & 0 & 0 \\ -1 & -2 & -1 \end{bmatrix} * C(4-2). \tag{13}$$

For the pixel points traversed horizontally and vertically, the final value of the point can be obtained through the following formula:

$$G = \sqrt{G_x^2 + G_y^{2\cdot}} \tag{14}$$

After studying Sobel operator, it is found that the main advantage of using Sobel operator for edge detection in the swimming field is that the processing speed is faster. The disadvantage is that the template with only two directions can only detect edges in two directions, namely, the vertical direction and the horizontal direction. The Sobel operator does not strictly distinguish the subject and the background of the image. In other words, the Sobel operator is not processed based on the grayscale of the image. Since the Sobel operator does not strictly simulate the human visual

$$\frac{1}{16} \times \begin{bmatrix} 1 & 2 & 1 \\ 2 & 4 & 2 \\ 1 & 2 & 1 \end{bmatrix} \qquad \frac{1}{273} \times \begin{bmatrix} 1 & 4 & 7 & 4 & 1 \\ 4 & 16 & 26 & 1 & 4 \\ 7 & 26 & 41 & 26 & 7 \\ 4 & 16 & 26 & 16 & 4 \\ 1 & 4 & 7 & 4 & 1 \end{bmatrix}$$

Figure 3: Common templates for Gaussian filtering.

physiological characteristics, the extracted image contour sometimes is not satisfactory. At this time, Sobel operator edge detection cannot achieve the desired effect for the pose processing scene with high accuracy requirements. At the same time, pixels with gray value greater than the threshold are regarded as edge points in this way. Some noise points with large gray value, such as large water waves, may also be judged as edges [22]. In order to test the edge detection performance of Sobel operator in swimming scene, MATLAB is used to detect the following pictures.

It can be seen from the results that there are many misjudgments about edges detected by Sobel operator, which are mainly reflected in the following three aspects:

(1) Water waves are often detected as edges

(2) The edge of the swimmer's swimsuit is misjudged as nonedge

(3) Too much internal information of the target will have a certain impact on the follow-up experiments

4.1.2. Canny Operator. Canny operator is a multilevel edge detection algorithm. The significance of Canny operator is to find the optimal edge of the image. The principle is as follows: firstly, the image is denoised. The purpose of denoising is that many noises belong to high-frequency signals, which will lead to misjudgment in edge detection. Although Gaussian filtering can reduce the probability of misjudgment, the edge information of the image may also belong to high-frequency signals, so it is also very important not to judge the edge as noise. Here, the grasp of the scale lies in the selection of an appropriate Gaussian blur radius [23]. The template is used to calculate each pixel, then the nonmaximum value is suppressed, and finally the double threshold detection is performed. The original graph processed by Canny operator obtains the research results. It can be seen from the results that Canny operator is more accurate and precise for human body edge detection. Only the edge of the foot cannot be accurately identified due to the large spray, and the spray part still detects the edge, but has little impact.

4.2. Detection of Key Information. After edge detection, in order to get the position information of key points, the system chooses to carry out Hough line detection on the image after edge detection. The purpose is to obtain the coordinates of the key position. The included angle of a key position can be determined by three coordinates. Hough transform is an algorithm that image processing must come into contact with. It detects objects with a specific shape through a voting algorithm. This process obtains a set conforming to the specific shape in a parameter space by calculating the local maximum value of the cumulative result. The Hough transform method can detect shapes such as circles, lines, ellipses, etc. In the lane line detection, one of the solutions initially considered is to use the Hough transform to detect the straight line for lane line extraction. Hoff line detection uses the duality of lines and points to detect. In line detection, the points in the parameter space correspond to the lines in the image space one by one. Similarly, the points in the image space correspond to the lines in the parameter space one by one. In the coordinate system, a line can be expressed as $y = kx + b$, K is the slope, and B is the intercept, both of which are constants [24]. The parameters of all straight lines passing through point $M(x_1, y_1)$ satisfy the equation, that is, the point determines a group of straight lines. If the equation is rewritten as $b = -kx, +y_1$, it represents a straight line in the parameter space, as shown in Figure 4.

If $B(x_2, y_2)$ and a point are added to the line $y = kx + b$, $B(x_2, y_2)$ also corresponds to a line in the parameter space, as shown in Figure 5.

In practical application, the image space is shown in Figure 6. If multiple pixel points in the source image form a straight line, the curve mapped to the parameter space can intersect at one point, and the intersection of the curve can be detected in the parameter space to determine the straight line.

After the original image is detected, the parameter space image is obtained. The linear direction is discretized, the direction R is obtained, and the results are obtained by statistical selection. The coordinates of the key position can be selected, and then, the key position information can be calculated according to the nearby coordinates. After the operation, the action information of the swimmer's key position can be obtained. After the action continuous frames are processed, the continuous information can be obtained, as shown in Figure 7.

4.3. Design and Application of Swimming Motion Evaluation Algorithm. The original intention of the system design proposed in this paper is to improve the swimmer s' turning movements. In the process of improving the swimming movements, athletes need to first locate their own problems and then improve to the standard movements. The

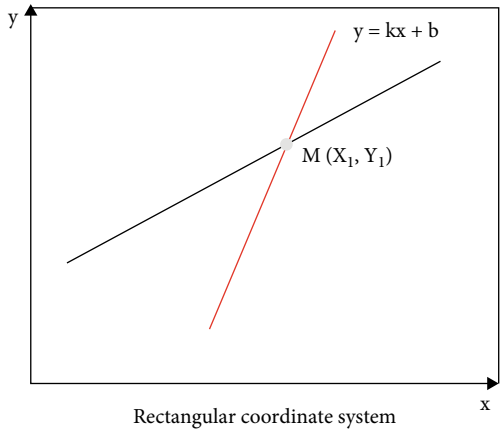

Figure 4: Mapping diagram of rectangular coordinate system and parameter space 1.

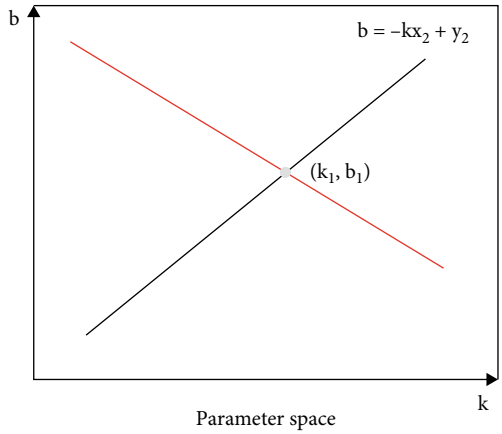

Figure 5: Mapping diagram of rectangular coordinate system and parameter space 2.

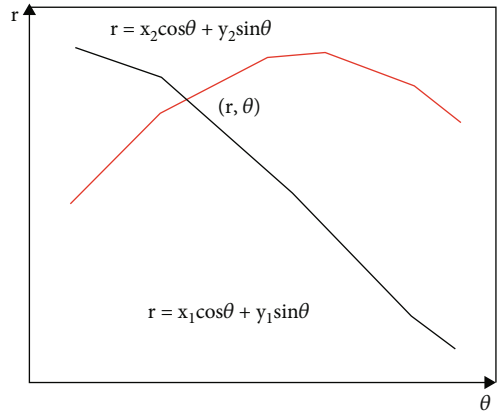

Figure 6: Mapping diagram of rectangular coordinate system and parameter space 3.

evaluation algorithm is added in the improvement process. After in-depth study of the key information in the swimming process, the following motion evaluation algorithm is designed. The action evaluation algorithm mainly includes two contents:

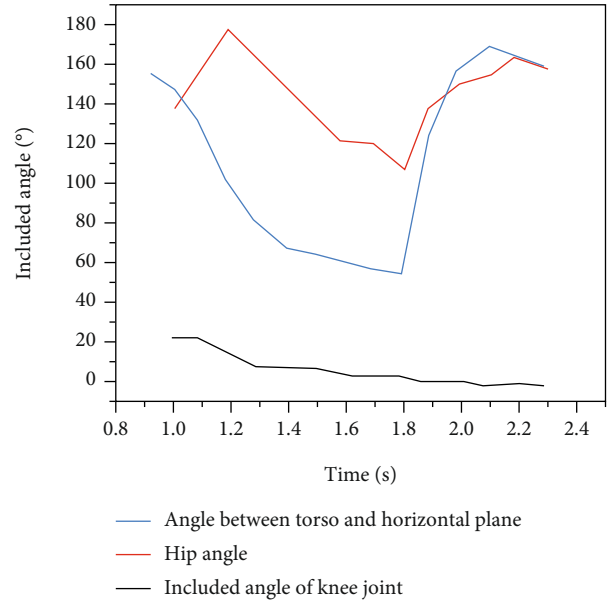

Figure 7: Key information of breaststroke movement of an athlete.

(1) Give users suggestions on optimizing the action standardization

(2) Quantifying the user's actions

The evaluation of the above two points is based on the comparison between the action of the observer and the standard action. The observation index is to analyze the accuracy of the athletes' swimming rhythm and observe whether the athletes' actions are standard [25]. Therefore, the order of importance of the three aspects of the evaluation system is as follows: whether the action cycle is standard, the proportion of standard action time, and whether the action amplitude is standard. The weights of these three points are defined as 50%, 30%, and 20%, respectively. Therefore, the comprehensive score formula is as follows:

$$CS = P + 50\% + T_{ps} * 30\% + A_{ps} * 20\%, \quad (15)$$

where CS is the comprehensive score, P is the score of the standard part of the action cycle, T_{ps} is the score of the proportion of the standard action time, and A_{ps} is the score of the standard part of the action. The obtained formula is as follows:

$$P = e^{-(x-28)^2/50} * 100. \quad (16)$$

Establish the amount data of the standard action, calculate the information of each key position through the above method, then adjust the cycle of each breaststroke action to the action cycle of the observer, and average the key information calculated in these 23 frames, that is, obtain the curve as shown in Figure 8. According to the proportion of standard action time and the scores of each link, the comprehensive scores of athletes are obtained.

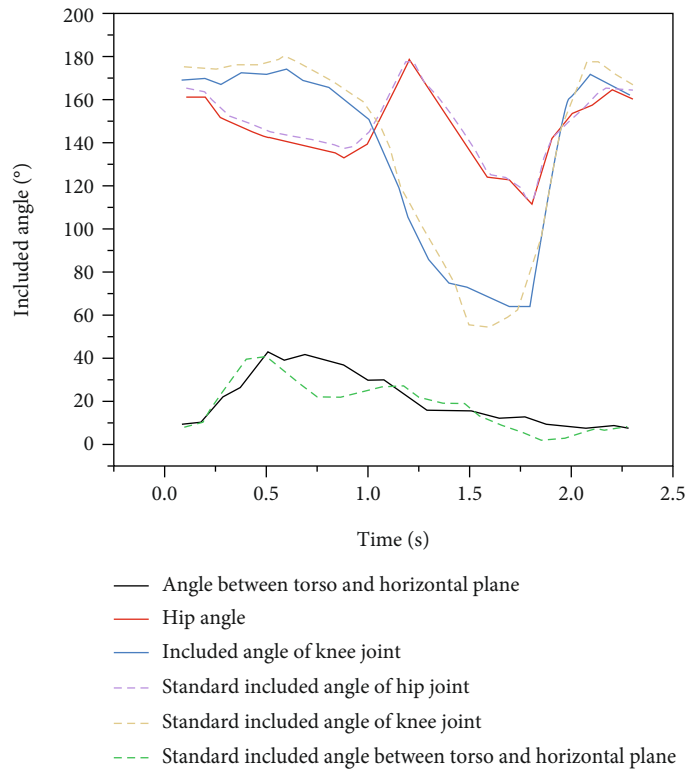

Figure 8: Comparison diagram of breaststroke action and standard action of an athlete.

5. Construction of Swimming Guidance System

The method of detecting breaststroke action in the previous chapter is extended to detecting breaststroke turning action. After detecting breaststroke turning action, the details of turning action are analyzed, standard action data are established, and comparison algorithm is designed [26]. A turning motion guidance system based on OpenCL technology is established to facilitate users to use the system and improve the real-time feedback ability of the system. OpenCL defines two different programming models: task parallelism and data parallelism. In the data parallel mode, computing data is divided and allocated to different computing units for simultaneous computing, which is suitable for computing tasks with independent data. Task parallelism refers to the fact that each step of the computing step has a front-to-back dependency, which makes it impossible for us to execute the computing tasks in parallel. Therefore, we can only parallelize the data of each step and then perform asynchronous/synchronous serial execution of the entire process. In order to coordinate the sequence of the entire process, OpenCL provides an event mechanism for process synchronization control.

5.1. Key Information Detection during Turning. The turning action in this chapter refers to the stage from the time when both hands touch the wall to the time when both feet leave the wall, such as Canny operator edge detection and Hoff line detection, to detect the breaststroke turning action of an athlete. Figure 9 is obtained. After the position of power, the goal of each stage, and the information of key nodes in the process of turning are clear, the evaluation algorithm of breaststroke turning can be designed.

5.2. Design and Application of Turning Motion Evaluation Algorithm. From the target and key node information pursued at each stage of the turning process, the breaststroke turning motion evaluation algorithm is similar to the breaststroke motion evaluation algorithm, but the difference lies in the data of the standard motion. Therefore, the comprehensive scoring link formula is consistent with the breaststroke action evaluation algorithm. In order to judge whether the athletes' turning movements are standard or not, it is necessary to clarify two points: first is the standard movement data; second is the algorithm of comparison with standard data. Select eight athletes and observe their action cycles to obtain the standard data curve as shown in Figure 10.

After analyzing the athletes' movements, the scores of the swimmers' strokes are evaluated, and the data of each link are substituted into the following formula:

$$\begin{aligned} CS = {} & p * 50\% + T_{ps} * 30\% \\ & + A_{ps} * 20\% CS = e^{-(30-28)^2/25} * 100 * 50\% \\ & + \left(1 - \frac{8}{30}\right) * 100 * 30\% + \left(1 - \frac{85.47 - 62.38}{62.38}\right) \\ & * 100 * 20\% CS = 43. \end{aligned} \tag{17}$$

The comprehensive scores are as follows: the swimmer's turning action score is low. In order not to strike the athletes'

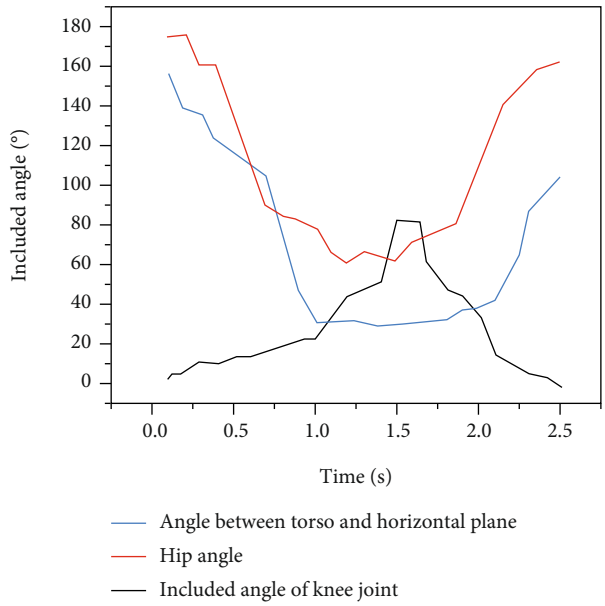

Figure 9: Key information of turning movement.

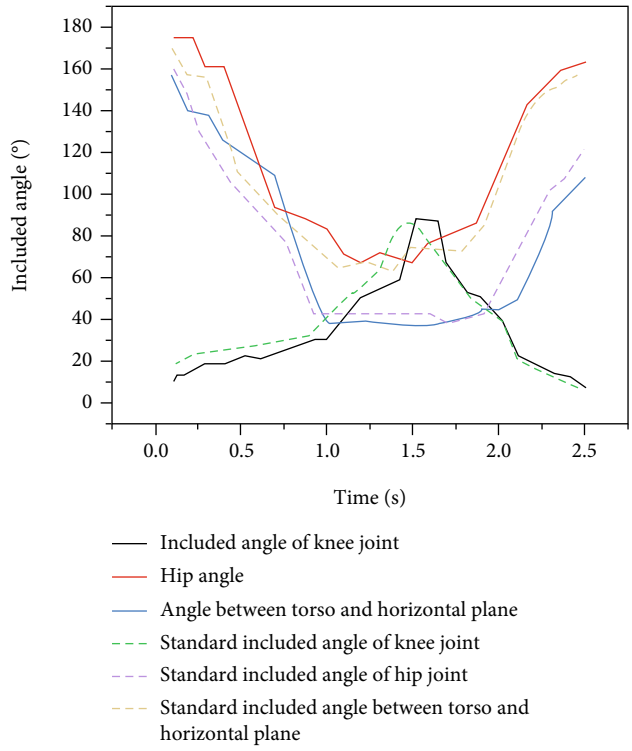

Figure 10: Comparison diagram of turning action and standard action.

psychology, the difficulty of the scoring system can be adjusted. By adjusting the variance of the Gaussian function and the definition of nonstandard actions, the range of standard actions can be expanded. For example, the difficulty can be reduced, and the score can be increased from 5% to 10%. In order to optimize swimmers' movements, it is necessary to establish a library of optimization suggestions, which can be set in advance according to different conditions of swimmers.

5.3. Construction of Turning Motion Guidance System Based on OpenCL Technology. OpenCL is an open computing language. It is mainly designed for parallel computing on heterogeneous computing platforms. Most heterogeneous computing platforms have at least two computing devices in the same operating system. The instruction set and hardware architecture of these devices are widely different. Heterogeneous computing platforms have a wide range of applications, among which the most famous combination is the combination of processor and graphics card, namely, CPU and GPU. The reason why CPUs and GPUs are so different is that they are designed for two different application scenarios. The CPU needs strong versatility to handle various data types and at the same time requires logical judgment, which will introduce a large number of branch jumps and interrupt processing. These all make the internal structure of the CPU extremely complex. GPUs, on the other hand, face large-scale data of highly uniform types, independent of each other, and a pure computing environment that does not need to be interrupted.

5.3.1. Hardware Level. In terms of hardware, it combines programmable logic embedded dual core cortex-a9 hard core processor, which is the latest processor in the field and can fully meet the flexibility of design. DE10-Nano is also equipped with high-speed DDR3 memory, digital simulation function, Ethernet, and other application functions.

5.3.2. Software Level

(1) Set up the working environment of OpenCL. Unzip the board level support package of DE10-Nano to the specified location. In order for the compiler to find the location of the DE10-Nano device, you need to create a new variable in the system environment variable. Then, in order for the windows system to find the relevant compilation commands of OpenCL, you need to conFigure the SDK with relevant environment variables. After configuring environment variables, it is necessary to verify the availability of heterogeneous systems to ensure the availability of heterogeneous platforms

(2) Write the source program. OpenCL programs are divided into host programs and kernel programs. The host program mainly provides the relevant environment and parameters to allow the kernel code to run in the device

(3) Download the Linux image of OpenCL BSP with DE10-Nano on the official website, burn it to the SD card, and then boot the development board through the SD card. After the development board is connected and powered on, ensure that the IP address of the development board is in the same network segment as the PC compiling the code and then copy the compiled code to the development board.

After entering the development board, initialize the runtime mechanism of OpenCL and finally run the host program. Hosts is a system file without an extension. Its basic function is to establish an associated "database" between some commonly used URL domain names and their corresponding IP addresses. When a user enters a URL that needs to log in in the browser, the system will automatically first find the corresponding IP address from the Hosts file. Once found, the system will open the corresponding web page immediately. If not found, the system will submit the URL to the DNS domain name resolution server for IP address resolution. If it is found to be a blocked IP or domain name, this page will be blocked from opening

This system is used to analyze the breaststroke turning movement of an athlete who has been trained for four years. After inputting the breaststroke turning movement video of the athlete, display the results on the screen connected to the development board. The results are more targeted to point out the problems of the athlete, and the suggestions given are also more targeted. Therefore, this system has a good effect in practical application.

6. Conclusion and Prospect

6.1. Conclusion. This system is put forward under the condition that the popularization rate of scientific training auxiliary equipment in the field of domestic swimming training is not high and the turning technology of domestic athletes is generally backward. It is intended to quantify the swimming movement, so that athletes can more conveniently optimize their technical movements, and then promote the country to a higher level in the competitive sports of swimming. Starting from the goal, because the turning movement has a great impact on the competition results, and breaststroke has a wide coverage of the crowd, this paper takes the breaststroke turning as the starting point of this system. In this paper, the appropriate image processing method is selected through the experimental method. After using the above methods to analyze the breaststroke and turning movements of the athlete, the data are collected into a chart, the change trend of each index and the logic driving its change are analyzed in detail, the standard action model is constructed, and the athlete's action is compared with the standard action. Then, the motion evaluation algorithm is designed. Through this algorithm, athletes can get targeted motion optimization suggestions and comprehensive evaluation scores. The purpose of using OpenCL technology on the FPGA system is to reduce the threshold for users to use the system by strengthening the portability of the system and helping the popularization of the system. First, the DE10-Nano development board is used to connect the system hardware. Then, at the software level, the OpenCL working environment is built to complete the preparation of host code and kernel code. After compilation, it is copied to the development board and run.

6.2. Prospect. The original intention of this system is to improve the standard of swimmers' movements scientifically and conveniently. Science means that the evaluation of swimmers' movements is accurate, and the suggestions given are highly targeted.

At the level of promoting scientificity

(1) The standard action data of the system still needs to be optimized. In the future, we can observe the movements of more professional athletes and then continuously optimize the standard data according to the algorithm

(2) Introduce more dimension data. Although these three angles can locate the important attitude information of the observer, they are still not comprehensive. In the future, more angles can be added or included angles that can show more information can be found to build more comprehensive and detailed posture information

(3) The algorithm for optimizing standard data needs to be further improved. The logic of the existing algorithm is to constantly average the posture data of high-level athletes with the standard action. In the future, we can consider adding weights of different athletes, that is, to enhance the impact of the posture data of top athletes on the standard action data

(4) The anti-interference ability of image processing still needs to be improved. Due to the complex underwater environment, the water quality may be turbid, the light may be weak, and the athletes' movement range may lead to more bubbles or even interference from other swimmers. At this time, the image processing algorithm needs to be further improved to obtain accurate data

At the convenience level

(1) Further optimize the degree of automation of the system. The existing system is unable to recognize the swimming pose for the time being. In the future, we will consider adding in-depth learning technology to allow the system to judge the user's swimming pose according to the user's actions and complete the selection and solution of key information

(2) As an app, it is carried into a waterproof smart phone. The popularity of existing smart phones is high. In the future, with the improvement of technology, the waterproof performance of mobile phones will also be improved. When waterproof smart phones are common, they can be considered to be carried into smart phones as apps

Data Availability

The datasets used and analyzed during the current study are available from the corresponding author on reasonable request.

Conflicts of Interest

The author declares no conflict of interest.

References

[1] C. Ma, J. Jia, Z. Liu, K. Zhang, J. Huang, and X. Wang, "Simulation of three-dimensional phase field model with LBM method using OpenCL," *The Journal of Supercomputing*, vol. 78, no. 8, pp. 11092–11110, 2022.

[2] A. M. Almomany, A. al-Omari, A. Jarrah, M. Tawalbeh, and A. Alqudah, "An OpenCL-based parallel acceleration of a Sobel edge detection algorithm using Intel FPGA technology," *South African Computer Journal*, vol. 32, no. 1, pp. 3–26, 2020.

[3] J. Ruokolainen, M. Hyttinen, J. Sorvari, and P. Pasanen, "Exposure of cleaning workers to chemical agents and physical conditions in swimming pools and spas," *Air Quality, Atmosphere and Health*, vol. 15, no. 3, pp. 521–540, 2022.

[4] Y. Li, N. Nord, G. Huang, and X. Li, "Swimming pool heating technology: a state-of-the-art review," *Building Simulation*, vol. 14, no. 3, pp. 421–440, 2021.

[5] E. Lang, S. Silva, and N. Persaud, "Are guidelines fueling inequity? A call to action for guideline developers and their panelists," *Chest*, vol. 159, no. 2, pp. 465-466, 2021.

[6] R. Yuan, Y. Han, and X. Lu, "Nonlinear random matrix-based intelligent management model for swimming place waters," *Mathematical Problems in Engineering*, vol. 2022, Article ID 7601021, 12 pages, 2022.

[7] S. Zhang, J. Dai, and Z. Nie, "Can swimming teaching prevent drowning? An experimental study of children in China," *Discrete Dynamics in Nature and Society*, vol. 2022, Article ID 6141342, 8 pages, 2022.

[8] S. Yanlin, Z. Chen, and W. Xie, "Swimming as treatment for osteoporosis: a systematic review and meta-analysis," *BioMed Research International*, vol. 2020, Article ID 6210201, 8 pages, 2020.

[9] R. Caas, J. Figueroa-Puig, R. Ramirez-Campillo, and M. Tuesta, "Plyometric training improves swimming performance in recreationally-trained swimmers," *Revista Brasileira de Medicina do Esporte*, vol. 26, no. 5, pp. 436–440, 2020.

[10] D. Selva, D. Pelusi, A. Rajendran, and A. Nair, "Intelligent network intrusion prevention feature collection and classification algorithms," *Algorithms*, vol. 14, no. 8, p. 224, 2021.

[11] N. Ishmukhametova, S. Ilin, and R. Garifullin, "Implementation of swimming classes in the physical education system of non-profiled universities and their impact on student bodies," *SCIENCE AND SPORT Current Trends*, vol. 8, no. 1, pp. 122–127, 2020.

[12] O. Ganchar, I. Ganchar, and I. Cherkun, "The methodical system aimed at forming swimming skills of the cadets majoring in marine profile in the process of training and improving," *Scientific bulletin of South Ukrainian National Pedagogical University named after K D Ushynsky*, vol. 3, no. 132, pp. 48–56, 2020.

[13] J. Yin, S. Huang, L. Lei, and J. Yao, "Intelligent monitoring method of short-distance swimming physical function fatigue limit mobile calculation," *Wireless Communications and Mobile Computing*, vol. 2021, Article ID 9919231, 6 pages, 2021.

[14] L. Zhang and W. Liu, "Swimming training evaluation method based on convolutional neural network," *Complexity*, vol. 2021, Article ID 4868399, 12 pages, 2021.

[15] X. Sun, F. Li, C. Wu, and F. Zhai, "Dynamic analysis of international swimming research using CITESPACE," *Mobile Information Systems*, vol. 2022, Article ID 1213708, 13 pages, 2022.

[16] A. Dorontsev and A. Svetlichkina, "Risk factors for the development of maladaptive reactions to different types of physical load in middle-aged men," *Human Sport Medicine*, vol. 20, no. 1, pp. 135–141, 2020.

[17] A. B. Gudkov, A. F. Shcherbina, O. N. Popova, and A. N. Nikanov, "Characteristics of indicators of central hemodynamics of cadets of marine university in the period of long swimming," *Marine Medicine*, vol. 7, no. 1, pp. 54–59, 2021.

[18] K. Y. Ozeker, M. Bilge, D. Selin, and Y. Kose, "The effect of dry-land training on functional strength and swimming performance of 10-12 years old swimmers," *Progress in Nutrition*, vol. 22, no. 2, pp. 1–10, 2020.

[19] M. Arandelovic, I. Stankovic, and M. Nikolic, "Swimming and persons with mild persistant asthma," *The Scientific World Journal*, vol. 7, Article ID 513291, 7 pages, 2007.

[20] M. O. Segizbaeva and N. P. Aleksandrova, "Adaptive changes of the ventilatory function in athletes with different training type," *Human Physiology*, vol. 47, no. 5, pp. 551–557, 2021.

[21] D. Kishore, S. Shubhajit, A. V. Chukwuka, and S. N. Chandra, "Behavioural toxicity and respiratory distress in early life and adult stage of walking catfish Clarias batrachus (Linnaeus) under acute fluoride exposures," *Toxicology and Environmental Health Sciences*, vol. 14, no. 1, pp. 33–46, 2022.

[22] M. R. F. Ramos, Y. A. C. S. Junior, and L. A. B. de Souza, "Swimming as treatment of scapular dyskinesis," *Case Reports in Orthopedics*, vol. 2019, Article ID 5607970, 3 pages, 2019.

[23] S. F. Masoomi, A. Haunholter, D. Merz, S. Gutschmidt, X. Q. Chen, and M. Sellier, "Design, fabrication, and swimming performance of a free-swimming tuna-mimetic robot," *Journal of Robotics*, vol. 2014, Article ID 687985, 7 pages, 2014.

[24] T. Zhang, R. Tian, C. Wang, and G. Xie, "Path-following control of fish-like robots: a deep reinforcement learning approach," *IFAC-PapersOnLine*, vol. 53, no. 2, pp. 8163–8168, 2020.

[25] K. Papadimitriou and S. Savvoulidis, "The effects of two different hiit resting protocols on children's swimming efficiency and performance," *Central European Journal of Sport Sciences and Medicine*, vol. 30, no. 2, pp. 15–24, 2020.

[26] C. Lequiniou, F. G. Schmitt, E. Calzavarini, S. Souissi, and Y. Huang, "Copepod swimming activity and turbulence intensity: study in the Agiturb turbulence generator system," *The European Physical Journal Plus*, vol. 137, no. 2, pp. 1–14, 2022.

Hindawi
Wireless Communications and Mobile Computing
Volume 2022, Article ID 7684586, 13 pages
https://doi.org/10.1155/2022/7684586

Research Article

An Analysis of Internet of Things Computer Network Security and Remote Control Technology

Hong Zhao and Lingxia Wang

Information Center, Lanzhou University of Arts and Science, Lanzhou 730000, China

Correspondence should be addressed to Hong Zhao; 1000190@luas.edu.cn

Received 29 May 2022; Revised 5 August 2022; Accepted 8 August 2022; Published 13 September 2022

Academic Editor: Jun Ye

In order to solve the problem of the specific application of Internet of Things computer network security monitoring technology in infrastructure construction, a method of remote network monitoring system design is proposed, taking tunnel security construction as an example. According to the characteristics of construction tunnel safety monitoring, this method provides theoretical guidance from several aspects, such as computer remote monitoring, data decision analysis, safety control, personnel positioning, and data management. Through experiments, it is found that in the safety detection experiment, when the data is extracted within 2 minutes for detection, the detection accuracy is higher than 80%, and if it is 4 minutes, the detection accuracy is higher than 90%; in the response time test, the local control response time is generally less than 1 s. In the remote control response time test, the response time can generally be within 3 s, and it may be greater than 5 s. The designed construction tunnel monitoring system transmits the collected data to the monitoring terminal remotely. Then, the sensor data is analyzed for timing decision-making. This method can effectively calculate the safety status of each monitoring unit of the current tunnel according to a certain algorithm and formulate corresponding emergency measures according to the safety status.

1. Introduction

With the rapid development of Internet of Things technology, its application scope is becoming wider and wider. At present, the Internet of Things has been widely used in intelligent building, smart city, smart transportation, smart home, logistics system, environmental detection, digital medical, energy conservation, fire protection, and other fields. With the continuous development of the transportation industry, more and more tunnels have been put into use. As the tunnel environment is bad and accidents are easy to happen, the safety of the tunnel has become a big problem of traffic safety. How to ensure the safe operation of the tunnel will have a very important significance. With the increase of China's investment in infrastructure construction, the safety of tunnel construction has been widely paid attention to. Common tunnel disasters include fire, excessive harmful gas, water inrush, and collapse. How to predict the disaster and control the safety after the disaster is a key point of tunnel construction monitoring. Construction of tunnel monitoring system is a huge system, involving multidisciplinary knowledge such as computers, communications, and software development. According to the characteristics of the construction of tunnel safety monitoring, exploratory research was carried on from the aspects of the data decision-making analysis, safety control, personnel positioning, data management, and so on. A construction tunnel safety monitoring solution based on Internet of Things was proposed in the paper. The environmental characteristics, safety protection requirements, and control requirements of the construction of tunnel were analyzed in detail. The disaster characteristics of the tunnel fire, harmful gas exceeding bid, water inrush, collapse, and main protection points were introduced in this paper. Combined with the actual situation of the tunnel construction, the method of combining the local control and remote control of tunnel safety control was put forward. When the level of tunnel disaster was low, the control command was sent through the monitoring

software to drive the control execution equipment in the tunnel field for control. When the level of tunnel disaster was high and the onsite danger was beyond local control, the monitoring software requested the remote assistance from the remote 3G terminal and reported the onsite situation. At the same time, in order to manage and monitor the construction personnel better, the construction tunnel monitoring system used ZigBee network to locate the construction personnel. The designed construction tunnel monitoring system conducted timing decision-making analysis of sensor data. The method could effectively calculate the current security status of each monitoring unit of the tunnel according to a certain algorithm and work out the corresponding emergency treatment measures according to the security status.

Taking the tunnel construction as an example in this paper, based on the Internet of Things computer network, timing decision-making analysis of construction tunnel monitoring system and sensor data were conducted. The current tunnel safety state of each control unit was calculated according to certain algorithm. According to the safety state, the corresponding emergency treatment measures were formulated, providing several sets of emergency response plan for the users to choose and implement.

The Internet of Things needs to ensure the security and confidentiality of computer network information transmission during the operation process and strengthen the management of network services. Illegal program codes in the Internet will destroy important data and control functions in the IoT system. Therefore, managers need to strengthen the management of illegal program codes and formulate effective control measures to ensure the security of the code running in the IoT system. IoT managers need to strengthen their awareness of network security prevention, formulate effective solutions for specific problems, and ensure the security of network communications. The application of remote control technology can meet the needs of remote data transmission and acquisition, and managers need to strengthen the management of network codes during the period. Prevent illegal code from damaging the IoT system and affect communication security.

2. Related Works

Shi and Zhou believed that it was of great significance to study remote tunnel monitoring system based on Internet of Things architecture. Ensuring the safe operation of tunnels was not only a management system issue but also required a reliable technical support [1]. Mansour et al. believed that doing a good job in the tunnel safety emergency command, it was necessary not only to establish a perfect safety management organization system but also to establish an efficient and intelligent information management system [2]. Chen et al. believed that the remote tunnel monitoring system could provide data support for management and decision-making for the management. The management could realize real-time monitoring and remote control of the tunnel conveniently, eliminate potential safety hazards in advance, and take emergency rescue measures in case of emergencies, reducing harm and loss and improving the intelligence of the system [3]. Tong and Sun believed that the development of Internet of Things technology in China was still in the initial stage. And various technologies and modes were not mature enough and the application scope was not very wide [4]. Wei et al. believe that the development of the Internet of Things focuses on the world, and China is no exception. The next major target of the information industry is the Internet of Things [5]. Honar Pajooh et al. believed that the application of IoT technology in tunnels not only improves the data level of tunnels but also promotes the development of the entire IoT industry [6]. Wei et al. believed that the safe operation of tunnels was an important part of the safety work of China's transportation construction industry [7]. The safety monitoring and emergency rescue work of tunnel operation can greatly improve the level of safety monitoring and emergency linkage in the whole traffic construction industry. Qiao believed that the research of the application of Internet of Things technology in tunnel remote monitoring system also had reference significance for the Internet of Things research on construction safety in transportation construction industry and the construction of unified safety monitoring and emergency command system [8]. The Internet of Things has grown rapidly since it was first proposed in 1995. Many universities in China have conducted in-depth researches on the automatic monitoring of the Internet of Things. Guo et al. believed that the Internet of Things was applied in various industries constantly and smart cities and smart transportation were advocated throughout the country [9]. At present, China's monitoring system based on the Internet of Things is also developing rapidly, but there are also some problems. Most of the monitoring systems are only simple technical improvements of the traditional monitoring systems, with lacking of the idea of thing-thing connecting. Zhang et al. believed that most monitoring systems only used a single sensor and a single communication mode and the integration degree was not high [10]. The whole process of monitoring system includes the data acquisition, communication, processing, evaluation, and visualization. Part of the link still does not involve the Internet of Things or the function is relatively weak. Most monitoring systems based on the Internet of Things are applied in logistics system, earthquake disaster, and other aspects, but there are few applications in engineering. Due to the limitation of precision, reliability, and durability of Chinese instruments, hardware from different countries and software from China are often adopted by large-scale monitoring systems based on the Internet of Things. And the system is not highly integrated. The traditional tunnel monitoring system in China mostly uses fieldbus technology to transmit the underlying data. There are some disadvantages in this way. The cost of wiring is a great overhead, and the complexity and difficulty of wiring and maintenance bring great trouble to the construction personnel. It cannot meet the requirement of dynamically adding monitoring points in the tunnel. If new monitoring points or monitoring quantity are needed, rewiring is required. The complexity and difficulty is imaginable. According to the characteristics of construction tunnel security monitoring, a construction tunnel security monitoring

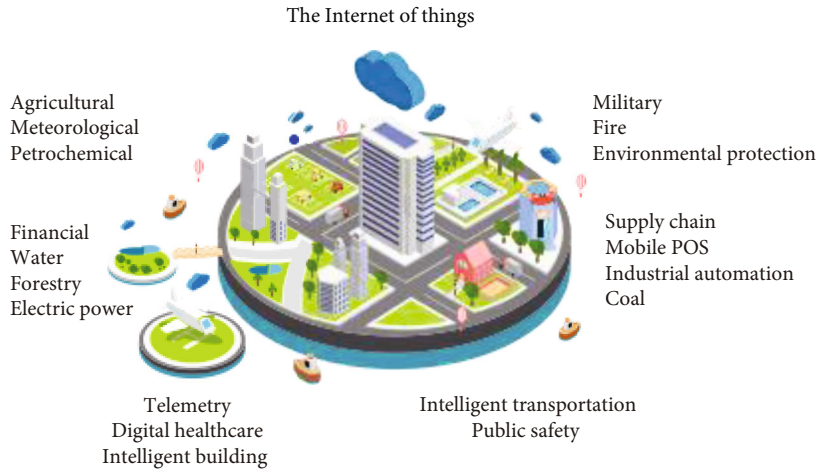

Figure 1: Analysis of Internet of Things computer network security and remote control technology.

solution based on wireless sensor network was proposed in the paper. The analysis of Internet of Things computer network security and remote control technology is shown in Figure 1.

3. Method

The monitoring system of construction tunnel is a concentration of sensor data collection, data analysis and processing, the disaster in situ processing equipment, the 3G remote linkage equipment, mobile positioning multifunction as one whole system, detecting all kinds of disasters in the tunnel real-timely, and reporting the data to the monitoring center. Monitoring software analyzes and processes the data. According to the level of risk, local tunnel processing equipment is called and 3G remote linkage mechanism was started, respectively, to ensure that losses caused by tunnel disasters are minimized. The hardware structure of tunnel monitoring system is composed of sensor network, 3G network, ZigBee network, and monitoring center [11]. Sensor network mainly accomplishes data acquisition. The data of acquisition include temperature, humidity, light, oxygen, carbon dioxide, carbon monoxide, smoke, nitric oxide, nitrogen dioxide, methane, dust, noise, wind speed, liquid level, stress, vibration, and displacement. Because wireless sensor nodes use batteries, the data acquisition is a way of a time interval for a period of time to collect data. Sensor nodes for each data set the alert value. Once the collected data exceeds the alert value, the node enters emergency pass-through mode. The node collects data uninterruptedly, so that policy-makers can timely grasp the change trend of the disaster. When the collected data falls below the safe value, the node exits the emergency pass-through mode. The collected data is sent to the wireless gateway through the WIAPA network and then sent by the gateway to the remote computer network monitoring center through the router [12, 13]. WIA network is an industrial wireless network in full compliance with the national standard for WIA-PA of process automation. A WIA network consists of at least one WIA gateway and one device and a WIA gateway can manage 100 devices at most. The application of WIA-PA technology will help to reduce the risks of the production and use of enterprise-related products, ensure industrial safety, and promote the realization of industrial energy conservation and emission reduction targets. Multiple WIA networks can form large-scale complex networks through Ethernet interconnection [14]. The 3G information is sent by the monitoring center to the 3G terminal equipment supplier through the Internet network, then to the 3G public network by the supplier's server, and finally to the 3G terminal equipment by the 3G public network [15]. ZigBee network consists of master node, mobile node, and anchor node. The host node acts as a network gateway and is responsible for collecting data from streamers and mobile phones. At the same time, the mobile phone counts the data location of the mobile phone together with the anchor point through the data extension. The positioning algorithm of ZigBee wireless positioning network adopts RF-TOF ranging positioning technology, and the position of construction personnel can be calculated by placing the sensor node on the helmet of construction personnel. In recent years, indoor positioning has gradually become a basic function in many terminal applications, including civil use, disaster protection, and peacekeeping missions. Indoor positioning technology has tended to mature. At present, it has been widely covered and applied to many scene management systems, providing cost-effective convenience for all-time managers and users. Compared with the satellite positioning which is only relied on outdoors, signal sources used for positioning are numerous in indoor scene. Due to different indoor location signal sources, a variety of indoor location algorithms are also produced. One of them is the location algorithm based on ranging, which depends on the hardware with direct ranging ability, namely, the location algorithm based on TOF.

The Internet of Things needs to analyze and process data information during the operation process, so as to ensure that the computer has enough space to store the data information. Once the data information in the Internet of Things is damaged, the damaged data can be automatically repaired with the support of the system, and the function of

automatic repair can be exerted. There are multiple technical control areas in IoT, and these technical control areas need to be isolated from each other. The effective isolation between technical control areas can avoid the damage to the network system by illegal intruders and ensure the security of the Internet of Things computer system as much as possible. In addition, in order to strengthen the management of Internet of Things computer network security, it is necessary to build corresponding operating norms, implement the responsibility system, and give operators certain operating rights.

In the research, the device provided these functions including signal sending and receiving, time stamp recording, and delay sending. When clocks were out of sync between hardware, single-sided two-way ranging (SS-TWR) could be adopted. The calculation formula of signal flight time was shown in

$$\mathrm{TOF} = \frac{1}{2} * ((T_3 - T_0) - (T_2 - T_1)). \tag{1}$$

This method was not commonly used, because there was a deviation between the clock of the base station and the tag and the standard clock, which was represented by the clock drift rate k ($k = 10\,\mathrm{ppm}$). Assuming that the tag delay time T_d was 3 ms and the signal flight time TOF was negligible compared with the delay time, the ranging error caused by the delay time T_d was shown in

$$|r| = \frac{1}{2} * |k_b - k_t| * T_d * c. \tag{2}$$

$|k_b - k_t| = 5\,\mathrm{ppm}$, and $|r| \approx 2.25\mathrm{m}$. $|k_b - k_t|$ was likely to be higher than 5 ppm in reality, which could bring a big ranging error. To reduce the effect of clock drift on ranging, a double-sided two-way ranging (DS-TWR) method was used. Based on SS-TWR, this method added another sending and receiving of delay and signal. The TOF calculation method of DS-TWR method was shown in

$$\begin{cases} T_{r1} = T_3 - T_0, T_{p1} = T_2 - T_1, \\ T_{r2} = T_5 - T_2, T_{p2} = T_4 - T_3, \\ \mathrm{TOF} = \dfrac{T_{r1} * T_{r2} - T_{p1} * T_{p1}}{T_{r1} + T_{r2} + T_{p1} + T_{p2}}. \end{cases} \tag{3}$$

The approximate calculation formula of ranging error caused by clock drift of the method was shown in

$$|r| \approx \mathrm{TOF} * \frac{1}{2} * |k_b + k_t| * c. \tag{4}$$

Both k_b and k_t were set as 20 ppm. If the distance between the base station and the tag was 200 m and TOF was about 666 ns, the ranging error was obtained, which was shown in

$$|r| = 666 * 10^{-9} * 20 * 10^{-6} * 3 * 10^8 \approx 0.004\mathrm{m}. \tag{5}$$

That is, the ranging error of DS-TWR method due to clock drift was mm level, so the DS-TWR method should be adopted in the actual TOF working mode. In the paper, ZigBee wireless communication technology was adopted to standardize PLC control system information communication. The filtering algorithm was adopted to filter the redundant noise of the data collected by the gateway. Considering that the state data of the system working environment was distributed discreetly, the system control variable was set to be numerically stable and the production equipment state data in the discrete time domain was represented by the Kalman filter. The expression was shown in

$$s(x) = \frac{As(x-1) + B + W(x)}{S(x) + V(x)}. \tag{6}$$

In the formula, $S(x)$ and $S(x-1)$ were the estimated value of production equipment state data at the moment of x and moment $x-1$, respectively. A and B were the defined parameters of the system. $W(x)$ and $V(x)$ were the noise of the system and the working environment, respectively.

Calculate the covariance $P(x/x-1)$ of the estimated value of state data at at the moment of x and $x-1$. The formula was shown in

$$P\left(\frac{x}{x-1}\right) = \frac{AH(x-1)H(x) + Q}{R}. \tag{7}$$

In the formula, $H(x-1)$ and $H(x)$ were the system observation matrices the moment of x and moment $x-1$, respectively. R was system covariance. Q was the gain coefficient.

$P(x/x-1)$ was further optimized to obtain the optimal estimation value $K(x)$ of the system time. The expression was shown in

$$K(x) = \frac{LK(x-1)}{P(x/(x-1)) + f}. \tag{8}$$

In the formula, $K(x-1)$ was the optimal estimation value of state data at $x-1$ moment. L was the covariance of $K(x-1)$ value. F was Gaussian white noise.

After the original data was filtered, PID controller optimization algorithm was adopted to make the production equipment state variables collected by the system closer to the real value of the environment. Each state data was abstracted as a particle, and the particle space position was determined according to the particle moving speed and inertia, so as to find the optimal path to reduce the system error. The PID controller weighting parameters E_1 and E_2 were defined. The expression was shown in

$$\begin{cases} E_1 = \dfrac{a1e1[I(x) - D(x) + a2e2[O(x) - D(x)]}{gv(x)}, \\ E2 = D(x) + v(x+1). \end{cases} \tag{9}$$

In the formula, a_1 and a_2 were particle accelerations. e_1 and e_2 were random parameters. (x) and $O(x)$ were the

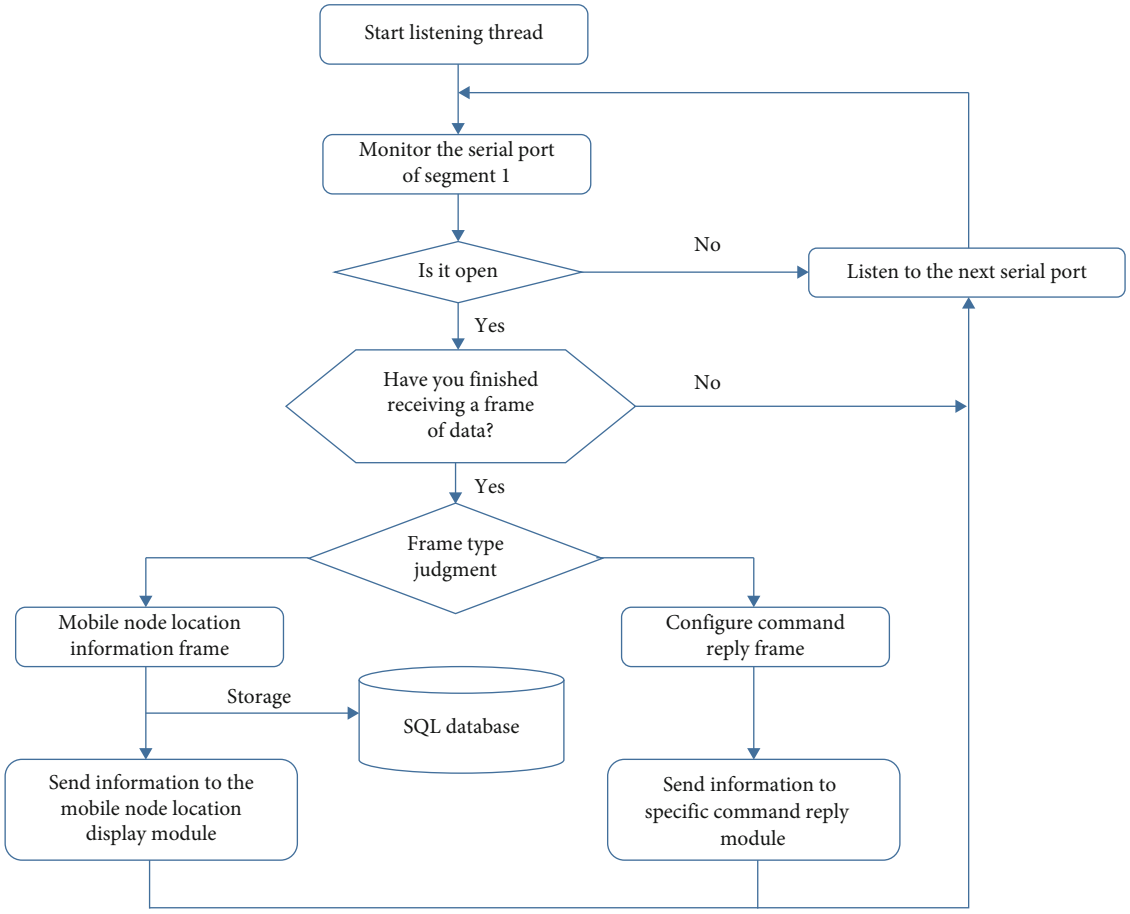

Figure 2: Multiserial port monitoring process.

positions of moment particle and particle swarm, respectively. $D(x)$ was the optimal position. g was inertial parameter. $v(x)$ and $v(x+1)$ were the velocity.

The system variance state equation was shown in

$$H(x) = E_1 \int_0^x P\left(\frac{x}{x-1}\right) dx + E_2 \frac{dp(x/(x-1))}{dx}. \quad (10)$$

In the formula, $P'(x/(x-1))$ was the optimized system variance.

The positioning system was completed by ZigBee network data collection management module. Due to the system to monitor three sections of the subway construction site at the same time, so the network also was composed of three subpositioning networks. Each network consisted of a master node, a reference node, and a mobile node. The master node was equal to the gateway to complete the work of the data receiving and sending of the reference node and mobile node. At the same time, the upward computer sent data through the serial port [16].

This system performs computer network remote monitoring for multiple construction threads at the same time. The subway construction site did not connect. Therefore, WIA network and ZigBee network were composed of three subnetworks, with collection and management of various blocks, respectively. They can resist various electromagnetic interferences used in industrial field, home automation control, and industrial telemetry remote control. And the data was sent to the PC at the same time. So the data collection and management module was composed of three different network management modules. The structure of data acquisition and management module is shown in Figure 2.

After the monitoring system collects the data, it stores the sensor data in the database of the remote computer. In order to get what the current state of the tunnel was, data fusion and the analysis of the state of the tunnel were necessary. The tunnel construction monitoring system is designed to show the real-time and automatic statistics of the construction site conditions and personnel activities to the management personnel. As an auxiliary means of construction safety management, it adds more guarantee for the safety of the tunnel construction. A block of the tunnel was long. Even if the sensor data of the tunnel was analyzed, which position was in danger could not be known according to the results [17].

The computer network remote control system can meet people's various needs and has been widely used in various fields, such as network monitoring, network automation management, and computer-aided teaching. The remote control system consists of different parts, such as server terminal, communication network, user terminal, and controlled

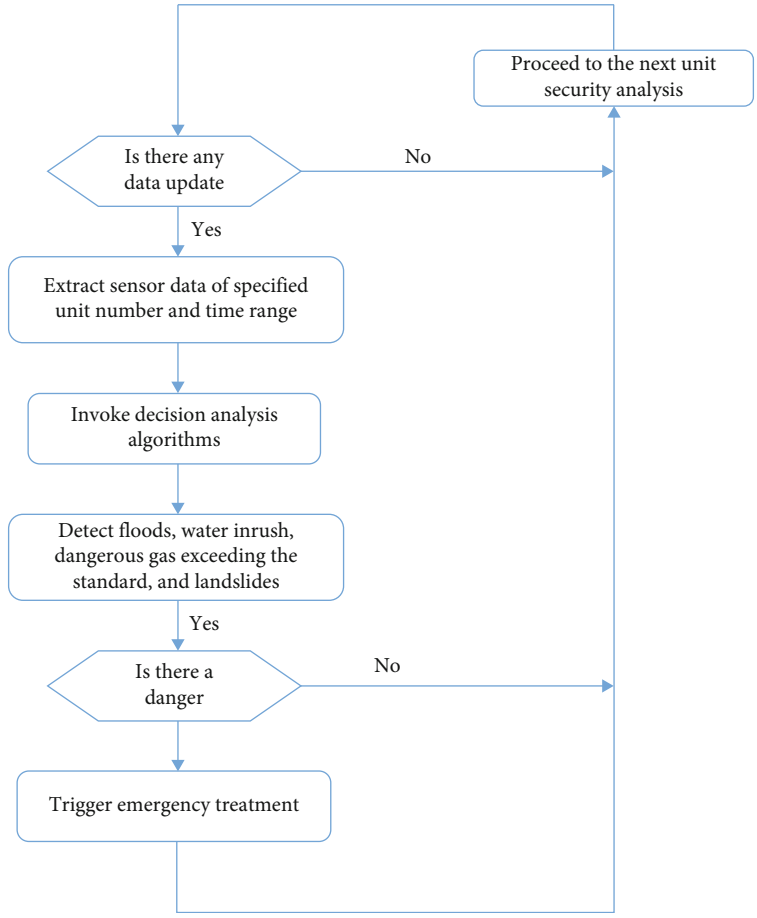

Figure 3: Flow chart of decision-making analysis and processing.

network. The main function of the controlled network is to receive commands issued by the master network and distribute them to each device. The operating systems of the master network and the controlled network can be Windows 7, Windows 8 or Windows XP.

Therefore, the system adopts the decision analysis method based on the computer network remote monitoring unit. A block of the tunnel is divided into a number of monitor units. Each unit could collect all kinds of sensor data and store the data in the database. Decision-making analysis was the analysis of a single state of monitoring unit. Decision analysis system is generally composed of interactive language system, problem system, database, model library, universal library, and knowledge base management system. This system detected four kinds of dangerous situations in the tunnel, including fire, dangerous gas exceeding bid, water inrush, and collapse and outputs the grade of the four kinds of danger of the unit. When the danger level exceeds the normal level, the computer will trigger corresponding emergency measures by itself, so as to respond to the dangerous situation as soon as possible. The flow chart of decision-making analysis is shown in Figure 3.

Monitoring software regularly carried out safety detection on the tunnel under construction, which mainly detected fire, harmful gases, water inrush, and collapse disaster. According to the data of different sensors, the tunnel disaster was divided into different levels, which were divided into five grades including normal, existence of hidden danger, danger treatment, emergency avoidance, and disaster relief. Correct and reasonable prevention and control measures will play a role in inhibiting or reducing the degree of disaster harm. On the contrary, if no attention or take wrong countermeasures, this will aggravate the degree of disaster and even play a role in inducing disaster. According to different levels of disasters, different measures were taken. Tunnel emergency treatment was to take different countermeasures for different categories and levels of disasters [18].

The emergency response measures were divided into the following kinds: rewrite the monitor view area color, send local control command, and start the remote linkage. The latter two needed to send control commands to the field and remote, with a relatively complex processing logic. In local control, monitoring center sent control commands to execution nodes by WIA gateway. After the transmission was completed, it was necessary to wait for the execution result of the terminal device. And then, the next control action was taken according to the execution result. The flow chart of local control and remote linkage control in tunnel emergency treatment is shown in Figure 4.

WIA Ethernet interface commands provided a software interface for managing and configuring the WIA network and sending and receiving data information of terminals

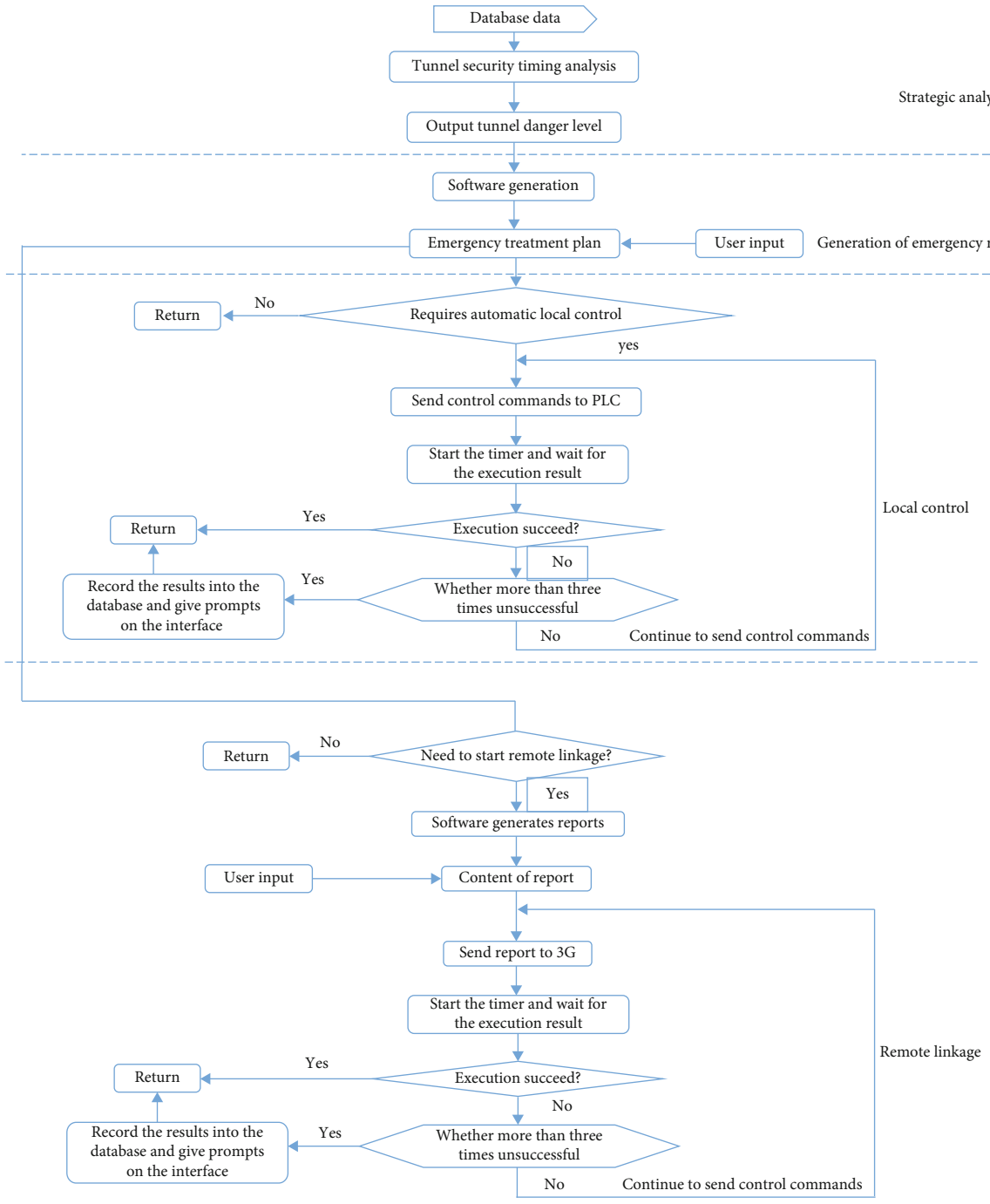

Figure 4: Flow chart of emergency processing.

over the Ethernet. WIA network information could be obtained by using Ethernet interface commands. The process of the specific processing is shown in Figure 5.

Construction tunnel safety inspection was based on a single unit for the unit. By analyzing all the extracted data uploaded by the unit node for a period of time in the database, the security level of the unit was concluded, in order to ensure the rapidity and accuracy of the data analysis. Choose to extract the data uploaded by the sensor nodes within 2-10 minutes from the field information collected through the monitoring network. If the time span is too long, it will take too long, and if the time span is too short, the results will be inaccurate and errors will occur. In terms of the weight of data, the closer the data was uploaded, the greater the weight should be [19, 20]. At the same time, in the analysis of tunnel danger, it should be analyzed according to the analysis of multiple sensor data. Each sensor data could represent the different importance. In fire detection, for example, temperature, humidity, oxygen, carbon monoxide, carbon dioxide, and smoke should be tested at the same

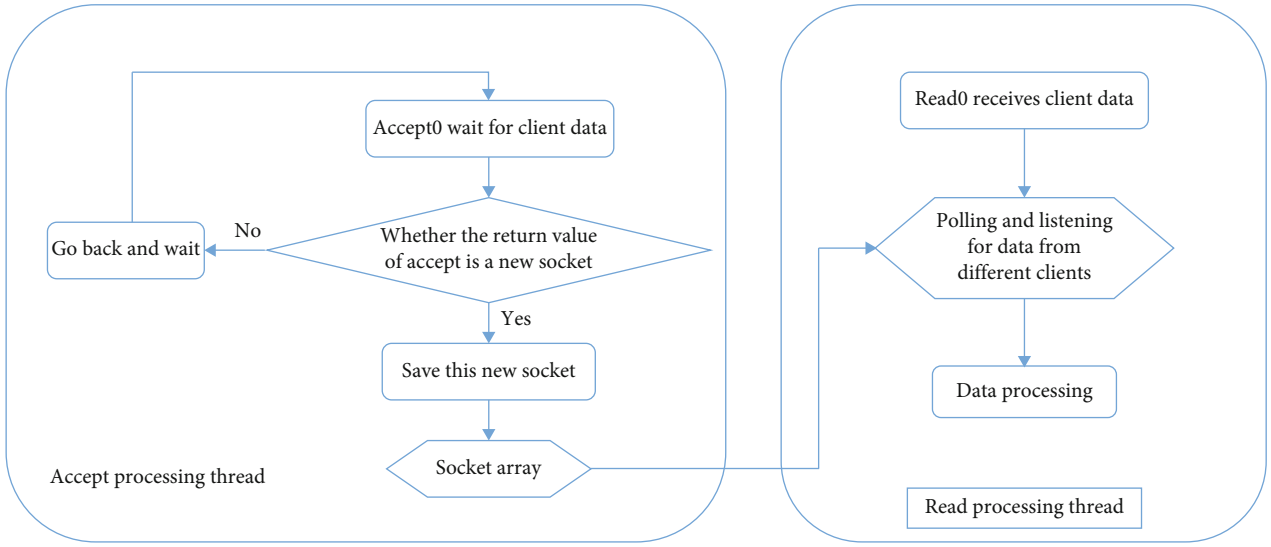

Figure 5: The flow chart of multiterminal network data processing.

time. Among them, temperature, carbon monoxide, carbon dioxide, and smoke for the effectiveness of temperature test were larger. Therefore, different types of sensors accounted for different weights. The decision-making algorithm of construction tunnel safety analysis is shown in Figure 6.

The calculation formula of tunnel danger level K was shown in

$$K = 0.2 * \frac{1}{n1} \sum_{t>0}^{t<80\%T} M_i\alpha + 0.8 * \frac{1}{n2} \sum_{t>80\%T}^{t<100\%T}. \quad (11)$$

n_1 was the number of sensors in the first 80%. n_2 was the number of sensors in the latter 20%. α was the weight value of sensors. And M_i was the warning level corresponding to the sensor value. The tunnel monitoring system adopted SQL Server 2005 for data management, which mainly completed system parameter saving, external data record storage, database data transfer function, data printing, and print preview function [21, 22]. The database management module managed the system data and stored the sensor network data, the location information of mobile nodes, and the system parameters in real time. At the same time, the data management module also provided data query interface. The users can query most of the data stored in the database, using reports or charts to describe the data.

There are two common communication protocols, namely, IP protocol and TCP protocol. Among them, the safety factor of the TCP protocol is relatively high, which can ensure the stability of the system operation. However, the protocol needs to occupy a lot of resources, and long-term operation will affect the system processing rate. When the TCP protocol runs, it needs two computers to transmit the data to be transmitted in the form of packets. If there are multiple network terminals, the IP protocol can be used at this time. The combination of the two protocols is a collection of network protocols.

4. Results Analysis

The main components of a controlled network are hardware and software, which work together to provide control services. The core of the controlled system is the control of the data collection, and the control system is centered on the computer. When designing a controlled system, it is necessary to adhere to the principle of security, pay attention to strengthening the protection of user information, and repair it immediately once a problem occurs. In order for the controlled network to function, it is necessary to strictly follow the prescribed operation steps and send the content of the remote transmission to the main control terminal. Remote control technology can realize the control of computer hardware equipment and software equipment and complete file transmission and management tasks.

Because fires and landslides were difficult to simulate, the method of field burning paper was used in the process of the tunnel danger simulation. Sensors were placed around the combustion for detection. Landslides could not be simulated in the laboratory environment. Therefore, the test method adopted was to simulate the change characteristics of support subplane during collapse by pressurizing the pressure sensor and changing the displacement value of the sensor. When testing whether harmful gases exceeded the standard or not, the analysis method of each gas exceeding the standard was similar. So the detection of harmful gases exceeding the standard was carried out according to the concentration of carbon dioxide [23]. Computer remote network monitoring security analysis test extracts data within 2 minutes and 4 minutes for decision analysis. In the decision-making analysis algorithm, it was concluded that the weight of the historical data and the data within 80% of the current time accounted for 80%. Therefore, when data of within 2 minutes was taken for testing, the detected disaster time was 24~30 s in theory. The detection accuracy was higher than 80%. The test results are shown in Table 1.

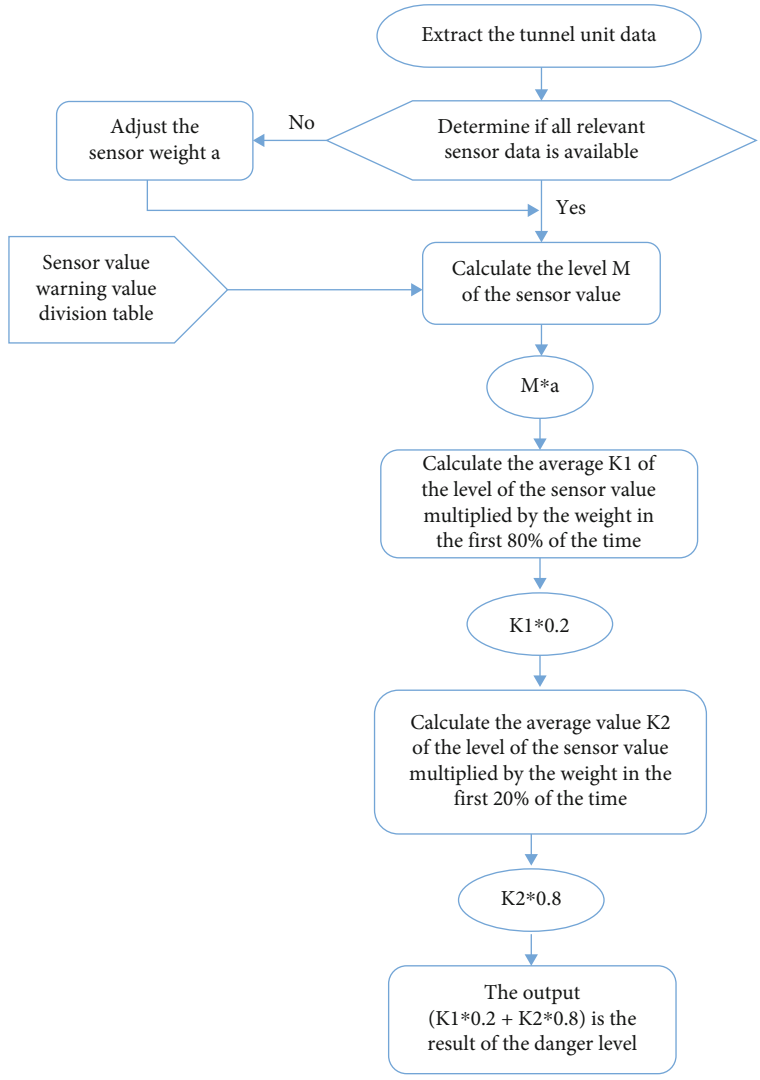

Figure 6: Decision-making algorithm for analysis of construction tunnel safety.

Table 1: Extracting historical data within 2 minutes for decision-making analysis.

Test items	Number of tests	Analysis time less than 30 s	Analysis time more than 30 s	Not to be detected	Detection accuracy
Fire (simulation)	25	13	8	4	84.00%
Water inrush	32	28	4	0	100%
Excess of harmful gas	42	34	6	2	95.23%
Landslide (simulation)	19	11	7	1	94.74%

However, if it was within 4 minutes, the results of the detection were obtained from 48 to 60 s normally. The detection accuracy was higher than 90%. The test results are shown in Table 2.

The local control command was executed by the controller PLC at the construction site. The monitoring software sent the control command to the WIA gateway through Ethernet and the WIA gateway sent the message to the underlying executing node according to the format of writing command. After receiving the data, the executing node sent the data to the serial port of RS232 to 485. Finally, data would be sent to the 485 interface of controller PLC to reach the end of each control device [24].

When the number of network nodes was 10, 20, and 40, the statistical results of the test were divided into four situations: response time less than 1 s, response time more than 1 s, response time less than 3 s, and no execution. The test results are shown in Table 3 and Figure 7.

Seen from the above results, the local control of the response time was generally less than 1 s. With the increase of network size, there would be a control command delay phenomenon of execution. And the larger the network size

Table 2: Extracting historical data within 4 minutes for decision-making analysis.

Test items	Number of tests	Analysis time less than 60 s	Analysis time more than 60 s	Not to be detected	Detection accuracy
Fire (simulation)	25	14	9	2	92.00%
Water inrush	32	26	6	0	100%
Excess of harmful gas	42	25	16	1	97.62%
Landslide (simulation)	19	11	8	0	100%

Table 3: The test results of local control response time.

Network scale (number of network nodes)	Number of tests	Response time less than 1 s	Response time more than 1 s less than 3 s	No execution
10	35	35	0	0
20	36	34	2	0
40	35	30	4	1

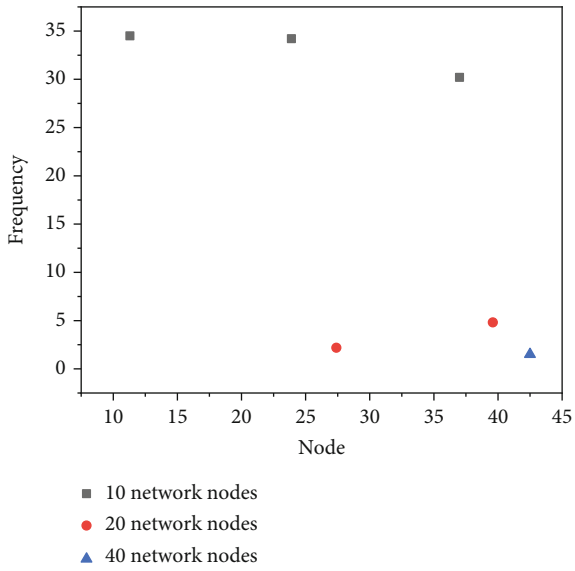

Figure 7: The test results of local control response time.

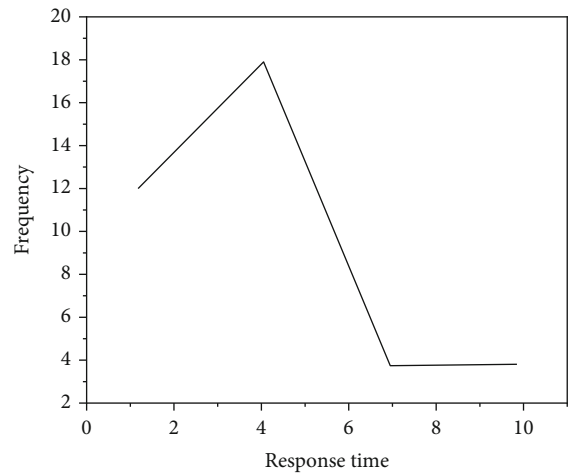

Figure 8: The test results of remote linkage network response time.

was, the delay phenomenon is more serious. The main cause was with the increase of network nodes, node processing capacity is limited: it includes node computing power configuration, backplane bandwidth, and forwarding buffer. The slice of time obtained by each node was smaller. When the network size reached 40 nodes, the control command would be executed (it was not executed within 30 s). Complex network is a special network structure, which is a network structure model that abstracts the elements in a complex system into nodes and the relations between the elements into edges. Therefore, the scale of the network should be reasonably considered when the network was laid out. And the sensor nodes in each bidding section should not be too many when the tunnel was managed and constructed by bidding section [25]. Remote linkage was that the scene situation was reported to the remote 3G terminal equipment. The communication process was that the information to be sent was packed by the monitoring software and was sent to the 3G terminal server through the Ethernet interface. Then, the message was sent to the terminal device by the server through 3G network. Therefore, in the process of testing remote linkage response, the time when the terminal receives the packet was recorded through sending a command to the terminal several times [26]. In the process of testing the response speed of 3G network, the data was sent to the 3G terminal device by hand and the response time from sending data to 3G terminal was calculated. The characteristics of response time and the distribution of response time are shown in Figure 8.

The test results showed that the response time of the 3G network distribution was relatively dispersed. Generally, the situation of within 3 s could appear. The cause was the external network information received by 3G terminal. Since the median value can only reflect problems with the median value, there is no more feedback, for example, I want to know within how many ms of 80% of the service's requests take, which require additional data metrics. The situation of more than 5 s could also appear. At the same time, the phenomenon of no response also could appear. The stability of the external network demand was high. So the phenomenon of receiving nothing could appear. Therefore, in the

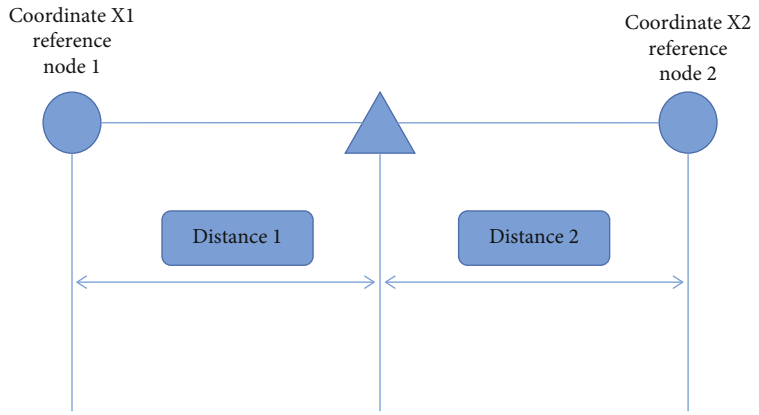

Figure 9: Schematic diagram of localization algorithm.

Table 4: The test results of positioning.

The test conditions		Valid data (within 3 m range)	Deviation from normal value (3 m)	Total test data	Minimum error (cm)	Maximum error (cm)	Valid data percentage
The square measure	Two reference nodes	31	6	37	4	293	83.78%
	Three reference nodes	24	4	28	12	225	85.71%
Corridor measuring	Two reference nodes	38	2	40	27	275	95.00%
	Three reference nodes	26	7	33	9	295	78.79%

design of the software, it was necessary to add a resending mechanism. When the information of the 3G terminal devices was not received within a certain period of time, the control command needed to be resent. In the construction tunnel, the tunnel was usually linear structure and the localization algorithm was relatively complex to implement, especially the two-dimensional localization system, which had a long algorithm development cycle. Therefore, the system currently adopted the one-dimensional localization system, which outputs the segment number of the moving node and the corresponding one-dimensional coordinate value [27, 28].

There are many researches on sensor network localization technology. And the basic localization algorithm is to locate the unknown location node through the known location node. ZigBee communication protocols were used in positioning network. Ranging algorithm used the time pulse to measure the distance (TOF). Mobile node sent waves to the reference node. Calculate the time to recover from the wave. Since the transmission time is proportional to the distance, the distance between the reference node and the mobile node can be calculated through the time difference, and finally, the location information of the mobile node can be obtained. For the location of the phone, determine the exact location of the data. The positioning diagram is shown in Figure 9.

The test was divided into corridor test in the experimental building and outdoor square environment test to test the positioning effect in different environments. The distance between the two reference nodes was 30 m. Due to the current conditions, the positioning effect was only tested in the case of 2 and 3 reference nodes. If the test result deviated too much from the true value (the error was more than 3 m), it was considered invalid. During the test, the deviation error value and the percentage of valid data were recorded. The test results of positioning are shown in Table 4.

In the test results, due to hardware instability and other factors, the measured results could appear the phenomenon of error more than 3 m. Seen from the test results of positioning, the test accuracy and test environment and the number of reference nodes had no connection. The environmental impact on positioning system was relatively small. But if the precision of positioning system was only about 80%, the precision was also needed to further improve.

5. Conclusion

The Internet of Things technology is the development trend of China's future society. The effective use of the Internet of Things in enterprises can improve the efficiency of resource sharing. During this period, technicians need to strengthen the management of the operating environment of the Internet of Things and further improve the functions of the remote control system to ensure its operational safety, and stability will better promote the long-term development of China's Internet of Things technology.

With the intensification of road traffic construction in China, more and more attention has been paid to the monitoring of construction tunnels. Common construction tunnel disasters include fire, harmful gas exceeding the standard, water inrush, and landslides. Computer remote construction tunnel monitoring system based on wireless sensor network collects 17 kinds of sensor values through the wireless sensor network to monitor the running state of the construction tunnel in real time. By analyzing the sensor data, the safety state of the tunnel is obtained. When the

tunnel is in different levels of danger, the monitoring software will take different measures. For emergency treatment plan, carry out local control and remote linkage control of construction tunnels and eliminate or reduce tunnel disasters. This paper mainly studies the following aspects:

(1) The analysis of tunnel safety: the safety analysis of each unit of the construction tunnel was carried out regularly. By extracting the recent historical data from the database, different weight values were allocated to the data of different time and data of different sensor types. And the status of each monitoring unit was calculated by decision-making analysis algorithm

(2) Network communication management based on multiterminal: construction tunnel monitoring system was composed of multiple network, including WIA sensor network, ZigBee positioning network, and 3G remote linkage. Monitoring system was based on multiple bid monitoring, with each bid being a subnetwork, so the multiple network management was one of the focuses of this system. The communication system with network multiple terminal system was studied. Finally, the multiterminal multinetwork management was realized

(3) Tunnel emergency treatment: in the construction tunnel monitoring, different emergency treatment measures need to be taken when the detection tunnel is in different danger levels. In this paper, according to the actual situation of the tunnel, a reasonable tunnel emergency treatment scheme was developed and the software emergency treatment process was designed and realized

(4) Remote linkage control: when the risk of construction tunnel is at high level, relying on control equipment of the field cannot control the situation effectively, with the need to send the remote linkage request. The integrated remote control scheme based on 3G communication was adopted in this system. Through the Ethernet interface, the report was sent to the equipment placed in fire department, emergency department, government department, etc.

(5) System monitoring view management: as the construction tunnel monitoring software, it is necessary to monitor the tunnel running condition in real time to understand the running state of each section of the construction tunnel as well as the running state of the fan and water pump and other execution equipment, realizing the graphical monitoring

(6) Database management: in the computer network remote monitoring system based on wireless sensor network, sensors continuously collect various sensor data, which is the basis for tunnel safety analysis on the one hand and the basis for postevent accident analysis on the other hand. Provide data dump, data query function, and data printing function

Data Availability

The datasets used during the current study are available from the corresponding author upon reasonable request.

Conflicts of Interest

The authors declare that they have no conflicts of interest regarding the publication of this paper.

References

[1] Y. Shi and Y. Zhou, "Gene extraction of Leizhou kiln porcelain patterns based on safety Internet of Things and its application in modern design," *IETE Journal of Research*, vol. 3, pp. 1–8, 2021.

[2] R. F. Mansour, M. M. Althobaiti, and A. A. Ashour, "Internet of Things and synergic deep learning based biomedical tongue color image analysis for disease diagnosis and classification," *IEEE Access*, vol. 9, pp. 94769–94779, 2021.

[3] G. Chen, F. Zeng, J. Zhang, T. Lu, and W. Shu, "An adaptive trust model based on recommendation filtering algorithm for the Internet of Things systems," *Computer Networks*, vol. 190, no. 15, article 107952, 2021.

[4] Y. Tong and W. Sun, "The role of film and television big data in real-time image detection and processing in the Internet of Things era," *Journal of Real-Time Image Processing*, vol. 18, no. 4, pp. 1115–1127, 2021.

[5] T. Wei, W. Feng, Y. Chen, C. X. Wang, N. Ge, and J. Lu, "Hybrid satellite-terrestrial communication networks for the maritime Internet of Things: key technologies, opportunities, and challenges," *IEEE Internet of Things Journal*, vol. 8, pp. 8910–8934, 2021.

[6] H. Honar Pajooh, M. Rashid, F. Alam, and S. Demidenko, "Multi-layer blockchain-based security architecture for Internet of Things," *Sensors*, vol. 21, no. 3, p. 772, 2021.

[7] D. Wei, H. Ning, F. Shi et al., "Dataflow management in the Internet of Things: sensing, control, and security," *Tsinghua Science and Technology*, vol. 26, no. 6, pp. 918–930, 2021.

[8] X. Qiao, "Integration model for multimedia education resource based on Internet of Things," *International Journal of Continuing Engineering Education and Life-Long Learning*, vol. 31, no. 1, p. 17, 2021.

[9] C. Guo, S. Su, K. Choo, P. Tian, and X. Tang, "A provably secure and efficient range query scheme for outsourced encrypted uncertain data from cloud-based Internet of Things systems," *IEEE Internet of Things Journal*, vol. 9, no. 3, pp. 1848–1860, 2021.

[10] W. Zhang, X. Wang, G. Han, Y. Peng, and M. Guizani, "SFPAG-R: a reliable routing algorithm based on sealed first-price auction games for industrial Internet of Things networks," *IEEE Transactions on Vehicular Technology*, vol. 70, pp. 5016–5027, 2021.

[11] S. Qu, Z. Wang, Z. Qin, Y. Xu, and Z. Liu, "Internet of Things infrastructure based on fast, high spatial resolution and wide measurement range distributed optic-fiber sensors," *IEEE Internet of Things Journal*, vol. 9, no. 4, pp. 2882–2889, 2021.

[12] L. Nie, Y. Wu, X. Wang, L. Guo, and S. Li, "Intrusion detection for secure social Internet of Things based on collaborative edge computing: a generative adversarial network-based approach," *IEEE Transactions on Computational Social Systems*, vol. 9, no. 1, pp. 134–145, 2021.

[13] P. Wei and F. He, "The compressed sensing of wireless sensor networks based on Internet of Things," *IEEE Sensors Journal*, vol. 21, pp. 25267–25273, 2021.

[14] Z. Yue, H. Sun, R. Zhong, and L. Du, "Method for tunnel displacements calculation based on mobile tunnel monitoring system," *Sensors*, vol. 21, no. 13, p. 4407, 2021.

[15] I. H. Chen, Y. S. Lin, and M. B. Su, "Computer vision–based sensors for the tilt monitoring of an underground structure in a landslide area," *Landslides*, vol. 17, no. 4, pp. 1009–1017, 2020.

[16] Y. Cao, X. Zhou, and K. Yan, "Deep learning neural network model for tunnel ground surface settlement prediction based on sensor data," *Mathematical Problems in Engineering*, vol. 2021, Article ID 9488892, 14 pages, 2021.

[17] P. Peng, Y. Jiang, L. Wang, and Z. He, "Microseismic event location by considering the influence of the empty area in an excavated tunnel," *Sensors*, vol. 20, no. 2, p. 574, 2020.

[18] D. Jia, W. Zhang, and Y. Liu, "Systematic approach for tunnel deformation monitoring with terrestrial laser scanning," *Remote Sensing*, vol. 13, no. 17, p. 3519, 2021.

[19] M. Barrow, F. Restuccia, M. Gobulukoglu, E. Rossi, and R. Kastner, "A remote control system for emergency ventilators during sars-cov-2," *IEEE embedded systems letters*, vol. 14, pp. 43–46, 2021.

[20] K. Jerwood, P. Lowy, L. Deeming, B. M. Kariuki, and P. D. Newman, "Remote control: stereoselective coordination of electron-deficient 2, 2'-bipyridine ligands to re (i) and ir (iii) cores," *Dalton Transactions*, vol. 50, no. 45, pp. 16459–16463, 2021.

[21] Z. Zhou, D. Liu, H. Sun, W. Xu, and Z. Wang, "Pigeon robot for navigation guided by remote control: system construction and functional verification," *Journal of Bionic Engineering*, vol. 18, no. 1, pp. 184–196, 2021.

[22] C. Chen, L. Ling, S. Zhu, and X. Guan, "On-demand transmission for edge-assisted remote control in industrial network systems," *IEEE Transactions on Industrial Informatics*, vol. 16, no. 7, pp. 4842–4854, 2020.

[23] C. Losada-Gutierrez, F. Espinosa, C. Santos-Perez, M. Marron-Romera, and J. M. Rodriguez-Ascariz, "Remote control of a robotic unit: a case study for control engineering formation," *IEEE Transactions on Education*, vol. 63, no. 4, pp. 246–254, 2020.

[24] E. Asadi, A. M. Salman, Y. Li, and X. Yu, "Localized health monitoring for seismic resilience quantification and safety evaluation of smart structures," *Structural Safety*, vol. 93, no. 1, p. 102127, 2021.

[25] U. Ramanathan, N. L. Williams, M. Zhang, P. Sa-nguanjin, J. A. Garza-Reyes, and L. A. Borges, "A new perspective of e-trust in the era of social media: insights from customer satisfaction data," *IEEE Transactions on Engineering Management*, vol. 69, 2020.

[26] W. Yan, L. Qiao, S. Krishnapriya, and R. Neware, "Research on prediction of school computer network security situation based on IoT," *International Journal of System Assurance Engineering and Management*, vol. 13, Suppl 1, pp. 488–495, 2021.

[27] M. M. Samy, W. R. Anis, A. A. Abdel-Hafez, and H. D. Eldemerdash, "An optimized protocol of m2m authentication for Internet of Things (IoT)," *International Journal of Computer Network and Information Security*, vol. 13, no. 2, pp. 29–38, 2021.

[28] S. S. Kumar and M. S. Koti, "An hybrid security framework using Internet of Things for healthcare system," *Network Modeling Analysis in Health Informatics and Bioinformatics*, vol. 10, no. 1, pp. 1–10, 2021.

Hindawi
Wireless Communications and Mobile Computing
Volume 2022, Article ID 2172580, 10 pages
https://doi.org/10.1155/2022/2172580

Research Article

Numerical Analysis and Optimization of English Reading Corpus for Feature Extraction

Wu Juan, Xiong Wei, and Liao Hongyi

Jiangxi University of Engineering, Xinyu 338029, China

Correspondence should be addressed to Liao Hongyi; b20160904213@stu.ccsu.edu.cn

Received 7 June 2022; Revised 10 August 2022; Accepted 18 August 2022; Published 6 September 2022

Academic Editor: Jun Ye

In order to solve the problem of comparative analysis ability of English reading corpus, meet the needs of the construction of language feature analysis system of English reading corpus, make up for the shortcomings of English reading corpus, and improve the wide application of English, the construction method of English reading corpus is proposed. For a long time, English has been an important communication tool in terms of national politics and final economic communication. Especially with the in-depth development of economic globalization, English plays a vital role in international communication. Therefore, the study of the semantics and features of English texts can provide important information materials for English learning and communication in nonnative English speaking countries. Taking this as the starting point, this paper focuses on the numerical analysis and optimization of English reading corpus based on feature extraction and puts forward a language feature analysis system of English reading corpus. At the same time, feature extraction and text classification are used to improve the comparative analysis ability of English reading corpus. The research shows that the feature extraction oriented English reading corpus can solve the problem of English reading learning and improve the ability of reading and analyzing English articles.

1. Introduction

Language itself is an important tool to assist life, and corpus is a special language material and language material based on language. Corpus is extracted from things actually applied in real life. The extraction of the text content is mainly used to specify the regular rules according to the text content, match, search, and extract the target content, and export it to a new file. Its content is generally composed of written and oral language, while corpus is an important method of modern linguistic research formed on the basis of language and corpus and after a large number of collection, sorting and processing of corpus according to special rules. With the support of corpus, people can obtain language application rules or grammatical phenomena more regularly and conveniently. English corpus is a more widely used corpus, which plays a vital role in linguistic research and English Curriculum Teaching [1]. Especially with the development of English popularization, the existence of English corpus provides strong convenience for people to analyze and learn English. In order to ensure that the search of English corpus is more convenient and accurate, we must deeply analyze and process the relevant corpus by word segmentation, sentence segmentation, and classification. Put the corpus in one database to meet all requirements. Therefore, this paper proposes a language feature analysis system of English reading corpus based on Java web and improves the comparative analysis ability of English reading corpus with the help of feature extraction and text classification [2]. The structure of the web application is shown in Figure 1.

2. Literature Review

Ahsan et al. said that the research on Chinese text classification started in the early 1980s [3]. It has generally experienced three stages: feasibility study, auxiliary classification system, and automatic classification system. Rahman et al. believe that the research on the classification of Chinese texts is also based on the classification of English texts and

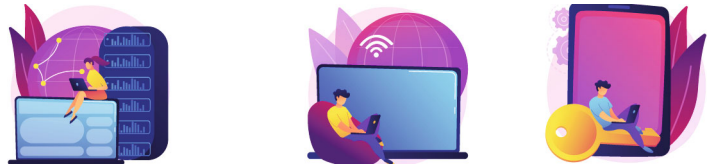

View
(i) ISP
(ii) Customize the tag library
(iii) XML

Controller
(i) XML configuration file
(ii) Servlet

Model
(i) JavaBean
(ii) EJB
(iii) Java entity class

Figure 1: Structure diagram of web.

combined with the characteristics of Chinese texts to adjust the method and realize its application [4]. Liu et al. said that the main research units include dozens of colleges and universities, including the Institute of Computing of the Chinese Academy of Sciences and Tsinghua University, and have made a series of corresponding research results and experimental systems [5].

Massei said that in recent years, special education or representative education has also attracted the attention of many scholars and has been widely used in the practice of natural language and culture, exchange rate changes, and achieved positive results [6]. In 2003, Cheng and Jin first applied the distributed representation of words (also known as word representation or word embedding) to the statistical language model [7]. Zhang et al. proposed a hierarchical log bilinear model in 2008 [8]. Xu first introduced the calculation method of word embedding proposed by them in 2008. In 2011, it was combined with convolutional architecture to develop a Senna system for sharing word representation among multiple natural language processing tasks such as language model construction, named entity recognition, semantic analysis, and syntactic analysis, and achieved the best effect at present at a speed exceeding the traditional methods [9]. Xu and He extended the skip gram (continuous skip gram) model of continuous word bag and opened source word2vec, a tool based on deep learning, which provides an effective implementation of continuous word bag and skip gram architecture for calculating word vector [10]. In addition, some scholars have also done some research on the comparison of these word vector methods. For example, Joseph Turian compared the effects of several word vectors in 2010. American scholars have also done some research work on cross domain learning classification tasks, such as Xavier Glorot's cross domain emotion classification based on deep learning in 2011 and Bengio's deep learning research on feature representation for transfer learning in 2012.

All research on the linguistic corpus in the United States is independently developed by relevant universities. Since the linguistic corpus generally studies English and English is mostly the mother tongue of developed countries, the research is also relatively developed. However, there are some disadvantages in some research software. The number of software is insufficient, and the application of Computer Science in phrasal analysis of linguistic corpus is not paid enough attention. Most software development time is too early, and there is no update and secondary development, which makes the function disconnected. At the same time, there is no connection between software and software, and the function integration is very poor. In the analysis software wordsmith 50, you can make a vocabulary list of the article you are studying. In the process of making, you can count the frequency of a word in the article, and you can choose the arrangement of frequency or the arrangement of words. After the production, you can view the statistical results of frequency. Its function is to study the types of words in the corpus, determine the common lexical chunks in the corpus, and compare the frequency of specific words in different texts. Then, query and count the frequency of one or some words or phrases in the specified text, mark their positions, restore the sentences of 8 words on the left and 8 words on the right, and form moves at the same time. At the same time, we can compare multiple word lists and analyze the subject words. The analysis method is the subalgorithm to determine the subject words (subject words refer to those words whose frequency is significantly higher or lower than that of the corresponding words in the reference corpus). This software lacks the location map of displaying words, the vocabulary list of making multiword chunks, and the analysis after segmentation in paragraphs. The processing speed is relatively slow, the interface is not friendly enough, and the installation is troublesome. In the research of linguistic corpus, the use of computer technology to support the research of this discipline is a short board and cannot be used in the mobile terminal, resulting in the fixed research location. If you change the environment, you need to reinstall the software and configure the computer environment, which is very complicated, this is because there are scattered software, no integration, and uneven functions. In the research process, we should do a lot of preliminary work for the research projects and functions, understand the functions of each software, analyze its functions, and carry out research planning in combination with the research methods of linguistic corpus at this stage, which occupies a lot of research time, and the methods used are old means. Although the research methods of linguistic corpus have experienced a certain development time, the scalability of existing software is still insufficient.

3. Method

3.1. Overview of Java Web Technology. Java web is composed of JSP and Servlet. The so-called website development is actually the combination of JSP and Servlet. In JSP and

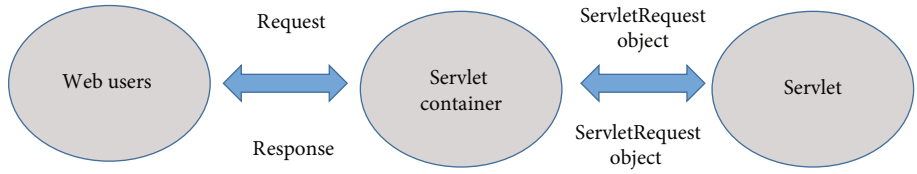

Figure 2: Servlet request process.

Table 1: Request response mode.

Name	Explain
HttpServletRequest	The Servlet container contains the HTTP request information in the HttpServletRequest object, and the Servlet component reads the user's request data from the request object. In addition, HttpServletRequest can store the shared data within the request range.
HttpServletResponse	The user generates HTTP response results.
Httpsession	The Servlet container creates an instance of Httpsession for each HTTP reply. Httpsession can store the shared data in the session range
ServletContext	The Servlet container creates a ServletContext instance for each web application, which can store the shared data of the application.

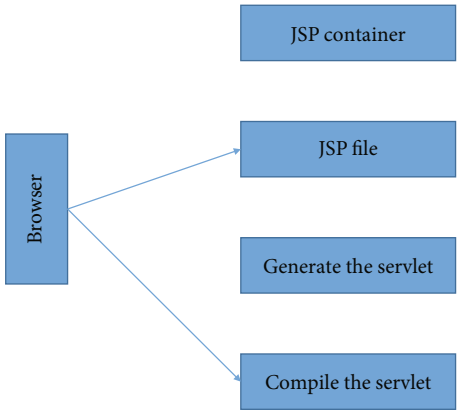

Figure 3: Analysis of JSP by container.

Servlet, JSP is responsible for realizing the function of front-end, while Servlet is responsible for realizing the function of background processing server. In the process of web project development, regardless of the choice of any framework structure, we need to rely on the mutual echo and combination of these two technologies to complete the development of web applications [11]. Servlet is responsible for processing technology and runs in the container, but its real running process is to perform its technology processing function when it is passively loaded in the container. For web applications, the working mode of Servlet is mainly to respond to the request of the client. Whenever the client initiates a request, the server will respond to the initiated request and push the results processed by the business layer to the client. There are two situations that will cause connection interruption. One is that the client request times out, and the other is that the browsing is disconnected. In the same Servlet container, each object corresponds to the corresponding request one by one. Then, the Servlet will fill the processed response results into the relevant attributes of the corresponding object Servlet response. The return process is in the charge of the container where it is located, and the content that the user can understand will be parsed by the browser and displayed in a corresponding way [12], as shown in Figure 2.

The following describes some of these classes, which are mainly used to deal with the corresponding methods of shared data and requests, as shown in Table 1.

JSP is similar to the principles of PHP/ASP and net/ASP. It is a tool for developing web applications based on HTML technology. The development languages used in the implementation of the server are different. There are two cases. The first is a single file. JSP will contain the file itself and the code content of the server and HTML. The second is multiple files. At this time, JSP will separate and save the code content of service order and HTML. When JSP recognizes Java code, it will add JSP tags before Java code to facilitate code reading [13], as shown in Figure 3.

3.2. Spring Overview. Spring's goal is to turn complexity into simplicity and make the coding and design of Java programs lively and interesting. This is one of the most important reasons why most Java programmers trace this open source framework [14]. Spring integrates modular programming, code writing, and testing, simplifies development steps, and provides convenience for Java programmers. According to the output function, the whole framework has five important output modules, including more than 1400 classes, as shown in Figure 4.

3.3. Bootstrap Overview. Bootstrap is an open source front-end development framework. Creating bootstrap is a framework for web front-end development used to build responsive websites [15]. Because bootstrap inherits the front-end development library of less (the latest version already contains the source code of SASS), many common CSS and JavaScript collections can be found in bootstrap, which is convenient for developers to call at any time. Bootstrap

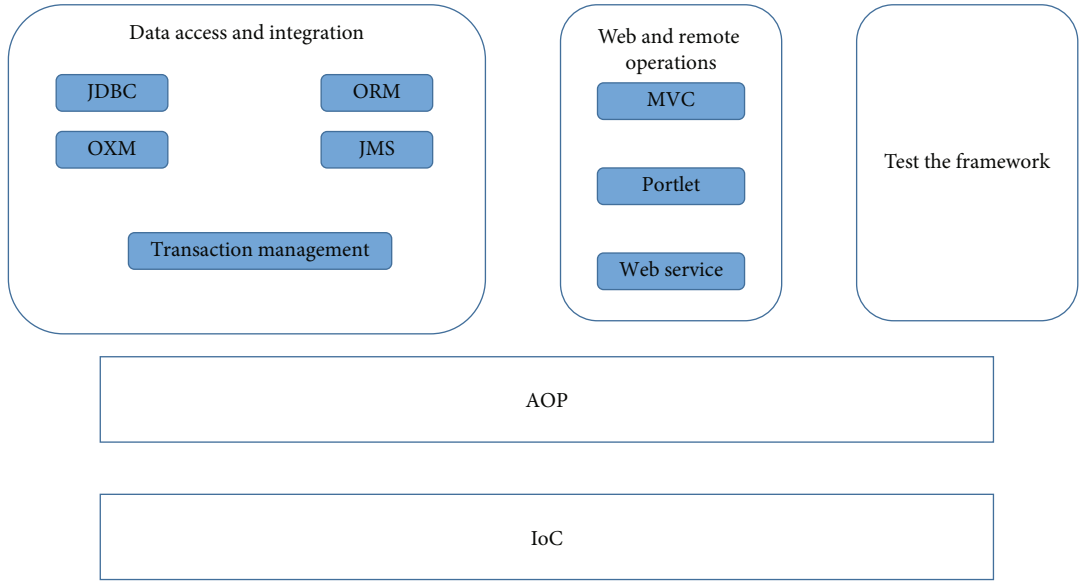

Figure 4: Spring framework.

has basic layout styles, JavaScript plug-ins, customized CSS style sheets, CSS components, grid system, and other functions [16].

(1) Basic layout style

Many layout styles can be found in bootstrap, such as tables, buttons, and forms. These styles can be applied to any HTML element. You only need to prestore the relevant CSS classes.

(2) JavaScript plug-in

Based on Jquery1.10 +, bootstrap has 12 JavaScript plug-ins. These plug-ins can provide rich user experience and website extension functions. When used in combination with the CSS group, these functions can achieve the effect of designing corresponding pages [17].

4. Results and Analysis

The system takes browser/server (B/S) as the basic architecture of the system, which is divided into three-tier structure of database, server, and user [18]. All the articles studied are stored in the English reading corpus in the form of text files. As the research corpus, they are retrieved by the server and used by users. Users can easily obtain the English reading corpus by accessing the web page through the browser. Pretrained models have been shown to generalize well to a given domain or into different modes. They show strong small-sample learning behavior and good learning ability. All business logic and functions are realized on the server side. The physical server is the analysis system server, while the logical server is the business server, database server, and web server. A computer software that manages resources and services users is usually divided into file servers, database servers, and application servers. The database (corpus) is connected with the database server. The user logs in through authentication and uses relevant functions. The user sends a service request to the server. The server accesses the query corpus through the connection with the corpus, completes the calculation of the required analysis function on the server, and then displays the analysis results to the user on the web page. Roles are divided into three categories: tourists, users, and administrators [19]. The relationships among the three types of roles are as follows:

Tourists use specific functions, which are described in the requirements analysis of the authentication module and will not be repeated here. Tourists log in as users through identity authentication and use the business functions in the server. From the administrator login portal, visitors can log in as administrators through authentication, add, delete, modify, and check the user data in the database server, and maintain the authority of the system [20].

An important part of the system is the English language analysis function. There are three problems to be solved in the realization of this part. The first is to carry out secondary development and integration by analyzing the past linguistic corpus analysis software and drawing lessons from the functions of Antconc, BFSU_Colloctor1.0, WordSmith5.0, Kf Nfram, and Claws4 software. The second aspect is to develop the analysis function after code assignment combined with the code assignment function of a university. The third aspect is to realize its research and analysis function. English reading corpus is a collection of English language materials stored on a computer to study how English is used, according to different research and analysis schemes (comparative study between corpus and corpus in corpus, comparative study between upload research factors and corpus in corpus, and comparative study between upload factors and upload factors). The system functions are divided into general functions, characteristic functions, and special functions according to the use frequency and research order. Common functions include English reading related data analysis and vocabulary search.

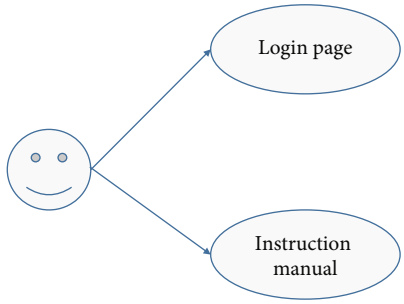

Figure 5: Use case diagram of tourist login role.

Corpus is the basic resource for corpus linguistics research and the main resource for empirical language research methods. It can be applied to lexicography, language teaching, traditional language research, and statistical or example-based research in natural language processing. Language feature analysis is inseparable from the choice of vocabulary or lexical chunks. There are simple and accurate search and complex regular expression search in the demand. Search is the basis of research and is used frequently [21].

4.1. Authentication Module

4.1.1. The Role of Tourists. The system is not a free and open source project, so set the identity of tourists. Tourists can only browse the user manual on the login page and consult the use methods and main functions of the system. If they are in a nonlogin state, they cannot use the functions of the system and can only have a better understanding. If you need to use the system, you need to contact the administrator to obtain the user name and password to use [22], as shown in Figure 5.

4.1.2. User Role. Visitors check the user name and password in the database through the user name and password to log in. After logging in, they become users, that is, they can use all the functions in the system. If you want to change your password or account name, or forget your user name or password, you need to contact the administrator to change or find your user name and password. When you add security questions when setting up your local account, you can answer security questions to log in again.

4.1.3. Administrator Role. The administrator is only responsible for adding, deleting, modifying, and querying users. The administrator is responsible for all permissions in the system. If tourists apply to use the system, contact the administrator. The administrator creates user account and password by default or according to the user's requirements [23]. If users want to change or query their user name or password, they also need to contact the administrator for operation, but the administrator cannot use the system and exists only as user management [24], as shown in Figure 6.

4.2. General Function Module

4.2.1. Vocabulary Search and Data Analysis. For a word in an article, match a selected phrase, an uploaded phrase, or

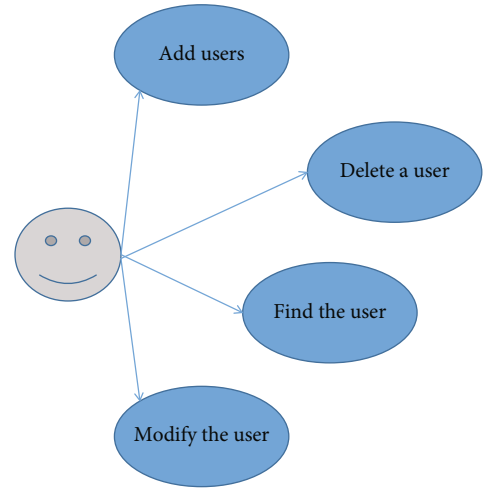

Figure 6: Use case diagram of administrator login role.

search to find it correctly. As required, finding a word in each sentence is the easiest task. The corpus contains the language material that appears in the actual use of a language, so it should not usually be counted as a corpus. By understanding the requirements, he discovered that the task was to search not just single words, but also word chunks, with many variations. Real research is aimed at improving and preparing future projects [25].

In the process of density analysis, in order to make the searched words or lexical chunks more intuitive, the function of black-and-white location map needs to be introduced. Black and white location map is an incidental function combined with density analysis. It is made up of a single point called pixels (picture elements). These points can be differently arranged and stained to form the pattern. Count and display the position of a single word or lexical chunk in the article or corpus, and show it with a black bar chart on a white background, which is equivalent to hot spot analysis. It intuitively displays the specific position of the text search word, so as to facilitate the researchers to identify the distribution of words or lexical chunks in the article or corpus [26].

4.2.2. MI Value. Mutual information value (MI value for short) is a common method used to calculate the collocation strength of words. Mutual information indicates whether the two variables X and Y are related to each other, and the relationship between them. The MI value is calculated in bits. The use of MI in linguistics is different from its common methods in finance, especially its numerical range [27]. In Information Science, the MI value is in the range of 0~1, while the MI value used between linguistic words is only separated by 0 bits. The larger the value, the greater the mutual encounter and attraction between words. Mutual information is actually a broader special case of relative independence. If the variables are not independent, then we can judge whether they are "close" to being mutually independent by examining the Kullback-Leibler divergence between the product of the joint probability distribution and the edge probability distribution. Specifically, the MI value calculates

the frequency of one word in the corpus and can provide information about the probability of another word [28].

For example, a and B are two random words divided by body, the total potential of body is w, and S is the interval. The actual observed frequencies of their bodies are $F(a)$ and $F(b)$, and the resulting frequency is $F(a, b)$. The MI value is calculated as shown in the following equation:

$$I(a, b) = \log_2 \bullet \frac{P(a, b)}{P(a) \bullet P(b) \bullet 2S} = \log_2 \bullet \frac{F(a, b) \bullet W}{F(a) \bullet F(b) \bullet 2S}. \quad (1)$$

If a body's potential is w-word determinant, $F(a)$ is a frequency test for multiword sequences or lexical-driven models, $F(b)$ is a collocation frequency test for multiple temporal or lexical-driven models a, and $F(a, b))$ is the frequency of the sum of the two parts of speech, and the MI value can be calculated according to the following formula:

$$I(a, b) = \log_2 \bullet \frac{W \bullet F(a, b)}{F(a) \bullet F(b)}. \quad (2)$$

4.2.3. Z Value. If the unit total capacitance is w and the nominal frequency of the integer in the body is C_1, then the average frequency of the integer in each function is calculated as C_1/W. If the collocation span is limited to s, the frequency of the collocation with each node word is $C_1 \cdot (2S + 1)/W$. $2S$ refers to the span position set on the left and right sides of the node word, and 1 is the word position occupied by the node word. However, this form can contain block words and similar phrases, so the word position in the design will not be 1. However, when determining the probability of occurrence of a word with probability frequency N, the theoretical probability P must be calculated according to the following equation:

$$P = \frac{C_1(2S + 1)}{s} \bullet \frac{N}{s}. \quad (3)$$

The desired coupling frequency of the coupling term can be obtained by giving the theoretical P value for the coupling produced by the potential W. Then, the combined frequency of the combination item and the instruction item is shown in the following equation:

$$SD = \sqrt{(2S + 1) \bullet N \bullet \left(1 - \frac{C_1}{s}\right) \bullet \frac{C_1}{s}}. \quad (4)$$

Next, calculate the difference of the collocation distribution in the text, as shown in the following equation:

$$E = \frac{C_1(2S + 1) \bullet N}{W}. \quad (5)$$

Divide the difference between the actual frequency C_2 and the expected frequency e of the node words of the collocation by the standard deviation to obtain the Z value. The value of Z value can be used to judge the strength of word collocation. The Z value of word collocation needs to be at the level of 0.01 to be significant, and the Z value must be equal to or greater than 2.576. By setting a critical value of 2.576, researchers can obtain significant word collocations and filter out accidental collocations that have no effect on node words, as shown in the following formula:

$$Z = \frac{C_2 - E}{SD}. \quad (6)$$

4.2.4. Log Likelihood Function Value. In linguistic English reading corpus, the value of log likelihood function is mainly used to determine the collocation relationship value of two words in the left and right span of node words, display the collocation rate in the left and right span, and quickly locate the search for effective collocation words near node words. When A is set as the vocabulary of corpus A, B is defined as the vocabulary of corpus B, c is the frequency of words in corpus A, and d is the frequency of words in corpus B, the algorithm is shown in the following formula:

$$\log - \text{likelihood} = 2c \bullet \log_e \frac{c}{A \bullet c + b/A + B} + 2d \bullet \log_e \frac{d}{B \bullet c + d/A + B}. \quad (7)$$

4.2.5. T Value. T value is a relative position quantity of the most common straight-line conversion standard score, which is used to represent the relative position of an individual in its group. In linguistics, it is to describe the weight of vocabulary in its research factor compared with that of another vocabulary in the same research factor. The basic principle is that the original score of an individual has several standard deviations above or below the average, which is the Z value. The time sharing obtained by expanding the Z score is the T value, as shown in the following formula:

$$T - \text{Score} = \frac{N \bullet F(n, c) - FN \bullet F(c)}{N \bullet \sqrt{F(n, c)}}. \quad (8)$$

4.2.6. K-SVD Algorithm. An over complete dictionary is used to represent any known signal. The number of atoms in the dictionary is K. After sorting all atoms according to the column vector, it is set as the following formula; then, the signal y can be approximately expressed as the following formulas:

$$D \in R^{n \times k}, \quad (9)$$

$$\{d_j\}_{j=1}^{K}, \quad (10)$$

$$y \approx Dx. \quad (11)$$

In the above formula, the sparse representation coefficient of signal y is $X \in R^k$. The solution process of signal sparse representation is transformed into the following optimization problem, as shown in the following formula:

$$\widehat{x} = \arg \min_x \|x\|_0. \quad (12)$$

The constraint conditions of this formula are shown in the following formula:

$$\|y - Dx\|_2 \leq \varepsilon. \quad (13)$$

In the above formula, the zero norm of x is $\|x\|_0$, which refers to the number of nonzero elements in vector x, and the smaller positive value is ε. In order to obtain the optimal dictionary D and the most sparse coefficient matrix X, the problem of solving the known signal $Y = \{y_1, y_2, \cdots, y_N\}$ is transformed into the optimization problem described by the following expression, as shown in the following formula:

$$\left(\hat{D}, \hat{X}\right) = \arg \min_x \|Y - DX\|_F^2. \tag{14}$$

The constraint conditions of this formula are shown in the following formula:

$$\|x_i\|_0 \le T_0, \forall i = 1, 2, \cdots, N. \tag{15}$$

In the above formula, the column vector of coefficient matrix X is x_i, the F norm of matrix A is defined as $\|A\|_F$, and the sparsity is defined by t0.

4.3. Special Functional Requirements. Concordance is a research method provided according to the needs of linguistic English reading corpus language feature analysis. Concordance retrieval is mainly used to study the frequency of random chunks in articles. Each discipline has different key points and keywords, and there are also differences in the mode of language expression. When it comes to professional knowledge, the composition of lexical chunks is different, resulting in different collocation of technical language. Consistency retrieval is mainly to analyze the above situation.

The function of thesaurus production is to serve the following functions of thesaurus production. Starting from the analysis of linguistic English reading features, the list of words can roughly know the main thrust of the article and predict the research direction of lexical chunks through the number of hits.

Keywords are the function of directly referring to the context and meaning words screened from the research factors, which is the top priority. Compare according to the theme words. Generally, the comparison is made between two theme words. The theme words of an article cannot be analyzed only according to the frequency of words or lexical chunks. The key function is the Keyness coefficient. The value of K determines the importance of words, and screen the high-frequency words of each article. Suppose A is the frequency of the same word or lexical chunk in corpus A, B the frequency of the same word or chunk in corpus B, C the vocabulary of corpus A, and D the vocabulary of corpus B. The algorithm is shown in the following formula:

$$\text{Keyness} = (A + B + C + D) \bullet \frac{[\|A * D - C * B\| - (A + B + C + D)/2]^2}{(A + C) \bullet (B + D) \bullet (A + B) \bullet (D + C)}. \tag{16}$$

The specific information of the model building platform is shown in Table 2.

As a Java toolkit in the field of natural language processing, HanLP has many advantages, such as efficient processing speed, real-time updating corpus, and user-defined processing mode. Moreover, the tool, including dictionary, is completely open source, with fast word segmentation speed and small memory occupation; Weka is one of the open source data mining platform tools, which is mainly used for data processing operations such as regression, classification, and acquisition of association rules.

Table 2: Statistics of development platform information.

Name	Content
Development language	Java
Development environment	Eclipse .JDK
Operating system	Uhuntu 14.04
Main tools	HanLP, Weka

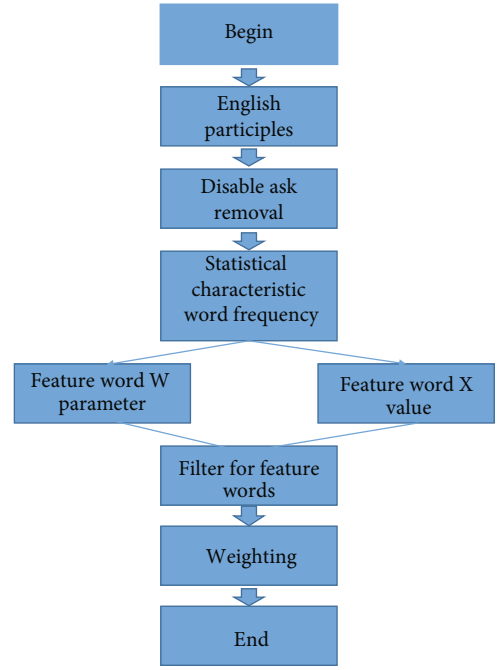

Figure 7: Schematic diagram of model operation flow.

The English reading corpus preprocessing module consists of three functions: word segmentation, removing stop words, and dependency parsing. After processing the input initial text data, two sets of output data are obtained, namely, the set of text feature words without stop words and the set of dependent word pairs. The four functions of effective dependent word pair acquisition, feature word frequency statistics, network edge weight determination, and directed network architecture are used to form a text network construction module for further processing the output data of the preprocessing module. The output data of this module is text network data and feature word frequency statistics. The feature extraction module is composed of three functions: inverse document frequency, feature word w parameter solution, and feature word extraction. The dimension-reduced feature space output data is obtained by calculating the output data of the previous module. The function of calculating the weight of feature words is the feature weighting

module, which is used to assign values to the feature items in the feature vector space.

The specific operation process of English reading corpus word segmentation feature extraction model is shown in Figure 7. The operation contents of each stage are described as follows:

(1) *Text Preprocessing Stage*. Use the open source language processing tool HanLP to perform word segmentation and dependency parsing on the input text data, and remove the stop words contained in the feature word set and dependency word pair set

(2) *Text Network Construction Stage*. After counting the word frequency of the feature word set, the feature word is used to construct the text network node to obtain the effective dependent word pair set, complete the construction of the text network edge and its weight, and obtain the weighted directed text network

(3) *Feature Extraction Stage*. The w parameter value of the feature word node is solved by the improved K-SVD algorithm, and the value of the corresponding feature word is solved according to the word frequency information of the feature word. After comparing the weight, the feature word screening is completed to realize feature extraction

(4) *Feature Weighting Stage*. Weigh the feature words after feature extraction. The operation method is the same as the feature extraction method. The weighted value of the feature words is the weight of the solved feature words

In order to verify the performance of the constructed model, a comparative verification experiment is designed. The experimental data selects English news reading materials in recent ten years as the corpus. The number of news articles is about 511065, and the number of sentences is about 21412825. The training data is randomly extracted from the news content. The overall iterative training of the English reading corpus takes about 3 days, and each training time is about 2 seconds.

(1) Comparative analysis of word segmentation feature output results

Under the same experimental data, the comparison experiment of word segmentation feature output accuracy is carried out by using design model and model *a* and model *B*. The comparison results of word segmentation feature output accuracy of the three models are shown in Figure 8.

As can be seen from Figure 8, for feature extraction, the model has a high accuracy of word segmentation feature output in the increasing experimental time, which shows that the design model has a better extraction effect and can better master the semantics and grammar of the original sentence. The output accuracy of word segmentation features of the two literature comparison methods shows a

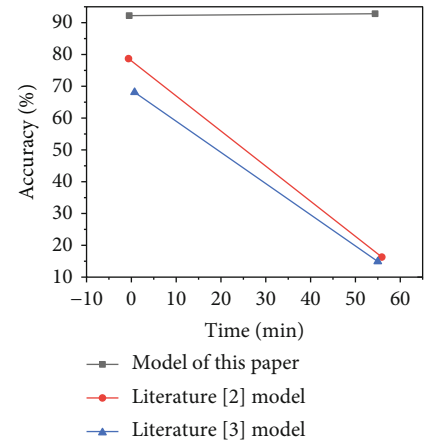

Figure 8: Comparison results of word segmentation feature output accuracy.

gradual downward trend. The above comparison results fully prove the good performance of the design model.

(2) Comparative analysis of accuracy and recall of output results

Using the model, the accuracy and recall of feature extraction are obtained. The accuracy and recall of the model have more significant advantages, and the feature extraction is more accurate. The reason is the introduction of K-SVD optimization algorithm, which considers the word length of feature words. After accurately screening word segmentation features and removing stop words, the model uses feature words to construct text network nodes, obtain an effective set of dependent word pairs, complete the construction of text network edges and their weights, obtain a weighted directed text network, achieve a relatively balanced accuracy and recall, and complete the effective extraction of word segmentation features.

5. Conclusion

In the word segmentation stage of English reading corpus, to remove redundant features and extract features conducive to classification, it is necessary to reduce the dimension of the feature vector space. Among them, one of the most commonly used and effective methods is feature extraction, which uses the most representative feature items of text category information to complete the component word task. Compared with the existing analysis system, there is only the comparison means between corpus and corpus. This system adds the function of corpus upload and comparison, which makes the system add the function of corpus and upload corpus and the function of comparative analysis between upload corpus and upload corpus, and expands the application scope of the system. The work of this paper will lay a solid foundation for the analysis of English language features of the linguistic corpus of a university and solve the embarrassing situation that linguistics has research means but does not realize methods to a certain extent. At

the same time, through the innovation of function and research object, the scientific research of linguistics has turned a new page. It is proved that the construction of language feature analysis system of English reading corpus can effectively solve the problem of comparative analysis ability of English corpus, meet the needs of global economic and trade exchanges, make up for the lack of comparative analysis ability of English reading corpus, and improve the development of global economy and trade.

Data Availability

The data used to support the findings of this are available on request from the corresponding author.

Conflicts of Interest

The authors declare that they have no conflicts of interest.

Acknowledgments

This study was supported by the Provincial Project for the 2019 Teaching Reform Research of Colleges and Universities in Jiangxi Province: analysis and research on the graded teaching of College English in private colleges (No.: jxjg-19-28-8).

References

[1] R. G. Hashish and M. Zeidouni, "Injection profiling through temperature warmback analysis under variable injection rate and variable injection temperature," *Transport in Porous Media*, vol. 141, no. 1, pp. 107–149, 2022.

[2] S. Kushwah, S. Parekh, H. Mistry, M. Bhatt, and V. Joshi, "A methodological study of leaf spring by material comparison and Taguchi's DOE," *International Journal on Interactive Design and Manufacturing (IJIDeM)*, vol. 16, no. 1, pp. 239–252, 2022.

[3] Z. Ahsan, H. Dankowicz, M. Li, and J. Sieber, "Methods of continuation and their implementation in the COCO software platform with application to delay differential equations," *Nonlinear Dynamics*, vol. 107, no. 4, pp. 3181–3243, 2022.

[4] A. U. Rahman, M. Saeed, and F. Smarandache, "A theoretical and analytical approach to the conceptual framework of convexity cum concavity on fuzzy hypersoft sets with some generalized properties," *Soft Computing*, vol. 26, no. 9, pp. 4123–4139, 2022.

[5] J. Liu, J. Li, Z. Wang, Y. Tian, and H. Wang, "Optimization of heating process for bearing rings in a vacuum furnace based on numerical analysis," *ISIJ International*, vol. 61, no. 1, pp. 302–308, 2021.

[6] S. Massei, "Some algorithms for maximum volume and cross approximation of symmetric semidefinite matrices," *BIT Numerical Mathematics*, vol. 62, no. 1, pp. 195–220, 2022.

[7] J. Cheng and H. Jin, "An adaptive extreme learning machine based on an active learning method for structural reliability analysis," *Journal of the Brazilian Society of Mechanical Sciences and Engineering*, vol. 43, no. 12, pp. 1–19, 2021.

[8] G. Zhang, Y. Song, S. Liao, L. Qu, and Z. Li, "Uncertainty measurement for a three heterogeneous information system and its application in feature selection," *Soft Computing*, vol. 26, no. 4, pp. 1711–1725, 2022.

[9] D. Xu, "Observability inequalities for Hermite Bi-cubic orthogonal spline collocation methods of 2-D integro-differential equations in the square domains," *Applied Mathematics & Optimization*, vol. 84, no. 2, pp. 1341–1372, 2021.

[10] S. Xu and B. He, "A parallel splitting alm-based algorithm for separable convex programming," *Computational Optimization and Applications*, vol. 80, no. 3, pp. 831–851, 2021.

[11] Y. Li, "Numerical analysis and optimization of feature extraction-oriented english reading corpus," *Mathematical Problems in Engineering*, vol. 2022, Article ID 9883201, 13 pages, 2022.

[12] F. Mohammaddokht and J. Fathi, "An investigation of flipping an English reading course: focus on reading gains and anxiety," *Education Research International*, vol. 2022, Article ID 2262983, 10 pages, 2022.

[13] L. Chang and G. O. Deák, "Adjacent and non-adjacent word contexts both predict age of acquisition of English words: a distributional corpus analysis of child-directed speech," *Cognitive Science*, vol. 44, no. 11, p. e12899, 2020.

[14] X. He, "An English reading and learning system based on web," *Scientific Programming*, vol. 2021, Article ID 7281269, 8 pages, 2021.

[15] G. Ling, "Corpus-driven resource recommendation algorithm for English online autonomous learning," *Computational and Mathematical Methods in Medicine*, vol. 2022, Article ID 9369258, 10 pages, 2022.

[16] F. Ghanami, G. A. Hodtani, B. Vucetic, and M. Shirvanimoghaddam, "Performance analysis and optimization of NOMA with HARQ for short packet communications in massive IoT," *IEEE Internet of Things Journal*, vol. 8, no. 6, pp. 4736–4748, 2020.

[17] A. K. Sarnaghi, A. Rais, A. Kovryga, W. F. Gard, and J. W. G. V. D. Kuilen, "Yield optimization and surface image-based strength prediction of beech," *European Journal of Wood and Wood Products*, vol. 78, no. 5, pp. 995–1006, 2020.

[18] Y. Ding and T. Wang, "Environmental affection-driven English tense analysis: a healthcare exercise-based corpus case study over public English environment," *Journal of Environmental and Public Health*, vol. 2022, Article ID 9497554, 8 pages, 2022.

[19] Z. Sun, "Development of corpus linguistic using lexical teaching to improve English writing," *Wireless Communications and Mobile Computing*, vol. 2022, Article ID 4024149, 7 pages, 2022.

[20] G. Yufang, W. Wu, M. White, H. Aziz, and K. Liew, "Evaluation of college English textbooks based on computer-aided analysis corpus," *Security and Communication Networks*, vol. 2022, Article ID 4648957, 7 pages, 2022.

[21] Q. Dai, "Construction of English and American literature corpus based on machine learning algorithm," *Computational Intelligence and Neuroscience*, vol. 2022, Article ID 9773452, 9 pages, 2022.

[22] S. Wang and X. Shi, "Research on correction method of spoken pronunciation accuracy of AI virtual English reading," *Advances in Multimedia*, vol. 2021, Article ID 6783205, 12 pages, 2021.

[23] S. Huang, "Optimization and simulation of an English-assisted reading system based on wireless sensor networks," *Journal of Sensors*, vol. 2022, Article ID 6823502, 11 pages, 2022.

[24] X. Yu and L. Zhang, "Effectiveness of interactive reading mode based on multisensor information fusion in English teaching," *Mobile Information Systems*, vol. 2022, Article ID 7993728, 12 pages, 2022.

[25] R. Futrell, E. Gibson, H. J. Tily et al., "The natural stories corpus: a reading-time corpus of English texts containing rare syntactic constructions," *Language Resources and Evaluation*, vol. 55, no. 1, pp. 63–77, 2021.

[26] L. Lowphansirikul, C. Polpanumas, A. T. Rutherford, and S. Nutanong, "A large English-Thai parallel corpus from the web and machine-generated text," *Language Resources and Evaluation*, vol. 56, no. 2, pp. 477–499, 2022.

[27] G. Fatima, R. M. A. Nawab, M. S. Khan, and A. Saeed, "Developing a cross-lingual semantic word similarity corpus for English-Urdu language pair," *Transactions on Asian and Low-Resource Language Information Processing*, vol. 21, no. 2, pp. 1–16, 2021.

[28] L. Plug, R. Lennon, and E. Gold, "Articulation rates' intercorrelations and discriminating powers in an English speech corpus," *Speech Communication*, vol. 132, pp. 40–54, 2021.

Hindawi
Wireless Communications and Mobile Computing
Volume 2022, Article ID 4771395, 13 pages
https://doi.org/10.1155/2022/4771395

Research Article

Design and Implementation of Coal Mine Safety Monitoring System Based on GIS

Junwen Zhang

Electrical and Mechanical Department, Lanzhou Resource & Environment Voc-Tech University, Lanzhou 730021, China

Correspondence should be addressed to Junwen Zhang; 2015223010027@stu.scu.edu.cn

Received 15 June 2022; Revised 26 July 2022; Accepted 9 August 2022; Published 5 September 2022

Academic Editor: Jun Ye

In order to further improve the safety production management capacity of coal enterprises and minimize the rate of coal mine safety accidents, based on the purpose of improving safety production efficiency, this paper constructs a coal mine safety detection system based on GIS technology. At the same time, on the basis of fixed-point positioning and remote monitoring at the PC end, this paper implements the whole process detection and monitoring of coal mine safety production with the help of mobile terminal intelligent system. The system software uses Java language to code it. In the first round of test, one function omission, three serious system errors, 14 general errors, and 21 minor errors are found. The accident passing rate of the second test is greater than 99.88%, and all performance indexes of the system meet the performance requirements, which proves the feasibility of the system.

1. Introduction

In recent years, with the exploitation of coal resources and the sustainable development of coal industry, China's coal industry has developed rapidly with the help of technological progress and other fields. However, in the process of continuous development, coal accidents have not been effectively controlled. Of course, for a long time, the Chinese government has attached great importance to the management of coal production safety and issued a number of safety production regulations one after another. The purpose is to enable coal enterprises to strengthen the management of coal production safety by adopting advanced science and technology. Even so, on the whole, the incidence of coal safety accidents in China is still "among the best" in the world. This paper takes this as the background and puts forward a coal mine safety detection system based on GIS technology for the purpose of further improving the safety production management of coal enterprises.

2. Literature Review

With the rapid development of computer network technology and integrated electrical technology in foreign countries, coal mine safety production management system has made a major breakthrough in technology, and many types of advanced sensor equipment have been produced at the mine side. These sensor devices can collect mine environmental data, including air data such as gas, CO, and methane, as well as electrical equipment data produced for coal mines. At the same time, they also have the ability to remotely control the equipment, and the system can set predetermined rules for some automatic operations. In terms of network, the monitoring network of coal mine safety production monitoring system is mainly constructed by using LAN technology and Internet technology to realize the interaction between the monitoring center system and mine side data. At the software application level of coal mine safety production monitoring system, the functions of the application system mainly include power environment monitoring, video monitoring, etc. at the same time, it is effectively connected with coal mine production scheduling system through data interface to escort coal mine safety production. At present, the more advanced coal mine safety production management systems abroad mainly include Liang system, promos system, and Dan system. In general, these systems adopt the distributed system structure of open system

interconnection model. The system is composed of the monitoring center on the upper side of the well and the monitoring substation on the underground side. The monitoring substation uses the Internet of things technology to connect all kinds of sensor equipment, which can adopt all kinds of data in real time and report to the monitoring center. The monitoring center can analyze the data, can automatically issue some control parameters, and has certain automation and intelligence ability. At present, the safety production accident rate of foreign coal mining enterprises is generally lower than that in China, which is mainly due to the role of coal mine safety production monitoring system [1].

Safety management of foreign mines has worked well in China and has spread to some major states of coal mines. At the same time, some coal mining companies and research and technology companies have begun to simulate and self-study the safety supervision of foreign mines. First, they introduced the K-type coal mine safety monitoring system that can monitor the operation of the coal mine under cover and store, manage, and analyze management information to of LAN technology. However, the monitoring at that time mainly focused on air monitoring. The monitoring parameters were mainly gas, and the monitoring results were more accurate, which played a certain role in coal mine safety production at that time. Because there are many coal mining enterprises in China, there is a lot of demand for gas sensor equipment. In order to meet this demand, some hardware manufacturers in China have strengthened the research on gas sensor. On the whole, the data acquisition stability and other convenience of gas sensors provided by early hardware manufacturers were not good, and the wireless transmission technology was not mature at that time, and wired transmission technology was adopted. To deploy gas sensors in the middle of the mine, wired lines need to be deployed, which not only increased the construction cost but also increased the workload of line repair and maintenance [2]. At the same time, the equipment in this period still has problems such as short service life and troublesome adjustment, which has a certain impact on the accuracy of data detection and restricts the function of coal mine safety production monitoring system.

3. Key Technologies of Safety Production Monitoring Based on GIS

3.1. Image Scaling. The commonly used interpolation algorithms include the nearest neighbor interpolation, bilinear interpolation, and cubic convolution interpolation. The nearest neighbor interpolation method is simple and fast, but when there is a slight change in gray level between the pixels of the image, the scaled image has traces of artificial processing [3]. Compared with the nearest neighbor interpolation method, a bilinear interpolation method has a large amount of calculation, the gray values of pixels are continuous, and the distortion of the scaled image is not obvious. The calculation amount of cubic convolution method is much larger than that of bilinear interpolation method, but the accuracy is high and the image edge details are maintained well. However, due to the limited logic resources of video real-time transmission application and the more complex the algorithm is, the more resources will be occupied. Therefore, a bilinear interpolation method is selected to scale the image in this paper [4]. The core idea of bilinear interpolation method is to obtain the pixels of the points to be interpolated by averaging the values of the four pixels close to the pixels to be interpolated. Its principle is shown in Figure 1.

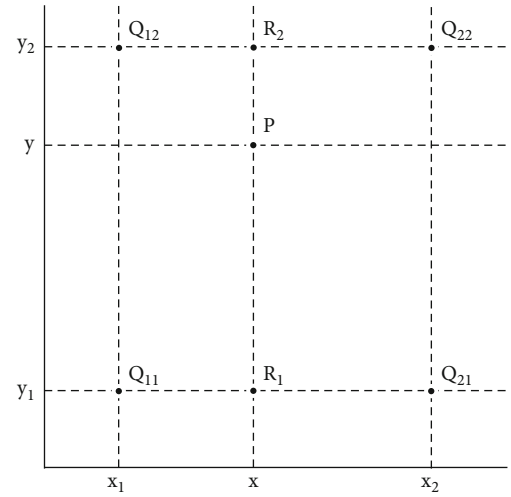

Figure 1: Bilinear difference principle.

Figure 1, $Q_{11}, Q_{12}, Q_{21}, Q_{22}$ are known pixels. According to the bilinear interpolation algorithm, the linear interpolation in the x direction is shown as follows:

$$f(R_1) = \frac{x2 - x}{x2 - x1} f(Q_{11}) + \frac{x - x1}{x2 - x1} f(Q_{21}), \tag{1}$$

$$f(R_2) = \frac{x2 - x}{x2 - x1} f(Q_{12}) + \frac{x - x1}{x2 - x1} f(Q_{22}), \tag{2}$$

where $f(R_1), f(R_2)$, respectively, represent the pixel values at two places, and $x1 - x2$ represents the distance between $x1$ and $x2$.

The linear interpolation in y direction is shown as follows:

$$f(a) = \frac{y2 - y}{y2 - y1} f(m1) + \frac{y - y1}{y2 - y1} f(m2), \tag{3}$$

where $f(a)$ represents the pixel value of point P, that is, the pixel value of the point to be interpolated.

3.2. RGB and YUV Conversion. RGB and YUV are important parts of video processing, and the conversion is the basis of coding. RGB and YUV are both a color space, that is, a method of coding a color. RGB is the most common color space in the computer. Each color can be represented by three variables: red, green, and blue. YUV is also a color space, which is commonly used in the field of analog video and television. In the process of video transmission, the RGB format video data captured by the camera is usually converted to YUV format, so as to reduce the burden of

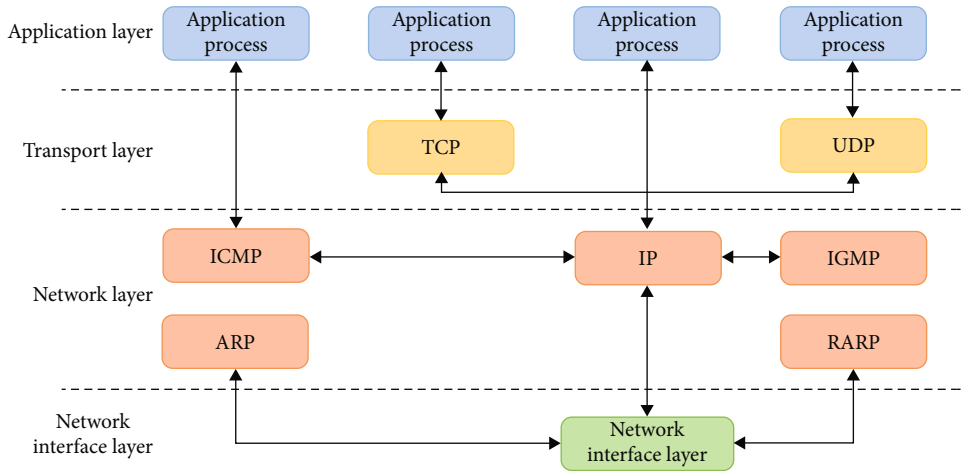

Figure 2: Four-layer structure of TCP/IP protocol.

storage and transmission, and then converted to RGB format before displaying the image [5]. The conversion formula between YUV and RGB is shown as follows:

$$\begin{bmatrix} Y \\ U \\ V \end{bmatrix} = \begin{bmatrix} 0.299 & 0.587 & 0.114 \\ -0.147 & -0.289 & 0.436 \\ 0.615 & -0.515 & -0.100 \end{bmatrix} \begin{bmatrix} R \\ G \\ B \end{bmatrix}, \quad (4)$$

$$\begin{bmatrix} R \\ G \\ B \end{bmatrix} = \begin{bmatrix} 1.000 & 0.000 & 1.140 \\ 1.000 & -0.395 & -0.581 \\ 1.000 & 2.032 & 0.001 \end{bmatrix} \begin{bmatrix} Y \\ U \\ V \end{bmatrix}. \quad (5)$$

3.3. Video Transmission Protocol. TCP/IP protocol is a transmission control protocol, which is represented by the four-layer structure of application layer, transmission layer, network layer, and network interface layer. As shown in Figure 2, data packets are transmitted layer by layer in the TCP/IP protocol stack from top to bottom or from bottom to top. Entities in one system communicate between the upper and lower layers through the interface, and the communication between entities and entities in the same layer of another system is carried out according to the protocol [6].

3.3.1. RTP and RTCP Protocols. The RTP protocol typically uses the UDP protocol to transmit multimedia files in a unicast or multicast network environment [7]: first the packet, then the time output of the news stream. Each RTP datagram has a header and a load. The first 12 bytes have the same header value, and the load is audio or video files. The details of the RTP datagram header are shown in.

RTP file header contains the basic data of streaming media real-time transmission, such as the type of transmission media, serial number, format, and whether there is additional data and timestamp. RTP protocol, which provides end-to-end transmission service of real-time multimedia data, is a transport layer protocol and cannot be connected. It moves the functions of some transport layer protocols (such as flow control) upward to the application layer to complete the functions of transport layer together with UDP; it also does not rely on the special network address format and does not provide any reliability mechanism. Therefore, the underlying transmission protocol is required to support segmentation and framing or managed by the application [8].

3.4. Multiple Linear Regression Analysis Method. Let y be a random variable that can be observed for many times, which is affected by p factors $x_1, \cdots, x_p$ and 1 random factor ε. The relationship between them is expressed by the following formulas:

$$y = \beta_0 + \beta_1 x_1 + \cdots + \beta_p x_p + \varepsilon, \quad (6)$$

$$\varepsilon \sim N(0, \sigma^2). \quad (7)$$

The following formula is called the theoretical regression equation:

$$E(y) = \beta_0 + \beta_1 x_1 + \cdots + \beta_p x_p. \quad (8)$$

Conduct n independent observations to obtain n groups of sample data, as follows:

$$(x_{i1}, x_{i2}, \cdots, x_{ip}; y_i), \quad i = 1, 2, \cdots, n. \quad (9)$$

The following formula is satisfied:

$$\begin{cases} y_1 = \beta_0 + \beta_1 x_{11} + \beta_2 x_{12} + \cdots + \beta_p x_{1p} + \varepsilon_1, \\ y_2 = \beta_0 + \beta_1 x_{21} + \beta_2 x_{22} + \cdots + \beta_p x_{2p} + \varepsilon_2, \\ \cdots, \\ y_n = \beta_0 + \beta_1 x_{n1} + \beta_2 x_{n2} + \cdots + \beta_p x_{np} + \varepsilon_n. \end{cases} \quad (10)$$

Among them, $\varepsilon_1, \varepsilon_2, \cdots, \varepsilon_n$ are independent of each other and obey $N(0, \sigma^2)$. The above formula is expressed in a

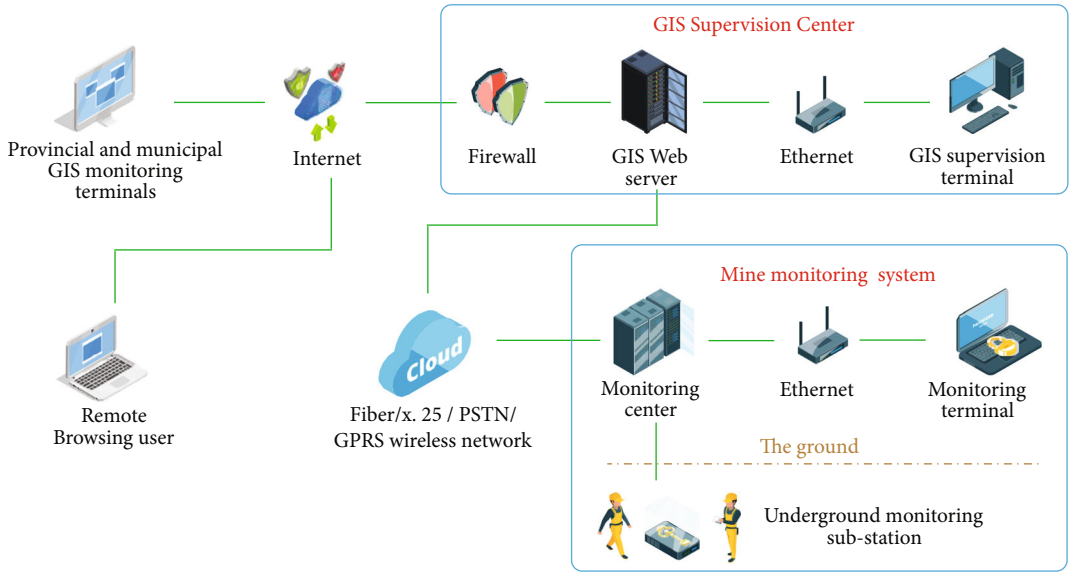

Figure 3: Coal mine remote safety monitoring system model.

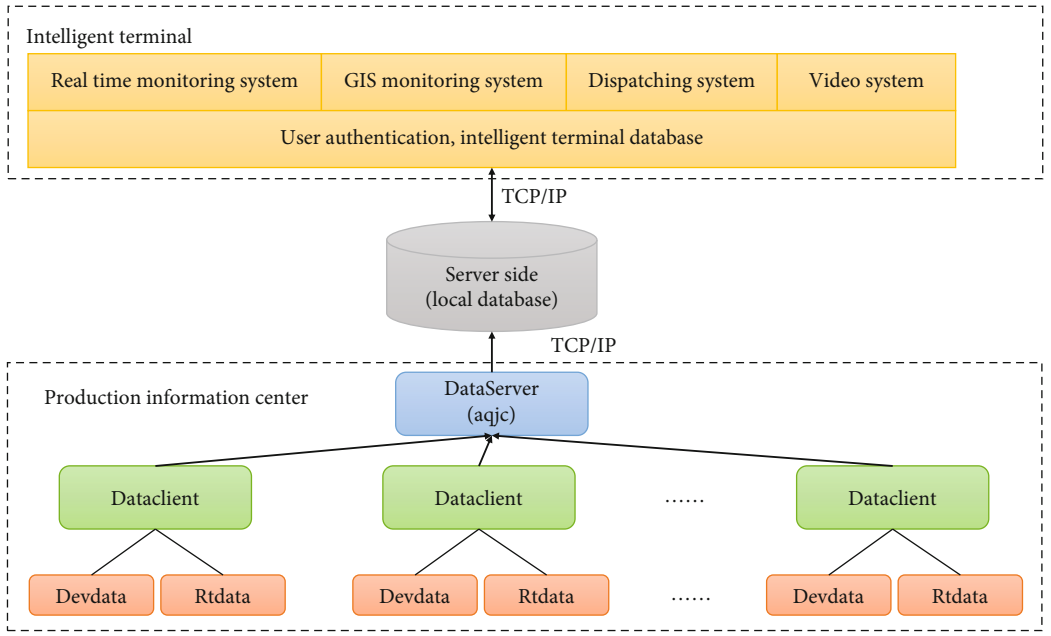

Figure 4: The working model of the smart terminal-based coal mine climate management system software.

matrix form as follows:

$$Y = X\beta + \varepsilon, \tag{11}$$

$$Y = (y_1, y_2, \cdots, y_n)^T, \tag{12}$$

$$\beta = \left(\beta_0, \beta_1, \cdots, \beta_p\right)^T, \tag{13}$$

$$\varepsilon = (\varepsilon_1, \varepsilon_2, \cdots, \varepsilon_n)^T, \tag{14}$$

$$\varepsilon \sim N_n\left(0, \sigma^2 I_n\right). \tag{15}$$

I_n is the n-order identity matrix, as shown in

$$X = \begin{bmatrix} 1 & x_{11} & x_{12} & \cdots & x_{1p} \\ 1 & x_{21} & x_{22} & \cdots & x_{2p} \\ \cdots & \cdots & \cdots & \cdots & \cdots \\ 1 & x_{n1} & x_{n2} & \cdots & x_{np} \end{bmatrix}. \tag{16}$$

4. Design of Coal Safety Detection GIS System Based on Mobile Terminal Platform

4.1. System Modeling. Coal mine remote safety monitoring system is a real-time monitoring system in the process of

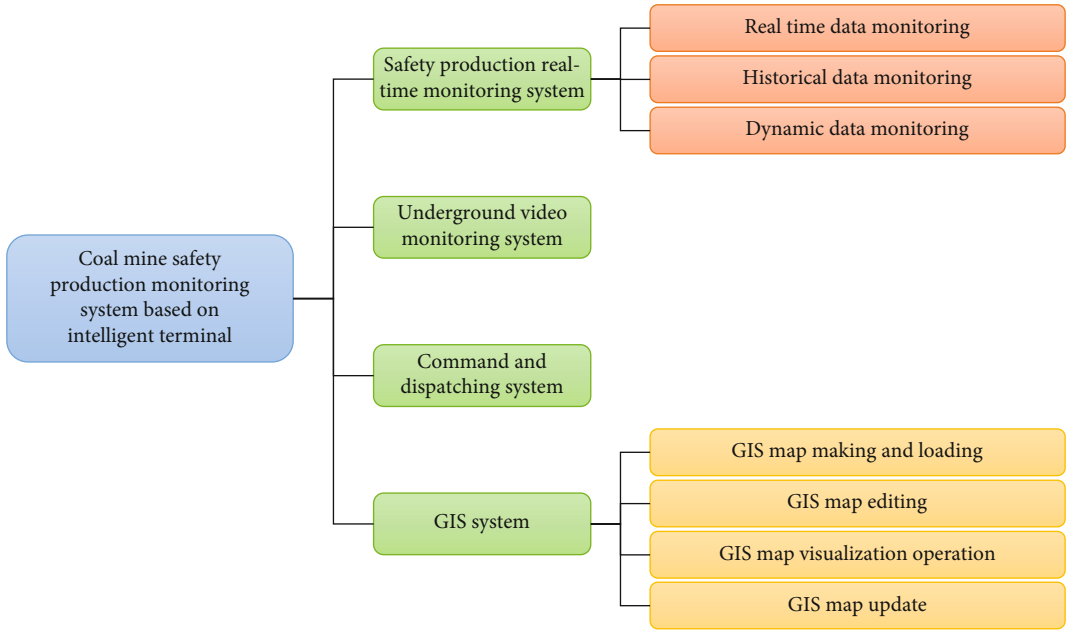

Figure 5: Functions of coal mine safety production monitoring system based on intelligent terminal.

digital mine production, safety, and management. It can make managers at all levels understand their responsibilities, so as to quickly, timely, and accurately obtain the relevant information of coal mine safety production, so as to avoid the occurrence of coal mine safety accidents. The general system model is shown in Figure 3.

The acquisition module is mainly responsible for the acquisition of various monitoring data in the mining area, including sensor information and video information.

The transmission module is mainly responsible for the real-time transmission of various collected data, including underground to underground data transmission and data transmission from within the mining area to outside the mining area.

The processing module is mainly responsible for the processing of various monitoring data.

The storage module mainly includes data centers based on a local database, such as mining area dispatching center, data center, and group information center, which is responsible for the real-time storage of monitoring data [9, 10].

The application module is mainly the realization of the overall function of the system and its application in practice, including the application of PC based terminal and mobile terminal.

4.2. Overall System Structure Analysis. The software model for the coal mine climate management product based on the smart terminal, as shown in Figure 4, has three main components, each of which has the following function: contains information, a server, and a smart terminal.

The server side stores the data managed by the DataServer at the data generator in real time, stored in the internal data, and then sent to the smart terminal. The terminal successfully divides the coal mine safety monitoring system into four systems according to the requirements of the position:

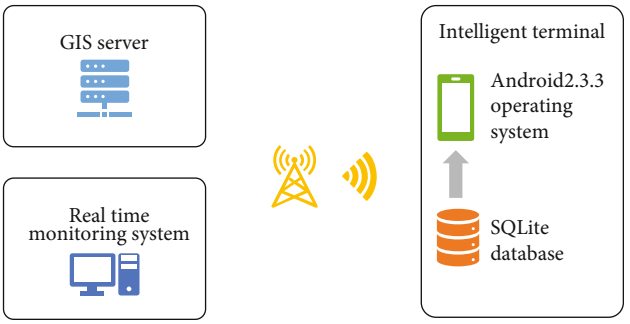

Figure 6: Overall structure of coal mine monitoring GIS system based on an Android platform.

real time monitoring system, covert video monitoring system, commands, and GIS system. As seen in Figure 5, it is synchronized with the existing coal mine safety monitoring system and has reliable and real-time performance.

4.3. Design and Implementation of GIS System

4.3.1. Overall Structure Design of GIS System. Coal mine safety monitoring GIS system based on intelligent terminal is a visual monitoring platform based on geographic data and the comprehensive use of geographic information system, mobile communication, network, and other technologies. It provides fast, accurate, and visual information services for the macro management, command, coordination, and dispatching of leaders and principals at all levels and changes the traditional coal mine management mode. As shown in Figure 6, the coal mine safety monitoring GIS system based on Android platform mainly includes three parts: GIS Server, intelligent terminal, and real-time monitoring system [11].

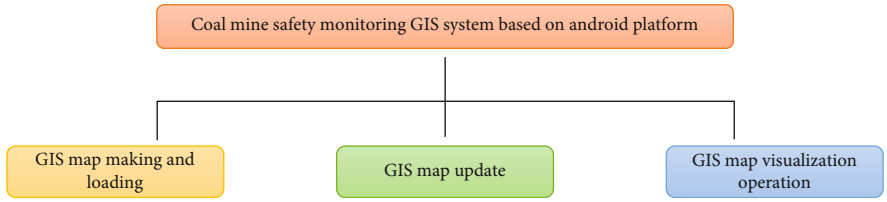

Figure 7: Functions of coal mine safety monitoring GIS system based on an Android platform.

Intelligent terminal, namely, mobile terminal, adopts Android2.3.3 operating system and SQLite database. It mainly realizes the update of GIS map and the visualization function of coal mine safety monitoring GIS system based on Android platform, including the enlargement, reduction and translation of mining area map, the query of measuring point information, and the alarm and early warning in case of abnormal data of measuring point sensor. All data queried are provided by SQLite database. The real-time monitoring system is mainly responsible for the real-time transmission of monitoring data between the central server and the intelligent terminal and stores the transmitted data in the SQLite database of the intelligent terminal in real time, forming a data linkage mode with the GIS system [12].

4.3.2. Functional Module Design of the System. The main functions of GIS-based map updating and GIS-based map making are shown in Figure 7.

(1) GIS Map Making and Loading. Realize the conversion from CAD engineering drawing of mining area to shape file format suitable for intelligent terminal, the generation and editing of GIS map, the creation of SD card of intelligent terminal, and the loading and display of GIS map of intelligent terminal.

(2) GIS Map Update. Realize the real-time update of GIS map in mining area, and update the map in real time according to the changes of sensors and roadways, including whether the map is updated or not and real-time map acquisition.

(3) GIS Map Visualization Operation. It realizes the visual operations such as zoom in, zoom out, translation, and survey point information query of the mining area map. According to the positioning search of sensors, roadways, and working faces, the found roadways, sensors, and other elements are displayed with corresponding flashes. Users can view their details (including attribute information and data information) by clicking the sensor elements.

(4) Design of Terminal Database. The main function of data management of intelligent terminal is to realize real-time data management. It is the core of the whole intelligent terminal software system. Its design is directly related to the efficiency of system execution and the stability of the system. At the same time, based on the security considerations in the coal mining industry, when the terminal system logs in to the central server to request services, it is necessary to set up a certain security authority inspection mechanism to provide the authentication function of the user's job identity, effectively distinguish the manager's own functional domain, prevent the illegal terminal from tampering and stealing the production information of the central server, and ensure the absolute security of production information [13]. The processing flow of user authority management is shown in Figure 8.

We choose SQLite as the intelligent terminal database, which mainly stores and manages the coal mine safety production data, monitoring coal mine information, dispatching user information, and other data. According to the above system requirements, we will establish various tables in the database and the corresponding words, field types, and field values in the table. The database Table name and the corresponding fields in each Table are Pinyin characters of Chinese names [14]. The intelligent terminal involves the data Table in Table 1.

Sensor attribute information includes measuring point number (cdbh), installation location (azdd), name (mc), type (lx), unit (dw), lower range limit (lcxx), upper range limit (lcsx), lower alarm limit (bjxx), and upper alarm limit (bjsx), as shown in Table 2.

Sensor data information includes sensor number (cgqbh), data volume (sjl), year month day (nyr), and time (sj), as shown in Table 3.

In order to meet the application environment, construct the optimal database, make it more effective to store and query data, and meet various operation needs of users; the following principles should be followed in the design of database GIS:

(1) Data conservation: during the design process, developers should check for remodeling if they are unsure about the availability of library design
(2) Registration: all lists of files, table names, and field names must comply with the common law to assist in the creation, modification, editing, and research
(3) Capacity control of library table: since SQLite is a lightweight database and the memory of handheld terminal is limited, the library Table should be cleared and updated in real time to ensure the real-time and effectiveness of intelligent terminal data [15]

4.4. GIS System Software Overall Design

4.4.1. Software Development Strategy. The Android operating system is divided into four stages: application layer, application layer, main library layer, and Linux kernel layer. Its structure is shown in Figure 9.

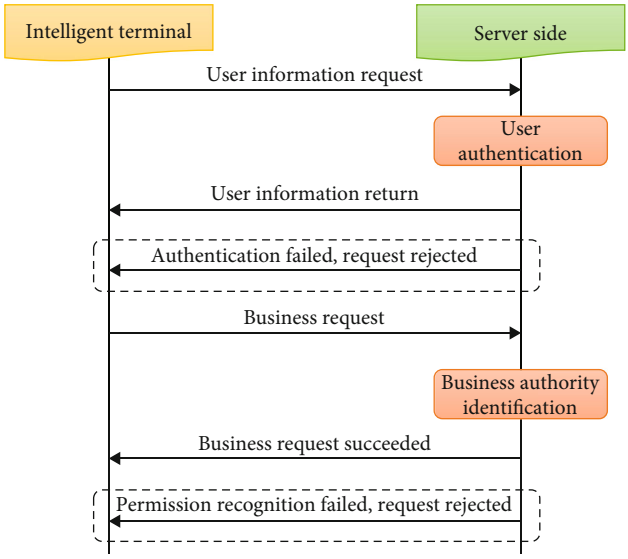

Figure 8: User authority authentication.

Table 1: Data Table in GIS database.

Table name	Name	Function
cgqsxb	Sensor property sheet	Description of sensor installation position, type, upper range limit and lower range limit
cgqsjb	Sensor data sheet	Real time monitoring data of sensor

Table 2: Message format of sensor attribute information package.

Field	Data type
cdbh	vachar
azdd	vachar
mc	vachar
lx	vachar
dw	vachar
lcxx	vachar
lcsx	vachar
bjxx	vachar
bjsx	vachar

Table 3: Format of sensor data packet message.

Field	Data type
cgqbh	vachar
sjl	vachar
nyr	vachar
sj	vachar

The application layer is a collection of a series of core applications of Android system, in which all applications are written in Java language. Its core programs include e-mail client, SMS (short message) sequence, calendar, Google map, and web browser.

An application layer is designed to create applications for the Android platform application layer. Developers have access to the API system used by the main application. The software architecture is used to facilitate the reuse of software products. Each program can publish its own task blocks, and any other program can publish task reports.

The base library layer contains C/C++ libraries used in various components of the Android system, including the main library, which provides most of the functions of Java programming languages at home [16].

The Linux kernel layer is the system kernel layer. Android core system services depend on the Linux 2.6 kernel, mainly adding a virtual CPU named goldfish and specific driver code required by Android runtime [17].

4.4.2. Software Function Model Design. The software model of coal mine safety monitoring GIS system based on Android platform mainly includes two parts: server and intelligent terminal, as shown in Figure 10.

The intelligent terminal mainly includes a map update module and a map visualization module [18]. The map update module mainly judges whether the map is updated or not. If there is a map update, it sends a download request to the server, receives the map file sent by the server, and saves it on the local disk. The map visualization module mainly completes the map enlargement, reduction, translation, survey point information query (query the data in the SQLite database table, including attribute information and data information), and monitoring point sensor alarm and early warning (query the SQLite database Table in real time to monitor the survey point, and if the data of the survey point sensor is abnormal, the survey point graphic element flashes) to realize the real-time monitoring of safety production in the mining area [19].

4.4.3. Design of GIS Map Visualization Function. The visualization function of coal mine safety monitoring GIS system based on Android platform mainly includes GIS map enlargement, reduction, translation, measuring point sensor information query, and alarm and early warning. Its visual function software model is shown in Figure 11.

The user enters the GIS monitoring system, starts the timer, opens the database, queries the data volume, alarm lower limit and alarm upper limit of all monitoring point sensors in the database table, and judges the abnormal data volume of the monitoring point. If the data quantity of the measuring point is less than the lower limit of the alarm or the data quantity is greater than the upper limit of the alarm, the element of the measuring point flashes an alarm warning; otherwise, continue to judge the abnormal data quantity of the measuring point.

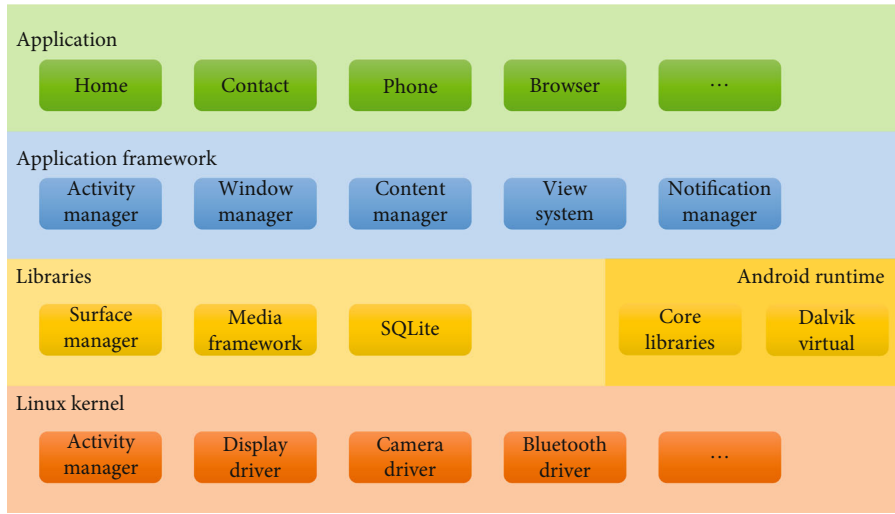

Figure 9: Android operating system.

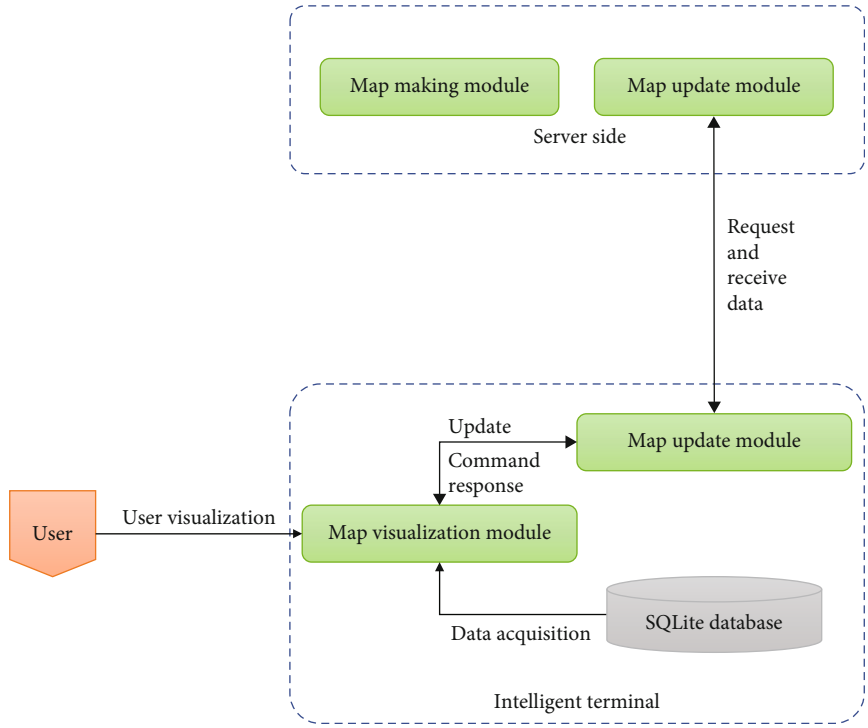

Figure 10: Software function model of coal mine safety monitoring GIS system based on Android platform.

5. System Function Test

5.1. System Test Environment. System testing is to check whether the developed application system meets the requirements in the system requirement specification. It is an important means to ensure the system quality and a necessary work before delivery to the target user [20]. Before the system test, the system test environment must be determined according to the selected development technology and system application scale to ensure the accuracy of the test results [21]. As the coal mine safety production monitoring system is composed of application layer system, network layer, and hardware layer, the actual test environment will be established during the specific test, and the function and performance of the application layer system will be tested with test tools. The test environment selected for this system test is as follows:

5.1.1. Software Environment. For the software environment, the following are used:

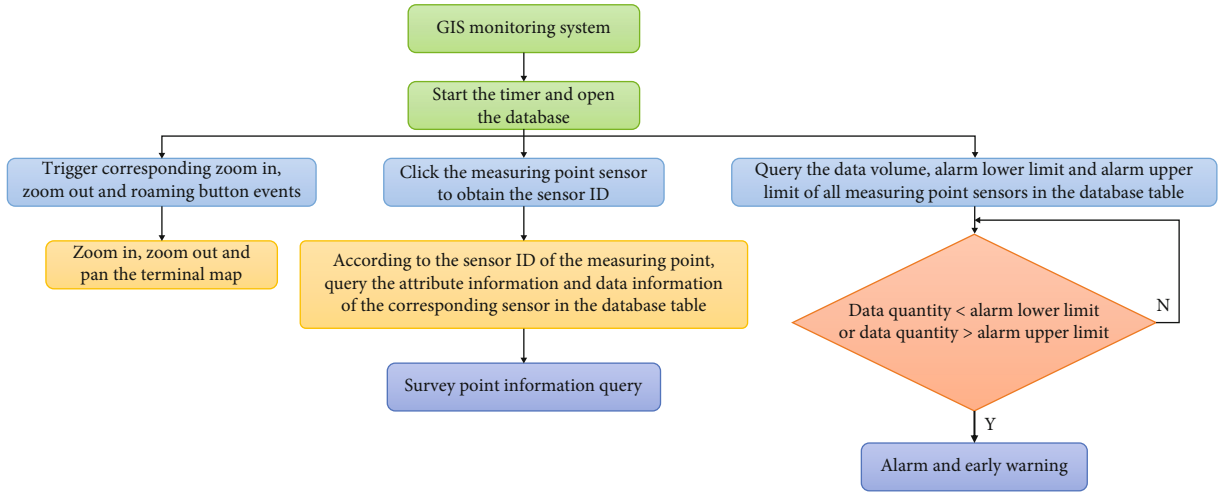

Figure 11: Schematic diagram of GIS visualization function software design.

(i) Operating system: Windows Server 2012 R2

(ii) Web server application tool: Java 1.8 + Tomcat 8

(iii) Database management software: Oracle 11g

(iv) Web browser tools: Firefox, Chrome, and other system versions

5.1.2. Hardware Environment. For the hardware environment, the following are used:

(1) Server hardware environment: Lenovo system x3650 M4 (Intel Xeon E5-2600 ∗ 2, ECC DDR332gb, eight 2.5-inch 300GB SAS hard disks)

(2) Client hardware environment: Lenovo Yangtian t4900v (Intel Core i5 4570; 4GB DDR3; 1TB hard disk)

5.1.3. Test Simulation Environment. In order to verify the actual test effect, a coal mine 2 mining area in Gansu Province was selected for the simulation test. The mining area 2 is located about 120 m underground, with a mine channel of 2 m wide and 2.5 m high, with a right angle bend in the middle. All kinds of sensor equipment required for transmission are deployed in the middle of the mining area; networking is carried out according to the network layer networking scheme and connected with the application system server of the monitoring center through the industrial Ethernet ring network [22].

5.2. System Function Test. After continuous development and improvement of software testing technology, some function testing methods have been produced in system function testing, and the most commonly used system function testing method is black box testing. A black box test means that the tester regards the tested system as a black closed box in the test process; that is, the tester only tests the external functional characteristics of the tested system on the premise of completely knowing the content, logical structure, and logical path of the tested system. It can be seen that the black box test is a test method focusing on the external functions of the tested system [23]. In the specific function test, the tester first designs the test case according to the system requirement specification and then simulates the operation from the perspective of the operator to verify that the system can correctly receive the data entered by the operator or initiate the business operation and that the system can output the correct operation results; that is, compare whether the expected output is consistent with the actual output. If it is consistent, the test item is considered to pass; otherwise, it is not passed [24].

The system will use the black box test to test the function, but because the system function is too complex, there are many test cases designed. The following only introduces the test process of some test cases [25].

5.2.1. Alarm Threshold Setting Function Test Process. The alarm threshold setting function test case is used to verify whether the functions of adding, editing, and deleting alarm threshold information meet the expected requirements. In the specific test process, based on the operator's point of view, simulate the input of corresponding data or initiate corresponding operations to verify whether the output results are consistent with the expected output results. The specific test process is shown in Table 4.

5.3. Substation Management Function Test Process. The substation management function test case is used to verify whether the information addition, editing, deletion, and query functions of substation information meet the expected requirements. The specific test process is shown in Table 5.

The above test process of the system function test is introduced through the test process of the two function test cases. Due to the limitation of the length of the paper, the above test process only discusses the test process under the condition of inputting effective data. Through the above test results, it is found that all the function tests of the two function tests pass under the condition of inputting effective data. In the actual test process, the tester carried out the test in strict accordance with the system requirement specification and considered the input of valid data, invalid data, and other situations, comprehensively, scientifically, and reasonably tested the function of the system. During the first

Table 4: Alarm threshold setting function test process.

Test function	Input action	Expected output	Test result
Alarm threshold information addition	Select the alarm threshold setting function of the secondary menu under the environmental monitoring subsystem, select "add" on the main page, and enter the alarm threshold on the add page	The system outputs a prompt message: "alarm threshold information added successfully!"	Pass
Alarm threshold information editing	Information, click "save"	The system outputs a prompt message: "alarm threshold information edited successfully!"	Pass
Alarm threshold information deletion	Select the alarm threshold setting function of the secondary menu under the environmental monitoring subsystem, select a record on the main page, and click the "Edit" button to enter the alarm threshold information editing page. Edit the information on the page and "save"	The system outputs a prompt message: "are you sure to delete this alarm threshold information?" Click "confirm" to complete the deletion and return to the main page of alarm threshold information setting; click "cancel" to return to the main page without deletion	Pass

Table 5: Substation management function test process.

Test function	Input action	Expected output	Test result
Substation information addition	Select the secondary menu substation management function under the system management subsystem, select "add" on the main page, enter substation information on the add page, and click	The system outputs a prompt message: "substation information added successfully!"	Pass
Substation information editing	Click save	The system outputs a prompt message: "substation information edited successfully!"	Pass
Substation information deletion	Select the secondary menu substation management function under the system management subsystem, select a record on the main page, and click the "Edit" button to enter the substation information editing page. Edit the information on the page and "save"	The system outputs a prompt message: "are you sure to delete this substation information record?" Click "confirm" to complete the deletion and return to the main page of substation management; click "Cancel" to return to the main page without deletion	Pass
Substation information query	Select the secondary menu substation management function under the system management subsystem, select a substation information record on the main page, and click "delete"	If the query criteria has data, the system outputs the substation records that meet the query results in a list. If no data is queried, the output prompt: "no data is queried, please re-enter the query criteria!"	Pass

round of testing, a total of 1 function omission, 3 serious errors, 14 general errors, and 21 minor errors were found. After finding the test problems, the errors and function omissions were repaired, and then, the regression test was carried out. Through the regression test, it was found that the problems found in the early stage had been modified and did not cause new problems, indicating that the system function test passed.

Although the system data collection does not have specific functions in the presentation layer, all monitoring data in the system come from the data collection in the background of the system. Since data acquisition is the basis of

Table 6: Test results of data acquisition.

	Reported data volume	Amount of data collected/accurate	Result
Acquisition success rate	3600	3600	100%
Data accuracy	3600	3600	100%

Table 7: System performance test results.

Performance index	Demand value	Test value	Test result
Average response time of all services	<3 seconds	1.976 seconds	Pass
Average response time of statistical analysis and query business	<5 seconds	2.779 seconds	Pass
Transaction pass rate	>99.88%	100%	Pass
Average CPU utilization of web application server	<65%	41.73%	Pass
Average memory utilization of web application server	<65%	57.31%	Pass
Average CPU utilization of database server	<65%	44.52%	Pass
Average memory utilization of database server	<65%	61.32%	Pass

the operation of the system, it is necessary to test the success rate and accuracy of data acquisition. In the specific test process, 30 sensors in the simulated 1 mining area are configured to report data every 30 seconds for 60 minutes, and the total amount of data reported is 3600 data records. At the same time, the data stored in the local sensor network node is recorded to compare the accuracy of the uploaded data. The specific test results are shown in Table 6.

Through the results in Table 6, it is found that the success rate and accuracy rate of data acquisition are 100%, meeting the acquisition requirements. According to the system performance requirements, the planned number of concurrent users of the system is 1000. This test environment is a single web application server and database server, and no load balancing scheme is built. During the specific test, 1000 virtual users are simulated through LoadRunner, and the test script and running scenario are configured according to the LoadRunner test process. In the configured running scenario, the concurrent load of 1000 virtual users is initiated on the system for 180 minutes. Various performance indicators are tracked in the whole process. The final performance test results are shown in Table 7.

According to the test results shown in Table 7, under the high load condition of 1000 virtual concurrent users, all performance indexes of the system meet the system performance requirements, indicating that the system performance is passed.

6. Conclusion

Firstly, by consulting a large number of documents, this paper compares and analyzes several popular operating systems based on mobile terminals. The results show that Android operating system is one of the most potential smartphone platforms at present and makes a simple study on the system architecture of Android platform. On this basis, this paper selects various key technologies, puts forward the overall research scheme and architecture of coal mine safety monitoring GIS system based on an Android platform, and describes in detail the overall design idea of the system and the code implementation of some functional modules, such as the visual operation of mining area map and real-time update of mining area map. The realization of the system provides a set of solutions suitable for the enterprise's own personnel movement, real time, and efficient office for the production of modern coal mining enterprises.

On the basis of mobile network, combined with the technical scheme and application mode of coal enterprise safety production monitoring system, a research scheme of coal mine safety production monitoring system based on intelligent terminal is proposed on the basis of the original fixed network coal mine safety production monitoring system. This paper makes a detailed demand analysis and design, architecture design, functional module design, and partial code implementation of the coal mine safety monitoring GIS system based on an Android platform. According to the mobile application solution, this paper studies the key technologies involved in the software development based on intelligent terminal, including the selection of intelligent terminal platform, the selection of GIS software suitable for intelligent terminal, and socket technology, and constructs a software development platform with strong universality.

According to the actual situation and the particularity and importance of mining area production information, the production, generation, real-time update, and real-time download of GIS map are realized on the GIS Server. This paper describes in detail the download process and code implementation of GIS Server-side software and terminal software, establishes the application mode of coal mine safety monitoring GIS system based on Android platform associated with mining area production real-time monitoring system and dispatching system, and realizes the seamless connection between coal mine safety production monitoring systems based on intelligent terminal in the real sense. The

system software uses Java language to code it. In the first round of test, one function omission, three serious system errors, 14 general errors, and 21 minor errors are found. The accident passing rate of the second test is greater than 99.88%, and all performance indexes of the system meet the performance requirements, which proves the feasibility of the system.

Data Availability

The datasets used and/or analyzed during the current study are available from the corresponding author on reasonable request.

Conflicts of Interest

The author declares that there are no competing interests.

References

[1] Y. Deng, L. Song, Z. Zhou, and P. Liu, "An approach for understanding and promoting coal mine safety by exploring coal mine risk network," *Complexity*, vol. 2017, Article ID 7628569, 17 pages, 2017.

[2] A. Susanto, D. O. Setyawan, F. Setiabudi, Y. M. Savira, and M. Tejamaya, "Gis-based mapping of noise from mechanized minerals ore processing industry," *Noise Mapping*, vol. 8, no. 1, pp. 1–15, 2021.

[3] N. M. Vusovic, M. Vlahovi, M. Ljubojev, M. Vlahovi, and D. Krzanovic, "Software solution for the mine subsidence prediction based on the stochastic method integrated with the gis," *Mining and Metallurgy Engineering Bor*, vol. 8, 2020.

[4] I. R. Orimoloye and O. O. Ololade, "Spatial evaluation of land-use dynamics in gold mining area using remote sensing and gis technology," *International journal of Environmental Science and Technology*, vol. 17, no. 11, pp. 4465–4480, 2020.

[5] Y. Liu, J. Liu, B. Yang, and S. Yuan, "Assessing water and sand inrushes hazard reductions due to backfill mining by combining gis and entropy methods," *Mine Water and the Environment*, vol. 40, no. 4, pp. 956–969, 2021.

[6] I. Minea, D. Boicu, O. E. Chelariu, M. Iosub, and A. Enea, "Assessment of recharge capacity potential of groundwater using comparative multi-criteria decision analysis approaches," *Journal of Geographical Sciences*, vol. 32, no. 4, pp. 735–756, 2022.

[7] A. Sobolewski and N. Sobolewski, "Holistic design of wetlands for mine water treatment and biodiversity: a case study," *Mine Water and the Environment*, vol. 41, no. 1, pp. 292–299, 2022.

[8] F. Fenando, "Sistem informasi geografis (sig) pemetaan lokasi pertambangan batu bara berbasis quantum gis (studi kasus: pt. hasil bumi kalimantan)," *Journal of Information Systems and Informatics*, vol. 3, no. 1, pp. 108–120, 2021.

[9] B. Li, T. Li, W. Zhang, Z. Liu, and L. Yang, "Multisource information risk evaluation technology of mine water inrush based on VWM: a case study of Weng'an coal mine," *Geofluids*, vol. 2021, Article ID 8812144, 12 pages, 2021.

[10] Z. Qiang, Y. Wang, K. Song, and Z. Zhao, "Mine consortium blockchain: the application research of coal mine safety production based on blockchain," *Security and Communication Networks*, vol. 2021, Article ID 5553874, 10 pages, 2021.

[11] R. Viradia, F. Annie, M. Kali, F. Pollock, and J. D. Hayes, "Hand injuries of coal miners in southern West Virginia: a pilot study on health-care resources in southern West Virginia," *Journal of Emergencies Trauma and Shock*, vol. 14, no. 1, pp. 18–22, 2021.

[12] Z. Yan, Y. Wang, and J. Fan, "Research on safety subregion partition method and characterization for coal mine ventilation system," *Mathematical Problems in Engineering*, vol. 2021, Article ID 5540178, 11 pages, 2021.

[13] F. Wenjun, Y. Xu, L. Liu, and L. Zhang, "Design and research of intelligent safety monitoring robot for coal mine shaft construction," *Advances in Civil Engineering*, vol. 2021, Article ID 6897767, 16 pages, 2021.

[14] N. Maksimovich, O. Berezina, O. Meshcheriakova, and A. Demenev, "Research of migration of technogenic bottom sediments with application of modern geoinformation systems," *Inter Carto Inter GIS*, vol. 26, no. 2, pp. 201–211, 2020.

[15] G. Bai and T. Xu, "Coal mine safety evaluation based on machine learning: a BP neural network model," *Computational Intelligence and Neuroscience*, vol. 2022, Article ID 5233845, 9 pages, 2022.

[16] D. P. Mishra, D. C. Panigrahi, P. Kumar, A. Kumar, and P. K. Sinha, "Assessment of relative impacts of various geo-mining factors on methane dispersion for safety in gassy underground coal mines: an artificial neural networks approach," *Neural Computing and Applications*, vol. 33, no. 1, pp. 181–190, 2021.

[17] I. Muhire, V. Manirakiza, F. Nsanganwimana, M. Nyiratuza, T. A. Inzirayineza, and A. Uworwabayeho, "The environmental impacts of mining on gishwati protected reserve in Rwanda," *Environmental Monitoring and Assessment*, vol. 193, no. 9, pp. 1–24, 2021.

[18] N. Singh, A. Shandilya, R. K. Tripathi, and K. K. Sharma, "Spatio - temporal landcover dynamics and environmental impact in coal mine area of Korba district (Chhattisgarh)," *IOP Conference Series Materials Science and Engineering*, vol. 1116, no. 1, article 012182, 2021.

[19] N. Vuovi, M. Vlahovi, and D. Kranovi, "Stochastic method for prediction of subsidence due to the underground coal mining integrated with gis, a case study in Serbia," *Environmental Earth Sciences*, vol. 80, no. 2, pp. 1–29, 2021.

[20] Y. Choi, J. Baek, and S. Park, "Review of gis-based applications for mining: planning, operation, and environmental management," *Applied Sciences*, vol. 10, no. 7, p. 2266, 2020.

[21] A. Sharma, R. Kumar, M. Talib, S. Srivastava, and R. Iqbal, "Network modelling and computation of quickest path for service-level agreements using bi-objective optimization," *International Journal of Distributed Sensor Networks*, vol. 15, no. 10, Article ID 5325116, 2019.

[22] J. Jayakumar, B. Nagaraj, S. Chacko, and P. Ajay, "Conceptual implementation of artificial intelligent based E-mobility controller in smart city environment," *Wireless Communications and Mobile Computing*, vol. 2021, Article ID 5325116, 8 pages, 2021.

[23] L. Xin, M. Chengyu, and Y. Chongyang, "Power station flue gas desulfurization system based on automatic online monitoring platform," *Journal of Digital Information Management*, vol. 13, no. 6, pp. 480–488, 2015.

[24] R. Huang, S. Zhang, W. Zhang, and X. Yang, "Progress of zinc oxide-based nanocomposites in the textile industry," *IET Collaborative Intelligent Manufacturing*, vol. 3, no. 3, pp. 281–289, 2021.

[25] C. Liu, M. Lin, H. Rauf, and S. Shareef, "Parameter simulation of multidimensional urban landscape design based on nonlinear theory," *Nonlinear Engineering*, vol. 10, no. 1, pp. 583–591, 2021.

Hindawi
Wireless Communications and Mobile Computing
Volume 2022, Article ID 8079543, 12 pages
https://doi.org/10.1155/2022/8079543

Research Article

Application of Inclination Sensor in Real-Time Remote Monitoring System of Tunnel Structure Deformation

YuFeng Xu,[1] **Yiming Li**,[1] **and Jianfa Qiu**[2]

[1]*School of Civil Engineering and Transportation, South China University of Technology, Guangzhou 510640, China*
[2]*Architectural Design Research Institute of South China University of Technology Co., Ltd., Guangzhou, 510640 Guangdong, China*

Correspondence should be addressed to Jianfa Qiu; jfqiu@scut.edu.cn

Received 2 July 2022; Accepted 28 July 2022; Published 31 August 2022

Academic Editor: Jun Ye

Through the "real-time monitoring system," the inclination sensor can realize the real-time automatic monitoring of the existing lines within the influence scope of the subway structural engineering, which can provide timely and reliable information for the construction unit, so as to evaluate the safety of the project during the construction and the impact of the construction on the existing line, as well as the possible hidden dangers or accidents that may endanger the construction and the environmental safety of the existing line subway. Make timely and accurate forecast, so as to take effective measures to eliminate hidden dangers and avoid accidents.

1. Introduction

During subway construction, the shield construction process of newly constructed tunnels not only affects the initial stress state of the surrounding soil but also disturbs the surrounding strata. It causes the loss of surrounding stratum and the seepage of water in the stratum, resulting in soil consolidation and settlement, which in turn causes horizontal or vertical displacement of the surrounding soil, thereby causing deformation of the surrounding work. The deformation value that the internal structure of the subway and the section equipment can withstand is limited, and serious safety accidents may occur after exceeding a certain limit [1].

Generally speaking, the occurrence of engineering hazards is predictable. Only sufficient monitoring frequency density can detect continuous signs of change from monitoring data and real-time automatic monitoring of existing lines within the influence scope of subway structural engineering; it can provide the construction unit with timely and reliable information to assess the safety of the project during construction and the impact of construction on the existing line and make timely and accurate forecasts for possible hidden dangers or accidents that may endanger construction and the environmental safety of existing subway lines, in order to take effective measures in time to eliminate hidden dangers and avoid accidents.

Tunnel deformation monitoring generally uses total station monitoring; the total station has the advantages of large instrument size and easily damaged measuring points and is easily limited by measurement conditions. It is difficult to continue to use in the absence of light, and the cost of the instrument is high, and the test accuracy is low. Real-time remote monitoring cannot be realized [2].

Inclination sensor is an instrument for measuring the horizontal angle of a structure, which is widely used in bridge erection and other aspects. However, its application in the deformation monitoring of subway tunnels is still relatively small. Compared with other deflection measurement methods, the inclination sensor has its unique advantages.

This paper takes the application of the inclination sensor in the real-time monitoring system of the tunnel structure deformation of a project as the background. The tilt sensor is easy to install, is not limited by measurement conditions, and has high accuracy, which provides accurate and reliable values for the tunnel structure deformation real-time monitoring system. In order to provide theoretical guidance and data support for the realization of the real-time monitoring system of tunnel structure deformation and by comparing

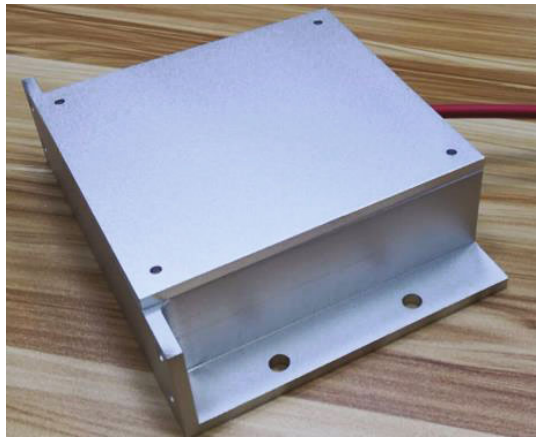

Figure 1: Inclination sensor.

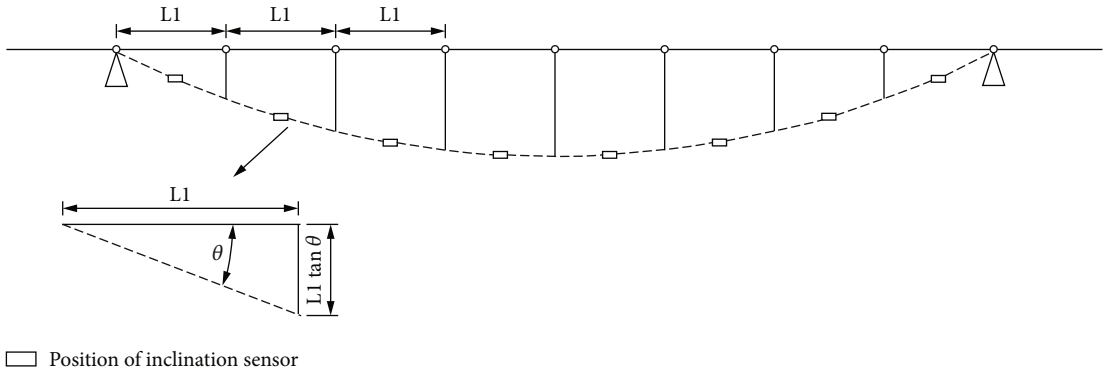

Figure 2: Schematic diagram of deflection calculation method.

the measurement of the inclination sensor with the measurement of the traditional total station, the feasibility of the real-time remote monitoring system for the deformation of the tunnel structure by the inclination sensor is verified.

2. Principle of Deformation Measurement by Inclination Sensor

Inclination sensor is an acceleration sensor that uses Newton's second law. It is a fixed inclination measurement instrument produced by using a dual-axis inclination sensor developed and produced by a microelectromechanical system as a sensitive element and combined with intelligent chip technology. It is used to observe the biaxial inclination angle of bridges, buildings, railways, and other structures relative to the horizontal [3]. It is suitable for the deformation of hidden parts that are difficult to be observed by conventional geodetic methods. It can be used for long-term testing with the automation system. The size of the tilt sensor is 120 mm × 150 mm × 40 mm, and the tilt sensor used is shown in Figure 1.

The schemes of converting deflection by inclination angle include using the least squares method to obtain a set of optimal solutions and directly integrating the inclination angle function to obtain the deflection value, but these methods involve relatively complex mathematical calculations [4]. Therefore, the simplest method of arranging measuring points and calculating deflection in the conversion process is selected for research: that is, select n positions on the structure to place the inclination sensor, as shown in Figure 2, assuming that the structural deformation is within the linear range. By loading the structure, the change value of the inclination angle before and after loading is obtained, and the tangent value of the inclination angle is multiplied by the distance of the segment to obtain the deflection value of the segment.

According to the knowledge of material mechanics, we know that the approximate differential equation of the deflection line of the beam is

$$\omega'' = -\frac{M(x)}{\mathrm{EI}}. \tag{1}$$

If it is a straight beam of equal cross-section, its bending stiffness EI is a constant, and the above formula can be rewritten as

$$\mathrm{EI}\omega'' = -M(x). \tag{2}$$

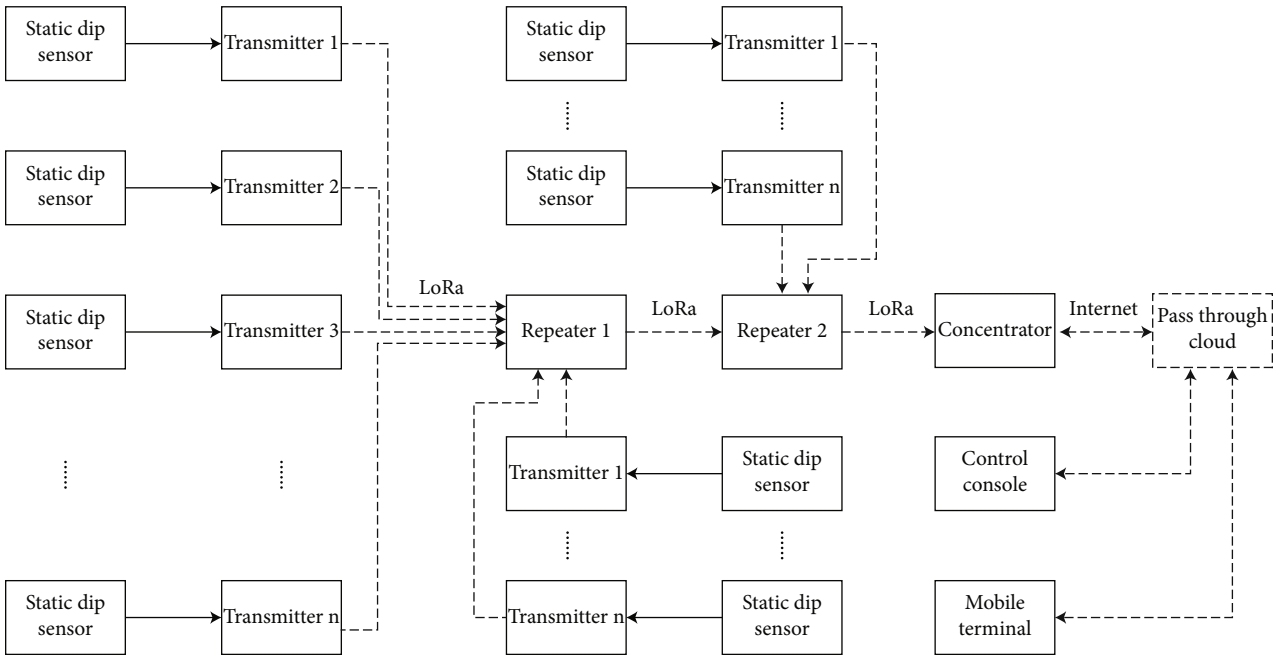

Figure 3: Flow chart of data acquisition.

Integrating the above equation once can get the angle equation of the beam:

$$\mathrm{EI}\omega' = -\int M(x)dx + C_1. \tag{3}$$

Integrate Equation (3) again to get the deflection curve equation of the beam.

To sum up, the corner of any section of the structure is equal to the corner of the deflection line at that point, that is, the angle between the tangent of the deflection line at this point and the x-axis [5]. There is a first-order integral relationship between the deflection of the beam and the corner. From this, we can obtain the deflection of the structure by measuring the angle of rotation at certain points when the structure is bent.

Given a beam of length L, divide the beam into n equal sections, each with a length of $L_1 = L/n$, a tilt sensor is placed at the midpoint of each segment. After the beam is loaded at a certain time, the beam deflects. The deflection increment for each segment is

$$\Delta\omega_i = L_1 \tan\theta_i. \tag{4}$$

Then, the deflection at the end of the i-th segment is the accumulation of the deflections of all segments in the previous $i-1$ segment, namely,

$$\omega_i = \sum_{1}^{i-1} L_1 \tan\theta_i, \tag{5}$$

where L_1 is the length of each segment, θ_i is the change value of the inclination angle at the midpoint of the i-th segment, that is, the measured value of the inclination sensor of this segment, $\Delta\omega_i$ is the deflection difference between the front and rear ends of the i-th segment, and ω_i is the deflection value at the end of the i-th segment. Calculation of deflection by measuring inclination is an indirect method, and deflection calculated by different mathematical models

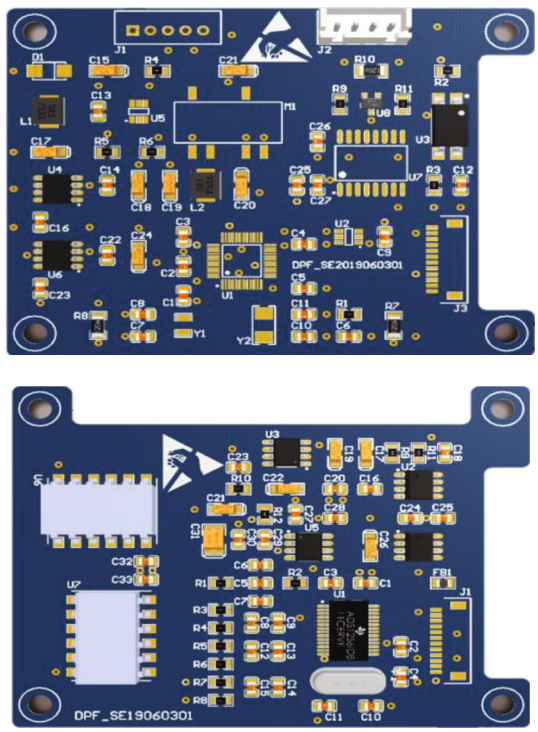

Figure 4: Inclination sensor base plate and expansion board.

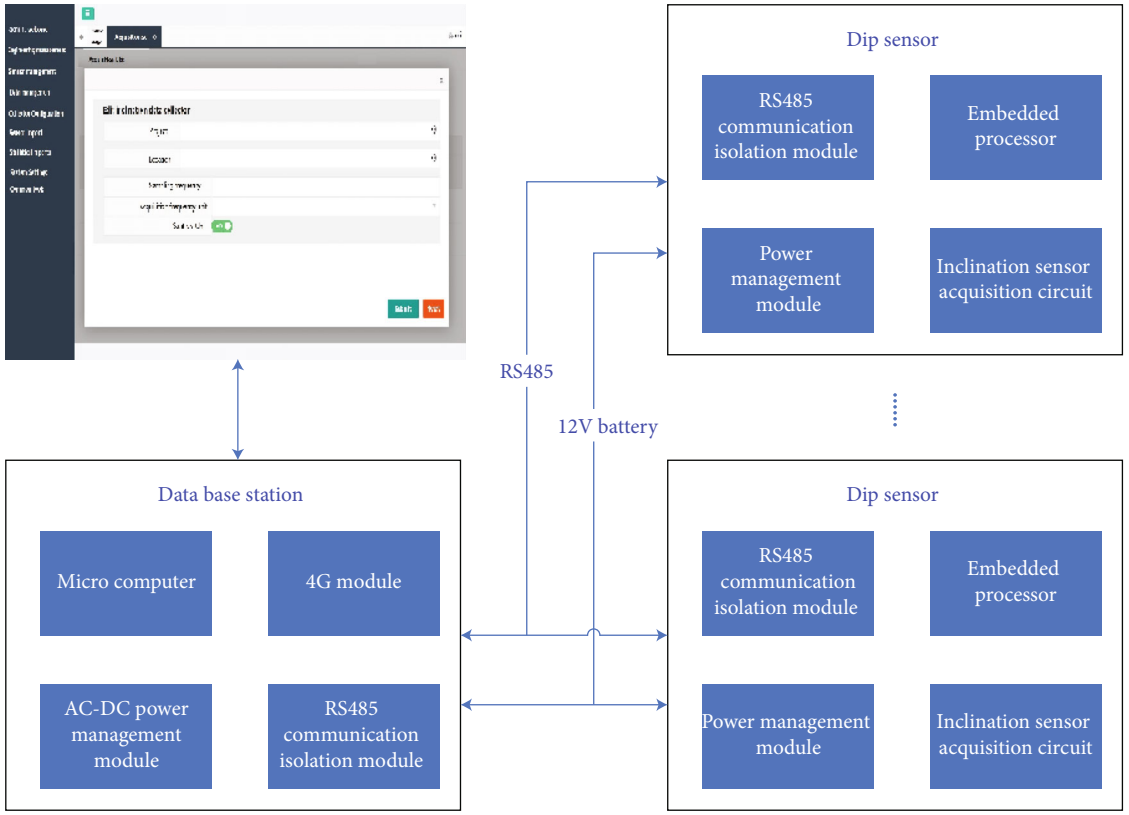

Figure 5: System topology.

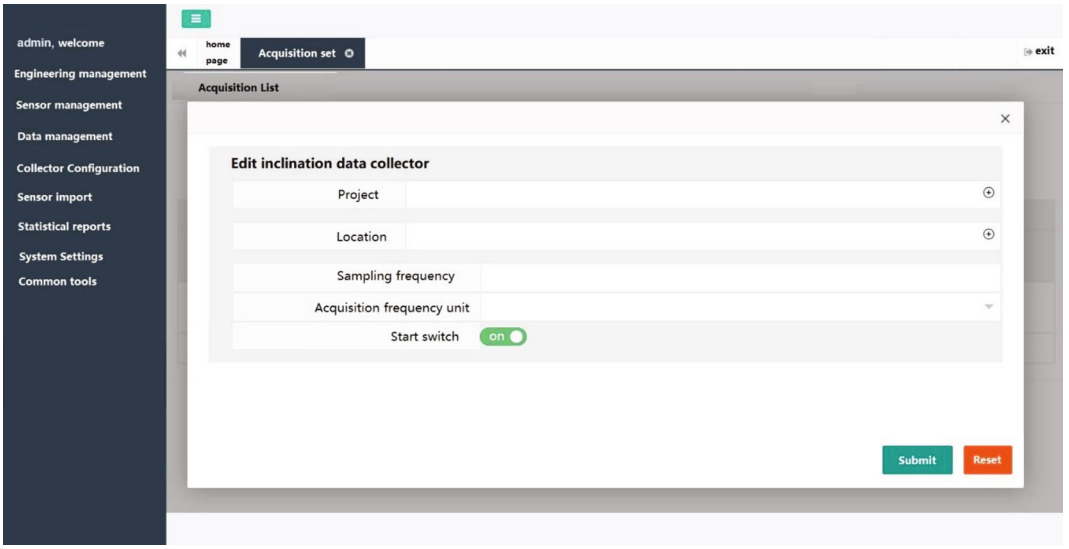

Figure 6: Data collection frequency setting diagram.

is an approximate result, not an exact deflection value. In this segmented calculation model, the calculation accuracy increases with the increase of the number of segments. Generally, when the number of segments is the same as the number of curves, the relative error between the calculated value and the actual value can reach a range of less than 5% [6].

3. Real-Time Monitoring System

The real-time monitoring system consists of four parts: inclinometer, data acquisition system, data transmission system, and main control computer terminal system. Data transmission adopts LoRa wireless network transmission. The relevant process is shown in Figure 3.

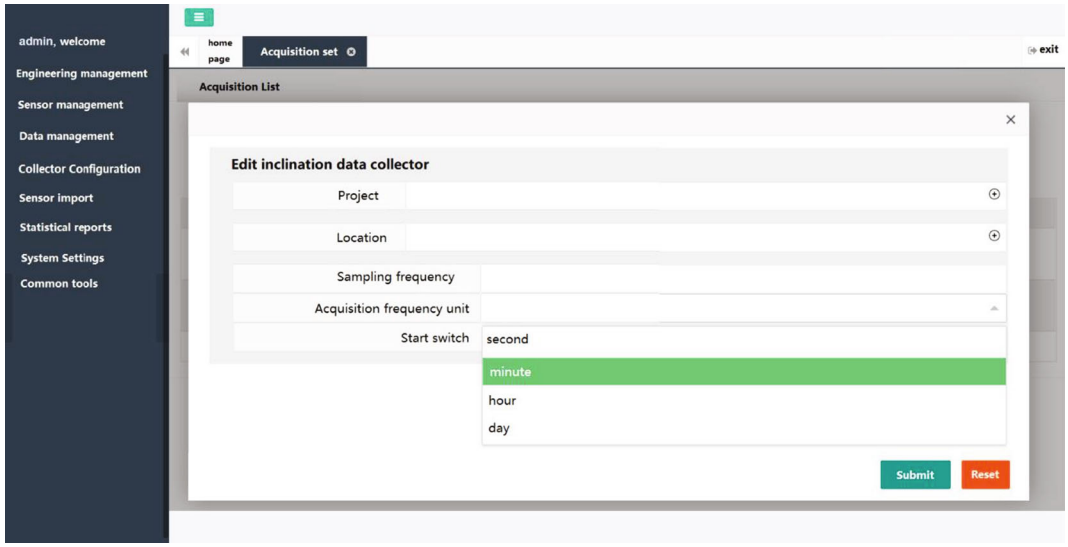

Figure 7: Data collection frequency setting diagram.

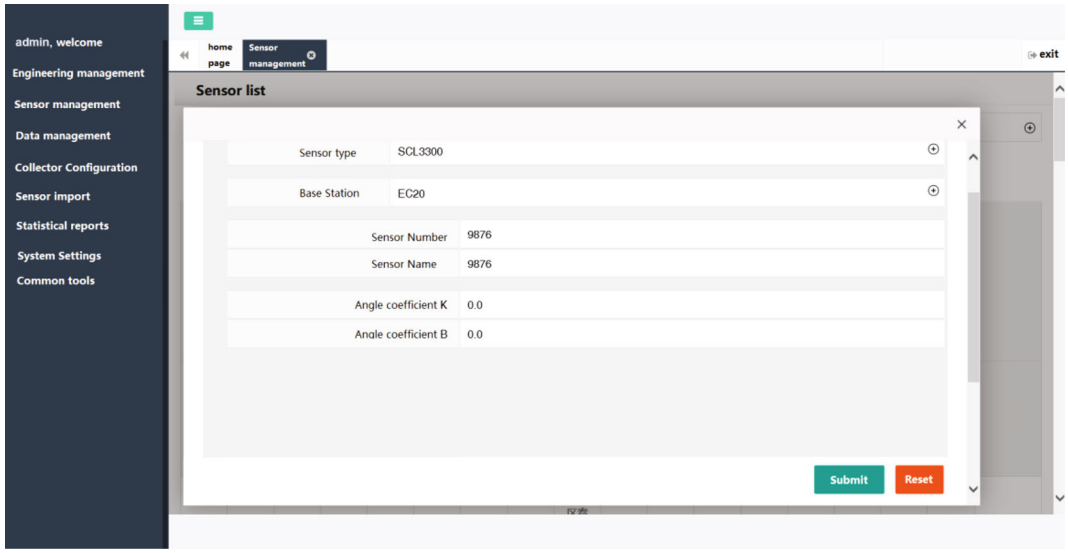

Figure 8: Start acquisition setup diagram.

The field implementation of the inclination sensor is carried out according to the following steps:

(1) 13 inclination sensors are arranged at the waist of the subway section, and the collection frequency and collection method are set on the collection software

(2) Click to start the measurement, and send the acquisition command to the sensor. The hardware can make all the inclination sensors receive the command at the same time. After receiving the command, the measurement is performed at the same time interval, and the measured data is stored in the sensor

(3) After sending the collection command, the sensor collects data at the same time interval. The collected data is first stored in the sensor, and then, the sensor returns the collected data to the terminal and decodes the data to obtain the sensor inclination value

4. Inclination Sensor Data Collection and Analysis

Currently, the on-board sensor has synchronous and synchronous detection, which is extremely important for structural measurements. The method of realizing synchronization can be realized by means of hardware and software, and the method of software can be realized by interpolation [7].

Synchronous acquisition technology is a bit synchronous communication technology. To achieve hardware

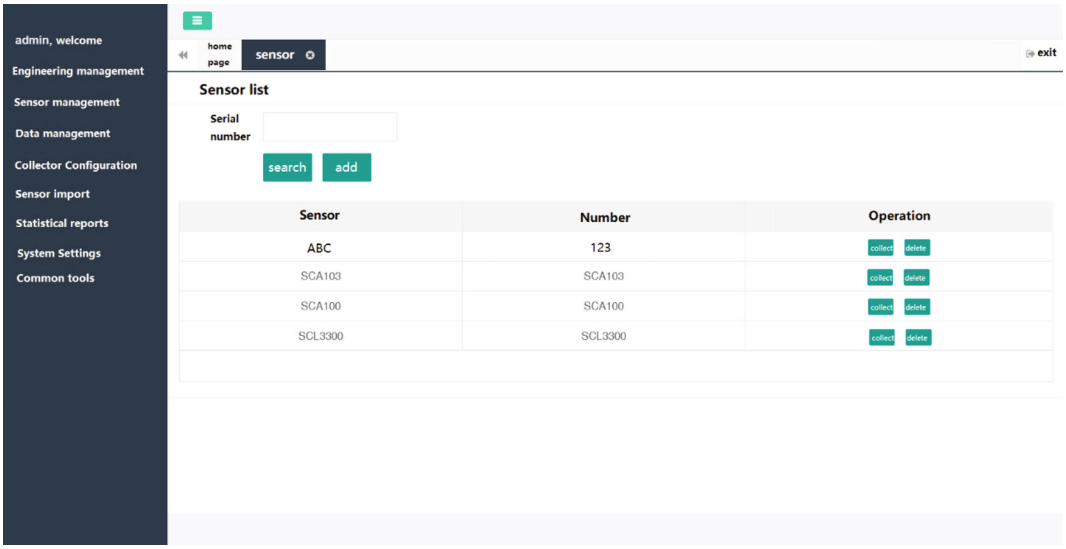

Figure 9: Collection result viewing diagram.

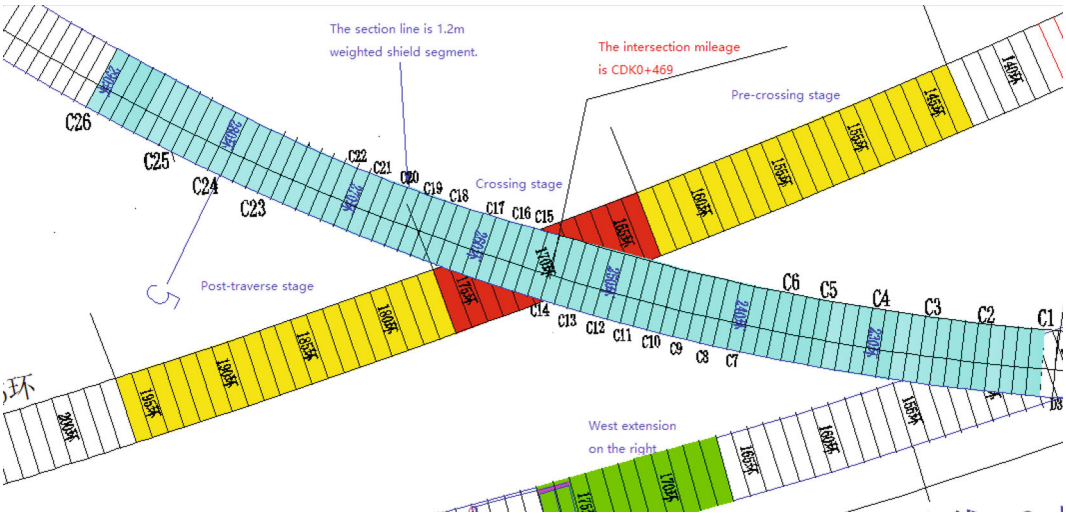

Figure 10: Layout of side points of total station.

synchronization, it is necessary for the sender and receiver to have clock signals with the same frequency and phase. When no data collection is required, the connection line is in the MARK state. When starting a measurement, the sender sends one or two sync characters. When the two sides are synchronized, they can send a large block of data continuously with a single character, so that the start and stop bits are no longer needed. During the sending process, both parties need to coordinate with a clock to determine the position of each bit in the serial transmission. When starting the measurement, the two sides use the synchronization character to keep the clock internally synchronized with the sender, and then input the data behind the synchronization character bit by bit, convert it into parallel format at the same time, and let the CPU read the data until the end character is received.

The synchronous acquisition adopts a common clock, and the synchronous acquisition has a high transmission frequency and realizes high-speed, large-capacity data transmission. The monitoring center application management system is at the heart of data analysis and display [8]. During data transmission, both parties must maintain complete synchronization, requiring the receiving and sending devices to have the same clock and maintain strict synchronization.

4.1. Technical Scheme of Inclination Sensor Acquisition. The system will adopt a bus topology [9] and connect the tilt sensor to the data base station through a 5-core shielded cable (12V, GND, D+, D-, S). The inclination sensor adopts the DPF_SE2019060301 version of the inclination sensor. As shown in Figure 4, the base plate and the expansion board of the inclination sensor are, respectively, packaged into an integrated inclination sensor through an aluminum casing. Electrical energy is the most precious resource of wireless sensor network, which determines the lifetime of wireless sensor network [10].

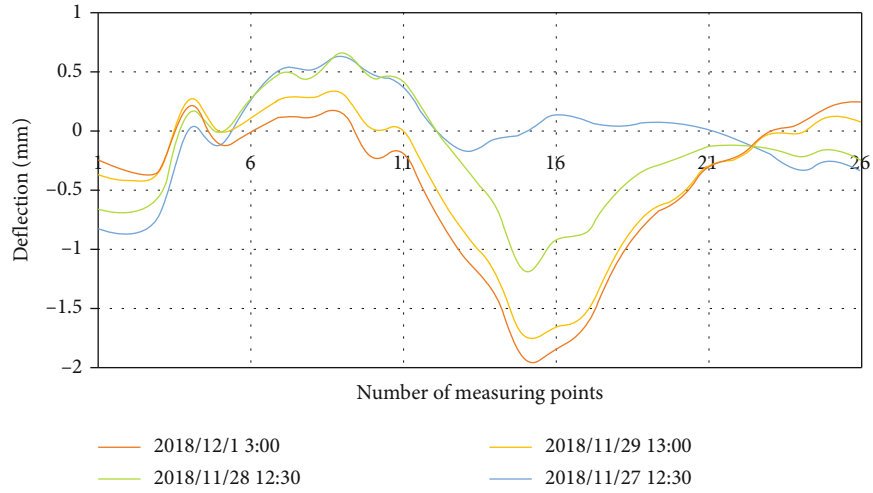

Figure 11: Deformation curve measured by total station.

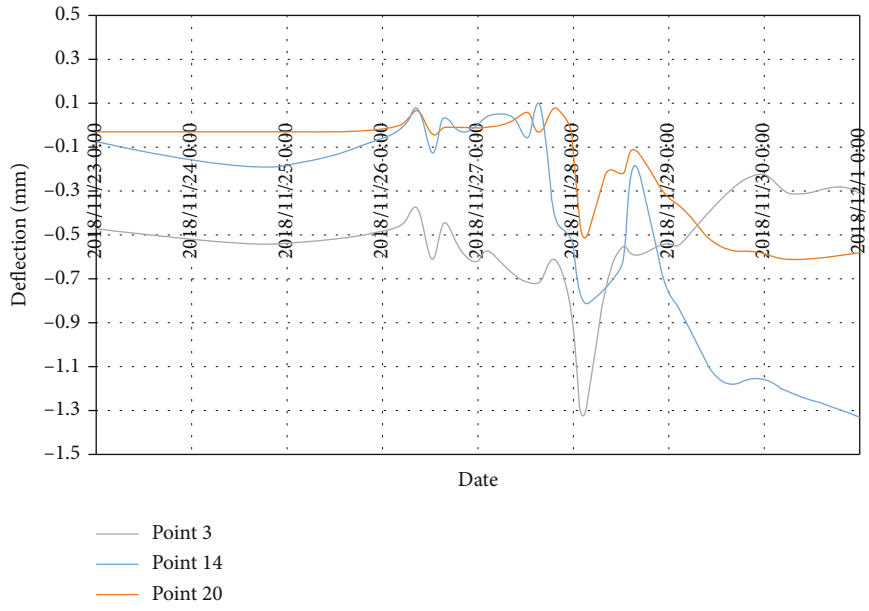

Figure 12: Deformation curve measured by total station.

The data base station uses the RS485 bus to connect with each sensor and realizes the synchronous acquisition between each sensor through the 12V level output. The incoming data from the pin sensors is uploaded via the 4G network to the server platform, which calculates and displays it. Real-time data transmission between the monitoring center and the monitoring terminal is realized [11].

In summary, the system consists of a server-side data processing platform, a data base station, and an inclination sensor to form a complete system topology, as shown in Figure 5.

4.2. User Data Collection Operation Steps

(1) 13 inclination sensors are arranged at the waist of the subway section, and the collection frequency and collection method are set on the collection software, as shown in Figures 6–9

The acquisition mode 0 in the figure means that after clicking to start acquisition, a measurement value is returned every 1 s, and the measurement value is the measurement value of the inclination sensor in the x-axis direction. If the frequency is 20 Hz, the returned value is the average of 20 numbers measured within 1 s.

The acquisition method 20 in the figure represents that measuring the inclination value of the wall angle sensor in the x and y directions, the first 20 s returns the inclination value in the x direction measured by the inclination sensor, and the second 20 s returns the inclination value in the y direction measured by the inclination sensor.

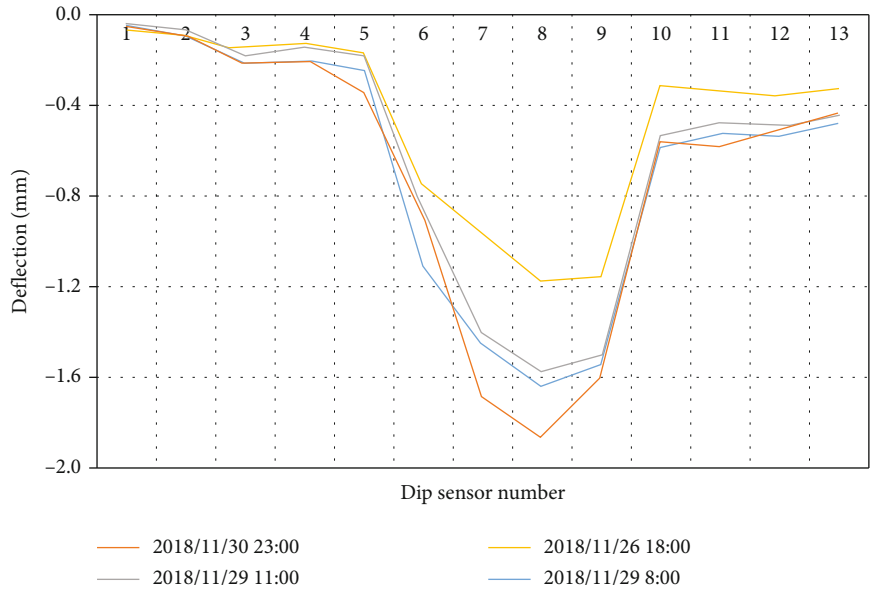

Figure 13: Measured deflection curve of inclination sensor.

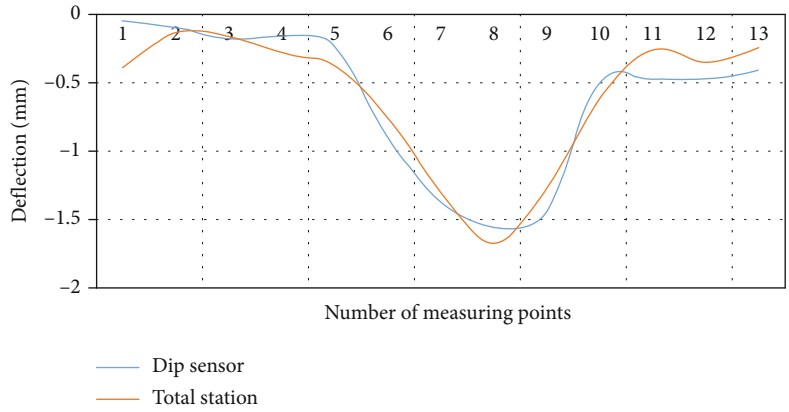

Figure 14: Measured deflection curve of inclination sensor and total station.

(2) Click to start measurement, and send the acquisition command to the sensor. The hardware can make all the inclination sensors receive the command at the same time, measure at the same time interval after receiving the command, and store the measured data in the sensor, as shown in Figure 8

(3) After sending the collection command, the sensor collects data at the same time interval. The collected data is first stored in the sensor, and then, the sensor returns the collected data to the terminal and decodes the data to obtain the sensor inclination value. The collection results are viewed as shown in Figure 9

Table 1: Measurement errors between inclination sensor and total station.

Point	Error (mm)	Point	Error (mm)
1	0.3	8	0.1
2	0.0	9	-0.2
3	0.0	10	0.1
4	0.1	11	-0.2
5	0.1	12	-0.1
6	-0.1	13	-0.2
7	-0.1	—	—

5. On-Site Measured Data Analysis

According to the measured data of the inclination sensor, the deformation curve of the subway tunnel and the deflection change of each sensor during the excavation process are analyzed, and the data of the inclination sensor and the total station data are compared with the theoretical curve to analyze the reasons.

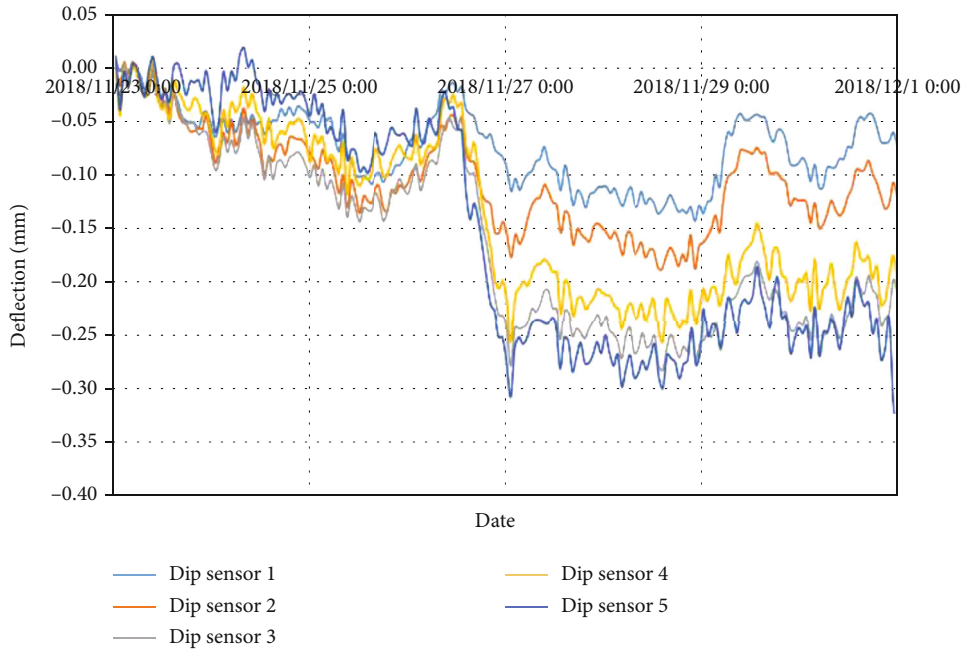

Figure 15: Curves of the measured deflections of 1~5# inclination sensors with time.

5.1. Point Layout and Data Analysis of Total Station. A total of 26 measuring points are arranged in the affected area of the subway by the total station, and 5 measuring points are arranged in each section. The total station has a total of 5 measuring points on the cut surface during the measurement process. To compare the data of the pillow sensors, data were selected that are identical in the cross-section of the pillow sensors: approximately 2# points. Tunnel preparations are carried out in the pre-, sluice-, and the replenishment phase. The location of the measuring point is shown in Figure 10.

Since the total station cannot perform real-time measurement, the data of the crossing stage is collected every half an hour, and part of the data of the crossing stage is taken for analysis, and the actual deformation curve of the tunnel is fitted as shown in Figure 11.

It can be seen from the above figure that as time goes by, the deflection value of the subway tunnel continues to increase. At 3 am on December 1, 2018, due to the end of the crossing stage, the deflection value reaches the maximum value of 1.91 mm, which is less than the maximum theoretical calculation. The value is 8.23 mm, which is less than the limit value of 10 mm, so the deformation of the existing tunnel structure meets the requirements.

It can be seen from the figure that the deformation curves of the affected area of the tunnel are basically the same, the deflection value of the measuring point in the crossing stage is larger, and the measured deflection value of other measuring points is relatively small due to the distance from the crossing stage. The accuracy of the theoretical calculation model can be verified.

The measured data were selected for analysis at the pretravel settlement, the transition stage, and the posttravel stage, respectively. The results are shown in Figure 12.

5.2. Inclination Sensor Acquisition Data Analysis. During the construction of the subway tunnel, the data of one week of a project passing through the existing tunnel section is taken for analysis, and the time period is 2018.11.23 0:00~2018.11.30 23:59, to achieve continuous data collection, and the user terminal can obtain an inclination angle acquisition value every minute. This allows an overview of the end of the tunnel, allowing the pin sensor and the positioning systems to be monitored in real time.

The tilt sensor can collect data 20 times within 1 s according to the frequency, and the data obtained by the user on the client is the average of 20 data within 1 s. Due to the large amount of real-time monitoring data, the values in one minute are averaged to obtain one value per minute. Take the measured inclination value from 0 : 00 to 23 : 59 on November 23, 2018.

Multiply the inclination value by the segment length to obtain the deflection value of each segment, and then obtain the deflection value of each point by the segment stacking method. During the excavation process, the deflection values at four different moments were analyzed and fitted into a deformation curve, as shown in Figure 13. Deflection measurement results of total station and inclination sensor are shown in Figure 14. Measurement errors between inclination sensor and total station are shown in Table 1.

It can be seen from the above figure that as time goes by, the deformation value of the existing tunnel increases continuously. Each inclination sensor is within the range of the crossing stage, and the existing tunnel is most affected. From the above figure, it can be seen that the maximum deflection value of the existing tunnel is 1.86 mm, which is less than the theoretical calculation value of 8.23 mm, which meets the requirement that the early warning value is less than 10 mm, and is relatively close to the measurement value

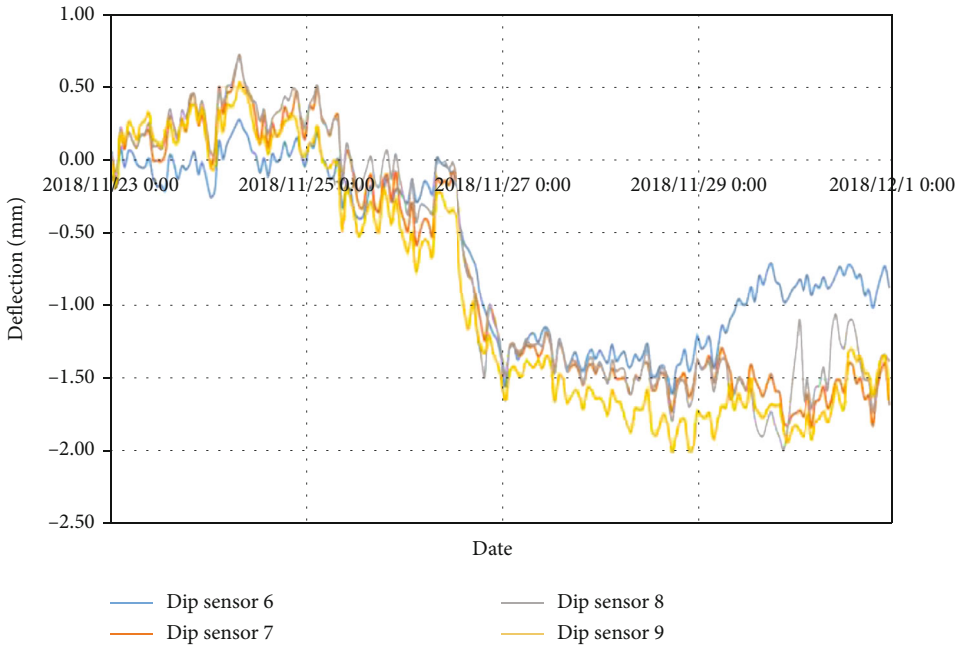

Figure 16: Curve of measured deflection with time of 6~9# inclination sensor.

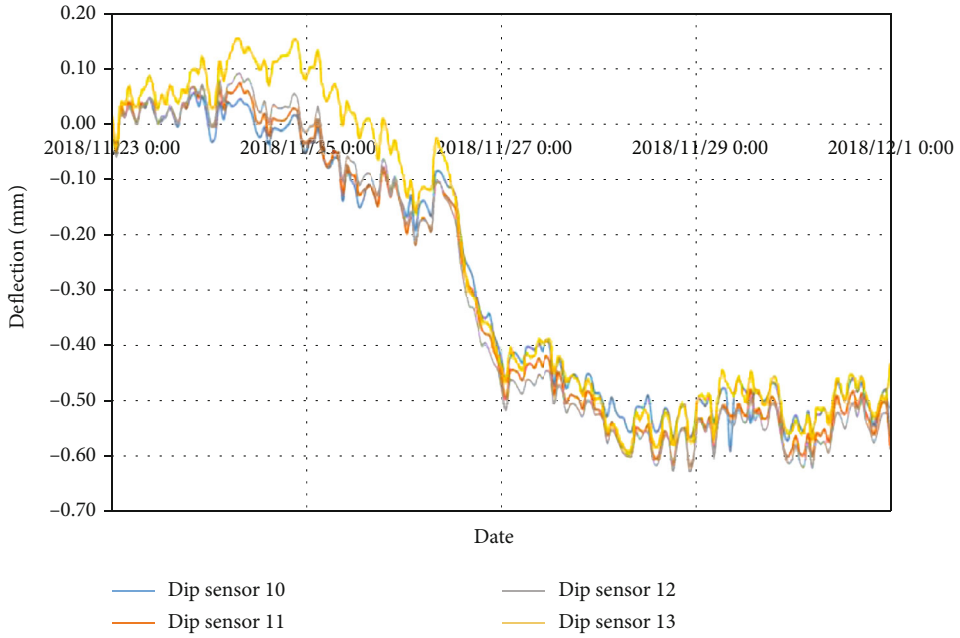

Figure 17: Curve of the measured deflection of the 10~13# inclination sensor with time.

of the total station. A method to measure the deflection of the tunnel is available.

The deflection changes of each inclination sensor during the crossing stage are plotted as shown in Figures 15–17.

Similar to the curve of the total station, the deflection values measured by the 13 inclination sensors all changed greatly around November 27, 2018, probably because the excavation was just below the existing tunnel. Among them, the deflection value of 6~9# tilt sensor has the largest change, and the change amount is 1.3 mm. The 1~5# inclination sensor, because it no longer passes through the section where the stage is located, has less influence and less deflection value change. The 10~13# inclination sensor is also not in the section of the crossing stage, so the deflection change is also relatively small. The above three graphs can reflect the real-time deflection change of the tunnel and can realize real-time monitoring.

5.3. Summary of Data Analysis. By converting the inclination value measured by the inclination sensor into the

deflection value, the deformation curve of the existing tunnel is obtained, and the maximum deformation value of the existing tunnel is obtained at the same time. Therefore, the following conclusions are drawn:

(1) The measured deflection curve obtained by the inclination sensor using the segmented superposition method has the same shape as the theoretical deflection curve, which shows the feasibility of the inclination sensor in tunnel deformation measurement

(2) The maximum deflection value measured by the inclination sensor is 1.86 mm, which is less than the theoretical calculation value of 8.23 mm and less than the early warning value of 10 mm. The existing tunnel will be affected by the tunnel excavation, but it is generally safe

(3) The measured value of the inclination sensor can reflect the real-time change of the structure, and the result is reliable

6. Conclusion and Outlook

6.1. In Conclusion

(1) The inclination sensor is small in size and easy to carry. Its size is 120 mm∗150 mm∗40 mm, which can be carried in large quantities

(2) The inclination sensor is easy to install, and the measuring point is not easy to be damaged. The aluminum casing can ensure its long-term use and is not limited by the measurement conditions and can be used in the absence of light

(3) Compared with the total station, the inclination sensor has low instrument cost and can be recycled

(4) The test accuracy of the inclination sensor is high, and the measured inclination can reach 9 decimal places, while the deflection value measured by the total station can only be accurate to two decimal places after the decimal point

(5) The tilt sensor can realize real-time monitoring in the office under the premise of unattended. Using the user platform and computer control, real-time monitoring can be achieved, which greatly reduces the workload and on-site testing time. And the acquisition of the inclination sensor can achieve high frequency; that is, 20, 50, and 100 numbers can be collected in 1 s, and real-time monitoring can be achieved

6.2. Outlook. The data acquisition method of the inclination sensor described in this paper, by comparing the data measurement and data acquisition of the total station and the inclination sensor, can reflect the advantages and feasibility of the inclination sensor in the real-time remote monitoring system for the deformation of the tunnel structure, which can be done faster. The purpose of strengthening real - time engineering monitoring is to eliminate potential safety hazards and avoid accidents. It has important practical engineering significance for the application and promotion of the inclination sensor in the real-time remote monitoring system of tunnel structure deformation.

Data Availability

The original data used to support the findings of this study have been deposited in the 4TU.ResearchData. The DOI of this data is 10.4121/20097617. You can download the data from this website https://figshare.com/s/9d5fdc8dd30c8dd4e5ab.

Conflicts of Interest

The authors declare that they have no conflicts of interest.

Acknowledgments

This work was funded by the 2020 Industry-University-Research Project (City-Level Industry-University-Research Project) "Three-Dimensional BIM Management System for Bridge Inspection Information" (Fund Number: x2tjB8200430) and the Fundamental Research Funds for the Central Universities in 2019 (Natural Science) "Bridge Inspection Information Three-Dimensional Management System" (Fund No. x2tjD2192960).

References

[1] Z. Keke, D. Xiaoyan, and H. Sa, "Design of deformation monitoring scheme for a certain underpass tunnel foundation pit," *Neijiang Science and Technology*, vol. 9, no. 9, pp. 55-56, 2019.

[2] H. Xie, *Research on Tunnel Deflection Measurement Based on Wireless Inclination Sensor*.

[3] T. Jun, "Application of wireless inclination measurement system in bridge deflection monitoring," *Traffic Construction and Management*, vol. 7, no. 7, 2014.

[4] P. Xu, *A Bridge Deflection Measurement Method and Experimental Research Based on Beam Rotation Angle*, Chongqing Jiaotong University, 2010.

[5] L. Hongwen, *Advanced Material Mechanics*, Higher Education Press, 1985.

[6] C. Deng, *Research on the Application of Key Technology of Inclination Sensor in Bridge Deflection Measurement*, South China University of Technology, Guangzhou, 2018.

[7] L. Zhaofeng, *Research on Application of Tilt Sensor in Deformation Monitoring of Arch Rib of Long-Span Arch Bridge*, South China University of Technology, Guangzhou, 2019.

[8] Z. Xihong, L. Funian, and Y. Yongyi, "Subway tunnel profile monitoring system based on IoT design," *Journal of Modern Electronic Technology*, vol. 41, 2018.

[9] C. Wang, *Research on the Comparison, Selection and Optimal Configuration of Tunnel Structural Health Monitoring Sensors*, Wuhan University of Technology, 2010.

[10] H. E. Cunfu, *Development and System Design of Wireless Force Sensor with Full Stand*, Instrument Technology and Sensor, 2017.

[11] J. Zhipeng, *Design of Outdoor Advertising Dip Angle Monitoring Terminal Based on Wireless Communication*, Modern Electronics Technology, 2015.

Hindawi
Wireless Communications and Mobile Computing
Volume 2022, Article ID 7624968, 10 pages
https://doi.org/10.1155/2022/7624968

Research Article

Evaluation of Motion Standard Based on Kinect Human Bone and Joint Data Acquisition

Xiaoning Zhang

School of Physical Education, Huaibei Normal University, Huaibei 235000, China

Correspondence should be addressed to Xiaoning Zhang; zhangxn@chnu.edu.cn

Received 5 June 2022; Revised 3 August 2022; Accepted 8 August 2022; Published 31 August 2022

Academic Editor: Jun Ye

In order to improve human bone and joint data, we propose a method to collect data and judge the standard of motion. Kinect is a 3D somatosensory camera released by Microsoft. It has three cameras in total. The middle is a color camera, which can take color images and obtain 30 images per second; on the left is the infrared projector, which irradiates the object to form speckle. On the right is the depth camera to analyze the infrared spectrum. On both sides are two depth sensors to detect the relative position of people. On both sides of Kinect are a set of quaternion linear microphone arrays for speech recognition and filtering background noise, which can locate the sound source. There is also a base with built-in motor below, which can adjust the elevation angle. It can not only complete the collection of color images, but also measure the depth information of objects. The experimental results show that we use MSRAction3D data set and compare the same cross-validation method with other latest research methods in the figures. The highest recognition rate of this method (algorithm 10) is the second, and the lowest and average recognition rates are the highest. The improvement in the lowest recognition rate is obvious, which can show that this method has good recognition performance and better stability than other research methods. Kinect plays a relatively important role in the movement of human bone and joint data acquisition.

1. Introduction

Body motion recognition has always been a hot issue concerned by people. However, there are still many basic problems in the field of computer vision that are not perfect and have not been reasonably solved. We live in the real three-dimensional world, and the images obtained by ordinary cameras are two-dimensional, which leads to the problem of lack of information and inaccurate recognition. Therefore, we use Kinect human bone data to identify human actions, which can reduce the lack of information in data collection. According to the knowledge of three views and projection introduced earlier, if we can use two-dimensional plane human body projection in three different directions to express human action, we can more truly show human motion in the three-dimensional world [1]. This chapter uses the two-dimensional plane projection feature of human bone data. The human action recognition method is to project the three-dimensional joint points into the two-dimensional space, construct the feature vector composed of three upward joint angles, represent the combination of translation and rotation through the changes of 17 joint angles of human body, and select the method of multiclassification support vector machine to classify 20 human actions in MSRAction3d data set [2]. The Kinect somatosensory device developed by Microsoft can directly capture the body movements of patients without requiring patients to wear and operate any peripheral devices. It has a more natural and convenient human-computer interaction mode and is more suitable for the development and adoption of community and family medical rehabilitation platforms [3]. Therefore, this paper selects Kinect somatosensory equipment as the human motion sensing carrier and designs a somatosensory rehabilitation training platform based on Kinect sensor. As shown in Figure 1, the platform integrates the functions of basic motion acquisition and rehabilitation evaluation, pre-sets typical rehabilitation training movements for the shoulder and elbow joints of the left and right limbs, and collects template motion flow data and training motion flow data through somatosensory sensors. Once the data was

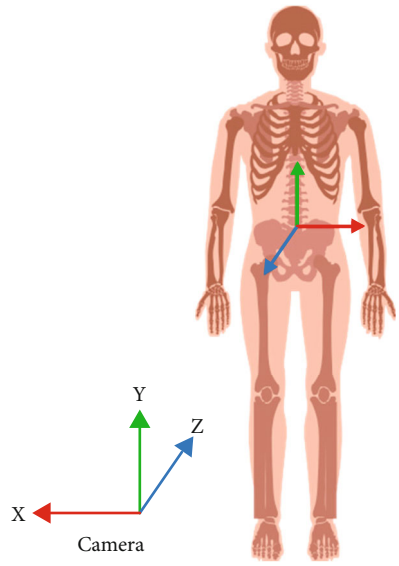

Figure 1: Data acquisition.

processed by the logic of the algorithm, the similarity of the data flows between the two groups of functions was calculated and examined by using the time dynamic control algorithm integration method and Hausdorff distance measurement algorithm. In addition, this paper examines the process of kinematic measurement of rehabilitation treatment to measure the effectiveness of rehabilitation treatment and perform interventions to clarify the algorithm and theoretical in paus [4].

2. Related Works

Since the 1980s, Internet information technology has been greatly developed. A series of human-computer interaction technologies, such as human-computer interaction and intelligent gesture recognition, have emerged one after another. Human-computer interaction means that human and computer user interface interact in some way to produce information data input and output. In real life, people can use gestures and language to complete the information input to the PC, and the computer can complete the data output through pictures, videos, and other ways, so as to realize the information interaction between people and computers. The human-computer somatosensory interaction is based on the acquisition of depth image. The acquisition of depth image mainly includes the following three ways: structure light, time of flight, and multicamera [5]. The Kinect device selected in this design mainly applies structure light detection technology. Prime sense names this depth measurement technology as light coding. Light coding is a kind of structured light technology, but the depth calculation method of light coding is different from that of other structured lights. Light coding is a depth detection algorithm independently developed by Cristache, C. M. It is a structured light technology using special depth calculation method. Compared with the conventional structured light algorithm, the light source of the light coding algorithm is the diffraction spot randomly generated by the laser passing through the ground glass, which has high randomness and is related to the pattern and distance [6]. Of course, the prior light source calibration process cannot be omitted. Compared with the traditional structured light algorithm, light coding algorithm is a kind of three-dimensional space coding, which is controlled by the chip product ps1080 of Kulczyk, T. when calibrating the light source [7]. Moreover, the measurement accuracy is only affected by the density of the calibrated reference plane and has nothing to do with the spatial geometric position of the reference object. The first generation of Kinect somatosensory devices adopts light coding algorithm technology to collect the depth information of three-dimensional space and compare it with the previously saved speckle reference image to obtain the distance between the target object in the Kinect field of view scene and the Kinect camera. However, according to Ma et al.'s paper on Kinect depth data accuracy analysis, with the increase of the distance between the object and the sensor, the random error of depth measurement will also increase, and increase from a few millimeters to 4 meters (when the maximum range of the sensor is reached) [8, 9]. For improving this accuracy, Naufal, A., Anam, C., Widodo, C. E., and Dougherty, G. put forward a theoretical error analysis, which can clarify what factors affect the accuracy of data. Vignesh et al. studied and developed a new somatosensory rehabilitation system, which aims to improve the enthusiasm of patients' rehabilitation training and improve the efficiency of patients' rehabilitation training [10]. In this system, the motion data of patients can be recorded in real time, and the obtained motion data can be compared with the corresponding standard motion data in the database, so as to judge the recovery of patients' condition. In the system Kinerehab, patients are reflected on the interface with the image of virtual animation, which has a good and natural human-computer interaction atmosphere, enhances the interest of rehabilitation training, makes patients interested in rehabilitation training, and stimulates patients to train independently. Fajri et al. studied and developed a rehabilitation training system based on human tracking technology, which is mainly aimed at the recovery of the shoulder and elbow [11]. The system takes the position information of the patient's key joint points through the sensor, modifies the effective position information of the key joint points according to the standard action position information, and then imports the modified standard action data information into the system model. The system can effectively reduce the wrong actions of patients in rehabilitation training and avoid the damage of wrong actions to human body. At the same time, the system also has a scoring mechanism to evaluate the recovery of patients. Kim designed and studied a rehabilitation training system aimed at improving patients' balance ability. In this system, sensors are used to obtain depth image information, reshape the 3D model of human body, and conduct human-computer interaction in the form of simple games through virtual reality scenes, so as to achieve the purpose of sports rehabilitation [12]. As a new rehabilitation training platform, robot is an effective clinical intervention means to assist doctors in the reconstruction of patients' motor

function, represented by the upper limb rehabilitation training system developed by Zhou, S. and others [13]. In the early stage, the motion rehabilitation robot provided resistance and active force through the spring support of free inertia balance. Wang et al. also used the human bone detection ability of Kinect somatosensory equipment to realize the imitation control of 16 joint humanoid robot for human action [14]. Their experimental results show that the time lag of the developed control system is only a short 200 ms. In addition, Afrieda. N. has developed humanoid robots that can recognize human joints in the whole body. They also use Kinect somatosensory equipment to solve the joint angle of the robot by using analytical geometry method, which can solve the kinematics of the robot more quickly [15].

3. Method

With the support of Kinect for windows SDK, it is possible to monitor the work of one or two human bones moving into the Kinect vision by controlling the bones, receiving data from human bone marrow, and then get a triangle integration of all joints [16]. The human skeleton frame design in this article is the first generation of Kinect. The number of each joint is shown in Figure 2 to support the description of the human skeleton.

According to the sequence of Kinect bone data acquisition, number 20 human bone joint points from a to t, as shown in Figure 2. Each number corresponds to the position coordinates of a human bone joint point, which represents different parts of the human body.

Table 1 is the naming of joint points corresponding to the number. 20 joint points represent the complete structure of human bones. Through the analysis of human motion, using the coordinate data of human joint points, every two adjacent joint points are formed into a joint vector, which contains the motion information of the joint [17]. It is also easy to construct the two-dimensional joint vector of the human body. Assuming that the coordinate data of the two-dimensional space of two adjacent joint points of the human body are $U(x_1, y_1)$ and $V(x_2, y_2)$, respectively, the joint vector of the two-dimensional space composed of them is

$$\mathrm{UV} = (x_2 - x_1, y_2 - y_1). \tag{1}$$

According to formula (1), set point $U(x_1, y_1)$ and point $V(x_2, y_2)$ to represent the joint points of the left ankle and left foot, respectively, and the vector in the formula represents the activity state of the end of the left foot in two-dimensional space, covering the details of the movement of the left leg. A total of 19 human two-dimensional joint vectors are composed of 20 human bone joint points.

If you look at different human functions in three-dimensional space from an angle, you will not be able to tell the truth of the order, because it will create a local block and covers some of the characteristics of movement. Therefore, we use three images of the human body and the projection method to reflect objects in three-dimensional space in two-dimensional planes, find the objects of motion at different plane angles, to vary class, and pay for defects. Consider only the features of motion in a triangle [18]. Because changes in the angle of the human joint affect the nature of translation and rotation, angular data can be used to determine the location of various movements. We consider the angle of the joints of the human body in three places inside the two planes, operate the plane from three different angles of view, and create the angles comfort in three different planes: the angle between the joints and the joints in the big picture and the anterior-posterior angular projection of the major plane of the human body. The angle of integration on the left watch is the projection of the joint from left to right of the left plane of the human body. The angle of inclination at the top is the approximate angle of inclination in the lower plane of the human body from the top to the bottom [19]. The angle of the selected human bone marrow is shown in Figure 3.

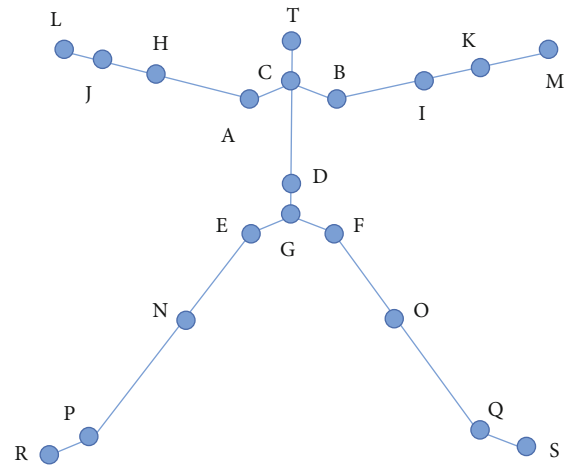

Figure 2: Numbering of 20 joint points.

Figure 3 shows 17 human joint angles selected by us. According to the 19 human two-dimensional joint vectors constructed above, the size of human bone joint angle can be calculated by using cosine similarity formula, as shown in the formula

$$\cos\theta(t) = \frac{U(t).V(t)}{\|U(t)\|.\|V(t)\|}. \tag{2}$$

θ is the angle of phase t of each bone data, and $U(t)$ and $V(t)$ are both vectors of phase t. Since the collected kinect bone data is in the form of three-dimensional coordinates (x, y, z), first, reduce the dimensionality of the three-dimensional bone data to make it become the bone data on the two-dimensional projection plane of the XOY surface, and then use the two-dimensional coordinates to Calculate the size of the joint angle. For example, during T, calculate the angle of inclination of the joint from the left wrist in both planes. The joint of the left wrist at time t is 11 $(x(t), y(t))$, the joint of the left elbow of t is 22 $(x(t)), y$

Table 1: Naming of 20 individual joint points.

Number	Name	Number	Name	Number	Name	Number	Name
A	Left shoulder	F	Right hip	K	Right wrist	P	Left ankle
B	Right shoulder	G	Hips	L	Left hand	Q	Right ankle
C	Neck	H	Left elbow	M	Right hand	R	Left foot
D	Spine	I	Right elbow	N	Left knee	S	Right foot
E	Left hip	J	Left wrist	O	Right knee	T	Head

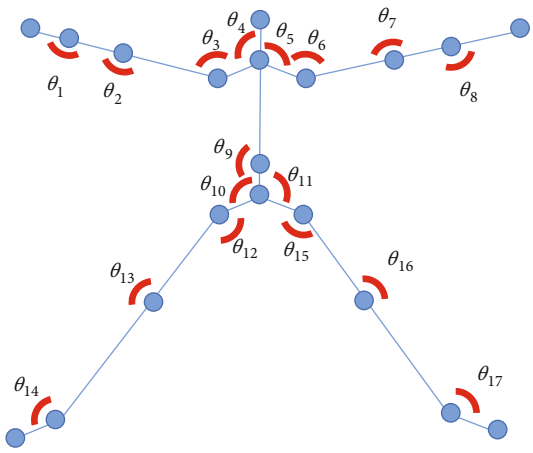

Figure 3: 17 joint angles of human body.

$(t))$, and the left wrist of t is 33 $(x(t), y(t))$ are shown as

$$\mathrm{JL}^{\{2\}}(t) = \left(x_1{}^{(t)}.y_1{}^{(t)}\right) - \left(x_3{}^{(t)}.y_3{}^{(t)}\right), \tag{3}$$

$$\mathrm{JH}^{\{2\}}(t) = \left(x_2{}^{(t)}.y_2{}^{(t)}\right) - \left(x_3{}^{(t)}.y_3{}^{(t)}\right), \tag{4}$$

$$\cos\theta^{\{2\}}(t) = \frac{\mathrm{JL}^{\{2\}}(t).\mathrm{JH}^{\{2\}}(t)}{\left\|\mathrm{JL}^{\{2\}}(t)\right\|.\left\|\mathrm{JH}^{\{2\}}(t)\right\|}. \tag{5}$$

4. Experimental Results and Discussion

On this basis, aiming at the problem of low accuracy and stability of human action recognition in complex environment with high noise, a method of human action recognition based on hierarchical feature fusion was proposed, which divided different parts of human body according to the composition of human body structure system. The layered strategy is adopted, which is conducive to the decomposition of complex human movements. Firstly, according to the bone joint coordinates obtained by Kinect, the features of human joint angles in two-dimensional space are extracted, and the actions are roughly classified by the support vector machine (SVM) method. Then, the body vector, angular velocity, and acceleration in 3d space were extracted, and the movements were classified by HMM.

With the knowledge of human models, the human body can be divided into five sections. Part I: physical. The body includes the head, neck, back, and hips. Part II: left hand. The left hand includes the forearm, left wrist, left elbow, and left shoulder. Part III: right hand. The right hand includes the arm, wrist, elbow, and shoulder. Part IV: left foot. The left leg includes the left foot, the ankle, the left knee, and the left thigh. Section V: right. Right foot includes the right foot, right ankle, right knee, and right foot. The body is an essential part of the human body. The motion feature information of some waists of the human body comes from this part of the joint points, and the motion feature information of the hands and feet comes from the joint points of the limbs [20].

By dividing the structure of the human body, it is possible to combine these five components to represent some of the most important functions of the human body. Therefore, in terms of proportions, this paper adopts a hierarchical concept. In step 1, first, divide the above five functions into categories with the same type of combination. For example, the two hands are a combination of the second and third sections. This is a rough proportion. The second layer redivides the functions of the same type of combination and filters the specific functions, which are the details of the process. We take the vector of the joint angle, including the projection of 17 joints on both sides of the three planes included in Chapter 3, according to the characteristics of the first rough decision and distribution of human activities. When distinguishing human actions with the same combination mode, we extract features from kinematics theory. A complete human action can be divided into main action and auxiliary action. The main action reflects the global state of the motion mode, and the auxiliary action reflects the local state of the motion mode. Only by combining the characteristics of the main and auxiliary actions can this action be expressed more accurately [21]. For the five parts of the human body divided above, we construct their limb vectors in three-dimensional space, respectively, shown as

$$GT^{\{3\}}{}_{(t)} = T^{\{3\}}{}_{(t)} - G^{\{3\}}{}_{(t)}, \tag{6}$$

$$AJ^{\{3\}}{}_{(t)} = J^{\{3\}}{}_{(t)} - A^{\{3\}}{}_{(t)}, \tag{7}$$

$$BK^{\{3\}}{}_{(t)} = K^{\{3\}}{}_{(t)} - B^{\{3\}}{}_{(t)}, \tag{8}$$

$$EP^{\{3\}}{}_{(t)} = P^{\{3\}}{}_{(t)} - E^{\{3\}}{}_{(t)}, \tag{9}$$

$$FQ^{\{3\}}{}_{(t)} = Q^{\{3\}}{}_{(t)} - F^{\{3\}}{}_{(t)}. \tag{10}$$

{3} represents in the three-dimensional space, t represents a certain time, and the joint points that are prone to drift at the end points of hands and feet are temporarily rounded off. Finally, the limb vectors in the three-dimensional space at all times of the five parts are

represented by $GT^{\{3\}}$, $AJ^{\{3\}}$, $BK^{\{3\}}$, $EP^{\{3\}}$, and $FQ^{\{3\}}$, respectively. According to the different contribution to the expression of human action, two joint angles are selected from each part, which are called the main action joint angle. The torso part selects angle θ_4 and angle θ_9, the left arm part selects angle θ_3 and angle θ_2, the right arm part selects angle θ_6 and angle θ_7, the left leg part selects angle θ_{12} and angle θ_{13}, the right leg part selects angle θ_{15} and angle θ_{16}, and the angular velocity of the joint angle is shown as

$$\omega(t) = \theta(t+1) - \theta(t). \tag{11}$$

The human action sequence is continuous and changes with time. The change of joint angle before and after forms the value of angular velocity ω. the limb vector and the angular velocity of active joint angle are the characteristics of active action, representing the overall movement of human limbs and trunk [22]. The bending of human limbs and trunk is reflected by the change of the distance between joint points. The human body is projected into the YOZ side plane from the left view direction. The distance between joint points of five bones is shown as

$$d_{GT}(y,z) = \sqrt{\left(y_G{}^{(t)} - y_T{}^{(t)}\right)^2 + \left(Z_G{}^{(T)} - Z_T{}^{(t)}\right)}, \tag{12}$$

$$\begin{aligned}
d_{GT}(y,s) &= \sqrt{\left(y_G^{(t)} - y_T^{(t)}\right)^2 + \left(s_G^{(t)} - s_T^{(t)}\right)^2},\\
d_{CL}(y,s) &= \sqrt{\left(y_C^{(t)} - y_L^{(t)}\right)^2 + \left(s_C^{(t)} - s_L^{(t)}\right)^2},\\
d_{CM}(y,s) &= \sqrt{\left(y_C^{(t)} - y_M^{(t)}\right)^2 + \left(s_C^{(t)} - s_M^{(t)}\right)^2},\\
d_{GN}(y,s) &= \sqrt{\left(y_G^{(t)} - y_N^{(t)}\right)^2 + \left(s_G^{(t)} - s_N^{(t)}\right)^2},\\
d_{GS}(y,s) &= \sqrt{\left(y_G^{(t)} - y_S^{(t)}\right)^2 + \left(s_G^{(t)} - s_S^{(t)}\right)^2},
\end{aligned} \tag{13}$$

where $d(y,z)$ represents the Euclidean distance between the two joints in the lateral plane and t represents the distance between the head and end joint points of the five parts of the human body at a certain time, reflecting the bending of the limbs and trunk in motion. The change of the distance before and after the time forms the speed v, and the acceleration is a physical quantity describing the speed of the change of human motion, as shown in

$$\begin{aligned}
v(t) &= d(t+1) - d(t),\\
\partial(t) &= [v(t)]'.
\end{aligned} \tag{14}$$

The distance between five joints in the lateral plane and the acceleration of motion are regarded as the characteristics of auxiliary action. The accelerations of the five parts are ∂_1, ∂_2, ∂_3, ∂_4, and ∂_5. The characteristics of main action and auxiliary action together constitute the characteristics of the second level fine classification of human action. Because everyone's height and arm length are different, even if two people make the same action posture, there will be some errors. In order to eliminate individual differences, divide the items in the formula by the shoulder width d_{AB} and the mean value $\bar{d}$ of the Euclidean distance between joints in the plane of YOZ side, as shown in

$$d_{AE}(x,y,s) = \sqrt{(x_A - x_E)^2 + (y_A - y_E)^2 + (s_A - s_E)^2}, \tag{15}$$

$$\bar{d}(y,s) = \frac{\sum_{t=1}^{n} d(t)}{n}, \tag{16}$$

where d_{AB} represents the width of each person's shoulder and D represents the average distance between the five major joints of the human body at all times in the YOZ side plane. The feature vector of the final rough classification is expressed as $[\theta_1{}^{\{2\}}, \theta_2{}^{\{2\}}, \theta_3{}^{\{2\}} \cdots \theta_{17}{}^{\{2\}}]$. The matrix composed of feature vectors of fine classification is expressed as

$$\begin{bmatrix}
GT^{\{3\}} & \omega_4 & \omega_9 & \partial_1\\
AJ^{\{3\}} & \omega_3 & \omega_2 & \partial_2\\
BK^{\{3\}} & \omega_6 & \omega_7 & \partial_3\\
EP^{\{3\}} & \omega_{12} & \omega_{13} & \partial_4\\
FQ^{\{3\}} & \omega_{15} & \omega_{16} & \partial_5
\end{bmatrix}. \tag{17}$$

Each row in the matrix represents a set of eigenvectors.

In this system, we will compare the similarity between the standard action data sequence template and the action data sequence collected in real time, so as to achieve the effect of rehabilitation evaluation. In reality, the time taken by the patient to complete a set of rehabilitation exercises is usually inconsistent with the time taken by the standard action template. Some patients with serious injuries take several times as long as the standard action template. For two sets of motion data sequences with different lengths, the operation of corresponding time points alone cannot meet the accuracy requirements of the current system. DTW, namely dynamic time warping algorithm, is a widely used speech recognition algorithm. At first, it is to solve the error caused by different tones in speech recognition. Compared with other algorithms, dynamic time warping algorithm expresses the relationship between two sequences with inconsistent length through the time warping function under certain conditions. At present, it is widely used in gesture recognition, language recognition, and other fields. The central idea of DTW is to extend or shorten two data sequences with different time lengths to ensure the consistency of the length of the two data sequences to be tested and select an appropriate path from the constructed distance matrix to minimize the sum of the distances obtained by the two sequences. In the recognition of human action sequence, it is actually to find the minimum distortion distance between the current sequence and the standard template.

It is assumed that the two sequences of the standard template and the template to be tested are R and T, and the length is m frames and N frames, respectively [23]

shown as

$$R = (R_1, R_2 \cdots R_{m-1}, R_m)\{R_m, m = 1, 2, \cdots M\},$$
$$T = (T_1, T_2 \cdots T_{n-1}, T_n)\{T_n, n = 1, 2, \cdots N\}. \quad (18)$$

In general, for two sequences with different lengths, it is necessary to construct a $m \times n$ matrix grid, and the matrix element (i, j) represents the distance $d(R_i, T_j)$ between R_i and T_j. The matrix is shown as

$$D = \begin{bmatrix} d(R_1, T_1) & d(R_1, T_2) & \cdots & d(R_1, T_n) \\ d(R_2, T_1) & d(R_2, T_2) & \cdots & d(R_2, T_n) \\ \vdots & \vdots & & \vdots \\ d(R_m, T_1) & d(R_m, T_2) & \cdots & d(R_m, T_n) \end{bmatrix}. \quad (19)$$

DTW algorithm is to find an optimal path through the grid matrix, and the grid points passed by this path are the points that need to be processed and calculated in the two sequences. Let this path be the regular path W, then the K -th element of W is defined as $W_k = (I, j)_k$. That is, the regular path is shown as

$$W = \{w_1, w_2, w_3 \cdots w_k\}(\max(m, n) \le K \le m + n - 1). \quad (20)$$

According to the constraints of continuity and monotonicity, the path of each grid point has only three directions. If the grid point is $(i.j)$ at this time, the path of the next grid point is only $(i + 1, j + 1)$, $(i, j + 1)$, $(i + 1, j)$. There are many regular paths that meet this condition, but the formula of minimum distortion distance is shown as

$$\mathrm{DTW}(R, T) = \min\left\{\frac{\sqrt{\sum_{k=1}^{k} w_k}}{k}\right\}. \quad (21)$$

The path meeting the minimum distortion distance needs to meet three conditions:

(1) The path must meet the requirements from the beginning $W(1, 1)$ of the sequence to the end $W_k(m, n)$ of the sequence

(2) The path needs to meet the sequence of time, namely $m + 1 \ge m\&\mathrm{n} + \ge n$

(3) The path selection needs to meet the monotonicity, and m and n increase by 0 or 1 in turn. That is, if $W_{k-1} = (i, j)$, W_k has three choices $(i + 1, j + 1)$, $(i + 1, j)$, and $(i, j + 1)$

The path with the smallest sum of cumulative distances of adjacent elements is the optimal regular path. According to the above formula, the DTW cumulative distance formula can be deduced as

$$D(i, j) = d(r_i, t_j) + \min\{D(i - 1, j - 1), D(i - 1, j), D(i, j - 1)\}. \quad (22)$$

A Kionix KXSD9 three-axis accelerometer is included in the Kinect internal structure to prevent the error caused by Kinect being placed on an uneven plane and improve the stability of Kinect's depth image acquisition. Among them, the camera in Kinect can be adjusted according to the needs of users. The moving touch drive motor in Kinect can adjust the elevation of the camera to match the user's position change. Kinect also has a focusing system. If the user exceeds the field of vision, Kinect can automatically drive the base motor to adjust vertically by ±28° [24]. The field of view of Kinect imaging is 43.5° vertical and 57.5° horizontal.

The maximum distance range that Kinect sensor can track and recognize is 0.8 m to 4 m, but in practice, in order to ensure accurate data, the recognition distance is 1.2 m to 3.5 m as shown in Table 2:

Kinect is a "pipeline" system functional architecture, as shown in Figure 4. The original sensor data stream includes depth data stream, color image data stream, and audio data stream. Researchers can directly develop applications based on the original data stream information obtained by Kinect SDK.

Kinect uses depth measurement technology in acquiring depth images, which is also known as light coding. That is to mark and code the space to be measured with light source. This technology belongs to structured light technology. Compared with other structured light technologies, the depth calculation method of this technology is different from other technologies. The light source of light coding is called "laser speckle." Laser speckle is the diffraction spot image formed after the light source irradiates the nonsmooth object or passes through the ground glass. These speckle images will constantly change with the distance of the light source, with a high degree of random variation. Generally speaking, the speckle images at any two places in the spatial environment are inconsistent. All speckle images in the whole space are saved and recorded, and then the structured light is irradiated into the space for marking. At this time, put a new object into the space and only view the speckle image generated by the object to obtain the specific position of the object [25].

Today, with the rapid development of science and technology, somatosensory technology has gradually matured. At present, in addition to being mainly used in entertainment games, there are also various human-computer interaction systems developed by many researchers. Therefore, at present, many companies at home and abroad are carrying out research and development in the field of motion sensing, designing, and manufacturing their own motion sensing equipment. Three of the most popular products on the market are the following.

Xtion, a motion sensing device designed and produced by ASUS, mainly uses the Structure Light detection technology to obtain depth images. The Structure Light is used to

Table 2: Effective sight distance of Kinect sensor.

Sensor characteristics	Effective sight distance
Color and depth	Default mode (0.8-4.0), close range mode (0.4-3.5)
Bone tracking	Default mode (0.8-4.0), close range mode (0.4-3.5)

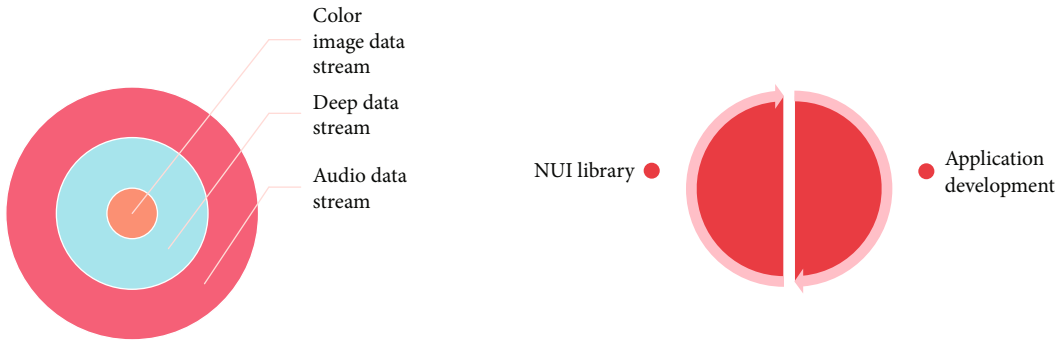

Figure 4: Interaction between application and Kinect sensor.

obtain spatial data and calculate other data, such as depth image and object skeleton. In the working process of the equipment, an infrared laser emitter emits the encoded near infrared light source. After the infrared light is reflected, it is captured by the infrared camera, and then the corresponding feature coding correspondence is calculated to determine the depth information.

Leap-motion, a motion-sensing device developed by Leap (USA), controls a person's hands by detecting their movements. Leap-motion uses multicamera detection technology. It has two infrared cameras and uses powerful data processing chips to quickly process the image data to detect the hand movements of the target. The leap-motion sensor's field of view detects the spatial shape of an inverted quad-pyramid with effective detection range of 25 mm to 600 mm. The product also has an open SDK (Software Development Kit), which can meet the needs of developers to develop and research on Windows, Linux, and Mac, the three mainstream operating system platforms.

Kinect for Xbox 360 is Microsoft's external motion sensing device that was officially unveiled on June 2, 2009. Structure Light detection technology is mainly used in obtaining depth images, which is the same as Xtion's principle. In terms of open source development, Microsoft has also designed SDK tools containing rich API interfaces, so developers can combine various languages to develop Kinect programming.

By comparing the above three kinds of motion sensing devices, it can be found that Kinect for Xbox 360 motion sensing devices is more convenient and high-precision for controlling people. Moreover, Microsoft also provides a large number of API interfaces in Kinect SDK, which is more advanced, so that Kinect can not only get the original depth data in the work, but also get the target object bone node data. Therefore, Kinect for Xbox 360 is selected as the somatosensory device in this design.

In order to obtain the coordinate information of human key joint points in real time to judge the similarity algorithm in the next step, Kinect sensor is used to track human joint points to obtain the motion data sequence in real time. The human skeleton is composed of human skeleton joint points, and each joint point has a relative position and direction. Kinect bone tracking module first detects the human body through the depth image information technology in Kinect and then corrects the human body posture. When the correction is successful, the measured human body can be tracked in real time, and the relevant bone information can be obtained in real time. When the correction fails, it will enter, while the cycle processes to calibrate again.

In the example provided by Kinect, the programs of two technologies of depth image data and bone tracking are provided, respectively, but there is no relevant program of data extraction. After learning the relevant application software, the two technologies of depth image and bone tracking are combined to successfully record and extract the data information of key bone joint points of human body. The base note is as follows: firstly, initialize the device environment, create new objects and create new user generators to store relevant data information, and facilitate subsequent calls. Secondly, register relevant callback functions and calibrate the skeleton. The functions to be called include the generation of new users and the detection of bone posture. Finally, bone tracking is performed, and relevant bone information is updated and read in real time. The flow chart of obtaining human bone information is shown in Figure 5.

The hardware setting of the simulation environment for the experiment in this chapter is Intel(R) Core(TM)i5-4210M CPU @2.60GHZ, 8GB RAM. Software settings are Windows 10, 64 bit operating system, and MATLAB R2017B. The MSRAction3D public data set is used. The data set contains 567 samples. Each action category is repeated by 10 different male and female subjects for 2~3 times. We take

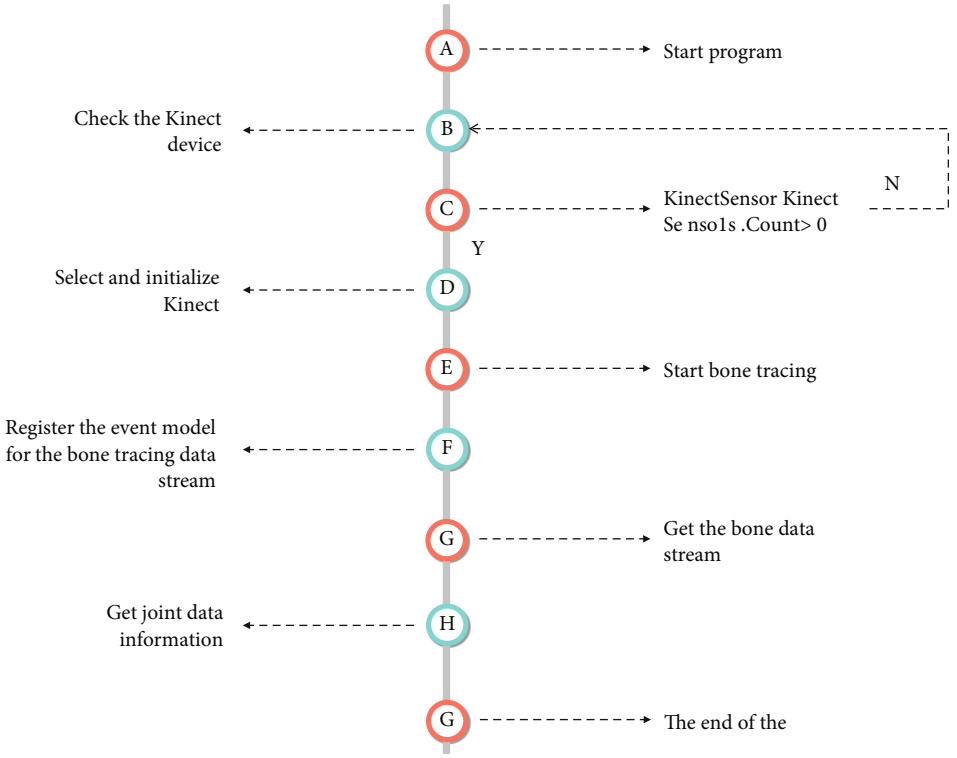

Figure 5: Flow chart of obtaining human body data information.

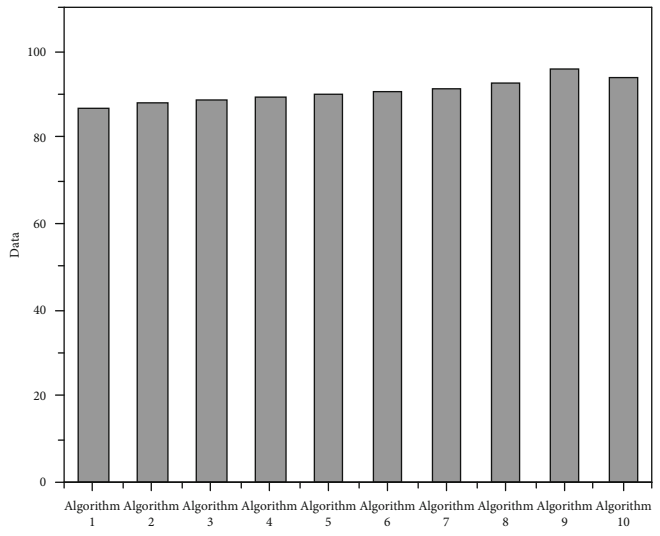

Figure 6: The highest recognition rate of this method and other methods.

547 samples for the test and remove 20 missing data samples. In the previous chapter, we directly classified 20 different human actions at one time. This chapter first roughly classifies these 20 actions into seven categories and then subdivides them: class I: single arm action; the second category: the movement of both arms; category III: single leg movements; the fourth category: trunk movement; category 5: the movement of both arms and legs; category 6: trunk plus arms; and category 7: trunk plus legs plus one arm. Because the number of subjects with different height and weight is not included in the study set, only the proportion of male and female subjects is included in the study set. We use MSRAction3D data set and compare the same cross-validation method with other latest research methods in Figures 6, 7, and 8. The highest recognition rate of this method (algorithm 10) is the second, and the lowest and average recognition rates are the highest. The improvement in the lowest recognition rate is obvious, which can show that this method has good recognition performance and better stability than other research methods.

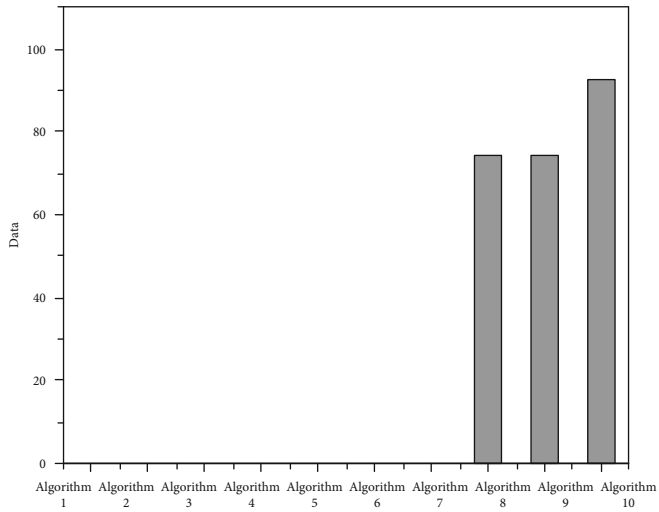

Figure 7: Minimum recognition rate of this method and other methods.

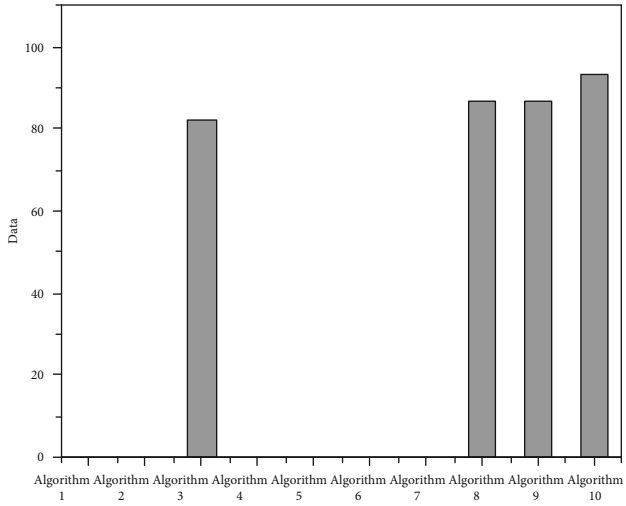

Figure 8: Average recognition rate of this method and other methods.

5. Conclusion

Based on Kinect human skeleton and joint data collection, the expression of human motion is completed through limbs, and all human bones together constitute human limbs. Rehabilitation exercise training is mainly to help people with movement disorders gradually recover their limb motor function through existing medical technologies and means. The traditional training methods are not suitable for patients to carry out rehabilitation training in family or community environment, regardless of the use cost or the complexity of operation. At the same time, the complex and cumbersome process of sports data acquisition often affects the rehabilitation doctors' judgment of patients' limb recovery. Therefore, this paper studies and designs a set of motion obstacle auxiliary evaluation training system based on Kinect. The system combines Kinect somatosensory sensor and virtual reality technology. By capturing and collecting human motion data information in real time and calculating relevant algorithms, patients can carry out rehabilitation training and complete the evaluation of rehabilitation training actions independently, so as to improve the rehabilitation efficiency of patients.

Data Availability

The data sets used and/or analyzed during the current study are available from the corresponding author on reasonable request.

Conflicts of Interest

It is declared by the author that this article is free of conflict of interest.

Acknowledgments

This study was supported by the 2011 Provincial Humanities and Social Sciences Research Project of Anhui Provincial Department of Education, "development of leisure sports in Huaibei from the perspective of folk entertainment culture in Huaibei" (2011sk223).

References

[1] R. Li, "Evaluation and simulation of medical sports health equipment multimedia image based on information asymmetry theory," *Multimedia Tools and Applications*, vol. 79, no. 15-16, pp. 9957–9976, 2020.

[2] A. N. Smirnov, N. V. Ababkov, V. V. Murav'Ev, and S. V. Fol'Mer, "Criteria for the evaluation of the technical state of the long-lived metal of HPP equipment based on acoustic structuroscopy," *Russian Journal of Nondestructive Testing*, vol. 51, no. 2, pp. 94–100, 2015.

[3] S. J. Seo, J. H. Lim, Y. Lee, C. W. Bark, and Y. G. Kim, "High-throughput analysis of new bone formation and bone substitutes after maxillary sinus floor elevation using synchrotron radiation micro-computed tomography," *Journal of*

Nanoscience and Nanotechnology, vol. 19, no. 2, pp. 680–686, 2019.

[4] M. Meglioli, A. Naveau, G. M. Macaluso, and S. Catros, "3D printed bone models in oral and cranio-maxillofacial surgery: a systematic review," *3D Printing in Medicine*, vol. 6, no. 1, p. 30, 2020.

[5] H. Lung, J. T. Hsu, Y. J. Wu, and H. L. Huang, "Biomechanical effects of diameters of implant body and implant platform in bone strain around an immediately loaded dental implant with platform switching concept," *Applied Sciences*, vol. 9, no. 10, p. 1998, 2019.

[6] C. M. Cristache, I. Tudor, L. Moraru, G. Cristache, and M. Burlibasa, "Digital workflow in maxillofacial prosthodontics—an update on defect data acquisition, editing and design using open-source and commercial available software," *Applied Sciences*, vol. 11, no. 3, p. 973, 2021.

[7] L. Zhang, "Research on the evaluation of sports events based on the concept of green environmental protection," *IOP Conference Series Earth and Environmental Science*, vol. 651, no. 4, p. 042028, 2021.

[8] Y. Ma, D. Liu, and L. Cai, "Deep learning-based upper limb functional assessment using a single kinect v2 sensor," *Sensors*, vol. 20, no. 7, p. 1903, 2020.

[9] A. Naufal, C. Anam, C. E. Widodo, and G. Dougherty, "Automate the calculation of human body height using a MATLAB-based Kinect camera for estimating body size: a pilot study," *AIP Conference Proceedings*, vol. 2346, no. 1, p. 040002, 2021.

[10] T. Vignesh, R. Mahadevan, and S. P. Harish, "Adherence to Kinect adventure games in individuals with Parkinson's disease – an experimental study from Mysore, India," *Journal of Evolution of Medical and Dental Sciences*, vol. 10, no. 33, pp. 2754–2760, 2021.

[11] B. R. Fajri, A. D. Samala, and F. Ranuharja, "Perancangan media interaktif gerak tari topeng patih pada wayang topeng malangan menggunakan sensor kinect," *INVOTEK Jurnal Inovasi Vokasional dan Teknologi*, vol. 20, no. 2, pp. 75–88, 2020.

[12] H. N. Kim, "Ambient intelligence: placement of Kinect sensors in the home of older adults with visual disabilities," *Technology and Disability*, vol. 32, no. 4, pp. 271–283, 2020.

[13] S. Zhou, F. Kang, W. Li, J. Kan, and Y. Zheng, "Point cloud registration for agriculture and forestry crops based on calibration balls using Kinect v2," *International Journal of Agricultural and Biological Engineering*, vol. 13, no. 1, pp. 198–205, 2020.

[14] Y. Wang, K. Junghyun, and S. G. Jahng, "Interactive research based on Kinect - focused on the work <Dream>," *TECHART Journal of Arts and Imaging Science*, vol. 7, no. 3, pp. 17–21, 2020.

[15] A. Procházka, O. Vyšata, M. Vališ, O. Ťupa, M. Schätz, and V. Mařík, "Use of the image and depth sensors of the Microsoft Kinect for the detection of gait disorders," *Neural Computing and Applications*, vol. 26, no. 7, pp. 1621–1629, 2015.

[16] Z. Feyziolu, S. Diner, A. Akan, and Z. C. Algun, "Is Xbox 360 Kinect-based virtual reality training as effective as standard physiotherapy in patients undergoing breast cancer surgery?," *Supportive Care in Cancer*, vol. 28, no. 9, pp. 4295–4303, 2020.

[17] Y. Chen, B. Zhang, J. Zhou, and K. Wang, "Real-time 3D unstructured environment reconstruction utilizing VR and Kinect-based immersive teleoperation for agricultural field robots," *Computers and Electronics in Agriculture*, vol. 175, no. 2020, p. 105579, 2020.

[18] N. Takeshima, T. Kohama, M. Kusunoki et al., "Development of simple, objective chair-standing assessment of physical function in older individuals using a Kinect™ Sensor," *The Journal of Frailty & Aging*, vol. 8, no. 4, pp. 186–191, 2019.

[19] L. E. N. Díaz, D. Pool, and M. Torres, "Development of an educational software as support for learning English and Mayan languages through the use of the Kinect sensor," *IARJSET*, vol. 6, no. 11, pp. 57–63, 2019.

[20] M. Mansoor, R. Amin, Z. Mustafa, S. Sengan, H. Aldabbas, and M. T. Alharbi, "A machine learning approach for non-invasive fall detection using Kinect," *Multimedia Tools and Applications*, vol. 81, no. 11, pp. 15491–15519, 2022.

[21] L. Wang, J. Liu, and J. Lan, "Feature evaluation of upper limb exercise rehabilitation interactive system based on Kinect," *IEEE Access*, vol. 7, pp. 165985–165996, 2019.

[22] R. Lozada-Yánez, N. La-Serna-Palomino, and F. Molina-Granja, "Augmented reality and MS-Kinect in the learning of basic mathematics: KARMLS case," *International Education Studies*, vol. 12, no. 9, p. 54, 2019.

[23] Y. S. Kang, S. T. Lu, C. C. Chiu, C. C. Tu, and Y. J. Chang, "Using Kinect v2 combined with Unity3D to design an agility training game," *International Journal of Computer Theory and Engineering*, vol. 11, no. 3, pp. 56–60, 2019.

[24] R. Bianchi, B. Yyelland, J. Yang, and M. McHarg, "Avatar Kinect: drama in the virtual classroom among L2 learners of English," *The Qualitative Report*, vol. 24, no. 13, pp. 6–6, 2019.

[25] M.-H. Nguyen, C.-C. Hsiao, W.-H. Cheng, and C.-C. Huang, "Practical 3D human skeleton tracking based on multi-view and multi-Kinect fusion," *Multimedia Systems*, vol. 28, no. 2, pp. 529–552, 2022.

Hindawi
Wireless Communications and Mobile Computing
Volume 2022, Article ID 7589727, 8 pages
https://doi.org/10.1155/2022/7589727

Research Article

Construction of Online English Corpus Based on Web Crawler Technology

Yanfei Qi[1,2]

[1]*School of Foreign Languages, Hanjiang Normal University, Shiyan 442000, China*
[2]*University of Perpetual Help System DALTA, Las Piñas 1740, Philippines*

Correspondence should be addressed to Yanfei Qi; qiyanfei@hjnu.edu.cn

Received 26 May 2022; Revised 16 July 2022; Accepted 25 July 2022; Published 28 August 2022

Academic Editor: Jun Ye

Using 100 random questionnaires, 89 people said they were increasingly dependent on the Internet for information, while the remaining 11 said they were not dependent much. Nowadays, the development of Internet technology is more and more mature, and the scale of the Internet is more and more large. At the same time, with the gradual deepening of global economic integration, English has become one of the indispensable language methods for international communication and cooperation. The development of network technology has been applied more and more widely in the process of English teaching; especially, the construction, research, and practical application of corpus have ushered in a broad development prospect. Based on web crawler technology, this paper focuses on the construction of web English corpus, which lays a foundation for English learning. Experiments show that crawler technology can effectively solve the collection and recognition of big data in English corpus.

1. Introduction

In recent years, with the in-depth development of my country's education reform, Chinese higher education is developing in the direction of international trade, communication, and information technology. The transformation and development of higher education has begun to pay attention to the use of information network media. The university websites of Chinese universities are gradually becoming more and more important. At the same time, most college websites have both Chinese and English versions. College English websites have become an important medium for their outreach, exchange programs and partnerships, finding different students and countries, and raising their profile globally [1]. There is no doubt that English language websites play an important role in international educational exchanges and participation, international school participation, and international student education. At present, most Chinese universities have opened English websites. Since then, good translation, good publicity, good communication, website construction, and internationalization of college English websites have also become new concepts studied by scholars. In this context, the development of online English corpus is particularly important. Therefore, this paper focuses on the development of online English corpus with the help of web crawler technology. On this basis, a web crawler graph is first created [2], as shown in Figure 1.

2. Literature Review

Buts and Jones said that before the big data revolution, the government and enterprises could not save all data for a long time, nor could they efficiently manage and analyze such a huge data set [3]. Ukraine said that under the traditional technology, the data storage is limited, the management is backward, and the cost is expensive [4]. In a big data environment, the most powerful new process is the collection, cleansing, and analysis of multiple files to ensure efficient, flexible, and efficient operations. According to Wang and He, from the government, industry, and all walks of life, big data becomes important for them to see new ideas and provide self-help [5].

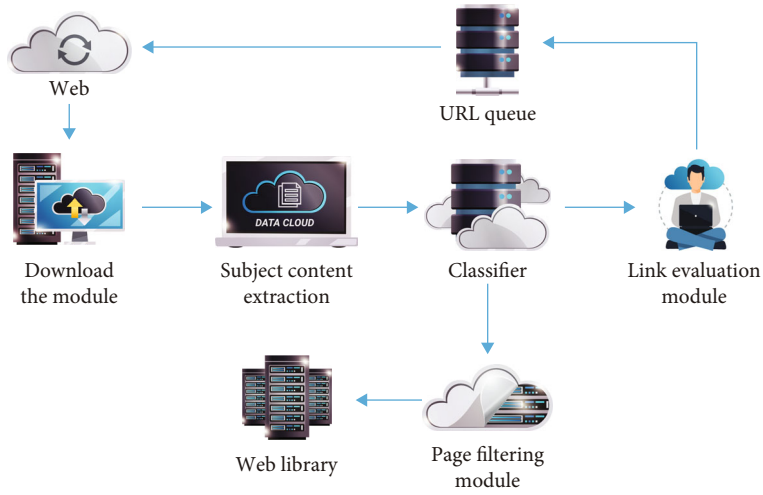

Figure 1: Architecture diagram of topic web crawler.

At present, Azazil has few research results on the application of corpus to college English websites [6]. Elgibreen et al., a corpus-based comparative analysis of English profiles of professors on English websites of Chinese and American universities, conducted a study on English profiles of Chinese and American professors from the perspective of evaluation theory [7]. In order to study the distribution of evaluation resources in the introduction discourse of English website professors in Chinese and American universities, Zhang et al. built a corpus and made a comparative analysis of the distribution of evaluation resources in the three subsystems of attitude, judgment, and grade difference under the framework of evaluation theory [8]. Kim and Davies selected 18 English profiles of Chinese and American university websites and built a micro corpus to study the public selection of high-frequency words of English profiles of Chinese and American university websites based on corpus [9]. Ding et al. conducted a corpus-based study on the core theme words of English profile of Chinese and American college websites. From minimal translation selections to full texts, these studies have started using the tools used to develop college English websites and completed some studies [10].

This paper makes a preliminary discussion on the translation of school website from the perspective of translation work. There are great differences in language and culture between English and Chinese college web pages. A full understanding of these differences is of great significance to the English translation of profiles. It is proposed that interpretative addition, modification or reorganization, and zero translation can be used as effective strategies for the translation of web profiles. Using the methods of case study and comparative study, this paper analyzes the English language news updated by four "985" colleges and universities in a city in 2021 and discusses the difficulties and solutions encountered in the network communication of college English websites. The audiences of college English websites mainly include students from various countries, overseas media, and brother colleges [11]. English websites must meet the needs of the above three groups of people in order to attract audiences and achieve the expected communication effect; this paper analyzes the problems existing in the translation of college English website propaganda and puts forward countermeasures and suggestions for the construction of college English websites from the following two aspects: on the one hand, through the comparison of parallel texts, analyze the similarities and differences in language and structure of global college English websites, and find out possible language translation errors, cultural translation errors, and functional translation errors; on the other hand, taking the text of college English website as the corpus, this paper investigates the translation initiator, translator, and audience and makes appropriate adjustments to the content and presentation of the source language, so as to make the translation meet the needs of the audience and make the college English website really play the role of external publicity.

3. Method

3.1. Overview of Web Crawler Technology. A web crawler (also known as a web spider and web bot) is a program or script that receives information from around the world through certain websites under certain laws. Web crawlers can skip a website's standard hyperlinks to search and store information. It starts with one page of the website, reads the content of the page, looks at other hyperlinks in the page, and then sees the next page through these hyperlinks [12]. Continue until all web pages on the Internet are captured. The broad classification of web crawler technology is shown in Figure 2.

Crawling means moving slowly in one direction. Technically speaking, web crawlers are tools used for data collection in search engines. They are called web crawlers, web spiders, or web robots. With the continuous development of technology, web crawlers are becoming more and more mature, which has gone beyond the definition of just a tool for search engines to collect data [13]. Generally speaking, a basic web crawler should have a set of seed URLs as input and a set of

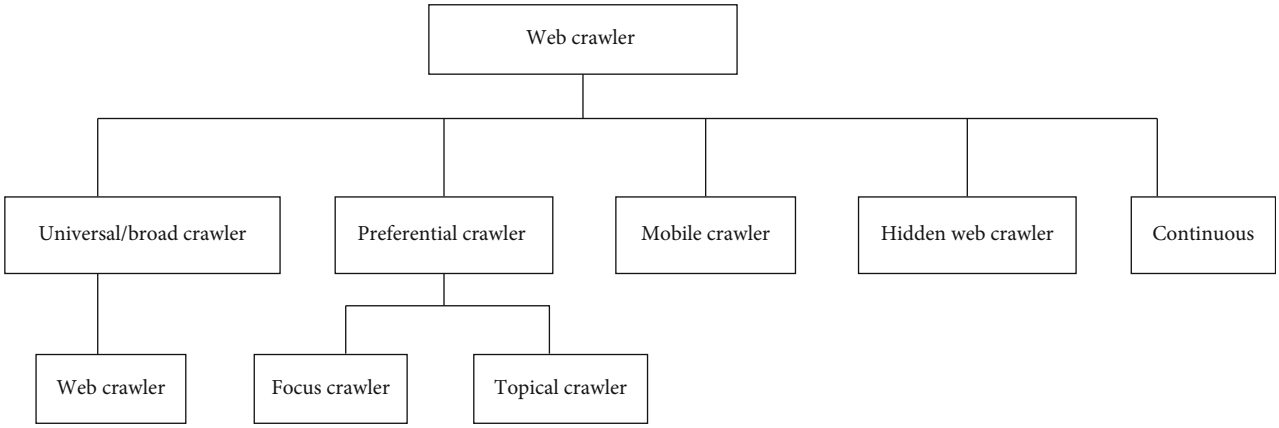

Figure 2: Classification of web crawlers.

crawled web pages as output. The specific workflow is as follows:

(1) Firstly, several initial URLs are selected as the starting position of web crawler according to the target

(2) Put the seed URL in the URL line to get it

(3) Read the URL through the URL line, resolve the DNS, and get the IP of the host. To pull the web page relative to the URL, identify the desired page, or remove the URL from the web page and place it on a line with the entry, and provide an entry for the URL in the URL field

(4) Compare the URL extracted from the web page with the crawled URL to remove the duplicate. Finally, put the deduplicated URL into the URL to be crawled, enter the cycle, and stop the web crawler when the stop condition is reached

3.2. Framework Comparison. Web crawler is the core tool for big data industry to obtain data [14]. Generally, when it comes to the collection task with small amount of data and simple capture logic, you can use self-made web crawler code for data collection. However, when it comes to the collection task with large amount of data and complex capture logic, if we continue to use the way of self-made web crawler for data collection, it will greatly increase the code development time, thus increasing the cost and time of the project. At present, there are many web crawler frameworks in the market, and different programming languages correspond to multiple web crawler frameworks. Table 1 gives some open source web crawler frameworks corresponding to programming languages in the current market.

Although there are many web crawler frameworks in the market at present, there are not many open source web crawler frameworks that are popular with developers and often used. The specific comparison can be seen in Table 2.

Scrapy is also an open source web crawler framework developed by python programming language [15]. Scrapy framework crawler has extremely powerful functions, high crawling efficiency, many related extension components, and very high degree of configurability and scalability and can flexibly customize crawling data. Scrapy can be used to download websites and extract output files from files without any issues on the page (Scrapy also provides users with options (links more like lxml) and cannot complete HTML code and simply delete files) and does a good job. For data mining, monitoring and automated testing, Scrapy can be easily customized as needed. Scrapy can be easily customized as needed. It supports the generation of crawler files from built-in definition templates, speeds up the creation of crawler code, and ensures that the code remains unchanged in large projects. In addition, scrapy also provides a variety of data export formats (JSON, CSV, XML, etc.), which can facilitate the connection with the database and data transmission in the project pipeline. The scrapy web crawler framework community has a large number of people and complete documents. It can deal with almost all current anticrawling websites. It is the most widely used web crawler framework in Python at present, as shown in Figure 3.

GitHub sets three options for open source project code: watch, star and fork, which can generally be used to indicate the activity and attention of the open source project code. The following table shows the comparison of watch, star and fork data of GitHub, an open source web crawler framework commonly used in the market so far (in descending order of star number, see Table 3) [16].

3.3. Algorithm Comparison. The most commonly used feature selection algorithms are data frequency, data gain, mutual data, and access statistics.

3.3.1. Document Frequency. The number of documents containing a word in corpus training is the frequency data for that word. The basic idea of this method is that words with low frequency often carry little information, so they cannot distinguish the categories well. Therefore, words with low frequency can be deleted, which can not only reduce the feature dimension but also improve the accuracy of classification.

Table 1: Web crawler framework corresponding to different programming languages.

Language	Web crawler framework
JAVA	Apache Nutch, webmagic, Heritriz3, WebCollector, craw1er4j, Spiderman, SeimiCrawler, jsoup-Gecco, and htmlunit
Python	Scrapy, pyspider, Newspaper, and Crawley
PHP	cola, Portia, python selenium, QueryList, phpspider, and PHPCrawl
Go	Beanbun, php selenium
C#	SmartSpider, Abot, xet, AngleSharp, HtmlAgilityPack, and CsQueryopen-source-sear ch-engine.Cobweb
C/C++	upton, Spidr, and Larbin
Ruby	wombat
node.js	node-crawler

Table 2: Comparison of web crawler frameworks.

Web crawler framework	Programing language	Describe
Apache Nutch	Java	It can collect all the contents of the website (general crawler and whole web crawler), regardless of the accuracy of collection and analysis. It is suitable for web search engines. However, nutch's crawler customization ability is relatively weak, modular design, and strong scalability; rich extraction page APIs. Support multithreading and distributed crawling. Support JS dynamic rendering page crawling. There is no framework dependency and can be flexibly embedded into the project.
Webmagic	Java	
Webcollector	Java	The Java crawler framework, which does not need configuration and is convenient for secondary development, can realize a powerful crawler with only a small amount of code. Support distributed.
Hretrix3	Java	The extensibility is enhanced to facilitate users to realize their own crawl logic. The biggest feature of the lightweight single machine open source crawler framework based on Java is simplicity. In addition, it also supports multithreading and proxy and can filter duplicate URLs.
Crawler4j		
scrapy	Python	A fast, simple, efficient and extensible web content capture framework developed entirely based on Python is used to extract the required data from the website. Scrapy has a wide range of uses and can be used for data mining, monitoring, information processing, and automated testing. Using scrapy, you can easily modify it according to your needs (scrapy is available).

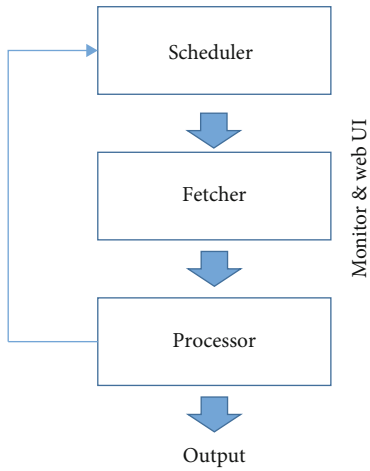

Figure 3: Pyspider architecture data flow diagram.

3.3.2. Information Gain. Information gain (IG) is to calculate the difference between the amount of information carried by the system when a feature appears and does not appear. For text classification, the difference between document frequency with and without feature word t represents the IG value of feature word t. IG value adopts the following formula, as shown in

$$\mathrm{IG}(t) = -\sum_{i=1}^{n} P(C_i)\log P(C_i) + P(t)\sum_{i=1}^{n} P(C_i|t)\log P(C_i|t) + P(\bar{t})\sum_{i=1}^{n} P(C_i|\bar{t})\log P(C_i|\bar{t}). \quad (1)$$

3.3.3. Chi Statistics. Chi statistics is often called square statistics, which is used to test whether two variables are independent. On the premise that the two variables are independent of each other, the deviation degree between the actual observed value and the theoretical value of the sample is calculated and expressed as chi value [17]. The larger the chi value, the two variables tend to be correlated; on the contrary, the two variables tend to be independent. The correlation between feature words and document categories can also be measured in this way. First, assume that the entry is independent of a category. The larger the chi value of the entry calculated on this basis, the greater the deviation between the result and the assumption, and the more relevant the entry is to the category. Therefore, the process of feature selection in this method is to calculate the chi value of each entry

Table 3: Comparison of GitHub data of web crawler framework.

Project	Language	Watch	Star	Fork
Scrapy	Python	1840	31956	7573
pyspider	Python	888	12865	3163
webmagic	JAVA	809	7730	3395
Colly	Go	219	7164	536
Pholcus	Go	441	5209	1331
node-crawler	node.js	256	4555	732
crawler4j	JAVA	307	3429	1719
WebCollector	JAVA	329	2294	1324
Apache Nutch	JAVA	245	1895	1135
QueryList	PHP	67	1469	250
Gecco	JAVA	133	1466	606
heritriz3	JAVA	174	1413	596
wombat	Ruby	53	1143	113

and category and sort it from large to small, and the top value is the feature. The calculation formula of chi value of word t for category CI is shown in

$$\mathrm{Chi}(t, C_i) = \frac{N \times (AD - CB)^2}{(A + C)(B + D)(A + B) + (C + D)}. \quad (2)$$

In the model, N represents all the data in the body, A represents the data that contains t and is Ci, B represents the data that contains t but does not contain Ci, C represents the number of data that does not contain t but belongs to Ci, and D represents no word t or data from Ci.

3.3.4. Mutual Information. In data theory, interpersonal data (MI) refers to the amount of data provided by two events. The greater the amount of mutual information, the greater the correlation. The mutual information calculation formula of word t and category Ci is shown in

$$\mathrm{MI}(t, C_i) \approx \log \frac{A \times N}{(A + C)(A + B)}. \quad (3)$$

The meaning of variables in formula (3) is consistent with that in formula (2).

3.4. Final Feature Extraction. Based on the candidate feature set, extract the final feature set. The specific steps are shown in Figure 4.

(1) Calculate the information gain value. The information gain value of each feature in the candidate feature set is calculated in the training corpus

(2) Get features. According to the decreasing order of information gain value, select some of the top features

(3) Get the final feature. Add the features obtained from the entity information to the feature set obtained in step (2), and take this feature set as the final feature set

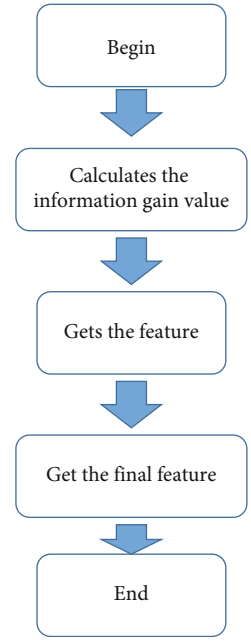

Figure 4: Final feature extraction process.

3.5. Classifier Based on Naive Bayesian Algorithm. The classifier is constructed by naive Bayesian algorithm [18]. Suppose that each instance a is represented by a feature set, and class c takes a value from a finite set C. A training example set and a test example $(a1, a2, \cdots, am)$ are provided.

The target of the instance A to be classified is to obtain the class tag c (a) of the instance $(a1, a2, \cdots, am)$, as shown in

$$c(a) = \arg\max_{c \in C} P(a_1, a_2, \cdots, a_m | c) P(c). \quad (4)$$

What we need to do now is to estimate the two probability values in equation (4) based on the training example set. Naïve Bayes classifiers assume that attribute values are conditionally independent of each other when a class tag is given. That is, the joint probability is exactly the product of each individual

feature probability. The specific formula is shown in

$$P(a_1, a_2, \cdots, a_m|c) = \prod_{j=1}^{m} P(a_j|c). \quad (5)$$

Substituting into formula (4), the classification formula of naive Bayesian classifier can be obtained, as shown in

$$c(a) = \arg\max_{c\in C} P(c) \prod_{j=1}^{m} P(a_j|c). \quad (6)$$

It can be simply calculated by calculating the occurrence frequency of different classes and eigenvalue combinations in the training example set. The specific formula is shown in

$$P(c) = \frac{\sum_{i=1}^{n} \delta(c_i, c)}{n}, \quad (7)$$

$$P(a|c) = \frac{\sum_{i=1}^{n} \delta(a_{ii}, a_j)\delta(c_i, c)}{\sum_{i=1}^{n} \delta(c_i, c)}. \quad (8)$$

Obviously, this approach leads to an underestimation of the results when the value of the zero-frequency property is present. In more severe cases, some values will be 0, making all numbers calculated by equation (6) to be 0. Laplace estimation is often used for smoothing to avoid the above problems. Equations (7) and (8) are rewritten, as shown in

$$P(c) = \frac{\sum_{i=1}^{n} \delta(c_i, c) + 1}{n + n_c}, \quad (9)$$

$$P(a|c) = \frac{\sum_{i=1}^{n} \delta(a_{ii}, a_j)\delta(c_i, c) + 1}{\sum_{i=1}^{n} \delta(c_i, c) + n_j}. \quad (10)$$

The workflow of naive Bayesian classifier based on entity link is as follows:

(1) The feature extraction method based on entity link is used for feature extraction [19]

(2) According to the obtained feature set, a naive Bayesian classifier is constructed and trained

(3) Preprocess the web page captured by the crawler, including topic information extraction, word segmentation, and other preprocessing, and then, quantify the web page

(4) The classifier is used to recognize the theme of the web page after vectorization processing. If the web page belongs to the theme class, the web page is saved to the theme page library; otherwise, the page is discarded [20]

4. Results and Analysis

For the evaluation of subject recognition effect, three indexes are mainly used: accuracy (P), recall (R), and F value. Accuracy is the proportion of the number of texts related to the topic accurately identified; recall rate is the ratio of the number of texts related to the topic accurately identified to the number of texts related to all topics in the training set; F value is a comprehensive evaluation index [21]. Suppose: in the training corpus, the text related to the subject and determined to be related to the subject is a, the number of texts unrelated to the subject but determined to be related to the subject is B, and the number of texts related to the subject but not determined to be related to the subject is C; then, the calculation formula of the three evaluation indexes is shown in

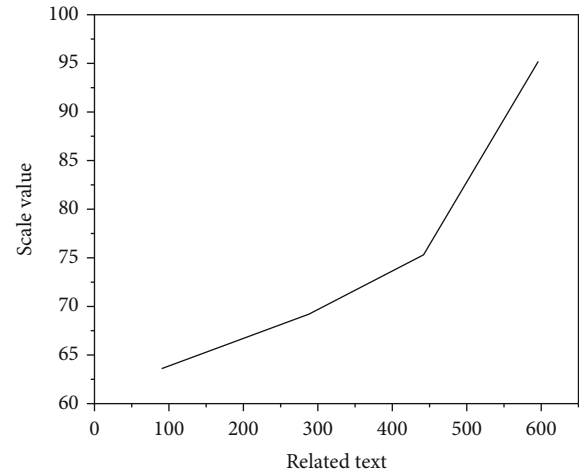

Figure 5: Experimental results (broken line).

Accuracy:

$$P = \frac{a}{a + b}. \quad (11)$$

The recall rate is shown in

$$R = \frac{a}{a + c}. \quad (12)$$

The F value is shown in

$$F = \frac{2 \times (P \times R)}{P + R}. \quad (13)$$

A total of 1443 military (587) and nonmilitary (856) articles were selected from Sogou news corpus as training corpus. The method based on entity link proposed in this chapter is used to construct naive Bayesian classifier for experiment [22]. The experimental results are shown in Figure 5.

From the experimental results, compared with the traditional naive Bayesian classifier, the introduction of entity link technology to improve it can achieve better results. As the entity link-based topic recognition algorithm can achieve good recognition effect, it lays a technical foundation for the construction of English corpus, because only efficient and accurate corpus recognition can build English corpus with richer content and more complete functions.

Table 4: Specific classification.

Common language	School profile, subject introduction, academic resume of professors, news activity reports, and introduction of institutions and departments.
Special terms	Organization department name (department, institute, institution, etc.), course name, major name, discipline name, and position name.

Corpus collection is the first step in the construction of a special English corpus for college English websites. In order to connect with international famous universities as soon as possible, improve the internationalization of Chinese university English website construction, standardize the classification system of Chinese university English website construction, and further improve the information content of Chinese university English website, we should focus on the current international first-class university English website construction, learn advanced experience, collect relevant corpus, and classify as a whole. So as to improve the Chinese expression of Chinese English and Chinese College English websites.

Use Baidu Encyclopedia, Wikipedia, and global college websites to collect information on the top ten colleges and universities in the United States. Classify and sort out the source language (English) texts of global university websites. Taking the English texts of global university websites (including website introduction, school brochures, and English version of teaching materials) as the research object, classify and sort out the corpus of Chinese and American university websites according to common terms and special terms, and construct "English original university website corpus" and "Chinese university English website corpus," respectively. This paper takes the special English of global college English websites as the research object, which mainly includes the Chinese and English versions of special English in two categories and ten subcategories of global college English websites. It mainly includes the Chinese and English versions of special English in two categories and ten subcategories of global college English websites. Each group of special texts should be no less than 10,000 words (English), and each special character text should be no less than 2,000 words (English). The specific classification is shown in Table 4.

From the results, a major problem in the development of English websites in Chinese colleges and universities is that there are too many Chinglish and Chinglish languages, and the language is incorrect. There are many news publicity materials and few practical application materials. There are many propaganda terms for Chinese audiences, but few actual contents for international scholars and international students. In particular, the construction of English websites of subordinate colleges and departments of Chinese universities, English websites of research institutions, and English websites of international students lags far behind that of the official website of Chinese universities.

On the basis of corpus collection, this paper describes the language characteristics of the English texts of "English original university website corpus" and "Chinese university English website corpus," respectively, and summarizes the unique language characteristics of the two kinds of corpus. Based on the two corpora established by the project, the world original vocabulary and vocabulary with Chinese characteristics are produced. The characteristics of vocabulary, syntax, and stylistic structure of college English websites are studied. Then, according to the characteristics of vocabulary, syntax, and stylistic structure of English websites, this paper explores typical sentence patterns and translation skills in the construction of college English websites. Through the comparative study, we find the similarities and differences between the English text of college websites translated from Chinese and the original English text and then put forward the similarities and differences between the two functions, so as to provide a real and objective basis for the subsequent improvement of the language quality of college English websites and the translation research of college English websites. Through corpus description and text analysis, we find that there are major differences between American college English official websites and Chinese college English websites in language style, discourse structure, vocabulary syntax, cultural connotation, and so on.

Generally speaking, the discourse structure of Chinese college English websites is influenced by Chinese discourse, focusing on parataxis and paying attention to the integrity, richness, and literary grace of the discourse. The English discourse of American college websites embodies the characteristics of English, focusing on hypotaxis and focusing on the form and logic of the discourse. Taking the above general introduction of the Tsinghua University and Princeton University as an example, it is not difficult to see that Tsinghua University advances linearly in chronological order, from the initial historical evolution to the introduction of the current school development in the middle and then to the final expression of the future vision and objectives of the school. On the whole, it is close to the structure of relevant Chinese texts on the school Chinese website, and the length is relatively long. The official website of the Princeton University first makes an overall introduction to the school in simple language to give readers a clear impression, and then, the detailed information classification in the website makes it easy for readers to find the practical information they want to know. In other words, a whole long text is divided into several short sub texts, which are introduced by classification, and the language introduced is mostly phrases and short sentences, which are concise and easy to understand.

5. Conclusion

The collection and recognition of corpus data is the foundation of English corpus construction, and web crawler technology has obvious advantages in data collection. Through experiments, this paper proves that web crawler technology can effectively identify and collect English corpus data, thus solving the core technical problems of English corpus construction. In addition, the construction of online English corpus based on web crawler technology is feasible, and it is very efficient in the collection and identification of corpus materials.

Data Availability

The data used to support the findings of this study are available from the corresponding author upon request.

Conflicts of Interest

The author declares that there are no conflicts of interest.

Acknowledgments

This work was supported by the fund project: The Phased Achievements of the Provincial Teaching Research Project (Research on School-Based Construction and Practice of Online and Offline Hybrid "First-Class Courses" of College English. No. 2020699) of Higher Education in Hubei Province in 2020 and Key Project of Science Research Plan of Hanjiang Normal University (Research on Information Literacy Based on Mobile Assisted Language Learning, No. XJ2020a01).

References

[1] A. E. Goldberg and T. Herbst, "The nice-of-you construction and its fragments," *Linguistics*, vol. 59, no. 1, pp. 285–318, 2021.

[2] J. Li, "Design, implementation, and evaluation of online English learning platforms," *Wireless Communications and Mobile Computing*, vol. 2021, Article ID 5549782, 11 pages, 2021.

[3] J. Buts and H. Jones, "From text to data: mediality in corpus-based translation studies," *MonTi Monografías de Traducción e Interpretación*, vol. 13, no. 13, pp. 301–329, 2021.

[4] Z. Ukraine, "English detached adjectival constructions with an explicit subject: a quantitative corpus-based analysis," *Journal of Linguistics/Jazykovedný casopis*, vol. 72, no. 2, pp. 465–474, 2021.

[5] R. Wang and J. He, "Social gender construction in political context: a corpus-based study of lexical differences across genders," *Linguistics and Literature Studies*, vol. 8, no. 3, pp. 114–124, 2020.

[6] L. Azazil, "Frequency effects in the l2 acquisition of the catenative verb construction – evidence from experimental and corpus data," *Cognitive Linguistics*, vol. 31, no. 3, pp. 417–451, 2020.

[7] H. Elgibreen, M. Faisal, M. A. Sulaiman, S. Abdou, and M. Algabri, "An incremental approach to corpus design and construction: application to a large contemporary Saudi corpus," *IEEE Access*, vol. 9, pp. 88405–88428, 2021.

[8] J. Zhang, T. Zou, and Y. Lai, "Novel method for industrial sewage outfall detection: water pollution monitoring based on web crawler and remote sensing interpretation techniques," *Journal of Cleaner Production*, vol. 312, no. 1–4, p. 127640, 2021.

[9] J. B. Kim and M. Davies, "English what with absolute constructions: a construction grammar perspective," *English Language and Linguistics*, vol. 24, no. 4, pp. 637–666, 2020.

[10] H. Ding, Y. Chen, and L. Wang, "College English online teaching model based on deep learning," *Security and Communication Networks*, vol. 2021, Article ID 8919320, 11 pages, 2021.

[11] A. H. Meftah, M. Qamhan, Y. Seddiq, Y. A. Alotaibi, and S. A. Selouani, "King Saud University emotions corpus: construction, analysis, evaluation, and comparison," *IEEE Access*, vol. 9, pp. 54201–54219, 2021.

[12] N. Li, X. Jin, and Y. Li, "Identification of key customer requirements based on online reviews," *Journal of Intelligent and Fuzzy Systems*, vol. 39, no. 1984, pp. 1–14, 2020.

[13] K. Thirugnanasambanthan, "A new approach to web crawling — dhekts crawler in comparison with various crawlers," *Indian Journal of Science and Technology*, vol. 14, no. 19, pp. 1580–1586, 2021.

[14] Z. Jiang, C. Chi, and Y. Zhan, "Research on medical question answering system based on knowledge graph," *IEEE Access*, vol. 9, pp. 21094–21101, 2021.

[15] G. Liu, S. Fei, Z. Yan, C. H. Wu, and J. Zhang, "An empirical study on response to online customer reviews and e-commerce sales: from the mobile information system perspective," *Mobile Information Systems*, vol. 2020, Article ID 8864764, 12 pages, 2020.

[16] N. A. Ismail, N. I. Ramzi, E. Su, and M. Razak, "Webometric analysis of institutional repositories of Malaysian public universities," *DESIDOC Journal of Library & Information Technology*, vol. 41, no. 2, pp. 130–139, 2021.

[17] U. K. Balajisaravanan, K. Karthick, S. Rajkumar, M. Murali, and N. Selvanathan, "Design of a personalized domain specific web crawler," *International Journal of Advanced Science and Technology*, vol. 29, no. 7, pp. 12162–12167, 2020.

[18] Y. Li, H. Wei, Z. Han, J. Huang, and W. Wang, "Deep learning-based safety helmet detection in engineering management based on convolutional neural networks," *Advances in Civil Engineering*, vol. 2020, Article ID 9703560, 10 pages, 2020.

[19] Y. Hao, X. Yan, J. Wu, H. Wang, and L. Yuan, "Multimedia communication security in 5G/6G coverless steganography based on image text semantic association," *Security and Communication Networks*, vol. 2021, Article ID 6628034, 12 pages, 2021.

[20] M. Li and J. Zhang, "Integrating Kano model, AHP, and QFD methods for new product development based on text mining, intuitionistic fuzzy sets, and customers satisfaction," *Mathematical Problems in Engineering*, vol. 2021, Article ID 2349716, 17 pages, 2021.

[21] Y. Yao, D. Hu, C. Yang et al., "The impact and mechanism of fintech on green total factor productivity," *Green Finance*, vol. 3, no. 2, pp. 198–221, 2021.

[22] Z. Zhai, X. Chen, Y. Zhang, and R. Zhou, "Decision-making technology based on knowledge engineering and experiment on the intelligent water-fertilizer irrigation system," *Journal of Computational Methods in Sciences and Engineering*, vol. 21, no. 3, pp. 665–684, 2021.

Hindawi
Wireless Communications and Mobile Computing
Volume 2022, Article ID 1926940, 13 pages
https://doi.org/10.1155/2022/1926940

Research Article

Application of Image Color Gamut Boundary Judgment Algorithm in Digital Media

Xuewei Li

College of Art, Northeast Electric Power University, Jilin Jilin 132000, China

Correspondence should be addressed to Xuewei Li; lixuewei@neepu.edu.cn

Received 18 May 2022; Revised 25 July 2022; Accepted 1 August 2022; Published 28 August 2022

Academic Editor: Jun Ye

Image chromatic aberration evaluation is one of the research hotspots and academic difficulties in the field of color science and imaging technology. Based on the algorithm theory of image color gamut boundary judgment, this paper constructs its application model in digital media. The model uses the threshold color difference image as a reference and applies it to the evaluation experiment of color difference above the threshold based on the quantitative estimation method. During the simulation process, the improved HAD dual-color image digital boundary judgment algorithm is programmed. For small color difference data at the threshold level, the calculated color difference of the boundary judgment algorithm framework is smaller than the visual perception color difference; for the large color difference data above the threshold, the boundary judgment algorithm framework is given. The research results of the threshold color difference experiment show that the perceptible color difference threshold and acceptable color difference threshold of image color gamut observers for image color difference are 1.85 AE and 3.63 AE, respectively, which are basically twice the relationship. The visually perceptible chromatic aberration threshold and acceptable chromatic aberration threshold for lightness parameters are higher than those of chroma and hue, which shows that the boundary judgment algorithm framework has certain advantages for the evaluation performance of color digital image threshold chromatic aberration and effectively improves the algorithm robustness.

1. Introduction

With the development of various display media technologies, the application of color digital images in people's work and life is becoming more and more extensive, so the color difference evaluation of color digital images becomes increasingly important [1]. However, since a color digital image is composed of a large number of pixels of different colors, it is an uneven and complex color sample, which is difficult to measure directly with a colorimetric instrument [2], and it is also more complicated than a uniform color sample to calculate, so it has always been a color science and research difficulties in the field of imaging technology [3, 4].

Image chromatic aberration evaluation is one of the research hotspots and academic difficulties in the field of color science and imaging technology. Objectively and effectively measuring and evaluating the color difference between different color samples is also a difficult problem and a key technology to be solved urgently in the industry. These color difference formulas have been widely used in textile, printing, and other industries [5, 6]. With the development of science and technology, display devices such as smart mobile phones, digital TVs, tablet computers, and desktop monitors also require an accurate color difference formula to evaluate the reproduction performance of their color digital images [7]. This brings huge losses to the self-interest of the original creator [8]. Therefore, the issue of intellectual property protection of digital media has attracted more and more attention, and the issue of digital media certification has become increasingly prominent [9–11].

This paper studies the application of the image model boundary judgment algorithm framework in image chromatic aberration evaluation. The research first verified CIELAB, CIEDE2000, S-CIELAB, S-CIEDE2000, and CAM02 through the psychophysical experimental method test of category determination. The performance of the six color difference formulas and models of UCS and boundary judgment algorithm in the evaluation of image color difference

and the parameters affecting the evaluation of image color difference were analyzed through visual data, and the relationship between lightness, chroma, hue, resolution, and sharpness was discussed. These three methods are the most used in current applications, so the algorithms in these three transform domains are introduced. The research results show that the boundary judgment algorithm framework based on the appearance model has the highest prediction accuracy for image color difference, followed by S-CIELAB, and CAM02-UCS has the worst performance in image chromatic aberration evaluation. The experimental results show that, compared with the traditional Krawtchouk transform, the boundary judgment algorithm of fractional Krawtchouk transform domain will have better robustness and invisibility of digital media after the appropriate fractional order is selected; compared with other transform domain (such as DCT and DWT) boundary judgment algorithms, the robustness of the algorithm in this paper is also higher.

2. Related Work

The researchers used the eigenvalue decomposition method to construct a one-dimensional fractional Krawtchouk transform and further extended it to a two-dimensional space; finally, a class of robust boundary judgment algorithms in the transform domain was designed by applying the fractional Krawtchouk transform [12]. By adjusting the fractional order, the robustness and invisibility of digital media can be enhanced. In addition, in the boundary judgment algorithm, the fractional order can be used as a key to enhance the security of digital media [13].

Dong et al. [14] modified the coefficients in the transform domain to embed digital media. These transforms include discrete Fourier transform (DFT), discrete cosine transform (DCT), and discrete boundary judgment transform (DWT). Bogert et al. [15] believe that it needs to transform the original image, the calculation is more complex, and the amount of data is large, but the digital boundary judgment algorithm in the transform domain can resist the influence of compression coding and low-pass filtering; it can effectively resist such as JPEG compression; the energy distribution in the transform domain is concentrated and easily combined with the human visual system (HVS) to determine the strength of embedded digital media. Wang and Cao [16] found that the method of embedding digital media based on transform domain has many advantages over the method of embedding digital media based on spatial domain, so it is very suitable for application in digital digital media technology. Vazquez and Bertalmío [17] proposed a digital boundary judgment algorithm based on the boundary judgment tree of important coefficients, which uses the boundary judgment of zero-tree coding and the masking of the human visual system to judge the boundary of the blue component (the least sensitive of the human eye) of the color image. Zuo et al. [18] verified that the algorithm has good invisibility, but various image color gamut processing has a greater impact on the blue component, digital media may be lost in various image processing, and the robustness is poor [19].

Compared with the spatial boundary judgment algorithm, the subsequently developed transform domain digital boundary judgment algorithm is more popular because it has many advantages [20]. Transform domain boundary judgment algorithm is to embed digital media information by changing transform domain coefficients. At present, there are commonly used boundary judgment algorithms based on DFT, boundary judgment algorithms based on DWT, and boundary judgment algorithms based on DWT. Then, the LSB algorithm in the spatial domain, the DCT-based boundary judgment algorithm in the transform domain, and the DWT-based digital media algorithm are compared in simulation experiments. The results show that the transform domain boundary judgment algorithm is more robust than the spatial domain boundary judgment algorithm as a whole [21], and the robustness of the boundary judgment algorithm based on DWT in the transform domain is stronger, so this paper selects the boundary judgment transformation to process the image and strives to obtain good robustness and invisibility. Scholars proposed a blind detection algorithm based on boundary judgment domain contrast and HVS characteristic adaptation [22]. The scheme embeds digital media into the detail subgraphs LH and HL by analyzing the boundary judgment transformation and performs the embedding intensity factor according to the boundary judgment contrast and HVS characteristics (i.e., brightness sensitivity, texture sensitivity, and contrast sensitivity) [23, 24]. Experimental results show that the scheme has strong invisibility and robustness without attacks [25] but is not robust after noise, median filtering, clipping, and JPEG compression attacks [26, 27].

3. Analysis of Image Color Gamut Boundary Judgment Algorithm

3.1. Image Gamut Scale. Two stimulus color samples are considered to have matching colors to a standard image gamut observer with normal color vision if they have the same tristimulus value. The image color gamut scale is to establish a prediction model that conforms to the characteristics of color visual discrimination, that is, each unique color should have a unique chromaticity parameter, and a coordinate system with each dimension perpendicular to each other can be used to express the chromaticity parameter of the response. And they reflect the main visual characteristics of color, such as lightness, chroma, and hue. The calculated color difference between two stimulus color samples should be proportional to the corresponding difference in visual perception.

$$\iint \frac{fin(t)}{1/x(t)} - \frac{fin(t+\sigma w(t))}{k(t,t-1)}\,dtdw = 0. \tag{1}$$

Usually, the three RGB channels of a color image pixel are represented as the three imaginary parts f, j, and k of the quaternion. That is, the quaternion method can represent a color image as a pure quaternion matrix. In this way, the three channels of the color image can be processed

as a whole. Suppose (m, n) is a color image of size $M \times N$, which can be expressed as a quaternion.

$$\begin{cases} fin(t + \sigma w(t)) = \dfrac{1}{x} - \dfrac{1}{t}, \\ fin(t - \sigma w(t)) = \sqrt{t}. \end{cases} \tag{2}$$

For the blind boundary judgment algorithm that adopts the quantization method, the plaintext digital media (meaningful binary image digital media) is usually selected. This type of method perturbs the selected transform domain coefficients (or coefficient expressions) according to the bit information (0 or 1) of the digital media after the original image is subjected to the overall orthogonal transform or the block orthogonal transform. Then, inverse transform is performed on the whole transform domain coefficients or the block transform domain coefficients in Figure 1 after perturbation to obtain an image added with digital media.

The image color gamut is decomposed into a series of subband signals with different spatial resolutions (different channels), different frequency characteristics, and directional characteristics. These subband image color gamuts have good local characteristics such as time domain and frequency domain, which can be used to represent the local features of the original image color gamut and then realize the localized analysis of the time and frequency of the image color gamut.

The LSB watermarking algorithm in the spatial domain, the DCT-based watermarking algorithm, and the DWT-based watermarking algorithm in the transform domain are compared by simulation experiments, respectively. The experimental results show that the digital watermarking algorithm based on DWT has stronger robustness than the LSB algorithm and the algorithm based on DCT, so this paper chooses to embed the watermark based on wavelet transform. The quantization formula is divided into an embedding formula and an extraction formula. For the convenience of description, we represent the digital media as a vector w, and f represents its i-th element with a value of 0 or 1; the selected transformation coefficients are represented as vectors C and S, representing its i-th element.

3.2. Combination of Boundary Judgment Conditions. In a mixed color composed of several color components, if one color changes continuously, the appearance of the mixed color will also change continuously. From this, the complementary color law and the intermediate color law of the boundary judgment conditions are obtained. The law of complementary colors: if a color is mixed with its complement in appropriate proportions, it will produce white or gray; if it is mixed in other proportions, it will produce a desaturated color that approximates the color with a larger specific gravity. The law of halftones: the mixing of any two noncomplementary colors produces a halftone whose hue depends on the relative amounts of the two colors, and the saturation in Table 1 depends on how far and near the two colors are in the hue order.

In order to verify the advantages and disadvantages of the algorithm and ensure the authenticity of the evaluation results, each image color gamut observer is required to adapt to the image for 30 minutes before determining the judgment result. Theoretically, if the transform used is an orthogonal transform, the coefficients obtained after transforming the protected image with digital media are equal to the perturbed coefficients (i.e., the values at points P1, P2, P3, and P4). When the values of quality are 90, 80, 70, and 60, respectively, the PSNR value of the algorithm HAD is higher than that before the improvement, but the NC value is lower than the original algorithm, but the NC value is also at a high level. This algorithm is attacked by JPEG compression. The robustness of the future image gamut is stronger.

3.3. Algorithm Recursion Analysis. In this experiment, we embed two digital media images into 96 carrier images, respectively, to obtain 192 algorithm recursion test combinations. In each group of experiments, the fractional order $a = b = 0.4$ is selected, and then, the PSNR value of the digital media image is obtained as the embedding step increases. The figure shows the change of the average PSNR value of the 192 test groups with the increase of the embedding step size. It can be seen from the figure that (1) with the increase of the embedding step size, the PSNR value of the digital media image decreases; (2) under the same quantization step size, the proposed FrKT domain boundary judgment algorithm is better than the Krawtchouk transform domain and score it.

$$\text{tinret}(h(x), x) = \begin{cases} 1 - \cos j(x) \sin h(x), \\ 1.5 \sin (x) \cos (h - x). \end{cases} \tag{3}$$

The boundary judgment algorithm of the order boundary judgment transform (DrFT) has a higher PSNR value, because after the FrKT transform coefficients are embedded in the digital media, the information of the digital media is more evenly distributed to the whole image through the inverse transformation. X, Y, and Z are the tristimulus values of the color sample, Xn, Yn, Zn is the tristimulus value of the CIE standard illuminator irradiated on the complete diffuse reflector and reflected to the eyes of the observer in the image color gamut, where $Yn = 100$, when the viewing angle of the image color gamut of the color sample is less than 30.

In this experiment, the CV value is used to represent the observer accuracy of the image gamut in Figure 2. Image gamut interobserver accuracy refers to the agreement between the experimental data of each image gamut observer and the experimental data of other image gamut observers. The CV values of the image gamut observer accuracy are shown. When viewing the field of view, the CIEl931 XYZ standard chromaticity system should be used; when the viewing angle of the image color gamut of the color sample is greater than 40 fields of view, the CIEl964 XYZ standard chromaticity system

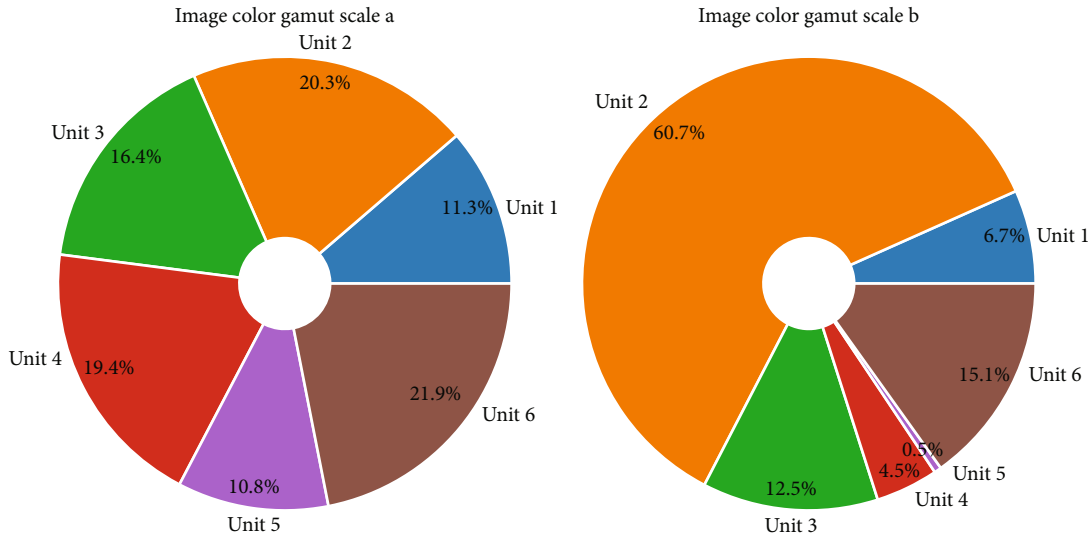

Figure 1: Coefficient distribution of image color gamut scale transform domain.

Table 1: Attributes of boundary judgment conditions.

Attribute number	Evaluation a	Evaluation b	Evaluation c	Evaluation d
10	0.87	1.98	0.46	-1.07
20	0.40	-0.44	0.13	-0.10
30	0.45	1.15	0.19	0.47
40	0.77	-0.43	0.82	-0.45
50	0.43	-1.68	0.49	-1.36
60	0.11	0.19	0.19	-0.05

should be used.

$$\begin{cases} \cos\left(2\text{delta}(x) + x\right) = r + t, \\ \sin\left(2\text{delta}(x) - x\right) = r - t. \end{cases} \tag{4}$$

The subscripts A and B, respectively, represent the two color difference formulas being compared, by comparing the F value with the critical value Fa. Fa is the critical value for determining the F distribution under the confidence interval. Generally, in order to have better robustness of digital media images, a larger quantization step size should be selected; however, a larger quantization step size will lead to a decrease in the visual quality of the image.

The related literatures are the watermarked image and the extracted watermarked image after JPEG compression attack with quality factor = 80 and quality factor = 40, respectively. Generally speaking, the PSNR value of the image embedded in the digital media should be at least close to 40 dB to ensure the invisibility of the digital media. In the following experiments, we selected a quantization step size of 25 for the boundary judgment algorithm of the Krawtchouk transform domain (the average PSNR was 40.72 dB at this time) and selected a quantization step size of 40 and 25 for the boundary judgment algorithm of the FrKT domain (this time the average PSNR was 40.72 dB). The time average PSNR is 42.25 dB and 46.43 dB, respectively.

4. Model Construction of Image Color Gamut Boundary Judgment Algorithm in Digital Media

4.1. Image Color Gamut Normalization Index Analysis. In the test of image color gamut normalization index stage, six modulation parameters including brightness, chroma, hue, contrast, resolution, and sharpness were selected for the test of image color difference parameters and color difference formula. Each parameter is modulated by functions, wherein the modulation of lightness, chroma, and hue is to modulate L, C, and h, respectively, in CIELAB space. Contrast modulation is divided into brightness contrast modulation and chroma contrast modulation, which use the sigmoid function and the inverse-sigmoid function, respectively, to increase and decrease the contrast. The modulation of the resolution adopts the method of double-cubic resampling, and the pixels of 2×2, 3×3, and 4×4 are averaged to the pixels of $l \times l$, respectively.

$$\frac{1 - y(x) - z(x) - x}{y(x) - z(x) - x} = \sum z(x) - x \sum y(x) - x. \tag{5}$$

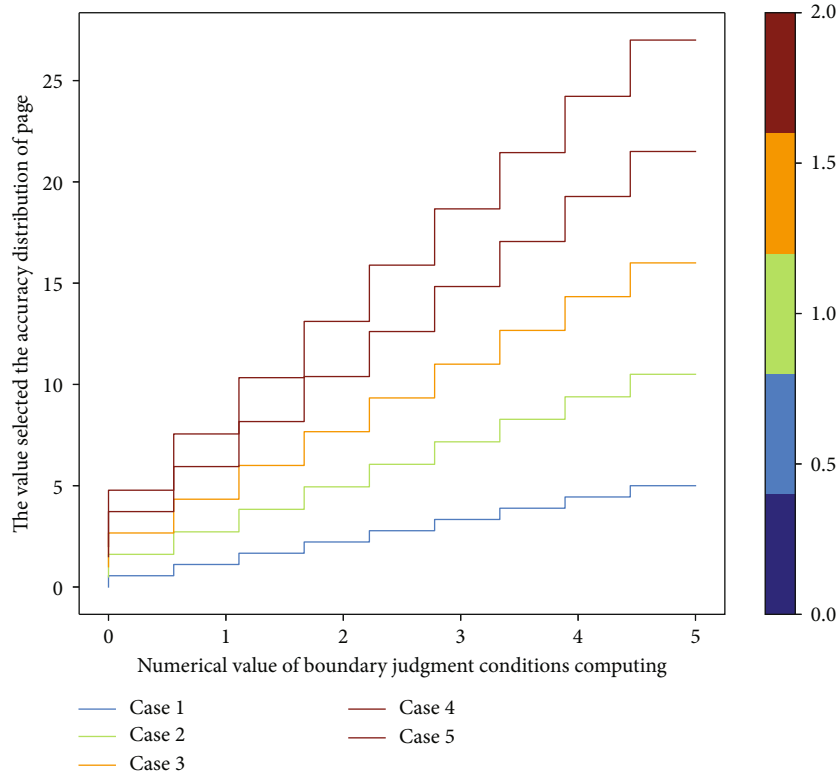

Figure 2: Accuracy distribution of boundary judgment conditions.

They embed "Deer" digital media into each original image and then calculate the PSNR value of the image after digital media, and it shows the change curve of the average PSNR value with the change of fractional order. It can be seen from the figure that (1) when the fractional order $a = b = l$, the PSNR value is the smallest, and FrKT degenerates into the traditional Krawtchouk transform; (2) when the PSNR value is the largest, $a = b = 0.4$ and 0.6. Further, digital media attack is carried out on each image embedded in digital media, and the robustness of the boundary judgment algorithm is analyzed with the change of fractional order.

$$\frac{dy(x)}{dx} - \frac{dz(x)}{dx} = \begin{cases} \frac{1}{2} fin\left(\frac{1-x}{1-y(x)}\right), \\ \frac{1}{2} fin\left(\frac{1-x}{1-z(x)}\right). \end{cases} \quad (6)$$

The article gives the situation that the average BER of all image extraction digital media varies with the fractional order under different attacks. It can be seen from the figure that the average BER is larger when $a = b = 0.1$ and 0.7, which indicates that the robustness of the boundary judgment algorithm is not good at this time. This is because when $a = b = 0.1$ or 0.7, the transformation coefficient we choose is small, even smaller than the quantization step size; after the image with digital media is attacked, the value of Figure 3 changes greatly.

The similarity between the detected digital media and the original digital media is measured by BER, and the BER is close to 0, and the more similar the detected digital media is to the original digital media, the higher the robustness of the digital media. It lists several types of image processing attacks used in the experiment and the corresponding attack parameters. For the rotation and scaling attack, the experiment firstly performs geometric transformation on the image and then performs geometric deformation correction on the transformed image to obtain the attacked image. In order to compare the robustness under different fractional orders, the fractional orders (0.4, 0.5) were selected for the FrKT transform in the experiment.

4.2. Boundary Judgment Coefficient Update. After the experiment of boundary judgment coefficient stage I, it is found that the modulation method of resolution is not very reasonable, and the modulation of chroma and contrast greatly changes the image content, and the sigmoid function of contrast modulation is inverse. The sigmoid function is more complex.

$$0.01 > \frac{\text{ziber}(x,y)}{\text{ziber}(x)} + \text{ziber}(y) - \text{ziber}(y) > 0.001. \quad (7)$$

Therefore, after further reviewing the literature, the modulation parameters and modulation methods selected in the evaluation experiment on the threshold and suprathreshold image chromatic aberration in phase II have been modified to a certain extent. The modulation parameters selected in the stage experiment are lightness,

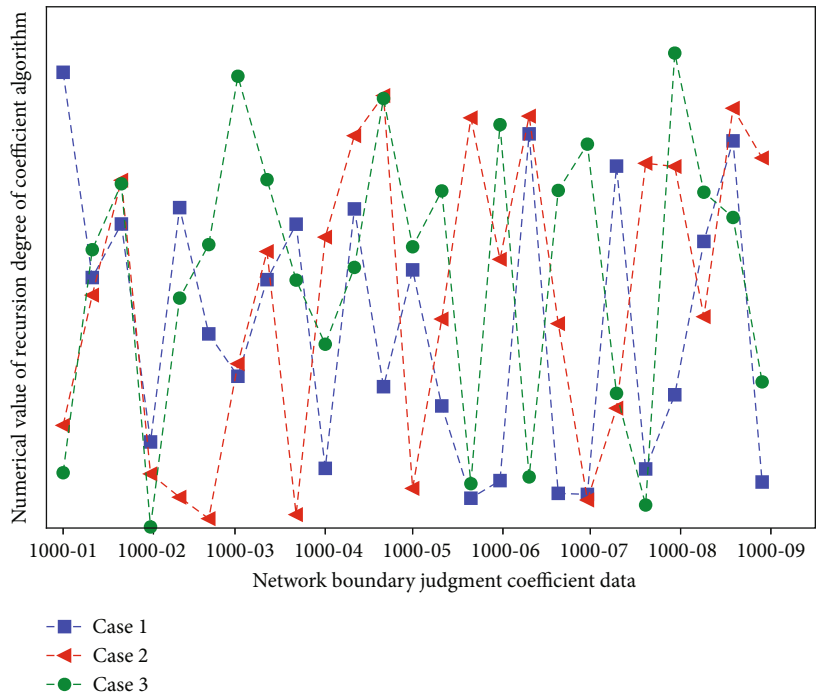

Figure 3: Recursion of boundary judgment coefficient algorithm.

chroma, hue, contrast, and sharpness, and the specific modulation functions and parameters are as shown. The modulation of lightness and chroma is divided into two types: multiplicative and power. For the modulation of contrast, another simple sigmoid function is used to modulate the brightness. The shift modulation of the hue angle and the modulation of the sharpness are the same as those of the phase I method. Finally, there are a total of 540 test images (6 original images × 90 modulations) for phase II experiments.

This kind of color gamut mapping is similar to the device-to-device color gamut mapping, and it is still the calculation from an input point in Figure 4 to an output point in the three-dimensional perceptual color space, regardless of the distance between adjacent pixels in the image color space relation. It can be seen that after the watermark embedding is performed according to the algorithm in this paper, the attacked watermark image has little visual impact, and the similarity between the extracted watermark image and the original watermark image is high, indicating that the algorithm in this paper can attack JPEG compression.

Most of the existing color gamut matching algorithms perform color conversion on an image pixel by pixel and only consider the color characteristics of the image and ignore the color correlation between image pixels. Since the out-of-gamut colors in the image are usually the border colors of the image, it is very important to protect the continuity of the color gamut border of the image. Nonspatially related mapping algorithms sometimes make different colors of the image border map to the same color, resulting in blurred borders or lost borders. Sometimes they are mapped to different colors but distort the facts and make similar colors adjacent in space appear dissimilar. This depends on the spatial properties of neighboring pixels.

$$\left[(\text{delta}(a)\text{\^{}}2 - a) + (\text{delta}(b)\text{\^{}}2 - b) + (\text{delta}(c)\text{\^{}}2 - c) + \frac{1}{abc}\right] = 1 - abc. \tag{8}$$

In contrast, the two boundary judgment algorithms using the DCT domain and the domain are more robust to histogram equalization, which is due to embedding digital media bits into the edge information of the image or using correlations between blocks to embed them. Digital media will increase the robustness of boundary judgment algorithms to histogram equalization.

4.3. Image Color Gamut Interpolation Fitting. In the image gamut interpolation experiments, we combined each binary image with 15 color original images separately to generate zero digital media for the image, generating a total of 105 experimental combinations. Common image processing attacks are then performed on each combined protected image, and digital media is extracted to analyze the robustness of the algorithm.

$$1 - \prod \frac{\text{inret}(\text{ciber}(m,n),m,n)}{m+n} - \prod \frac{\sqrt{\text{inret}(\text{ciber}(m,n),m,n)}}{1-m-n} = \frac{1}{m-n}. \tag{9}$$

More generally, we randomly generate 0-1 matrices of size 64 × 64 as digital media to verify the robustness of the algorithm. Use this matrix to generate the verification information of 15 color images, and then perform various image processing attacks on each image to obtain the average value

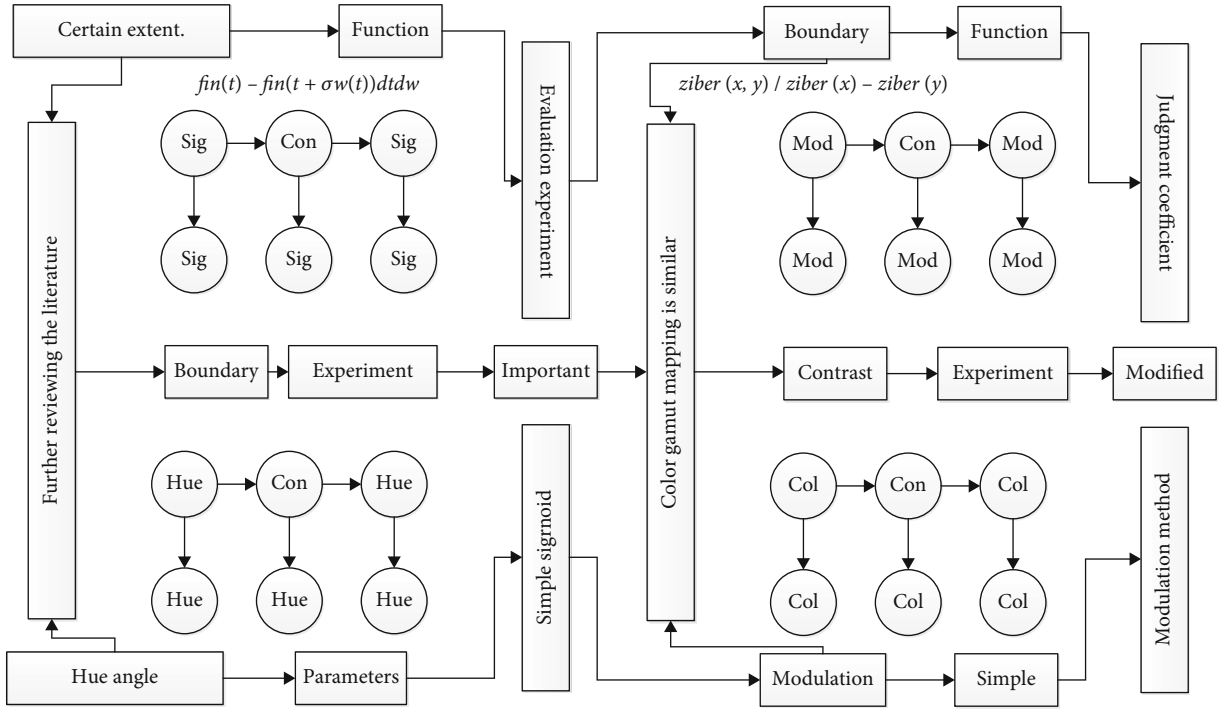

Figure 4: Mapping relationship of boundary judgment coefficients.

of the extracted digital media. It can be seen from the figure that the BER value of the proposed algorithm is lower than that of the existing methods under most attacks, which verifies the robustness of the algorithm in Figure 5.

In this algorithm, the invisibility of digital media depends on the distortion step size parameter, the quantization step size J, and the object parameter in TDFT. Generally speaking, the larger the quantization step size, the better the robustness of the digital media; but the larger quantization step size will lead to the degradation of the image quality of the digital media. According to the experiment, first we choose $g = 700$ and then analyze the influence of a.

$$\frac{\tan \text{gent}(x, y, z)/\text{heter}(x)\text{heter}(y)\text{heter}(z)}{1 - \text{heter}(x, y, z)} \in R. \quad (10)$$

In this experiment, we combined "Deer" digital media with the original images, respectively, to obtain 20 test combinations. The BER value of the paper considers geometric attacks on digital media and the combination of common image gamut processing attacks and ensemble attacks, including the following: image rotation, image scaling, image rotation+scaling, image translation, image cropping, image rotation+scaling+median filter, image rotation+scaling +mean filter, image rotation+scaling+salt and pepper noise, image rotation+scaling+Gaussian white noise, and image rotation+scaling+JPEG compression.

4.4. Quantization of Digital Media. The digital media quantization steps are divided into the following: (1) the original image is resized to make the generated hash robust against scaling operations, and the generated hash is not affected by the image size, and the image is converted to YCrCb

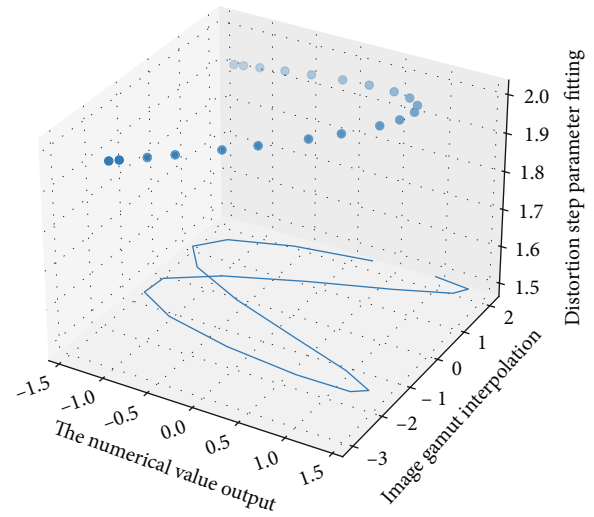

Figure 5: Image color gamut interpolation distortion step parameter fitting.

space; (2) the zemike moment feature of the Y component and the zemike moment feature of extracting the absolute value of the difference between the Cr and Cb components use the values of the first 5-order zemike moments as the global feature, so a total of 22 real eigenvalues except 0-order 1; (3) we perform salient feature extraction on the image, take the first 6 largest salient regions and then extract 4 features of each region including 2 position coordinates and length and width and extract 4 texture features, thus obtaining a total of 48 real local parts.

By extending the boundary judgment transformation in Figure 6 to a two-dimensional situation, the approximate

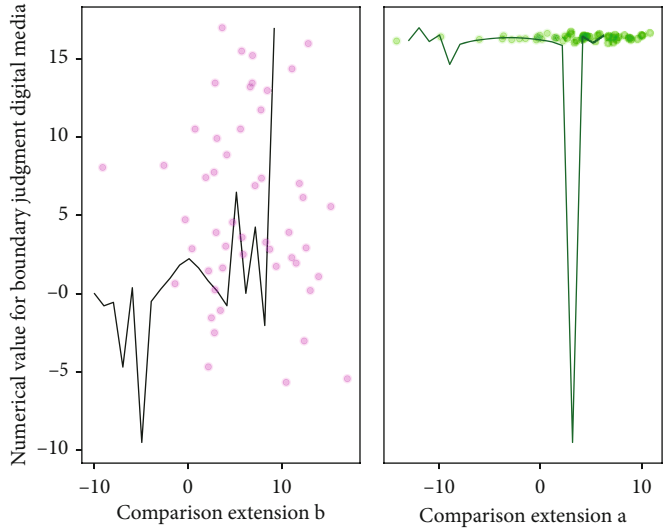

Figure 6: Digital media quantization boundary judgment transformation extension.

components and detail components of the original image in different scales and directions can be obtained. After the image is transformed by multiscale boundary judgment, the coefficients present a pyramid-like structure. And the image energy is redistributed; most of the energy is distributed on the boundary judgment coefficient of the lowest frequency.

$$\left.\begin{aligned} \nabla da &= da(i) - da(j) \\ \nabla db &= db(i) - db(j) \\ \nabla dc &= dc(i) - dc(j) \end{aligned}\right\}. \tag{11}$$

The design of the system content and the construction of the experimental platform are parameterized: the watermark image and the extracted watermark image after the Gaussian noise attack with a mean of 0 and a variance of 0.005 are added. Since both FrBFM and BFM can construct the rotation and scaling invariance of the image, in the case of only geometric attack, FrBFM and BFM have similar robustness, the difference is not very big, and the BER is close to 0.

$$\begin{bmatrix} \sqrt{da(i) + da(j) - 1} \\ \sqrt{db(i) + db(j) - 1} \\ \sqrt{dc(i) + dc(j) - 1}, \cdots, 1) \end{bmatrix} = \sum dxdi. \tag{12}$$

It refers to the relationship between the visual perception chromatic aberration of the observer in the image color gamut and the parameter k after linear modulation of lightness or chroma with parameter k. It can be seen that the error bars of the visual perception chromatic aberration for lightness and chroma vary with the modulation parameter k, that is, the greater the lightness difference or chroma difference, the greater the influence of the image content on the visual perception chromatic aberration of the image gamut observer, it can also be said that the small color difference data between the images is less affected by the image content, while the large color difference data between the images may have a great relationship with the image content.

5. Model Application and Analysis of Image Color Gamut Boundary Judgment Algorithm in Digital Media

5.1. Preprocessing of Image Color Gamut Boundary Data. Using Komca Mmolm company's spectroradiometer CS2000 was measured at a distance of 1.3 m from the display, as shown in the image gamut boundary data. According to the IEC standard, the measurement is carried out in a dark room. The size of the color block to be measured is 5 cm × 5 cm and displayed in the center of the screen. All measurements are performed on this color block, and other areas of the screen are set to black. The tested color blocks are $17 \times 4 = 68$ sets of training samples consisting of red, green, blue, and gray in the range of 0-255 with 16 sampling intervals, and 100 randomly generated test sample data are measured at the same time.

$$\begin{bmatrix} fin(i - \sigma w(i)) \\ fin(j - \sigma w(j)) \\ fin(k - \sigma w(k)) \end{bmatrix} = \begin{bmatrix} i - w'(i) \\ j - w'(j) \\ k - w'(k) \end{bmatrix}. \tag{13}$$

On the whole, the value of the boundary judgment algorithm model for the prediction results of the brightness parameters of the six images is the smallest, that is to say, the correlation between the brightness difference calculated by the boundary judgment algorithm model and the visual perception color difference is the best; especially for the "Street" and "Ski" images, the prediction accuracy of the boundary judgment algorithm was evaluated by F. After

the test, it is significantly better than other color difference formulas.

There are some influences, but it can be recognized, indicating that the algorithm has good resistance to Gaussian noise attack, but it is worse than salt and pepper noise attack. The prediction accuracy of the S-CIELAB model is second only to the boundary judgment algorithm model; especially for the images "Fruits" and "Flower," the prediction accuracy of the S-CIELAB model is very close to the boundary judgment algorithm model, but the S-CIELAB model is for others. The prediction accuracy of the 4 images is slightly different from the boundary judgment algorithm model.

The prediction accuracy of CIELAB and S-CIEDE2000 color difference formula for the image in Figure 7 is very close, while the prediction accuracy of CIEDE2000 is slightly worse than that of CIELAB and S-CIEDE2000, CAM02. The prediction accuracy of UCS on the brightness parameter is most affected by the image content. Its prediction accuracy for the image "Street" is the worst, and its prediction accuracy for the image "Tree" is better, second only to the boundary judgment algorithm model.

$$\frac{\partial \text{delta}(\text{case}(x)-x)}{\partial \text{delta}(x)}+\frac{\partial \text{delta}(\text{case}(y)-y)}{\partial \text{delta}(y)}+\frac{\partial \text{delta}(\text{case}(z)-z)}{\partial \text{delta}(z)}=\sqrt{1-\text{case}(x,y,z)}. \tag{14}$$

This may be because the image "Street" contains a lot of complex high-frequency information and is not suitable for CAM02-UCS, a color difference model based on a single color block calculates color difference, and the image content of "Tree" is relatively simple, so CAM02 is used.

5.2. Implementation of Digital Media Simulation. In order to further compare the performance of the ULPM method and the IULPM method for extracting digital media, we put these two methods in the test image sets data 1 and data 2 for simulation tests. Each test image in the test image set data 1 undergoes a step size of 0.1 from 50 to 100. From this, we can observe the image color gamut that the proposed IULPM method extracts the average NC value of digital media close to 0.9, while the average NC value of the ULPM method is between 0.1 and 0.9. We also tested the 1800 angles of Figure 8 from 0 to 1800 with a step size of 0.10, and the experimental results show similar results.

If the original image is a color image converted to YCrCb space, only the luminance Y component is used, and the resizing makes the generated hash robust against scaling operations and the generated hash is not affected by the image size, for a robust rotation-resistant operation, the image performs a rotation projection to obtain a second image. As shown, this operation converts the rotation of the image into a translation of the second image, and then combines the rotation, and invariant features are obtained by translation invariance.

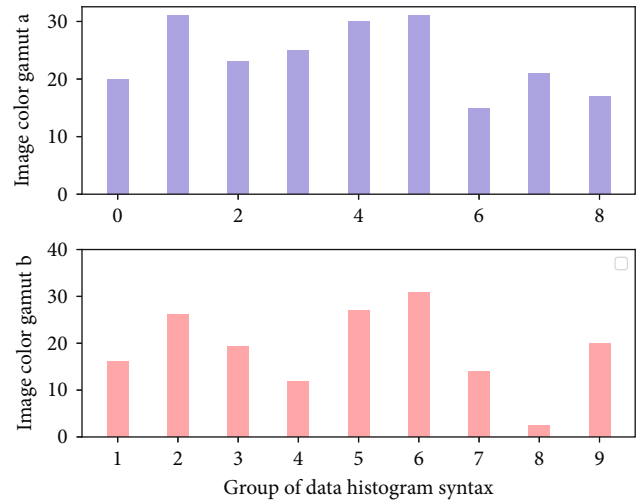

Figure 7: Histogram of image color gamut boundary data.

All methods are tested on the dataset data 1 in Figure 9. For a fair comparison, the PSNR value of all images embedded in digital media is ensured to be close to 40 dB by adaptively adjusting the respective digital media embedding strength, and the results are obtained by all methods use their respective algorithms. The parameter IV indicates the number of intervals of the polar axis, which determines the accuracy of the rotation correction. When IV is set to 360, as is set by the ULPM method, their rotation correction accuracy is only 0.5 degrees. The IULPM method proposed by us increases the IV to 1800 and adds a new "zero-to-one" mapping rule, so that the rotation correction accuracy of the proposed method reaches 0.1. For example, if the data samples of the original image color gamut are 1000, the data of each channel after filtering is 1000, and the total is 2000. Therefore, according to the Nyquist sampling theorem, a downsampling method is proposed, that is, one for every two sample data in each channel is taken.

5.3. Example Application and Analysis. The image color gamut boundary data shows that 216 test images and their original images form 216 test image pairs, and the image color gamut observers evaluate the 216 test image pairs twice to avoid the continuous experiment time being too long and causing the image color gamut. At the beginning of each experiment, all test image pairs are generated in a random display order, and the left and right display positions of the original image and the test image in each test image pair are also random to avoid the nonuniformity of the display affecting the experimental results. The background of the display was set to 20% neutral gray, and the test image pairs were displayed in the center of the display with 10 viewing angle intervals.

In addition, due to the particularity of DFT transformation, the symmetric embedding method should be considered when embedding watermarks to ensure that the data obtained during inverse transformation are real numbers. The image color gamut observation distance of the

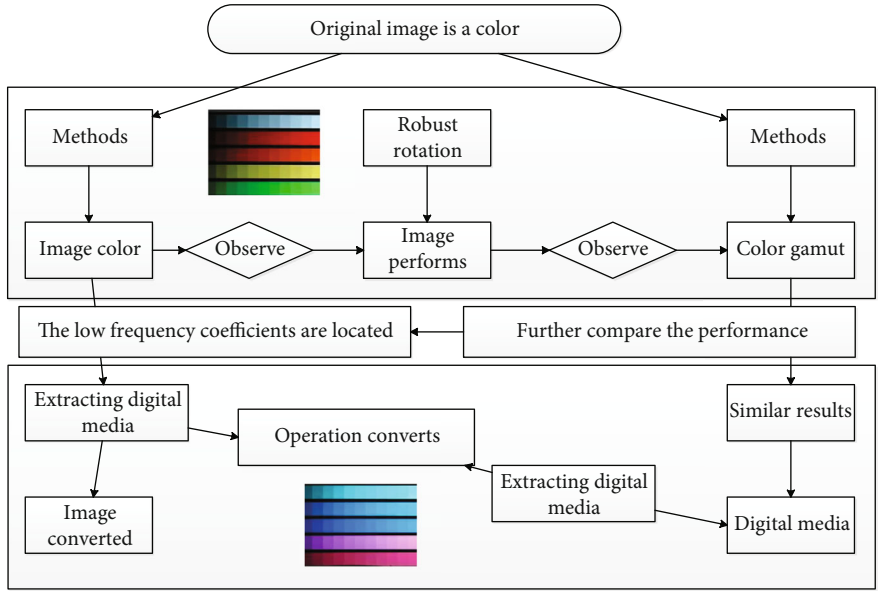

Figure 8: Digital media result topology.

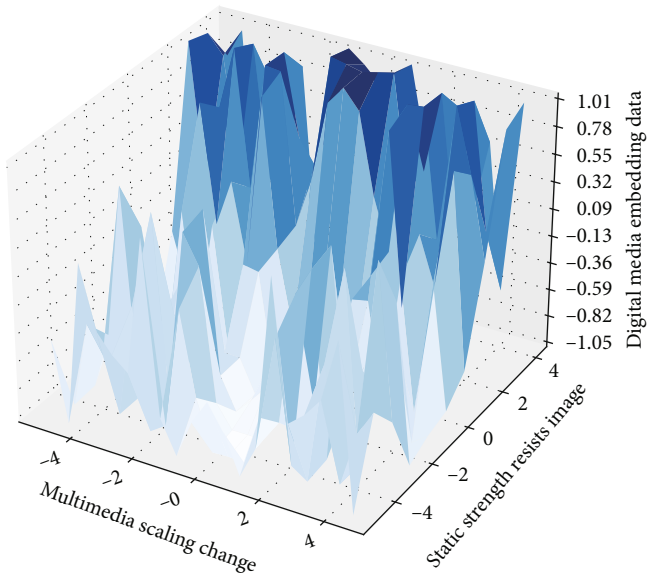

Figure 9: Digital media embedding strength resists image scaling.

image color gamut observer is 80 cm, and then, it is calculated that the horizontal image color gamut observation angle is 22.50, and the vertical image color gamut observation angle is 14.250.

In this experiment, the CV value is used to represent the observer accuracy in Table 2 of the image color gamut. Image gamut interobserver accuracy refers to the agreement between the experimental data of each image gamut observer and the experimental data of other image gamut observers. The intraobserver accuracy of the image color gamut refers to the consistency between the two evaluation data of the image color gamut observer himself for the same test image pair, that is, the repeatability accuracy of the image color gamut observer. The CV values of the image gamut observer accuracy are shown. The larger these two parameters, the higher the robustness of the system, and the worse the imperceptibility of digital media. Based on the experiments in Figure 10, as far as our method is concerned, when the setting range is [0.3, 0.5], and it is set to 24500, the proposed method achieves the best compromise in terms of robustness and imperceptibility of digital media.

In this experiment, a total of 10 image gamut observers with normal color vision participated, all of whom were graduate students, including 6 males and 4

Table 2: Algorithm distribution of image gamut boundary.

Algorithm text	Image gamut boundary code
Their original images form case(x)	For i in range(k):
Causing the image color gamut	Getlabel = labels[sortdisindex[i]]
The image color ∂delta(x)	Classcount[getlabel] = classcount.get(getlabel, 0) +1
Time being too long and $da(i) + da(j)$	Datasize = data.shape[0]
The continuous experiment	X = np.tile(inputx, (datasize, 1)) - data
Gamut boundary $k - \sigma w(k)$	Xpositive = x ∗∗ 2
The image ziber(x) color gamut	Xdistances = xpositive.sum(axis=1)
Test image pairs twice to $1 - x$	Distances = np.sqrt(xdistances)
Observers evaluate the heter(x)/heter(y)	Print(sortclass[0][0])
Test image pairs $\nabla dc = dc(i) - dc(j)$	Knnclassify(inputx, data, labels, k)
Test images and gent(x, y, z)	Return sortclass[0][0]

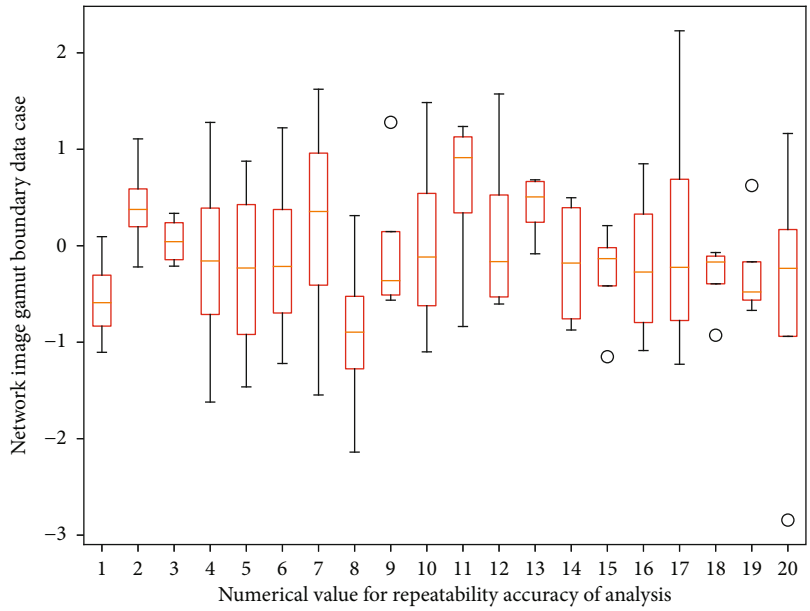

Figure 10: Repeatability accuracy of image color gamut boundary data.

females, aged between 20 and 33. Five of the image gamut observers performed two evaluations to analyze the interobserver accuracy of the image gamut. Therefore, there are 2700 visual evaluation data obtained in this experiment (10 image color gamut observers × 216 test image pairs + 5 image color gamut observers × 108 test image pairs). And the selection of CIECAM02 as the intermediate connection space has wider significance compared to CIELAB. First of all, the Euclidean distance of two colors can be used to describe the color difference in the uniform color space, which is not only simple to calculate but also can reflect the difference between two colors more intuitively, which provides convenience for the application of color industry. Secondly, from the comparison of the design purposes of the two models, CIECAM02 can predict the color perception of the environment according to the parameters of the environment, while CIELAB can only predict the color properties under a specific light source, so choosing CIECAM02 as the intermediate connection space can meet the current color transfer requirements.

6. Conclusion

This paper studies the problem of color difference evaluation of color digital images. Through the design and implementation of related psychophysical experiments, a large amount of visual evaluation data is obtained to test and compare the performance of different color difference formulas in image color difference evaluation and to analyze the influence of color digital images for chromatic aberration evaluation. Compared with the traditional boundary judgment algorithm based on quaternion boundary judgment transformation, the algorithm in this paper has higher robustness and embedding capacity, and there is no energy loss in the boundary judgment algorithm based on quaternion

boundary judgment transformation. The perceptible chromatic aberration thresholds of the image color gamut observers were obtained through psychophysical experiments, and the prediction performance of the image color difference above the threshold of the boundary judgment algorithm framework was discussed. Experiments show that embedding a watermark into the blue component can preserve the perceptual quality of the original image better than embedding digital media into other color components. The scrambling method of changing the gray value does not change the position of the pixel point but changes the gray value of the original image into a new gray value, thereby generating a chaotic image to achieve the purpose of image scrambling. The digital media extracted by the digital media after being attacked has the background information of the original image, which is more conducive to proving the copyright of the image. Therefore, the research in this paper has an important role in promoting the progress of color science and the development of color digital image-related industries.

Data Availability

The data that support the findings of this study are available from the corresponding author upon reasonable request.

Conflicts of Interest

The author declares no conflicts of interest.

References

[1] M. Zhang, Y. Xue, Y. Ge, and J. Zhao, "Watershed segmentation algorithm based on luv color space region merging for extracting slope hazard boundaries," *ISPRS International Journal of Geo-Information*, vol. 9, no. 4, p. 246, 2020.

[2] Y. Zhu, "Color management of digital media art images based on image processing," *Ingénierie des Systèmes d'Information*, vol. 25, no. 4, pp. 445–452, 2020.

[3] K. Zhou, Z. Zhang, R. Yuan, and E. Chen, "A deep learning algorithm for fast motion video sequences based on improved codebook model," *Neural Computing and Applications*, pp. 14–16, 2022.

[4] L. Xu, B. Zhao, and M. R. Luo, "Color gamut mapping between small and large color gamuts: part II gamut extension," *Optics Express*, vol. 26, no. 13, pp. 17335–17349, 2018.

[5] X. Long and J. Sun, "Image segmentation based on the minimum spanning tree with a novel weight," *Optik*, vol. 221, article 165308, 2020.

[6] R. Xu, "Fuzzy C-means clustering image segmentation algorithm based on hidden Markov model," *Mobile Networks and Applications*, vol. 27, no. 3, pp. 946–954, 2022.

[7] Y. Xue, J. Zhao, and M. Zhang, "A watershed-segmentation-based improved algorithm for extracting cultivated land boundaries," *Remote Sensing*, vol. 13, no. 5, p. 939, 2021.

[8] J. Huang, H. Obracht-Prondzynska, D. Kamrowska-Zaluska, Y. Sun, and L. Li, "The image of the City on social media: a comparative study using "Big Data" and "Small Data" methods in the Tri-City Region in Poland," *Landscape and Urban Planning*, vol. 206, article 103977, 2021.

[9] L. Jing and S. Lv, "Art image processing and color objective evaluation based on multicolor space convolutional neural network," *Computational Intelligence and Neuroscience*, vol. 2021, 10 pages, 2021.

[10] W. Chen, C. He, C. Ji, M. Zhang, and S. Chen, "An improved K-means algorithm for underwater image background segmentation," *Multimedia Tools and Applications*, vol. 80, no. 14, pp. 21059–21083, 2021.

[11] F. Zheng, C. Yang, P. H. Chong, G. Wang, G. M. Ali, and P. Lam, "Deep learning algorithm for picture frame detection on social media videos," in *Internet of Things and Intelligence Systems (IoTaIS)*, pp. 149–155, Bandung, Indonesia, November 2021.

[12] P. Kandhway and A. K. Bhandari, "An optimal adaptive thresholding based sub-histogram equalization for brightness preserving image contrast enhancement," *Multidimensional Systems and Signal Processing*, vol. 30, no. 4, pp. 1859–1894, 2019.

[13] R. Li, K. Zou, and W. Wang, "Application of human body gesture recognition algorithm based on deep learning in non-contact human body measurement," *Journal of Ambient Intelligence and Humanized Computing*, pp. 10-11, 2020.

[14] H. Dong, Y. Jiang, Y. Fan, Y. Wang, and G. Gui, "Secondary segmentation extracted algorithm based on image enhancement for intelligent identification systems," *International Journal of Distributed Sensor Networks*, vol. 14, no. 12, 2018.

[15] E. Bogert, A. Schecter, and R. T. Watson, "Humans rely more on algorithms than social influence as a task becomes more difficult," *Scientific Reports*, vol. 11, no. 1, pp. 5–9, 2021.

[16] Y. Wang and Y. Cao, "Leukocyte nucleus segmentation method based on enhancing the saliency of saturation component," *Journal of Algorithms & Computational Technology*, vol. 13, p. 173, 2019.

[17] J. Vazquez and M. Bertalmío, "Spatial gamut mapping among non-inclusive gamuts," *Journal of Visual Communication and Image Representation*, vol. 54, pp. 204–212, 2018.

[18] J. Zuo, Z. Jia, J. Yang, and N. Kasabov, "Moving object detection in video sequence images based on an improved visual background extraction algorithm," *Multimedia Tools and Applications*, vol. 79, no. 39-40, pp. 29663–29684, 2020.

[19] Z. Ying, H. Niu, P. Gupta, D. Mahajan, D. Ghadiyaram, and A. Bovik, "From patches to pictures (PaQ-2-PiQ): mapping the perceptual space of picture quality," *Computer Vision and Pattern Recognition*, pp. 3575–3585, 2020.

[20] D. Liu, Q. Su, Z. Yuan, and X. Zhang, "A fusion-domain color image watermarking based on Haar transform and image correction," *Expert Systems with Applications*, vol. 170, article 114540, 2021.

[21] W. Yang, J. Luo, X. Wu, X. Li, Z. Jiang, and Z. Pan, "Image tactile perception with an improved jseg algorithm," *International Journal of Performability Engineering*, vol. 14, no. 1, p. 77, 2018.

[22] B. Krajancich, N. Padmanaban, and G. Wetzstein, "Factored occlusion: single spatial light modulator occlusion-capable optical see-through augmented reality display," *IEEE Transactions on Visualization and Computer Graphics*, vol. 26, no. 5, pp. 1871–1879, 2020.

[23] S. Faraj, S. Pachidi, and K. Sayegh, "Working and organizing in the age of the learning algorithm," *Information and Organization*, vol. 28, no. 1, pp. 62–70, 2018.

[24] X. Yu, X. Ye, and S. Zhang, "Floating pollutant image target extraction algorithm based on immune extremum region," *Digital Signal Processing*, vol. 123, article 103442, 2022.

[25] D. Komura and S. Ishikawa, "Machine learning approaches for pathologic diagnosis," *Virchows Archiv*, vol. 475, no. 2, pp. 131–138, 2019.

[26] Y. Oishi, H. Ishida, and R. Nakamura, "A new Landsat 8 cloud discrimination algorithm using thresholding tests," *International Journal of Remote Sensing*, vol. 39, no. 23, pp. 9113–9133, 2018.

[27] Y. A. Sari, J. M. Maligan, Y. S. Adinugroho, and Y. G. Bihanda, "Multiple food or non-food detection in single tray box image using fraction of pixel segmentation for developing smart NutritionBox prototype," *International Journal of Innovative Technology and Exploring Engineering (IJITEE)*, vol. 9, no. 3, p. 13, 2020.

Hindawi
Wireless Communications and Mobile Computing
Volume 2022, Article ID 2370745, 15 pages
https://doi.org/10.1155/2022/2370745

Research Article

The System of the Dissemination Characteristics of Internet Public Opinion Big Data Based on Artificial Intelligence

Xiaobo Wu[1] and Sitong Liu[2,3]

[1]*School of Business, Lingnan Normal University, Zhanjiang 524048, Guangdong, China*
[2]*School of Journalism and Communication, Nanjing University, Nanjing 210023, Jiangsu, China*
[3]*School of Management, Guilin University of Aerospace Technology, Guilin 541004, Guangxi, China*

Correspondence should be addressed to Sitong Liu; liusitong@guat.edu.cn

Received 21 May 2022; Revised 22 July 2022; Accepted 29 July 2022; Published 26 August 2022

Academic Editor: Jun Ye

In the era we live in today, the network is often used to analyze a large number of complex systems. With the development of the information society, there are more and more ways to disseminate public information through social networks. Public opinion dissemination refers to the process of disseminating public opinion information through social networks. Because the dissemination of public opinion is the basis for the exchange of ideas among multiple communicators of public opinion, the network community will certainly have an impact on the dissemination and development of public opinion. This article is based on artificial intelligence to study the network public opinion big data dissemination characteristic analysis system, introduces the network public opinion analysis system based on the characteristics of the network public opinion, introduces in detail multiple methods and clustering algorithms for extracting the text information of Internet public opinion, and proposes the Kmeans + Canopy + semantic similarity algorithm, and uses the A event to compare the parameters of the network clustering coefficient, the correlation measure and the degree centrality measure, and the performance of the Kmeans + Canopy algorithm and the Kmeans + Canopy + semantic similarity algorithm. The results of the experiment found that the clustering coefficient of "People's Daily" in the network dissemination of A event was 0.038, which was the highest among all nodes. It shows that 3.8% of the nodes established by the "People's Daily" can interact one-to-one to deliver information and intelligence resources. Although the complexity of the algorithm has increased and the time consumed by the system has increased, the accuracy of clustering has been improved, especially for cultural articles, the accuracy rate has been as high as 75%, and entertainment articles can reach up to 70%, and stabilize at around 70%.

1. Introduction

1.1. Background. Public opinion can always be defined as the attitudes and ideas of a person or group that touches and connects the emotions and ideas of social groups to each other in a fixed time and angle for many public events. From a sociological point of view, citizenship itself is a full response to the will of the people. The complex network we want to study, as a network close to real life, plays an important role in the research of public opinion communication, and has attracted the attention of various fields. The traditional big data dissemination of public opinion on the Internet has always been in need of improvement in terms of expansion and accuracy, and the research results in the combination with artificial intelligence are not ideal. Artificial intelligence realizes intelligent resource management for wireless communication through powerful learning and automatic adaptation capabilities. On the other hand, in wireless communication resource management, the use of artificial intelligence requires new network architecture and system models and standardized interfaces/protocols/data formats to promote the large-scale deployment of artificial intelligence in future B5G/6G networks.

1.2. Significance. With the advent of the Internet, more and more netizens pay attention to public opinion events through online media. With the spread of comments by

netizens on emergencies, negative public opinion topics and confrontations related to these incidents are also widely spread on the "self-media" network. Gradually, this phenomenon has aroused the attention of academia as well as the attention of all sectors of society. People search all kinds of hot news on the Internet to express their thoughts. However, due to the openness and authenticity of the Internet, the spread of negative events can even affect social stability. Due to the large number of public opinion events that occur at the same time, and the public opinion events also contain a large amount of information, management departments must quickly and regularly guide the fermentation of public opinion events on the Internet, which is of great significance for determining the emotional intensity of Internet users. Public events are hot topics of social concern, which can easily arouse enthusiastic discussions among viewers and netizens, thereby forming general public opinion on the Internet. Public opinion on public events has a major impact on the development and maintenance of public events, and the wrong direction will affect the implementation of public events.

1.3. Related Work. The "self-media" network is real time and open. This kind of network lacks a gatekeeping system. Starting from the characteristics of the "self-media" network public opinion elements, Wang G constructed a multidimensional network model oriented to the "self-media" network public opinion topology. Based on the real process of generating and disseminating multiple topics of the same event, he designed a topic detection algorithm suitable for these multidimensional public opinion networks. The research results are mainly summarized from the following three aspects: (1) The multidimensional network model can effectively describe the communication characteristics of multiple topics on the "self-media" network. (2) Using a multidimensional topic detection algorithm, 70% of public opinion topics related to case study events have been effectively detected, which shows that the algorithm is effective in detecting topics in the information flow on the "self-media" network. (3) By defining the psychological scores of single and paired Chinese keywords in public opinion information, using topic detection algorithms to determine the emotional tendency of each topic, revealing the negative topics discussed on the "self-media" network, but the research results have not yet been obtained wide range of applications [1]. Metadata is the information about the organization of data, data domains, and their relationships. Traditionally, information science has been the center of metadata research. Mayernik MS introduced 5 key sociotechnical characteristics of metadata in digital networks. He said that the nature and importance of metadata in network communication systems are rarely discussed in the information science community. Without such metadata, network communications cannot exist. If we want to have meaningful discussions about our digital traces, or make wise decisions about new policies and technologies, then we must develop theoretical and empirical frameworks for explaining digital metadata. But the practicality is not strong [2]. As Internet users use tags when posting and searching for information on social media, it is important to understand who built the tag network and how the information is spread across the network. Kim J unleashes the potential of the AlphaGo tag network by solving the following problems. His current research examines whether traditional opinion leadership (that is, the influence hypothesis) or the grassroots participation of the public (that is, the interpersonal relationship hypothesis) promotes the dissemination of information in the tag network. Finally, it tested the correlation between the attributes of key users (i.e., the number of followers and followers) that have a significant impact on the distribution of information and their central position in the network. The results show that the main participants in the network actively receive information from their followers, rather than acting as an intermediary between participants, but the experimental process is too complicated [3]. Cyberspace is reshaping the way companies manage sales and marketing assets. Gang LI's research in these network applications and services found that some public relations companies hire staff to post product reviews on different online communities and social networks, and the hired has not even consumed these services or products. Although online paid posters can be used as an effective e-marketing strategy, they can also conduct malicious behavior by spreading rumors or negative information about competitors. More specifically, a set of paid posters can cooperate with good marketing to produce the expected results of positive or negative opinions to attract attention or stimulate curiosity. However, how to use social media to sell better still remains to be considered [4]. Modern malware uses advanced techniques to hide static and dynamic analysis tools. Therefore, investigating how to use general indicators (such as the energy consumed by the device) to reveal the presence of malware is very important. From this perspective, Caviglione L uses two detection methods based on artificial intelligence tools, such as neural networks and decision trees, to find malware that hides the exchange of data. In order to verify its effectiveness, seven covert channels have been implemented and tested on the measurement framework using Android devices. Experimental results show that this method can effectively detect hidden data exchanges between applications, but it requires a lot of initial investment [5]. How to fully tap the potential of artificial intelligence (AI) technologies in future wireless communications, such as beyond 5G (B5G) and 6G, is a very popular interdisciplinary research topic worldwide. Lin M reviewed the latest developments in resource management authorized by artificial intelligence from a framework perspective to a methodology perspective, not only considering the management of radio resources (such as spectrum), but also other types of resources, such as computing and caching. He also discussed the challenges and opportunities faced by AI-based resource management in the widespread deployment of AI in future wireless communications, but further research is needed to achieve intelligent resource management [6]. However, because of the relative virtual nature of the network, it is of great practical significance to quickly and effectively dig out important information from the massive network information and to understand the public opinion dynamics of the people and control them in time.

1.4. Innovation. This paper studies the analysis system based on artificial intelligence on the dissemination characteristics of network public opinion big data. Aiming at the characteristics of Internet public opinion, this article introduces in detail multiple methods and clustering algorithms for extracting text information of Internet public opinion. In order to improve the clustering convergence and the accuracy of network information detection, this paper considers that the results of calculating similarity between Chinese words are still not ideal. Because there are many synonyms in Chinese words, this paper proposes a method of combining Kmeans + Canopy and semantic similarity algorithm, and compares it with Kmeans + Canopy, and the effect is very good.

2. Method of Network Public Opinion Big Data Dissemination Characteristic Analysis System Based on Artificial Intelligence

Following the three major media, newspapers, radio, and television, the Internet has been given an important mission as the "fourth media" and has penetrated into all aspects of human life. Through social networks, people can check some popular news and social events that interest them and express their opinions. In recent years, due to the development of the Internet era, the number of mobile Internet users has increased significantly, as shown in Figure 1 [7]. As one of the most convenient Internet products, mobile phones have become an indispensable tool for Internet users. At the same time, because the Internet is so open and free, more and more netizens express their attitudes, ideas, opinions, and problems quickly, directly, and honestly through the Internet. The Internet has become an important platform for the development and dissemination of public opinion [8].

Public opinion refers to an individual's expression of social reality events in a certain period of time and is an objective expression of group attitudes, thoughts, feelings, and problems. Public opinion is exposed and spread through the Internet. To a certain extent, people can use these media to express their reactions and emotions to events and express their thoughts, and even personal remarks can easily trigger the fermentation of certain events [9]. The way to start forwarding without understanding the comprehensiveness of the event also belongs to the category of online public opinion, which will have a negative impact on economic development and social stability. Therefore, timely detection of online public opinion, and appropriate response measures based on its development and changes, and effective monitoring of it have become important tasks for government departments.

The social network public opinion communication process is divided into 4 stages, as shown in Figure 2 [10].

Because most of the Internet public opinion information appears in Chinese texts, the relevant processing of Chinese Internet public opinion texts has become a research focus. The following mainly introduces various knowledge of processing public opinion text, such as Chinese preprocessing, feature extraction and representation, text similarity calculation, and text clustering knowledge [11]. Figure 3 is the network public opinion analysis system.

The network-based public opinion analysis system is a web-based application system. For big data processing technology, Hadoop is a distributed system infrastructure developed by the Apache Foundation. Users can develop distributed programs without understanding the underlying details of the distribution and make full use of the power of the cluster for high-speed computing and storage. Hadoop's MapReduce parallel computing framework is a computing model running on HDFS distributed storage system. The main purpose of this design is to achieve sharing and overcome the problems of the overall system, which can greatly reduce the initial communication consumption during data transmission [12]. In the processing of network public opinion data, the subsystem preprocesses the collection of public data for public opinion analysis and analysis and prediction of the basic system. The data collected by the collection system is mainly stored locally in the form of webpage text and cannot be used directly [13]. A subsystem that pregenerates each automatically encoded information and recognizes the received web page text, then removes network noise, extracts text information, and provides Chinese word segmentation to the public opinion analysis and prediction subsystem for further processing.

The public opinion analysis and prediction subsystem is an important part of the entire public opinion analysis and planning framework and is used to perform the key functions of the system. The public opinion prediction and analysis system analyzes the public network information previously processed through public opinion data. The main content usually includes the following aspects:

(1) Subject search and tracking, from general network information such as news and blogs on the Internet, through data mining, automatically search and retrieve the public opinion topics contained therein, and identify each follow-up report of the subject, to achieve the completeness of tracking the birth, development, and demise of the theme [14].

(2) Hot topic recognition, for most of the titles found, according to their news source sequence, visit volume, number of comments, number growth rate, and comment time intensity, to identify the headline information on the Internet hotspot

(3) Sensitive topic recognition, based on detailed analysis of various sensitive words found on the Internet, using keywords to manage, identify "suspicious" topics, and generate relevant warnings

The public network database is essentially composed of a network public opinion information database, a network public opinion analysis database, a system management database, a sensitive word database, and a user database. The specific situation is shown in Figure 4 [15]. According to the characteristics of the quantity, size, growth rate, and type of data stored in different databases, different data

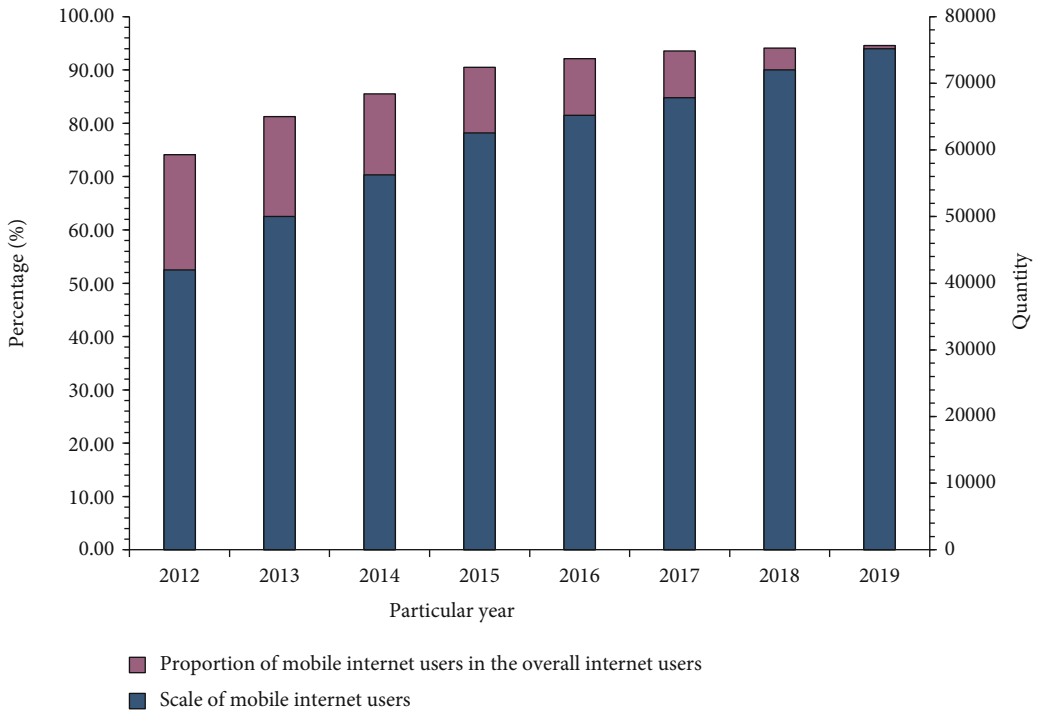

Figure 1: Scale of Internet users and Internet penetration in China.

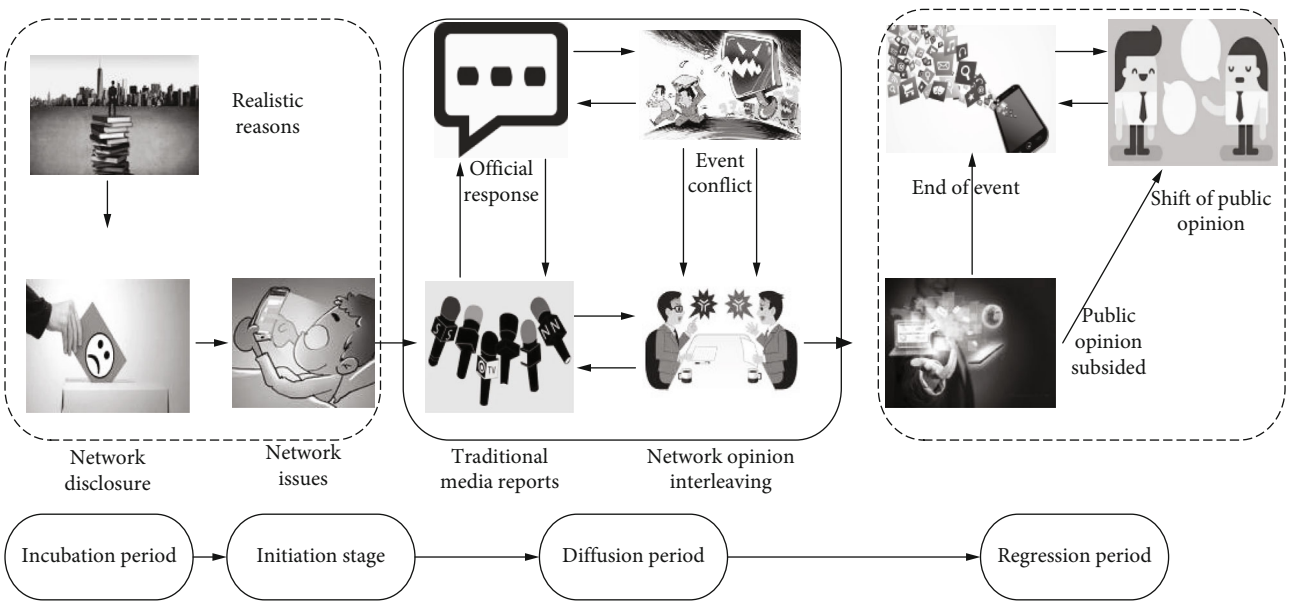

Figure 2: Network public opinion dissemination model diagram of social events.

systems are used to determine the database and control. Network public opinion data storage and management are collected through a network data collection system, which provides preconditions for the processing of network public opinion data [16].

2.1. Preprocessing of Online Public Opinion Information Text. With the advent of the big data era, the data on the Internet is showing a trend of doubling. How to efficiently obtain and use the content of interest on the Internet is an important direction of value-added in the current data mining field. For this purpose, web crawlers have ushered in a new wave of revitalization and have become a hot technology that has developed rapidly in recent years. Web crawler is a program that automatically extracts web pages according to certain rules. It can automatically crawl web pages on the Internet through the network [17]. Figure 5 shows the design form of the web crawler. The various text information on the webpages obtained by the web crawler contain a large amount of unorganized original webpage data, and there are

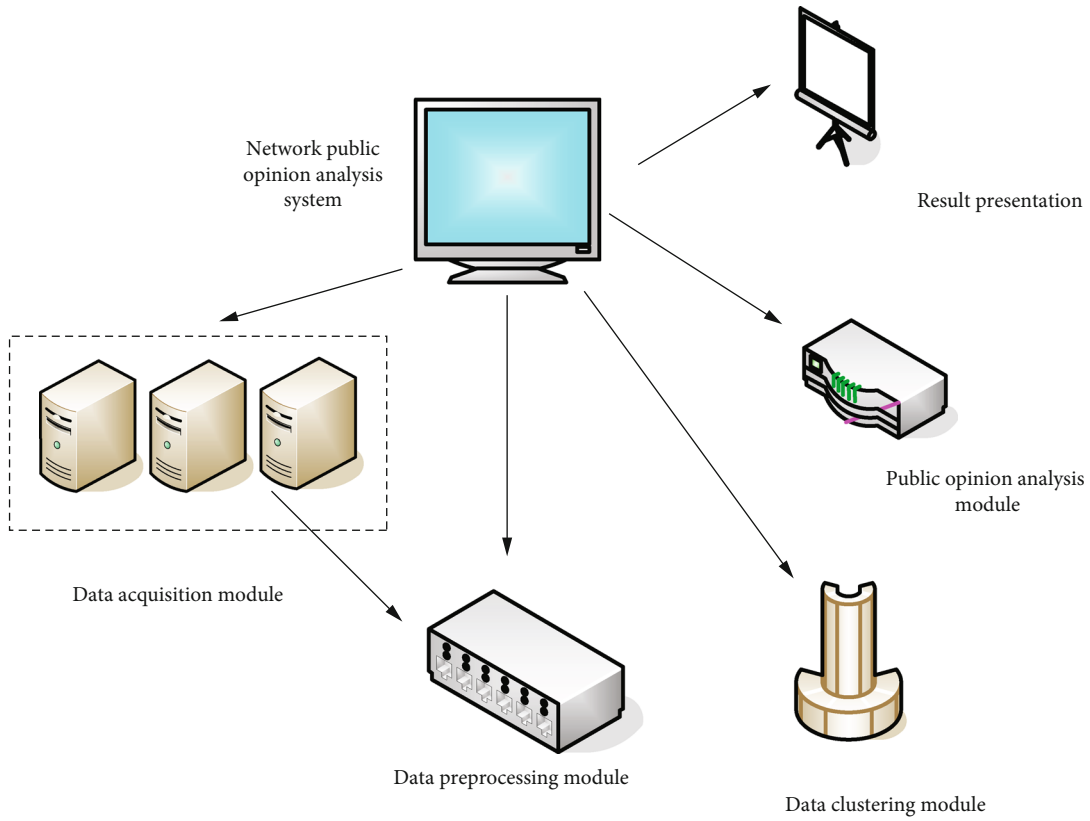

Figure 3: The composition of the network public opinion analysis system.

many repetitive downloading webpages and information with little relevance. Therefore, it is very important to preprocess the text of the network public opinion information.

Text information is composed of many words, punctuation marks, spaces, and important characters. It belongs to the unstructured data. Word segmentation is the first step of preprocessing, the process of combining rules into words [18]. English word segmentation is relatively concise, based on basic unit words, with obvious divisions, which is convenient for computer processing. In our understanding, Chinese word segmentation depends on the word as a meaningful language. It is more complicated and difficult due to the simplicity of the combination of words and the diversity of meanings. But in order to extract relevant keywords from the text, word segmentation is a very important step in generating information. With the development of Chinese information processing, related technologies have been significantly improved, including Chinese word segmentation technology, and many word segmentation algorithms have appeared [19]. Existing word segmentation algorithms include string-based word segmentation, understanding-based word segmentation, statistics-based word segmentation, and semantic-based word segmentation. This article will perform word segmentation processing on the network public opinion information text. The system includes functions such as Chinese word segmentation, part-of-speech tagging, and new word recognition and supports user dictionaries. After the word segmentation process, only part of the text is planned, since there is no unified standard for the Chinese stop word list; in this case, a corresponding stop word list is established according to the feature set. As some modal auxiliary words, conjunctions, and prepositions have no practical meaning and have little effect on the vocabulary, select an effective set of feature items, thereby reducing the feature space dimension, which can save storage space and calculation time, which can improve performance and accuracy [20].

2.2. Text Feature Extraction

2.2.1. Mutual Information Method. Mutual information is mainly used to measure text features and categories. The main idea is as follows: If a word has a higher frequency in a certain category and is higher than other categories, then the amount of common information between the word and the corresponding category is greater [21, 22]. The mutual information method can improve the efficiency of classifier training and application by reducing the effective vocabulary space. The operation process is relatively simple, which is convenient for everyone to understand and use. Mutual information can be used as a measure to measure the correlation between text feature w and category l, which can be defined as $\mathrm{OR}(w, l)$, and the formula is shown in

$$\mathrm{OR}(w, l) = \log p(w, l)/p(w)p(l), \tag{1}$$

where $p(w)$ represents the proportion of the number of texts containing the feature w to the total number of texts, $p(l)$

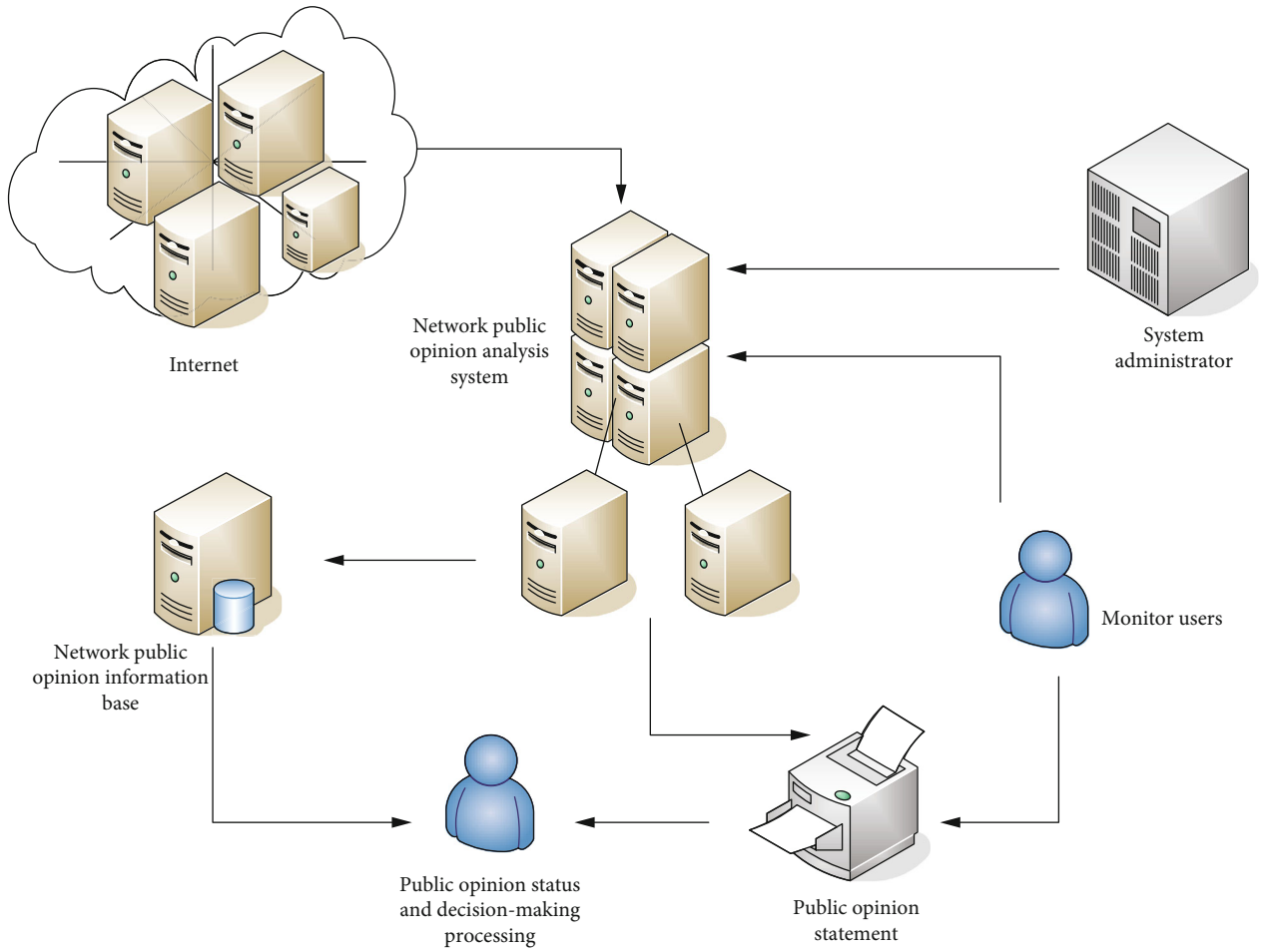

Figure 4: Business flow chart of network public opinion analysis system.

represents the proportion of the number of texts contained in the category l to the total number of texts, and $p(w, l)$ represents the probability of the occurrence of the feature w in the texts contained in the category l. It can be understood that if the probability of feature w appearing in a certain category l is significantly higher than that of other categories, it means that the probability of using feature w as a feature item of category l will be greater. Set the set of all classes of text to s; then, the average value of mutual information $\mathrm{OR}(w)$ can be defined as:

$$\mathrm{OR}(w) = \sum_{i=1}^{s} p(l_i)\mathrm{OR}(w, l_i). \tag{2}$$

If the mutual information value is equal to 0, it means that the feature w does not belong to type l at all. Similarly, when the mutual information value reaches the maximum, it means that the feature w belongs to type l only. However, in the mutual information, the frequency of the feature w is not considered, so it is likely to ignore the high-frequency vocabulary with obvious characteristics, and instead select the low-frequency vocabulary as the best feature item of the text. Therefore, the extracted feature information can be guaranteed by increasing the dimensionality of the feature space, but this will increase the calculation time and space utilization.

2.2.2. χ^2 Statistical Method. χ^2 Statistics can also be used to measure the correlation between features and categories. The formula of χ^2 statistical method between feature w and category l is:

$$M = \left[p(w, l)p(\bar{w}, l) - p(\bar{w}, l)p\left(w, \bar{l}\right)\right]^2, \tag{3}$$

$$\chi^2(w, l) = \frac{\mathrm{NM}}{p(w)p(\bar{w})p(l)p\left(\bar{l}\right)}, \tag{4}$$

In the above formula, when the value of $\chi^2(w, l)$ is smaller, it means that the correlation between feature w and category l is greater, and the distinguishing ability of feature w in category l is more obvious. Therefore, we must pay attention to the size of the value. Usually, the average statistics and maximum statistics of χ^2 statistics can also be calculated. If the total number of text categories is s, it can be defined as:

$$\chi^2_{\mathrm{avg}}(w) = \sum_{i=1}^{s} p(l_i)\chi^2(w, l_i), \tag{5}$$

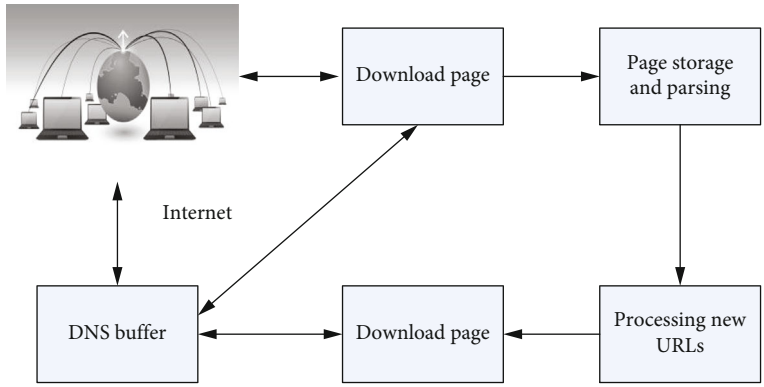

Figure 5: The design form of the web crawler.

$$\chi^2_{\max}(w) = \max\left\{\chi^2(w, l_i)\right\}. \tag{6}$$

The accuracy of χ^2 statistics in feature selection is very high, and the sensitivity to the training set is relatively low, so it is relatively stable.

2.2.3. Information Gain Method. The metric of information gain is the amount of information that a feature item carries in the clustering process. The greater the amount of information, the more important the feature is. Information gain is a statistical method based on entropy, and this entropy is the amount of information the feature carries in the clustering system [23].

Assuming that the feature is w and $\bar{w}$ represents the feature other than w, the information gain formula for the feature and category l is:

$$I(w) = \sum_{i=1}^{s} p(l_i) \log\left(1/p(l_i)\right) - p(w) \sum_{i=1}^{s} p(l_i \wedge w) \log\left(1/p(l_i \wedge w)\right) - p(\bar{w}) \sum_{i=1}^{s} p(l_i \wedge \bar{w}) \log\left(1/p(l_i \wedge \bar{w})\right), \tag{7}$$

where $p(l_i)$ represents the proportion of the number of texts contained in category l to the total number of texts, $p(w)$ represents the proportion of the number of texts containing feature w to the total number of texts, and $p(l_i \wedge w)$ represents the probability of feature w belonging to category l.

Information gain only considers the effect of features on the entire classification,

$$\mathrm{IDF}_i = \log \frac{S}{s_i}. \tag{8}$$

Formula (8) does not consider the relationship between features and categories, so it is very restrictive, which will greatly reduce the efficiency of feature extraction.

2.2.4. Term Frequency-Inverse Document Frequency (TF-IDF). When the importance of a word or phrase in a document needs to be determined to extract the features of the text, the TF-IDF method is used to calculate the vector density of the feature to establish a field vector model. The TF-IDF method is the most commonly used method in data update. The main idea of TF-IDF is: If a word or phrase appears in the article with a high frequency of TF, but rarely appears in other texts, it can be considered that the word or phrase has good distinguishing ability, and then, it is beneficial to classification. TF (word frequency) is used to indicate the frequency of occurrence of the word in the text of the document. The main idea of IDF (inverse document frequency) is as follows: If only a few documents contain the keyword, that is, the smaller s, the IDF is larger, indicating that the keyword is easy to distinguish. Therefore, the TF-IDF weight can be calculated to reflect the importance of keywords in a specific document.

In the TF-IDF method, the total number of documents is set to S, the keywords appear in each document, $n_{i,j}$ is the number of times the keyword appears in the document, and then, the frequency of the keyword appearing in the document is $\mathrm{TF}_{i,j}$. As shown in Equation (8), the denominator of this equation represents the sum of the number of occurrences of all words in the document. The calculation process of IDF_i of the keyword is expressed in Equation (8). Equation (9) expresses the importance of keywords in the document through a weight of $w_{i,j}$.

$$\mathrm{TF}_{i,j} = \frac{n_{i,j}}{\sum_k n_{k,j}}, \tag{9}$$

$$\mathrm{IDF}_i = \log \frac{S}{s_i}, \tag{10}$$

$$w_{i,j} = \mathrm{TF}_i \times \mathrm{IDF}_i. \tag{11}$$

2.3. Text Representation. After extracting text feature items, in order to facilitate quantitative expression of the relationship between the texts, the text can be expressed as a text vector composed of feature items to describe and replace the text. The commonly used text representation models are as follows:

2.3.1. Vector Space Model (VSM). The concept of the vector space model is easy to understand. It is used to express the meaning of the document in text, and only needs to

represent the feature item representing the document and the frequency of its appearance, without considering other things such as position, order, and factor.

The main idea of using the space vector model to represent text is to use a vector in the vector space to represent a single text, and the dimension of the vector space is represented by the feature items representing the corresponding text. And the dimension value corresponds to the weight of the feature vocabulary, which can be calculated by the TF-IDF method.

Assuming that in the text set A, there are m feature items t for each text a and the feature items are independent of each other, then:

$$a = (e_1, e_2, \cdots, e_m). \tag{12}$$

Assuming w_i is the weight of feature e_i in text a, with $(e_1, e_2, \cdots, e_m)$ as the coordinate axis of the m-dimensional space and $(e_1, e_2, \cdots, e_m)$ as its corresponding coordinate value, then:

$$a = (t_1 w_1, t_2 w_2, \cdots, t_m w_m). \tag{13}$$

The weight of the feature item is used to construct the feature vector of text a, and then, the feature vector $\bar{V}_d$ of text a can be expressed as:

$$\bar{V}_d = (w_1, w_2, \cdots, w_m). \tag{14}$$

Therefore, the text set A can be formally expressed as:

$$A = \begin{bmatrix} \vec{V}_{d_1} \\ \vec{V}_{d_2} \\ \cdots \\ \vec{V}_{d_n} \end{bmatrix} = (e_1, e_2, \cdots, e_m) \times \begin{pmatrix} w_{11} & \cdots & w_{1m} \\ \cdots & \cdots & \cdots \\ w_{n1} & \cdots & w_{\mathrm{nm}} \end{pmatrix}. \tag{15}$$

It can be seen from the above that the vector field model is very useful in the field of information retrieval. This method of word processing reduces the complexity of the problem and improves the performance of statistical data. However, the vector field model also has certain limitations. If the words are independent of each other, it is difficult to achieve literal association. The weight of the structured text is read according to TF-IDF, and a certain amount of data in the storage library is required to reflect the calculation effect; the text vector produced by the field vector model is high and sparse, which will increase the storage capacity [24, 25].

2.3.2. Probability Model. The probability model uses the probability relationship between distinguishing words and distinguishing words and between distinguishing words and text to retrieve information. The first is to divide the content in the text into related text information, and the rest are less important content. Then, by selecting the probability value corresponding to the distinguishing word, the probability of the distinguishing word appearing in the two types of text is displayed, and then, the correlation between the terms is calculated. The probability model is largely based on theory. If it has a different understanding of correlation, there will be different probability models and different ranking results. The basis of the probability recovery model is the basis of relevance, and the technical problem of the probability recovery model is the data source and probability calculation. Because of this, there will be unpredictable situations and corresponding evaluation criteria for each probability model, which is not conducive to specific use and requires a large-scale calculation.

2.3.3. Boolean Model. Boolean model is a simple information retrieval model based on Boolean algebra theory. In the standard Bolianian model, the text information is expressed as:

$$d = (w_{i1}, w_{i1}, \cdots, w_{\mathrm{in}}). \tag{16}$$

The model also represents a single text as a vector, and the weight w_{ik} of the feature item in the vector is represented by 0 or 1, respectively, indicating whether the feature word appears in the text. It can be seen from this that the Boolean model is a special form of the above-mentioned space vector model.

In the Boolean model, it is assumed that the relationship between the feature words and the text only includes appearance and non-appearance, so the Boolean model vector is composed of all the different feature words in the text. That is, the dimensionality of the vector is determined by the number of different feature words, and the corresponding weight value is 1 or 0.

The structure of the Boolean model is simple, easy to understand, and highly maneuverable. However, there are many limitations. For example, the matching conditions are too harsh, which will affect the accuracy of text retrieval; the Boolean model can only be used in information retrieval to calculate the relevance of a query and a document, but it cannot calculate the similarity between documents in depth.

2.3.4. Clustering Algorithm. For processing large data sets, clustering algorithms are relatively scalable and efficient, which will be of great help to the processing of online public opinion text information. Text clustering is the core step of the public opinion analysis system, and the selection of the clustering algorithm directly affects the result of topic detection. The function of text clustering is to divide the mixed text collection into several categories. The text similarity in each category is very high, but the text similarity between the categories is very low. The main clustering algorithms include Kmeans clustering algorithm and Canopy algorithm.

Kmeans algorithm: randomly select k data points as the initial value of each cluster center; remove the initial center point; calculate the distance from all other points to the center of each cluster; and then, classify the data point closest to the center point into the cluster; according to the new cluster, find the point with the smallest distance from other points in the cluster as the new cluster center point; repeat the above

steps until convergence. The Kmeans algorithm is widely used in real-life clustering applications due to its simple and effective analysis method. The specific process is shown in Figure 6.

Canopy clustering algorithm: The parallelization of Canopy clustering algorithm is similar to Kmeans clustering algorithm. First, it needs to set two thresholds T1 and T2, T1 > T2; one of the clusters is called the Canopy set, which is empty at the beginning; reading the data as a Canopy in the collection, then read the data, calculate the distance between it and all Canopy in the collection, if it is less than T1, divide the data into this Canopy; when the space is less than T2, the data cannot be considered as the center of other Canopy; otherwise, a new Canopy will be introduced.

Therefore, the Canopy algorithm is usually used in combination with the Kmeans algorithm, the original data is clustered through the Canopy algorithm, the parameter K and the first cluster center are determined, and then, the Kmeans algorithm is used for clustering to obtain the final result.

For the evaluation index of the effect of network public opinion text clustering, the most commonly used index is to use the accuracy rate and the recall rate when obtaining information and calculate the break-even point P to make a judgment. Assuming that R is the number of texts that are classified correctly, W is the number of texts that should be classified, and C is the number of texts that are actually classified in this category, and then, the accuracy and recall and P values are:

$$\text{Precision} = \frac{R}{C} \times 100\%, \tag{17}$$

$$\text{Recall} = \frac{R}{W} \times 100\%, \tag{18}$$

$$Q = \frac{1}{\text{Precision}} + \frac{1}{\text{Recall}}, \tag{19}$$

$$P = \frac{2}{Q}. \tag{20}$$

2.3.5. Analysis of the Dissemination Characteristics of Online Public Opinion. In the process of spreading online public opinion, there are two ways of spreading, namely, linear spreading and decentralized spreading. Because of the differences between the media and the content of the communication, the mode of communication will have different effects. In real life, the information exchange between individuals belongs to linear communication, and even the exchange of opinions between small groups can also be classified as linear communication. Although it seems that the spread speed is not fast, it can also spread widely, and the growth effect of the exponential function is the same. At the same time, it can meet high requirements on the accuracy and completeness of information dissemination. Linear propagation can be regarded as a single-line connection between individuals, with high correlation and good information connectivity, so the scope is relatively small, information update is more convenient, and the next level of individuals is prevented from getting erroneous information. There is a big difference between decentralized communication and linear communication. Decentralized communication usually occurs in groups, with a wider spread and greater intensity. Therefore, attention should be paid to the correctness and function of the control information at the source of the dissemination. Because the feedback will take a long time, and the probability of feedback will be extremely low, therefore, there will generally be cases where relevant departments directly respond to the incident.

3. Analysis Experiment on the Dissemination Characteristics of Internet Public Opinion Big Data

3.1. Clustering Coefficient Measurement. The clustering coefficient represents the topological characteristics of the network and reflects the relative scale of the social network. The clustering coefficient represents the average size of all participants in the network, which is equal to the actual number of cores in the neighborhood/the maximum number of cores in the neighborhood. Therefore, its coefficient is always greater than 0 and less than 1, and its size indicates the degree of integration of the entire network. This article extracts a hot event A for network analysis.

3.2. Relevance Measure and Degree Centrality Measure. Relevance measurement: The measurement represents the relationship between members in the network and reflects the breadth of information dissemination. Common indicators are diameter and average path. The diameter refers to the shortest line distance between any two nodes in the network, that is, the shortest distance between all nodes. The larger the diameter, the more links the entire network passes through, the smaller the diameter, the fewer the links, and the faster the spread of information. The smaller the number of segments, the greater the breadth of information dissemination, and vice versa.

Degree centrality demonstrates the ability of an individual to interact and connect with other individuals in the network. The larger its value, the closer to the center of the network, the greater the weight, and the more it will affect others. The degree centrality is divided into degree centrality and degree centrality. The degree centrality is the number of connections to the nodes in the network. The larger its value, the greater the number of connections. The degree centrality indicates the degree of integration and overall continuity between the members of the network and represents the overall consistency of the network center. The larger its value, the more compact and consistent the network system.

3.3. Intermediate Centrality Measure and Close Centrality Measure. The measure of intermediate centrality represents the centrality of the individual in the whole of all networks. There are intermediate centrality and intermediate centrality. The middle centrality indicates the degree of control over resource information. In other words, if a node is on the shortest route of other parties as a "bridge," individuals must use this "bridge" to obtain information and resources, and this route will master the sources of other components. With some control, other individuals can even be guided to

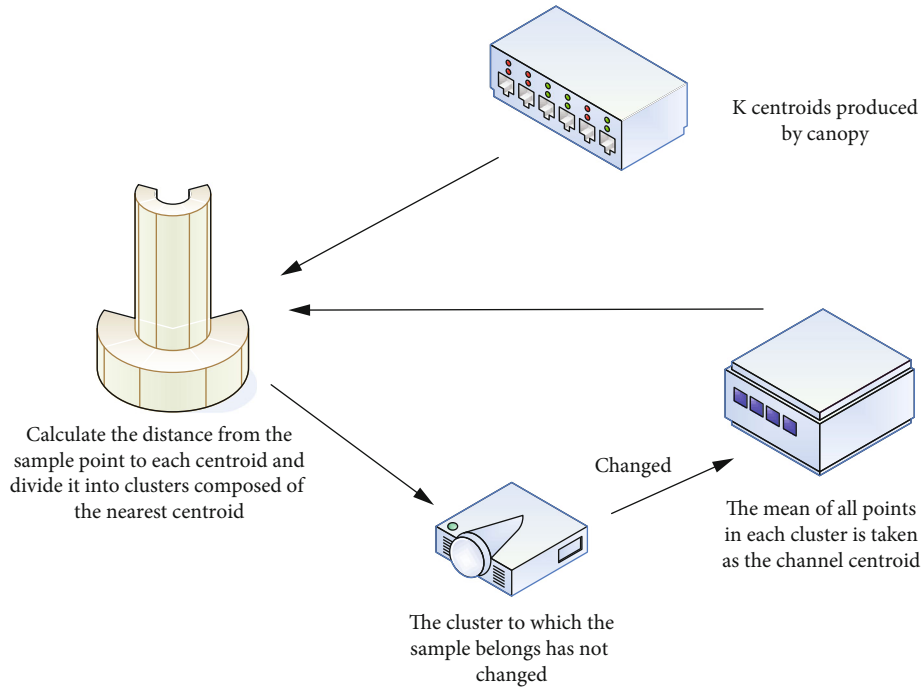

Figure 6: Flow chart of Kmeans algorithm.

obtain wrong information to achieve their goals. The intermediate central potential refers to the difference between the center of the highest node in the network and the centers of other nodes.

Proximity centrality measure: In social networks, neighboring nodes will distribute information sources more flexibly. It represents the degree to which one individual in the network is not restricted by other individuals. These include near central potential and near centrality. The proximity centrality is the sum of the shortest distances between an individual and all other individuals in the network. If it is farther from the center, it means that the restriction between this individual and other groups of individuals is higher. That is to say, the closer to the center, the deeper the core position in the network, the smaller the effect on information retrieval and retrieval sources, and the lower the weight.

3.4. Network Density Measurement. The general network depends on the structure of the entire network. According to the types of social network components and the diversity of their relationships, there are many general networks. The communication relationship between general networks can be considered as a "virtual interpersonal network" between individuals. The number of actors in this network is 100, which means there are 100 segments. The size of the network affects the relative structure of the network and the distance between nodes. As one of the key indicators of network structure, network density represents the approximate level of connections between individuals in social network relationships. The density is directly related to the relative density between nodes. If there are X connections and n nodes, there are $n(n-1)$ connecting lines, and the calculation formula for network density Y is:

$$Y = \frac{X}{n(n-1)}. \tag{21}$$

Generally speaking, the magnitude of the Y value and the relative density between the segments of the network are directly related to the impact on the individual. The larger the value of Y, the more useful it is in providing sources of information for individuals, but because the relationship between individuals is so close, the same individual may receive feedback from different individuals on the same information, which leads to the superposition of sources and information, increases the tedious degree of work, and is not conducive to the development of individuals in the network. In order to explain the closeness of the social network members in event A, the network density will be tested.

In the experiment, a cluster system consisting of 2 hosts was used. Each host is connected to a switch through a 100 M network card to form a local network and is connected to the Internet through the current stable Gigabit Ethernet card. Hadoop-2.6.0 was selected as the test platform, and designed a general network public opinion analysis system, and compared the performance of the Kmeans + Canopy algorithm and the Kmeans + Canopy + translation algorithm. Two of the hosts are configured as shown in Table 1.

4. The Experimental Analysis of the Dissemination Characteristics of Big Data of Online Public Opinion

Table 2 is the clustering coefficient measurement of the network public opinion of the A event.

Table 1: Configuration information of two hosts.

Project	Host 1	Project	Host 1
CPU	Intel Xeon (TM) 2.8 GHz	CPU	Intel Xeon (TM) 2.8 GHz
Memory	2 G	Memory	2 G
Hard disk	100 G	Hard disk	100 G
Host IP	192.168.1.211	Host IP	192.168.1.212

Table 2: Cluster coefficient measurement of event a network public opinion.

Node	Clus Coef	nPairs
Today's headlines	0.021	732
People's daily	0.038	602
Surging news	0.034	596
Tencent news	0.028	852
NetEase news	0.024	623

It can be seen from Table 2 that in the spread of this incident, the clustering coefficient of "People's Daily" is 0.038, which is the highest among the news software surveyed. It shows that 3.8% of the associated nodes have established contact with the "People's Daily" and can communicate with each other, provide information and understand the source. The nPairs size of "Tencent News" is 852, which is the largest among all nodes, indicating that "Tencent News" is the actor with the most network segments and connections. It can be seen from the results that the average size of the entire network is much higher. Some of them, such as "Tencent News" and "People's Daily," have greater relative proximity and are more likely to establish relationships with other parts.

The results of the relevance measurement results of the network public opinion dissemination of the A event and the degree centrality of the network public opinion dissemination data are shown in Table 3.

There are no unconnected nodes in the network public opinion dissemination of the A event; that is, all the nodes spreading in the network of this event can be directly connected or established by other participants. The average network path of "People's Daily" and "Netease News" is 4.9, and the power of information dissemination in public networks is stronger, access to the network is better, and information can be widely disseminated.

The degree centrality of "Tencent News" is 39, which is the highest among all nodes on the entire network. It reflects the great influence gained through media communication in the information network, and its high central position in the communication of online public opinion, which also confirms the role and appeal of active media and popular online actors.

Proximity to the center describes the closeness of participants in the network to other participants and refers to the information exchange capability of the entire network. The size of the proximity to the center is inversely proportional to the degree of information dependence between network participants. The results are shown in Table 4 for

Table 3: Correlation measurement results of network public opinion communication and degree centrality results of network public opinion communication data.

Node	Average path	Degree centrality
Today's headlines	5.2	36.00
People's daily	4.9	33.00
Surging news	5.1	32.00
Tencent news	5.0	39.00
NetEase news	4.9	37.00

Table 4: Calculation results of intermediate centrality of event a public opinion communication and proximity centrality of network public opinion.

Node	Intermediate centrality	Near centrality
Today's headlines	482.32	1462
People's daily	512.35	1528
Surging news	500.49	1546
Tencent news	493.26	1501
NetEase news	481.52	1623

calculating the intermediate centrality of the public opinion propagation of the A event and the close centrality of the network public opinion.

It can be seen from the results that in event A, "People's Daily" and "The Paper" have a high degree of centrality. They have a higher degree of control over information sources and have a greater role as a "bridge." Obviously, their power and influence are enormous. In the network dissemination of event A, "Today's Toutiao" has a close relationship with other nodes, is highly independent, has a low degree of dependence on other parties, and is not easy to control. "Tencent News" and "Netease News" followed closely behind. These network segments are close to the core of the network and have advantages in receiving information and capacity.

For the measurement of "individual network density" in the general network, the public opinion data of event A in Ucinet is shown in Figure 7.

It can be seen from Figure 7 that "Tencent News" has 39 network node relationships, which is the largest in the network scale. This shows that 39 nodes have established an interactive relationship with it. There are 49 connections established with "Tencent News," and the average network can have up to 190 relationships, and the ratio of the total number of associations to the maximum number of possible relationships is 4.2. On the whole, the personal network

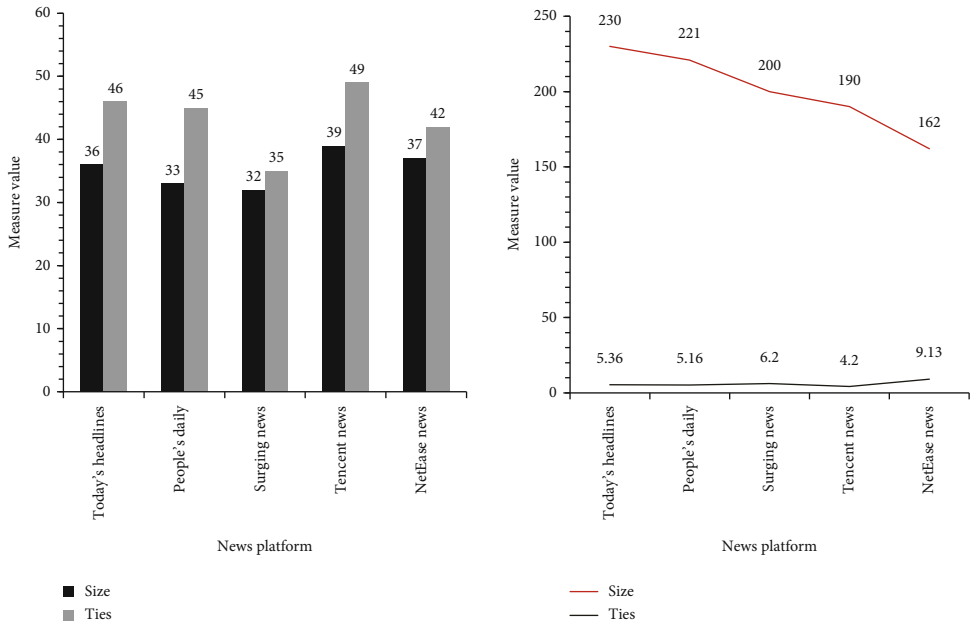

Figure 7: Measurement of "individual network density" in the overall network of public opinion of event a network.

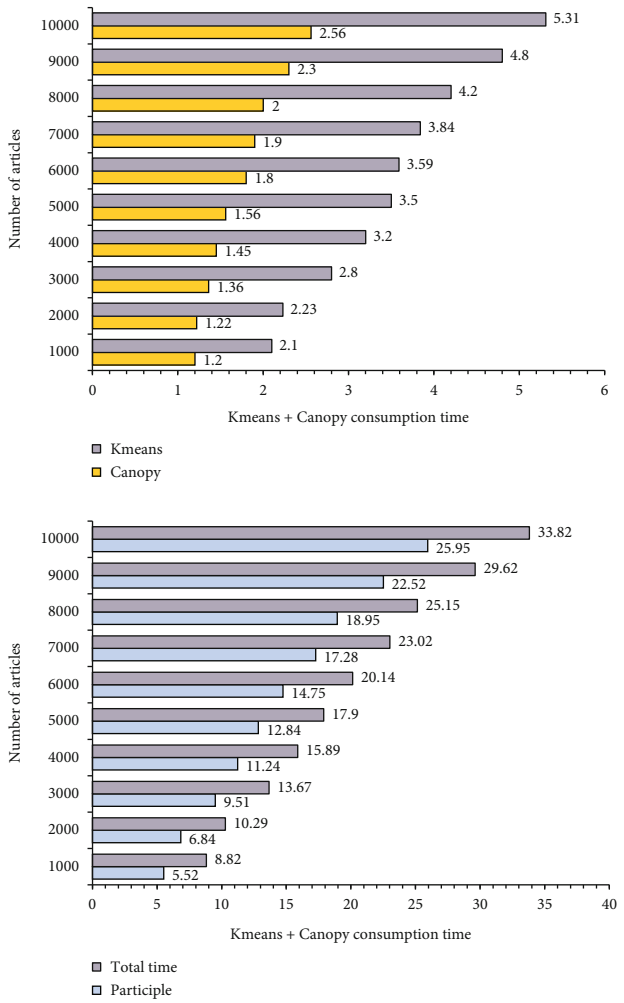

Figure 8: Time consumption of Kmeans + Canopy in each stage.

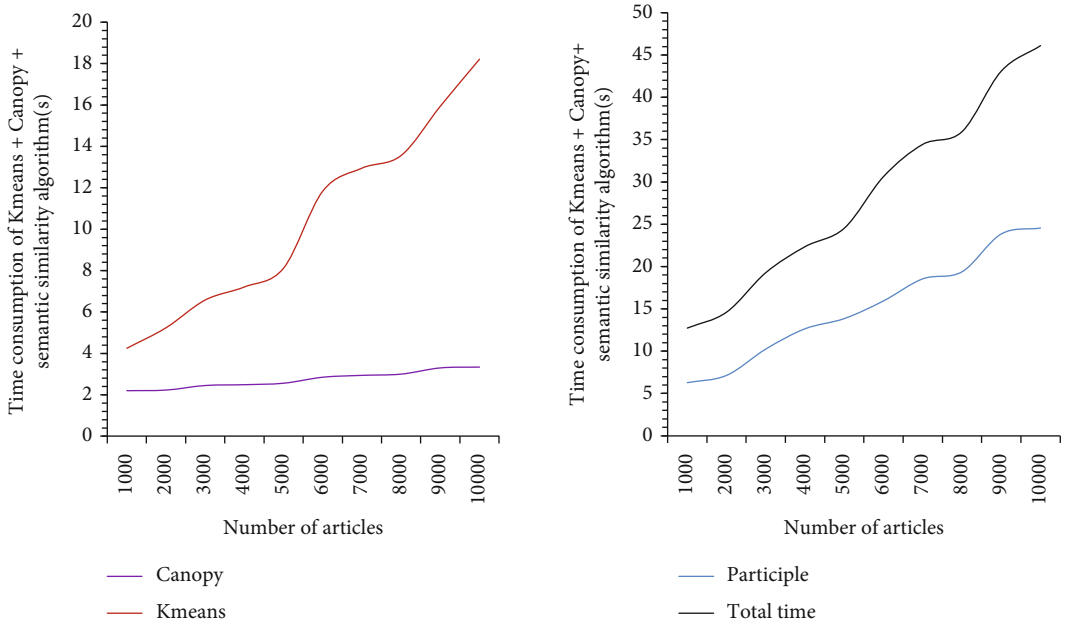

Figure 9: Time consumption of Kmeans + Canopy + semantic similarity algorithm.

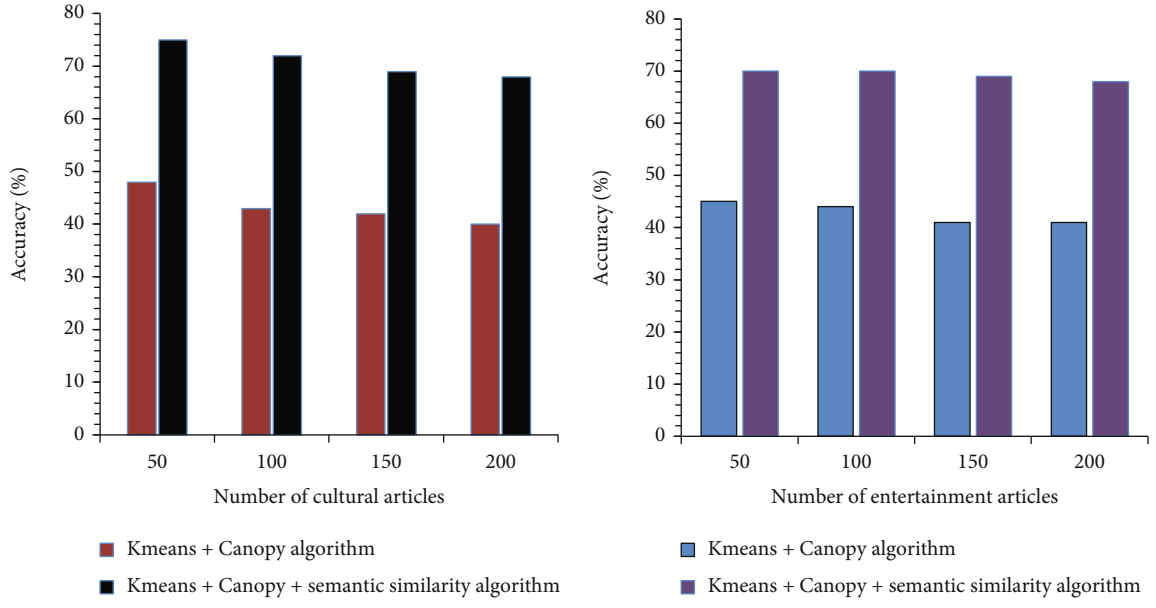

Figure 10: Accuracy comparison results of the two algorithms.

density of "Tencent News" is relatively high. The network density among all participants on the network is closely related to other nodes. This reflects the important role of authoritative media and online opinion leaders.

The Kmeans + Canopy algorithm and the Kmeans + Canopy + semantic similarity algorithm process 1000-10000 articles, respectively. The time consumed in each stage of the two clustering algorithms is shown in Figures 8 and 9.

Figures 8 and 9 analyze the time consumed by the Kmeans + Canopy algorithm and Kmeans + Canopy + semantic similarity in the three stages of word segmentation, Kmeans, and Canopy. Experimental results show that the two algorithms generally spend the most time in the word segmentation stage, and the Canopy stage spends the least time. The complexity of the Kmeans + Canopy + semantic similarity algorithm has increased, and the time spent in each stage of word segmentation, Canopy, and Kmeans has increased accordingly. Among them, the increased time in the word segmentation and Canopy phases is not obvious. The time consumed in the Kmeans phase is roughly twice that before the improvement, but the total time consumed does not exceed twice the time before the improvement.

The Kmeans + Canopy algorithm and the Kmeans + Canopy + semantic similarity algorithm process 50, 100,

150, and 200 cultural articles and 150 entertainment articles, respectively, and the accuracy comparison results are shown in Figure 10, respectively.

From the experimental results obtained in Figure 10, it can be seen that the clustering algorithm of Kmeans + Canopy is used to cluster the mixed two types of articles into multiple topic categories, the clustering convergence is poor, and the effect is very poor; using the clustering algorithm combining semantic similarity and Kmeans + Canopy, the two types of mixed articles are clustered into two topic categories, and the clustering effect is very ideal. Comparing the two algorithms, it can be seen that the clustering effect of the clustering algorithm using the combination of semantic similarity and Kmeans + Canopy is greatly improved, and the effect of corresponding public opinion analysis is also improved.

5. Conclusion

Artificial intelligence is a branch of computer science, a science that studies intelligent technology, that is, the use of artificial intelligence technology to develop smart devices or smart systems to simulate and expand human cognitive behavior. With the development of society, the spread of public opinion on the Internet has become an unstoppable trend. At the same time, more and more netizens pay attention to public opinion events through online media, and they actively comment on online public opinions, so proper regulation of online information is an inevitable trend. Therefore, based on the development trend of online public opinion, this article analyzes the collection method of online public opinion information. This article first analyzes the concept of online public opinion, introduces an online public opinion analysis system, and focuses on the development of textual information on online public opinion. In the clustering module, according to Chinese characteristics, such as synonyms and polysemous words, this paper proposes a clustering algorithm that combines Kmeans, Canopy, and semantic similarity and compares the performance of Kmeans + Canopy algorithm and Kmeans + Canopy + semantic similarity algorithm. Experiments have found that although the algorithm complexity increases and the system use time increases, the accuracy of clustering is improved. Especially for cultural articles, the accuracy rate is as high as 75%, and entertainment articles are as high as 70%, and stabilized at around 70%, thereby improving the discovery ability of online public opinion and achieving good research results. However, due to time and personal abilities, this article may have many areas for improvement. For example, this article only focuses on articles with large differences in content styles between culture and entertainment, the experimental data may not be representative, and multiple types of articles should be analyzed together.

Data Availability

Data sharing is not applicable to this article as no new data were created or analyzed in this study.

Conflicts of Interest

The author states that this article has no conflict of interest.

Acknowledgments

This work was supported by the Natural Science Youth Program of Lingnan Normal University QN2116 and the Youth Fund for Humanities and Social Sciences Research Project of Ministry of Education: "Research on the Audience Communication of Network Rumors in the Big Data Era" (Project number: 18YJC860021).

References

[1] G. Wang, Y. Chi, Y. Liu, and Y. Wang, "Studies on a multidimensional public opinion network model and its topic detection algorithm," *Information Processing & Management*, vol. 56, no. 3, pp. 584–608, 2019.

[2] M. S. Mayernik and A. Acker, "Tracing the traces: the critical role of metadata within networked communications," *Journal of the American Society for Information Science and Technology*, vol. 69, no. 1, pp. 177–180, 2018.

[3] J. Kim, "How did the information flow in the #Alpha Go hashtag network? A social network analysis of the large-scale information network on twitter," *Cyberpsychology, Behavior and Social Networking*, vol. 20, no. 12, pp. 746–752, 2017.

[4] G. Li, W. Niu, L. Batten, and J. Liu, "New advances in securing cyberspace and curbing crowdturfing," *Concurrency and Computation: Practice and Experience*, vol. 29, no. 20, article e4162, 2017.

[5] L. Caviglione, M. Gaggero, J. F. Lalande, W. Mazurczyk, and M. Urbanski, "Seeing the unseen: revealing mobile malware hidden communications via energy consumption and artificial intelligence," *IEEE Transactions on Information Forensics and Security*, vol. 11, no. 4, pp. 799–810, 2016.

[6] M. Lin and Y. Zhao, "Artificial intelligence-empowered resource management for future wireless communications: a survey," *China Communications*, vol. 17, no. 3, pp. 58–77, 2020.

[7] A. Chuan, "The national geographic characteristics of online public opinion propagation in China based on WeChat network," *Geoinformatica: An international journal of advances of computer science for geographic*, vol. 22, no. 2, pp. 311–334, 2018.

[8] E. Davidov, "Nationalism and constructive patriotism: a longitudinal test of comparability in 22 countries with the ISSP," *International Journal of Public Opinion Research*, vol. 23, no. 1, pp. 88–103, 2011.

[9] Y. Ming, J. Yang, J. Cao, Z. Zhou, and C. Xing, "Distributed energy sharing in energy internet through distributed averaging," *Tsinghua Science and Technology*, vol. 23, no. 3, pp. 233–242, 2018.

[10] A. Mandes and P. Winker, "Complexity and model comparison in agent based modeling of financial markets," *Journal of Economic Interaction and Coordination*, vol. 12, no. 3, pp. 469–506, 2017.

[11] F. Wang, Y. Zhang, Q. Rao, K. Li, and H. Zhang, "Exploring mutual information-based sentimental analysis with kernel-based extreme learning machine for stock prediction," *Soft Computing*, vol. 21, no. 12, pp. 3193–3205, 2017.

[12] H. Lu, Y. Li, M. Chen, H. Kim, and S. Serikawa, "Brain intelligence: go beyond artificial intelligence," *Mobile Networks and Applications*, vol. 23, no. 7553, pp. 368–375, 2018.

[13] K. Lin, C. Li, D. Tian, A. Ghoneim, M. S. Hossain, and S. U. Amin, "Artificial-intelligence-based data analytics for cognitive communication in heterogeneous wireless networks," *IEEE Wireless Communications*, vol. 26, no. 3, pp. 83–89, 2019.

[14] L. D. Raedt, K. Kersting, S. Natarajan, and D. Poole, "Statistical relational artificial intelligence: logic, probability, and computation," *Synthesis Lectures on Artificial Intelligence and Machine Learning*, vol. 10, no. 2, pp. 1–189, 2016.

[15] S. Jha and E. J. Topol, "Adapting to artificial intelligence," *JAMA*, vol. 316, no. 22, pp. 2353-2354, 2016.

[16] S. Makridakis, "The forthcoming artificial intelligence (AI) revolution: its impact on society and firms," *Futures*, vol. 90, no. jun., pp. 46–60, 2017.

[17] R. Li, Z. Zhao, X. Zhou et al., "Intelligent 5G: when cellular networks meet artificial intelligence," *IEEE Wireless Communications*, vol. 24, no. 5, pp. 175–183, 2017.

[18] R. Liu, B. Yang, E. Zio, and X. Chen, "Artificial intelligence for fault diagnosis of rotating machinery: a review," *Mechanical Systems & Signal Processing*, vol. 108, no. AUG., pp. 33–47, 2018.

[19] J. H. Thrall, X. Li, Q. Li et al., "Artificial intelligence and machine learning in radiology: opportunities, challenges, pitfalls, and criteria for success," *Journal of the American College of Radiology*, vol. 15, no. 3, pp. 504–508, 2018.

[20] M. Hutson, "Artificial intelligence faces reproducibility crisis," *Science*, vol. 359, no. 6377, pp. 725-726, 2018.

[21] J. Cao, E. M. van Veen, N. Peek, A. G. Renehan, and S. Ananiadou, "EPICURE: ensemble pretrained models for extracting cancer mutations from literature," in *2021 IEEE 34th international symposium on computer-based medical systems (CBMS)*, pp. 461–467, Aveiro, Portugal, 2021.

[22] J. Zhao, D. Zeng, J. Qin, H. M. Si, and X. F. Liu, "Simulation and modeling of microblog-based spread of public opinions on emergencies," *Neural Computing and Applications*, vol. 33, no. 2, pp. 547–564, 2021.

[23] F. Xiao, "Multi-sensor data fusion based on the belief divergence measure of evidences and the belief entropy," *Information Fusion*, vol. 46, pp. 23–32, 2019.

[24] Y. Zhang, H. Huang, L. X. Yang, Y. Xiang, and M. Li, "Serious challenges and potential solutions for the industrial internet of things with edge intelligence," *IEEE Network*, vol. 33, no. 5, pp. 41–45, 2019.

[25] O. I. Khalaf and G. M. Abdulsahib, "*Optimized dynamic storage of data (ODSD) in IoT based on blockchain for wireless sensor networks*," *Peer-to-Peer Networking and Applications*, vol. 14, no. 5, pp. 2858–2873, 2021.

Hindawi
Wireless Communications and Mobile Computing
Volume 2022, Article ID 3178571, 11 pages
https://doi.org/10.1155/2022/3178571

Research Article

3D Indoor Scene Synthesis System Based on Collaborative Retrieval

Yu Weijun

College of Art and Education, Chizhou University, Chizhou, China

Correspondence should be addressed to Yu Weijun; 0120030309@czu.edu.cn

Received 23 May 2022; Revised 25 July 2022; Accepted 1 August 2022; Published 21 August 2022

Academic Editor: Jun Ye

In order to solve the research problem of collaborative retrieval 3D indoor scene synthesis system, an automatic synthesis method of 3D indoor scene is proposed. In the research fields of computer graphics and computer vision, the modeling of various 3D scenes has always been a hot spot and a very valuable research topic for Chinese and foreign scholars. GMM is used to fit the position of the object on the support surface, and the position distribution model is obtained. Firstly, a file is created to store the normalized position of the counted object on the support surface. The number of coordinates represents the number of times the object appears in the scene library. Then, the Gaussian mixture model is used to fit the content of the file to obtain the location distribution model. For the initial indoor scene and the description of small objects to be added to the scene given by the user, select small objects with the help of the material library. Shapenetcorcv2 is the core part of the database, with a total of 55 categories and more than 50000 model instances. The automatic placement of these small objects is realized by using the scene synthesis algorithm, which shows the continuous enrichment of the evolution process of simple scenes to solve various problems of 3D indoor scene modeling. This method not only reflects the design requirements of users but also avoids cumbersome manual operation.

1. Introduction

With the rapid development of computer software and hardware technology, the application field of computer graphics has gradually expanded. Virtual reality, scientific visualization, and computer animation have become the three major research directions of computer graphics in recent years. The so-called virtual reality (VR) refers to the highly realistic virtual space generated by computer. Virtual reality technology (abbreviated as VR) is a new practical technology developed in the 20th century. Virtual reality technology includes computer, electronic information, and simulation technology. With the continuous development of social productivity and science and technology, the demand for VR technology in all walks of life is growing. VR technology has also made great progress and has gradually become a new field of science and technology. Within a certain range, it is highly similar to the real environment in terms of vision, hearing, and touch, so that users can experience as if they were in the real world and have an immersive feeling. Virtual reality is a multidisciplinary integrated technology. Virtual reality also known as spiritual world technology is an advanced computer human-machine interface with immersion, interactivity, and conception as the basic characteristics. It comprehensively utilizes computer graphics, simulation technology, multimedia technology, artificial intelligence technology, computer network technology, parallel processing technology, and multisensor technology; simulate the functions of human sense organs such as vision, hearing, and touch, so that people can be immersed in the virtual realm generated by the computer; and can communicate with them in natural ways such as language and gestures. Real-time interaction creates a human-friendly multidimensional information space. The development of various disciplines has also promoted the progress of virtual reality technology, making it widely used in military, medical, education, science and technology, entertainment, construction, industry, and commerce. 3D modeling technology is the key technology of virtual reality. At present, the modeling methods of objects can be roughly divided into three types:

the first method is to use three-dimensional software for modeling, the second method is to collect information through instruments and equipment for modeling, and the third method is to use image or video for modeling. In many applications of computer games, virtual reality, augmented reality, and hybrid reality, a large number of realistic 3D scenes are needed for users to carry out various interactive activities. Three-dimensional scene is the data basis for the interaction between human and virtual world, and indoor scene is widely used because it can better reflect the interaction between human and virtual scene. Nowadays, the rapid development and increasing popularity of the Internet make the acquisition, aggregation, storage, transmission, processing, and analysis of a large amount of data more and more convenient. After the digital age, information age, and Internet age, mankind has entered the era of big data. Various types of media data are growing rapidly. Although the number of three-dimensional data is less than that of pictures and video data, there are some well-known large-scale three-dimensional model scene databases, such as 3D Warehouse, which makes the acquisition of three-dimensional models more convenient than traditional modeling methods. The massive data resources contained in it provide the necessary data basis for the research of 3D scene analysis. Based on the analysis of existing resources and with the help of computer technology, the automatic generation of 3D scene will greatly improve the efficiency of scene modeling and provide a variety of virtual interactive environments for related applications, as shown in Figure 1.

2. Literature Review

With the improvement of living standards, people began to pay attention to interior home design and unified home decoration style. Ji and others feel that most ordinary users have very limited understanding and mastery of interior design and furniture style matching, and it is difficult to complete the design by themselves [1]. Therefore, usually, many users will hand over the interior design work to special interior designers. Fu and others said that traditional interior design often needs to spend higher labor and time costs and requires effective communication between customers and designers to obtain satisfactory design [2]. Wang and others said that in recent years, the emergence of indoor home intelligent design platform has simplified the design process and reduced the operation difficulty for users. Users can display a satisfactory indoor scene layout through simple drag and drop. After putting out a satisfactory layout, users will be concerned about the overall style of home decoration and the compatibility of furniture [3]. At present, interior home design platforms only classify furniture based on style categories (classical Chinese style, new Chinese style, classical European style, pastoral style, rural style, etc.). Kouadria and others said that users have to manually select appropriate furniture for matching in the same style category. However, even furniture of the same style is not necessarily matching. In the two scenes, all furniture models are modern Chinese style. It can be seen that the scene on the left has more style consistency than the scene on the right [4]. Therefore, if we can analyze the style consistency of the furniture model in the three-dimensional indoor scene and realize the furniture recommendation based on style consistency, we can automatically synthesize the three-dimensional indoor scene with style consistency. Bhangale and Mohanaprasad said that scene synthesis based on style consistency can better and faster help users choose furniture, synthesize indoor scenes that better meet users' needs, and reduce users' time consumption in indoor home design, which is of great significance to the whole home decoration design industry [5]. Zhang and others think that in the process of 3D indoor scene synthesis based on style consistency, the furniture model in the final synthesized scene should not only be the same in the type of home style but also reflect the compatibility and coordination of materials and colors between furniture [6]. However, Dong and others said that in the field of computer graphics and computer vision, the relevant methods of scene synthesis and layout design usually only consider the semantic information of furniture without constraints on the style of synthetic scenes [7]. The scene is a reasonable imagination based on the actual situation of the space, and it is a reasonable experience based on the designer's true feelings in the situation. Whether the analysis and setting of the space scene are successful or not basically determines the style and artistic height of furniture design. Chen and others think that in recent years, with the development of computer graphics and computer vision, style methods based on single model have attracted attention. These methods can obtain the shape characteristics of furniture models under the same style by analyzing the shape characteristics of models [8]. However, these methods often cannot distinguish more detailed shape characteristics under the same style. On the other hand, Wang and others said that the 3D furniture model with style consistency in the same indoor scene not only has similarity in shape but also has consistency in material and texture information to some extent. However, the current 3D model style analysis method does not discuss this information together with shape feature information, so it cannot be directly used for furniture retrieval with style consistency [9]. Therefore, Song and others said that it is still a very challenging problem to design a measurement method of style consistency of 3D furniture model; realize feature extraction including material, texture, and shape; analyze the style similarity of different types of objects; and synthesize indoor scenes on this basis [10].

3. Method

This paper proposes an indoor scene synthesis method based on collaborative retrieval. The process of this method is as follows: after the user decides the layout of the scene and selects the favorite style furniture, the style consistency analysis method is proposed to extract the style of the selected style furniture model and then conduct the corresponding furniture collaborative retrieval combined with the model style features in the model retrieval database and the scene layout information and place the retrieved furniture model in a reasonable position. In order to ensure the

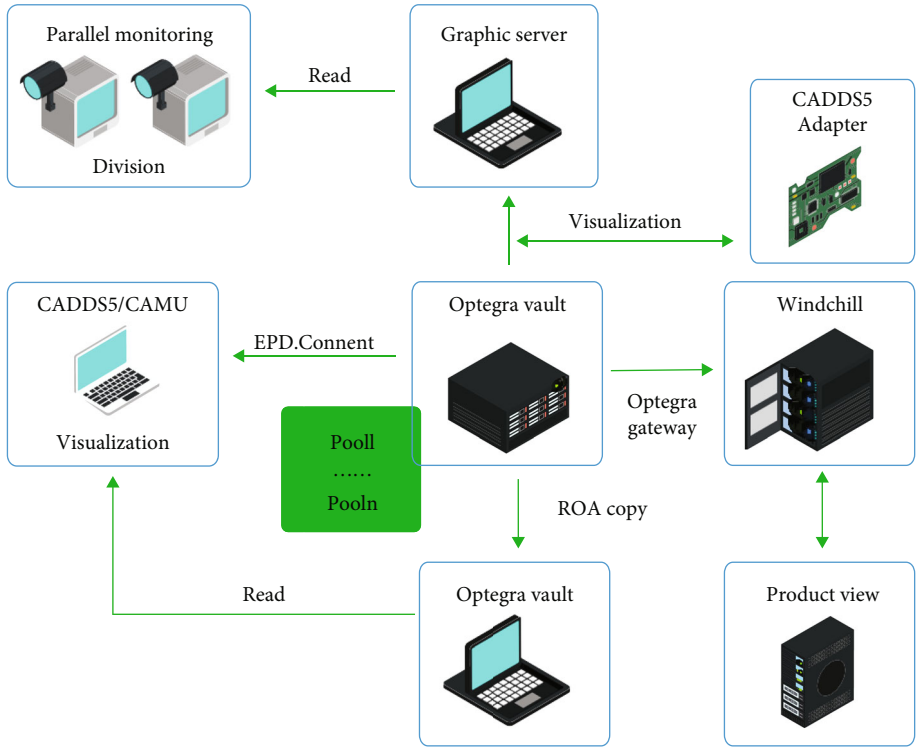

Figure 1: Research on 3D indoor scene synthesis system based on collaborative retrieval.

reasonable and authentic placement of the final furniture model, this chapter uses the furniture model position adjustment method based on constraints. In the process of scene synthesis, the style consistency of the furniture model of the synthetic scene and the consistency of the location and size of the scene furniture model with the layout information of the original scene should be ensured, as shown in Figure 2.

The main goal of style consistency information extraction is to extract the style features of the furniture models in the user selected style furniture and model retrieval database. The 256 dimensional features obtained by the consistency analysis framework are directly used as the style consistency features of each model. Scene layout information extracts the layout information of the scene, including the category and position and size of walls, doors, and each furniture object. This information is used as the limiting condition for user input to constrain the furniture models and their positions in the final synthesized scene [11]. In collaborative retrieval based on style consistency and layout information, after extracting the style consistency information and scene layout information of furniture model, the next step is to retrieve scene furniture. If the best matching retrieval is directly carried out for each furniture object category existing in the scene layout, the consistency between furniture models may be ignored, and it is difficult to achieve satisfactory results. Collaborative retrieval between furniture objects can not only ensure the style consistency of retrieved furniture but also ensure the consistency with the category and shape information of the corresponding furniture model in the layout information of the scene input by the user [12].

In object position adjustment in order to ensure the rationality of the furniture position of the synthetic scene, it is necessary to judge and adjust the position of each object in the scene. After obtaining the candidate furniture data of each furniture node, the combination optimization process based on style consistency features and scene layout information will be carried out. This paper uses formula (1) as a cost function to evaluate the quality of a specific candidate furniture combination and measures the style consistency of the furniture model set C selected from the candidate furniture set, the style consistency between the furniture model set C and the style furniture model provided by the user, and the consistency between the size of the furniture model in C and the size of the corresponding furniture object in the scene layout. $a.w$ and $a.h$ represent the length and width of the surrounding of furniture object a, respectively. Cong, Cong, and Zha are set to 1, 0.5, and 2.0, respectively, in practice, as shown in formulas (1), (2) and (3).

$$F(C) = \lambda_1 \sum_{a,b \in c} d(f_a, f_b) + \lambda_2 \sum_{c \in C} d(f_c, f_{\text{user}}) + \lambda_3 \sum_i d_s(s_i^{\text{user}}, s_i^c), \tag{1}$$

$$d(a, b) = \lambda \|a - b\|^2, \tag{2}$$

$$d_s(a, b) = \max\left(\|a.w - b.w\|^2, \|a.h - b.h\|^2\right). \tag{3}$$

In order to minimize the best combination of candidate furniture in formula (3), a simple way is to enumerate all possible combinations and directly select the one that can make the largest furniture combination. Since each furniture

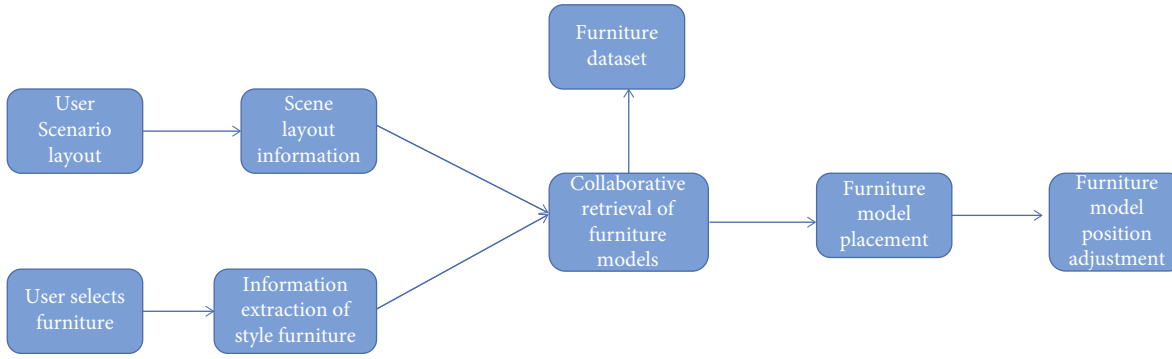

Figure 2: Scene synthesis process based on collaborative retrieval.

selects the first 10 optimal matches as the candidate furniture set, for a scene layout with n furniture nodes, the time complexity of judging all possible combinations is $0(10^N)$, which obviously has a very expensive computational cost [13]. A heuristic algorithm based on cluster search is used to approximate the optimization process. It intuitively explains that if the current combination is optimal, at least one or more subsets of the combination are likely to be optimal. Before adjusting the position, you need to set some constraint information to guide the placement process of each 3D model. In order to ensure that the synthetic scene conforms to the law of the real world, the extracted room contour polygon and the bounding box of each furniture object need to set some hard constraints. These hard constraints are not allowed to occur at any time. Once they occur, it means that the synthetic scene does not meet the physical authenticity. These hard constraints are as follows: overlap rule: when placing an object, the object cannot intersect or overlap with the bounding box of any other object. For two 3D furniture models i and j, this paper calculates the intersection area of two polygons to judge whether the bounding boxes BB_i and BB_j of two objects intersect. If the intersection area of two bounding boxes is O, it means that they do not overlap, as shown in the following formula:

$$C_1(i,j) = \begin{cases} 1, & \mathrm{area}\left(\mathrm{BB}_i \cap \mathrm{BB}_j\right) = 0, \\ 0, & \mathrm{else}. \end{cases} \tag{4}$$

Through wall rule: when placing an object, the object cannot be placed outside the wall or intersect with the wall. For the three-dimensional furniture model i, this paper calculates the intersection area of the bounding box BB_i of the model and the contour polygon P_{wall} composed of the room wall. If the intersection area is equal to the area of the bounding box of the model, it means that the object is placed inside the room, as shown in the following formula:

$$C_2(i,j) = \begin{cases} 1, & \mathrm{area}(\mathrm{BB}_i \cap P_{\mathrm{wall}}) = \mathrm{area}(\mathrm{BB}_i), \\ 0, & \mathrm{else}. \end{cases} \tag{5}$$

Door blocking rule: in real life, in order to ensure that people can enter an indoor scene from the outside. When placing an object, the bounding box of the object cannot overlap with the extended area of the door. In order to judge whether the three-dimensional furniture model I blocks the door J, this paper first extends the door j by 1.2 meters along the interior direction of the room, and the extended area can be represented by a rectangle. Thus, this paper calculates the intersection area between the bounding box BB_i of the model and the rectangular $R_{\mathrm{door}j}$ of the extended area of the door to judge whether there is a door, as shown in formula (5):

$$C_3\left(i, \mathrm{door}_j\right) = \begin{cases} 1, & \mathrm{area}\left(\mathrm{BB}_i \cap R_{\mathrm{door}_j}\right) = 0, \\ 0, & \mathrm{else}. \end{cases} \tag{6}$$

Proximity rule: the distance between each object and adjacent objects should be consistent with the layout information as far as possible. Firstly, we need to define the distance between two objects and describe the specific setting of proximity constraint. For two objects i and j, this paper uses the minimum value d_{ij} of the point distance on the bounding box of two objects as the distance between the two objects. C is the relative distance of objects i and j in the layout provided by the user, and a is the coefficient manually set, which is set to 0.1 in this paper, as shown in the following formula:

$$C_4 = \sum_{i,j} e^{-a\left(d_{ij} - \partial^i_{\mathrm{wall}}\right)}. \tag{7}$$

If one of the objects in the search box is placed against the wall, it should also be placed against the wall. The specific setting of the wall constraint is described. The distance d between the object i and the wall is equal to the minimum value of the distance from the point on the bounding box of the object to the wall polygon. d^i_{wall} is the relative distance between the object 1 and the wall in the layout provided by the user. Compared with the proximity constraint, the influence of the wall constraint is greater. Therefore, it is

set as 10 in this paper, as shown in the following formula:

$$C_5 = \sum_{i,j} e^{-\beta\left(d^i_{\text{wall}} - \partial^i_{\text{wall}}\right)}. \quad (8)$$

Based on the discussion of the above constraint information, the position adjustment process can be regarded as the solution process of numerical optimization. Because the layout position provided by the user can be used as a good initial solution, this paper uses the mountain climbing algorithm to solve the local optimal value. First, define the solution goal. According to the previous rule definition, this paper uses the following formula as the optimization goal, as shown in the following formula:

$$C_{\text{all}} = \prod_{i,j} C_1(i,j) \cdot \prod_i C_2(i) \prod_{i,\text{door}j} C_3\left(i, \text{door}_j\right) \cdot C_4 \cdot C_5. \quad (9)$$

In order to verify the effectiveness of the scene synthesis method proposed in this chapter, this section will conduct corresponding experimental analysis on the collaborative retrieval based on style consistency and scene layout information and the location adjustment method based on local optimization mountain climbing algorithm. The corresponding experiments are as follows: collaborative retrieval and top-1 retrieval effect comparison experiment, collaborative retrieval effect comparison experiment with different parameter ratios, scene synthesis effect comparison experiment with or without position adjustment process, and user survey of the comparison between indoor scene synthesized by this method and indoor scene synthesized by experts [14]. Gaussian distribution is a very important continuous probability distribution function in the fields of machine learning, computer, mathematics, physics, and engineering. It describes a random variable distributed around a single value aggregation. At the same time, Gaussian distribution is also the most widely used type of distribution. Gaussian model is used to quantify things with Gaussian distribution and decompose a thing into several models based on Gaussian distribution. It can be divided into a single Gaussian model (SGM) and Gaussian mixture model. The definition of multidimensional Gaussian distribution (normal distribution) probability density function is shown in the following formula:

$$N\left(x, \mu, \sum\right) = \frac{1}{\sqrt{(2\Pi)|\Sigma|}} \exp\left[-\frac{1}{2}(x-\mu)^T \Sigma^{-1}(x-\mu)\right]. \quad (10)$$

Different from the one-dimensional Gaussian distribution, sample x is the n-dimensional sample vector, μ is the expectation of the model, and Σ is the variance of the model. For the single Gaussian model, because it can be clear whether the training sample belongs to the Gaussian model (for example, when training the face skin color model, the skin color part in the face image is segmented to form the training sample set), μ is usually replaced by the mean value of the training sample and Σ by the sample variance. In order to apply Gaussian distribution to pattern classification, it is assumed that the training sample belongs to category A, as shown in the following formula:

$$N\left(\frac{x}{A}\right) = \frac{1}{\sqrt{(2\Pi)|\Sigma|}} \exp\left[-\frac{1}{2}(x-\mu)^T \Sigma^{-1}(x-\mu)\right]. \quad (11)$$

Formula (11) describes the probability value that the sample belongs to category a. Substituting any observation sample x_i into formula (10) can obtain a scalar value $N(x_i, \mu, \sum)$. If the value is greater than the threshold value, it can be determined that the observation sample belongs to category A. When analyzing a three-dimensional indoor scene, one of the key links is to extract and analyze the spatial relationship between objects in the scene, including support relationship and proximity relationship. These are two different spatial relationships, but they have a certain correlation with each other, so priority should be considered in detection. The basis for determining the priority is that after the detection of the spatial relationship with higher priority is completed, the detection results can facilitate the detection of the spatial relationship with lower priority or simplify the algorithm steps and improve the efficiency of the algorithm. In general, the priority of support relationship is higher than that of proximity relationship [15]. Therefore, firstly, the support relationship between objects in the scene is detected. When judging the relationship of objects, the support relationship will be judged first. After the judgment of all supporting relationships is completed, the judgment of proximity relationship can be carried out. In the 3D scene, there will be the relationship between supported and supported objects. This paper detects the relationship by extracting the algorithm of supporting relationship. The flow chart of this algorithm is shown in Figure 3.

The algorithm mainly consists of three steps: preliminary judgment: judge whether two BBB bounding boxes intersect. If the center distance of the BBB bounding box of two objects is not within the preset off value range (set this off value to 4.0), we can directly draw a conclusion: there is no supporting relationship between the two objects. Otherwise, make the next judgment. This step is a preliminary screening process. The purpose is to exclude some object pairs that obviously have no support and supported relationship, so as to save the running time of the algorithm and improve the efficiency of detailed judgment. If the AABB bounding boxes of the two objects intersect, it indicates that the two objects may have a relationship between support and supported. It is necessary to further detect the GOBB bounding box with good tightness to judge whether there is a support relationship between the GOBB bounding boxes of the two objects. If it exists, it can indicate that there is a supporting and supported relationship between the two objects. Otherwise, proceed to the next step of detection [16, 17]. If the AABB bounding boxes of two objects intersect, but the GOBB bounding box has no support and supported relationship, it is necessary to detect the triangular patch level to finally judge whether the two objects have a support relationship. If the triangle of one object is in contact with the

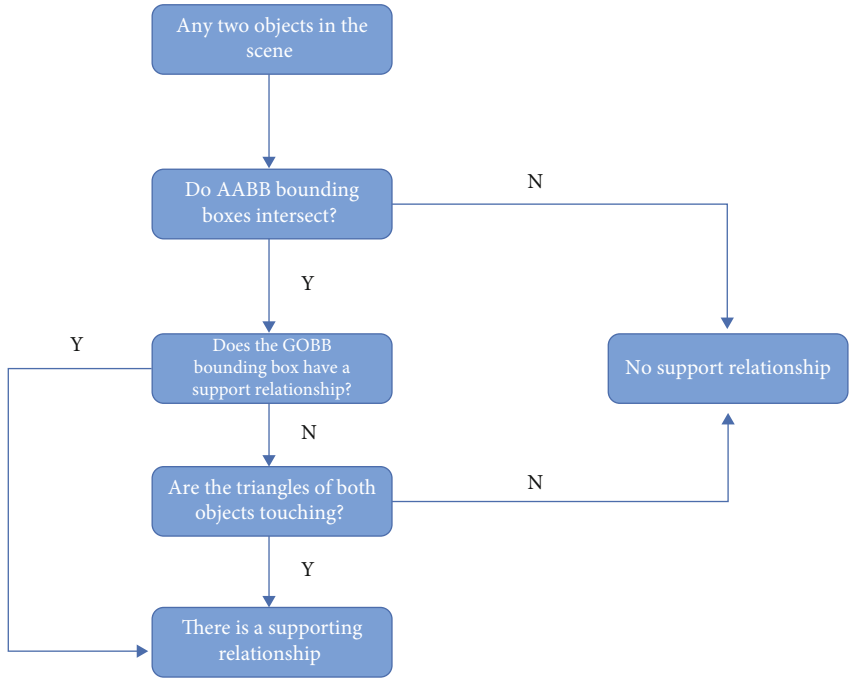

Figure 3: Algorithm flow of extracting support relationship.

triangle of another object, it can be determined that there is a support relationship between the two objects.

4. Experiment and Analysis

Home synthesis system integrates the proposed three-dimensional model analysis method of style consistency with the scene synthesis method based on style consistency retrieval and designs and implements a prototype system for home design. The purpose of this system is to help ordinary users without relevant design experience to quickly carry out indoor home design and meet the requirements of users for style consistency design. The system can not only enable ordinary users to carry out home design but also become an auxiliary tool for home style research by professionals in the home design industry. The system provides relevant data structures and can easily support the expansion of relevant technologies [18]. Today's indoor home design platform can assist users in the actual indoor scene design, but users need to choose the appropriate furniture model for placement. Although the design platform will show some excellent sample rooms for users' reference, a fixed number of sample rooms still cannot meet the diversified user's personalized design needs. It still takes a lot of time for users to migrate directly from house type to template. Taking this as the starting point, based on the research results of style consistency analysis of 3D indoor scenes, a relevant prototype system based on style consistency analysis and 3D scene synthesis will be designed and implemented [19]. The system can not only analyze the style consistency of the current indoor scene but also assist users in the design of indoor scene, realize the style consistency index and recommendation of furniture model, and place the corresponding correct position. While reducing the user interaction time, the system can design and synthesize the indoor scene satisfactory to users. The overall flow chart of the system is shown in Figure 4.

According to the analysis and research on the style consistency of the front three-dimensional indoor scene and the design objectives of the system in this chapter, the main functional modules of the HorneSynthesis system are shown in Table 1.

After determining the process and function of home synthesis system, it is necessary to conduct data analysis for each process and its required functions. The system is written using synthesis.

4.1. Home Security System. The home security system mainly includes home fire prevention, gas prevention, anti-theft, and waterproof leakage. It is composed of sensors, computers, and corresponding control systems. The sensor detects the light, temperature, smell, and other parameters of the home, and if there is a dangerous situation, it will transmit the relevant information to the computer.

4.2. Automatic Control System. The automatic control system is the centralized management of electrical appliances such as air conditioners, washing machines, refrigerators, and cleaners. It consists of two major parts: a home computer and a controller. For example, it can automatically control the air conditioner to automatically adjust the indoor temperature and humidity according to different weather conditions, so that the family can always be in a comfortable environment.

4.3. Home Information System. Household information systems are mainly computer-controlled telephones, televisions, etc., which are connected to the social information

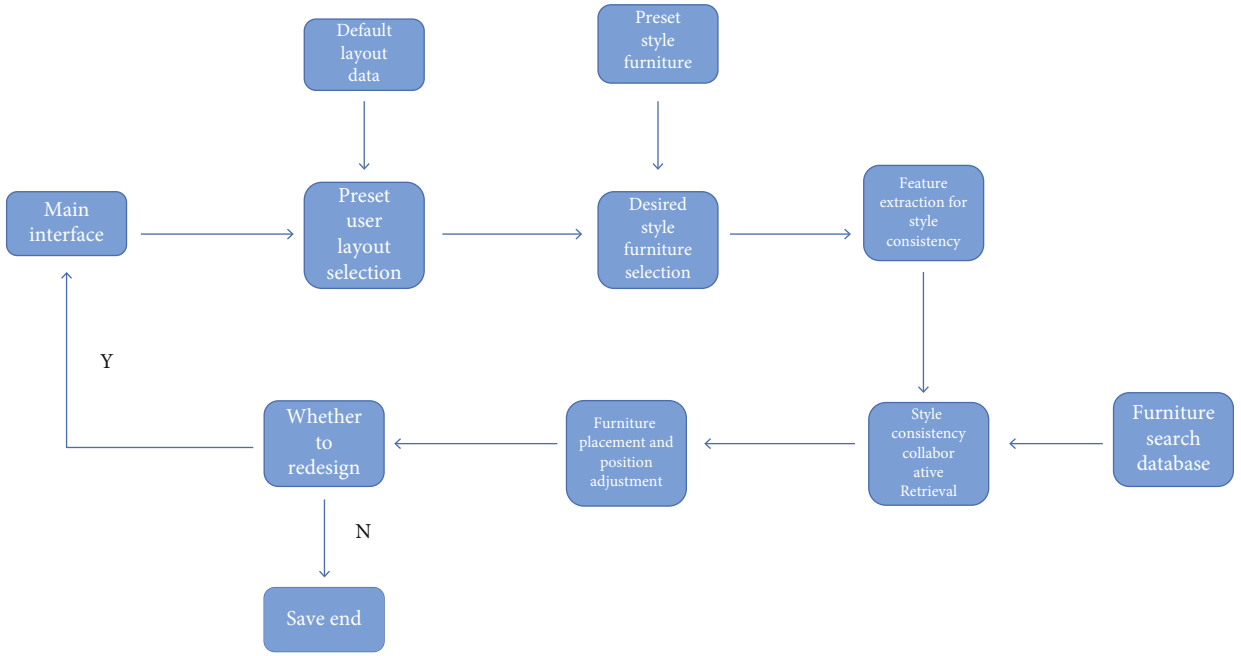

Figure 4: System flow chart.

Table 1: System functions.

Processing process	Specific functions
User information processing	Select preset layout
	Layout information processing
	User style furniture selection
	Feature extraction of user style furniture
Scene synthesis	Furniture retrieval
	Furniture placement
	Furniture position adjustment
	Visual synthetic scene

center through communication lines to obtain various information. The home information system can be used for health management, such as temperature measurement, blood pressure measurement, and pulse measurement, and the home system also realizes home office, truly experiencing the convenience brought by the information age.

The position adjustment class corresponds to the position optimization process proposed in Section 3. Finally, the synthesized scene is rendered by OpenGL. The detailed data structure design is shown in Table 2.

The whole system is divided into four modules: input module, scene analysis module, scene synthesis module, and output module. The description of each module in the algorithm is as follows: input. It refers to the rough scene with only large furniture specified by the user as the initial scene, as well as the type and quantity of objects planned to be put into the scene. In the scene analysis module, it includes two main contents: the analysis of the geometric relationship between objects in the scene and the training of the position distribution model of object placement. For the analysis of geometric relationship, four parts are mainly done: support surface extraction, intersection detection, support relationship and proximity relationship detection, and symbiotic relationship analysis. The function of each part is as follows: support surface extraction: extract the support surface contained by each object in the scene. This part is the basis and support of the whole scene synthesis algorithm. The analysis of intersection relationship, support relationship, proximity relationship, symbiosis relationship, and the training of position distribution model can be completed only after the support surface is extracted [20, 21]. For intersection detection, avoid overlapping objects during placement. The intersection detection algorithm based on bounding box is adopted. In detection of support relationship and proximity relationship, detect the support relationship and proximity relationship between each two objects in the scene to prepare for the analysis of symbiotic relationship, you can try to directly violently return the coordinate information. For example, the yolo detection series yolo contains a foreground probability + 4 coordinates + each

Table 2: System data structure.

Class	Attribute	Attribute property
Layout information class	Layout bounding box	It is used to determine the location of the room layout. The layout information is represented by four point coordinates of a rectangle. The type is list
	Wall information	Save the polygon composed of walls, which is represented by the vertex coordinates of the polygon. The type is list
	Door information	Save the position of each door. Ignore the thickness and height of the door. It is represented by the coordinates of two points. The type is list
	Furniture information	The position, category, size, and orientation information of each furniture in the layout. The type of category information is int and the other types are list
Furniture	Furniture category	Record the category information of furniture. The type is int
	Furniture size	Record the size of the furniture bounding box. The type is list
	Shape feature	Record the shape features of the furniture model for collaborative retrieval. The type is list
	Projection feature	Record the projection features of the furniture model for collaborative retrieval. The type is list
Scene class	Scene model collection	It is used to visualize the display scene
	Scene layout information	Wall, door, and other information used to display the scene
Furniture retrieval	Retrieve candidate sets	The candidate furniture model is calculated during furniture collaborative retrieval, and the type is list
	Optimal retrieval set	The currently calculated optimal candidate retrieval set. The type is list

category probability for each point on the feature map. You can make appropriate magic changes and add four coordinates to return to the associated target boxes, such as the face and human body; of course, this can only be used for simple target associations. The priority of the support relationship is higher than the proximity relationship. In symbiosis analysis, with the help of the data set of three-dimensional scene, the types and frequency of objects that can be supported by various types of supports in the scene are counted. It provides a basis for the algorithm of placing the specified support surface in scene synthesis. For the position distribution training of object placement, firstly, with the help of three-dimensional scene data set, count the position of objects on the same category of supports, normalize the data, and then, fit these data with Gaussian mixture model to train the position distribution model, as shown in Figure 5.

The object random automatic placement algorithm is the first stage of scene synthesis. The goal is to select one of the supports contained in the scene and then randomly select a support plane from the support to randomly place small objects on the plane. The algorithm flow is shown in Figure 6.

(1) The algorithm mainly includes three small algorithms: randomly selecting the support surface, generating candidate placement points, and intersection detection. Firstly, the method of randomly selecting the support plane from the selected supports is introduced. The uniform sampling algorithm of 3D model surface is given. In this algorithm, triangles are randomly selected according to the area of triangles. Inspired by this, we randomly select the support surface according to the area of the support surface. It can be seen that the probability of each plane being selected is proportional to the area of the plane [22]. After accepting the sample, we place it on the support surface based on the rejection. Accept and reject sampling is referred to as reject sampling. The basic idea of this algorithm is as follows: if the function form of target distribution is complex and sampling is difficult. By sampling the distribution of another function that is simple in form and close to the objective function, the invalid data points other than the objective distribution can be discarded, and the rest are effective sampling points [23, 24]. In this paper, the last selected support surface is made into a square according to its longest edge, so that this square contains the whole support surface. Suppose the selected support surface is rectangular, as shown in Figure 7.

It can be seen from the foregoing that the supporting surfaces in the scene are parallel to the xy plane, so the random selection of points on the supporting surface is the random selection of x and y coordinates. The probability of each point being selected on both sides of the square is the same, so the selection of points in the square area conforms to the uniform distribution [1]. After selecting any data point, it is also necessary to detect whether the data point falls within the support surface area. As shown in Figure 7, the support surface area is a rectangular area surrounded by a solid line. If the selected data point is $p(x_1, y_1)$, the data point is within the support surface area, so it is a valid data point. If the selected data point

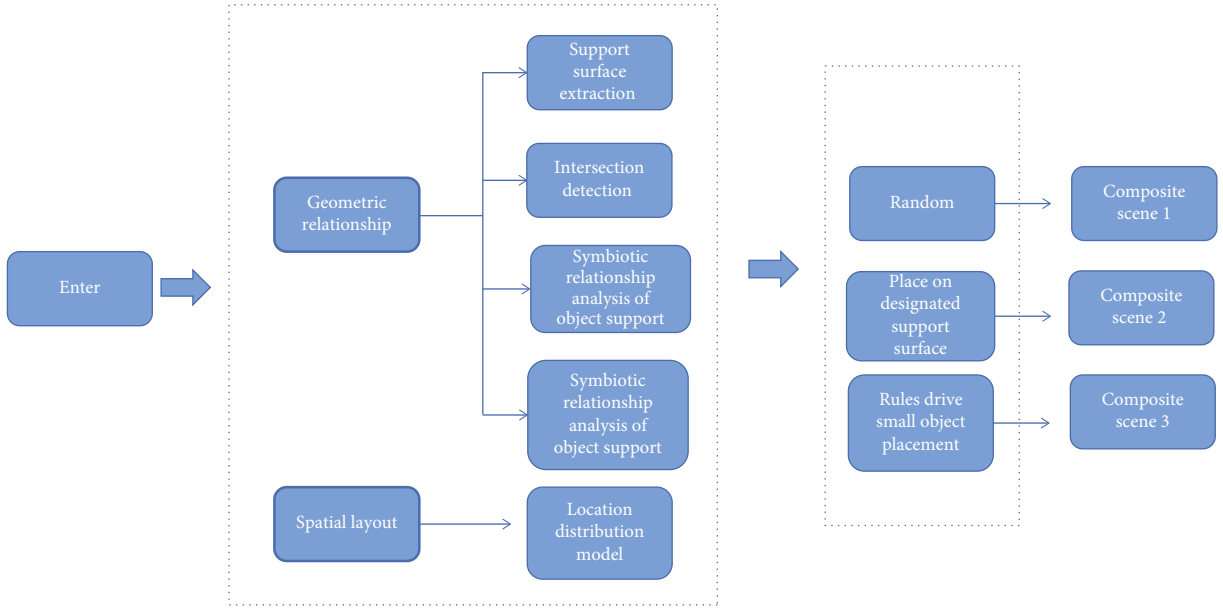

Figure 5: User-guided scene synthesis.

is $p\,(x_2, y_2)$, the data point is outside the support surface area, so it is an invalid data point, which needs to be discarded and recollected [25, 26]. Based on the previous experimental analysis, it can be explained that using shape features and projection features at the same time can more accurately analyze the style consistency of 3D models. However, how can shape features and projection features be effectively combined and how can the dimension of each feature be designed. In this paper, experiments are carried out on different feature dimension combinations in order to analyze the optimal dimension combination scheme. This paper selects different feature dimension combination schemes (128 and 128, 128 and 256, 256 and 128, 256 and 256). Firstly, 20% of the inter template data is reserved for testing, and 100 quads are constructed as the test data. The effect of each combination on the generalization ability of deep learning network is judged by analyzing the loss change curve of the test quads in the training process. The four curves represent the change process of test loss using a specific feature dimension combination, in which SF represents shape feature and PF represents projective feature. It can be seen from the figure that when the shape features and projection features are 128 dimensions, the generalization performance of the network is the best, as shown in Figure 8.

The style analysis method of 3D furniture model based on depth measurement learning is integrated with scene synthesis based on style consistency retrieval, and the corresponding home synthesis prototype system is designed and implemented [27]. From the perspective of software development, this paper introduces the composition module and important data structure of the system and expounds the implementation effect of the main functions of the system through an example. The system can help users without any interior design experience to carry out interior design more effectively. Users need to input a three-dimensional interior scene and the target style furniture object, and the system automatically realizes the scene synthesis of the corresponding style. The system can be used as a tool for furniture style analysis and can also help users quickly synthesize 3D indoor scenes with consistent style.

5. Conclusion

3D scene analysis and synthesis have always been a research hot spot in the field of computer graphics and computer vision. With more and more scene data available, the use of deep learning method can effectively analyze the objects in the scene and extract the common information of objects in a scene. This paper proposes a style consistency analysis method of 3D indoor scene objects, which can extract the style features of furniture objects in 3D indoor scene and use this feature to realize the 3D indoor scene synthesis method based on style consistency retrieval. In this method, the stylistic features of 3D furniture objects are extracted and retrieved together with the scene layout information provided by the user, and then, the position of the placed furniture model is slightly adjusted to meet some position constraints. The work of this paper is mainly reflected in the following three aspects: the style consistency analysis method of 3D model based on metric learning. The style consistency of three-dimensional furniture model means that the furniture model in the same scene should not only be the same in the type of home style but also maintain the compatibility and coordination, reflecting the consistency and aesthetic feeling of color and material. In this paper, the four-tuple depth measurement network based on shape features and projection features is used to analyze the style consistency features of three-dimensional models. This method provides a basis for 3D style consistent scene synthesis. Based on the style consistency feature analysis method, after the user provides the layout information of

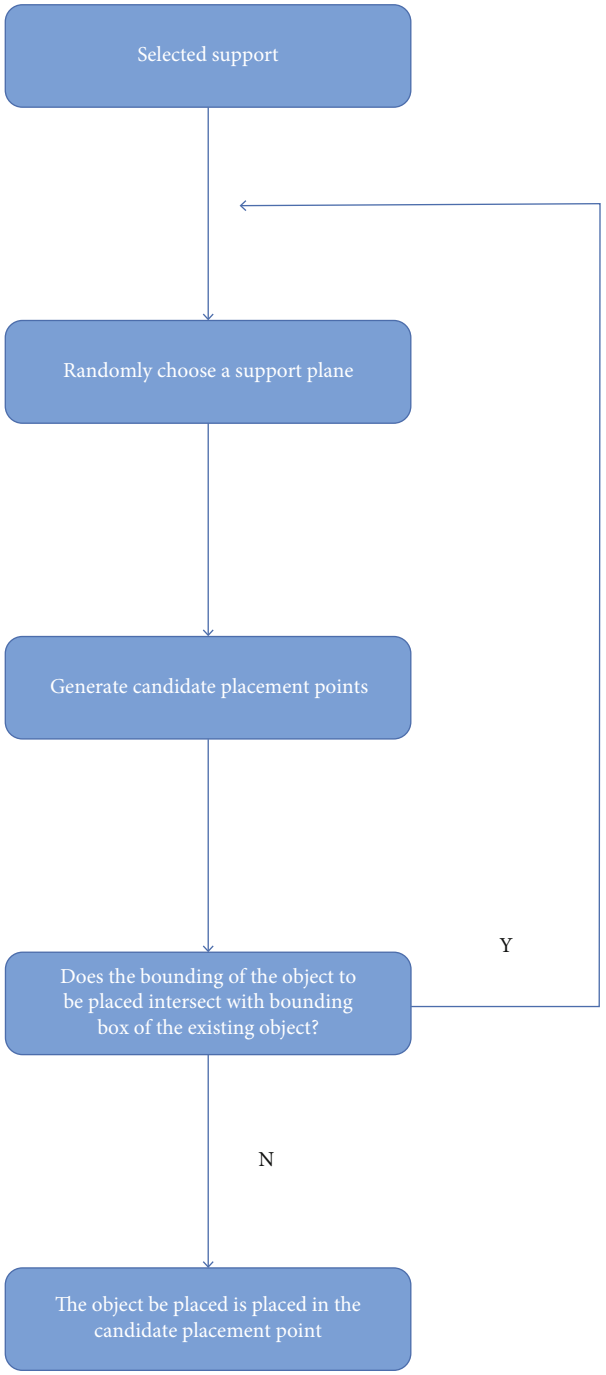

Figure 6: Flow chart of random placement algorithm.

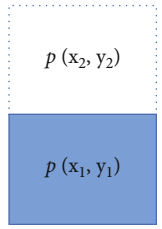

Figure 7: Receive reject sampling.

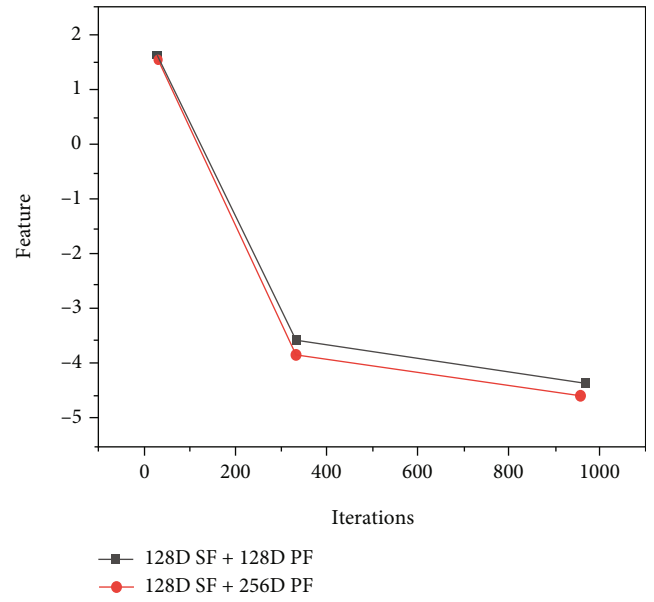

Figure 8: Comparative experimental results of different style feature dimensions.

the indoor scene and the furniture of the target style, this paper proposes a 3D indoor scene synthesis method based on style consistency retrieval, which can automatically synthesize the indoor scene with consistent layout information and style consistency provided by the user. Combined with the research contents of the first two parts, this paper integrates the style feature analysis based on style consistency with the scene synthesis method and designs and implements the corresponding home synthesis prototype system. This paper expounds the structure and effect of the system from the perspective of data development.

Data Availability

The data that support the findings of this study are available from the corresponding author upon reasonable request.

Conflicts of Interest

The author declared no potential conflicts of interest with respect to the research, authorship, and/or publication of this article.

References

[1] P. Ji, D. Qin, P. Feng, T. Lan, and G. Sun, "Research on indoor scene classification mechanism based on multiple descriptors fusion," *Mobile Information Systems*, vol. 2020, Article ID 4835198, 14 pages, 2020.

[2] X. Fu, Y. Zhang, W. Zhang, Q. Li, and T. Kong, "Research on the size of ring forgings based on image detection and point cloud data matching method," *The International Journal of Advanced Manufacturing Technology*, vol. 119, no. 3-4, pp. 1725–1735, 2021.

[3] J. Wang, J. H. Zhang, J. L. Zhang, F. M. Lu, R. G. Meng, and Z. Wang, "Research on fault recognition method combining

3D Res-UNet and knowledge distillation," *Applied Geophysics*, vol. 18, no. 2, pp. 199–212, 2021.

[4] A. Kouadria, O. Nouali, and M. Y. H. Al-Shamri, "A multi-criteria collaborative filtering recommender system using learning-to-rank and rank aggregation," *Arabian Journal for Science and Engineering*, vol. 45, no. 4, pp. 2835–2845, 2020.

[5] K. B. Bhangale and K. Mohanaprasad, "Content based image retrieval using collaborative color, texture and shape features," *International Journal of Innovative Technology and Exploring Engineering*, vol. 9, no. 3, pp. 1466–1469, 2020.

[6] S. H. Zhang, S. K. Zhang, Y. Liang, and P. Hall, "A survey of 3D indoor scene synthesis," *Journal of Computer Science and Technology*, vol. 34, no. 3, pp. 594–608, 2019.

[7] Y. Dong, B. Q. Hu, S. L. Zhang, Y. L. Huang, G. C. Nong, and H. Xin, "Research on North Gulf distributed big data submarine 3D terrain computing system based on remote sensing and multi-beam," *Soft Computing*, vol. 24, no. 8, pp. 5847–5857, 2020.

[8] Y. Chen, Z. Li, T. Zeng, Y. Ning, and Z. Bin, "Research and design of 3D reconstruction system based on binocular vision," *International Core Journal of Engineering*, vol. 5, no. 12, pp. 29–35, 2019.

[9] Z. Wang, Z. Zhang, Y. Luo, Z. Huang, and H. T. Shen, "Deep collaborative discrete hashing with semantic-invariant structure construction," *IEEE Transactions on Multimedia*, vol. 23, pp. 1274–1286, 2020.

[10] Q. Song, N. Zhang, and H. Liang, "Review of the Chinese internet philanthropy research (2006-2020) : analysis based on CiteSpace," *The China Nonprofit Review*, vol. 13, no. 1&2, pp. 4–4, 2021.

[11] L. Kruesi, F. Burstein, and K. Tanner, "A knowledge management system framework for an open biomedical repository: communities, collaboration and corroboration," *Journal of Knowledge Management*, vol. 24, no. 10, pp. 2553–2572, 2020.

[12] G. Xiong, Q. Fu, H. Fu, B. Zhou, and Z. Deng, "Motion planning for convertible indoor scene layout design," *IEEE Transactions on Visualization and Computer Graphics*, vol. 27, pp. 4413–4424, 2020.

[13] M. Li, A. G. Patil, K. Xu et al., "GRAINS," *ACM Transactions on Graphics*, vol. 38, no. 2, p. 1, 2019.

[14] H. Li, "3D indoor scene reconstruction and layout based on virtual reality technology and few-shot learning," *Computational Intelligence and Neuroscience*, vol. 2022, Article ID 4134086, 9 pages, 2022.

[15] J. T. Lin, Y. Z. Lee, and J. Lalevee, "Efficacy modeling of new multi-functional benzophenone-based system for free-radical/cationic hybrid-photopolymerization using 405 nm led," *Journal of Polymer Research*, vol. 29, no. 3, pp. 1–9, 2022.

[16] G. Alhudhud, H. Al-Baity, D. H. Alsaeed, A. S. Al-Humaimeedy, and I. Al-Turaiki, "3D echolocating system for the visually impaired based on bat sonar approach," *Bioscience Biotechnology Research Communications*, vol. 12, no. 2, pp. 356–361, 2019.

[17] Y. Wu, X. Gu, Z. Tu, and Z. Zhang, "System dynamic analysis on industry-university-research institute synergetic innovation process based on knowledge flow," *Scientometrics*, vol. 127, no. 3, pp. 1317–1338, 2022.

[18] R. R. Herrera and J. E. R. Martínez, "Voice synthesis system based on recursive functions designed by graphs," *Research in Computing Science*, vol. 148, no. 10, pp. 347–355, 2019.

[19] V. N. Shvedenko, V. V. Shvedenko, and O. V. Shchekochikhin, "A process control methodology based on digital twins of production system objects," *Automatic Documentation and Mathematical Linguistics*, vol. 55, no. 5, pp. 210–218, 2021.

[20] W. Li, G. Junhua, B. Chen, and J. Han, "Incremental instance-oriented 3D semantic mapping via RGB-D cameras for unknown indoor scene," *Discrete Dynamics in Nature and Society*, vol. 2020, Article ID 2528954, 10 pages, 2020.

[21] Y. Luo, Z. Huang, Y. Li, F. Shen, and P. Cui, "Collaborative learning for extremely low bit asymmetric hashing," *IEEE Transactions on Knowledge and Data Engineering*, vol. 33, no. 12, pp. 3675–3685, 2020.

[22] X. Zhang, J. Yao, L. Dong, and N. Ye, "Research on 3D architectural scenes construction technology based on augmented reality," *Journal of Computational Methods in Sciences and Engineering*, vol. 21, no. 1, pp. 1–17, 2020.

[23] Z. Wu, C. Ren, X. Wu, L. Wang, and Z. Lv, "Research on digital twin construction and safety management application of inland waterway based on 3D video fusion," *IEEE Access*, vol. 9, pp. 109144–109156, 2021.

[24] Y. G. Kabaldin, D. A. Shatagin, and M. S. Anosov, "Synthesis of new metallic materials on the basis of nonlinear dynamics and artificial intelligence," *Russian Engineering Research*, vol. 41, no. 9, pp. 824–828, 2021.

[25] Z. Zhu, D. Li, Y. Hu, J. Li, D. Liu, and J. Li, "Indoor scene segmentation algorithm based on full convolutional neural network," *Neural Computing and Applications*, vol. 33, no. 14, pp. 8261–8273, 2021.

[26] L. V. Hùng, "3d hand pose estimation in point cloud using 3D convolutional neural network on egocentric datasets," *Research and Development on Information and Communication Technology*, vol. 2020, no. 2, pp. 87–97, 2021.

[27] M. Gorlachova and B. Mahltig, "3D-printing on textiles – an investigation on adhesion properties of the produced composite materials," *Journal of Polymer Research*, vol. 28, no. 6, pp. 1–10, 2021.

Hindawi
Wireless Communications and Mobile Computing
Volume 2022, Article ID 9906100, 12 pages
https://doi.org/10.1155/2022/9906100

Research Article

Research on Reconfiguration of Distribution Network considering Three-Phase Unbalance

Xuejie Wang[1,2] **Yanchao Ji**[1] **Jianze Wang**[1] **Yi Zhao**[2] **Peng Ye**[2] **Lei Qi**[3] **Shuo Yang**[4] **and Siqi Liu**[4]

[1]*School of Electrical Engineering &Automation, Harbin Institute of Technology, Harbin 150001, China*
[2]*School of Electric Power, Shenyang Institute of Engineering, Shenyang 110136, China*
[3]*Liaoning Provincial Institute of Safety Science, 110004 Shenyang, China*
[4]*Fushun Power Supply Company, State Grid Liaoning Electric Power Supply Co Ltd, Fushun 113008, China*

Correspondence should be addressed to Xuejie Wang; wangxj1@sie.edu.cn

Received 16 April 2022; Revised 21 June 2022; Accepted 6 July 2022; Published 18 August 2022

Academic Editor: Jun Ye

In the distribution network, the addition of distributed power sources can improve the voltage part of the distribution system, provide uninterrupted power supply, and reduce network losses. The location of the power supply and its output will also directly affect the system voltage and power loss. Therefore, determining the optimal installation location and capacity of distributed power generation is of great significance to the distribution network. However, in the actual system, due to the unbalanced load distribution and the three-phase unbalance of the transmission line, the power distribution system presents the characteristics of unbalanced distribution. As the number of electric vehicles increasing, the imbalance of the distribution network has become more prominent.

1. Introduction

Distribution network reconfiguration is of great significance to the planning and operation of the distribution network. Reconfiguration can determine the topology of the network to improve the economy and stability of the operation of the system. Distributed power has aggravated the three-phase imbalance of system. The goal of the reconfiguration program is to determine the optimal network topology path by controlling the switch state, to meet the system's minimum network loss and load balance objective function, and to some given distribution network operation constraints [1, 2]. Due to the nonlinearity of power flow and the discreteness of switching states, the problem of distribution network reconstruction can be regarded as a mixed integer nonlinear problem in mathematics. In the previous theoretical research, heuristic algorithms have been studied in depth [3, 4]. In addition, many global optimization algorithms are applied, such as genetic algorithm [5], artificial neural networks [6], and particle swarm optimization [7]. The calculations of these methods are usually more complicated, and they cannot guarantee the global optimal solution. In mathematical optimization problems, reconstruction models are usually expressed as linear programming problems [8], quadratic programming problems [9], etc. Although a lot of results have been obtained in the algorithm for solving the reconstruction problem, most of the existing algorithms are obtained under the assumption that the distribution network is a three-phase balanced system. In the actual system, due to the unbalanced load and network structure, the distribution network operates in a three-phase unbalanced state. In order to solve the above imbalance problem, the literature [10] proposed a real-time distribution network reconstruction algorithm for three-phase unbalanced systems.

2. Three-Phase Unbalanced System Model

In a three-phase unbalanced power distribution system, the relationship between voltage and current can be expressed in Figure 1.

$$\begin{bmatrix} \boldsymbol{V}_i^a \\ \boldsymbol{V}_i^b \\ \boldsymbol{V}_i^c \end{bmatrix} = \begin{bmatrix} \boldsymbol{V}_j^a \\ \boldsymbol{V}_j^b \\ \boldsymbol{V}_j^c \end{bmatrix} + \begin{bmatrix} z_{aa} & z_{ab} & z_{ac} \\ z_{ba} & z_{bb} & z_{bc} \\ z_{ca} & z_{cb} & z_{cc} \end{bmatrix} \cdot \begin{bmatrix} \boldsymbol{I}_i^a \\ \boldsymbol{I}_i^b \\ \boldsymbol{I}_i^c \end{bmatrix}. \tag{1}$$

The load model can be regarded as a negative sequence injection current in the system, and each load is assumed to be a constant power component, a linear combination of a constant impedance component, and a constant current component. Therefore, the three-phase injection current at the i bus can be expressed as

$$[\boldsymbol{I}_{L,i}]_{abc} = \alpha_{1,i} \cdot [\boldsymbol{I}_{\mathrm{P},i}]_{abc} + \alpha_{2,i} \cdot [\boldsymbol{I}_{\mathrm{Z},i}]_{abc} + \alpha_{3,i} \cdot [\boldsymbol{I}_{\mathrm{I},i}]_{abc}, \tag{2}$$

where $[\boldsymbol{I}_{P,i}]_{abc}$ is the constant power three-phase injection current component; $[\boldsymbol{I}_{\mathrm{Z},i}]_{abc}$ is the constant impedance three-phase injection current component; and $[\boldsymbol{I}_{\mathrm{I},i}]_{abc}$ is the three-phase injection current component of constant current.

The distributed power model at the i bus can be regarded as the positive sequence injection current as

$$[I_{\mathrm{DG},i}]_{abc} = \left[\frac{P^{\mathrm{a}}_{\mathrm{DG},i} - jQ^{\mathrm{a}}_{\mathrm{DG},i}}{V_{\mathrm{i}}^{a^*}} \quad \frac{P^{\mathrm{b}}_{\mathrm{DG},i} - jQ^{b}_{\mathrm{DG},i}}{V_{\mathrm{i}}^{b^*}} \quad \frac{P^{c}_{\mathrm{DG},i} - jQ^{c}_{\mathrm{DG},i}}{V_{\mathrm{i}}^{c^*}} \right]^T, \tag{3}$$

where $P^{\mathrm{a}}_{\mathrm{DG},i}$, $P^{\mathrm{b}}_{\mathrm{DG},i}$, and $P^{c}_{\mathrm{DG},i}$ are, respectively, the three-phase active power of the distributed power supply at bus i and $Q^{\mathrm{a}}_{\mathrm{DG},i}$, $Q^{b}_{\mathrm{DG},i}$, and $Q^{\mathrm{c}}_{\mathrm{DG},i}$ are, respectively, the three-phase reactive power of the distributed power supply at bus i.

When the distributed power supply operates in constant power operation mode, the equivalent injection current can be directly derived from Equation (3). When the distributed power supply operates in constant voltage mode, a double-loop calculation is required to obtain the equivalent injection current. The inner-loop calculation yields the amount of distributed power supply reactive power required to keep the bus voltage in a fixed range. The outer-loop calculation can obtain the injection current from the initial active power and the calculated reactive power. In a three-phase asymmetric system with two-phase or single-phase branches, the impedance of the missing phase in Equation (1) is zero, and the voltage and current of the missing phase can be excluded from the calculation results. Correspondingly, the current values of the missing phases in Equations (2) and (3) can be set to zero.

Distribution network reconfiguration is generally viewed as feeder reconfiguration optimization problem, and it is usually assumed that only three-phase feeder branches are available for reconfiguration. Any line is equipped with three-phase switching equipment, and the switch states can be defined as

$$S_j = \begin{cases} 1, \text{Switch j is closed, consistent with the initial direction} \\ 0, \text{Switch j is off} \\ -1, \text{Switch j is closed, opposite to the initial direction} \end{cases}, \tag{4}$$

where the direction of reference is determined by the direction of current.

The network connectivity of the distribution network is characterized by the node-branch correlation matrix. If the system is an ideal three-phase symmetric system, a single-phase equivalent circuit is usually adopted, as well as the node-branch correlation matrix $\boldsymbol{A}_{balanced}$ determined by the structure of system. The initial test state of the distribution network assumes that the switches are all closed. The initial node-branch correlation matrix A_0 of the network is symmetric, and A_0 is constant for a given network.

where a_{ij}^0 is the matrix elements of $\boldsymbol{A}_0$.

If the distribution network is a three-phase asymmetric system, the node-branch correlation matrix is three-phase and is obtained by multiplying $\boldsymbol{A}_{balanced}$ by a unit matrix of order 3:

$$A(i,j) = \begin{bmatrix} a_{ij} & 0 & 0 \\ 0 & a_{ij} & 0 \\ 0 & 0 & a_{ij} \end{bmatrix} = \begin{bmatrix} a_{ij}^0 & 0 & 0 \\ 0 & a_{ij}^0 & 0 \\ 0 & 0 & a_{ij}^0 \end{bmatrix} \cdot S_{\mathrm{j}}. \tag{5}$$

And

$$\boldsymbol{I}_{bus} = \left(\boldsymbol{A} \cdot \boldsymbol{Y}_{branch} \cdot \boldsymbol{A}^T\right) \cdot \boldsymbol{V}_{\mathrm{bus}} = \boldsymbol{Y}_{\mathrm{bus}} \cdot \boldsymbol{V}_{\mathrm{bus}}. \tag{6}$$

Among them,

Where $\boldsymbol{I}_{bus}$ is the node injection current vector; $\boldsymbol{V}_{\mathrm{bus}}$ is the bus voltage vector; $\boldsymbol{Y}_{\mathrm{bus}}$ is the nodal conductivity matrix; and $\boldsymbol{Y}_{branch}$ is the tributary conductivity matrix.

$$\boldsymbol{I}_{bus} = \boldsymbol{I}_{DG} - \boldsymbol{I}_L, \tag{7}$$

where $\boldsymbol{I}_{DG}$ is the distributed power injection current vector and $\boldsymbol{I}_L$ is the load injection current vector.

According to Equations (6) and (7), the tidal current calculation can be expressed as follows: the initial voltage $\boldsymbol{V}_{\mathrm{bus}}^{k-1}$ is given, the nodal injection current $\boldsymbol{I}_{\mathrm{bus}}^{k}$ can be solved by Equation (7), and $\boldsymbol{V}_{\mathrm{bus}}^{k}$ is calculated by substituting $\boldsymbol{I}_{\mathrm{bus}}^{k}$ into Equation (6). When the termination condition is satisfied, the iterative termination calculation in turn leads to the system nodal voltage and branch current values.

Equation (7) can in turn be expressed as

$$\boldsymbol{I}_{\mathrm{bus},i}^{l} = \sum_{k=1}^{n} \sum_{p=a}^{c} t_{ik}^{lp} \cdot v_k^p, l = phase\ a, b, c. \tag{8}$$

In the formula, $t_{ik}^{lp} = \sum_{j=1}^{m} (a_{ij}^0 a_{kj}^0 y_j^{lp}) \cdot S_j^2 \triangleq g_{ik}^{lp} + j b_{ik}^{lp}$.

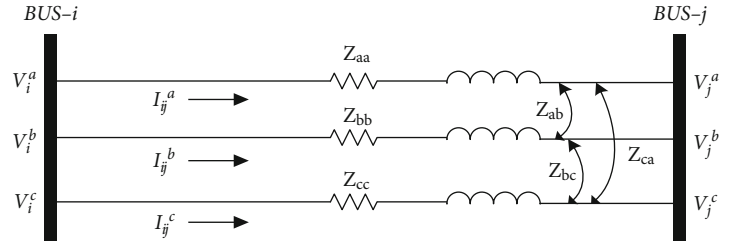

Figure 1: Improved hierarchical decentralized reconstruction method process.

$[y_j^{aa}, y_j^{ab}, y_j^{ac}; y_j^{ba}, y_j^{bb}, y_j^{bc}; y_j^{ca}, y_j^{cb}, y_j^{cc}]$ is the conjugate inverse matrix of the jth branch impedance matrix. Due to the existence of the relation of Equation (9):

$$\boldsymbol{I}_{bus,i}^{l} = \frac{P_{inject,i}^{l} - j \cdot Q_{inject,i}^{l}}{e_i^l - j \cdot f_i^l}, \tag{9}$$

where $P_{inject,i}^{l}, Q_{inject,i}^{l}$ is the active and reactive injected power at node i of a phase.

The tide calculation formula can be obtained as

$$\begin{cases} P_{inject,i}^{l} = \sum_{k=1}^{n} \sum_{p=a}^{c} \left\{ e_i^l \left(g_{ik}^{lp} \cdot e_k^p - b_{ik}^{lp} \cdot f_k^p \right) + f_i^l \left(g_{ik}^{lp} \cdot f_k^p - b_{ik}^{lp} \cdot e_k^p \right) \right\} \\ Q_{inject,i}^{l} = \sum_{k=1}^{n} \sum_{p=a}^{c} \left\{ f_i^l \left(g_{ik}^{lp} \cdot e_k^p - b_{ik}^{lp} \cdot f_k^p \right) - e_i^l \left(g_{ik}^{lp} \cdot f_k^p + b_{ik}^{lp} \cdot e_k^p \right) \right\} \end{cases}. \tag{10}$$

In power loss, in an unbalanced system, the result of power loss in the branch is the input power minus the output power of each phase, so we can obtain

$$A^T \cdot V_{bus} = Z_{branch} \cdot I_{branch}. \tag{11}$$

Substituting Equations (1) and (5) into Equation (11), the total active power loss can be obtained as

$$\begin{aligned} P_{loss} &= \mathrm{Re} \left\{ \sum_{j=1}^{n} \left[\sum_{k=a}^{c} \left(V_j^{k^*} \cdot \sum_{i=1}^{n} \left(\sum_{p=a}^{c} V_i^p \cdot \left(\sum_{i=1}^{m} a_{il}^0 a_{jl}^0 y_l^{pk} \cdot s_l^2 \right) \right) \right) \right] \right\} \\ &= \sum_{j=1}^{n} \sum_{k=a}^{c} \sum_{i=1}^{n} \sum_{p=a}^{c} \left\{ e_j^k \cdot \left(e_i^p \cdot g_{ij}^{pk} + f_i^p \cdot b_{ij}^{pk} \right) \right. \\ &\quad \left. + f_j^k \cdot \left(f_i^p \cdot g_{ij}^{pk} - e_i^p \cdot b_{ij}^{pk} \right) \right\}. \end{aligned} \tag{12}$$

The magnitude of the voltage depends on the network topology of the system and the output power of the distributed power supply, which are the two variables that satisfy the power loss minimization objective function. In addition to this, the operational constraints have to be satisfied:

2.1. Voltage Amplitude Constraint.

$$V_{imin} \le |V_i^a|, \left| V_i^b \right|, |V_i^c| \le V_{imax}, i = 1, 2, \cdots, N, \tag{13}$$

where V_{imin} and V_{imax} are the allowable minimum and maximum voltages of node i, respectively, so that V_{imin} is 0.95 times the rated voltage and V_{imax} is 1.05 times the rated voltage.

2.2. Node Voltage Imbalance Constraint. Voltage imbalance can be obtained by dividing the maximum voltage deviation by the average voltage amplitude of the three phases. According to ANSI C84.1-2011, the voltage imbalance should be controlled within 3%. Therefore, the voltage imbalance constraint can be expressed as

$$\left| \frac{\left| V_i^p \right| - avg_i}{avg_i} \right| \le 3\%, \text{ where, } avg_i = \sum_{p=a}^{c} \left| V_i^p \right| / 3, p = a, b, c. \tag{14}$$

2.3. Current Constraint.

$$\left| I_{branch,i}^{p} \right| \le I_{\mathrm{i,max}}, \tag{15}$$

where $I_{\mathrm{i,max}}$ is the load capacity of branch i.

2.4. Network Radiation-like Structural Constraints. Network constraints and balanced systems are systems where the distribution network remains radial in operation. The network of unbalanced system is radial network.

$$\sum_{k=1}^{M} |S_k| = N - d, \tag{16}$$

where d is the number of all balancing nodes.

All loads are supplied with uninterrupted power supply, rank $(A) = N - d$. At least one branch in each loop is open and closed.

$$\sum_{i=1}^{M_k} |S_i| \le M_k - 1, \tag{17}$$

where M_k is the number of branches of loop k.

3. Optimal Planning of DG Units

According to the literature [11], the results show that the factors affecting the system power loss include the network topology, the location, and the output power of DG units. The sensitivity of the injected active power loss per bus can

be used to determine the optimal bus location for installing the distributed power units.

3.1. DG Optimal Location of the Unit. Since the integration of distributed power units increases the bus active power injection, the best installation location is the bus with the maximum negative active loss sensitivity [12] so that power loss will be effectively controlled. Define the power loss Equation (13) as

$$P_{loss} = g(e, f). \tag{18}$$

The relationship between the voltage vector and the injected power is determined from Equation (10):

$$h\left(e, f, P_{inject}, Q_{inject}\right) = 0. \tag{19}$$

If the small variation $[\Delta P, \Delta Q]^T$ is added to the injected power vector $[P_{inject}, Q_{inject}]^T$, the variation of the voltage vector can be solved by Equation (15):

$$\left[\frac{\partial h}{\partial e} \quad \frac{\partial h}{\partial f}\right]\Bigg|_{x^0} \cdot \begin{bmatrix} \triangle e \\ \Delta f \end{bmatrix} + \left[\frac{\partial h}{\partial P_{inject}} \quad \frac{\partial h}{\partial Q_{inject}}\right]\Bigg|_{x^0} \cdot \begin{bmatrix} \triangle P_{inject} \\ \Delta Q_{inject} \end{bmatrix} = 0. \tag{20}$$

Therefore, the amount of change in power loss caused is shown in Equation (21):

$$\triangle P_{loss} = \left[\frac{\partial g}{\partial e} \quad \frac{\partial g}{\partial f}\right] \cdot \begin{bmatrix} \triangle e \\ \triangle f \end{bmatrix}. \tag{21}$$

Then, the power loss sensitivity vector for each bus injected power is

$$M_s = -\left[\frac{\partial g}{\partial e} \quad \frac{\partial g}{\partial f}\right] \cdot \left(\left[\frac{\partial \mathrm{h}}{\partial e} \quad \frac{\partial h}{\partial f}\right]\right)^{-1} \cdot \left(\left[\frac{\partial \mathrm{h}}{\partial P_{inject}} \quad \frac{\partial h}{\partial Q_{inject}}\right]\right). \tag{22}$$

The sensitivity vector is solved to obtain the power loss sensitivity of the injected power of each phase of the busbar. It is considered that only the busbars of three phases can be used as candidate installation locations; then, the sensitivity of each busbar is taken as the average of the sensitivity of the three phases.

3.2. Optimal Capacity of DG Units. The optimal capacity of the DG unit minimizes the power loss in the unit in an unbalanced system that keeps the initial topology constant [13].This case can be considered an undesirable situation in reconfiguration studies, due to the fact that the DG unit needs to emit the maximum power and there is no other way to additionally support the reconfiguration. The influence of the optimal capacity of distributed generation is as follows: The optimal capacity of the DG unit is solved so that the power loss of the unit can be minimized in the unbalanced distribution system with initial topology. This scenario can be considered the worst case in reconfiguration research. Because DG units must generate maximum power into the grid, there is no need for additional support to reconfigure the network. After installing the DG unit and arranging its optimum capacity, the power loss of the system has been minimized under the initial system structure. Power optimization may be further reduced if the system is reconfigured. In addition, due to time-varying load, power losses are not always minimized in the case of a fixed network structure and constant DG output power. It is therefore necessary to reconfigure the network and reduce the DG power from time to time [14].

The optimization problem of the optimal capacity can be expressed as

$$\min_u J = P_{loss}(x, u) \quad s.t. \begin{cases} f(x, u) = 0 \\ g(x, u) \le 0 \end{cases}. \tag{23}$$

In the formula: $x = [e, f]^T$, $u = [P_{DG}, Q_{DG}]^T$, $f(x, u)$ is the tidal equation, and $\mathrm{g}(x, u)$ denotes the inequality constraint of Equations (13)–(17). The inequality constraint can be eliminated by introducing a penalty function in the objective function, and Equation (23) can be expressed as

$$\min J_{uc} = P_{loss}(x, u) + \sum_{i=1}^{H} \phi_i(\beta_i, g_i), \tag{24}$$

where H is the total number of inequality constraints.

Each penalty function is defined as

$$\phi_i(\beta_i, g_i) = \begin{cases} 0, & \text{if } g_i \le 0 \\ \beta_i, g_i^2, & \text{if } g_i > 0 \end{cases} \text{and} \beta_i > 0. \tag{25}$$

The tide calculation is first performed to obtain the power loss such that the equation constraint $f(x, u)$ is always satisfied. Thus, Equation (25) becomes an unconstrained optimization problem, and its minimum can be solved using the proposed Newtonian numerical method; the differentiation of Equation (26) is

$$\mathrm{F(u)} = \frac{dJ_{uc}(\mathrm{x}, \mathrm{u})}{du} = \frac{dP_{loss}(\mathrm{x}, \mathrm{u})}{du} + \frac{d}{d_u}\sum_{i=1}^{H} \phi_i(\beta_i, g_i). \tag{26}$$

In the formula, the first part of the rightmost side of the equation is the same as the sensitivity matrix, whose matrix columns represent the bus of the selected DG unit. The second term can be obtained by differentiating the inequality constraint. Since the second-order partial derivative

equation of the multivariate function is difficult to solve, the minimum of Equation (26) can be solved by the cutline method with positive definite cutline update.

$$\begin{aligned} u_{k+1} &= u_k - H_k^{-1} \cdot F(u_k), \\ s_k &= u_{k+1} - u_k, y_k = F(u_{k+1}) - F(u_k), \\ H_{k+1} &= H_k + \frac{y_k \cdot y_k^T}{y_k^T \cdot s_k} - \frac{H_k \cdot s_k \cdot s_k^T \cdot H_k}{s_k^T \cdot H \cdot s_k}. \end{aligned} \tag{27}$$

4. Network Reconfiguration of DG Units

After installing the DG units and adjusting their optimal capacity as described above, the system network losses are at their lowest level under the initial network topology. A network reconfiguration is required to bring the power loss down further. In addition, due to the fluctuating load, the power loss is not always minimal with a constant topology and a constant DG [15]. Therefore, in each operational interim period, the objective function is defined as minimizing the total cost of power loss and limiting the output power of the DG set. The problem is described as

$$\begin{aligned} \min J = & \left(\begin{array}{c} w_1 \cdot P_{loss}(S, PQ_{DGact}) + w_2 \sum_{i=1}^{k} \sum_{p=a}^{c} \left(P^p_{DG\ \max,i} - \left(P^p_{DGact,i} \right)_t \right) \\ + w_3 \sum_{i=1}^{k} \sum_{p=a}^{c} \left(Q^p_{DG\ \max,i} - \left(Q^p_{DGact,i} \right)_t \right) \end{array} \right) \cdot \triangle T \\ & s.t. (13) \sim (17), \text{and} \\ & \left(P^p_{DGact,i} \right)_t \le P^p_{DG\ \max,i}, \left(Q^p_{DGact,i} \right)_t \le Q^p_{DG\ \max,i}, \\ & i = 1 \sim k, p = a, b, c, t = 1 \sim 24. \end{aligned} \tag{28}$$

where T is the number of contact switches; K is the number of DG units; ΔT is the scheduled running time in hours; $P^p_{DG\ \max,i}$, $Q^p_{DG\ \max,i}$ is the optimal capacity of the i-th DG unit; and $(P^p_{DGact,i})_t$, $(Q^p_{DGact,i})_t$ is the p ($p = a,b,c$) phase active and reactive power output by the ith DG unit at time t of operation.

Since the optimization problem of distribution network reconfiguration considering three-phase imbalance is a second-order partial derivative equation solution problem for multivariate functions, therefore, an improved hierarchical decentralized reconstruction method is adopted to simultaneously reconstruct the optimal topology of the distribution network considering the three-phase imbalance and regulate the DG output power. The flowchart is shown in Figure 2:

4.1. Network Decomposition. Loops are more easily identified by the difference between closed contact switches and segmented opens for differentiation. In order to easily distinguish between tightly connected partitions and loosely connected partitions [16], the connectivity between the subdivisions is defined as follows:

$$\mathrm{D(A, B)} = \frac{\text{Number of public bus}}{\min\left(\text{Total number of busbars in zone A, Total number of busbars in zone B}\right)}, \tag{29}$$

If $\mathrm{D(A, B)} = 0$, it means that partition A and partition B are independent of each other. Given a threshold δ, if, means that partition A and partition B are tightly connected and if $\mathrm{D(A, B)} \le \delta$ means that partition A and partition B are loosely connected. However, if the threshold δ is set too small, the loosely connected partitions are not easily identified; if the threshold δ is set too large, the loosely connected partitions are easily expanded. Therefore, it is generally reasonable to choose a threshold δ of 0.2.

The specific steps of network decomposition are as follows.

The set of cut vertices of a connected graph $\mathrm{G} = (\mathrm{V}, \mathrm{E})$ is a vertex set $U \subseteq V$ satisfying the following conditions: G-U is not connected; G-K is connected, $K \subset U$; every vertex u of U in a connected graph G is connected to at least one vertex in every partition of G-U. A set of cut vertices is a cut vertex if there is only one vertex in the set.

(a) The value of the modified adjacency matrix **C** is acquired. Let $\boldsymbol{m}$ be the number of loops, and the modified adjacency matrix is an m-dimensional square matrix

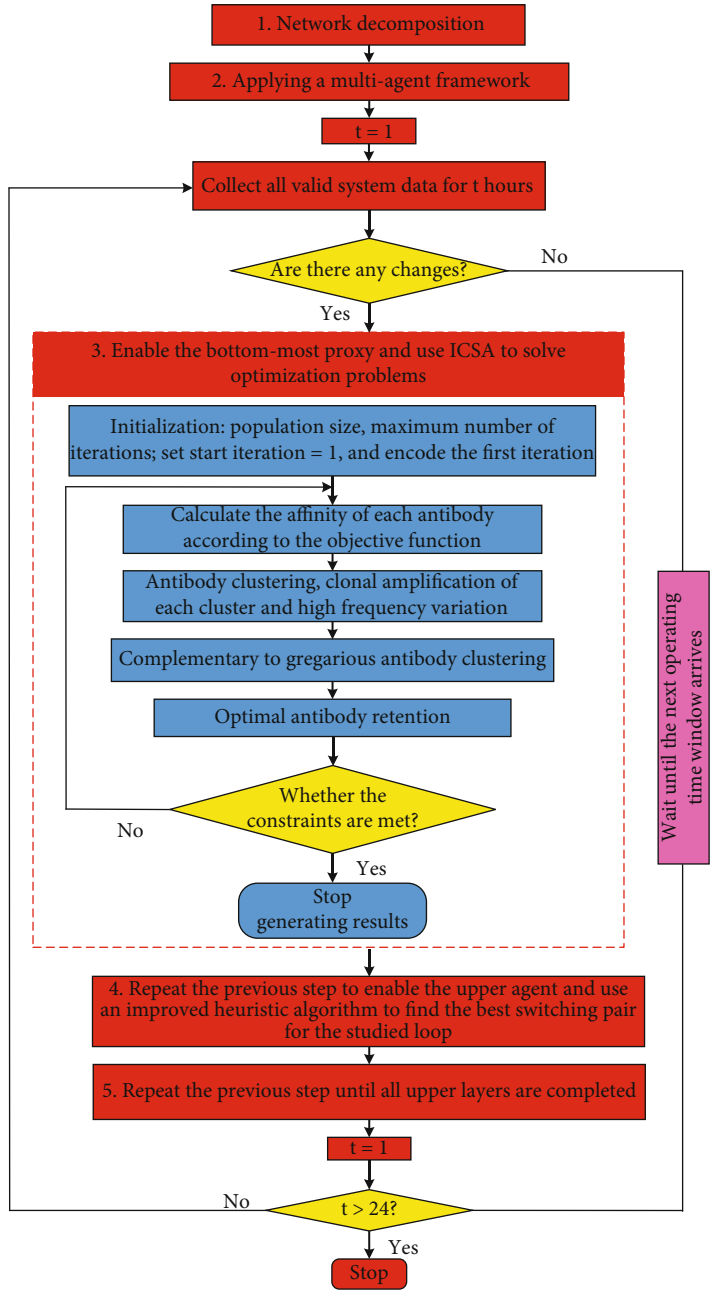

Figure 2: Improved hierarchical decentralized reconstruction method process.

(b) If there are no partitions with a common bus other than the source node, these partitions are defined as basic partitions. Two basic partitions are connected to each other by a contact switch. The following steps are used for all basic partitions

(c) Draw the connectivity graph. In the connectivity graph $G = (V, E)$, the set of vertices $V = \{v_1, \cdots, v_n\}$ represents **1 – n** loops. The edge **E** connecting the vertices indicates that the loops are coupled to each other. The vertices are drawn in the studied region to represent the loops, and if the element C (i, j) is not zero, an edge is added between the vertices v_i and v_j. If loop **i** is loosely connected to loop **j**, then it is noted as L; otherwise, it is noted as **T**

(d) Be sure to check graph G for connectivity. If not, the isolated vertices need to be found, denoted as *S*. The corresponding loop of the isolated vertex contains the first member of the decomposition system

(e) Determine the cut vertex set of G-s. The search starts from the parent node, and the cut vertex set node is found from the child nodes associated with the parent node. If the cut vertex set is empty, the search moves to the vertex associated with the child node.

Table 1: The structure of chromosomes.

OS_1-OS_T	P_{1a}	Q_{1a}	P_{1b}	Q_{1b}	P_{1c}	Q_{1c}	…	P_{Ka}	Q_{Ka}	P_{Kb}	Q_{Kb}	P_{Kc}	Q_{Kc}

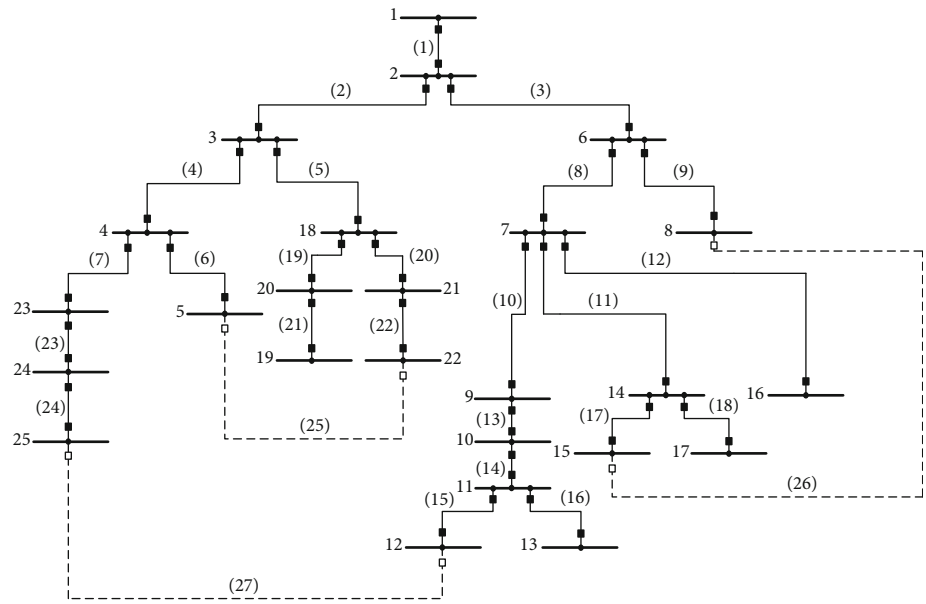

Figure 3: The single-line diagram of the 25-bus unbalanced distribution system.

Table 2: Optimal capacity of DG units for three scenarios.

Scenario	Installation site	Optimal capacity region					
		Phase A		Phase B		Phase C	
		Active (kw)	Reactive (KVar)	Active (kw)	Reactive (KVar)	Active (kw)	Reactive (KVar)
1	12	356.2	362.4	420.5	368.3	258.4	189.3
	Three − phase minimum voltage = [0.966,0.965, 0.956 pu] Power loss =224.2 kW; maximum voltage imbalance =2.236%						
2	12	220.5	158.2	210.8	172.4	214.8	165.9
	13	214.8	156.7	208.6	163.2	212.4	162.5
	Three − phase minimum voltage = [0.964,0.965,0.963 pu] Power loss = 192.8 kW; maximum voltage imbalance = 0.562%						
3	12	136.5	103.6	145.2	106.3	148.6	108.2
	13	135.2	104.5	143.8	102.6	146.3	105.8
	11	152.6	116.2	160.5	116.5	162.6	115.6
	Three − phase minimum voltage = [0.963, 0.965, 0.965 pu] Power loss = 186.2 kW; maximum voltage imbalance = 0.358%						

If the cut vertex set is found, the cut vertex set is removed, and the associated edges define two separate components. Continue searching for each component's cut vertex set until there are no more cut vertex sets. Each component represents the decomposed system, and the contact switch corresponding to the cut vertex set represents the decomposed system by the links between them

(f) In case two vertices are connected to the edge marked with ***L***, their corresponding rings are decomposed into two subsystems. If two loosely connected vertices are tightly connected to another vertex, the contact switch corresponding to that vertex is an interconnection between the two subsystems. In the lowest level subsystem forming the basis of the entire system, which includes all busbars, loads, and DG units. Each higher-level subsystem consists of several subsystems representing the entire system

4.2. Applying a Multi-Agent Framework. Intelligent agents consisting of data units, computation units, and decision units need to be assigned to each subsystem for solving subproblems of the assigned subsystem and exchanging

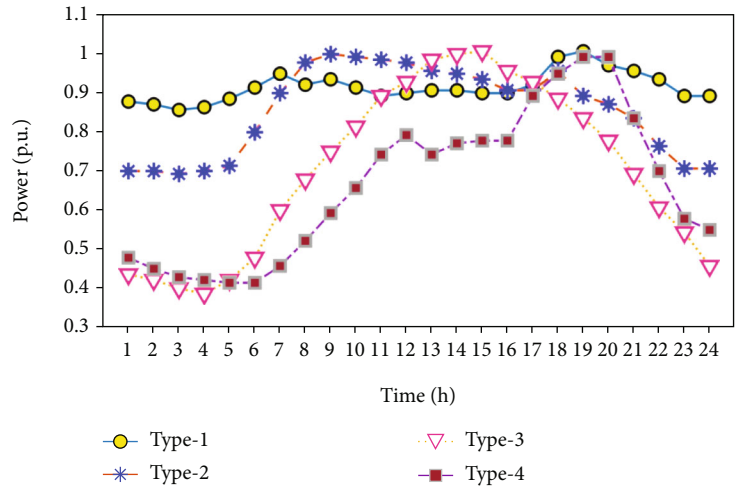

Figure 4: Four groups of load shapes.

Table 3: The optimal switching plan.

Time window	Open switches	Time window	Open switches	Time window	Open switches
0-1 h	15, 17, 22	9-10 h	15, 17, 22	17-18 h	15, 17, 22
2-3 h	15, 17, 22	10-11 h	17, 24, 6	18-19 h	15, 17, 22
3-4 h	15, 17, 22	11-12 h	15, 17, 22	19-20 h	15, 17, 22
4-5 h	15, 17, 22	12-13 h	17, 24, 22	20-21 h	15, 17, 22
5-6 h	15, 17, 22	13-14 h	15, 17, 22	21-22 h	15, 17, 22
6-7 h	15, 17, 22	14-15 h	17, 24, 22	22-23 h	17, 24, 6
7-8 h	17, 24, 6	15-16 h	17, 24, 6	23-24 h	15, 17, 22
8-9 h	15, 17, 22	16-17 h	15, 17, 22		

information with other agents. Since DG units may exist in the bottom most subsystem, the bottom most agent should be able to decide the optimal topology and the best DG output of the local system. The optimization problem for each bottom most agent layer is represented by Equation (29), and all variables are refined into local variables for its subsystem. Based on the decision plan solved by the lower layer agents, all upper layer agents ought to judge whether the common contact switch is off or not; hence, each embedded optimization problem is a pure reconstruction problem with the equation:

$$\min J = P_{loss}\left(S_{subsystem}, S_{solved}, PQ_{solved}\right) \cdot \Delta T. \quad (30)$$

In the formula, $S_{subsystem}$ is the set of switching states to be solved; S_{solved} is the set of switching states already solved by the lower layer agent; and PQ_{solved} is the actual output power of the DG unit of the lowest layer agent.

4.3. Optimization Problems for the Lowest-Level Agent. The optimization problem defined in the bottom-most agent is a mixed-integer nonlinear problem, switch states, and DG outputs selected as decision variables. The immune clonal selection differential evolution algorithm is utilized to solve the mixed integer nonlinear optimization problem defined in the bottom-most surrogate [17]. Due to the presence of DG in the decision variables, some changes have been made to the algorithm. A considerable number of antibody groups are generated from genes that determine antibodies, which are used as the initial antibody groups for the differential evolution algorithm of immune clone selection as shown in Table 1.

The definition of antibody genes is shown in Table 1, and there are T +6 K genes in total: The first T gene represents the open switch; the following 6 K genes are the active and reactive power generated by the Kth DG unit. Antibody clustering, clonal expansion, and high-frequency mutation randomly select a gene i from T +6 K genes; get high-frequency mutation to randomly change a selected gene, and introduce new information into offspring. The selected gene could represent the open switch. Before evaluating fitness values for new antibody clusters, all duplicate antibodies were removed, and the viability of each progeny was assessed by sequentially examining system structural constraints and voltage/current constraints. Then, the fitness values of all viable progeny are calculated, and the best antibody is selected. Finally, the optimal topology of all the lowest-level subsystems and the optimal output of the DG unit are solved. The agents coordinate when necessary, passing the final result to the upper agent to activate the computation. The network reconstruction problem is solved separately and decomposed into different subproblems. A hierarchical structure is used to assign independent agents to subproblems to realize parallel computing. Each agent is made up of three units. The data unit collects local information and communicates with other agents. The computational unit realizes the improved heuristic algorithm to solve the local reconstruction problem, and the decision unit completes the coordination control. The calculation result of the lower agent is transmitted to the data unit of the upper agent. The final optimal configuration is completed by the collaboration between multiple agents.

4.4. Upper Layer Proxy Startup Issues. A heuristic algorithm based on branch-and-switch and single-loop optimization is

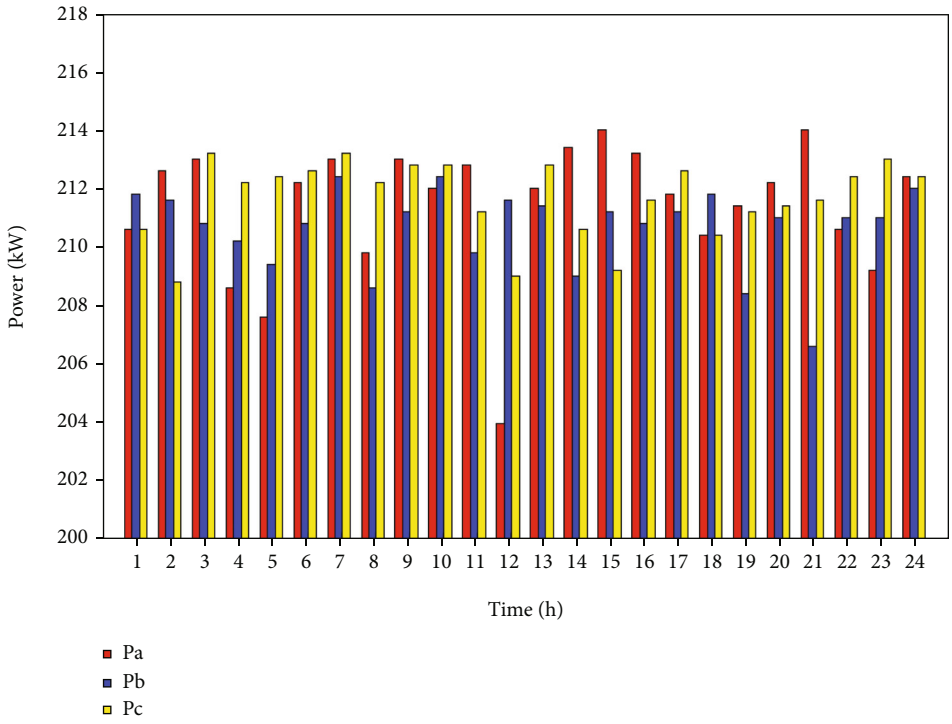

Figure 5: Active output power of the DG unit at Bus-12.

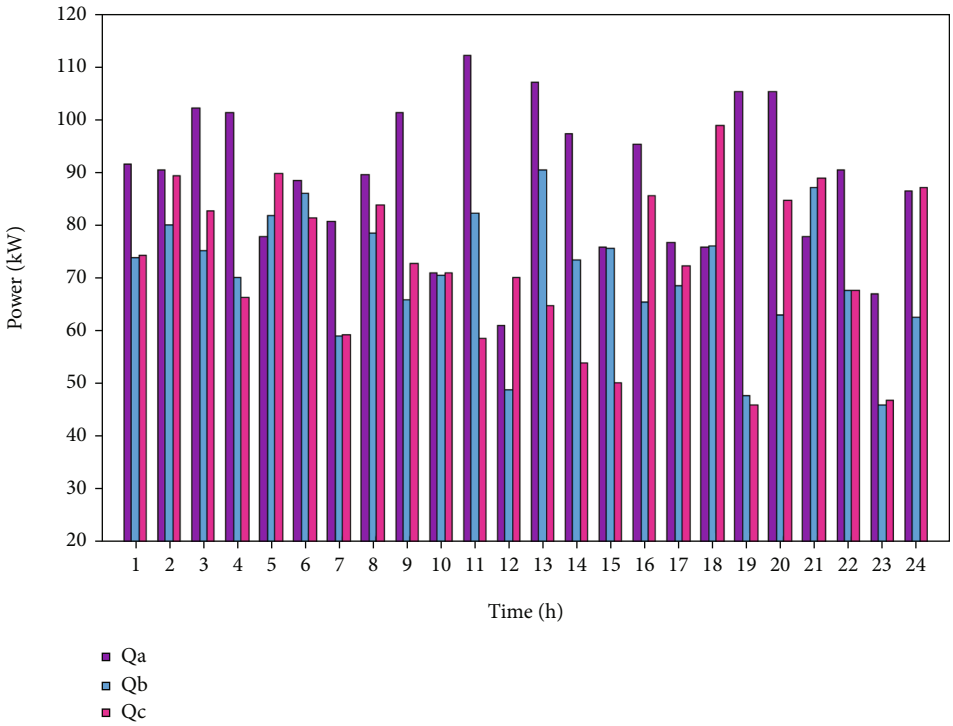

Figure 6: Reactive output power of the DG unit at Bus-12.

adopted to solve the optimal topology of the upper-level subsystem with the known switching states and DG outputs solved in the lower-level agent. Then, the optimal topology of the whole distribution system and the actual output power of all DG units are obtained based on real-time data within the current time window. At this point, the distribution reconfiguration is completed, and the DG units are in the optimal operating state, which will remain unchanged until the next time window when the scheduling plan for the next cycle is re-evaluated.

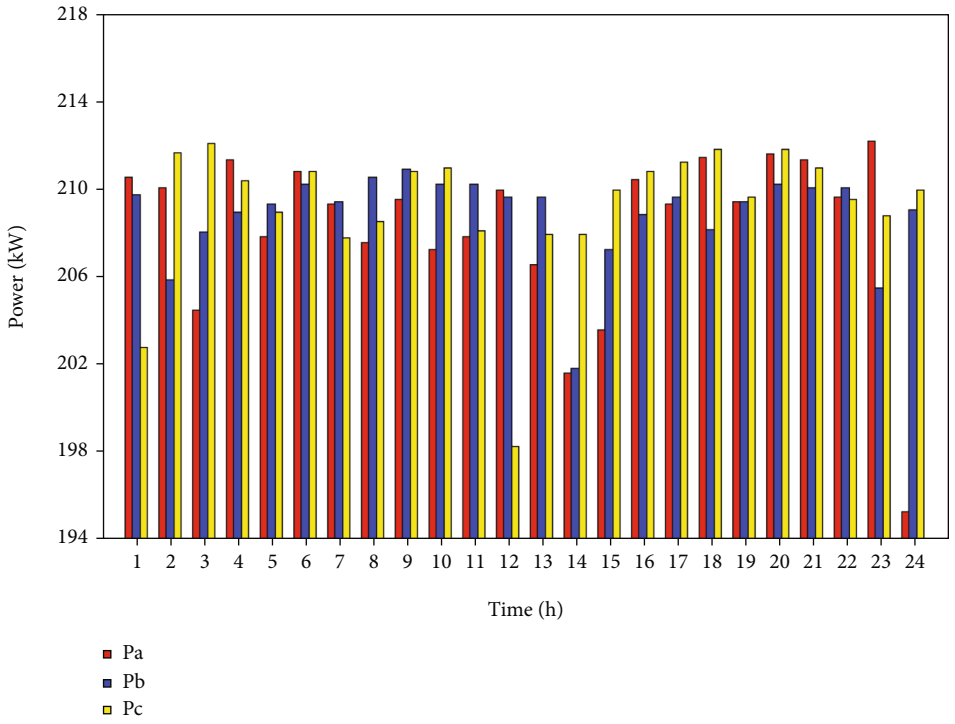

Figure 7: Active output power of the DG unit at Bus-13.

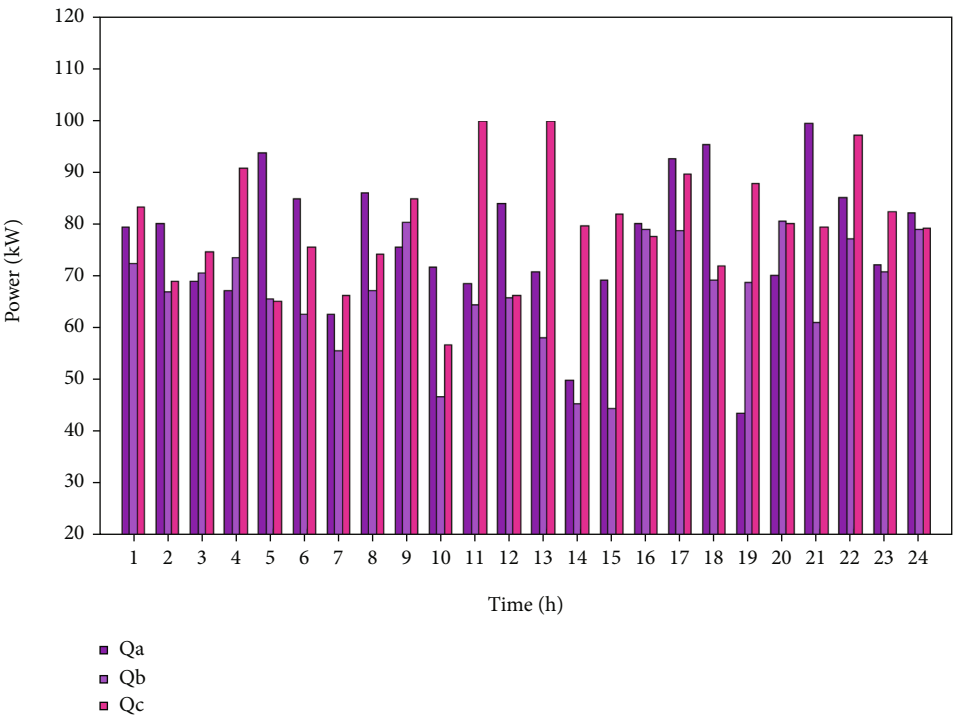

Figure 8: Reactive output power of the DG unit at Bus-13.

5. Algorithm Simulation

The simulated system of the distribution network used in this paper is a 25-node unbalanced system [18] with unbalanced line impedance and load distribution as shown in Figure 3.The system has three tie switches, 25, 26 and 27, respectively. Under normal operation, the interconnection switch is open. The initial three-phase power loss is 450.38 kW, and the minimum voltage is 0.93 pu.

In this paper, the load is modeled with a Gaussian mixture model (GMM) proposed in the literature [19], and the probability density function of the GMM is determined by

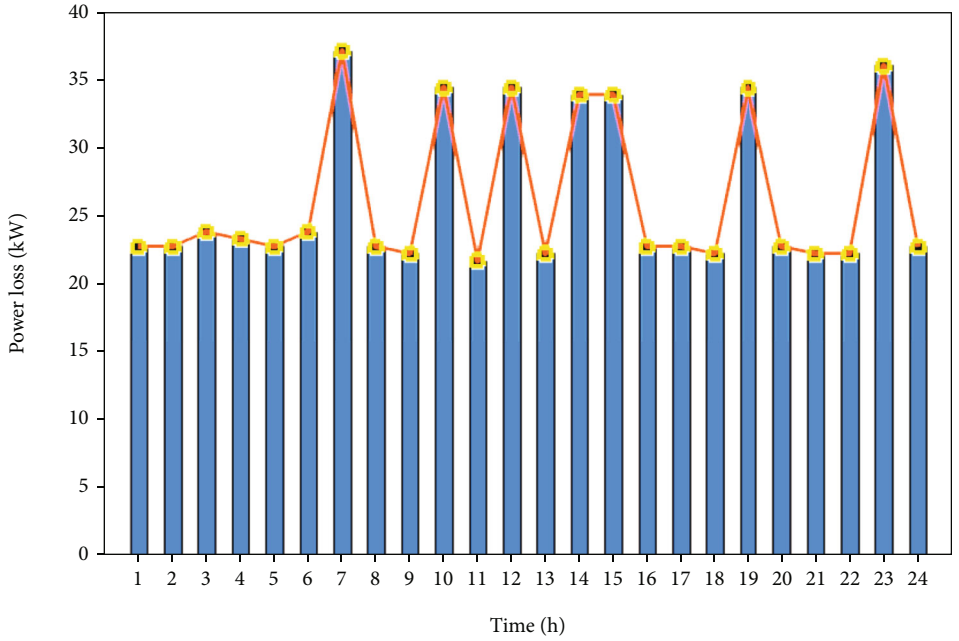

Figure 9: System power loss within 24 hours.

the following equation:

$$f(z) = \sum_{i=1}^{AM} w_i N(\mu_i, \sigma_i). \tag{31}$$

In the formula, AM is the number of components in the mixture model, μ_i is the mean, σ_i is the standard deviation, and w_i is the weight.

A GMM is applied randomly to each load. So the actual load power is obtained by multiplying the initial value by the unit value generated by the GMM. Monte Carlo simulations were performed, and the results showed that buses 12, 13, 11, 10, 15, 17, 14, and 9 were consistently the most sensitive 8 buses out of all 200 samples. To demonstrate the effectiveness of power loss reduction by installing DG units on the most sensitive buses, a system with 8 DG units on each of the 8 buses mentioned above is installed. After the DG unit locations are determined, the optimal capacity of each DG unit can be solved. Three scenarios are tested with a capacity limit of 500 kW/500kVA per phase DG, and the proposed Newton algorithm converges quickly after 5 to 20 iterations for different scenarios. The optimal capacities of DG units for the three scenarios are given in Table 2:

(1) Install a DG unit at the most sensitive bus 12

(2) Install a DG unit at bus 12 and 13, respectively

(3) Install a DG unit at bus 12, 13 and 11, respectively

Tests were conducted on several scenarios, and the results are shown in Table 2.

The results show that the optimal capacity of the DG units can be successfully solved while satisfying all system constraints. The integration of DG units helps to reduce power losses, increase voltage, and reduce voltage imbalance. The results of scenarios 2 and 3 are significantly better than those of scenario 1, indicating that the integration of multiple decentralized small-capacity DG units is more helpful than the integration of one large-capacity DG unit. Comparing the results from scenarios 2 and 3, the integration of two DG units already reduces the losses significantly, and adding a third DG unit does not help much. Therefore, the final decision was made to install two DG units at buses 12 and 13.

The operation period is set to 1 h, and the starting point is 0 : 00. 4 sets of 24-hour load curves are input to the system as real-time load data as shown in Figure 4.

The optimal switching scheme is shown in Table 3:

The following graphs give the actual output of the DG unit for 24 hours as shown in Figures 5–9.

6. Conclusion

A hierarchical decentralized distribution network reconfiguration method is proposed based on the characteristics of three-phase unbalanced distribution network reconfiguration. Network decomposition and multi-agent architecture are used to obtain the optimal reconfiguration scheme. In addition, although multiple agents are set up, the necessary information exchange between them is only the switching status of their subsystems, so the information transfer is low. The network reconfiguration algorithm has been applied in an unbalanced 25 node system. The simulation results show that the algorithm can reduce the power loss and the imbalance degree of the system.

Data Availability

Data sharing is not applicable to this article as no new data were created or analyzed in this study.

Conflicts of Interest

The author states that this article has no conflict of interest.

Acknowledgments

This work was supported by the Scientific research fund project of Education Department of Liaoning Province of China No. JL-2020.

References

[1] M. E. Baran and F. F. Wu, "Network reconfiguration in distribution systems for loss reduction and load balancing," *IEEE Power Engineering Review*, vol. 4, no. 2, pp. 101-102, 1989.

[2] M. W. Siti, D. V. Nicolae, A. A. Jimoh, and A. Ukil, "Reconfiguration and load balancing in the Lv and Mv distribution networks for optimal performance," *IEEE Transactions on Power Delivery*, vol. 22, no. 4, pp. 2534–2540, 2007.

[3] G. K. V. Raju and P. R. Bijwe, "An efficient algorithm for minimum loss reconfiguration of distribution system based on sensitivity and heuristics," *IEEE Transactions on Power Apparatus and Systems*, vol. 23, no. 3, pp. 1280–1287, 2008.

[4] F. V. Gomes, S. Carneiro, J. L. R. Pereira, M. P. Vinagre, P. A. N. Garcia, and L. R. D. Araujo, "A new distribution system reconfiguration approach using optimum power flow and sensitivity analysis for loss reduction," *IEEE Transactions on Power Apparatus and Systems*, vol. 21, no. 4, pp. 1616–1623, 2006.

[5] N. Gupta, A. Swarnkar, and K. R. Niazi, "Distribution network reconfiguration for power quality and reliability improvement using genetic algorithms," *International Journal of Electrical Power & Energy Systems*, vol. 54, pp. 664–671, 2014.

[6] M. A. Kashem, G. B. Jasmon, A. Mohamed, and M. Moghavvemi, "Artificial neural network approach to network reconfiguration for loss minimization in distribution networks," *International Journal of Electrical Power & Energy Systems*, vol. 20, no. 4, pp. 247–258, 1998.

[7] W. C. Wu and M. S. Tsai, "Application of enhanced integer coded particle swarm optimization for distribution system feeder reconfiguration," *IEEE Transactions on Power Apparatus and Systems*, vol. 26, no. 3, pp. 1591–1599, 2011.

[8] J. A. Taylor and F. S. Hover, "Convex models of distribution system reconfiguration," *IEEE Transactions on Power Apparatus and Systems*, vol. 27, no. 3, pp. 1407–1413, 2012.

[9] M. Lavorato, J. F. Franco, M. J. Rider, and R. Romero, "Imposing radiality constraints in distribution system optimization problems," *IEEE Transactions on Power Apparatus and Systems*, vol. 27, no. 1, pp. 172–180, 2012.

[10] J. C. Wang, H. D. Chiang, and G. R. Darling, "An efficient algorithm for real-time network reconfiguration in large scale unbalanced distribution systems," *IEEE Transactions on Power Apparatus and Systems*, vol. 11, no. 1, pp. 511–517, 1996.

[11] S. K. Goswami and S. K. Basu, "A new algorithm for the reconfiguration of distribution feeders for loss minimization," *IEEE Transactions on Power Delivery*, vol. 7, no. 3, pp. 1484–1491, 1992.

[12] B. Currie, C. Abbey, G. Ault et al., "Flexibility iskey in New York: new tools and operational solutions for managing distributed energy resources," *IEEE Power and Energy Magazine*, vol. 15, pp. 20–29, 2017.

[13] H. F. Zhai, M. Yang, B. Chen, and N. Kang, "Dynamic reconfiguration of three-phase unbalanced distribution networks considering unbalanced operation constraint of distributed generation," *International Journal of Electrical Power & Energy Systems*, vol. 99, pp. 1–10, 2018.

[14] Y. Haichuan, Z. Bide, and W. Haiying, "Distribution network dynamic reconfiguration method for improving distribution network's ability of accepting DG," *Power System Technology*, vol. 40, no. 5, pp. 1431–1436, 2016.

[15] X. Bai, Y. Mavrocostanti, D. Strickland et al., "Corrigendum: distribution network reconfiguration validation with uncertain loads - network configuration determination and application," *IET Generation, Transmission & Distribution*, vol. 11, no. 2, pp. 582–582, 2017.

[16] H. M. Ahmed, A. B. Eltantawy, and M. M. Salama, "A planning approach for the network configuration of AC-DC hybrid distribution systems," *IEEE Transactions on Smart Grid*, vol. 9, no. 3, pp. 2203–2213, 2018.

[17] X. Wang, Y. Ji, J. Wang, Y. Gao, and L. Qi, "Research on distribution network reconfiguration based on microgrid," *Journal of Ambient Intelligence and Humanized Computing*, vol. 11, no. 9, pp. 3607–3615, 2020.

[18] J. B. V. Subrahmanyam and C. Radhakrishna, "A simple method for feeder reconfiguration of balanced and unbalanced distribution systems for loss minimization," *Electric Power Components & Systems*, vol. 38, pp. 72–84, 2010.

[19] R. Singh, B. C. Pal, and R. A. Jabr, "Statistical representation of distribution system loads using Gaussian mixture model," *IEEE Transactions on Power Systems*, vol. 25, no. 1, pp. 29–37, 2010.

Hindawi
Wireless Communications and Mobile Computing
Volume 2023, Article ID 9789176, 1 page
https://doi.org/10.1155/2023/9789176

Retraction

Retracted: Construction of Accounting Internal Control Management Platform Based on IoT Cloud Computing

Wireless Communications and Mobile Computing

Received 17 October 2023; Accepted 17 October 2023; Published 18 October 2023

This article has been retracted by Hindawi following an investigation undertaken by the publisher [1]. This investigation has uncovered evidence of one or more of the following indicators of systematic manipulation of the publication process:

(1) Discrepancies in scope
(2) Discrepancies in the description of the research reported
(3) Discrepancies between the availability of data and the research described
(4) Inappropriate citations
(5) Incoherent, meaningless and/or irrelevant content included in the article
(6) Peer-review manipulation

The presence of these indicators undermines our confidence in the integrity of the article's content and we cannot, therefore, vouch for its reliability. Please note that this notice is intended solely to alert readers that the content of this article is unreliable. We have not investigated whether authors were aware of or involved in the systematic manipulation of the publication process.

Wiley and Hindawi regrets that the usual quality checks did not identify these issues before publication and have since put additional measures in place to safeguard research integrity.

We wish to credit our own Research Integrity and Research Publishing teams and anonymous and named external researchers and research integrity experts for contributing to this investigation.

The corresponding author, as the representative of all authors, has been given the opportunity to register their agreement or disagreement to this retraction. We have kept a record of any response received.

References

[1] L. Song, "Construction of Accounting Internal Control Management Platform Based on IoT Cloud Computing," *Wireless Communications and Mobile Computing*, vol. 2022, Article ID 9552118, 13 pages, 2022.

Hindawi
Wireless Communications and Mobile Computing
Volume 2022, Article ID 9552118, 13 pages
https://doi.org/10.1155/2022/9552118

Research Article

Construction of Accounting Internal Control Management Platform Based on IoT Cloud Computing

Li Song

Inner Mongolia University of Finance and Economics, Chifeng, 024000 Inner Mogolia, China

Correspondence should be addressed to Li Song; 1808180062@mail.bnuz.edu.cn

Received 29 March 2022; Revised 28 April 2022; Accepted 6 May 2022; Published 16 August 2022

Academic Editor: Jun Ye

The Internet of Things is a network that interconnects all items on the Internet through radiofrequency identification, infrared sensors, global positioning systems, laser scanners, and other sensing equipment according to the agreed communication protocol to achieve intelligent identification, positioning, analysis, monitoring, and management. Internal accounting control is an accounting measure established for the enterprise to identify and analyze the operating conditions and to be responsible for the enterprise assets. Accounting internal control is the core of internal control, and the rational use of internal control theory is conducive to promoting the healthy development of enterprises. According to the control object, it can be divided into financial risk control, operational risk control, human resource risk control, strategic risk control, and information distortion control. This paper is aimed at studying the construction of an accounting internal control management platform based on the Internet of Things cloud computing. How the internal accounting control system adapts to the development of the socialist market economy is the current research focus. In view of the current development status of the control system, this paper combines the internal control with the accounting information system and explores the enterprise management from the strategic management level and the operational management level. This paper mainly builds an accounting big data analysis platform based on cloud computing and believes that the platform should have the function of financial comprehensive analysis. The experiment in this paper found that the actual management cost of the company in 2017 was 2630 million yuan, and the predicted management cost was 2600 million yuan. The gap between the predicted data and the actual data is getting closer and closer, indicating that the prediction platform is effective.

1. Introduction

The Internet of Things has attracted the attention of all countries in the world because of its good economic benefits. At the same time, the Internet of Things has also become an important booster for the recovery of the world economy. The good development of an enterprise requires not only external assistance but also internal management. Therefore, this paper combines IoT cloud computing with internal accounting control management, hoping to promote the development of enterprises through the combination of internal management and external technology.

The internal control system adopts various control methods for the storage and use of property and materials, which can prevent and reduce the damage of property and materials, and prevent the occurrence of problems such as waste and corruption. The scientific internal control system can reasonably control, coordinate, and evaluate the various functional departments and personnel within the enterprise, to ensure the efficient operation of the enterprise. Correct and reliable accounting data is a necessary condition for business managers to understand the past, control the present, predict the future, and make decisions. The internal control system can effectively prevent the occurrence of errors and malpractices by formulating and implementing business processing procedures, so that the accounting data can be controlled under the condition of mutual restraint.

This paper proposes to implement control from two levels of strategy and operation and use the control method combining result control and behavior to control enterprise risk. This paper points out from the enterprise management level that the main purpose of internal control is to improve

the enterprise's ability to resist risks and promote the realization of the enterprise's long-term goals.

2. Related Work

Scientific management of enterprises helps enterprises to create more value and develop in a more scientific direction. Vakhrushina and Prunenko confirm that the significance of domestic and management accounting processes is objectively increasing in the context of the economic crisis. They identified the likelihood and manner of inclusion of processes of management accounting into internal control processes and concluded that some of the existing duplicated processes were finally confirmed to be in line with the principles ensuring success of the implementation thereof [1]. The knowledge economy puts forward higher requirements for accounting information resources of enterprises. Wei designed and implemented the enterprise accounting management platform based on data mining. First, he designed the accounting information implementation process to meet the needs of the enterprise and conducted relevant inspections of the platform. The results show that the enterprise accounting platform constructed by the experiment can realize most of the functions of accounting and financial management and provide a certain basis for the financial management decision of enterprises. Practice has proved that the platform can be effectively applied to accounting work and is feasible [2]. In response to the management requirements, Mikhnenko analyzes the behavior of the internal environmental elements of the enterprise, formulates management solutions, and improves the effectiveness of its behavior. The high quality of the solution is provided by the information model, which is a highly adequate image of the specific object being controlled, and the ability to control the volume of the device to fully perform its inherent function. In this case, the digital transformation of the analytical process is based on its own information platform and should use breakthrough digital technologies. The study uses methods such as system analysis to summarize modern concepts of economic systems management, the development of digital technologies, and their introduction into the management decision-making process [3]. As a management tool, accounting serves management and ensures the connection between the operating system and the entity's administrative management system. Ciuhureanu emphasizes that management accounting systems involve the internal management of a business and provide managers with important information in several interrelated areas: forecasting, costing and analysis, coordination, decision-making, control, and evaluation. He begins by highlighting the necessity and usefulness of management, accounting information for management, and through a selective study of a sample of 301 subjects, aims to analyze the opportunities for providing information through management accounting systems. He came to a series of conclusions based on established associations [4]. Ponomareva and Slinykov present research on the formation of accounting and control systems that provide information and analytical support for management objectives. In forming strategically oriented financial indicators, the company's cost of capital occupies a fundamental position. According to the research results, the information and analysis of the developed accounting and control system support the company's market management objectives and its business processes are integrated with other management systems in a parallel automated manner [5]. Crespo-Perez understands the convergence of cloud computing, machine learning, and IoT as a framework for decision support system development, and to develop this framework, he analyzed and synthesized 35 research articles from 2006 to 2017. The results show that when the amount of data is large, computational algorithms and sophisticated analytical techniques are required. The IoT combines a large amount of data accumulation and data mining to improve the learning of business automatic intelligence [6]. There is currently no unified way to represent, share, and understand IoT data. Antunes et al. discusses the limitations of current storage and analysis solutions, points out the advantages of semantic methods for context organization, and extends unsupervised models to automatically learn word categories. The scheme is evaluated on the Miller–Charles dataset and the IoT semantic dataset extracted from popular IoT platforms with a correlation of 0.63 [7]. Although these theories have explored IoT cloud computing and internal accounting control to a certain extent, the combination between the two is less and not practical.

3. Construction Method of Accounting Internal Control Management Platform Based on IoT Cloud Computing

3.1. IoT System. RFID is an easy-to-operate, simple, and practical application technology, and the external environment can be ignored during its use [8]. For example, short-range RF products are not afraid of harsh environments such as oil stains and dust pollution and can replace barcodes. With the development of the Internet of Things, the way of information collection has also changed from manual collection to the current automated collection. The current IoT perception technology is mainly radiofrequency identification technology, which combines radio broadcasting technology and radar technology. Radiofrequency identification technology first appeared in aircraft radar detection technology, mainly for military operations [9]. With the continuous deepening of scientific research and technology, radiofrequency identification has also been gradually applied from the military field to the Internet of Things field. Generally speaking, a complete RFID system includes four parts: tag, antennas, management system, and reader [10, 11], the basic working principle of the radio frequency identification system: the electronic tag enters an effective magnetic field, and if it receives a special radiofrequency signal launched by the reader through the transmitting antenna, the electronic tag is activated. Therefore, the energy obtained by the induced current will send the encoded information stored in the chip through the built-in radiofrequency antenna, or actively send a certain frequency signal. The receiving antenna of the reader receives the reflected

microwave synthesis signal, and after decoding by the antenna regulator, the valid information is sent to the central information system for related data processing. The central information system recognizes the code of the tag according to the code, makes the corresponding processing and control according to different settings, and finally sends out an instruction signal to the control reader to complete the corresponding read and write operations, as shown in Figure 1.

The antenna of the radiofrequency identification system is responsible for receiving and transmitting radiofrequency information, and the role of the antenna in this process is to convert the received electromagnetic wave information into a current signal, or convert the current signal into an electromagnetic wave and send it out [12, 13]. In this process, the energy emitted by the antenna will form an electromagnetic field, which has a certain effect on the identification of the electronic tag, and the electromagnetic wave magnetic field formed is the scale range of the reader. However, the number of antennas in the RFID system needs to be analyzed in detail [14].

The electronic tag in the RFID system consists of a chip and an antenna [15]. The data information of the target object exists in the electronic tag, and its existence form can be in a read-only state or a compatible state. During the operation, the reader sends a signal and the tag receives it, and the electronic tag converts the electromagnetic wave information into DC power [16, 17]. The specific situation is shown in Figure 2.

The main purpose of the RFID reader is to "communicate" with the electronic tag and receive the control commands issued by the system [18]. The transmission frequency of the RFID system is controlled by the reader, and the range of information communication is also limited by the reader [19]. From the perspective of the structure of the reader, it can be divided into a reading device and a writing device, as shown in Figure 3.

IOT is a network-based and service-oriented integrated message treatment technics. It has enabled a quantum leap not only in the communication methods among individuals but also among people and things. In a word, IoT technology has turned the whole world into a whole [20]. Networking, materialization, interconnection, automation, perception, and intelligence are the basic characteristics of the Internet of Things. Despite the powerful functions of IoT, the basis of IoT is still the Internet, only that IoT has been expanded and extended on the basis of the Internet. From the current research progress, IoT may be classified into sensing level, application level and web level, illustrated in Figure 4.

The job of the recognition layer is to identify the target. In what process web-based sensitive or identifier devices will be engaged, the exact target detection can be achieved only with the cooperation of multiple technologies.

The application layer consists of data acquisition and supervision and power consumption control. The managed architecture covers accounting and administrative features. In summary, the application tier is the technique of combining IoT technologies with the rest of the domain to get a new kind of clever settlement.

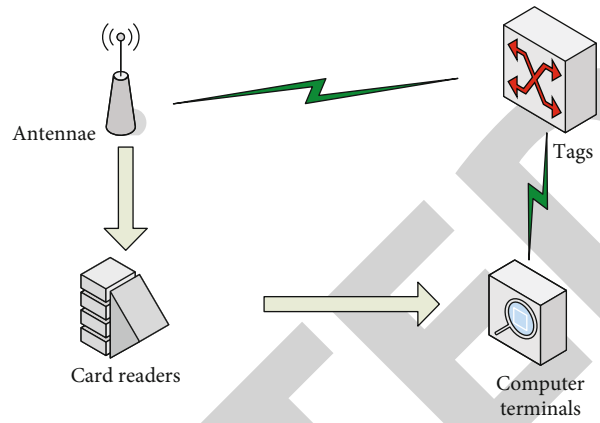

Figure 1: RFID system architecture.

The IoT technology is the heart of IT. In the field of IoT, all entities can talk to every other and just share messages through IoT technology with the help of the below features. It connects any item to the Internet through information sensing equipment and according to the agreed protocol and conducts information exchange and communication, to realize a network of intelligent identification, positioning, tracking, monitoring, and management.

(1) Transportability IoT technology enables information delivery by complying with protocols

(2) Integrated perceptibility, IoT has the ability to self-organize and break technology dependency

(3) Automatic control, which is intelligently managed through the use of fuzzy knowledge technology

(4) Intelligent processing, using data processing technology to process the raw data and transmit it to the user

3.2. Distributed Algorithms. The distribution optimization problem can be traced back to the early 1980s, but due to technical problems, it has not been developed much until the rise of networking in recent years, and distribution optimization has reappeared. Distributed optimization is the task of effectively realizing optimization through cooperation and coordination among multiple agents and can be used to solve large-scale and complex optimization problems that are incompetent for many centralized algorithms. Some scholars have proposed a distributed convex optimization algorithm based on gradually reducing the step size and discussed the constraints at the same time. Figure 5 is a schematic diagram of a distributed storage structure.

Multiagents can be divided into the directed graph and undirected graph. The function expression of a directed graph can be expressed as

$$C_{hf} = \begin{cases} 1 \\ 0 \end{cases}, (h, f) \in \alpha, \quad (1)$$

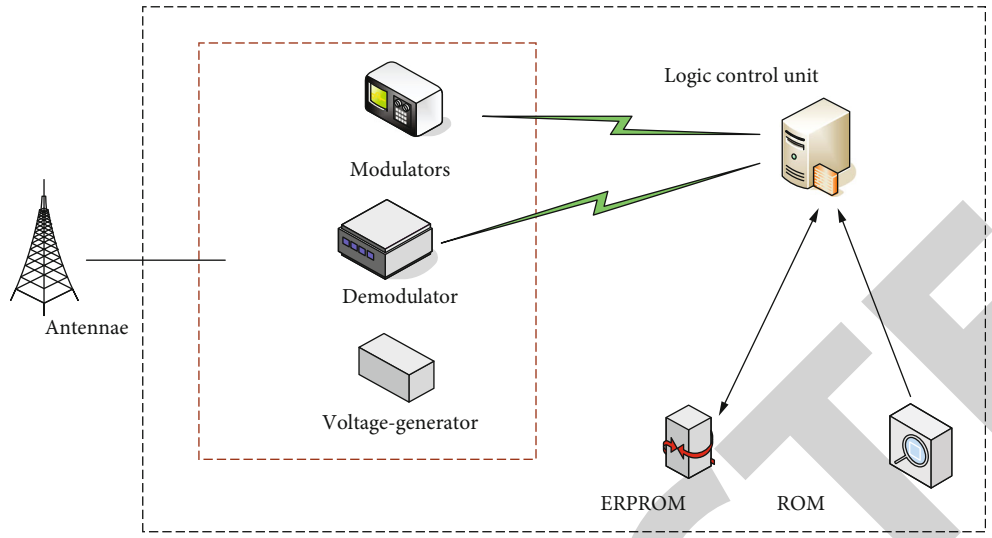

Figure 2: Electronic tagging.

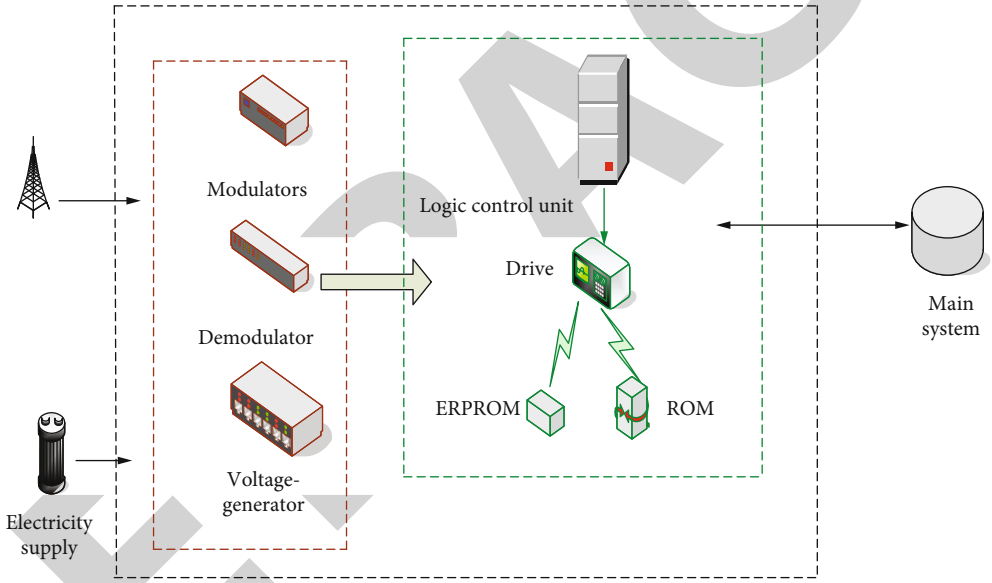

Figure 3: Structure of the reader.

where C_{hf} represents the weight of the directed edge and h, f represent the directed node.

$$k_{hl}(h) = \sum_{f=1}^{l} C_{hf},$$
$$k_{\text{out}}(h) = \sum_{f=1}^{l} C_{hf}, \tag{2}$$

The in-degree matrix is $K_{hl} = \lfloor k_{hf} \rfloor$, and the out-degree matrix is $K_{\text{out}} = \lfloor k_{fh} \rfloor$. When $K_{hl} = K_{\text{out}}$, we consider it to be a weighted flat map.

The dynamic formula of a multiagent system composed of multiple agents can be expressed as:

$$s_a(k) = y_i(k), \tag{3}$$

where $s_a(k)$ is the state of agent a and $y_a(k)$ is the control law to be designed. The cooperation of multiple agents to solve a multidimensional optimization problem can be expressed as

$$\min_{a \in W^J} g(a) = \sum_{k=1}^{h} g_k(a). \tag{4}$$

Because the calculation formula is too complicated, it can be solved separately in the actual application process.

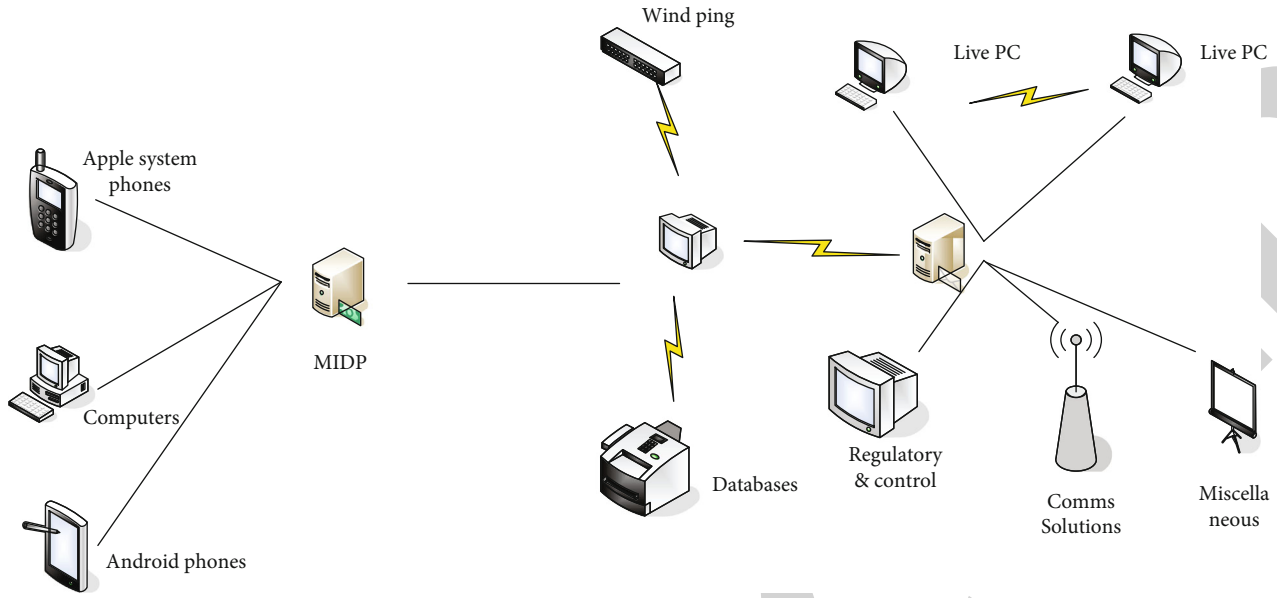

Figure 4: Internet of Things platform architecture diagram.

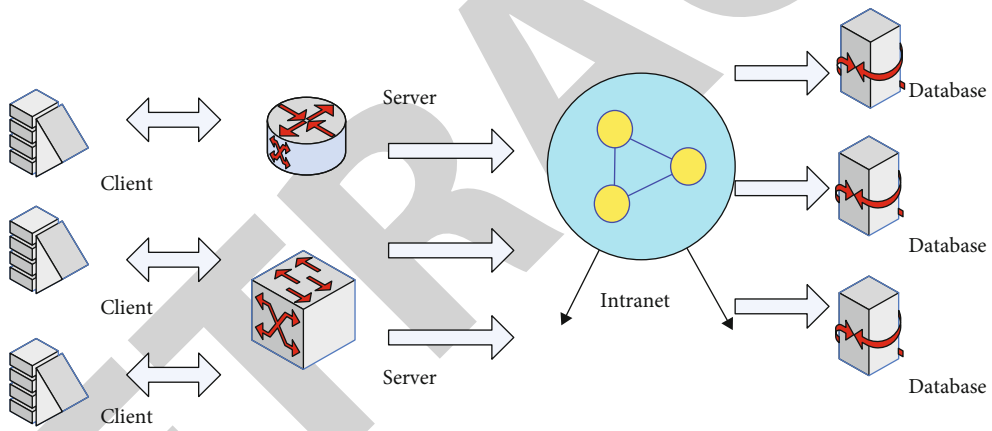

Figure 5: Distributed storage structure.

A single part gets a cost function, and the agent can jointly update its state with each part.

The basis of Bayesian classification is probabilistic reasoning, that is, the process of deriving unknown variable information from known variable information.

$$P(C|x_1, x_2, x_3, \cdots, x_n) = \frac{P(C)P(x_1, x_2, x_3, \cdots, x_n|C)}{P(x_1, x_2, x_3, \cdots, x_n)}. \quad (5)$$

Bayesian probabilistic models assume that each feature $x_j (i \neq j)$ is conditionally independent of other features, namely,

$$P(x_i|C, x_j) = P(x_i|C), i \neq j. \quad (6)$$

Therefore, the categorical variable of the conditional distribution of C can be obtained, namely,

$$P(C|x_1, x_2, x_3, \cdots, x_n) = \frac{1}{C}P(C)\prod_{i=1}^{n} P(x_i|C). \quad (7)$$

If the gait data is divided into two categories, using the Bayesian formula, it can be expressed as

$$P(w_j|x) = \frac{P(x|w_j)P(w_j)}{P(x)}. \quad (8)$$

It is possible to obtain completely equivalent decision rules. There are two forms of these two minimum error

Bayesian classification methods; one is the posterior probability form, namely,

$$P(w_1|x) > P(w_2|x). \tag{9}$$

The other is a class of conditional probability density forms, namely,

$$P(x|w_1)P(w_1) > P(x|w_2)P(w_2), \tag{10}$$

$$g_{hf} = \begin{cases} -c_{hf}, h \neq f, \\ k_{hm}(h), h = f, \end{cases} \tag{11}$$

where $g(hf)$ represents a directed graph matrix, (μ, A, B) represents the probability space of variables, μ represents the basic event, A is a subset of μ, and B is the probability. $Y = (y_{cx})$ represents the continuous uniform Markov process transition rate matrix. We can generalize it to the following function expression:

$$B\{\alpha_{v+z} = d|\alpha_v = c\} = \begin{cases} 1 + y_{cx}z + f(z), c = z, \\ y_{cx}z + f(z), c \neq z, \end{cases} \tag{12}$$

Among them $y_{cx} = -\sum_{c\neq x} y_{cx}, y_{cx} \geq 0, \lim_{z\longrightarrow 0} f(z)/z = 0$. For discrete Markov process, its transition probability matrix can be expressed as

$$g_{cx} = B\{\alpha_{v+z} = d|\alpha_v = c\}, v \in M, \tag{13}$$

where g_{cx} represents the Markov transition probability matrix.

The compact form of the closed-loop system composed of multiagent distributions can be expressed as

$$H = -\varepsilon G(\varphi_v)H - \alpha\nabla f(H) - M, \tag{14}$$

$$M = \alpha\varepsilon H(\varphi_V)H. \tag{15}$$

Among them $H = |h_1, \cdots, h_m|^v, M = |m_1, \cdots, m_n|^v$.

When the derivative of the closed-loop system is zero, we get

$$G(\varphi_V)H^* = 0, \tag{16}$$

$$M^* + \partial\nabla f(H^*) = 0. \tag{17}$$

To make the system distribution reach the optimal level, related researchers proposed a distributed optimization algorithm under the continuous Markov switching topology:

$$\varphi_d = -\varepsilon \sum_{f\in C_d} k_{df}(\phi_o)\left(t_d - t_f\right) - \alpha\nabla j_d(t_d) - \kappa_d, \tag{18}$$

$$\kappa_d = \alpha\varepsilon \sum_{f\in C_d} k_{df}(\phi_0)\left(t_d - t_f\right), \tag{19}$$

where α, ε represent the constant. If $\alpha < 1, \beta$ satisfies the following conditions, it can be expressed as

$$i_1 = \alpha\bar{\kappa} - \frac{\eta\alpha^2\nu^2}{2} > 0. \tag{20}$$

3.3. Overview of Cloud Computing. Cloud computing is a SERVICE delivery model that provides ubiquitous, on-demand network access to a configurable pool of shared computing resources. These resources include computing resources, network resources, and storage resources. The cloud computing model has nine characteristics: IT capabilities are provided as services, user self-service, network access, open service access interfaces, resource aggregation into pools, continuous service updates, elastic expansion, automated management, and resource usage metering. Cloud computing is a disruptive technology that has the potential to enhance collaboration, agility, scalability, and availability and potentially reduce costs through optimization and efficient computing. Cloud computing has advantages that traditional IT architectures do not have. First, cloud computing can improve resource utilization. The on-demand acquisition of cloud computing ensures the effective allocation and use of resources, while the elastic expansion mode ensures the recovery and reuse of resources. Therefore, the utilization rate of resources is effectively improved. The industrial system of cloud computing consists of cloud computing service industry, cloud computing manufacturing industry, infrastructure service industry, and supporting industry. The cloud computing service industry is used to utilize cloud service resources to provide services to cloud computing consumers. According to the different types of services provided, the service modes of cloud computing can be divided into three types: software as a service, platform as a service, and infrastructure as a service.

3.4. Overview of Internal Control. Although the internal control thought appeared in China in the Shang and Zhou dynasties, the systematic research on internal control thought started relatively late. From the perspective of China, internal control can be divided into ancient internal control—emerging period; contemporary internal control—planned control, mainly referring to the control system of planned economy; modern internal control—adaptive control. In fact, China did not formally apply the internal control theory until after its accession to the WTO. With the continuous in-depth exploration of the internal control idea, countries around the world also have some differences on the internal control theory. Taking the United States as an example, they believe that internal control needs to pay attention to the goals of the enterprise, and China believes that internal control needs to protect the safety of assets. Reasonable use of internal control theory can prevent employees from irregular behavior, protect enterprise property safety, prevent enterprise risks, and make enterprises develop in a more scientific direction. Internal control is a systematic project, which requires the cooperation of multiple departments and multiple control methods. Internal control is a dynamic process. Internal control is not only

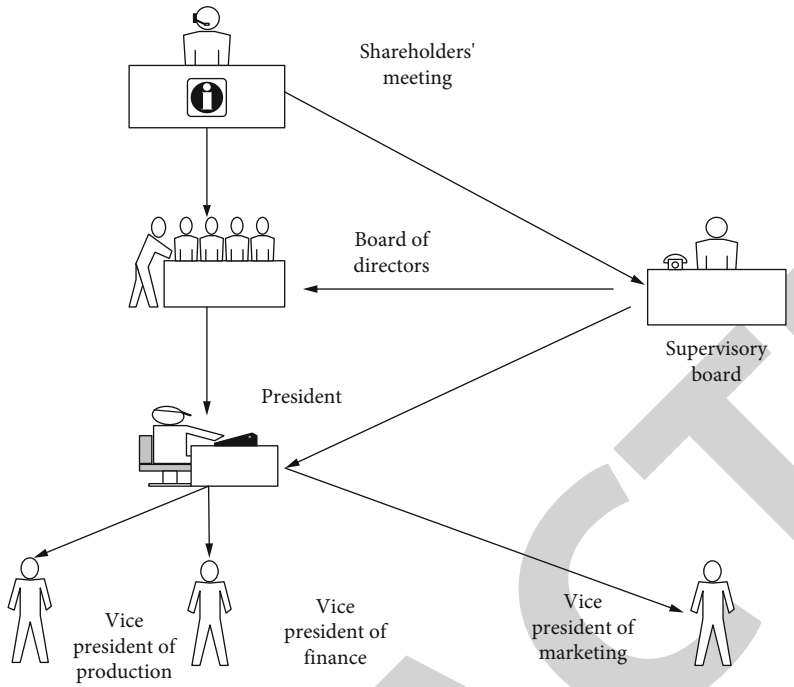

Figure 6: Organizational structure of enterprise internal control.

affected by the external environment, market, government, etc. but also by the internal corporate culture, organizational structure, and organizational scale. Changes in the environment will inevitably require internal control to be adjusted accordingly. Figure 6 shows the organizational structure of the internal control of the enterprise.

4. Construction Experiment of Accounting Internal Control Management Platform Based on Internet of Things Cloud Computing

4.1. Experimental Parameters. This paper discusses the construction of the accounting internal control management platform of the Internet of Things cloud computing; therefore, this experiment needs to rely on IoT, and the hardware of the system with various sizes may also have various impacts on the operation. Table 1 shows the parameters of our hardware for this simulation.

4.2. Internal Accounting Control Structure. The goal of corporate governance is to ensure that the company operates in the correct and favorable direction, to prevent directors, managers, and other senior executives from doing behaviors that endanger the interests of shareholders out of their own selfishness, so that the company can achieve maximum benefits. The main goal of internal accounting control is to standardize accounting behavior, ensure the authenticity of accounting information, eliminate hidden dangers, and prevent and timely discover and correct errors and fraudulent behaviors, to protect the safety and integrity of the unit's assets and ensure the implementation of relevant national laws, regulations and internal rules, and regulations of the unit; its basic goal is still to ensure the realization of the company's goals. Therefore, corporate governance and internal accounting control are unified in the realization of corporate goals.

According to the data in Table 2, this experiment illustrates the shareholding situation of a large enterprise in city C. According to the specific data in Table 3, when the company was listed, S Group held 5.2 million shares, accounting for 42% of the total shares. Transportation enterprise B holds 615,000 shares, accounting for 5% of the total shares. The trading company holds 610,000 shares, accounting for 4.95% of the total shares. D chemical group holds 455,100 shares, accounting for 3.7% of the total shares. Among the top five shareholders of the enterprise, the fifth is the individual shareholder, which holds 159,900 shares, accounting for 0.13% of the total shares. According to the shareholding data of shareholders, S group has the largest number of holdings, has the absolute right to speak in the company, and has no other similar major shareholders, which will lead to decision errors and is not conducive to the normal operation of the company.

4.3. Evaluation of Cost-Benefit Indicators. A large enterprise in city C built an accounting big data analysis platform based on cloud computing and improved it before the trial. The details are as follows.

According to the data in Table 3, the accounting big data analysis platform using cloud computing has brought different degrees of influence to enterprises. From the perspective of platform development, before the construction of the cloud computing accounting big data analysis platform, software development costs 500,000 yuan, and software maintenance costs 120,000 yuan; after the cloud computing

Table 1: System parameters.

Systems	Memory	Hard disk	Mainframe
Domain controller	3G	30G	2 core
Attendance system operating environment	3G	30G	1 core
V center server	6G	30G	2 cores
Database server	3G	30G	2 cores
ESXI server	3G	30G	2 cores

Table 2: Description of the shareholding of a large company in City C.

Shareholder information	Number of listed shareholdings	Shareholding
S group enterprises	52000000	42%
B transport enterprise	6150000	5%
A trading company	6100000	4.95%
D chemical group	4551000	3.7%
U (individual)	159900	0.13%

accounting big data analysis platform is built, it will cost 260,000 yuan for software development and 110,000 yuan for software maintenance. According to the data, it can be seen that accounting big data analysis platform of cloud computing greatly reduces the software cost. Judging from the report, it took 15 days to sort out the report before the platform was built, and the accuracy of the report was 67%. Collating the report requires the participation of the entire team. After the platform is built, it takes 2 hours to organize the report. The accuracy of the report is 96.9%, and the platform can automatically complete the report. According to this situation, the accounting big data analysis platform of cloud computing reduces the workload of staff and improves the accuracy of reports. From the perspective of financial analysis, the financial analysis before the platform construction was concentrated on the surface, and each analysis took about 7 days, and the analysis accuracy was maintained at about 72%. After the platform is built, the financial analysis is concentrated in the deep layer, and each analysis is carried out in real time, and the analysis accuracy is maintained at about 98%. According to the data, the cloud computing accounting big data analysis platform can carry out in-depth analysis, shorten the analysis time, and improve the accuracy of the analysis.

5. Construction of Accounting Internal Control Management Platform Based on IoT Cloud Computing

5.1. Test Analysis of Cloud Computing Accounting Big Data Analysis Platform. Accounting data is a collection of unprocessed numbers, letters, and special symbols expressed in the form of "documents, certificates, accounts, and tables" in the processing of accounting matters. In fact, the most important thing in big data analysis is financial analysis. Using the accounting big data analysis platform to analyze the company's financial affairs can clearly see the company's development status.

According to the data in Figure 7, the assets of an enterprise in city C in June were 4,000,000 yuan, and the liabilities were 320,000 yuan; in July, the assets were 4,080,000 yuan, and the liabilities were 3,54,830 yuan. In August, the assets were 4,102,160 yuan, and the liabilities were 365,450 yuan; in September, the assets were 4,105,670 yuan, and the liabilities were 368,560 yuan. In October, the assets were 4,156,750 yuan, and the liabilities were 385,610 yuan; in November, the assets were 4,106,530 yuan, and the liabilities were 386,120 yuan. According to the data, the asset level of the company in 6 months is relatively stable, and it has basically maintained a stable upward state. However, from the perspective of liability, although the overall difference is not large in terms of data, its growth rate is greater than that of assets, indicating that the company needs to adjust its strategy.

Looking at the company's operating profit margin, the growth was 36.7% in June and 32.3% in July; the growth was 15% in August and 4.6% in September; growth was 30.4% in October and 20.4% in November. Looking at the company's return on assets, the growth rate was 6.7% in June and 7% in July; the growth was 2.8% in August and 7% in September; growth was 12.5% in October and 6.9% in November. According to the data, the company's operating profit and asset income fluctuated greatly, the overall development in August and September was poor, and the development in June, July, and October was better. This shows that the company should change its development strategy in the summer.

According to the data in Figure 8, the company's sales in different regions will be different. In the district A, the sales revenue is 3.15 million yuan, and the company's revenue in the same period is 4.86 million yuan. In district B, the sales revenue was 1.96 million yuan, and the company's revenue in the same period was 2.83 million yuan. In district C, the sales revenue was 2.74 million yuan, and the company's revenue in the same period was 2.91 million yuan. In district D, the sales income is 2.8 million yuan, and the company's income in the same period is 7 million yuan. In district E, the sales revenue was 2.11 million yuan, and the company's revenue in the same period was 2.91 million yuan. In district F, the sales income was 2.74 million yuan, and the company's income in the same period was 3.56 million yuan. According to the data, although the sales in district D are generally good, the sales situation is poor compared with the same period, so district D should change its strategy.

Table 3: Comparative analysis table before and after platform application.

Projects		Comparative analysis		Conclusion
		Before	After	
Platform costs	Development	500,000	260,000	Reduce software costs
	Maintenance	120,000	10,000	
Statements	Time	15 days	2 hours	Improves efficiency
	Accuracy	67%	96%	
	Workload	Whole group	Automatic	
Financial analysis	Levels	Surface	Deep	Improve analysis accuracy
	Time	7 days	Real time	
	Accuracy	72%	98%	

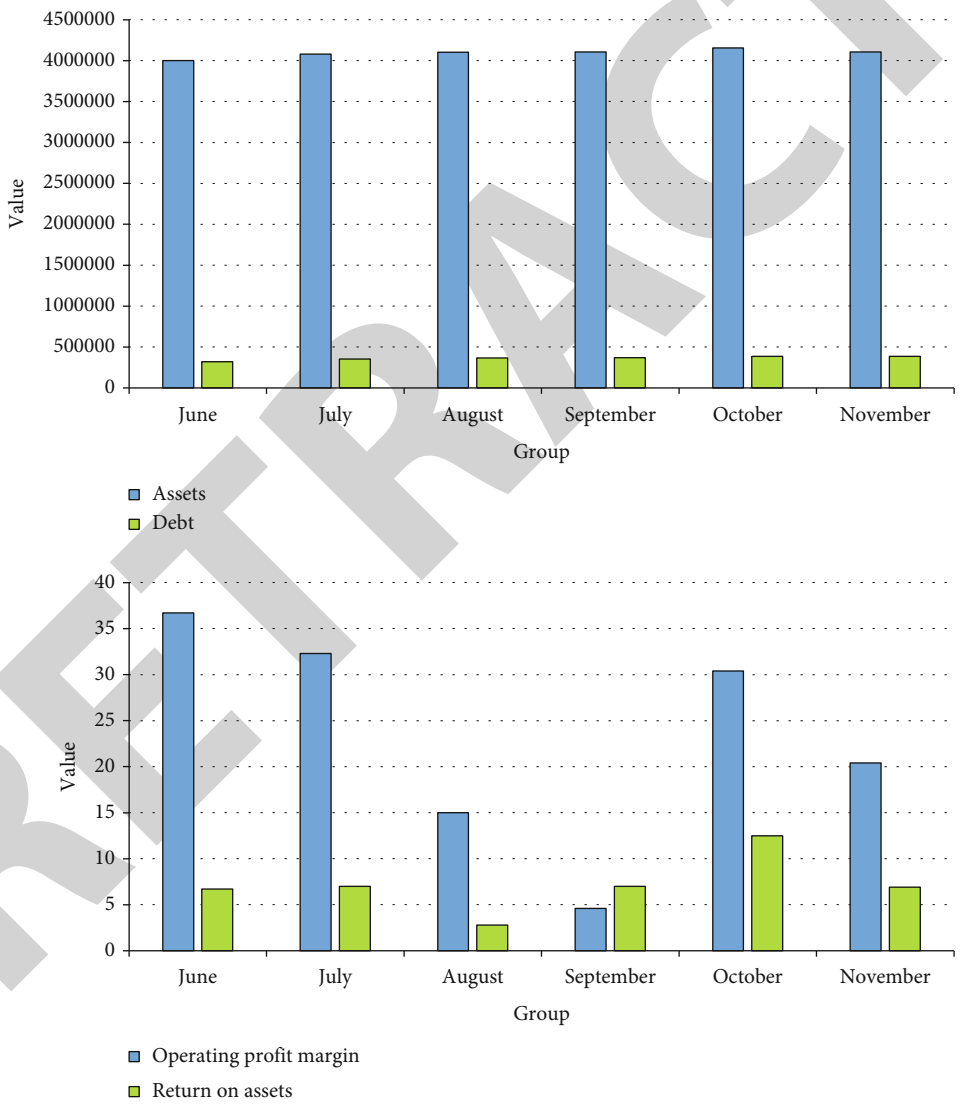

Figure 7: Financial analysis situation.

Judging from the company's overall sales, the company's actual sales in June were 15.83 million yuan, accounting for 103% of the month's sales. The company's actual sales in July was 16 million yuan, completing 110% of the month's sales. The company's actual sales in August was 14.93 million yuan, completing 113% of the month's sales. The company's actual sales in September was 17.3 million yuan, completing 112% of the month's sales. The company's actual

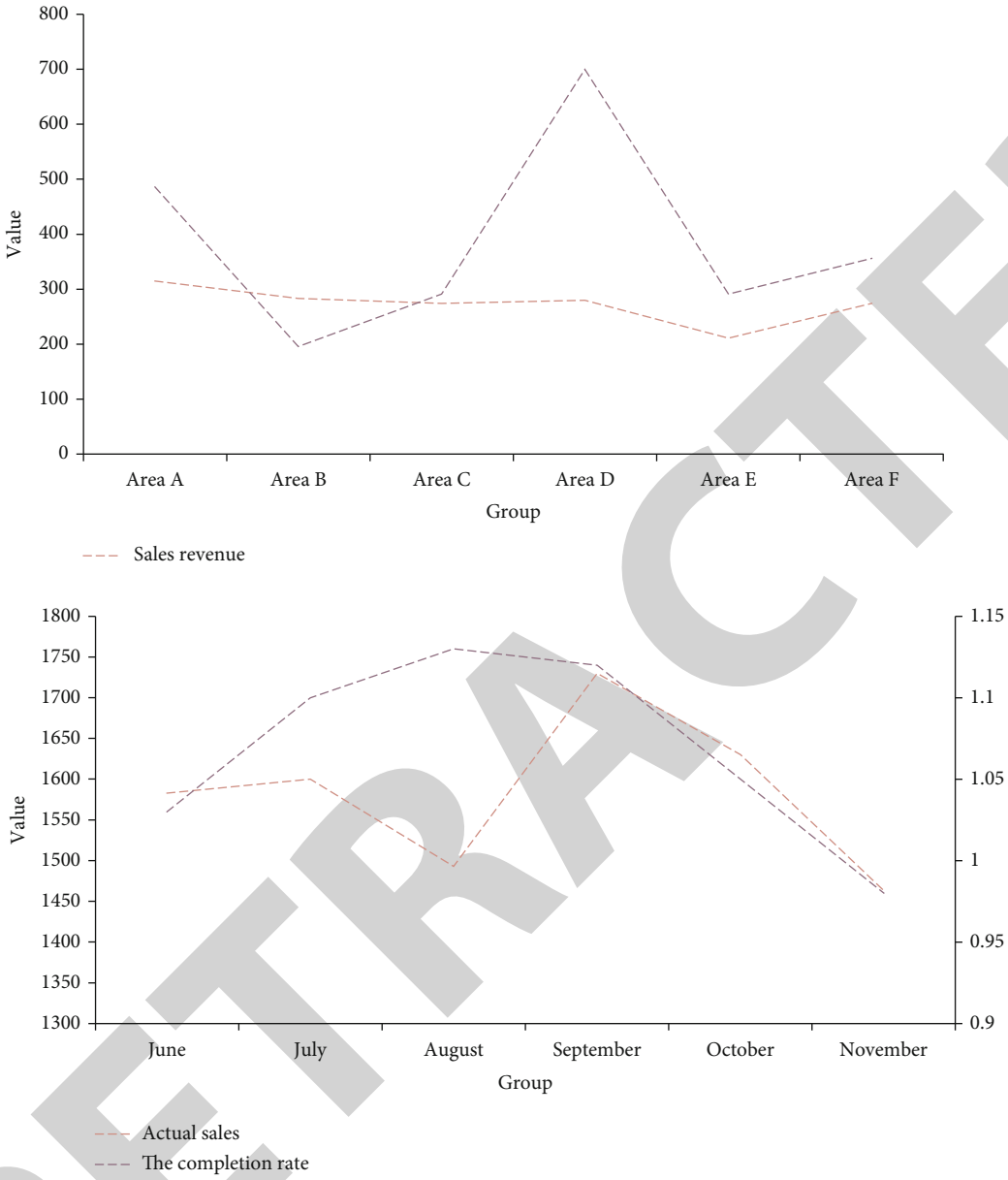

Figure 8: Schematic representation of the company's sales.

sales in October was 16.3 million yuan, completing 105% of the month's sales. The company's actual sales in November was 14.63 million yuan, accounting for 98% of the month's sales. According to the data, the company's sales have basically met the expectations, indicating that the company's basic strategy is correct, but it is too conservative.

5.2. Financial Forecast Function. To analyze the prediction function of the accounting big data analysis platform, we conducted an experiment on it, and the details are as follows:

According to the data in Figure 9, from the perspective of operating income, the actual income in 2012 was 27,000 million yuan, and the predicted income was 25,479 million yuan. The actual revenue in 2013 was 27,964 million yuan, and the forecast revenue was 28,963 million yuan. The actual revenue in 2014 was 35,789 million yuan, and the forecasted revenue was 36,890 million yuan. The actual revenue in 2015 was 57,869 million yuan, and the forecasted revenue was 56,782 million yuan. The actual revenue in 2016 was 78,951 million yuan, and the forecast revenue was 77,541 million yuan. The actual revenue for 2017 was 80,154 million yuan, and the forecast revenue was 80,000 million yuan. According to the data, the difference between the operating income forecast and the actual forecast income is small, indicating that the accounting big data analysis platform is effective.

In terms of operating cost, the actual operating cost in 2012 was 19,850 million yuan, and the predicted operating cost was 19,953 million yuan. The actual operating cost in 2013 was 20,000 million yuan, and the forecast operating cost was 22,156 million yuan. The actual operating cost in 2014 was 25,000 million yuan, and the forecast operating

Figure 9: Financial forecasting functional analysis.

cost was 26,450 million yuan. The actual operating cost in 2015 was 31,450 million yuan, and the forecast operating cost was 30,453 million yuan. The actual operating cost in 2016 was 43,250 million yuan, and the forecast operating cost was 42,360 million yuan. The actual operating cost in 2017 was 57,480 million yuan, and the predicted operating cost was 57,000 million yuan. According to the data, it can be seen that the gap between the predicted value and the actual value of the big data analysis platform is constantly narrowing, indicating that the big data analysis platform is effective.

5.3. Predictive Analysis of Operating Costs. Operating costs refer to all costs of the daily needs of the enterprise, including the cost of goods, wages, management expenses, and sales expenses. This part of the expenditure will have an important impact on the enterprise.

According to the data in Figure 10, the actual management expenses of the company in 2012 were 1500 million yuan, and the predicted management expenses were 1086 million yuan. In 2013, the company's actual management expenses were 1589 million yuan, and the forecast management expenses were 1580 million yuan. The company's actual management expenses in 2014 were 2013 million yuan, and the forecast management expenses were 1993 million yuan. In 2015, the company's actual management expenses were 2265 million yuan, and the forecast management expenses were 2196 million yuan. In 2016, the

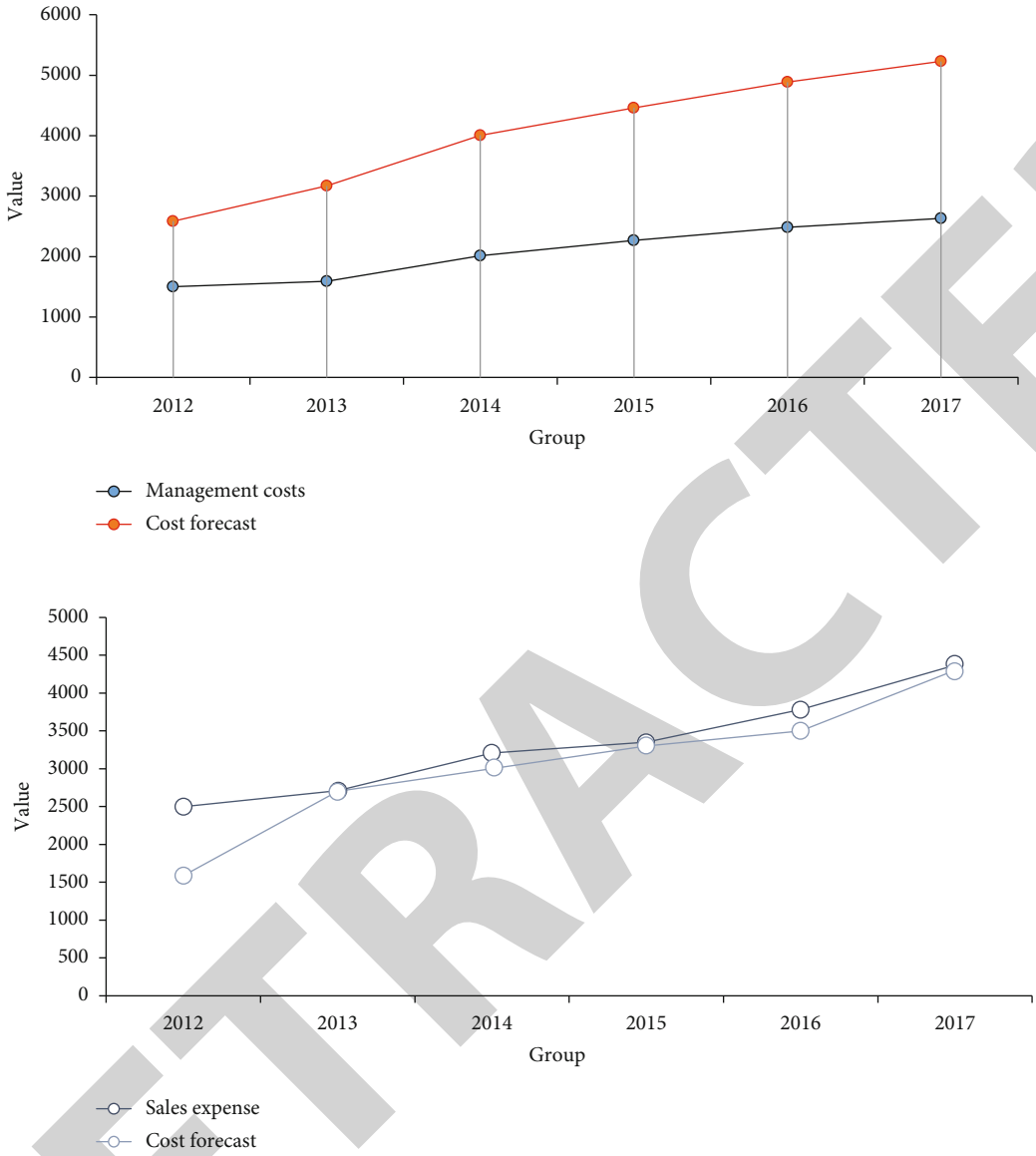

Figure 10: Operational cost forecast analysis.

company's actual management expenses were 2486 million yuan, and the forecast management expenses were 2400 million yuan. In 2017, the company's actual management expenses were 2630 million yuan, and the forecast management expenses were 2600 million yuan. According to the data, the prediction value of the big data analysis platform had a large gap in 2012, and then, the gap gradually narrowed, indicating that the platform's management cost prediction ability is relatively accurate.

In terms of selling expenses, the actual selling expenses of the company in 2012 were 2500 million yuan, and the predicted selling expenses were 1590 million yuan. In 2013, the company's actual sales expenses were 2710 million yuan, and the predicted sales expenses were 2700 million yuan. In 2014, the company's actual sales expenses were 3210 million yuan, and the predicted sales expenses were 3\000 million yuan. In 2015, the company's actual sales expenses were 3350 million yuan, and the predicted sales expenses were 3300 million yuan. In 2016, the company's actual sales expenses were 3780 million yuan, and the predicted sales expenses were 3500 million yuan. In 2017, the company's actual sales expenses were 4370 million yuan, and the forecast sales expenses were 4300 million yuan. According to the data, although the predicted value of the platform fluctuates, the difference is constantly shrinking, indicating that the accuracy of the platform's sales expense prediction is constantly improving.

6. Conclusions

With the development of science and technology, especially the promotion of Internet of Things technology, the combination of enterprise management and technology has become a common phenomenon today. Internal factors are the fundamental factors for the development of things, so the development of enterprises should not only rely on

Hindawi
Wireless Communications and Mobile Computing
Volume 2022, Article ID 9144951, 9 pages
https://doi.org/10.1155/2022/9144951

Research Article

Digital Media Art Creation Based on Virtual Reality and Semantic Feature Fusion

Yue Dai

College of Mathematics and Information Science, Nanjing Normal University of Special Education, Nanjing, 210038 Jiangsu, China

Correspondence should be addressed to Yue Dai; 250032@njts.edu.cn

Received 30 April 2022; Revised 29 June 2022; Accepted 21 July 2022; Published 12 August 2022

Academic Editor: Jun Ye

With the development of the times and science and technology, virtual reality technology as a high-tech technology has gone into people's vision and deeps into every aspect of people's lives and plays a more and more important role. In today's era, with the rapid development of digital new media technology and the gradual formation of a diversified media pattern, virtual reality technology generates a three-dimensional realistic virtual environment with its three-dimensional graphics generation technology, multisensing interaction technology, and high-resolution display technology. A special interactive device is required to enter the virtual environment. This is a brand-new comprehensive information technology, which is more and more widely used in various important fields of modern digital media design. This paper introduces a variety of digital media to promote the creation of virtual reality creation technology. Virtual reality technology in digital media art is more convenient, and more creative forms continue to emerge. The popularity of the virtual reality technology will undoubtedly promote the progress and development of the times and gives the digital media art more forms and volumes. In this paper, using virtual reality technology to digital media art, the forms of technology are summarized, and the way to cite examples is illustrated. This paper is aimed at analyzing and summarizing the virtual reality technology in the digital media art application, and virtual reality technology can give more valuable things in the digital media art creation and also hope to be able to bring some thinking and creative inspiration to writers or readers.

1. Introduction

Virtual reality technology as the name suggests is a technique of simulating realistic scenes with advanced science and technology; as an advanced science technology, it integrates sensor technology, sensor technology, computer graphics technology, multimedia technology, and network technology. The scientific and technical technique for designing multidisciplinary techniques such as human sensor technology, stereo technology, and simulation technology is based on technical means developed in the computer. Simple understanding of virtual reality technology is a 360° surrounding virtual scenario created in conjunction with various high-tech techniques. With this technical man, you can give full play to your imagination, and you will find the scenes, things, and expectations of expectations and play a role in virtual scenes. The fundamental purpose of virtual reality is to make the effect of the experience reach the most authentic feel. Through natural skills, human-computer interaction can be used, and the system that can achieve such a target is called virtual reality technology.

Virtual reality technology is an emerging technology and has been widely used in various fields. The emergence of this emerging technology is not late. About half a century ago, the prototype of virtual reality technology has appeared: two square displays that can be buckled on the human eye, controlling the control through certain instrument control, the human eye sees the contents of the display, generating the body's feelings, will have physical action with the change or movement of the content in the monitor, and follow changes or move, and it is easy to generate a certain psychological or emotional resonance. A few years ago, Oculus launched a virtual reality headset display, which officially unveiled in front of people, and gradually emerged on the stage of digital media.

Virtual reality technology is based on high-level science technology, through various sensory feelings to create a

virtual environment and users with dedicated input and output devices to pass reality with virtual world and have good interactivity. Virtual reality technology has the following features:

1.1. Immersion. Immersion refers to people immersed in the virtual reality technology to create a virtual space or atmosphere. Immersion is divided into semi-immersed and completely immersed virtual reality technology. In semi-immersive virtual reality technologies such as desktop virtual reality technology, the viewer can experience the shock caused by the virtual scene but also by the impact of the surrounding environment. Virtual reality technology means that the user is completely immersed in entering into a completely virtual space to create a scene, which is not affected by the external environment. What they all have in common is that they all require external devices to achieve, and can enable users to have different levels of immersion.

1.2. Interactivity. Virtual reality technology can be quickly accepted by the mass group and spread in the market, it is important to interact, and its technical features can communicate with people to form exchanges and dialogue, building a realistic scene, through similar real scenes through interaction with people, affecting the behavior of people, and making the user a real interaction experience.

1.3. Imagination. Virtual reality technology provides a better way of playing space for designers or users a nd better achieving people of things about future world, unknown world, and ideal world imagination. For example, the character designer can realize the image design of the characters in the virtual space, and the scene designer can simulate the simulation scene in the virtual space. Fans can realize their design dreams according to their own imagination.

Digital media art is a comprehensive art course, which is a small combination of art and science in traditional painting, contemporary art, art design, dance, and film by implanting technology and advanced technological means. Make art scientific, not only integrate each other but also have different disciplines. If we say that technology is a "tool," it is a noun. The reason of things lies in the internal reasons of things. "Tao" is "Tao," and any artistic creation should abide by it. As a science and technology, virtual reality technology has emerged a new art form in artistic creation, that is, digital media art. No matter what science and technology are incorporated into artistic creation, the basic laws of artistic creation are inseparable from the basic laws of artistic creation and the artistic accomplishment of the creators of art. In the process of digital media art creation, it is necessary to follow the inner "Tao" and create "tools" in order to create good digital media art. The rise and development of virtual reality technology have injected fresh blood into digital media art. In recent years, many new art forms have appeared in people's vision, such as trendy sound art, real-time dialogue, dynamic games, electronic sculpture, network performance equipment, and experimental imaging related to digital technology [1].

2. Literature Review

2.1. VR Technology Makes Digital Media Art Creations More Convenient. QuickTime VR technology is hotter in the current virtual reality technology family, and a wide range of technologies were applied. QuickTime VR is a primary virtual reality technology based on static images in the microcomputer platform. It can not only view the panoramic view of the three-dimensional graphic image but people can also see the feelings of a three-dimensional virtual space in a flat observation platform, and feel the immersive experience of the 360° environment. With this same, QuickTime VR technology not only has a good display of 3D objects or space but also gives a good experience. At the same time, it has a convenient and excellent editing function. The new media and participants under QTVR virtual reality technology are more interactive, and the viewer can master the process of playback and can participate in the contents of the play and can also be based on the participants. It requires at any time adjustment to meet many different needs of different users. QuickTime VR technology can pass through various input devices such as cameras and SLR, and almost any electronic input device can be combined with the input device. For example, by inputting photos from the camera into the QuickTime VR plug-in, viewers can freely edit, grade, and edit various pictures and videos in the camera. The unique feature is that multiple photos can be connected to form a video image [2]. Connecting the image content, you can also achieve the smooth expression of the image, not only the image perception but also give the viewer more contentive story [3]. The emergence of QuickTime VR technology makes the production of digital media art more convenient and free [4]. Because the price of QuickTime VR technology is not high, the scope of use is wide, and the space is widely accepted by the public. At the same time, QuickTime VR technology provides more creative opportunities for web browser plug-ins for educational, entertainment, and business networks, adding new tastes [5]. The purpose of Moreno is to reflect on the new status of museums in the digital age. Works using new media must be understood as a space for nonhierarchical communication, the role of the artist is diminished, and the public becomes the user who completes the public process [6]. Kessler et al. provide insights into new approaches and perspectives on the use of digital technologies to treat trauma-related disorders [7]. Ceranoglu discusses key interventions for parents and clinicians to help adolescents who are dependent on digital media, as well as opportunities for public health interventions by advocacy groups and the digital media industry [8]. The objective of Chan et al. was to understand how digital media technologies can facilitate the rehabilitation of offenders in correctional institutions [9].

2.2. VR Technology Makes Digital Media Art Creations More Flexible. Virtual reality technology provides more flexible way of creative ways to traditional paintings. With the improvement and progress of virtual reality and enhance reality technology, many artists began to make use of virtual

space concepts and TILT Brush VR technology [10] such as software that can be used and created in virtual space. It combines traditional art paper pen with the creation of computers 3D. Cherker can directly perform virtual forms with virtual reality technology tools. Tilt Brush is an application that draws stereoscopic images in a virtual space. It uses tools such as headners, envelopes, hand-standing equipment [11]. Cherker is created in virtual space according to the inner idea, with the mobile device of the handheld device, creator. It can be expressed smoothly, and some people say this is a way of creative ways. Creators were created in virtual space, and they can also review and appreciate their work in virtual spaces. The form of creation is novel, not only is more flexible but also brought better participation and experience to the creators. This painting work created with Tilt Brush VR is also collected by Google's world's first virtual reality art exhibition in San Francisco. This technology has brought more creations to animation creation, increasing the true feelings of characters and scene creations, and provides more possibilities for creation [12].

2.3. VR Technology Makes Digital Media Art Creations More Free. VR technology provides more convenient and free-playing shapes for the shape of stereo space. Through the architectural design procedure XRTISAN [13], designers can "build" houses directly in the virtual space in this procedure. Through the handheld device operating lever, the designer can change the size and height of the object in the virtual space and provide convenience to the object additional material as needed. The designer only needs to operate in a virtual space, and you can get the most authentic effect [14]. This technique enables more work to be done in less time, not only increasing the efficiency of design work, but also the quality of the work. Through an external equipment helmet, the designer can walk in the construction of the house, and the effect of the experience is like walking in the renovated house. Similar software programs also have HoloStudio [15], and creators can perform three-dimensional modeling directly within the virtual space according to the user's gesture and add materials and colors. More advanced is to print the work directly with a 3D printer [16]. There are also similar practical programs Quill in the field of film and television scholarships, which is a program that specializes in animation and film creation, participating in split script creation and drawing movie conceptual drawings and art design. This software adds time dimensions for painting while achieving linear editing features.

The creation of digital interaction arts, of course, is the cornerstone of human-machine interaction as the in-depth development of itself. There are two aspects of this, on the one hand, research people's interaction mentality and interaction behavior, and on the other hand, it is to study how to improve the interaction of the machine, so that the machine can be more natural in the interaction of people. The study of these two aspects also matched the interaction concepts analyzed by the German media art theory and comment experts mentioned in the previous section—ideological and scientific skills. To put it bluntly, it is a direction focused on studying the role of "people" in interaction art in the human machine [17]. The other is also the most direct research content is the ability of human-computer interaction "machine" to express people's cultural spirit.

The most recent works of Morgan Rauscher 2 belong to this category. This is a professional interactive artwork using robots, which is an artificial intelligence technology [18]. 32 customized acrylic materials "face" in the gallery, and each face is controlled by computer, using sports capture technology to make this 32 "face" to react to passible customers [19]. Author's thinking about this type of human machine interaction problem in the gallery and gaze, watching and gazing, watching and gazing, watching and watching, survived in a particular space [20].

2.4. "Machine" Research Became the Cornerstone of Creation. For digital interaction art, "machine" research has become the cornerstone of creation [21]. The authors grasp the ability and application skills and determine the expression of the author's computer art language [22]. The ability to make cold-ice-ice machine specific expression of cultural spirit is not easy, because computer interaction art requires many practical technical issues. These include the following aspects.

2.4.1. Research on Input Mode. Input mode can also be generally divided into several research directions: the first is to change the existing input device. For example, after disassembling the keyboard or mouse, connect other buttons to the original device contacts through the cable. This technique is high in the end of the 1990s, especially in the exhibition of many museums [23].

The second direction is to use various types of sensors. After the analog signal is converted into a digital signal, input the computer. This type of modification is easier to attract the audience in the first time [24], but the disadvantage is that the interactive form lacks change, and there will be aesthetic fatigue after the audience has a long time operation. There is an Australian new media artist Jeffrey Sauore 1 (the Legible City "belongs to this type. Jeffrey mounted the sensor on a pedal bearing of a bicycle, which can convert the speed of the bearing into a digital signal into the computer [25]. The audience rides on the bike, and you can use the car to control the direction, the foot pedal control speed, and travel in the virtual city that is cast. The architectural exterior of the street is a three-dimensional text model generated by computer, while the audience has a physical cycle action in the real world (cycling action). The viewer can control your speed and direction and swim in the three-dimensional text maze. The author hopes that the audience can take a stroll in a virtual scene to choose the story behind these buildings that they want to read. This interaction reflects the creation of computer interactive art in the 1990s.

The third direction is a person's behavior or action as an input method. With the gradual maturity of machine vision technologies, more and more artists try to introduce this technology into the input interface of "interaction" into computer interaction art works. Among them, American digital artist Jim Campbell's interactive art device "hallucination" is a representative work that uses this technology early.

When the viewer approaches the lens, the camera will record the entire screen in real time, while the audience can also see the image under real-time records in the 50-inch backpoint TV. As the audience makes actions, the audience in the image will suddenly pull out the flames and accompany the "ZIZI" burning, and let people have the illusion of truth and illusion. Side of the audience can see the bears' fierceness from the TV, this magical feeling will make people experience the martial arts master in China's martial arts novels, and this experience may only have art work to express this charm. This work is an early representative of machine vision technologies and uses the camera to capture external image signals. The target detection is performed by the frame difference method of the universal image sequence in the machine vision. This viewer can detect the different regions of the front and rear frames in the image sequence frame as long as the audience can detect the different regions of the two frames in the image sequence frame. This area is the audience. During the area of action, the artist is in this area through artistic techniques, including increasing various simulation effects to express the author's ideas and ideas.

3. Preliminaries

3.1. Two-Dimensional Defined Matrix of Digital Interactive Art Disciplines. Digital interactive art has no longer development time and belongs to a multidiscipline cross-shaped discipline, but which disciplines professionalism, how to intersect, but have no relevant books that give corresponding answers. This section will define the discipline matrix of digital interaction art with a discipline definition method of computer science.

In the spring of 1985, ACM and IEEE-CS jointly formed a research group, started the existence of "calculation as a discipline", and published the results on the "ACM Communication" in January 1989. The report gives the concept of calculating the second-dimensional definition matrix of disciplines and refines its content, as shown in Table 1.

With this scientific method, we can discuss the definition of digital interactive discipline matrix, and the digital interactive artistic process was summarized in three parts: perceptual, rational knowledge, and practice (design), from perceptual to rational knowledge, then by rational understanding of back to practice. In the field of interactive digital art, "perceptual" refers to the creative process of generating phase method; "rational knowledge" refers to the inspiration, ideas into practical programs and plans, similar to the system architecture in the field of computer science; "practice" will complete the final work to achieve specific technology through specific graphic design, programming and so on.

As shown in Table 2, the "horizontal" relationship in the matrix reflects the creation process of digital interaction art, which reflects the interaction between inductive understanding, rational understanding, and design and production.

The content of the "longitudinal" relationship is the common content of the discipline in the field of disciplines, which helps us to cognition digital interaction art and helps us better use methodology. Ideological series digital interaction art creation is as follows: the following will be introduced and described in the context of "longitudinal" in the context of digital interaction art.

Table 1: Calculate the two-dimensional definition matrix.

Three processes in the discipline
1.Discrete structure
2. Programing basic
3. Algorithm and structural
4. Architecture
5. Operating system
6. Network computing
7. Programming language
8. Human-machine interaction
9. Graphics and visualization calculation
10. Smart system
11. Information management
12. Software engineering
13. Social and professional issues
14. Scientific computing

The animation production in two-dimensional animation and traditional sense is not the same concept. He focuses on computer generated process animation, including the motion of the physical engine and collision. The three laws are the extremely important basic course for digital interaction art.

Discrete structures study discrete amounts of structures, and interrelationships are the main objectives and provide a strong mathematical tool for solving its basic problems in various branches, especially inductive to rational transition, which is important in transformation of sensibility cognition into rational cognition method. The discrete structure is self-evident for the importance of computer science. In recent decades, because of its application of computer science, since the operation target is discrete, the mathematical basis of computer science is basically discrete. We can say that the mathematical language of computer science is discrete mathematics. The most typical case of digital interaction art is the most typical case of the "particle system" 1, William Thomas Riv is under the guidance of the discrete method, and has been proved by experiments that aerosols can be considered as thousands of discrete and discontinuous. The particles are constituted, and each particle is an independent individual including attributes such as initial speed, acceleration, motion direction, gravity, health, and the particle or particle and external space that follow the classic Newtonian law, so that the first creation is simulated in the computer.

It can be seen from the two-dimensional definition matrix chart that the visual art and science and technology are almost a single autumn. At present, domestic digital art education is mainly due to two major camps: one is based on the field of college, and the other is a digital art or computer graphic education in computer science. The former teachers stated that the source of life is mainly from art students and more biased toward visual performance and

Table 2: Digital interactive art subject 2D defined matrix.

Subject area	Sensual knowledge	Sense of understanding	Rational understanding	Design production
Visual art	Plane, color, stereo composition	○	○	
Visual art	Graphic semantics	○		
Artistic theory	Modern design history	○		
Mathematical method	Discrete structure	○	○	
Computer science	Programming language		○	
Computer science	Graphics and visualization calculation	○	○	
Computer science	Human-machine communication		○	
Computer science	Artificial intelligence	○	○	○
Machinery automation	Systemism and control		○	○
Electronic engineering	Machine visual	○	○	○
Visual art	Single-chip principle	○	○	○
Visual art	Plane graphics, image processing			○
Two-dimensional animation	Web design			○
Computer animation	Plane animation			○
Film and television art	Postediting			○

Table 3: Comparison of creative modes.

Creative mode works	Independent artist	Independent creative, production outsourcing	Reactive team	University, research institution
Personal style	Strong	Strongest	Moderate	Weaker
Social critical	Strong	Strong	Moderate	Weaker
Overall packaging	Weaker	Strong	Moderate	Strongest
Novelty	Weaker	Moderate	Strongest	Strong
Technique level	Weaker	Moderate	Strongest	Strong
Artistic appeal	Moderate	Strongest	Moderate	Moderate

software operations, and the latter has more emphasized relatively strong programming capabilities to make students pay more attention to function and practicality. However, there is a significant resistance to digital interactive art education in the university stage.

In summary, the three-dimensional definition matrix of digital interaction art disciplines constitutes the basic content of this major, covering many fields. The determination of the discipline definition will not only help to correctly understand the creative thinking methods contained in the Digital Interactive Art Discipline but also contribute to the development, construction, and talent cultivation of digital interaction art.

3.2. Configuration in Mode. From the data listed in Table 3, it can compare the advantages and disadvantages of several creative modes. These comparison results are not constant, depending on the corresponding changes that depend on the specific work, but overall, the works under the four creative methods have their own long.

Of course, the composition of the above four categories of works is not isolated. Some artists and art groups may gradually switch between these creative methods according to their own characteristics during their creative careers for several years or even decades. For example, Du Zhenjun is a digital artist traveling in France that the author knows, which is a typical case of completing the transition from type one to type two. In his early years, he studied Chinese painting at the Academy of Fine Arts of Shanghai University. After studying abroad, he learned more support and assistance from new technologies for artistic expression; so, he decided to choose French Regional School of Fine Arts of Rennes for further study. In 1999, he obtained a master's degree in "Digital Space." During his studies, he began to study technology and created a series of works. He became one of the few independent digital multimedia artists overseas. Du Zhenjun's early works mainly focused on image interaction at the technical level. For example, the interactive work "Cleaning" on the ground projection shows that when the audience enters the image area, the computer obtains the information of the audience's location through the sensor device and then plays the cleaning at the corresponding location. The worker bends down to wipe and clean the image of the audience's feet. In 2007, the large-scale computer interactive art installation "Fireball" created by him at the Shanghai Electronic Arts Festival uses a temperature sensor. When the audience lights a lighter and the flame burns above 60 degrees in front of the sensor, the sensor will trigger an image of the raging fire. The feeler of the top image, the flag floating in the flame is a metaphor for the

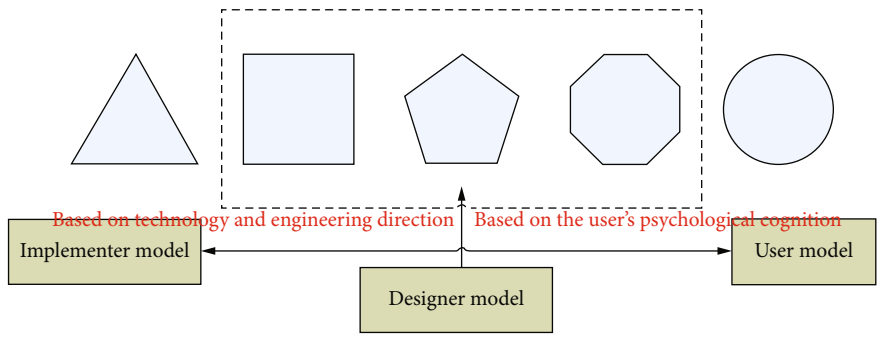

Figure 1: The relationship between designer model, implementer model, and user model.

blurring of national boundaries under globalization and the contradictory thoughts that come with it. As an independent artist, the author, from the early conception and creation of his own work to the realization of the technology, is all done by himself, to the increase in the scale, technical difficulty, and visual effects of the work in recent years. It is also the gradual transition of computer interactive art from the early personal work to the individual. The idea is then completed by the outsourced producer to complete the stage of technology and effect realization.

4. Digital Media Artistic Creation Achievements under Virtual Reality Technology

Interaction rules are a set of expressions that control the relationship between the work and the audience or participants. Any interaction of the audience or participants within the allowed range of the rules will cause the final display state of the work. The interaction process in this ideal state is somewhat similar to the butterfly effect in chaos theory. This effect shows that the result of the development of things has a very sensitive dependence on the initial conditions, and a very small deviation of the initial conditions will cause great differences in the results. The above theory also shows that after the audience participates in the interactive process of digital interactive artwork, they hope that no matter how much their participation is, they can produce the corresponding effects or even unpredictable random effects. If the final effect is too predictable, it will make the audience. The participation and interactivity of works are greatly reduced.

Under the macroscopic concept of creative methods, art creation methods refer to the methods used by artists when creating works, including the whole process from selecting themes and determining the subject matter, to actual production and completion of the work. The artist's worldview and artistic outlook have a decisive influence on the creative method. Some of them focus on creating works based on certain abstract concepts and models, some focus on creating works based on objective reality, and some focus on creating works based on the artist's own spiritual feelings. When artists choose specific art creation methods according to their own worldview and artistic outlook, they mainly solve the problem of the relationship between content and form. The same subject matter content is shown in different forms by artists with different creative methods. It is not uncommon in the history of art. For example, both the neoclassical painter Ingres and the romantic painter Delacroix have painted the theme of "Hero Perseus rescues Andalomeda," forming works of different styles; the Spanish painter Goya expresses their opposition The French aggressors slaughtered the Spanish patriots in an angry protest. They used realistic creative methods to create "The Shot on May 3, 1808" and used romantic creative methods to create "The Devil Satan Eats the Son of Mankind."

According to the abovementioned macrodescription of the theory of creative methods, does digital interactive art also have corresponding methods or laws? The current digital interactive art creation is very similar to interactive design methods and software engineering; so, it can be discussed with the help of design models in computer interface design. There are usually two modes: one is technology-centric creative mode, and the other is human-centric.

For the first type, there are usually three models according to the interface design model: designer model (designer model), implementor model (implementation model), and user model (user model). The relationship between the three models is shown in Figure 1. The designer model usually focuses on the object, performance, interaction process, etc.; the user model usually focuses on the goal, emotion, etc., is the user's "mental model" in the process of interacting with the work, and is the operation that the user feels about the work; the implementer model focuses more on technical implementation issues such as data structures, algorithms, and databases and is a model of how works work. One of the important goals of the designer is to make the designer model and the user model as close as possible, but the technology-centric creative model often lacks this process and is often subject to technical constraints. The result is that the final effect is biased towards the implementer. The model may only reflect the technological content, while ignoring the psychological model of users and audiences.

Human-centered design patterns pay more attention to user models. The user model of an interactive system is the mental image formed subconsciously when the user interacts with the system. Under normal circumstances, a huge user model will be concealed under the dazzling visual effects and novel interaction methods. Norman believes that user

models are related to each person's experience, experience, and cognitive level, and it is often difficult for people to describe their user models, and even in many cases, people are not aware of their existence. The user model is based on each user's expectation and understanding of the system, including the functions and objects provided by the system, how to feedback when the user interacts with the system, and the goals that the user wants to complete during the interaction. According to different user experience, each user's point of view will be slightly different, which also makes the study of user models a more complicated issue, but the user model is still useful as a framework for analyzing, understanding, and judging user behavior. Interaction design expects that different users can interact predictably and intuitively from different perspectives. Therefore, the closer the designer model is to the user model, the user will feel the understanding and ease of use of interactive operations.

The above two types of realization method models are often used in product design and interface design and have great reference significance for digital interactive art creation, but art works are different from products after all. The blind emphasis on listening to the audience will cause complexity in the design of the work on the one hand and weaken the creativity and originality of the artist on the other, making the work lose its spiritual value and practical significance. At the same time, the creation is too much restricted by technical means, which makes the technology-centric creation model also have obvious defects: "Natural Interface-Research on Interaction Design Methods in the Post-PC Era." In the fourth chapter, the waterfall model of the interaction design process model is designed and drawn, which is adapted from the Royce waterfall model in software engineering. The author of this article divides the interaction design process into five steps: research and vision, goal and positioning, technology and design plan, functional prototype, and interactive system model. Each step is linked by evaluation or testing and evaluation.

The core idea of the waterfall model is to simplify the problem according to the process, separate the realization of the function from the design, and facilitate the division of labor and cooperation; that is, the logical realization and the physical realization are separated by the structured analysis and design method. As can be seen in Figure 2, the waterfall model of the interaction design process roughly mimics the development process of the Reuss waterfall model. Each development step is based on the completion of the previous step, and the results of the previous step should be checked when doing the next task, carrying out tests and evaluations, one step at a time, with clear processes and clear responsibilities. All this seems quite perfect, but after careful consideration, many artists will question: is this development and creation process too clear, that is to say, is it too idealistic? Because it is basically impossible to separate the steps so clearly, in each artistic creation process, it enters the design stage when the requirements are clear and completely determined and then enters the construction execution stage when the design is completed until the final completion of the work and product. In the actual operation process, often in the initial stage of creation, the artist may

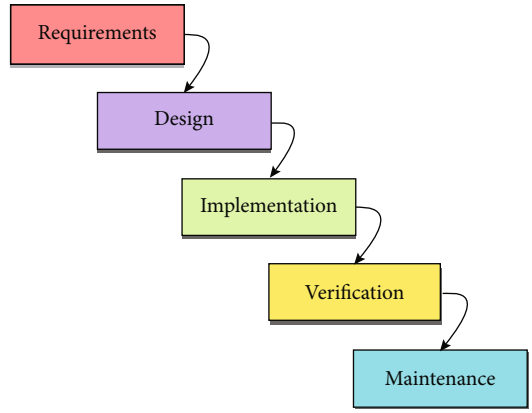

Figure 2: Royce Falls model.

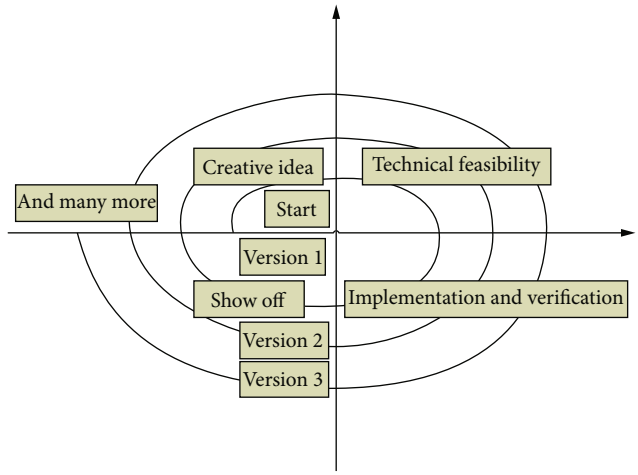

Figure 3: Digital interactive art creation method using the spiral model.

only have a vague and general direction and may not have a complete and clear goal, let alone an accurate demand analysis. Therefore, the interactive creation process based on the waterfall model is too ideal. In the actual creation process, it is necessary to find a more practical and effective model method to optimize the waterfall model.

4.1. Application Examples of Creation and Realization Methods. The characteristics of the spiral model itself are as follows: how to apply this model to digital interactive art creation and ensure that this method really promotes the creation of works. The biggest feature of the spiral model is that it introduces risk analysis that other models do not have, so that the software has the opportunity to stop when major risks cannot be excluded to reduce losses. One of the ways to answer this type of question is to use examples. Successful works can usually help understand the use of models and thus serve as examples for future works creation. Figure 3 shows a digital interactive art creation method using the spiral model.

Version 1 is as follows: creative conception—similar to proposition creation, derived from an exhibition plan of the Organizing Committee of the Liverpool Biennale in 2009, concerning the reconstruction of the Liverpool

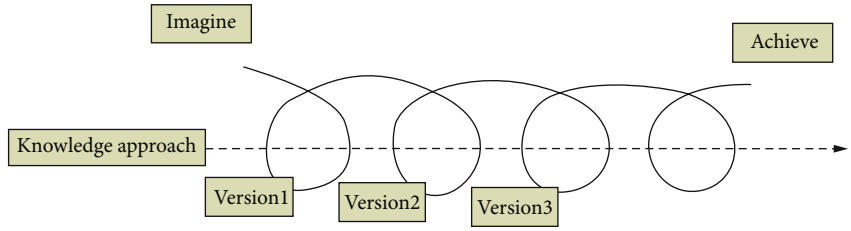

Figure 4: Spiral model entering the iterative process.

suburban canal. The canal connects Liverpool and Newcastle and is an important transportation link and economic artery in the past. In recent years, due to changes in transportation methods, the canal has gradually been abandoned after losing its main transportation function, and the factories beside the river have gradually moved away. Based on this, the Liverpool Biennale has planned a project that hopes to use public art to awaken the residents of Liverpool to renew their attention and remembrance of the canal and to improve the cultural life of the residents in the communities around the canal. According to the background materials provided by the curator, the artist hopes to build a large-scale installation on the bank of the canal, consisting of 72 transparent glass tubes, in which blue spheres made of light materials are placed in advance. When the audience or local residents pass by the device, the corresponding infrared switch is triggered, and the sphere in the tube gradually rises, just like an undulating blue wave, and more like a young girl stretching out her slender hands and dancing in front of you. This is a visual impact and the touch of the heart. Technical feasibility is as follows: there is no doubt that the whole work uses a computer control system. These computers are directly connected to external sensing devices and the air pump in the glass tube. They need to respond to events generated by external hardware and send out corresponding control signals. The designer considers that the work is located outdoors and does not have relatively fixed maintenance personnel. Therefore, when making the technical feasibility plan, the designer hopes to make the entire control system an embedded system and develop an independent single-chip microcomputer as the system control. Realization and verification are as follows: the single-chip microcomputer is triggered by the infrared switch, and the signal to control the air pump switch is sent to achieve the creative effect. In specific practice, the following problems are encountered. First, the friction coefficient between the ball and the pipe wall needs to be reduced to achieve the smooth undulation effect of the ball in the pipe; the second is to reduce the delay of the air pump switch; and the last is the stability of the air pump and many more.

The above process is the complete spiral of version 1. When the concept changes, the second spiral that enters the model is the second iteration of the iterative process. In the creation of digital interactive art, there are many factors that cause the adjustment of ideas, such as technical stability, maturity, funding, venue, and space. Any factor may cause the final work to be inconsistent with the original plan. Due to time and site factors, the project was adopted by Shanghai Shentong Metro Company and will be placed in the Houtan Station of Shanghai Metro Line 7 Expo Park. Although the plan was approved, due to the large differences in site and space, version 2 naturally entered the spiral model.

Version 2 was as follows: creative concept—as there is no direct sunlight underground in the subway station, the artist correspondingly increased the lighting to bring out the crystal clear and suspended effect of the sphere; secondly, there is a large flow of people in the subway station to avoid agglomeration. The effect is that the interaction between the sphere and the audience is changed so that the sphere fluctuates up and down with the rhythm of the music in the station. Technical feasibility is as follows: the overall control is transferred from the outdoor to the indoor control box, a server is used as music data collection, and then the control signals are, respectively, transmitted to each air pump. Realization and verification were as follows: LED spotlights are added in the tube, and designers need to consider the shock absorber structure to alleviate the collision of the sphere with the lights; the method of controlling the air pump switch in version 1 is affected by speed and cannot be synchronized with the rhythm of music. In another way, the air pump is always on, but the control gas displacement is less than the size of the blown sphere, and then the stepless regulator is used to modulate the gas displacement according to the music control signal.

The laws of art are dialectics that exist objectively in art practice as shown in Figure 4. If an artist wants to control his creation, he must understand and correctly use these artistic laws. Naturally, digital interactive art cannot get rid of this rule. The laws of traditional art creation have mature rules and theories in terms of cognition, creation techniques, and aesthetic taste. Therefore, this chapter draws on the knowledge of cognitive psychology, software engineering, and other disciplines and aims at the digital interactive art creation relative to other art types. It puts forward relevant laws and methods for its creative conception and realization method due to its particularity.

5. Conclusion

Through a simple understanding of virtual reality technology and digital media art, it can be seen that there is a great correlation and availability between the two. Digital media art creation based on virtual reality technology is richer in imagination and more diverse. The expressive power and more shocking visual effects have opened the door to a new world for creators and users, thereby making artistic

expression and future development more possible. As an emerging technology, virtual reality technology has certain advantages. Applying it to digital media art creation can effectively make up for the shortcomings of traditional creation and realize the innovative reform of art creation. Therefore, art workers should take a correct view of virtual reality technology, continuously innovate and upgrade virtual reality technology in practice, and give full play to the advantages of virtual reality technology to help digital media art creation industry and digital media art creation workers create. Higher-quality works of art meet the public's requirements for digital media works of art, thereby further promoting the long-term development of the digital media industry. All in all, under virtual reality technology, the forms, styles, and types of digital media art creation are becoming more and more diversified. Ordinary people can use virtual reality technology to create digital media art. Digital media art creation under virtual reality technology provides a good platform for enriching and developing people's imagination and creativity. It is believed that in the near future, as virtual reality technology continues to mature, the integration of virtual reality technology and digital media art creation will further deepen and continue to promote the in-depth development of digital media art creation.

Data Availability

No data were used to support this study.

Conflicts of Interest

The author declares that there are no conflicts of interest regarding the publication of this article.

References

[1] Y. Li, "Application of virtual reality technology in digital media art creation," in *International Conference on Cognitive based Information Processing and Applications (CIPA 2021)*, B. J. Jansen, H. Liang, and J. Ye, Eds., vol. 85 of Lecture Notes on Data Engineering and Communications Technologies, pp. 820–825, Springer, Singapore, 2022.

[2] P. Christiane, *Digital Art*, Thames & Huson (World of Art), New York, 2008.

[3] M. Rush, *New Media in Art*, Thames & Huson (World of Art), New York, 2005.

[4] C. Paul, "New media in the white cube and beyond: curatorial models for digital art," *Leonardo Reviews Quarterly*, vol. 1, no. 2010, p. 33, 2008.

[5] M. Tribe and R. Jana, *New Media Art*, Taschen Gmbh, 2006.

[6] L. Moreno, "Museums and digital era: preserving art through databases," *Collection Building*, vol. 38, no. 4, pp. 89–93, 2019.

[7] H. Kessler, L. Dangellia, S. Herpertz, and A. Kehyayan, "Digitale medien in der psychotherapie – neue ansätze und perspektiven in der behandlung von traumafolgestörungen," *PPmP-Psychotherapie·Psychosomatik Medizinische Psychologie*, vol. 70, no. 9/10, pp. 371–377, 2020.

[8] T. A. Ceranoglu, "Inattention to problematic media use habits: interaction between digital media use and attention-deficit/hyperactivity disorder," *Child and Adolescent Psychiatric Clinics of North America*, vol. 27, no. 2, pp. 183–191, 2018.

[9] J. Chan, J. Yeung, N. Wong, R. Tan, and N. Musa, "Utilising digital media as enabling technologies for effective correctional rehabilitation," *Safer Communities*, vol. 18, no. 1, pp. 30–40, 2019.

[10] B. Wands, *Art of the Digital Age*, Thames & Huson, New York, 2007.

[11] J. Blais and J. Ippolito, *At the Edge of Art*, Thames & Huson, 2006.

[12] S. K. Card, T. P. Moran, and A. Newell, *The Psychology of Human-Computer Interaction*, Lawrence Erlbaum Associates, Hillsdale, NJ, 1983.

[13] A. D. Norman, *The Design of Everyday Things*Doubleday/Currency, New York.

[14] M. Banzi, *Getting started with Arduino*, O'Reilly media, 2009.

[15] D. M. I. Lopes, *A Philosophy of Computer Art*, Routledge, 2010.

[16] S. Poole, "Trigger Happy: Videogames and the Entainment revolution," *Arcade Publishing*, vol. 29, p. 226, 2000.

[17] A. Bentkowska-Kafel, *Digital Visual Culture: Theory and Practice (Computers and the History of Art)*, Chicago University Press, 2009.

[18] A. Bentkowska-Kafel, *Digital Art History: Computers and the History of Art*, Chicago University Press, 2005.

[19] S. Wilson, *Art Science Now: How Scientific Research and Technological Innovation Are Becoming Key to 21st-Century Aesthetics*, Thames & Hudson, 2010.

[20] M. Lovejoy and D. Currents, *Art in the Electronic Age*, Routledge, 2004.

[21] R. Colson, *The fundamentals of digital art*, Bloomsbury Publishing, 2007.

[22] W. Lieser, *The world of digital art*, Ullmann Publishing, 2010.

[23] L. Candy and Z. Bilda, "Understanding and evaluating creativity," in *Proceedings of the 6th ACM SIGCHI Conference on Creativity & Cognition*, pp. 303-304, Washington, DC, USA, 2009.

[24] X. X. Zhu, D. Tuia, and L. Mou, "Deep learning in remote sensing: a comprehensive review and list of resources," *IEEE Geoscience & Remote Sensing Magazine*, vol. 5, no. 4, pp. 8–36, 2017.

[25] X. Wang, L. Gao, and S. Mao, "CSI phase fingerprinting for indoor localization with a deep learning approach," *IEEE Internet of Things Journal*, vol. 3, no. 6, pp. 1113–1123, 2016.

Hindawi
Wireless Communications and Mobile Computing
Volume 2023, Article ID 9783176, 1 page
https://doi.org/10.1155/2023/9783176

Retraction

Retracted: Design and Application of Land Resource Management System Based on Internet of Things

Wireless Communications and Mobile Computing

Received 17 October 2023; Accepted 17 October 2023; Published 18 October 2023

This article has been retracted by Hindawi following an investigation undertaken by the publisher [1]. This investigation has uncovered evidence of one or more of the following indicators of systematic manipulation of the publication process:

(1) Discrepancies in scope
(2) Discrepancies in the description of the research reported
(3) Discrepancies between the availability of data and the research described
(4) Inappropriate citations
(5) Incoherent, meaningless and/or irrelevant content included in the article
(6) Peer-review manipulation

The presence of these indicators undermines our confidence in the integrity of the article's content and we cannot, therefore, vouch for its reliability. Please note that this notice is intended solely to alert readers that the content of this article is unreliable. We have not investigated whether authors were aware of or involved in the systematic manipulation of the publication process.

Wiley and Hindawi regrets that the usual quality checks did not identify these issues before publication and have since put additional measures in place to safeguard research integrity.

We wish to credit our own Research Integrity and Research Publishing teams and anonymous and named external researchers and research integrity experts for contributing to this investigation.

The corresponding author, as the representative of all authors, has been given the opportunity to register their agreement or disagreement to this retraction. We have kept a record of any response received.

References

[1] Q. Song, "Design and Application of Land Resource Management System Based on Internet of Things," *Wireless Communications and Mobile Computing*, vol. 2022, Article ID 2726673, 14 pages, 2022.

Hindawi
Wireless Communications and Mobile Computing
Volume 2022, Article ID 2726673, 14 pages
https://doi.org/10.1155/2022/2726673

Research Article

Design and Application of Land Resource Management System Based on Internet of Things

Qian Song

School of Land Science and Technology, China University of Geosciences, Beijing 100083, China

Correspondence should be addressed to Qian Song; songqian@cugb.edu.cn

Received 25 May 2022; Revised 4 July 2022; Accepted 11 July 2022; Published 11 August 2022

Academic Editor: Jun Ye

In order to further solve the problems existing in the process of land resource management of relevant departments of land and resource management, realize the information management of land resources, and promote the efficient utilization of land resources and scientific information management, this paper proposes a land resource management system based on Internet of things technology. With the help of resource allocation and management algorithm based on the needs of Internet of things users and land resource management requirements, this paper constructs a land resource management system based on Web and mobile network platform. The system development takes Java as the background programming language, constructs the database based on Oracle 9i, and uses GIS/GPS and other electronic map functions to realize the accurate display and resource sharing of land resource information. In the system test, 60, 120, 240, and 360 concurrent users are simulated to access the system at the same time. The connection success rates of the corresponding system are 97.2%, 97.5%, 98.3%, and 96.6%, respectively, which fully verifies the good performance of the system; it can be widely used in land resource information management.

1. Introduction

Land resource is an important basic guarantee resource of a country and region, which can provide a strong basic guarantee for the economic development of a country and region. At the same time, on the premise of providing people with the necessary material basis for production and life, the use of land has also attracted much attention. For a long time, as a large agricultural country with a land area of 9.6 million square kilometers, we have always attached great importance to land management. With the rapid development of information technology, relevant departments have also begun to actively carry out information construction. The system uses the application of information technology to strengthen the protection of land resources and the scientific management of land resources [1]. As the land and resource departments pay more and more attention to the acceleration of information construction, some information systems related to land resource management have also appeared one after another. However, at present, there are still some problems in the existing system and information development direction, such as untimely data update and inconvenient query, in terms of land resource information retrieval and project change, which also hinders the scientific development, management, and application of land resources [2]. Therefore, we must strengthen the application of land resource management technology and further improve the efficiency of land resource management with the help of information technology such as the Internet of things.

2. Literature Review

Foreign countries are widely used in the field of information technology. They have been involved in the application of GIS for a long time and have developed a series of software platforms to provide developers with use, so as to improve the development and application of GIS. As early as the 1990s, they have begun to provide GIS information for office staff [3]. Mobile GIS was initially applied in outdoor data collection and gradually developed and applied to today's mobile positioning system, real-time navigation system,

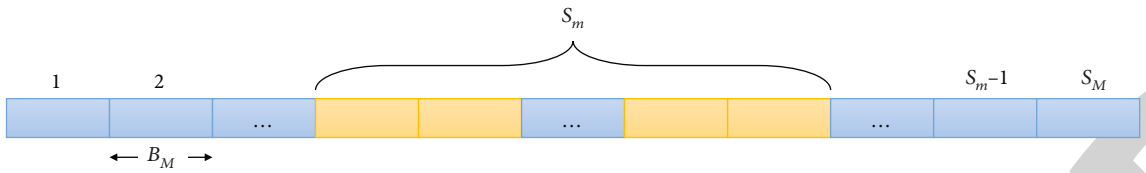

Figure 1: Subchannel allocation.

location-based information service (LBS), and other aspects, with great success [4]. Autodesk onsite launched by a foreign company is a mobile service solution. It provides a comprehensive set of tools for mobile terminal development. With these tools, developers can provide perfect technical implementation for mobile development and complete synchronous or offline processing in data processing [5]. If you cannot connect to the network, you can work offline to ensure that the data can be submitted centrally after the user is connected to the network. Onsite provides rich functions: navigation, zooming, and zooming to the selected figure; feature selection and viewing; display symbols in proportion; hot connect to database report; add labels to relevant contents; pop up feature labels; and support color and monochrome display. There are more than 800 kinds of arbitrary coordinate representation diagrams, support standard data format, reliable and compressed data transmission, etc. MapX Mobile launched by some companies is a MapX platform that can be used in Pocket PC [6]. It can be developed and used as a third-party plug-in in the software system and can be well applied to the software development process of computer and mobile terminal. MapX Mobile is a natural extension of MapX and MapXtreme for Windows, through which Windows programmers can develop mobile software [7]. Similarly, Chinese experts and scholars, especially some university researchers, are also studying the GIS on mobile devices with the help of various means. With the help of data collection and processing in the experimental area, some scholars have realized the collection and management of land information on Trimble GeoXT Mobile GIS equipment. At the same time, they can update the land information in time and realize the submeter precision processing of land information through the differential processing method [8]. Through the analysis, it can be seen that the research results play a great role in China's land information collection and management. It can be popularized and used in China's land information collection and research. Some scholars put forward the Ninghai County Land Information Management System based on mobile GIS. The system completes the comprehensive statistical analysis of the land situation of Ninghai County through the comprehensive use of electronic map technology and mobile positioning technology, which makes the land management mode realize the information transformation. The system can complete the services such as land positioning, information viewing, and information query and realize the concept of providing services for land information [9].

3. Algorithm of User Demand Resource Allocation and Management System Based on Internet of Things

3.1. System Model. This section mainly describes a broadband IoT communication scenario using in-band deployment, in which only a single base station is deployed. Make the MTC welcome you according to the NB-bT standard, and all MTCES share a PRB bandwidth for uplink data transmission [10]. The MTCES in single base station NB-IoT network are divided into two types: delay-sensitive equipment and non-delay-sensitive equipment. The two types of equipment are randomly deployed in the network.

Suppose the number of DS devices in the network system is M, the number of non-DS devices is U, and the DS devices are expressed as

$$M = \{m_1, \cdots, m_M\}. \tag{1}$$

The number of non-DS equipment is

$$U = \{u_1, \cdots, u_U\}. \tag{2}$$

Each DS device has a data packet that needs to be uploaded to the base station, and it is required to fully upload the task within the specified delay. The upload task of DS device is expressed as

$$\{p_m, d_m, t_m^{\max}\}, \tag{3}$$

where p_m represents the transmission power of the DS device, d_m represents the packet size uploaded by the DS device to the base station, $t_m^{\max}$ represents the minimum delay requirement of the device, and the maximum value of $t_m^{\max}$ will not exceed $T_{\max}$. On the contrary, non-DS equipment only requires data packets to be successfully uploaded to the base station without delay requirements, which can be described as $\{p_u, d_u\}, u \in U$, where p_u represents the power of the transmission equipment and d_u represents the size of data packets to be uploaded by the equipment [11]. Next, we will focus on the system modeling in this scenario, that is, communication model and subcarrier allocation model.

(1) Communication model

It is shown in Figures 1 and 2.

The resource allocation method of DS equipment is to jointly allocate time slot resources and spectrum resources.

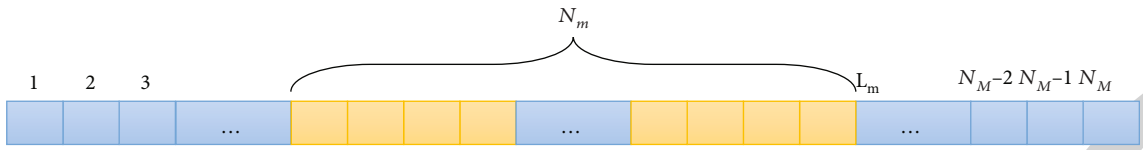

Figure 2: Time slot allocation.

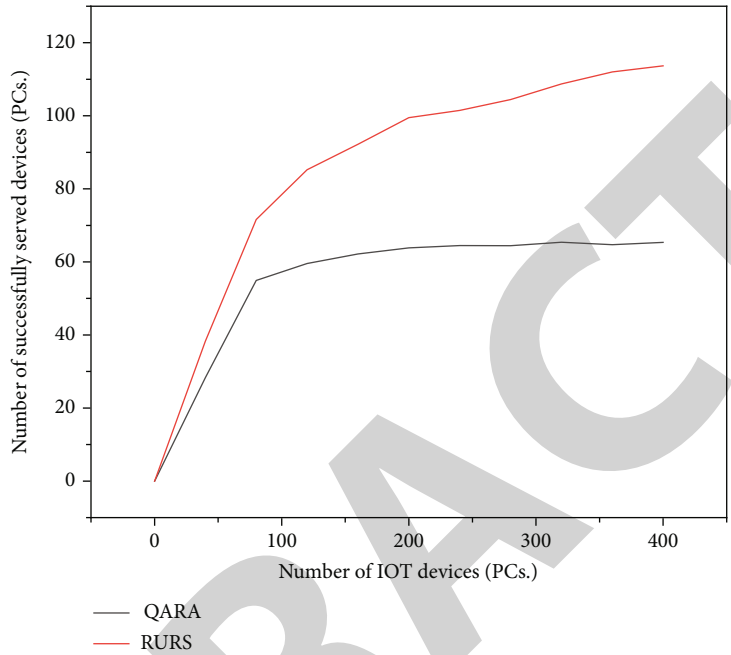

Figure 3: Variation curve of the number of successful service devices with the total number of devices.

Spectrum resources and time slot resources are allocated continuously, as shown in Figures 1 and 2. Based on the allocated number of subcarriers S_m, the uplink transmission rate r_m obtained by DS device m can be expressed as

$$r_m = S_m B_M \log_2\left(1 + \frac{|h_m|^2 p_m}{S_m B_m N_o}\right), \quad \forall_m \in M, \tag{4}$$

where S_m represents the subcarrier bandwidth of the system, N_o represents the noise power spectral density, and h_m represents the channel gain with the base station due to factors such as propagation and fading [12]. According to the time slot resource N_m allocated to the device by the system, the amount of data that the DS device can upload to the base station can be expressed as

$$D_m = r_m N_m T_{\text{slot}}, \quad \forall_m \in M, \tag{5}$$

where T_{slot} represents the size of a single time slot.

According to the time slot and spectrum resources allocated by the system to DS device m, the minimum transmission amount D_m that m can complete can be calculated. The data transmission amount should be greater than the data packet uploaded by DS device, that is,

$$D_m \geq d_m, \quad \forall_m \in M. \tag{6}$$

Meanwhile, the data uploading process of DS device m must meet its own delay requirements, as shown in the following formula:

$$L_m T_{\text{slot}} \leq t_m^{\max}, \quad \forall_m \in M, \tag{7}$$

where L_m represents the time slot position for completing the data packet upload. The following content mainly introduces the communication model of non-DS device u. According to the number S_u of NB-IoT network subcarriers allocated to u, the uplink rate obtained by device u can be expressed as

$$r_u = S_u B_U \log_2\left(1 + \frac{|h_u|^2 p_u}{B_u N_o}\right), \quad \forall_u \in U, \tag{8}$$

where B_U represents the subcarrier bandwidth of the non-DS device and h_u represents the channel gain between the non-DS device u and the base station due to factors such as propagation and fading [13]. Through the number of allocated time slots N_u, the amount of data D_u transmitted by device u can be obtained, which can be expressed as

$$D_u = r_u N_u T_{\text{slot}}, \quad \forall_u \in U. \tag{9}$$

Since non-DS equipment only requires to upload data

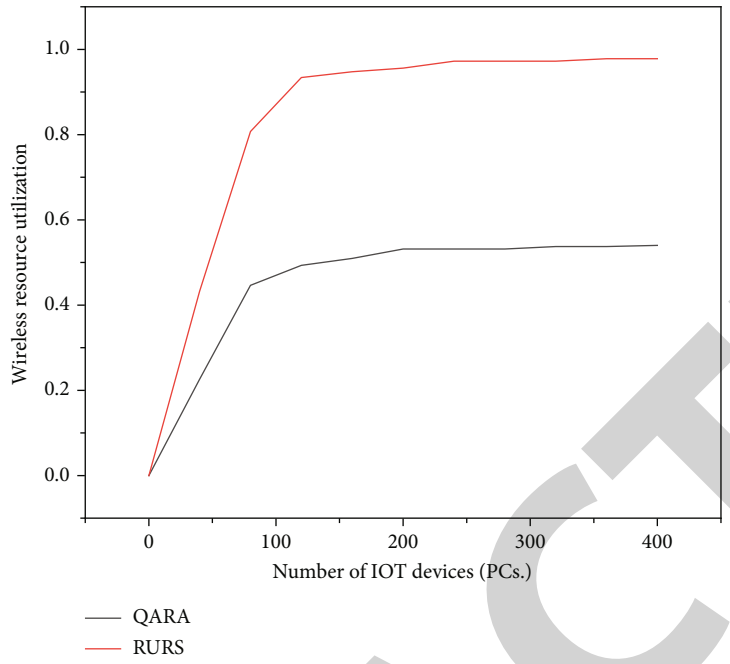

Figure 4: Variation curve of resource utilization rate with the total number of equipment.

packets, the amount of data that can be uploaded D_u should exceed the uploaded data packets of non-DS equipment, that is, d_u:

$$D_u \geq d_u, \quad \forall_u \in U. \tag{10}$$

(2) Subcarrier allocation model

For the resource allocation algorithm of non-DS equipment, the available spectrum resources of the system are divided into S_U subcarriers, and the subcarrier bandwidth is expressed as B_U. According to the difference between DS and non-DS devices, the total time slot resource is divided into two parts, which are denoted as and respectively [14]. The constraints between N_M and N_U are as follows:

$$N_M + N_U = N. \tag{11}$$

The model stipulates that a single time slot under the same subcarrier can only be allocated to a single DS device or a single non-DS device. This restriction is as follows:

$$\begin{aligned} \sum_{m \in M} o_{s,n,m} \leq 1, \quad & s = 1, \cdots, S_M, n = 1, \cdots, N_M, \\ \sum_{u \in U} p_{s,n,u} \leq 1, \quad & s = 1, \cdots, S_U, n = 1, \cdots, N_U. \end{aligned} \tag{12}$$

According to NB-IoT standard, it has the following constraints on subcarrier bandwidth selection and subcarrier allocation. The uplink transmission bandwidth of NB-IoT system is 180 kHz and supports the interval between two subcarriers, which is expressed as set $B = \{3.75\,\text{kHz}, 15\,\text{kHz}\}$. When the subcarrier is 3.75 kHz, the system only supports single-carrier transmission, while when the subcarrier is 15 kHz, the system supports both single-carrier transmission and multicarrier transmission [15]. According to the above situation, the constraints can be obtained:

$$B_M, B_U \in B. \tag{13}$$

In addition, NB-IoT standard imposes constraints on subcarrier allocation, especially for multicarrier transmission. In the multicarrier transmission mode, the standard stipulates that a single device can be allocated 1, 3, 6, or 12 consecutive subcarriers, represented by set $C = \{1, 3, 6, 12\}$. Thus, the subcarrier allocation constraints of the device are as follows:

$$\begin{aligned} S_m \in C, \quad & \forall_m \in M, \\ S_u \in C, \quad & \forall_u \in U. \end{aligned} \tag{14}$$

3.2. Algorithm Design and Implementation. The main idea of this algorithm is to decompose the above problem into two subproblems: DS device resource algorithm and non-DS device resource allocation algorithm [16]. It is assumed that the devices are randomly deployed within the coverage of the base station, and the number of non-DS devices is greater than that of DS devices. The total time slot resources are divided into two parts according to the proportion of the two devices, which can be expressed as

$$N_M = \begin{cases} N_1, & N_1 \leq N_2, \\ N_2, & N_1 > N_2, \end{cases} \tag{15}$$

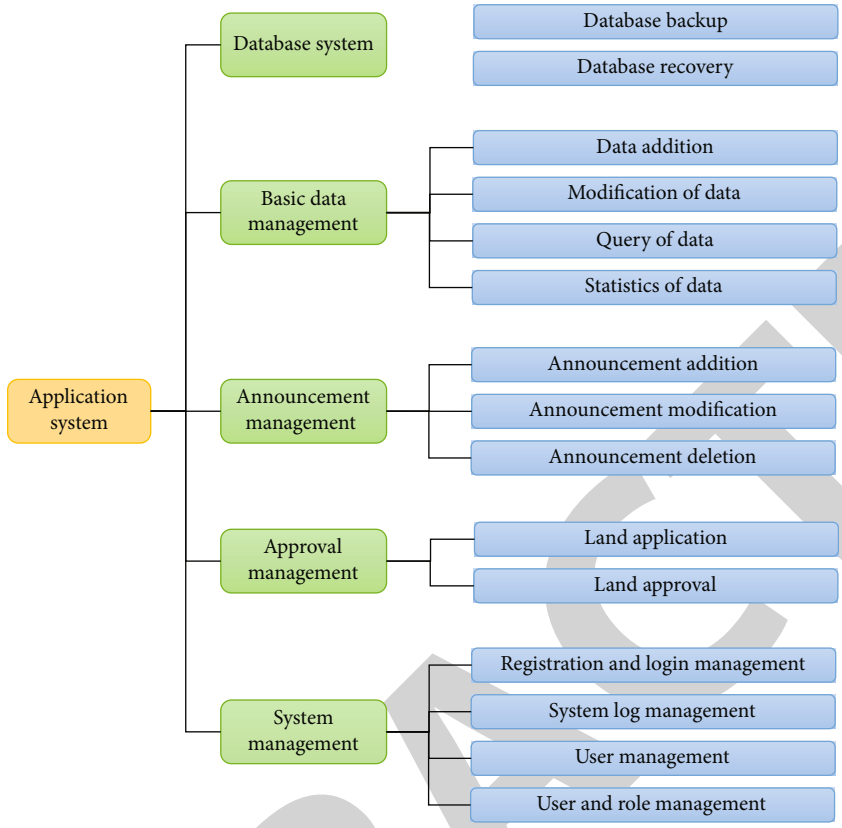

Figure 5: Function module diagram.

where

$$N_1 = \left[\frac{T_{\max}}{T_{\text{slot}}}\right], \quad N_2 = \left[N \times \frac{U}{U+M}\right]. \tag{16}$$

In the whole algorithm, due to the delay demand of DS equipment, the front part of the overall time slot resources is allocated to DS equipment, and the remaining time slot resources are allocated to non-DS equipment. Considering the effectiveness and rationality of overall resource allocation, these two parts of resources adopt different resource allocation algorithms [17]: the first half adopts dynamic continuous multicarrier allocation algorithm, and the second half adopts single-carrier proportional fair allocation algorithm.

3.3. Algorithm Simulation Results. Figure 3 shows the curve of the number of devices successfully served by NB-IoT system with the total number of devices. In the process of simulation, it is assumed that the ratio of non-DS to DS equipment is 1 : 1, and the number distribution interval of equipment is [0400]. It can be seen from the figure that the curve of RURS algorithm first increases linearly; then, the growth rate slows down, and finally, the curve converges. And then, the number of service devices requested in the network gradually tends to the capacity of the system. Therefore, the curve increases slowly. When the number of service devices requested by the system is much greater than the system capacity, the limitation of system wireless resources leads to the stability of RURS curve [18]. The reason for the linear growth of RURS algorithm curve is that the available wireless resources of the system are greater than the resources requested by the overall equipment, and then, the number of service devices requested in the network gradually tends to the capacity of the system. Therefore, the curve increases slowly. When the number of service devices requested by the system is much greater than the system capacity, the limitation of system wireless resources leads to the stability of RURS curve. The curve trend of QARA

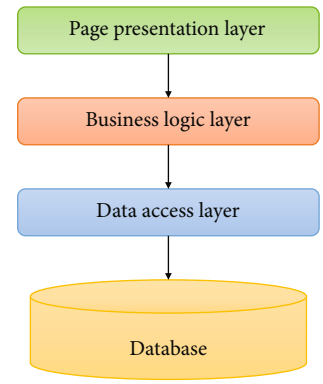

Figure 6: Architecture design of land resource management system.

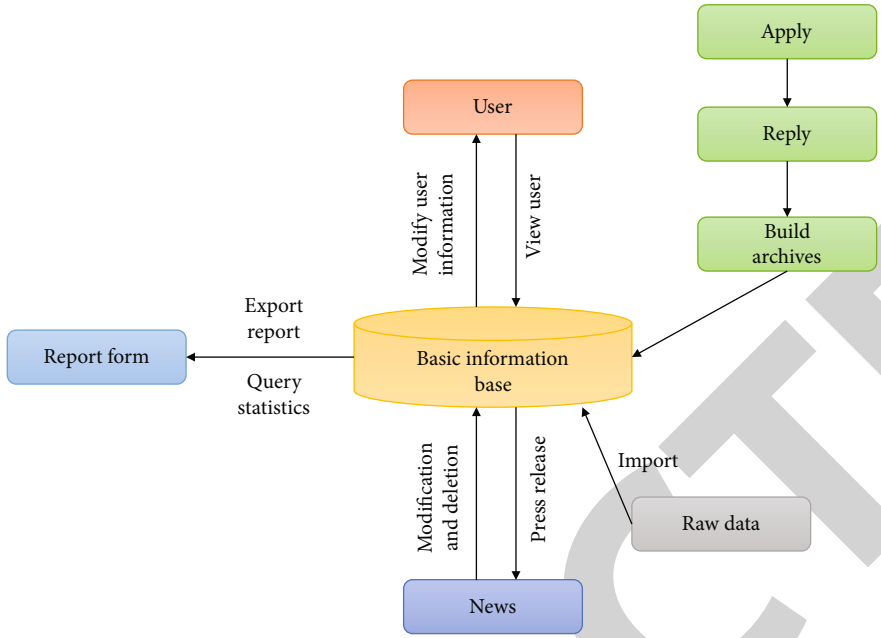

Figure 7: System data flow chart.

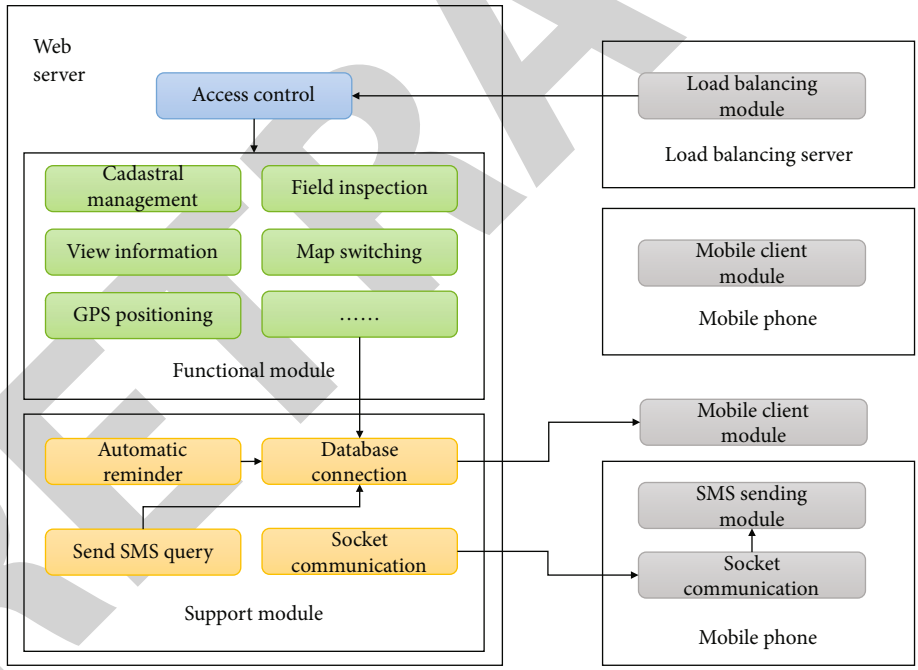

Figure 8: System logic structure diagram.

algorithm is also linear first, and then, the growth rate slows down, but the curve of QARA does not tend to be stable in the end but grows at an extremely slow rate. To a certain extent, low QoS devices are easy to meet the demand. With the gradual increase of randomly generated low QoS devices, the number of successful service devices increases very slowly under the condition of equal resources [19]. Finally, the reason why the curve does not tend to be stable is that due to the proportional fairness algorithm based on system capacity, to a certain extent, low QoS devices are easy to meet the demand. With the gradual increase of randomly generated low QoS devices, the number of successful service devices increases very slowly under the condition of equal resources. By comparing the curves of RURS algorithm and QARA algorithm, it can be seen that QARA algorithm performs better than RURS algorithm in terms of the performance index of the number of successful service devices of the system, and QARA algorithm is nearly 80% higher than

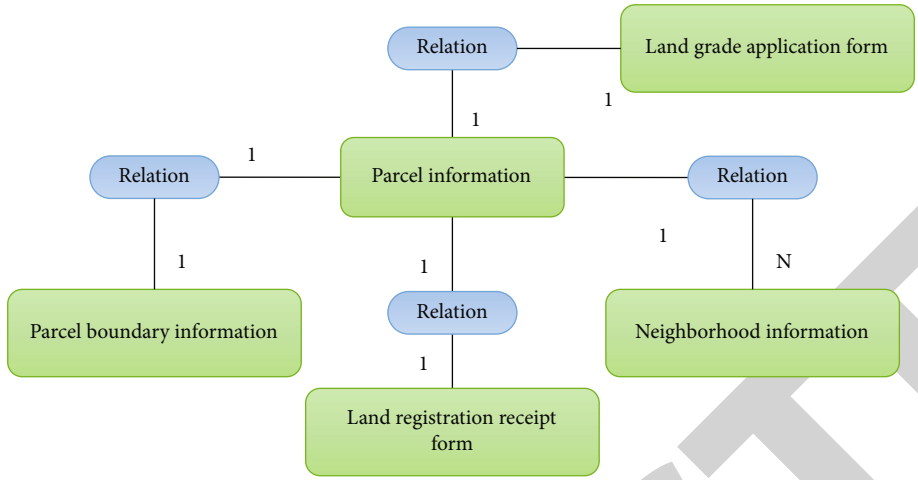

Figure 9: System E-R diagram.

RURS algorithm when the algorithms are close to convergence.

Figure 4 shows the change curve of system wireless resource utilization with the total number of system equipment. In the process of simulation, it is assumed that the ratio of non-DS to DS equipment is 1 : 1, and the number distribution interval of equipment is [0400]. The growth rate of RUQRS algorithm is linear, and then, the growth rate of RUQRS algorithm is linear. The reason for the initial linear growth is that the number of devices is far less than the system capacity, resulting in the linear growth of the wireless resources actually allocated to devices. When the sum of DS and non-DS devices requesting services approaches the system capacity, the growth rate slows down due to the competition of wireless resources between devices. Finally, both QARA and RURS algorithms converge because the wireless resources of the system are limited. When the number of devices requesting services is far greater than the system capacity, the proportion of resources successfully used reaches a constant value. By comparing the curves of RURS algorithm and QARA algorithm, it can be seen that the system resource utilization rate of QARA algorithm is always higher than that of RURS algorithm. When both converge, QARA algorithm improves the wireless resource utilization rate by nearly 80% compared with RURS algorithm. The reasons why the performance of QARA algorithm is better than RURS are as follows: (1) the size of Ru is limited, so that the resources allocated to design economy cannot be fully utilized in RURS; and (2) the time slot resources allocated to the equipment in the RURS algorithm cannot meet the communication requirements of the equipment and waste resources [20].

The simulation results show that QARA algorithm, a dynamic resource allocation algorithm based on user QoS, breaks the performance constraints of large-scale scenarios in NB-IoT networks. From the simulation results, it can be seen that QARA algorithm has greatly improved the performance index of the number of successful service devices of the system. The simulation results shown in Figures 3 and 4 show that QARA algorithm has stronger applicability and can improve or maintain the original performance in scenarios with higher and lower QoS requirements. Through the above description, we can prove that the narrowband Internet of things resource allocation algorithm proposed in this chapter is scientific and effective.

4. Overall System Design

4.1. System Function Design. Land resource management information system mainly includes the management of basic land data, database management, announcement release management, system management, and other main functions.

(1) Land data management

The contents involved in land data management are relatively comprehensive, mainly including the management of various data of mining area, road, well pad, and station site.

(2) Database management

The database management includes database backup and recovery functions.

(3) Information release management

The information release management includes the release, modification and deletion of notices, announcements and other contents

(4) System management

Users verify their identity when logging in to determine their operation permissions. Only users with permissions can enter the management system for relevant operations. Different users have different permissions, etc. [21].

The functions of the system are shown in Figure 5.

The land resource management information system adopts the typical system architecture mode of ASP.NET Web application: database-data access layer-business logic layer-page presentation layer, as shown in Figure 6.

Table 1: Scheme of one book four.

Field name	Chinese name	Data type	Can it be blank	Remarks
Specification No.	Instruction serial number	nvarhcar	No	Primary key
AssociatedNo.	Item serial number association	nvarhcar	No	Foreign key
ResponsiblePerson	Principal	nvarhcar	No	Foreign key
Applicant Name	Name of applicant	nvarhcar	No	
Project Name	Entry name	nvarhcar	No	
ProjectC/BName	Project county/city/batch name	nvarhcar	No	
AppITotalArea	Total area of applied land	nvarhcar	Yes	
NewLand area	New land area	nvarhcar	Yes	
TotalS ituation	Total current situation_total	nvarhcar	Yes	
TotalCurrent SitO	Total current situation_state owned land	nvarhcar	Yes	
TotalCurrent SitC	Total current situation_collective land	nvarhcar	Yes	
TotalAgriculturalLand	Agricultural land_total	nvarhcar	Yes	
OwnedAgricuLand	Agricultural land_state-owned	nvarhcar	Yes	
CollecAgricuLand	Agricultural land_collective	nvarhcar	Yes	
Total arable land	Cultivated land_total	nvarhcar	Yes	
State-owned farmland	Cultivated land_state-owned	nvarhcar	Yes	
CollectiveFarmland	Cultivated land_collective	nvarhcar	Yes	
TotalBasicFarmland	Basic farmland_total	nvarhcar	Yes	
State-ownedFarmland	Basic farmland_state-owned	nvarhcar	Yes	
BasicFarmland _ collective	Basic farmland_collective	nvarhcar	Yes	
TotalWoodland	Woodland_total	nvarhcar	Yes	
State-ownedForest	Woodland_state-owned	nvarhcar	Yes	
Woodland _ collective	Woodland_collective	nvarhcar	Yes	
Total1	Total 1	nvarhcar	Yes	
Total2	Total 2	nvarhcar	Yes	
Total3	Total 3	nvarhcar	Yes	
Owned1	State-owned 1	nvarhcar	Yes	
Owned2	State-owned 2	nvarhcar	Yes	
Owned3	State-owned 3	nvarhcar	Yes	
Group1	Collective 1	nvarhcar	Yes	
Group2	Collective 2	nvarhcar	Yes	
Group3	Collective 3	nvarhcar	Yes	
ConnAssoBounSur	Association survey boundary connection	nvarhcar	Yes	
AssodAddiLand	Cultivated land connection	nvarhcar	Yes	
AssesAgen	Evaluation authority	nvarhcar	Yes	
EvaluReportNo	Appraisal report no	nvarhcar	Yes	
ProjectAppTime	Project approval time	nvarhcar	Yes	
DesignAppTime	Design approval time	nvarhcar	Yes	
ConstruFunds	Composition of construction funds	nvarhcar	Yes	
ProjectConsPeriod	Project construction period	nvarhcar	Yes	
AddLandWay	Supplementary cultivated land mode	nvarhcar	Yes	Foreign key
Remarks	Remarks	nvarhcar	Yes	

4.2. Module Design. The process of data flow and storage in the process of land resource management can be vividly represented by business flow chart and table distribution chart. Data flow diagram (DFD) is a tool to describe the system data flow. It can get rid of the physical content and describe the context and actual flow of information in a graphical way [22]. It is the most important tool to describe the logical model of management information system. The operation flow chart of some modules of the system is shown in Figure 7 below.

4.3. System Logic Architecture. There are many users accessing the system. In order to ensure the stable operation of the system, the system sets up a load balancing module. In

Table 2: District land supply information.

Field name	Chinese name	Data type	Can it be blank	Remarks
PartitionNo	Partition serial number	nvarhcar	No	Primary key
ReportingInstructionsNo	Serial number of submission instruction	nvarhcar	No	Foreign key
ProvideWays	Mode of provision	nvarhcar	No	Foreign key
FunctionPartitionName	Function partition name	nvarhcar	No	
ForArea	Land supply area	Float	No	
SettingUses	Set purpose	nvarhcar	No	
AssessPrice	Evaluation price	Float	Yes	
PriceProposed	Proposed unit price	Float	Yes	
LandLife	Land use years	Float	Yes	Unit (month)

Table 3: Agricultural land conversion scheme.

Field name	Chinese name	Data type	Can it be blank	Remarks
ReportingInstructionsNo	Serial number of submission instruction	nvarhcar	No	Primary key
TotalA griculturalLand	Agricultural land_total	nvarhcar	No	
OwnedLandArea	State owned land area	Float	No	
CollectiveLand Area	Collective land area	Float	No	
TotalArable	Cultivated land_total	Float	No	
OwnedArable	Area of state-owned cultivated land	Float	No	
FarmlandArea	Collective cultivated land area	Float	Yes	
NationalPlanning	In line with national planning	nvarhcar	Yes	
ProvincialPlanning	In line with provincial planning	nvarhcar	Yes	
CityPlanning	In line with municipal planning	nvarhcar	No	
CountyPlanning	In line with county-level planning	nvarhcar	No	
TownshipPlanning	In line with township planning	nvarhcar	No	
AdjustNationalPlanning	Adjust national planning	nvarhcar	No	
AdjustProvincialPlanning	Adjust provincial planning	nvarhcar	Yes	
AdjustCityPlanning	Adjust municipal planning	nvarhcar	Yes	
AdjustCountyPlanning	Adjust county-level planning	nvarhcar	Yes	
AdjustTown shipPlanning	Adjust township level planning	nvarhcar	Yes	
PlanTargets	Planned indicators of this year	nvarhcar	Yes	
CarryoverPlanTargets	Carry forward plan indicators	nvarhcar	Yes	
UseAgriculturalLandTargets	Proposed agricultural land index	nvarhcar	Yes	
UseFarmlandIndex	Proposed cultivated land index	nvarhcar	Yes	
PlanTargetsDescription	Indicator description of carry forward plan	nvarhcar	Yes	

Table 4: Development system and some related tools.

Name	Edition
Operating system	Windows Server 2008
Database	Oracle 9i
Application server	Tomcat7.0
Development system	Eclipse4.4
Android development documentation and debugging tools	Android SDK Software Development Kit
Struts development kit	Version 3.0
Plug-in unit	Android Development Tools (ADT)

Table 5: System operation software environment.

Server side	Windows 2008 or IIS7.0 operating system
Client	Android system

order to ensure the security of the system, the access rights open to each type of users are different. The system sets up an access control module to control the access rights based on user roles to ensure the security of the system. The functional modules of the system mainly include cadastral management, field patrol, GPS positioning, information viewing, and map switching. Each module collaborates independently and realizes information interaction through universal standard and extensible interface. In the application management system based on smart phones, the socket communication module is essential, and the corresponding function module is SMS sending module. Land information is managed by relational database. Among them, the system logic architecture design is shown in Figure 8.

4.4. Database Design

(1) Design principles

The design requirements of the database are very high, and the design is carried out in accordance with the specifications. The specific requirements of the system are as follows:

(1) Normative requirements: the data table must be named according to the standard of "T_ English Table name," so that when developers call each other, they can know what function the table is designed to achieve by looking at the database name. For the naming of fields, they must be named in capital letters, and easy-to-understand English should be used for naming as much as possible [23]

(2) Modification principle: the management of land resources is affected by many factors. Once these factors change, the database of the system may change, such as adding a field, deleting a field, and modifying a field type. These operations must be completed by the database administrator, and others have no authority to modify the able structure

(3) Paradigm control principle: in order to pursue perfection, some systems need the database to reach the third paradigm. In this system, due to more access to the database, especially the query business, the requirements for database specification are not so strict. When necessary, effective redundant fields can be set to realize the query of a large amount of data, so as to avoid the use of connection symbols in the retrieval process and improve the access efficiency

(2) Entity relationship design

According to the system data analysis and business research, the entities involved in the system mainly include parcel information, land registration application form, land registration receipt form, and parcel boundary information. A parcel is associated with multiple neighborhood information, so the relationship between them is $1:n$; A parcel of land information is associated with a land registration application form, so the relationship between the two is 1 : 1. A parcel information is associated with a parcel boundary information, so the relationship between the two is 1 : 1. A parcel of land information is associated with a land registration receipt table, so the relationship between the two is 1 : 1. As shown in Figure 9, various business entities that will be used in the system are sorted out, and finally, the E-R diagram is formed.

(3) Design data sheet

First is one book and four schemes.

One book and four schemes are mainly used to record the information of the construction land application submitted by the construction unit to relevant units, including the name of the application unit, project name, total area of applied land, area of newly added land, agricultural area, and cultivated land area; among them, the logical structure design of the information table of one book and four schemes is shown in Table 1.

Second is district land supply information.

The regional land supply information table is mainly used to record the land information approved by each construction land application unit. The main fields include regional serial number, serial number of submission specification, mode of supply, land supply area, set purpose, evaluation price, and land use years; among them, the logical structure design of the regional land supply information table is shown in Table 2.

Third is agricultural land conversion scheme.

In the process of land use, due to the needs of urban planning, agricultural land may be converted to construction land. The information table of agricultural land conversion scheme is used to record this conversion scheme. The fields mainly include serial number of submission specification, agricultural land area, state-owned land area, collective land area, provincial planning, and municipal planning. Among them, the logical structure design of agricultural land conversion scheme information table is shown in Table 3.

4.5. System Realization

(1) Implementation environment

Due to the compatibility of Java language with multiple systems and combined with practical analysis, the program development language of this subject is Java language [24]. A series of development systems and development tools involved in the whole process of system development and design are shown in Table 4.

The requirements of system operation software environment are shown in Table 5.

The hardware environment requirements required by the system are shown in Table 6.

Table 6: Hardware environment requirements.

	Configuration requirements
The server	The main frequency of CPU is 2.5 to 3.0 GHz, with more than 2 G memory, and the server has a backup hard disk. The minimum configuration requires that the main frequency is not less than 2.0 GHz and the memory is not less than 1 G
Network bandwidth	Bandwidth system with high speed, stability, and excellent network environment
Client	Android smartphone

Table 7: User login test.

Project	Function and description
Case name	User login function test case
Function description	When entering the system, the user needs to enter the user name, password, and other relevant information in the login interface. After clicking "login," the system will judge whether this information matches the information in the database. If it passes the verification, it will log in to the system. Otherwise, it will give information prompt
Execution process	Open the system login page, enter user information in the text box, and then click the "login" button
Input	User name: 1001, password: 1, user type: inspector
Expected output	Log in to the inspector system interface of smartphone terminal software
Actual output	Log in to the inspector system interface of smartphone terminal software

Table 8: Information release function test table.

Project	Function and description
Case name	Information release function test case
Function description	After entering the system, the administrator of the land department will create a new "information release" information of land resources. After filling in the release content, the system will automatically verify and click the "release" button. If it is complete, call the save method to save it to the database. If it is incomplete, prompt the user to modify and improve it
Execution process	(1) Successfully logged in to the system (2) Select information type (3) Enter release information (4) Integrity verification, incomplete to 5, complete to 6 (5) Prompt users to modify and improve (6) Save publishing information (7) End
Input	Mandatory parts and some necessary non mandatory parts of the information to be published
Expected output	If the information is incomplete, the system will give a prompt. If the information is complete, the system will save and return the result
Actual output	After all the required inputs are entered, the information is published successfully, and the system returns the corresponding operation results; the system can also give a prompt when the required input content is incomplete.

(2) Implementation of Web services

The EJB service endpoint does not need a corresponding Home interface, and SOAP does not implement reference transfer, so it is impossible to transfer a reference from a Web service interface or Home interface to a remote interface. In addition, it is also impossible to create and delete a Web service, so the Home interface does not need to be defined.

(3) Service description

If JAX-RPC belongs to the specification of the agreed Web service client, WSDL is the corresponding specification of the agreed Web service server and makes relevant detailed conventions and descriptions for the Web service specification, in which the description mainly includes the three most basic characteristics of the Web service:

What the service does: the operations or methods provided and supported by the service.

How to access the service: the supported data format details the necessary protocols related to the operation of accessing the service.

Where the service is located: the relevant network address determined through a specific protocol, such as URL.

Next is through the login service in the public service in the training and examination management system with typical characteristics, i.e., authority authentication service, as an analysis case.

Table 9: Summary of function test results.

Test item	Result			Test item	Result		
	Success times	Number of errors	Success rate (%)		Success times	Number of errors	Success rate (%)
Hyperlink jump check	100	0	100	Data update check	99	1	99
Submission check of duplicate data	97	3	97	Input and inspection of non-conforming data	97	3	97
Specified number of input values	99	1	99	Information addition function check	100	0	100
Information modification function check	98	2	98	Information query function check	100	0	100
Data saving check	99	1	99	System user permission check	100	0	100
Information deletion check	99	1	99				

Table 10: Server software performance test.

Content	Test result			
Server software	Server software			
Number of clients	60	120	240	360
CPU usage (%)	6	6	8	7
Physical memory usage (M)	122	124	137	133
One time connection success rate of client (%)	98.3	98.5	97.2	96.7

4.6. System Test

(1) Function test

The purpose of testing is to find problems in the developed software system this morning and solve them in time, so as to avoid more investment in maintenance after delivery to users. According to the requirements of software system development, this is the last step before delivery to users. After the system test, the problems found in the system should be quickly modified and improved [25]. In the test phase, the function test of the system adopts the method of black box test, and professional testers write test cases and form standard test reports.

First is login function test.

The login function of the system is fully tested, and the designed test table is described in Table 7.

Second is information release function test.

This function is mainly aimed at the operation of the administrator of the system. The test process design of land resource information release function is described in Table 8.

The summary table of function test results includes eleven items, including hyperlink jump check, submission check of duplicate data, input of specified number of values, information modification function check, data saving check, and system information deletion check. The summary table and test conditions are described in Table 9.

(2) Performance test

The system provides an interface for users to submit land use application information or view land resource use information through the interface; because the use information of land resources is very important, especially when measuring land use, relevant data should be submitted and saved to the server in time, so it is necessary to verify and save these data. If incomplete, give a clear and simple hint. If complete, call the save interface. In the process of statistical analysis of land resources utilization, it is necessary to analyze a large number of experimental data submitted by investigators. One or two or even thousands of land resource information cannot reflect the complete utilization of land resources. Therefore, in order to improve the pertinence of the system test and the persuasion of the data, the system simulates 300 concurrent users to access the query and statistics function at the same time, and the amount of statistical data reaches 8 million. After executing the test script, the test result is within 1 s, which meets the needs of users.

It is mainly to conduct destructive test on the bearing capacity of the server, so as to determine the service capacity of the server. There are about 200 users using the system. During the test, the paper simulates 60, 120, 240, and 360 concurrent users to access the system at the same time and records the changes of various parameters of the server. The statistical results are shown in Table 10.

After analyzing the test contents and data in Table 10, it can be seen that the resource occupancy rate is relatively low, the response is relatively timely, and the system performance is good and meets the nonfunctional requirements. Through the analysis of the above test results, it can be seen that the functional design of the system meets the needs of users and can accept the concurrent operation requests of the required number of users; the server has good performance, can process the statistical analysis and summary of big data,

and can improve the work efficiency and ensure the accuracy of land resource information in the process of land resource management. The paper makes a comprehensive test on the implemented system, writes test cases, executes test scripts, and generates concurrent users. The test results show that the system has complete functional design, stable performance, and long-term and stable operation and supports the operation and use of users. The server has good performance and can handle the statistical analysis and summary of big data. It can improve the work efficiency and ensure the accuracy of land resource information in the process of land resource management. On the whole, the system has passed the test.

5. Conclusion

In this study, the mobile development platform based on Android, combined with ArcGIS Server, map tile, ArcGIS Server API for Android, and mobile positioning technology, takes the current situation of land resource management as the starting point, takes the early data and map information as the data source, and develops the "land resource management system based on mobile platform" through the analysis of land resource management business. The system can be installed on smart phones or tablets with different operating systems. The updated GIS service obtains ArcGIS Server map service through 4G network, which realizes the query of land information anytime and anywhere in land management. Through the shared API, the editing and updating of geographic data attributes, GPS positioning, and field inspection are realized. The playback of the path can be realized through the intelligent terminal. It can also publish land resource information. The development of this system is not only a part of the information construction of the land department but also a challenge for the crossplatform application of mobile GIS. In the future, crossplatform mobile GIS will have more mobile application markets. The main content is to test the function and performance of the system. The proportion of software testing in the whole system R & D cycle is very large. System testing is not the last stage of the system R & D cycle but runs through the whole system R & D cycle. System testing is a key step to verify the quality and stability of the system. In the system test, 60, 120, 240, and 360 concurrent users were simulated to access the system at the same time. The corresponding system connection success rates were 98.3%, 98.5%, 97.2%, and 96.7%, respectively. The system finally passed the test and met the needs of users. The paper makes a comprehensive test on the implemented system, writes test cases, executes test scripts, and generates concurrent users. The test results show that the system has complete functional design, stable performance, and long-term and stable operation and supports the operation and use of users. The server has good performance and can handle the statistical analysis and summary of big data. It can improve the work efficiency and ensure the accuracy of land resource information in the process of land resource management. On the whole, the system has passed the test.

Data Availability

All the data supporting the results were shown in the paper and can be available from the corresponding author.

Conflicts of Interest

The author declares that there is no conflict of interest regarding the publication of this paper.

References

[1] C. Guo, S. Su, K. Choo, P. Tian, and X. Tang, "A provably secure and efficient range query scheme for outsourced encrypted uncertain data from cloud-based Internet of Things systems," *IEEE Internet of Things Journal*, vol. 9, no. 3, pp. 1848–1860, 2021.

[2] A. D. Nawkhare, P. H. Vaidya, M. K. Ghode, and N. S. Titirmare, "Assessment of soil quality of Babhalgaon village of Latur district for soil health and land resource management by using remote sensing and GIS techniques," *International Journal of Current Microbiology and Applied Sciences*, vol. 9, no. 7, pp. 4009–4023, 2020.

[3] W. Zhang, X. Wang, G. Han, Y. Peng, and M. Guizani, "SFPAG-R: a reliable routing algorithm based on sealed first-price auction games for Industrial Internet of Things networks," *IEEE Transactions on Vehicular Technology*, vol. 70, no. 5, pp. 5016–5027, 2021.

[4] E. Juhi Jasiha and R. R. Dr, "Implementation of ABMS with Cuk converter for enhanced battery life using Internet of Things," *International Journal for Modern Trends in Science and Technology*, vol. 7, no. 5, pp. 107–111, 2021.

[5] K. Ding, W. Li, J. Sun, X. Xiao, and Y. Wang, "Convolutional neural network for voltage sag source azimuth recognition in electrical Internet of Things," *Wireless Communications and Mobile Computing*, vol. 2021, Article ID 6656564, 2021.

[6] D. Zheng, Y. Yang, L. Wei, and B. Jiao, "Decode-and-forward short-packet relaying in the internet of things: timely status updates," *IEEE Transactions on Wireless Communications*, vol. 20, no. 12, pp. 8423–8437, 2021.

[7] A. Sharma and R. Kumar, "Risk-energy aware service level agreement assessment for computing quickest path in computer networks," *International Journal of Reliability and Safety*, vol. 13, no. 1/2, p. 96, 2019.

[8] Q. H. Han, "Research on the construction of cold chain logistics intelligent system based on 5G ubiquitous Internet of Things," *Journal of Sensors*, vol. 2021, no. 1, Article ID 6558394, 11 pages, 2021.

[9] L. Rosa, F. Silva, and C. Analide, "Mobile networks and internet of things infrastructures to characterize smart human mobility," *Smart Cities*, vol. 4, no. 2, pp. 894–918, 2021.

[10] X. Xie, "Construction of innovative computer training education mode under the environment of multiple intelligences Internet of Things," *Journal of Intelligent and Fuzzy Systems*, vol. 41, no. 13, pp. 1–11, 2021.

[11] M. Ghosh and D. Gope, "Hydro-morphometric characterization and prioritization of sub-watersheds for land and water resource management using fuzzy analytical hierarchical process (FAHP): a case study of upper Rihand watershed of Chhattisgarh State, India," *Applied Water Science*, vol. 11, no. 2, pp. 1–20, 2021.

Hindawi
Wireless Communications and Mobile Computing
Volume 2023, Article ID 9805273, 1 page
https://doi.org/10.1155/2023/9805273

Retraction

Retracted: Enterprise Management Resource Protection System Based on Digital Information Technology

Wireless Communications and Mobile Computing

Received 17 October 2023; Accepted 17 October 2023; Published 18 October 2023

This article has been retracted by Hindawi following an investigation undertaken by the publisher [1]. This investigation has uncovered evidence of one or more of the following indicators of systematic manipulation of the publication process:

(1) Discrepancies in scope
(2) Discrepancies in the description of the research reported
(3) Discrepancies between the availability of data and the research described
(4) Inappropriate citations
(5) Incoherent, meaningless and/or irrelevant content included in the article
(6) Peer-review manipulation

The presence of these indicators undermines our confidence in the integrity of the article's content and we cannot, therefore, vouch for its reliability. Please note that this notice is intended solely to alert readers that the content of this article is unreliable. We have not investigated whether authors were aware of or involved in the systematic manipulation of the publication process.

Wiley and Hindawi regrets that the usual quality checks did not identify these issues before publication and have since put additional measures in place to safeguard research integrity.

We wish to credit our own Research Integrity and Research Publishing teams and anonymous and named external researchers and research integrity experts for contributing to this investigation.

The corresponding author, as the representative of all authors, has been given the opportunity to register their agreement or disagreement to this retraction. We have kept a record of any response received.

References

[1] W. Zhou, "Enterprise Management Resource Protection System Based on Digital Information Technology," *Wireless Communications and Mobile Computing*, vol. 2022, Article ID 3277750, 13 pages, 2022.

Hindawi
Wireless Communications and Mobile Computing
Volume 2022, Article ID 3277750, 13 pages
https://doi.org/10.1155/2022/3277750

Research Article

Enterprise Management Resource Protection System Based on Digital Information Technology

Wenya Zhou

School of Economics, Sichuan University, Chengdu, 610065 Sichuan, China

Correspondence should be addressed to Wenya Zhou; 18409494@masu.edu.cn

Received 11 April 2022; Revised 11 June 2022; Accepted 4 July 2022; Published 10 August 2022

Academic Editor: Jun Ye

Enterprise management resource protection is a system management activity in which an enterprise conducts comprehensive planning, allocation, utilization, and development of its resources, and it is the process of organizing, planning, coordinating, supervising, and controlling the allocation, utilization, and development of enterprise resources. The purpose of this paper is to analyze the system that digital information technology applies to enterprise management by constructing models and combinations based on digital information technology so that the built models and combinations have a more effective analysis and research. This paper first gives a general introduction to digital information technology, then analyzes the theory of enterprise management resource protection, then establishes a model for information technology to act on enterprise management, and finally analyzes the combination of information technology and enterprise management and compares the two through enterprise case analysis. The experimental results show that in the case of enterprise management in various regions, the efficiency of enterprise management based on digital information technology is obviously higher, and the enterprise resources can be better protected. From 2018 to 2021, the development of enterprise management resource protection in various regions is basically showing an upward trend; it increased from 3.443, 5.414, 6.473, 4.382, 2.997, 3.751, 0.506, and 2.974 in 2018 to 6.187, 7.658, 8.601, 7.518, 5.932, 6.516, 3.877, and 6.243 in 2021. This is a good demonstration of the effectiveness of the protection of enterprise management resources based on digital information technology.

1. Introduction

With the rapid development of the domestic economy, the protection of enterprise resources in enterprise management has become a hot issue in the current business circle. Many scholars believe that resources are an important factor that increases people's work pressure, which in turn affects people's physical and mental health. In recent years, scholars have paid more and more attention to the theoretical research of enterprise resource protection based on enterprise management. Digital information technology mainly uses geographic information system, communication network, and multimedia technology to build a digital system, so as to organize, process, transmit, query, and display the collected information, in order to assist the decision-making in enterprise resource protection in enterprise management and comprehensively guide the progress of enterprise management resource protection.

Today, with the rapid development of Internet technology, the whole country is a "digital city." This paper uses digital information technology to provide a technical support for solving the problem of enterprise resource protection in enterprise management, provides a standardized and scientific information management for it, and builds an effective enterprise management system. This also has a very far-reaching impact on the development of the enterprise. The application scope of digital information technology is very wide, and the use of digital information technology can meet the comprehensive management of enterprises. But in recent years, the research on digital information technology for enterprise management is relatively less. Therefore, the application of digital information technology to the research

of enterprise management resource protection has certain theoretical and practical significance.

2. Related Work

With the progress of society, more and more people have studied digital information technology. Theis proposed that "Moore's Law" will open a new era, and the focus of information technology research and development will shift from miniaturization of time-honored technologies to coordinated introduction of new devices, new integration technologies, and new architectures for computing [1]. However, many such studies have emerged and may be lacking in innovation. Later, Habib studied the use of mathematical information automation technology to carry out a new management of higher education institutions and successfully provided experience to higher education academia [2]. However, this research system still has some limitations, and it has not been able to successfully identify the characteristics of the system. Wang studied the hypothetical association between digital birth and four common IT addictions. He employed a multidimensional digital information technology approach to compare the associations between specific attributes of digital soundtracks and each type of IT addiction [3]. However, it is clear that the final results did not reach the expected state, and further research is needed. Following this, Li studied the use of these modern information technologies in libraries for common applications through a case study of digital libraries in China. He concluded that artificial intelligence can improve the service level of existing digital libraries from three aspects: resource construction, information organization, and information service [4]. However, the cases he studied were too scattered to fully present his views. Based on research by academics, Given found that the digital technologies used by humanists support traditional ways of working within their disciplines, while also creating potential for new academic practices. The heterogeneous nature of the research practices of humanities scholars is explored and thus has implications for the design of digital tools [5]. However, his research does not take into account the practical significance and is too theoretical. Through his research results, Vanpoucke proposed the use of information technology and found that more and more companies exchange information with each other in order to better cooperate closely with supply chain partners. In his paper, he showed that information exchange was indispensable for business integration [6]. However, such studies are too complex to be appropriate as survey studies for small companies. Subsequently, Yadav studied the design of an optimal low-power digital phase-locked loop. DPLLs use modulators or demodulators in wireless or wired communications to compute fast speeds, low noise or jitter, large bandwidth, and very fast acquisition times [7]. However, this design is not yet complete and has not yet been applied in practice.

The innovation of this paper is as follows: (1) In the enterprise management resource protection project, digital information technology can be used to quickly collect, process, integrate and process resources, and then transmit and display them. It is convenient and effective to apply digital information technology to enterprise management, and it can also better conduct a comprehensive management of enterprises. (2) Creating two models for comparison to get better test results. In addition, the advantages and characteristics of digital information technology are deeply studied, and the effective function of applying it to enterprise management resource protection is found out, so as to obtain a better system combination of digital information technology and enterprise management resource protection.

3. Application of Digital Information Technology in Enterprise Management

3.1. Function of Digital Information Technology in Enterprises

3.1.1. The Meaning of Digital Technology and Information Technology. Digital technology is a science and technology that accompanies electronic computers. It refers to a technology that converts various information (such as picture, text, sound, and image) into binary numbers that can be recognized by electronic computers with the help of certain equipment and then operates, processes, stores, transmits, propagates, and restores the numbers [8]. It is also called digital technology, computer digital technology, etc., because it is necessary to use computers to encode, compress, and decode information in operations, storage, and other links. Digital technology is also called digital control technology. Information technology (IT for short) refers to the technology that expands human information functions under the guidance of the basic principles and methods of information science. Generally speaking, information technology is the sum of technologies that realize the functions of information acquisition, processing, transmission, and utilization as the main means of electronic computers and modern communication; it is also a general term for related methods, means, and operating procedures for the management, development, and utilization of information resources.

3.1.2. Judgment Formula of Digital Information Technology. The use of digital information technology can make a comparison and evaluation of things in the enterprise and achieve the standard of fuzzy comprehensive evaluation. Generally, the formula for dealing with multilayer comprehensive evaluation problems is as follows:

$$P = Q \bullet W = Q \bullet \begin{bmatrix} Q_1 \bullet W_1 \\ Q_2 \bullet W_2 \\ \vdots \\ Q_M \bullet W_M \end{bmatrix}. \tag{1}$$

Among them,

$$W_1 = \begin{bmatrix} Q_{1_1} \bullet W_{1_1} \\ Q_{1_2} \bullet W_{1_2} \\ \vdots \\ Q_{1_M} \bullet W_{1_M} \end{bmatrix}, \cdots, W_1 = \begin{bmatrix} Q_{M_1} \bullet W_{M_1} \\ Q_{M_2} \bullet W_{M_2} \\ \vdots \\ Q_{M_N} \bullet W_{M_N} \end{bmatrix}. \tag{2}$$

While,

$$W_{1_1} = \begin{bmatrix} O_1 \\ O_2 \\ \vdots \\ O_o \end{bmatrix}, \cdots, W_{m_n} = \begin{bmatrix} T_1 \\ T_2 \\ \vdots \\ T_t \end{bmatrix}. \tag{3}$$

In the formula, O is the overall comment set on which the judgment is made; $Q; \mathrm{Q}_1 \cdots Q_M; \mathrm{Q}_{\mathrm{M_N}}$ is the weight matrix of each layer; $W_1 \cdots \cdots W; W_{1_1} \cdots \cdots W_{M_N}$ is the judgment transformation matrix of each layer [9].

Since,

$$Q_1 \cdot W_1 = Q_1 \cdot \begin{bmatrix} O_1 \\ O_2 \\ \vdots \\ O_7 \end{bmatrix} = (0.1, 0.1, 0.1, 0.1, 0.1, 0.3, 0.2) \cdot \begin{bmatrix} 0.6 & 0.2 & 0.1 & 0.1 \\ 0.5 & 0.4 & 0.1 & 0 \\ 0.2 & 0.2 & 0.5 & 0.1 \\ 0.3 & 0.5 & 0.2 & 0 \\ 0.2 & 0.4 & 0.3 & 0.1 \\ 0.3 & 0.4 & 0.2 & 0.1 \\ 0.8 & 0.1 & 0.1 & 0 \end{bmatrix} = (0.3, 0.3, 0.2, 0.1), \tag{4}$$

$$Q_2 \cdot W_2 = Q_2 \cdot \begin{bmatrix} D_1 \\ D_2 \\ \vdots \\ D_7 \end{bmatrix} = (0.1, 0.1, 0.2, 0.2, 0.1, 0.3) \cdot \begin{bmatrix} 0.6 & 0.5 & 0.2 & 0.1 \\ 0.5 & 0.3 & 0.2 & 0 \\ 0.4 & 0.3 & 0.3 & 0 \\ 0.3 & 0.4 & 0.3 & 0 \\ 0.3 & 0.4 & 0.3 & 0 \\ 0.4 & 0.3 & 0.3 & 0 \\ 0.5 & 0.4 & 0.1 & 0 \end{bmatrix} = (0.3, 0.3, 0.2, 0.1). \tag{5}$$

Similarly, it can be calculated as

$$Q_3 \bullet W_3 = (0.3, 0.2, 0.2, 0.1). \tag{6}$$

So then, it can get

$$O = Q \cdot W = Q \cdot \begin{bmatrix} Q_1 \cdot W_1 \\ Q_2 \cdot W_2 \\ Q_3 \cdot W_3 \end{bmatrix} = (0.5, 0.2, 0.3) \cdot \begin{bmatrix} 0.3 & 0.3 & 0.2 & 0.1 \\ 0.3 & 0.3 & 0.2 & 0.1 \\ 0.3 & 0.2 & 0.2 & 0.1 \end{bmatrix} = (0.3, 0.3, 0.2, 0.1). \tag{7}$$

This result is normalized to obtain O = (0.33, 0.33, 0.22 , 0.11).

After a calculation of the set digital informatization formula to the enterprise evaluation system, the final result O is obtained. Overall, the application of informatization to enterprises is very effective [10].

3.1.3. Digital Information Technology and Enterprise Management. In the new era, enterprises are facing the challenges of intensified competition and accelerated innovation. In this context, mastering digital information technology becomes more and more important. First of all, digital information technology can expand the information sources of enterprises and enrich the innovation resources of enterprises. This effect is not only reflected in technology, but also in the market, and this is the key point that enterprises value most. As shown in Figures 1 and 2, the logical structure of digital information technology highlights the characteristics of enterprise innovation management mode after using digital information technology.

From this, it can be seen that the application of digital information technology in enterprise management has a very high value. Digital information technology has the function of innovation and integration of different professions.

3.2. Enterprise Management System

3.2.1. Concept of Management System. The enterprise management system mainly stipulates the functional scope, responsibilities, authority, and working procedures and methods of management of various management departments, management positions, and various professional management businesses [11]. The value of enterprise management lies in enabling different employees to work together to achieve enterprise goals; the management system can be regarded as the sum of the rules for regulating and coordinating the behaviors of various departments and personnel, integrating resources, and constraining and adjusting various behaviors and their relationship with resource elements in business management activities [12].

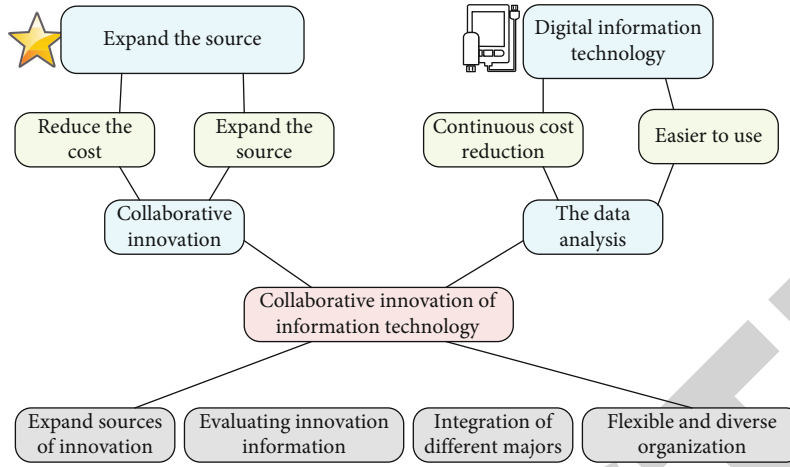

Figure 1: Schematic diagram of digital information technology innovation management model.

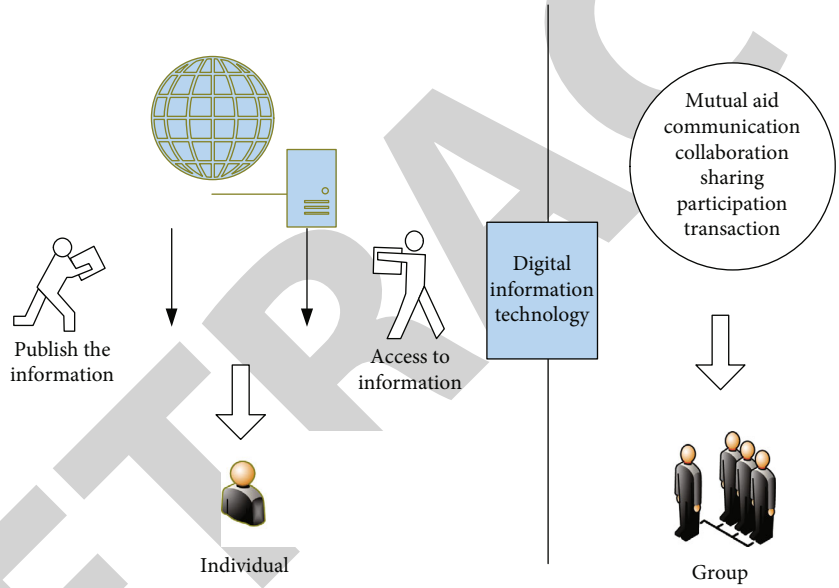

Figure 2: Digital information technology applications.

The management process is also an indispensable part of the enterprise, and the management system can co-evolve with the management process as shown in Figure 3.

The management system is more dependent on the vertical level of the organizational structure, and the process operation is more inclined to the horizontal coordination between departments. The two are parallel in the management system and do not conflict. In practical applications, the two are often combined.

3.2.2. Management system. In the management system, it is assumed that Y and X are two topological spaces; $Z: Y \longrightarrow Y, V: X \longrightarrow X$ are the self-maps of Y and X, respectively. If there is a homeomorphism c from Y to X: $Y \longrightarrow X$, make $c[Z(T)] = K[c(T)]$; then, Z and K are said to be topologically conjugated, denoted as $Z \sim K$. If the inverse $c^{-1}(T)$ of $c(T)$ is substituted into the above formula T, we have

$$c\{Z[c^{-1}(T)]\} = K\{c[c^{-1}(T)]\} = K(T), \tag{8}$$

So it can be concluded that

$$c^{-1}[K(T)] = c^{-1}\{Z[c^{-1}(T)]\} = Z[c^{-1}(T)]. \tag{9}$$

It can also be proved that

$$c[Z^2(T)] = c[Z(Z(T))] = K[c(Z(T))] = K[k(c(T))] = K^2[c(T)]. \tag{10}$$

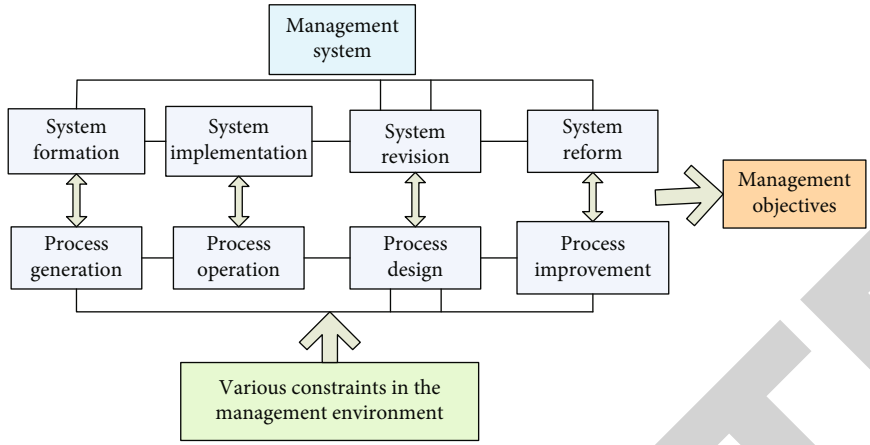

Figure 3: Co-evolution of management system and management process.

The implementation of management system can play the functions of planning, organization, leadership, control, etc. to coordinate organizational resources and improve overall performance and the process of implementation and effectiveness of management system, that is, the process of coordinating and planning the various elements of the enterprise and their interrelationships [13]. Supposing $P = [R_1(A), R_2(A) \cdots R_M(A)]^E$ is the operation of various resource elements of the enterprise, A represents time, and B_X represents the many ways in which the management system coordinates and integrates various resources of the enterprise. Then, the following differential equations can be obtained:

$$\frac{SR_X(A)}{SA} = B_X[R_1(A), R_2(A) \cdots R_M(A)]. \tag{11}$$

Assuming that the function on the right-hand side of the equation is considered in a system of m-dimensional constant coefficient linear differential equations, assuming that B is a 22-constant square matrix, and Y is simplified to a two-dimensional columnwise number, we can obtain

$$\frac{SY}{SA} = BY. \tag{12}$$

Then, the solution that satisfies the initial condition $Y(0) = Y_0$ is

$$Y = W^{SA}Y_0 = \varnothing(A, Y_0). \tag{13}$$

Not only that, $\phi(A, Y_0)$ also has the following properties:

$$\varnothing(A_1 + A_2, Y) = \varnothing(A_2, \varnothing(A_1, Y)). \tag{14}$$

For the convenience of analysis, we consider a two-dimensional constant coefficient dynamical system. Assuming that the system matrix $B = \begin{bmatrix} Q & W \\ E & R \end{bmatrix}$, Y is simplified to $Y = \begin{bmatrix} y \\ x \end{bmatrix}$; the plane constant coefficient homogeneous differential equation can be obtained:

$$\begin{cases} \dfrac{RY}{RA} = QY + Wx \\ \dfrac{Rx}{RA} = EY + Rx \end{cases}. \tag{15}$$

Obviously, $\begin{cases} y = 0 \\ x = 0 \end{cases}$ is a singular point, (QW - ER≠0), which is a non-singular matrix. It can be concluded that

$$\begin{bmatrix} y \\ x \end{bmatrix} = K \begin{bmatrix} \aleph \\ \mu \end{bmatrix} = \begin{bmatrix} t_{11} & t_{13} \\ t_{12} & t_{14} \end{bmatrix} \begin{bmatrix} \aleph \\ \mu \end{bmatrix}. \tag{16}$$

Then, Equation (15) can be transformed into

$$\frac{R}{RA} \begin{bmatrix} \aleph \\ \mu \end{bmatrix} = K^{-1} \begin{bmatrix} Q & W \\ E & R \end{bmatrix} K \begin{bmatrix} \aleph \\ \mu \end{bmatrix}. \tag{17}$$

A non-singular matrix K can be taken such that

$$K^{-1} \begin{bmatrix} Q & W \\ E & R \end{bmatrix} K = P. \tag{18}$$

The management system also has the characteristics of multidimensionality and diversification. Due to various disturbances from the outside of the enterprise, it coordinates various elements and resources of the enterprise in a relative space as a high-dimensional vector field. The dynamic

Table 1: Manage business process design content.

Scholars	Concept	Definition
Davenport and Short	BP redesign	Analysis and design of workflow or various processes within or between organizations
Morrow and Hazel	BP redesign	Examine activities and information flows in key processes for simplification, cost reduction, quality improvement, and flexibility
Short and Venkatraman	BP redesign	The restructuring of internal business processes to improve customer, product distribution, and delivery performance
Short and Venkatraman	BN redesign	Restructure some of the critical products and services that are part of the larger enterprise network
Johansson et al.	BP redesign	It is the means by which an organization obtains radical changes in cost, cycle, service, and quality. It requires a multitool approach with an emphasis on customer-facing core processes
Krajewski and Ritzman	BP redesign	The selection of input elements, resources, workflows, and methods needed to transform inputs into outputs
Kaplan and Murdock	CP redesign	A fundamental rethink of how the enterprise is run, a simultaneous and integrated redesign of workflow, decision-making, organizational, and information systems
Loewenthal	Organizational redesign	To focus on the core competitiveness of the enterprise, the fundamental thinking and redesign of the enterprise process and organizational structure, in order to achieve a huge improvement in organizational performance

equation in the previous section is slightly expanded to get:

$$\frac{RY}{RA} = Q(A)Y. \tag{19}$$

The meaning of the letter remains unchanged, except that it changes from Q to Q(A), and the institutional constraints become a function of time rather than the original constant matrix, which is more in line with the actual situation [14]. Its formula can be:

$$J(A) = \begin{vmatrix} Y_{11(A)} & \cdots & Y_{nl(A)} \\ Y_{\ln(A)} & \cdots & Y_{nn(A)} \end{vmatrix}. \tag{20}$$

Then, Formula (19) has a general solution:

$$Y(A) = \sum_{O=1}^{M} E_O Y_O. \tag{21}$$

3.2.3. Management Process Design. The definition of process design is mentioned in the literature review part of this paper, and some are listed in Table 1. The management business process realizes the implementation of most management systems through the content decomposition of the specific business process and the objective description of the time and space requirements. The research on the management process design must focus on the actual problems in the implementation of the enterprise management system, clarify the role and characteristics of the management process on the realization of management functions, and then explain its formation mechanism and related influencing factors. Based on these interpretive studies, a methodological study of management process design was carried out [15].

Table 2: The clear situation of employees at all levels of P company on their own job responsibilities.

	Ordinary	In the middle	At the top
Very ambiguous	3.85%	0%	0%
Not clear	7.69%	8.23%	33.3%
More clear	23.08%	63.20%	66.7%
Very clear	65.38%	28.57%	0%

3.2.4. Employees' Awareness of the Management System. The compilation of management system is the main form of management system. For example, Company P is an enterprise with only a few hundred employees, and its system compilation is complex, with 15 articles, 154 chapters, and more than 400,000 words, and it is ready to be further expanded. Such a compilation of management systems, even corporate executives may not have the patience and time to read them through [16]. The employees' attention and understanding of the management system also determine its performance effect. The survey results in Table 2 show the degree of clarity of employees at all levels in the company's system to their own-related job responsibilities:

3.3. Theory of Enterprise Resource Protection

3.3.1. The Theoretical Significance of Resource Protection. The theory of resource protection means that enterprises maintain, protect, and gather resources with all their strength and the threat that enterprises face is that they will lose or lose these precious resources. Assuming that the enterprise faces the threat of resource loss, lacks resources, and does not get the corresponding resource return after investing a lot of resources, it will promote the psychological pressure of employees [17]. However, other resources can be used to offset the negative impact of the lack of resources,

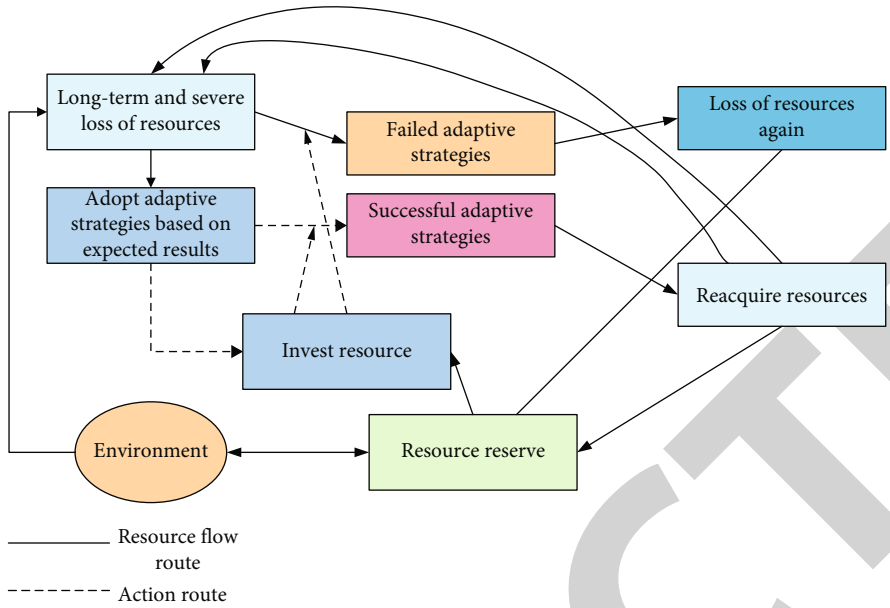

Figure 4: Resource protection model.

and enterprises can replace resources. For example, re-employment of people can greatly reduce the feelings of depression and anxiety caused by long-term unemployment. If people cannot directly replace the resource, indirect or symbolic replacement methods can be used.

3.3.2. Resources in the Theory of Enterprise Resource Protection. Enterprises will seek the resources they need according to the order of physical resources, social resources, and psychological resources. Through the resource conservation theory, maintaining and gathering resources is the main purpose of the enterprise. Therefore, enterprises will not only protect the resources because of the value generated by the resources themselves, but also because the resources help enterprises obtain and protect other meaningful resources. In the theory of "resource protection," resources include physical objects, personal characteristics, identities, abilities, and other resources that employees value, as well as physical objects, personal characteristics, situations, or abilities that enable employees to obtain precious resources [18]. According to the relevant data, the resource protection model can be drawn as shown in Figure 4. It can be seen that a successful enterprise adaptability strategy is to make a circular input in resources to obtain resources.

4. System Demonstration of Enterprise Management Resource Protection after the Application of Information Technology

4.1. Information Technology Panel Model

4.1.1. Ordinary Panel Model. The ordinary panel model can be used to test the linear impact of information technology on enterprise resources. However, the impact of information technology on total factor enterprise resources is not a simple linear relationship and may show a nonlinear relationship with the changes of heterogeneous factors such as the level of information technology and human capital of enterprises in various regions. In order to further judge whether heterogeneous factors such as information technology level and human capital level will cause the influence of information technology on total factor productivity to be nonlinear, this paper uses the panel threshold model to test [19].

There are many variables in the model, such as the degree of opening to the outside world (FDI), the level of marketization (Mar), the level of human capital (Huma), and the level of industrialization (Indu). The descriptive statistics for these variables are shown in Table 3: It can be seen that the marketization level (Mar) has the highest average value of 1.636, indicating that it is most deeply influenced by information technology.

The panel regression results of information technology on the technical efficiency of enterprise resource protection are shown in Table 4. Model (1) and model (2) examine the impact of information technology on technical efficiency under fixed effects and random effects, respectively [20]. And according to the test results, the choice of model (1) is more suitable. From the results, the elastic coefficients of the degree of opening to the outside world, the level of marketization, and the level of industrialization are 0.0002, 0.0007, and 0.0017, respectively, and they all passed the 5% significance test. This shows that the degree of opening to the outside world, the level of marketization, and the level of industrialization have a significant positive impact on technical efficiency.

The impact of information technology on the technological progress of enterprise resources is shown in Table 5. The test results also indicate that model (1) is more suitable. From the results, the elasticity coefficient of information technology after introducing other influencing factors such as the degree of opening to the

Table 3: Descriptive statistics of variables.

Variable	The mean	The standard deviation	The minimum value	The maximum
Total factor productivity (TFP)	**0.005**	**0.011**	**− 0.015**	**0.037**
Technical efficiency (TEC)	**− 0.003**	**0.004**	**− 0.013**	**≤0.001**
Technological progress (TCH)	**0.011**	**0.012**	**− 0.014**	**0.045**
Information technology (IT)	**4.792**	**2.197**	**− 1.937**	**9.399**
Openness (FDI)	**− 4.361**	**1.069**	**− 8.232**	**− 2.606**
Marketization level (mar)	**1.636**	**0.322**	**0.267**	**2.328**
Human capital level (Huma)	**0.556**	**0.096**	**0.302**	**0.862**
Industrialization level (Indu)	**− 0.802**	**0.222**	**-1.697**	**-0.488**

Table 4: Panel regression results of information technology on the technical efficiency of enterprise resource protection.

Variable	(1) FE	(2) RE
IT	− 0.0016∗∗∗ (− 18.484)	− 0.0022∗∗∗ (− 13.075)
FDI	0.0003∗∗ (2.262)	0.00045∗∗∗ (3.407)
Mar	0.0008∗∗ (1.974)	0.0008∗∗ (2.224)
Huma	(0.798) Indu 0.0018∗∗∗	(2.338) 0.0021∗∗∗
Constant	(3.493) − 0.0092∗∗∗	(3.386) 0.0109∗∗∗
F/Wald test Hausman test	347.32 188.61∗∗∗	1132.27
Observations R-squared	390 0.8304	390 0.8246

Note: *, **, and *** represent the significance levels of 0.1, 0.05, and 0.01, respectively.

Table 5: Panel regression results of information technology on the technological progress of enterprise resource protection.

Variable	(1) FE	(2) RE
IT	0.0006∗ (1.708)	− 0.0012∗∗∗ (− 13.074)
FDI	− 0.0001∗ (− 0.362)	0.00054∗∗∗ (3.436)
Mar	0.0049∗∗∗ (1.983)	0.0009∗∗ (2.234)
Huma	(0.797) Indu 0.0017∗∗∗	(2.439) 0.0020∗∗∗
Constant	(3.462) − 0.0092∗∗∗	(3.395) 0.0138∗∗∗
F/Wald test Hausman test	347.33 188.61∗∗∗	172.28
Observations R-squared	390 0.8603	390 0.6249

Note: *, **, and *** represent the significance levels of 0.1, 0.05, and 0.01, respectively.

outside world is 0.0005, and its impact on technological progress is significant at the 10% level. It can be seen that this is very different from the above. This shows that information technology can change the impact of technological progress on enterprise resources by coupling other factors. From this, it can be concluded that improving absorptive capacity will help to improve technological progress through opening to the outside world [21].

5. Three-Threshold Model

This paper starts with a complex three-threshold model using Stata software. As shown in Figure 5, the *P* values of the single threshold and the double threshold are both 0.008, and they have passed the 1% significance test. However, the *P* value of the three thresholds is not significant at the levels of 1%, 5%, and 10%, so the double threshold type should be used [22].

According to the threshold value test results in Figure 6, when the enterprise management resources are used as the threshold variable, the estimated values of the double thresholds are 0.486 and 0.578, respectively, and both have passed the LR test. Based on the double threshold value, the sample is divided into three regions: low level of management resources, medium level of management resources, and high level of management resources [23].

According to the use of the threshold model, it is possible to conduct threshold research on enterprises in different regions. Figure 7 reflects the development of enterprise management resource protection by region from 2018 to 2021. Basically, there is a rising area, from 3.443, 5.414, 6.473, 4.382, 2.997, 3.751, 0.506, and 2.974 in 2018 to 6.187, 7.658, 8.601, 7.518, 5.932, 6.516, 3.877, and 6.243 in 2021. From the average point of view, the highest enterprise management resources in each region are the eastern coastal areas.

5.1. Information Technology Centralized Verification of the Implementation Effect of Enterprise Resource Protection. Information technology can promote technological progress by accelerating the speed of technology introduction and diffusion [24]. The rapid development of information technology has greatly accelerated the speed of information exchange between enterprises and strengthened the technical exchange and cooperation between enterprises. The development of information technology provides a platform and channel for the introduction and diffusion of technology so that enterprises in less developed areas farther away have the opportunity to contact and learn advanced technology and increase exchanges and learning in technology, so as to help narrow the differences in the technical level of enterprises between regions and achieve balanced development. The operation of centralized accounting of information technology also helps to strengthen the management and

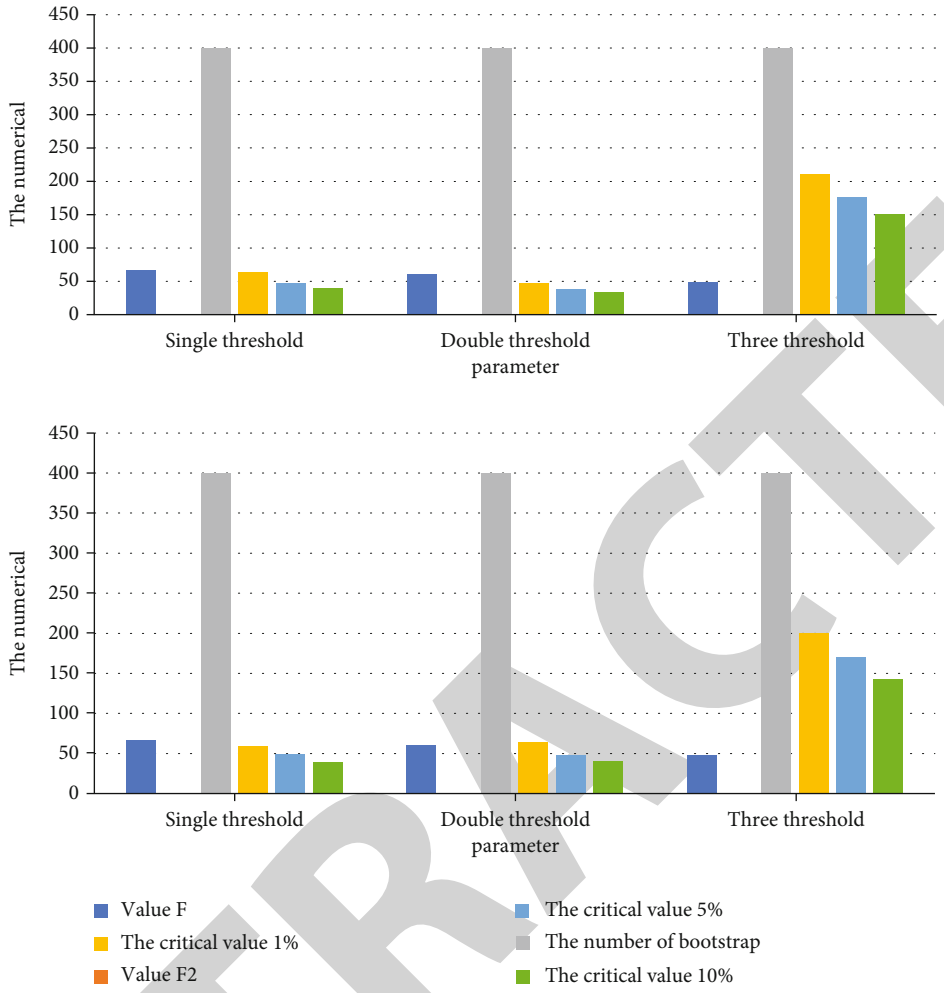

Figure 5: Test results of the three-threshold model and the two-threshold model.

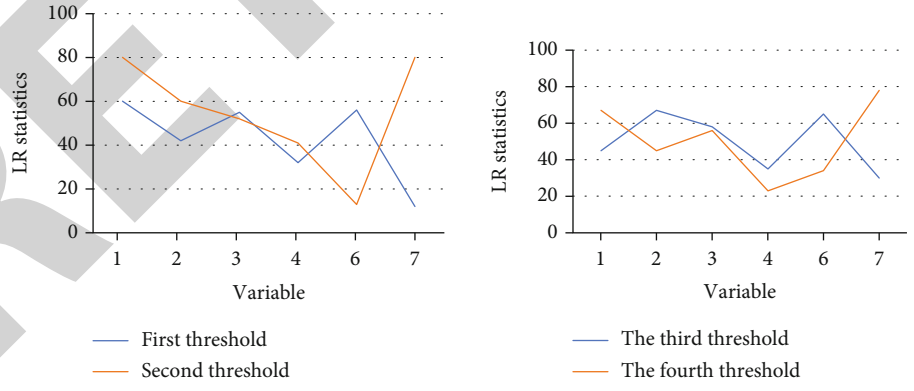

Figure 6: Threshold test (taking enterprise management resources as the threshold variable).

effect of the head office on the prefecture and city branches. Compared with before operation, the leaders of the head office can conduct pre-examination of large-amount matters in information technology accounting and increase supervision and control. At the same time, the financial information system can automatically generate vouchers, and the information technology only needs to check whether the automatically generated vouchers are correct, and there is no need to manually enter the account and amount, which reduces the subjective error of vouchers and improves the quality of enterprise resource accounting.

According to the model system created above, we investigated the data of Company P from 18 to 21 years before and after the implementation of centralized accounting,

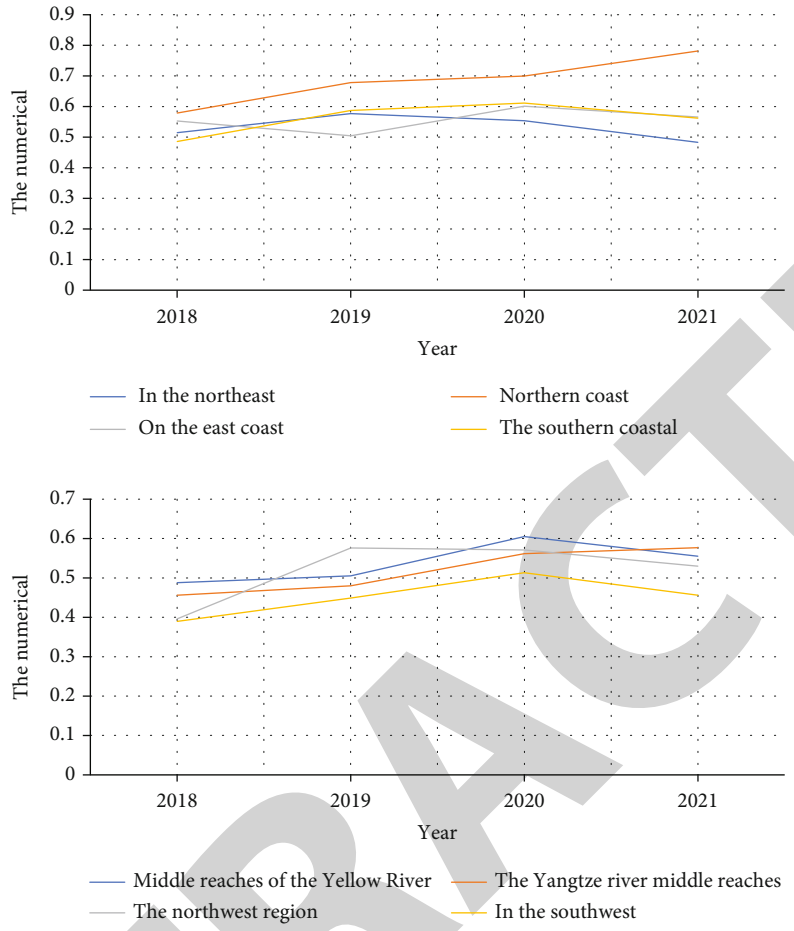

Figure 7: Development of regional enterprise management resources from 2018 to 2021.

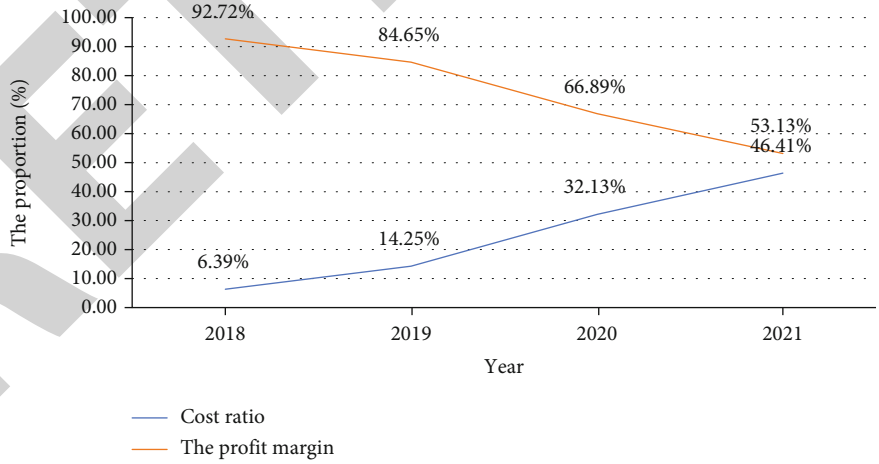

Figure 8: The cost ratio and profit margin of Company P in 2018-2021 year.

and obtained Figure 8 and the conclusion: Since 2020, when the centralized accounting of information technology was implemented, the cost and expense ratio of Company P decreased from 66.85% in 19 years to 53.4% in 20 years. For a company, it is not easy to reduce the cost and expense ratio by 15 points. This also shows from the side that company A has greatly improved its cost control after implementing centralized accounting of information technology.

In addition, we can also find from the comparison of receivables and income and their growth rates in Figure 9: After the implementation of centralized accounting of information technology in 2020, the growth rate of receivables will

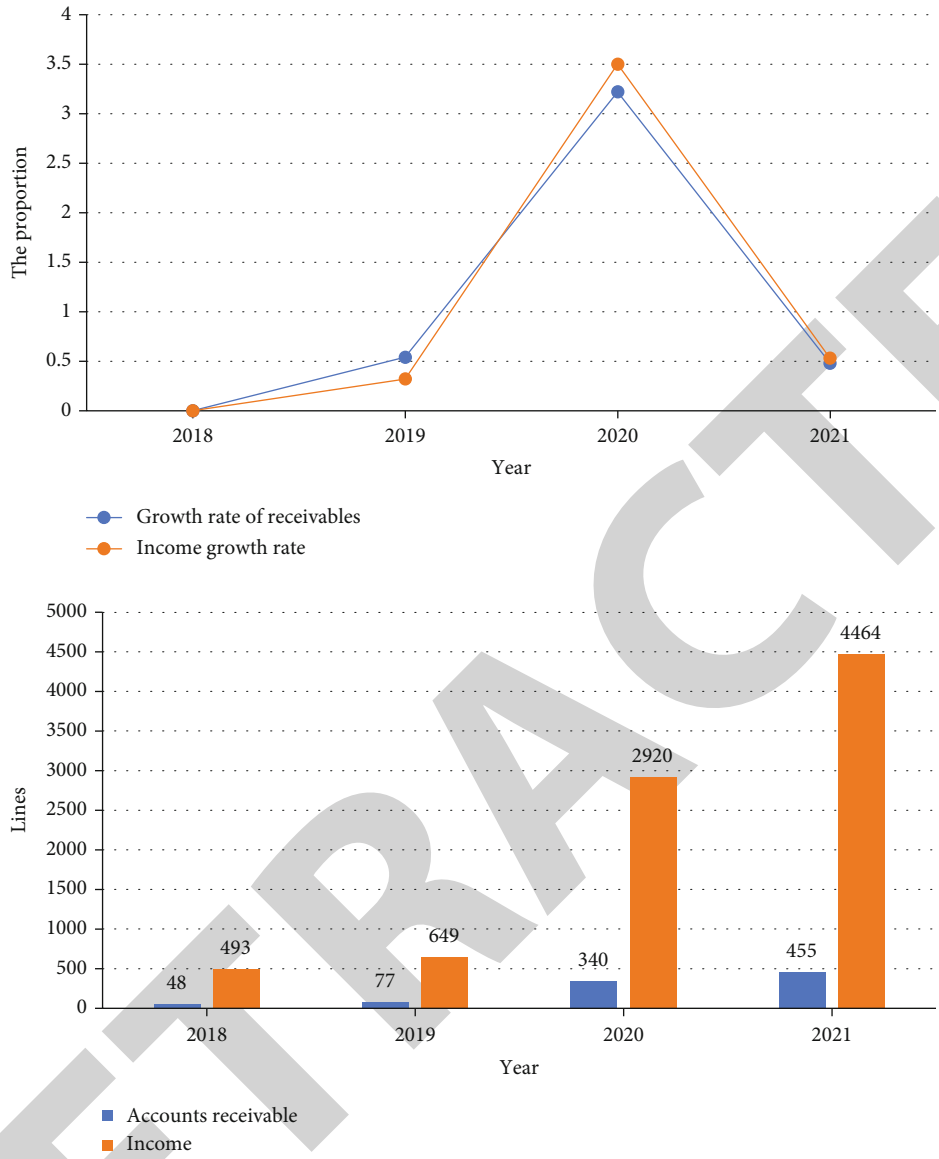

Figure 9: Receivables and revenue growth rate and revenue data graph.

be smaller than the growth rate of revenue. And the company's management of outstanding payments has improved.

But how to evaluate the impact of information technology centralized accounting on enterprise resource protection? Operating income and profit are two important metrics, which we can see from Figure 10: From 2019 to 2020, before and after the implementation of information technology centralized accounting, the main business income increased by 52.67%, and the pre-tax profit also increased significantly. It is true that the growth of revenue and profit is influenced by many factors, such as market conditions and employee compensation. But the impact of changes in financial management models on revenue, expenses, and profits cannot be ignored.

5.2. Application of Digital Information Technology in Enterprise Management Resource Protection. In the development process of enterprise resource management, information technology and computer network technology are constantly expanding the scope of application, especially the application of digital information technology, which plays an irreplaceable role in the protection of enterprise management resource. In addition, the introduction of digital information technology has revolutionized the innovative way of enterprise management resource protection. By introducing digital information technology in the work, managers only need to control the relevant software and use convenient operation means to design the management model. Then, the information can be stored in the software system and the background database, which provides convenience for the later management, processing, and production. The use of digital information technology and the effective application of computer software technology can improve the efficiency and quality of enterprise work and overcome the shortcomings of traditional enterprise management models.

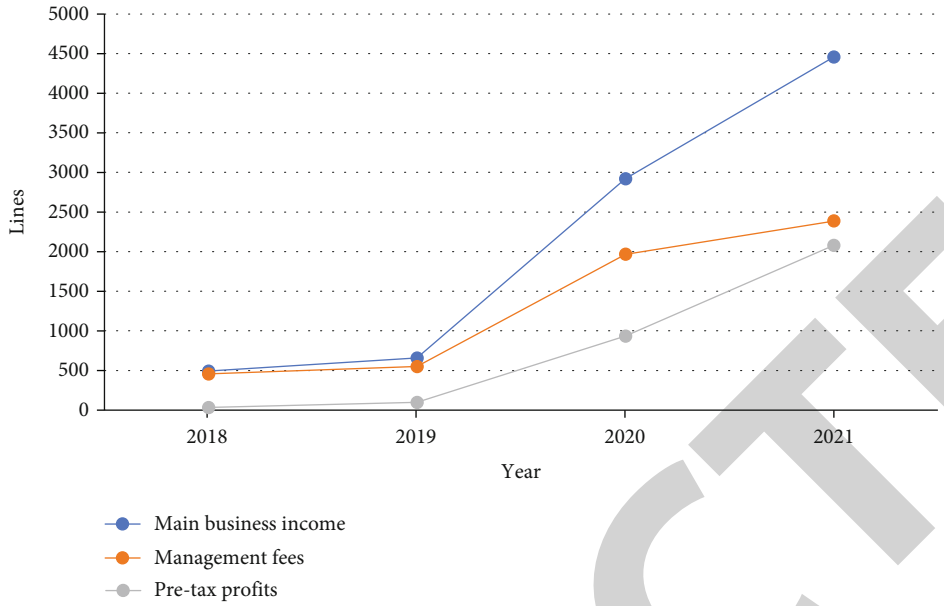

Figure 10: P Company income profit line chart.

6. Discussion

This paper is devoted to research and design based on digital information technology and applies it to the complex analysis and processing of enterprise management resource protection. For the research of digital information technology, this paper starts by introducing the concept of information technology, then establishes two models for comparison, and successfully combines improved enterprise management resources and information technology. In the stage of empirical analysis, the created model is used to analyze enterprise instances, and the results show that the obtained results are in line with the actual situation.

Through the analysis of this case, it is shown that the enterprise management resource protection combination based on digital information technology is more effective than a single type of resource management and enterprise managers apply digital information technology to implement management. In this way, the loss of enterprise resource projects can be greatly reduced, and optimization decisions of multi-project portfolios can be made. In the specific practical decision-making, develop the resource combination strategy of the enterprise, select the project reasonably and flexibly, substitute the information technology into the enterprise combination decision-making for calculation and analysis, and quickly obtain the information combination plan, so as to make the most effective management decision.

7. Conclusions

Through the case study, important conclusions were drawn: In the current enterprise management mode, using digital information technology, enterprise managers can more effectively prevent the loss of enterprise resources and better protect the cycle of enterprise management resources. As the two models created in this paper, according to the change of enterprise resource parameters after the use of information technology, a more detailed study and quantitative analysis of the protection of enterprise management resources based on digital information technology are carried out, and it determines the role and way of introducing information technology. The project discussed in this paper is a research on the protection of enterprise management resources based on digital information technology, which successfully demonstrates the effectiveness and efficiency of information technology for the protection of enterprise management resources. However, the selection of projects is relatively limited, and large enterprises will often face many combinations of choices, so further in-depth research is required.

Data Availability

No data were used to support this study.

Conflicts of Interest

The authors declare that there are no conflicts of interest regarding the publication of this article.

References

[1] T. N. Theis and H. Wong, "The end of Moore's law: a new beginning for information technology," *Computing in Science & Engineering*, vol. 19, no. 2, pp. 41–50, 2017.

[2] M. N. Habib, W. Jamal, U. Khalil, and Z. Khan, "Transforming universities in interactive digital platform: case of city university of science and information technology," *Education and Information Technologies*, vol. 26, no. 1, pp. 517–541, 2021.

[3] H. Y. Wang, L. Sigerson, and C. Cheng, "Digital nativity and information technology addiction: age cohort versus individual difference approaches," *Computers in Human Behavior*, vol. 90, pp. 1–9, 2019.

Hindawi
Wireless Communications and Mobile Computing
Volume 2022, Article ID 8783355, 11 pages
https://doi.org/10.1155/2022/8783355

Research Article

Application of Virtual Reality Technology in Adolescent Mental Health Science Education

Xiaoyang Wang,[1,2] **Xiaowen Zhu**,[1] **and Jingjing Lin**[3]

[1]*Humanities and Social Sciences School, Xi'an Jiaotong University, Xi'an, Shanxi 710049, China*
[2]*Zhejiang Ocean University, Zhoushan, Zhejiang 316000, China*
[3]*Nanhai Experimental School, Zhoushan, Zhejiang 31600, China*

Correspondence should be addressed to Xiaoyang Wang; xyangwang@zjou.edu.cn

Received 21 May 2022; Revised 16 July 2022; Accepted 25 July 2022; Published 9 August 2022

Academic Editor: Jun Ye

The 21st century is a time of rapid advances in science and technology, and scientific knowledge and literacy are highly relevant to the development of the country. Science education is the main means of learning scientific and cultural knowledge, and its teaching quality determines the formation of national scientific literacy. In addition, information technology teaching assistants are one of the main research areas in the field of educational technology, and they have long attracted the attention of researchers in the field of education. Based on these facts, this research introduces virtual reality technology into science education to make a favorable influence on the psychological well-being of young people, through color feature extraction, gray-level cooccurrence matrix feature extraction, Marching Cubes algorithm, and image synthesis technology to be scientifically and effectively combined with science education, and the popularization rate of students receiving science education has increased by 26.9%. As a result, the mental health of students was improved, and the number of students with subhealth mentality decreased by 16.9%. Adolescence is a transitional period for adolescents from immaturity to maturity. Adolescents are prone to fall into depression, anxiety, rebellion, autism, and other emotions, which will have a damaging impact on the growth of adolescents' mental health. The use of virtual reality technology in science education has opened up a new field of virtual teaching and learning. This pattern of education will make a huge influence on the future growth of education and the creation of teaching concepts.

1. Introduction

In recent years, virtual reality technology (virtual reality, VR for short) has developed rapidly. This is a kind of computer technology that helps users create virtual worlds and obtain simulation experience, breaking the shackles of time and space and giving users an immersive interactive experience. Virtual reality has made great contributions to medicine, entertainment games, and education. Applying virtual reality technology to education can mobilize learners' sensory stimulation in an all-round way, enhance learners' sensibility, and stimulate learning motivation. It has realized situational learning and has the effect of knowledge transfer, so virtual reality technology is suitable for education and teaching. Combining virtual reality technology with science education will produce a brand-new teaching model. Under the premise of grasping the essence of teaching, virtual reality technology can give full play to its advantages and bring qualitative improvement to science education.

The rapid development and popularization of computer technology have accelerated the development process of virtual reality technology. The current virtual reality technology is designed in many disciplines and related technical theories, including artificial intelligence, image processing, pattern recognition, graphics, and other high performance. The application and development of computing virtual technology should also cover many disciplines, such as mathematics, communication, aesthetics, physics, and psychology.

The mental health of adolescents is not only related to the happy life and healthy growth of individuals but also

relevant to the improvement of the national health status, and it is also an important guarantee for the development of national competition and internationalization. The application of virtual reality technology in science education to solve the mental health problems of adolescents and address the physical health problems of adolescents at different levels is of great importance to raising the physical health of Chinese adolescents. Using virtual reality technology to solve adolescents' mental health problems in scientific education is of great significance to improving the mental health of our country's adolescents.

2. Related Work

With the popularity of smartphones, the spread of virtual reality (AR) and virtual reality (VR) apps that utilize smartphone technology is also on the increase. However, the virtual reality technology of intelligent collection still needs to be strengthened, and many effects and technologies in the allocation of resources of smart phones are not achievable. Despite the widespread use of AR and VR technologies in education, there is still a lack of evidence-based research to test the discrepancies between AR and VR technologies in terms of educational impact. The purpose of Huang et al.'s exploratory research is to resolve this lacuna in the literature by contrasting the effects of AR and VR technologies on acquisition results (such as retrieval of scientific information). In particular, Huang et al. used a dual-condition (AR and VR) between-subject design to examine the retention of scientific knowledge by auditory and visual information rendered on the Samsung S4 smartphone app. The results of Huang et al.'s research ($<i>N = 109$) show that VR is considerably more absorbing and attractive via the regime of space existence. However, AR appears to be a more efficient medium for transmitting audible information via space presence, which may be due to the heightened awareness need related to immersive experiences. Therefore, an essential meaning of design is that when the experience is consumed, the educational component should be incorporated into the visual form [1]. Virtual reality (VR) is becoming recognized as a worthwhile tool for preparing dental students, and its usage is increasing in dental schools all over the world. Towers et al. timely review the literature related to the use of VR in dental education to ensure that educators fully understand the current areas of investigation and areas that require further investigation in order to make an appropriate decision on whether to adopt VR as an appropriate decision. The teaching tool used the methodology outlined by Arksey and O'Malley for a scoping review. The survey determined 68 related articles. As a result of the review, four educational topic areas related to "simulation hardware," "simulation authenticity," "scoring system," and "verification" emerged. The literature reveals some weaknesses and hypotheses. It suggests areas for extra inquiry to develop a greater foundation of evidence for the usefulness of VR in dental education and to inform its future development [2]. Background mixed reality technologies, consisting of virtual reality (VR) and augmented reality (AR), are seen as potential tools in science teaching and learning. It can cultivate positive emotions, encourage independent learning, and improve learning outcomes. Zhou X research proposed a VR/AR-based technology-assisted biological microscope learning system. The construction of the microscope is portrayed in a detailed three-dimensional model, and each element is indicated by the relationship and correlation between them. The interaction behavior of the model is defined and a standard operation instruction is produced. Motion control of the simulation elements on the basis of collision recognition. Combining immersive VR devices and AR technology, Zhou et al. worked on a virtual microscope subsystem and a mobile virtual microscope guiding system. The system thus consists of a VR subsystem and an AR subsystem. The VR subsystem has an emphasis on simulating the operation of the microscope and the related interactional behavior, allowing the user to view and manipulate the parts of the 3D microscope model through natural interaction in an immersive scene [3]. As the size of the software program code base in software development projects increases, the insight and understanding of its underlying dependency structure pose a challenge to programmers. The availability of virtual reality (VR) systems continues to increase, bringing VR-based program code structure visualization into the actual applications of software developers, and can support program understanding and insight. However, the full visual immersion of VR will bring cognitive burden and potential interference. So far, the potential motivation and program understanding factors for applying gamification to this VR visualization function have not been fully studied. Oberhauser and Lecon profiled and assessed a program code VR digital gamification method called VR Gamification Immersive Software Structure (VR-GaImS), which applies digital gamification to the multimetaphorical VR visualization of software program structure. The results of preliminary empirical investigations using the prototype of Oberhauser and Lecon's research show that it has the potential to enhance enjoyment and motivation, focusing on and encouraging inquiry into software architecture [4]. Virtual reality technology has captured the attention of people. This technology has been used in many fields such as medicine, industry, education, video games, or tourism. Perhaps, its greatest area of interest is recreation and amusement. The Martín-Gutiérrez study found that no matter which industry, the implementation of virtual reality or enhanced reality has a few limitations: it is pricey, has poor ergonomics, or means that too much work is required to produce the content. The most recent technological developments, which include the fast social adoption of smartphones, have boosted anyone's exposure to virtual and augmented reality. Moreover, a few major corporations such as Apple, Facebook, Samsung, and Magic Leap have invested more in these technologies in order to increase their availability in the coming years. Educational establishments will profit from better access to virtual technology, which will permit teaching in virtual environments that cannot be visualized in a physical environment [5]. Background virtual reality (VR) fusion technology has grown in popularity in recent years, and a number of prior studies have used it in laboratory education. However, due to the lack of evidence

to assess the impact of virtual reality convergence technology on VR education, many designers have chosen to forego this expensive and sophisticated technology. In this research, Qian et al. studied the influence of virtual reality convergence on immersion, presentment, and learning performance through experiments. Every player is allocated randomly to one of the following three states: a PC environment manipulated by a mouse (PCE), a VR environment manipulated by a controller (VRE), or a VR environment running virtual reality fusion (VRVRFE), manipulated by a real person. Findings of analysis of variance (ANOVA) and t-tests for immersion and co-efficacy showed considerable variation between the PCE ∗ VR − VRFE condition pairs. In addition, the results show that PCE ∗ VRVRFE and VRE ∗ VR − VRFE have significant differences in the intrinsic value of learning performance, and the difference between the immersive group is slightly significant. In conclusion, the results show that, compared with the traditional PC environment, virtual reality fusion can provide a better sense of immersion, presence, and self-efficacy, as well as the intrinsic value of better learning performance [6].

3. The Role of Science Education in the Mental Health of Young People

3.1. Overview of the Mental Health of Adolescents. Regarding mental health, self-confidence, no inferiority, no complaints in social life, and no extreme handling of things, regardless of whether real life is good or bad for them, they can calmly face the pressure from life and have a mature attitude and ability to love and be loved. They should also have certain management and organization capabilities, and be able to handle one's own affairs well in the interpersonal relationship of complex social life, with a certain degree of independence. Do not rely on others, behave rationally, have independent opinions, and listen to reasonable suggestions.

When necessary, they can make major decisions and be willing to take responsibility.

There is a good organization [7], a long-term plan, and a good self-control, using our own will to consciously control ourselves to achieve the desired goals.

This is the manifestation of our psychological maturity.

Adolescence is the transitional period between children and adults and the initial stage after adulthood. They are in a critical period of exploring identity and establishing identity. After entering puberty, self-awareness increases, inner conflicts increase, they are curious about the opposite sex, psychologically sensitive, caring about other people's opinions, having mood swings, and susceptible to surrounding events. This is a period of high incidence of psychological problems. It is an important period of life development. Different mental activities are very active and form different psychological qualities, but this does not seem to be a strong trend. They move quickly and have greater plasticity. With the rapid economic growth and major changes in lifestyles, young people are more likely to be affected by negative mental health problems than other groups [8].

3.2. Adolescents' Mental Health Status and Reasons. Based on the particularity of adolescents' psychological problems, academic circles at home and abroad have conducted in-depth studies on them, and the application of psychological scales has played a very important role in these studies. At present, the measurement tools used in the research of adolescents' psychological problems are mainly divided into four categories: the first category is a symptom-oriented psychological diagnosis scale, the second category is an adaptation-oriented scale, the third category is a mental health quality scale, and the fourth category is a scale focusing on adolescents' mental subhealth. The most widely used is the first category of symptom-oriented psychological diagnostic scales. The reason is that the first type of tools can be tested in a relatively wide range, with freedom of time and location, and most of them are self-evaluated. The symptom-oriented psychological diagnostic scales are more commonly used in research. It mainly includes Mental Health Diagnostic Test (MHT), Mental Health Scale for Chinese Middle School Students, Symptom Self-Rating Scale (SCL-90), Depression Self-Rating Scale (SDS), and Anxiety Self-Rating Scale (SAS). These measurement tools are based on mental illness factors such as anxiety, mood disorders, obsessive-compulsive symptoms, paranoia, hostility, and depression [9].

Based on the above multiple testing methods, a cross-sectional survey of the general conditions of adolescents was conducted using stratified cluster random sampling methods to analyze the detection rates of Chinese adolescents' mental subhealth of different genders, as shown in Table 1.

The detection rate of male mental subhealth symptoms is lower than that of females, and the mental subhealth status is higher than that of females. The comparison is statistically significant.

Analyze the detection rate of adolescents' mental subhealth for the age group from junior high to senior ones, as shown in Table 2.

The table shows that the detection rate of mental health among college students is the highest and that of junior high school students is the lowest. Moreover, the detection rate of mental subhealth symptoms and mental subhealth state of junior high school students is the highest among the three ages [10].

The test results of adolescent SCL-90 are shown in Table 3.

The factor scores of adolescent SCL-90 are measured in comparison to those of the control group. The average score of adolescent SCL-90 factors is between 1.37 and 1.84. The higher item is interpersonal relationship, and the lower score is somatization, as shown in Table 4.

When analyzing factors that affect the mental health of adolescents, structural equations are used for analysis. Five latent variables including school atmosphere, family atmosphere, objective family environment, academic pressure, and peer effect are included in the system to analyze whether they have an influence on the mental health of the latent variables. According to relevant literature and research, the assumptions made in this paper for the structural equation model of adolescent mental health are as follows:

Table 1: Detection rate of mental subhealth of Chinese adolescents of different genders.

Psychological condition	Boys	Girl	Overall	x^2 value	p value
Mood	2158 (25.9)	2061 (25.1)	4219 (25.5)	1.166	0.280
Conduct	2166 (26.0)	1976 (24.1)	4142 (25.0)	7.658	0.006
Social adaptation	1435 (17.2)	1215 (14.8)	2650 (16.0)	17.456	0.001
Mental health	4070 (48.8)	3975 (48.5)	8045 (48.9)		

Table 2: Analysis of the detection rate of adolescents' mental subhealth for different age groups.

Grade	Number of people	Mental health	Mental subhealth
Junior high school	6827	2996 (43.9)	2291 (33.61)
High school	6843	3267 (47.7)	2163 (31.6)
University	2875	1782 (62.0)	792 (27.5)
x^2 value		317.239	
p value		0.001	

First, the school atmosphere has a favorable influence on the psychological well-being of adolescents.

Second, the family atmosphere has a favorable influence on the psychological well-being of adolescents.

Third, the objective family environment has a positive effect on the psychological well-being of adolescents.

Fourth, academic pressure has a harmful effect on the psychological health of adolescents.

Fifth, the peer effect has a favorable influence on the psychological well-being of adolescents.

Sixth, the objective family environment has a positive effect on the family atmosphere.

Seventh, the family's objective environment has a negative impact on academic pressure.

Eighth, the peer effect has a positive effect on the school atmosphere.

Ninth, the school atmosphere has a negative effect on academic pressure, as shown in Figure 1.

A comparative analysis of the proportion of different grades that affect their physical and mental health due to school atmosphere, family atmosphere, objective family environment, academic pressure, peer effect, etc. is shown in Figure 2.

From the chart data, it is not difficult to find that the mental health of junior high school students is mainly affected by the school atmosphere and peer effect, while the influencing factors of the mental health of high school students are mostly academic pressure.

3.3. Science Education. The science curriculum in elementary schools in our country comes from the term "Gezhi." It spread to our country after the Westernization Movement. The main problem of learning lies in the acquisition of scientific knowledge through experimental questions. Later, the name of the course was changed to "Nature," and the Ministry of Education officially announced in 2001; the name of the course was changed to "Science," and the "National Standard for Basic Science Courses" was announced [11]. This change extends the curriculum teaching to the entire field of natural sciences, including the relationship between scientific nature and human society. An important purpose of basic science courses should be observation. It is because most of the science courses are based on experiments, which requires students to have the ability to observe to discover problems and to have the courage to question and innovate and research-based learning experiments to cultivate students' ability to discover and think about problems. However, it is not appropriate for all children to have the opportunity to take science courses. The popularity of statistical science education in various regions is shown in Figure 3:

Science education should form quality education, which is recognized by science teachers. Mental health education is an important part of quality education, but some science teachers neglect the mental health education of students [12]. Although science teachers are responsible for cultivating children's scientific literacy, education is still partial to exams. The fraction theory is probably the reason why many teachers ignore it. We must moisturize things silently in the mental health of students. Experimental teaching is an important part of science teaching, and it is also a valid method to cultivate students' rigorous scientific attitude, fearless scientific courage, and active and innovative scientific thinking. Therefore, it is very necessary to apply virtual reality technology to science education.

4. Virtual Reality and Technology

4.1. Virtual Reality. Virtual reality technology is VR technology. This technology is a kind of information technology with complex characteristics that appeared at the end of the 20th century and realized the fusion of multimedia technology, numerical image treatment, sensor technology, and computer graphics [13]. VR technology can produce three-dimensional visual and sound impacts. Because human-machine interaction is an amicable and concordant state that relies on natural skills and 3D virtual reality technology can transform the reactive and exhausted situation between man and machine, the status quo of traditional multimedia teaching has therefore had a significant impact. Virtual reality technology has applications in many fields, such as medicine, art design, and games, as shown in Figure 4.

As shown in Figure 5, virtual reality technology has high immersion, high interactivity, and high conception.

Table 3: The total detection rate of SCL-90 factor score problems in adolescents and control groups.

Factor name	Boys	Girl	Total
Somatization	7 (16.46)	15 (25.84)	22 (12.54)
Obsessive-compulsive symptoms	26 (45.62)	28 (53.26)	54 (14.56)
Man-machine relationship	21 (40.12)	25 (18.65)	46 (14.69)
Depression	17 (25.12)	20 (23.06)	37 (41.59)
Anxiety	26 (26.56)	16 (23.12)	42 (14.59)
Hostility	15 (23.21)	14 (15.21)	29 (12.89)
Paranoid	5 (9.61)	8 (21.21)	12 (15.65)
Spirituality	6 (11.52)	2 (12.21)	8 (54.21)

Table 4: Comparison of the factor scores of adolescent SCL-90 with those of the control group.

Factor name	Test group	Control group	T
Somatization	1.32 + −0.37	1.41 + −0.43	-0.405
Obsessive-compulsive symptoms	1.73 + −0.51	1.82 + −0.60	-0.963
Interpersonal relationship	1.81 + −0.50	1.84 + −0.52	-0.065
Depression	1.68 + −0.42	1.71 + −0.49	-0.344
Anxiety	1.53 + −0.48	1.58 + −0.56	-0.049
Paranoid	1.59 + −0.46	1.63 + −0.42	-0.033
Psychotic	1.54 + −0.52	1.57 + −0.47	-0.030

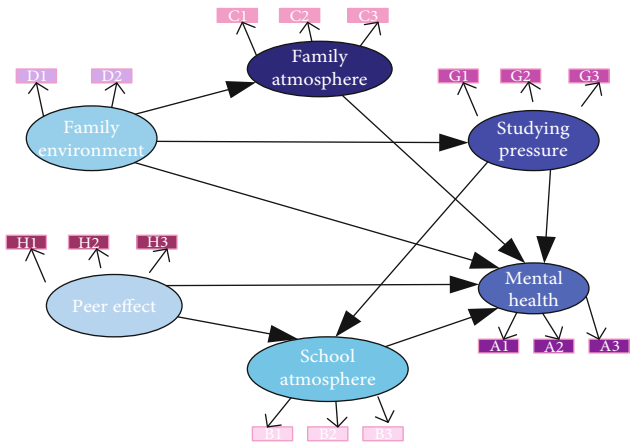

Figure 1: The original path diagram of the factors affecting the mental health of adolescents.

4.2. Virtual Reality Technology

4.2.1. Color Feature Extraction. Because the image pixel value array is a series of values, therefore, it is essentially possible to use some simple mathematical statistics to achieve a representation of the overall color characteristics of the image [14]. The most popular color feature is the calculation of moments per channel on the basis of the RGB color space. RGB color is the most common in virtual reality technology; besides this, there is HIS color space.

The first-order moments mean the calculation formula for the mean is

$$\eta = \sum_{j=0}^{M} \frac{1}{M} P_{ij}, \tag{1}$$

where P_{ij} represents the value of the ith color channel at pixel position j and N represents the total number of pixels. Second-order moment is the standard deviation, which is the square root of the distribution difference. The calculation formula can be expressed as

$$\alpha = \sqrt{\frac{1}{M} \sum^{M} \left(P_{ij} - \eta\right)^2}. \tag{2}$$

Third-order moment stands for skewness, which gives a measure of the asymmetry of the pixel value distribution. The calculation formula can be expressed as

$$\text{Skewness} = \sqrt[3]{\left(\frac{1}{M} \sum_{j=1}^{M} \left(P_{ij} - \eta_i\right)^3\right)}. \tag{3}$$

In the process of image processing, the RGB color space is usually converted to the HIS color space. There are two most commonly used color spaces for color feature extraction, RGB and HIS, but compared with the two color spaces,

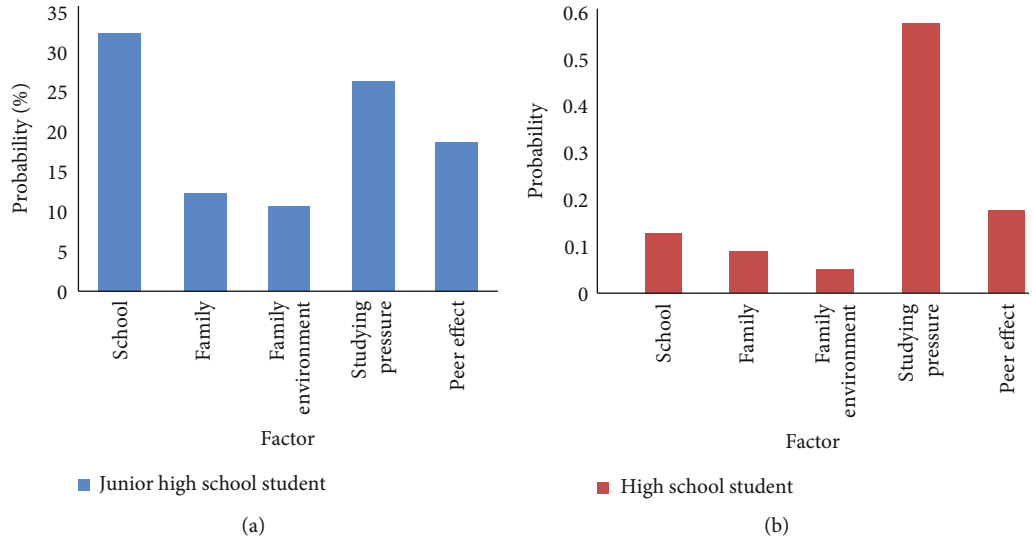

Figure 2: Different comparisons of the physical and mental health of junior high school students and high school students due to school atmosphere, family atmosphere, objective family environment, academic pressure, peer effect, etc.

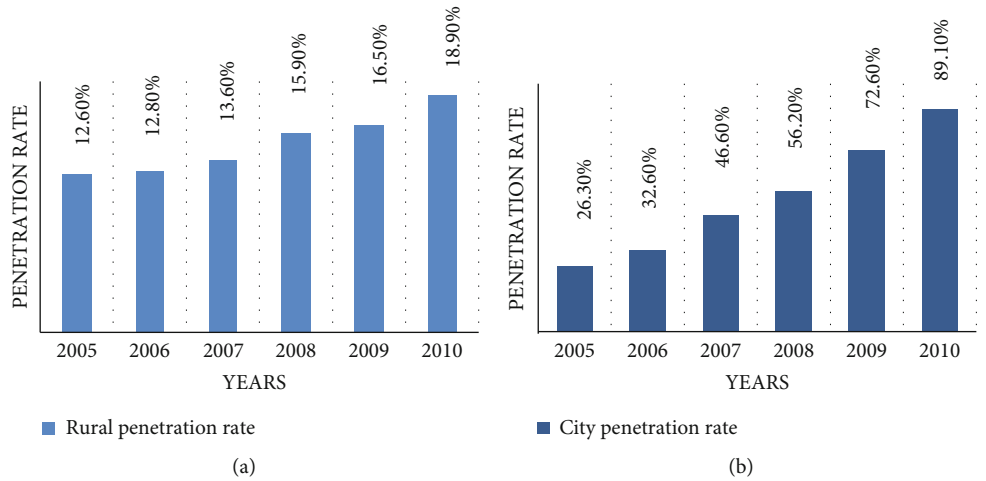

Figure 3: The penetration rate in urban and rural areas from 2015 to 2020.

HIS is more accurate and efficient in the calculation process. The conversion formula is as follows:

$$E = COS^{-1}\left\{\frac{(1/2)[(O-G)+O-B]}{\sqrt{(O-G)^2+(O-G)(G-B)}}\right\}, \quad (4)$$

$$Z = 1 - \frac{3}{O+G+B}\min(O,G,B).$$

4.2.2. Feature Extraction of Gray-Level Cooccurrence Matrix. Texture is an intrinsic characteristic of an image related to the surface material of a material, and it includes a lot of significant information about the surface structure and its relationship to the surrounding environment [15]. Texture can be thought of as the gray scale of an image in some form in color space, and it is one of the characteristics in common with images. Because the texture of an image is also formed by the repetition of grayscale distribution, there must be a specific connection between two pixels in the image space domain. We call it the spatial correlation of the pixels of the image, that is, the grayscale. The hierarchical cooccurrence matrix is based on the spatial correlation of pixels to describe the texture characteristics of the image [16]. Obtain the gray-level cooccurrence matrix from the gray-level image. According to statistics, at a certain distance in the four directions of 0°, 45°, 90°, and 135°, the gray value of gray pixel i and the value of gray pixel j appear at the same time. The result is shown in Figure 6.

Where D is the distance, suppose there is 6×6 image pixel data with gray levels of 0, 1, 2, and 3. A cooccurrence matrix count is conducted for the horizontal and vertical orientations around each pixel, and the results are shown in Figure 7.

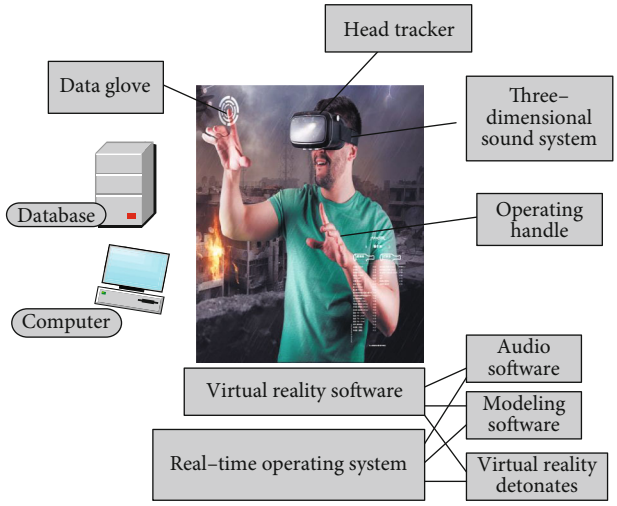

Figure 4: Virtual reality game.

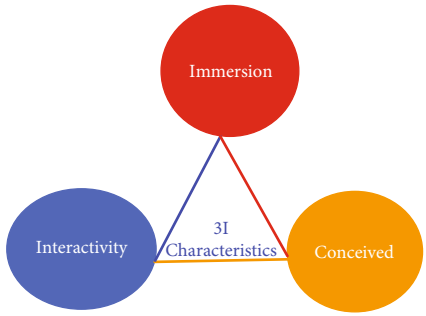

Figure 5: Three characteristics of virtual reality.

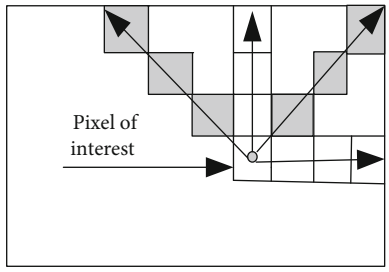

Figure 6: Matrix.

Then, in the 0 direction, the gray level cooccurrence matrix with a distance of 1 is

$$P_{1,0} = \begin{bmatrix} 4310 \\ 3454 \\ 2565 \\ 0654 \end{bmatrix}. \tag{5}$$

According to the gray-level cooccurrence matrix obtained by statistics, the following related attributes of the texture can be calculated:

0	0	1	2	3	1
0	0	1	2	3	1
1	1	2	2	0	2
1	1	2	2	1	3
2	2	3	3	3	2
2	3	1	3	1	0

Figure 7: 6×6 image pixel data.

$$\begin{aligned} \text{Contrast} &= \sum_{i,j} |i-j|^2 p(i,j), \\ \text{Correlation} &= \sum_{i,j} \frac{(i-\eta i)(j-\eta j)p(i,j)}{\alpha_i \alpha_j}, \\ \text{Energy} &= \sum_{i,j} p(i,j)^2. \end{aligned} \tag{6}$$

4.2.3. Marching Cubes Algorithm. The essence of MC algorithm is to find isosurface from volume data, so MC algorithm is usually called isosurface extraction algorithm. It is the most classic and most commonly used algorithm among the three-dimensional reconstruction surface rendering methods [17].

Marking the corner points of the voxel can simplify the solving of the isosurface. The specific method is as follows: in a voxel, we set the corner points with a pixel value greater than the threshold as the marked points and mark them with black dots; the corner points whose pixel value is less than the threshold are set as marked points without any marking, as shown in Figure 8.

Generally, there are two methods to find the coordinates of the equivalent point and the normal vector of the triangle surface: linear interpolation and the method of selecting the midpoint.

Linear interpolation

$$\begin{aligned} B &= \frac{B_1(\text{is covalue} - W_1)(B_2 - B_1)}{W_2 - W_1}, \\ N &= \frac{N_1(\text{is covalue} - W_1)(N_2 - N_1)}{W_2 - W_1}. \end{aligned} \tag{7}$$

Choose the midpoint method:

$$\begin{aligned} B &= \frac{|B_2 - B_1|}{2}, \\ N &= \frac{|N_2 - N_1|}{2}. \end{aligned} \tag{8}$$

So we can use the gradient vector of the point to represent the normal vector of the point, and the gradient formula of any point on the isosurface is

$$g(a,b,c) = \oplus f(a,b,c). \tag{9}$$

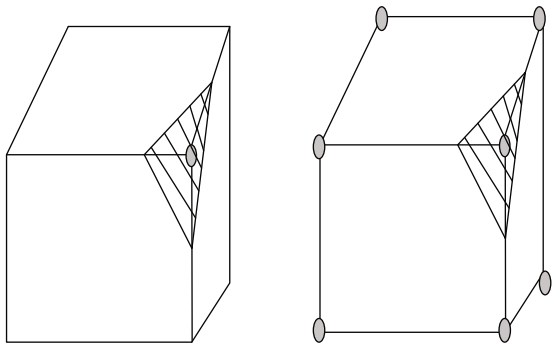

Figure 8: Schematic diagram of marked and unmarked points.

The gradient at the corner points of the voxel can be obtained using the central difference method:

$$g_a = \frac{f(a_{i+1}, b_j, c_k) - f(a_{i-1}, b_j, c_k)}{2 \oplus a},$$
$$g_b = \frac{f(a_i, b_{j+1}, c_k) - f(a_i, b_{j-1}, c_k)}{2 \oplus b}, \quad (10)$$
$$g_c = \frac{f(a_i, b_j, c_{k+1}) - f(a_i, b_j, c_{k-1})}{2 \oplus c}.$$

4.3. Image Synthesis. Before the final image is obtained, image synthesis must be performed in a specific way. According to the scanning direction of the ray in space, we can roughly divide the image synthesis methods into the following two categories:

Back-to-front image synthesis method: this method starts from the ray farthest from the viewpoint. The color value and transparency value of the pixels on the ray are synthesized along the direction from the ray to the viewpoint, until the viewpoint position is reached [18]. The calculation is as follows:

$$C_k = C_j(1 - \partial_i) + C_i\partial_i. \quad (11)$$

Continue to iterate and simplify the available formula:

$$C = C_0\varphi_1\varphi_2 \cdots \varphi_n + C_1\partial_1\varphi_2\varphi_3 \cdots \varphi_n + \cdots C_n\partial_n,$$
$$C_0 = \prod_{i=1}^{n} \varphi_i + \prod_{i=1}^{n} C_i\partial_1 \prod_{j=i+1}^{n} \varphi_j. \quad (12)$$

Front-to-back image synthesis method: the front-to-back image synthesis method is very similar to the back-to-front synthesis method. The only difference is that the initial position of the ray is at the viewpoint, and it is projected from the viewpoint to the farthest point, the same as above.

5. Virtual Reality Is Used for Science Education

5.1. Analysis of Virtual Phenomenon Applied Teaching. Science education often includes the explanation of many natural phenomena and the accumulation of common sense in life, requiring students to combine theory and practice to deepen the internalization of knowledge [19]. Primary school science curriculum is an integral part of overall science education. In order to support the advancement of basic science education, long-term education researchers have conducted related research and research outside of teaching and discovered the current problems in basic science education in China: teaching fills ducks, insufficient training, and lack of curriculum resources. Therefore, the current low level of science education in elementary schools in our country hinders the development of science education in China. In order to better improve the science curriculum and solve the shortcomings of traditional teaching, researchers in the education field are gradually trying to use new technical methods to support the development of educational activities [20]. Thanks to virtual reality technology, students can feel themselves in the real world through various technical means, such as three-dimensional computer technology, interactive technology, computer technology, and man-machine interface, to get a real educational experience. The easy-to-use virtual teaching software allows teachers to improve scientific teaching methods and enhance teaching software resources. At the same time, it can effectively improve students' interest in learning, complete the content, and teach more effectively. For "virtual reality application education," its academic attention index is shown in Figure 9.

It is not difficult to see the application and popularity of virtual reality from this data. The research on virtual reality application education began to grow exponentially, indicating that the application research of virtual reality technology in education has gradually become a hot spot in the past two years. This is also related to the maturity of virtual reality technology.

5.2. The Application of Virtual Phenomena to the Analysis and Design of Science Education. To investigate virtual reality technology from the standpoint of educational technology, use this technology as a novel educational technology, and design a novel field of study linked to educational technology—virtual teaching and learning. Virtual teaching is a new learning method that integrates information technology with contemporary talent development, which takes people into a virtual learning environment. Virtual learning utilizes virtual reality technology to build a virtual learning environment and then uses the generated objectified reality to replicate key knowledge points. It guides students to take in information in a virtual environment using their senses, such as sight, and hearing; to receive information in a virtual environment; and to improve students' interest in learning and awareness of innovation. With the use of virtual reality in teaching, we found that most of the teaching based on virtual reality usually gives control of body movements, as shown in Figure 10.

The interest and attitude of students in the classroom based on virtual reality games are more active, which is better than traditional online learning platforms. Therefore, based on the theory of embodied cognition, we can think that the teaching environment in virtual reality or mixed reality environment has a positive impact on teaching activities. It is on basis of the design of learning activities on basis

Figure 9: Academic analysis and publication volume of virtual reality technology education in the next few years of 2010.

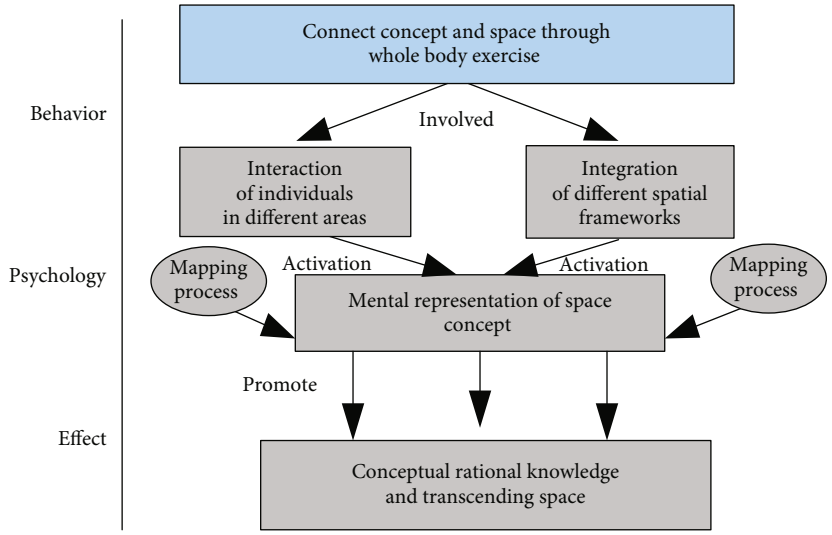

Figure 10: Process model diagram of embodied interaction to promote conceptual understanding.

of the activity theory, combined with the characteristics of virtual reality technology, and on the basis of the existing learning activity theory, adding the element of "teaching context," as shown in Figure 11.

5.3. The Preparation and Implementation of Virtual Phenomena Applied to Scientific Education Analysis and Design Experiments. 10 virtual reality-based learning activity cases of elementary school science courses were designed, and teaching experiment research was carried out in the fourth grade of an affiliated experimental elementary school in the autumn semester. The specific teaching experiment research process is shown in Figure 12.

This study uses questionnaire surveys and learning tests to study the changes in learning motivation and the comparison of test scores between the experimental group and the control group, through the interview method and questionnaire survey method to explore the learning subject's experience and evaluation of science courses based on immersive

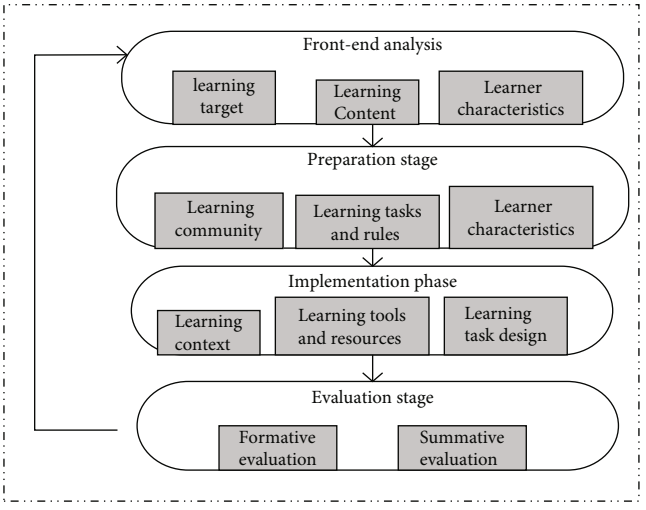

Figure 11: Virtual reality classroom teaching design process.

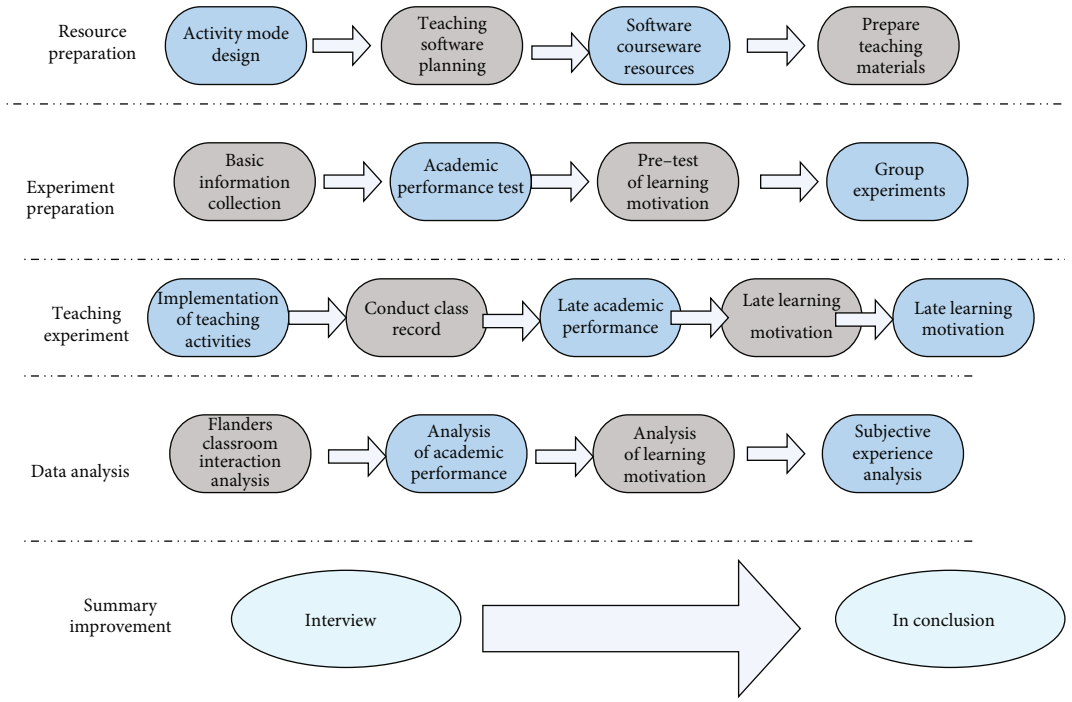

Figure 12: Teaching experiment research process.

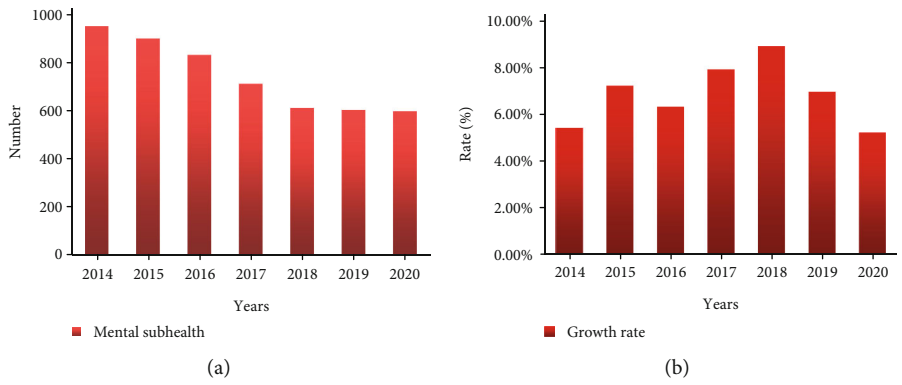

Figure 13: The number of mentally subhealthy people in the school from 2014 to 2020 and the rate of decrease.

virtual reality. And after a long-term experiment course, the students were tested by this test and found that the mental subhealth of the students in the school was gradually decreasing, as shown in Figure 13.

It is found that the school's insistence on combining science courses with virtual reality during the past few years has been quite effective in curing students' mental health. The rate of decrease in 2016 was relatively fast, but the rate of decrease afterwards was relatively slow. This is related to the pressure of the current society, but the overall situation is positive.

6. Conclusion

Teaching and learning activities require reliance on certain technological tools. As a result, with the reform of teaching technology, changes in teaching models and teaching activities will take place. Teaching technology is getting more and more sophisticated, making the present misunderstanding of education and teaching progressive and human educational thinking and awareness increasing. Thus, with the appearance and popularity of virtual reality technology, virtual education has breached the traditional education and teaching model and has given the field of education a distinctive approach to innovation and an unprecedented educational model. This education model will have a huge influence on the future growth of education and the creation of teaching ideas. Future directions are as follows: (1) improve teaching process: combine current experimental research data to improve elementary school science classroom teaching process based on immersive virtual reality technology. (2) Enriching experimental objects: choose

learners from different regions and different age groups to conduct related experiments in different subjects, enrich the experimental research objects, and obtain more complete experimental data. (3) Expand the software function: realize the use of virtual reality software to collect students' learning data, realize the function of online score generation and analysis, and reflect the teaching application effect of virtual reality technology to the greatest extent.

Data Availability

No data were used to support this study.

Conflicts of Interest

The authors declare that there are no conflicts of interest regarding the publication of this article.

References

[1] K. T. Huang, C. Ball, J. Francis, R. Ratan, J. Boumis, and J. Fordham, "Augmented versus virtual reality in education: an exploratory study examining science knowledge retention when using augmented reality/virtual reality mobile applications," *Cyberpsychology, Behavior and Social Networking*, vol. 22, no. 2, pp. 105–110, 2019.

[2] A. Towers, J. Field, C. Stokes, S. Maddock, and N. Martin, "A scoping review of the use and application of virtual reality in pre- clinical dental education," *British Dental Journal*, vol. 226, no. 5, pp. 358–366, 2019.

[3] X. Zhou, L. Tang, D. Lin, and W. Han, "Virtual & augmented reality for biological microscope in experiment education," *Virtual Reality & Intelligent Hardware*, vol. 2, no. 4, pp. 316–329, 2020.

[4] R. Oberhauser and C. Lecon, "Towards gamifying software structure comprehension in virtual reality," *Control and Intelligent Systems*, vol. 47, no. 2, pp. 56–62, 2019.

[5] J. Martín-Gutiérrez, C. E. Mora, B. Añorbe-Díaz, and A. González-Marrero, "Virtual technologies trends in education," *Eurasia Journal of Mathematics Science & Technology Education*, vol. 13, no. 2, pp. 469–486, 2017.

[6] J. Qian, Y. Ma, Z. Pan, and X. Yang, "Effects of virtual-real fusion on immersion, presence, and learning performance in laboratory education," *Virtual Reality & Intelligent Hardware*, vol. 2, no. 6, pp. 569–584, 2020.

[7] C. Cao and R. J. Cerfolio, "Virtual or augmented reality to enhance surgical education and surgical planning," *Thoracic Surgery Clinics*, vol. 29, no. 3, pp. 329–337, 2019.

[8] H. H. S. Ip, S. W. L. Wong, D. F. Y. Chan et al., "Enhance emotional and social adaptation skills for children with autism spectrum disorder: a virtual reality enabled approach," *Computers & Education*, vol. 117, pp. 1–15, 2018.

[9] M. G. Blumstein, B. B. Zukotynski, B. N. Cevallos et al., "Randomized trial of a virtual reality tool to teach surgical technique for tibial shaft fracture intramedullary nailing," *Journal of Surgical Education*, vol. 77, no. 4, pp. 969–977, 2020.

[10] J. Lenoir, S. Cotin, C. Duriez, et al.W. o. v. r. interaction, and p. simulation, "Interactive physically-based simulation of catheter and guidewire," *Journal of Preventive Medicine Information, 2017*, vol. 61, no. 13, pp. 2132–2141, 2005.

[11] D. Freeman, S. Reeve, A. Robinson et al., "Virtual reality in the assessment, understanding, and treatment of mental health disorders," *Psychological Medicine*, vol. 47, no. 14, pp. 2393–2400, 2017.

[12] M. C. Howard, "A meta-analysis and systematic literature review of virtual reality rehabilitation programs," *Computers in Human Behavior*, vol. 70, no. MAY, pp. 317–327, 2017.

[13] J. Thies, M. Zollhofer, M. Stamminger, C. Theobalt, and M. Nießner, "FaceVR: real-time facial reenactment and eye gaze control in virtual reality," *ACM Transactions on Graphics*, vol. 37, no. 2, 2018.

[14] T. Kay and A. Asl, "Virtual reality systems for rodents," *Current Zoology*, vol. 63, no. 1, pp. 109–119, 2017.

[15] L. P. Berg and J. M. Vance, "Industry use of virtual reality in product design and manufacturing: a survey," *Virtual Reality*, vol. 21, no. 1, pp. 1–17, 2017.

[16] J. Munafo, M. Diedrick, and T. A. Stoffregen, "The virtual reality head-mounted display oculus rift induces motion sickness and is sexist in its effects," *Experimental Brain Research*, vol. 235, no. 3, pp. 889–901, 2017.

[17] E. Roy, M. M. Bakr, and R. George, "The need for virtual reality simulators in dental education: a review," *Saudi Dental Journal*, vol. 29, no. 2, pp. 41–47, 2017.

[18] H. Zhang, "Head-mounted display-based intuitive virtual reality training system for the mining industry," *International Journal of Mining Science and Technology*, vol. 27, no. 4, pp. 717–722, 2017.

[19] E. Biffi, E. Beretta, A. Cesareo et al., "An immersive virtual reality platform to enhance walking ability of children with acquired brain injuries," *Methods of Information in Medicine*, vol. 56, no. 2, pp. 119–126, 2017.

[20] K. Jensen, F. Bjerrum, H. J. Hansen, R. H. Petersen, J. H. Pedersen, and L. Konge, "Using virtual reality simulation to assess competence in video-assisted thoracoscopic surgery (VATS) lobectomy," *Surgical Endoscopy*, vol. 31, no. 6, pp. 2520–2528, 2017.

Hindawi
Wireless Communications and Mobile Computing
Volume 2022, Article ID 6904653, 12 pages
https://doi.org/10.1155/2022/6904653

Research Article

Interactive Multimedia Data Coscattering Point Imaging for Low Signal-to-Noise Ratio 3D Seismic Data Processing

Jianbo Fei and Yanchun Wang

School of Geophysics and Information Technology, China University of Geosciences, Beijing 100083, China

Correspondence should be addressed to Jianbo Fei; 3010190018@cugb.edu.cn

Received 30 May 2022; Revised 14 July 2022; Accepted 22 July 2022; Published 4 August 2022

Academic Editor: Jun Ye

In this paper, low signal-to-noise ratio 3D seismic data are processed by the method of coscattered point imaging, and the imaging method is analyzed in combination with interactive multimedia for 3D seismic data. The reconstruction is carried out using a convex set projection algorithm based on the curvilinear wave transform. The track set is extracted from the 3D data body and transformed into the common offset distance-center point tract set to achieve the reconstruction of seismic data in the common offset distance track set domain and through comparison. It is concluded that the reconstruction effect is better in the common. The reconstruction results are better in the common offset distance track set domain. To shorten the processing time and obtain better reconstruction results, this paper proposes the idea of direct reconstruction of frequency slices. Experiments on the actual seismic three-component wavefield based on velocity-type and acceleration-type three-component geophones are carried out to reveal the signal characteristics of the actual seismic wavefield under the mining space. Due to the limitation of the construction observation space and the particularity of the actual needs of mine detection, the application of the scattered wave imaging method in the mine must be based on the corresponding detection space and detection purpose. The implementation of this thesis improves the signal-to-noise ratio, resolution, and fidelity of the 3D seismic data of the Shawan Formation, which is more conducive to the search for lithological traps. Combined with the seismic geological data, several traps were finally found and implemented, indicating that the fidelity of the resultant information is good and can meet the needs of interpretation and comprehensive research. The multiwave scattering imaging method in this paper can complete multiwave field imaging of longitudinal, transverse, and slot waves, which has the advantages of data redundancy, high superposition number, and more accurate imaging than conventional reflection wave imaging and provides field application value for ensuring mine safety production.

1. Introduction

Seismic signal noise suppression to improve the signal-to-noise ratio is the primary task of seismic data processing. Because seismic signals are affected by complex geological structures and surface environment, exploration instrument interference, and other unavoidable environmental factors, the acquired seismic signals contain random noise and regular noise. Random noise has a wide frequency and no fixed propagation direction; regular noise is also equivalent to coherent noise [1]. Coherent noise contains surface waves, multiple waves, refractive waves, acoustic waves, and other noise with certain dynamics, which have regular main frequencies and apparent velocities and are relatively easy to distinguish. The nature of the noise is different, and the suitable denoising methods are different. There are differences in frequency and apparent velocity between effective seismic waves and coherent noise, so coherent noise can be removed by one-dimensional frequency filtering and two-dimensional apparent velocity filtering [2]. With the rapid advancement of computer technology, seismic data processing can also fully rely on advanced processing technology, which requires not only the resolution and fidelity to be guaranteed but also the processing efficiency to be improved to a great extent to adapt to the complexity and difficulty of exploration work. Processing the acquired large-scale data and displaying them visually

using computer graphics and imaging to achieve convenient human-computer interaction provide an effective technical means for the technical personnel at the exploration site to observe and interpret the data [3]. It is also a very large part of the workload invested by researchers in seismic data processing.

The surface observation seismic profile is to excite seismic waves at some points near the surface and at the same time to observe at some points arranged along the surface measurement line; the vertical seismic profile is also to excite seismic waves at some points near the surface, but it is to observe at some points arranged at different depths along the borehole [4]. The former geophone is placed on the surface, and the measurement line is arranged along the ground, so it is also called a horizontal (or ground) geophone profile; the latter geophone is placed in the well, and the measurement line is arranged vertically along the wellbore, so it is called vertical geophone profile. In the horizontal seismic profile, because the geophone is placed on the ground, only upward waves from the subsurface can be received in addition to the direct and surface waves propagating along the surface; in the vertical seismic profile, because the geophone is placed inside the formation through the well, both upward and downward waves propagating from the bottom can be received. In the field of geological exploration, before the emergence of three-dimensional visualization technology, researchers often obtain geological information through cross-sectional images [5]. This method of interpreting three-dimensional information by two-dimensional means has great limitations, making it difficult to grasp the underground structure, resulting in most of the data being wasted and low utilization of resources. Records are presented as half-branch of the hyperbola. As the CSP gather deviates from the scattering point, the equivalent offset of the effective scattered wave increases, and the small equivalent offset signal lacks data and appears as a hyperbolic far-branch signal in morphology. The 3D visualization of seismic data can provide geologists with a visual reference of the geological structure and geological model, and it can help to reveal the intrinsic laws of geological data, which can lead to activities such as energy exploration and thus generate great economic benefits.

The experiments on the actual three-component wavefield of mine seismic based on velocity-type and acceleration-type three-component geophones were carried out to reveal the signal characteristics of the actual seismic wavefield under the mining space by analyzing the differential characteristics of the coal seismic waves in the time-frequency domain and polarization parameters, to evaluate the field applicability of the two types of geophones, and to provide application guidance for mine seismic exploration.

2. Related Works

Among the data visualization methods, the research of 2D visualization algorithms started earlier, and there are many mature 2D visualization software. As the visualization research progressed, researchers began to favor 3D visualization methods with higher data utilization, trying to find better 3D visualization and use its richer expressive power to overcome some limitations of 2D visualization [6]. At present, the purpose of 3D visualization of seismic data is to reflect the inline information between data more efficiently to improve the accuracy of oil and gas exploration and accelerate the exploration process, rather than pursuing more detailed and realistic 3D scenes; however, due to the increasingly large amount of 3D seismic data obtained by advanced data acquisition techniques, although the emergence of GPU has eased the pressure of CPU in processing 3D geometric operations, GPU is also limited by the size of memory and cannot directly cope with the massive data exceeding the memory scale, so it is difficult to load the data completely into the memory and then process it in the process of data visualization and other applications [7]. The traditional body data rendering process is exactly loading the body data completely into memory at one time, and the rendering module only gets the data from memory, so this approach fails for large seismic data that exceeds the memory scale [8].

Bakulin et al. proposed a wavefront method for interpreting seismic refraction waves, i.e., using Huygens' principle to reconstruct the wavefront field based on the recorded first-to-wave travel time at two gun sites, and then calculate the depth of the refraction layer based on the velocity above the refraction layer, but when the stratigraphy changes drastically, the circular wavefront theory does not match the actual situation and cannot be applied to this geological condition [9]. Shiraishi et al. proposed the delay time method to identify the refraction layer by calculating the relationship between the reciprocal time and the intercept time, but this method is limited in the imaging effect in subsurface formations with large dip angles and multiple media layers [10]. Schaaf and Bond further proposed the addition and subtraction method based on Thornburgh's wavefront method, in which the travel time of two-gun points to each geophone can be added to obtain [11]. This method calculates the exact value from the refractive layer to the surface through the "plus line" and "minus line." The generalized reciprocal method is a technique to image the undulating refractive layer at any depth based on the seismic refractive wave data consisting of forward and reverse travel times and to analyze the velocity of the refractive layer based on the travel times recorded by the geophone [12]. Using the upper cover velocity and refractive wave travel time data, the method can be used to calculate refractive layer images with higher resolution in complex near-surface structures [13].

Whether in the time domain or the frequency domain, the co-offset distance channel set seismic data reconstruction effect is the best with less loss of effective information. However, for the three-dimensional seismic data body, only one direction of information is utilized, and the reconstruction effect has a greater possibility of improvement. Therefore, two-dimensional random sampling is performed on the time slice of this data body, and the reconstruction process is the same as that of the above one-dimensional random undersampling missing seismic data, but the sampling data processed are the common gunpoint-checkpoint direction and the common offset distance-center point direction. The reconstruction accuracy of the reconstruction results is

significantly improved compared with the 1D random undersampling reconnection results. However, the reconstruction results of the common offset distance-center point under two-dimensional random sampling are not much better than the reconstruction results of the common gunpoint-checkpoint channel set, because the slope of the homophase axis of the reflected wave in the center point channel set is larger and the wave field is more complicated when the two directions are sampled.

3. Interactive Multimedia Data Coscattering Point Imaging Design

At present, mine seismic mainly serves to solve the problems of mine full-space hazard source detection and anomalous structure imaging accuracy, and the lithology of the actual mine site is usually known, so the subsequent study in this paper is carried out from simple to complex, using the uniform isotropic medium as the background. Due to the limitation of the construction observation space and the specificity of the actual demand for mine detection, the application of the scattered wave imaging method in mines must be based on the corresponding detection space and detection purpose, so the study of the mapping method for the set of scattered wave coscattered point paths in different typical detection modes is essential [14]. The purpose of utilizing the scattered wave signal in the transmission recording cannot be achieved. In the process of transforming the transmitted wave of the working face, all other possible travel time compensation methods were tried, but this fundamental problem could not be avoided. On this basis, scattered wave imaging and multiwave multicomponent methods can be integrated into the field of mine seismic to form a practical multiwave scattering imaging method for mines and make theoretical and application innovations.

The model is shown in Figure 1. The background velocity of the model is 3000 m/s, the scattering point velocity is 2000 m/s, the detection point is arranged at $X = 0{\sim}50$ m, $Z = 0$ m, the single gunpoint is arranged at $X = 50$ m, $Z = 0$ m, the channel spacing is 2.5 m, and the scattering point is located at $X = 100$ m, $Z = 0$ m.

The virtual survey line is established at $X = 50$ m, and the virtual survey line is in the range of $Z = -50{\sim}50$ m, and the mapping parameters of the coscattering point channel set of the overdetection are the following: the maximum equivalent offset distance is 100 m, the equivalent offset distance interval is 2 m, and the CSP point interval is 2 m. This method can transform the linear reflection wave in front of the original record into a scattered wave with hyperbolic arrival characteristics and significantly increase the number of signal superpositions. Under this equivalent method, the CSP channel set only has the signal of one side of the equivalent offset distance, and the record is presented as the half branch of the hyperbola because the actual gun check positions are located on one side of the detection area. As the CSP channel set deviates from the scattering point, the equivalent offset distance of the effective scattered wave increases, and the signal of small equivalent offset distance is missing data, which appears as the distant branch signal of the hyperbola in morphology and causes difficulties in the judgment of the top point of the scattered wave [15]. The CSP channel set under this equivalent method may still have scattered waves that may cause imaging artifacts even when it is not at the scattering point position, cannot avoid the arc drawing phenomenon of the conventional oversurvey offset imaging, and cannot distinguish the real scattering point signal.

When the source-receiver point is in the alleyway on both sides of the working face, the essence is the conventional transmission wave method observation system at the working face, and the detection area is the area between the source and receiver points. Specifically, for a certain scattering point, the travel time and path of the scattered wave are dynamic and known during mapping, then for any sampling point signal in the records of different shot detection pairs, the corresponding polarization factor. According to Huygens' principle, transmitted waves also belong to the category of scattered waves, and scattered waves will be generated when the transmitted waves encounter scattering points during the propagation of transmitted waves. From this, it is obtained that the equivalent offset distance of the source-receiver point on the working face side of the double-aisle is dominantly given by

$$h_e = v_e\left(\frac{t}{2}\cdot\frac{t_0}{t_i} - t_0^2\right)^{1/2}. \tag{1}$$

Suppose the source point is in the track lane and the receiving point is in the belt lane, currently, due to the change of the propagation path of the scattered wave. We try to introduce a new propagation travel time t_{rv} according to the equivalent offset distance; t_{rv} is the travel time of the scattered wave from the receiving point R to the vertical virtual receiving point $R^{'}$ of the opposite lane so that the total travel time of the scattered wave from the source point S through the scattering point to the receiving point R:

$$t = \left[t_0^2 - \frac{h_s^2}{v_s^2}\right]^{1/2} - \left[(t_{rv} - t_0)^{1/2} - \frac{h_s^2}{v_s^2}\right]^{1/2}. \tag{2}$$

The travel times of the scattered waves at different depth scattering points under the concept of equivalent offset distance do not satisfy the hyperbolic relationship when the source and receiver points are located in the alleyways on both sides of the working face, and the purpose of using the scattered wave signals in the transmission record cannot be achieved. In the process of working surface transmission wave modification, various other possible travel time compensation methods were tried but could not circumvent this fundamental problem, which originated from the nature of the actual observation system. Although it is difficult to solve this problem with the current method, it will be an important research direction to use the new method to modify the transmission wave so that its time distance satisfies the hyperbolic relationship, which in turn satisfies the conventional seismic processing method, greatly improves the data

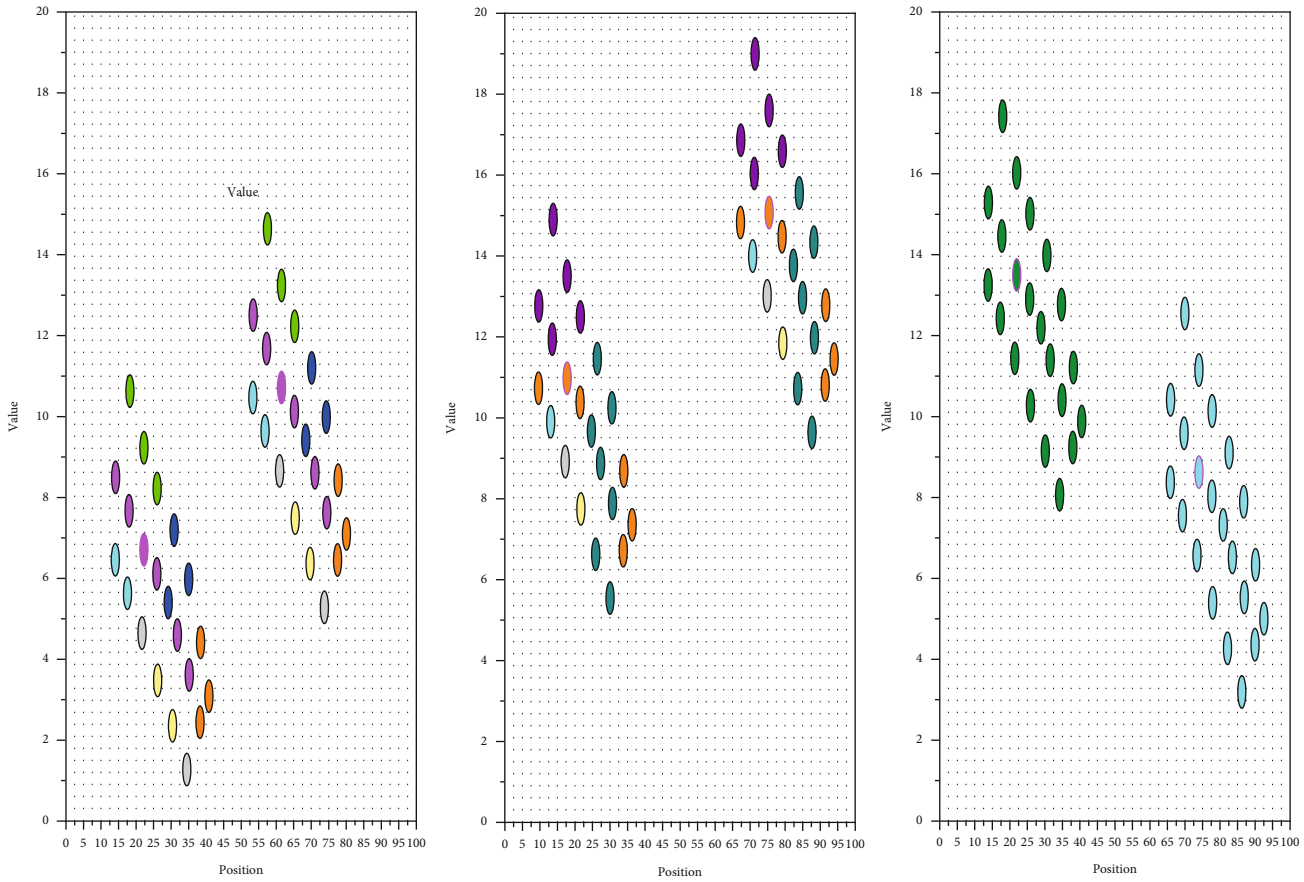

Figure 1: Coscattering point channel set for the overdetection single-point model.

utilization in transmission detection engineering, and ensures the redundancy of seismic wave imaging in the in-plane detection:

$$u(t+\Delta t) = s\sum_{m=2}^{2M}\frac{\nabla t}{k!}\frac{\partial k}{\partial t}u(t). \tag{3}$$

To resolve geological anomalies on one side of the working face roadway or other explored roadway in the direction of the following layer, multiwave imaging of one side area is performed using scattered waves. It should be noted that the mapping of the channel set is limited by two parameters, namely, travel time and spatial path, and the corresponding polarization filtering function is also changed with these two parameters; specifically for a scattering point, the travel time and path of the scattering wave are dynamic and known at the time of mapping, then the corresponding polarization factor and directional filtering factor for any sampling point signal in the records of different gun inspection pairs [16]. The directional filter factors are all dynamically obtainable. In this way, the vector wavefield separation process is completed for a specific type and region of scattered waves:

$$\rho\frac{\partial V_x^X}{\partial t} - d(x)V_x^X = \frac{\partial \sigma_{xx}}{\partial x}, \tag{4}$$

$$\rho\frac{\partial V_x^Z}{\partial t} + d(x)V_x^Z = \frac{\partial \sigma_{xx}}{\partial x}. \tag{5}$$

In the ideal field of seismic data acquisition, it is required to acquire regular and dense high-quality raw data without exceeding the project cost; however, the data acquisition is often affected by various factors, and the seismic trace data are often missing. To effectively recover the missing seismic traces, this paper proposes a high-precision seismic data reconstruction method to obtain regular and complete pre-stack seismic data, which provides an excellent data environment for subsequent data interpretation and final judgment. This paper presents an in-depth study of the data reconstruction aspects and analyzes the critical steps that affect the reconstruction effect.

As shown in Figure 2, some longitudinal and transverse lines are arranged on the ground in the vibration zone, a geophone is placed on them, and the reflected wave superimposed signals of each stratigraphic subinterface in the ground received by the geophone are sampled once every time after the source explosion, and finally, the sampled data are brought back and filtered, corrected, antifolded, etc., which finally form the longitudinal line (also called the main line), transverse line (also called contact line), and time axis line data, and are stored in Seg-Y format.

The purpose of classifying bulk data by data values is to correctly assign different color and transparency values to

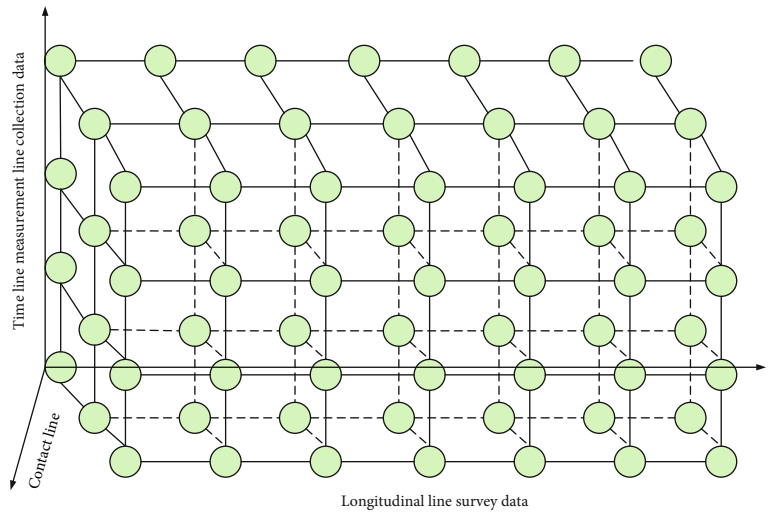

Figure 2: Logical distribution of data in 3D space.

different classes of data to correctly represent the different distributions of multiple substances or the different properties of a single substance. To achieve this, it is necessary to map the different classifications to different colors and opacities using transfer functions.

However, it is often very difficult to find a suitable transfer function to classify and map the data body, and the organization is often quite complex when many different materials coexist. For example, for seismic data, rocks of the same lithology often have different gray values depending on the layer depth, and pixels of the same gray value may belong to rocks of different lithology [17], to correctly represent the different distributions of multiple substances or the different properties of a single substance. Therefore, this problem is still an urgent research problem in the 3D visualization technology of body data. At present, for 3D data bodies with simple material composition, the two most used methods are the threshold classification method and the probabilistic classification method, and the following is a brief description of the classification of seismic body data using the threshold method.

4. Low Signal-to-Noise Ratio 3D Seismic Data Processing Design

In the analysis of time-varying signals with frequency variations over time, time-frequency analysis can represent the one-dimensional signal on a two-dimensional coordinate map with time and frequency as the horizontal and vertical coordinates, which can clearly show the time-frequency characteristics of the signal and reflect some useful information needed in signal processing. The high resolution of time-frequency representation is of great significance to the description of geological formations, and time-frequency analysis is closely related to the study of stratigraphic structure, sedimentary properties, and reservoirs.

From the theory of absorption and attenuation of seismic waves, it is known that the fluctuation equation satisfied by the displacement vector in a viscoelastic medium without physical force when seismic waves propagate in a nonperfectly elastic rock is

$$\rho \frac{\partial^2 u}{\partial t^2} = \frac{(\lambda - \mu)\nabla \mathrm{divu} + \left(\lambda' - \mu'\right)\nabla \mathrm{divu}}{\partial t} - \mu^2 \frac{\partial u}{\partial t}. \quad (6)$$

In the traditional seismic prestack data set, the first two types of tracts are generally used, the reflected wave holography is hyperbolic, and the refracted and direct wave homography is linear, with different dip angles of homography superimposed on each other, damaging the effective wave information. The signal structure is simple, and the combination of the data body before stacking with the curvilinear wave transform with scale, direction, and curvilinear singularity will theoretically achieve a more satisfactory reconstruction effect.

To further compare the different effects between the three threshold parameter formulas, first set the maximum number of iterations to 50, and draw a graph of the relationship between the number of iterations and the signal-to-noise ratio, as shown in Figure 3. To achieve this, it is necessary to map the different categories to different colors and opacities through a transfer function. From Figure 3, we can see that when the signal-to-noise ratio of 15 dB needs to be achieved, the linear threshold parameter cannot be achieved within 50 iterations, and the exponential threshold parameter needs about 27 iterations to be achieved, while the new exponential threshold parameter applied in this chapter can be completed in only 18 iterations, and the convergence speed is much faster.

In other words, the signal-to-noise ratio of the new exponential threshold parameter is higher for the same number of design iterations, and the new exponential threshold parameter is more advantageous for industrial production considerations:

$$\rho \frac{\partial^2 \varphi}{\partial t^2} = \frac{\mu' \nabla \mathrm{divu}}{\partial t} + \mu^2 \frac{\partial u}{\partial t}. \quad (7)$$

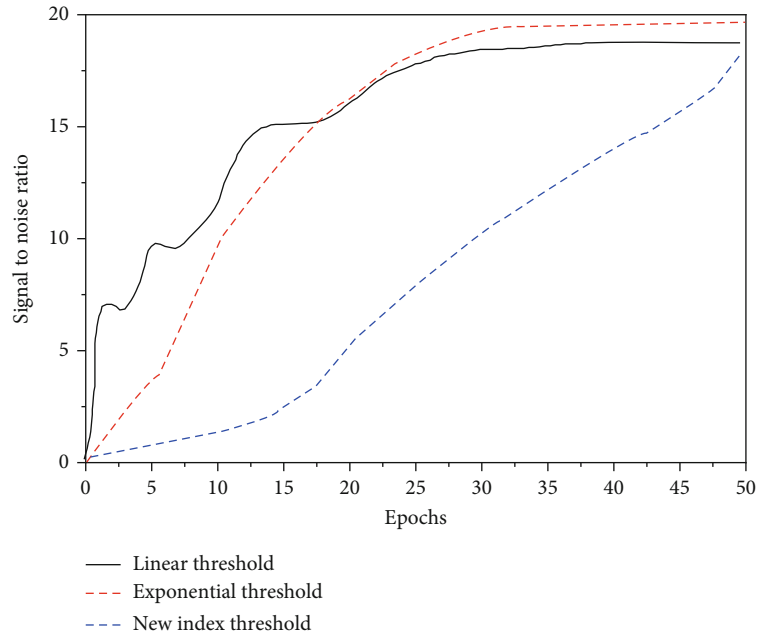

Figure 3: Number of iterations versus signal-to-noise ratio graph.

In this paper, to improve the reconstruction accuracy, the complex-valued curvilinear transform is used, but there is still a certain shortage for the computation time aspect. For this reason, this paper proposes a reconstruction method based on the frequency-domain complex-valued curvilinear transform, i.e., the Fourier transform is used first to transform the reconstruction data from the time domain to the frequency domain, and then, the reconstruction is carried out using the algorithm of this paper. Since the reconstruction data are sparse by Fourier transform before the reconstruction by curvilinear transform, the low energy effective wave coefficients are not filtered out when the convex set projection algorithm is applied, so that the in-phase axes containing high and low energy amplitudes can be reconstructed simultaneously, which is more effective than the previous reconstruction by curvilinear transform alone [18].

Moreover, since the complex-valued curvilinear transform is used, the computation time is the same whether the reconstruction is done in the time domain or the frequency domain. Although the computation time is required for transforming the time domain to the frequency domain and conjugate valuation, it is negligible compared to the computation time of the complex-valued curvilinear transform when processing a large amount of seismic data. Moreover, the time-frequency transformation process can make the data sparser, which is more conducive to the reconstruction of seismic data in the compressed sensing framework, and theoretically, the reconstruction results will be better.

The plane wave amplitude is influenced by the geometric diffusion in addition to the stratigraphic attenuation. To eliminate the influence of geometric diffusion on plane wave amplitude, the method of measuring two samples, i.e., reference sample and rock sample, can be used in petrophysical tests. The time-domain signal is converted to the frequency domain by Fourier transform as a signal in complex form, with the real part being the amplitude spectrum and the imaginary part being the phase spectrum. In the case of ignoring the phase information, only the amplitude and frequency are considered, and the reference subwave is corrected by different Q values until it can reach a certain degree of agreement with the subwave signal at the receiving point, and this method is called the spectrum simulation method. The method loses the phase information, and although it is possible not to focus on the fit at the time point, only to compare the similarity of the corresponding frequencies, the information does bring unavoidable errors, as shown in Figure 4.

Since the mapped texture elements may not be aligned with the coordinates in the texture space where the corresponding data points are located, they need to be resampled to obtain more accurate texture values. The simplest way to handle this is to use the trilinear interpolation of the mapping results of the eight nearest data points for a sample point in the texture slice to obtain a more accurate texture value for that sample point.

The wavelet coefficients are in different scales, i.e., the representation of the original signal at multiple resolutions [19]. It can clearly show the time-frequency characteristics of the signal, reflecting some useful information needed in signal processing. It is easier to distinguish the effective signal from the random noise under multiscale decomposition by the transmission characteristics because the wavelet coefficients of the signal increase with scale while the coefficients representing the noise decrease. Thus, we can choose an appropriate threshold to extract the effective signal and smooth the noisy signal. In the near-surface loose sediment layer, the geometric seismology based on elastic wave theory is no longer fully applicable, and the dispersion characteristics possessed by the surface waves are directly related to the layered structure of the medium, which provides a basis for

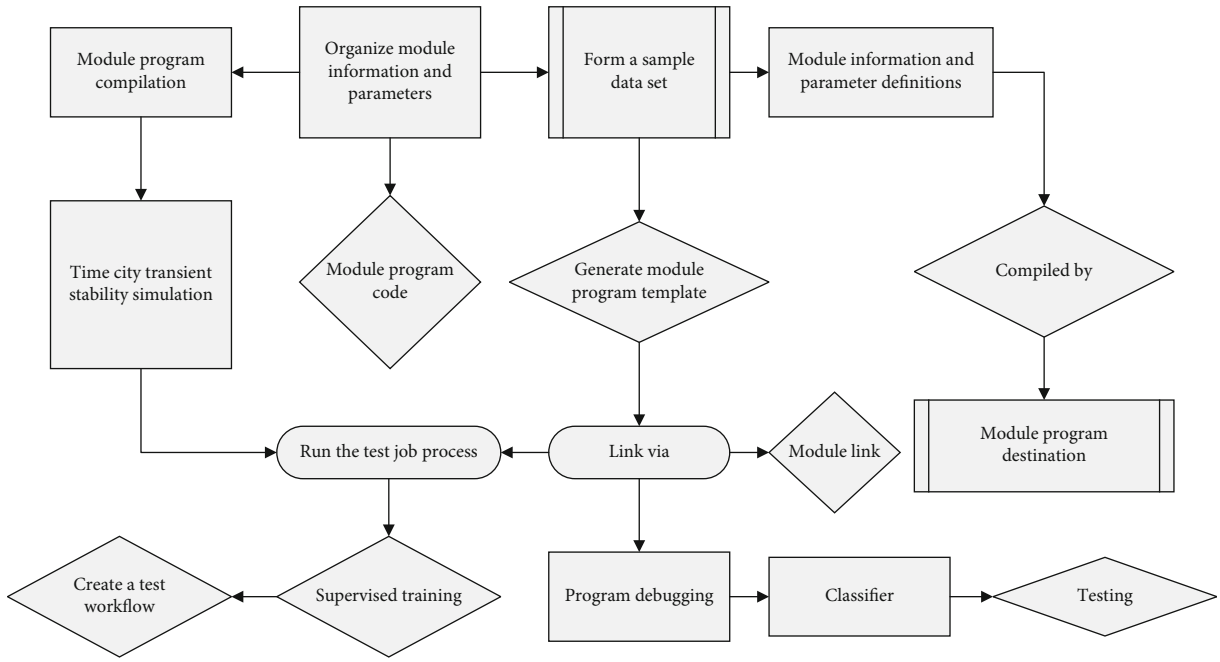

Figure 4: Processing steps.

estimating the near-surface property parameters using the surface wave dispersion characteristics.

$$f_{\max} = \frac{1}{|\partial t/\partial l|\nabla l}. \tag{8}$$

5. Experimental Design of Imaging

The offset/antioffset aperture is an important parameter in the Kirchhoff-type prestack offset/antioffset implementation technique. The size of the aperture determines the range of seismic traces that contribute to the pixels of the imaged spot. It is difficult to accurately calculate the optimal offset or counteroffset aperture during the actual calculation. Therefore, the best offset/counteroffset aperture value for imaging can be selected based on the actual processing experience, considering the burial depth, dip angle, and other factors. For a certain seismic record, the coordinates of its centerpoint can be determined, and the cone with this center point coordinate as the vertex will be used as the offset/antioffset aperture. The size of the aperture gradually increases with depth, and the size of the desired aperture can be defined by choosing the appropriate offset angle. The actual calculation process usually takes a relatively small offset angle in the vertical measurement line direction and a relatively large offset angle along the measurement line direction. The reverse offset aperture is selected as above.

There is no higher frequency component in the seismic data body than the maximum temporal frequency, which represents the maximum temporal frequency to avoid artifacts at the intersection of the trace and the operator trajectory as a function of the local operator dip and trace spacing. In order not to generate operator spurious frequencies, the sampling sequence of the summed seismic trace data superimposed along the offset/antioffset operator trajectory needs to satisfy the Nyquist sampling criterion:

Firstly, a prestack depth offset is applied to the arbitrary nonzero gun-check distance seismic data, and then, a zero gun-check distance inverse offset is applied to the offset imaging data to output the zero gun-check distance data, and the reflection coefficients can be maintained during the transformation process.

In near-surface velocity structure imaging, the first-to-wave walk-time tomography method usually produces a smooth velocity model. When there is a low-velocity weathering layer overlying the high-velocity bedrock in the near-surface structure, the first-to-wave travel time planimetric imaging method may not be able to invert the sharp boundary. However, based on the same travel time information, the refracted wave travel time offset method can accurately calculate the location of the refracted layer. The method obtains the position information of the refractive layer by downward extension of the refractive wave walk-time profile and a given overlying layer velocity. In this chapter, the joint inversion method of refractive wave travel-time offset imaging and velocity is proposed, as shown in Figure 5.

The method first calculates the position of the refractive layer by the refractive wave walk-time offset method and further constrains the first-to-wave walk-time laminar imaging inversion by transforming the refractive layer obtained from the offset into a discontinuity of the regularization term in the inversion objective function. The refractive layer position shape and velocity model obtained by the offset is updated simultaneously in each subsequent iteration. To accommodate more complex cases, the method is further extended to the multilayer medium case [20]. Although

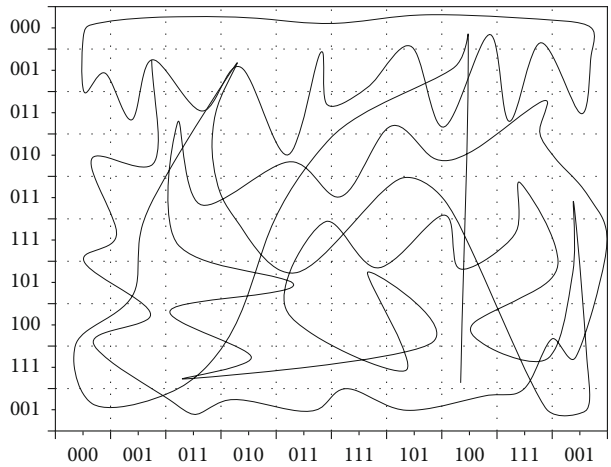

Figure 5: Third-order 3D gray curve.

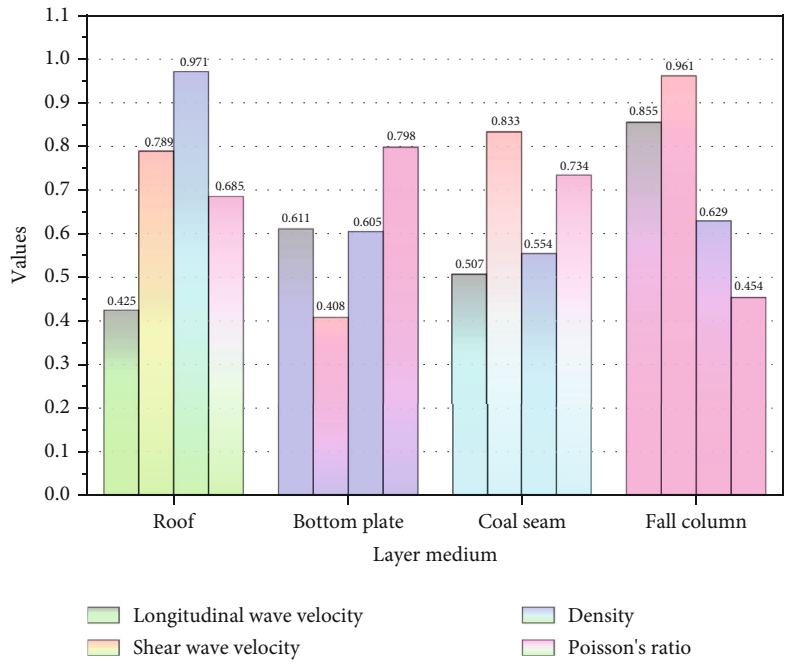

Figure 6: Parameters of the 3D model of the working surface.

transforming the time domain to the frequency domain and conjugate evaluation requires computational time, this is not the case when dealing with large amounts of seismic data. Theoretical model tests show that the joint inversion method demonstrates superiority in reconstructing near-surface models with strong velocity contrast compared to the conventional Tikhonov regularized first-to-wave walk-time laminar imaging method and the delay time method. In practical data applications, the near-surface velocity model obtained by this joint inversion method can calculate more accurate long-wavelength static correction values and make the reflection layer energy more concentrated in the superimposed profile.

When geologists continuously browse the 3D seismic data body, the data block corresponding to each frame is determined by the viewpoint coordinates and observation direction of the current frame, and the viewpoint coordinates and angle change continuously as the browsing progress, forming the viewpoint motion trajectory. Therefore, by fitting the viewpoint trajectory and predicting the viewpoint coordinates at the next moment, the potential domain data can be obtained from the predicted coordinates to realize the preloading operation of the predicted data blocks and reduce the lagging sensation during the continuous viewing of the frames, as shown in Figure 6.

The basis of the Hilbert-R tree is to map the location coordinates of data in high-dimensional space to the encoded values of the corresponding filled curves. Therefore, a stable fractal curve with high filling quality is one of the conditions to ensure the query performance of the Hilbert-R tree.

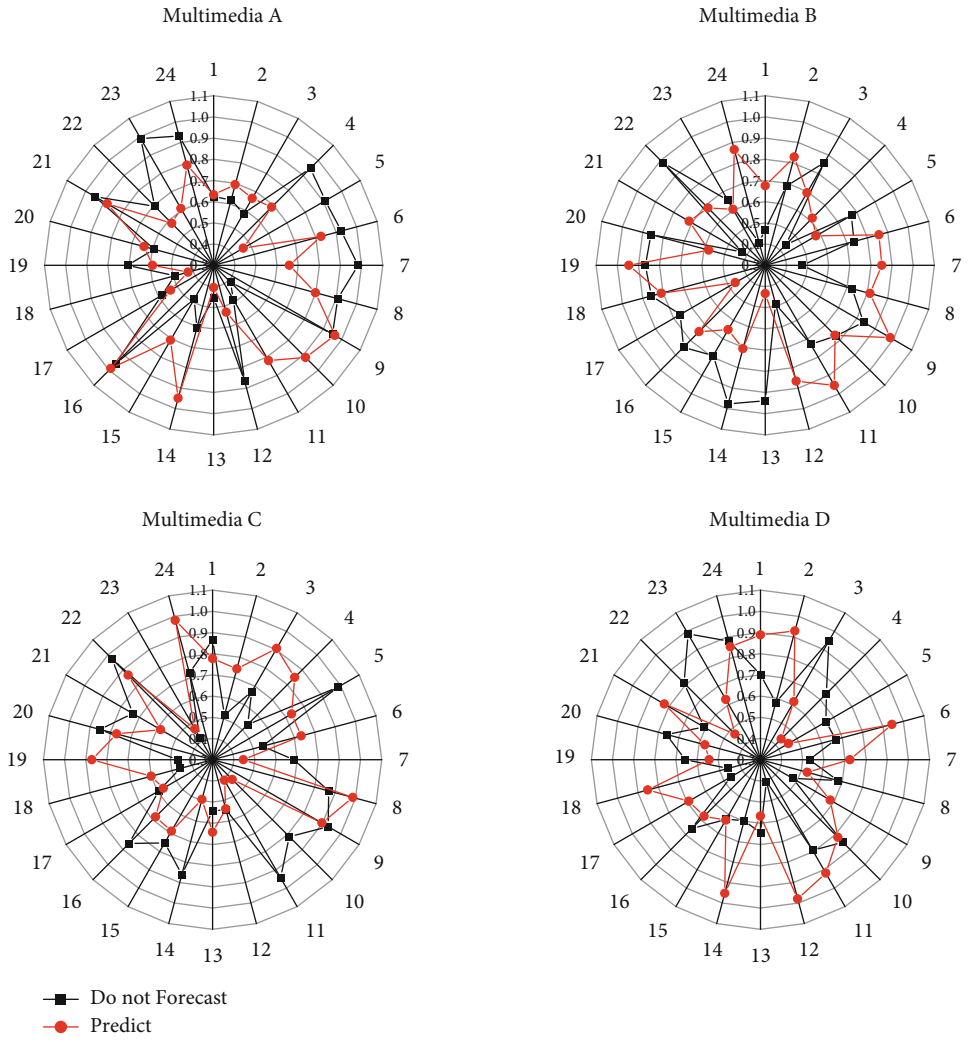

Figure 7: Efficiency comparison.

6. Analysis of Results

In the three-dimensional visualization process, excluding the rendering time, the indexing time of the target data block accounts for most of the total time consumed. In general, the query time of the node is greater than the indexing time of the target data within the node, so it can be said that the access efficiency of the node determines the time consumed by the data indexing in the display process.

This enhancement is based on the superiority of the Hilbert-*R* tree structure using clustering technology: the Hilbert-*R* tree is faster than octree, for all its nodes; except the last node at each level, the rest of the nodes are filled, i.e., for the same volume of data bodies, the number of subblocks generated by the Hilbert-*R* tree is often much less than that of the octree, so its indexing speed is higher than that constructed by the octree structure. By analyzing the different characteristics of coal seam seismic waves in the time-frequency domain and polarization parameters, the signal characteristics of the actual seismic wave field in the mine space were revealed, and the field applicability of the two types of geophones was evaluated. The Hilbert-*R* tree based on cure clustering, based on the Hilbert-*R* tree, performs clustering operations on data bodies in advance to ensure that the Hilbert code values of adjacent MBC centroids

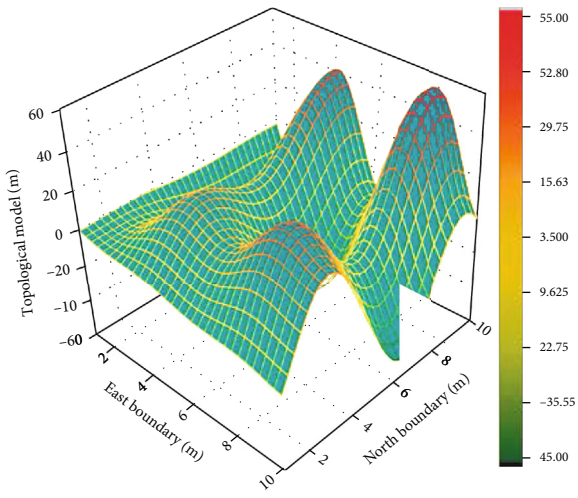

Figure 8: Sounding vibration effect.

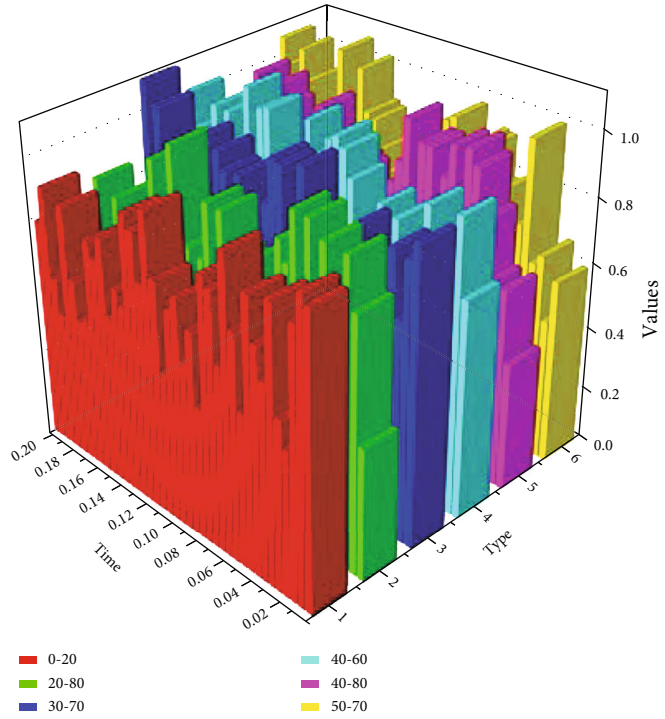

Figure 9: Estimated Q values for different fitted bands.

generated at the end are also similar, i.e., for data adjacent to each other in the spatial structure, their storage locations are also similar, thus effectively reducing the number of disk accesses and thus improving indexing efficiency.

To ensure that the 3D visualization of large-scale seismic data will not be stalled or stuttered, it is necessary to keep the frame rate of the rendering at 24 fps or more. The average frame rate was recorded and compared with the frame rate without prediction, and the results are shown in Figure 7.

The proposed preloading method based on viewpoint motion prediction not only has a high frame rate for visualization of data A and B with small data volume but also maintains a frame rate of about 24 fps for data body C with a size of 10 GB. Compared with the method without preloading, the frame rate increases by 3.2%~46.54% as the data volume increases.

For strong surface waves, low-frequency chirp vibration, wild value interference, and low-frequency strong energy interference, the adaptive coherent noise attenuation technology with high fidelity and split-frequency high-energy noise suppression technology are selected to effectively suppress them. Amplitude preserving noise suppression needs to meet the requirements of maintaining the relative amplitude, waveform, frequency, and phase and suppression filtering as far as possible to meet the requirements of zero phase, amplitude all-pass, and denoising process specifically using four methods to evaluate the denoising effect. The effective signal cannot exist in the suppressed noise. Before and after the suppression, the spectrum can only show the frequency range of the noise. In the single-frequency noise suppression process, the effective signal of the same frequency band cannot be damaged. After the noise suppression, the relative relationship between the effective signal amplitude and energy remains unchanged, and no false frequency phenomenon occurs.

Due to the wide frequency band of the surface wave, the use of an adaptive coherent noise attenuation technique will cause the phenomenon of false frequency; the treatment of the surface wave for the low-frequency band and the high-frequency band of two frequency bands was repeatedly suppressed to maximize the fidelity of the denoising. The collected seismic signals contain random noise and regular noise. The low-frequency chirp developed in the work area is attenuated using the adaptive coherent noise attenuation technique and the predictive antifold technique. The spectrum analysis before and after the chirp suppression in Figure 8 shows that not only the chirp is successfully suppressed but also the effective wave energy is not hurt, and the relative fidelity is achieved in the process of suppressing the surface wave.

The use of split-frequency high-energy noise suppression technology attenuates wild-value interference and strong energy interference in each frequency band. Because the abnormal amplitude energy difference between low and high frequency is large, the low-frequency effective signal may also be mixed with the high-frequency noise signal; wanting to eliminate noise at the same time to protect the effective signal needs to be divided into frequency noise attenuation. The split-frequency high-energy noise suppression technique is to calculate the weighting curve based on the numerical relationship between noise and signal in different frequency bands, perform noise reduction, and then reconstruct the seismic record.

Through fine spherical diffusion and two surfaces' consistent amplitude compensation, the amplitude attenuation caused by the absorption of frequency by the earth is eliminated. It is ensured that the splicing energy of different

blocks of data is consistent, and the relative amplitude curves of the conventional processing profiles and the high-fidelity processing profiles are compared, and the high-fidelity processing maintains the amplitude properties of the data better. Not only the resolution and fidelity are required to be guaranteed but also the processing efficiency needs to be greatly improved to adapt to the complexity and difficulty of exploration work. In the application process, the relative strength and weakness of the amplitude are not artificially changed, and the amplitude can objectively and effectively reflect the subsurface geological interface information and achieve amplitude fidelity as much as possible.

It is generally believed that once the extracted subways are correct, the folded processing will preserve the amplitude, but the extraction of subwaves is affected by various factors such as noise, so the folded processing can only preserve the amplitude relatively, and the good control technology is used to judge the fidelity effect in the process of improving the resolution. The error between the seismic data and the actual well data is gradually reduced so that each step of the resolution improvement process for the Shawan Formation can be based on evidence, and relative fidelity is achieved in the process of resolution improvement, as shown in Figure 9.

The Q value estimation accuracy is the highest and most stable in the frequency range of 40-60 Hz, and the absolute error of Q value estimation is about 2%. The reason is that 40-60 Hz is the closest to the main frequency of seismic subwaves, and the frequency band concentrates the main energy of seismic waves. 0-120 Hz range has the highest estimation error, and the error becomes larger as the seismic wave propagation time increases, and the amplitude decreases as the seismic wave propagates to the deeper part of the ground due to the energy attenuation caused by the absorption and attenuation of the ground, and there is also the effect of the pickup error of the first-to-wave time.

Comparing the estimation results in two different frequency bands, 30-70 Hz and 50-70 Hz, we can see that the estimation results in 30-70 Hz are more stable, indicating that the seismic wave absorption and attenuation in the low-frequency band are lower than the seismic wave absorption and attenuation in the high-frequency band, and the analysis results are consistent with the seismic wave absorption and attenuation theory in which the attenuation of high-frequency seismic waves is stronger. Only the upgoing waves from the subsurface can be received; in the vertical seismic section, because the geophone is placed inside the formation through the well, it can receive both the upgoing waves propagating from the bottom up and the upgoing waves propagating from the top down. Therefore, when estimating Q values using actual seismic data, a reasonable fitting band should be selected within the effective frequency bands of different data, which can effectively avoid the errors caused by noise interference.

7. Conclusion

The equivalent offset distance scattered wave imaging method has good scattered wave extraction capability with a high superposition number and low signal-to-noise ratio requirement. The adaptive instantaneous polarization parameter acquisition method based on the Hilbert transform with a time window can dynamically acquire accurate polarization parameters for each sampling point signal, and the dynamic polarization filtering function can be established by combining with the typical seismic wave polarization characteristics of the mine. The polarization filter function is invalid for conversion waves with the same type of polarization characteristics, and the relevant interference waves can be eliminated by the conversion wave velocity difference that can be designed as a suppression factor. In the roadway overdetection, the original observation system can be changed to expand the offset distance by establishing an equivalent virtual survey line perpendicular to the roadway direction; in the workforce transmission wave observation, the scattered wave travel time of different depth scattering points under the concept of two-dimensional equivalent offset distance does not satisfy the hyperbolic relationship, and the purpose of using the scattered wave signal in the transmission record cannot be reached, while the three-dimensional equivalent offset distance method in the workforce can extend the detection direction. The method can extend the detection direction to the depth direction of the top and bottom plates of the working face, to carry out the scattered wave imaging of the top and bottom plates. It is more helpful to reveal the inherent laws of geoscience data, to carry out activities such as energy detection, and then generate huge economic benefits. In the roadway overdetection, the original observation system can be changed, and the offset distance can be expanded by establishing an equivalent virtual survey line perpendicular to the roadway direction; in the workforce transmission wave observation, the scattered wave travel time of different depth scattering points under the concept of two-dimensional equivalent offset distance does not satisfy the hyperbolic relationship, and the purpose of using the scattered wave signal in the transmission record cannot be achieved, while the workforce three-dimensional equivalent offset distance method can extend the detection. The 3D equivalent offset distance method of the working face can extend the detection direction to the depth direction of the top and bottom of the working face, to carry out the scattered wave imaging of the top and bottom of the working face.

Data Availability

No data were used to support this study.

Conflicts of Interest

The authors declare that there is no conflict of interest with any financial organizations regarding the material reported in this manuscript.

References

[1] D. Liu, W. Wang, X. Wang, C. Wang, J. Pei, and W. Chen, "Poststack seismic data denoising based on 3-D convolutional

neural network," *IEEE Transactions on Geoscience and Remote Sensing*, vol. 58, no. 3, pp. 1598–1629, 2020.

[2] M. Waage, S. Bünz, M. Landrø, A. Plaza-Faverola, and K. A. Waghorn, "Repeatability of high-resolution 3D seismic data," *Geophysics*, vol. 84, no. 1, pp. B75–B94, 2019.

[3] S. Yuan, S. Wang, C. Luo, and T. Wang, "Inversion-based 3-D seismic denoising for exploring spatial edges and spatio-temporal signal redundancy," *IEEE Geoscience and Remote Sensing Letters*, vol. 15, no. 11, pp. 1682–1686, 2018.

[4] N. Lebedeva-Ivanova, S. Polteau, B. Bellwald, S. Planke, C. Berndt, and H. H. Stokke, "Toward one-meter resolution in 3D seismic," *The Leading Edge*, vol. 37, no. 11, pp. 818–828, 2018.

[5] N. Salaun, H. Toubiana, J. B. Mitschler et al., "High-resolution 3D seismic imaging and refined velocity model building improve the image of a deep geothermal reservoir in the Upper Rhine Graben," *The Leading Edge*, vol. 39, no. 12, pp. 857–863, 2020.

[6] H. Karbalaali, A. Javaherian, S. Dahlke, R. Reisenhofer, and S. Torabi, "Seismic channel edge detection using 3D shearlets—a study on synthetic and real channelised 3D seismic data," *Geophysical Prospecting*, vol. 66, no. 7, pp. 1272–1289, 2018.

[7] A. Malehmir, A. Tryggvason, C. Wijns et al., "Why 3D seismic data are an asset for exploration and mine planning? Velocity tomography of weakness zones in the Kevitsa Ni-Cu-PGE mine, northern Finland," *Geophysics*, vol. 83, no. 2, pp. B33–B46, 2018.

[8] M. Protasov, V. A. Tcheverda, and A. P. Pravduhin, "3D true-amplitude anisotropic elastic Gaussian beam depth migration of 3D irregular data," *Journal of Seismic Exploration*, vol. 28, no. 2, pp. 121–146, 2019.

[9] A. Bakulin, P. Golikov, M. Dmitriev, D. Neklyudov, P. Leger, and V. Dolgov, "Application of supergrouping to enhance 3D prestack seismic data from a desert environment," *The Leading Edge*, vol. 37, no. 3, pp. 200–207, 2018.

[10] K. Shiraishi, G. F. Moore, Y. Yamada, M. Kinoshita, Y. Sanada, and G. Kimura, "Seismogenic zone structures revealed by improved 3-D seismic images in the Nankai Trough off Kumano," *Geochemistry, Geophysics, Geosystems*, vol. 20, no. 5, pp. 2252–2271, 2019.

[11] A. Schaaf and C. E. Bond, "Quantification of uncertainty in 3-D seismic interpretation: implications for deterministic and stochastic geomodeling and machine learning," *Solid earth*, vol. 10, no. 4, pp. 1049–1061, 2019.

[12] S. Cordery, "An effective data processing workflow for broadband single-sensor single-source land seismic data," *The Leading Edge*, vol. 39, no. 6, pp. 401–410, 2020.

[13] H. Wang, W. Chen, W. Huang et al., "Nonstationary predictive filtering for seismic random noise suppression—a tutorial," *Geophysics*, vol. 86, no. 3, pp. W21–W30, 2021.

[14] G. Bellefleur, S. Cheraghi, and A. Malehmir, "Reprocessing legacy three-dimensional seismic data from the Halfmile Lake and Brunswick No. 6 volcanogenic massive sulphide deposits, New Brunswick, Canada," *Canadian Journal of Earth Sciences*, vol. 56, no. 5, pp. 569–583, 2019.

[15] Z. Wang, H. Di, M. A. Shafiq, Y. Alaudah, and G. AlRegib, "Successful leveraging of image processing and machine learning in seismic structural interpretation: a review," *The Leading Edge*, vol. 37, no. 6, pp. 451–461, 2018.

[16] A. El-Emam, M. Al-Otaibi, and C. Koeninger, "Workshop explores advances in land seismic data processing," *The Leading Edge*, vol. 38, no. 12, pp. 960–965, 2019.

[17] M. Mohammadi, B. Soleimani, and M. Mahmoudian, "Predicting abnormal formation pressure using 3D seismic velocity, in Kupal Oil Field," *Journal of Petroleum Research*, vol. 27, no. 96-6, pp. 103–115, 2018.

[18] H. Cheng, K. Xie, C. Wen, and J. B. He, "Fast visualization of 3D massive data based on improved Hilbert R-tree and stacked LSTM models," *IEEE Access*, vol. 9, pp. 16266–16278, 2021.

[19] A. Malehmir, M. Markovic, P. Marsden et al., "Sparse 3D reflection seismic survey for deep-targeting iron oxide deposits and their host rocks, Ludvika Mines, Sweden," *Solid Earth*, vol. 12, no. 2, pp. 483–502, 2021.

[20] Y. Chen, "Fast dictionary learning for noise attenuation of multidimensional seismic data," *Geophysical Journal International*, vol. 222, no. 3, pp. 1717–1727, 2020.

Hindawi
Wireless Communications and Mobile Computing
Volume 2022, Article ID 8110399, 8 pages
https://doi.org/10.1155/2022/8110399

Research Article

Networked Fitness Management System Based on Internet of Things

Haikun Wu

Teaching Department of Basic Course, Yinchuan University of Energy, Yinchuan 750100, China

Correspondence should be addressed to Haikun Wu; 160706226@stu.cuz.edu.cn

Received 7 June 2022; Revised 5 July 2022; Accepted 15 July 2022; Published 3 August 2022

Academic Editor: Jun Ye

In recent years, with the rapid development of Internet of things and other technologies, the digitalization, networking, and intelligence of sports have become the current research focus. In this paper, the fitness management system based on the Internet of things is studied. By analyzing the system function and performance requirements, the design of fitness client (small tablet) of networked fitness management system is based on Internet of things. Receiving the fitness data uploaded by the fitness device through Bluetooth, the fitness data can be processed and displayed in real time with graphics. After the exercise, the fitness data can be uploaded to the central computer through Wi-Fi wireless. Taking barbell as an example, by analyzing the movement characteristics of barbell, Bluetooth MPU6050 module is used for data acquisition; the data collected includes angle, number, etc.; the relevant functions of barb-dumbbell movement are analyzed and designed; and the Bluetooth communication module and Wi-Fi communication module in the small tablet software system are designed and implemented. The relevant experiments were carried out based on the developed software and hardware platform. Recognition experiments on 7 classes of actions show that the proposed deep neural network learns well on small datasets, achieving an action recognition accuracy of 97.61%, and the SVM also achieves a recognition accuracy of more than 96%. In the 50 action cycle calculation experiments, the number statistics algorithm reached 100% calculation accuracy, and the action cycle calculation results are also close to the real value, proving the effectiveness of the periodic calculation method.

1. Introduction

Today, the times are constantly developing, and people's requirements for material life will gradually improve. While their living standards are met, they begin to pursue a healthy lifestyle, basically based on physical exercise? The Internet of things uses the network and various sensing devices to collect information and connect people, people and things, and things and things to achieve intelligent remote management and control. In the context of the current mobile Internet, the information acquisition technology is based on the Internet of things, as the fourth generation data acquisition technology, with its superiority and times, it will play an increasingly important role in the field of information technology. The intelligent sports health management system based on big data mining and Internet of things is composed of seven layers, namely, user layer, Internet of things layer, communication layer, network layer, function layer, rule layer, and data layer. Running is one of the important activities for people to conduct physical exercise. It is the most popular fitness activity in the world. It is highly evaluated in both the medical and sports circles, and it is also the most scientific and effective way to maintain a person's body and mind. The health management system designed based on Internet of things technology can provide remote monitoring and health guidance for patients, so as to promote personal health. Experimental results show that the system has achieved the expected effect.

(1) *User Layer*. The user layer is a collection of resident application interfaces, and users interact with the Internet of things layer and input or view personal

information through fitness APP, WeChat mini program, user interface of fitness equipment, and computer web page

(2) *Internet of Things Layer*. The IoT layer includes hardware such as wearable devices, phones or computers, smart fitness equipment, smart fitness venues, smart trails, virtual reality (VR), and augmented reality (AR) devices. In the hardware device, the interface program that interacts with the user and the calculation and storage model of fitness data is stored in advance, which can realize simple information query, evaluation, prediction, and other functions. The network layer is the Internet network, which complies with the international standard of network settings and information transmission, transmits the user information to the scheduled website, or transmits the information required by the user from the scheduled website to the user interface

(3) *Communication Layer*. The communication layer mainly includes 4G and 5G wireless networks. Through the wireless network, the user information is transmitted to the Internet or the Internet information is transmitted to the user

(4) *Function Layer*. Function layer is the core part of intelligent sports health management system. This layer obtains the fitness data to be calculated from the data layer and selects the appropriate operation rules from the rule layer to calculate the data, after the calculation results are obtained, the recommended information such as health status assessment information, sports injury and disease prediction information, and scientific fitness methods are pushed to the users through the network layer, communication layer, and Internet of things layer

(5) *Rule Layer*. Rule layer is the intelligent part of intelligent sports health system, including sports injury and disease evaluation model base, data mining method base, and scientific fitness knowledge base

(6) *Data Layer*. The data layer stores users' sports information, including personal basic sports database and personal sports status database

In the digital network era, people have higher requirements for sports and fitness; in the future, sports and fitness not only need good fitness equipment and environment but it also needs more convenient and intelligent health management, service guidance, social entertainment, and other refined fitness services. The innovation of sports and fitness equipment in digital network era will depend on the development of information technology and network technology. Using the Internet of things technology, it can connect residents, wearable devices, smart trails, smart fitness equipment, smart fitness venues, etc.; collect data for the intelligent sports and health management system; and push scientific fitness methods recommended by the system to residents. IoT has unique advantages in fitness data collection and information output.

With the development of science and technology, at present, the integration and application of network technology in the field of physical fitness are one of the most important trends to promote the development of national fitness. At present, the portable equipment or large medical equipment used to monitor the basic parameters of the human body basically does not reflect the other value of, except for recording and monitoring. With the rapid development of embedded devices, wireless sensor networks, mobile computing, and other technologies, the public lives in an omnipresent network formed by the integration of communication networks, Internet, sensor networks, and so on. There is a growing body of research on how science, technology, and humanity can be combined, using new technologies and complex systems theory to digitize and dynamic humanistic knowledge, which is traditionally limited to language level and static.

Taking this as a starting point, a fitness client of networked fitness management system based on the Internet of things is designed. The related functions of health management system are analyzed and designed, and the Bluetooth communication module and Wi-Fi communication module in the small tablet software system are designed and implemented [1].

With the development of the times and the progress of society, the popularization of computer network technology and information technology in China is accelerating, and the Internet of things technology also appears in people's vision and gradually recognized by people. In this era of big data, it has brought huge challenges to all walks of life. Gao et al. put forward the method of applying the Internet of things technology to the research and development of data asset management system of graph database [2]. In order to monitor the classroom environment, control electrical equipment to reduce energy consumption, and analyze the classroom environment and utilization rate, Zhu et al. developed an intelligent classroom management system based on the Internet of things [3].

In the process of physical training, it is the key point of scientific physical training to adjust and control the strength of physical load in real time, accurately and effectively, and make it conform to the predetermined training plan. In view of the current problems in the field of sports and fitness, Shan and Mai designed and implemented a dynamic management technology of sports and fitness based on the concept of Internet of things and blockchain [4]. Li, based on the Internet of things (IoT), studied the method of using linear acceleration energy estimation model to evaluate athletes' special physical ability. A real-time monitoring platform for athlete training is designed [5]. Zhou's application management system of outdoor fitness equipment for all people based on big data of Internet of things will provide enough power for physical and social health of all people through intelligent terminals, Internet of things, and big data analysis [6]. Huang et al. designed an intelligent physical fitness monitoring system based on Internet of things technology [7] in view of the current demand for the popularization

Figure 1: Intelligent fitness management of the Internet of things.

of smart phones and athlete training monitoring. Yang and Paik studied fitness games based on the Internet of things [8]. He and Amp discussed the information visualization design of health management application in the digital information age. This paper analyzes the basic steps of visual information creation from four aspects: information acquisition, architecture, presentation, and interaction, and summarizes the visual design method and interface design method of sports information of fitness management APP [9]. Rekha et al. designed a Web application for fitness management system [10]. Dong et al. proposed a design scheme for a physical test management system, which was mainly developed by Python language, and Django framework was used as the Web framework [11].

On this basis, the fitness management system based on the Internet of things is studied. Through the system function and performance requirements analysis, the fitness client (small tablet) of the Internet of things based on network fitness management system is designed. Figure 1 shows the main functions of the intelligent fitness management system of the Internet of things [12].

2. Research Methods

It mainly designs and realizes the small tablet fitness system. At present, mobile phones, tablets, and other terminal products on the market basically provide Bluetooth function and Wi-Fi connection and communication function; the small tablet and central machine of the system are both tablets based on Android platform; in order to realize the seamless connection between small tablet and fitness equipment and central machine, considering the transmission distance and speed, the system uses Bluetooth and Wi-Fi wireless communication technologies to realize the system networking mode, that is, the fitness device communicates with the small tablet by connecting Bluetooth through the external serial port, the small tablet communicates with the central computer through Wi-Fi technology, and it makes full use of the built-in functions of the existing hardware devices and simplifies the networking mode of the whole system.

The small tablet mainly processes and stores the fitness data uploaded by the fitness device through Bluetooth wireless technology, real time graphic display is adopted, and the fitness users can view their fitness data at a glance, at the same time, according to the small board to evaluate the effect of exercise and remind fitness users to adjust the state of exercise, so as to achieve efficient and healthy physical fitness. The formula for Bluetooth wireless technology is shown in the following formula:

$$c = h\lambda. \tag{1}$$

The electromagnetic spectrum has a frequency range ranging from 1 to 10 at 25 times, ranging from thousands of meters to atomic size.

According to the formula provided by the Exercise Medicine Association is as follows:

$$\text{Male}: \text{BMR} = 13.7 * \text{weight} + 5.0 * \text{height-}6.8 * \text{age} + 66. \quad (2)$$

$$\text{Female}: \text{BMR} = 10 * \text{weight} + 6.25 * \text{height-}5 * \text{age-}161. \quad (3)$$

The data indicate that the basal metabolic rate in men is higher than that in women.

In normal life, the purpose of daily metabolism is to maintain the daily intake of calories, and the body weight will not increase or decrease based on the calorie intake. The formula of normal daily metabolism of human body is

$$\text{TDEE} = \text{BMR} * \text{Factor}. \quad (4)$$

In the design stage of the client, a small Android tablet of Rainbow brand i803Q1 is used, and it only provides real-time display of fitness graphics, so the small tablet hardware platform can meet the needs of the system.

Taking the bar dumbbell exercise as an example, the bar dumbbell exercise can be simplified to the fixed axis rotation of the forearm and upper arm by analyzing the characteristics of the bar dumbbell exercise; therefore, it is necessary to monitor the angle change of arm swing during the movement; and at the same time, it is necessary to collect the number of completed movements. Therefore, for the bar dumbbell movement, the fitness data to be collected include angle, number, start time, and duration. Before each fitness exercise, NFC certification must be carried out to ensure the security of fitness information, while providing identity information for the system to store fitness data. Through the demand analysis of the bar-dumbbell movement, its functional structure design is shown in Table 1.

Bar dumbbell itself cannot collect fitness data, the need for an external sensor to collect fitness data. Bluetooth MPU6050 module is used for data acquisition. The sensor is composed of Bluetooth HC-06 module and serial port MPU6050 module, data can be sent through Bluetooth, and each frame data sent is divided into acceleration packet, angular velocity packet, and angle packet. By detecting and analyzing the collected data, it can accurately obtain the current fitness status, and the detailed technical parameters of the wireless sensor module MPU6050 are shown in Table 2.

Table 1: Movement function of bar dumbbell.

The serial number	Bar dumbbell movement function
1	The identity authentication
2	Bluetooth transmission
3	Real-time display
4	The number of statistics
5	Data is stored
6	Quality evaluation

Table 2: Technical parameters of the MPU6050.

Indicators	Parameter
Current	<10 mA
Appearance	15.24 mm∗15.24 mm∗2 mm
Voltage	3V ~6 V
Measure the dimensions	Acceleration: 3D, angular velocity: 3 D, attitude angle: 3 D
Range	Acceleration: 16 g, angular velocity: 2000°/s
Resolution	Acceleration: 6.1E-5 g; angular velocity: 7.6E-3°/s
The stability	Acceleration: 0.01 g, angular velocity: 0.05°/s
Baud rate	115200 kps/9600 kps

Table 3: Pendulum amplitude parameters of bar dumbbell movement.

The serial number	Action	Amplitude (°)	Maximum angular velocity (°/s)
1	Bending	135	135
2	Levelly obeying	90	90
3	Before resting	90	90
4	Bent arm	90	90
5	Bent over for bending	135	135
6	Elect	120	120
7	The bench press	90	90
8	The birds	90	90

3. Result Analysis and Discussion

Taking the analysis and design of functions related to barbell movement as an example, the Bluetooth communication module and Wi-Fi communication module in the small tablet software system are designed.

3.1. Bar Dumbbell Movement Analysis. For so many kinds of bar dumbbell movement, how to distinguish the standard of action is particularly important in the process of action. Through simple calculation and analysis, the movement amplitude of the bar dumbbell's typical movement is listed as shown in Table 3.

The amplitude of bar dumbbell movement is an important index to judge whether the movement is qualified. The amplitude comparison of 8 bar dumbbell actions is shown in Figure 2.

As can be seen from the figure, the maximum amplitude of bend lift and bend lift is 135°, and the maximum motion range is required. Push lift is 120°, and the rest of the movements are 90°.

3.2. Bar Dumbbell Movement Statistics and Frequency Analysis. The MPU6050 sensor is equipped with a Bluetooth chip, so during the exercise process, the sensor constantly collects the fitness data of the fitness user and transmits it to the small tablet through the Bluetooth chipr, and data

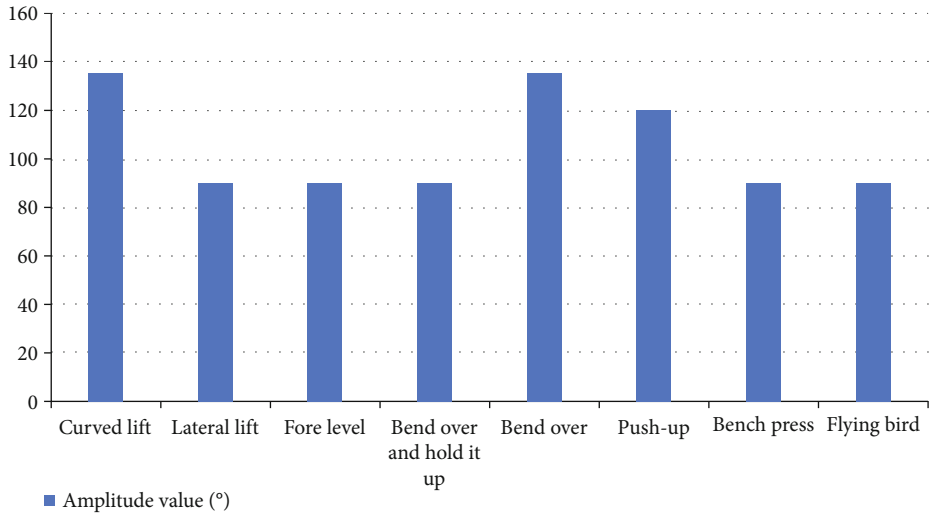

Figure 2: The amplitude of each bar dumbbell action.

Table 4: Data frame format of output angle of MPU6050 sensor.

Data number	The data content	Meaning
0	0 × 55	Baotou
1	0 × 53	Identify the package as an angle package
2	RollL	x-axis angle low byte
3	RollH	x-axis angle high byte
4	PithL	y-axis angle low byte
5	PithH	y-axis angle high byte
6	YawL	z-axis angle low byte
7	YawH	z-axis angle high byte
8	TL	Temperature low byte
9	TH	Temperature high byte
10	Sum	The checksum

frames transmitted mainly include three data packets of acceleration, angular acceleration, and swing angle of dumbbell motion. The frame structure of data is shown in Table 4.

The standard setting of the limit value and effective limit angle of X-axis detected by bar dumbbell movement types is shown in Table 5. Figure 3 shows the specific performance of the initial extremum and peak extremum of each action limit angle.

The limit angle and effective limit angle of bar dumbbell movement are mainly used for the statistics of the effective movement times of bar dumbbell movement, in the recognition of bar dumbbell movement, you have to define it by the y-axis angle, to realize the function of automatically recognizing the movement categories of barbell in the small tablet software, at the same time, the change of the angle of the Y -axis and the Z-axis should also be detected, but because the angle of the Z-axis is greatly offset, therefore, only according to the angle change of X-axis and Y-axis can we initially identify the same type of movement and count the number of movements. For example, in the bar dumbbell movement shown in the table above, the arm swing angle can only be recognized as bar dumbbell bending when the initial angle is -90, and the peak angle is 45 degrees.

3.3. Bar Dumbbell Action Recognition. Action recognition adopts two modes of automatic recognition and key selection. In this system design, there are fewer sports to be automatically recognized, and the accuracy of automatic recognition is low due to the lack of z-axis positioning, the key selection mode is to carry out a specific movement, and the data of the movement is analyzed.

Through the analysis of the system function and performance requirements, the fitness client of the network fitness management system based on the Internet of things is designed. The width and speed of the IOT bandwidth are calculated as follows:

$$C = \frac{(L + S) = 6}{2} * 1.1, \tag{5}$$

$$\text{Bandwidth} = \frac{\text{speed}}{8}. \tag{6}$$

In order to realize the seamless connection between the small tablet computer and the fitness equipment and the central machine, considering the transmission distance and speed, the system adopts Bluetooth and Wi-Fi wireless communication technology to realize the system network mode.

In the automatic recognition mode, the effective angle of each movement is divided into five stages, when the motion angle changes in accordance with the corresponding five stages, then the type of movement can be determined and the number of effective movements completed can be counted. This method can eliminate some small fluctuation interference, but when there is unqualified action between two effective actions, it cannot be excluded. Otherwise, it will affect the research of fitness management system of Internet of things.

In order to operate the fitness management system conveniently and efficiently, create a bar dumbbell motion

Table 5: Parameter standard of dumbbell movement recognition.

The serial number	Action	The limit angle		Effective limit angle	
		The initial extremum (°)	Peak extremum (°)	α_{min} (°)	α_{max} (°)
1	Bending	-90	45	-50	25
2	Levelly obeying	-90	-180	-160	-110
3	Before resting	-90	-180	-160	-110
4	Bent arm	-90	-180	-160	-110
5	Bent over for bending	-90	45	-45	25
6	Elect	-30	90	-10	70
7	The bench press	0	90	20	70
8	The birds	0	90	20	70

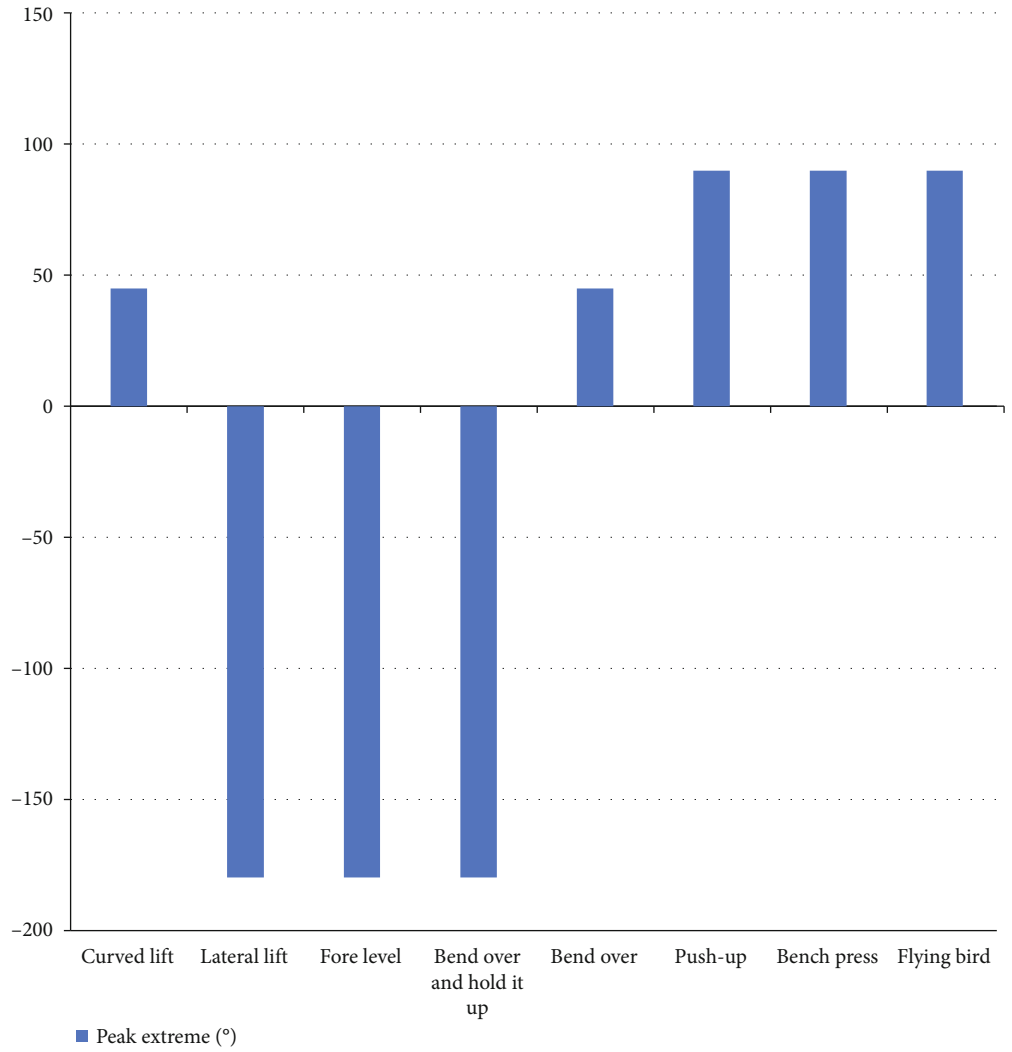

Figure 3: Limit values of X-axis angles detected by each movement type of bar dumbbell.

option list, as shown in Table 6. Set a different key number for each movement, and select the specified movement to exercise.

3.4. Design and Implementation of Bluetooth Communication Module. In the designed fitness management system, each fitness program must be equipped with a small tablet installed with the fitness App designed in this paper, and it is convenient for fitness users to watch the trend of fitness data and adjust exercise movements in real time. In order to reduce the trouble of wiring the fitness equipment, Bluetooth technology is adopted to realize the connection between the fitness equipment and the small tablet and upload of fitness data. Therefore, Bluetooth communication has become a bridge of

Table 6: Movement options of rigid dumbbell.

The serial number	Action options
1	Bending
2	Levelly obeying
3	Before resting
4	Bent arm
5	Bent over for bending
6	Elect
7	The bench press
8	The birds

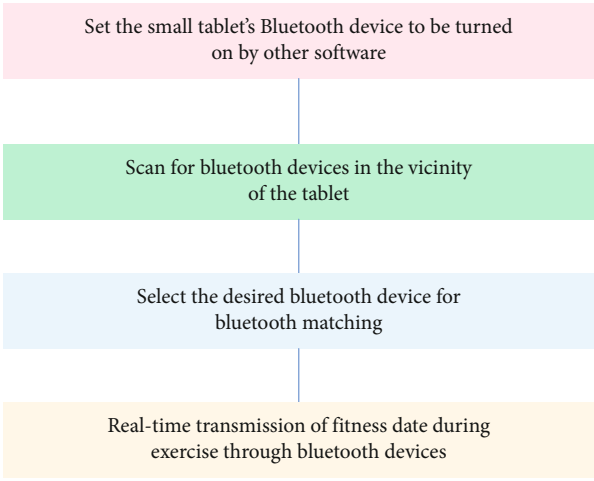

Figure 4: Four steps of Bluetooth communication program module.

data interaction between fitness equipment and small tablet; in this system, the Bluetooth communication program module is divided into the following four steps, as shown in Figure 4.

This system realizes the software program of Bluetooth communication by calling the built-in Bluetooth API of Android system. After launching the fitness App on a small tablet, the fitness software will automatically search for nearby Bluetooth devices and display them in a pop-up dialog box in the form of a list. Select the locked Bluetooth for connection. With the development of the Internet of things technology, wireless is the neural system of the Internet of things and also meets the needs of industrial production and material connection, and its transmission technology formula is as follows:

$$P = I * CPI * T. \tag{7}$$

Fitness application is convenient for fitness users to watch fitness data in real time. In order to reduce the trouble of fitness equipment wiring, Bluetooth technology is adopted to realize the connection between fitness equipment and small tablet computers. You can see that the aerobic heart rate during exercise is

$$\text{RATE} = (220\text{-age}) * (85\%\text{-}60\%). \tag{8}$$

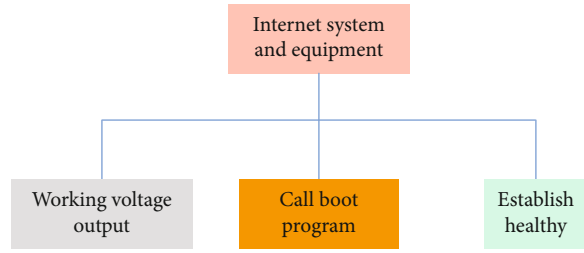

Figure 5: Connectivity of IoT devices.

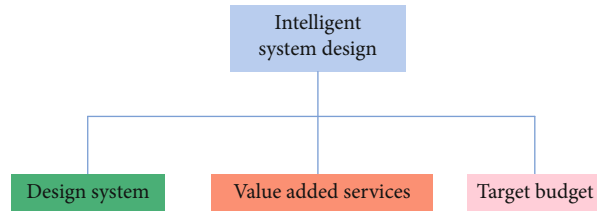

Figure 6: Internet of things system setup.

3.5. Wi-Fi Communication Module Design. According to the initial system requirements and overall design, fitness data is transmitted between the small tablet and the central computer through Wi-Fi wireless communication technology. Similar to the operation mechanism of Bluetooth communication module, Wi-Fi communication technology also adopts Socket programming based on TCP/IP protocol. It works much like Bluetooth communication, by calling the bind function to bind the port between the small tablet and the central computer; under the C/S architecture, the small tablet software system can be used as the client and the central computer software system as the server, we register a listening event with the system by calling the listen function, if the information is dynamic, the port of the data processed by the TCP/IP system process is the same as the defined mapping, insert the message into the listen sequence of events, and wake up the receiving process to receive the message, as shown in Figures 5 and 6.

4. Conclusions

This paper mainly studies the fitness management system based on the Internet of things. From the point of view of the fitness person, it does not bring the best fitness effect to the fitness person. Through the system function and performance requirements analysis, based on the internet of things network fitness management system fitness client (small tablet) design, the fitness data uploaded by the fitness equipment can be received through Bluetooth, and the fitness data can be processed and displayed in real time with graphics, after the exercise, the fitness data can be uploaded to the central computer through Wi-Fi. Taking barbell as an example, by analyzing the movement characteristics of barbell, Bluetooth MPU6050 module is used for data collection, including angle and number. The relevant functions of bar dumbbell movement are analyzed and designed, and the Bluetooth communication module and Wi-Fi communication module in the small tablet software system are designed

to realize the communication and data processing of the small tablet. Achieving an action recognition accuracy of 97.61%, the SVM also achieves a recognition accuracy of more than 96%. In the 50 action cycle calculation experiments, the number statistics algorithm reached 100% calculation accuracy, and the action cycle calculation results are also close to the real value, proving the effectiveness of the periodic calculation method. There are many health and exercise parameters, and only two of them are selected in this paper to realize the basic prototype system. In the next step, a variety of health data and exercise data can be added to obtain multiple health parameters and exercise parameters, so as to provide more detailed data analysis for people's fitness and improve their fitness effects.

In the process of research, there are still the following parts to be improved: (1) the system adopts the single sensor collection of limb movement data, this way is more convenient to use, but can only be used for a single limb movement, and follow-up research can install multiple sensors and multiple sensors of data fusion, to realize the identification of complex limb movements. (2) Limited to the experimental conditions, the number of training data sources is small. In addition, the experiment uses the computer in the LAN to replace the cloud server. In subsequent studies, the number of subjects can be increased and the number of remote servers runs by processing system software.

Data Availability

The data used to support the findings of this study are available from the corresponding author upon request.

Conflicts of Interest

The authors declare that there are no conflicts of interest with respect to the research, authorship, and/or publication of this article.

References

[1] H. Liu and X. Zhu, "Design of the physical fitness evaluation information management system of sports athletes based on artificial intelligence," *Computational Intelligence and Neuroscience*, vol. 2022, Article ID 1925757, 10 pages, 2022.

[2] L. Gao, Q. Yang, B. Zou, Q. Liu, and C. Wang, "Research on data asset management system of graph database based on internet of things," *Journal of Physics: Conference Series*, vol. 1802, no. 3, article 032134, 2021.

[3] Z. M. Zhu, F. Q. Xu, and X. Gao, "Research on school intelligent classroom management system based on internet of things," *Procedia Computer Science*, vol. 166, pp. 144–149, 2020.

[4] Y. Shan and Y. Mai, "Research on sports fitness management based on blockchain and internet of things," *EURASIP Journal on Wireless Communications and Networking*, vol. 2020, 13 pages, 2020.

[5] J. Li, "Evaluation method of athletes' special physical fitness based on internet of things," *Revista Brasileira de Medicina do Esporte*, vol. 27, no. spe2, pp. 62–65, 2021.

[6] L. Zhou, "Application and management of universal outdoor fitness equipment based on big data of internet of things," *Journal of Shazhou Professional Institute of Technology.*, vol. 10, no. 4, pp. 22–25, 2019.

[7] Z. Huang, Q. Chen, L. Zhang, and X. Hu, "Research on intelligent monitoring and analysis of physical fitness based on the internet of things," *Access*, vol. 7, pp. 177297–177308, 2019.

[8] W. Yang and J. Paik, "Fitness game based on internet of things," *TECHART Journal of Arts and Imaging Science*, vol. 7, no. 1, pp. 1–5, 2020.

[9] P. He and G. V. Amp, "Research on information visualization design of app for fitness management," *China Computer & Communication*, vol. 20, no. 3, pp. 46–48, 2019.

[10] V. S. Rekha, B. Mani, and M. Sujithra, "FIT BIT- a web application for fitness management system," vol. 5, no. 2, pp. 22–25, 2020.

[11] X. Dong, L. I. Bo, and J. Zhang, "Design of physical fitness test management system," *Henan Science and Technology*, vol. 3, no. 4, pp. 3–7, 2019.

[12] T. Frikha, A. Chaari, F. Chaabane, O. Cheikhrouhou, and A. Zaguia, "Healthcare and fitness data management using the IoT-based blockchain platform," *Journal of Healthcare Engineering*, vol. 2021, Article ID 9978863, 12 pages, 2021.

Hindawi
Wireless Communications and Mobile Computing
Volume 2022, Article ID 4461165, 8 pages
https://doi.org/10.1155/2022/4461165

Research Article

Tourist Attraction Recommendation Method Based on Megadata and Artificial Intelligence Algorithm

Laiyan Yun,[1] Huihua Jiao,[2] and Kai Lu[3]

[1]*College of Finance and Economics, Hainan Vocational University of Science and Technology, Haikou, 571126 Hainan, China*
[2]*Inetwork and Educational Technology Center, Qiongtai Normal University, Haikou, 571127 Hainan, China*
[3]*Department of Public Safety Technology, Hainan Vocational College of Political Science and Law, Haikou, 570100 Hainan, China*

Correspondence should be addressed to Huihua Jiao; jhh@mail.qtnu.edu.cn

Received 21 May 2022; Revised 6 July 2022; Accepted 15 July 2022; Published 3 August 2022

Academic Editor: Jun Ye

As China's economy continues to grow of informational technology and mobile Internet industry, the online tourism industry has received more and more extensive attention and use. However, as an emerging industry, users often need to spend a lot of time to choose travel services that match their needs because of the complex amount of relevant information. Under such circumstances, this paper studied the recommendation method in travel platform. First, the big data is used to extract user data. Secondly, the current online travel business recommendation for users has the problem of low accuracy. The reason is that the services provided are still in traditional recommendation algorithm. In this paper, the Bayesian network is used to evaluate the user's attribute preference and generate a data model, using effective methods in artificial intelligence algorithms to improve collaborative filtering algorithms and finally generate hybrid recommendation algorithms. Compared with the traditional recommendation method, the experimental results showed that the research can improve the recommendation accuracy of tourist attractions by 6.55%, increase the user's satisfaction for the platform, and enhance the visit rate and retention rate of the tourist attraction recommendation platform.

1. Introduction

At present, in order to accurately grasp the user's preferred tourist attractions and improve the visit rate and retention rate of the tourism recommendation platform, the tourism industry has gradually deepened the research on the recommendation algorithm for tourist attractions. However, the current personalized recommendation algorithm still has the problem of low recommendation accuracy. This paper applies big data and artificial intelligence algorithms to improve the recommendation method, which is conducive to improving users' satisfaction with the platform and improving the visit rate and retention rate of the tourist attraction recommendation platform. Improving the visit rate and retention rate of the tourist attraction recommendation platform, it is of great significance to the good development of the online tourism industry.

Liu et al. proposed that it is the most widely used of the personalized recommendation methods. The principle of the algorithm is based on the user's model labels and the user's ratings and comments on the recommended entities [1]. Han et al. subdivided the collaborative filtering algorithm into two types: one type is the collaborative filtering algorithm based on high similarity, and the other is the collaborative filtering algorithm based on the data model. The collaborative filtering method based on the high similarity of neighbors focused on analyzing the relationship between users and entities; the model-based collaborative filtering algorithm learned the prediction model through the user's rating of the entity or other behaviors, built the feature association between the user and the entity, and recommended the entity with high user preference to the users [2]. Many scientists had studied collaborative filtering algorithms based on data models, such as Ngaffo AN's research on matrix factorization factor models. The matrix factorization factor model is widely used. The matrix factor algorithm is used to extract hidden factors from the evaluation matrix of user objects, and these factors are used to describe users and

entities, as well as users' estimated values of other entities [3]. Besides, Angadi et al. discussed Naive Bayes model. The model had a solid mathematical theory and steady-state classification efficiency as the basis, and the algorithm required by the model was relatively simple, and the main content of the algorithm was to solve some parameters with incomplete data [4]. In addition, there is an analysis of the hidden semantic analysis model performed by Cai. The model used statistical econometrics to analyze large amounts of text, extracted implicit semantic structures that exist between words, and used this kind of implicit semantic structure to reconstruct sentences [5].

Problems of the current recommendation algorithm: (1) the problem of cold start. A study by Villanueva-Polanco and Angulo-Madrid pointed out that a cold start is when a new entity that has never been evaluated is added to the system and its associated data is extremely scarce. In addition, when a newly registered user joins the system, the user's data is extremely lacking, and it is also impossible to recommend [6]. Karacan et al. proposed and applied a novel overlapping method that employs overlapping techniques as a tool to deal with the shortcomings of clustering techniques. The advantage of overlapping techniques is to allow users to feedback their behavior and ratings in social networks, belonging to multiple clusters simultaneously [7]. (2) The problem of sparsity: Chen et al. combines the evaluation of individual cognitive behaviors, user cognitive relationships, and time decay coefficients into a probability matrix decomposed by a single model, combined with the social interaction coefficient for personalized recommendation, for the use of social interaction factor for personalized recommendations [8]. Rodpysh et al. pointed out that the reason for the sparse data is that most users have a very limited number of reviews for the product. Second, as the total number of products and users increases, the number of products viewed by users will only decrease. The proportion of evaluation items to the total is even lower [9]. The sparsity problem can cause inefficiency, low precision, and low adequacy for similarity computation. (3) Real-time questions: according to the research of Paddock, the total number of items and users for calculating similarity keep increasing, so when all the sparse matrices are passed, the time spent increases exponentially, and users' demands for real-time recommendation will be difficult to meet [10].

At present, the research on the recommendation method of tourist attraction recommendation platform had achieved certain results, but there still had a problem about poor recommendation accuracy. This paper applied big data and artificial intelligence algorithms to the improvement of recommendation algorithms, and payed attention to solve the problem of low recommendation accuracy. This paper can accurately discover the needs of users, help users to obtain recommendation results efficiently and accurately, and meet the personalized needs of users.

2. Tourist Attraction Recommendation System

The tourist attraction recommendation system can enable users to obtain attractions that match their preferences, save a lot of time for users, and improve users' satisfaction with the platform, thereby increasing the visit rate of the tourist attraction recommendation platform and enhancing its market competitiveness. The recommendation system is based on the recommendation algorithm. Firstly, the user data is extracted from the big data, and the data is simply analyzed and interpreted. Then, the data is mined, and the user model is generated. Finally, the hybrid recommendation algorithm improved by the artificial intelligence algorithm module completes the prediction of the user's scenic spot preference. It is shown in Figure 1.

2.1. Big Data Module. Because the data collection of big data is very large, the requirements for data retrieval, storage, control, and analysis are very high [11]. It has four characteristics of large scale, fast flow, diverse types, and low value density. The commonly used big data technologies are actually based on the Hadoop ecosystem [12]. Hadoop uses a decentralized system infrastructure. In other words, its data storage and processing processes are distributed and completed by multiple machines. Through such parallel processing, security and data processing scale are improved. The main designs of the Hadoop platform: HDFS and MapReduce [13]. HDFS provides massive storage, and MapReduce provides massive computing. When submitting computing tasks to the MapReduce platform, the computing tasks are first divided into different partitions, each partition processes some input data and then sinks to different nodes. When the Map task is completed, Reduce will combine the outputs of several previous maps and then output. It is equivalent to using distributed machines to complete large-scale computing tasks.

Therefore, this paper drew inspiration from the Hadoop ecosystem and built a big data module for building a tourist attraction recommendation system. In this system, the data sources of users and attractions are extensive and diverse, and a complex data environment is formed in parallel, which brings a problem that must be solved for big data processing. Therefore, the big data module must obtain, clean, and integrate the required data sources in order to obtain the essence and relationship of the data. After a series of reconstructions, the data is emptied and stored in a similar structure to ensure high data quality and reliability. The module composition is shown in Figure 2.

Data extraction is not a brand new technology and has been relatively mature in the traditional database field [14]. Data retrieval is the process of filtering the desired data using specific criteria, transferring the data to a target file, and searching the entire data source. As the first step of data processing, data mining plays an important role.

The principle of data cleaning is to use the existing technical means to transform the low-quality data in the source data into data that can meet the quality requirements by analyzing the existing format and the reasons for redundant data, so as to ensure the data quality of the datasets generated by the later data integration [15]. Data integration integrates scattered but interrelated data into a unified dataset according to a certain logic, so that the unity and utilization efficiency of the overall data can be guaranteed [16]. Data

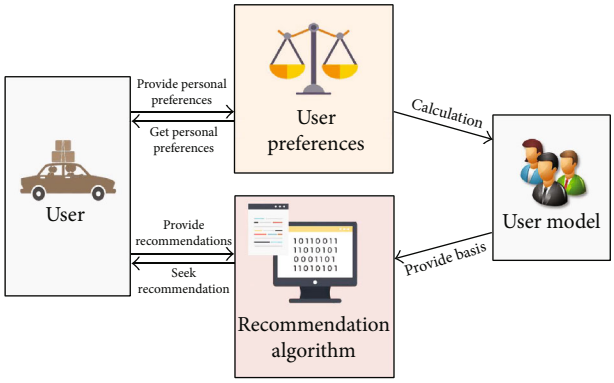

Figure 1: Tourist attraction recommendation system.

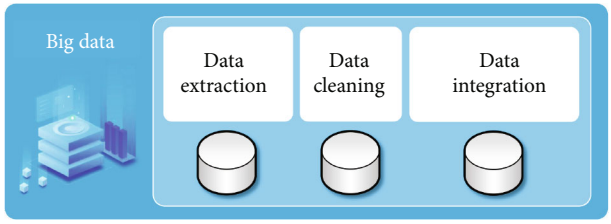

Figure 2: Big data module.

integration can provide comprehensive data sharing and provide an integrated data source access interface that is convenient for other modules to access the big data module.

2.2. Engine Service Module. Engine service module consists of data mining group and user model. The reason it is called "engine service" is that this module is at the heart of the whole system [17]. Its final result will produce a related user model, which contains various data of the user: age; gender; travel time; travel footprint; travel mode of transportation; distance between tourist attractions and residence. The data will be compiled into three types of attributes: interest preference, explicit feedback, and implicit feedback. Only when the generated user model data is accurate can the artificial intelligence algorithm make accurate recommendations; otherwise, it is water without a source and a tree without roots. The module composition is shown in Figure 3.

In this module, the data mining group will reanalyze the data processed by the big data module and generate a user model that includes three attributes: interest preference, explicit feedback, and implicit feedback.

2.3. Artificial Intelligence Algorithm Module. Artificial intelligence has become a broader term nowadays. In the past, a large number of the term artificial intelligence is regularly used interchangeably with subfields such as machine learning and deep learning. However, they differ from each other in a number of ways. Machine learning, for example, focuses on building systems that can learn or improve performance based on the data they use [18]. In other words, all machine learning is artificial intelligence, but not all artificial intelligence is machine learning. In order to give full play to the value of artificial intelligence, scholars have gradually deepened their research on data science. Data science is an interdisciplinary field that combines professional skills and knowledge from science, data statistics, computer science, and other disciplines, supplemented by other methods to extract data value and conduct a comprehensive and detailed study of data collected and generated from multiple sources analysis [19].

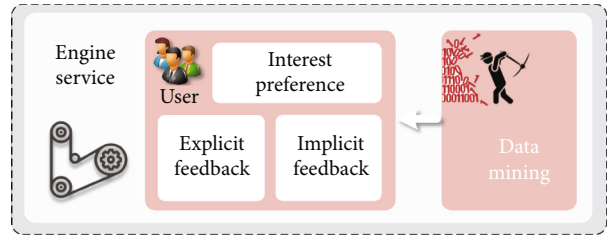

Figure 3: Engine service module.

The artificial intelligence algorithm module studied in this paper includes four aspects: data processing, feature engineering, model evaluation, and machine learning. The focus of this module is machine learning, mainly generating data models through Bayesian networks and improving hybrid recommendation algorithms through artificial intelligence algorithms. The module composition is shown in Figure 4.

3. Algorithm for Tourist Attraction Recommendation

3.1. Introduction to Bayesian Networks. Bayesian network is a graphical model whose operations contain probabilistic content, so it is often used to analyze and predict the relationship between two objects [20]. As shown in Figure 5, it is a classic Bayesian network diagram. If the probability of X_4 is calculated, it needs to rely on X_1, X_2, and X_3. It can be seen that the Bayesian network involves probability problems. The following is a preliminary introduction to Bayesian probability.

The Bayesian formula is a conditional probability formula, such as $P(A|B)$, which represents the probability of A under the condition of B, where $P(A|B)$ represents the probability of A and B occurring at the same time. From this, the calculation formulas of $P(A|B)$ and $P(B|A)$ can be obtained as follows:

$$P(A|B) = \frac{P(A,B)}{P(B)}, \tag{1}$$

$$P(B|A) = \frac{P(A,B)}{P(A)}. \tag{2}$$

The formula for calculating the Bayesian posterior probability after processing is as follows:

$$P(A|B) = \frac{P(A)P(B|A)}{P(B)}. \tag{3}$$

3.2. Bayesian Algorithm. Bayes' theorem is often used to calculate the probability of a condition occurring by

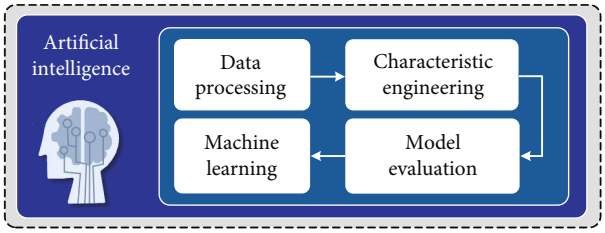

Figure 4: Artificial intelligence algorithm module.

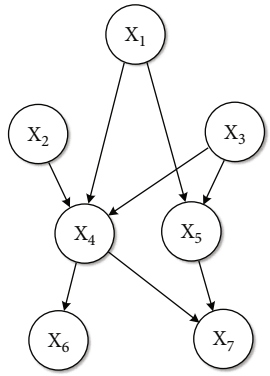

Figure 5: Bayesian network.

quantifying the relationship between two objects. For example, let X be the head precursor data, which contains unknown attributes whose value is $(x_1, x_2, \cdots, x_n)$. For the classification problem, after X is determined, the probability of assuming that H is established is $P(H|X)$, which means that under the condition X is the posterior probability of H . Bayes' Theorem provides a method consisting of $P(H)$, $P(X)$, and $P(X|H)$, similar to Formula (3), where $P(H|X)$ operates as follows:

$$P(H|X) = \frac{P(X|H)P(H)}{P(X)}. \tag{4}$$

$P(H)$ is the prior probability of H, $P(X|H)$ is the posterior probability of X under condition H, and $P(X)$ is the prior probability of X. Bayes satisfies the condition that each feature data in a special set is independent of each other. And from the probability theory, it can be concluded that when A and B are independent of each other, $P(AB) = P(A)P(B)$. The calculation formula of its $P(X|H)$ is as follows:

$$P(X|H) = \prod_{k=1}^{n} P(x_k|H) = P(x_1|H)P(x_2|H)\cdots P(x_n|H). \tag{5}$$

3.3. Application of Bayesian Network in Scenic Spot Recommendation. In the stage of predicting user preference, it is necessary to calculate the user's preference for an entity. The probability formula can be derived to express the user's preference for an entity, and a data model can be evaluated and generated. The generation process is as follows: first, define the user set and the scenic spot set: define the user model as a set, which is used to represent n users, and the set is $U = \{u_1, u_2, \cdots, u_n\}$. Among them, ui(i ∈ n) represents the user feature vector, and all the features are aggregated to represent a user feature vector. The scenic spot set is defined as $A = \{a_1, a_2, \cdots, a_m\}$, which represents m users, where a(ii ∈ m) represents the scenic spot feature vector. All features collectively represent an attraction record. The best choice is obtained by improving formula (5). The calculation formula of the user's preference for the scenic spot is as follows:

$$P(a_i|u_j) = \frac{P(a_i)P(u_j|a_i)}{P(u_j)}. \tag{6}$$

3.4. User Model Generated by Bayesian Network. The formula for calculating the user's preference for scenic spots generated by the Bayesian network is reanalyzed to generate a user model.

Definition $P(a_i|u_j)$ represents the probability of recommending a certain scenic spot to a user, that is, the user's scenic spot recommendation degree. The attribute coincidence between users is defined, which is used to judge the similarity of users' preference attributes for scenic spots. The calculation formula is as follows:

$$\mathrm{Sim}_b(u,k) = \frac{N_{fu} \cap N_{fk}}{N_{fu} \cup N_{fk}}. \tag{7}$$

Define Sim$b(u,k)$ to represent the similarity of behavior between users, and its calculation formula is as follows:

$$\mathrm{Sim}_b(u,k) = \frac{\sum_{a \in c_{u,k}} Ns_{u_a} Ns_{k_a}}{\sqrt{\sum_{a \in c_u} Ns_{u_a}^2} \sqrt{\sum_{a \in c_k} Ns_{k_a}^2}}. \tag{8}$$

$C_{u,k}$ represents the attractions visited by both user u and user k, $N_{s_{u_a}}$ represents the number of check-ins by user u at attraction a, $N_{s_{k_a}}$ represents the number of times user k has checked in at attraction a, C_u is the number of attractions that user u has checked in, and C_k is the number of attractions that user k has checked in number. Definition Sim(u,k) represents the similarity between user u and user k, including user behavior similarity and user attribute similarity. The calculation formula is as follows:

$$\mathrm{Sim}(u,k) = b\mathrm{Sim}_b(u,k) + (1-b)\mathrm{Sim}_f(u,k). \tag{9}$$

b is a weighting factor used to adjust the similarity of user behavior and the similarity of user attributes, and the proportion of a certain factor is increased according to the actual situation. If the user is a new user without any information record, then define b = 0 at this time, thus solving the problem that the new user has no data under

the cold start problem. Define $R_{u,a}$ to represent user u's rating for attraction a, and its calculation formula is as follows:

$$R_{u,a} = \gamma \frac{N_{u,a}}{\sum_{j \in A} N_{u,j}}. \tag{10}$$

$N_{u,a}$ represents the number of check-ins of user u at attraction a, $\sum_{j \in A} N_{u,j}$ represents the number of check-ins of user u, and A table indicates the set of user attractions, and γ is the adjustment factor to prevent the value of $R_{u,a}$ from being too small. So far, the user model has been created.

3.5. Introduction to Leapfrog Algorithm. Hybrid leapfrog algorithm be called SFLA for short belongs to artificial intelligence algorithm. The "frog" group is initialized, and information is transmitted according to the differentiated groups, and the global optimal solution of the problem is obtained by combining the deep subgroup search function and the overall global information exchange function of the frog group. The SFLA algorithm not only has the faster global optimization capability of the particle swarm optimization algorithm but also has the local optimization capability and can perform the evolutionary algorithm faster. The algorithm has the advantages of convenient implementation, fast optimization, and strong global search ability and has became one of the most popular research fields for researchers. The concept diagram of hybrid leapfrog search is shown in Figure 6.

In the SFLA algorithm, group of frogs is composed of several frog individuals, and each group is divided into several subpopulations containing a random number of frogs. The data of frog individuals in different subpopulations are different, and each frog in the subpopulation has certain special data, which will affect other individuals. Then, after the local search is performed, data is exchanged in each subpopulation, and the local optimal solution can be found in the subpopulation.

3.6. Improved Hybrid Recommendation Algorithm Based on Artificial Intelligence. The SFLA algorithm in the artificial intelligence algorithm and the collaborative filtering algorithm are introduced for fusion and improvement to generate a hybrid recommendation algorithm. The mathematical model of the algorithm can be interpreted as: all kinds of substitutes and measurement relations used by the algorithm during the execution process will automatically organize the data into a mathematical model, which is conducive to the analysis of the algorithm. Next, analyzing and explaining the mathematical model of the SFLA algorithm: randomly generate P frog individuals to form the initial frog population $Q = \{F_1, F_2, \cdots, F_p\}$, and the ith frog in Q is denoted as $F_1\{x_{i1}, x_{i2}, \cdots, x_{il}\}$. This formula represents a solution to the problem, where l refers to the dimension of the solution space. Arranging all the frogs in the population in descending order of fitness and dividing the population into m subpopulations, each subpopulation has n frogs, and the initial

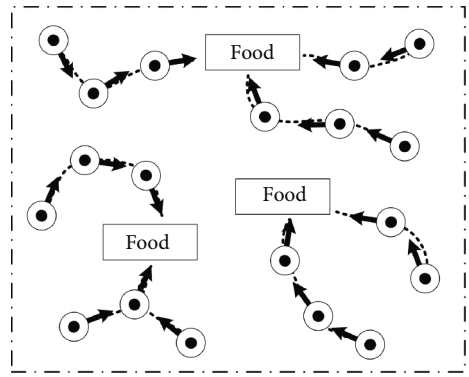

Figure 6: Hybrid leapfrog search.

total number P of frogs satisfies $P = m \times n$. When the population is divided into subpopulations, the rules described by the formula are used to divide, where F^k refers to the kth frog subpopulation.

$$F^k = \left\{ F_{k+m(j-1)} \in P \middle| 1 \le j \le n \right\}, \quad 1 \le k \le m. \tag{11}$$

Local search is carried out in each subpopulation and iteratively updated, that is, the position of the frog Fw with the worst fitness in each subpopulation is continuously updated iteratively. The updated rules are as follows:

$$D_i = \text{rand}\,(0, 1) \times (F_b - F_W), \tag{12}$$

$$\text{new}F_w = F_w + D_i - D_{\max} \le D_i \le D_{\max}. \tag{13}$$

In the formula, rand $(0, 1)$ refers to a random number between 0 and 1, while D_i refers to the distance movement value in the i direction, and $D_{\max}$ refers to the upper limit of the single position movement of each frog. After the location update operation is performed, if the fitness of newF_w is better than that of F_w, use newF_w instead of F_w. The fitness of newF_w is not as good as that of F_w, replacing F_g with F_b and performing the update operation again.

The normal distribution theory is introduced to solve the optimization problem of local minima. The basic theory of normal distribution is as follows: a random variable x that obeys the normal distribution of mathematical expectation is u, and the variance is σ^2 which can be expressed as N (u, σ^2), and the standard normal distribution is the normal distribution when $\sigma = 1$, $u = 0$. Its probability density function is as follows:

$$f(x) = \frac{1}{\sqrt{2\pi}\sigma} \exp\left(-\frac{(x-u)}{2\sigma^2}\right). \tag{14}$$

A variation factor that follows a normal distribution is added to the update strategy of the worst frog, where $N(0, 1)$ refers to the standard normal distribution. The improved strategy is as follows:

$$\text{new}F_w = F_w + N(0, 1) \times D_i - D_{\max} \le D_i \le D_{\max}. \tag{15}$$

The mutation strategy of the fittest is added to the SFLA algorithm to improve the lower limit of the quality of the population. The addition of the variation factor can reduce the blindness of optimization, thereby improving the execution speed of the algorithm.

$$\text{new}F_{mij} = F_{mij} + N(0,1)_{mij} \times F_{mij}. \tag{16}$$

On this basis, the winning mutation mechanism is added to make the population move towards a better solution, and it is easier to find the optimal solution. The winning mutation strategy can be expressed as:

$$\text{new}F_{bj} = F_{bj} * \left(1 + \xi N(0,1)_{bj}\right). \tag{17}$$

The similarity value of the target user u and the U' element in the nearest neighbor set can be used as the fitness function, and the final expression of the algorithm is obtained as follows:

$$f(F_k) = \sum_{n=1}^{N} x_{kn} \text{sim}\left(u, u'\right). \tag{18}$$

In order to verify whether the algorithm is effective, two high-dimensional unimodal functions, the Sphere function and the Rosenbrock function, are selected to test the performance of the algorithm. The detailed mathematical formulas and characteristics of the functions are as follows.

The Sphere function is often used to measure the accuracy of an algorithm. In the value range, the function only obtains the globally unique optimal value 0 when the point is (0,0,…,0). That is to say, the optimal value of the function is $f(0, 0, \cdots, 0) = 0$.

$$f_1(X) = \sum_{i=1}^{n} x_i^2, x_i \in [-100, 100]. \tag{19}$$

The Rosenbrock function has the characteristics of nonconvex and asymmetric and is generally used to measure the operating efficiency of the algorithm. The function only obtains the globally unique optimal value 0 when the point is (1,1,…,1). In other words, the optimal value of the function is $f(1, 1, \cdots, 1) = 0$.

$$f_2(X) = \sum_{i=1}^{n-1} \left[\left(x_{i+1} - x_i^2\right)^2 + (x_i + 1)^2\right], x_i \in [-30, 30]. \tag{20}$$

4. Data Sources

Taking the data obtained online as a dataset, records of 1000 users and 2851 tourist attractions were obtained. User attributes include user ID, gender, age, location, and check-in time; scenic spots include scenic spot identification, user ID, scenic spot description, scenic spot location, scenic spot label, and check-in times. The process of processing the dataset is as follows: first, the operation of prescreening

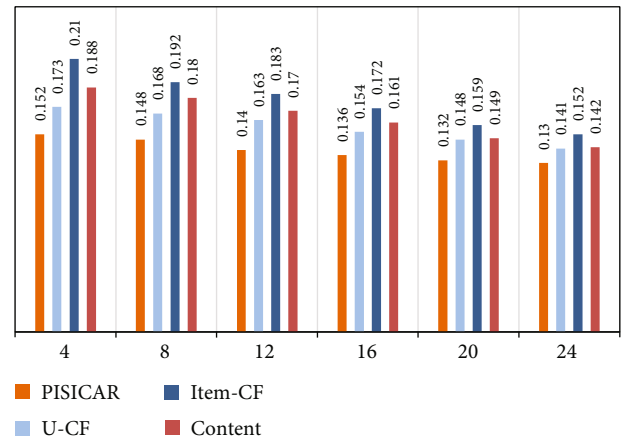

Figure 7: The effect of the number of adjacent users on the mean absolute error.

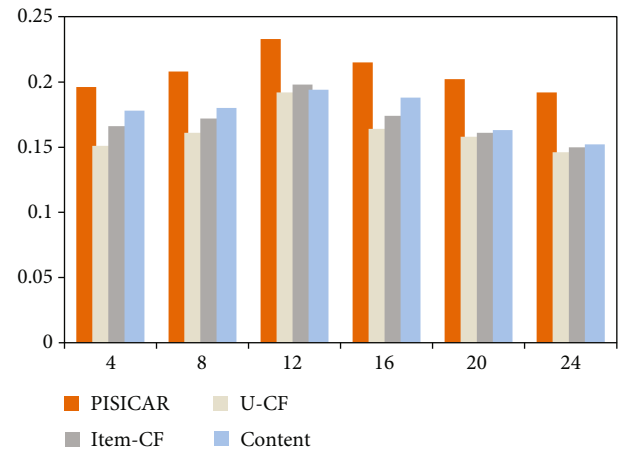

Figure 8: Accuracy comparison.

and processing the dataset is carried out; the purpose is to decompose the users who generate a very low number of travel records, so as to improve the accuracy of recommendation. Then, according to the ratio of 8 to 2, the dataset is divided into training set and test set. The training set is used to construct the tourist attraction recommendation algorithm model, and the test set is used to verify the accuracy of the tourist attraction recommendation algorithm.

5. Experiment of Recommendation Algorithm

The improved algorithm was named PISICAR, performing experimental analysis on the dataset after processing the data required for the experiment. According to the proposed tourist attraction recommendation algorithm and experimental analysis, it is concluded that the mean absolute error of the algorithm recommendation results is associated with the amount of relevant factors selected as users in the experiment. Therefore, this experiment accepted a different number of adjacent user selections and used PISICAR as a collaborative user filtering-based attractions recommendation algorithm, as well as element-based collaborative filtering and content-based algorithms used in the comparative

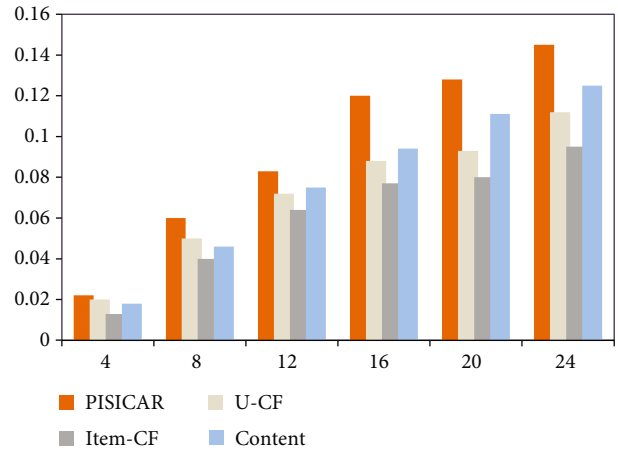

Figure 9: Recall comparison.

experiments for comparison. U-CF is used to present a recommendation algorithm for tourist attractions based on joint user filtering, Item-CF is used to present a recommendation algorithm for filtering objects of joint tourist attractions, and Content is a content-based tourism used to present the details of attractions. This paper presents the strength of the algorithm performance by calling the parameters of the mean absolute error value. The specific experimental results are shown in the figure.

Neighboring user sets are called for comparison of mean absolute error values in the experiments. The number of its calls is different, and the corresponding mean absolute error value will also change, but the whole is gradually stable with the amount of the growth of the users of the mean absolute error value. By comparing the difference of the number of adjacent user parameters of different algorithms in Figure 7, the average absolute error value of the recommendation algorithm proposed in this paper is much lower than that of the other three algorithms.

The accuracy comparison is shown in Figure 8.

The recall comparison is shown in Figure 9.

From Figures 8 and 9, the precision rate and the recall rate increase with the number of recommendations. However, the accuracy rate reached an inflection point when the number of recommendations increased to a certain extent and then showed a downward trend. It is shown that the accuracy and recall of the algorithm change when the number of tourist attractions recommended to the user changes. A comparison of the algorithm proposed so far in this paper with three other commonly used unimproved algorithms shows that the algorithm proposed in this paper has higher precision and recall. Further analysis showed that the recommendation accuracy of this algorithm is 6.55% higher than that of the unimproved algorithm.

6. Conclusion

For a travel recommendation platform, a higher recommendation accuracy rate can bring users a better user experience. Based on big data and artificial intelligence algorithms, this paper improved the tourist attraction recommendation algorithm. There were still shortcomings in the research on the recommendation algorithm of tourist attractions. There are several aspects that can be improved:

(1) In the aspect of recommendation algorithm research, the method used to formulate label parameters for the user model lacks pertinence, and the multifaceted behavior patterns of users cannot be added to the user model. Also, there are not enough labels to cluster sights. Subsequent research will optimize these two aspects

(2) In this paper, the research depth of tourist attraction method based on big data and artificial intelligence algorithm is not enough. The next step is aimed at addressing new users and new attractions. In addition, it is also necessary to introduce scenario factors for scenario analysis to provide extensive and in-depth support for the recommendation of tourist attractions

(3) The big data processing platform still needs to be improved, and there is still a lot of room for improvement in the processing mechanism in the face of diverse and complex data. The next step is to optimize the data algorithm and add it to the data warehouse to better carry out the work of online analysis

Data Availability

No data were used to support this study.

Conflicts of Interest

The authors declare that there are no conflicts of interest regarding the publication of this article.

Acknowledgments

This work was supported by the Scientific Research Project of Colleges and Universities in Hainan Province (grant no. Hnky2021ZD-26, Research on key technologies of student credit investigation and certificate deposit based on blockchain), Hainan Provincial Natural Science Foundation of China (grant no. 621RC1082), and Research Fund Project of Qiongtai Normal University (qtyb201810).

References

[1] Y. Liu, M. Yin, and X. Zhou, "A collaborative filtering algorithm with intragroup divergence for POI group recommendation," *Applied Sciences*, vol. 11, no. 12, pp. 5416–5416, 2021.

[2] X. Han, Z. Wang, and H. J. Xu, "Time-weighted collaborative filtering algorithm based on improved mini batch K-means clustering," *Advances in Science and Technology*, vol. 105, no. 2, pp. 309–317, 2021.

[3] A. N. Ngaffo, W. E. Ayeb, and Z. Choukair, "Service recommendation driven by a matrix factorization model and time series forecasting," *Applied Intelligence*, vol. 52, no. 1, article 2478, pp. 1110–1125, 2022.

[4] U. B. Angadi, A. Rai, and G. Uma, "MBFerns: classification and extraction of actionable knowledge using multi-branch ferns-based Naive Bayesian classifier," *Soft Computing*, vol. 25, no. 13, pp. 8357–8369, 2021.

[5] A. Cai, "A latent semantic analysis-based image tag optimisation method," *International journal of applied decision sciences*, vol. 13, no. 1, pp. 109–121, 2020.

[6] R. Villanueva-Polanco and E. Angulo-Madrid, "Cold boot attacks on the supersingular isogeny key encapsulation (SIKE) mechanism," *Applied Sciences*, vol. 11, no. 1, article app11010193, pp. 193-194, 2021.

[7] H. Karacan, H. Karacan, and Y. E. Yenice, "A novel overlapping method to alleviate the cold-start problem in recommendation systems," *International Journal of Software Engineering and Knowledge Engineering*, vol. 31, no. 9, pp. 1277–1297, 2021.

[8] R. Chen, Y. S. Chang, Q. Hua, Q. Gao, X. Ji, and B. Wang, "An enhanced social matrix factorization model for recommendation based on social networks using social interaction factors," *Multimedia Tools and Applications*, vol. 79, no. 19-20, pp. 14147–14177, 2020.

[9] K. V. Rodpysh, S. J. Mirabedini, and T. Banirostam, "Correction to: employing singular value decomposition and similarity criteria for alleviating cold start and sparse data in context-aware recommender systems," *Electronic Commerce Research*, vol. 22, no. 1, article 9497, pp. 223–223, 2022.

[10] A. Paddock, "Real-time data," *International Journal of Computer Applications*, vol. 175, no. 32, pp. 28–31, 2020.

[11] L. Cui, "Construction of big data technology training environment for vocational education based on edge computing technology," *Wireless Communications and Mobile Computing*, vol. 2022, 9 pages, 2022.

[12] E. V. Nikulchev, A. V. Tatarintsev, and V. Belov, "Choosing a data storage format in the Apache Hadoop system based on experimental evaluation using apache spark," *Symmetry*, vol. 13, no. 2, pp. 195–198, 2021.

[13] A. Smm, A. As, and B. Ant, "Cross-map reduce: data transfer reduction in geo-distributed map reduce," *Future Generation Computer Systems*, vol. 115, no. 3, pp. 188–200, 2021.

[14] N. E. Zamri, M. A. Mansor, and M. Kasihmuddin, "Amazon employees resources access data extraction via clonal selection algorithm and logic mining approach," *Entropy*, vol. 22, no. 6, pp. 596-597, 2020.

[15] A. M. Venkatachalam, A. Perera, S. E. Stutzman, D. W. M. Olson, V. Aiyagari, and F. D. Atem, "Methods for cleaning and managing a nurse-led registry," *Journal of Neuroscience Nursing*, vol. 52, no. 6, pp. 328–332, 2020.

[16] J. Zhu and P. Wu, "Towards effective BIM/GIS data integration for smart city by integrating computer graphics technique," *Remote Sensing*, vol. 13, no. 10, pp. 1889–1895, 2021.

[17] J. Ong, A. Selvam, and J. Chhablani, "Artificial intelligence in ophthalmology: optimization of machine learning for ophthalmic care and research," *Clinical and Experimental Ophthalmology*, vol. 49, no. 5, pp. 413–415, 2021.

[18] K. S. Lee, I. S. Song, E. S. Kim, H. I. Kim, and K. H. Ahn, "Association of preterm birth with medications: machine learning analysis using national health insurance data," *Archives of Gynecology and Obstetrics*, vol. 305, no. 5, pp. 1369–1376, 2022.

[19] J. Torres, A. Zalapa-Damián, and F. J. Domínguez-Mota, "Data science and machine learning technique for predicting electrical resistivity in recycled concrete with nopal as addition," *Forum*, vol. 40, no. 8, pp. 43–62, 2021.

[20] Z. Duan, L. Wang, and M. Sun, "Efficient heuristics for learning Bayesian network from labeled and unlabeled data," *Intelligent Data Analysis*, vol. 24, no. 2, pp. 385–408, 2020.

Hindawi
Wireless Communications and Mobile Computing
Volume 2022, Article ID 4436016, 12 pages
https://doi.org/10.1155/2022/4436016

Research Article

Application of Machine Learning Algorithms in the Development and Consumption Trend of Green and Intelligent Vehicles under the Background of Big Data

BenShuang Liang, Jing Yang, Yaxin Guo, and Xin Guo

Automotive Consumer Research, China Automotive Technology and Research Center Co., Ltd., Tianjin 30000, China

Correspondence should be addressed to BenShuang Liang; liangbenshuang@catarc.ac.cn

Received 6 May 2022; Revised 23 June 2022; Accepted 5 July 2022; Published 27 July 2022

Academic Editor: Jun Ye

In the face of global warming, air pollution, and other difficulties, electric vehicles have become an industry strongly supported by various countries due to their good environmental protection characteristics. In the context of big data, people are exposed to more and more information, and the convenience brought by big data is also increasing. Based on this background, the development of green and intelligent vehicles is getting faster and faster. This paper is aimed at studying the application of machine learning algorithms in the development and consumption trends of green and intelligent vehicles in the context of big data. This paper proposes machine learning algorithms based on big data, as well as support vector machine algorithms and so on. Machine learning algorithms specialize in how computers simulate or implement human learning behaviors to acquire new knowledge or skills and to reorganize existing knowledge structures to continuously improve their performance. The test results of this paper show that, starting from 2014, China has begun to vigorously develop green and intelligent vehicles. In 2014, the production volume of green and intelligent vehicles in China was 3,675, and the sales volume was 2,790. The development of green and intelligent vehicles is not very good and has not been fully accepted by the public. However, since 2017, the production and sales of green and intelligent vehicles have been slowly increasing. By 2020, the production of green and intelligent vehicles will be 24,360 and the sales will be 24,090. It can be seen that with the development of time, green and intelligent vehicles are gradually being recognized.

1. Introduction

Since the reform and opening up, China's economy has developed rapidly, but problems such as insufficient energy resources and environmental degradation have become more and more prominent. In order to fundamentally solve these problems, we must start from the economic system, energy system, and environmental system. China proposes a green development plan, proving that China's green development path is unstoppable. Energy conservation and emission reduction and environmental policies can also help lead the purification of green technology innovation activities. Big data, or huge amount of data, refers to the amount of data involved that is so large that it cannot be acquired, managed, processed, and organized into information that helps companies make more active decisions within a reasonable time through mainstream software tools.

In the past, automobiles mainly used nonrenewable resources such as gasoline and diesel to supply electricity. However, China's per capita oil resources are seriously insufficient and need to be imported in large quantities. The increase in the number of conventional vehicles has led to a sharp increase in the use of gasoline and diesel, which has added to the pressure on China's energy supply. Therefore, improving the exhaust control technology of vehicles, reducing emissions, and using clean energy are very important for energy conservation and emission reduction, as well as the green transformation of the automotive industry.

The innovations of this paper are: (1) This paper introduces the theoretical knowledge of big data and machine

learning algorithms and uses machine learning algorithms to analyze how machine learning algorithms play a role in the development of green and intelligent vehicles and the application of consumption trends. (2) This paper expounds the support vector machine and the BP neural network. Through experiments, it is found that the machine learning algorithm can effectively analyze the development and consumption trends of green and intelligent vehicles.

2. Related Work

With the development of the times, people's economic level is constantly improving, and more and more people use smart cars. Rajalakshmi and Rajakumar found that people faced problems when parking their vehicles in parking spaces, and the existing parking systems were not able to accommodate the flexibility of people's travel. So they came up with a sensor network-based system that can classify cars and track parking spaces based on their length. The images of the cars are compared with the images stored in the database, and according to their length, each car is entered and the information is displayed in the LCD. The system can accurately detect vehicles in both indoor and outdoor areas. In response to the problem of insufficient parking spaces, Rajalakshmi and Rajakumar proposed a sensor network-based system, but it has not been proved by actual experiments [1]. Chang et al. found that the unprecedented growth of wireless traffic not only poses challenges to the design and evolution of wireless network architectures but also brings great opportunities to promote and improve future networks. At the same time, the evolution of communication and computing technology can make the edge of the network become more intelligent, rich in computing and communication capabilities. They suggested exploring big data analytics to improve edge caching capabilities, which are seen as a way to improve network efficiency and alleviate the high demands of future networks. Chang et al. proposed that the opportunity brought by the unprecedented growth of wireless traffic should also be discovered, but did not specify how to seize this opportunity [2]. Shen and Chan found that sharing forecast information helps all aspects of the supply chain to better match demand and supply, and they believe that sharing forecast information can improve supply chain performance. In the era of big data, supply chain managers have the ability to process massive amounts of data through big data technology and analysis. Big data technologies and analytics provide more accurate predictive information and provide opportunities to transform business models. They analyzed the forecast information sharing of supply chain management in the era of big data. Shen and Chan only saw the benefits brought by big data but did not see the challenges [3]. Zhou and Luo found that big data is a dataset that is suitable for capturing, managing, and possessing the ability to process data within a short period of time. In smart cities, available resources can be used safely, sustainably, and efficiently to achieve positive, measurable economic, and social outcomes. Most of the challenges of big data in smart cities are multidimensional and can be addressed from different multidisciplinary perspectives. They combined the fuzzy logic model and entropy weight method to conduct an empirical study of feasible urban public safety evaluation modeling. Zhou and Luo did not mention how to combine the two methods and what is the specific effect of the combination [4]. Li et al. found that the Internet of Things (IoT) and big data are the two most talked about technology topics in recent years, and they are closely related, and these devices will be able to generate big data that people need to analyze. Therefore, IoT and big data have the potential to revolutionize the entire telecom industry. Li et al. saw the advantages of big data in the future and also saw that big data can bring benefits to the telecommunications industry, but they did not make a specific analysis of big data [5]. Epelde et al. found that in recent years, the digitization of human-generated information flows from traditional manual processes leading to the massive availability of heterogeneous data in most areas of life. This is due to lower costs and improved capabilities of information and communication technology (ICT) for storage, processing, and transmission. They realized that there was a lot of information in the information flow that could be exploited but did not see that manual processes would waste a lot of time and cost [6]. Khosravi et al. found that accurate forecasting of renewable energy plays a key role in the grid. They proposed the use of machine learning algorithms to predict hourly solar irradiance, and the predictive models were developed based on two types of input data. To this end, they developed Multilayer Feedforward Neural Network (MLFFNN), Radial Basis Function Neural Network (RBFNN), Support Vector Regression (SVR), Fuzzy Inference System (FIS), and Adaptive Neuro-Fuzzy Inference System (ANFIS). Khosravi et al. knew that predictive models were developed based on two types but did not conduct a comprehensive analysis of both types [7]. Yang et al. found that the photovoltaic-thermoelectric hybrid system can realize the full spectrum utilization of the solar spectrum, but the surface reflection has always been an important reason for inhibiting its power conversion efficiency. Therefore, they proposed a novel composite nanostructure to reduce surface reflections in a certain range by means of the finite difference time domain (FDTD) simulation method. Although Yang et al. proposed a new type of composite nanostructure, no explanation was given for this new type of composite nanostructure [8].

3. Machine Learning Algorithms in the Context of Big Data

3.1. The Concept of Green and Intelligent Vehicles. With the increase in the number of automobiles in China, the problem of automobile exhaust pollution and its large energy demand is becoming more and more serious. Promoting the green innovation of automobile enterprises and developing the new energy automobile industry are very important for energy conservation and emission reduction [9]. At present, the development of China's new energy vehicle industry is faced with the characteristics of high technology, high investment, and high risk, which requires policy guidance and strong support from the government. A green smart car is shown in Figure 1.

Figure 1: Green smart car.

As shown in Figure 1, with the further expansion of car ownership in China, the energy crisis and air pollution have become increasingly prominent, becoming the main problems hindering the development of automobiles. Energy-saving, green, and intelligent new vehicles will be the direction of future automobile development. At present, major automakers have invested a lot of manpower and material resources in the research of alternative energy and new power. New energy vehicle technologies represented by hybrid power, fuel cells, advanced diesel, and alcohol gasoline have shown a rapid development trend. In the process of the rapid increase of automobiles, the pollution of automobile exhaust to China's environment cannot be ignored. Many studies have shown that traffic pollution, especially automobile exhaust, is an important cause of urban smog in China. If the electric energy used by electric vehicles comes entirely from fossil fuels, the emissions of air pollutants produced by electric vehicles will exceed that of ordinary fuel vehicles [10]. Therefore, more and more electric vehicle charging stations will be equipped with certain photovoltaic power generation equipment to supply the electric energy required for electric vehicle charging. The performance of the electric vehicle is shown in Figure 2.

As shown in Figure 2, the worldwide problems of energy depletion and environmental pollution are becoming more and more serious, and the development of new energy vehicles is the top priority for energy conservation and emission reduction in China and the world. Compared with some well-known enterprises, China is relatively backward in new energy vehicle drive technology and power battery material technology and is much behind in the patent strategy construction plan [11].

3.2. Relevant Machine Learning Algorithms in the Context of Big Data. Everyone recognizes the importance of big data, but there are different opinions on the definition of big data. Big data is an abstract concept. In addition to a large amount of data, big data has several characteristics that determine the difference between big data and the concepts of "large data" and "very large data." In a general sense, big data is a key factor of production to promote the development of the digital economy. The development of the digital economy is the only way to achieve high-quality economic development and build a modern economic system. Promoting the digital transformation of the economy and society is actually the transition from the era of industrial economy to the era of digital economy. Big data refers to the identification, acquisition, management, processing, and collection of data that cannot be provided by traditional IT technology, hardware, and software tools within a limited time [12]. The components of big data are shown in Figure 3.

As shown in Figure 3, the value chain of big data can be divided into four stages: data generation, data collection, data preservation, and data analysis. Data analysis is the last important stage of the big data value chain and the basis for realizing the value and application of big data. Its purpose is to extract useful value, provide judgmental recommendations, or support decision-making analysis, which has the potential to yield different levels of potential value [13]. With the rapid development of the global economy, the demand for energy is also increasing, the reserves of traditional fossil energy are shrinking, and environmental problems such as global warming have become increasingly prominent. Energy issues have become the focus of attention around the world. The new energy power generation technology and application represented by solar energy and wind energy have become the research hotspots in various countries [14].

3.2.1. Support Vector Machine (SVM). Support vector machines and kernel methods are important methods in the field of machine learning, and their basic theories and practical engineering applications are relatively mature. Initially, support vector machines were used for classification and regression tasks, after which some of these important problems were studied in depth. Together, these vectors support the classification hyperplane and are therefore called support vector machines [15]. The schematic diagram of SVM is shown in Figure 4.

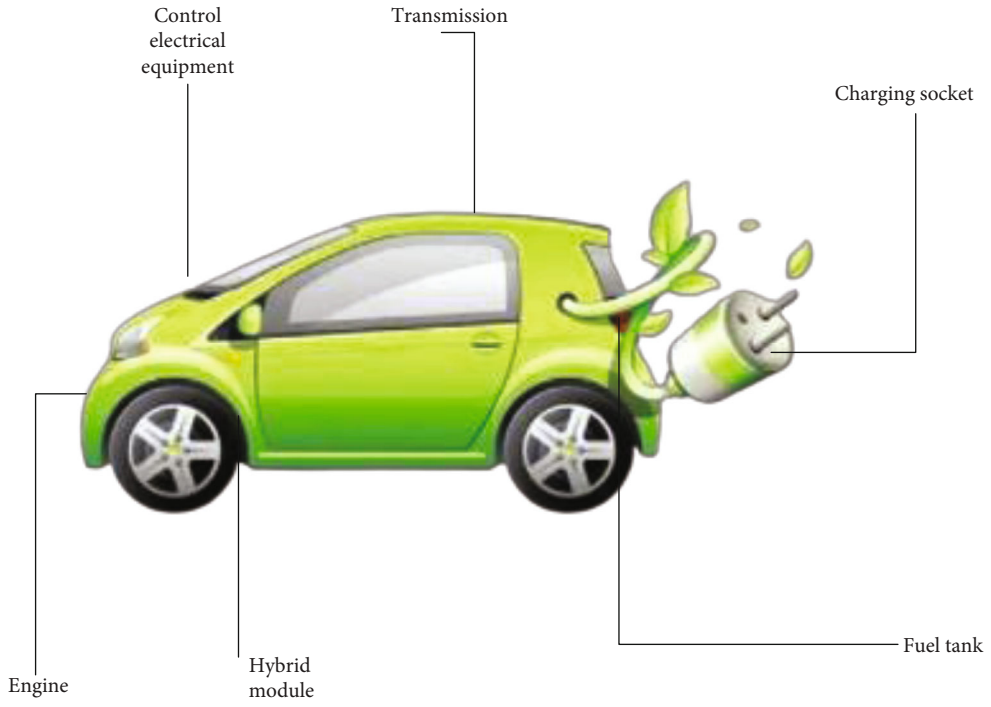

Figure 2: Performance of electric vehicles.

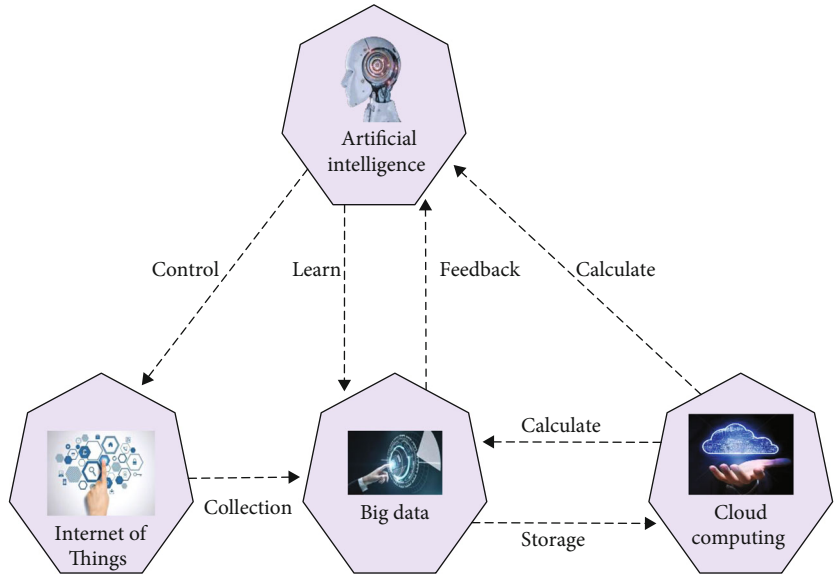

Figure 3: Components of big data.

As shown in Figure 4, the final decision function of SVM is only determined by a small number of support vectors, and the computational complexity depends on the number of support vectors, not the dimension of the sample space, which avoids the "curse of dimensionality" in a sense. SVM has the strongest robustness to samples in this classification. Robustness is the ability of a system to survive abnormal and dangerous situations. For example, whether the computer software cannot crash or crash under the condition of input error, disk failure, network overload, or intentional attack is the robustness of the software. The classification to be solved can be described using

$$w^T a + b = 0, \tag{1}$$

where $w = (w_1, w_2, \cdots, w_d)$ is the normal of the classification hyperplane and the distance from the training sample

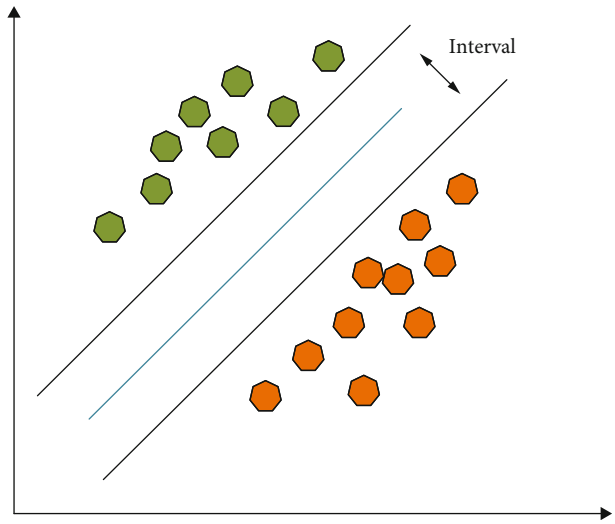

Figure 4: SVM schematic.

to the hyperplane can be expressed as

$$r = \frac{|w^T a + b|}{|w|}. \tag{2}$$

For a linearly classifiable sample set, if hyperplane (w, b) can correctly classify all samples, then for any sample $(a_i, b_i) \in D$, there is

$$\begin{cases} w^T a_i + b \geq +1, & b_i = +1, \\ w^T a_i + b < -1, & b_i = -1. \end{cases} \tag{3}$$

The point closest to the classification surface is called the support vector, and the distance from the support vector to the classification hyperplane is

$$r = \frac{1}{|w|}. \tag{4}$$

To find the so-called "maximum interval" classification hyperplane, it is necessary to find (w, b) that satisfies formula (3) and maximize r, that is,

$$\text{s.t.} \quad b_i\left(w^T a_i + b\right) \geq 1, \quad i = 1, 2, \cdots, m. \tag{5}$$

Formula (5) can be obtained by solving the desired classification hyperplane. This is a quadratic planning problem; note that it can be solved by using the related method of the quadratic planning problem. But *S*-gradient solution, least squares, etc. can also be used to solve such problems [16]. The least square formula is a mathematical formula, called curve fitting in mathematics, which includes not only linear regression equations but also matrix least squares.

3.2.2. Introduction to the Variant Form of Support Vector Machine. Compared with traditional statistical learning methods, support vector machines have obvious advantages in preventing overfitting and high training accuracy. Therefore, with the in-depth study of SVM by a large number of scholars, many variant algorithms of SVM appear. These methods mainly have certain advantages in a certain aspect by changing coefficients, adding function terms and so on. Compared with previous statistical learning methods, SVMs have obvious advantages to prevent overfitting and achieve high training accuracy [17]. Therefore, according to the detailed study of SVM by most scholars, quadratic relaxation C-SVM, LS-SVM, and other methods have appeared. These methods have specific advantages in specific aspects, mainly by changing the coefficients and adding correlation terms.

The quadratic relaxation C-SVM is based on the original C-SVM, replacing ζ on the objective function with ζ^2, so the original problem is transformed into

$$\min\ (w, b) = \frac{1}{2}\|w\|^2 + C\sum_{i=1}^{n}\zeta_i^2, \tag{6}$$

where ζ^2 is also used to characterize the degree of misclassification of the sample by the hyperplane. By solving the Lagrange multiplier method, it is easy to obtain its dual formula as

$$\min\ \alpha = \frac{1}{2}\sum_{i=1}^{n}\sum_{j=1}^{n} a_i a_j \left[K\left(a_i a_j\right) + \frac{1}{2C}\right]. \tag{7}$$

Since the slack variable in the objective function of the original problem has become a quadratic form, it also considers both the empirical risk and the minimum model complexity, which conforms to the principle of structural risk minimization [18].

LS-SVM is the least square support vector machine, which is a kind of SVM (support vector machine), but it is simpler to calculate than SVM. In order to solve the problem that C-SVM needs to use the least square method to calculate the complexity, this paper proposes LS-SVM, the objective function uses the least square method, and the formula constraint is used instead of the inequality constraint, which can effectively solve the linear formula and simplify the calculation. Its original objective function is

$$\min\ \alpha = \frac{1}{2}\|w\|^2 + \frac{1}{2}C\sum_{i=1}^{n}\zeta_i^2. \tag{8}$$

Among them, ζ_i must be nonnegative. When $\zeta_i = 0$, the minimum value is still satisfied; then, $\zeta_i < 0$ makes the target problem larger, and the solution of formula (8) about ζ_i is a nonnegative value, which is

$$\begin{bmatrix} 0 & Y^T \\ Y & Q + \dfrac{1}{C}I \end{bmatrix} \begin{bmatrix} b \\ a \end{bmatrix} = \begin{bmatrix} 0 \\ I \end{bmatrix}. \tag{9}$$

Weighted support vector machines believe that various samples play various roles in constructing the optimal

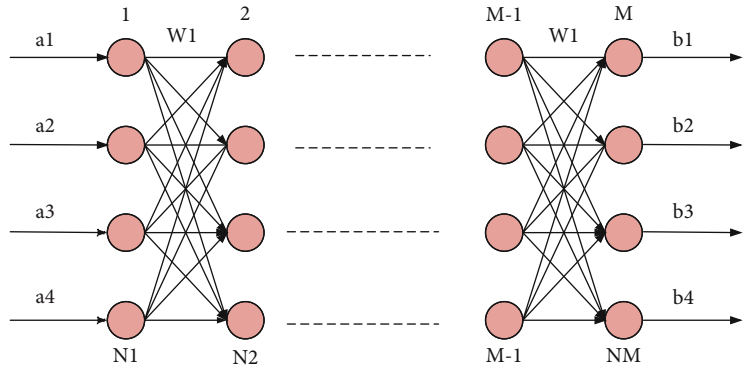

Figure 5: BP neural network structure diagram.

Table 1: Comparison table of different network error rates.

Network code	Number of network layers	1-5 experiments' error rate	6-10 experiments' error rate
A	11	26.7	9.5
B	12	25.9	8.4
C	15	24.9	8.3
D	15	24.8	7.2
E	18	24.8	7.2

classification decision hyperplane. Such problems often occur in practical real-world applications [19].

3.3. BP Neural Network. A BP neural network is a multilayer feedforward neural network trained according to the error back propagation algorithm, and it is one of the most widely used neural network models. The BP neural network has a complete theoretical system and learning mechanism and builds a multilayer model by imitating the response process of human brain neurons to external signals. It is learned iteratively through two processes of signal forward propagation and error feedback adjustment [20]. It has good correlation and can effectively solve complex problems such as nonlinear classification, function approximation, and medical detection. The structure diagram of BP neural network is shown in Figure 5.

As shown in Figure 5, the BP neural network is usually a 3-layer neural network consisting of a single input layer, a single output layer, and a single hidden layer. Each layer is composed of multiple neurons with processing functions, and the neurons in each layer are connected to each other, and there is no connection between internal neurons [21].

Assuming that the output vector of the i-th layer is $O_i = (o_{i1}, o_{i2}, \cdots, o_{\mathrm{iN}})^T$, the input vector of the $i+1$-th layer is

$$\mathrm{net}_{i+1} = W_i O_i^T. \tag{10}$$

The i-th layer output vector is

$$O_i = f(\mathrm{net}_i + B_i). \tag{11}$$

Among them, $f(\cdot)$ is the neuron excitation function, and the sigmoid function is generally selected. In a mathematical formula such as

$$f(a) = (1 + e^{-ax})^{-1}, \tag{12}$$

where a is a constant, the shape of the sigmoid function is like an S shape, also known as the S function, and its shape changes as a becomes smaller and becomes flat. The sigmoid function is a common sigmoid function in biology, also known as the sigmoid growth curve. In information science, the sigmoid function is often used as the activation function of neural network because of its monoincrease and inverse function monoincrease properties.

O_M is the actual output, and $D = (d_1, d_2, \cdots, d_{NM})$ is the expected output, so the objective function of the BP algorithm is

$$E = \frac{1}{2}(Y - D)^T (Y - D). \tag{13}$$

The traditional BP algorithm does not consider the gradient descent direction of the $t-1$-th iteration. If there is a relatively flat area in the error surface, it is easy to fall into the area near the local minimum and cannot jump out and converge to the overall minimum. The momentum term reflects the adjustment experience accumulated before and acts as a damping effect on the adjustment at time t. When the error surface fluctuates suddenly, the oscillation trend can be reduced and the convergence speed can be improved. Therefore, a momentum term needs to be added as in

$$\Delta w_{ijk}(t) = \Delta w_{ijk}(t-1) + \lambda \delta_{ik} o_{ij}. \tag{14}$$

In formula (14), $\Delta w_{ijk}(t-1)$ is the momentum term, although $\lambda \delta_{ik} o \longrightarrow 0$ and $\Delta w_{ijk}(t-1)$ is not 0, it can make it jump out of the local minimum faster and speed up the network convergence rate and performance.

3.4. VGGNet Model. The VGGNet model is a deep convolutional neural network. It explores the relationship between the depth of convolutional neural networks and their performance. With the widespread use of convolutional neural networks in the field of computer vision, many methods

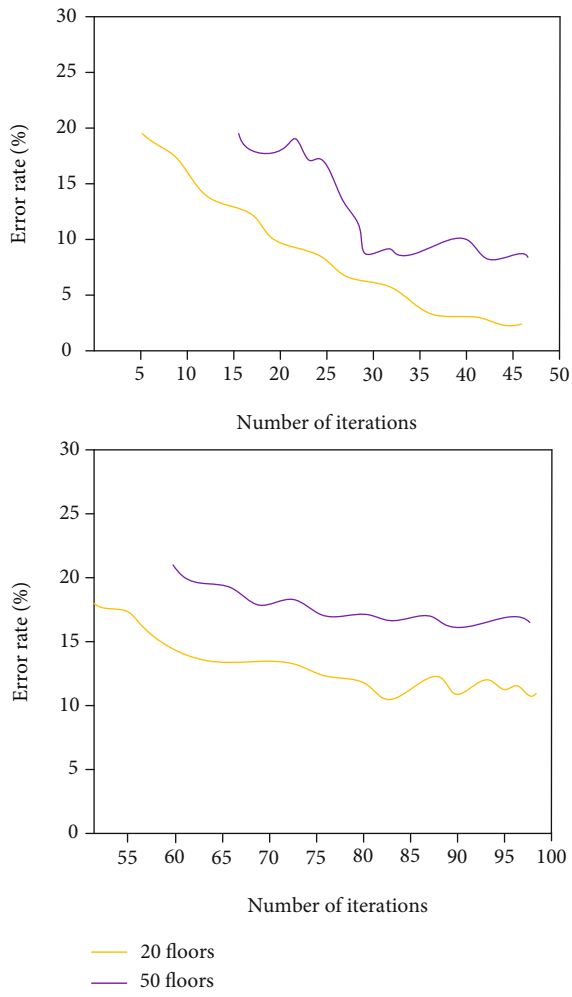

Figure 6: Two network training set error rates.

have been tried to improve the network. In terms of datasets, using multiscale maps of the entire image during training and testing can also improve recognition accuracy. In a research work, people try to study the relationship between network depth and recognition accuracy [22]. Experimental studies show that deeper networks can achieve better recognition results, as shown in Table 1.

As shown in Table 1, at the same time, without fine-tuning, the training results of VGGNet are used for feature extraction, and then SVM is used as a classifier for other datasets, and very good results have been achieved.

Vanishing or exploding gradients are the main reason that makes neural networks harder to train. There are some methods to solve this problem, such as normalizing the initial value and adding normalization layers in the middle of the network; these techniques can make the neural network with dozens of layers converge under the action of stochastic gradient descent and backpropagation. Normalization is a dimensionless processing method, which makes the absolute value of the physical system value into a relative value relationship, simplifies the calculation, and reduces the magnitude of the effective method.

When the deeper network starts to converge, a degradation problem is exposed. With the deepening of the network layers, the accuracy of the network reaches the highest and decreases rapidly. Unexpectedly, this reduction in accuracy is not due to overfitting, as shown in Figure 6.

As shown in Figure 6, the degradation of accuracy on the training set shows that not all deep networks are easy to train. Now, suppose there are a shallower neural network and an equivalent deeper neural network. Such a structure proves that a deeper network should not have a higher error rate than a corresponding shallower network.

3.5. Scenario Analysis of China's Energy Consumption Based on Green Development. Green development is a method of social development aimed at improving the happiness of human life. Everyone should play their role in saving resources, reducing the emission of polluting gases, and promoting green development. Green development has become an important trend. Many countries take the development of green industries as an important means to promote economic restructuring.

The factors closely related to the energy consumption structure are GDP, population, industrial structure, and environment. If China wants to achieve the goal of green development, it must first make a rational allocation plan for the energy consumption structure. The environmental load model can also be referred to as the IPAT model. This model accurately describes the relationship between the environment, economy, and energy and plays an important role in the study of green development. The environment can be described in terms of the amount of information delivered to the individual, a concept known as the load of the environment. A high-load environment is an environment that transmits a large amount of sensory information; a low-load environment is an environment with less stimulus information. In all other conditions being equal, the high-load environment had a stronger arousal effect than the low-load environment. The general form of the IPAT model is

$$I = P \cdot A \cdot T = P \cdot \frac{Y}{P} \cdot \frac{I}{Y}. \tag{15}$$

In the formula, I refers to the environmental load; P refers to the total population; Y refers to the gross domestic product (GDP). Using the carbon dioxide emissions generated by energy consumption to reflect the environmental load and replacing I with C, the above formula will become

$$C = P \cdot \frac{Y}{P} \cdot \frac{C}{Y}. \tag{16}$$

Energy consumption will produce carbon dioxide in the use, but the carbon dioxide produced per unit of energy of different varieties is different. This difference is expressed by the carbon dioxide emission coefficient, and the total

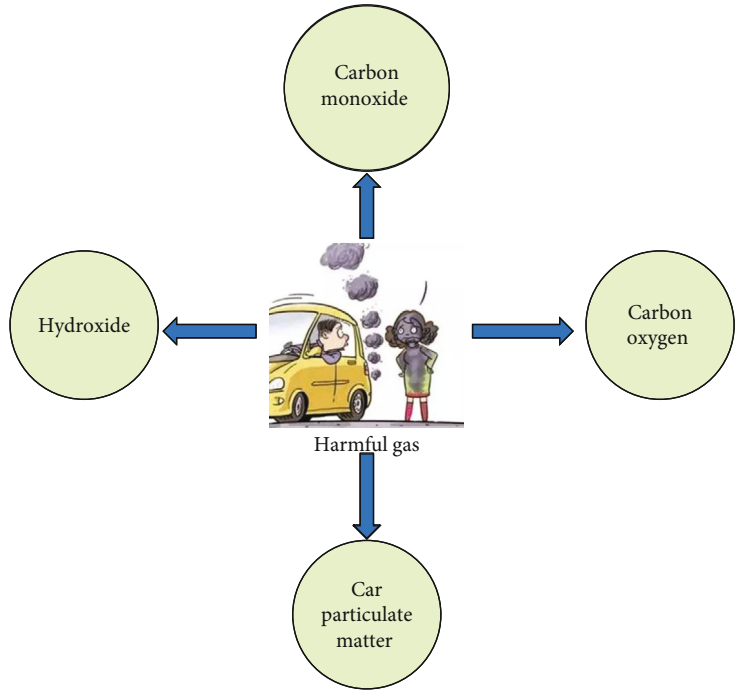

Figure 7: Hazardous gas emissions.

Table 2: The number of cars and the number of drivers.

Years	Motor vehicles (100 million units)	Drivers (100 million)	Sewage discharge (100 million tons)
2015	1.99	2.01	4.57
2016	2.59	3.15	5.78
2017	3.10	3.85	6.89
2018	4.90	5.12	7.98
2019	5.14	5.30	10.65
2020	6.98	7.03	12.09

carbon dioxide emission can be expressed as

$$C = \sum_{i=1}^{4} E^i \cdot f^i. \tag{17}$$

E represents the total energy consumption; E^i represents different energy consumption varieties; that is to say, in the total energy consumption, the ratio of the i-th energy consumption to the total energy consumption. f^i is the amount of carbon dioxide gas released by the i-th unit of energy consumption. According to the relationship between energy and GDP, the total energy consumption can be expressed as

$$E = Y \times \frac{E}{Y} = Y \times \sum_{Y}^{E^i}. \tag{18}$$

China attaches equal importance to economic development and environmental protection. With the continuous advancement of technology, China's economic development has become more and more rapid, but the promotion of China's industrial structure and energy intensity is relatively small. China still has to take economic development as the first task, so the demand for energy is still very large.

3.6. Necessity to Promote the Consumption of Energy-Saving and Environment-Friendly Vehicles. Increasing the consumption of energy-saving and environment-friendly vehicles will help alleviate the contradiction between China's energy supply and demand. With the increasingly serious environmental pollution and the aggravation of the contradiction between energy supply and demand, the transformation of automobile energy demand is imperative. Countries are accelerating the formulation and implementation of technological innovations for energy-saving and environment-friendly vehicles and supporting the energy-saving and environment-friendly vehicle industry. Harmful gas emissions are shown in Figure 7.

As shown in Figure 7, while automobiles consume a lot of resources, the exhaust gas they emit will seriously affect human health. Carbon monoxide in car exhaust binds to hemoglobin in the blood 250 times faster than oxygen. Therefore, even a small amount of carbon monoxide inhalation may cause terrible hypoxic injury. With the rapid increase in automobile consumption, the exhaust gas brought by fuel vehicles includes harmful and toxic gases such as carbon dioxide, lead compounds, and carbon monoxide, which will seriously threaten the ecological environment and human health.

(1) To reduce harmful gas emissions, it is necessary to increase the proportion of consumption of energy-saving and environment-friendly vehicles

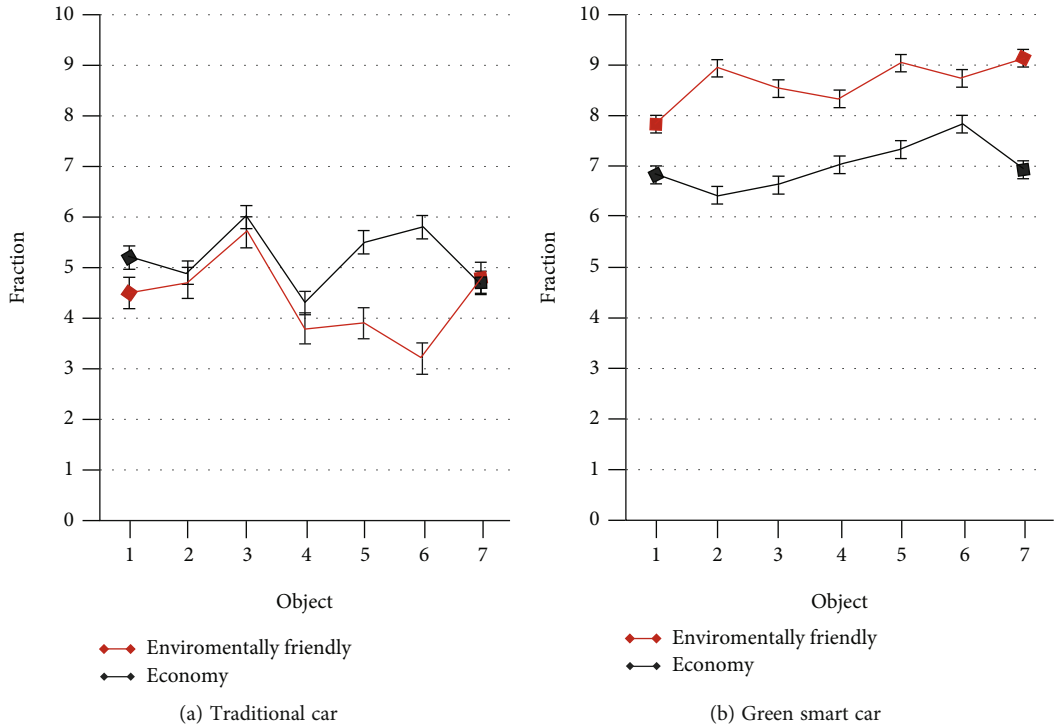

Figure 8: Characteristics of conventional cars and green smart cars.

The exhaust emissions of traditional fuel vehicles mainly include carbon monoxide, carbon oxides, nitrogen oxides, and automobile particulate matter, and the emissions of the four main exhaust emissions of automobiles are increasing year by year. Carbon monoxide has the highest annual emissions of the four major emissions.

(2) Increasing the proportion of energy-saving and environment-friendly automobile consumption will help ease the pressure on China's crude oil supply

At present, the power of the automobile industry in various countries is mainly provided by petroleum, and China is no exception. At this stage, the number of new energy vehicles and low-displacement vehicles has not been accepted by the majority of Chinese consumers. Under the circumstance that the number of vehicles in China continues to rise, the amount of gasoline used in vehicles is rising. Oil is the blood of modern economic and social development, and it is also a strategic resource of a country. Excessive dependence on foreign countries will seriously restrict the harmonious and healthy development of economy and society. Therefore, increasing the consumption ratio of energy-saving and environment-friendly vehicles will help curb the rising trend of China's dependence on foreign oil and change the increasingly serious contradiction between China's oil supply and demand.

(3) To seize the dominance and development rights of the new generation of automobile technology, it is necessary to adjust the development concept in advance

The research and development of energy-saving and environment-friendly vehicles are still in its infancy in the world, and the early research and development of new technologies require a lot of financial support. According to the product cycle theory, the funds invested in the product development stage are mainly compensated in the product maturity stage, and the development of the automobile industry has its own particularity. The automobile industry is one of the important pillar industries of the country. It involves a long industrial chain, a long R&D cycle, and a large capital investment. In the global automobile industry, China belongs to the emerging market. Although it develops rapidly, there is still a big gap between it and the developed economies, especially in the energy saving and environmental protection automobile industry.

4. Experiment and Analysis on the Development and Consumption Trend of Green and Intelligent Vehicles

4.1. Characteristics of Green and Intelligent Vehicles. Since the 21st century, with the rapid development of the automobile industry and the rapid growth of car ownership, the problem of environmental pollution caused by motor vehicle exhaust has become increasingly prominent. Motor vehicles will emit various air pollutants with complex composition during driving, as shown in Table 2.

As shown in Table 2, many countries in the world have issued preferential tax and subsidy policies for electric vehicles and related industries to promote the rapid development of electric vehicles. With the support of policies, the number

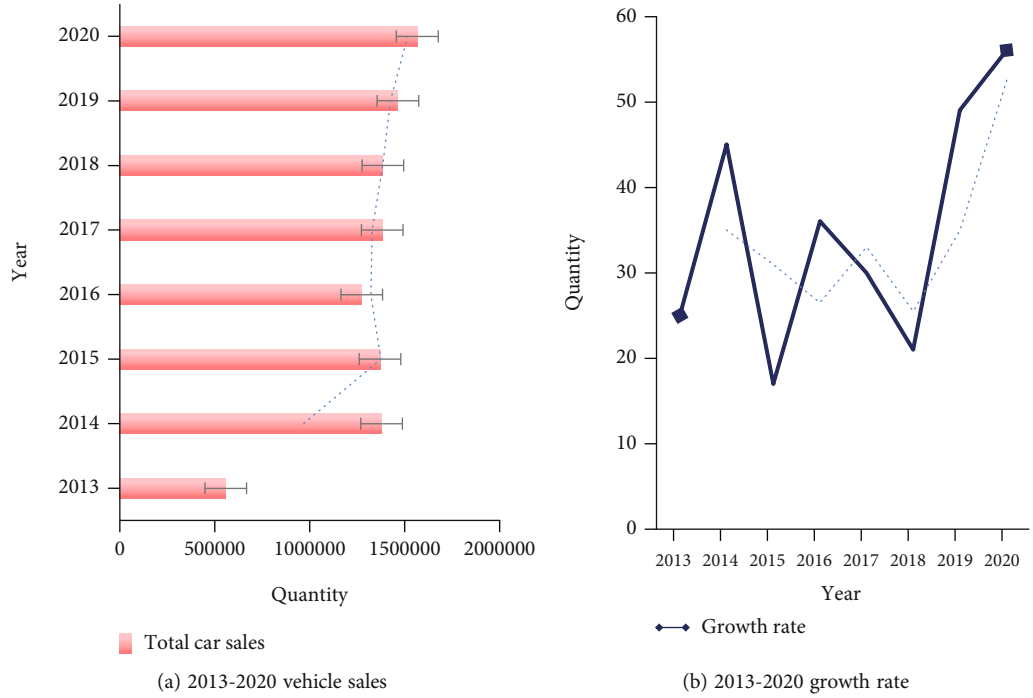

(a) 2013-2020 vehicle sales

(b) 2013-2020 growth rate

Figure 9: 2013-2020 car sales and annual growth rates.

Table 3: Sales volume of new energy vehicles (units) and its proportion in total vehicle sales (%).

Years	Total car sales	Sales volume	Proportion
2014	556818	3675	0.66%
2015	1376190	2890	0.21%
2016	1368571	4790	0.35%
2017	1272250	5089	0.40%

of electric vehicles in China has grown rapidly. This paper compares traditional cars and green smart cars, as shown in Figure 8.

As shown in Figure 8, electric vehicles have high hopes for solving air pollution and global warming. However, studies have shown that if the electricity used by electric vehicles comes entirely from fossil fuels, the emissions of CO_2 and air pollutants produced by electric vehicles will exceed that of ordinary fuel vehicles. Therefore, in order to make electric vehicles fully play the role of improving air quality and alleviating global warming, electric vehicles should use the electricity generated by the conversion of renewable energy such as wind energy and solar energy as much as possible.

4.2. Overall Trend of Automobile Consumption in China. Since the reform and opening up, China's economy has grown significantly, and economic growth will continue to grow rapidly for a long time. Economic growth will surely drive the overall income of residents to continue to increase, and the purchasing power of residents for automobiles will also continue to increase. Especially in the successive introduction of national policies to strengthen and benefit farmers, it will change the slow growth of rural residents' income in the past, and rural residents' income growth has entered a fast lane. Therefore, the potential market for automobile consumption will be gradually released in rural areas. With the growth of residents' income, more and more people will cross the threshold of automobile consumption, which will promote the continuous growth of automobile consumption. The car sales from 2013 to 2020 and the annual growth rate are shown in Figure 9.

As shown in Figure 9, at the same time, in order to cope with climate change, save oil resources, protect the environment, and build an environment-friendly society. The state has increased policy support for the consumption of new energy vehicles year by year, so that the whole society can form a unified understanding of the consumption of new energy vehicles. The sales volume (units) of new energy vehicles and the proportion (%) in total vehicle sales are shown in Table 3.

As shown in Table 3, the main consumers of these energy-saving and environment-friendly vehicles are government units and urban public transport systems, and the majority of residents choose small-displacement vehicles and conventional hybrid vehicles when purchasing energy-saving and environment-friendly vehicles. The consumption of new energy vehicles in China increased from 3675 in 2014 to 5089 in 2017, but the sales of new energy vehicles in 2017 were very small. Compared with the rapidly increasing total vehicle consumption, the proportion of new energy vehicle sales in total vehicle consumption is still very low. After hovering between 2014 and 2017, its proportion was still at 0.40%, but since 2017, the proportion has maintained a stable upward trend.

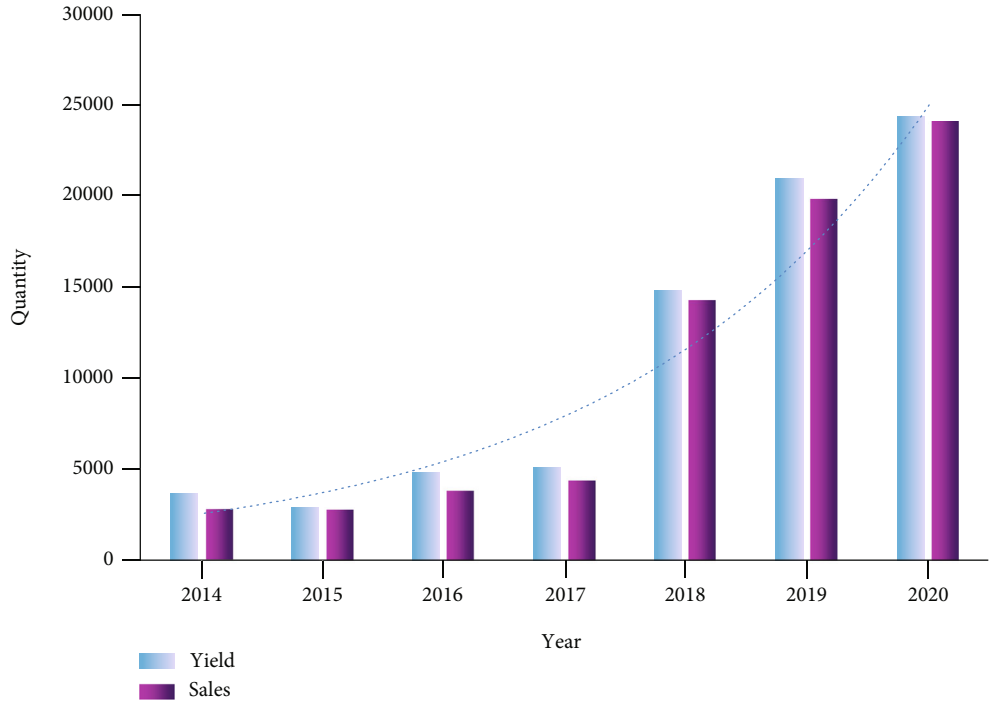

Figure 10: 2014-2020 green and intelligent vehicle production and sales and trends.

This paper analyzes the production and sales volume and trends of green and intelligent vehicles from 2014 to 2020, as shown in Figure 10.

As can be seen from Figure 10, the production and sales of new energy vehicles increased rapidly after 2017, breaking through the stagnant state of production and sales in the previous period. This is mainly due to the targeted fiscal and tax policies implemented by the Chinese government in recent years, which has made the situation of the new energy vehicle industry tend to be good. Effective policy support makes new energy vehicles not only recognized by consumers but also help China to accelerate the pace of rapid development of the industry.

5. Conclusions

In this era of faster and faster development, people are not only pursuing material needs but also have more and more needs for the environment. China has always advocated vigorously developing green environmental protection, protecting the ecological environment and saving energy. The use of automobiles brings a lot of harmful gases to the living environment. Therefore, people begin to study green and intelligent automobiles. This paper mainly focuses on the application of machine learning algorithms in the development and consumption trends of green and intelligent vehicles in the context of big data. Therefore, this article describes the machine learning algorithm and the concept of green and intelligent vehicles. In the method part, this paper summarizes the machine learning algorithms. Based on the machine learning algorithms, it also proposes support vector machines and neural network algorithms. According to the analysis, these two methods have better classification and recognition effects. In the experimental part, this paper analyzes the development of traditional vehicles and new energy vehicles in recent years and investigates the characteristics of traditional vehicles and new energy vehicles. In the end, it was found that green and intelligent vehicles not only are environment-friendly but also can reduce costs.

Data Availability

The data that support the findings of this study are available from the corresponding author upon reasonable request.

Disclosure

A preprint has previously been published [1]. Based on that version, we add more than 80% new content in this paper.

Conflicts of Interest

The authors declare that they have no conflicts of interest.

References

[1] https://dokumen.pub/2021-international-conference-on-applications-and-techniques-in-cyber-intelligence-applications-and-techniques-in-cyber-intelligence-atci-2021-data-engineering-and-communications-technol-1st-ed-2021-3030791963-9783030791964.html.

[2] R. Rajalakshmi and S. Rajakumar, "A noval approach for intelligent car parking system," *Iosr Journal of Electronics & Communication Engineering*, vol. 13, no. 2, pp. 54–60, 2018.

[3] Z. Chang, L. Lei, Z. Zhou, S. Mao, and T. Ristaniemi, "Learn to cache: machine learning for network edge caching in the big data era," *IEEE Wireless Communications*, vol. 25, no. 3, pp. 28–35, 2018.

[4] B. Shen and H. L. Chan, "Forecast information sharing for managing supply chains in the big data era: recent development and future research," *Asia-Pacific Journal of Operational Research*, vol. 34, no. 1, pp. 1740001–1740144, 2017.

[5] Q. Zhou and J. Luo, "The study on evaluation method of urban network security in the big data era," *Intelligent Automation & Soft Computing*, vol. 24, no. 1, pp. 133–138, 2018.

[6] H. Li, R. Lu, and J. Misic, "Guest editorial big security challenges in big data era," *IEEE Internet of Things Journal*, vol. 4, no. 2, pp. 521–523, 2017.

[7] G. Epelde, A. Beristain, R. Alvarez et al., "Quality of data measurements in the big data era: lessons learned from MIDAS project," *IEEE Instrumentation and Measurement Magazine*, vol. 23, no. 7, pp. 18–24, 2020.

[8] A. Khosravi, R. N. N. Koury, L. Machado, and J. J. G. Pabon, "Prediction of hourly solar radiation in Abu Musa Island using machine learning algorithms," *Journal of Cleaner Production*, vol. 176, pp. 63–75, 2018.

[9] L. Yang, Z. Huang, and B. Shi, "Compound nanostructure capable of realizing full-spectrum utilization of solar energy for PV-TE hybrid systems," *Applied Optics*, vol. 58, no. 17, pp. 4726–4733, 2019.

[10] M. F. Wahid, R. Tafreshi, M. Al-Sowaidi, and R. Langari, "Subject-independent hand gesture recognition using normalization and machine learning algorithms," *Journal of Computational Science*, vol. 27, pp. 69–76, 2018.

[11] S. Raghu and N. Sriraam, "Classification of focal and non-focal EEG signals using neighborhood component analysis and machine learning algorithms," *Expert Systems with Applications*, vol. 113, pp. 18–32, 2018.

[12] A. Whyte, K. P. Ferentinos, and G. P. Petropoulos, "A new synergistic approach for monitoring wetlands using sentinels -1 and 2 data with object-based machine learning algorithms," *Environmental Modelling and Software*, vol. 104, pp. 40–54, 2018.

[13] J. Liu, Y. Ye, C. Shen, Y. Wang, and R. Erdélyi, "A new tool for CME arrival time prediction using machine learning algorithms: CAT-PUMA," *The Astrophysical Journal*, vol. 855, no. 2, pp. 109–109, 2018.

[14] Y. Huichun, P. Panpan, Y. Yong, and L. Yunhong, "Coupled electronic nose and BP neural network to study on the predicting model of zearalenone and aflatoxin B_1," *Journal of the Chinese Cereals and Oils Association*, vol. 32, no. 5, pp. 117–121, 2017.

[15] H. Zhu, F. Liu, Y. Ye et al., "Application of machine learning algorithms in quality assurance of fermentation process of black tea– based on electrical properties," *Journal of Food Engineering*, vol. 263, pp. 165–172, 2019.

[16] H. Y. Tsao, P. Y. Chan, and C. Y. Su, "Predicting diabetic retinopathy and identifying interpretable biomedical features using machine learning algorithms," *BMC Bioinformatics*, vol. 19, no. S9, pp. 111–121, 2018.

[17] T. C. Chuah and L. L. Ying, "Intelligent RAN slicing for broadband access in the 5G and big data era," *IEEE Communications Magazine*, vol. 58, no. 8, pp. 69–75, 2020.

[18] K. C. Montgomery, J. Chester, and T. Milosevic, "Children's privacy in the big data era: research opportunities," *Pediatrics*, vol. 140, Supplement_2, pp. S117–S121, 2017.

[19] W. Xu, H. Zhou, N. Cheng et al., "Internet of vehicles in big data era," *IEEE/CAA Journal of Automatica Sinica*, vol. 5, no. 1, pp. 19–35, 2018.

[20] X. Ma, Y. Ji, Y. Fan, and C. Yi, "Exploring the evolution of passenger flow and travel time reliability with the expanding process of metro system using smartcard data," *Journal of Harbin Institute of Technology (New Series)*, vol. 26, no. 1, pp. 17–29, 2019.

[21] M. Asif, M. A. Hassanain, K. M. Nahiduzzaman, and H. Sawalha, "Techno-economic assessment of application of solar PV in building sector," *Smart and Sustainable Built Environment*, vol. 8, no. 1, pp. 34–52, 2019.

[22] E. Ayanoglu, "Editorial launching IEEE transactions on green communications and networking," *IEEE Transactions on Green Communications & Networking*, vol. 1, no. 1, pp. 1-2, 2017.

Hindawi
Wireless Communications and Mobile Computing
Volume 2022, Article ID 6585189, 13 pages
https://doi.org/10.1155/2022/6585189

Research Article

Detection and Function of Elastic Wave Tomography of Foundation Piles of High-Rise Buildings under the Background of Internet of Things

Wannan Guo[1] **and Yang Liu**[2]

[1]*School of Mechanics and Engineering, Liaoning Technical University, Fuxin, 123000 Liaoning, China*
[2]*School of Management, Dalian Polytechnic University, Dalian, 116034 Liaoning, China*

Correspondence should be addressed to Yang Liu; 20071120200726@xy.dlpu.edu.cn

Received 28 April 2022; Revised 23 June 2022; Accepted 4 July 2022; Published 25 July 2022

Academic Editor: Jun Ye

Foundation piles are a widely used foundation form for high-rise buildings. Its main function is to reduce the settlement of buildings. In recent years, in areas with good upper soil conditions, in order to reduce the amount of earthwork excavation and transportation, more and more engineering buildings use foundation piles. Therefore, the status of foundation piles in construction projects is becoming more and more important. The high-rise building foundation pile project belongs to the underground concealed project. In the construction process, it is greatly affected by factors such as construction technology and geology. After the construction is completed, it is difficult to observe the changes inside the foundation pile with the naked eye as time goes by. A series of problems such as building collapse, settlement, and cracking often occur, thus affecting normal use and causing some safety accidents. In order to solve these series of problems, this paper proposes an elastic wave tomography detection method. It performs imaging inversion calculation on the inside of the foundation pile, and many methods are used in it. In the canonical Gaussian-damped Newton method in tomography, its iteration rate is 3.5% higher than that of the canonical Gaussian-Newton method, the convergence speed is accelerated, the accuracy is high, and the error is small. In the process of detection, this method is more suitable to detect the integrity and quality of foundation piles.

1. Introduction

Elastic wave tomography technology is a computer detection system based on the Internet of Things. It involves many subjects such as mathematics, physics, computer, engineering, and materials and has a wide range of application value. Tomography is also called computer-aided tomography. It is a reconstruction technique from data to image. It can reflect the internal quality of the tested material or workpiece through pseudocolor images and conduct qualitative and quantitative analysis of defects, thereby improving the reliability of detection. Due to the misjudgment or design error of the bearing capacity of the foundation by the exploration unit, a series of problems such as building collapse, shortening of service life, construction quality, cutting corners, and incomplete foundation pouring are caused. This brings security risks to the project. The detection of building foundation piles has been paid more and more attention. In this paper, elastic wave tomography technology is used to detect the interior of high-rise building foundation piles, and the elastic wave equation model, cross-hole CT observation system, tomography forward, and inversion methods are used. The purpose is to detect the bearing capacity of the foundation pile and the integrity of the pile body and analyze the defects of the pile body.

Elastic wave tomography can quickly and effectively determine the physical and mechanical properties of rock or concrete. Using the computer imaging results of the Internet of Things, the acoustic parameters are accurately given to determine the stability of the building foundation piles.

It lays the foundation for the comprehensive detection of foundation piles of high-rise foundation buildings from single strength measurement to crack measurement, defect measurement, damage layer thickness measurement, and elastic parameter measurement.

China classifies residential buildings with more than 10 floors and other civil and industrial buildings with a height of more than 24 meters as high-rise buildings. Generally, the service life of high-rise buildings is about 70 years. After decades of load-bearing use, the foundation piles of buildings undergo uneven deformation, uneven settlement, or inclination over time. This leads to loose and aged pile structures, cracks, fractures, and collapses, causing a series of safety problems. In response to this set of issues, Asaue et al. performed preventive and proactive maintenance on in-service concrete slabs to determine civil engineering forecasts. To determine the maintenance system based on the predictions of the concrete slabs, they evaluated the evolution of fatigue damage and internal defects. They research and develop acoustic emission (AE) tomography and elastic wave tomography as innovative nondestructive testing (NDT) methods for the detection of concrete quality. The three-dimensional velocity distribution within the panel is determined by the method described above, and damaged or degraded areas are identified. The results show good agreement between the predicted low-velocity region and the damage region estimated from crack distribution, displacement, and strain. At locations where cracks are strongly observed, the velocity drops below 3400 m/s. In addition, regions with velocities below 2700 m/s were also observed in slabs reaching the fatigue limit [1]. According to photoacoustic computed tomography (PACT) technology, Mitsuhashi et al. used optical contrast and ultrasonic detection principles to form images of photoacoustic-induced initial pressure distribution in tissues to detect internal damage of high-rise building foundation piles. The PACT reconstruction problem corresponds to an inverse source problem, where the initial pressure distribution is recovered from measurements of the radiated wavefield. When ultrasonic waves propagate in a medium, absorption, scattering, and mode conversion from longitudinal to transverse waves occur. In this paper, a forward model based on time-domain finite-difference discretization of the three-dimensional elastic wave equation is established, and the corresponding adjoint calculation method of the forward operator is given. A large scale of these operators employing multiple graphics processing units has also been developed and implemented [2]. Huang et al. investigated the dynamical effective parameters and crack arrest behavior of multidegree-of-freedom locally resonant metamaterials. Based on the Wiener-Hopf method, the energy release rate, which characterizes the crack splitting resistance, is deduced, and the influence of material parameters is discussed. Compared with single-atom lattice chains and locally resonant metamaterials composed of single-degree-of-freedom unit cells, this new multidegree-of-freedom-coupled periodic structure exhibits some fundamental features during crack propagation. The results show that the dynamic crack propagation in elastic wave metamaterials exhibits a lower energy release rate due to the coupling of different displacements. This shows that it has better fracture resistance and crack arrest properties. This work is expected to provide a way to improve the crack growth resistance of advanced materials and structures [3]. He et al. proposed a new elastic wave metamaterial. It consists of vertical and lateral resonators and orthogonal stiffeners. An active feedback control system is used to extend the tunable range in the low and high frequency regions and to change the acoustic structure coupling characteristics. The effective mass density under different feedback constants is discussed. To reflect the effect of fluid-solid interactions, they considered immersing elastic wave metamaterials in different fluid media and calculated their acoustic transmission loss (STL). This work provides a feasible method for building mechanical/acoustic models with multifunctional potentials [4].

Depending on the form or material of the foundation piles, there may be an unacceptable decrease in the foundation bearing capacity of buildings and structures under construction. To control the quality of cast-in-place reinforced concrete piles, based on the analysis of the excited and recorded elastic wave parameters in the piles, Lozovsky et al. combined ultrasonic monitoring of concrete integrity using sensors in access pipes installed in reinforced cages. Numerical simulations of the propagation of elastic waves are carried out. Their research was carried out on a series of 2D bored pile models. These bored piles had no defects, but had soil inclusions, or access pipes and concrete debonding. The possibilities and limitations of this method are summarized. The location and geometry of the defect, as well as the influence of the adhesion failure of the access pipe and concrete on the measurement results, are demonstrated. It requires additional studies of abnormal wellbore tomography before drawing conclusions about the possibility and further using the pile as part of the foundation. General recommendations are given regarding the number of access pipes arranged in the pile and the selection of the time interval for calculating the attenuation. Their results show that it is incorrect to calculate the strength of the pile material by the speed of wave propagation [5]. Cui et al. used the finite element software ABAQUS to simulate the process of detecting piles by ultrasonic transmission method. The influence of the inclined acoustic tube on the test results of foundation piles is analyzed. The results show that after the pile is completed, due to the inclination of the sound tube, the sound depth curve velocity of the received signal is inclined to one side, and the sound velocity deviates seriously from the normal value. When the pile body has defects, due to the inclination of the acoustic tube, the defect signal is not obvious, and it is easy to miss or misjudge the pile body defect. In order to solve the problem of tilting the sound tube, a mathematical model of the positional relationship of the sound tube is established, and the sound velocity correction method based on the angle of the sound tube is deduced. Validation showed that the corrected acoustic signal was able to accurately determine the defect and its location in the pile. This effectively reduces the influence of the inclined sound tube on the detection signal, which is beneficial to improve the accuracy of the detection of the pile body [6].

The realization of tomography has two basic processes: forward and inversion. For forward inversion research, Espinosa et al. used the full waveform inversion (FWI) method to solve the inverse problem, imaging high acoustic impedance contrast experimental data of different test targets. The method is based on a high-resolution numerical simulation of the wave-medium interaction forward problem, considering the full time series. To reduce the complexity of numerical implementation, the model takes into account fluid media. Therefore, they aimed to evaluate the accuracy of reconstruction under this assumption for materials with varying degrees of shear wave attenuation and to investigate the limitations of this assumption. The sound velocity images obtained with experimental data are given, and the reconstruction accuracy is evaluated. Their future work should include viscoelastic materials [7]. The above studies on elastic waves, tomography, and forward and inversion are in-depth and have reference significance for this article.

Elastic wave tomography is a new type of geophysical method, mainly used for nondestructive testing of concrete structures. In this paper, the elastic wave tomography detection method is used to perform tomography detection on the foundation piles of high-rise buildings. It combines ultrasonic detection technology, cross-hole CT observation system, and tomography forward and inversion technology to perform inversion imaging analysis on the inner medium of high-rise building foundation piles. In this way, the quality of foundation piles can be evaluated, and some potential safety hazards caused by damage to foundation piles can be avoided.

2. Detection Method of Foundation Pile Elastic Wave Tomography

Tomography technology is based on ray scanning, inversion calculation of the obtained information. It reconstructs the image of the distribution law of the elastic wave and electromagnetic wave parameters of the rock mass within the measured range, to achieve a geophysical inversion interpretation method for delineating the geological anomaly. Elastic wave tomography is one of the classification of tomography techniques and is often used in the detection of building foundation piles [8]. Elastic wave tomography has the characteristics of high exploration accuracy, good reliability, intuitive and clear images, small site requirements, and strong anti-interference ability [9].

2.1. Elastic Wave Tomography Detection

(1) Imaging principle of elastic wave tomography and elastic wave equation model

The elastic wave tomography detection technology mainly uses an Internet of Things detection system. The dry ray beam formed by the propagation of elastic waves in different media forms a tangent surface of the object during the detection process. Then, according to the parameter changes of the wave-initial signal on the cut plane, discrete image reconstruction is performed in the Internet of Things computer to generate an internal image of the object. It goes on to infer the technology of the internal physical properties and states of objects [10]. As shown in Figure 1, it is a schematic diagram of fan-shaped wave ray projection detected by elastic wave tomography. First, the elastic wave is used to detect from the outside of the object, and the projection data is obtained. Finally, the data is overlapped in small blocks, the internal image of the object is quantified, and then, the internal information of the object is reconstructed. When an elastic wave penetrates a medium, the speed of the wave is related to the integrity, density, elastic modulus, and shear modulus of the medium. In the application of nondestructive testing of concrete structures, the higher the density, the higher the strength, and the better the integrity of the detected object, the faster the elastic wave propagates and the smaller the attenuation. If the detected object is broken loose, not vibrated tightly, and the strength is low, the elastic wave will not only reduce the transmitted wave speed but also attenuate rapidly.

The elastic wave displacement equation of motion can be obtained from the imaging principle:

$$(\alpha + \beta)\nabla(\nabla \cdot w) + \beta\nabla^2 w + \wedge = \rho\ddot{w}. \tag{1}$$

When $\wedge = 0$, in a small medium, if the compressive deformation and volume expansion change are ignored, and only the rotational or shear deformation inside the medium is considered, then the case of no scattered field displacement is expressed by the equation:

$$\nabla \cdot w = 0. \tag{2}$$

Substituting the equation for free-field displacement into the equation yields:

$$\nabla^2 w = \frac{\rho}{\beta}\ddot{w} = \frac{\ddot{w}}{c_e^2}. \tag{3}$$

When the medium is in a uniform state, the propagation velocity of the shear wave can be obtained by the following equation:

$$c_e^2 = \frac{\rho}{\beta}. \tag{4}$$

When the curl of the medium displacement is equal to 0, it represents the position change of the particle, which is a directed line segment from the initial position to the final position. Its size has nothing to do with the path, and the direction is from the start point to the end point. It is a physical quantity with magnitude and direction, that is, a vector.

It can get:

$$\nabla \times w = 0. \tag{5}$$

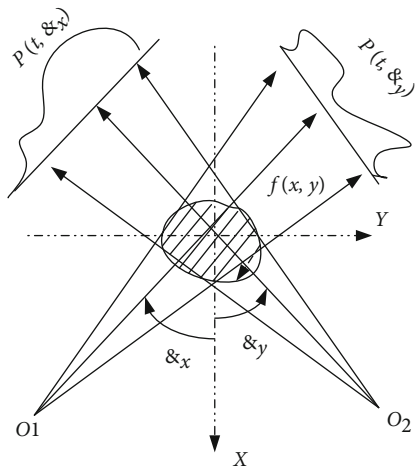

Figure 1: Schematic diagram of fan-wave ray projection for elastic wave tomography detection.

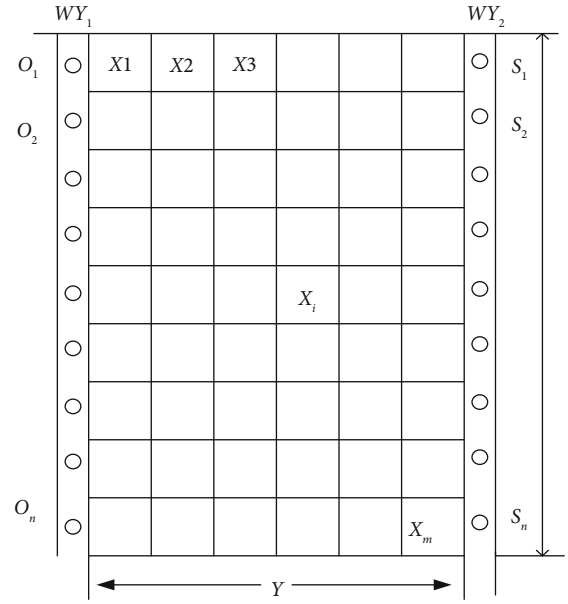

Figure 2: The layout of borehole CT measurement.

Also because:

$$\nabla^2 = \nabla(\nabla \cdot w) - \nabla \times \nabla \times w = \nabla(\nabla \cdot w). \tag{6}$$

Substituting the above equation into the elastic wave displacement equation of motion, it can get:

$$\nabla^2 w = \frac{\rho}{\partial + 2\beta} \ddot{w} = \frac{\ddot{w}}{c_R^2} c_R^2 = \frac{\partial + 2\beta}{\rho}. \tag{7}$$

This is the elastic wave equation for expansion and contraction waves. When the curl of displacement is 0, under the premise of no rotational deformation, when the unit inside the elastic medium expands, deforms, or compresses, the elastic mass only reciprocates at the position centered on the equilibrium position. Its motion direction is consistent with the propagation direction of elastic waves [11]. Among them, the displacement is a vector, and the landmark is a scalar. Displacement is the straight-line distance from the start point to the end point, and the distance is the length of the path.

2.2. Cross-Bore CT Observation System. The cross-hole CT observation system is to perform tomography of transmitted waves between two drilled plates. The cross-hole CT observation system is often used for high-precision interhole formation imaging detection. In the first hole, the transmitter transmits the transmitted wave and reaches the second hole and is received by the detector. The data is transmitted to the transmission recorder for postprocessing analysis, and the transmitted wave propagation paths are superimposed and then imaged, as shown in Figure 2. WY_1 is the excitation hole, and a row of excitation points is arranged along the excitation hole. WY_2 is the receiving hole, and the row next to the receiving hole is the receiving point.

First, the section between the excitation hole and the receiving hole is divided into several squares of equal area, and the space of the forming area is discretized. Assuming that the number of squares in the horizontal space is y, and the number of squares in the vertical space is l, then the total number of squares is $f = y \times l$. The size of the square can be determined according to the size of the object to be detected and the amount of data.

Assuming the inverse of the wave velocity of the jth square, the ray equation for each ray wave can be obtained:

$$u_1 w_1 + u_2 w_2 + \cdots + u_m w_m = f_1, \tag{8}$$

$$\sum_{j=1}^{m} u_j w_j = f_i, i = 1, 2, \cdots, n. \tag{9}$$

Among them, f_i is the arrival time of the wave during the propagation of the ith ray, and u_j is the length of the i th ray in the jth square.

If the depths of the excitation of the two boreholes are different during the measurement process, and x times are received, X-ray equations can be obtained. The matrix equation for the resulting ray travel time equation is:

$$\begin{bmatrix} u_{11} u_{12} \cdots u_{1m} \\ u_{21} u_{22} \cdots u_{2m} \\ \cdots\cdots\cdots\cdots \\ u_{x1} u_{x2} \cdots u_{xm} \end{bmatrix} \begin{bmatrix} u_1 \\ u_2 \\ \cdots \\ u_m \end{bmatrix} = \begin{bmatrix} f_1 \\ f_2 \\ \cdots \\ f_x \end{bmatrix}. \tag{10}$$

The above equation can be abbreviated as:

$$AU = f. \tag{11}$$

The size of x and m depends on the number of rays. When solving this system of equations, the wave slowness

values within the squares give the result. Then, take the reciprocal value to get the distribution diagram of the wave velocity value between holes.

2.3. Acoustic Detection Method. The line source of elastic wave tomography detection technology is elastic wave [12]. In elastic wave detection, the most commonly used emission waves are ultrasonic waves and seismic waves, of which ultrasonic waves are one of the most commonly used methods for engineering detection [13]. The difference between elastic waves and ultrasonic waves: the energy of elastic waves is greater than that of ultrasonic waves, and ultrasonic waves decay quickly. The propagation speed of elastic waves in the medium is relatively stable, while the speed of ultrasonic waves is relatively high. One excitation point in elastic waves can form multiple rays. The speed of the elastic wave when passing through the medium reflects the integrity and density of the medium. Acoustic tomography technology obtains information by penetrating the medium and inverts the imaging through the Internet of Things computer. Finally, the sound wave velocity distribution map of the medium is obtained to judge the quality of the medium [14]. Ultrasonic testing has the characteristics of high precision and accurate positioning of abnormal points and is one of the most commonly used defect detection methods. As shown in Figure 3, it is the process of ultrasonic testing.

There are many types of transducers for ultrasonic testing of concrete, such as flat type (high frequency), Langevin type (low frequency), radial supercharged type, and one-shot double-received type. According to the different positions of the ultrasonic transducer in the foundation pile, ultrasonic detection can be divided into three different ways. The first is the ultrasonic transmission method in the foundation pile. The second is the ultrasonic transmission method outside the foundation pile. Both methods are single-hole transmission, as shown in Figure 4. The third is the transhole transmission method in the pile, as shown in Figure 5.

Ultrasonic testing mainly judges the quality of the medium through the wave speed. The elastic properties of concrete itself enable ultrasonic waves to reflect the compositional relationship of their internal structures when propagating in concrete. Generally speaking, the greater the speed of sound within a certain range, the greater the strength of the concrete, and the quality of the concrete can be guaranteed. The smaller the speed of sound, the lower the concrete strength, and the quality of the concrete of the pile body is defective. If the area with low speed of sound is large and the measuring points are continuous, it will bring security risks to the use of the project [15]. Therefore, the ultrasonic sound velocity plays an important role in judging the quality of foundation piles.

Taking the foundation piles of high-rise buildings as the detection object, the foundation piles of general buildings are completed with concrete pouring. In the sound velocity evaluation, for the foundation piles with good quality, the fluctuation state of the sound velocity is consistent with the fluctuation of the concrete quality, and both obey the normal distribution [16]. In practice, the method often used to analyze the speed of sound is the probabilistic method. Another method is the lower limit value method of sound speed. When the critical value of the abnormal sound speed is too small, the probability method cannot judge the defect. The basic principle of the probability method is to judge the quality of the foundation pile by whether the sound velocity generated by the ultrasonic wave in the concrete foundation pile obeys the normal distribution law.

It arranges the sound velocity of any profile survey point in order of largest to smallest:

$$s_1 \geq s_2 \geq \cdots s_i \geq \cdots s_{p-k} \geq \cdots s_{p-1} \geq s_p. \tag{12}$$

Among them, i represents the sound velocity measurement value of the ith measuring point; p is the number of measurement points on the value plane; k refers to the number of the smallest value in the final sequence.

The equation for the statistical calculation value:

$$s_0 = s_e - \partial_{Fs}, \tag{13}$$

$$s_e = \frac{1}{p - k\sum_{i=1}^{p-k} s_i}, \tag{14}$$

$$W_s = \sqrt{\frac{1}{p-k-1}\sum_{i=1}^{p-k}(s_i - s_e)^2}. \tag{15}$$

Among them, s_0 is the judgment value for criticizing the abnormality of the medium; s_e is the average of the number of (p-k); W_s is the standard deviation of the number of (p-k); ∂ is the corresponding number of (p-k).

The basic principle of the PSD criterion is that the measured sound on any section is continuously derivable with the change of the height of the measuring point. When the concrete has defects, the relationship between the two is discontinuous and nonderivative [17]. This criterion discards the assumption that the acoustic time values are normally distributed. It is based on the mutation of the properties of the ultrasonic propagation medium at the defect. The variation law of the defect area of the acoustic time value is a discontinuous function. The equation expression of the PSD criterion is:

$$F_i = \frac{(y_i - y_{i-1})^2}{(k_i - k_{i-1})}. \tag{16}$$

Among them, y_i, y_{i-1} represents the acoustic time value between two adjacent measurement points, and k_i, k_{i-1} represents the depth value between two adjacent measurement points. Practice has proved that the PSD criterion is very sensitive to defects, and the time-to-acoustic changes caused by nondefect factors are all gradual processes [18].

The most commonly used waveforms for ultrasonic nondestructive testing are shear wave and longitudinal wave [19]. The propagation speed of transverse waves

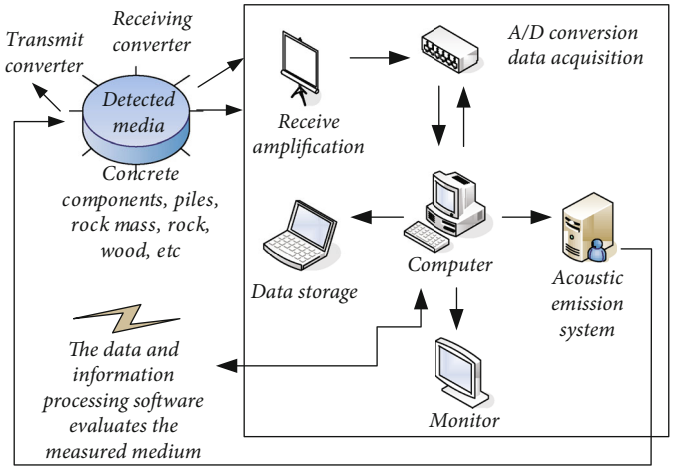

Figure 3: Ultrasonic testing process diagram.

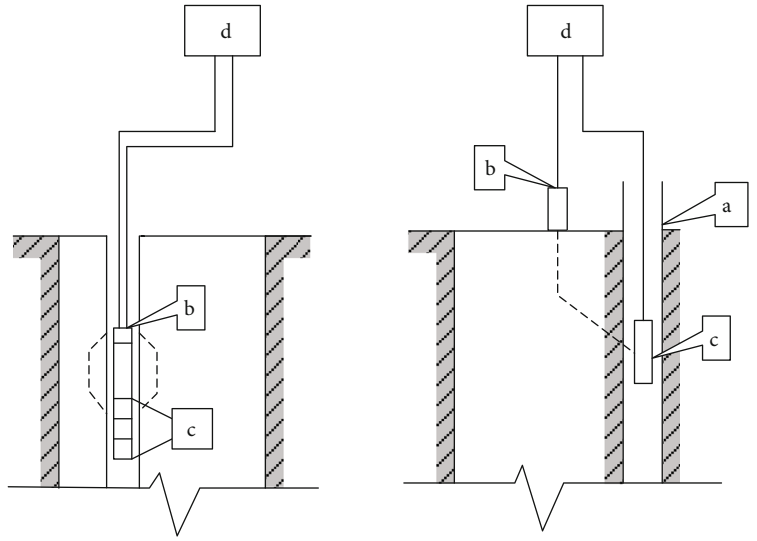

Figure 4: Ultrasonic transmission method inside and outside the foundation pile.

and longitudinal waves are different, and the particle will cause the superposition of the two vibrations, and then, the conversion of vibration modes will occur. Surface waves whose amplitude decays as they go deeper into the surface appear at the free interface of a solid. The propagation of sound waves in bounded solids also produces guided waves, which are waves with more complex vibrations. The difference between longitudinal waves and transverse waves is that the former is a wave with parallel propagation directions, and is a propelling wave, which is less destructive. The latter is a wave whose propagation direction is vertical, and is a shear wave, which is more destructive.

(1) The longitudinal wave velocity of an infinite body, expressed by the elastic constant:

$$d_g = \sqrt{\frac{F(1-\beta)}{\rho(1+\beta)(1-2\beta)}}. \tag{17}$$

Among them, F represents the elastic modulus; $\beta < 0.5$ represents Poisson's ratio, dimensionless; ρ refers to the density of the medium.

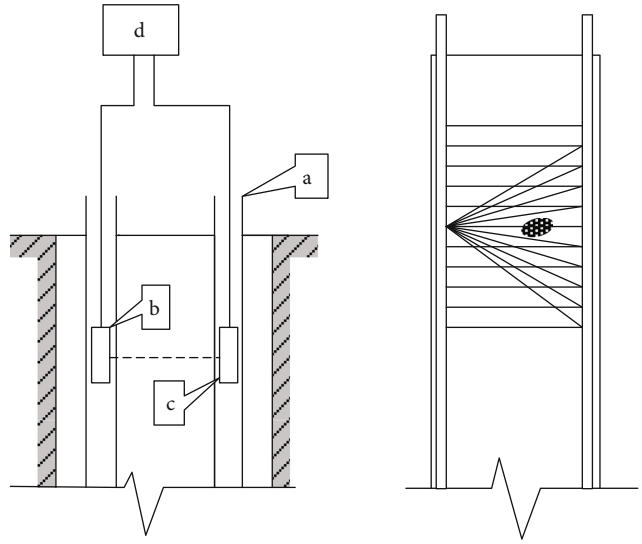

a. Acoustic tube
b. Transmitting transducer
c. Receiving transducer
d. Ultrasonic detector

Figure 5: Schematic diagram of cross-hole transmission method in foundation pile.

(2) Infinite bulk shear wave velocity, expressed by elastic constant

$$d_p = \sqrt{\frac{S}{\rho}} = \sqrt{\frac{F}{2\rho(1+\beta)}}. \tag{18}$$

In the equation, S represents shear modulus; other parameters are the same as above.

(3) The ratio of longitudinal wave velocity to shear wave velocity

$$\frac{d_g}{d_p} = \sqrt{\frac{2(1-\beta)}{(1-2\beta)}}. \tag{19}$$

In the equation, when $\beta = 0.25$, $d_g/d_p = \sqrt{3} = 1.7321$. The β of concrete is between 0.2 and 0.25, and the β of dense rock is 0.25, so it can be seen that the sound speed of transverse waves is smaller than that of longitudinal waves.

(4) The surface wave velocity of an infinite body, expressed by the elastic constant:

$$d_R = \frac{0.87 + 1.12\alpha}{1+\beta}\sqrt{\frac{S}{\rho}} = \frac{0.87 + 1.12\beta}{1+\beta} d_p. \tag{20}$$

2.4. Tomographic Forward and Inversion. The realization of tomography has two basic processes: forward and inversion. There is a certain energy relationship between forward and inversion. Forward modeling is the basis for full waveform inversion. The inversion imaging results are related to the forward calculation results [20]. Figure 6 is the staggered grid of forward calculation.

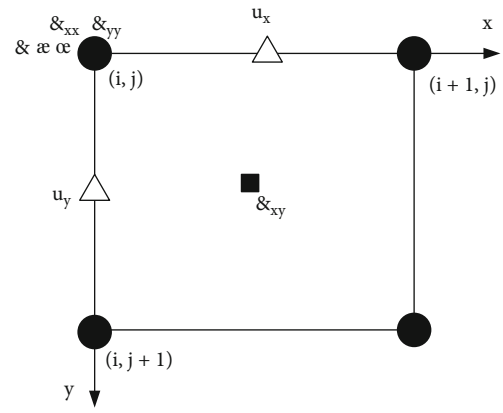

Figure 6: Staggered grid for forward calculation.

Forward modeling is the analysis basis for the three major links of acoustic wave data acquisition, data processing, and interpretation evaluation and is the basis for inversion calculation. Forward modeling assumes the simulated structure of the acoustic wave propagation medium. On this basis, according to the physical law of sound wave propagation, the sound wave data information obtained at the sound wave receiving place is predicted, that is, the sound wave record [21]. Forward modeling has the following functions: first, it provides a theoretical basis for the acquisition and processing of acoustic data and can evaluate the scientificity and feasibility of the method. The second is to detect the authenticity of the results and the accuracy of the inversion algorithm.

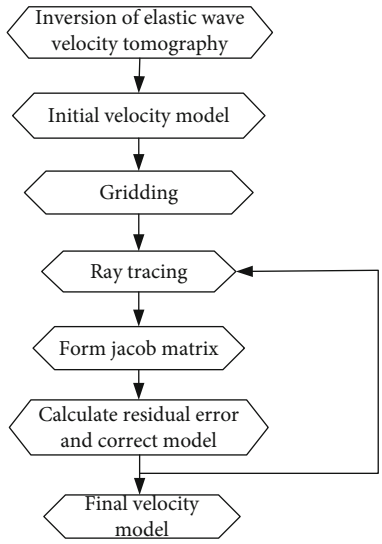

Figure 7: Flow chart of elastic wave tomography inversion calculation

Table 1: List of detection parameters.

Stake number	Survey line	Interval of measuring points (m)	Test pile length (m)
1	AB	0.5	30.4
	BC	0.5	30.4
	AC	0.5	30.6
2	AB	0.5	36.0
	BC	0.5	36.0
	AC	0.5	36.0
3	AB	0.5	36.0
	BC	0.5	36.0
	AC	0.5	36.0
4	AB	0.5	46.0
	BC	0.5	46.5
	AC	0.5	46.0
5	AB	0.5	46.5
	BC	0.5	46.5
	AC	0.5	46.5

Through the canonical Gauss-Newton method and forward calculation, it can obtain the observation return $w = k(m)$ about the acoustic wave and the medium eucalyptus, where w is the data information and m is the model information [22]. K are generalized mapping operators, which represent the relationship between the model and the data. The inversion calculation is to obtain the parameters of the model by solving the observation equation, that is, the velocity model. The most suitable velocity model can be directly found through the observation equation calculated by the forward calculation. This makes the final observation data the closest to the real data, finding the minimum value of the objective function [23]. In this paper, statistical theory is used to calculate the inversion problem. To sum up in principle, the tomography can be interpreted with the following inversion algorithm steps, as shown in Figure 7.

Table 2: Summary of test results.

Stake number	Survey line	Pile evaluation and defect location	Comprehensive evaluation
1#	AB	Complete	I
	BC	Complete	
	AC	Complete	
2#	AB	Complete	I
	BC	Complete	
	AC	Complete	
3#	AB	26.5 m defective	III
	BC	Complete	
	AC	25.5 m, 26.5 m defective	
4#	AB	Complete	I
	BC	Complete	
	AC	Complete	
5#	AB	Complete	I
	BC	Complete	
	AC	Complete	

(1) Regular Gauss-Newton method for statistical inversion

Derivative for any component, it can get:

$$\frac{\alpha L_\beta(T)}{\alpha T_q} = \frac{2}{G}\sum_{p=1}^{G}\frac{\alpha A(T)_p}{\alpha T_q}\left[A(T)_p - \widehat{F}_p\right] + \lambda\frac{2}{K}\sum_{q=1}^{K}\left[T_q - Y\left(T_q\right)\right]. \tag{21}$$

The gradient in the equation yields:

$$\nabla L_\beta(T) = \frac{2}{G}\nabla A(T)^R\left[A(T) - \widehat{F}\right] + \beta\frac{2}{G}\left[T - Y(T)\right]. \tag{22}$$

The Hesse matrix of the objective function is:

$$\nabla^2 L_\beta(T) = \frac{2}{G}\nabla A(T)^R\nabla A(T) + \beta\frac{2}{G}I_{M\times M}. \tag{23}$$

(2) Regular Gauss-damped Newton method for statistical inversion

In the iterative equation of the regular Gauss-Newton method, in order to speed up the iterative convergence process, it is determined whether the Hesse matrix is positive

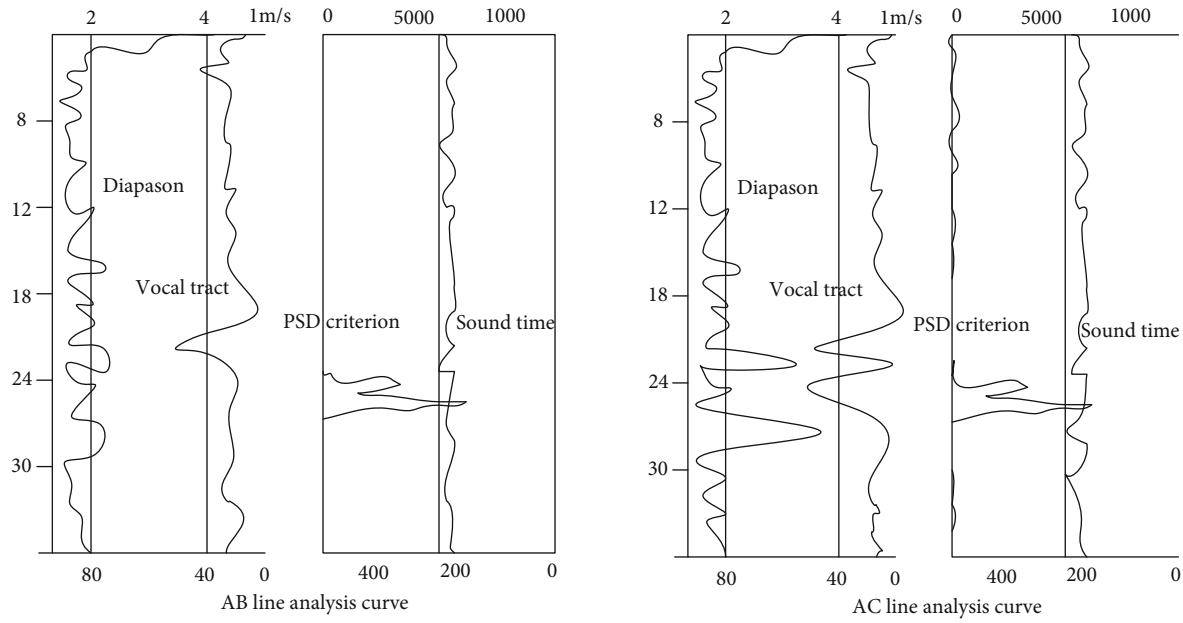

Figure 8: Analysis curve of AB survey line and AC survey line in no. 3 foundation pile.

Table 3: Profile inspection data.

	Sound velocity (km/s)	Amplitude (dB)	Sound time (μs)	PSD (μs^2/m)	Frequency (kHz)
Maximum	5.09	104.6	228	5780	49.019
Minimum value	3.728	73.3	167	0	19.607
Average value	4.614	97.85	185.7	121.03	37.523
Standard deviation	0.189	4.71	9.5		3.832
Deviation	4.10%	4.81%	5.10%		10.21%

definite. Given the regularization parameter $\beta \geq 1$, compute the process gradient:

$$\nabla^2 L_\beta\left(T^{(l)}\right) = \frac{2}{G}\nabla A\left(T^{(l)}\right)^R \nabla A\left(T^{(l)}\right) + \beta\frac{2}{G} I_{M\times M}. \quad (24)$$

Newtonian directions are calculated:

$$g^{(l)} = -\left[\nabla^2 L\left(T^{(l)}\right)\right]^{-1} \nabla L\left(T^{(l)}\right). \quad (25)$$

2.5. Role of Elastic Wave Tomography Detection

(1) As a method of engineering quality detection, elastic wave layer imaging technology is more convenient and simple, with high detection accuracy, light instrument, high work efficiency, and fast image reconstruction and analysis. It can accurately detect the defects of high-rise building foundation piles, and the detection effect is good [24]

(2) Elastic wave tomography detection can quantitatively give the distribution map of physical property parameters inside the medium. The physical and mechanical properties of rock or concrete can be determined quickly and efficiently. According to the imaging results, the acoustic parameters are accurately given to determine the stability of the building foundation piles, which brings convenience to the internal detection activities

3. Experiment on Elastic Wave Tomography of Foundation Piles of High-Rise Buildings

3.1. Effectiveness of Elastic Wave Tomography Detection on Foundation Piles. The pile foundation has good performance such as high bearing capacity, small settlement, and can withstand a certain level and uplift force. It is widely used in bridge engineering, deep-sea and shallow-sea oil production platforms, and special soils such as frozen soil and expansive soil. The basic task of an ultrasonic detector for concrete quality testing is to emit ultrasonic pulse waves to the tested concrete. At the other end of the concrete, the sound wave is received by the receiving transducer, and the sound signal is converted into an electrical signal. After the data acquisition is completed, it is automatically displayed

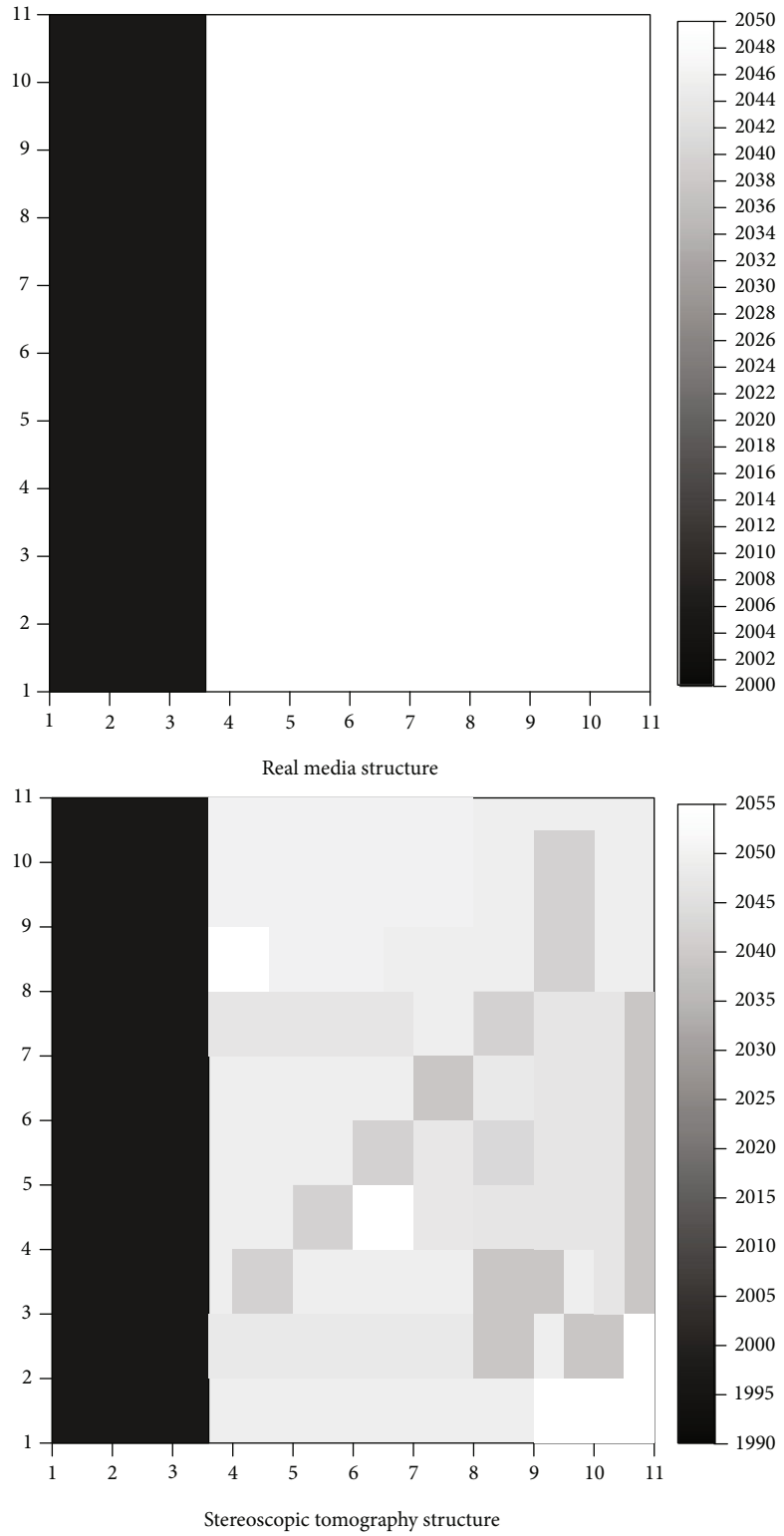

Figure 9: Real-medium structure diagram and stereo tomography results.

on the display after being processed and calculated by the software, and the data is stored in the storage system at the same time. Taking the high-rise building foundation pile as an example for tomographic analysis, the diameter of the high foundation pile is 800 mm. It is assumed that the length of the foundation pile is 11.8 m, which is made of general concrete, and the bearing layer at the bottom of the foundation pile is strongly weathered sandstone. The test depth of

Table 4: Inversion calculation workload of medium model parameters.

Numerical simulation and algorithm		Number of iterations (times)	CPU time consuming (points)	$\frac{V - V^*}{V^*}$
Numerical simulation 1	Algorithm 4.1	60	36.835	0.021332
	Algorithm 4.2	54	34.186	0.040343
	Algorithm 4.3	35	29.211	0.050868
Numerical simulation 2	Algorithm 4.1	62	34.797	0.020848
	Algorithm 4.2	52	33.940	0.025816
	Algorithm 4.3	34	29.176	0.055962

elastic wave in the experiment is -9~-13.25 m. The integrity of the foundation piles of the project is tested by ultrasonic projection method to judge the quality of the project. According to the algorithm, it is judged whether there are defects such as fracture and subsidence. For example, Table 1 is a preview of the detection parameters, and Table 2 is the detection results of all foundation piles.

The results show that, in the no. 3 foundation pile, the positions of the main defects detected in the two survey lines AB and AC are at 26.5 m of AB, 25.5 m, and 26.5 m of AC. Other pile bodies have no defects found so far. It shows that the quality of most of the pile bodies is relatively good. Figure 8 is the analysis curve of the AB survey line and the AC survey line in the no. 3 foundation pile.

It can be seen from the analysis of the imaging curve that the sound speed and the wave amplitude are greater than the critical value of the sound speed and the wave amplitude, indicating that the internal condition of the foundation pile is good, and the quality of the concrete is relatively good. However, during the detection process of the sub-3 piles, the sound velocity and wave amplitude near 25~26 m fluctuated greatly and decreased at the same time, which was lower than the normal critical value. This indicates that the pile at this location is defective. In the same pile, AC imaging of piles between 25 and 26 m also showed that the detected sound velocity and amplitude were lower than normal critical values. The curve of acoustic parameters and depth of profile shows abnormal changes of PSD parameters at AB and AC. The speed of sound changes. After analysis, these two points are measured values at discontinuous intervals, and the speed of sound is greater than the critical value of the speed of sound. Defects are therefore detected. Combined with the above survey line analysis curve, the detection data of the profile can be obtained, as shown in Table 3.

The parameters such as sound time, sound speed, sound amplitude, and frequency of concrete at other survey lines are normal. The dispersion is 5.10%, 4.10%, 4.81%, and 10.21%. It can be judged that there is no defect in the internal structure. When there is a defect in the concrete, since the speed of sound of impurities such as soil and air in the defect area is much lower than that of the sound concrete, the transit time increases significantly, and the sound time value also increases accordingly. It can be seen that the acoustic time value is an important parameter for judging whether there is a defect in the concrete. During the inspection of the no. 3 pile, the acoustic parameters at 25-26 m changed significantly, so another judgment was made that there was a defect inside the no. 3 pile.

3.2. Tomographic Forward and Inversion Experiments. Taking the foundation piles of high-rise buildings as the experimental object, the inversion simulation is carried out by the regular Gauss-Newton method of statistical inversion in the two foundation piles, and two simulation graphs are obtained. According to the nonlinear least squares method, the velocity model is updated, and the step factor is searched. Although the velocity model is updated, it is necessary to ensure that the value of the objective function does not change. It iterates the velocity model once, and then goes through multiple inversion iterations. This makes little change in the velocity model, and the final result of the volume tomographic image after iteration can be obtained.

Figure 9 shows the real medium structure diagram and the stereo tomography results. The velocity model is established by model meshing. When the y-axis coordinate is greater than or equal to 100, the velocity value is 2050. The velocity value of the y-axis coordinate less than 100 is 2000, and the initial velocity value is set to 1900. According to the above inversion iteration results, the relative error between the inversion result and the exact value is obtained, as shown in Table 4.

As can be seen from the table, the canonical Gauss-damped Newton method for statistical inversion tends to converge faster. In Algorithm 3, the number of iterations is only 35, the time spent is 29.211, and the number of iterations is less. And each iteration takes less time on average, so it speeds up the iterative process. But the relative error between the inversion result and the exact value can be seen that the relative error of using the regular Gauss-Newton method is small. During simulation 1 and simulation 2, the iteration time of the regular Gauss-damped Newton method is about 3.5% faster than that of the regular Gauss-Newton method, and the iteration rate is increased. Therefore, in the case of less knowledge of the background experience of the inversion, it can be seen from the simulation effect that the regular Gauss-damped Newton method is more suitable. Therefore, it is not difficult to see from the previous theoretical derivation and numerical test results that these algorithms are all effective algorithms for inversion calculation of medium model parameters and demonstrate the efficiency and practicability of the algorithms.

4. Discussion

In this paper, the principle of elastic wave tomography is introduced first. Then, the elastic wave equation model is introduced, and some technical method principles are extended from elastic waves. In the experimental part, elastic wave tomography technology and ultrasonic technology are used to detect the damage of high-rise building foundation piles. The method is applied to the actual operation process, and the role of these methods is expounded. From elastic wave tomography and distribution, inversion and forward modeling are carried out through experiments to obtain experimental data. The experimental results show that the elastic wave tomography technology plays an important role in detecting whether the foundation piles of high-rise buildings are defective.

5. Conclusions

This paper focuses on the detection process and role of elastic wave tomography in high-rise building inspection in the context of the Internet of Things. The defects and damages of high-rise buildings are analyzed from four major perspectives: elastic wave, cross-hole CT observation system, acoustic wave defect detection, and tomography forward and inversion. Based on the applicability and function of detection, the computer imaging is analyzed. It judges whether the internal medium is damaged from parameters such as sound time, sound speed, sound amplitude, and frequency, thereby improving the safety of foundation piles. This effectively solves the influence of construction technology, geology, and other factors during the construction process. After the construction is completed, a series of building collapses, settlements, and cracks will affect the normal use of foundation piles and cause some safety accidents over time. However, during the experiment, many problems were encountered, and the experimental data was not comprehensive enough, so it looked forward to future research to have better solutions.

Data Availability

The data that support the findings of this study are available from the corresponding author upon reasonable request.

Conflicts of Interest

The authors declare that they have no conflicts of interest.

References

[1] T. Asaue, T. Nishida, T. Maeshima et al., "Evolution of fatigue damage in wheel-loading tests evaluated by 3D elastic-wave tomography," *Journal of Disaster Research*, vol. 12, no. 3, pp. 487–495, 2017.

[2] K. Mitsuhashi, J. Poudel, T. P. Matthews, A. Garcia-Uribe, L. V. Wang, and M. A. Anastasio, "A forward-adjoint operator pair based on the elastic wave equation for use in transcranial photoacoustic computed tomography," *SIAM Journal on Imaging Sciences*, vol. 10, no. 4, pp. 2022–2048, 2017.

[3] K. X. Huang, G. S. Shui, Y. Z. Wang, and Y. S. Wang, "Enhanced fracture resistance induced by coupling multiple degrees of freedom in elastic wave metamaterials with local resonators," *Journal of Elasticity*, vol. 144, no. 1, pp. 33–53, 2021.

[4] Z. H. He, Y. Z. Wang, and Y. S. Wang, "Sound transmission tuned by active feedback control attached to elastic wave metamaterials immersed in water," *Journal of Applied Mechanics*, vol. 88, no. 7, pp. 1–28, 2021.

[5] I. N. Lozovsky, R. A. Zhostkov, and A. A. Churkin, "Numerical simulation of ultrasonic pile integrity testing," *Russian Journal of Nondestructive Testing*, vol. 56, no. 1, pp. 1–11, 2020.

[6] Y. Cui, Z. Ma, Y. Yang, and D. Song, "Acoustic velocity correcting method for the tilted acoustic tube in testing of pile by ultrasonic transmission," *Advances in Civil Engineering*, vol. 2020, Article ID 8824739, 8 pages, 2020.

[7] L. Espinosa, E. Doveri, S. Bernard, V. Monteiller, R. Guillermin, and P. Lasaygues, "Ultrasonic imaging of high-contrasted objects based on full-waveform inversion: limits under fluid modeling," *Ultrasonic Imaging*, vol. 43, no. 2, pp. 88–99, 2021.

[8] L. Yi, L. Sun, X. Ming, and M. Zou, "Full-depth spectral domain optical coherence tomography technology insensitive to phase disturbance," *Biomedical Optics Express*, vol. 9, no. 10, pp. 5071–5083, 2018.

[9] A. L. Perchuk and A. A. Serdyuk, "Phase relations in spinel Lherzolite KLB-1 according to results of thermodynamic modeling up to 30 GPa: peculiarities of mineral assemblages and geodynamic effects," *Petrology*, vol. 30, no. 2, pp. 198–211, 2022.

[10] J. Xie, M. H. Ritzwoller, and S. J. Brownlee, "Inferring the oriented elastic tensor from surface wave observations: preliminary application across the western United States," *Geophysical Journal International*, vol. 201, no. 2, pp. 996–1021, 2015.

[11] J. Li, Z. Feng, and S. Gerard, "Wave-equation dispersion inversion," *Geophysical Journal International*, vol. 208, no. 3, pp. 1567–1578, 2017.

[12] R. Grzeszick, A. Plinge, and G. A. Fink, "Bag-of-features methods for acoustic event detection and classification," *IEEE/ACM Transactions on Audio Speech & Language Processing*, vol. 25, no. 6, pp. 1242–1252, 2017.

[13] D. Vangi, M. Bruzzi, and J. N. Caron, "Compact probe for non-contact ultrasonic inspection with the gas-coupled laser acoustic detection (GCLAD) technique," *Experimental Mechanics*, vol. 62, no. 3, pp. 403–415, 2022.

[14] B. Zheng, J. Zhang, and T. Feng, "Large deformation mechanics of gob-side roadway and its controlling methods in deep coal mining: a case study," *Advances in Civil Engineering*, vol. 2020, Article ID 8887088, 13 pages, 2020.

[15] M. Song and W. Zhu, "Elastic wave propagation in strongly nonlinear lattices and its active control," *Journal of Applied Mechanics*, vol. 88, no. 7, pp. 1–25, 2021.

[16] Z. Li, Y. Wang, and Y. Wang, "Tunable three-dimensional nonreciprocal transmission in a layered nonlinear elastic wave metamaterial by initial stresses," *Applied Mathematics and Mechanics*, vol. 43, no. 2, pp. 167–184, 2022.

[17] N. P. Aleshin, A. A. Kirillov, and L. Y. Mogilner, "A general solution of the problem of elastic-wave scattering by a plane crack," *Doklady Physics*, vol. 66, no. 7, pp. 202–208, 2021.

[18] X. Yang, Z. Li, and H. Liu, "Using refined theory to studied elastic wave scattering and dynamic stress concentrations in plates with two cutouts," *Journal of Applied Mathematics and Physics*, vol. 8, no. 12, pp. 2999–3018, 2020.

[19] G. Sha, "Attenuation and phase velocity of elastic wave in textured polycrystals with ellipsoidal grains of arbitrary crystal symmetry," *Acoustics*, vol. 2, no. 1, pp. 51–72, 2020.

[20] N. U. Kuldoshov, N. R. Kulmuratov, and M. R. Ishmamatov, "Numerical solution of the problem of the action of a plane unsteady elastic wave on cylindrical bodies," *Theoretical & Applied Science*, vol. 91, no. 11, pp. 352–360, 2020.

[21] Z. Li, H. Liu, and W. Zhen, "Elastic wave scattering and dynamic stress concentrations around double holes in piezoelectric media," *Journal of Applied Mathematics and Physics*, vol. 8, no. 12, pp. 3060–3069, 2020.

[22] B. Afa and C. Ipab, "A novel method for investigation of acoustic and elastic wave phenomena using numerical experiments," *Theoretical and Applied Mechanics Letters*, vol. 10, no. 5, pp. 307–314, 2020.

[23] S. J. Horning, M. E. Juweid, H. Schöder et al., "Interim positron emission tomography scans in diffuse large B-cell lymphoma: an independent expert nuclear medicine evaluation of the Eastern Cooperative Oncology Group E3404 study," *Blood*, vol. 115, no. 4, pp. 775–777, 2010.

[24] L. Nguyen, "A family of inversion formulas in thermoacoustic tomography," *Inverse Problems & Imaging*, vol. 3, no. 4, pp. 649–675, 2009.

Hindawi
Wireless Communications and Mobile Computing
Volume 2022, Article ID 5443237, 13 pages
https://doi.org/10.1155/2022/5443237

Research Article

Moving Target Detection Technology Based on UAV Vision

Sining Cheng, Jiaxian Qin, Yuanyuan Chen, and Mingzhu Li

TJ-YZ School of Network Science, Haikou University of Economics, Hainan, 571127 Haikou, China

Correspondence should be addressed to Sining Cheng; siningcheng@163.com

Received 17 May 2022; Revised 24 June 2022; Accepted 11 July 2022; Published 22 July 2022

Academic Editor: Jun Ye

The detection of moving objects by machine vision is a hot research direction in recent years. It is widely used in military, medical, transportation, and agriculture. With the rapid development of UAV technology, as well as the high mobility of UAVs and the wide range of high-altitude vision, the target detection technology based on UAV vision is applied to traffic management such as vehicle tracking and detection of vehicle violations. The moving target detection technology in this study is based on the YOLOv3 algorithm. It implements moving vehicle tracking by means of Mean-Shift and Kalman filtering. In this paper, the Gaussian background difference technology is used to analyze the illegal behavior of the vehicle, and the color feature extraction technology is used to identify and locate the license plate, and the information of the illegal vehicle is entered into the database. The experiment compares the moving target detection of UAV vision and the traditional target detection in four aspects: recognition accuracy, recognition speed, manual time, and divergent results. The results show that the average accuracy rates of UAV vision-based moving target detection and traditional pattern recognition are 98.4% and 87.8%, respectively. The recognition speeds are 24.9 (vehicles/sec) and 10.6 (vehicles/sec), respectively. However, the artificial time and divergence results of moving target detection based on UAV vision are only 1/3 of the traditional mode. The moving target detection based on UAV vision has a better moving target detection ability.

1. Introduction

With the continuous development of technologies such as digital information and image recognition, the research on UAVs has been deepening in recent years, and UAVs have also achieved remarkable results in many fields. It is widely used in military reconnaissance, agricultural irrigation, field fire protection, urban transportation, and so on. Facing the increasing number of vehicles and complex traffic problems year by year, traditional vehicle photography technology can identify vehicle information and determine the location of the vehicle to a certain extent. However, complex traffic problems such as illegal parking, speeding, and occupation of emergency lanes often occur in vehicle traffic, as well as the immaturity of traditional vehicle detection technology, which leads to a series of defects in the traditional vehicle photography technology, such as low vehicle recognition, slow calculation and recognition, and long manual inspection time. By taking advantage of the UAV's high-altitude field of view and superior stability, it is combined with moving target detection technology. Through aerial photography of road scenes, it can obtain stable and broad vehicle pictures. Through the corresponding technical identification of the vehicle picture, it realizes the effective detection of road vehicles.

2. Related Work

With the development of the times, there are more and more vehicles, and traffic accidents also occur frequently, so the motion detection of vehicles is particularly important. Many people have studied moving target detection technology. Among them, Xu et al. experiment studied moving vehicles through an adaptive filter and obtains the relevant factors of moving vehicle detection [1]. Pan et al. proposed a Fourier transform to compensate for motion loss to improve the accuracy of moving object detection [2]. The Kalra et al. experiment can effectively detect ground-moving targets. They used probability distribution functions to predict the movement of moving objects and form an effective motion dataset [3]. Minaeian et al. proposed a new visual object detection technology. Through unmanned vehicles

to detect some dangerous areas, they have achieved good results [4]. Tah et al. acquired moving targets in the form of camera monitoring by deploying Kalman filtering. And they analyzed and achieved effective detection and tracking of moving targets [5]. Although target detection technology can achieve the detection and tracking of moving targets to a certain extent, it cannot fully utilize the advantages of moving target detection due to the lack of effective detection carriers.

Because UAVs are light and stable and have a high field of view, relevant workers have combined moving target detection with UAVs for research. Among them, Yundong et al. used drones to detect railway information and propose a technical means of segmenting pictures to solve the technical defects of small target detection [6]. Micheal et al. proposed a deep learning detector to train pictures taken by drones, so as to achieve a better motion recognition effect [7]. In the Escobar and Sandoval experiment, 8000 test images were taken by drones, and the accuracy of the test can reach 95% through the detection of image features [8]. In order to improve the accuracy of moving target detection in UAV recognition, Li et al. proposed an extraction method of cross-features [9]. Doukhi et al.'s research showed that the YOLO algorithm and deep learning can realize the visual moving target detection of UAV [10]. Taking the UAV as the carrier, moving target detection is effectively carried out through techniques such as image feature processing, but the use of the algorithm is not optimal.

This paper combines UAV vision and target detection technology and adopts a variety of vehicle detection technology and vehicle behavior recognition analysis technology. It effectively detects vehicle traffic problems and compares them with traditional object detection techniques. It analyzes the advantages and disadvantages of the two target detection methods. Innovation points are the following: (1) through a variety of vehicle recognition technologies, this paper comprehensively introduces the application of UAV target detection in vehicle management and detection, and (2) this paper compares vehicle detection with traditional target detection technology.

3. Moving Target Detection Method Based on UAV Vision

UAV has the advantages of high maneuverability, small size, and sensitive operation. It is widely used in transportation, military, scientific research, and other fields [11–13]. The development of computer technology and image recognition technology has made moving target detection technology more and more mature, and the use of unmanned aerial vehicles can make moving target detection technology to a higher level. This paper will use the moving target detection technology of UAV vision to study the vehicle traffic problem [14, 15]. The five aspects of vehicle detection, vehicle tracking, vehicle violation behavior analysis, license plate positioning and recognition, and illegal vehicle information input data database are studied through algorithm calculation. The moving target detection architecture diagram of UAV vision is shown in Figure 1.

3.1. Moving Target Detection Technology of UAV Vision. In order to adapt to the constantly changing scene of UAV aerial photography, this paper studies the target detection algorithm based on YOLOv3 and collects vehicle data through UAV aerial photography for training.

3.1.1. YOLO Algorithm. YOLO is a common detection algorithm that extracts image features through an artificial neural network and then uses the regression algorithm to achieve the effect of image detection. It is widely used in vehicle detection [16]. Based on the convolutional neural network, YOLO divides the image input into the system into $r \times r$ units. Each grid detects the corresponding part of the image, and the unit predicts the cell border and the confidence of the cell border. The predicted probability of the cell border is generally represented by P_B:

$$P_B = \begin{cases} 0, & \text{no goal,} \\ 1, & \text{have goal.} \end{cases} \tag{1}$$

In formula (1), a cell prediction probability of "0" indicates that there is no object in the frame, and "1" indicates that there is an object.

The cell border confidence P_C is expressed as

$$P_C \longrightarrow (a, b, c, d, e). \tag{2}$$

In formula (2), a and b are the cell center offsets, c and d are the border width and height, and e is the border confidence.

3.1.2. YOLOv3 Algorithm. YOLOv3 is an improvement of the YOLO algorithm, which deepens the network structure through residuals on the basis of the original convolutional network structure. YOLOv3 performs frame prediction in a clustering manner and uses the predicted 4 values as the parameters to determine the frame prediction. They are the horizontal and vertical axes of the center point of the frame and the width and height of the frame [17]. The four parameters work together to predict the frame, and the determination of the frame target is expressed by the confidence, and the value range of the confidence is $[0, 1]$. The larger the value, the greater the probability that the frame contains objects. When the confidence level is 1, it means the real object and the bounding box are completely covered, and when the confidence level is 0, it means that the priority of the bounding box is lower [18]. The algorithm structure of YOLOv3 is shown in Figure 2.

In Figure 2, the algorithm structure of YOLOv3 is input from the picture to the downsampling layer, then undergoes 5 residual processing, and finally detects and generates the detection result. The loss function of the YOLOv3 network consists of three parts, the frame prediction error, the presence or absence of the target error, and the error during classification. The loss function of the YOLOv3 network is

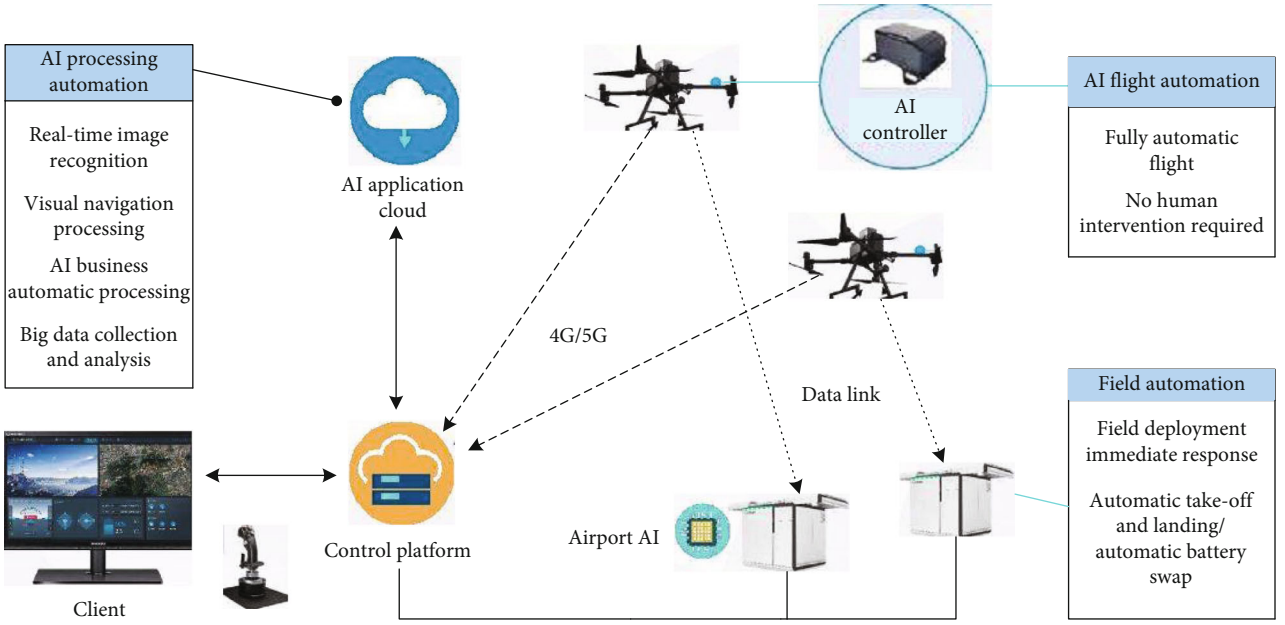

Figure 1: Architecture of moving target detection in UAV vision.

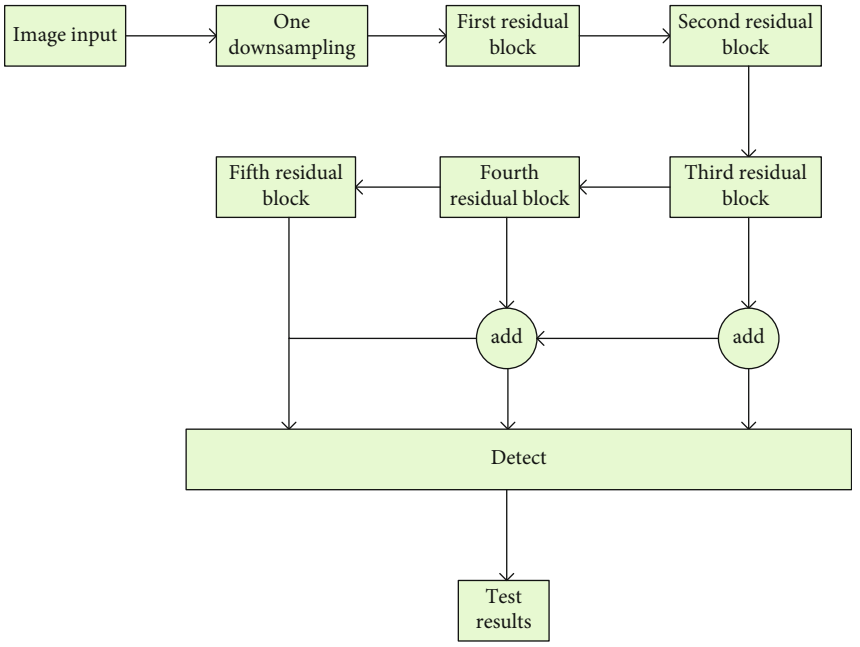

Figure 2: Algorithm diagram of YOLOv3.

expressed as

$$
\begin{aligned}
L = {} & \lambda_{\text{coord}} \sum_{i=0}^{r^2} \sum_{j=0}^{B} k_{ij} \left[(a_i - \overline{a_i})^2 + \left(b_i - \overline{b_i} \right)^2 \right] \\
& + \lambda_{\text{coord}} \sum_{i=0}^{r^2} \sum_{j=0}^{B} k_{ij} \left[\left(\sqrt{c_i} - \sqrt{\overline{c_i}} \right)^2 + \left(\sqrt{d_i} - \sqrt{\overline{d_i}} \right)^2 \right] \\
& + \sum_{i=0}^{r^2} \sum_{j=0}^{B} k_{ij} (e_i - \overline{e_i})^2 + \sum_{i=0}^{r^2} \sum_{j=0}^{B} k_{ij} (e_j - \overline{e_j})^2 \\
& + \sum_{i=0}^{r^2} k_{ij} \sum_{h \in \text{class}} \left[P_i(h) - \overline{P_i}(h) \right]^2.
\end{aligned} \tag{3}
$$

In formula (3), r represents the number of grids, and the explanation of a, b, c, d, and e is shown in formula (2). B represents the number of real boxes predicted by the grid, k_{ij} represents the detection target of the jth predicted box in the ith grid, and $P_i(h)$ represents the probability of detecting the h type. Class represents the data type.

3.2. Vehicle Tracking Technology Based on UAV Vision. The vehicle tracking technology based on UAV vision is mainly aimed at harsh conditions such as overspeed movement,

ultralow speed movement, and occlusion of highway vehicles. This paper proposes an algorithm combining Kalman filter and Mean-Shift. It first uses the Kalman filtering algorithm to predict where the target may appear in the next frame. It then uses the Mean-Shift algorithm to search and match in the candidate area, so that it can adapt to different situations to achieve real-time, accurate, and effective tracking of vehicles.

3.2.1. Mean-Shift Algorithm. The Mean-Shift algorithm is a target tracking algorithm based on a color histogram, which initializes the tracking target in the way of human-computer interaction and tracks the target in a given area [19, 20]. Region locking is generally determined using region circles, which are scaled using length and width [21].

The core of the Mean-Shift algorithm is to accurately calculate the position information of the next target:

$$A(x) = \begin{cases} \frac{1}{2} c_d^{-1} (b+2)\left(1 - x^T x\right), & x^T x \le 1, \\ 0, & \text{other.} \end{cases} \tag{4}$$

In formula (4), b is the offset to the next target, c is the coefficient, and $A(x)$ is the kernel function. T is a mathematical notation for transpose.

Then, the contour function is

$$a(x) = \begin{cases} \frac{1}{2} c_d^{-1} (b+2)(1-x), & x \le 1, \\ 0, & \text{other.} \end{cases} \tag{5}$$

In the case of formula (5), $a'(x)$ is a constant.

The flow chart of the Mean-Shift algorithm is shown in Figure 3.

3.2.2. Kalman Filter Algorithm. In describing the position of moving objects, the Kalman filter can be used, which has a very good position prediction effect. It mainly judges the next motion state of the object according to the previous motion state of the object, such as motion speed, direction, and other information, so as to realize the tracking of the target [22, 23].

(1) Bayesian Estimation. In most scientific calculations, it is necessary to preestimate the dependent variable over time. Bayesian estimation is a good way to solve the dynamic state of discrete time. The definition of Bayesian estimation is

$$s_k = F_k(s_{k-1}, g_{k-1}). \tag{6}$$

In formula (6), $g_{k-1} \in \Re^m$ represents a vector with dimension m at time $k-1$, and F_k is a nonlinear state transition function. s_k represents the motion state of the predicted object at time k.

The association of observation vectors $y_k \in \Re^a$ and F_k is an observation model:

$$y_k = D_k(s_k, f_k). \tag{7}$$

In formula (7), f_k is the observation vector of dimension and D_k is a nonlinear observation model.

The core of Bayesian estimation is to construct a probability density function from all the available information. Before transitioning the state, the prior probability must be predicted, and a transition state with the highest prior probability is selected by comparison. Then, the next state is predicted by the new observation and its corresponding probability function [24, 25]. Bayesian estimation is to use the observed value r and the probability density to calculate the confidence of the system state s.

Bayesian prediction process:

$$P(s_k|r_{k-1}) = \int P(s_k|s_{k-1}) P(s_k|s_{k-1} r_{k-1}). \tag{8}$$

In formula (8), the process does not include a priori probability at time k.

Bayesian update observation procedure:

$$P(s_k|r_k) = \frac{P(r_k|s_k) P(s_k|r_{k-1})}{P(r_k|r_{k-1})}. \tag{9}$$

If both the state transition model and the observation model exhibit a linear correlation, and the states at all times belong to a Gaussian distribution, then the Bayesian estimator is a Kalman filter under this particular condition.

(2) Kalman Filter. Kalman filter is a dynamic state linear programming process, each prediction is made on the basis of the previous state, and only the previous state is retained after the best prediction state is determined. As a result, systems employing Kalman filters have small storage space and thus have the ability to make fast, real-time predictions [26].

Since the Kalman filter is a linear prediction model, its state transition model and sensing model are both linear formulas. The expressions of these two models under the Kalman filter are

$$s_k = C_k s_{k-1} + G_k \mu_{k-1} + r_{k-1}. \tag{10}$$

In formula (10), C_k represents a state transition matrix and G_k represents a state input matrix. r represents the sensing model:

$$y_k = D_k s_k + f_k. \tag{11}$$

The core algorithm of the Kalman filter is the following.

Knowing the prior state and posterior state at time k, the covariance of prior prediction error and posterior prediction

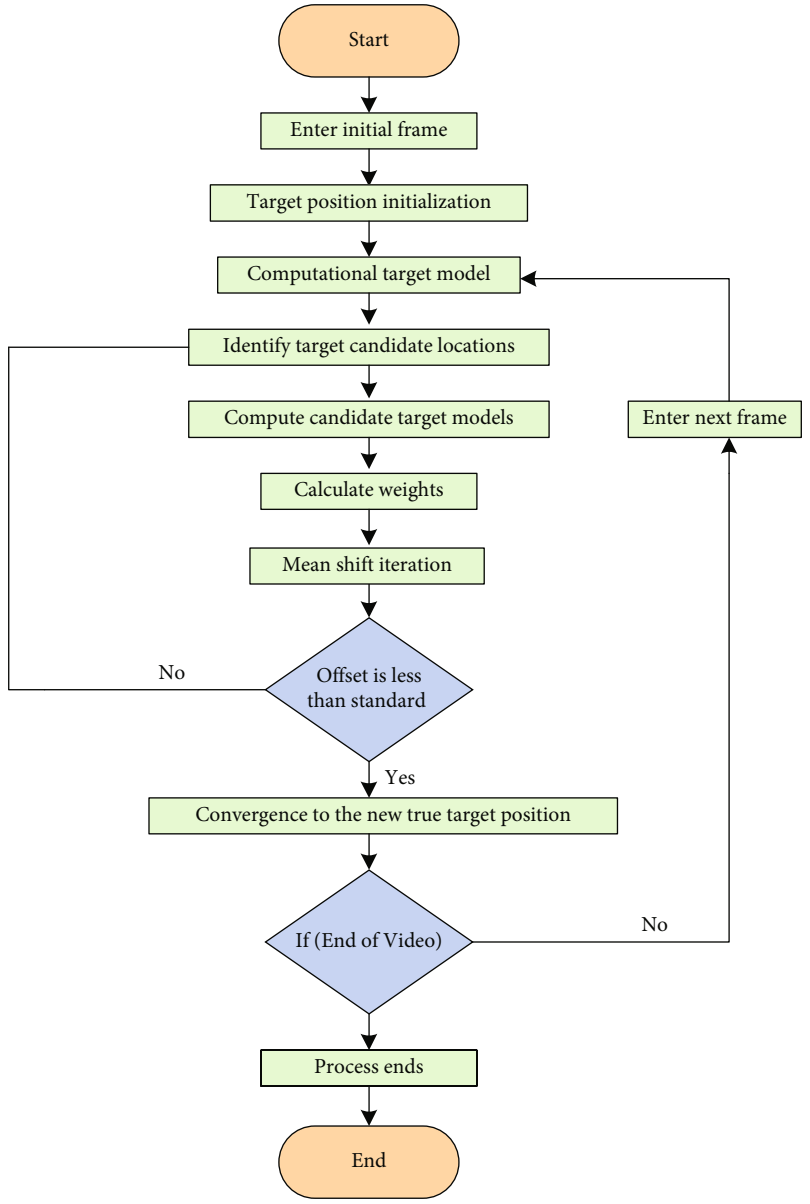

Figure 3: Flow chart of the Mean-Shift algorithm.

error is expressed as

$$d_k^- = s_k - \widehat{s}_k^-, \tag{12}$$

$$d_k = s_k - \widehat{s}_k. \tag{13}$$

Then, the prior prediction error covariance is expressed as

$$\phi_k^- = E\left[d_k^- d_k^{-T}\right]. \tag{14}$$

The posterior prediction error covariance is expressed as

$$\phi_k = E\left[d_k d_k^T\right]. \tag{15}$$

Then, the formula for the Kalman filter is

$$\widehat{s}_k = \widehat{s}_k^- + W_k\left(y_k - D\widehat{s}_k^-\right). \tag{16}$$

Deforming formula (16), W_k can be obtained:

$$W_k = \frac{P_k^- D^T}{DP_k^- D^T + R}. \tag{17}$$

It can be seen from formula (17) that W_k represents the

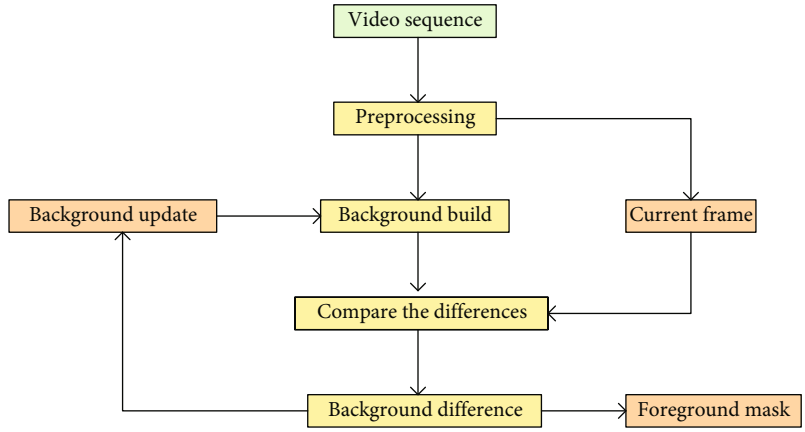

Figure 4: Background difference process diagram.

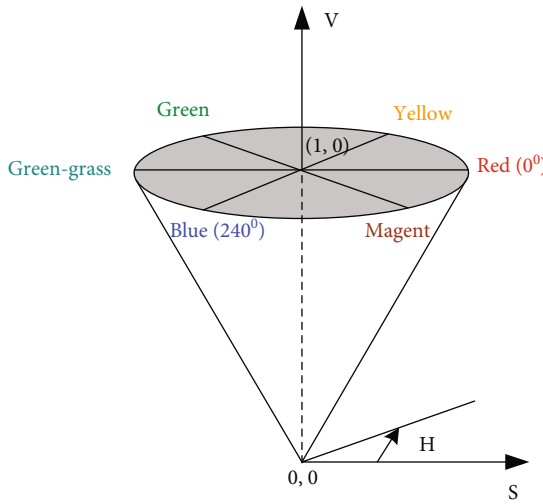

Figure 5: *HSV* model diagram.

Table 1: *HSV* license plate color threshold range.

HSV components	Blue	Yellow	White	Black
H	[200, 250]	[20, 50]	—	—
S	[0.3, 1]	[0.3, 1]	[0, 0, 1]	—
V	[0.34, 1]	[0.34, 1]	[0.9, 1]	[0, 0.3]

gain, and the smaller the observation covariance R, the greater the gain. At the same time, the smaller the P_k^-, the larger the gain value. T stands for transpose.

3.2.3. Combination of Mean-Shift and Kalman Filtering Algorithms. In the tracking of the vehicle, it is necessary to determine each frame of the vehicle motion, establish a Kalman filter to predict the vehicle position, and let the state vector of the vehicle be $s_k = [s_k\ y_k\ \hat{s}_k\ \hat{y}_k]^T$. The first two components are the vector values of the vehicle on the x-axis and y-axis, and the last two components are the speed of the vehicle on the x-axis and y-axis [27].

According to the kinematic theorem,

$$\begin{aligned} s_k &= s_{k-1} + \hat{s}_{k-1}t + \frac{1}{2}at^2, \\ y_k &= y_{k-1} + \hat{y}_{k-1}t + \frac{1}{2}at^2. \end{aligned} \tag{18}$$

In formula (18), a represents acceleration and t represents time.

Then, the vehicle motion model is expressed as

$$\begin{bmatrix} s_k \\ y_k \\ \hat{s}_k \\ \hat{y}_k \end{bmatrix} = \begin{bmatrix} 1\,0\,t\,0 \\ 0\,1\,0\,t \\ 0\,0\,1\,0 \\ 0\,0\,0\,1 \end{bmatrix} \begin{bmatrix} s_{k-1} \\ y_{k-1} \\ \hat{s}_{k-1} \\ \hat{y}_{k-1} \end{bmatrix} + \begin{bmatrix} \frac{t^2}{2} \\ \frac{t^2}{2} \\ t \\ t \end{bmatrix} a. \tag{19}$$

The combined process of Mean-Shift and Kalman filtering algorithm is the following.

The position of the moving picture of the vehicle is marked, which records the state at the initial moment with the Kalman filter. The position predicted by the Kalman filter is iterated to the Mean-Shift method, and the position obtained by the iteration is updated to the Kalman filter, and then, the position is updated iteratively to realize the real-time tracking of the vehicle.

3.3. Vehicle Violation and Recognition Technology Based on Moving Image. Aiming at the characteristics of high traffic flow and fast speed on the expressway, this paper does not make further analysis of the normal driving vehicles. It only screens and identifies vehicles whose motion trajectory change rate exceeds the threshold (overspeed detection), the rate of change is lower than the threshold (ultralow speed and parking detection), movement track reverses (reverse), and the motion trajectory is within the emergency lane for a long time (occupying the emergency lane).

It marks the trajectory of the offending vehicle. It detects vehicle violations by means of background difference. It

compares the image changes before and after by means of background difference to detect vehicle violations [28].

Background difference is a method of extracting the background image and the previous frame background image. And it analyzes the difference between the two images, and comparing the images can determine whether the vehicle has violated the rules such as speeding or ultra-low speed. The process of the background difference method is shown in Figure 4.

The calculation steps of the background difference are the following.

Let the picture or video sequence be $g_1(x, y)$, $g_2(x, y)$, $\cdots$, $g_n(x, y)$, the result of background analysis is

$$G_k(x, y) = |g_k(x, y) - H_k(x, y)|. \tag{20}$$

In formula (20), $H_k(x, y)$ represents the background model, and $G_k(x, y)$ represents the analysis result of the background difference.

Arrange $G_k(x, y)$ to get

$$L_k(x, y) = \begin{cases} 1, & G_k(x, y) > T, \\ 0, & G_k(x, y) \le T. \end{cases} \tag{21}$$

In formula (21), $L_k(x, y)$ is the binarization of the difference result. T represents the threshold value of the difference method judgment, which is a constant.

3.4. License Plate Location and Recognition Technology Based on License Plate Color and Texture Features. Aiming at the position of the marked illegal vehicle trajectory, the license plate area is quickly located, and the template matching method is used to identify the license plate characters. The location and recognition of the license plate are realized by the color and texture features of the license plate. Due to the different manufacturers of license plates or different production processes, the background colors of license plates are not the same, and the RGB color model covers all color representations.

By projecting the color of the license plate onto the three planes of *RG*, *GB*, and *BR*, it can be observed that the depth relationship of the color is $R < G < B$. Since the location of the license plate requires color features, it is possible to convert RGB to HSV for research. Among them, H represents chromaticity, S represents purity, and V represents lightness. The model of *HSV* is shown in Figure 5.

The background colors of license plates are generally blue, yellow, black, and white. Through the collection of a large number of license plate data, the color threshold ranges of the four license plate background colors of *HSV* are obtained, as shown in Table 1.

When the license plate color is blue or yellow,

$$\bar{H} = \frac{1}{m}\sum_{j=1}^{m} H_j, \tag{22}$$

$$\bar{S} = \frac{1}{m}\sum_{j}^{m} S_j, \tag{23}$$

$$\begin{cases} H_r = \dfrac{1}{m-1}\sum \left(H_j - \bar{H}\right)^2, \\ S_r = \dfrac{1}{m-1}\sum \left(S_j - \bar{S}\right)^2. \end{cases} \tag{24}$$

In formula (24), H_r and S_r are the components on the H and V axes.

When the background color of the license plate is black or white, the calculation method is the same as formulas (22), (23), and (24).

In addition to using color features, the location and recognition of license plates also need to use the texture features of license plates. The human eye can only observe more than 20 levels of gray. However, when the gray level drops below level 5, characteristic texture information will be generated, so the noise reduction processing of the level 5 gray level can effectively locate and recognize the license plate. The flow chart of license plate texture recognition is shown in Figure 6.

Finally, for illegal vehicles, the key frame images are intercepted, and the license plate and illegal information are recorded in this paper and entered into the database.

4. Experiment of Moving Target Detection Based on UAV Vision

Moving target detection technology plays an important role in actual production and life. The processing process of the traditional moving target detection method is preprocessing of the target image, selecting the target area, extracting the target feature vector, and classifying with the help of a classifier. Although it can achieve effective target detection to a certain extent, with the development of image recognition and other technologies, the photographic level of traditional target detection technology is not good. However, with the development of image recognition and other technologies, the traditional image recognition technology of target detection technology has many shortcomings. There are many defects in traditional object detection methods. This paper will take the UAV as the carrier to compare and analyze the moving target detection technology under the UAV vision and the traditional target detection technology. The experimental object of this paper is the moving vehicle.

4.1. Effectiveness of Moving Target Detection

4.1.1. Sample Data. In order to make a comprehensive comparison between the moving target detection technology of UAV vision and the traditional moving target detection technology, the experimental samples must be strictly screened, and the selection of samples must be representative and gradient. In order to ensure the validity of the experiment, the experiment will select 12 kinds of moving target detection systems, 6 of which are in the field of view of the UAV, and the other 6 are not equipped with UAV equipment. In this paper, the index data that has a great

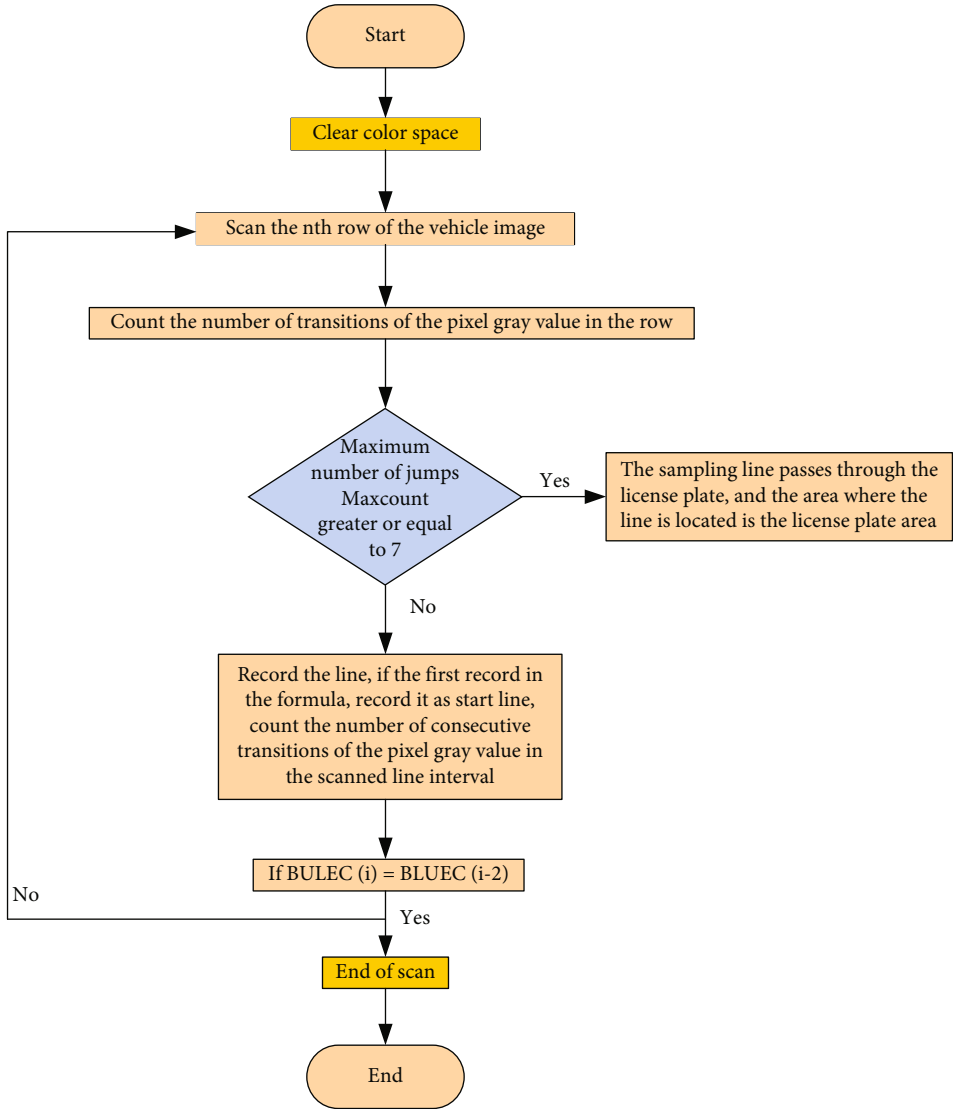

Figure 6: Flow chart of license plate texture recognition.

Table 2: Moving target detection index table.

Moving target detection index	Moving target detection under UAV vision	Traditional object detection
The accuracy of moving target detection and recognition	92%	83%
The speed of moving object detection	90%	81%
Human time spent on moving object detection	93%	89%
Divergent results from moving object detection	95%	92%
Frequency of moving object detection	13%	8%
Image size for moving target detection	25%	14%

influence on the detection of moving objects is counted. Table 2 is the index table of moving object detection.

From the data in Table 2, it can be seen that among the indicators of moving target detection, the accuracy of moving target detection and recognition, the speed of moving target detection, the labor time spent on moving target detection, and the divergence results generated by moving target detection have a great influence. The frequency of moving object detection and the image size of moving object detection have little effect.

4.1.2. Correlation Analysis of Samples. The selection of moving target detection samples will directly affect the experimental results, so when selecting moving target detection

Table 3: Correlation analysis table of moving target detection.

Number of sample groups	Moving target detection index	Relevance
1	The accuracy of moving target detection and recognition	0.284
2	The speed of moving object detection	0.248
3	Human time spent on moving object detection	0.252
4	Divergent results from moving object detection	0.216

sample indicators, it is also necessary to analyze the degree of correlation between the sample indicators and moving target detection. The correlation analysis of samples is to amplify the characteristic information of the experimental data to better compare the experimental results. Through the data in Table 2, it can be found that the first four indicators have a great influence on the detection of moving objects, which is more than 90%. The impact of the latter two is not very large, so the first four indicators in Table 2 will be selected for correlation analysis of moving target detection. Table 3 is the correlation analysis table of moving target detection.

From the analysis of the data in Table 3, it can be seen that the correlation between the accuracy of moving target detection and recognition and moving target detection is the highest at 0.284. The lowest difference is 0.216 for moving target detection, but the overall difference is not large, and the data dimension of this experiment is not high. Therefore, all the moving target detection indicators in Table 3 are used as factors to measure the quality of the moving target detection system.

4.1.3. Validity Analysis of Samples. In order to compare whether the experiment of moving target detection technology based on UAV vision and traditional moving target detection technology is effective, the experiment will use the k-fold cross-validation method for data verification. k-fold cross-validation is designed to allow each data to be tested and verified. In this experiment, the 7-fold cross-validation method is selected; the test selects 3500 vehicles as the test data, of which 3000 vehicles are the test set and 500 vehicles are the test set. The experimental results of the validity analysis of two different motion detection techniques are shown in Table 4.

From the data analysis in Table 4, it can be seen that the average effectiveness of the above four moving target detection indicators for two different target detection systems is 88.2% and 86.8%, respectively. Therefore, the two target detection systems can be compared and analyzed through the above four indicators.

4.2. Comparison Experiment of Moving Target Detection under UAV Vision and Traditional Moving Target Detection

4.2.1. The Accuracy of Moving Target Detection and Recognition. The accuracy of moving target detection and recognition is the most basic indicator of the moving target detection system. In order to better compare the UAV-based moving target detection and recognition accuracy with the traditional detection and recognition accuracy, the experiment will select 6,000 vehicles for the test experiment. Among them, there are 2,000 small cars, 2,000 medium-sized cars, and 2,000 large cars. By continuously increasing the experimental data, this paper compares the target recognition accuracy of the two methods. Figure 7 shows the experimental results of the accuracy of moving target detection and recognition in two ways.

It can be seen from Figure 7 that with the increase of the model, the recognition accuracy will be improved. However, the overall UAV vision moving target detection and recognition accuracy is 10.7%; the highest recognition accuracy can reach 99%.

4.2.2. Speed of Moving Target Detection. The speed of moving target detection is to judge the ability of the detection system to process data, because the detection speed of vehicles will be affected by scene factors. Therefore, the experiment selects two scenarios, crossroads and ordinary roads, to detect the passing vehicles. The experimental results of the moving target detection speed of the two methods are shown in Figure 8.

From the analysis of Figure 8, it can be seen that the target detection speed at the intersection is slightly lower than that of ordinary intersections, and the moving target detection speed of UAV vision is 14 vehicles per second more than the traditional moving target detection and recognition accuracy.

4.2.3. Manual Time Spent on Moving Target Detection. Part of moving target detection is a mode of human-computer interaction, and image recognition is required when moving objects are detected. However, manual selection is sometimes required when selecting an image target. If the manual selection time is short or manual operation is not required, the performance of the moving target detection system will be greatly improved. To this end, an experiment will be done to compare the manual time spent on the two methods of moving target detection. The experimental environment is set with different vehicle ratios, which are 40% and 80%, respectively. By detecting the increase of vehicles, this paper observes the labor time spent, and the labor time spent in the two methods of moving target detection is shown in Figure 9.

From the data analysis in Figure 9, it can be seen that the more vehicles account for the components, the longer the manual detection takes. However, the manual detection of moving objects based on UAV vision generally takes much less time than the traditional method. When the vehicle ratio is 40%, the average labor time of the two is 2.25 s and 12.25 s,

Table 4: Validity analysis table of moving target detection.

Moving target detection index	Moving target detection under UAV vision	Traditional object detection
The accuracy of moving target detection and recognition	94.3%	86.8%
The speed of moving object detection	75.7%	75.2%
Human time spent on moving object detection	93.1%	88.3%
Divergent results from moving object detection	89.8%	85.7%
Average	88.2%	84%

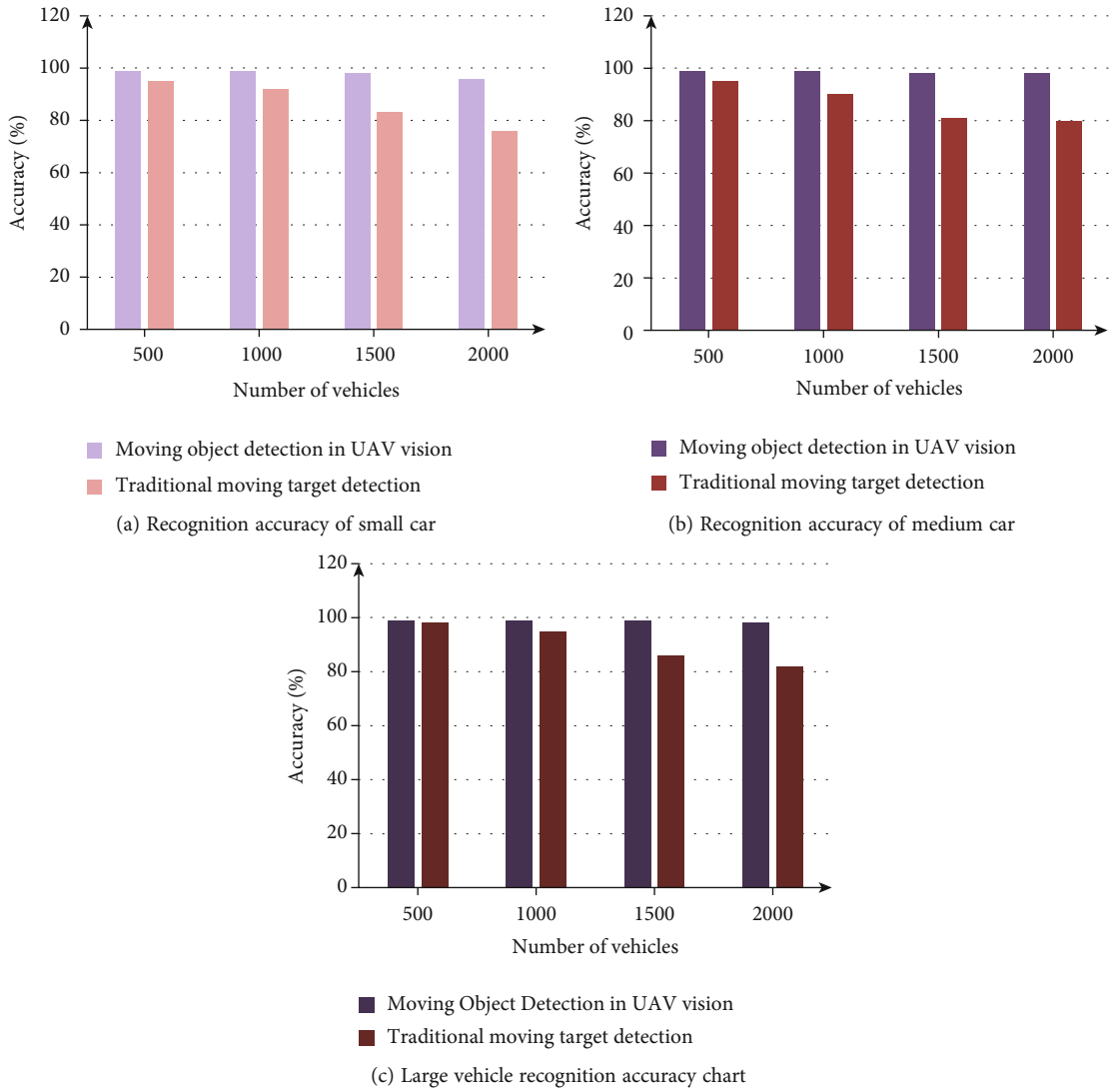

Figure 7: The accuracy of moving target detection and recognition in two ways.

respectively. When the vehicle ratio is 80%, the average labor time of the two is 3.31 s and 16.12 s, respectively.

4.2.4. Divergent Results from Moving Target Detection. When the moving target detection is not accurate enough, there will be differences in the results, which will cause errors in the current detection results and even affect future detections. Its effective reduction or even elimination of divergence results is the ability of a good moving target detection system. In this experiment, 50 intersections and 50 ordinary intersections are selected to detect objects at the intersections. Observing the proportion of differences in the results of the two methods of moving object detection, the differences in the results of the two methods of moving object detection are shown in Figure 10.

From the data analysis in Figure 10, it can be seen that the proportion of divergent results of moving target detection based on UAV vision is much less than that of traditional methods. On different road types, the divergence results of moving target detection based on UAV vision are

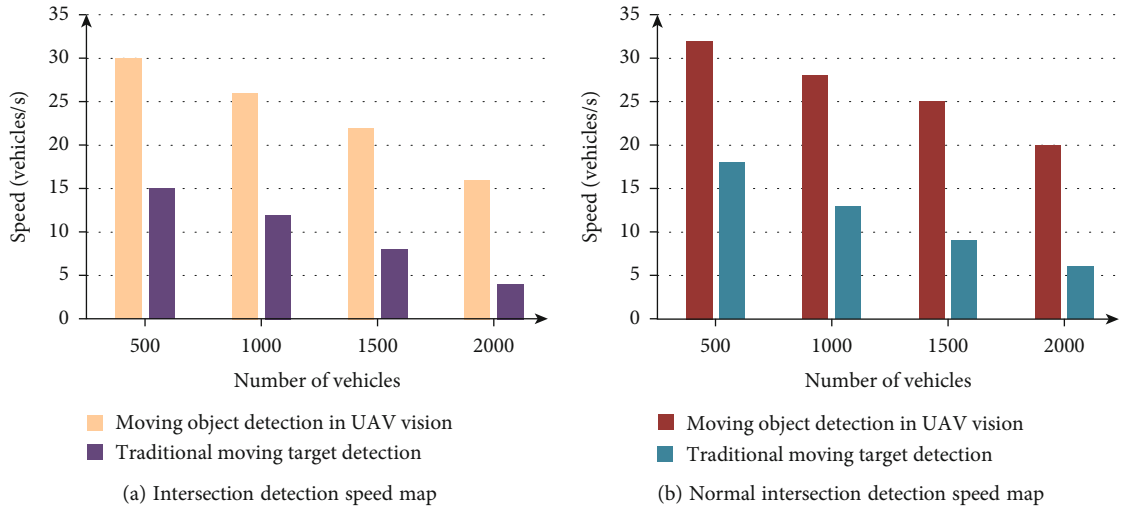

(a) Intersection detection speed map

(b) Normal intersection detection speed map

Figure 8: The speed diagram of moving target detection in two ways.

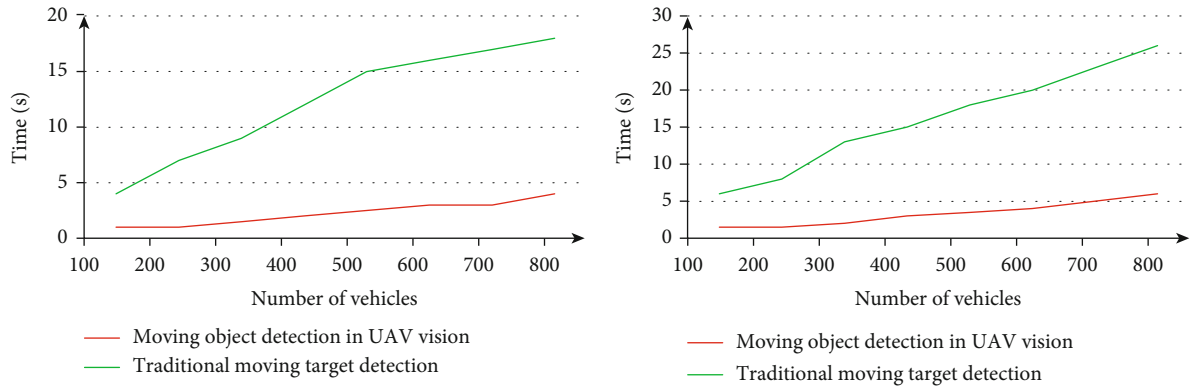

(a) 40% vehicle ratio

(b) 80% vehicle ratio

Figure 9: The labor time diagram of moving target detection in two ways.

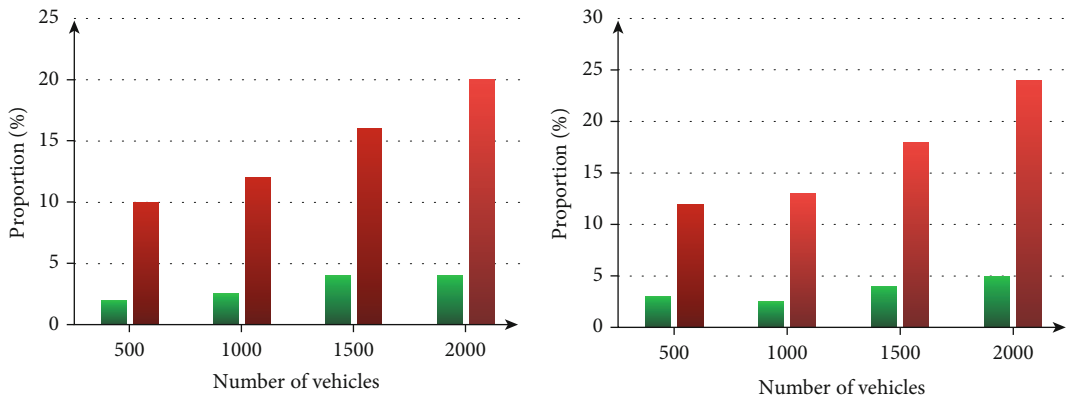

(a) Divergence result map of ordinary intersection

(b) Divergence result map of intersection

Figure 10: Difference results of moving target detection in two ways.

Table 5: Average data comparison table of four dimensions.

Type of moving target detection	Recognition accuracy	Recognition speed (vehicles/sec)	Manual time (s)	Proportion of divergent results
Moving target detection based on UAV vision	98.4%	24.9	2.8	3.5
Traditional moving target detection	87.8%	10.6	14.2	15.3
Difference	10.6%	14.3	11.4	11.8

very low. The average disagreement results at intersections and common intersections are 3.25% and 3.75%.

4.3. Experiment of Two Kinds of Moving Target Detection. The experiment compares the moving target detection based on UAV vision and the traditional moving target detection from four dimensions: the accuracy of moving target detection and recognition, the speed of recognition, the time spent manually, and the divergent results. The average data comparison of the four dimensions is shown in Table 5. It can be seen that the moving target detection based on UAV vision has better performance than the traditional moving target detection.

5. Discussion

The development of UAVs and the combination with multiple fields have greatly promoted the progress of society. In terms of traffic control, traditional target motion detection often fails to achieve the detection effect of prefetching. It achieves effective detection of moving targets by utilizing the unmanned aerial vehicle's supervision capability, improved image feature extraction, and powerful recognition and prediction technology.

6. Conclusion

Through experiments, the UAV vision-based moving target detection and the traditional moving target detection are compared in four aspects: recognition accuracy, recognition speed, labor time, and divergent results. This paper draws the following conclusions: (1) The average recognition accuracy of moving target detection based on UAV vision is 98.4%, which is 10.6% more than the traditional moving target detection. In terms of recognition speed, the average recognition speed of moving target detection based on UAV vision is 24.9 vehicles per second, which is 14.3 vehicles per second more than the traditional moving target detection. (2) The proportion of manual time spent and divergent results of moving target detection based on UAV vision is only about 1/3 of that of traditional moving target detection. Moving target detection based on UAV vision is far superior to traditional moving target detection in terms of detection and recognition. Detection and recognition algorithms and UAV vision are the core of UAV moving target detection. Therefore, finding better detection and recognition algorithms and improving UAV vision will be the direction of future research.

Data Availability

The data that support the findings of this study are available from the corresponding author upon reasonable request.

Conflicts of Interest

The authors declared no potential conflicts of interest with respect to the research, authorship, and/or publication of this article.

Acknowledgments

This work was financially supported by the Natural Science Foundation of Hainan Province, China, Item number: 621QN0899.

References

[1] S. W. Xu, P. L. Shui, X. Y. Yan, and Y. H. Cao, "Combined adaptive normalized matched filter detection of moving target in sea clutter," *Circuits Systems & Signal Processing*, vol. 36, no. 6, pp. 2360–2383, 2017.

[2] J. Pan, Q. Zhu, Q. Bao, and Z. Chen, "Coherent integration method based on radon-NUFFT for moving target detection using frequency agile radar," *Sensors*, vol. 20, no. 8, p. 2176, 2020.

[3] M. Kalra, S. Kumar, and B. Das, "Moving ground target detection with seismic signal using smooth pseudo Wigner–Ville distribution," *IEEE Transactions on Instrumentation and Measurement*, vol. 69, no. 6, pp. 3896–3906, 2020.

[4] S. Minaeian, L. Jian, and Y. J. Son, "Vision-based target detection and localization via a team of cooperative UAV and UGVs," *IEEE Transactions on Systems Man & Cybernetics Systems*, vol. 46, no. 7, pp. 1005–1016, 2016.

[5] A. Tah, S. Roy, P. Das, and A. Mitra, "Moving object detection and segmentation using background subtraction by Kalman filter," *Indian Journal of Science & Technology*, vol. 10, no. 19, pp. 1–11, 2017.

[6] L. I. Yundong, D. O. Han, L. I. Hongguang, X. Zhang, B. Zhang, and X. I. Zhifeng, "Multi-block SSD based on small object detection for UAV railway scene surveillance," *Chinese Journal of Aeronautics*, vol. 33, no. 6, pp. 1747–1755, 2020.

[7] A. A. Micheal, K. Vani, S. Sanjeevi, and C. H. Lin, "Object detection and tracking with UAV data using deep learning," *Journal of the Indian Society of Remote Sensing*, vol. 49, no. 3, pp. 463–469, 2021.

[8] J. Escobar and S. Sandoval, "Unmanned aerial vehicle (UAV) for sea turtle skeleton detection in the Mexican Pacific," *Remote Sensing Applications Society and Environment*, vol. 1, no. 1, pp. 4–12, 2021.

[9] Z. Li, C. Meng, F. Zhou et al., "Fast vision-based autonomous detection of moving cooperative target for unmanned aerial vehicle landing," *Journal of Field Robotics*, vol. 36, no. 1, pp. 34–48, 2019.

[10] O. Doukhi, S. Hossain, and D. J. Lee, "Real-time deep learning for moving target detection and tracking using unmanned aerial vehicle," *Journal of Institute of Control*, vol. 26, no. 5, pp. 295–301, 2020.

[11] B. K. Kim, J. Park, S. J. Park et al., "Drone detection with chirp-pulse radar based on target fluctuation models," *ETRI Journal*, vol. 40, no. 2, pp. 188–196, 2018.

[12] W. Wang, X. Li, L. Xie, H. Lv, and Z. Lv, "Unmanned aircraft system airspace structure and safety measures based on spatial digital twins," *IEEE Transactions on Intelligent Transportation Systems*, vol. 23, no. 3, pp. 2809–2818, 2022.

[13] Z. Lv, "The security of Internet of drones," *Computer Communications*, vol. 148, pp. 208–214, 2019.

[14] Z. Lv, D. Chen, H. Feng, R. Lou, and H. Wang, "Beyond 5G for digital twins of UAVs," *Computer Networks*, vol. 197, p. 108366, 2021.

[15] Y. Khosiawan, Y. Park, I. Moon, J. M. Nilakantan, and I. Nielsen, "Task scheduling system for UAV operations in indoor environment," *Neural Computing and Applications*, vol. 31, no. 9, pp. 5431–5459, 2019.

[16] G. Hu and C. Wen, "Traffic sign detection and recognition based on improved YOLOv4 algorithm," *International Journal of Computer Applications Technology and Research*, vol. 10, no. 6, pp. 161–165, 2021.

[17] C. Liu and J. Li, "Self-correction ship tracking and counting with variable time window based on YOLOv3," *Complexity*, vol. 2021, no. 3, 9 pages, 2021.

[18] Z. Zhang, Y. Zhang, Y. Wen, K. Fu, and X. Luo, "Intelligent defect detection method for additive manufactured lattice structures based on a modified YOLOv3 model," *Journal of Nondestructive Evaluation*, vol. 41, no. 1, pp. 1–14, 2022.

[19] C. Fu, Y. He, F. Lin, and W. Xiong, "Robust multi-kernelized correlators for UAV tracking with adaptive context analysis and dynamic weighted filters," *Neural Computing and Applications*, vol. 32, no. 16, pp. 12591–12607, 2020.

[20] J. Liu, N. Sha, W. Yang, T. Jia, and L. Yang, "Hierarchical Q-learning based UAV secure communication against multiple UAV adaptive eavesdroppers," *Wireless Communications and Mobile Computing*, vol. 2020, Article ID 8825120, 15 pages, 2020.

[21] S. Jiao, H. Gao, X. Zheng, and D. Liu, "Fault tolerant control algorithm of hexarotor UAV," *Journal of Robotics*, vol. 2020, Article ID 8829329, 16 pages, 2020.

[22] X. Fan, C. Huang, F. Bin, S. Wen, and X. Chen, "UAV-assisted data dissemination in delay-constrained VANETs," *Mobile Information Systems*, vol. 2018, Article ID 8548301, 12 pages, 2018.

[23] H. Zhu, H. Wei, B. Li, X. Yuan, and N. Kehtarnavaz, "Real-time moving object detection in high-resolution video sensing," *Sensors*, vol. 20, no. 12, p. 3591, 2020.

[24] H. Bi, J. Ma, and F. Wang, "An improved particle filter algorithm based on ensemble Kalman filter and Markov chain Monte Carlo method," *IEEE journal of selected topics in applied earth observations and remote sensing*, vol. 8, no. 2, pp. 447–459, 2015.

[25] A. Israr, E. H. Alkhammash, and M. Hadjouni, "Guidance, navigation, and control for fixed-wing UAV," *Mathematical Problems in Engineering*, vol. 2021, Article ID 4355253, 18 pages, 2021.

[26] Z. Yin, G. Li, C. Du, X. Sun, J. Liu, and Y. Zhong, "An adaptive speed estimation method based on a strong tracking extended Kalman filter with a least-square algorithm for induction motors," *Journal of Power Electronics*, vol. 17, no. 1, pp. 149–160, 2017.

[27] L. Yue, R. Yang, Y. Zhang, L. Yu, and Z. Wang, "Deep reinforcement learning for UAV intelligent mission planning," *Complexity*, vol. 2022, Article ID 3551508, 13 pages, 2022.

[28] C. W. Chen, "Drones as internet of video things front-end sensors: challenges and opportunities," *Discover Internet of Things*, vol. 1, no. 1, p. 13, 2021.

Hindawi
Wireless Communications and Mobile Computing
Volume 2022, Article ID 4314734, 13 pages
https://doi.org/10.1155/2022/4314734

Research Article

Blockchain Consensus Mechanism for Distributed Energy Transactions

Jiangyao Wu,[1] Ye Liu,[1] Jiefei Cai ,[2] and Shuhui Su[2]

[1]*Guangdong Power Grid Co., Ltd., Guangzhou, Guangdong 510600, China*
[2]*China Southern Power Grid Digital Grid Research Institute Co., Ltd., Guangzhou, Guangdong 510630, China*

Correspondence should be addressed to Jiefei Cai; caijf1@iotosaas.com

Received 2 April 2022; Revised 10 June 2022; Accepted 29 June 2022; Published 15 July 2022

Academic Editor: Jun Ye

In order to reduce the cost of grid dispatching and increase the transparency of energy transactions, the distributed energy transaction model based on blockchain is constructed. At the same time, in order to improve the high communication overhead and low throughput of the traditional PBFT algorithm in the consortium blockchain, an efficient Byzantine fault-tolerant consensus mechanism (DE-BFT) for the energy blockchain is designed. The algorithm improves from two aspect: *node election* and *main chain consensus*. In the stage of *node election*, the model uses a health score evaluation and a verifiable random function to improve the security and randomness of node selection. In the stage of *main chain consensus*, the efficient data consistency interaction protocol decreases the complexity of the communications between nodes, down to a constant term level from exponential one. The result shows that, compared with other consensus algorithm, the DE-BFT algorithm performs better in terms of consensus delay, communication overhead, throughput, and consensus node reliability.

1. Introduction

Distributed energy transaction [1] has the characteristics of long business process, many participants, and wide distribution. These characteristics lead to serious data silos, difficult credit transfer, and prominent transaction risks in distributed energy transactions. Blockchain is famous for its openness, transparency, traceability, tamper resistance, and decentralization. Exploring blockchain-based energy-distributed transactions can help reduce grid dispatch costs and increase transaction transparency. According to the degree of decentralization, blockchain is divided into three modes: *public blockchain* [2], *consortium blockchain* [3], and *private blockchain* [4]. The multicenter characteristics of *consortium blockchain* are more suitable for the status quo of power reform in China. Therefore, most of the distributed energy transaction research based on blockchain currently adopts the application mode of *consortium blockchain* [5–8]. Consensus algorithm is the key technology that determines the performance and security of blockchain systems. Compared with the traditional *Byzantine fault tolerance (BFT) algorithm* [9], the *practical Byzantine fault tolerance (PBFT) algorithm* [10] reduces the overhead execution of network, which makes it becomes more practical. However, PBFT still has some problems, such as security loopholes in the selection of consensus nodes and excessive communication overhead in the case of multiple nodes, which have become important factors restricting the development of blockchain.

Distributed energy transaction platforms requires lower latency and higher security. Therefore, the performance of the consensus algorithm is an important factor affecting the development of energy blockchain. Literature [11] proposed an effective real-time distributed blockchain consensus algorithm for energy transactions. The algorithm manages a large number of transactions in partitions to ensure the real-time improvement of system transactions but manages multiple systems at the same time, so the security of the system cannot be guaranteed. Literature [12] proposed *delegation Byzantine fault tolerance (DBFT) consensus*

algorithm to improve the efficiency of energy transactions. Compared with PoW and PoS, DBFT solved the efficiency problem. Although the algorithm verifies the security of transactions through entrustment, it increased the complexity of communication, and the complexity is $O(n^2)$. The security is not as high as PoW and PoS. Therefore, literature [13] proposes an energy trade deal algorithm based on the blockchain mechanism of consensus. First of all, according to PBFT, the lack of a dynamic problem in the VPBFT voting mechanism was introduced. The node system is divided into four types with different responsibilities and gives the number of relations between nodes. When the number of nodes is changed, it can be calculated according to the quantity relation, ensuring dynamic. Second, a data anonymous transaction and authentication protocol are designed. In the protocol, when the seller sells data, the mapping relationship between the real identity and the false identity of the data owner is blinded and sent to the buyer. When the buyer wants to verify their identity, the seller's identity can only be verified with the authentication of the blockchain. The complexity of the protocol is also $O(n^2)$, resulting in insufficient real-time performance of the protocol. Literature [14] proposed a secure energy transaction method based on blockchain consensus. The *Byzantine general problem (BGP)* protocol is used for developing transactions, by reducing the number of system attacks to ensure the safe operation of the system. However, the efficiency of the algorithm decreases rapidly with the increase of the number of nodes and the communication complexity is $O(n^2)$, so the real-time performance of the system is insufficient. Literature [15] proposed PBFT protocol, an energy-efficient consensus node selection mechanism is designed, and VRF is used to ensure the security of leader. In addition, in the case of multihop neighbor nodes, the authority of the node is evaluated by selecting the relay node by extending the centrality, which may lead to centralization of nodes' colluded interests, and communication complexity is the same as literature [14]. Literature [16] guarantees the fairness of transaction resource allocation by introducing the active reputation value of the entity. In the consensus process, the reputation is used to select the master node to reduce the traffic of duplicate nodes, and its communication complexity is $O(m * n)$ (where m is a constant). Since the selection of the master node must be very safe, the burden on the master node is increased. The above research found that the existing research results focus on the combination of blockchain and energy trading but ignore the real-time and security of energy trading. Research on an efficient consensus mechanism for distributed energy transactions is an urgent problem to be solved in energy blockchain research [17].

This paper comprehensively considers the security and efficiency of energy transaction scenarios based on blockchain and designs a distributed energy transaction mode based on blockchain. This mode improves the traditional PBFT algorithm from the two stages of block node election and main chain consensus. In the block node election stage, a health score evaluation mechanism is designed to reliably evaluate the consensus behavior of nodes. In order to improve the randomness of the node election process and the antiattack capability of the network, a verifiable random function is used to randomly elect candidate nodes and master nodes according to their health scores. In the main chain consensus stage, consensus is reached between nodes based on the efficient data interaction protocol provided by HSBFT [18], which further improves the transaction throughput of the distributed energy trading platform based on block chain and reduces the transaction delay.

2. Preliminary Knowledge

2.1. Verifiable Random Function. Verifiable random function (VRF) can generate specific outputs from specific inputs [19]. Its biggest feature is that it can verify that the output result is correct without knowing the input. So VRF is essentially a pseudorandom function with a verifiable function. If a specific value and private key are input, VRF outputs a random number and a proof by generating a function group. Combined with the public key, the verifier can use the proof function group to verify whether the random number is generated by the input. This process does not need to expose the private key of the input, so the VRF is safe. VRF contains the following two function groups [20].

2.1.1. Generating Function Group. Generating function: nodes use a generating function to generate a hash random output R and a hash proof P, respectively. SK is the private key of the node. M is a specific input value set by the system.

$$\begin{aligned} R &= \text{VRF\_Hash}(SK, M), \\ P &= \text{VRF\_Proof}(SK, M). \end{aligned} \tag{1}$$

2.1.2. Proof Function Group. PK is the public key of the verified node.

$$\begin{aligned} R &= \text{VRF\_P2H}(P), \\ &\text{VRF\_Verify}(PK, M, P). \end{aligned} \tag{2}$$

VRF satisfies three properties of verifiability, uniqueness, and randomness. Verifiability means that through the above steps, the verification node can still verify whether the R and P values are generated by the PK holder according to M without knowing the private key of the verified node. The uniqueness means that for any PK and M, there is a unique output R, and R can be verified. The randomness means that output R of VRF_Hash is distinguishable from the random number M.

Verifiable random functions have two characteristics:

(1) For different inputs, the output values are random and uniformly distributed within the range of values

(2) For the same input, the output it gets must be the same

The role of the VRF in the consensus mechanism of this paper is that even if the private key of the random number node is unknown, other nodes can verify that a certain random number is generated by the node that issued the

random number. It can be verified that a random output is indeed generated by a specific node under the premise of not exposing the private key.

2.2. PBFT Consensus Algorithm. The PBFT consensus mechanism mainly achieves the consensus of all nodes through the consensus protocol and the view-change protocol. Among them, the view-change protocol is to replace the master node with a slave node when it cannot continue to perform its duties and to ensure that requests that have been executed by non-Byzantine servers will not be tampered with. The premise of PBFT to ensure security and activity is that the number of Byzantine nodes in the system does not exceed 1/3 of the total number of nodes in the system.

The PBFT algorithm is divided into three stages, namely, preprepare, prepare, and commit. Figure 1 is a flowchart of the execution of the PBFT algorithm. The detail is as follows:

(1) Request: the client sends a request to the master node

(2) Preprepare: after the master node receives the request sent by the client, it assigns a sequence number to the client's request and sends a preprepare message to all replica nodes

(3) Prepare: the replica node receives the preprepare message and verifies the authenticity of the message. After passing the verification, it broadcasts the prepare message to other replica nodes

(4) Commit: when the replica node receives $2f$ prepare messages as same as the above preprepare message, it steps into commit phase and broadcasts the commit message to all replica nodes

(5) Response: after the replica node receives $2f + 1$ the same commit messages, it replies with a corresponding message to the client. If the client receives $f + 1$ the same reply message, the request execution is completed

All nodes in the PBFT algorithm work under the same configuration information, which is called a view, and each view is uniquely determined by a master node. The master node has core capabilities such as serial number allocation and initiating proposals in the entire system. Other replica nodes participate in the voting process. When the master node fails, the view-change protocol will be triggered. The master node is going to be replaced and step into the next view stage. The PBFT consensus mechanism adopts the method of $p = v \bmod |N|$ for selecting master nodes. As the selection method is fixed, it is easily to be exposed at next round of master nodes and thus be attacked.

3. Blockchain-Based Distributed Power Transaction Model

Figure 2 shows a distributed power transaction model based on blockchain. The nodes is mainly classified as user nodes on the power consumption side, distributed energy nodes on the power generation side, power grid enterprises, data centers, and small power stations. The power consumption side and the power generation side calculate electricity data and release electricity purchase/selling plans to the blockchain trading platform rely on smart ammeter. After being matched, the transaction records are stored on the blockchain to ensure that each transaction is verifiable and traceable and cannot be tampered with.

The blockchain-based power distributed transaction is mainly divided into the following stages.

(1) Node initialization stage: each user or enterprise needs to go through the authorization and authentication of the central management node (the central management node is authorized by the power grid enterprise and is responsible for the identity authentication and authorization of the nodes in the blockchain) when it newly joins the blockchain network. At the same time, the central management node conducts authority and trust base evaluation and divides the trust base into three levels: A (high), B (medium), and C (low). Considering the advantages of high performance and high reliability of the data center compared with other nodes in the transaction model, the trust base of the data center is A. The trust base of small power stations is B as their performance are relatively weak even though endorsed by the power grid. For other distributed power generation nodes or user nodes newly joining the network, the trust base is set as C

(2) Smart contract initialization stage: all participating nodes in the power blockchain jointly build smart contracts. All nodes jointly agree on a certain smart contract including triggering conditions, response rules, and logical processes. The contract is signed by all parties with their private key, which ensures the validity, and uploaded to the blockchain network. Each node will receive a copy of the contract and save it in the memory at once, waiting for a new round of consensus phrase in the system, triggering the consensus execution of the contract. After reaching a consensus, the stage of the smart contract initialization is completed

(3) Transaction stage: before the transaction, the smart ammeter will conduct statistical analysis on the user's generation/consumption during this period and formulate an appropriate power purchase/sale plan for the user according to the analysis. This plan will release to a transaction platform. The smart contract carries out intelligent matching of this online transaction

(4) Transaction consensus on-chain stage: after the online transaction negotiation is completed, a consensus is reached among the distributed nodes and finally stored in the blockchain. A power transaction can be officially completed only after the consensus of the nodes

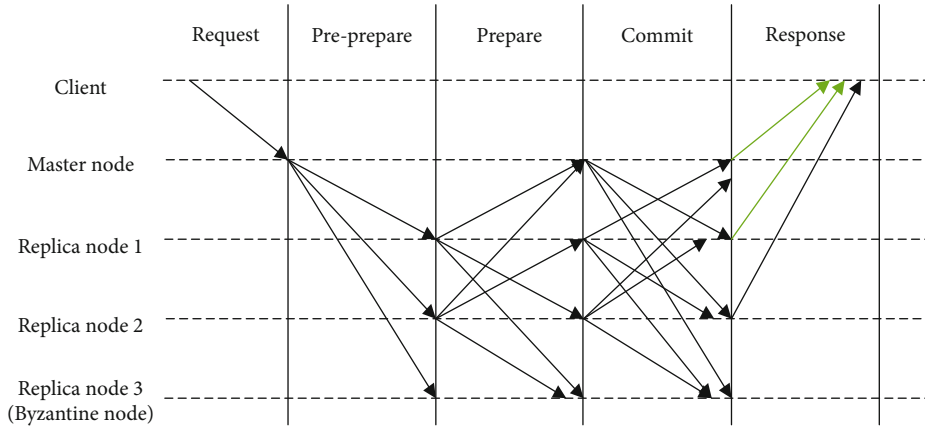

Figure 1: PBFT consensus consistency protocol.

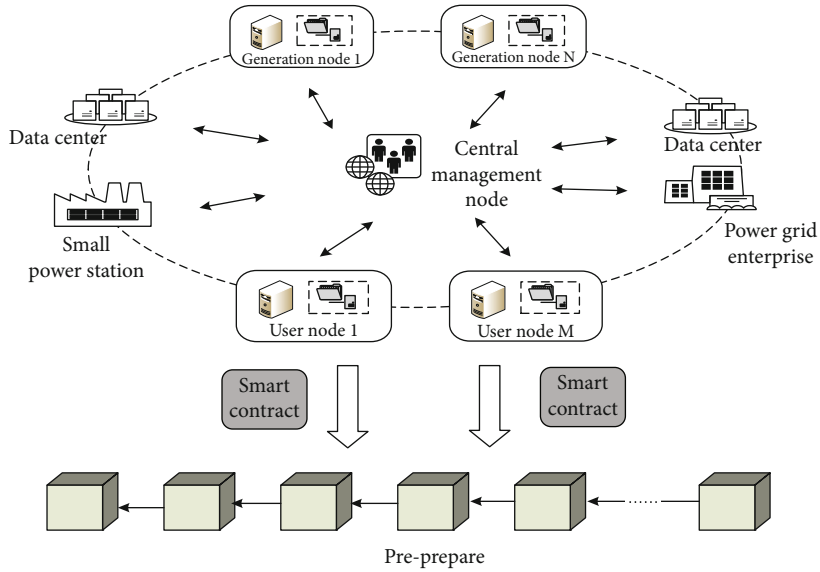

Figure 2: Blockchain-based distributed power transaction model.

The speed of the power transaction consensus on the chain directly affects the user's transaction experience and transaction efficiency. At the same time, in order to make the data finally stored on the blockchain reliable, the security and antiattack of the consensus process must be executed. Consensus failure will lead to transactions that cannot be carried out smoothly, hindering the normal operation of the power transaction model. Therefore, the consensus mechanism is crucial to the stability and safety of the blockchain-based power distributed transaction model.

4. DE-BFT Consensus Algorithm

4.1. Node Type and View Number. The distributed nodes participating in the consensus are divided into the following types according to their functions:

Master node: the master node is responsible for packaging transactions in the blockchain network and submitting new blocks

Candidate node: the candidate node is in charge of verifying and reaching consensus, the blocks of transactions generated during periods. It is also in charge of the election of the master node and consensus committee members

Follow node: follow node revolves the election of candidate nodes and copies the final block data on the blockchain

Byzantine node: it is a malicious node in the system, or a node exhibits malicious behavior due to being attacked. The malicious behavior of Byzantine nodes in the energy blockchain will cause transaction delays or untrustworthy transaction settlements, affect user experience, and hinder the development of power blockchain

Central management node: in power transaction model, as the joining and exiting status of each distributed power node changes dynamically, an authoritative and credible central node is required to manage identity authentication and to maintain the status of all nodes in the system. Based on the characteristics of the consortium chain, which ensures the reliability of the joining nodes. This paper

Table 1: Node status table.

Serial number	Trusted Base	Status	Health score	Acting as master node times
1	A	Master node	0.9	2
2	B	Candidate node	0.6	—
3	B	Candidate node	0.5	—
4	C	Follow node	0.4	—

introduces a new concept of a central management node. As an authority and leader in the power field, power grid companies are endorsed by national credit. Therefore, a branch office of power grid is generally in charge of the central management node. In order to prevent the centralization of power transaction system, the central management node does not revolve any power transactions such as transaction verification and block submission in the system

View number: it represents the position and status of the current master node. The view number is described as the term of $p - t$. p represents the number of the master node, and t represents that how many times that p is the master node. By this way, it ensures that no two views have the same view number throughout the entire period

4.2. Block Producer Election Mechanism

4.2.1. Health Score Evaluation Strategy. The health score evaluation strategy calculates the credibility of each node based on the behavior of the node in the process of participating in the block consensus. As part of the consensus protocol, the health score evaluation is deployed on the blockchain through smart contracts and can be performed in each node which participates in the consensus, and the evaluation results will be sent to the central management node. As shown in Table 1, the central management node maintains all nodes status in a node status table. Each time, the node status table is updated completely. The result will be synchronized to the blockchain, for all nodes to view. For each node newly added to the system, its initial health score value will be evaluated according to the analysis results of the trusted base of the CA certification center in the distributed power transaction model in this paper. If the trust base is B, the initial health is set to 0.5, and if the trust base is C, it is set to 0.4. For example, when a certified data center joins the network, considering its high performance and high reliability advantages compared to other nodes in the blockchain, the trust base of the data center is set as A; that is, the initial value of the health score is 0.6; if a small power station newly joins the network, since it is endorsed by the power grid, its trust base can be set as B; that is, the initial value of the health score is 0.5; similarly, when a user node joins the network, the trust base can be set as C, and the initial value of health score is set to 0.4 accordingly. The node health score evaluation algorithm is shown in Algorithm 1. The algorithm detail is described as below.

(1) Health Score Evaluation of Master Node. For the master node, if a new block is generated during the t^{th} round of consensus process of the current view which the current master node participates in, the health score of the master node will increase accordingly, but the health score value does not exceed the threshold of 1 set by the system. If the current view number of the master node has not changed, the growth rate of the master node's health score will be slower. In order to avoid centralized processing of the system, when the health score value is 1 and the number of blocks packaged by the master node reaches the threshold k, the view-change protocol will be triggered to select new master node.

$$H_i(t) = \begin{cases} \min\left\{1, H_i(t-1) + \frac{1}{k}[1 - H_i(t-1)]\right\} & \text{, Send consistent messages in a timely manner,} \\ H_i(t-1) \times \frac{1}{t} & \text{, Consistency messages not sent in time,} \\ 0 & \text{, Send inconsistency messages,} \end{cases} \tag{3}$$

$$H_i(t) = \begin{cases} \min\left\{1, H_i(t-1) + \frac{1}{k}[1 - H_i(t-1)]\right\} & \text{, Send consistent messages in time,} \\ H_i(t-1) \times \frac{1}{t} & \text{, Message not sent in time,} \\ H_i(t-1) \times \frac{1}{t+1} & \text{, The message sent is different from most,} \\ 0 & \text{, Send inconsistency messages.} \end{cases} \tag{4}$$

Algorithm: Health Score Evaluation Algorithm
Input (smart contract trigger condition): New node joins and a round of consensus ends.
Output: Node health score value.
1. When new nodes are added
Trigger health score evaluation smart contract.
2. If trust base = "A"
health score =0.6
3. If trust base = "B"
health score =0.6
4. If trust base = "C"
health score =0.4
5. End if
6. when a round of consensus ends / a new block is generated.
Trigger health score evaluation smart contract
7. If node type = primary
If the master node sends messages consistently during the consensus phase
Calculate the master node health score value according to formula (3) :
$H_i(t) = \min\{1, H_i(t-1) + (1/k)[1 - H_i(t-1)]\}$
If the master node does not send the message in time.
Calculate the master node health score value according to formula (3):
$H_i(t) = H_i(t-1) \times (1/t)$
If the master node sends messages inconsistently
$H_i(t) = 0$
Execute the view-change protocol
8. If node type = candidate
If candidate nodes send consistent messages
Calculate the candidate node health score value according to formula (4):
$H_i(t) = \min\{1, H_i(t-1) + (1/k)[1 - H_i(t-1)]\}$
If the candidate node did not send the message in time
$H_i(t) = H_i(t-1) \times (1/t)$
If the candidate node sends a message different from other nodes
$H_i(t) = H_i(t-1) \times (1/t+1)$
9. End if
10. End

Algorithm 1: Algorithm description of node health score evaluation strategy.

The specific evaluation of the master node's health score is shown in formula (3), where $H_i(t)$ is the health score value of the t^{th} round of consensus and k is the threshold of the consensus round. If the master node does not send messages to the candidate node in time during the view process, resulting in no new block being generated, its health score will drop. If the master node sends inconsistent messages to other candidate nodes, its health score will drop directly to 0 and be kicked out of the candidate node set, triggering the view replacement protocol to replace the master node and view.

(2) Health Score Evaluation of Candidate Node. For a candidate node, if the same message is sent to other nodes during the t^{th} consensus process of the current view and it is consistent with the final consensus result, the node's health score will slowly increase, but again, it will not exceed the system setting threshold 1. As the number of consensuses in the same view increases, the rate of increase in health score also decreases. If a candidate node does not participate in the consensus process in a certain round, that is, does not send any messages to other nodes, its health score will be reduced in a certain proportion. If a candidate node participates in the consensus process but sends a message that is inconsistent with the final result, its health score will also decrease. The technical solution will reduce the health score value of nodes at different speeds according to the different behavior of nodes. If it is detected that the same consensus node has sent different information lists, the node will be regarded as a malicious node, its health score value will be reduced to 0, and it will be removed from the current candidate node set. The health score evaluation of candidate node is shown in formula (4).

4.2.2. Primary Node Election Protocol. The master node is generated in the candidate node set and follows the nodes whose health score exceeds 0.5 into the candidate node set. After the selection of candidate node is completed, each candidate node independently performs VRF calculation. If the calculated hash output meets the requirements for becoming the master node output threshold, then node broadcasts its own VRF output and proof and requests authentication from other nodes in the candidate node set. The specific verification process of the master node is shown in Figure 3.

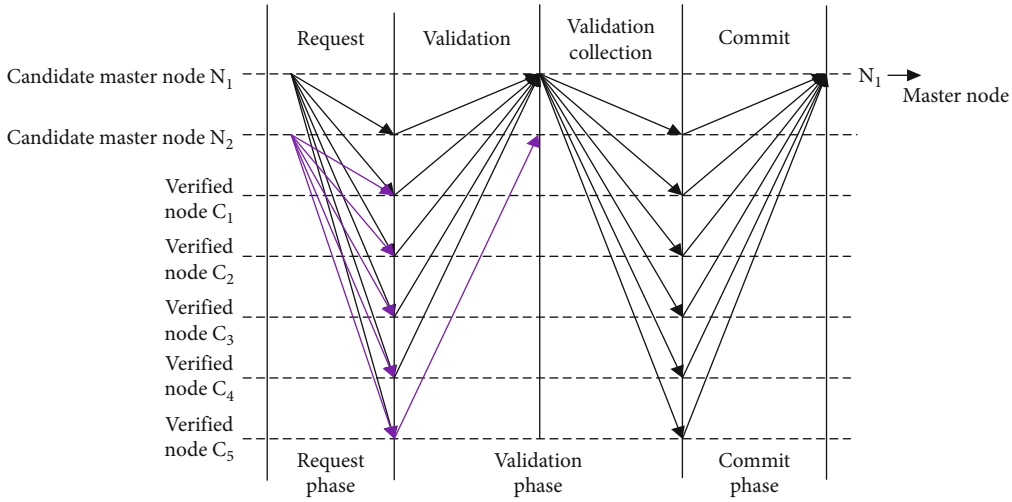

Figure 3: The process of the master node election protocol.

(1) Request Phase. The verifiable random function VRF hash outputs of candidate master nodes N_1 and N_2 are all within the threshold range set by the system, then these two nodes obtain their own proof values through the proof function, and then, N_1 and N_2, respectively, send the request verification message encrypted by digital signature to the consensus committee node. The format of the request message is

$$\langle \text{request}, R_i, P_i, T, H_i \rangle_{\text{sig}(N_i)(i=1,2)}. \tag{5}$$

(2) Validation Phase. In the validation phase, other candidate nodes start the timer when they receive the first validation request message. When the timer stops, they no longer receive any request validation messages and start to verify the received request validation messages. The validation process requires the following:

(a) Check whether the signatures of nodes N_1 and N_2 are correct; if not, delete the message directly

(b) Check whether the value sent by the node is correct; if not, delete the message directly

(c) Compare the health score values of all the verified nodes received during the timer period, and select the node with the highest health score as the master node

Assuming that in the above verification, the $C_1 - C_4$ verification nodes finally select N_1 as the master node, then a verification message will be returned to the node N_1. The format of the validation passed message is

$$\langle \text{verify}, T, m, \Phi \rangle_{\text{sig}(C_i)}, \tag{6}$$

where T represents the timestamp when the node verified the return message to the verified node, m represents the proof message digest that the node selects N_1, Φ represents the set of request messages received by the node, and sig(C_i) represents the digital signature of the consensus committee node, which is used to prove that the message is indeed sent by the node and cannot be tampered with by others.

(3) Validation Collection Phase. In this step, all candidate master nodes that meet the VRF output conditions and send the request verification message will receive the verification pass messages from other verification nodes and collect and package these messages. When the node receives a verification pass message from more than $f + 1$ different candidate nodes, it means that the node has obtained the approval of most nodes to be selected as the master node and records this status in its own local log, switches to the view of its elected master node, and modifies the number of view. Then, the master node returns a confirmation message to all other consensus nodes. The format of the message is

$$\langle \text{confirm}, T, \Psi \rangle_{\text{sig}(N_i)(i=1,2)}, \tag{7}$$

where Ψ is the set of verification pass messages received by the master node from other different nodes, as shown in Figure 3. N_2 only received the verification passing messages from C_5, so it cannot become the master node.

(4) Confirmation Stage. In the confirmation stage, after other consensus committee nodes receive the confirmation message from the N_1 node, they need to verify the correctness of all messages in the message set and verify whether the signature of the master node is correct. Consensus records the state change of the master node in the local log, switches to the view number where the current master node is located, and sends a confirmation message back to node N_1. After node N_1 receives the confirmation state change message from other nodes, it officially becomes the master node, assumes its role in the system at this stage, and begins to process incoming requests in the system. Algorithm 2 describes the algorithm of the master node election process.

Algorithm: Master Node Election Algorithm
Input: Candidate Node Set$\{N_1, N_2, \cdots, N_i\}$.
Output: Master Node Serial Number.
1. Trigger the smart contract to call a random verifiable function to generate a random number for this round of elections
2. The candidate node calls the random verifiable function to generate the random number of this round
$R_i = \text{VRF\_Hash}(SK, M)$
Calculate:
$P_i = \text{VRF\_proof}(SK, M)$
3. If candidate node generates random numbers$R_i \le v$.
Broadcast the request verification message$\langle \text{request}, R_i, P_i, T, H_i \rangle_{sig(N_i)}$.
4. When the consensus node receives the first request verification message
Timer start
Verificatesig(N_i)
If signature is incorrect
Delete this message
VerificateR_i, P_i
If $R_i, P_i$is incorrect
Delete this message
End timer
Compare < the health score value of all requesting verification nodes >
Selectmax $\{H_i, i \in \{\text{A set of candidate nodes conforming to random numbers.}\}\}$
5. Broadcast master node serial number
6. End

Algorithm 2: Description of primary node election algorithm.

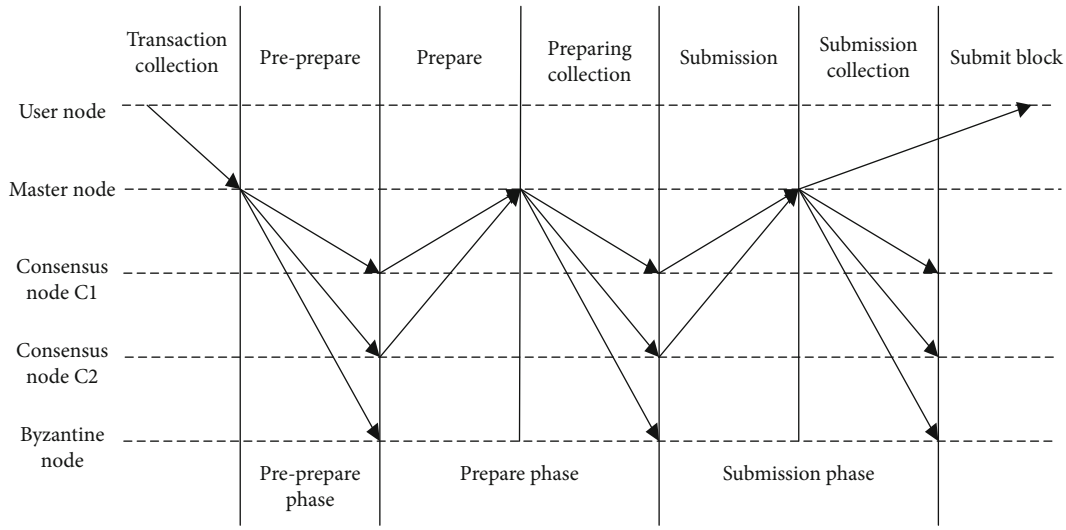

Figure 4: Data consistency interaction protocol.

4.3. Main Chain Consensus Protocol. In the main chain consensus stage of the traditional PBFT algorithm, the communication complexity between nodes is very high, which makes the Byzantine consensus algorithm difficult to apply in practical systems. HSBFT is an efficient data exchange protocol. In general, its communication complexity is at a constant level. Therefore, in our energy blockchain consensus mechanism, in order to improve the transaction confirmation speed, ensure the real-time information transmission, and provide a good user experience, this paper adopts HSBFT's efficient data consistency interaction protocol as the main chain consensus protocol. The specific process is shown in Figure 4.

The following describes the main stages of the consensus protocol operation process described above in detail:

(1) Preprepare stage: after the master node packages the transactions collected in the memory transaction pool into blocks, it multicasts a prepreparation message to the consensus node set, appends this message to its own local log, and starts timer $T1$. The consensus node verifies the message when it receives the prepreparation message. After the verification is passed, it officially receives the message, enters the preparation stage, and replies the preparation message to the master node

```
Algorithm: Main Chain Consensus Algorithm
Input: Transaction Collection
Output: New Block
1. The master node sends the packaged transaction set to the blockchain network
2. Broad coast pre-prepare message to consensus node
3. The master node starts the timer
4. When the consensus node receives the pre-preparation message
        Perform verification
        If verification passed
            Send prepare message back to master node
        If the number of messages received by the master node within the timer ≥ 2f
            Then multicast a prepare message
        Else
            End this round of consensus
5. When the consensus node receives the prepare message
        Perform verification
          If verification passed
            Then send a commit message to the master
            When the number of commit messages received by the master node ≥ 2f
              The master node sends a commit collection message to the non-master node
              When the non-master node receives the commit collection message
                Perform verification
                If verification passed
                    Then copy the new block content to the local
                End if
            End if
6. End
```

Algorithm 3: Description of the main chain consensus algorithm.

(2) Prepare stage: when the master node receives the preparation message sent by the nonmaster node, it will also verify the messages sent by each nonmaster node one by one. The verification process is similar to the verification process of the prepreparation message. When the master node receives more than $2f$ correct prepare messages from different nodes, the master node multicasts a prepare message to all active nonmaster nodes. The nonmaster node enters the submission phase after passing the verification of the prepare message

(3) Submission stage: the data interaction and verification process in the submission stage is similar to that in the preparation stage. When the nonmaster node enters the submission stage, it sends a message representing entering the submission stage to the master node. When the master node receives at least $2f$ messages from different nonmaster nodes, after the correct message is submitted by the master node, the master node sends a submission collection message to the nonmaster node, and the master node submits the block to the blockchain, and the nonmaster node verifies the message after receiving the submission collection message, after the message is authenticated successfully, copying the block data. The consensus process ends

Through the data interaction protocol in the above three stages, the final block consensus is realized to ensure the reliability and consistency of the data stored on the chain. It can be seen intuitively from Figure 3 that, compared with the traditional PBFT algorithm, the communication complexity of this protocol is reduced to a constant level. Therefore, the low complexity of the consensus protocol is more suitable for the real-time requirements of distributed energy transactions, and the transaction confirmation speed is faster. Algorithm 3 describes the main chain consensus algorithm in detail.

5. Experimental Results and Analysis

5.1. Experimental Configuration. This article uses the same test machine for experiments, the processor is AMD A4-Series A4-5000 quad-core, the operating system is 64-bit Windows 7 flagship SP1, and the memory is 4 GB. It is programmed using DVE-C++5.1 software.

5.2. Security Analysis. The traditional PBFT consensus mechanism uses the remainder of $p = v \bmod |N|$ to elect the master node, where v and N represent the current view number and the number of nodes, so the values of v and N are easy to know. The attacker can predict the next node in advance. The position of the main node of the round is attacked in advance, which destroys the consensus process of the system and easily leads to poor real-time energy

transactions. The efficient and secure consensus mechanism proposed in this paper uses a verifiable random function to elect block-generating nodes and uses the node's private key as the input of the VRF function. And the result can be verified by the public key. The attacker does not know the private keys of other nodes in the network, so that the position of the next master node cannot be predicted in advance and an attack on a node cannot be launched in advance. At the same time, the consensus mechanism proposed in this paper will evaluate the health score of nodes according to the behavior of nodes in the consensus process. Nodes with low health scores will not be able to participate in the election of consensus nodes and master nodes, thereby enhancing the reliability and security of block producing nodes. Therefore, the consensus mechanism proposed in this paper can enhance the security and randomness of block node election, so as to effectively resist DDoS attacks.

5.3. Feasibility Analysis

5.3.1. Algorithms Based on Verifiable Random Functions. Most of the existing solutions use a fixed order to select the master in turn, which is the current mainstream master selection method. When the order in which the backup node becomes the master node is fixed, the master node is vulnerable to DDoS attacks by the adversary and destroys the system activity. In this paper, an algorithm is designed to improve the selection method of the consensus node set. First, a verifiable random function is used to randomly select the node set, and the health score is used as the basis for selection. For the selection of the master node, all nodes can be easily verified, and finally, the selection result is reached through consensus to ensure the randomness and reliability of node election. The main process of selecting a verifiable random function, due to its randomness and zero-knowledge proof characteristics, can effectively resist DDoS attacks and ensure the activity of the system.

5.3.2. Feasibility Analysis of View-Change. In PBFT, the view-change protocol is triggered by at least $2f + 1$ consistent view-change messages from different nodes. If the current consensus fails, the system switches to a new view with the help of the view-change protocol for normal operation. However, in the PBFT optimized in this paper, the consensus mechanism follows the concept of PBFT. When the master node fails, the system will trigger the view-change protocol to conduct a new round of node election. According to the health score as the reference for selecting the master node, the selected master node is verified in combination with the verifiable random function. In this paper, a timeout mechanism is set to improve the efficiency of selecting the master node. If the master node is successfully verified within the specified time, replace the primary node. Otherwise, it fails, and the health score is used as a reference again, and the master node is verified by the verifiable random function again until the master node is successfully selected. Compared with the traditional PBFT, the selected master node has higher reliability, reduces the possibility of failure of the master node, reduces the communication overhead caused by view-change, and increases the algorithm throughput.

Table 2: Communication complexity comparison table.

Algorithm	Total number of communications	Communication complexity
PBFT	$f(n) = 2n^2$	$O(n^2)$
ES-BFT [22]	$f(n) = 2n^2 + n + 1$	$O(n^2)$
EPBFT [21]	$f(n) = n^2 + 3n + 1$	$O(n^2)$
RBFT [23]	$f(n) = n^2 + n$	$O(n^2)$
DE-BFT	$f(k) = 5k + 2(k \le n)$	$O(n)$

Table 3: Transaction types table.

Transaction type	Number of test groups
Deploy smart contracts	4
Call smart contracts	4
Query the ledger status	4

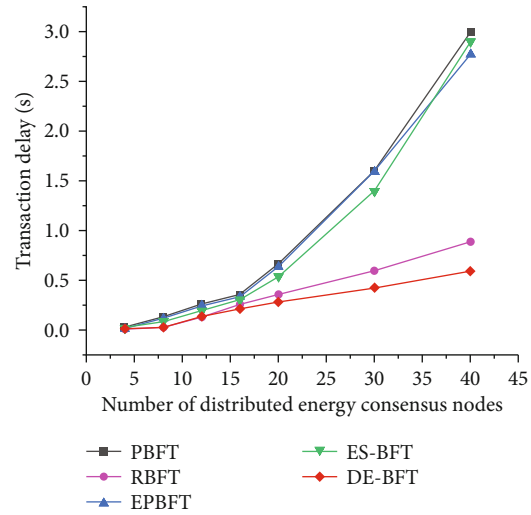

Figure 5: Comparison of transaction delays.

5.4. Stability Analysis of the System. The master node generated based on the VRF algorithm has randomness and unpredictability. The probability that the consensus node manipulated by malicious nodes is the master node is very small. When a malicious node operates on other slave nodes, it will not affect the correct consistency of the entire consensus result, because it is not the node responsible for producing blocks. Most nodes are honest. If a malicious node successfully deceives the master node, honest nodes in the consensus set can ensure that illegal blocks are not passed. At the same time, the health score set by the system can filter the behavior of malicious nodes, reduce their health score, and eliminate them from the consensus collective. Furthermore, the health score is

Table 4: Experimental parameter configuration table.

Parameter type	Parameter value
Test round	8
Number of transactions	1000
Number of concurrent processes	5

updated every n rounds, which also limits the ability of malicious nodes to manipulate security parameter choices to manipulate the identity of the master node. In contrast, the PBFT algorithm can neither identify Byzantine nodes nor guarantee the privacy of key nodes. The chosen master node is vulnerable to malicious nodes.

5.5. Communication Complexity Analysis. In this paper, the communication complexity is set as the number of times the system needs to communicate between nodes to complete a new block submission. In this section, the paper will select 4 similar algorithms for horizontal comparison and calculate the communication complexity in distributed energy trading, respectively. The statistics are shown in Table 2.

In the PBFT algorithm, the number of communications in the *request* phase is 1. The *preprepare* phase is $n-1$. The *prepare* and *commit* phases are n^2-n. The *response* phase is n. The total number of communications is $f(n) = 1+n-1+2(n^2-n)+n = 2n^2$. Therefore, the communication complexity of PBFT is $O(n^2)$.

The algorithm EPBFT [21] has a total of 5 stages. In *preprepare* and *prepare-1* phases, the number of communication is n. In *commit-1* phase, the primary only sends a *commit-1* message to backup 1. So the number of communication is 1. In *prepare-2* phase, the honest node will send messages to n nodes. The communication times in this stage is n^2, and the communication times in the final *commit-2* phase is n. In summary, the total communication time is $f(n) = n^2+3n+1$, and the communication complexity is $O(n^2)$, in distributed energy transaction.

The algorithm ES-BFT [22] also has 5 stages. Its total number of communications is $f(n) = 2n^2+n+1$.

Compared with PBFT, the algorithm RBFT [23] lacks the *prepare* phase. So there are three stages in total, and the total communication time is $f(n) = n^2+n$. Communication complexity is both $O(n^2)$.

Due to the introduction of VRF, the algorithm DE-BFT communication times at each stage can be set as $k(k \le n)$. As can be seen from DE-BFT data consistency interaction protocol, the data interaction protocol goes through five stages. So the total communication time is $f(k) = 5k+2(k \le n)$. Therefore, the communication complexity of DE-BFT is $O(n)$.

5.6. Delay. Delay indicates the time interval from the client initiating a transaction request to the request being confirmed and the chain being connected. The smaller the delay is, the faster the transaction is confirmed. In this paper, 7 groups of delay test experiments were set up according to different numbers of distributed energy consensus nodes.

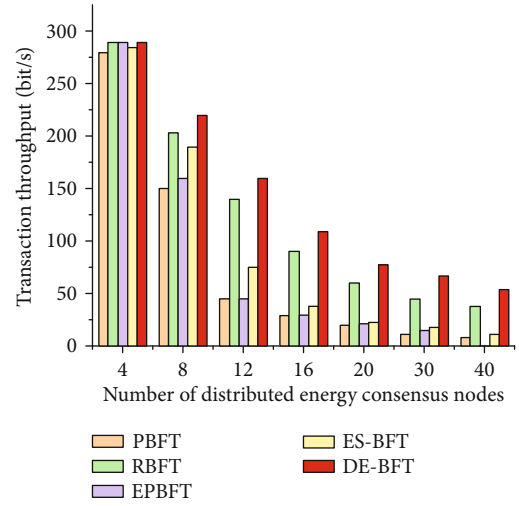

Figure 6: Comparison of transaction throughput.

Each group of experiments tested the chain time required by 12 groups of the same type of transaction request under PBFT algorithm environment, EPBFT algorithm environment, ES-BFT algorithm environment, RBFT algorithm environment, and consensus protocol environment. The distribution of specific test transaction types is shown in Table 3, and its average value is taken as the final delay data.

Figure 5 shows the comparison of transaction delay results of various consensus algorithms in the application of distributed energy trading. With the increasing number of nodes, due to the differences in communication complexity and consensus mechanism among consensus algorithms, the delay of other consensus algorithms has an obvious linear relationship with the number of nodes. The more nodes, the greater the delay. In contrast, DE-BFT and RBFT proposed in this paper have relatively slow delay growth rate. When the number of nodes is small, RBFT and DE-BFT have similar delay, but with the increase of the number of nodes, the consensus algorithm proposed in this paper has more advantages. Distributed energy transaction will face a large number of distributed energy nodes, and the consensus algorithm proposed in this paper is more suitable for the increasing of distributed nodes.

Therefore, the consensus protocol of the energy blockchain solution proposed in this paper has a more stable performance with low latency when dealing with complex and flexible energy application scenarios.

5.7. Throughput. In this paper, 7 experiments of throughput have been set up according to different numbers of distributed energy consensus nodes. Each experiment has passed professional pressure test in PBFT algorithm environment, EPBFT algorithm environment, ES-BFT algorithm environment, RBFT algorithm environment, and consensus protocol environment in this paper with the same parameters by several professional pressure test tools. The parameter configuration is shown in Table 4, and the experimental results are shown in Figure 6.

When the number of distributed energy consensus nodes is greater than 12, the throughput of PBFT, ES-BFT, and EPBFT decreases significantly. This is because the dramatic increase in traffic during consensus puts pressure on network bandwidth, increasing the time required for consensus. Therefore, ES-BFT, PBFT, and EPBFT are not suitable for multinode blockchain environment.

RBFT and DE-BFT are in the same system environment of consensus nodes. When there are fewer consensus nodes, the throughput trends of RBFT and DE-BFT are consistent. Because the number of nodes is small, the number of communications is small. When there are more nodes, the throughput of DE-BFT is significantly higher than that of RBFT. Because the total number of communications in DE-BFT increases slowly, and the communication complexity is $O(n)$. In addition, DE-BFT uses VRF to select the master node, which can reduce the possibility of changing views and has higher reliability.

In general, the consensus protocol in this paper uses the health score reputation system to designate consensus nodes more reasonably and achieves good performance in the energy industry from the aspect of actual indicators.

6. Conclusion

Blockchain-based distributed energy transactions can effectively reduce grid dispatch costs and increase transaction transparency. This paper proposes a blockchain consensus mechanism for distributed energy transactions by analyzing the decentralization characteristics of blockchain and the noncentralized characteristics of distributed energy, aiming at the real-time and secure requirements of distributed energy trading platforms. This paper improves the traditional PBFT consensus algorithm of the consortium chain in the two stages of block node election and main chain consensus. First, in the block-generating node election stage, the health score combined with the verifiable random function is used to randomly select the master node from the candidate node set, and based on the health score, the node with the highest health score is selected as the block producer from the randomly selected candidate master nodes. In the consensus stage of the main chain, an efficient data consistency interaction protocol is adopted to reduce the communication complexity between nodes. Through experiments and analysis, it is proved that the improved consensus algorithm DE-BFT can reduce the communication complexity between nodes in the consensus stage down to $O(n)$. At the same time, compared with the traditional PBFT consensus algorithm and other improved PBFT algorithm, e.g., EPBFT, DE-BFT provides higher throughput and lower latency. The improved consensus algorithm ED-BFT not only improves the efficiency of distributed energy transactions but also ensures the security in the transaction.

Data Availability

No data were used to support this study.

Conflicts of Interest

The authors declare that there are no conflicts of interest regarding the publication of this article.

Acknowledgments

This work was supported by the Research and Demonstration Project of Key Technologies of Energy Blockchain Application for Industrial Internet (037800KK52200005 and GDKJXM20201754).

References

[1] Y. He, W. Xiong, B. Y. Yang et al., "Distributed energy transaction model based on the alliance blockchain in case of China," *Journal of Web Engineering*, vol. 20, no. 2, pp. 359–386, 2021.

[2] Z. Yao, H. Pan, X. Si, and W. Zhu, "Decentralized access control encryption in public blockchain," in *International Conference on Blockchain and Trustworthy Systems*, pp. 240–257, Springer, Singapore, 2019.

[3] S. Guo, C. Huang, Y. Yan, L. Chen, and S. Shao, "Trusted digital asset copyright confirmation and transaction mechanism based on consortium blockchain," in *International Conference on Artificial Intelligence and Security*, pp. 703–714, Springer, Cham, 2021.

[4] P. B. Honnavalli, A. S. Cholin, A. Pai, A. D. Anekal, and A. D. Anekal, "A study on recent trends of consensus algorithms for private blockchain network," in *International Congress on Blockchain and Applications*, pp. 31–41, Springer, Cham, 2020.

[5] Y. F. Li, Y. L. Chen, T. Li, X. J. Ren, and C. M. Chen, "A regulatable data privacy protection scheme for energy transactions based on consortium blockchain," *Security and Communication Networks*, vol. 2021, Article ID 4840253, 11 pages, 2021.

[6] H. Zhao, M. Zhang, S. Wang, E. Li, Z. Guo, and D. Sun, "Security risk and response analysis of typical application architecture of information and communication blockchain," *Neural Computing and Applications*, vol. 33, no. 13, pp. 7661–7671, 2021.

[7] M. Saracevic and N. Wang, "New model of sustainable supply chain finance based on blockchain technology," *American Journal of Business and Operations Research*, vol. 3, no. 2, pp. 61–76, 2021.

[8] Z. Xu, "Computational intelligence based sustainable computing with classification model for big data visualization on map reduce environment," *Discover Internet of Things*, vol. 2, no. 1, p. 2, 2022.

[9] M. Castro and B. Liskov, "Practical byzantine fault tolerance," *OsDI*, vol. 1999, no. 99, pp. 173–186, 1999.

[10] K. Driscoll, B. Hall, H. Sivencrona, and P. Zumsteg, "Byzantine fault tolerance, from theory to reality," in *International Conference on Computer Safety, Reliability, and Security*, pp. 235–248, Springer, Berlin, Heidelberg, 2003.

[11] M. J. M. Chowdhury, M. Usman, M. S. Ferdous et al., "A cross-layer trust-based consensus protocol for peer-to-peer energy trading using fuzzy logic," *IEEE Internet of Things Journal*, vol. 3, no. 8, pp. 1–1, 2021.

[12] K. V. Amit, H. W. Zhong, and N. S. Yatindra, "Consensus mechanism for peer-to-peer energy trading," in *Recent Trends in Electronics and Communication*, pp. 355–364, Springer, Singapore, 2022.

[13] Y. Pan, "A novel trade transaction agreement algorithm using blockchain consensus mechanism," *Scientific Programming*, vol. 2021, Article ID 5343337, 9 pages, 2021.

[14] A. Sheikh, V. Kamuni, A. Urooj, S. Wagh, N. Singh, and D. Patel, "Secured energy trading using byzantine-based blockchain consensus," *IEEE Access*, vol. 8, pp. 8554–8571, 2020.

[15] X. Q. Xu, G. Sun, and H. F. Yu, "Au efficient blockchain PBFT consensus protocol in energy constrained IoT applications," in *2021 International Conference on UK-China Emerging Technologies (UCET)*, pp. 152–158, IEEE, Chengdu, China, 2021.

[16] J. W. Hu, Y. L. Chen, X. J. Ren, Y. Yang, X. Qian, and X. Yu, "Blockchain-enhanced fair and efficient energy trading in industrial internet of things," *Mobile Information Systems*, vol. 2021, Article ID 7397926, 13 pages, 2021.

[17] W. Hu and L. Huanhao, "A direct transaction model for energy blockchain mobile information system based on hybrid quotation strategy," in *International Conference on Human-Computer Interaction*, pp. 33–51, Springer, Cham, 2020.

[18] Y. Jiang and Z. Lian, "High performance and scalable byzantine fault tolerance," in *2019 IEEE 3rd information technology, networking, electronic and automation control conference (ITNEC)*, pp. 1195–1202, IEEE, Chengdu, China, 2019.

[19] G. L. Guo, Y. Zhu, E. Chen, G. Zhu, D. Ma, and W. C. C. Chu, "Continuous improvement of script-driven verifiable random functions for reducing computing power in blockchain consensus protocols," *Peer-to-Peer Networking and Applications*, vol. 15, no. 1, pp. 304–323, 2022.

[20] H. Wang and W. A. Tan, "Block proposer election method based on verifiable random function in consensus mechanism," in *2020 IEEE International Conference on Progress in Informatics and Computing (PIC)*, vol. 18, pp. 304–308, Shanghai, China, 2020.

[21] H. Tang, Y. Sun, and J. Ouyang, "Excellent practical byzantine fault tolerance," *Journal of Cybersecurity*, vol. 2, no. 4, p. 167, 2020.

[22] R. H. Wang, S. Y. Xing, and Q. Q. Xu, "Efficient byzantine fault-tolerant algorithm with supervision mechanism," *Computer Engineering and Applications*, vol. 57, no. 18, pp. 142–148, 2021.

[23] P. L. Aublin, S. B. Mokhtar, and V. Quéma, "Rbft: redundant byzantine fault tolerance," in *2013 IEEE 33rd International Conference on Distributed Computing Systems*, pp. 297–306, IEEE, Philadelphia, PA, USA, 2013.

Hindawi
Wireless Communications and Mobile Computing
Volume 2022, Article ID 6796160, 11 pages
https://doi.org/10.1155/2022/6796160

Research Article

New Path of Stranger Interaction Platform and Network Cross-Cultural Communication in the Omnimedia Era

Ruixian Li

School of Journalism and Communication, Wuhan University, Wuhan, 430000 Hubei, China

Correspondence should be addressed to Ruixian Li; liruixian@jou.edu.cn

Received 25 May 2022; Accepted 24 June 2022; Published 12 July 2022

Academic Editor: Jun Ye

The Internet is a new medium for disseminating information. The emergence of online information dissemination tools has overcome the limitations of time and space in the early information dissemination tools, and online information dissemination has extraordinary attractiveness in all walks of life. Online communication is the dissemination of information, including news, knowledge, and other information, through computer networks. The benefits of high speed, high volume, interactivity, immediacy, vividness, openness, ease of discovery, and online communication over time, across different fields and media, enable people to appreciate online media in a new way. The Internet is rapidly becoming the new preferred means of communication due to its unparalleled advantages. The research on cross-cultural communication on the Internet is based on the globalization of economy, the globalization of information dissemination, and the development of cultural marketing. This paper has conducted a research experiment on the new path of stranger interaction platform and network cross-cultural communication in the all-media era. The experimental data show that the paths of cultural dissemination account for 39% of introductions by others and 26% of social platforms such as WeChat. Promotional information on other platforms accounted for 17%, app stores accounted for 12%, and others accounted for 6%. It can be seen that the introduction and recommendation of others are the main way of cross-cultural communication. After studying the interactive platform for strangers in the all-media era, we learned from the Internet that cross-cultural communication has gradually become the main way.

1. Introduction

In the 1990s, globalization became a concern. Globalization mainly refers to economic globalization, which develops rapidly with the development of international division of labor and international cooperation. It is a real and irrefutable reality. However, globalization is not only economic globalization but also cultural globalization. Its cross-border activities will inevitably bring about the collision, exchange, and integration of different national cultures. Since the 1990s, the global economic integration has developed well, and cross-cultural communication has gradually become a key issue for communication to promote development. In cross-cultural communication, western capitalist countries have become the most important intermediaries with their relatively developed economies and communication industries. Due to globalization, some cultures influence and merge with others, and some cultures consciously develop into "strong cultures." Under the background of today's economic globalization, various cultures are experiencing a period of conflict, division, and integration, and cross-cultural communication is becoming an increasingly important means of cultural communication. Its influence surpasses even any other communication content, becoming one of the most powerful factors of economic and cultural globalization [1, 2].

With the acceleration of the process of globalization, the rapid development of information technology, and the rise of knowledge economy, the clash of civilizations caused by different cultural forms is a major challenge facing mankind in the 21st century. On the one hand, the Internet facilitates the exchange of different cultural forms because it provides speed and convenience for cultural exchange [3, 4]. On the other hand, due to the hegemonic and

subversive nature of western cultural exchanges and the new injustices and inequalities it brings, it creates an inherent crisis in cross-cultural communication online. Ignoring this crisis will deepen the inherent contradictions of human society and hinder the exchange and spread of human culture.

This paper studies the new path of stranger interaction platform and network cross-cultural communication in the all-media era. Its data shows that "online radio channels" accounted for 15.4%, "video channels" accounted for 16.6%, "live channels" accounted for 12.4%, and "news information channels" accounted for 26.3% of the total selections. The specific gravity is significantly higher than several other options. Among several other channels, "translation channels" accounted for 18.6% of all ticks. The lowest proportions are e-commerce channels and tourism culture channels, accounting for 4.7% and 5.4%, respectively. It can be seen from the above data that the news information channel, as the main channel of the platform, has been widely recognized by users. The news content on the platform is high-quality and the presentation forms are rich, so its news information channel is widely loved by users and has become the preferred channel for users on this new media platform. This is also of great significance for promoting the development of new paths of current network cross-cultural communication.

2. Related Work

This paper studies some technologies of the new path of network cross-cultural communication, which can be fully applied to the research in this field. Lee et al. proposed a theoretical framework. They explained that the effect of exclusion depends on the extent to which exclusion is transmitted in a cultural normative or counter-normative manner, rather than in an explicit or implicit manner [5]. Qin and Fedorovskaya believed that in the context of modern globalization, research in the field of cross-cultural communication has become particularly important [6]. Combined with individual interviews, Huang and Yang's study further analyzed the deep-seated reasons for the formation of the mixed mode of implicit theory in cross-cultural groups. They found that school evaluation methods and the definition of student achievement affect teachers' implicit creativity theory [7]. Based on the community network structure and the improved classical network propagation model, Chen constructed a susceptible infection recovery model for the grassroots propagation of engineering safety culture. He discussed the law of basic-level dissemination of engineering safety culture [8]. Stanislavova and Solovyova worked on issues related to "intercultural communication" issues. This shows the complexity and relevance of this issue to the stage of modern cultural development [9]. These methods provide some references for our research, but due to the short time and small sample size of the relevant research, they have not been recognized by the public.

Based on the interactive platform of strangers, this paper has reviewed the following relevant materials to optimize the research on the new path of network cross-cultural communication. The study by Liao et al. is based on the new characteristics of news consumption and the resulting new problems. They made an in-depth analysis of the capabilities that contemporary news audiences should possess, including the selection, decoding, and encoding of news information [10]. Xu focused on the business value and business intelligence of social media, such as examining customers' online commenting behavior and the impact of social media on business performance [11]. Moreno aimed to reflect on the new status of museums in the digital age. Works using new media must be understood as a space for nonhierarchical communication, where the role of the artist is diminished and the public becomes the user to complete the opening process [12]. Radu et al. believed that social media can be useful by posting information about discounts, offers, and the advantages of accessing products offered by an institution. It is used in advertising and promotion strategies [13]. Deng et al. believed that media convergence enables professionals in the mass media field to use various media to publish news and present information and entertainment [14]. The findings of Ismail et al. showed that the spread of liberal ideology and secular ideology goes hand in hand. Its widespread growth is consistent with the rapid development of communication media in the era of convergence [15]. These methods provide sufficient literature basis for us to study the new path of stranger interaction platform and network cross-cultural communication in the all-media era.

3. All-Media Interactive Platform and Network Cross-Cultural Communication

Cross-cultural communication is a comparative study of information dissemination between different cultural boundaries. The rapid development of information technology, the simultaneous cooperation between globalization and regional economies, and the efforts of multinational corporations to expand their overseas activities have defined the framework for cross-cultural communication in the new century. In this paper, by studying the interactive platform of strangers in the all-media era, the development of a new path of network cross-cultural communication has reached a new level.

3.1. Omnimedia Stranger Interaction Platform. Standing at the front end of the 21st century, it is surprising to find that the media world is showing an increasingly wonderful landscape. With the continuous emergence and development of physical media such as mobile phones and tablets or virtual media such as Weibo, Tianya Community, and Renren.com, the boundaries between spoken media, print media, electronic media, and online media, which were originally separate, are gradually disappearing. It is replaced by an era of omnimedia that is changing with each passing day [16].

Regarding the concept of all media, at present, there is no unified normative definition in academia. The term originated from a cleaning company in the United States that provided full service in residential areas. Founded in 1999, the company owns and operates a variety of media formats, including magazines, books, news apps, TV shows,

radio shows, and websites that promote home services and products, although the media forms covered by the company at that time, compared with the wide variety of media forms today, may only show a concept of multimedia, which is not comprehensive. However, at the end of the last century, the development trend of the media, which was not gradually prosperous until this century, was revealed. In the first decade of this century, the connotation of omnimedia has been continuously enriched. So far, it includes newspapers, magazines, radio, television, audio and video, film, publishing, the Internet, telecommunications, and satellite communications that use human sight, hearing, sight, and touch. So far, there are two main research dimensions on the concept of omnimedia: one is omnimedia based on the fusion of multiple media forms and the other is omnimedia based on the fusion of different media management models.

Omnimedia has developed from traditional media and new media. Therefore, before discussing the communication modes of all media, it is necessary to first explain the communication modes of traditional and new media.

Traditional media disseminate information in a linear fashion. The most important features of linear communication are the absence of interruptions and the certainty of direction. Propagation is described as a linear, one-way process. The first stage is that the source sends the information, the sender converts it into a signal to be transmitted, and after transmission, the receiver converts the received signal into information and sends it to the receiver. That is to say, in this process, it is a linear communication process starting from the communicator, going through the medium, and ending with the recipient. For example, in television, a program is created and broadcast. Each program has a time slot, and viewers who want to watch it must strictly adhere to the time of the broadcast program, which can neither be advanced nor delayed. In this mode, viewers' choices are limited and they cannot watch the show in its entirety to their liking. In traditional mass media, the individual needs of the audience are partially satisfied by their own choices of information products on the mass market [17].

Nonlinear propagation is one of the main characteristics of new media. Nonlinear communication emphasizes the autonomy of the listener, who can selectively absorb information according to their preferences. Circular patterns are described in the article "How Propagation Works." This model is very different from the straight line model. In the process of communication, the concept of the communicator and receiver does not exist, but both appear in the feedback loop as participants in the communication behavior by sending and receiving information. A good example of this is the use of digital television. Due to the development of digital technology, TV programs are clearer, faster, and more informative. Different from traditional TV, the viewing of digital TV is not limited by the broadcast time of the program, and the audience can watch the program on demand at any time according to their viewing habits.

The nature of information dissemination in the traditional media era is one-way, while in the new media era, it is interactive, and the nature of information dissemination in the omnimedia era is multidimensional development. The difference between all-media news communication and traditional news communication is shown in Figure 1.

From the communicator's point of view, information does not depend on a single channel, television, radio, the Internet, etc. Communicators can spread information in all directions through different media in order to convey information as effectively as possible in the shortest time possible. In the media age, the boundaries between senders and receivers of information are becoming more and more blurred, the sender is also the receiver, and the content of information is becoming more and more abundant. This is reflected in the fact that many stories are not first reported by professional media organizations but are recorded by eyewitnesses at the scene with mobile phones and posted online [18].

In the media age, information travels faster and easier. What happens in one place can be monitored through different terminals, and events are relayed immediately.

Stranger socializing is when two people that do not know each other socialize. It obtains the opportunity to get in touch through a certain channel and produces social behavior, which is a social behavior of material exchange and spiritual exchange. Stranger social platforms refer to tools and channels used by strangers to socialize. Stranger social platforms survive with different forms of products, such as live broadcasts, games, and interest communities. Not long after the socialization of strangers became popular on the Internet, it appeared in everyone's field of vision. Despite its various controversies, this way of socializing has evolved over two decades. Technological innovation has also played a positive role in the development of strangers' social platforms, and the major leap in the development of strangers' social platforms depends on the popularization of LBS technology. LBS, a location-based service, needs to be implemented on mobile devices. At the beginning of the 21st century, application software with positioning as the core function appeared widely, and social networking with strangers developed rapidly. The conceptual diagram of the stranger interactive platform is shown in Figure 2.

In the rapidly developing stranger social market, different platforms have their own unique characteristics and appeal. This gives users a great choice and also makes the stranger social market more vibrant [19]. From the point of view of the purpose of users using stranger social platforms, stranger social platforms are divided into two categories. They are social platforms for strangers for the purpose of obtaining information and making friends. From the perspective of the friendship mode of stranger social platforms, stranger social platforms are divided into three categories. These three categories are the three most common matching modes in stranger social platforms: sliding matching, LBS-based geographic location matching, and smart matching. With the continuous improvement of technology and products, there are many new models emerging, but the stranger social market is still dominated by these three models [20].

This paper analyzes the algorithm of the interactive platform based on cluster analysis. Cluster analysis is to cluster different datasets, and each different dataset has its own

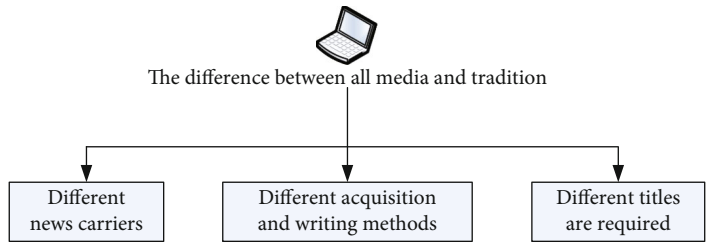

Figure 1: The difference between all-media news communication and traditional news communication.

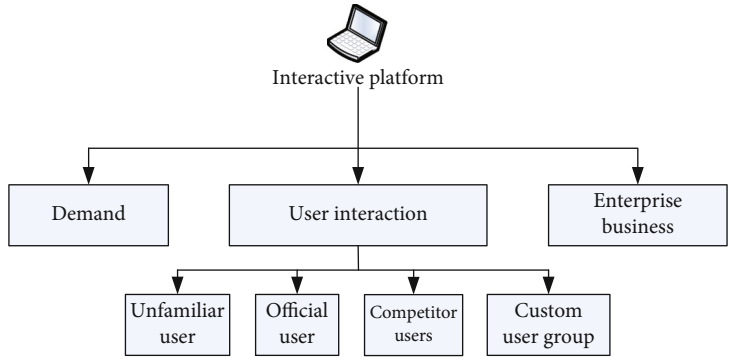

Figure 2: Conceptual diagram of the stranger interactive platform.

different needs. The general situation of the cluster analysis is as follows. (1) The algorithm is adaptable to multiple nodes. (2) It can also work well for mixed data. (3) It can handle datasets of any shape well. (4) The less input from people, the better. (5) It is not sensitive to useless data or duplicate data. (6) The order of the user's input data has no effect on the clustering results. (7) The dataset has a multiattribute problem. (8) It employs constraint-based clustering. (9) The clustering results are easy to understand.

The degree of difference or similarity between different datasets can be determined by calculating the squared difference between two points m_i and m_j. The calculation formula of the squared difference used is the Euclidean distance, and the specific formula content is as follows:

$$d(i,j) = m_{i1} - m_{j1}^2 + m_{i2} - m_{j2}^2 + \cdots + m_{ik} - m_{jk}^2, \quad (1)$$

where i belongs to $(m_{i1}, m_{i2}, \cdots, m_{ik})$ and j belongs to $(m_{j1}, m_{j2}, \cdots, m_{jk})$; they all represent a k-dimensional data. Manhattan distance is another commonly used square difference calculation formula; the formula is as follows:

$$d(i,j) = m_{i1} - m_{j1} + m_{i2} - m_{j2} + \cdots + m_{ik} - m_{jk}. \quad (2)$$

Both Euclidean distance and Manhattan distance need to meet the following requirements: the distance between any two objects is not negative; the distance between the object and itself is 0. The distance from one object to another is the same as the distance from the other to this object; the distance between two objects must be the shortest distance.

The Minkowski distance is a generalization of Euclidean distance and Manhattan distance [21]; the formula is as follows:

$$d(i,j) = \left(m_{i1} - m_{j1}^p + m_{i2} - m_{j2}^p + \cdots + m_{ik} - m_{jk}^p \right)^{\frac{1}{p}}, \quad (3)$$

where p is a positive integer. If each object has a weight, the Euclidean distance is calculated as follows:

$$d(i,j) = w_1 m_{i1} - m_{j1}^2 + w_2 m_{i2} - m_{j2}^2 + \cdots + w_k m_{ik} - m_{jk}^2. \quad (4)$$

The data processing method of clustering objects generally adopts the method of sum standardization, which is to first obtain the sum of the data corresponding to all objects and then divide each object by this sum, and the formula is as follows:

$$m_{ij} = \frac{m_{ij}}{\sum_{i=1}^{x} m_{ij}} \quad (i = 1, 2, \cdots, x; j = 1, 2, \cdots, y). \quad (5)$$

The object obtained in this way satisfies that the sum of all objects is 1, as shown in the following formula:

$$\sum_{i=1}^{x} m_{ij} = 1 (j = 1, 2, \cdots, y). \quad (6)$$

The k-means algorithm is a simple clustering method, which uses the difference between samples as a benchmark. Assuming that the clustered k clusters are $M_1, M_2, \cdots, M_k$

and the initial cluster centers of each cluster are $r_1, r_2, \cdots, r_k$, the dataset M is represented as follows:

$$M = \{m_i | m_i \in R^y, i = 1, 2, \cdots, y\}. \tag{7}$$

The Euclidean distance between two data is as follows:

$$d(m_i, n_j) = (m_{i1} - n_{j1})^2 + (m_{i2} - n_{j2})^2 + \cdots + (m_{iy} - n_{jy})^2. \tag{8}$$

The objective function formula is as follows:

$$E = \sum_{i=1}^{k} \sum_{p \in m_i} d(m_j, r_i). \tag{9}$$

The mean shift algorithm is a density estimation algorithm that requires no input. The mean shift algorithm can be called in a continuous loop, which can quickly make the sample points converge to the place where the density function is the largest [22].

Assuming a sample set M_d in a space (d represents the dimension of the sample), there are y sample points m_i in its space, $i = 1, 2, \cdots, y$. By taking one of the sample points m randomly from the sample, then the formula of the kernel density of the sample can be formed according to the kernel function $k(m)$ of the sample point. The density expression for this sample point is as follows:

$$f(m) = \frac{1}{y} \sum_{i=1}^{y} K_H(m - m_i). \tag{10}$$

The expression for $K_H(m)$ is as follows:

$$K_H(m) = |H|^{-\frac{1}{2}} K\left(H^{-\frac{1}{2}} m\right). \tag{11}$$

If the similarity between the sample and the kernel should be represented by this kernel function $k(m)$, then the improved formula of the algorithm is as follows:

$$f_{h,k}(m) = \frac{C_{k,d}}{yh^d} \sum_{i=1}^{y} k\left(\left\| \frac{m - m_i}{h} \right\|\right), \tag{12}$$

where h is the radius of the kernel function and $C_{k,d}$ and yh^d are the unit density [23].

The mean shift vector looks like this:

$$x_{h,G}(m) = \sum_{i=1}^{y} m_i g\left(\left\| \frac{m - m_i}{h} \right\|\right) - m, \tag{13}$$

$$x_{h,G}(m) = \sum_{i=1}^{y} g\left(\left\| \frac{m - m_i}{h} \right\|\right) - m. \tag{14}$$

Let $xh, G(m) = 0$; the final coordinates of the vector can be obtained:

$$m = \sum_{i=1}^{y} m_i g\left(\left\| \frac{m - m_i}{h} \right\|\right), \tag{15}$$

$$m = \sum_{i=1}^{y} g\left(\left\| \frac{m - m_i}{h} \right\|\right). \tag{16}$$

3.2. Network Cross-Cultural Communication. Intercultural communication has a long history and has existed in a broad sense since the emergence of human society. In theory, intercultural communication is the communication of information and cultural exchanges among people, organizations, and countries belonging to different cultural systems. The essence of intercultural communication is its "interculturality."

Cross-cultural communication penetrates into the entire human society and is the driving force for change and development. It can be said that without the interaction between cultures, there will be no survival and development of human society, let alone human development and civilization [24, 25]. The British philosopher pointed out: "The communication between different civilizations is the cornerstone of the development of human civilization. Greece learns from Egypt, and Arabia learns from the Roman Empire. Medieval Europe learns from Arabia, and Renaissance Europe imitates the Byzantine Empire." Through the development of primitive society, slave society, and feudal society, human society has brought people from different regions, races, and nationalities together through cross-cultural interaction. It promotes the development of human culture and social change [26].

Chinese cross-culture is in a passive position in the international "image war." Imports of expensive Hollywood movies almost dominate China's cinemas every year. Japanese cartoon books and cartoons fill Chinese newsstands and TV channels. Internet broadcasting technology has developed steadily, and the latest Korean and American dramas are translated into Chinese with subtitles within 24 hours. More than ever, people can enjoy cultural products created through cross-cultural interaction and experience the latest cultural developments brought about by globalization. However, cross-cultural differences and multiple cultural identities are not what one might think. According to the clothing, etiquette, and behavior of the people in these films, as well as the cultural phenomenon they represent, it is easy to form an overall image of a country. Ideas such as western cultural centralism, cultural imperialism, postcolonialism, old and new racism are implicit in cross-cultural products. While these products satisfy the cultural life of China, they also deconstruct and construct people's cognition and attitude towards the world.

From a broader perspective, there are two main forms of intercultural interaction. The first one is regional cultural exchanges. It refers to the interaction of people from different cultural backgrounds, ethnic groups, and social groups

in different regions. It generally refers to the interaction between traditional culture and modern culture, national culture, and group culture, and its internal interaction within a country or region, immigration, urbanization, economic development, and education level are important factors affecting the interaction between cultures. The second one is international cultural exchange. It refers to the interaction and communication between people from different countries and cultures [27].

In a general sense, cross-cultural communication refers to cultural exchanges and cultural communication activities between different cultural forms and communication objects under different cultural backgrounds. This communication and dissemination process reflects the transmission of cultural information and the maintenance of cultural interaction among different cultural communication objects. Intercultural communication is the process of exchange, mutual penetration, contact, transformation, and sharing of cultural elements in different cultural forms on a global scale. These activities and processes involve countries, nations, groups, and even human societies of different cultures around the world.

From the perspective of cultural dissemination, the greatest significance of Chinese culture going across cultures to the world lies in the effectiveness of its dissemination form. That is, the cross-cultural factor is added to the traditional form of communication and its related factors, which greatly expands the scope and depth of the field. The Lasswell 5W propagation mode is shown in Figure 3.

The specific content process of the 5W model: who, what, through what channel, to whom, and what effect, will be produced. The 5W propagation model is the most commonly used propagation model in communication.

The study of the path of communication is a key issue in the study of cross-cultural communication theory. At present, there are many academic viewpoints on this research topic in the academic world, and a lot of inductive analyses have been done on the paths and methods of cross-cultural communication. Intercultural communication is the process of communicating, sharing, and integrating cultural information between different cultural forms. Under normal conditions, the process of cross-cultural communication is the interaction between the communication subject and the communication topic. That is to say, the communication subject does not blindly output information, and the communication object is not completely passive when receiving information, but both objects are dynamic, interactive, and mutually influencing. The interaction and mutual influence between the dissemination subject and the dissemination audience are accomplished by the media transmitting information.

Intercultural communication is an important part of the overall communication activities of human society, representing the important interaction among individuals, groups, nations, and countries. Intercultural interactions maintain the dynamic balance of social structures and systems. It "unites" people from different regions, groups, nations, and countries, promotes the development of world culture, and makes human culture have the characteristics of "worldliness." It can be said that intercultural communication has promoted the development of human culture and the emergence of world civilization.

Figure 3: Lasswell 5W propagation mode.

4. Multiangle Omnimedia and Cross-Cultural Communication

4.1. Cross-Cultural Communication of Chinese Element Advertisements. Advertising communication refers to the communication activities related to the brand, brand identity, brand positioning, and brand personality that the brand owner communicates to the target audience through communication tools. It takes planning as the core, it takes creativity as the key, and it pays the advertising management department in return. The main purpose of advertising communication is to promote brand image and establish brand identity. In order to achieve this goal, it needs the help of advertising creativity. Therefore, it puts into practice the advertising creativity with Chinese elements. On the one hand, because the foundation of brand internationalization is in the Chinese market, relying on the recognition psychology of Chinese audiences can rapidly expand market awareness. Secondly, Chinese element advertising also helps enterprises to create a unified brand image in various regions, enhance the professionalism of the brand in the minds of consumers, and improve the intimacy between consumers and the brand. In the practice of internationalization of Chinese brands, well-known enterprises such as Haier, Midea, Huawei, and Tsingtao Brewery have taken the lead in using Chinese-style advertising to create labels for national brands. However, due to the lack of experience of multinational enterprises and the backward awareness of advertising, products of the same level are frequently defeated in business competition with other countries.

In order to more intuitively reflect the competition in China's advertising industry, this paper makes a statistical analysis of the awards in China from 2011 to 2017 at the Cannes Lions International Festival of Creativity. As an industry event leading the development of global advertising, the Cannes Lions International Festival of Creativity represents the world's highest-quality advertising production technology and creativity. It is widely recognized by the international community and the industry. Therefore, the sample has a certain reference value. The proportion of award-winning advertising agencies at the Cannes Lions International Festival of Creativity in the past seven years is shown in Figure 4.

As can be seen from Figure 4, Chinese advertising agencies accounted for only 8% in the seven years, and US advertising agencies accounted for 10%. Multinational advertising agencies account for 82%, and multinational advertising agencies have covered almost all the advertising production services in the two countries in the past seven years. The trend of award-winning advertising agencies in China at

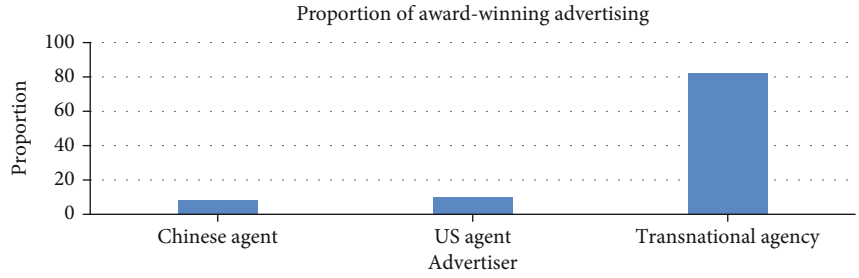

Figure 4: Proportion of award-winning advertising agencies at Cannes Lions in the past seven years.

the Cannes Lions International Festival of Creativity in the past seven years is shown in Figure 5.

As can be seen from Figure 5, in the 2011 competition, only one was on the list, and after that, Chinese advertising agencies encountered the same situation of only one for many years. In 2015, the number of participants from China was as high as 260, but the submitted works were eliminated except for two companies that won awards. It was not until 2017 that Chinese advertising agencies ushered in a small-scale "explosion," and a total of 3 Chinese advertising agencies made the list. It has occupied "half of the country" of China's advertising agencies for nearly seven years. These phenomena are enough to show that China's advertising industry is in a weak position in terms of competitiveness. The proportion of Cannes International Creative Award-winning advertisers in the past seven years is shown in Figure 6.

From the perspective of advertisers, the international awareness of Chinese advertisers has increased in the past seven years, accounting for 34%. American advertisers account for 20%, and multinational advertisers account for 46%. There is still a gap between Chinese advertisers and multinational advertisers. Statistics show that in the past seven years, the basis of multinational advertisers has dominated. The growth trend of award-winning advertisers in China at Cannes Lions in the past seven years is shown in Figure 7.

As can be seen from Figure 7, Chinese advertisers only briefly overtook in 2015, and the overall fluctuation was not large. In addition, all Chinese advertisers on the list also include government agencies and social welfare organizations. This part of the data dilutes the true level of Chinese brand internationalization to a certain extent. In fact, only two mobile Internet companies have the capability of "self-promotion," and the rest of the Chinese companies are almost all smart multinational advertising agencies.

Importantly, there is no shortage of excellent advertising creative companies in China. In this regard, the legend of Yingyang is the best example. The company once used the advertising slogan "Mom, I did the work for you" to make Diao brand washing powder famous overnight. It has successfully knocked on the door of thousands of Chinese consumers. Then, because of its deep understanding of the essence of Chinese culture, it has been trusted by many Chinese companies. It has successfully helped national brands to develop international markets and created many excellent advertising works that are deeply rooted in the hearts of the people. Therefore, the ability of Chinese enterprises to use "Chinese elements" to build national brands should be no less than that of multinational enterprises. Instead, it relies on long-term study of the Chinese market and Chinese culture. It can enhance its competitiveness by virtue of its low-cost and high-quality services and flexible operation methods, and it has become the main force for the dissemination of national culture. In addition, Chinese companies have spared no effort to incorporate "Chinese elements" into brand advertisements when developing new markets, adding value to their products with a unique and attractive culture. It gradually gained a firm foothold in the "foreigner circle." There is reason to believe that the successful dissemination of these "Chinese elements" will surely help Chinese brands to shape one legend after another.

4.2. Cross-Cultural Communication of Sino-Russian Headline Media. This part uses the questionnaire survey method to conduct the survey. A total of 225 questionnaires were distributed, and 220 valid questionnaires were recovered. The statistics and analysis results of the questionnaires are as follows.

In terms of the widespread use and promotion of Sino-Russian Toutiao, among the 220 questionnaires collected this time, the proportion of people who know the use of Sino-Russian Toutiao is shown in Table 1.

According to Table 1, there are 132 people who know about Sino-Russian headlines, accounting for 60% of the respondents. There are 30 people who do not know about Sino-Russian Toutiao, accounting for 14% of the respondents, and 125 people who are using Sino-Russian Toutiao, accounting for 57% of the respondents. Judging from the number and proportion, the respondents are not very familiar with Sino-Russian Toutiao, but even fewer actually use them.

According to the statistics of the question of "Which channel did you learn about Chinese and Russian headlines?" in this survey, the proportion of introductions by others was 39% and the proportion of social platforms such as WeChat was 26%. Promotional information on other platforms accounted for 17%, app stores accounted for 12%, and others accounted for 6%. It can be seen that the introduction and recommendation of others are the main way for the interviewed groups to understand Sino-Russian headlines. Through inquiries to some of the interviewees, we learned that most of them learned about the new media platform Sino-Russian Toutiao through exchanges with

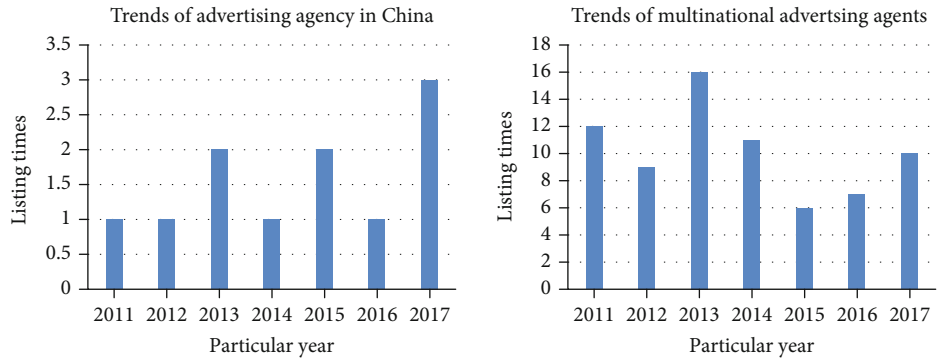

Figure 5: Trend of award-winning advertising agencies in China at Cannes Lions in the past seven years.

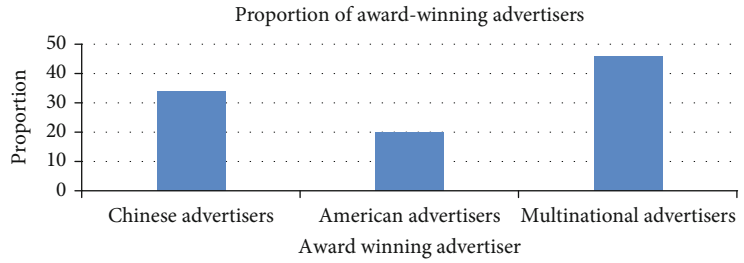

Figure 6: Proportion of Cannes International Creative Award-winning advertisers in the past seven years.

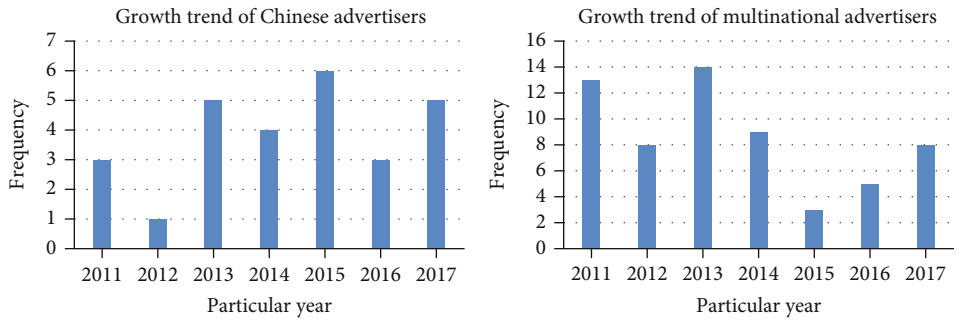

Figure 7: Growth trend of award-winning advertisers in China at Cannes Lions in the past seven years.

Table 1: The proportion of people who know that they use Sino-Russian headlines.

	Number of people	Proportion
Know	132	60%
I do not know	30	14%
In use	125	57%

teachers and people who have been studying longer than them after learning Chinese. Relatively few people learned about Sino-Russian headlines after seeing promotional information on other online platforms.

Sino-Russian headlines are functionally divided into news channels, online radio channels, video channels, live channels, translation channels, e-commerce channels, and tourism and culture channels. Each channel has different characteristics and complements each other in content and presentation form to meet the diverse needs of users. In this questionnaire, we investigated which channels the respondents often use or like, so as to grasp the attractiveness of different channels to users. The statistical results are shown in Figure 8.

As shown in Figure 8, "online radio channels" accounted for 15.4%, "video channels" accounted for 16.6%, and "live channels" accounted for 12.4%. "News and information channel" was checked 115 times, accounting for 26.3% of all checks. Its weight is significantly higher than several other options. Among the other channels, the number of "translation channels" checked was 81, accounting for 18.6% of the total number of checks, and the proportion was slightly

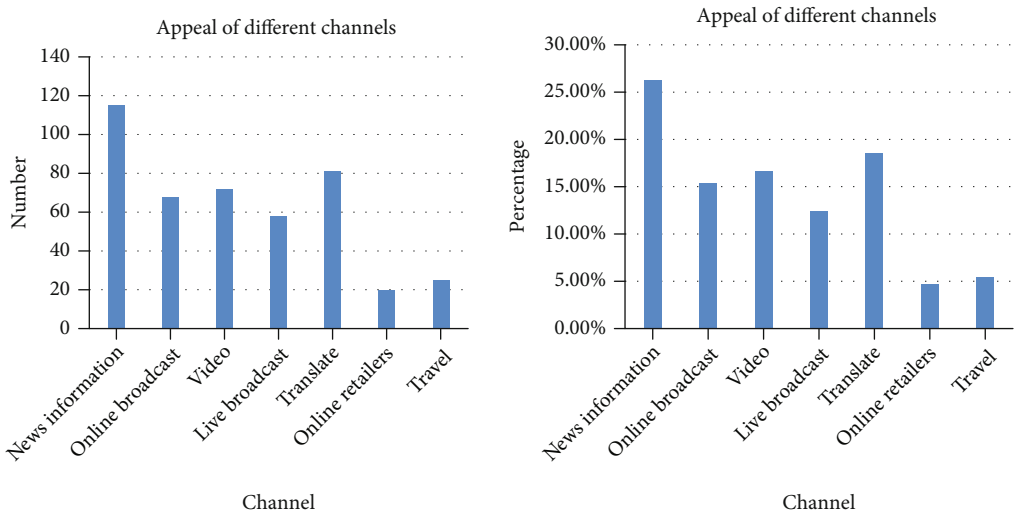

Figure 8: The attractiveness of different channels to users.

higher. The lowest proportions are e-commerce channels and tourism culture channels, accounting for 4.7% and 5.4%, respectively.

It can be seen that the news information channel, as the main function of "China-Russia Toutiao," has been widely recognized by users. "China-Russia Toutiao" is committed to building a flagship of Sino-Russian bilateral information and builds a bridge between China and Russia through authoritative and professional news. The news content on the platform is high-quality, and the presentation forms are rich, so its news information channel is widely loved by users. It has become the user's preferred channel on the new media platform. This has also laid a good foundation for "China-Russia Toutiao" to convey China's voice and deepen mutual understanding between China and Russia. The relationship between users' perception of the popularity of Sino-Russian headlines and user stickiness is shown in Table 2.

Judging from users' perception of the popularity of "China-Russia Toutiao," among the users who choose to continue to use the platform, those who think that the platform is well known account for only 13% of the total number. In contrast, more people think that the platform is less well-known and very low, accounting for 19% and 16% of the total number of people, respectively. This shows that in the eyes of some loyal users of "China-Russia Toutiao," the popularity of the platform still needs to be improved. The relationship between users' trust in Sino-Russian Toutiao and user stickiness is shown in Table 3.

From the point of view of user trust, 55% of the users who will continue to use "China-Russia Toutiao" said they trust the platform very much, and 39% of them trust the platform. Only 6% of them expressed low trust in the platform. Among the users who choose not to continue to use "China-Russia Toutiao," the proportions of "relatively distrust" and "very distrust" of the platform are 46% and 7%, respectively. The remaining 40% and 7% chose to be somewhat trusting and very trusting. Compared with popularity, users' preference for trust in "China-Russia Toutiao" is obviously more obvious, and respondents generally have a higher degree of trust in the platform. This not only shows that users feel that the news information published on the platform is authentic and reliable but also reflects that users have a better experience during use. It has a strong sense of security.

As shown in Tables 2 and 3, according to the trend test made on the statistical results, both groups of tests have reached a significant level. It shows that there is a correlation between the tested variables. This means that platform popularity and user trust will have an impact on user stickiness. Through investigation and analysis, it can be seen that platform popularity and user trust are closely related to user

Table 2: The relationship between users' perception of the popularity of Sino-Russian headlines and user stickiness.

	Will continue to use	Will not continue to use
High visibility	17 (13%)	2 (7%)
High popularity	66 (52%)	2 (7%)
Low popularity	25 (19%)	11 (79%)
Low visibility	20 (16%)	2 (7%)
Total	128	17

Table 3: The relationship between users' trust in Sino-Russian Toutiao and user stickiness.

	Will continue to use	Will not continue to use
Very trust	71 (55%)	2 (7%)
More trust	49 (39%)	6 (40%)
More distrustful	8 (6%)	7 (46%)
Very distrustful	0 (0%)	2 (7%)
Total	128	17

stickiness. Therefore, "China-Russia Toutiao" should focus on the improvement of these two aspects in the future development process. By increasing its popularity and expanding its influence, it has created a more reliable Sino-Russian bilateral information platform. It allows more users to choose and continue to use "China-Russia Toutiao," so as to achieve a better communication effect.

5. Conclusion

New media has brought a lot of convenience to people in terms of clothing, food, housing, and transportation. The interactivity and immediacy, diversity and hypertext, and exchange and virtuality of new media provide people with the possibility to surpass traditional media. Communication between people is no longer limited to traditional methods such as face-to-face conversations and written correspondence. Various new interpersonal communication tools have emerged, such as WeChat, Weibo, online games, and forums. Changes in the environment of social interaction have a large impact on the youth groups in society. How to thoroughly, deeply, and accurately understand and implement the impact of new media on interpersonal communication is a topic of constant debate in academic circles. Through the research on all media, this paper puts forward practical suggestions for building a new path of network cross-cultural communication, which has important theoretical and practical significance. Based on the research on the new path of stranger interaction platform and network cross-cultural communication in the all-media era, it is also of great significance to promote the development of current network cross-cultural communication.

Data Availability

The data that support the findings of this study are available from the corresponding author upon reasonable request.

Conflicts of Interest

The author declared no potential conflicts of interest with respect to the research, authorship, and/or publication of this article.

References

[1] Z. Zhao, "Analysis of museum cultural creation from the perspective of cultural industry," *Scientific Programming*, vol. 2022, Article ID 8138574, 8 pages, 2022.

[2] J. Y. Hong, H. Ko, and J. H. Kim, "Cultural intelligence and ARCS model for digital era," in *Proceedings of The 9Th International Conference on Web Intelligence, Mining and Semantics*, Seoul, Korea, June 2019.

[3] Z. Liang, Y. Duan, Q. Wang et al., "Study on the relationship between conspicuous need and group cultural identity of fashion cultural consumption," *Advances in Materials Science and Engineering*, vol. 2022, Article ID 3541548, 9 pages, 2022.

[4] S. M. Aljaberi and A. S. Al-Ogaili, "Integration of cultural digital form and material carrier form of traditional handicraft intangible cultural heritage," vol. 5, no. 1, pp. 21–30, 2021.

[5] J. Lee, L. J. Shrum, and Y. Yi, "The role of cultural communication norms in social exclusion effects," *Journal of Consumer Psychology*, vol. 27, no. 1, pp. 108–116, 2017.

[6] X. Qin and N. A. Fedorovskaya, "Specifics of Russian-Chinese cross-cultural communication in the field of fine art of the second half of the 20th — early 21st century," *Observatory of Culture*, vol. 17, no. 6, pp. 582–593, 2021.

[7] S. Huang and B. Yang, "A comparative study on Chinese teachers' implicit theories of creativity in the context of cross-cultural communication," *International Journal of Learning and Teaching*, vol. 7, no. 1, pp. 20–24, 2021.

[8] W. Chen and B. In, "Modeling and simulation of cultural communication based on evolutionary game theory," *Complexity*, vol. 2021, Article ID 6115606, 12 pages, 2021.

[9] I. Stanislavova and G. Solovyova, "Modernism and the problem of cross-cultural communication," *Herald of Omsk University*, vol. 25, no. 2, pp. 75–80, 2020.

[10] B. L. Liao and A. Yanran, "Composition and improvement strategies of news audience's media literacy in the omnimedia era," *Contemporary Social Sciences*, vol. 24, pp. 128–137, 2020.

[11] X. Xu, "Editorial: studies in the globalisation era," *International Journal of Logistics Economics and Globalisation*, vol. 6, no. 4, pp. 253-254, 2017.

[12] L. Moreno, "Museums and digital era: preserving art through databases," *Collection Building*, vol. 38, no. 4, pp. 89–93, 2019.

[13] G. Radu, M. Solomon, C. M. Gheorghe, M. Hostiuc, I. A. Bulescu, and V. L. Purcarea, "The adaptation of health care marketing to the digital era," *Journal of Medicine & Life*, vol. 10, no. 1, pp. 44–46, 2017.

[14] M. Deng, X. Zheng, and L. Chen, "Inheritance of sports intangible cultural heritage and the construction of physical education in colleges and universities under the wireless communication microprocessor," *Wireless Communications and Mobile Computing*, vol. 2022, Article ID 7124632, 13 pages, 2022.

[15] A. M. Ismail, W. K. Mujani, and Z. A. Rahman, "Liberalism, extremism and media in the era of convergence," *International Journal of Civil Engineering and Technology*, vol. 9, no. 10, pp. 831–840, 2018.

[16] M. Puluhulawa and R. Husain, "Body shaming through social media as a digital crime in the era of disruption," *Jambura Law Review*, vol. 3, no. 1, pp. 112–123, 2020.

[17] Y. Gao and F. Latif, "An intelligent teaching strategy of cross-cultural business communication course based on big data," *Security and Communication Networks*, vol. 2022, Article ID 9809952, 9 pages, 2022.

[18] M. Butabayeva, "Pragmatics in eflteaching: avoiding pragmatic failure in cross-cultural communication," *ACADEMICIA An International Multidisciplinary Research Journal*, vol. 10, no. 12, pp. 1424–1427, 2020.

[19] Q. Xu and G. Wang, "Cross-cultural communication of regional images based on multimodal discourse analysis and network security," *Mobile Information Systems*, vol. 2021, Article ID 9956593, 10 pages, 2021.

[20] V. Ahieieva, "Types of interference as the manifestation of cross-cultural communication in translation," *Humanities Science Current Issues*, vol. 1, no. 29, pp. 4–9, 2020.

[21] A. V. Lentovskaya, "Information and communication technologies and the formation of cross-cultural communication skills in a foreign language environment," *Science*, vol. 26, no. 4, pp. 76–88, 2020.

[22] V. Jakuionyt, "Cross-cultural communication: creativity and politeness strategies across cultures. A comparison of Lithuanian and American cultures," *Creativity Studies*, vol. 13, no. 1, pp. 164–178, 2020.

[23] T. A. Sharypina and M. K. Men'Shchikova, "Literary canon in the context of cross-cultural communication," *Proceedings of Petrozavodsk State University*, vol. 43, no. 1, pp. 119–121, 2021.

[24] J. Zhang, Y. Xie, and Q. Wen, "A review on the study of Confucius institutes and their significance in foreign cultural communication —— research based on national social science fund project," *Linguistics*, vol. 3, no. 1, pp. 137–144, 2021.

[25] E. Alyousuf and F. Almansour, "The CoP's role in introducing new technology in cultural organizations," *American Journal of Business and Operations Research*, vol. 5, no. 2, pp. 91–123, 2021.

[26] M. A. Keijzer, M. Mäs, and A. Flache, "Communication in online social networks fosters cultural isolation," *Complexity*, vol. 2018, Article ID 9502872, 18 pages, 2018.

[27] X. Li, X. Deng, and H. Xu, "Interactive cultural communication effect in VR space of intelligent mobile communication network," *Wireless Communications and Mobile Computing*, vol. 2022, Article ID 9689272, 11 pages, 2022.

Hindawi
Wireless Communications and Mobile Computing
Volume 2022, Article ID 1299434, 9 pages
https://doi.org/10.1155/2022/1299434

Research Article

Optimization of Dynamic Obstacle Avoidance Path of Multirotor UAV Based on Ant Colony Algorithm

Yuexin Yang[1] **and Zhuoxun Chen**[2]

[1]*Changzhou University, Changzhou 213164, China*
[2]*George School, Newtown 18940, USA*

Correspondence should be addressed to Yuexin Yang; yangyuexin2021@mail.chzu.edu.cn

Received 21 March 2022; Revised 16 May 2022; Accepted 25 May 2022; Published 7 July 2022

Academic Editor: Jun Ye

In this paper, the real-time path avoidance problem of multirotor UAV in the case of sudden obstacles in two-dimensional environment is studied. The principle, model, and application of ant colony algorithm are analyzed. On this basis, the adaptive dynamic window ant colony algorithm is proposed, and the adaptive dynamic window method is designed; the heuristic function of adding obstacle detection factors and the double pheromone update strategy are made to the ant colony algorithm, and the improved ant colony algorithm is used to replan the path within the dynamic window that can be automatically adjusted to achieve the purpose of obstacle avoidance. A real-time simulation experiment of path planning was conducted by constructing an environment map in MATLAB. The simulation results show that with the continuous increase of the number of sudden obstacles, the real-time replacement path of multirotor UAV also gradually increases, and when approaching the obstacles, the replacement path is more dense, indicating that the adaptive window ant colony algorithm can be applied to dynamic path replacement, and the multirotor UAV can realize dynamic obstacle avoidance path optimization under the condition of sudden obstacles in a short time.

1. Introduction

Unmanned aerial vehicles (UAVs) are generally unmanned. Human-controlled vehicles are particularly prominent in the growing development of aerial vehicle technology. UAVs are usually equipped with a variety of sensors, as well as graphic and communication equipment, in order to achieve tasks such as terrain reconnaissance, patrolling, mapping, and rescue due to their good maneuverability and to complete various flight maneuvers under the operator's action commands [1]. The common ones in the market are rotary-wing UAVs, of which quadratics and operators are more popular due to their stable flight. The military most of the fixed-wing UAVs are equipped with high-definition cameras and weapon systems for military reconnaissance missions [2]. Drones are exclusive not only in military applications but also in commercial applications to improve human life. Thus, the research topics and commercial applications related to UAVs are constantly emerging with new technological developments. However, with intelligent computers and high technical requirements for collecting and processing transmitted information, the mission of UAVs has become challenging and more difficult for human control, and relying solely on human control of UAVs in the face of unknown environmental situations has placed higher demands on individual capabilities [3, 4]. The development trend of UAVs is toward autonomy, and one of the outstanding issues in the development of autonomous and intelligent systems for UAVs is path planning. The path planning of UAVs is similar to the ground robot path planning problem, where a route is planned from the starting point in the playable area to the target point without contact with obstacles, in how to constitute the route and a better choice of route is the main element explored in the problem [5]. UAVs sometimes need to execute flight paths in fixed height mode free mode due to different operational difficulties and mission requirements, and the use of path planning techniques can not only obtain optimal collision-free paths

but also minimize path length, flight time, and energy consumption [6].

Currently, UAVs, both in military and civilian applications, mainly perform reconnaissance, aerial photography, and monitoring tasks in the open field plains and high-altitude domains, and path planning lacks autonomy and practicality in the face of unknown environments in cities [7]. Path planning technology is still immature and still requires human control and has a high accident rate. UAVs make poor autonomous flight decisions when facing unknown situations such as neighborhoods, schools, and other buildings, and often collide in the presence of unknown obstacles, which greatly reduce the maneuverability of UAVs. Under the urban low-altitude environment, UAV has weak application ability in rescue reconnaissance, road monitoring, traffic law enforcement and other aspects.

In order to solve the above problems, UAV needs to solve the problem of path planning in the face of unknown environment. The first problem to be solved is environmental perception, and the UAV is retrofitted with sensors to realize the perception of the surrounding environment, which is the prerequisite for the UAV to make path planning decisions [8]. Current environmental sensors for UAVs are mainly 2D planar LIDAR, millimeter wave, ultrasonic rangefinders, monocular vision and binocular vision cameras, and infrared range sensors, all of which can sense the 3D external environmental information faced by the UAV. Another major issue is the judgment and detection of obstacles in the environment, whereby the UAV control decision system can make path planning and control the UAV to fly along the planned path [9].

In this paper, the research of environment perception problem in path planning is carried out based on binocular vision sensors for rotary-wing UAVs, which perceive the environment with buildings similar to campus community and realize the reconstruction of 3D environment and obstacle detection; meanwhile, the ant colony algorithm is used as the path planning algorithm for UAVs in unknown environment and the applicability is improved so as to realize the autonomous flight in unknown environment.

2. Related Work

2.1. Environmental Sensing Technology. Since UAVs themselves lack the ability to perceive the environment, in order to ensure the UAV's understanding and grasp of the environment, it is necessary to enable the UAV to acquire information including the obstacles in the surrounding environment, other actions exhibited by the obstacles, nonobstacle areas that the UAV can pass through, and flexible actions. The technique to obtain this information by fusing data from multiple sensors such as LIDAR, cameras, and millimeter wave radar is the environmental sensing technique [10].

In this paper, binocular stereo vision from environmental perception technology is used as the UAV environmental perception function, and since binocular vision relies on computer computing power. It has produced many research results as the technology level improves both at home and abroad. Srikanthakumar S et al. extended the research work on 2D image vision to the visual study of 3D object structures, especially the detailed analysis of the relationship between 3D structures similar to polyhedra such as columns in the spatial coordinate system [3]. Hu J et al. proposed a new vision theory, namely, the Marr stage vision theory, which proposes a three-stage vision processing to obtain a true 3D map, standardizing the visual representation at different angles to relate the specific structures to the actual object realization [11]. Huang X et al. used binocular vision techniques in mobile robots to perform behavioral perception of moving objects in the environment and dynamic processing based on behavioral information of objects that can move in the outside world [12]. Benjamin M R et al. worked out a stereo vision system using dual camera baseline elongation to achieve accurate self-localization and path navigation of the detector [13]. The system logarithmically optimizes and probabilistically estimates the captured images at different locations to obtain high accuracy parallax and calculates the individual 3D spatial coordinates of the objects in the recognized images, allowing the detector to perform real-time 3D reconstruction of the surrounding environment.

Lolla T et al. achieved target recognition of a larger number of objects in the environment using a newly developed binocular vision system, which improved the autonomous navigation performance of the soccer robot [14]. Chamitoff G E et al. improved the accuracy of the robot in grasping the target objects through binocular vision multiangle positional fusion estimation and real-time depth estimation [15]. Li H et al. applied binocular vision technology in the measurement of vehicle safety distance, built a binocular parallel lateral system, and calculated the vehicle and camera distances from the left and right images acquired in the high-speed real-time motion of the vehicle, which was applied to the safety warning system of the vehicle [16].

2.2. UAV Path Planning Technology. UAV path planning has been an important research area in the western developed countries since 1960. Initially, the UAV flight was controlled by the operator of the vehicle by constantly observing changes in the surrounding environment and thus by radio remote control. With the popularization of artificial intelligence in recent years, intelligent path planning technology began to develop and mature with the extensive use of intelligent algorithms and sensors [17].

In [18], the existing SVM and APF algorithms were loaded into the processing computer and a vision system was attached to initially complete the path planning in the room. Ling F et al. used a combination of inertial guidance and vision in path planning technology, and performed a fusion of positional and environmental information processing to achieve UAV path planning under obstructed conditions in an outdoor environment [19].

Taghavifar H et al. based on binocular vision technology enables the UAV to obtain obstacle information in an unknown environment by the probabilistic method and determine the planning of 3D paths by the determination rules of obstacle information [20]. Yan B et al. detect and identify obstacles in a complex and variable environment,

and make fast commands through the autonomous judgment of the flight control system, thus performing collision-free navigation [21]. Roy S et al. studied the control and path planning methods for micro and small UAVs [22].

2.3. Path Planning Algorithm. The main UAV path planning methods are Voronoi diagram method, PRM path planning method, RRT planning method, and so on. Among them, Voronoi diagram method is to use the method of connected geometry in mathematics to turn the obstacle area into a constructible connected graph, and then the boundary of the graph is connected into a flightily path phase, and the minimum initial path is searched in the boundary connection, which greatly reduces the difficulty in path search but at the same time the obtained flight path does not conform to the UAV flight characteristics. The probabilistic map PRM algorithm was proposed in [23]. The algorithm divides the flight space freely, randomly samples the solutions, and connects the sampled adjacent solutions as a path connectivity map.

Korayem M H et al. proposed the genetic algorithm, which appropriately encodes each path, followed by randomly generating paths of a certain size, evaluating the paths, and selecting them according to certain rules; simulating the genetic operation and simulating the process of cyclic biological inheritance to obtain the optimal solution (path) [24]. Benjamin M R et al. introduced a differential variation strategy into a genetic algorithm applied to UAV path planning to solve the problem of local minima [25]. In [26], the particle swarm algorithm sets the particles as local attraction points and dynamically corrects the unknown of the particles in the distance of the passable range boundary, which can improve the ability of the algorithm to search for the global optimal solution and get the solution faster.

3. Adaptive Dynamic Window Ant Colony Algorithm

In the previous chapters, the UAV environment perception problem was studied, and the UAV was made to have environment perception capability through scene reconstruction and detection of obstacles in the environment by binocular cameras. The autonomous flying rotor UAV has the ability of environment perception and also needs to have the function of intelligent path planning, and needs to have the path planning algorithm applicable to the unknown environment. In this chapter and afterwards, we start to study the application of ant colony algorithm for UAV path planning when there are unknown obstacles in two-dimensional and three-dimensional environments.

Currently, UAV path planning in many cases is applicable to offline planning in two-dimensional environments, i.e., static obstacles knew to exist in the environment are considered in advance, and all obstacle information in the environment is mastered in advance. The global path planning is used once in the UAV to follow the planned route and reach the target point. However, due to inadequate understanding of the unknown factors of the actual flight environment, there are still some unexpected situations. In order to ensure that the UAV can perform reasonable obstacle avoidance in the case of sudden obstacle discovery, its ability of replanning the path needs to be improved. This chapter firstly analyzes and introduces the basic principle of ant colony algorithm, and based on this proposes an ant colony algorithm with adaptive dynamic window.

3.1. Basic Ant Colony Algorithm. Biologists have observed that ants have single and compound eyes but are unable to obtain information about their surroundings through their eyes in the natural environment, and they use their own secreted pheromones to sense changes in information about their surroundings when searching for food and thus choose their paths. Ants randomly choose unknown intersections in the environment and release pheromones in the path they take, where the change of pheromones is related to the length of the path.

3.2. Mathematical Model of the Basic Ant Colony Algorithm. The mathematical model of the ant colony algorithm is based on the combination of random events and the probabilistic selection of ants as they travel, shifting to surrounding points in unit steps, and the path points that have been traveled can be discarded. Assuming that the pheromone concentration of ants is τ and there are a number of m ants from the starting point to the target point in search of food, the probability that the kth ant will travel from a point i to a point j at this point in time t is p_{ij}^{k} expressed by the following equation:

$$p_{ij}^{k} = \begin{cases} \dfrac{\tau_{ij}^{\alpha}(t).\tau_{ij}^{\beta}(t)}{\sum_{S\in \text{allowed}} \tau_{ij}^{\alpha}(t).\tau_{ij}^{\beta}(t)}, & j \in \text{allowed}_k. \end{cases} \quad (1)$$

In Equation (1), allowed_k represents the path node to be chosen by the ant next, α is the information heuristic factor, and α represents the importance of a small section of the path walked by the ant to influence the whole path taken by the ant colony. If the value of α is too large, the higher the degree of influence of the pheromone, the more ants will choose the path with the β larger value. β is the expected heuristic factor, and if β is too large, the importance of the heuristic information is better than the influence of the pheromone. The heuristic information can be interpreted as whether the ants can easily judge the selectivity of the next path node. The contraindication table 888 is used to store the path nodes selected by each ant. $\text{allowed}_k = \{C - \text{tabu}_k\}$ denotes the next path node chosen by ant k.

The mathematical model of the ant colony algorithm also has heuristic functions that enable the ranking of the alternatives in the search algorithm in each branch step according to the available information to decide which branch function to follow, which approximates the exact solution. It can also be understood as the degree of expectation, which in the solution path planning process is defined as:

$$\eta_{ij}(t) = \frac{1}{d_{ij}}, \tag{2}$$

where d_{ij} is the distance from a point i to another point j.

In the process of ants looking for the target point, there is a process of replacing the old pheromone with the new pheromone. The pheromone volatilization speed ρ is used to adjust the pheromone update. The concept of its own speed determines the volatilization speed of pheromone on the path. The larger ρ is, the faster it will be. This regulation state is in a balance state, which neither volatilizes pheromone too fast nor makes its stock too small. The update function of pheromone is as follows:

$$\tau_{ij}(t+n) = (1-\rho)\tau_{ij}(t) + \Delta\tau_{ij}(t), \tag{3}$$

$$\Delta\tau_{ij}(t) = \sum_{k=1}^{m} \Delta\tau_{ij}(t). \tag{4}$$

The pheromone retained between two path nodes i, j is $\Delta\tau_{ij}^{k}$ and the pheromone in t is $\Delta\tau_{ij}(t)$. After another period of time n, the pheromone changes to $\tau_{ij}(t+n)$.

3.3. Basic Ant Colony Algorithm Path Planning Implementation. The steps for implementing the basic ant colony algorithm applied to path planning are as follows.

(1) Set the target point to be reached at the start point of the planning, set the basic parameters of the algorithm, the number of path nodes, etc., and initialize and establish the abstracted environment model

(2) Reset Tabu, the algorithm starts to search for the path, and then searches for the path node according to the transfer probability formula, keeps the length information from the start point of the selected node to the current path point, and determines whether the target point is reached or the node is zero; if so, the search stops. Otherwise, the search continues

(3) After one search, the pheromone on the path will be updated according to Equation (3) as a whole

(4) End the search path when the number of searches is N

(5) Output saved optimal path information and the algorithm ends

The flow chart of the algorithm is shown in Figure 1.

3.4. An Improved Approach to the Ant Colony Algorithm. (1) Improvement based on the algorithm itself, mostly seen in parameter optimization methods, improvement methods of heuristic information, and improvement of pheromone update rules. (2) Adding ant colony types, such as parallel ant colony algorithms and sequential multi-ant colony algorithms. (3) Combining with other algorithms to become fusion algorithms.

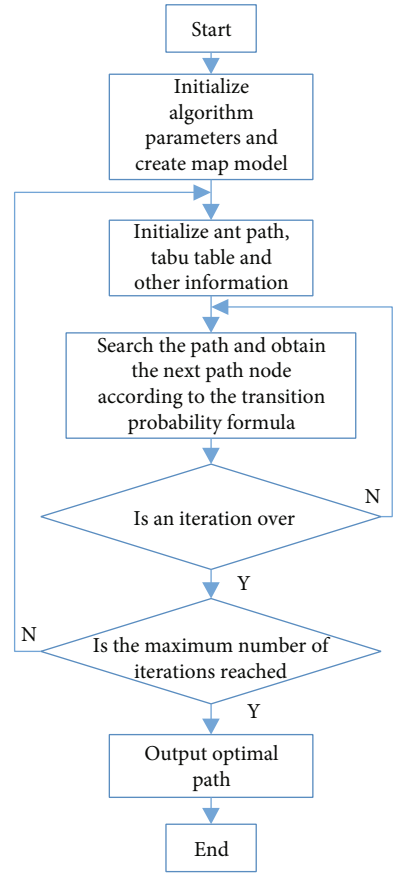

Figure 1: Algorithm flow chart.

4. Design of Adaptive Dynamic Window Ant Colony Algorithm

There are two methods of path avoidance planning due to sudden obstacles: the first case is to discard all the previously planned paths offline when facing sudden obstacles, and plan a new path from the location to the target point again. In the other case, only the local replanning is carried out within the set range, and after avoiding the obstacles, a suitable path point is chosen nearby to fly back to the previously set path point. Since the global planning effect of ant colony algorithm is good, the Lupin performance is strong, and it is easy to combine with other methods; this paper integrates the advantages of the above two methods and adopts the dynamic window area within the ant colony algorithm replacing—discard the original path—the idea of "outputting the local optimal point and using the secondary planning of ACOA to the target point" is adopted to make full use of the advantage of global planning of ACOA.

4.1. Design of Adaptive Dynamic Windows. Based on the analysis of the shortcomings of the general traditional dynamic window method, an adaptive dynamic window is designed in this section, and the specific design process is as follows.

(1) Choosing a suitable window can enable the computational power to be improved and the optimization-seeking effect to meet the real-time UAV path planning. The purpose of automatically adjusting the size of the dynamic window is to ensure that the UAV avoids obstacles while meeting the flight speed, the algorithm takes less time, the planning effect is good, and the UAV completes replanning before reaching a new path point

(2) The determination of the adaptive dynamic window boundary, assuming that the UAV flight process advances according to the unit distance, the determination of the window size is based on the UAV as the starting point, and the determination of the adaptive window boundary $4w^2$ is the distance from the window determination point, i.e., the starting point for local planning, to the local optimal point in the process of local path planning. In general, the dynamic window boundary is fixed. The smaller the window boundary is, the better the path planning is in real time. The adaptive dynamic window takes a range of $(0, 4w^2)$, where $4w^2$ represents the range of the area that can be covered by the dynamic window. When using the adaptive dynamic window method, w can be taken to any finite value in the covered subregion. The specific scheme is as follows

In the path planning process, the flight area is divided into a $100 * 100$ raster with three dynamic windows of different sizes are large window $4 * 10 * 10$, medium window $4 * 7.5 * 7.5$, and small window $4 * 5 * 5$. The size of the dynamic window is determined based on the maximization probability and minimization probability. The range of the windows is shown in Figure 2.

The yellow box indicates the small window range, and the yellow triangle represents the current position of the drone. Similarly, the orange window indicates the medium window range, the blue box indicates the large window range, and the triangle is the position of the drone.

As shown in Figure 3, the adaptive dynamic window selection process is: the initialized window detects new obstacles as it moves with the UAV and determines the replaced dynamic window based on the proportion of the range of the obstacle grid occupying the initial dynamic window, and the size of the dynamic window is constant from the beginning after the optimal local path point is replaced. As the UAV travels to the next path point, a new window is determined. In the window division diagram, the total number of unit grids in the area covered by the yellow box is 100; the number of unit grids in the blue box is 400, and the percentage of obstacles is 0.25 and 0.5. Based on the principle of maximum and minimum probability, a large window is selected when, a medium window is selected when, and a small window is selected when. Where is the upper threshold of the dynamic window, which means that the obstacle cannot occupy the dynamic window completely in the planning, and the UAV has replanned to avoid the obstacle in advance before the obstacle occupies the window

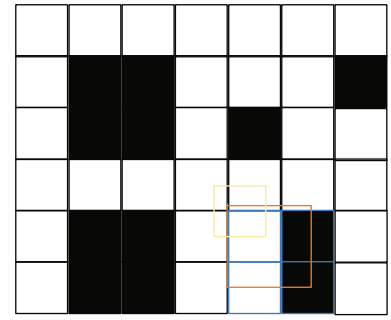

Figure 2: Window creation and division.

completely. When the obstacle occupancy ratio reaches the threshold value, the dynamic window range will be enlarged to the upper limit.

4.2. UAV Path Cost Function Design. Firstly, the UAV flight range needs to be rationalized and the path cost function needs to be determined in the UAV path planning. The design of the cost function is good or bad, which determines whether a flight path with less loss can be planned. In this paper, the path cost function should be described as the calculation of the cost function in a weighted manner according to the shortest travel of the path and the path that can be explored in the window to be able to replan. The UAV calculates the path cost of two adjacent points during the flight and then sums the whole path of each section of the city. Its cost function is as follows:

$$F = \sum_{i,j \in N}^{N} \left[\lambda \cdot c_f^{ij} + (1 - \lambda) . c_t^{ij} \right]. \tag{5}$$

All the path points in this path are N, λ is the weight factor, c_f^{ij} is the path of adjacent points i, j, and c_t^{ij} is the threat cost of the path between the nodes of all adjacent two points i, j. The threat cost of a path edge is:

$$c_t^{ij} = 1/\min\left(l_1, l_2, l_3, \cdots, l_{\text{end}}\right), \tag{6}$$

where $(l_1, l_2, l_3, \cdots, l_{\text{end}})$ is the distance from the path point to the center of the obstacle.

4.3. Double Pheromone Update Rule. To improve the ability of the algorithm to find the global optimal solution, a dual pheromone update strategy is used in this paper.

In the basic ant colony algorithm, the size of the pheromone concentration residual factor ρ has a large impact on the algorithm's ability to find the optimal solution, especially when the algorithm proceeds to a certain level. If a larger value is set, the algorithm will find the nonoptimal solution faster, i.e., it will select the path nodes that have been searched before. If the value is set to a smaller value, the pheromone concentration decreases rapidly, so that many path nodes are not selected and the optimal path is not found.

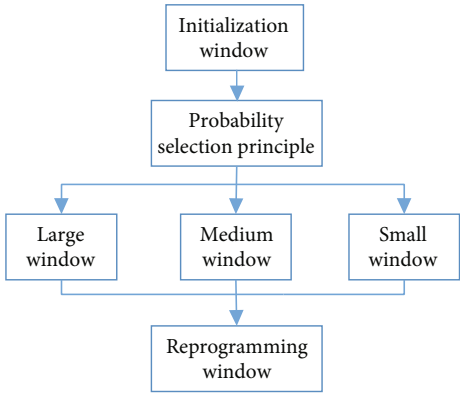

Figure 3: Adaptive dynamic window determination rules.

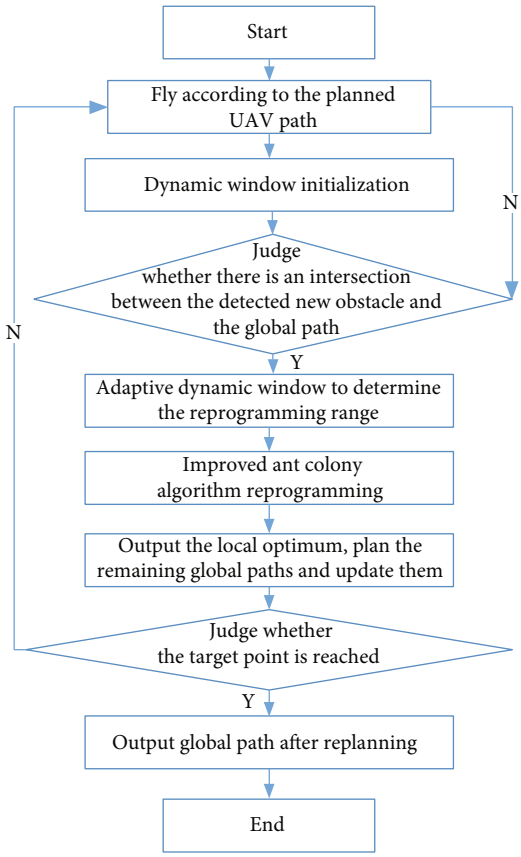

Figure 4: Flow chart of improved ant colony algorithm based on adaptive dynamic window.

Therefore, in this paper, when designing the pheromone concentration update rule, the residual factor ρ is set within a certain range between the high and low threshold values to avoid the phenomenon of "premature" nonoptimal solutions found too early by the ant colony algorithm. The pheromone update rule combines the variable range of pheromone concentration with the local information of the ratio of maximum and minimum paths in each iteration to achieve the purpose of combining the whole and the part and to improve the algorithm's ability and speed of finding

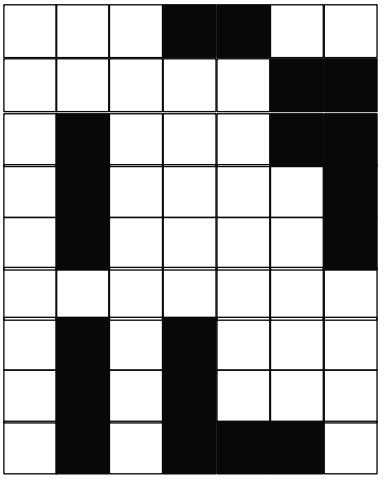

Figure 5: Initial map.

the best solution. The pheromone concentration update rule is as follows:

$$\begin{cases} \tau_{ij}(t+n) = \rho_{\min}\tau_{ij}(t) + \Delta\tau_{ij}(t) + \sqrt{d_{\max}/d_{\min}}, \tau_{ij}(t) > \tau_{\max} \\ \tau_{ij}(t+n) = \rho\tau_{ij}(t) + \Delta\tau_{ij}(t) + \sqrt{d_{\max}/d_{\min}}, \tau_{\min}(t) < \tau(t) < \tau_{\max}, \\ \tau_{ij}(t+n) = \rho_{\max}\tau_{ij}(t) + \Delta\tau_{ij}(t) + \sqrt{d_{\max}/d_{\min}}, \tau_{ij}(t) < \tau_{\max} \end{cases} \tag{7}$$

where $d_{\max}$ denotes the longest path in which the algorithm performs the optimal solution process at one time and $d_{\min}$ denotes the shortest distance. $\tau_{\max}$ is the maximum value of pheromone concentration on the path and $\tau_{\min}$ is the minimum value of pheromone concentration.

4.4. Algorithm Implementation Flow. The flow chart of the adaptive dynamic window-based ant colony planning algorithm is shown above, with the following operational steps.

(1) Determine the departure position of the UAV, as well as the global path with known environmental information

(2) Initialize the dynamic window and determine its initial value as $4 * 10 * 10$

(3) The UAV flies according to the path point and judges whether the newly discovered obstacles have intersection with the global path according to the window range; if not, it continues to fly according to the original planned path. If there is, the window range is replanned according to the adaptive dynamic window determination rule

(4) Call the improved ant colony algorithm to output the optimal local path (see Figure 4 for the steps of the improved ant colony algorithm).

(5) Update the local path to pass, i.e., ensure that the UAV avoids the obstacle. The drone flies according to the updated path

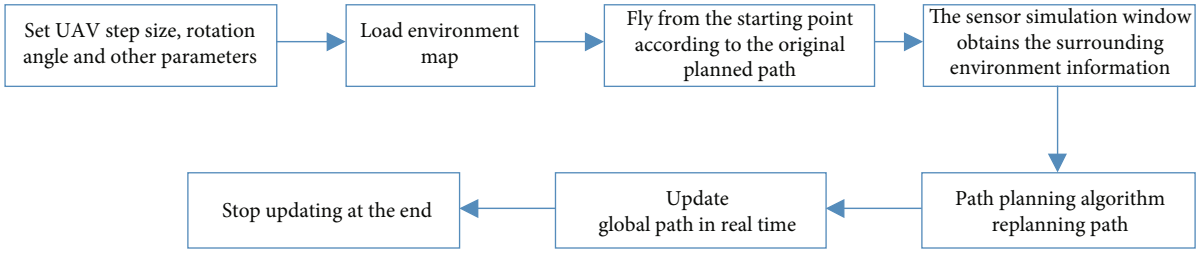

Figure 6: Matlab real-time simulation process diagram.

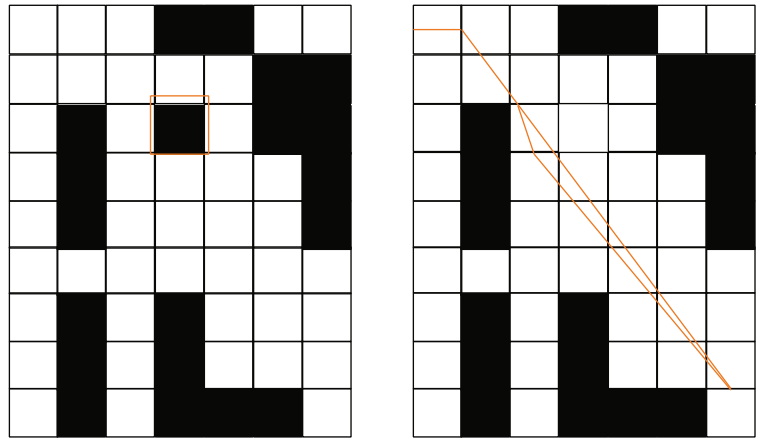

(a) The number of newly detected obstacles is 1 (b) UAV replanning path

Figure 7: Simulation results of path replanning for a single sudden obstacle.

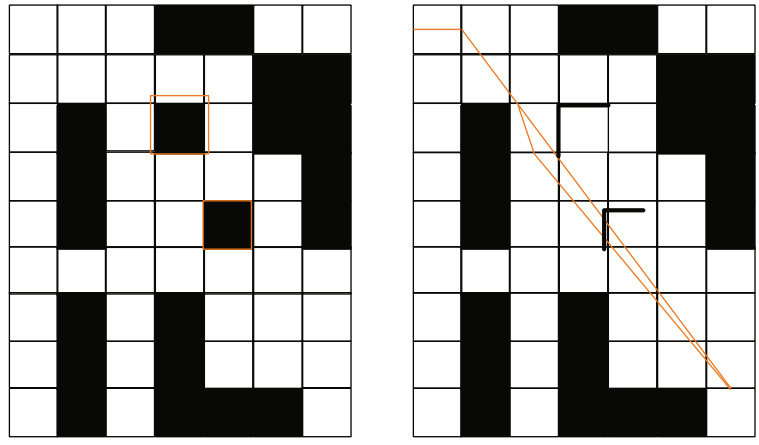

(a) The number of newly detected obstacles is 2 (b) The UAV replans its path

Figure 8: Simulation results of path replanning with the number of sudden obstacles being 2.

(6) Determine whether the final target point is reached; if not, return to step (3). If yes, output the updated path

5. Simulation Experiments and Results Analysis

The experimental simulation environment of this paper is MATLAB2019b and the system environment is Windows 7. In order to visually simulate the real-time replanning process of UAV, this paper calls the range Sensor module in MATLAB Navigation Toolbox to simulate the dynamic window, whose detectable range is 0-20 unit distances and the detecting range is adjustable (simulating adaptive window). The maximum horizontal detection angle is $[-\pi, \pi]$. The flight environment is simulated by setting up a $100 * 100$ grid map with distance units in meters. Set up the flight environment as shown in Figure 5.

The Matlab real-time dynamic reprogramming simulation process is shown in Figure 6.

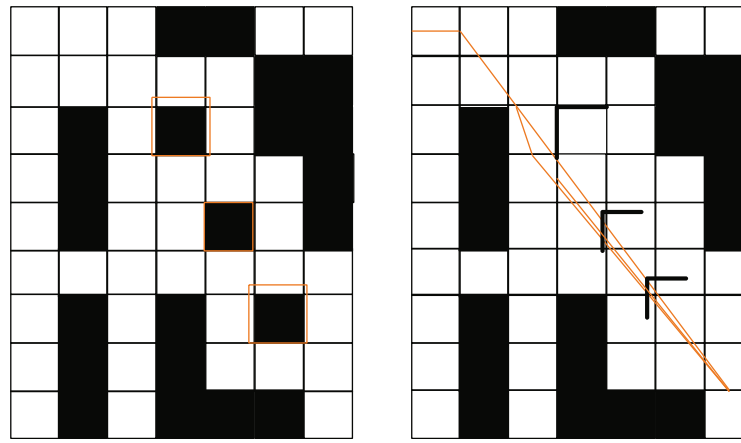

(a) The number of new obstacle detections is 3 (b) Replanning the path 3

Figure 9: Simulation results of path replanning with the number of sudden obstacles being 3.

Table 1: Comparison of the results of different methods under the same initial conditions.

Project	Number of sudden obstacles	Number of replanning	Optimal replanning path length (m)	Simulation run time
Use fixed window	1	2	132.569	15.25687
Ant colony	2	5	150.089	27.54623
Replanning	3	8	161.258	37.26534
Adaptive window	1	1	125.605	13.82569
Ant colony	2	2	136.789	25.59299
Replanning	3	4	145.140	32.45474

The path has been planned in the simulation environment. When the number of newly discovered obstacles is 1, the simulation result is shown in Figure 7.

When the number of newly detected obstacles is 2, the simulation results are shown in Figure 8.

When the number of newly detected obstacles is 3, the simulation result is shown in Figure 9.

In Figures 7–9, obstacles are marked with orange boxes, and orange solid lines represent the replacement path of real-time update recorded in the case of sudden obstacles. It can be seen that the real-time replanning paths are less in the case of the number of burst obstacles is 1. As the number of burst obstacles increases, the real-time replacing paths gradually increase and are denser when they are close to the obstacles, indicating that the adaptive window ant colony algorithm can be applied to dynamic path replacing.

Table 1 shows that the number of planning increases with increasing obstacles and the time consumed by the algorithm increases. As mentioned in the previous section, the purpose of this paper is to improve the replanting effect and make the time-consuming decrease. The data show that the ACO with adaptive window can obtain a better replacing path under the condition of reasonable obstacle avoidance of the UAV, i.e., the final output replacing path is shorter and the replanting times are less, i.e., the algorithm is better than the ACO with fixed window in terms of time consumption.

6. Conclusions

In this paper, UAV real-time path replanning problem in the case of sudden obstacles in a two-dimensional environment is studied. The principle, model, and application of ant colony algorithm are analyzed. On this basis, the adaptive dynamic window ant colony algorithm is proposed, and the adaptive dynamic window method is designed; the heuristic function of adding obstacle detection factors and the double pheromone update strategy are made to the ant colony algorithm, and the improved ant colony algorithm is used to replan the path within the dynamic window that can be automatically adjusted to achieve the purpose of obstacle avoidance. A real-time simulation experiment of path planning was conducted by constructing an environment map in the matter. The simulation results show that the UAV has a strong path-replacing capability under sudden obstacle conditions, and the time consumption is short.

Data Availability

The data used to support the findings of this study are available from the corresponding author upon request.

Conflicts of Interest

The authors declare no conflicts of interest.

References

[1] N. Xiong, X. Zhou, X. Yang, Y. Xiang, and J. Ma, "Mobile robot path planning based on time taboo ant colony optimization in dynamic environment," *Frontiers in Neurorobotics*, vol. 15, article 642733, 2021.

[2] J. Dreo and P. Siarry, "Continuous interacting ant colony algorithm based on dense heterarchy," *Future Generation Computer Systems*, vol. 20, no. 5, pp. 841–856, 2004.

[3] S. Srikanthakumar, C. Liu, and W. H. Chen, "Optimization-based safety analysis of obstacle avoidance systems for unmanned aerial vehicles," *Journal of Intelligent & Robotic Systems*, vol. 65, no. 1-4, pp. 219–231, 2012.

[4] G. L. Qin, "An improved ant colony algorithm based on adaptively adjusting pheromone," *Information and Control*, vol. 31, no. 3, p. 198, 2002.

[5] Y. Zhang, X. X. Yang, and W. W. Zhou, "Velocity obstacles-based collision avoidance feasible trajectory planning optimization algorithm for multiple UAV," *Systems Engineering and Electronics*, vol. 37, no. 2, pp. 323–330, 2015.

[6] M. S. Kran, E. Özceylan, M. Gündüz, and T. Paksoy, "A novel hybrid approach based on particle swarm optimization and ant colony algorithm to forecast energy demand of Turkey," *Energy Conversion and Management*, vol. 53, no. 1, pp. 75–83, 2012.

[7] X. Gu, L. Shen, C. Jing, Y. Zhang, and W. Zhang, "A virtual motion camouflage approach for cooperative trajectory planning of multiple UCAVs," *Mathematical Problems in Engineering*, vol. 2014, Article ID 748974, 15 pages, 2014.

[8] Q. Wu, Z. Chen, L. Wang et al., "Real-time dynamic path planning of mobile robots: a novel hybrid heuristic optimization algorithm," *Sensors*, vol. 20, no. 1, p. 188, 2020.

[9] F. Andert and F. Adolf, "Online world modeling and path planning for an unmanned helicopter," *Autonomous Robots*, vol. 27, no. 3, pp. 147–164, 2009.

[10] L. Liu, Y. Gao, and Y. Wu, "Speed optimization control for wheeled robot navigation with obstacle avoidance based on viability theory," *Automatika*, vol. 57, no. 2, pp. 428–440, 2016.

[11] J. Hu, L. Zhang, M. Lin, and W. Liang, "An integrated safety prognosis model for complex system based on dynamic Bayesian network and ant colony algorithm," *Expert Systems with Applications*, vol. 38, no. 3, pp. 1431–1446, 2011.

[12] X. Huang, X. Dong, J. Ma et al., "The improved a ∗ obstacle avoidance algorithm for the plant protection UAV with millimeter wave radar and monocular camera data fusion," *Remote Sensing*, vol. 13, no. 17, p. 3364, 2021.

[13] M. R. Benjamin, M. Defilippo, P. Robinette, and M. Novitzky, "Obstacle avoidance using multiobjective optimization and a dynamic obstacle manager," *IEEE Journal of Oceanic Engineering*, vol. 44, no. 2, pp. 331–342, 2019.

[14] T. Lolla, P. Lermusiaux, M. P. Ueckermann, and P. J. Haley Jr., "Time-optimal path planning in dynamic flows using level set equations: theory and schemes," *Ocean Dynamics*, vol. 64, no. 10, pp. 1373–1397, 2014.

[15] G. E. Chamitoff, A. Saenz-Otero, J. G. Katz, S. Ulrich, B. J. Morrell, and P. W. Gibbens, "Real-time maneuver optimization of space-based robots in a dynamic environment: theory and on-orbit experiments," *Acta Astronautica*, vol. 142, pp. 170–183, 2018.

[16] F. Ling, Q. Li, Y. Qian, Z. Jiang, R. Liu, and W. Li, "Research on attenuation law and application of elastic wave propagation in multi-coal seam fracture," *IOP Conference Series: Earth and Environmental Science*, vol. 861, no. 5, article 052029, 2021.

[17] H. Taghavifar, B. Xu, L. Taghavifar, and Y. Qin, "Optimal path-planning of nonholonomic terrain robots for dynamic obstacle avoidance using single-time velocity estimator and reinforcement learning approach," *IEEE Access*, vol. 7, pp. 159347–159356, 2019.

[18] B. Yan, G. Z. Yan, X. G. Fu, and D. H. Tang, "Minimal energy trajectory plan of weld inspection manipulator for intersected pipes based on genetic algorithm," *Journal of Shanghai Jiaotong University*, vol. 39, no. 6, pp. 914–918, 2005.

[19] S. Roy, "Dynamic obstacle avoidance in multi-robot motion planning using prediction principle in real environment," *Automation Control and Intelligent Systems*, vol. 1, no. 2, p. 16, 2013.

[20] Y. D. Zhang and L. N. Wu, "Bankruptcy prediction by genetic ant colony algorithm," *Advanced Materials Research*, vol. 186, pp. 459–463, 2011.

[21] M. H. Korayem, M. Nazemizadeh, and H. N. Rahimi, "Trajectory optimization of nonholonomic mobile manipulators departing to a moving target amidst moving obstacles," *Acta Mechanica*, vol. 224, no. 5, pp. 995–1008, 2013.

[22] S. Farí, X. M. Wang, S. Roy, and S. Baldi, "Addressing unmodeled path-following dynamics via adaptive vector field: a UAV test case," *IEEE Transactions on Aerospace and Electronic Systems*, vol. 56, no. 2, pp. 1613–1622, 2019.

[23] B. Liao, X. Li, W. Zhu, R. Li, and S. Wang, "Multiple ant colony algorithm method for selecting tag SNPs," *Journal of Biomedical Informatics*, vol. 45, no. 5, pp. 931–937, 2012.

[24] M. H. Korayem, A. K. Hoshiar, and M. Nazarahari, "A hybrid co-evolutionary genetic algorithm for multiple nanoparticle assembly task path planning," *The International Journal of Advanced Manufacturing Technology*, vol. 87, pp. 3527–3543, 2016.

[25] Y. Ma, H. Wang, Y. Xie, and M. Guo, "Path planning for multiple mobile robots under double-warehouse," *Information Sciences*, vol. 278, pp. 357–379, 2014.

[26] N. Demirel and M. D. Toksar, "Optimization of the quadratic assignment problem using an ant colony algorithm," *Applied Mathematics & Computation*, vol. 183, no. 1, pp. 427–435, 2006.

Hindawi
Wireless Communications and Mobile Computing
Volume 2022, Article ID 2304820, 10 pages
https://doi.org/10.1155/2022/2304820

Research Article

Application of Spatial-Temporal Behavioral Trajectory Analysis in the Space Design of Digital Villages

Jun Li

College of Fine Art and Design, Hubei Engineering University, Xiaogan, 432000 Hubei, China

Correspondence should be addressed to Jun Li; lijun4059@hbeu.edu.cn

Received 9 April 2022; Revised 25 May 2022; Accepted 4 June 2022; Published 1 July 2022

Academic Editor: Jun Ye

From the perspective of the environment-behavior science, this paper takes the space design of a digital village in Youzhaqiao Village on the outskirts of Guangshui City, for example, to record and track the behavior of residents and tourists in the area via mobile phone motion track recording software. Based on the collection, selection, and collation of the trajectory data, the valid data has been counted and analyzed; finally, the field investigation and questionnaires have been integrated to propose optimization strategy for the use and design of the space of Youzhaqiao Village from aspects such as human perception, cognition, and behavior.

1. Introduction

An important part of achieving rural modernization is the steady advancement of digitization and the sustainable vitalization of the traditional countryside. In particular under the situation where smart cities, IT applications, and intelligent technologies are constantly being promoted, the scope of rural space design has been greatly widened by the strategies of integration of digital village and smart agriculture, providing strong momentum to rural tourism planning and opening up a new economic situation of urban-rural integration and digitization development as well [1]. This paper will study how the intelligent technology and behavioral trajectory data can be integrated into the rural space design.

From the perspective of the environment-behavior science, this paper takes the space design of a digital village in Youzhaqiao Village on the outskirts of Guangshui City, for example, to record and track the behavior and activity of residents and tourists in the area via mobile phone motion track recording software. Based on the collection, selection, and collation of the trajectory data, the valid data has been counted and analyzed; finally, the field investigation and questionnaires have been integrated to propose an optimization strategy for the use and design of the space of Youzhaqiao Village from aspects such as human perception, cognition, and behavior.

2. Research Background and Significance

2.1. Research Background. An important part of achieving rural modernization is the steady advancement of digitization and the sustainable vitalization of the traditional countryside. In particular under the situation where smart cities, IT applications, and intelligent technologies are constantly being promoted, the scope of rural space design has been greatly widened by the strategies of integration of digital village and smart agriculture, providing strong momentum to rural tourism planning and opening up a new economic situation of urban-rural integration and digitization development as well [1]. This paper will study how the intelligent technology and behavioral trajectory data can be integrated into the rural space design.

With villages as a vital and inseparable part of the country, rural revitalization and rural tourism are inextricably linked, while the planning and designing of rural tourism are unique from other types of planning and designing which need to consider the sustainability of agricultural development and rural landscape layout under the premise of sound rural function and reasonable industrial layout. And the rapid development of intelligent terminals and location-based services (LBS) and smart terminals led by GPS navigators and smartphone apps (especially sports

and health categories) not only facilitates the public's travel but also provides data support for the study of spatial-temporal behavior patterns [2].

The analysis of tourists' behavioral characteristics is one of the most important bases for landscape design. Compared with field investigation and questionnaires, which are the most widely used methods of information collection, the spatial-temporal behavioral trajectory analysis has more advantageous continuity and accuracy in respect of time and space, better reflecting the tourists' behavioral features. The spatial-temporal behavioral trajectories of experimental subjects can be collected via the recording data of these subjects' GPS, which have been combined with the time geography to compute and visualize human behavior patterns geographically by scholars such as Guan et al. [2]. As for the vast tourist GPS data, foreign scholars such as Orellana et al. have proposed to analyze the data with both MSPs (Movement Suspension Patterns) and GSPs (Generalized Sequential Patterns), while MSPs represent places where tourists stop moving for interests and GSPs represent the general time order of places visited by tourists [3]. Huang and other scholars have utilized ArcGIS technology to realize three-dimensional visualization of space-time route from GPS track points, evaluating and analyzing the length of route, time, speed, and coverage of sightseeing. And combining the concept of space-time-route theory with two-pole emotions of tourism experience model, they also have proposed a concept of "Tourism Emotional Path" (TEP) to study the black box of tourists' emotions in their tourism experience [4].

From the perspective of the environment-behavior science, this paper takes the space design of a digital village in Youzhaqiao Village on the outskirts of Guangshui City, for example, to record and track the behavior and activity of residents and tourists in the area via mobile phone motion track recording software. Based on the collection, selection, and collation of the trajectory data, the valid data has been counted and analyzed; finally, the field investigation and questionnaires have been integrated to propose an optimization strategy for the use and design of the space of Youzhaqiao Village from aspects such as human perception, cognition, and behavior.

2.2. Research Significance

2.2.1. It Has Practical Guiding Significance for the Spatial Layout of Rural Tourism. Through the analysis of the spatial characteristics and dilemmas of rural tourism and the feasibility analysis of digital applications, empirical cases are studied, and typical spatial planning models are extracted, which provides important technical support and practical reference for the formulation of digital rural spatial development strategies and policies in Hubei Province. Based on this, it has the following three practical guiding significances: first, guide local governments to effectively manage the use of rural tourism resources, scientifically guide the layout of rural tourism landscapes, and promote the construction of a digital rural tourism system; second, provide references for the design of policies and systems for rural tourism spatial planning in Hubei Province; and third, provide technical and methodological support for the preparation of rural planning in Hubei Province.

2.2.2. Provide Technical Support for Improving Digital Rural Tourism Planning. Innovatively integrating spatio-temporal behavior trajectory data analysis technology into rural tourism spatial planning and solving its compatibility problem will significantly enhance the application value of digital technology in rural lagging areas, highlight its basic supporting role for the optimization of rural tourism space layout, and further improve the accuracy and appropriateness of digital rural tourism space planning strategies, which has strong practicality.

2.2.3. Explore and Improve the Optimization Path of Digital Rural Tourism Spatial Layout. Based on multiple elements, this paper accurately identifies the spatial characteristics and spatial distribution law of rural tourism and clearly captures the landscape structure, functional distribution, behavior analysis, development direction, and tourist agglomeration effect of rural tourism.

3. Analysis of the Current Space Situation in Youzhaqiao Village

3.1. Advantages

3.1.1. Excellent Transportation Accessibility. Roads pass through the village within the 10-minute reach of the urban area of Yingshan City, which is feasible for one-day tour line.

3.1.2. Beautiful Natural Landscape. Ponds and hillocks are surrounded by lucid waters and lush mountains, which are the foundation for the development of leisure and sightseeing agriculture and rural tourism.

3.1.3. Rich in Cultural Sites. The existing well-protected cultural and historical resources include the old paths of the Tea Horse Road, the old-style private school site, and the old battlefield site of the New Fourth Army and the traditional edible oil extracting workshop.

3.2. Disadvantages

3.2.1. Disorganized Layout of Farm Houses. Youzhaqiao Village has many natural winding roads, with ordinary farmhouses scattered around which are various in building time and style. There exists interference between the daily life of villagers and the tour routes of tourists.

3.2.2. Narrow and Limited Space in This Village. The layout of the farm settlements is rather haphazard, the villagers' farmhouses are located with small spaces between each other, and there are sloppily built-up buildings, which make scarce land available for construction for rest and relaxing, landscape installations, or fitness facilities.

3.2.3. Public Service Facilities, such as Toilets and Other Infrastructure Facilities, Need to Be Improved. Village roads need widening and upgrading because insufficient traffic capacity and low road grade, recreational areas and activity centers, and tourism support services should be supplemented.

3.3. Principles of Digital Rural Space Construction Compared with Other Regions. Villages have their own ecosystems, but this environmental carrying capacity is low, and environmental quality is susceptible to natural and human factors. Therefore, the antidisturbance ability of the ecosystem in ecologically fragile areas is weak; the environmental quality and ecological balance are more susceptible to extensive management behavior, while the sustainable development of rural tourism is to maintain the sustainable use of tourism resources and ecological balance [5], so the sustainable development of rural tourism in this area is more likely to be affected by extensive management behaviors, and the development concept and business methods are more measurable for the sustainable development of rural tourism in the region. According to this, more relevant research and measurement indicators highlight the impact of geomorphological climate, development concept, and operation modes on the sustainable development of rural tourism in ecologically fragile areas and pay more attention to geomorphological and climatic characteristics, tourism resources, etc.: the measurement of sustainable development of rural tourism in ecologically fragile areas and the analysis of influencing factors such as climate and geology. Conditions, quality of tourism resources, degree of regional cultural display, tourism experience, etc.

4. The Common Tools of Environment Spatio-Temporal Behavior Research

As China's urban construction gradually turns to the stock era, planning and design have new requirements for research tools and analysis methods. The traditional research process mainly adopts observation, photography, interview, questionnaire, and manual counting, which is not only difficult to record data with low accuracy and strong subjectivity but also costs a lot of energy in the subsequent analysis. In the era of big data, a number of fast and convenient intelligent research tools have gradually emerged. This paper will introduce a comprehensive tool of track recording in the investigation of environment spatio-temporal behavior [6].

Trajectory data is the data information obtained by sampling the movement process of one or more moving objects in the space-time environment, including the location, sampling time and speed of sampling points, etc., which constitute the trajectory data according to the sequence of sampling. For example, for smart phones with positioning function, the track data reflects the mobile phone holder's action status in a certain period of time. Mobile Internet can locate the location of the phone through wireless signals and then sample and record and form the mobile phone holder's movement track data by connecting the sampling points. GPS positioning terminals can also collect trajectory data [6].

By processing the track data in ArcGIS, the core density of human flow, residence time, and average speed can be analyzed. Among them, the average trajectory speed can reflect the comfort or landscape attraction, and the average trajectory stay time can reflect the activity attraction [6].

5. Research Method Based on Spatial-Temporal Behavior Trajectory

5.1. The Acquisition of Spatial-Temporal Behavior Trajectory. With the spatial temporal behavior trajectory, the main research and analysis method of this paper, we have invited tourists and local volunteers to record their behavioral trajectories by using the mobile phone app and collected and filed the data as GPX formatted trajectory files, from which we have obtained the basic information about their behaviors, including walking path length, walking speed, traveling time, and staying position. We then import the files into processing software such as ArcGIS and then overlay and classify multiple data to finally conduct behavioral pattern analysis. Our train of thought in spatial-temporal behavioral trajectory analysis is as follows.

5.1.1. Comparative Analysis of the Spatial-Temporal Behavior Trajectory of Tourists and Residents. Firstly, we collect and analyze the behavioral trajectories of tourists and residents separately to find the contradictions in spatial use between them. Taking Youzhaqiao Village as an example, we search for contradictions and propose corresponding optimization strategies and then put forward a purposeful landscape design based on the contradictions and optimization strategies.

5.1.2. Analysis of the Most Beautiful Tourist Route. After resolving the contradictions in spatial use between residents and tourists, we analyze the spatial and temporal behavioral trajectories of tourists, paying particular attention to the most traveled routes and the most visited areas, combining this with questionnaires to collect information on the history and culture of local attractions and the location of scenic spots which is worth to visit. In the case of Youzhaqiao Village, we recommend the most beautiful tour routes for tourists.

5.1.3. Analysis of Categorical Planning and Tourism Design. We categorize the tourists from an age perspective, referring to the three age groups proposed by the WHO (World Health Organization), namely, young people under 44, middle-aged people between 45 and 59, and older people over 60. Based on this, we have analyzed the characteristics of each age group and the route of their spatial and temporal behavior and have developed different types of tourism designs for different age groups.

5.2. Questionnaires and Field Investigation. Questionnaires and field investigation are one of the most important information collection methods for tourism landscape design, and the results collected by this method will be used as a subjective supplement in this paper to make up for the defects of spatial-temporal behavior trajectory data in terms of human history and local condition. Therefore, questionnaires and field investigation are used to collect data on the daily life, age distribution, history, culture, and folk customs of the residents of Youzhaqiao Village. A total 200 questionnaires were distributed, and 188 valid questionnaires were recovered (as shown in Table 1). By combining

Table 1: Behavior analysis table of Youzhaqiao Village.

Statistical analysis of behavior types in Youzhaqiao Village	The number	The proportion
Take a rest	15	7%
Pass by	25	13.2%
Leisure and entertainment	22	11.7%
Experience local customs	38	20.2%
Visit cultural and historical sites	25	13.2%
Sightseeing orchard tea garden	35	18.6%
Repast	22	11.7%

the spatial-temporal behavioral trajectories of the residents, we are able to analyze the local conditions in Youzhaqiao Village more thoroughly and thus design and formulate subjective optimization strategies from an objective perspective based on the trajectories.

5.3. Data Sources. The questionnaire set up 14 statistical variables, in line with the principle of being representative, evaluable, and easy to answer, from October 10 to 18, 2019, in the Guangshui oil and oil bridge village tourist site and the location of government departments, in the form of in-depth interview presurvey, with the village tourism operators and managers to demonstrate, after the questionnaire is improved, from October 19, 2019, to August 25, 2020, in the case of rural tourism, in the form of field distribution of questionnaires to investigate. A total of 188 valid questionnaires and 12 invalid questionnaires were collected, and the effective questionnaire rate was 94%, including 140 tourists, 30 rural tourism operators, and 10 rural tourism managers *74.4% of tourists, 21.5% of operators, and 6.6% of managers, respectively). The data of the valid questionnaire were collected, and the data of the two variables that were not related to the sustainable development indicators of rural tourism in the case area were excluded, and the remaining data were valid data, and the valid data were the data sources of the empirical analysis.

6. Analysis of Spatial-Temporal Behavior Trajectory Data in Youzhaqiao Village

6.1. Paradoxical Analysis of Residents and Tourists' Behavior Trajectories. We have collected 200 pieces of information on the spatial-temporal behavioral trajectories of tourists and local residents, respectively, through the smart terminal of the mobile phone app. According to their spatial distribution characteristics, before getting the road planning, it can be seen from the picture in Figure 1 that tourists have a long time to stay at the entrance of the village due to the limited public car parks and the insufficient width of the roads in the village, as well as the insufficient number of public toilets and long waiting times (as shown in Figure 1).

In tea plantations and orchard areas, the spatial-temporal behavioral trajectories of residents and tourists frequently intersect, where the contradiction in spatial use is most serious. We also observe that in the residents' questionnaires and field investigation, pig and cattle farming in the village is predominantly free range, which has led to a disorganized spatial-temporal behavioral trajectory for the residents. In the areas where the residents live and work, tourists pick, trample, and destroy crops at will, causing some damage to the environment of the cultivated farms (Figure 2). As for the above-mentioned areas including the ancient tea horse paths, they are within the essential routes to tourist attractions where tourists stay for a long time. Therefore, the most serious contradictory impacts are on the areas of tea plantations and orchards, for which spatial optimization and guidance measures are proposed.

6.2. Countermeasures for Contradictory Space Optimization. We have planned ecological public car parks in separate points to alleviate the parking demand of tourists and to renovate the motorways in the village. Focusing on renovating and upgrading space between lotus and tea plantations, we suggest transforming the mountainous area into a multifunctional sightseeing tea gardens and orchards, building a spatial pattern where agricultural production keeps pace with tourism. In addition, we choose the hillside land far from the village and water system to build a centralized farming area and build the sewage system.

6.3. Analysis of the Best Tour Route. The best tour route is recommended by considering three aspects: firstly, the attractiveness calculated by the density of tourists' trajectories; secondly, the degree of attraction of the scenic spots along the route; and thirdly, the length of the tour route, meaning that tourists can spend a limited amount of time appreciating more beautiful spots. Combining the overall geographically spatial distribution of the village, the distribution of the main historical and cultural attractions, and the most prevailing trajectory of tourists, we recommend taking the "one axis, two zones" of the leisure and tourism agricultural structure for tourism. The axis is the transportation development axis (the ancient Tea Horse Road), linking the two sides of Shima Road and being the main traffic axis for the development of modern agricultural industry in Youzhaqiao Village. The two zones are the recreational agriculture zone and the space lotus zone. Through experiments, we can find the best tour route, which can fully reflect the comprehensive effect of nature, ecology, and environment, combining agricultural production with science, education, agricultural experience, and tourism in a scientific way and giving visitors multiple choices (as shown in Figure 3).

Rural tourism scenic spots often have many scenic spots, large regional areas, and complex routes in the area; among the many attractions in the village, choose a satisfactory tourist route, so that tourists can visit at the time; the cost and the tourism experience can be satisfied, which is a problem that tourists expect and scenic planners and managers are studying. Based on the thinking of this problem, the system will collect the relevant registration information of the user (age, gender, hobbies, things, city, etc.) data, using the background server to recommend the analysis of the algorithm rational, accurate to provide tourists with reasonable tourism routes. Using this method can both allow tourists to avoid travel at peak of the crowd, save travel time, see

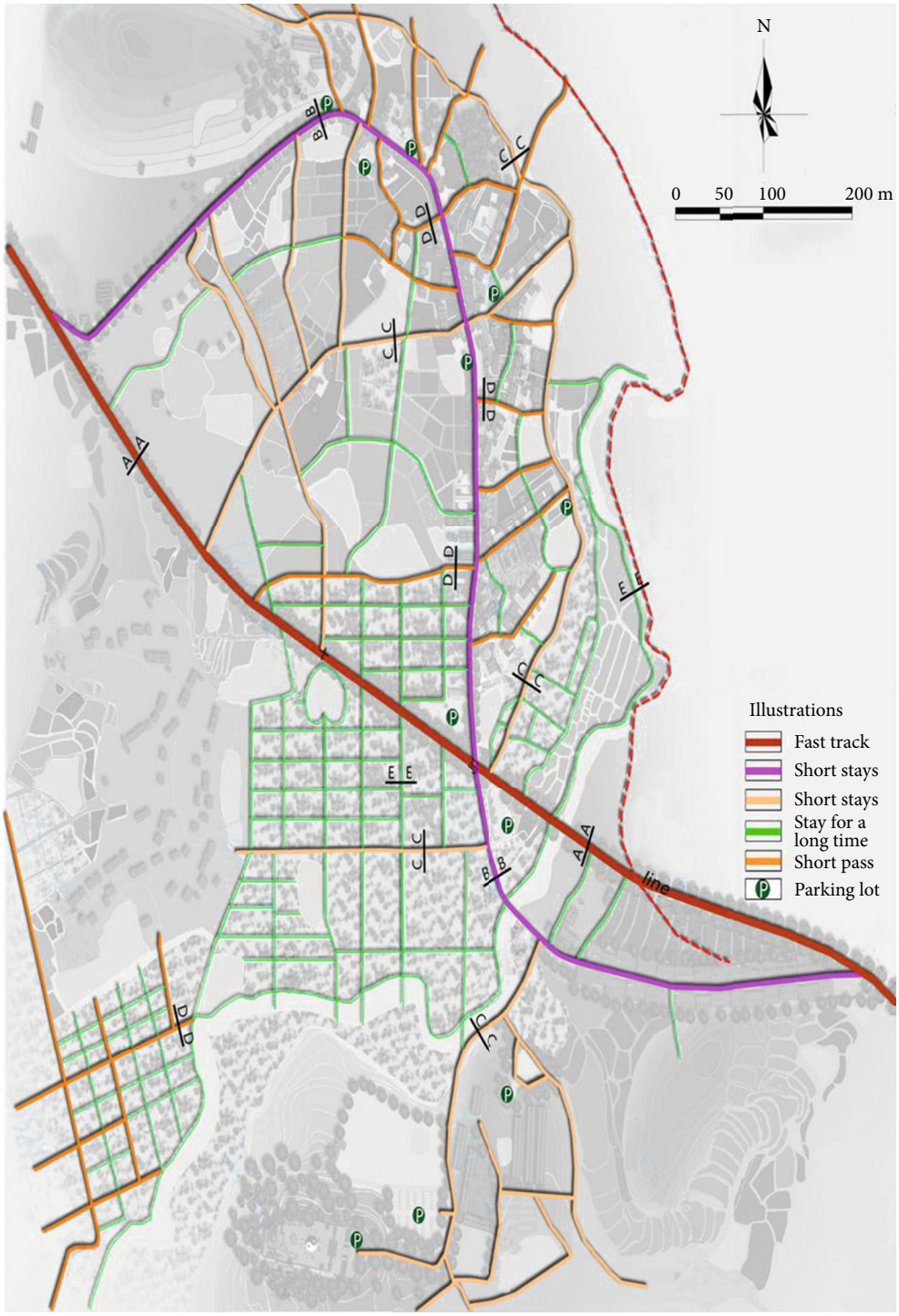

Figure 1: Map of residents' behavior patterns and stay time in Youzhaqiao Village.

the most popular attractions, and choose the one that suits their physical strength. The tour distance can improve the turnover efficiency of scenic spots [7].

6.4. Analysis Based on Age Classification and Tour Design. For the 200 behavioral trajectory data collected from tourists, by calculating the density and stay time of short time behavioral trajectories, we can get the difference in vitality and attractiveness of each spot in the village's scenic space (as shown in Table 2). We can classify visitors as young, middle-aged, and elderly. The elderly focus on and enjoy history and culture; therefore, the most frequent trajectory of the elderly is set as a cultural tour route including the space lotus cultural square, the theme exhibition hall, and the tourist tea plantations. The young and middle-aged are more interested in leisure, entertainment, and enjoyment, so the most common route for the young and middle-aged is the recreational route, which is more

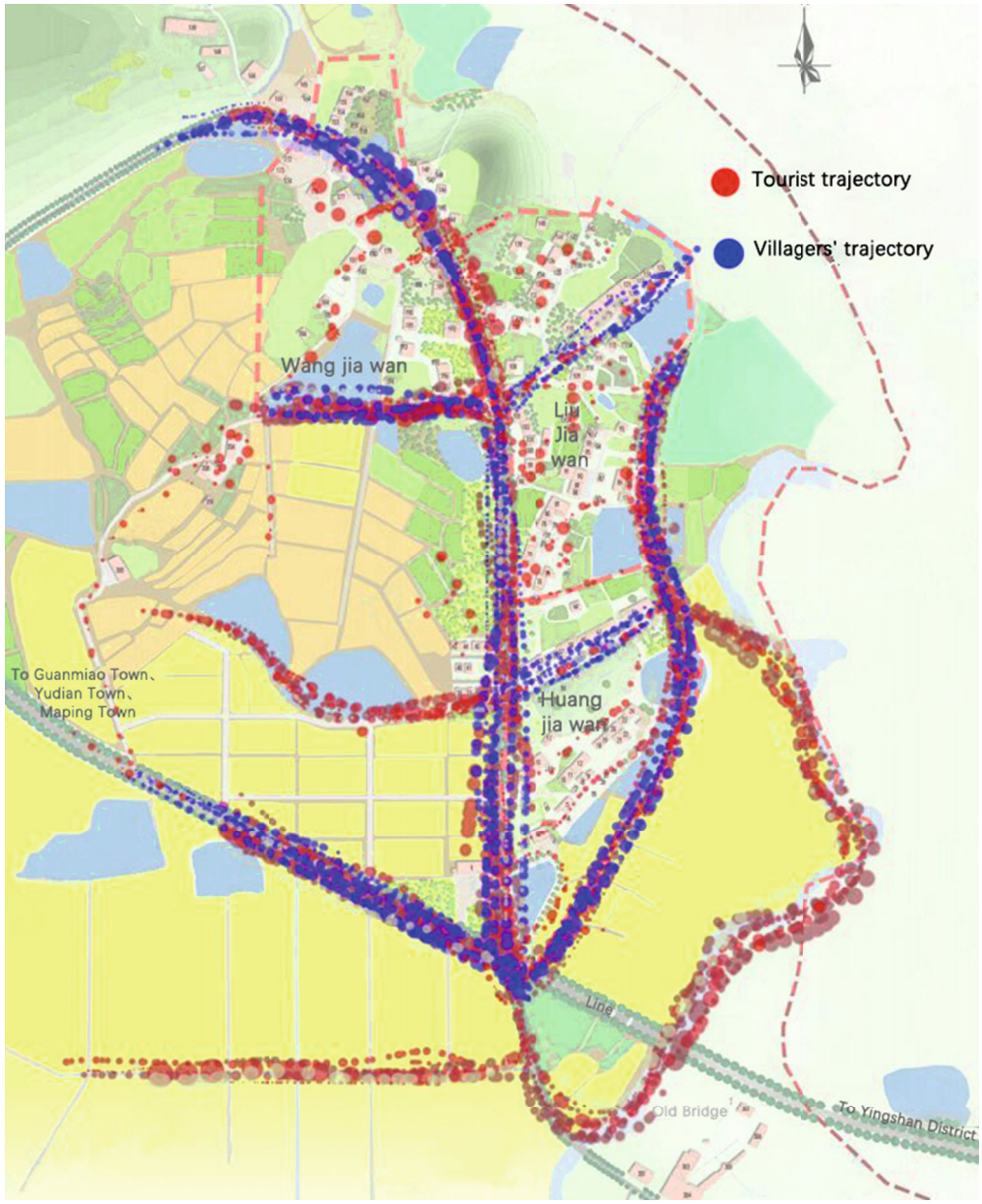

Figure 2: Map of tourists' and villagers' behavior trajectory.

inclined towards entertainment and food shopping and links the farmhouse enjoyment in Huangjiawan and Wangjiawan, the lotus-picking wharf square, vicinity of ancient Youzhaqiao bridge, the imperial city temple square, the shopping and commercial street, and the space lotus trade market (as shown in Figure 4).

6.5. Based on Behavior and Public Service Facility Evaluation Model. In this paper, residence time and supply time of public service facilities are used as two variables to measure the adaptability of regional supply and demand. Behavior trajectory data reflects the demand of tourists and combined with the superposition analysis of existing stay facilities can reflect the supply-demand relationship between this space and stay behavior (as shown in Figure 5).

(1) Determine supply levels

$$X\mathrm{ti} = \mathrm{Fi}\, T. \tag{1}$$

The supply level of stopover facilities at time t in grid I is X. Among them, the supply level of the stay facilities in the period in the first grid is the number of facilities in the first grid and the supply time of the facilities in the grid.

(2) Determine demand levels

$$Y\mathrm{ti} = (R\mathrm{ti} - S\mathrm{ti} + T\mathrm{ti}) \times T\mathrm{Ati}. \tag{2}$$

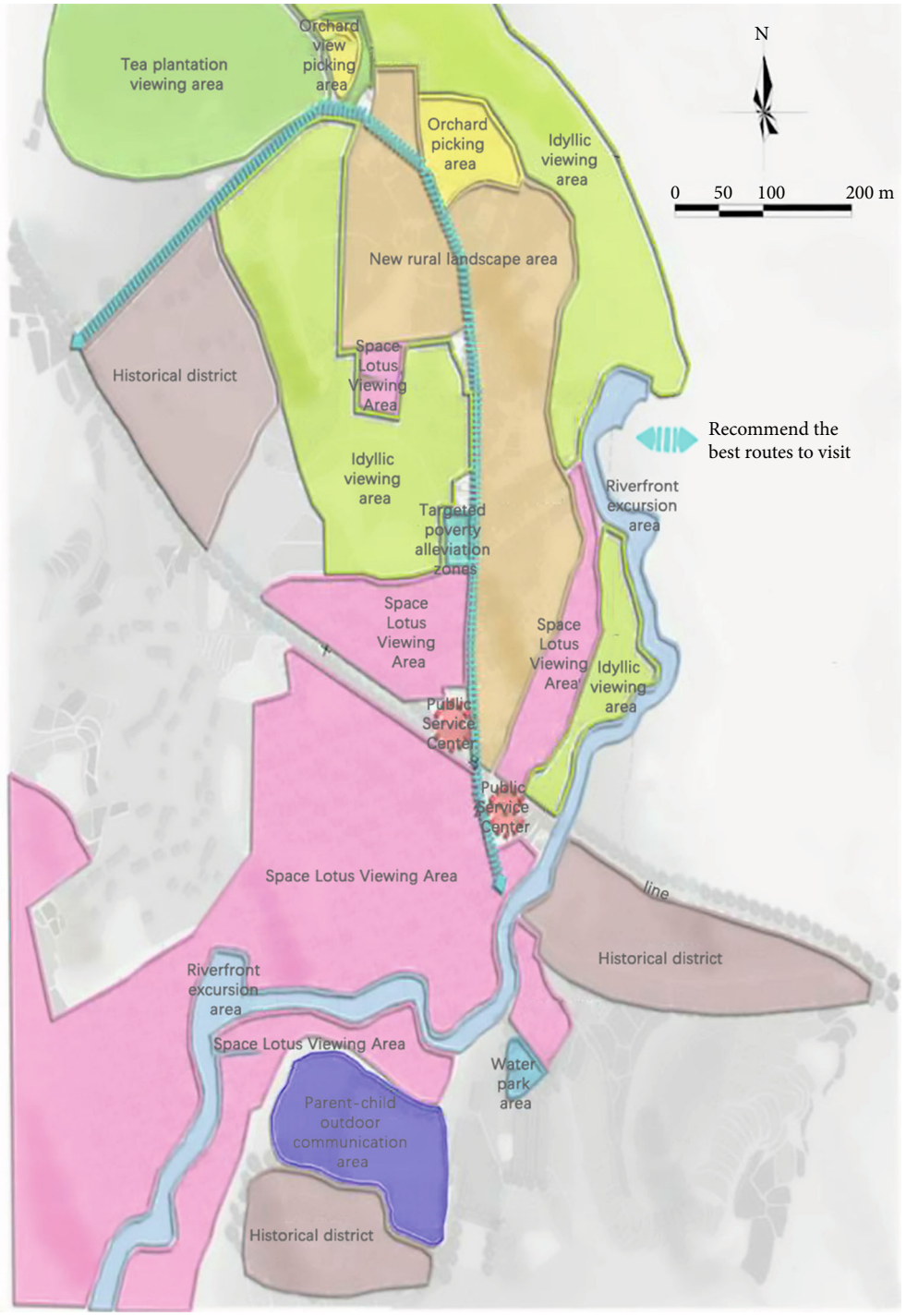

Figure 3: Recommendation of the best tour route based on analysis of trajectory data.

Table 2: Space vitality evaluation form.

	Sightseeing tea garden	Space lotus culture square	The ancient Tea Horse Road	Theme exhibition hall	Agritainment	Food shopping
Frequency	Lower	Higher	Lowest	Lower	Higher	Highest
Stay time	Higher	Lower	Lower	Higher	Higher	Highest
Overview	Landscape vitality	Lowest vitality	Traffic vitality	Higher vitality	Higher vitality	Highest vitality

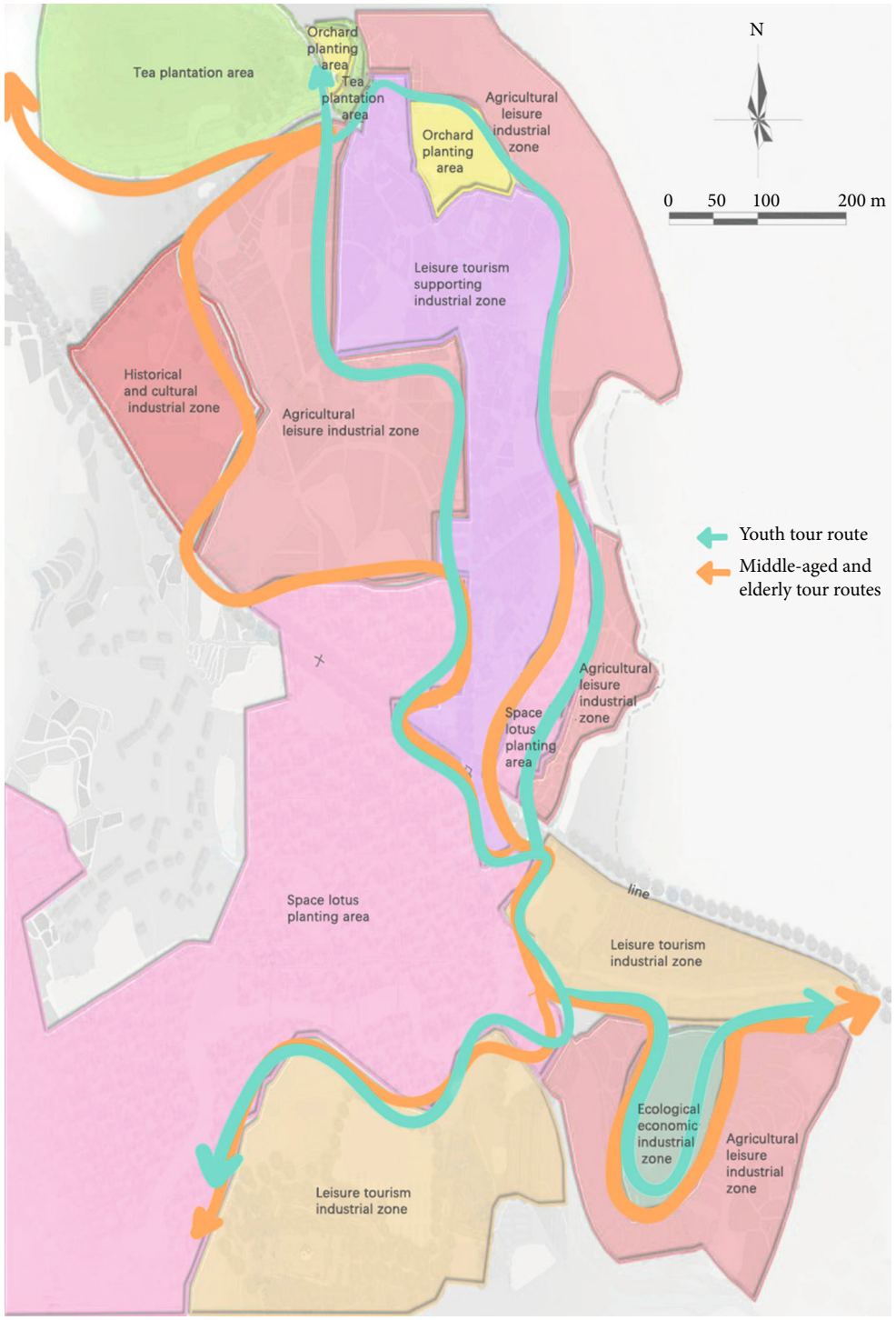

Figure 4: Recommendation of the tour route for young and middle-aged tourists based on analysis of trajectory data.

Demand level in period t in grid I is Y = (regional inflow number in period T in grid I − outflow number in period T in grid I + fixed number of people in period T in grid I) × per capita residence time in period T in grid I TAti. Among them, the demand level of the period in the first grid is the number of people flowing in the period of the first grid, the number of people flowing out of the period in the grid, the fixed number of people in the period of the first grid, and the per capita stay time in the grid period.

(3) Overlay analysis

$$B\text{ti} = \frac{Y\text{ti}}{X\text{ti}} \tag{3}$$

Demand level is Yti/supply level Xti = supply − demand relationship Bti. Among them, it is the relationship between

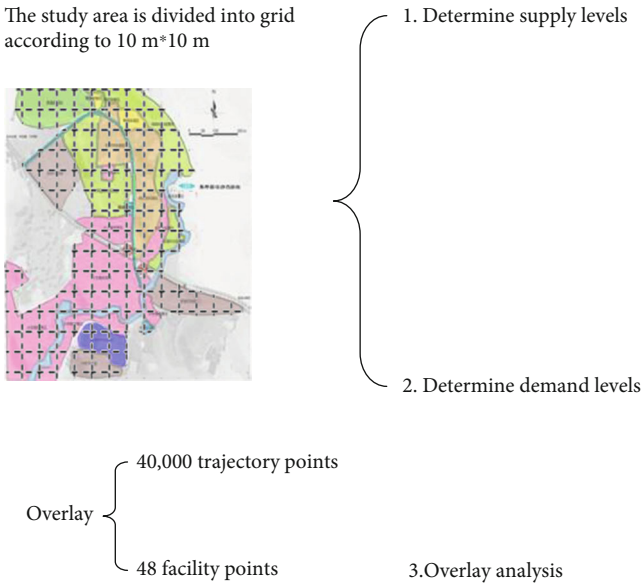

Figure 5: Grid diagram.

supply and demand, the level of demand, and the level of supply.

In essence, the balance of supply and demand is to keep a balance between the supply quantity and composition of public service facilities and the demand and composition of tourists and to provide different aspects of supply according to different needs, to seek a more harmonious and long-term development of rural tourist attractions.

According to the statistical analysis, in the areas with stopover or stopover facilities, the proportion of areas with demand greater than supply is as high as 78.6%, areas with demand less than supply account for 8.3%, and areas with good supply and demand only account for 5.2%.

6.5.1. Lack of Vitality. Excess space resources and areas where the supply of public service facilities exceeded the demand accounted for 8.3%, mainly in some areas of sightseeing tea gardens and space lotus culture square. The above areas have less people flow and few stay, and public service facilities are generally idle.

6.5.2. Rational Use. In space supply and demand balance, areas where supply equals demand account for 5.2%, mainly in space lotus culture square and theme exhibition hall. The above-mentioned area stay facilities are set appropriately to reasonably meet the needs of the crowd to stay.

6.5.3. Overload. Excessive demand for space is 78.6% of the regions where the supply is less than the demand, including theme exhibition hall, agritainment, and food shopping. Covering most of the activity areas of rural tourism scenic spots, the area has few stay facilities, which cannot meet the normal stay needs of tourists.

On the whole, the supply and demand of stay facilities in the rural core landscape area are extremely unbalanced. There are insufficient quantities, single type, and low frequency of partial use.

The optimization of the use of space stay facilities in scenic spots is mainly through reasonable adjustment of the number of public service facilities and flexible increase in the area with a large demand or by changing the composition of rural space landscape, analyzing the specific reasons for the oversupply of service facilities in areas, and guiding people to use stay facilities or transform them into other use spaces through design [8].

This paper evaluated the supply and demand status of rural spatial stopover facilities by using the GIS analysis method based on the characteristics of stopover facility layout and trajectory stay time information and provided new research ideas and design references for the characteristics of rural digital space.

Under the influence of the global spread of COVID-19 in 2020, the demand for outdoor social communication activities is increasing, which is of great significance to the spatial development of digital rural tourism [8]. In addition to meeting basic needs, it is more important to improve the spatial quality of rural digital tourism through stay facilities.

7. Conclusion

The design of the digital village space is a complex and large systematic project. Through data analysis based on the spatial-temporal trajectory data analysis in this spatial environment survey of Youzhaqiao Village, the behavioral patterns and distribution characteristics of residents and tourists can be intuitively and objectively found, and the best and most optimal routes can be recommended, providing reliable support for the design [4]. As an innovative data collection method, spatial-temporal behavioral trajectory data analysis has its advantages of realistic, real-time information and wide coverage, largely compensating for the ambiguity of traditional survey methods of collecting behavioral data and providing real-time, accurate, and rich information of various kinds, playing an important role in the space design of digital villages. Hence, the combination of trajectory data of spatial-temporal behavior and traditional survey methods will become an important approach to environmental behavior research [5].

Data Availability

Data sharing is not applicable to this article as no datasets were generated or analyzed during the current study.

Conflicts of Interest

The author declares that he has no conflicts of interest.

Acknowledgments

This study was financially supported by the Provincial Teaching Research Project of Colleges and Universities in Hubei Province: Research on Reform of Practical Teaching of Major Courses of Environmental Design Based on Immersive Virtual Simulation Technology in 2020 (no. 2020631).

References

[1] P. Chao, "The logic in the advancement of digital villages strategy," *The People's Forum*, vol. 33, pp. 72-73, 2019.

[2] G. Meibao, S. Yue, Z. Ying, and C. Yanwei, "Method in the research of time geography: geographical calculation and visualization of behavioral pattern of human beings," *International Metropolitan Design*, vol. 25, no. 6, pp. 18–26, 2010.

[3] D. Orellana, A. K. Bregt, A. Ligtenberg, and M. Wachowicz, "Exploring visitor movement patterns in natural recreational areas," *Tourism Management*, vol. 33, no. 3, pp. 672–682, 2012.

[4] H. Xiaoting, L. Meixuan, Z. Haiping, and Q. Qianlong, "Study of tourism spatial-temporal Bevavior assessment based on GPS data," *Tourism Journal*, vol. 31, no. 9, pp. 40–49, 2016.

[5] H. Xiaoting, "Study of the process of the tourism emotional experience based on spatial-temporal routes-taking the Hong Kong Ocean park as an example," *Tourism Journal*, vol. 30, no. 6, pp. 39–45, 2015.

[6] EBSD Research Group Public Account, *Research Toolkit*, p. 10, 2021.

[7] S. Zexiao, Z. Banghong, Q. Anchen, and Z. Kexi, "Analysis of sustainable development measurement and influencing factors of rural tourism in ecologically fragile areas: a case study of Dongchuan District, Kunming City," *Rural Science and Technology*, vol. 10, 2019.

[8] Z. Xia and W. Shucheng, *Evaluation and Application of Stay Behavior Adaptability in Wuhan University Campus Open Space Based on Behavior Trajectory Data Analysis*, vol. 1, Published in Huazhong Architecture, 2022.

Hindawi
Wireless Communications and Mobile Computing
Volume 2022, Article ID 3696817, 11 pages
https://doi.org/10.1155/2022/3696817

Research Article

Hierarchical Coordinated Control of DC Microgrid Based on Recursive Fuzzy Neural Network Algorithm

Haotian Wu,[1,2] **Zhong Wei**,[1] **Shiwen Liu**,[3] **and Ming Shi**[1]

[1]*Shanghai Investigation, Design & Research Institute Co., Ltd, Shanghai 200335, China*
[2]*North China Electric Power University, Beijing 102206, China*
[3]*Shanghai University of Electric Power, Shanghai 200000, China*

Correspondence should be addressed to Haotian Wu; 50201603@ncepu.edu.cn

Received 16 April 2022; Revised 19 May 2022; Accepted 28 May 2022; Published 23 June 2022

Academic Editor: Jun Ye

In order to realize the stable operation of the DC microgrid, a hierarchical coordinated control method of the DC microgrid based on the recursive fuzzy neural network algorithm is designed in this article. Based on the analysis of the working mode and topology of the DC microgrid, the droop control coefficient is calculated through power flow calculation, and then, a three-layer control strategy is designed combined with a hierarchical coordinated control algorithm to realize the distributed coordinated control of DC microgrid. Combined with the recursive fuzzy neural network algorithm, the real-time amplitude limiting and convergence of the output of the distributed coordination controller are realized. Experimental results show that under the control of this method, the changes in current and voltage at each port of the DC microgrid are relatively stable during off-grid switching. In addition, this method effectively reduces the fault rate of power grid lines, which fully proves the feasibility and reliability of this method.

1. Introduction

With the increasing proportion of renewable energy such as solar energy and wind energy connected to the power grid, microgrid has been widely used as an important form of distributed energy access [1]. Since the microgrid contains a large number of DC power supplies, such as photovoltaic, fuel cells, and energy storage, as well as DC loads, such as LED lighting and electric vehicles, the traditional AC microgrid needs the connection of commutators to access these power supplies and loads, which increases the cost and loss. Therefore, in recent years, the DC microgrid has attracted more and more attention from academic and industrial circles at home and abroad [2]. With the continuous development of power electronics technology, insulated gate bipolar transistor (IGBT) and digital signal processing (DSP) appear one after another. A voltage source converter (VSC) is mainly composed of IGBT, and its control system is mainly composed of DSP. VSC can be self-commutating without an AC system providing commutation voltage. Secondly, VSC can independently control the output of active and reactive power through IGBT. Finally, when the power flow reverses, the direction of DC current reverses, and the DC voltage remains unchanged. This is the theoretical basis of parallel multiterminal flexible DC (VSC-MTDC). Nowadays, VSC-MTDC is the main topology of the DC microgrid. The construction of a DC microgrid based on VSC-MTDC is an effective way to solve DC load grid connection and DC power consumption [3].

The multiterminal DC microgrid based on VSC-MTDC has high control ability and flexibility compared with the traditional AC microgrid, but its operation control strategy is relatively complex. In particular, the control of DC voltage is the most important control goal of a multiterminal DC microgrid because it is related to the stability of DC power flow. At present, the mainstream control strategies of multiterminal DC microgrids are mainly divided into two categories: one is single-point DC voltage control, and the other is multipoint DC voltage control. Among them, single-point DC voltage control is divided into master-slave control and voltage margin control, and multipoint DC voltage control is divided into voltage slope control and segmented voltage

slope control [4]. Based on the background of multiterminal flexible DC transmission, Reference [5] discusses the development status and main control modes of multiterminal DC microgrid and discusses the advantages and disadvantages, existing problems, and protection methods of various control modes. Reference [6] designed the DC microgrid distributed coordination method based on finite time consistency. In this control method, voltage secondary control and power generation cost operation control are introduced based on the original droop control, and each power generation unit is only communicated with the adjacent communication unit, and multiple control objectives such as voltage stability and power generation cost minimization are achieved by the finite time consistency algorithm. In Reference [7], a multisource coordinated control method for DC microgrid based on virtual voltage is designed. Combined with the idea of virtual voltage and autonomous decentralized control, this method firstly analyzes the influence of line resistance on current-sharing control in detail, proposes a current-sharing control strategy based on virtual voltage, and then proposes an improved dynamic consistency algorithm, which can dynamically track and control the busbar voltage at the outlet of each converter and quickly converge the consistent value.

In the past few years, the neural network has been used to identify and control the real-time value of a nonlinear system, and the DC microgrid is essentially a nonlinear input-output system. The recursive fuzzy neural network (RFNN) combines many advantages of recurrent neural network (RNN) and fuzzy control. It has the advantages of low-level learning and computing ability, as well as high-level human-like thinking and reasoning of fuzzy theory. Reference [8] proposed a servo-driven adaptive hybrid control system of permanent magnet synchronous motor (PMSM) based on self-evolving fuzzy neural network (RRSEFNN) based on recursive radial basis function network (RBFN). RRSEFNN combines the advantages of the self-evolving fuzzy neural network, recursive neural network, and RBFN. The simulation results show that this method has accurate dynamic response ability. In Reference [9], a backstepping control system with specified tracking performance using tracking error constraints and recursive fuzzy neural network (RFNN) is proposed for strict feedback nonlinear dynamic systems. Through the control of a nonlinear system and a manipulator, the effectiveness of the control method is verified. However, the real-time output of the DC microgrid controller is usually unstable, so a recursive fuzzy neural algorithm can be used to optimize the output of the DC microgrid controller to maintain the amplitude limitation and convergence of controller output.

In view of the above problems, a distributed coordinated control method of DC microgrid based on power flow calculation is designed in this article. Based on the analysis of the working mode of the DC microgrid, the droop control coefficient of the DC microgrid is calculated through power flow calculation, and then, combined with the hierarchical control strategy, a three-layer control mode is designed to enhance the feedback connection of the control process. Among them, the first layer is equipment-level control, and the second and third layers are system-level control to realize the distributed coordinated control of the DC microgrid. In the third layer control of system level, a recursive fuzzy neural network algorithm is introduced to optimize the output of the hierarchical controller, so as to maintain the amplitude limitation and convergence of output and improve dynamic response ability of the controller.

2. Analysis of Working Mode of DC Microgrid

The topology of the DC microgrid is one of the research hot spots at home and abroad. Many scholars have proposed different types of DC microgrid topologies. For example, the Royal Swedish Institute of Technology proposed a mesh structure interconnected by multiple converters; the Swedish CIGRE Institute proposed a ring network structure similar to multiterminal DC transmission. The layered structure of the DC microgrid is proposed by Aachen University of Technology according to different voltage levels. At present, common topologies mainly include parallel dendrite topology and ring network topology, as shown in Figure 1.

In Figure 1, the solid line represents the positive electrode, and the dotted line represents the negative electrode. The DC microgrid structure in this article adopts a ring network topology. In this article, the working modes of DC microgrid are summarized into five situations, the specific contents of which are as follows:

Mode (1): grid-connected operation. The power generation system runs in MPPT (Maximum Power Point Tracking) mode, the battery converter and two-way AC/DC adopt voltage sag control, and the battery works in charging or standby state according to the charge.

Mode (2): grid-connected operation. The power generation system operates in MPPT mode with a heavy load. The bidirectional AC/DC works in the current-limiting state of full power and needs to be discharged by the battery to maintain the load terminal voltage stability.

Mode (3): off-grid operation. The power generation system operates in MPPT mode, and the load terminal voltage is kept stable by the battery.

Mode (4): off-grid operation under light load (load power is less than the output power of PV MPPT mode control). The battery is full (SOC > 90%), and the power generation system operates in constant voltage mode to keep the load terminal voltage constant.

Mode (5): off-grid operation. Under heavy load (load is greater than the output power of PV MPPT control), the battery has reached the maximum discharge current or the discharge is too low (SOC < 40%), the power generation system operates in MPPT mode, and part of the load needs to be removed to keep the voltage at the load end constant, so as to ensure the power supply of important loads.

In modes (1) and (2) in the parallel operation mode and mode (3) which is the off-grid run time, the battery converter and bidirectional AC/DC converter use droop control, load voltage fluctuates with the load, and some is more sensitive to voltage change of load to maintain a constant voltage, so it needs to compensate the voltage of the load [10, 11]. In modes (4) and (5), the load terminal voltage is

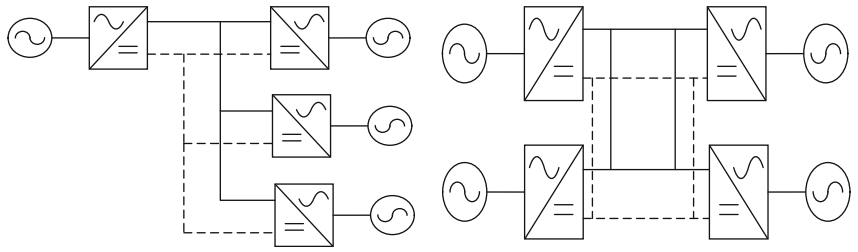

(a) Parallel dendrite topology (b) Ring network topology

Figure 1: Common topology of DC microgrid.

accomplished by the photovoltaic DC/DC converter. Therefore, the load terminal voltage control error needs to be transmitted to these three converters [12].

3. Power Flow Calculation

Based on the consideration of droop control, this article realizes the inwards calculation. The DC microgrid structure studied in this paper is shown in Figure 2.

In Figure 2, DC bus voltage stability is mainly achieved by the AC power source and battery. The AC power source is connected to the DC microgrid through a two-way AC/DC rectifier. The battery is connected to the DC microgrid through a DC/DC converter. The photovoltaic source is connected to the DC microgrid through a DC-DC converter and mainly operates in the MPPT mode. The load connected to the DC microgrid is set as a constant power load.

In the DC microgrid power flow, nodes can be divided into two types [13]. In this study, they are defined as W nodes and Q nodes, where the node power equation of Q node is

$$Q_{dci} = U_{dci}\sum_{j\in i} Y_{ij}U_{dcj}, \tag{1}$$

where $j \in i$ means that node j after $\sum Y_{ij}$ must be directly connected to node i. Therefore, the nonlinear equations of the voltage of each node can be written according to the power column of each node. According to the power control of DC microgrid photovoltaic grid inverter and wind power, constant power load equipment can see as Q node, but the energy storage device (such as battery and supercapacitor) converter and two-way parallel converter can neither as Q node nor as W here to define it as node WD, and the need to meet

$$\begin{cases} Q_{dci} = U_{dci}\sum_{j} Y_{ij}U_{dcj}, \\ U_{dci} = U_{0i}^{\text{ref}} - k_{di}I_{dci}, \\ I_{dci} = \dfrac{Q_{dci}}{U_{dci}}. \end{cases} \tag{2}$$

After sorting out formula (2), we can get

$$U_{0i}^{\text{ref}} = U_{dci} + k_{di}\sum_{j} Y_{ij}U_{dcj}. \tag{3}$$

When the bidirectional converter and battery grid-connected converter is controlled by drooping and the PV is controlled by MPPT, the power flow calculation formula is as follows when the load is constant power load:

$$\begin{aligned} U_{\text{dc\_}s}^{\text{ref}} &= k_s\left[\left(\frac{1}{r_{12}}+\frac{1}{r_{13}}\right)U_{\text{dc\_}s} - \frac{U_{\text{dc\_}b}}{r_{12}} - \frac{U_{\text{dc\_}l}}{r_{13}}\right] + U_{\text{dc\_}s}, \\ U_{\text{dc\_}b}^{\text{ref}} &= k_b\left[\left(\frac{1}{r_{12}}+\frac{1}{r_{24}}\right)U_{\text{dc\_}b} - \frac{U_{\text{dc\_}s}}{R_{12}} - \frac{U_{\text{dc\_}p}}{r_{24}}\right] + U_{\text{dc\_}b}, \\ Q_l &= U_{\text{dc\_}l}\left[\left(\frac{1}{r_{13}}+\frac{1}{r_{34}}\right)U_{\text{dc\_}l} - \frac{U_{\text{dc\_}s}}{r_{13}} - \frac{U_{\text{dc\_}p}}{r_{34}}\right], \\ Q_{\text{pv}} &= U_{\text{dc\_}p}\left[\left(\frac{1}{r_{24}}+\frac{1}{r_{34}}\right)U_{\text{dc\_}p} - \frac{U_{\text{dc\_}b}}{r_{24}} - \frac{U_{\text{dc\_}l}}{r_{34}}\right]. \end{aligned} \tag{4}$$

Given the node power of Q node and the reference voltage value and sag coefficient at WD node, the voltage of each node can be obtained by solving equation (4), and then, the power flow of each branch can be obtained [14]. According to formula (4), the influence of reference voltage, droop coefficient, and line impedance must be considered in the coordinated control. For example, suppose the PV adopts the MPPT mode to output power of 5 kW, and the power of constant power load is 10 kW. If the output of the AC/DC converter and battery converter is expected to be equal, the sagging control parameters of the two converters can be set to be the same; that is, when $U_{\text{dc\_}s}^{\text{ref}} = U_{\text{dc\_}b}^{\text{ref}} = 520$ V, $k_s = k_b = 0.5$, and $r_{12} = r_{13} = r_{24} = r_{34} = 2\Omega$, the voltage and injected power of each node are shown in Table 1.

Obviously, bidirectional converter and battery converter controlled by voltage sag use the same reference voltage value and sag coefficient, their output is not the same, which is related to the network topology and line resistance, and the output of each converter can be changed by changing the reference voltage value and sag coefficient [15]. For example, the reference voltage of the power battery increases as $U_{\text{dc\_}b}^{\text{ref}} = 525$ V, other parameters are constant, the AC/DC converter and battery converter output, respectively, 2.2 kW and 3.2 kW, and output of the storage battery is the

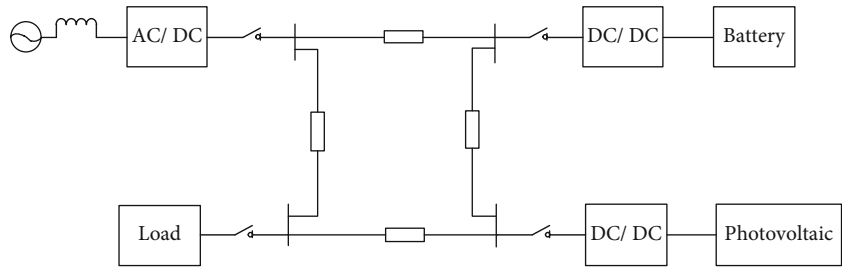

Figure 2: DC microgrid structure drawing.

Table 1: Voltage and power injection at each node.

Node	Voltage (V)	Power (kW)
AC/DC converter	515	5
Accumulator converter	518	2
Constant power load	496	10
Photovoltaic converter	517	5

proportion of increase; reducing the reference voltage of the power battery, the battery output will decrease, even by the discharge mode into charging mode. Similarly, changing the droop coefficient can also change the output of the converter.

To sum up, in the coordinated control of a DC microgrid, power flow calculation must be carried out first to verify whether the setting of the voltage reference value and sag coefficient matches the expected value of output power of each converter [16].

4. Hierarchical Coordinated Control of DC Microgrid

On the basis of the power flow calculation of the DC microgrid above, the droop control coefficient is calculated. Then, the structure and algorithm operation of the recursive fuzzy neural network are analyzed. The recursive fuzzy neural network algorithm is used to enhance the feedback connection of the control process, and a three-layer control strategy is designed.

The three-layer control strategy can be divided into device-level control and system-level control. Device-level control is based on local information to accomplish some basic control objectives similar to load distribution; system-level control is used to manage and optimize the whole system. The control objectives include the secondary regulation of DC bus voltage and the improvement of system operation efficiency, so as to achieve optimal operation. In this study, layer 1 is device-level control and layer 2 and layer 3 are system-level control.

4.1. Recursive Fuzzy Neural Network Analysis. The DC microgrid controller is a complex dynamic system with nonlinear and large time-varying characteristics. Its mechanism model is difficult to establish by conventional methods, and the stability of complex system control is particularly important in operation. Therefore, we limit and modify the output of the DC microgrid controller through a recursive fuzzy neural network to improve its convergence and dynamic performance. The control structure diagram based on the recursive fuzzy neural network algorithm in this paper is shown in Figure 3.

4.1.1. Structure Design of RFNN Identifier. The recursive fuzzy neural network is a kind of optimal recursive neural network, which uses the recursive network to realize fuzzy inference of the output results of the neural network. It has the advantages of both recursive neural network and fuzzy logic, which not only can reflect the dynamic mapping relationship between the output results of the neural network but also has the ability of qualitative knowledge expression, which is easy to determine the structure of the network and the parameters of neurons.

The recurrent fuzzy neural network model can be stored in the form of feedback connection inside information, making the network output not only affected by the current of input data but also influenced by historical input and output data, thus forming a global or local recursive network structure, which more effectively deals with the DC microgrid nonlinear mapping problem. The network structure of the recursive fuzzy neural network (RFNN) algorithm is shown in Figure 4.

In Figure 4, the recursive fuzzy neural network is divided into six levels, namely, the input layer, the membership layer, the rule layer, the recurrent layer, the TSK fuzzy layer, and the output layer.

Layer 1 is the input layer. Each node of this layer is directly connected with the input vector, and the input value can be transmitted to the next layer. The input-output relationship of the network is

$$o_i^{(1)} = x_i. \tag{5}$$

Layer 2 is the membership layer. Usually, the membership function is a Gaussian function, and each node in this layer represents a membership function:

$$o_{ij}^{(2)} = \exp\left[-\frac{1}{2}\left(\frac{u_j^{(2)} - \mu_{ij}^p}{\sigma_{ij}^p}\right)^2\right], \quad j = 1, 2, \cdots, m, \tag{6}$$

where $\mu_{ij}^{(2)}$ represents the mean of the jth membership function of the ith input variable of the pth output mapping

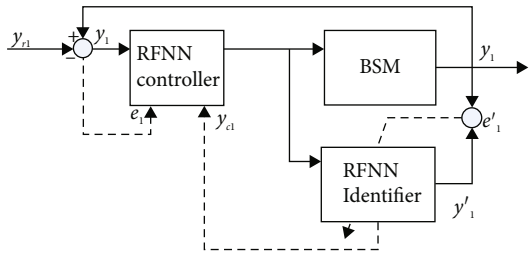

Figure 3: The control structure diagram based on recursive fuzzy neural network.

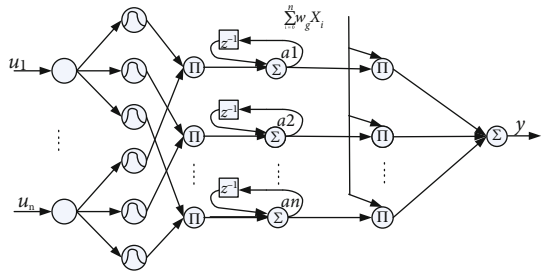

Figure 4: The network structure of RFNN.

relationship, $\sigma_{ij}^{(2)}$ represents the variance of the jth membership function of the jth input variable of the pth output mapping relationship, m is the number of membership functions of each input variable, and $o_{ij}^{(2)}$ is the ith output value.

Layer 3 is the rule layer. The activation function is the product function adopted by this layer, and a fuzzy logic rule is a node:

$$o_{pj}^{(3)} = \prod_{j=1}^{n} u_{pj}^{(3)}, \tag{7}$$

where the degree to which the input data conforms to the rule is expressed by the output strength of the jth rule node, which is $o_j^{(3)}$:

$$J_{\text{sum}} = \sum_{j=1}^{m} o_j^{(3)}, \tag{8}$$

$$J_{\max} = \arg \max_{1 \le j \le m} \left(o_j^{(3)} \right), \tag{9}$$

$$J_{\min} = \arg \min_{1 \le j \le m} \left(o_j^{(3)} \right), \tag{10}$$

where the minimal activated degree of the rules is $J_{\min}$ and the maximal activated degree is $J_{\max}$, respectively.

Layer 4 is the recurrent layer. In the recursive layer, the internal variable q_j is introduced into the feedback link. The activation function of the feedback link is a linear summation function, and this link is dynamic feedback:

$$o_j^{(4)} = u_j^{(4)}(k) + p_j(k), \tag{11}$$

$$p_j(k+1) = a_j o_j^{(4)}(k), \tag{12}$$

where $a_j \in (0, 1)$ is a constant value and the output of the jth internal feedback variables is represented as $p_j(k)$ and $a_j \in (0, 1)$.

Layer 5 is the T_S fuzzy layer. Use T_S type fuzzy rules sum of each node. The operation is

$$o_j^{(5)} = o_j^{(4)} \sum_{i=0}^{n} w_{ij} x_i, \tag{13}$$

where the ith input variable is x_i and the jth consequent weight of the ith input variable is w_{ij}.

Layer 6 is the output layer. The calculation equation of nodes is

$$o = \frac{\sum_{j=1}^{m} o_j^{(5)}}{\sum_{j=1}^{m} o_j^{(4)}}, \tag{14}$$

where $i \in 1, 2, \cdots, n$; $j \in 1, 2, \cdots, m$.

4.1.2. Structure Design of RFNN Controller. The structure of the RFNN controller is the same as that of the RFNN identifier, as shown in Figure 4, and its input-output relationship expression is

$$\mathbf{Y^C}(k) = \mathrm{G}^C\left(X_1^C(k), X_2^C(k), u^C(k)\right), \tag{15}$$

where $u^c(k)$ is the error e between the set value of the controller output and the actual output value, ${x_1}^c(k)$ represent the nonlinear mapping relationship of e in the rule layer, and ${x_2}^c(k)$ represent the nonlinear mapping relationship of e in the T_S fuzzy layer.

4.1.3. Parameter Learning. The gradient descent method is set as the parameter learning algorithm of the RFNN controller and RFNN identifier, and their forward parameters and consequent parameters are both online learning parameters. The online learning performance index is set to

$$J = \frac{1}{2} \sum_{p=1}^{N_0} \left(y_p - y_p' \right)^2. \tag{16}$$

According to the structural design of the RFNN identifier in the previous section, as shown in Figure 4, the approximation of ${y_1}'$ to y_1 is recursive convergence during parameter learning. Therefore, the analysis shows that the parameter update formula of the identifier network is

$$w_{ij}^p(k+1) = w_{ij}^p(k) - \eta_{ij}^w \frac{\partial J(k)}{\partial w_{ij}^p}, \tag{17}$$

$$\sigma_{ij}^p(k+1) = \sigma_{ij}^p(k) - \eta_{ij}^\sigma \frac{\partial J(k)}{\partial \sigma_{ij}^p}. \tag{18}$$

At time k, the gradient value of each parameter of the RFNN controller can be calculated by the gradient algorithm, and the specific calculation equation is shown in formulas (19) and (20). Since the RFNN controller adopts the same design structure as the RFNN identifier, the parameter learning of the RFNN controller also adopts the gradient descent method. The model information provided by the identifier for the output of the DC microgrid controller is shown in formula (21). Based on the model information of formula (21), formulas (17)(–)(20) are consistent with the parameter update process of the RFNN controller and will not be described in detail:

$$\begin{aligned}\frac{\partial J}{\partial w_{ij}^{p}} &= \frac{\partial J}{\partial y_p}\frac{\partial y_p}{\partial w_{ij}^{p}} = \frac{1}{2}\frac{\partial \sum_{p=1}^{N_0}\left(y_p - \dot{y_p}\right)^2}{\partial y_p}\frac{\partial y_p}{\partial w_{ij}^{p}} \\ &= e_p\frac{\partial\left(y_p - \dot{y_p}\right)}{\partial y_p}\frac{\partial y_p}{\partial w_{ij}^{p}} = -e_p\frac{o_{pj}^{(4)}}{\sum_{j=1}^{M} o_{pj}^{(4)}},\end{aligned} \tag{19}$$

$$\frac{\partial J}{\partial \sigma_{ij}^{p}} = -e_p\frac{\partial y_p}{\partial \sigma_{ij}^{p}} = \frac{-2\times e_p\left(W_{ij}^{p}x_i o_{pj}^{(4)} - o_{pj}^{(5)}\right)\times\left(u_j^{(2)} - \mu_{ij}^{p}\right)^2\times o_{pj}^{(3)}}{\left(\sum_{j=1}^{M} o_{pj}^{(4)}\right)^2\times {\sigma_{ij}^{p}}^3}, \tag{20}$$

$$\tilde{y_p} = \frac{-2\times e_p\left(W_{ij}^{p}x_i o_{pj}^{(4)} - o_{pj}^{(5)}\right)\times\left(u_j^{(2)} - \mu_{ij}^{p}\right)\times o_{pj}^{(3)}}{\left(\sum_{j=1}^{M} o_{pj}^{(4)}\right)^2\times \sigma_{ij}^{p}}. \tag{21}$$

4.1.4. Adaptive Learning Algorithm and Its Convergence Analysis. The learning rate is the most important determinant of the neural network algorithm in the learning process. A too high learning rate will cause the instability of the neural network algorithm and then make the whole learning process fail. A too low learning rate will lead to the whole learning process being too slow. To solve this problem, the adaptive change method based on the Lyapunov framework is adopted as the learning algorithm in this paper. The formula is as follows:

$$\eta^{w}(t) = \frac{1}{\max_k\left(\partial y_p(t)/\partial w_{ij}^{p}\right)^2}, \tag{22}$$

$$\eta^{\sigma}(t) = \frac{1}{\max_k\left(\partial y_p(t)/\partial \sigma_{ij}^{p}\right)^2}. \tag{23}$$

On the premise of ensuring the convergence of neural networks, in order to speed up the convergence process of the neural network, this paper adopts the adaptive variable learning rate. The convergence proof of adaptive learning rate can be obtained by constructing the Lyapunov function. Firstly, the Lyapunov function is constructed, as shown in the following formula:

$$V(t) = J(t) = \frac{1}{2}\sum_{p=1}^{N_0} e_p^2. \tag{24}$$

It can be obtained from formula (24):

$$\Delta V(t) = V(t+1) - V(t) = \frac{1}{2}\sum_{p=1}^{N_0}\left(e_p^2(t+1) - e_p^2(t)\right). \tag{25}$$

When $\Delta V \le 0$, the neural network algorithm is convergent and stable, which is determined by the Lyapunov stability principle. According to the model structure of the recursive fuzzy neural network algorithm, the following equation can be obtained:

$$\Delta V(t) = \Delta V_1(t) + \Delta V_2(t) + \cdots + \Delta V_{N_0}(t), \tag{26}$$

$$\Delta V_p(t) = V_p(t+1) - V_p(t) = \frac{1}{2}\left(e_p^2(t+1) - e_p^2(t)\right). \tag{27}$$

According to Reference [9], formula (28) can be obtained:

$$\Delta e(t) = e(t+1) - e(t) \cong \left[\frac{\partial e(t)}{\partial X}\right]^{\mathrm{T}}\Delta X, \tag{28}$$

where

$$\left[\frac{\partial e(t)}{\partial X}\right] = \left[\frac{\partial e(t)}{\partial w}\ \ \frac{\partial e(t)}{\partial \sigma}\right], \tag{29}$$

$$\Delta X = \left[\Delta w\ \Delta\sigma\right]^{T}. \tag{30}$$

Theorem 1. *When it is satisfied,*

$$\eta^{w}(t) = \frac{2}{\max_k\left(\partial y_p(t)/\partial w_{ij}^{p}\right)^2}, \tag{31}$$

$$\eta^{\sigma}(t) = \frac{2}{\max_k\left(\partial y_p(t)/\partial \sigma_{ij}^{p}\right)^2}. \tag{32}$$

This neural network learning algorithm is convergent and stable.

Proof of Theorem 1. Formulas (33) and (34) can be obtained from formulas (17), (20), (26), and (28):

$$\begin{aligned}\Delta e_p(t) = -e_p(t)\Bigg[&\sum_{j=1}^{N_p}\sum_{i=0}^{n}\eta_{ij}^{w}\left(\frac{\partial y_p(t)}{\partial w_{ij}^{p}}\right)^2 + \sum_{j=1}^{N_p}\sum_{i=0}^{n}\eta_{ij}^{\mu}\left(\frac{\partial y_p(t)}{\partial \mu_{ij}^{p}}\right)^2 \\ &+ \sum_{j=1}^{N_p}\sum_{i=0}^{n}\eta_{ij}^{\sigma}\left(\frac{\partial y_p(t)}{\partial \sigma_{ij}^{p}}\right)^2\Bigg],\end{aligned} \tag{33}$$

$$\Delta V_p(t) = -\frac{1}{2}e_p^2(t)\left\{\sum_{j=1}^{N_p}\sum_{i=0}^{n}\eta_{ij}^{w}\left(\frac{\partial y_p(t)}{\partial w_{ij}^{p}}\right)^2\left[2-\eta_{ij}^{w}\left(\frac{\partial y_p(t)}{\partial w_{ij}^{p}}\right)^2\right] + \sum_{j=1}^{N_p}\sum_{i=1}^{n}\eta_{ij}^{\mu}\left(\frac{\partial y_p(t)}{\partial \mu_{ij}^{p}}\right)^2\left[2-\eta_{ij}^{\mu}\left(\frac{\partial y_p(t)}{\partial \mu_{ij}^{p}}\right)^2\right] + \sum_{j=1}^{N_p}\sum_{i=1}^{n}\eta_{ij}^{\sigma}\left(\frac{\partial y_p(t)}{\partial \sigma_{ij}^{p}}\right)^2\left[2-\eta_{ij}^{\sigma}\left(\frac{\partial y_p(t)}{\partial \sigma_{ij}^{p}}\right)^2\right]\right\}. \tag{34}$$

$e_p^2 \geq 0$ can be obtained according to equation (34). For $\Delta V \leq 0$, formula (34) in braces is not less than zero. It is obtained:

$$\eta_{ij}^{w}(t) < \frac{2}{\left(\partial y_p(t)/\partial w_{ij}^{p}\right)^2}, \tag{35}$$

$$\eta_{ij}^{\sigma}(t) < \frac{2}{\left(\partial y_p(t)/\partial \sigma_{ij}^{p}\right)^2}. \tag{36}$$

For each type of parameter, in order to unify the learning rate standard, the unified standard of the learning rate of each type of parameter can be formulated by

$$\eta^{w}(t) < \frac{2}{\max_k\left(\partial y_p(t)/\partial w_{ij}^{p}\right)^2}, \tag{37}$$

$$\eta^{\sigma}(t) < \frac{2}{\max_k\left(\partial y_p(t)/\partial \sigma_{ij}^{p}\right)^2}. \tag{38}$$

Therefore, when the change of learning rate satisfies formulas (37) and (38), the algorithm is convergent and stable, and Theorem 1 is correct. □

4.2. Layered Coordinated Control Process Design. On the basis of the above analysis of the recursive fuzzy neural network, the recursive fuzzy neural network algorithm is used to enhance the feedback connection of the control process, so as to form a three-layer coordinated control strategy.

4.2.1. Layer 1 Control. In the first layer control, each unit only depends on its own injected power and port voltage and other internal information, according to their own droop characteristics to carry out load distribution, so as to achieve supply and demand power balance [17, 18]. As for the uncontrollable clean energy, such as photovoltaic power supply, which generally generates electricity according to the maximum power, it can be considered as a whole with energy storage as controllable clean energy. In this case, the droop method can be applied for control.

The droop control can be expressed as a linear function of voltage and power. Therefore, the governing equation of the first-layer control is set as follows:

$$\begin{cases} v_0 = V_{\text{ref}} - d_i P_i + \Delta v, \\ d_i = d_{i0} - \Delta d. \end{cases} \tag{39}$$

In the formula, v_0 represents the voltage value of the current operating point; V_{ref} represents the reference voltage of sag control; d_i represents the improved sag coefficient; d_{i0} represents the original reference value of sag coefficient, which is proportional to their respective capacities; and Δv and Δd represent the changes in output voltage and sag coefficient, respectively, which are determined by the control results of the second and third layers, respectively.

4.2.2. Layer 2 Control. In the second layer, each control unit calculates the average voltage value of the system through the finite time consistency algorithm based on the voltage information of itself and its connected communication units.

The voltage iteration formula of control unit i is

$$v_i(m+1) = w_{ii}(m)v_i(m) + \sum_{j\in i} w_{ij}(m)v_j(m), \tag{40}$$

where $v_i(m)$ represents the output voltage value calculated by element i after the mth iteration and $w_{ii}(m)$ and $w_{ij}(m)$ represent weights, which can adapt to the changes of system communication topology and meet the requirements of "plug and play" of distributed power supply. The average uniform voltage of each unit is obtained after g iterations, and its value is shown in

$$\bar{v} = v_1^g = v_2^g = \cdots = v_i^g = \frac{1}{n}\sum_{i=0}^{n} v_{i0}, \tag{41}$$

where $\bar{v}$ represents the average voltage, v_i^g represents the voltage value calculated by element i after the gth iteration, and v_{i0} represents the initial voltage of each element. At the end of iteration, in view of the problem of voltage deviation caused by droop control, the recursive fuzzy neural network algorithm is used to fuzzy the voltage of each generation unit to realize the voltage correction and control. The voltage deviation Δv_i is obtained by comparing the average voltage with the given reference voltage. The calculation process is as follows:

$$\Delta v_i = \left(K_{pv} + \frac{K_{iv}}{s}\right)(V_{\text{ref}} - \bar{v}), \tag{42}$$

where K_{pv} and K_{iv} represent fuzziness coefficient and membership coefficient, respectively.

4.2.3. Layer 3 Control. The primary objective of layer 3 control is to minimize the cost of generating electricity. In this paper, uncontrollable clean energy, such as wind power and photovoltaic, is matched with energy storage units to change the situation that wind power and photovoltaic are unimpeachable. Therefore, the distributed power supply in the DC microgrid can be divided into internal combustion power supply and clean energy for discussion.

For the internal combustion type generation unit, the fuel cost is much larger than the converter loss, so the cost function mainly considers both the fuel cost and the maintenance cost. For the ith internal combustion type generation unit, P_{Gi} is its output power, and the cost function is shown as follows:

$$C_{GiP_{Gi}} = M_{Gi}P_{Gi} + F_{Gi}\left(\alpha_{Gi} + \beta_{Gi} + \lambda_{Gi}P_{Gi}^2\right), \quad (43)$$

where C_{Gi} represents the cost of power generation, M_{Gi} represents the maintenance cost per unit power generation unit i of the internal combustion engine, F_{Gi} represents the cost of fuel per kilo calorie, and α_{Gi}, β_{Gi}, and λ_{Gi} represent the fuel cost coefficient of the gas turbine.

Clean energy generally outputs power through the converter; at this time, the converter loss value becomes an important factor affecting the cost of power generation. Therefore, the cost function of controllable clean energy of fuel cells includes three parts: fuel cost, maintenance cost, and converter loss. For the jth controllable clean energy generation unit, P_{Qj} is its output power, and the cost function can be expressed as

$$C_{Qj}\left(P_{Qj}\right) = \left(M_{Qj} + F_{Qj}\right)\left(a_{Qj} + b_{Qj}P_{Qj} + c_{Qj}P_{Qj}^2\right). \quad (44)$$

In formula (44), P_{Qj} represents the output power unit of the converter, M_{Qj} represents the maintenance cost per unit power of the clean energy generation unit j, F_{Qj} represents the cost per unit power of the fuel cell, and a_{Qj}, b_{Qj}, and c_{Qj} represent the loss coefficient of the converter, corresponding to the no-load loss, resistance loss, and power device loss of the converter, respectively.

In the cost of wind power and photovoltaic power generation, fuel costs are not taken into account, and the cost of energy storage is mainly taken into account in terms of maintenance costs. Therefore, the cost functions of both can be expressed in formula (44), except that the value of PQ_j is 0 at this time. Since the whole composition of scenery and energy storage is taken into account in this paper, the overall cost function is finally expressed in the form of formula (44).

In the process of stable operation, each generation unit should also meet a series of constraints, including supply and demand power balance constraints and maximum and minimum power constraints. Formula (45) is the constraint function:

$$\begin{cases} \sum_{i=1}^{m} P_{Gi} + \sum_{j=1}^{n} P_{Qj} - \sum_{k=1}^{l} P_{Lk} = 0, \\ P_{Gi,\min} \le P_{Gi} \le P_{Gi,\max}, \\ P_{Qj,\min} \le P_{Qj} \le P_{Qj,\max}, \end{cases} \quad (45)$$

where P_{Lk} represents the power consumed by the load.

When all generating units and loads meet the inequality constraint conditions, the fuzzy correction value of the droop coefficient can be obtained after processing by the recursive fuzzy neural network algorithm. The calculation process is as follows:

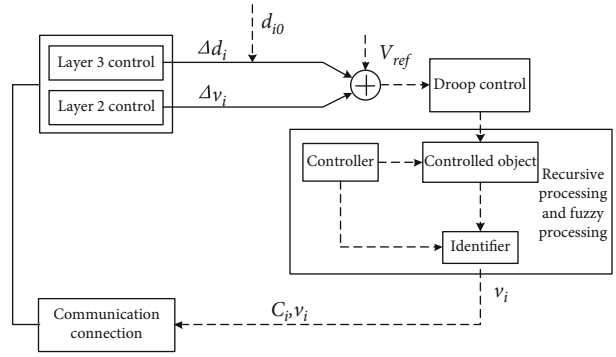

Figure 5: Block diagram of distributed coordinated control of DC microgrid.

$$\Delta d_i = \left(K_{pc} + \frac{K_{ic}}{s}\right) \times C. \quad (46)$$

In the formula, K_{pc} and K_{ic} represent the correction coefficients of the recursive layer and the fuzzy layer, respectively, and C represents the average cost, that is, the cost of each generation unit after iterative convergence.

This enables layer 3 control. It can be seen that the units with high generation costs bear less output power, so as to realize the economic operation of the system while satisfying the proportional distribution of load.

To sum up, this study carried out distributed and coordinated control for the DC microgrid based on the above working mode analysis and power flow calculation results. The recursive fuzzy neural network algorithm is used to enhance the feedback connection of the control process, and the three-layer coordinated control can be formed [19].

In the recursive fuzzy neural network, an identifier and a controller are set. Among them, the controller can output the control signal according to the system error, combined with the adaptive control law, and is used for the controlled object, making the output result of the object load the expected value range. The identifiers can identify the controlled objects and provide object information for the adaptive adjustment of the controller.

Because processing layer 3 of the recursive fuzzy neural network contains the dynamic feedback connection link, when using the discriminator to identify the controlled object, only the output value of the controlled object at the previous time and the control signal value at the current time are used as the input of the network, which can greatly control the process.

Thus, the specific idea of the layered coordinated control method for DC microgrid based on the recursive fuzzy neural network algorithm is shown in Figure 5.

Before the method is started, each unit is controlled by the traditional droop control method. With this method enabled, each cell relies on its local controller to exchange information with its neighboring cells, including its own

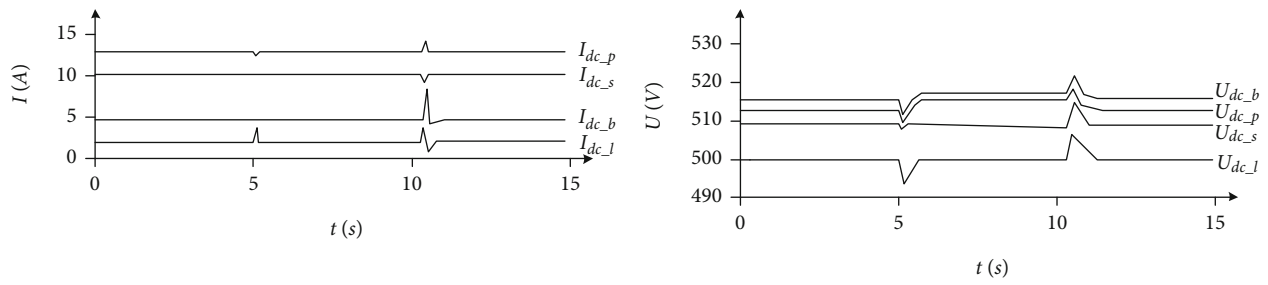

(a) Current variation

(b) Voltage variation

Figure 6: Changes in the current and voltage of each port during grid-connected–off-grid–grid-connected switching.

operating voltage and cost. After the initial cost is iteratively averaged in the third layer of control, Δd_i is used to modify the sag coefficient to obtain d_i, and the new operating point voltage is obtained. The voltage was substituted into control layer 2 to calculate the average voltage, then compared with V_{ref} to get the voltage deviation Δv_i, and then substituted Δv_i into formula (39) to get the final control equation. Through the final control equation, each control unit can realize the load distribution based on the minimum generation cost and finally effectively maintain the bus voltage stability.

5. Experiment and Analysis

In order to verify the feasibility of the hierarchical coordinated control method of DC microgrid based on the recursive fuzzy neural network algorithm designed above, the following experiments were designed in the MATLAB platform to verify.

The experiment takes a DC microgrid as the object, and its operation is as follows: the DC bus voltage of the DC microgrid is 500 V; the two-way AC/DC converter is connected to the 220 V AC grid through a 2 : 1 transformer, with a capacity of 5 kW, a reference voltage of 515 V, and a sag coefficient of 0.5. Of photovoltaic power generation unit capacity of 5 kW, the energy storage unit adopts the rated power of 3 kW battery, its capacity is 220 V/50 Ah, the rated discharge current is 10 A, battery SOC upper and lower are 90% and 40%, respectively, the battery converter of three reference voltage values is 515 V, 512.55 V, and 510 V, corresponding to the discharging and charging, automatic mode, and droop coefficient of 0.25, and dead zone limit is +/-2.5 V, allowing the load side of plus or minus 10 V DC bus voltage variation.

5.1. Check the Effect of Seamless Switch Control of Grid-Connected–Off-Grid–Grid-Connected. Firstly, the method in this paper is used to carry out grid-off grid-connected seamless switching control for DC microgrid, and its control effect is tested. When the load resistance is 40 Ω (12.5 A), the photovoltaic converter has been working in MPPT mode; the port, the change of the voltage, and current are shown in Figure 6.

As can be seen from Figure 6, the AC/DC bidirectional converter operates in the voltage sag control mode during 0-5 s, and the battery converter reference voltage is 514 V and is in the automatic switching mode. At this point, due to the relatively light load, the battery is in standby mode. After 5 s, disconnect the AC/DC bidirectional converter, the DC microgrid changes from grid-connected operation to off-grid operation, the battery automatically switches to discharge mode, and the load terminal voltage is maintained at 500 V. At 10.5 s, the grid connection is restored, and the AC/DC bidirectional converter operates in voltage sag mode. The voltage at the negative end is maintained at 500 V. After a short transient process, the battery converter returns to a standby state. In the grid–off-grid switching, the operating mode of each converter is automatically switched. During the switching process, the voltage of each port will fluctuate. Under the steady-state condition that the voltage fluctuation of the load terminal is less than 10 V, both the grid-connected and off-grid terminals will remain at 500 V. Thus, it can be shown that this paper has achieved a better control effect. It can be seen from the figure that after the step of voltage and current, they both can quickly return to a stable state. It shows that after the improvement of the recursive fuzzy neural network algorithm, the DC microgrid control system has good robustness, stability, and fast convergence speed.

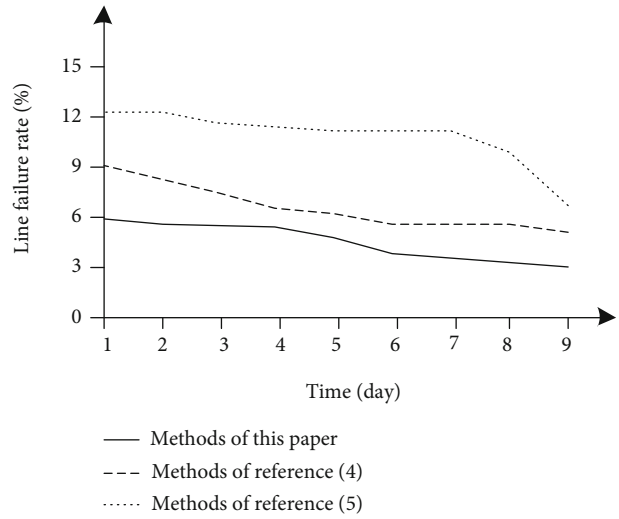

Figure 7: The line failure rate is compared under different control methods.

5.2. Check the Failure Rate of DC Microgrid Line. On this basis, in order to further highlight the effectiveness of the proposed method, the application performance of the proposed method, the Reference [6] method, and the Reference [7] method is verified by taking the failure rate of the DC microgrid line as the index. The line failure rate can reflect the operation safety of the DC microgrid, and it is a key index to evaluate the control effect and reflect the effectiveness of the control method.

A line in the experimental area was randomly selected as the experimental object to verify the failure rate of DC microgrid lines under the control of different methods. The results are shown in Figure 7.

According to the results shown in Figure 7, under the control of different methods, the failure rate of the circuit decreases over time. Under the control of methods of Reference [6], the fault rate of the circuit is slightly higher than that of the methods of this paper. Under the control of methods of Reference [7], the line failure rate is obviously higher. Under the control of methods of this paper, the line failure rate decreases from 6% to 3%. The above results fully demonstrate that the methods of this paper can realize effective coordinated control of fault frequency of DC microgrid lines, so as to ensure the operation safety of the DC microgrid.

6. Conclusion

In this article, a hierarchical coordinated control method of DC microgrid based on the recursive fuzzy neural network algorithm is designed. On the basis of droop control, the coordinated and optimal control of the DC microgrid is realized through a three-layer hierarchical control structure, so as to achieve the purpose of stable operation of the DC microgrid. At the same time, the recursive fuzzy neural network algorithm is used to optimize the system-level control of the third layer in the hierarchical control structure, so as to ensure the real-time amplitude limiting, convergence, and stability of the DC microgrid controller. The experimental results show that under the control of the intelligent control algorithm in this paper, the current and voltage changes of each port of the DC microgrid are relatively stable in the process of off-grid switching, and the power grid line fault rate is low, which fully proves the effectiveness of this method. In the following research, we can further optimize the method in this paper from the perspective of shortening the control reaction time, so as to comprehensively improve its application performance.

Data Availability

No data were used to support this study.

Conflicts of Interest

The authors declare that there are no conflicts of interest regarding the publication of this article.

Acknowledgments

This research was funded by the scientific research project of Shanghai Investigation, Design & Research Institute Co., Ltd (2021QT(831)-001).

References

[1] R. C. Zhang, D. J. Zhai, and Y. Zhang, "DC microgrid distributed coordinated control strategy including hybrid energy storage system," *Journal of Ordnance Equipment Engineering*, vol. 41, no. 4, pp. 232–236, 2020.

[2] Y. Mi, Y. W. Wu, H. P. Ji, F. Yang, and C. S. Wang, "Coordinative control based on dynamic load allocation among multiple energy storages for is landed DC microgrid," *Electric Power Automation Equipment*, vol. 37, no. 5, pp. 170–176, 2017.

[3] J. D. Wu, K. Y. Wang, X. Huang, C. Qi, G. J. Li, and Y. Zhang, "Distributed coordinated control scheme of parallel DC-DC converters in isolated DC microgrids," *Power System Protection and Control*, vol. 48, no. 11, pp. 76–83, 2020.

[4] B. Liu, "Logistics distribution route optimization model based on recursive fuzzy neural network algorithm," *Computational Intelligence and Neuroscience*, vol. 2021, 10 pages, 2021.

[5] G. Tang, X. Zheng, S. Liu, Y. L. Gu, Y. Lu, and P. Qiu, "Novel DC voltage control strategy for multi terminal flexible DC transmission system," *Power system automation*, vol. 37, no. 15, pp. 125–132, 2013.

[6] Y. L. Li, P. Dong, M. B. Liu, and Y. Lin, "Distributed coordinated control of DC microgrid based on finite-time consensus algorithm," *Automation of Electric Power Systems*, vol. 42, no. 16, pp. 96–103, 2018.

[7] W. Q. Xie, M. X. Han, H. J. Wang, R. Li, and M. Wu, "Multisource coordinated control strategy of DC micro-grid based on virtual voltage," *Proceedings of the CSEE*, vol. 38, no. 5, pp. 1408–1418, 2018.

[8] F. F. M. El-Sousy, "Adaptive hybrid control system using a recurrent RBFN-based self-evolving fuzzy-neural-network for PMSM servo drives," *Applied Soft Computing*, vol. 21, no. 8, pp. 509–532, 2014.

[9] S. I. Han and J. M. Lee, "Recurrent fuzzy neural network backstepping control for the prescribed output tracking performance of nonlinear dynamic systems," *ISA Transactions*, vol. 53, no. 1, pp. 33–43, 2014.

[10] C. Dou, Y. Dong, J. M. Guerrero, X. Xie, and S. Hu, "Multiagent system-based distributed coordinated control for radial DC microgrid considering transmission time delays," *IEEE Transactions on Smart Grid*, vol. 8, no. 5, pp. 2370–2381, 2017.

[11] B. K. Chaitanya, A. Yadav, and M. Pazoki, "Wide area monitoring and protection of microgrid with DGs using modular artificial neural networks," *Neural Computing and Applications*, vol. 32, no. 7, pp. 2125–2139, 2020.

[12] H. M. Peng, L. Chang, Y. C. Guo, S. H. Li, and H. Li, "Dynamic interval power flow calculation of microgrid under master-slave control," *Power System Technology*, vol. 42, no. 1, pp. 195–202, 2018.

[13] K. M. Bhargavi and N. S. Jayalakshmi, "Leader–follower-based distributed secondary voltage control for a stand-alone PV and wind-integrated DC microgrid system with EVs," *Journal of Control, Automation and Electrical Systems*, vol. 17, no. 3, pp. 1–14, 2020.

[14] G. Y. Lee, B. S. Ko, J. Cho, and R. Y. Kim, "A distributed control method based on a voltage sensitivity matrix in DC microgrids with low-speed communication," *IEEE Transactions on Smart Grid*, vol. 10, no. 4, pp. 3809–3817, 2019.

[15] X. Liu, Z. Xie, Q. Sun, and Z. Wang, "A novel protection scheme against fault resistance for AC microgrid," *Mathematical Problems in Engineering*, vol. 2017, Article ID 8419257, 2017.

[16] Y. Han, Y. Pu, Q. Li et al., "Coordinated power control with virtual inertia for fuel cell-based DC microgrids cluster," *International Journal of Hydrogen Energy*, vol. 44, no. 46, pp. 25207–25220, 2019.

[17] L. Gao, L. Yao, H. Ren, and J. M. Guerrero, "A DC microgrid coordinated control strategy based on integrator current-sharing," *Energies*, vol. 10, no. 8, pp. 1116–1123, 2017.

[18] G. H. Philipo, Y. A. C. Jande, and T. Kivevele, "Clustering and fuzzy logic-based demand-side management for solar microgrid operation: case study of Ngurudoto microgrid, Arusha, Tanzania," *Advances in Fuzzy Systems*, vol. 2021, Article ID 6614129, 2021.

[19] R. Atassi and K. Yang, "An integrated neutrosophic AHP and TOPSIS methods for assessment renewable energy barriers for sustainable development," *International Journal of Neutrosophic Science*, vol. 18, no. 2, pp. 157–173, 2022.

Hindawi
Wireless Communications and Mobile Computing
Volume 2022, Article ID 6767960, 10 pages
https://doi.org/10.1155/2022/6767960

Research Article

User Experience Evaluation of B2C E-Commerce Websites Based on Fuzzy Information

Jieqiong Huang and Xiaozhi Wang

Department of Management Engineering, Hebei Petroleum University of Technology, Chengde, 067000 Hebei, China

Correspondence should be addressed to Xiaozhi Wang; cdpc_wxz@cdpc.edu.cn

Received 31 March 2022; Revised 20 May 2022; Accepted 30 May 2022; Published 18 June 2022

Academic Editor: Jun Ye

With the popularization of personal computers and the development of the Internet, the number of netizens is increasing. The emerging B2C e-commerce platform shows the fierce competition in the e-commerce market. B2C e-commerce distribution is faced with the problems of high distribution cost, long time, and poor quality, which leads to the poor user experience of B2C online shopping and the lack of trust in e-commerce enterprises. This research mainly discusses the user experience evaluation of B2C e-commerce websites based on fuzzy information. First, the AHP analytic hierarchy process is used to construct a hierarchical evaluation system, and then, the two-by-two judgment matrix is compared to the index factors at all levels, and experts are invited to score the method to determine the weight of each index to test whether it meets the consistency requirements. Finally, the fuzzy comprehensive evaluation method is used to perform fuzzy conversion of the original weight, and the membership degree set of the user experience evaluation factors is given, and the fuzzy comprehensive calculation result of the B2C website performance level is calculated. By combining in-depth interviews with website users and questionnaire surveys to analyze the behavioral characteristics of user information navigation, summarize the demand list for product search, product selection, product comparison, and product detail page browsing, and provide a reference for the design and development of information navigation. Calculating the decision model, mainly using fuzzy calculation, calculate the foreground value under each attribute and get the comprehensive foreground value. By comparing with the decision-making behavior model constructed by expected utility theory, it is found that the behavioral decision-making model constructed in this paper based on prospect theory can be closer to the actual situation. In this study, the satisfaction with the function provided reached 68 points, the emotional response 66 points, the aesthetic response 70 points, and the information construction 64 points. Through empirical research, the key factors affecting user satisfaction of B2C e-commerce logistics distribution are summarized, and a B2C e-commerce logistics distribution evaluation system based on user experience is established. This research will provide methods and ideas for the research on user experience design of e-commerce websites and the research and development of related network products. The article helps to draw out the countermeasures and suggestions for the development of the current B2C e-commerce logistics distribution.

1. Introduction

E-commerce is affecting every corner of the world; it has changed the current business system and profoundly changed the way people trade and consume. With the rapid development of information technology, economy, and society, e-commerce has become an important retail format, and online shopping has become an important way for people to shop. The biggest difference between e-commerce and online shopping and physical sales is that the products can only reach the consumer terminal, namely, the customer, through the ways that can be presented online (text, sound, image, etc.), and the intuitive perception and trial of the products are greatly restricted.

E-commerce simplifies trade processes, improves logistics systems, reduces transaction costs, increases trade opportunities, and promotes business restructuring and economic restructuring of enterprises, which will greatly increase productivity, completely change the nature of trade activities, and form a new set of trade activity framework.

The level of e-commerce development will directly affect the competitiveness of future international trade. In online shopping transactions, all physical products need logistics and distribution services to be realized. Such a huge amount of online shopping has great temptation for the logistics and distribution industry, which is increasingly competitive.

With the gradual maturity of online shopping service model in the online shopping market is heating up and tends to mainstream, its user scale continues to grow. The level of e-commerce in China is still in the early stage, and its function is mainly used for information exchange. The mutual promotion relationship between e-commerce and logistics cannot be recognized by most enterprises. A meta-analysis by Kim and Peterson examined the role of online trust in business-to-consumer e-commerce. An analysis of 16 pairs of relationships from 150 empirical studies involving online trust shows that online trust exhibits significant relationships with selected antecauses (e.g., perceived privacy and perceived quality of service) and consequences (e.g., loyalty and willingness to repeat purchases). Even so, additional analysis showed that methodological characteristics such as study design, type of site, and type of project used to measure trust structure modulated some online trust relationships. The relationship between online trust and its respective antecedents and consequences is also more specific, complex, and nuanced than previously thought. He discusses the impact of analysis on theory, practice, and future research [1]. Mero provides methods and systems for analyzing information about the online actions of multiple users. His analytical methods and systems allow the creation of new online and offline business approaches based on online consumer behavior. His method and system can include information about multiple users online action of the input data set, the input data set into a common file format data file, and each data file corresponding to a user in multiple users and include the user identifier and the multiple associated with the user's online operation uniform resource location (URL), access online information related to search terms and web pages and identify one or more metrics of user behavior, including "vertical" metrics and "search term" metrics [2]. Sullivan and Kim enhance the existing literature on online trust by integrating consumer product evaluation models and technology adoption models in the e-commerce environment. They investigated how perceived value affects online buyers' perceptions of online trust and their willingness to repurchase from the same site. They came up with a research model. Perceived quality is affected by competitive price and website reputation perception and then affects perceived value. Perceived value, website reputation, and perceived risk affect online trust and then repurchase intention [3]. Lal believes that the growth of social media has changed the online commerce landscape for organizations and customers. The introduction of social commerce sites has changed consumers' purchasing decisions from personal shopping to social shopping. His research is aimed at determining the factors that influence individuals' decisions to use social commerce sites in the Indian environment. It identifies six factors that influence individuals' intentions to use social commerce and divides them into three categories: social factors (information support and community commitment), trust (to members and community), and site quality (ease of use and quality of service). The structural equation model is used to verify the research model. All six factors are positively correlated with individuals' intentions to use social commerce sites. In addition, his research found that information support is the most important factor affecting individuals' intention to use social commerce sites, followed by trust in members, service equality, trust in community, convenience of navigation, and community commitment [4]. Gs et al. consider e-commerce to be the purchase and provision of goods or management through electronic media, such as the Internet and other PC systems. It is largely called e-commerce transaction and business capability. Since the broad base of the Internet, the level of exchange led electronically has grown tremendously. A wide variety of exchanges are conducted through e-commerce, including electronic asset transfer (EFT), supply chain management, online promotions, search vehicle displays, online exchange preparation, electronic information trade, and inventory management frameworks. These basic terms of e-commerce are essential to secure business behavior on the network. In addition to the key adage of e-commerce, vendors must guard against a number of different external security threats, most notably denial of service (DOS) [5]. Pansari and Kumar highlighted the need for customer engagement (CE) and developed a framework by reviewing marketing literature and analyzing popular news articles. By understanding the evolution of customer management, they believe partners care about each other when a relationship is satisfying and emotionally connected. Therefore, the components of customer involvement include both direct and indirect contributions from CE. Based on theoretical support, we propose a framework that illustrates the components of CE as well as its antecedents (satisfaction and emotion) and consequences (tangible and intangible outcomes). They also discuss how convenience, company nature (B2B vs. B2C), industry type (service vs. product), brand value (high vs. low), and degree of participation (high vs. low) mediate the connection between satisfaction and direct contribution, as well as the connection between CE's mood and indirect contribution [6]. Berne-Manero and Marzo-Navarro believe that although online social media shoppers' channel choice behavior has a significant impact on purchasing decisions in online and online markets, it has been neglected. The aim of his study was to examine the effects of transactive memory system (TMS) factors (specialization, trustworthiness, and coordination), knowledge sharing (KS), and communication quality on online social media channel selection for shopping activities. Partial least squares (PLS) analysis was used for structural equation modeling (SEM) to examine the measurement model and structural model of reflection structure. A total of 336 online questionnaires were collected from users of collaborative projects, social networking sites, blogs, content communities, virtual gaming worlds, and virtual social worlds. TMS factors, KS, and communication quality have positive influence on online channel selection [7]. In addition, specialization, credibility, and coordination contribute statistically to TMS as a second-order structure [8]. The security of B2C website includes the website's credit system, payment system, and security system. This subindicator will

be better and truly experienced in the actual operation and use process of users. E-commerce is a new thing that only appeared at the end of 90s. Due to the short time, coupled with this is a very rapid development of the field, the industry's understanding of e-commerce has yet to be further developed and improved in practice; therefore, there is no unified definition of e-commerce.

Fuzzy information, as a new description tool for uncertain decision-making information, has broad application prospects in real multiattribute decision-making problems. This article will use extension theory to explore a method to solve the quantitative evaluation of B2C e-commerce logistics services based on related theories such as service quality and logistics service quality, combined with the status quo and characteristics of B2C e-commerce logistics services. In the fuzzy comprehensive evaluation, it is necessary to calculate a fuzzy relationship matrix of each index to the comment level. According to the above description, the comment level is divided into five levels: very satisfied, satisfied, fair, not satisfied, and dissatisfied. The article studies how to build a semantic database reflecting different characteristics, and select appropriate classification mining technology to classify the content of the online word-of-mouth text; through sentiment analysis and statistics to reflect the evaluation preferences of online groups.

2. B2C E-Commerce Website User Experience Evaluation Research Methods

2.1. Selection of Website Evaluation Indicators. When establishing the website evaluation index, this article chooses the index from two aspects. From the perspective of website construction, we selected four indicators: website traffic ranking, number of visitors per million people, average daily IP volume (there is the concept of traffic here, which is the number of visitors to a website in a day) in the past month, access speed, and backlinks. At the same time, taking into account the user's attractiveness to the website, two indicators have been added: the average number of pages viewed by each visitor and the page dwell time. Considering the promotion and construction of the website, another indicator has been added: website link. Website links can effectively guide consumers to browse products [9]. Browse the product evaluation index as shown in Table 1.

The factor loading is recorded as the sum of squares of the elements in each column of matrix A as [10]:

$$q = \chi_{ij} \sum_{i=1} a^2. \quad (1)$$

χ_{ij} represents the total influence of the jth factor on all components, that is, the contribution of the jth factor to X. This is a measure of the relative importance of the jth factor [11].

2.2. Measurement Model of Logistics Service Quality. How to effectively measure and evaluate logistics service quality is the focus of scholars. From the perspective of enterprises and customers, the established logistics service quality evaluation system is different. Based on the perspective of the enterprise, the representative method is to use the 7Rs theory mentioned above to analyze the accuracy of goods, the goodness of goods, accurate product information, delivery on time rate, delivery accuracy, and timeliness in the logistics service process. 7 factors such as price and price are measured and evaluated.

Therefore, the established logistics service quality measurement model considers the influencing factors of physical service quality and customer service quality and is divided into two extremes of ordering and receiving, focusing on the following 9 factors: personnel communication quality, error handling, goods integrity, quality of goods, accuracy of goods, timeliness, order release quality, ordering process, and information quality.

Whether the logistics services provided by B2C e-commerce merchants can satisfy customers needs to be comprehensively considered from the six aspects of economics, transparency, completeness, timeliness, reliability, and empathy of logistics services, which is the index system. This article will use the theory of extenics to determine the weight of each index and establish a mathematical model for comprehensive evaluation, so as to evaluate the satisfaction of B2C e-commerce logistics service quality. The construction of a B2C e-commerce website is shown in Figure 1.

2.3. User Experience Evaluation. In order to collect user navigation experience information and to obtain user demographic data, as well as the user's online shopping habits and information navigation needs, therefore, this article mainly uses interviews, questionnaires, field observations, and other forms to collect user demand information and summarize the design focus. Interviews and questionnaire surveys are typical methods to understand users' subjective feelings and impressions of the product, especially when it comes to understanding the objectively difficult amounts, questions related to user subjective satisfaction, and possible worries. They are very useful in many and have a wide range of applications in the field and research. In the field of usability engineering, they can help us collect data and information about users' awareness, attitudes, usage, problems encountered in the use of the product, and expectations of the product [12].

2.4. Determine the Evaluation Criteria for Performance Indicators. Commonly used corporate performance evaluation standards mainly include the following three: corporate budget as the standard, corporate historical performance as the standard, and benchmark corporate operating data as the standard. In the research of this article, we combined the above three methods, that is, the financial indicators of website performance can use budget standards; the indicators of website operation can use historical standards; the indicators of website design and customer satisfaction can be selected in the industry. For benchmarking companies, evaluate the benchmarking companies and make necessary adjustments based on the actual situation of website development [13]. "Benchmarking enterprise" refers to an enterprise that has achieved remarkable results in

Table 1: Evaluation index data.

Site name	$X1$ average number of pages viewed by each visitor	$X2$ backlink	$X3$ access speed	$X4$ daily average IP amount	$X5$ the number of people visiting the website per million people
Tmall	4.92	30024	17.28	22120750	49100
Jingdong mall	26.00	10217	13.78	565250	510
Eslite	6.74	5773	17.73	7 6950	110
Suning online market	4.99	5735	328.92	1980750	3500
Amazon China	6.26	13292	48.70	1249250	2750
Yihaodian	8.30	2421	15.46	311125	570
Gome	4.17	4392	368.18	1467750	3300
Dangdang	7.86	12751	54.29	279775	570
Jumeiyoupin	7.36	3578	29.19	118275	170

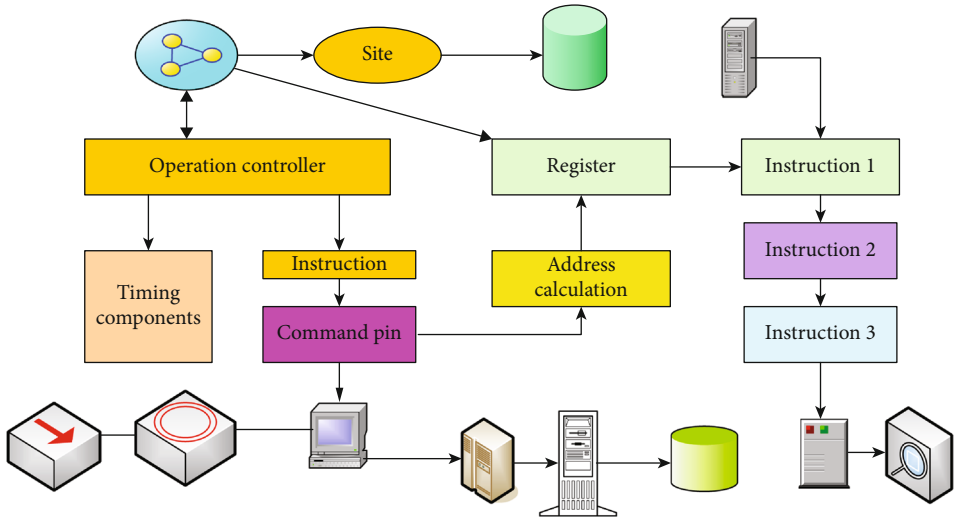

Figure 1: Construction of B2C e-commerce website.

information construction, progressiveness (including some aspects), exemplary, and industry representative. It is generally an enterprise with high popularity, good reputation, development potential, and strong comprehensive strength.

2.5. E-Commerce Website Evaluation Model Based on Analytic Hierarchy Process

(1) Preselection of experts. Find out the 5 most important experts for e-commerce website evaluation through the form of online, telephone, and on-site appointments. The criteria for judgment include the frequency of online shopping, the ability of website technology construction, the ability of website testing, and the level of mastery of domain knowledge and experience

(2) Determine the expert plan. Through comparison, the final selected experts include: 1 Taobao diamond-level online shopping expert, 1 testing technology expert with 2 years of software testing experience, 2 technical experts with 3 years of website construction and maintenance technical post experience, and master website construction, test theoretical knowledge, and 1 experienced expert who frequent online shopping

(3) Scoring by experts. Send the prepared evaluation index form to an expert via email for scoring and clarify the requirements and rules. At the same time, communicate with the expert through online and instant communication tools to instantly solve the vague and unclear problems in the form

(4) Comprehensive expert scoring result. Summarize the scoring results of experts, and make fixed-point consultation feedback revisions on the parts with large differences. Finally, the final result is determined by the weighted average method [14, 15]

For the reliability analysis of questionnaires with qualitative factors such as opinions and satisfaction, the α

coefficient (i.e., alpha reliability coefficient) method is currently used more frequently, which can clearly illustrate the inherent consistency of the scales of various item items. The formula is as follows [16]:

$$\alpha = \frac{k}{k-1}\left(1 - \frac{\sum Q}{Q}\right). \tag{2}$$

Among them, K is the number of questions in a certain level of the questionnaire, and Q is the variance of the ith item [17].

Refer to the fuzzy comprehensive evaluation principle, select the appropriate synthesis operator, and determine the comprehensive evaluation vector ZP [18]:

$$Z = W * \begin{pmatrix} R_{11} & \cdots & R_{1M} \\ \cdots & \cdots & \cdots \\ R_{P1} & \cdots & R_{PM} \end{pmatrix}. \tag{3}$$

To determine the comment set, the comment level should be assigned when using fuzzy comprehensive evaluation. Collecting consumers' possible judgments on logistics services under B2C e-commerce forms a comment level. The information of the degree of membership of the logistics service quality to the review level is reflected by the fuzzy vector. Usually, the number of reviews is between 4 and 9, and the number should not be too much or too little. Too many comment levels are not suitable for people to understand, and customers may misinterpret them when they understand, which will affect the evaluation results. Too few comment levels cannot reflect consumers' actual evaluation of B2C e-commerce logistics service quality. Therefore, the five comment levels are convenient for consumers to judge (very satisfied, satisfied, average, not satisfied, and dissatisfied).

Search design points:

(1) The design of the search category box is generally not easy to be too often. According to the longest sentence length of the secondary classification, it will generally not exceed 16 characters in length. The search category is generally displayed in the form of a drop-down menu list. It is collapsed in the default state. When expanding, pay attention to the corresponding color or action response when the mouse touches each tag category. If there are too many secondary categories, it should design the sidebar pull-bar or drop-down button, not all categories can be displayed together; otherwise, the expanded form is too long to be easy to read and takes up space on the page. In addition, the interval of each category is either a blank interval or a horizontal line interval, so that users can clearly distinguish each category

(2) Search input box and search button design. The input box and search button are often placed together, so they are analyzed together. Both need to pay attention to the width and length. The input box is the most important visual and function in the search design. Its size and shape determine the shape and size of the entire search area. The search button needs to be unified with the input box, and the button needs to have clear outlines and bright colors. Let users know and click at a glance

2.6. Data Reliability. For the objective indicators in the data, the article uses a variety of network monitoring tools and network statistics methods, such as Alexa, 360 website evaluation, price comparison websites, Gtmetrix, and webmaster tools. The final data is determined by the method, which guarantees the validity of the data.

B2C website can be said to be the website with the most complex information structure in interactive advertising. In the process of creating a better user experience, the visual design of the soft interface interaction mechanism is very important. Through its research, it can improve the perceptual interactivity of the interface and the website, thereby improving the actual interactivity of users and enabling consumers to experience online shopping more easily and happily. This positively affects consumers' attitudes towards the website, brand attitudes, and purchase intentions. It is hoped that the research on this basis can give reference and help to other websites and software and other soft interface design, so that the soft interface interaction mechanism of interactive advertising can better serve consumers and make users more beautiful. Experience natural was interaction without a sense of interaction. At the same time, it helps to improve the operation and long-term development of B2C websites and more effectively improves user experience. Make the interactive communication mechanism effective circulation. In this way, the corporate brand can grow well and healthily and establish a long-lasting and beautiful image. Standardize variables in the data that have large differences in dimensions or levels of data [19, 20]:

$$Z = \frac{X - \bar{X}}{\beta}. \tag{4}$$

$\bar{X}$ is the average value.

The integrated optimization mathematical model of forward and reverse logistics of B2C distribution system with fuzzy random demand is as follows [21]:

$$(Q, r, x, y)_{\min} = \sum_{j=1}^{m} Fy + \sum_{j=1}^{m}\left\{\frac{Fy}{Q} + C\left[\frac{Q}{2} + xr - (1 - e\lambda)LD\right]\right\}y. \tag{5}$$

The constraint conditions of the repair rate χ and the scrap rate ϑ are as follows [22]:

$$\chi = \sum_{i=1}^{m} \frac{\phi D(1 - e\gamma)C}{Q}, \tag{6}$$

$$\vartheta = \sum_{i=1}^{m} (\lambda BD + \eta dC). \quad (7)$$

3. E-Commerce Website User Experience Evaluation Results

It can be seen that the eigenvalues of the first two common factors are 3.695 and 2.083, respectively, which are both greater than 1, and the cumulative contribution rate of the two reached 82.534%, which summarizes the vast majority of the total variance; according to the evaluation of the B2C e-commerce website if necessary, these two common factors can be used to replace the original 5 variable indicators, and the characteristic root contribution rates of these two common factors can be obtained directly according to the chart as 52.783% and 29.751%. The contribution rate of SPSS characteristic root is shown in Table 2.

The results of this questionnaire survey involve a wide range of people, and the comprehensive results show that they can basically reflect the situation of online shopping or are familiar with online shopping, and the basic statistics of the questionnaire are shown in Table 3.

There are 14 websites with an average value of 6.0490969 or more, namely, Taobao, Tmall, JD.com, Alibaba, Suning.com, eBay, Dangdang, Gome, Amazon, Paipai, No.1 shop, Vancl Eslite, Dream Bazaar, and China Flower Network; in order to describe the overall comparison level of the website more intuitively and concisely, the value of the passing line is set to 6.0000, and there are 15 websites with a passing score, including 14 on the average score line and Lefeng.com. The comprehensive levels of Taobao and Tmall are significantly higher than those of other websites. The evaluation of different searches is shown in Figure 2.

Through the summary, it can be found that Baidu's word-of-mouth data is basically the service quality evaluation of the direct-operated B2C e-commerce platform published by online consumers. The data collected by the Sina Weibo platform is classified into three different types: industry or corporate news, product promotion and promotion essays, and customer-published evaluation information on the service quality of e-commerce platform companies. There are many types of information and more evaluation objects. It is complicated, and a large amount of data does not meet the requirements of the follow-up research of this article. After data screening, 1528 online reputations of each platform are retained, including 551 in Jingdong Mall, 504 in No. 1 Store, and 473 in Dangdang, providing data support for subsequent classification and sentiment analysis research. After data screening, the number of word-of-mouth of each platform mall is shown in Table 4.

In the B2C online shopping market in 2019, JD.com has a market share of 18.6%, Dangdang has a market share of 1.3%, and Vipshop has a market share of 2.9%. The market share is shown in Figure 3.

When the important parameters of each individual cost in the system change from -50% to 50%, that is, when the rate of change reaches 100%, the impact on the total cost is shown in Figure 4. The total cost increases with the increase of the individual cost parameters, vice versa. When the site selection cost changes, the total cost changes range of 36.16%; when the unit inventory holding cost changes, the total cost changes range of 6.96%; when the unit transportation cost changes, the total cost changes range of 46.60%; when the unit return processing cost changes, the total cost varies within 3.42%. It can be seen that changes in location costs, unit inventory holding costs, unit transportation costs, and unit return processing costs will all have an impact on the total cost.

Purpose of shopping: 67% of users browse shopping websites with a clear shopping goal. 21% of users will pay attention to some shopping platforms that they usually visit when they are idle and bored. Will drive oneself to buy two situations. 12% of users will pay attention to website

Table 2: SPSS feature root contribution rate.

Element	Initial eigenvalue		Total
	Variance	Accumulation%	
1	52.783	52.783	3.695
2	29.751	82. 534	2.083
3	13.455	95.988	0.0942
4	3.650	99.638	0.255
5	0.360	99.998	0.0025

Table 3: Basic statistics of the questionnaire.

Basic situation	Classification	Quantity	Ratio
Gender	Male	70	43.75%
	Female	90	56.25%
Age	18 or less	3	1.88%
	18-25	97	60.63%
	26-35	44	27.50%
	35 or more	16	10.00%

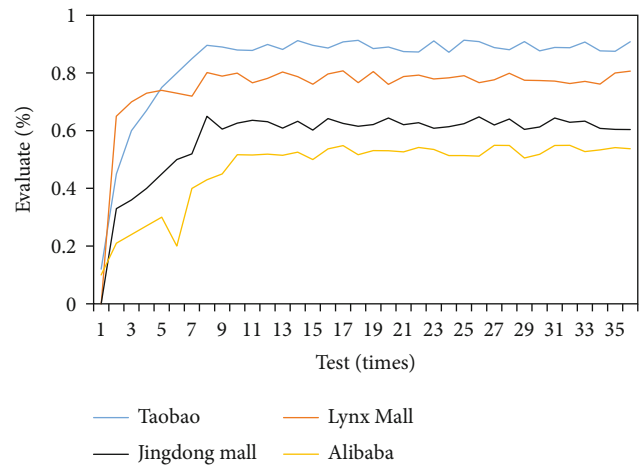

Figure 2: Evaluation of different searches.

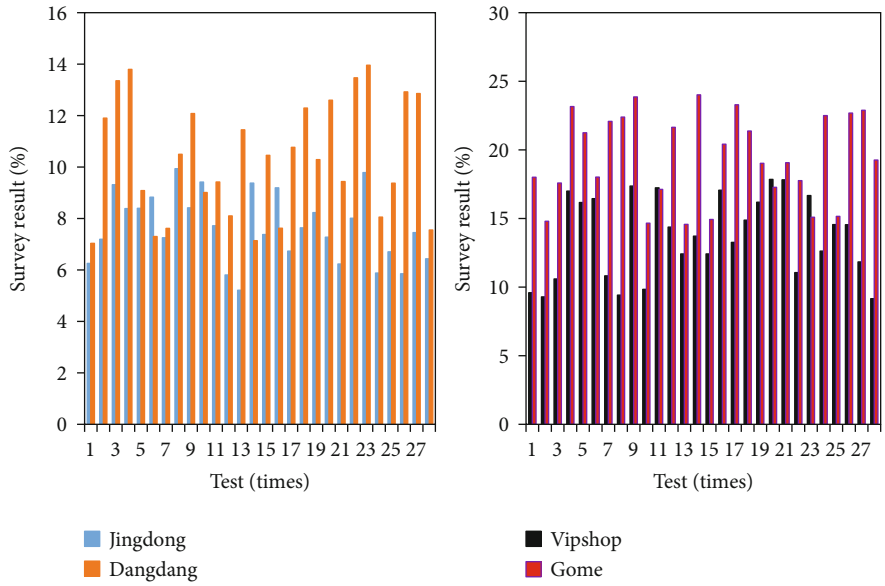

Figure 3: Market share.

promotion information. The purpose of shopping is shown in Figure 5.

On the whole, users have generally completed the task of product search, product selection and comparison, and selection of shopping products for purchase. It is found that the overall usability problems of the current design scheme and the number of pain points of experience have been significantly reduced, and the satisfaction with the provided functions reached 68 points, the emotional response 66 points, the aesthetic response 70 points, and the information construction 64 points. However, some users said that some functions are not perfect enough, and these existing problems and deficiencies need to be improved. The user experience evaluation is shown in Figure 6.

Table 4: After data screening, the number of word-of-mouth in each platform mall.

Directly operated B2C mall	Number of Weibo word-of-mouth screening	The number of Baidu word-of-mouth screening	Summary
Jingdong mall	302	249	551
Dangdang	351	112	473
Shop number 1	367	137	504
Total	1020	498	1528

4. Discussion

With the rapid development of B2C e-commerce, the impact of logistics circulation on e-commerce has become more and more significant. Efficient, fast, and low-cost logistics circulation system plays an important role in promoting the formation and maintenance of B2C enterprises' core competitiveness and has become a hot issue in current research [23].

Using the basic principles of the fuzzy possible mean method, the fuzzy random expected value method, and the fuzzy random simulation method, the clarification transformation method of the fuzzy random CLRIP model is constructed, and the improved genetic algorithm based on the adaptive selection mechanism and the TS- and SA-based methods are designed. Methods such as the two-stage hybrid heuristic algorithm to solve the clarification model effectively solve the problem of solving the complex fuzzy random CLRIP model [24].

Regarding the further investigation of logistics service quality, from the perspective of two studies, there is a certain difference between logistics service quality customers and logistics service providers. Logistics service providers should start from the subjective factors of the logistics provider, what type of logistics services they provide to customers, pay more attention to their own quantitative value, and create value for customers. The important thing in the service industry is the understanding of customer service quality. Therefore, more and more scholars began to discuss the meaning of logistics service quality from the perspective of customers [25].

User experience refers to the user's psychological feelings on the readability, ease of operation, and interactivity of the website's interface, functions, and related information during the process of visiting the website. Whether it is a design researcher, interaction designer, and high-level corporate decision-maker, user experience is also a problem they care about and strive to solve reasonably and with high quality [26].

Although B2C e-commerce has developed rapidly, the accompanying problems need to be solved urgently. E-commerce has grown up with the rapid development of the Internet. After customers purchase products online,

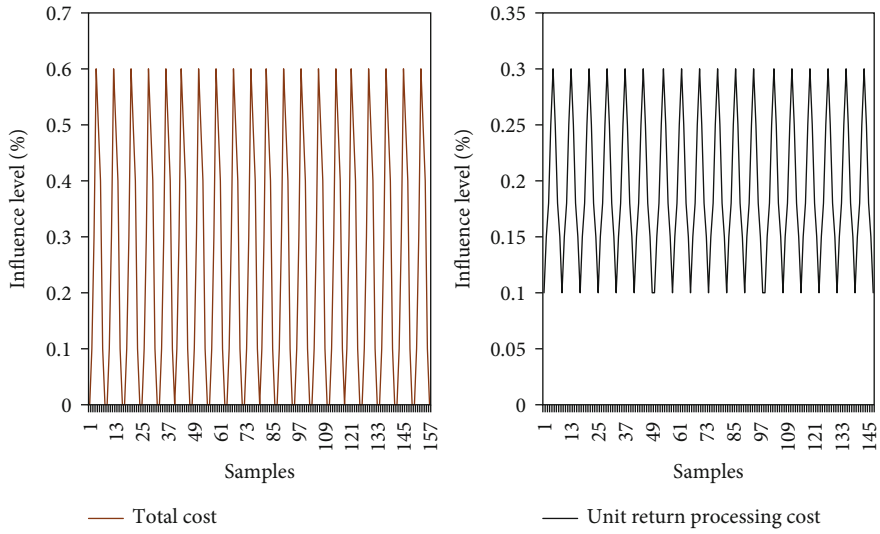

Figure 4: Impact on total cost.

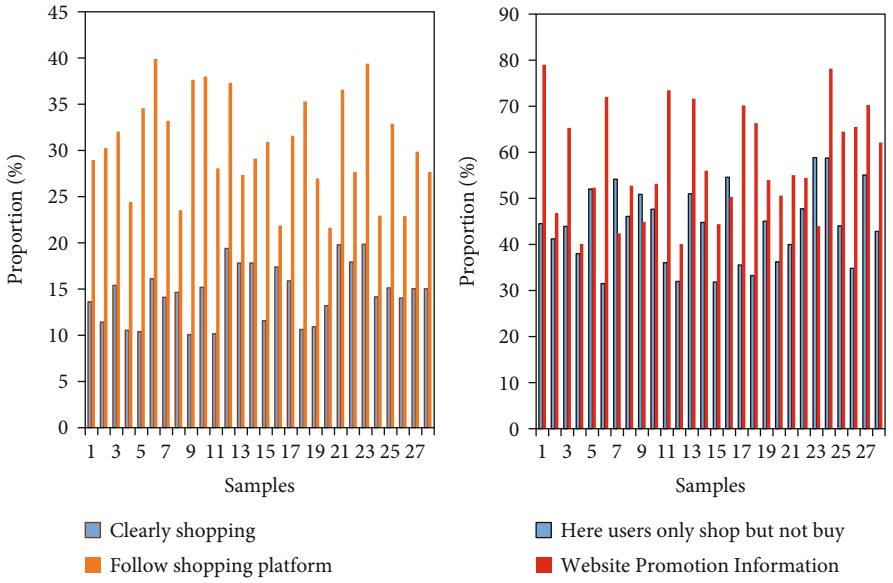

Figure 5: Purpose of shopping.

merchants distribute the products, which was involves three aspects: online payment, network security, and logistics. The problems in these three aspects hinder the development of e-commerce to some extent. With the continuous progress of network technology, network security and payment issues have been greatly improved, but the quality of e-commerce enterprise logistics services has not been significantly improved.

Especially with the improvement of people's living standards, the products purchased by customers are no longer daily necessities, but more electronic products and entertainment products. Traditional B2C commercial logistics services are not just pure physical sports, but based on traditional logistics, pursuing short-time flexible services, and high-value-added services. Therefore, the quality of logistics services plays an increasingly important role in the development of B2C e-commerce [27].

At present, some B2C e-commerce companies are using third-party logistics, and some have established their own logistics. Different models have different distribution ranges and capacities. Generally speaking, the service quality of China's B2C e-commerce logistics providers is low, especially the information services have big defects, which hinder the development of e-commerce enterprises. Therefore, it is imperative to judge the service quality of B2C e-commerce logistics, find out the defects of development, and improve the service quality.

With the rapid development of Internet technology and information technology, advertising operators are changing their promotion methods and forms from traditional media

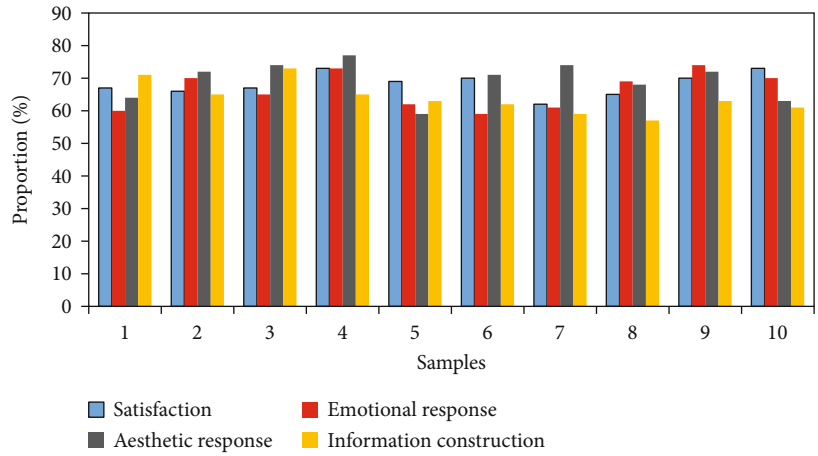

Figure 6: User experience evaluation.

to networks, mobile terminals, digital television, and other carriers. With the development of information technology and digital interactive media, with the emergence of new advertising forms such as text link advertising, web page advertising, search advertising, and mobile SMS advertising, the advertising forms have also undergone great changes. The public and advertising have more communication and interaction. Consumers have more control and speaking opportunities [28].

This article focuses on how to achieve a good interaction and experience through visual design in the search mechanism, control mechanism, user registration mechanism, and product browsing mechanism in the soft interface interaction mechanism of the B2C website. Based on a good user experience-centered design thinking, visual-related elements are designed, including fonts, colors, input boxes, buttons, and layouts. Reflect experience design and aesthetic design. In the process of visual design, integrated design is carried out through universal aesthetic principles, cognitive theories, and design principles. Use scientific usability testing to verify the design. Based on the above-mentioned research, the key points of visual design in the soft interface interaction mechanism that are in line with a good user experience are studied, and the consideration criteria that should be considered for excellent design are summarized. Enhance the user experience of the entire B2C website [29].

5. Conclusion

The research objects of this article are highly pertinent and based on the problems in the context. In-depth research can be conducted through extensive collection of comment data under multiple cultural backgrounds and comparative analysis, and there may be richer research findings; the research objects can also ask various forms of e-commerce such as C2C and B2B are expanded to improve the relevant theories of online reviews. In the measurement and calculation of objective indicators of the website, this article adopts the method of combining quantitative calculation of indicators and scoring by experts to analyze and evaluate all levels of indicators. Based on prospect theory as the theoretical basis, this paper analyzes the behavior patterns of consumers in the process of B2C e-commerce services with B2C enterprises as the research object and uses fuzzy mathematics to establish a consumer behavior decision model that conforms to this process. Through the mining of Internet word-of-mouth, and successively through classification, clustering, sentiment analysis, and other methods, the decision-making model is quantified.

Data Availability

No data were used to support this study.

Conflicts of Interest

The authors declare that there are no conflicts of interest regarding the publication of this article.

Acknowledgments

This work was supported by the Chengde Bureau of Science and Technology's research and development program (202001B001).

References

[1] Y. Kim and R. A. Peterson, "A meta-analysis of online trust relationships in E-commerce," *Journal of Interactive Marketing*, vol. 38, no. may, pp. 44–54, 2017.

[2] J. Mero, "The effects of two-way communication and chat service usage on consumer attitudes in the e-commerce retailing sector," *Electronic Markets*, vol. 28, no. 2, pp. 205–217, 2018.

[3] Y. W. Sullivan and D. J. Kim, "Assessing the effects of consumers' product evaluations and trust on repurchase intention in e-commerce environments," *International Journal of Information Management*, vol. 39, no. APR., pp. 199–219, 2018.

[4] P. Lal, "Analyzing determinants influencing an individual's intention to use social commerce website," *Future Business Journal*, vol. 3, no. 1, pp. 70–85, 2017.

[5] R. Gs, S. Lingam, and A. M. Sudhakara, "Security troubles in E-commerce website," *International Journal of Computer Engineering & Technology*, vol. 8, no. 4, pp. 42–52, 2017.

[6] A. Pansari and V. Kumar, "Customer engagement: the construct, antecedents, and consequences," *Journal of the Academy of Marketing Science*, vol. 45, no. 3, pp. 294–311, 2017.

[7] C. Berne-Manero and M. Marzo-Navarro, "Exploring how influencer and relationship marketing serve corporate sustainability," *Sustainability*, vol. 12, no. 11, p. 4392, 2020.

[8] S. Rezaei and K. Wan, "Examining online channel selection behaviour among social media shoppers: a PLS analysis," *International Journal of Electronic Marketing and Retailing*, vol. 6, no. 1, pp. 28–51, 2014.

[9] A. Bahri, S. Sarkar, and J. Song, "On the integral cohomology ring of toric orbifolds and singular toric varieties," *Algebraic & Geometric Topology*, vol. 17, no. 6, pp. 3779–3810, 2017.

[10] I. K. Yanson, N. L. Bobrov, C. V. Tomy, and D. M. Paul, "Electron–quasiparticle interaction in DyNi 2B 2C measured by point-contact spectroscopy," *Physica C Superconductivity & Its Applications*, vol. 334, no. 3, pp. 152–162, 2017.

[11] J. Chen, L. Guan, and X. Cai, "Analysis on Buyers' cooperative strategy under group-buying price mechanism," *Journal of Industrial & Management Optimization*, vol. 9, no. 2, pp. 291–304, 2013.

[12] T. W. Hudiburg, P. E. Higuera, and J. A. Hicke, "Fire-regime variability impacts forest carbon dynamics for centuries to millennia," *Biogeosciences Discussions*, vol. 14, no. 17, pp. 1–24, 2017.

[13] E. M. T. A. Alsaadi, "Building and developing E-commerce website," *International Journal of Science and Research (IJSR)*, vol. 3, no. 9, pp. 1419–1425, 2020.

[14] M. Pradana and M. Ichsan, "Analysis of an Indonesian E-commerce website: gap between actual performance and users' expectation," *Jurnal Manajemen dan Bisnis Indonesia*, vol. 6, no. 1, pp. 65–75, 2018.

[15] J. F. Andry, K. Christianto, and F. R. Wilujeng, "Using Webqual 4.0 and importance performance analysis to evaluate E-commerce website," *Intelligence*, vol. 5, no. 1, pp. 23–31, 2019.

[16] A. Vegesna, P. Jain, and D. Porwal, "Ontology based chatbot (for E-commerce website)," *International Journal of Computer Applications*, vol. 179, no. 14, pp. 51–55, 2018.

[17] L. Wang and H. Song, "E-commerce credit risk assessment based on fuzzy neural network," *Computational Intelligence and Neuroscience*, vol. 2022, Article ID 3088915, 10 pages, 2022.

[18] T. Hariguna, "Implementation of search engine optimization (SEO) in e-commerce website using on page SEO and off page SEO," *International Journal of Advanced Trends in Computer Science and Engineering*, vol. 9, no. 4, pp. 5481–5484, 2020.

[19] P. Purwanto and K. Kuswandi, "Effects of flexibility and interactivity on the perceived value of and satisfaction with E-commerce (evidence from Indonesia)," *Trite/market*, vol. 29, no. 2, pp. 139–159, 2017.

[20] P. Astuti and A. Utama, "E-commerce website as seller media for end user at Banyuwangi mall," *International Journal of Engineering & Technology*, vol. 7, no. 2.13, pp. 425–428, 2018.

[21] L. Liu, "e-commerce personalized recommendation based on machine learning technology," *Mobile Information Systems*, vol. 2022, Article ID 1761579, 11 pages, 2022.

[22] S. Bai, Z. Liu, and Y. Lv, "Evolutionary game analysis of consumer complaint handling in E-commerce," *Discrete Dynamics in Nature and Society*, vol. 2022, Article ID 3792080, 15 pages, 2022.

[23] Z. Zhang, G. Xu, and P. Zhang, "Research on E-commerce platform-based personalized recommendation algorithm," *Applied Computational Intelligence and Soft Computing*, vol. 2016, Article ID 5160460, 7 pages, 2016.

[24] Z. Dong, "Construction of mobile E-commerce platform and analysis of its impact on E-commerce logistics customer satisfaction," *Complexity*, vol. 2021, Article ID 6636415, 13 pages, 2021.

[25] H. Sun, G. Wang, and S. Xia, "Text tendency analysis based on multi-granularity emotional chunks and integrated learning," *Neural Computing and Applications*, vol. 33, no. 14, pp. 8119–8129, 2021.

[26] X. Zheng, G. Zhu, N. Metawa, and Q. Zhou, "Machine learning based customer meta-combination brand equity analysis for marketing behavior evaluation," *Information Processing and Management*, vol. 59, no. 1, article 102800, 2022.

[27] F. T. A. Hussien, A. M. S. Rahma, and H. B. A. Wahab, "A secure environment using a new lightweight AES encryption algorithm for E-commerce websites," *Security and Communication Networks*, vol. 2021, Article ID 9961172, 15 pages, 2021.

[28] N. Daries, E. Cristobal-Fransi, and B. Ferrer-Rosell, "Implementation of website marketing strategies in sports tourism: analysis of the online presence and E-commerce of golf courses," *Journal of Theoretical and Applied Electronic Commerce Research*, vol. 16, no. 3, pp. 542–561, 2021.

[29] A. Freij, K. Walid, and M. Mustafa, "Deep learning model for digital sales increasing and forecasting: towards smart E-commerce," *Journal of Cybersecurity and Information Management*, vol. 8, no. 1, pp. 26–34, 2021.

Hindawi
Wireless Communications and Mobile Computing
Volume 2022, Article ID 2478186, 10 pages
https://doi.org/10.1155/2022/2478186

Research Article

Online Monitoring of Automotive Engine Lubricating Oil Based on Internet of Things Technology

Jun Wang and Yimin Mo

Wuhan University of Technology, Wuhan 430070, China

Correspondence should be addressed to Jun Wang; wangjun666@whut.edu.cn

Received 23 March 2022; Revised 17 May 2022; Accepted 30 May 2022; Published 17 June 2022

Academic Editor: Jun Ye

In order to realize the online monitoring of automotive engine lubricating oil, a method based on Internet of Things technology is proposed. This method uses the self-organizing neural network of the Internet of Things to fuse the original multidimensional feature data to obtain the fusion value. The Parzen window method is used to formulate the limit value of fusion value, and the samples are divided into three states: normal, warning, and abnormal. Weka software is used to extract rules from oil data. This method can identify different wear state information from oil spectral data, extract knowledge rules, and use them to build the knowledge base of automobile engine wear diagnosis system, so as to realize the automation and intelligence of automobile engine fault diagnosis based on lubricating oil spectral wear data. The measurement method of the lubricating oil sensor is mainly to comprehensively reflect the relationship between oil quality and electrical signal, so as to effectively provide users with reliable information. After many studies, it is concluded that the conductivity of lubricating oil has a good linear relationship with its acid value, metal particles, moisture content, and the change of additive content. Measuring the change of conductivity is an effective means to detect the change of lubricating oil quality. The experimental results show that using the extracted knowledge rules to verify the state of samples, the recognition rate is 97.47%. In order to more fully explain the difference between important element fusion and all feature fusion, all features are extracted. At the same time, the fault diagnosis and recognition rate of all features is not high, only 62.39%. It is proved that the Internet of Things technology can effectively realize online monitoring of the automotive engine lubricating oil.

1. Introduction

The oilfield has main production equipment such as water injection pump, oil transfer pump, natural gas compressor, and generator set, which has the characteristics of continuous operation, large impact load, high working temperature, and fast movement speed. Once these major key equipment fails, it will cause huge economic losses to the oilfield and even endanger personal safety. Therefore, there are strict requirements for the safety performance and operation reliability of the equipment. At present, relying on the lubrication station and laboratory, the oilfield has carried out offline physical and chemical analyses and element analysis of the lubricating oil for generator sets, water injection pumps, natural gas compressors, and other equipment, which has played a positive role in finding the inducement of equipment failure in time, the development of early failure and ensuring the safe and reliable operation of equipment. However, this detection method is not intelligent and cannot be interconnected. It can only give isolated detection results, and the effect of guiding equipment maintenance is not obvious. Especially in the environment where the oilfield vigorously develops the Internet of Things technology and establishes a digital oilfield, this oil monitoring system is separated from the whole oilfield digital system and becomes an information island. It is a short board for building an intelligent digital oilfield system. Therefore, the construction of lubricating oil online monitoring to monitor and evaluate the lubrication and wear status of oilfield equipment in real time is

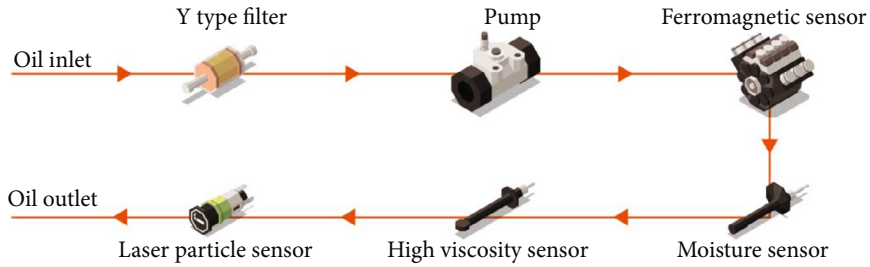

Figure 1: Sensor layout diagram of gear oil online monitoring module.

an effective means to realize predictive maintenance and active maintenance, which is of great significance to ensure the safe, economic, and efficient operation of equipment [1].

Lubricating oil online monitoring technology is to continuously detect the physical and chemical parameters and wear particles of lubricating oil by installing various sensors on the equipment. Generally, the technical method of trend analysis is used to determine the service status of lubricating oil and equipment. It has the characteristics of real-time, continuity, synchronization, rapid analysis, high degree of automation, and informatization. The moisture in lubricating oil will make the oil emulsified and oxidized and reduce the viscosity and oil film strength, and the formation of lubricating oil oxides and polluting impurities will reduce the fluidity of lubricating oil and lead to the increase of viscosity. Moisture and viscosity are an important basis for measuring the lubricating ability of oil. Ferromagnetic and nonferromagnetic wear elements in lubricating oil exist in the form of particles. Monitoring their quantity is of great significance to judge the equipment wear of nonferrous and metal parts. When the oil is aged or polluted, the content of polar molecules and particles in the oil changes, and the dielectric constant of the oil also changes. At the same time, due to friction and wear, worn metal particles and other highly conductive compounds will also change the dielectric constant of the lubricating oil [2]. By monitoring the dielectric constant and AC impedance of lubricating oil, the information of oil quality and wear fault can be reflected. For the main drive gear oil, the main monitoring indicators are temperature, viscosity, moisture, dielectric constant, ferromagnetic particles, and pollution degree. Therefore, the high viscosity sensor, moisture sensor, ferromagnetic sensor, and laser particle sensor are designed in the main bearing gear oil online monitoring module to collect the above indicators in real time. The sensor arrangement is shown in Figure 1.

According to the actual working conditions of the equipment, the three-dimensional six index system of lubricating oil online monitoring is determined, namely, physical and chemical indexes, wear index, and comprehensive quality index. Physical and chemical indexes include moisture and viscosity. Wear indicators include ferromagnetic particles and nonferromagnetic particles. The comprehensive quality indexes include dielectric constant and AC impedance. The three indexes compensate each other, which can scientifically and reasonably determine the working state of lubricating oil and the wear state of equipment [3].

2. Literature Review

According to relevant statistics, more than 50% of the malignant faults of mechanical equipment are caused by lubrication failure and excessive wear. Therefore, the research and application of oil online monitoring and diagnosis technology has important practical significance. At present, many scholars have done more research on the application of oil monitoring technology. Singh et al. mainly studied oil detection technology [4]. Fan et al. mainly introduced the application of oil detection technology in equipment fault diagnosis [5]. Wang et al. introduced the application of offline detection technology in shield. However, with the continuous improvement of automation and integration of shield and the increasing number of shield, the detection technology based on offline detection can not meet the needs of long-term continuous monitoring of modern equipment [6]. Yi et al.'s analysis of the transport fleet (6.4 L, 6.7 L engines) using conventional mineral oil (15 W-40) and fully synthetic oil (5 W-40) shows that the current 5000 mile oil change interval can be extended. Moreover, there are significant differences in oil performance and chemical degradation between 6.4 L and 6.7 L engines. The approximate life of 6.41 engine oil is 8000 miles (about 12800 km), while the approximate life of 6.7 L engine oil is 12500 miles (about 20000 km) [7]. Bo and Qin studied the oil change cycle of vehicle lubricating oil. Sg15W-40 general internal combustion engine oil is selected to conduct tracking test on five civil cars. The collected oil samples are analyzed for physical and chemical properties. Combined with statistical analysis method, it is obtained that the failure mileage of lubricating oil is 7600 km at 90% confidence level [8]. Zhao et al. conducted several groups of driving tests on sf5W-30 engine oil, studied the oil change cycle of sf5W-30 engine oil by using pressure differential scanning calorimeter (PDSC) and infrared spectrometer, and took the vulcanization value in the lubricating oil as the oil change index. When the vulcanization value in the lubricating oil reaches the set threshold (25 A/cm), the running mileage of the driving test vehicle is 9000-9400 km, and this is the engine oil failure time [9]. For Ashwini et al., according to the differences of vehicle operating conditions, different vehicle models are selected for driving test, and the viscosity, flash point, fuel dilution, and other indexes of engine oil (sm5w-30) with different operating mileages are tested. The test results show that after the five test vehicles run for 10000 km, the vehicle runs without abnormality, and the oil still has good oxidation stability, cleaning dispersion capacity, and lubrication performance [10]. Wang et al. based on Jiefang

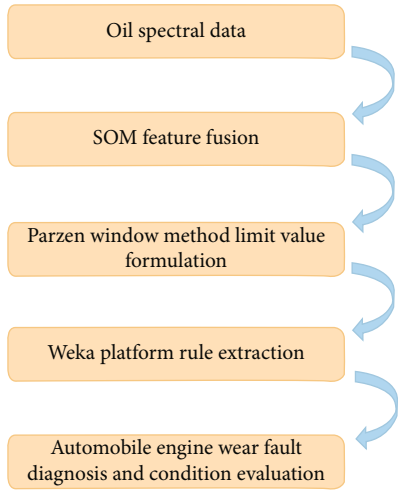

Figure 2: Flow chart of knowledge acquisition method.

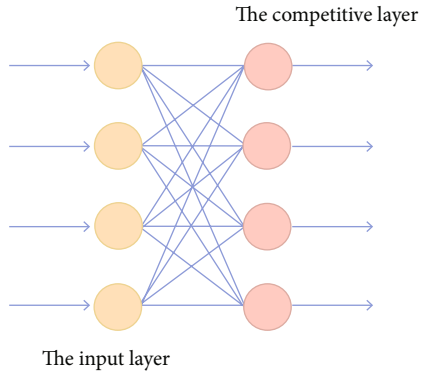

Figure 3: Structure of the self-organizing neural network.

J6 heavy tractor carried out the technology development and research on 1×10^5 km long oil change cycle of e410w-40 engine oil. Combined with bench test, driving test, and engine disassembly test, it shows that all indexes of lubricating oil are within the range specified in the national standard, and the wear of engine parts is also within the normal range, and in August 2015, China First Automobile Co., Ltd. took the lead in applying this long oil change cycle technology in China [11]. Yuldashev et al. believe that developing a sensor that can facilitate the real-time online monitoring of lubricating oil installed on the vehicle should not only monitor the deterioration degree and pollution of lubricating oil but also accurately remind the best time to replace new oil. When the lubricating oil deteriorates to the extent that it will harm the engine or exceed the predetermined threshold of parameter indicators, it will send an alarm to the user in time to remind the user to replace the lubricating oil. At present, it is a very urgent work for people. The development of this sensor should have the following characteristics: fast analysis speed, low cost, real-time monitoring, accurate judgment, simple operation, etc., so that each user can easily master its operation method [12]. Zhang et al. believe that at present, oil detection technology is mainly applied in engineering technology, large mining enterprises, petroleum oil detection, and other fields. The main method is to extract a certain amount of samples from its equipment and send them to the oil detection center, and then, professionals will detect and analyze the oil products of the oil samples to determine their pollution degree and deterioration status, so as to provide reference for its equipment to replace oil and diagnose faults [13].

Based on the current research, this paper proposes a method based on Internet of Things technology. This method uses the self-organizing neural network of the Internet of Things to fuse the original multidimensional feature data to obtain the fusion value. The Parzen window method is used to formulate the limit value of fusion value, and the samples are divided into three states: normal, warning, and abnormal. Weka software is used to extract rules from oil data. This method can identify different wear state information from oil spectral data, extract knowledge rules, and use them to build the knowledge base of automobile engine wear diagnosis system, so as to realize the automation and intelligence of automobile engine fault diagnosis based on lubricating oil spectral wear data. The measurement method of the lubricating oil sensor is mainly to comprehensively reflect the relationship between oil quality and electrical signal, so as to effectively provide users with reliable information. After many studies, it is concluded that the conductivity of lubricating oil has a good linear relationship with its acid value, metal particles, moisture content, and the change of additive content. Measuring the change of conductivity is an effective means to detect the change of lubricating oil quality.

3. Wear Fault Diagnosis Knowledge Acquisition Method Based on Oil Spectrum Data Fusion

3.1. Method and Process. Figure 2 shows the flow chart of knowledge acquisition method for automobile engine wear fault diagnosis based on oil spectrum data fusion, mainly including feature fusion based on SOM, boundary value formulation based on the Parzen window method and knowledge rule extraction based on Weka platform. The flow chart of knowledge acquisition method is shown in Figure 2.

3.2. Self-Organizing Neural Network Learning Algorithm. Self-organizing neural network, also known as self-organizing feature mapping and Koho Nen network, is a neural network with self-organizing ability trained by unsupervised learning. It can conduct self-organizing training and judgment on the input mode and finally divide it into different types. With its low-dimensional organization ability of high-dimensional data, SOM has many successful applications in data mining fields such as classification, clustering, fusion, and prediction [14]. Figure 3 shows the structure of the self-organizing neural network.

SOM's competitive learning algorithm process:

(1) Set the variable and parameter $X[n] = [x_1(n), x_2(n), \cdots, x_N(n)]^T$ as the input vector, or training sample. $W_i[n] =$

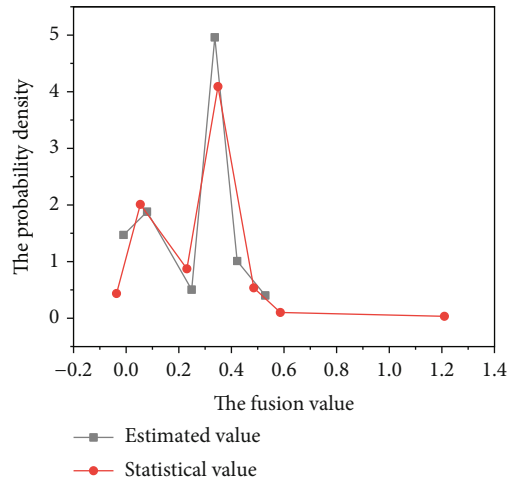

Figure 4: Comparison of probability density function between estimation and statistics.

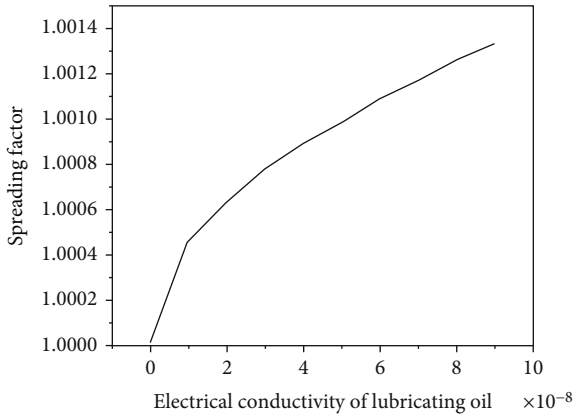

Figure 5: Relationship between the propagation factor and change of lubricating oil conductivity (frequency 10 MHz).

$[w_{i1}(n), w_{i2}(n), \cdots, w_{iN}(n)]^T$ is the weight loss, $i = 1, 2, .., M$. The number of iterations is K

(2) Initialization: initialize the weight vector W_i with a small random value. Set the initial learning rate $\eta(0)$. Normalize all input vectors X and initial values $W_i(0)$ of weight vectors:

$$X' = \frac{X}{\|X\|}, \tag{1}$$

$$W_i'(0) = \frac{W_i(0)}{\|W_i(0)\|}, \tag{2}$$

where

$$\|W_i(0)\| = \sum_{j=i}^{N} \left[w_{ij}(0)\right]^2, \tag{3}$$

$$\|X\| = \sum_{i=1}^{N} (x_i)^2. \tag{4}$$

They are the European norm of weight vector and input vector, respectively

(3) Sampling, approximate matching: select the training sample X' from the space and pass the standard of minimum Euclidean distance

$$\left\|X' - W_c'\right\| = \min_i \left\|X' - W_i'\right\|, i = 1, 2, \cdots, M, \tag{5}$$

to select the winning neuron C, so as to realize the competition process of neurons

(4) Update: Hebb learning rules are used for excited neurons in the topological neighborhood $N_c(n)$ of winning neurons:

$$W_i'(n+1) = W_i'(n) + \eta(n)\left(X' - W_i'(n)\right). \tag{6}$$

Update the weight vector of neurons, so as to realize the cooperation and update process of neurons

(5) Update the learning rate $\eta(n)$ and topological neighborhood and renormalize the learned weights:

$$N_c(n) = \mathrm{INT}\left[N_c(0)\left(1 - \frac{n}{N}\right)\right], \tag{7}$$

$$W_i'(n+1) = \frac{W_i'(n+1)}{\left\|W_i'(n+1)\right\|} \tag{8}$$

(6) Judge whether the number of iterations n exceeds K. If $n \le K$, increase the value of N by 1 and go to step 3. Otherwise, end the iteration process

3.3. Feature Fusion Based on SOM. The steps of feature fusion based on SOM are as follows.

3.3.1. Extract Normal Samples. Because the weights of the training samples are normal, we need to extract the features of the SOM network through the normal samples. The steps of extracting normal samples are as follows.

(i) Step 1: create a self-organizing neural network. Set the parameters of network training and carry out SOM training for all samples X. Among them, the number of output neurons is $m_1 \times n_1$ and the number of training K_1. m_1 and n_1 represent the number of rows and columns of output neurons, respectively

(ii) Step 2: identification of clustering samples. After training, a certain number of samples will be gathered on each output neuron. Therefore, sample identification is carried out with the help of SOM toolbox function in MATLAB [15]

(iii) Step 3: screening of normal samples. Because the topological structure on the neural network structure diagram shows the number of samples corresponding to neuron clustering. The color distribution on the nearest neighbor neuron map reflects the proximity between adjacent neurons. The lighter the color, the closer the distance between two neurons, and the darker the color, the farther the distance between two neurons; At the same time, according to the sample value size on each neuron, the normal sample is extracted and recorded as y

3.3.2. Normal Sample Training. Carry out SOM network training for normal samples, reset the number of output neurons $m_2 \times n_2$ and the number of network iterations K_1, and obtain the weight vector w of normal sample training. Where m_2 and n_2, respectively, represent the number of rows and columns of output neurons, the number of columns of weight vector w is equal to the sample dimension, and the number of rows is equal to the number of output neurons, i.e., $m_2 \times n_2$.

3.3.3. Feature Fusion. Calculate the minimum matching distance d from all samples x to the weight vector w of normal samples, and then fuse a curve to achieve the purpose of feature fusion [16].

$$d = \min_j \left\| X - W_j \right\|, \tag{9}$$

where j is the number of output neurons.

3.4. Formulation of Limit Value Based on Parzen Window Method. The traditional limit value formulation methods assume that the oil monitoring data obey the normal distribution, but the distribution law of the actual data is not necessarily normal, and its probability distribution is often unknown. At this time, it is necessary to estimate the probability density function of the data from a large number of data and obtain the probability distribution of the sample according to the probability density function; then, the limit value of wear diagnosis is obtained according to the estimated probability distribution.

To estimate the probability density function,

$$F(x) = P(X \le x) = \int_{-\infty}^{x} p(t)dt. \tag{10}$$

It is necessary to find the solution of linear operator

$$\int_{-\infty}^{\infty} \theta(x-t)p(t)dt = F(x), \tag{11}$$

where

$$\theta(x) = \begin{cases} 1, x > 0, \\ 0, x \le 0. \end{cases} \tag{12}$$

And the solution must also meet the following two conditions:

$$p(x) \ge 0, \int_{-\infty}^{\infty} p(x)dx = 1 \tag{13}$$

In equation (9), the expression of the distribution function $F(x)$ is unknown, but a set of samples $x_1, \cdots, x_l$ are given. According to the probability theory, this group of samples is independent and identically distributed. Now, use sample $x_1, \cdots, x_l$ to construct the empirical distribution function, where l is the number of samples [17].

$$F_l(x) = \frac{1}{l} \sum_{i=1}^{l} \theta(x - x_i). \tag{14}$$

The Parzen window estimation method is a nonparametric estimation method that uses known sample points to estimate the overall probability density distribution, that is, it uses the average value of the density of each point in a certain range to estimate the overall probability density. Due to its solid theoretical foundation and excellent performance, Parzen window technology has become a widely used the nonparametric density estimation method.

Generally, let x be a point in d-dimensional space, the total number of samples selected is n, in order to estimate the distribution probability density $P(x)$ at x, make a hypercube V_N centered on X, and its side length is h_N; then, the expression of volume is $V_N = h_N^d$. To calculate the number of samples k_n falling into hypercube V_N, it is necessary to construct a function so that

$$\phi(u) = \begin{cases} 1, \text{when} \left| u_j \right| \le \frac{1}{2}, j = 1, 2, \cdots, d, \\ 0, \text{other}. \end{cases} \tag{15}$$

If $\phi(u)$ satisfies the condition of equation (13), the number of samples falling into the hypercube is

$$k_N = \sum_{i=1}^{N} \phi\left(\frac{x - x_i}{h_N} \right). \tag{16}$$

Substitute equation (14) into:

$$\widehat{P}_N(x) = \frac{k_N / N}{V}, \tag{17}$$

$$\widehat{P}_N(x) = \frac{1}{N} \sum_{i=1}^{N} \frac{1}{V_N} \phi\left(\frac{x - x_i}{h_N} \right). \tag{18}$$

3.5. Conductivity Is the Main Basis for Evaluating the Quality

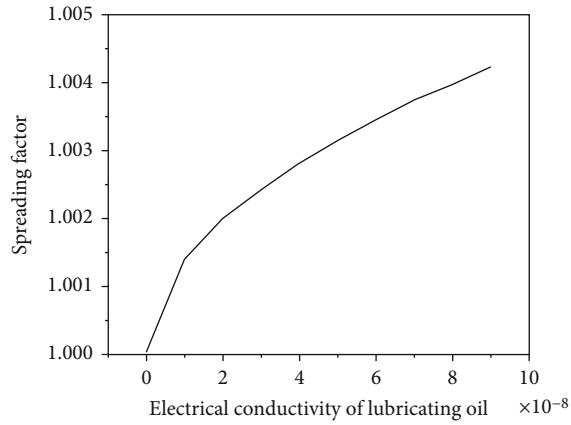

Figure 6: Relationship between propagation factor and change of lubricating oil conductivity (frequency 100 MHz).

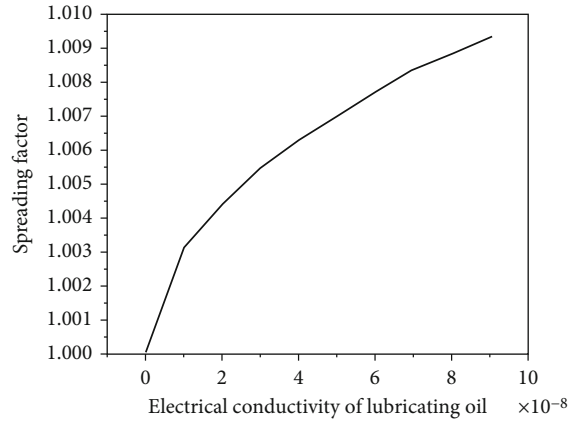

Figure 7: Relationship between the propagation factor and change of lubricating oil conductivity (frequency 500 MHz).

of Lubricating Oil. If its composition changes, or there is invasion of external substances, or its own oxidation, etc., they will change the conductivity of lubricating oil. Therefore, as long as we know the change of the conductivity value of the lubricating oil, we can easily judge the quality of the lubricating oil.

As early as 1994, Ford Motor Company had passed the laboratory evaluation and driving test. Finally, it was concluded that the online monitoring of lubricating oil can be done by measuring the conductivity of the lubricating oil. The measurement method of the lubricating oil sensor is mainly to comprehensively reflect the relationship between oil quality and electrical signal, so as to effectively provide users with reliable information. After many studies, it is concluded that the conductivity of lubricating oil has a good linear relationship with its acid value, metal particles, moisture content, and the change of additive content. Measuring the change of conductivity is an effective means to detect the change of lubricating oil quality. In the quality identification of lubricating oil, permittivity and conductivity are two important parameters to evaluate the electrochemical performance of oil. The permittivity of different oil products has little difference; however, the conductivity of different oil products varies greatly due to the change of oil components, generally ranging from 10-7 to 10-15 s/m, with a variation range of about 8 orders of magnitude. Therefore, when evaluating whether the quality of lubricating oil has deteriorated, it can be judged by accurately measuring the conductivity. Therefore, measuring conductivity will be a comprehensive way to reflect the change of lubricating oil quality. Therefore, this paper will study the theoretical method based on the physical quantity of conductivity and preliminarily design the online lubricating oil sensor [18].

3.6. Extraction of Wear Element Rules Based on Weka Platform. The knowledge rule extraction of engine wear elements is mainly carried out with the help of Weka platform. Weka is a comprehensive data mining system developed by Waikato University in New Zealand. It not only provides a variety of data mining methods (classification, clustering, association rules, etc.) but also provides data preprocessing functions suitable for any data set and a variety of algorithm performance evaluation methods. The rule extraction function of Weka software relies on the decision tree classification algorithm, namely, C4.5 algorithm. It is a guided inductive learning algorithm, which inherits all the advantages of ID3 algorithm and improves it. It is especially suitable for occasions with large amount of mining data and high requirements for relative efficiency and performance.

4. Experimental Results and Analysis

In order to verify the effectiveness of this method, 2089 oil spectral data of a military aircraft engine are used to verify the method. Seven commonly used important elements are selected for fault diagnosis, including Fe, Al, Cu, Cr, Ag, Ti, and Mg, so the characteristic dimension of the data is 7.

4.1. Feature Fusion. Firstly, the original spectral data are normalized to avoid the influence of magnitude difference on the fusion results. Then, SOM training is carried out on the normalized original data. Then, by comparing the distance distribution between neurons, the number of samples gathered on each neuron, and the value size, 401 samples on the third neuron are selected as normal samples and trained and fused to obtain the fusion value of the samples. Finally, the characteristic data of the sample and the fusion features are formed into a new vector matrix, which is adjusted in ascending order according to the value of the fusion value based on the fusion value. The concentration value of each element is compared with the fusion value one by one, and it is concluded that the wear element and the fusion value show the same change trend. It can be seen that the fusion eigenvalue can reflect the change trend and law of engine wear state [19].

4.2. Formulation of Limit Value. It can be seen from Figure 4 that the fitting effect of probability density function curve of statistics and estimation is good. Therefore, the limit value of the fusion value is formulated, and the data samples are divided into normal, warning, and abnormal.

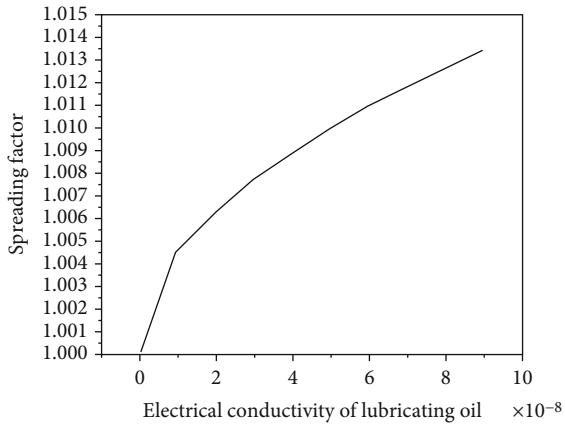

Figure 8: Relationship between propagation factor and change of lubricating oil conductivity (frequency 1 GHz).

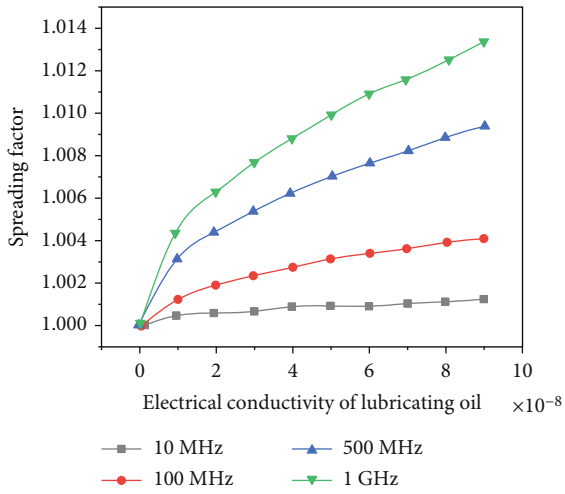

Figure 9: Relationship between electromagnetic wave propagation factors of different frequencies and changes of lubricating oil conductivity.

Figure 5 shows the propagation of electromagnetic wave with frequency of $F = 10$ MHz in lubricating oil. The relationship between electromagnetic wave propagation factor and lubricating oil conductivity is simulated by MATLAB. The abscissa represents the electrical conductivity of lubricating oil, the ordinate represents the propagation factor of electromagnetic wave, and the black curve in the figure represents the changing relationship between these two physical quantities.

It can be seen from Figure 5 that when the conductivity of lubricating oil $\sigma = 10^{-15}$S/m, the propagation factor of electromagnetic wave is about equal to 1. When the conductivity increases to $\sigma = 10^{-8}$S/m, the propagation factor of the corresponding electromagnetic wave is about 1.0004. When the conductivity continues to increase to $\sigma = 5 \times 10^{-8}$S/m, the propagation factor of the corresponding electromagnetic wave is 1.0010. Finally, when the conductivity $\sigma = 9 \times 10^{-8}$ S/m, the propagation factor of electromagnetic wave is about 1.0013. The increasing trend of conductivity can be roughly divided into two stages. The first stage: $\sigma = (10^{-15} \sim 10^{-8})$S/m ($\Delta\gamma$ represents the change rate of propagation factor) and the corresponding electromagnetic wave propagation factor changes to $1 \sim 1.0004$ ($\Delta\gamma = 0.0004$). At this stage, the electromagnetic wave propagation factor changes slowly with conductivity. The second stage: $\sigma = (10^{-8} \sim 9 \times 10^{-8})$S/m, the corresponding electromagnetic wave propagation factor changes from 1.0004 to 1.0013 ($\Delta\gamma = 0.0009$) [20]. At this stage, the electromagnetic wave propagation factor changes rapidly with the conductivity. Through comparative analysis of these data changes, it is easy to conclude that with the increase of lubricating oil conductivity, the propagation factor of electromagnetic wave also increases, and their change relationship is nearly linear in these two stages.

Figure 6 shows the propagation of electromagnetic wave with frequency of $F = 100$ MHz in lubricating oil. The black curve in the figure shows the relationship between the transmission coefficient of lubricating oil and the change of electrical conductivity of lubricating oil. It can be seen from Figure 6 that when the conductivity of lubricating oil $\sigma = 10^{-15}$S/m, the propagation factor of electromagnetic wave is about equal to 1. When the conductivity increases to $\sigma = 10^{-8}$S/m, the corresponding propagation factor of electromagnetic wave is about 1.0014. When the conductivity continues to increase to $\sigma = 5 \times 10^{-8}$S/m, the corresponding propagation factor of electromagnetic wave is 1.0031. Finally, when the conductivity $\sigma = 9 \times 10^{-8}$S/m, the propagation factor of electromagnetic wave is about 1.0042. Similarly, the increase of conductivity is roughly divided into two stages. The first stage: $\sigma = (10^{-15} \sim 10^{-8})$S/m, the change value of corresponding electromagnetic wave propagation factor is $1 \sim 1.0014$ ($\Delta\gamma = 0.0014$). It can be seen from the figure that the change of electromagnetic wave propagation factor with conductivity is relatively slow at this stage; The second stage: $\sigma = (10^{-8} \sim 9 \times 10^{-8})$S/m, the change value of electromagnetic wave propagation factor is 1.0014~1.0042 ($\Delta\gamma = 0.0028$). At this stage, the electromagnetic wave propagation factor increases rapidly with the increase of conductivity. It is easy to conclude from the data change that as the conductivity of lubricating oil increases, the propagation factor of electromagnetic wave in the whole process also increases: especially from Figure 6, it can be intuitively found that the relationship between the propagation factor and the change of conductivity is a star near linear relationship [21].

Figure 7 shows the propagation of electromagnetic wave with frequency of $F = 500$ MHz in lubricating oil. The black curve in the figure shows the relationship between the propagation coefficient and the conductivity. It can be clearly seen from Figure 7 that when the conductivity of lubricating oil is $\sigma = 10^{-15}$S/m, the propagation factor of electromagnetic wave is about equal to 1. When the conductivity increases to $\sigma = 10^{-8}$S/m, the corresponding propagation factor of electromagnetic wave is about 1.0031. If the conductivity continues to increase to $\sigma = 5 \times 10^{-8}$S/m, the propagation factor value of electromagnetic wave is 1.0071; finally, when the conductivity increases to $\sigma = 9 \times 10^{-8}$S/m, the propagation factor value of electromagnetic wave is about 1.0095. Similarly, the increase of conductivity is

Table 1: Summary of rules.

Rule 1	Condition	$c(\mathrm{AI}) \le 0.4$
	Conclusion	Normal
Rule 2	Condition	$0.4 < c(\mathrm{AI}) \le 0.8$ and $c(\mathrm{Ag}) \le 0.1$
	Conclusion	Normal
Rule 3	Condition	$c(\mathrm{Fe}) \le 0.2$ and $0.4 < c(\mathrm{AI}) \le 0.8$ and $c(\mathrm{Ag}) > 0.1$
	Conclusion	Normal
Rule 4	Condition	$c(\mathrm{Fe}) > 0.2$ and $0.4 < c(\mathrm{AI}) \le 0.8$ and $c(\mathrm{Ag}) > 0.1$
	Conclusion	Warning
Rule 5	Condition	$c(\mathrm{AI}) > 0.8$
	Conclusion	Warning

roughly divided into two stages for comparative analysis. The first stage: $\sigma = (10^{-15} \sim 10^{-8})$S/m, the variation range of corresponding electromagnetic wave propagation factor is $1 \sim 1.0031$ $(\Delta\gamma = 0.0031)$. At this stage, the electromagnetic wave propagation factor increases slowly with the increase of conductivity. However, in the second stage: $\sigma = (10^{-8} \sim 9 \times 10^{-8})$S/m, the corresponding electromagnetic wave propagation factor changes from 1.0031 to 1.0095 $(\Delta\gamma = 0.0064)$. In this stage, the electromagnetic wave propagation factor increases with the increase of conductivity. It can be concluded from the figure and table that the change law of these data can be obtained. When the conductivity of lubricating oil increases, the propagation factor of electromagnetic wave also increases, and their change relationship is also nearly linear in the first and second stages [22].

Figure 8 shows the propagation of electromagnetic wave with frequency of $F = 1$ GHz in lubricating oil. The black curve in the figure shows the relationship between the transmission coefficient of lubricating oil and the electrical conductivity of lubricating oil. It can be seen from Figure 8 that when the conductivity of lubricating oil $\sigma = 10^{-15}$S/m, the propagation factor value of electromagnetic wave is about 1. As the conductivity increases to $\sigma = 10^{-8}$S/m, the propagation factor of electromagnetic wave is 1.0045. When the conductivity continues to increase to $\sigma = 5 \times 10^{-8}$S/m, the propagation factor of electromagnetic wave is 1.0100. Finally, when the conductivity $\sigma = 9 \times 10^{-8}$S/m, the corresponding propagation factor of electromagnetic wave is about 1.0134. The change of conductivity can be roughly divided into two stages. The first stage: $\sigma = (10^{-15} \sim 10^{-8})$S/m, the variation range of corresponding electromagnetic wave propagation factor is $1 \sim 1.0045$ $(\Delta\gamma = 0.0045)$. At this stage, the electromagnetic wave propagation factor increases slowly with the change of conductivity. The second stage: $\sigma = (10^{-8} \sim 9 \times 10^{-8})$S/m, the change value of the corresponding electromagnetic wave propagation factor is $1.0045 \sim 1.0134$ $(\Delta\gamma = 0.0089)$. At this stage, the electromagnetic wave propagation factor changes rapidly with the conductivity. It can be seen from the figure that the change relationship between these two change stages is also nearly linear. From the relationship between the propagation factors of the above electromagnetic waves with different frequencies in the lubricating oil and the conductivity, the graphics drawn by MATLAB show that they all have a common feature: in the two different stages of conductivity change, they all have a nearly linear relationship [23].

In Figure 9, the abscissa is the variation range of electrical conductivity of lubricating oil, ordinate is the size of propagation factor, black is the electromagnetic wave with a frequency of 10 MHz, red is the electromagnetic wave with a frequency of 100 MHz, blue is the electromagnetic wave with a frequency of 500 MHz, and green is the electromagnetic wave with a frequency of 1 GHz. It can be concluded that the change of the conductivity factor is very linear, but it is not completely linear at several turning points in the curve of the propagation factor $\sigma = 10^{-8}$S/m. From the variation law of several curves, it can be concluded that with the increase of the frequency of electromagnetic wave, under the same change of conductivity, the change of propagation factor also increases, that is, it can be understood that the higher the frequency, the higher the sensitivity of electromagnetic wave to the change of conductivity [24, 25]. Through the simulation of the relationship between the electromagnetic wave propagation factor and the conductivity of lubricating oil by MATLAB software, it is verified that the change between propagation factor and conductivity is nearly linear.

4.3. Rule Extraction. In order to verify the effectiveness of the method, 1/2 samples in the divided state are randomly selected for rule extraction and the other 1/2 samples for rule verification. Based on the fusion of important elements, the rules of samples are extracted with the help of Weka software to build the knowledge base of fault diagnosis. The mined rules are shown in Table 1.

The extracted knowledge rules are used to verify the state of samples, and the recognition rate is 97.47%. In order to more fully explain the difference between important element fusion and all feature fusion, all features are extracted. At the same time, the fault diagnosis and recognition rate of all

features is not high, only 62.39%. This means that not all features play a positive role in the fault diagnosis of the automobile engine wear state.

5. Conclusion

An automobile engine wear fault diagnosis algorithm based on SOM feature fusion based on Internet of Things technology is proposed. Through the feature fusion of multifeature data, the fusion value is obtained, and then, the boundary value of the fusion value is formulated to divide the sample state. Finally, Weka software is used to extract the knowledge rules of oil data. The relationship between the propagation factor of the excitation signal in the sensor in the lubricating oil and the change of the conductivity of the lubricating oil is simulated, and the curve between the output signal of the sensor and the conductivity of the lubricating oil is simulated. It can be seen at a glance that the lubricating oil sensor designed in this paper is feasible and practical. The automation and intellectualization of fault diagnosis of automotive engine lubricating oil spectral wear data are realized. According to the actual wear data of automobile engine, the proposed method is used for wear fault diagnosis, and the recognition rate is 97.47%, which shows that this method has a high recognition rate for fault state.

Data Availability

The data underlying the results presented in the study are available within the manuscript.

Conflicts of Interest

The authors declare that they have no conflicts of interest.

Acknowledgments

Guangxi scientific research and technology development plan project: "development and industrialization of 1.5 L turbocharged gasoline engine suitable for hybrid vehicles" (No.: guike ac16380026) supported this study.

References

[1] Z. D. Yuan, H. Li, X. Q. Cheng, and Y. Zhang, "Research on regeneration technology of internal combustion engine lubricating oil," *Journal of Physics: Conference Series*, vol. 1635, no. 1, article 012012, 2020.

[2] J. Zhao, D. Wang, F. Zhang et al., "Real-time and online lubricating oil condition monitoring enabled by triboelectric nanogenerator," *ACS Nano*, vol. 15, no. 7, pp. 11869–11879, 2021.

[3] K. Bezerra, T. Neto, C. Souza, L. O. Gomes, and N. Filho, "Monitoring of lubricating oils used in diesel engine by biodiesel contamination from fuel dilution," *Lubrication Science*, vol. 33, no. 8, pp. 432–438, 2021.

[4] P. Singh, S. R. Chauhan, V. Goel, and A. K. Gupta, "Impact of binary biofuel blend on lubricating oil degradation in a compression ignition engine," *Journal of Energy Resources Technology*, vol. 141, no. 3, 2019.

[5] H. Fan, Y. Zhu, W. Zheng, X. Qin, D. Wu, and D. Zhong, "Research on on-line monitoring and regulation technology of pressure of high voltage transformer," *IOP Conference Series: Earth and Environmental Science*, vol. 446, no. 4, article 042083, 2020.

[6] Y. Wang, G. Xu, Q. Zhou, and J. Chen, "Design of intelligent detection system for diesel engine main oil duct hole based on s7-300 control," *IOP Conference Series Earth and Environmental Science*, vol. 693, no. 1, article 012011, 2021.

[7] P. Yi, W. Long, L. Feng, L. Chen, J. Cui, and W. Gong, "Investigation of evaporation and auto-ignition of isolated lubricating oil droplets in natural gas engine in-cylinder conditions," *Fuel*, vol. 235, no. JAN.1, pp. 1172–1183, 2019.

[8] H. Bo and M. Qin, "Real-time online monitoring and protection control system for automobile generator based on artificial intelligence," *Journal of Physics: Conference Series*, vol. 1345, no. 5, article 052060, 2019.

[9] L. Zhao, Y. Zhou, I. Matsuo, S. K. Korkua, and W. J. Lee, "The design of a remote online holistic monitoring system for a wind turbine," *IEEE Transactions on Industry Applications*, vol. 56, no. 1, pp. 14–21, 2020.

[10] M. Ashwini, S. Gowrishankar, and Siddaraju, "Internet of Things based intelligent monitoring and reporting from agricultural fields," *International Journal of Control Theory and Applications*, vol. 14, no. 2, pp. 119–128, 2019.

[11] Y. Wang, J. Yan, Z. Yang, Y. Zhao, and T. Liu, "GIS partial discharge pattern recognition via lightweight convolutional neural network in the ubiquitous power Internet of Things context," *Technology*, vol. 14, no. 8, pp. 864–871, 2020.

[12] Z. M. Yuldashev, A. M. Sergeev, and N. S. Nastueva, "Perspectives for the use of the Internet of Things in portable online cardiac monitors," *Biomedical Engineering*, vol. 55, no. 3, pp. 210–214, 2021.

[13] Z. Zhang, H. Zhou, and Z. Zhou, "Research on monitoring method of impulse vibration in large transformer transportation," *Journal of Physics: Conference Series*, vol. 1621, no. 1, article 012069, 2020.

[14] A. Marchioni, M. Mangia, F. Pareschi, R. Rovatti, and G. Setti, "Subspace energy monitoring for anomaly detection @sensor or @edge," *IEEE Internet of Things Journal*, vol. 7, no. 8, pp. 7575–7589, 2020.

[15] G. Elumalai and R. Ramakrishnan, "A novel approach to monitor and maintain database about physiological parameters of (Javelin) athletes using Internet of Things (IoT)," *Wireless Personal Communications*, vol. 111, no. 1, pp. 343–355, 2020.

[16] F. Li, R. Xie, Z. Wang, L. Guo, and W. Z. Song, "Online distributed IoT security monitoring with multidimensional streaming big data," *IEEE Internet of Things Journal*, vol. 7, no. 5, pp. 4387–4394, 2020.

[17] L. Du, "Preventive monitoring of basketball players' knee pads based on IoT wearable devices," *Microprocessors and Microsystems*, vol. 82, no. 8, article 103899, 2021.

[18] A. Reethika, T. M. Prakash, S. K. Pranao, D. K. Raj, and K. R. Kumar, "Automatic sensor network analysis for landslide detection system," *Journal of Physics: Conference Series*, vol. 1916, no. 1, article 012120, 2021.

[19] M. H. Majhool, H. Alrikabi, and M. S. Farhan, "Design and implementation of sunlight tracking based on the Internet of Things," *IOP Conference Series: Earth and Environmental Science*, vol. 877, no. 1, article 012026, 2021.

[20] T. Chen, S. Barbarossa, X. Wang, G. B. Giannakis, and Z. L. Zhang, "Learning and management for Internet of Things: accounting for adaptivity and scalability," *Proceedings of the IEEE*, vol. 107, no. 4, pp. 778–796, 2019.

[21] G. X. Liu, L. F. Shi, and D. J. Xin, "Data integrity monitoring method of digital sensors for Internet-of-Things applications," *IEEE Internet of Things Journal*, vol. 7, no. 5, pp. 4575–4584, 2020.

[22] S. Krishnan, S. Lokesh, and M. R. Devi, "An efficient Elman neural network classifier with cloud supported Internet of Things structure for health monitoring system," *Computer Networks*, vol. 151, pp. 201–210, 2019.

[23] T. Monika and R. Nagarajan, "Lubricating oil remaining useful life prediction using multi-output Gaussian process regression," *IEEE Access*, vol. 8, pp. 128897–128907, 2020.

[24] Z. P. Wang, X. Xue, H. Yin, Z. X. Jiang, and Y. F. Li, "Research progress on monitoring and separating suspension particles for lubricating oil," *CompLex*, vol. 2018, no. 1-9356451, pp. 1–9, 2018.

[25] B. Andrés, V. Alberto, G. Eneko, F. Susana, and J. R. Juan, "Using ensembles of regression trees to monitor lubricating oil quality," in *Modern Approaches in Applied Intelligence*, pp. 199–206, Springer, 2011.

Hindawi
Wireless Communications and Mobile Computing
Volume 2022, Article ID 4757016, 15 pages
https://doi.org/10.1155/2022/4757016

Research Article

Smart Community Emergency Evacuation Management System and Risk Assessment Based on Mobile Big Data

Yongjun Han,[1,2] Li Huang,[1,3] Tao Xiao,[1,4] Aihua Yuan,[1,5] Yi Yu,[6,7] Yanfei Feng,[1,4] Junshuai Cheng,[1] Ling Di,[1] Jiabao Zheng,[1,4] and Zengshu Ye[2]

[1]*Institute of Industrial Development and Governance Innovation, Zhejiang Guangsha Vocational and Technical University of Construction, Jinhua, 322103 Zhejiang, China*
[2]*School of Journalism and Communications, Communication University of Zhejiang, Hangzhou, 310018 Zhejiang, China*
[3]*School of Business, Yulin Normal University, Yulin, 537000 Guangxi, China*
[4]*School of Education and Humanities, University Tun Abdul Razak, Kuala Lumpur, 50400 Kuala Lumpur, Malaysia*
[5]*College of Business Administration, University of the East, Manila, 40441 Manila, Philippines*
[6]*College of Art Design, Hangzhou Vocational & Technical College, Hangzhou, 310018 Zhejiang, China*
[7]*Art Theory, Krirk University, Bangkhen, 10220 Bangkok, Thailand*

Correspondence should be addressed to Li Huang; hl1338@zjgsdx.edu.cn

Received 12 April 2022; Revised 16 May 2022; Accepted 23 May 2022; Published 16 June 2022

Academic Editor: Jun Ye

In recent years, with the continuous expansion and development of cities, urban population has become more and more dense. At present, there are few researches on community emergency evacuation management system in China. Therefore, the establishment of community emergency evacuation management system based on mobile big data can not only meet the efficient, fast, smooth, and orderly evacuation and settlement needs of the masses but also minimize emergencies. All kinds of losses and influences caused by accidents have very important practical significance. In this paper, an emergency evacuation management system is developed and designed on smart community platform based on mobile big data technology. In the process of development, it is found that the service integration method of mobile big data and application model is the best combination of this system. The construction process of community emergency evacuation management system framework is introduced in detail. Through the research and design of the system, and then test and analysis of the experiment, the sixth grade teachers and students of a primary school group experiment, there are 50 people in each group. The experimental group is familiar with the system operation in advance, and the knowledge of emergency evacuation management is previewed in advance. It is concluded that the class with emergency evacuation management system has much faster response time and decision-making time to emergencies than the class without emergency evacuation management system, and the injury situation of the class is much better. The study shows that the emergency evacuation management system plays an important role in dealing with emergencies, improving the escape rate and reducing the number of injured. I believe it will be further promoted in the future.

1. Introduction

1.1. Background and Significance. Before 2003, research on emergency management mainly focused on disaster management research. Since the mid-to-late 1970s, with the intensification of earthquakes, floods, and droughts, a number of important research results have been achieved in Chinese academic circles in individual disasters, regional comprehensive disasters, disaster theory, disaster mitigation strategies, and disaster insurance. With the rapid social and economic development and the continuous increase of urban population, problems such as the serious vulnerability

of urban lifelines have become increasingly obvious. In recent years, urban disasters have occurred frequently, causing serious losses to the country and people. The establishment and improvement of urban emergency evacuation systems have received more and more attention from the state. The community is the basic unit of the city. After responding to emergencies, community workers will promptly place people in the area to a safe zone. This is an important measure to prevent and reduce casualties and avoid secondary disasters. Therefore, in order to reduce disaster losses, it is necessary to rely on big data smart technology to implement disaster risk emergency management system for the community.

1.2. Related Work. In recent years, research on emergency evacuation in densely populated areas in cities has attracted widespread attention from scholars. Bo et al. have established a research framework for emergency evacuation of urban business circles in view of the particularity of emergency evacuation in urban business circles with dense floating population and concentrated commerce [1]. Huixian et al. designed a simulation experiment system for the emergency evacuation of urban complexes to provide decision-making assistance and support for the virtual drill and emergency rescue of urban disaster events [2]. Diantao et al. proposed an indoor positioning evacuation solution based on iBeacon base station on the current situation of fire emergency evacuation [3]. Zhang SP et al. designed a building emergency evacuation navigation system based on mobile terminals for complex building emergency evacuation problems [4]. Yang and Zhu used PyroSim software to establish the fire model and evacuation model of the terminal building, and conducted simulation analysis on this, and proposed a targeted terminal evacuation design plan [5]. Mingmin et al. proposed targeted emergency evacuation strategies for the emergency evacuation of people in subway stations, their research proves that targeted emergency evacuation strategies can effectively avoid most incident losses [6]. In summary, it can be seen from the previous research status of emergency evacuation that most of them are studying emergency evacuation strategies and using model construction to study how to propose emergency evacuation strategies, but few design an emergency evacuation strategy based on models and technologies, management system to assist and support emergency evacuation decisions.

1.3. Innovation in this Article. Based on previous research on emergency evacuation systems, this article applies mobile big data to community emergency evacuation management systems and makes the following innovations: (1) apply the GIS theory and technology based on location services to the emergency evacuation model; (2) proposed a spatial data organization method of subscale and level; (3) use .NET component programming technology to develop emergency evacuation management system framework; (4) E-R diagrams are used to describe the topic of emergency evacuation; and (4) the designed system obtains the data result through test analysis and comparison.

2. Related Theories and Technologies for the Development of Community Emergency Evacuation Management System Based on Mobile Big Data

2.1. Related Theories Based on Mobile Big Data. "Mobile big data" can not only capture accurate data information in real time but also create detailed customer portraits to indicate accurate customer data information [7]. Mobile data mainly refers to the medium of mobile Internet, from the application of mobile user terminal access to huge amounts of data in the process of flow, within a reasonable period of time to manage the processing and analysis, and as for human interpretation by the numbers according to the floorboard of the information. At present, in the academia for mobile data, there is no uniform definition and there is no systematic classification. Typical application fields of mobile big data can be classified into entertainment content, service, life, shopping, consumption, Internet, collaboration, and other fields.

2.1.1. Practical application of Mobile Big Data

(1) Combination of Mobile Big Data and Electronic Maps. The combination of mobile big data and Baidu deeply integrates the location service technology of mobile big data into Baidu Maps. With life services as the core, it reflects the commercial value of Baidu Maps; AutoNavi is a very good digital map content, navigation, and location service solution in China. The solution provider, the Gaode map developed by the solution provider, not only provides accurate free map navigation products but also has become the "new favorite" of many companies with its advanced mobile big data technology [8].

(2) Combination of Mobile Big Data and the Internet of Things. Based on the application of location services on the Internet of Things, it mainly provides users with integrated positioning services such as GPS and base stations. Users can track vehicles or goods by installing positioning terminals. The Internet of Things mobile big data application is a comprehensive application of various remote sensing technologies. Through radio frequency identification, infrared sensors, global positioning systems, laser scanners, and other information sensing equipment, according to the agreed agreement, items are connected to the Internet and information exchange and communication. The Internet of Things can realize the connection of most items to the network, facilitate identification, management, and control, and bring more convenience to people's lives. Human society will gradually enter the era of the Internet of Things, and the combination of mobile big data and the Internet of Things can combine location service function of mobile big data that is maximized. In other words, when the Internet of Things era comes, the spring of mobile big data location marketing will also come [9].

(3) Combination of Mobile Big Data and WeChat APP. WeChat "people nearby" is one of the most accurate

marketing and promotion methods. In this way, you can locate an area most effectively and then send preferential information to users in this area. The effect is usually good. After the merchant clicks to view "people nearby," it finds nearby WeChat users based on their geographic location and pushes promotional messages to nearby users for accurate delivery. The emergence of mobile big data has further enhanced the marketing power of WeChat. WeChat uses mobile big data for precise positioning. You can set any point as the center. As long as there are people nearby using WeChat, they can send their own information through greetings. The arrival rate is 100%, and the effect is relatively intuitive. And WeChat mobile big data is very suitable for many industries, such as hotel, real estate, and education. However, WeChat officially launched the mobile big data service [10–12]. When Tencent launched the 2.5 version in 2011, it added the mobile big data function, which attracted vendors such as streetside, shopper, and Kaikai, and provided very strong support for the development of mobile big data. Domestic mobile big data vendors have sprung up, but due to the lack of support from social networks, initial development is more difficult, and many users are still relatively unfamiliar with the concept of mobile big data. Therefore, the emergence of WeChat mobile big data has broken the barriers between QQ friends, Tencent Weibo, and mobile phone address books. The seamless replication of the user's friend relationship is realized. The addition of social networks has made the development of mobile big data smooth [13].

2.2. Related Theories of Emergency Evacuation

2.2.1. Types of Emergency Evacuation. When an emergency is approaching or has already occurred, the organized transfer of people in the dangerous area to a safe area is an emergency evacuation. Emergency evacuation includes two types: local evacuation and large-scale urban evacuation. When an emergency is about to occur or has occurred, the type, nature, characteristics, and possible impact of the emergency should be used to determine what type of emergency evacuation is to be organized. And to do these points, (1) keep calm, make correct judgments, and act quickly; (2) learn to protect yourself and avoid tripping and collision during evacuation; and (3) obey the command and evacuate according to the predetermined order and line [14]. Specifically, there are the following types:

The emergency evacuation system includes evacuation command agencies, evacuation plans, evacuation drills, evacuation sites, and evacuation guarantees. Chinese attaches great importance to the construction of an emergency evacuation system. Today, the construction of an emergency evacuation system in each city has followed Chinese system for many years, and the civil defense department is responsible for the specific implementation.

The evacuation command organization is the leading department that conducts evacuation drills in peacetime and organizes and implements urban emergency evacuation during emergencies and wartime. Its main responsibility is to lead the public security, fire protection, transportation, civil air defense, communications, medical, rescue, and other departments to participate in urban emergency evacuation and to coordinate the work of various departments.

The evacuation plan is a guiding plan for the organization and implementation of urban emergency evacuation. The evacuation plan clarifies the evacuation conditions, actual conditions, number of people, organization and command organization, the correspondence relationship between communities and evacuation areas, evacuation routes, and evacuation guarantees under various emergencies. The evacuation plan specifically includes evacuation marshalling methods, marshalling plans, vehicle security, determination of assembly areas, determination of evacuation routes, and control and adjustment of evacuation traffic flow. Streets and communities are the main bodies that ultimately implement the evacuation plan, and the evacuation plan of the superior must be strictly implemented [15].

Evacuation sites are the final destinations for urban evacuation. Evacuation points, evacuation bases, and evacuation areas constitute a "three-in-one" urban emergency evacuation system, which satisfies different types, properties, and emergencies with different consequences. Urban emergency evacuation needs under incident conditions.

2.2.2. Features of Emergency Evacuation

(1) Suddenly. Due to the sudden nature of emergency events, for urban emergency evacuation decision-making departments, the organization and implementation of urban emergency evacuation is also carried out without preparation; at the same time, the general public also received evacuation instructions without any expectation. People have made great progress in predicting natural disasters, but they are still at a loss for man-made emergencies.

(2) Urgency. Urgency is a distinctive feature of urban emergency evacuation. Since emergencies have the characteristics of suddenness, uncertainty, destructiveness, and proliferation, once the emergencies are handled improperly and the evacuation time is delayed, it will cause significant loss of people's lives and property. The urgency of urban emergency evacuation runs through the entire process of emergency evacuation. From emergency warning to release, from emergency evacuation decision-making to deployment and implementation, it reflects the urgency of time.

(3) Organized. The task of urban emergency evacuation is to transfer the population in dangerous areas to safe areas in an orderly and rapid manner. From the urban emergency evacuation task, it can be concluded that organization is another characteristic. Loss of organization can easily cause confusion, affect the efficiency of emergency evacuation, and cause unnecessary casualties.

(4) Uncertainty. Urban emergency evacuation is uncertain. First, the organization and implementation of urban emergency evacuation is uncertain. Due to the different types and nature of emergencies, the scope of impact and consequences is also different; second, the process of urban emergency evacuation is uncertain.

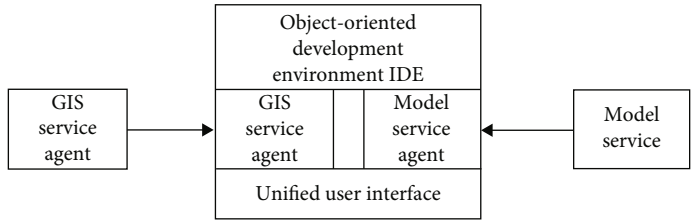

Figure 1: Service integration method of GIS and application model.

2.3. GIS Technology. GIS is a processing tool and technology for spatial data information. It can collect, store, process, and analyze spatial data information. After years of development, it has become a separate subject independently. The application of GIS technology can play the role of route command, obstacle handling, and advance induction in community emergency evacuation management [16]. In the past few years, it has received widespread attention and ushered in a development climax in the continuous research and application process. Driven by the continuous advancement of information technology, the digital age has fully arrived. From a theoretical point of view, GSI can play its own value and role in any industry. From the perspective of disciplines, GIS has already become a single subdiscipline under computer science. From the system point of view, the structure and functions of the GIS system are very reasonable and complete. In terms of technology and application, this technology can effectively solve many space problems. In terms of functions, GIS technology can complete a series of tasks for spatial data, such as data collection, storage, presentation, editing, and analysis. In summary, GIS is a system that can analyze and manage spatial object information. The most significant difference between it and DBMS is that it belongs to geographic information system, while DBMS belongs to the category of information system [17].

The biggest feature of GIS lies in the following: First, it is a computerized technical system in form. It includes multiple subsystems that are widely and closely related to each other. It is a system for processing spatial data and can be used to analyze the geographic target composed of points, lines, and areas. Second, the advantage of GIS technology lies in its realization of data integration, simulation and spatial analysis functions, and more attention and importance to the organization system and the role of people. The GIS system provides powerful functional support for the entire process from data collection to application. The system is mainly used to solve these problems: location problems, condition problems, model problems, simulation problems, and forecast changes [18, 19]. The realization of GIS technology is based on data collection technology, communication technology, software technology, information security technology, virtual reality technology, etc. GIS technology can not only effectively manage various resource and environmental information with spatial attributes, conduct rapid and repeated analysis and testing of resource and environmental management and practice models, facilitate decision-making, and conduct scientific and policy standard evaluations but also can effectively dynamic monitoring, analysis, and comparison of resource and environmental conditions, and changes in production activities during the period, data collection, spatial analysis, and decision-making processes can also be integrated into a common information flow, which can significantly improve work efficiency and economic benefits and provide technical support to ensure sustainable development [20, 21].

2.4. GIS and Application Model Set Service Integration Method. Based on web service technology, the functions of GIS are released in the form of services, and the application model is encapsulated and released in the form of services. The integration of GIS and application mode services solves complex geographic environment problems.

As shown in Figure 1, service integration has the characteristics of openness, maintainability, transparency, and reusability and is an advanced mode for GIS and application model integration. In the service-based integration method, GIS and application models are provided to developers in the form of services. Application models can be run in different locations, on different servers, or even on different platforms. However, the description method of application models, the dynamic discovery and integration of application model services, and the specific implementation technology of GIS services and application model services are still to be studied [22].

2.5. NET Component Programming Technology. .NET is a free and open source development platform for building a variety of applications, web applications, etc. and can be developed using a variety of languages, editors, and libraries [23]. .NET is a new generation of Intel-based distributed computing application platform launched by Microsoft. .NET framework has three core parts: common language runtime environment CLR, common class library, and ASP.NET. CLR realizes the independence of programming language based on .NET through mechanisms such as intermediate language (CIL).

At the same time, CLR also brings platform independence to the .NET framework. The .NET class library provides developers with a unified object-oriented, asynchronous, hierarchical, and scalable class library, including many highly available types and interfaces. The .NET platform not only supports procedural languages but also has nearly perfect support for object-oriented languages. ASP.NET is built using the class library provided by the .NET framework and provides a web application model, which consists of a set of controls and a basic structure. In the software development process, developers can directly call the ASP.NET control

set, which makes it very easy to build web applications. The specific .NET component development process is as follows:

(i) Build .NET components

(ii) Define the component interface

(iii) Realize component functions

(iv) Register deployment components

2.6. Related Model Formulas

2.6.1. Personnel estimation of accurate demographic data. When the building entity in the database contains information about the permanent population, the emergency evacuation population should be estimated based on accurate demographic data. Assuming that an evacuation area T is given, the population that needs to be evacuated in the area T is equal to the sum of the permanent residents of the buildings in the area. The calculation formula is as follows:

$$Z_{N\mu m} = \sum_{i=1}^{n} \alpha B_N, \tag{1}$$

$$\alpha = \frac{B_{s1}}{B_s}. \tag{2}$$

In the formula, (1) $Z_{N\mu m}$ is the total population to be evacuated; (2) B_{S1} is the area where building B falls into evacuation area T, B_S is the total area of the building, and α is the ratio of the area of the building falling into the evacuation area to the building area [24].

2.6.2. Building Classification and Population Density. In the case of building classification, the characteristics of population distribution can be found while analyzing each building type, and the population density function of each building can be established separately. The population density function must reflect the influence of time on population distribution. Assuming that the population density of the same type of buildings is the same, there are the following population density functions:

(1) Density of Residents. According to the characteristics and laws of the population distribution of residents, the population density is a function of the urban permanent population, the bottom area of the residential buildings, and the number of floors. The formula for calculating the population density established in this article is as follows:

$$d_1 = \beta_1 \frac{P_T}{\sum_{i=1}^{n}\sum_{j=1}^{m} S1_{ij} \times N1_{ij}}. \tag{3}$$

In the formula, (1) d_1 is the population density of the residential area, unit: person/㎡; (2) P_T is the urban permanent population, unit: person; (3) $S1_{ij}$ is the bottom area of the jth building in the ith residential area, unit: ㎡, $S1_{ij}$ obtained from the base map of the residential area; (4) $N1_{ij}$ is the number of floors of the jth building in the ith residential area; and (5) β_1 is the population density correction coefficient of the residential area, and its value is between (0 and 1). the β_1 value is 1 between 22 : 30 at night and 7 : 00 the next day.

(2) The Office Population Density Formula. Office population density can be calculated based on the city's total population of office buildings, government agencies, and enterprises and institutions, and the bottom area and number of floors of office buildings. The population density calculation formula established in this article is as follows:

$$d_2 = \beta_2 \frac{P_2}{\sum_{i=1}^{n}\sum_{j=1}^{m} S2_{ij} \times N2_{ij}}. \tag{4}$$

In the formula, (1) d_2 is the population density of the office area, unit: person/㎡; (2)P_2 is the total number of people in the city working in office buildings, government agencies, and enterprises and institutions, unit: person; (3) $S2_{ij}$ is the ith office area. The bottom area of the jth building, unit: ㎡, $S2_{ij}$ can be obtained from the base map of the office area; (4) $N2_{ij}$ is the number of floors of the jth building in the ith office area; and (5) β_2 is the population density correction coefficient of the office area. Suppose here that working hours are from 9 to 5, the population density of the office area reaches the maximum, $\beta_2 = 1$, and the rest of the time period, $\beta_2 = 0$.

(3) School Population Density. The population density of a school can be obtained from the sum of the number of teachers and the number of students in the school, as well as the bottom area and number of floors of the buildings in the school. The school population density formula established in this article is as follows:

$$d_3 = \beta_3 \frac{P_3}{\sum_{i=1}^{n}\sum_{j=1}^{m} S3_{ij} \times N3_{ij}}. \tag{5}$$

In the formula, (1) d_3 is the population density of the school, unit: person/㎡; (2) P_3 is the total number of teachers and students in the school (excluding universities, which are counted as residential areas), unit: person; (3) $S3_{ij}$ is the ith. The area of the bottom of each building, unit: square meters, $S3_{ij}$ can be obtained from the base map of the campus building; (4) $N3_{ij}$ is the number of floors of the jth building in the ith campus; and (5) β_3 is the correction coefficient of the campus population density. Time (8 : 00-12 : 00 in the morning, 14 : 30-17 : 00 in the afternoon) campus population density reaches its maximum, $\beta_3 = 1$; in the rest of the time, $\beta_3 = 0$.

(4) Population Density of Commercial District. The population density of a business district can be obtained from the sum of the number of employees in the business district

and the number of urban residents attracted by the business district, as well as the bottom area and number of floors of the business district buildings. The formula for calculating population density established in this article is as follows:

$$d_4 = \beta_4 \frac{P_4 + \gamma_4 + P_T}{\sum_{i=1}^{n}\sum_{j=1}^{m} S4_{ij} \times N4_{ij}}. \quad (6)$$

In the formula, (1) d_4 is the population density of the commercial area, unit: person/㎡; (2) P_4 is the total number of people working in the commercial area in the city. You can refer to the commercial population data in the statistical yearbook published by the city, unit: person; (3) $S4_{ij}$ is the bottom area of the jth building in the ith commercial area, unit: ㎡, and $S4_{ij}$ can be obtained from the base map of the commercial area; (4) $N4_{ij}$ is the number of floors of the jth building in the ith commercial area; and (5) γ_4 is the absorption rate of urban residents in the business district. It is assumed here that the shopping mall is not in business hours (22 : 30-7 : 00 the next day), $\gamma_4 = 0$; the absorption rate in business hours can be purchased from urban residents circumstances.

(5) Population Density of Catering, Accommodation and Cultural, Sports, and Entertainment Places. The population density of catering, accommodation and cultural, sports, and entertainment venues can be obtained from the sum of the number of people working in these venues and the number of citizens attracted, as well as the bottom area and number of floors of buildings in these venues. The formula for calculating the population density of catering accommodation and problem entertainment venues established in this article is as follows:

$$d_5 = \beta_5 \frac{P_5 + \gamma_5 + P_T}{\sum_{i=1}^{n}\sum_{j=1}^{m} S5_{ij} \times N5_{ij}}. \quad (7)$$

In the formula, (1) d_5 is the population density of catering, accommodation and cultural, sports, and entertainment venues, unit: person/m^2; (2) P_5 is the total number of people working in catering, accommodation and cultural, sports, and entertainment in the city, unit: person; (3) $S5_{ij}$ is the area of the bottom of the jth building in the i dining (accommodation, sports, and entertainment) place, unit: ㎡, $S5_{ij}$ can be obtained from the base map of the catering accommodation and cultural, sports, and entertainment venues; (4)$N5_{ij}$is the$i$th dining (accommodation, sports, and entertainment) number of floors of the$j$th building in the place; (5) γ_5 is the attraction rate of catering accommodation and problem entertainment places to urban residents; and (6) β_5 is the correction coefficient of population density of catering accommodation and problem entertainment places.

(6) Hospital Population Density. The population density of a hospital can be obtained from the sum of the number of doctors in the hospital and the number of patients absorbed, as well as the bottom area and number of floors of the buildings in the hospital. The formula for calculating hospital population density established in this article is as follows:

$$d_6 = \beta_6 \frac{P_6 + \gamma_6 + P_T}{\sum_{i=1}^{n}\sum_{j=1}^{m} S6_{ij} \times N6_{ij}}. \quad (8)$$

In the formula, (1) d_6 is the population density of the hospital, unit: person/㎡; (2) P_6 is the total number of doctors in the city, unit: person; (3) $S6_{ij}$ is the bottom area of the ith building, unit: ㎡, $S6_{ij}$ can be obtained from the base map of the hospital building; (4) $N6_{ij}$ is the number of floors of the jth building in the ith hospital; (5) γ_6 is the hospital to urban residents; and (6) β_6 is the correction coefficient of the hospital population density. Since the population in the hospital is constantly changing in different periods, the population density correction coefficient needs to be introduced.

(7) Warehouse Population Density. The population density of the warehouse can be calculated based on the total number of employees in the warehouse and the bottom area and number of floors of the warehouse building. The formula for calculating the population density of the suffering population established in this article is as follows:

$$d_7 = \beta_7 \frac{P_7}{\sum_{i=1}^{n}\sum_{j=1}^{m} S7_{ij} \times N7_{ij}}. \quad (9)$$

In the formula, (1) d_7 is the warehouse population density, unit: person/㎡; (2) P_7 is the total number of people working in the warehouse, unit: person; (3) $S7_{ij}$ is the bottom area of the jth building in the ith warehouse, unit: square meters, $S7_{ij}$ can be obtained from the base map of the heron building; (4) $N7_{ij}$ is the number of floors of the j building in the i warehouse site; and (5) β_7 is the warehouse population density correction coefficient.

2.6.3. Estimation of Population in Evacuated Area. After calculating the population density of each type of building above, the population of a given area can be estimated. The total population of a given evacuation area U is equal to the sum of the product of each type of building area and the corresponding population density in the U area. The specific calculation formula is as follows:

$$P_N = \sum_{i=1}^{m}\left(\sum_{j=1}^{n} \alpha_{ij} \times d_i\right). \quad (10)$$

In the formula, (1) P_N is the estimated total number of people in the evacuation area; (2) α_{ij} is the area of the jth building in the area with building type i; (3) d_i is the population density with building type i; and (4) i represents buildings. The type of $i = 1, 2, \cdots, n$.

2.6.4. Emergency Accident Model

(1) Leakage of Hazardous Substances. The leakage of hazardous substances has a serious impact, which will directly affect the safety of surrounding people and property. The analysis of the leakage of hazardous substances includes the area of the leakage, the type of the leakage, and the diffusion rate of the leakage. It is of great significance for the emergency management of the leakage of hazardous substances to measure hazardous substances according to a unified standard. The concept of "poison load" puts forward by the European department can measure the degree of harm of leakage.

$$\mathrm{TL} = K \times C^n \times t^m. \tag{11}$$

In the formula, (1) TL is the toxic load, which mainly measures the degree of poisoning of personnel; (2) K is a constant coefficient, generally <1; (3) C is the concentration of the substance expanded; (4) N is the degree of influence of toxic substances on humans; (5) t is the incident in which the person received poison; and (6) m is the impact on the person in the contact incident.

(2) Fire Accident. The fire contains a lot of radiation, which will have an impact on the surroundings, and in severe cases, it can cause serious damage to surrounding buildings, personnel, and property. The loss caused by a fire generally depends on the impact and damage caused by the fire on people and objects. Through the division of units, the calculation formula for thermal radiation is as follows:

$$Q = \eta \mathrm{QoHe}. \tag{12}$$

In the formula, (1) Q is the unit quantity of radiation; (2) η is the fire radiation coefficient, which can be 0.35; and (3) Qo is the radiation speed and He is the heat.

(3) Explosion Accident. Explosion accidents are a kind of disaster with relatively large impact. Explosion accidents generally include the explosion of gas, compressed gas, and liquefied gas.

When the gas explodes, the energy released is

$$E = \frac{\mathrm{PV}}{10(\gamma\text{-}1)}\left[1\text{-}\left(\frac{10^5}{p}\right)\right]^{\gamma-1/\gamma}. \tag{13}$$

In the formula, (1) P is the pressure inside the gas; (2) V is the volume of the container; and (3) γ is the specific heat capacity of the gas.

When compressed gas explodes, the resulting explosion is

$$E = \frac{\Delta P^2\text{-}\mathrm{V}\beta}{2}. \tag{14}$$

In the formula, (1) ΔP is the change in volume after the explosion; (2) V is the volume of the container; and (3) β is the compression ratio.

When the liquefied gas explodes, in addition to the volume expansion caused by the treatment, it will also boost the explosion of the container:

$$E = (H_1\text{-}H_2)\text{-}[(S_1\text{-}S_2)T_1]W. \tag{15}$$

According to the energy of the explosion, the impact range of the explosion can be drawn.

3. Design of the Community Emergency Evacuation Management System Framework Based on Location Services

3.1. System Framework Goals. The goal of the system framework is to realize a GIS system for community emergency evacuation. Computer, GIS, network, database, and auxiliary decision support technologies are applied to emergency evacuation of emergencies to provide auxiliary decision support information for community emergency evacuation. In peacetime, it can also provide decision makers with supporting information on shelter construction, evacuation drills, etc. and provide the general public with the latest information and trends of community emergency evacuation through the emergency evacuation information network. People can inquire about emergency evacuation information related to themselves; in case of emergencies, it can provide decision makers with timely, rapid, scientific, and reasonable decision-making support: realize the scientific determination of the emergency evacuation area, the accurate calculation of the population in the evacuation area, and the optimal choice of emergency evacuation route strength, so as to improve the scientificity of the emergency evacuation area, save emergency evacuation resources, improve emergency evacuation efficiency, and effectively reduce casualties, lives, and property purpose of the loss [25].

3.2. System Framework Requirement Analysis. The modification and analysis of community emergency evacuation management system is the basis of the overall design of community emergency evacuation, and it is related to whether the system built can meet the needs of community emergency evacuation. The following is a demand analysis for community emergency evacuation.

3.2.1. Management of Community Basic Geographic Environment Information. Graphicalization is the most intuitive and effective means of conveying information. The basic geographic environment information of the community should be conveyed to decision makers in the form of graphics and images. The basic geographic environment information of the community is the basis for carrying out the emergency evacuation work in the community. Whether it is the site selection of the usual refuge site or the emergency evacuation decision of the community in the event of an emergency, it is inseparable from the basic community geographic environment information support [26].

3.2.2. Management of Thematic Elements of Emergency Evacuation. The management of thematic elements of emergency evacuation mainly includes the spatial distribution of community shelters, the maximum number of people that can be evacuated, the use of shelters, infrastructure construction, corresponding street communities, the spatial distribution of emergency rescue teams, the size and scope of responsibilities of emergency rescue teams, and medical and fire fighting. Information such as the size of the unit's spatial distribution directly affects community emergency evacuation decisions under emergencies.

3.2.3. Disaster Model Management. The disaster model is the basis for scientific and reasonable decision-making in the event of large events. The system should be able to support the addition, modification, and improvement of disaster models. Decision makers can schedule and use these disaster models during emergencies, which has reached a quantitative analysis of the impact of disasters and improved the level of decision-making [27].

3.2.4. Decision-Making Assistance. The system should provide simple auxiliary decision-making tools such as distance measurement, area measurement, and slope and aspect analysis tools: with the support of the auxiliary decision-making model, it can obtain the service scope of the refuge site, dispatch the rescue team with the farthest distance, and select the best evacuation routes, etc.

3.2.5. Evacuation Plan Management. The evacuation plan is the basis for community emergency evacuation drills and the organization and implementation of urban emergency evacuation for emergencies. With the support of the model, according to the type, nature, and characteristics of emergencies, evacuation plans for various emergencies can be formulated more quickly, and the evacuation plans can be modified and updated.

3.2.6. Evacuation Information Release and User Query Analysis. With the support of network technology, the system should be able to determine and release the latest emergency evacuation plan, laws and regulations, common sense, and precautions for emergency evacuation. With the support of the back-end database and server, the community can freely inquire about the assembly points, emergency rescue vehicles, shelters, docking families, and other information that correspond to them during emergencies on the Internet. At the same time, they can also perform map measurement and analysis.

3.3. System Framework Design Principles

3.3.1. Practicality. Emergency evacuation GIS is related to the safety of people's lives and property and social harmony and stability. Therefore, the construction of the system should put the practicality in a prominent position.

3.3.2. Scalability. The system uses today's most mature software development technology and concept-component technology to ensure that the system has good scalability. When a new disaster model needs to be added, the user can add new disaster model components to achieve system function expansion.

3.3.3. Reliability. Reliability means that the decision support information provided by the system must have a strict mathematical and theoretical basis, so that the decision support information obtained has reference value and significance. At the same time, reliability is also reflected in the design of disaster models and auxiliary decision support models.

3.3.4. Security. System security is an important content of system construction. Because the system adopts a mixed architecture of C/S and B/S, the security of the system is placed in a more prominent position. The system takes certain measures to physically separate the intranet and the extranet to prevent the illegal intrusion of the intranet by users from the extranet. At the same time, it classifies the community emergency evacuation topic information and the basic geographic environment information with higher security requirements and sets the corresponding browsing authority.

The contingency and urgency of emergencies require efficient emergency evacuation decisions. When designing disaster model and auxiliary decision-making model, the system adopts the best theoretical technology to shorten the emergency evacuation time from the decision-making level [28].

3.4. Overall Framework Design of the System. The system framework is shown in Figure 2. The overall system framework includes a community emergency evacuation application platform, a community emergency evacuation service platform, a community emergency evacuation comprehensive database, and a community emergency evacuation hardware platform. The community emergency evacuation application platform is mainly to meet the emergency evacuation decision-making and the public's demand for emergency evacuation information by the emergency departments and civil defense departments at all levels in the city; the community emergency evacuation service platform includes a basic geographic information sharing platform and a special emergency evacuation information sharing platform; the emergency evacuation comprehensive database is the basis of the application platform and service platform; and the community emergency evacuation hardware platform includes computer network systems, communication network systems, and safety systems [29]. The E-R relationship of important entities in the community emergency evacuation GIS database is shown in Figure 3.

3.5. Architecture Design Based on the Combination of C/S and B/S. The software architecture of GIS application system is divided into client mode (C/S) and server mode (B/S). In the client mode, GIS applications need to be loaded. Most business processing is done by the client. The GIS data is concentrated on the server, and the server is responsible for processing part of the transaction. The advantage of this mode is high security and can realize complex GIS spatial analysis functions. The working principle is that the client

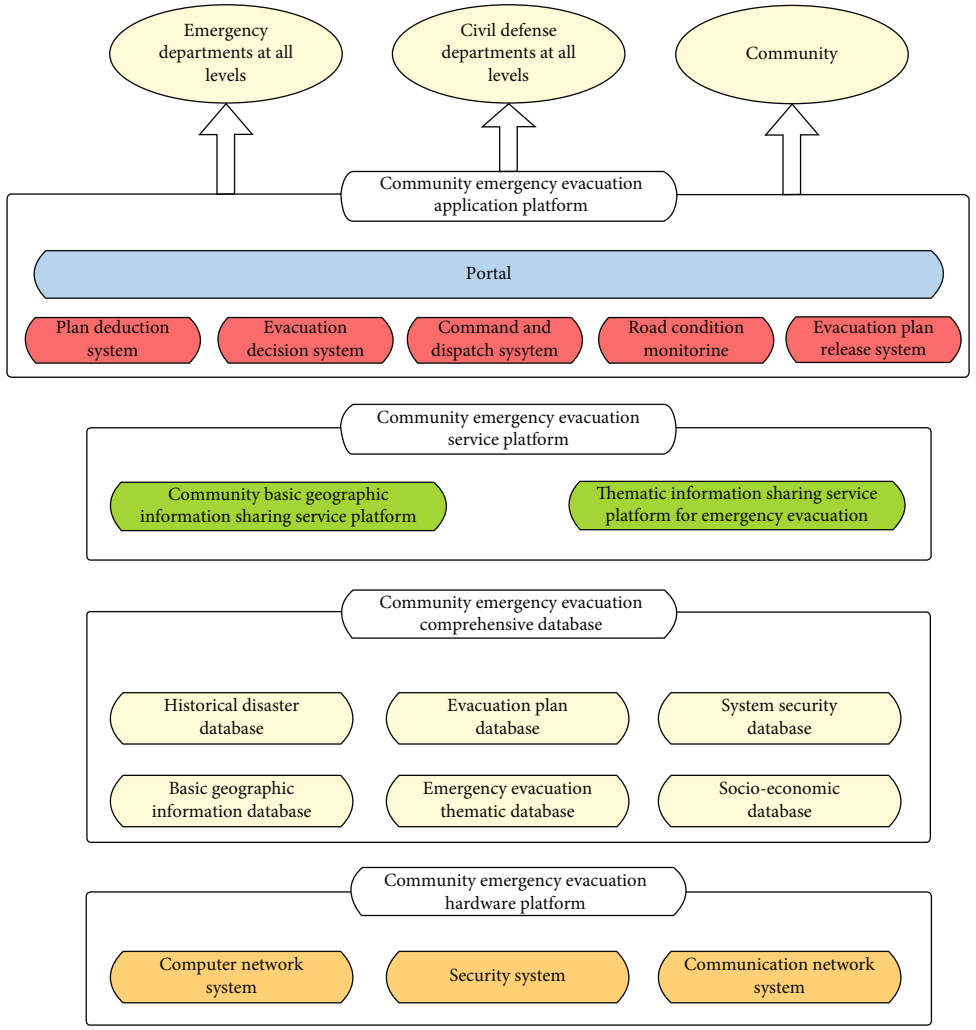

Figure 2: Community emergency evacuation GIS management system framework.

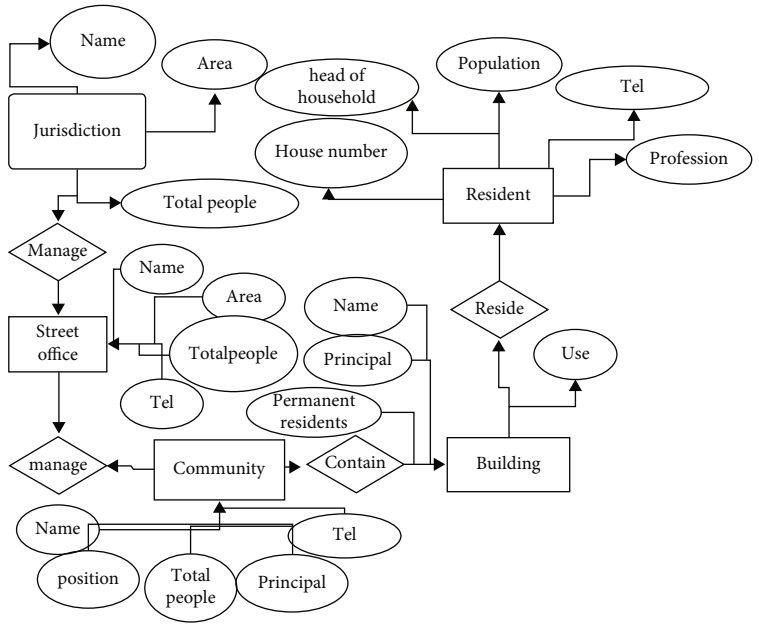

Figure 3: The E-R relationship of important entities in the community emergency evacuation GIS database.

Table 1: Community attribute table design.

Field name	Field type	Field length	Description
SmID	Long integer	4	Primary key
SmUserID	Long integer	4	Foreign key
Area	Double precision	8	Cannot be empty
SmJdID	Long integer	4	Foreign key
Name	Text type	50	—
Address	Text type	50	—
Total houses	Long integer	4	—
Total population	Long integer	4	—
Principal	Text type	20	—
Tel	Text type	20	—
SmSqID	Text type	20	—

Table 2: Design of building attribute table.

Field name	Field type	Field length	Description
SmID	Long integer	4	Primary key
SmUserID	Long integer	4	Foreign key
Area	Double precision	8	Cannot be empty
Perimeter	Long integer	8	Cannot be empty
SmSqID	Text type	4	Foreign key
Area	Long integer	50	—
Number of layers	Long integer	4	—
Total population	Long integer	4	—
Permanent residents	Text type	4	—
Principal	Text type	20	—
Tel	Text type	20	—
Use	Text type	50	—
SmJzWID	Long integer	4	Cannot be empty
SmYbID	Long integer	4	Cannot be empty
SmJzDID	Long integer	4	Cannot be empty

sends a request to the server, and the server processes the user request and transmits the processing result to the user in the form of pictures. This architecture client does not need to install any GIS plug-ins, and the network load is light. The client only needs to install a standard IE browser. The system adopts a hybrid system architecture combining C/S and B/S, giving full play to the advantages of C/S and B/S, and achieving complementary advantages.

The C/S and B/S hybrid architecture has the same database. In order to ensure the integrity and consistency of the database, users in the C/S mode are given the authority to manage the database, and ordinary users in the B/S mode only have the authority to query the database, at the same time, simple spatial analysis functions are realized by sending a request to the application server. This design model not only takes advantage of the strong spatial analysis capabilities and high security of the C/S model but also allows the majority of community residents to query and analyze the emergency evacuation information of the city they care about through the Internet.

Table 3: Comparison of community demographics and estimates.

	Statistical population	Estimated population	Error (%)
JinShan	38756	35011	-9.8
DaZheHu	32012	27915	-9.6
QiaoKou	5339	5771	30
BaiShaZhou	13468	13404	5.6
DingZiWan	14532	13331	-7.5
HuangJinYuan	5469	6003	6.4
XinKang	27956	25301	-8.7
ChaTing	33688	29876	-9.2

3.6. System Database Design. Database design occupies an important position in the construction of community emergency evacuation system. Database design directly affects system application, maintenance management, and data update. The content and structure of the database determine the quality and function of the system and directly affect the use of the system by users. Therefore, designing a database with a reasonable structure, rich attribute information, and strong current status is the key to determining whether the urban emergency evacuation system can provide effective auxiliary decision support information.

To realize the storage of GIS spatial data and attribute data in the spatial database requires a certain spatial data model and the design of spatial data model. The design of spatial data model includes conceptual model design, logical model design, and physical model design. The detailed steps of building the community emergency evacuation GIS database are as follows:

(i) Determine the entities in the urban emergency evacuation GIS database

(ii) Determine the attributes of each entity

(iii) Determine all connections between entities

(iv) Draw a spatial E-R diagram representing a solid unit

(v) Combine and optimize the spatial E-R diagrams of each unit

(vi) Transform the spatial E-R diagram into a data model acceptable to GIS software and RDBMS

(vii) Determine the storage method in the computer

It mainly includes the following: analysis of spatial database requirements, determining the relationship between geographic entities and entities to be expressed, logical expression of spatial entities, selecting appropriate data models, and organizing spatial data sets.

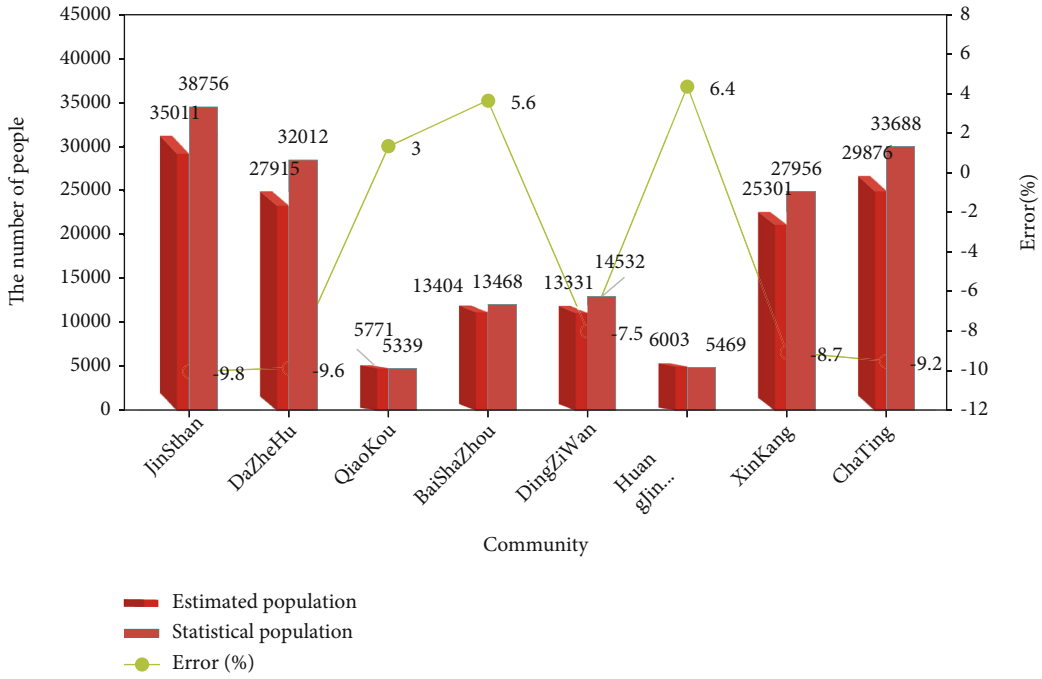

Figure 4: Comparison of community demographics and estimates.

Table 4: Adaptation system of different age groups.

	Reaction time	Evacuation time	Arrival time	Optimal path selection
0-18	3	4	8	0
18-38	2	3.5	7.5	3
38-58	2.5	4.5	8.5	5
58+	4	6	10	8

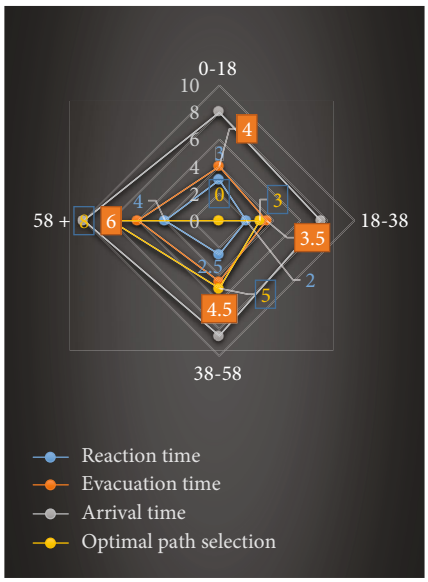

Figure 5: Adaptation system conditions of different age groups.

4. Organization and Realization of the Framework of Community Emergency Evacuation Management System Based on Location Services

4.1. System Framework Entity Modeling Expression

4.1.1. Express Conceptual Model with E-R Diagram. The database contains a series of entities such as jurisdictions, neighborhood offices, communities, buildings, households, and heads of households. These entities are related to each other. For example, a jurisdiction includes many neighborhood offices, a neighborhood office includes many communities, and neighborhood offices can only belong to one jurisdiction. Similarly, a community only belongs to one street office. Therefore, there is a one-to-many relationship between the jurisdiction and the street office and the street office and the community. Therefore, it is most appropriate to use E-R diagram modeling to express entity attribute information.

4.1.2. Supplement to the Logical Model Design of the System Framework. Logical data model refers to the description of the content and structure of data in the community emer-

Table 5: Group test results under different conditions.

	Reaction time	Decision time	Evacuation time	Arrival time	Injuries
A1	15	23	40	78	5
B1	8	11	28	57	0
A2	13	25	43	64	2
B2	7	10	30	47	0

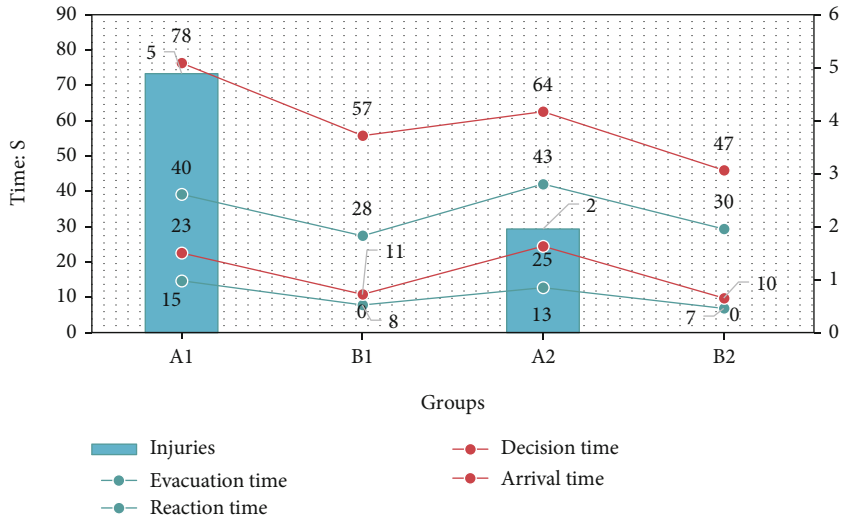

Figure 6: Group test results under different conditions.

gency evacuation database. It is the logical structure of data organization and the middle layer of data abstraction. This article uses relational data model to express the entities in the community emergency evacuation GIS database, as shown in Tables 1 and 2.

4.2. System Framework Application Test Analysis

4.2.1. Comparison of Population Statistics and Estimates by the System. Based on the data from the 2010 Statistical Yearbook of a certain city, this article exemplifies the population density of a certain city. Eight communities with accurate demographic data were randomly selected, and the demographic data of the community was analyzed and compared with the demographic data estimated in the article based on the use and area of the building. The comparison results are shown in Table 3 and Figure 4.

From Table 3 and Figure 4, it can be concluded that the system framework needs to be strengthened in calculation and analysis capabilities in practical application tests. The maximum estimation error of the data is -9.8%, and the minimum estimation error is 3%. The error between the estimated population data and the accurate population statistics data is within 10%. Judging from the error of the data, the estimated population is biased. There are two cases of overestimation and underestimation.

4.2.2. Comparison of Adaptability to Emergency Evacuation Management System of Different Age Groups in the Community. In order to test the adaptation of the emergency evacuation management system for people of different ages in the community, 10 people from 0 to 18 years old, 10 people from 18 to 38 years old, 10 people from 38 to 58 years old, and 10 people over 58 years old were randomly selected from a certain community. People are arranged to use the system in the same community for fire drills to evacuate from the community to the designated destination. The test data includes time-consuming reaction, time-consuming evacuation, time-consuming to reach the destination, and

Table 6: Group test results of different grades.

	Reaction time	Decision time	Evacuation time	Arrival time	Injuries
D1	12	26	31	63	2
D2	13	24	28	60	1
D3	10	25	32	61	1
D4	9	20	34	52	0
D5	9	19	28	48	0
D6	8	21	30	45	0

the number of evacuation persons who choose the optimal route. The test data results are shown in Table 4 and Figure 5.

As shown in Table 4 and Figure 5, it can be seen that the reaction time-consuming ratio is in order 18-38 years old>0-18 years old>38-58 years old>58 years old and over; the evacuation time-consuming order is 18-38 years old>0-18 years old>38-58 years old>58 years old; the order of arrival time is 18-38 years old>0-18 years old>38-58 years old>58 years old; the number of optimal route selections is 58 years old above>38-58 years old>18-38 years old>0-18 years old. From the data results, young people are better than the elderly in terms of reaction time, evacuation time, and arrival time because of their good physical fitness. However, the most people who choose the optimal route are the elderly, especially those over 58 years old. In this fire drill, 8 people chose the best route to reach the designated destination. In summary, young people are more adaptable to the emergency evacuation management system, and the elderly are less adaptable to the emergency evacuation management system except for choosing the optimal path. This is also the place where the emergency evacuation management system needs to be strengthened later.

4.2.3. Comparative analysis of community emergency evacuation management system testing. After the design of the community emergency evacuation management system,

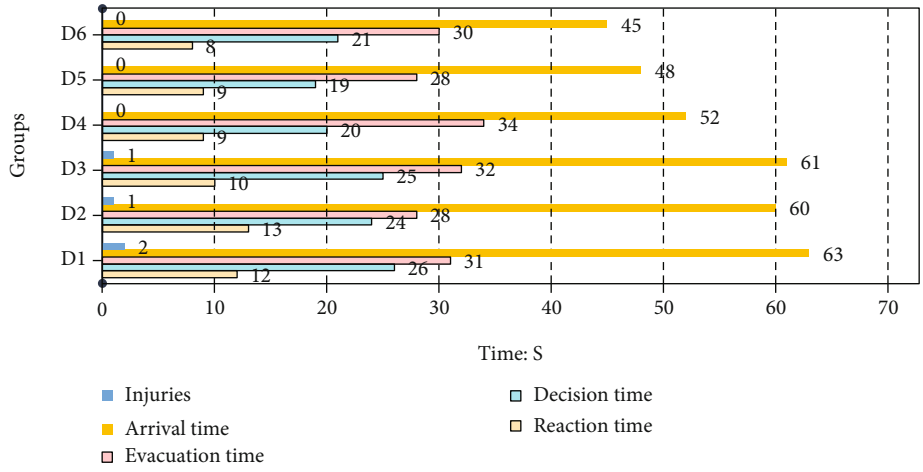

Figure 7: Group test results of different grades.

it is necessary to carry out actual test analysis, that is, the test uses the system and the unused system to compare with each other to find out whether the community emergency evacuation management system has an impact on the community's emergency evacuation work. This article takes a city's elementary school as an example, takes teachers and students as the experimental objects for test analysis and comparison, divides the 6th grade teachers and students into four groups, each with a fixed number of 60 people, and conducts the first round of grouping in the same teaching building on the same floor. Specific grouping situation is as follows: A1 group type is unused system and no advance notice; A2 group type is unused system and advance notice; B1 group type is used system and no advance notice; and B2 group type is used system and advance notice, test data including time-consuming evacuation (time-consuming to reach the flat ground on the first floor of the teaching building), time-consuming decision-making, time-consuming response, time-consuming destination (time from the teaching building to the playground), and the number of injured. The specific situation is shown in Table 5 and Figure 6.

It can be seen from Table 5 and Figure 6 that the data difference between using and not using the community emergency evacuation management system is still quite large. Among the number of injured, 5 people were injured in group A1, no one was injured in group B1, 2 people in group A2 were injured, and in B2, no one was injured in the group; the fastest response in the reaction time was 7 s in group B2, followed by B1, A2, and A1; the first two groups with the fastest decision time were also B1 and B2; the longest evacuation time was A2 Group, followed by group A1, B1, and B2 are the shortest; the fastest time to reach the destination is 47 s in group B2, and the slowest is 78 s in group A1.

In summary, it can be concluded that the emergency system can organize personnel to evacuate to the designated evacuation area in the fastest time. Most groups that do not use the emergency evacuation management system waste a lot of time, whether it is to withdraw from the teaching building. Or the command is unreasonable and unscientific. Regardless of whether the group is notified in advance, it is still much slower than the group that has used the system, which further confirms the importance of the community emergency evacuation management system. Time is of the utmost importance for emergencies. The fastest time to make the most correct decision is the assistance of the emergency evacuation management system.

In the second round of grouping, teachers and students in grades 1 to 6 use the system as experimental objects to test whether teachers and students of different grades have an impact on the work of the emergency evacuation management system. They are divided into 6 groups by grade: D1 group (grade 1), group D2 (grade 2), group D3 (grade 3), group D4 (grade 4), group D5 (grade 5), and group D6 (grade 6); test data includes evacuation time (arriving to the teaching building) time-consuming on the ground floor on the first floor, time-consuming decision-making, time-consuming response, time-consuming destination (time from the teaching building to the playground), and the number of injured.

It can be seen from Table 6 and Figure 7 that the time to reach the destination in different grades can be divided into two types, one is the slower time to reach the destination in grades 1 to 3, and the other is the time to reach the destination in grades 4 to 6. The time of evacuation, reaction time, and decision-making time is relatively fast, and it can be seen from the number of injured that only the students from grades 1 to 3 were injured, and there were no injured students from grades 4 to 5; evacuation time, reaction time, and decision-making time after using the system time data to the sixth grade are very close, indicating that the system's auxiliary support for decision-making can help decision makers make scientific and reasonable suggestions. To sum up, because the physical fitness of the lower grades is significantly lower than that of the upper grades, the experimental data has a large deviation in the time of arrival at the destination. Therefore, it can be concluded that the lower and upper grades of the experiment will not affect the emergency evacuation work.

5. Conclusions

The acceleration of the urbanization process has led to the continuous construction of new urbanized communities,

and the high concentration of community population has made the safety of the community gain more attention. New urbanized communities have the characteristics of both urban and rural communities. They are densely built, complex in structure, large in personnel flow, difficult in management, generally weak in disaster-bearing capacity, and have difficulties in the evacuation of people after a disaster, which are one of the difficulties in urban governance. Therefore, it is very important to design an evacuation management system that can help decision makers make emergency responses in the face of emergencies.

This paper applies location-based GIS technology, database technology, application model technology, network technology, component technology, and platform building technology to the community emergency evacuation process and realizes the model expression of each link of community emergency evacuation. Combined with the successful development of the community emergency evacuation management system framework, good simulation results have been achieved. This article mainly completes the following aspects: (1) research on the related theories, practical applications, and technologies of GIS technology based on location services. The concept of emergency evacuation is explained, and the characteristics and principles of emergency evacuation are summarized; (2) established a service integration method of GIS and application models; and (3) put forward the goal of emergency evacuation system construction, established development principles, designed the overall framework of the system, proposed a subscale and layered spatial data organization method, described the thematic elements of community emergency evacuation with E-R diagrams, design the main entity attribute table, and design the system structure and functional category composition.

Emergency evacuation is a very systematic work. When an emergency occurs, whether the decision of the decision-making department is scientific and reasonable is related to the success or failure of emergency evacuation. Therefore, improving the scientific and reasonable decision-making of community emergency evacuation is to reduce the loss of people's lives and property.

Data Availability

The data that support the findings of this study are available from the corresponding author upon reasonable request.

Conflicts of Interest

The authors declare that they have no conflicts of interest.

Acknowledgments

This work was supported by the Zhejiang Humanities and Social Sciences Foundation (No 19NDJC172YB).

References

[1] T. Bo, H. Jiaying, and Q. Jinan, "Spatial layout and route optimization of emergency evacuation in urban commercial districts: taking Shangxiajiu commercial district in Guangzhou as an example," *Regional Research and Development*, vol. 37, no. 4, pp. 92–97, 2018.

[2] J. Huixian, N. Mingxuan, W. Juan, and W. Guang, "Simulation experiment of emergency evacuation in urban complex based on disaster-escape population prediction," *Journal of Catastrophe Science*, vol. 32, no. 4, 2017.

[3] B. Diantao, Z. Junna, and P. Yue, "The principle and technology of indoor positioning navigation escape rescue system," *Fire Science and Technology*, vol. 37, no. 11, pp. 108–111, 2018.

[4] S. P. Zhang, H. X. Jiang, M. F. Zhang, and X. L. Wang, "Design of building emergency evacuation navigation system based on mobile terminal," *Journal of Fujian Normal University (Natural Science Edition)*, vol. 33, no. 1, pp. 22–27, 2017.

[5] S. Yang and L. Zhu, "Research on fire emergency evacuation of civil airport terminal building," *Fire Science and Technology*, vol. 35, no. 10, pp. 1384–1387, 2016.

[6] Z. Mingmin, C. Zhiyong, and Y. Shidong, "Research on emergency evacuation of people in a subway station based on numerical simulation," *Safety*, vol. 40, no. 4, pp. 22–25, 2019.

[7] Z. Jun and C. Hongyan, "Application technology and development trend based on location services," *Science of Surveying and Mapping*, vol. 41, no. 4, pp. 171–176, 2016.

[8] X. Yang, M. Liu, J. Fu, and F. Li, "Dynamic analysis of land resource use based on GIS technology," *International Journal of Earth ences and Engineering*, vol. 9, no. 6, pp. 2551–2556, 2016.

[9] L. Weihao, C. Jin, and L. Hui, "Privacy protection scheme based on location service privacy self-association," *Journal on Communications*, vol. 40, no. 5, pp. 57–66, 2019.

[10] S. Yuanyuan and Y. Wen, "A mobile recommendation model based on location service information," *Computer Applications and Software*, vol. 33, no. 12, pp. 202–206, 2016.

[11] R. Pandi Selvam, "Performance of MAODV and ODMRP routing protocol for group communication in mobile ad hoc network," *Communication*, vol. 1, no. 1, pp. 26–32, 2020.

[12] K. Kiruthika, S. Gayathri, R. Hemalatha, and P. Menaga, "Design and development of Mobile healthcare application for "Ayurvedic" based clinical Documents," *Human Computer Interaction*, vol. 1, no. 1, pp. 18–27, 2021.

[13] Z. Wei, "Research on emergency evacuation guidance of people in public places," *China Work Safety Science and Technology*, vol. 12, no. 9, pp. 164–170, 2016.

[14] W. Qiang, X. Hua, D. Yuanze, X. Zhang, and Y. Zhao, "Emergency evacuation simulation system and engineering application of mine flood (permeation) disasters," *Journal of China Coal Society*, vol. 42, no. 10, pp. 2491–2497, 2017.

[15] Y. Liu, X. Fang, C. Cheng et al., "Research and application of city ventilation assessments based on satellite data and GIS technology: a case study of the Yanqi Lake Eco-city in Huairou District, Beijing," *Meteorological Applications*, vol. 23, no. 2, pp. 320–327, 2016.

[16] Z. Min, D. Hairong, X. Huichun, L. Yidong, and W. Feiyue, "Basic concept, system framework and application of parallel emergency evacuation system," *Zidonghua Xuebao/Acta Automatica Sinica*, vol. 45, no. 6, pp. 1074–1086, 2019.

[17] K. Shankar, "Recent advances in sensing technologies for smart cities," *Communication*, vol. 1, no. 1, pp. 5–15, 2020.

[18] Z. Jicheng and S. Wenjie, "Research on emergency evacuation model based on multi-agent," *Modern Electronic Technology*, vol. 43, no. 8, pp. 135–138, 2020.

[19] S. Mansoori, A. Bozorgi-Amiri, and M. S. Pishvaee, "A robust multi-objective humanitarian relief chain network design for earthquake response, with evacuation assumption under uncertainties," *Neural Computing and Applications*, vol. 32, no. 7, pp. 2183–2203, 2020.

[20] Y. Huang and D. Cao, "Decision response of subway evacuation signs based on brain component features," *Neural Computing and Applications*, vol. 34, no. 9, pp. 6705–6719, 2022.

[21] D. Chen, P. Wawrzynski, and Z. Lv, "Cyber security in smart cities: a review of deep learning-based applications and case studies," *Sustainable Cities and Society*, vol. 102655, 2021.

[22] J. Yu, J. Wen, Y. Chen, B. Liao, and S. Du, "Spatial configuration of urban refuges based on simulation of emergency evacuation agent model: a case study of Jing'an District, Shanghai," *Acta Geographica Sinica*, vol. 72, no. 8, pp. 1458–1475, 2017.

[23] Y. Shen and Z. Pan, "Research on emergency evacuation system based on multi-technology integration," *Jiangsu Architecture*, vol. 189, no. 2, pp. 114–117, 2018.

[24] C. Yinbo and C. Yang, "Application analysis of intelligent fire emergency evacuation system in comprehensive pipe gallery project," *Smart City*, vol. 4, no. 24, pp. 75-76, 2018.

[25] Y. Sun, H. Song, A. J. Jara, and R. Bie, "Internet of Things and big data analytics for smart and connected communities," *IEEE Access*, vol. 4, pp. 766–773, 2016.

[26] J. Wen and Q. Qiming, "Research on the vulnerability of road network emergency evacuation based on GIS," *Remote Sensing for Land and Resources*, vol. 31, no. 1, pp. 277–282, 2019.

[27] Z. Beilei, P. Xiao, and W. Qiongfang, "Research on the allocation method of emergency evacuation sites in urban communities: taking Xueyuan community in Beilun District as an example," *Journal of Disaster Prevention and Mitigation*, vol. 34, no. 4, pp. 99–105, 2018.

[28] W. Wu, S. Ma, Y. Su, and C. Wu, "Double-layer learning, leaders' forgetting, and knowledge performance in online work community organizations," *Journal of Organizational and End User Computing (JOEUC)*, vol. 33, no. 1, pp. 92–117, 2021.

[29] Y. Yichen and K. Lingyong, "The current situation and countermeasures of traffic management for predictable disaster emergency evacuation," *Energy Conservation and Environmental Protection in Transportation*, vol. 15, no. 5, pp. 65–76, 2019.

Hindawi
Wireless Communications and Mobile Computing
Volume 2022, Article ID 8479040, 13 pages
https://doi.org/10.1155/2022/8479040

Research Article

Practical Research on the Assistance of Music Art Teaching Based on Virtual Reality Technology

Jing Zhang

College of Music, Jilin Normal University, Siping, 136000 Jilin, China

Correspondence should be addressed to Jing Zhang; zhangjing@jlnu.edu.cn

Received 28 March 2022; Revised 28 April 2022; Accepted 11 May 2022; Published 16 June 2022

Academic Editor: Jun Ye

Music education in our country has a long history, but modern teaching started relatively late. In recent years, our country has continuously accelerated the pace of learning in the field of music education. The use of advanced Internet of Things virtual reality has become an important way for the development of music art education in our country. This paper studies the practical effects of music art teaching combined with the aid of the Internet of Things virtual reality technology. This article takes the Internet of Things virtual reality technology-assisted music art teaching as the research object and analyzes the effects and advantages of virtual reality technology in music art teaching. Search for topics such as "music" and "VR" through Google to find literature related to music and art. Get the latest rankings of different types of electronic music on YouTube, and through the audition and BPM screening, download music that meets the classroom practice of this article. Research results show that a teaching system that combines VR and augmented reality technology can shorten teaching time by 65%. The virtual reconstruction of music art using VR technology allows students to visually observe the form of music art. The combination of VR technology and traditional teaching methods significantly increases the initiative, interest, effectiveness, and participation of students in learning and can achieve better teaching results. VR system is used in music teaching. DentSim system, Moog Simodont, and dental trainer system can effectively help students master the basic methods of note preparation and actively improve the teaching quality of music professional courses.

1. Introduction

Music education in China has a long history, but modern education started late. In recent years, the pace of learning in the field of music education in China has been accelerating. The use of advanced computer-assisted virtual reality has become an important method for the development of Chinese music and art education. However, most of the current researches focus on the music art itself and separate the music art to study its characteristics. There are still shortcomings in the comprehensive music art combined with virtual reality technology of the Internet of Things to assist education. Virtual reality is a combination of multiple technologies, including real-time 3D computer graphics, wide-angle (wide-field) stereoscopic display, and tracking of the observer's head, eyes, and hands, as well as tactile/force feedback, stereo, network transmission, and voice input and output technology.

The Han Y experiment proved that the virtual music room has an irreplaceable role in promoting students' learning music structure [1]. Jiang Z proposed that the "Musical Note Art" course is a high-pitched and low-pitched artistic training based on the standard note form. It is a practical training course to help students master the note form. It is the first technical course for music and art students, which can effectively train. The ability of students to combine hands and eyes has a vital role in cultivating students' operating habits [2]. On the basis of traditional musical note art, virtual art is added. The main conclusions of Rubinstein R's research are the same. The original virtual reality ecological music is mainly original and unique folk music produced in different natural arts, which is the life of local residents [3]. Slizovskaia O's many related achievements on "Music Art Teaching" and his attention to "Soundscape Art" are closely related to the artistic diversity of ethnic regions [4]. Peeters G discussed the relationship between

the aesthetic theory of art philosophy and the diversity of music culture and put forward the idea of strengthening "artistic rationality" to facilitate the symbiosis of cultural diversity. He believed that in Chinese culture, Laozi proposed the concept of "harmony" and "artistic rationality" [5].

Allen also compares the diversity of music and art teaching with the "intraspecies diversity" in art and believes that the diversity of individuals within the population of organisms is a means to prevent intraspecies organisms from suffering from genetically similar epidemics, while maintaining national culture. Diversity is one of the prerequisites to ensure the sustainable and healthy development of various human civilizations [6]. Dutã M proposed 9 research directions of music aesthetics worthy of attention, which are important achievements of guiding value in the research of art aesthetics in the music industry in our country [7]. Wang DX elaborated on the level of music art aesthetics research and the direction of combining virtual reality art music aesthetics research with art aesthetics [8]. Zhao SM analyzed the integration of music and nature insisted in Taoist music aesthetics. From the perspective of music criticism, he analyzed the artistic aesthetics of the ancients' music thoughts and discussed the ancients' artistic philosophy from different perspectives [9]. Shi YJ put forward three states of the relationship between man and nature and explained the interdependence and mutual recognition of nature, human and musical instruments from the production of Chinese musical instruments, and the characteristics of playing sound and their breathing characteristics [10].

This paper studies the practical effects of music art teaching combined with the aid of virtual reality technology. This article uses virtual reality technology to assist music art teaching as the research content and analyzes the effects and advantages of virtual reality technology in music art teaching. The music used in this research is divided into fast-paced music, and the music type is electronic music. Through consultation with music art course coaches and electronic music producers, combined with relevant literature, it can be known that music art is most suitable for a fast-paced music environment. Search for topics such as "music" and "VR" through Google to find literature related to music and art. Get the latest rankings of different types of electronic music on YouTube, and through the audition and BPM screening, download music that meets the classroom practice of this article.

2. Virtual Reality Technology and Music Art

2.1. The Internet of Things Virtual Reality Technology and Music Aesthetics. Music is the expression of human emotions and thoughts. It has multiple functions and values. The origin of music in human society can be traced back to the very ancient times. When human beings have not yet produced language, they already know how to express their meaning and feelings by using the level and strength of sounds. With the development of human labor, the chants of unified labor rhythm and the shouting of information are gradually produced. This is the most primitive form of music; when people celebrate the harvest and share the fruits of labor, they often beat stone tools and wooden tools to express joy; this is the prototype of the original musical instrument [11]. When discussing music art teaching in the USA, music art teaching has made a systematic interpretation of the functions of music. He brilliantly summarized the value of music functions as "We are perfec. The human nature of the people needs to be embodied by music," emphasizing that the value of music lies in the emotional expression of the rhythm of life and the reproduction of poetic romance [12]. From a variety of perspectives and from the perspective of their respective disciplines, the consensus on the function of music is to highly agree that music is an invisible spiritual force and an indispensable source of wisdom for the civilization and development of human society. At the same time, music is closely connected with nature and culture [13]. The development of musicology needs to conduct cross-research with other disciplines, which has been widely recognized in the industry, reflecting the artistic awakening of literature and art and the distinctive characteristics of synchronous development with the times [14]. Music art emphasizes "a kind of center," advocating order and elite culture, belonging to the category of the beauty of reason, and insisting on modernism of rationality, universality, and order. However, postmodernism has had a huge impact on the development of musicology, especially a breakthrough in the traditional aesthetic order [15]. The rise of "music art" has enabled musicology to embed the concept of artistic beauty into the creation of works under the idea of respecting differences and pursuing diversity, so as to guide the people's artistic attention and enhance the people's artistic sentiment [16].

The Internet of Things (IoT) is a network based on information carriers such as the Internet and traditional telecommunication networks, which enables all ordinary objects that can perform independent functions to achieve interconnection [17]. The Internet of Things has developed since its birth, and it has the most complete professional product series in the industry, covering various applications from sensors, controllers, to cloud computing. Its products and related services cover smart home, transportation and logistics, environmental protection, agricultural production, public safety, intelligent fire protection, industrial monitoring, personal health, and other fields. The Internet of Things will be the next "important productive force" to promote the rapid development of the world. On the one hand, it can improve economic efficiency and greatly save costs; on the other hand, it can provide technical impetus for the recovery of the global economy.

The rise of virtual reality stems from the crisis caused by art issues to human survival, and the world has begun to reexamine the development model of human society and the relationship between man and nature [18]. Virtual reality, also known as virtual technology and virtual environment, is a brand new practical technology developed in the twentieth century. Users feel as if they are there, seeing things in three-dimensional space instantly and without restrictions. These worldwide actions are several major leaps in the implementation of the concept of sustainable development by mankind and demonstrate the seriousness of the art problem [19]. From the perspective of the time sequence of academic development, Chinese art aesthetics is mainly established based on the originality of Chinese culture. It has profound background and great potential for tapping.

It emerged from the art protection movement and green development triggered by the global art crisis. Music and art education and all kinds of virtual reality art music are important components included in it [20].

Virtual reality art music also has titles such as green music and environmental music. Therefore, it can be summarized as "in order to praise the harmonious beauty of nature and all kinds of life in it, or to satirize and criticize special nature and social bad phenomena, and to promote artistic values and music protection ideas are the collective name of music whose main content is," which belongs to the category of artistic aesthetics [21]. This type of music explores the relationship between man and nature from the perspective of creation and auditory perception [22]. The research in this area existed and developed before Ellens Allen proposed "Ecomusicology", especially in areas such as music art teaching and biomusicology [23]. In fact, China's early artistic ideology had a profound impact on the value of virtual reality art and music. Some scholars call it "pre-modern." The philosophical point of view is to treat man and nature as a whole. Many philosophical thoughts of ancient Chinese have also been absorbed in the postmodern context about music and nature and music and culture [24]. Therefore, the study of music aesthetics in our country should attach great importance to the excavation of artistic ideas in Chinese classical music, highlighting the national cultural self-confidence [25].

2.2. Music Development and VR Music. Musicians use the adjustment function of "VR music" to participate in the research of noise management, use sound adjustment methods to eliminate noise pollution to improve the living sound, or play the psychological adjustment role of VR music to improve the work efficiency of workers. In the 1970s, the Japanese musician Hattori published the book "VR Music Aesthetics," which is the result of joint research by experts in Japanese literature, sound engineering, music psychology, architectural engineering, and media. In this multidisciplinary research, art and music are considered to be the constituent disciplines governing sound art. Combining the strategic needs of building an artistic civilization, Zhang Jianguo put forward in VR music research that "music originates from objective art and affects subjective art [26]. The popularization of environmental awareness has provided aesthetic standards for the humanized service of VR music, and other viewpoints, which clearly summarize and express the function and meaning of music art. Music art psychology is also a branch subject where musicology and art science intersect. Research in this area pays more attention to artistic issues. Li Shuangyan systematically discussed interdisciplinary research issues in various fields.

Soundscape research is a way of expression in the form of "Apocalypse.". Researchers in this field in our country are mostly concentrated in the fields of physical acoustics, architectural acoustics, and art science. Music scholars' interdisciplinary research in this area is still relatively weak, and their results are only seen in postgraduate papers, and they are the current research status at home and abroad. For example, Tao Bo analyzed, categorized, and interpreted the literature design examples of domestic sound landscape research and put forward some suggestions and opinions. Jiao Ying's thesis is about the exploration of the development of virtual reality art musicology and music acoustics in our country. Han Baoqiang and Zi Minjun also covered this aspect in their writings on the value of music in the universe and human life. At the Biomusicology Symposium held in Florence, it was established that the main research directions in this field are evolutionary musicology, comparative musicology, and neuromusicology, especially animal song types with cultural characteristics and various forms, and human music, comparing music scores to grasp the characteristics of animals. Compared with other cross-border research, it is more difficult, so the results are relatively few. Although research in this field is still in its infancy, it is a subject that interests researchers in many disciplines, and it is also of great significance to the study of virtual reality art and music.

Some studies have put forward the development and research focus of virtual reality art musicology from the perspective of research goals; that is, virtual reality art musicology research should answer the three questions of the relationship between music and nature, how music depends on nature, and how music reflects nature. Define what is virtual reality art musicology. The main purpose of this definition is to clarify three issues: One is that the main subject of virtual reality art musicology is still musicology, and it has a "species-genus" relationship with musicology; the other is that it is affected by the background of its production. The special focus is on the issues of art and sustainable development facing human society. The purpose is to use the educational function of musicology to arouse people's awareness of art protection and the cultivation of artistic civilization quality; the third is to persist in and follow the artistic beauty of music creation and the concept of an important power source, through the intersection and absorption of related theories and research methods, to expand the horizon of music creation, and to better play the function of musicology in serving society and educating people. This definition also answers two basic questions. The first is whether "virtual reality art musicology" meets the cross-disciplinary conditions, and virtual reality art musicology meets the subject "cross-border" research, which mainly reflects the following: First, the subject is clear, and it is still musicology; second, it follows modern art, the role of the academic paradigm of science, and the practice of cross-research in aesthetics and the expansion of musical expressions; and third, it has the development potential to expand to a wider range of academic theory and a deeper level of discipline. The second question answered is the main interface between "musicology" and "art sciences", which is discussed in detail below with respect to the three research goals proposed by Aaron. However, the cross-border research of virtual reality art musicology involves many disciplines and related fields such as work creation, soundscape art, art science, biology, and art. The research object is also a socio-economic-natural composite art system, which has a "cross-dissolving" multiple cross-border research conditions and advantages.

2.3. Music and Art Mixed Data Training Model of Virtual Reality. As mentioned in the overview of this article, reliance on the labels of training data is now a major limitation of hybrid data analysis and recognition. Deep neural networks

refer to new speech recognition software that works by imitating the way the human brain thinks, allowing the software to recognize speech faster and with higher accuracy [27]. Specifically in the field of mixed music analysis, the training process of deep neural network (DNN) and other methods must first mark the mixed data for training:

$$E = \frac{\sum_{j=1}^{k}\sum_{h=1}^{k}\sum_{t=1}^{n_j}\sum_{r=1}^{n_h}\left|y_{ij} - y_{hr}\right|}{2n^2u}. \tag{1}$$

These labels are generally manually labeled with a lot of work and usually only include the main instrument type labels. They have no ability to measure the intensity changes of secondary instruments, and the accuracy of the labels cannot be guaranteed for mixed data composed of several components of similar intensity:

$$D_A = E_w + E_{nb} + E_t - Ic. \tag{2}$$

Assuming that there is a data y sample and two different sparse dictionaries Da, Db where Da and y are used for data set training, and Db is used for data set training alone, formula (3) can be obtained:

$$y = (\mathrm{Da} \times \mathrm{Db}) - 1, \tag{3}$$

$$E_j = \frac{1/2u_j\sum_{i=1}^{n_j}\sum_{r=1}^{n_j}\left|y_{ji} - y_{jr}\right|}{n_j^2}, \tag{4}$$

$$Ew = \sum_{j=1}^{k} G_{jj}p_j s_j. \tag{5}$$

Therefore, if the sample y uses Da and Db to model the coefficient vectors, respectively, va, vb, it is easy to know

$$\begin{aligned} V_b &= \frac{\sum_{Z=1}^{h_j}\sum_{r=1}^{n_h}\left|y_{ji} - y_{hr}\right|}{n_j n_h\left(u_j + u_h\right)}, \\ Va &= \sum_{j=2}^{k}\sum_{h=1}^{j-1} G_{jh}\left(p_j s_h + p_h s_j\right)D_{jh}, \\ y_t &= \sum_{j=2}^{k}\sum_{h=1}^{j-1} G_{jh}\left(p_j s_h + p_h s_j\right)D_{jh}\left(1 - D_{jh}\right). \end{aligned} \tag{6}$$

By analogy, all the components in y have higher maximum correlation with the dictionary Da, and the expected value of single coefficient is higher. It can be seen that the sparse dictionary with more concentrated energy and better sparsity performance of coefficient vector has higher matching ability with the samples; that is, if the energy distribution of coefficient vector can be accurately measured, the measurement result will be given clear semantic information in the matching degree between the data sample and the dictionary of specific components. In this way, we can only use labeled single component data and unlabeled mixed source data to realize mixed source data identification and further data analysis on semantic level without relying on mixed source data labels.

$$M = \frac{d_{jh} - P_{jh}}{d_{jh} + P_{jh}}. \tag{7}$$

Because the music signal itself is composed of a small number of determined single tones, and the random artistic intensity of the music signal set is relatively low, the data set must have sparsity, so it is suitable to use the sparse decomposition algorithm for analysis. When the music index is regarded as a sparse feature, the calculation formula can be defined as follows:

$$\begin{aligned} \ln\left(\frac{FI_{it}}{FI_{it} - 1}\right) &= \alpha + \beta \ln FI_{it} - 1 + \phi X_{it} - 1 + \nu_i + \tau_t, \\ d_{jh} &= \int_0^{\infty} dF_h(y)\int_0^{y}(y - x)dF_j(y). \end{aligned} \tag{8}$$

Parameter selection is one of the most important factors affecting the performance of sparse decomposition algorithm, including frame length, dictionary modulus, and sparsity constraint (the number of atoms used in sparse modeling). For the more common music signal with 44.1 KHz sampling rate, the central C (261.63 hz) can be taken as the reference to ensure at least one complete waveform in each frame. Generally speaking, 256 sampling points is an appropriate frame length

$$\begin{aligned} f(x) &= \frac{1}{Nh}\sum_{i=1}^{N} k\left(\frac{X_i - x}{h}\right), \\ k(x) &= \frac{1}{\sqrt{2\pi}}\exp\left(z - \frac{x^2}{2}\right). \end{aligned} \tag{9}$$

In general, 1024 or 2048 dimensional dictionaries can meet the requirements of most solo or chamber music audio analysis. Considering the multiple harmonics and artistic conditions in the general music signal, the optimal sparsity constraint for solo and chamber music is generally no more than 10, while that for symphony is about 35.

$$\begin{aligned} h_t &= \tanh\left(w_c x_t + u_c(r_t \Theta h_{t-1}) + b_c\right), \\ h_t &= z_t \Theta h_{t-1} + (1 - z_t)\Theta h_t. \end{aligned} \tag{10}$$

The output of the simulation (i.e., the fitness values of all members of the sub population) is sent back to the master node to perform evolutionary operations (i.e., selection, cross-over, and mutation) and finally select the first generation of pareto fronts.

$$P = \sigma t = \frac{\sqrt{1/n\sum_{i=1}^{n}(FI_{it} - FI_{it})^2}}{FI_{it}},$$
$$u_{(j|i)} = w_{ij}A_i, \tag{11}$$
$$s_j = \sum_i c_{ij}u_{(j|i)}.$$

After determining the dictionary learning parameters, it is necessary to train the dictionary for each basic instrument or instrument combination. All dictionaries need to use the same parameter training, especially the sparsity constraint, to ensure that the calculated SPI value will not be affected. According to different recognition needs and data conditions, we can arbitrarily select the dimension of component dictionary and SPI features. Taking string quartet as an example, we can train four kinds of dictionaries, namely, violin, viola, cello, and string quartet, respectively. Each frame sample uses these four kinds of dictionaries to model and calculate SPI.

$$\ln\left(\frac{PI_{it}}{PI_{it}-1}\right) = \alpha + \beta \ln PI_{it} - 1 + v_i + \Im_t. \tag{12}$$

In order to improve the recognition accuracy, more dictionaries can be trained, and more SPI time series feature vectors can be obtained by introducing the data of several instrument ensemble, or only a few instrument training dictionaries with reliable data can be used, which gives higher flexibility to the application of this method. Due to the uncertainty of the sparse decomposition algorithm, the SPI time series need to be smoothed for observation and analysis

$$\ln\left(\frac{FI_{it}}{FI_{it}-1}\right) * k_{t1}[i] = \sum_j \cos\left(w_i^1, w_j^2\right) + \alpha + \beta \ln FI_{it} - 1 + \phi X_{it} - 1 + v_i + \tau_t,$$
$$\theta = -\frac{1}{T}\ln(1+\beta). \tag{13}$$

The longer the window length, the better the stability of the algorithm, but the time resolution will decrease accordingly. When the frame length is 256 sampling points and the overlap between frames is 50%, 400-800 frames is a suitable range. Because the smoothing window will cover a certain length of time, the analysis results will produce a fixed length of delay when compared with the real music signal changes.

3. Music Art Teaching Assisted by Virtual Reality Technology

3.1. Objects. This paper takes the virtual reality technology-assisted music art teaching as the research object and analyzes the effect and advantages of virtual reality technology in music art teaching.

3.2. Methods

3.2.1. Get Music. Through Google to search "music" and "VR" and other topics, find music art-related literature. Google is recognized as the world's largest search engine company and has ranked first in the "Top 500 World Brands" list compiled by the World Brand Lab. Get the latest ranking of different types of electronic music on YouTube, and download the music in line with the classroom practice of this article through audition and BPM screening.

3.2.2. Teaching Environment. The music used in this study is divided into fast-paced music, and the music type is electronic music. Through the consultation of music art course coach and electronic music producer, combined with the relevant literature, we can know that music art is the most suitable in the fast-paced music environment. Because the beat of this kind of music is 120-140 bpm (beats per minute), it is beneficial to enhance the secretion of excitatory hormone in music.

3.2.3. Teaching Equipment. Teaching equipment is divided into music equipment, measuring instruments, and music environment to create suitable music. Professional high and low sound equipment and adjustment equipment are used in the music environment, and professional DJ controller and playing software are used in the music player to ensure the output quality of music.

4. The Internet of Things Virtual Reality Technology-Assisted Music Art Teaching Practice

4.1. VR Music Art Teaching Auxiliary Education System Model Analysis. The whole system based on VR is shown in Figure 1. It is composed of VR music art teaching guidance service system, music art, and virtual reality art. By using DT technology, the equipment data parameters in music art are input into VR music art teaching guidance service system. The service system integrates teaching process data to drive teaching guidance solution, so as to establish virtual connection between music art and virtual reality art.

As shown in Table 1, VR technology, as a product of teaching reform in the information age, has been widely used in the theoretical learning and practical training of music courses. This teaching method helps to realize the idealization of teaching and the high efficiency of learning. Specifically, it can improve the teaching method, optimize the training mode, and enhance the combination of foundation and classroom. But at present, VR technology is not perfect; its clarity, comfort, accuracy, scope of application, and modeling ability still need to be improved; and the next stage still needs further research to improve the existing technology.

As shown in Figure 2, a model system is built by taking teaching equipment as an example. Among them, the VR auxiliary system for music art teaching mainly includes note recognition and matching, data processing of teaching objects, virtual art music teaching, natural interaction, and music art teaching guidance. Virtual reality art includes the construction of mixed reality development art, the design of virtual reality assistance systems, the model of teaching equipment, the construction of note IDs, and the matching of guidance process segments.

As shown in Figure 3, with the help of twin data, the sensor data from music art can be fused, and the note category data, teaching scene data, three-dimensional music data, and

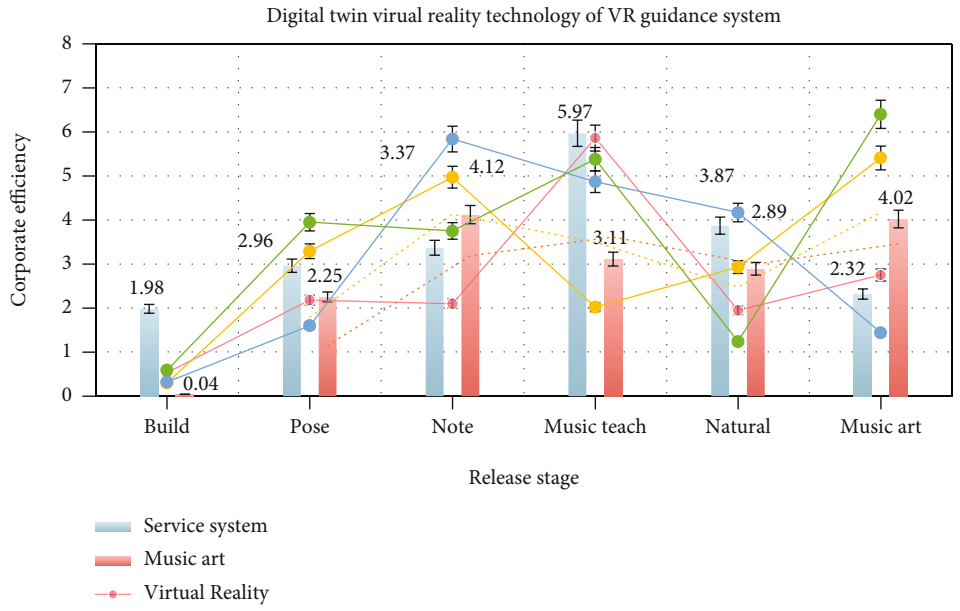

Figure 1: Digital twin virtual reality technology of VR guidance system.

Table 1: Theoretical learning and practical training of music courses.

Item	Service system	Music art	Virtual reality	DT technology	Drive teaching	Guide solution
Build	1.98	0.04	0.53	0.3	0.32	0.59
Pose calibration	2.96	2.25	2.18	3.29	1.6	3.95
Note	3.37	4.12	2.1	4.97	5.84	3.75
Music teaching	5.97	3.11	5.86	2.02	4.87	5.38
Natural	3.87	2.89	1.95	2.93	4.17	1.24
Music art	2.32	4.02	2.75	5.41	1.44	6.4

interactive instruction data can be input into virtual reality art to realize the data drive of virtual reality art by the service system, make music art and virtual reality technology realize the integration of virtual and reality, two-way mapping and simulation early warning provide valuable teaching data information for teaching staff, and realize data interaction between people and virtual reality system.

As shown in Table 2, the whole system is operated interactively with GUI operation panel. The teaching art perception module realizes the collection of 3D data feature points, the tracking of teaching objects, and the pose calculation of the camera in the real teaching scene. The virtual reality art music teaching module restores the three-dimensional scene coordinate points, matches the VR spatial coordinate system in hololens glasses, adopts the matching method based on natural feature points, and carries out music teaching between the teaching guidance solution and the real teaching scene, so as to realize the virtual reality fusion and registration visual experience effect.

As shown in Figure 4, in the complex teaching process, the virtual reality solution must be superimposed on the key parts of the equipment in the real scene and maintain a high degree of geometric consistency, note consistency, and time consistency with it. The system needs to track the object and students' observation position in real time to achieve high-precision 3D music in virtual space.

As shown in Table 3, the collected note signal is sent to the teaching guidance service system to classify the note data, match the teaching guidance solution, and call the corresponding solution stored in the music and art teaching guidance process library. Through the camera on hololens, teachers can collect the teaching art on site and feed it back to the service system to revise the teaching guidance process in real time. If the music notes are difficult to judge, remote expert online guidance can be used to intervene the on-site teaching art, so as to realize the two-way mapping of music art teaching data between virtual reality art and music art.

4.2. Implementation Method of VR Assistant System for Music Art Teaching Oriented to Virtual Reality. The technical framework of VR auxiliary system for music art teaching of virtual reality technology is shown in Figure 5, which mainly includes note recognition and matching module and music art teaching guidance module. Note recognition and matching module are responsible for collecting the sensor signal on the real device, recognizing and classifying the

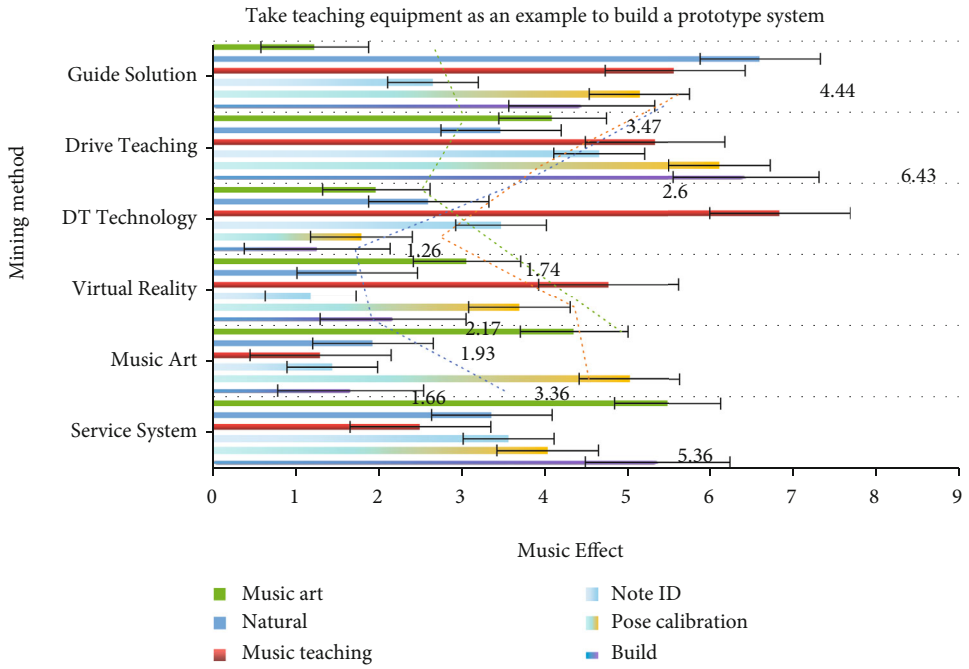

Figure 2: Take teaching equipment as an example to build a prototype system.

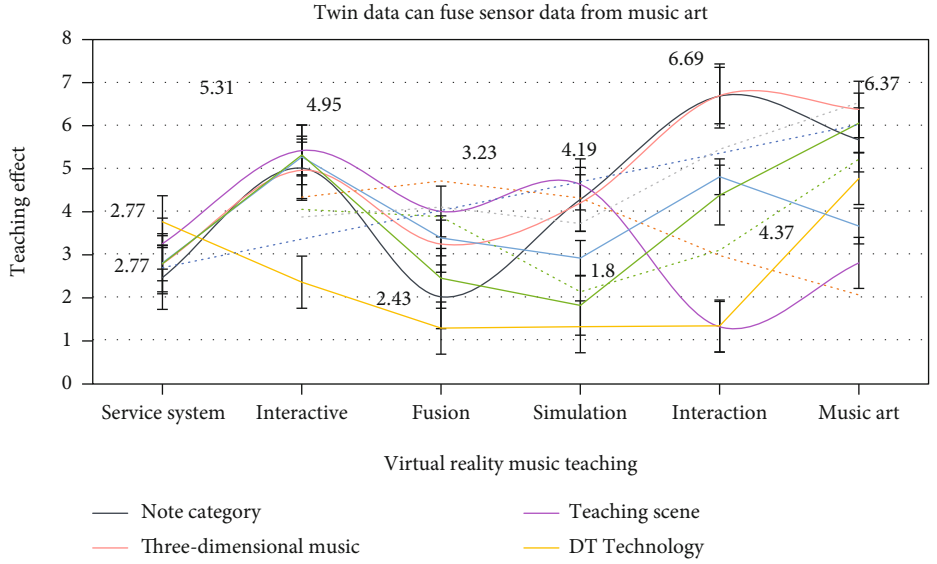

Figure 3: Twin data can fuse sensor data from music art.

Table 2: Interactive operation of the entire system combined with GUI operation panel.

Item	Note category	Teaching scene	DT technology	Drive teaching	Guide solution
Service	2.45	3.24	3.75	2.79	2.77
Interactive	5	5.41	2.34	5.26	5.31
Fusion	2	3.99	1.27	3.37	2.43
Simulation	4.27	4.62	1.3	2.9	1.8
Interaction	6.68	1.3	1.32	4.8	4.37
Music art	5.66	2.79	4.76	3.65	6.05

note signal, establishing the note tree model of the key parts of the device, forming the note ID identification number, and storing it in the note collection library to match with the teaching guidance solution in the music art teaching guidance module.

As shown in Table 4, the music art teaching guidance module integrates scientific teaching guidance methods according to different types of teaching virtual reality technology teaching technical manuals, stores them in the music art teaching database, conducts virtual simulation of teaching guidance process in the virtual interactive interface, and presents the teaching experience in combination with teaching history videos,

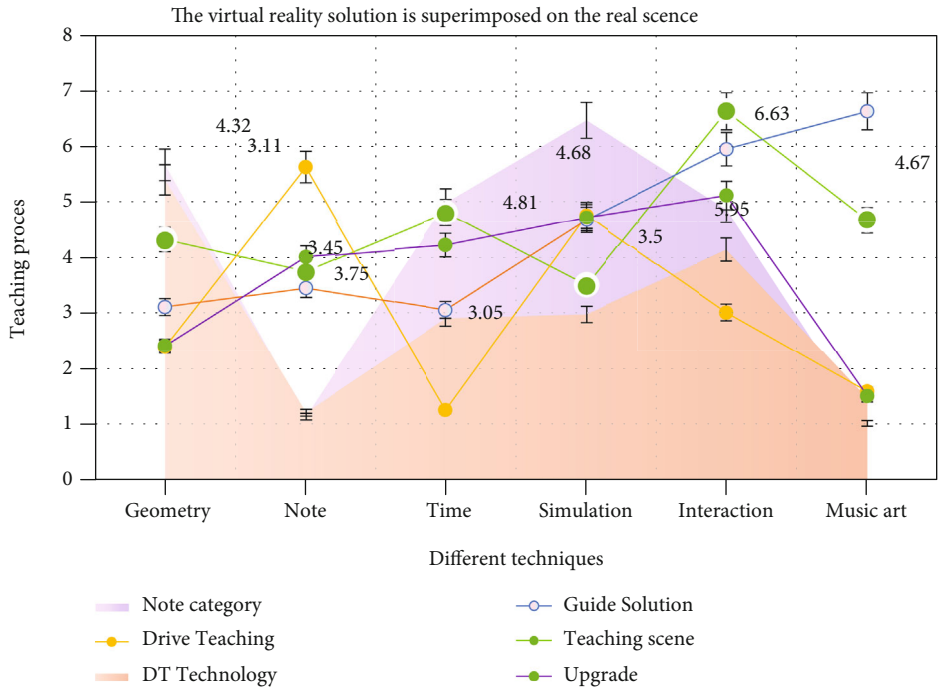

Figure 4: The virtual reality solution is superimposed on the real scene.

Table 3: Teaching guidance service system classifies its musical note data.

Item	Note category	Teaching scene	DT technology	Drive teaching	Guide solution	Upgrade
Geometry	5.67	4.32	5.4	2.39	3.11	2.41
Note	1.13	3.75	1.2	5.63	3.45	4.01
Time	4.99	4.81	2.9	1.25	3.05	4.22
Simulation	6.47	3.5	2.97	4.76	4.68	4.72
Interaction	4.87	6.63	4.14	3.01	5.95	5.12
Music art	1.01	4.67	1.46	1.58	6.63	1.5

teaching guidance process fragments, remote expert guidance, and other methods of learning guidance program.

As shown in Figure 6, virtual and real music teaching algorithms commonly used in hybrid reality technology include music algorithm based on virtual reality and music algorithm based on natural feature points. Both methods can solve the problem of spatial geometry consistency in 3D music teaching technology. As shown in Table 5, the music algorithm based on virtual reality has high accuracy and strong robustness, and can achieve stable positioning effect, but the actual teaching art is bad, which is easy to cause virtual reality damage. Compared with the virtual reality music algorithm, the music algorithm based on natural feature points can better satisfy the unmarked music in the teaching process. However, due to the complexity of teaching physics and art, it is easy to have the cumulative error of key frames, which easily leads to the loss of teaching target tracking in the teaching process. According to the characteristics of system development, the research of music algorithm based on natural feature points of video sequence is more in line with the interactive psychology of teaching staff.

The teaching process of virtual reality music art is shown in Figure 7, which is mainly divided into the steps of extracting scene feature points, feature point matching, camera pose estimation, pose correction, and camera pose confirmation. The system compares the reference frame image in the database with the current frame image collected by the hololens camera, matches its image feature points, and superimposes the virtual scene to realize virtual reality and fusion display of the guidance scheme in the real teaching scene.

As shown in Figure 8, the current music practice class mainly focuses on the art of note form, but ignores the music training of music art, which makes it more difficult for students to learn craniofacial music. Music is an interdisciplinary basic subject. Due to the lack of classroom experience and weak abstract thinking ability, the traditional "cramming" teaching makes it difficult for students to understand the relevant knowledge thoroughly, and it is more difficult for them to

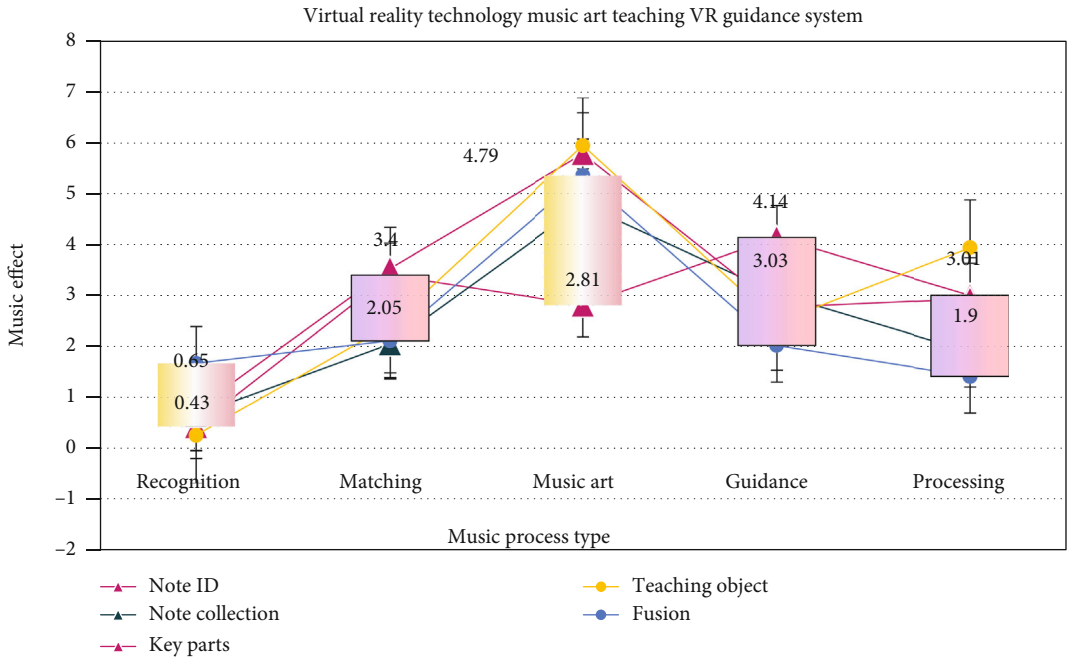

Figure 5: Virtual reality technology music art teaching VR guidance system.

Table 4: Music art teaching guidance module according to different models.

Item	Note ID	Note collection	Key parts	Teaching object	Fusion
Note recognition	0.43	0.65	0.77	0.26	1.67
Matching module	3.4	2.05	3.53	2.42	2.11
Music art	2.81	4.79	5.78	5.94	5.35
Teaching guidance	4.14	3.03	2.77	2.47	2.02
Data processing	3.01	1.9	2.94	3.94	1.42

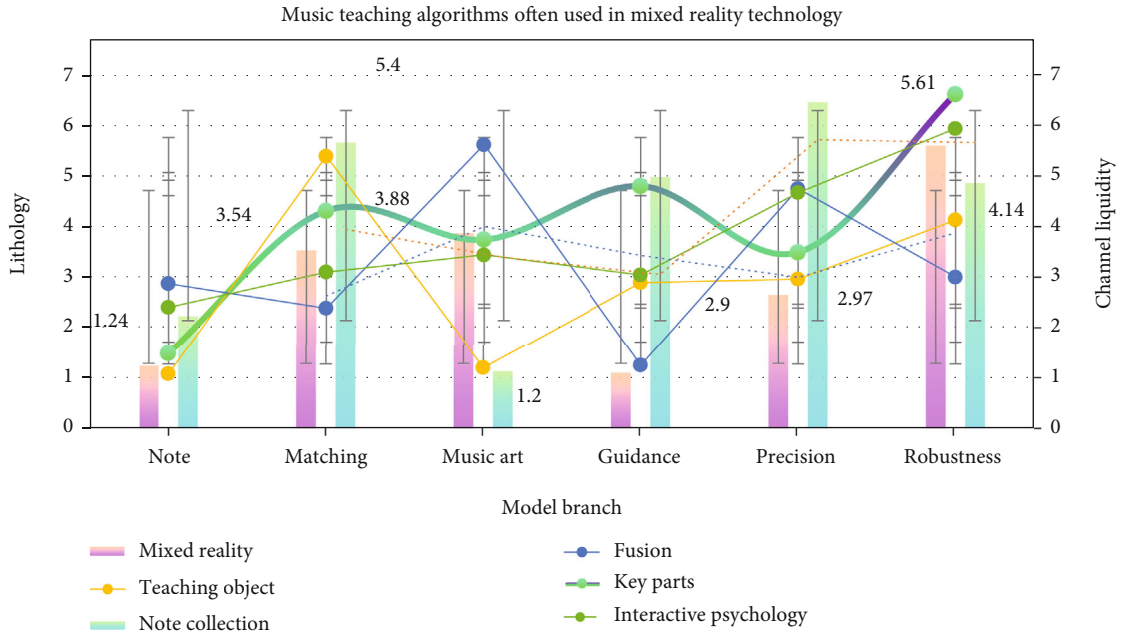

Figure 6: Music teaching algorithms often used in mixed reality technology.

Table 5: Music algorithm based on virtual reality.

Item	Mixed reality	Note collection	Teaching object	Fusion	Interactive psychology
Note recognition	1.24	2.23	1.08	2.88	2.41
Matching module	3.54	5.67	5.4	2.39	3.11
Music art	3.88	1.13	1.2	5.63	3.45
Teaching	1.1	4.99	2.9	1.25	3.05
Precision	2.66	6.47	2.97	4.76	4.68
Robustness	5.61	4.87	4.14	3.01	5.95

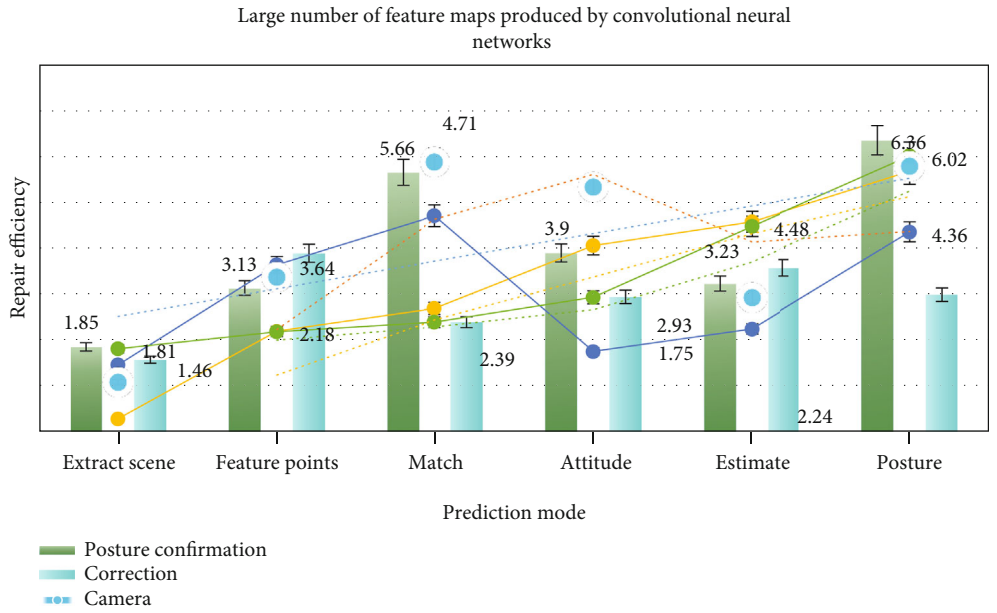

Figure 7: Large number of feature maps produced by convolutional neural networks.

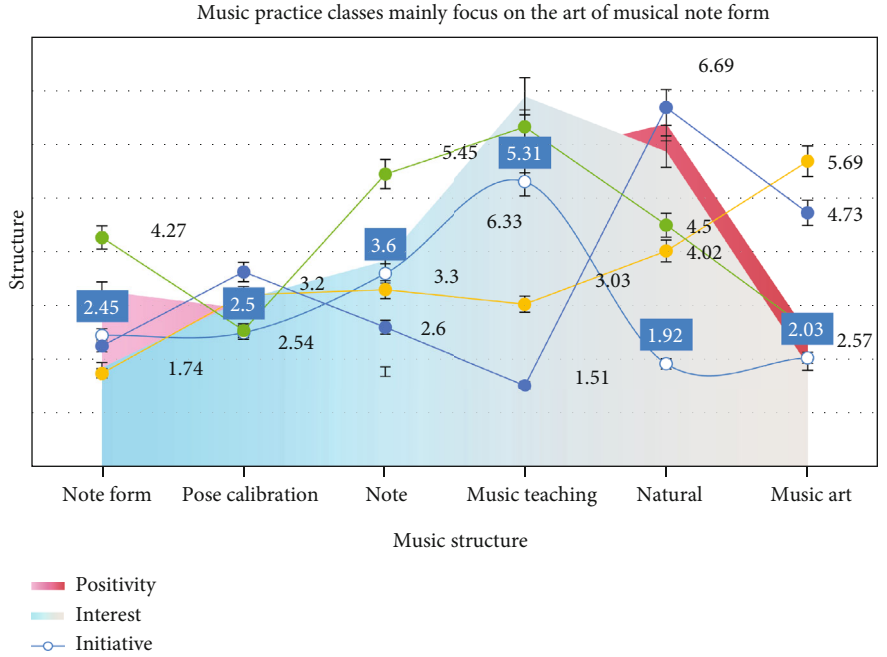

Figure 8: Music practice classes mainly focus on the art of musical note form.

Table 6: Traditional teaching methods are difficult to show abstract musical structure.

Item	Posture confirmation	Camera	Correction	Music art	Teaching	Precision
Extract scene	1.85	1.08	1.57	0.28	1.46	1.81
Feature points	3.13	3.38	3.89	2.19	3.64	2.18
Match	5.66	5.89	2.39	2.69	4.71	2.39
Attitude	3.9	5.34	2.94	4.06	1.75	2.93
Estimate	3.23	2.93	3.57	4.58	2.24	4.48
Posture	6.36	5.8	2.99	5.68	4.36	6.02

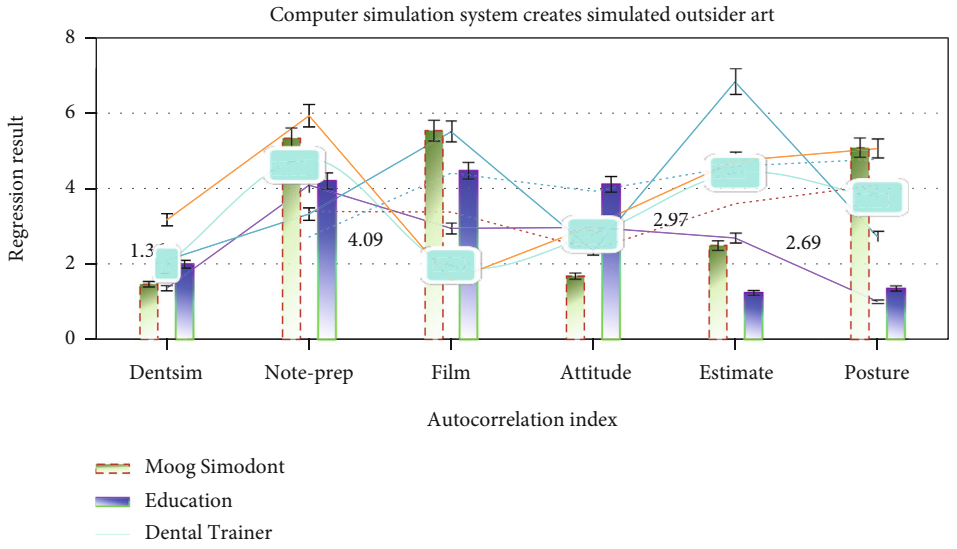

Figure 9: Computer simulation system creates simulated outside art.

Table 7: VR has been reported to be used to train classroom skills.

Item	Moog Simodont	Dental trainer	Education	Military	Music	Design
DentSim	1.47	2	2	1.36	2.1	3.17
Note-prep	5.33	4.79	4.2	4.09	3.32	5.93
Film	5.53	1.96	4.47	2.94	5.51	1.56
Attitude	1.68	2.78	4.11	2.97	2.35	3.02
Estimate	2.49	4.41	1.24	2.69	6.83	4.73
Posture	5.08	3.76	1.35	1	2.73	5.06

enter into an efficient learning state, thus undermining their learning enthusiasm, initiative, and interest and reducing their learning efficiency.

As shown in Table 6, traditional teaching methods are difficult to show abstract music structure. Music as a basic music course, its teaching content is rich, and its concept is abstract and obscure. At present, the commonly used music teaching methods, such as the Internet, 2D pictures (Atlas), and corpse music, have some limitations. For example, when explaining art music, students need to master many abstruse and abstract professional terms, music levels, and adjacent relationships in a short time. If 2D pictures are used for teaching, 3D spatial structure cannot be displayed directly; if specimens are used for teaching, although 3D structure is used, the relationship between music levels cannot be clearly presented.

As shown in Figure 9, computer simulation technology is involved in the creation of many external disciplines. VR has a wide range of applications, including film and television, education, military, music, design, and other fields. As shown in Table 7, VR has been reported to be used to train classroom skills, study human musicology, design surgical procedures, and treat patients with voice phobia. At present, a variety of VR systems have been applied in music teaching. Dentsim system, Moog Simodont, and dental trainer system can effectively help students master the basic methods of

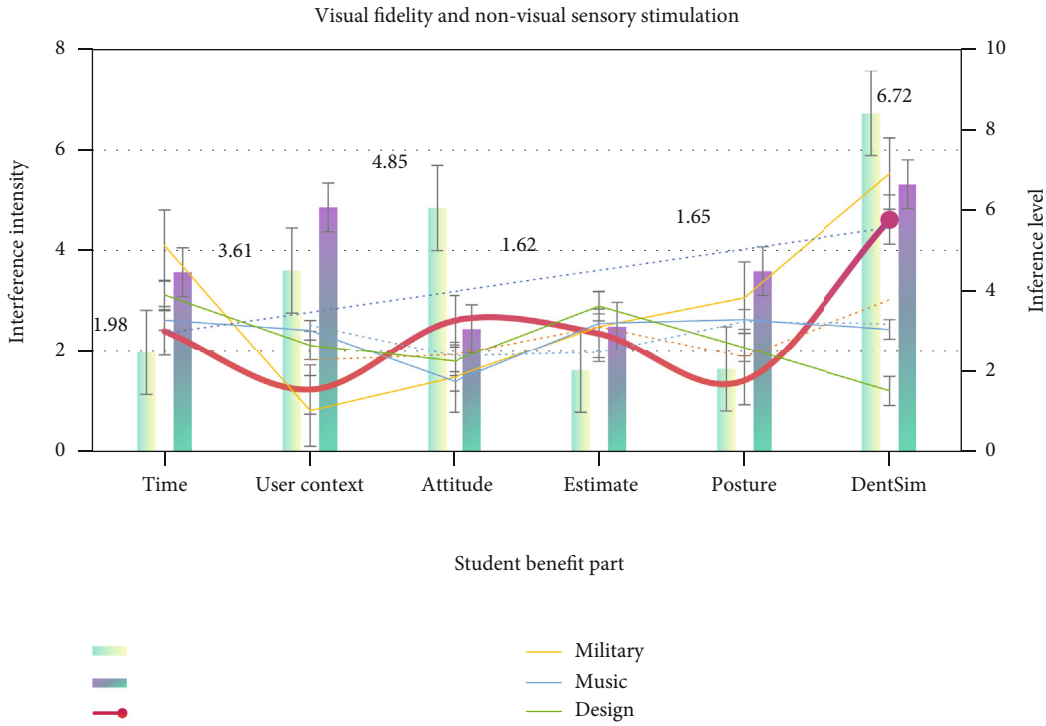

Figure 10: Visual fidelity and nonvisual sensory stimulation.

note preparation and actively improve the teaching quality of music professional courses.

As shown in Figure 10, virtual art created by VR can help users' episodic memory by adjusting students' visual fidelity and nonvisual sensory stimulation. Through data analysis, we know that VR and augmented reality teaching system can shorten the teaching time by 65%. Using VR technology to reconstruct music art can make students observe the form of music art intuitively. The combination of VR technology and traditional teaching methods can significantly increase students' learning initiative, interest, effectiveness, and participation; achieve better teaching effect; and make full preparation for the next classroom learning and practice. Training course is the most effective way to mobilize students' thinking in image. VR technology can be used to establish various virtual laboratories and carry out virtual training in them.

5. Conclusions

Music art teaching is closely related to art science. To some extent, its theoretical basis is the principle of artistic diversity. The metaphorical analogy between the diversity of music and the diversity of biology and art can be regarded as a pioneer in the study of music art teaching. In the study of music anthropology in Papua New Guinea, it is found that the artistic presentation of natural sound is the core expression of local folk music, and the sensitive experience of local residents on soundscape is completely through music to reflect the close relationship between nature and human culture. Sound anthropology is a branch of science that studies the close relationship between nature and human culture through music. Science is rigorous, and art is creativity. In vocal music teaching, we must not only adhere to the scientific nature, but also follow the artistic nature of vocal music, break through the purely technical concept of vocal music teaching, and realize the coordinated and unified development of science and art.

Music is the carrier of the world's national culture, and each nation has a unique way of thinking to form and inherit and nourish the national morality, religion, science and art, and other cultural genes. In ancient China, "music is to adjust the wind" and "music is to save the wind" are trying to express the expectation of good weather through music. Most of the world's folk songs are characterized by the artistic consciousness of integrating the beauty of landscape and natural landscape with regional style. This is the most common embodiment of the relationship between music and nature. Most of the masterpieces handed down from generation to generation are music works praising natural art. Different from the description of art by art science and art scholars, the lyric language of musicologists is discontinuous, metaphorical, and qualitative. Some music works are important evidence for the study of art history.

This paper believes that the Internet of Things technology is a comprehensive technology and a systematic project. At present, no institution or company in China can take full responsibility for the entire system planning and construction of the Internet of Things, but its theoretical research has been in all walks of life; the Internet of Things is only limited to the interior of certain industries in its practical application. Therefore, "virtual reality art Musicology" needs a definition that can clearly reflect its research scope. Based on this, we try to define it as "virtual reality art musicology"

which is based on the theory of musicology, by absorbing the theories and methods of art science and modern art science and studying the relationship and interaction between the formation of music culture, work creation, type characteristics, and function value and art.

Data Availability

The data that support the findings of this study are available from the corresponding author upon reasonable request.

Conflicts of Interest

The author declares that they have no conflicts of interest.

References

[1] Y. Han, S. Lee, J. Nam, and K. Lee, "Sparse feature learning for instrument identification: effects of sampling and pooling methods," *The Journal of the Acoustical Society of America*, vol. 139, no. 5, pp. 2290–2298, 2016.

[2] Z. Jiang, Z. Lin, and L. S. Davis, "Label consistent K-SVD: learning a discriminative dictionary for recognition," *IEEE Transactions on Pattern Analysis & Machine Intelligence*, vol. 35, no. 11, pp. 2651–2664, 2013.

[3] R. Rubinstein, T. Peleg, and M. Elad, "Analysis K-SVD: a dictionary-learning algorithm for the analysis sparse model," *IEEE Transactions on Signal Processing*, vol. 61, no. 3, pp. 661–677, 2013.

[4] O. Slizovskaia, E. Gómez, and G. Haro, "Automatic musical instrument recognition in audiovisual recordings by combining image and audio classification strategies," in *13th Sound and Music Computing Conference*, vol. 4no. 1, pp. 442–447, Germany, 2016.

[5] G. Peeters, B. L. Giordano, P. Susini, N. Misdariis, and S. McAdams, "The timbre toolbox: extracting audio descriptors from musical signals," *Journal of the Acoustical Society of America*, vol. 130, no. 5, pp. 2902–2916, 2011.

[6] A. S. Allen, "Ecomusicology: music, culture, nature, and change in environmental studies," *Journal of Environmental Studies & Sciences*, vol. 2, no. 2, pp. 192–201, 2012.

[7] M. Dutã, C. I. Amariei, C. M. Bogdan, D. M. Popovici, N. Ionescu, and C. I. Nuca, "An overview of virtual and augmented reality in dental education," *Oral Health Dentist Management*, vol. 10, no. 1, pp. 42–49, 2020.

[8] D. X. Wang, Y. R. Zhang, J. X. Hou et al., "iDental: a paptic-based dental simulator and its preliminary user evaluation," *IEEE Transactions on Haptics*, vol. 5, no. 4, pp. 332–343, 2012.

[9] S. M. Zhao and T. Li, "Preliminary evaluation of a virtual reality dental simulation system on drilling operation," *Bio-Medical Materials and Engineering*, vol. 26, no. 1, pp. S747–S756, 2020.

[10] Y. J. Shi, "Six degree-of-freedom haptic simulation of probing dental caries within a narrow oral cavity," *IEEE Transactions on Haptics*, vol. 9, no. 2, pp. 279–291, 2016.

[11] Z. Lv, X. Li, H. Lv, and W. Xiu, "BIM big data storage in web VRGIS," *IEEE Transactions on Industrial Informatics*, vol. 16, no. 4, pp. 2566–2573, 2019.

[12] R. H. Chu, Y. R. Zhang, H. D. Zhang, W. Xu, J. H. Ryu, and D. Wang, "Co-actuation: a method for achieving high stiffness and low inertia for haptic devices," *IEEE Transactions on Haptics*, vol. 13, no. 2, pp. 312–324, 2020.

[13] A. Banerjee, J. E. Frencken, F. Schwendicke, and N. P. T. Innes, "Contemporary operative caries management: consensus recommendations on minimally invasive caries removal," *British Dental Journal*, vol. 223, no. 3, pp. 215–222, 2017.

[14] P. Ntovas, N. Loubrinis, P. Maniatakos, and C. Rahiotis, "Evaluation of dental explorer and visual inspection for the detection of residual caries among Greek dentists," *Journal of Conservative Dentistry*, vol. 21, no. 3, pp. 311–318, 2018.

[15] L. Thomas and E. Autio, "Emergent equifinality: an empirical analysis of ecosystem creation processes," in *Proceedings of the 35th DRUID Celebration Conference*, pp. 36–40, Spain, 2020.

[16] R. Adner and R. Kapoor, "Innovation ecosystems and the pace of substitution: re-examining technology S-curves," *Strategic Management Journal*, vol. 37, no. 4, pp. 625–648, 2016.

[17] G. Dartmann, H. Song, and A. Schmeink, *Big Data Analytics for Cyber-Physical Systems: Machine Learning for the Internet of Things*, Elsevier, 2019.

[18] C. Leong, S. L. Pan, S. Newell, and L. Cui, "The emergence of self-organizing e-commerce ecosystems in remote villages of China: a tale of digital empowerment for rural development," *MIS Quarterly*, vol. 40, no. 2, pp. 475–484, 2016.

[19] R. F. Lusch, S. L. Vargo, and A. Gustafsson, "Fostering a trans-disciplinary perspectives of service ecosystems," *Journalof Business Research*, vol. 69, no. 8, pp. 2957–2963, 2016.

[20] T. Meynhardt, J. D. Chandler, and P. Strathoff, "Systemic principles of value co-creation: synergetics of value and service ecosystems," *Journal of Business Research*, vol. 69, no. 8, pp. 2981–2989, 2016.

[21] S. K. Jha, A. Pinsonneault, and L. Dubé, "The evolution of an ICT platform-enabled ecosystem for poverty alleviation: the case of eKutir," *MIS Quarterly*, vol. 40, no. 2, pp. 431–445, 2016.

[22] Y. W. Liang, A. S. Lee, and S. F. Liu, "A study on design-oriented demands of VR via ZMET-QFD model for industrial design education and students learning," *Eurasia Journal of Math-ematics, Science and Technology Education*, vol. 4, no. 5, pp. 1205–1219, 2016.

[23] G. Li, J. A. Anguera, S. V. Javed, M. A. Khan, G. Wang, and A. Gazzaley, "Enhanced atten-tion using head-mounted virtual reality," *Journal of Cognitive Neuroscience*, vol. 6, no. 10, pp. 1434–1454, 2020.

[24] A. Cranmer, J. D. Ericson, A. E. Broughel, B. Bernard, E. Robicheaux, and M. Podolski, "Worth a thousand words: presenting wind turbines in virtual reality reveals new opportunities for social acceptance and visualization research," *Energy Research & Social Science*, vol. 67, no. 10, article 101507, 2020.

[25] A. Chung, W. M. To, and I. Vong, "Integrating artificial intelligence with virtual reality for soundscape appraisal," in *INTER-NOISE and NOISE-CON congress and conference proceedings*, Americon, 2018.

[26] T. K. Huang, C. H. Yang, Y. H. Hsieh, J.-C. Wang, and C.-C. Hung, "Augmented reality (AR) and virtual reality (VR) applied in dentistry," *The Kaohsiung Journal of Medical Sciences*, vol. 34, no. 4, pp. 243–248, 2018.

[27] O. I. Khalaf and G. M. Abdulsahib, "Optimized dynamic storage of data (ODSD) in IoT based on blockchain for wireless sensor networks," *Peer-to-Peer Networking and Applications*, vol. 14, no. 5, pp. 2858–2873, 2021.

Hindawi
Wireless Communications and Mobile Computing
Volume 2022, Article ID 9291319, 10 pages
https://doi.org/10.1155/2022/9291319

Research Article

Multisource Target Data Fusion Tracking Method for Heterogeneous Network Based on Data Mining

Hongyan Guo[1] **and Xintao Li**[2]

[1]*College of Information Engineering, Henan Open University, Zhengzhou, Henan 450046, China*
[2]*College of Innovation and Entrepreneurship, Henan Open University, Zhengzhou, Henan 450046, China*

Correspondence should be addressed to Hongyan Guo; guohongyan123@stu.ahu.edu.cn

Received 15 March 2022; Revised 28 April 2022; Accepted 6 May 2022; Published 10 June 2022

Academic Editor: Jun Ye

This research is on heterogeneous network fusion method of multisource target data based on data mining. Firstly, it is a distributed storage structure model for building heterogeneous network multisource target data. Then, using the phase space reconstruction method, a grid distribution structure model for data fusion tracking is constructed, and realize visual scheduling and automatic monitoring of multisource target data. Finally, according to the feature extraction results, analyze the statistical characteristics of multisource target data in heterogeneous networks, combined with the fuzzy tomographic analysis method, multilevel fusion, and adaptive mining of multisource target data, extract the associated feature quantities in it, and realize the fusion tracking of data. The simulation results show that, in relatively simple heterogeneous networks, the feature mining error of the proposed method is nearly 2.11% lower than the two traditional methods. In relatively complex heterogeneous networks, the feature mining error of the proposed method is nearly 6.48% lower than the two traditional methods. It can be seen that this method has better adaptability for fusion tracking of heterogeneous network multisource target data, the anti-interference ability is strong, and the tracking accuracy in the data fusion tracking process is also improved.

1. Introduction

As the scale of heterogeneous networks continues to expand, the amount of multisource target data in heterogeneous networks is also gradually increasing; therefore, it is necessary to perform visual reconstruction and fusion tracking and identification of heterogeneous network multisource target data and ensure the stability of the network. Usually, in the process of fusion tracking and identification of multisource target data in heterogeneous networks (Figure 1), it is necessary to establish a heterogeneous network multisource target data fusion tracking model, and combined with big data mining and information reconstruction methods, the fusion detection and feature analysis of heterogeneous network multisource target data are carried out; thereby, the detection, tracking, and identification capability of multisource target data in heterogeneous networks is improved. And the related research on multisource target data fusion tracking method in heterogeneous network has received great attention. In general, for heterogeneous networks, the fusion tracking and identification of multisource target data are based on data fusion detection and feature analysis. This process can improve the ability to detect and identify multisource target data in heterogeneous networks, thereby improving the retrieval and access capabilities of multisource target data in heterogeneous networks [1].

The rapid development of database technology and machine learning disciplines makes data mining as a new technology on the stage of history. This is a database and other media to store data, and use machine learning algorithms to extract the knowledge that people are interested in from the data. Due to the continuous progress of machine learning in artificial intelligence, look at the rapid development of information technology: at the beginning, it was just a simple collection and creation of databases; the rapid development of data mining technology has been promoted;

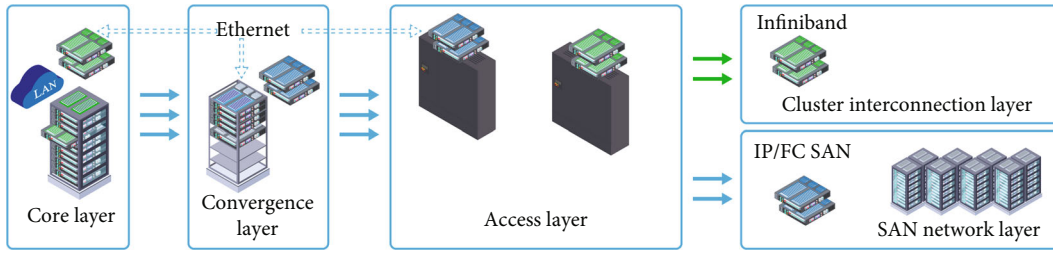

Figure 1: Data center heterogeneous network.

take a look at the development of information technology. The beginning is just a simple collection and sampling of data and the establishment of a database; then, start managing this data, such as the following: data storage, retrieval, and database transaction processing. Then, it developed to the analysis, understanding, and prediction of data, and then, data warehouse and data mining technology appeared. With the development of network information technology, database technology, etc., the amount of information stored in the database by humans increases over time, and adding and deleting technologies of the database are perfected; it provides conditions for the development of data mining technology; the increase in the amount of data also indicates that a technology for processing massive data is bound to emerge [2].

2. Related Works

At present, there are experts and scholars in the field of multisource target data tracking and identification; some more mature research results are presented, such as association feature detection method, fuzzy C-means cluster analysis method, and K-means cluster analysis method. Meng et al. proposed a method to simultaneously analyze resource content information and resource network topology information, probabilistic topic models, and tag recommendation methods for unified modeling; in order to carry out the fusion of multisource heterogeneous network information, the data can be more accurate for fusion analysis [3]. Wang et al. studied the wireless body area network multisensor; due to the large amount of data collected, the data types are complicated and it is difficult to effectively integrate multidimensional data, using the algorithm based on manifold learning, the high-dimensional data points, and their corresponding low-dimensional data points; the Euclidean distance is used as the conversion condition of the probability matrix, and a multidimensional data fusion model is constructed through finite iterations [4]. In addition, Wan et al. proposed a multisource target data fusion tracking method based on data mining in heterogeneous networks, in order to improve the detection and recognition ability of heterogeneous network multisource target data [5]. In addition, in the study of Liu et al., by extracting multilayer convolution features, the target data represented by it is more comprehensive, and calculate the correlation response of the data; then, dynamically fuse all the historical data and the target position in the real-time data response, so as to realize the positioning and dynamic tracking of target data [6]. In the study of Yi et al., using the fusion redetection mechanism to track the network target data and integrating the correlation filter into the network in the training phase, extract multisource data features through end-to-end training. In the tracking stage, the residual value is used to connect and fuse different source data, and a redetection mechanism is introduced to achieve real-time tracking [7]. Li et al. believe that data mining itself is not a new technology; after decades of research and development, people have mastered a large number of data mining algorithms and developed many data mining tools. However, these theories and tools are not necessarily applicable to large datasets [8]. Liu believes that traditional data storage methods cannot carry big data. Before the era of big data, traditional relational databases, e.g., were common tools for structured data storage. For the level of data volume, the storage efficiency of relational databases can fully meet the basic needs. And relational databases provide rich and flexible structured query statements, as well as features such as stored procedures, indexes, and database transactions [9]. Alqerm and Shihada believe some domestic scientific research institutions and universities have started research on data mining, a subject with great potential and practical application value; the domestic data mining research institutions are mainly universities, research institutes, or companies [10]. Ishaq et al. believe that the abovementioned specifications emphasize the completeness of geographic information, making the exchange format itself enormous; data reception and transmission overhead are too high for both software and hardware; this is contrary to the fast and efficient properties of dynamic target information itself; it is not conducive to the transmission of real-time information, so it is not suitable to use the spatial data format exchange standard as a reference [11].

However, when existing methods perform fusion tracking on heterogeneous network multisource target data, there are problems such as poor adaptability, high computational complexity, and poor data tracking ability. The author proposes a multisource target data fusion tracking method based on data mining in heterogeneous networks.

3. Research Methods

3.1. Data Collection. Data mining technology includes the following steps: data preparation, data mining, conclusion representation, and interpretation.

3.1.1. Data Preparation. The data preparation stage is the beginning of the whole mining process; this stage is very important; how well the data preparation stage is executed will determine the efficiency of the subsequent steps of the

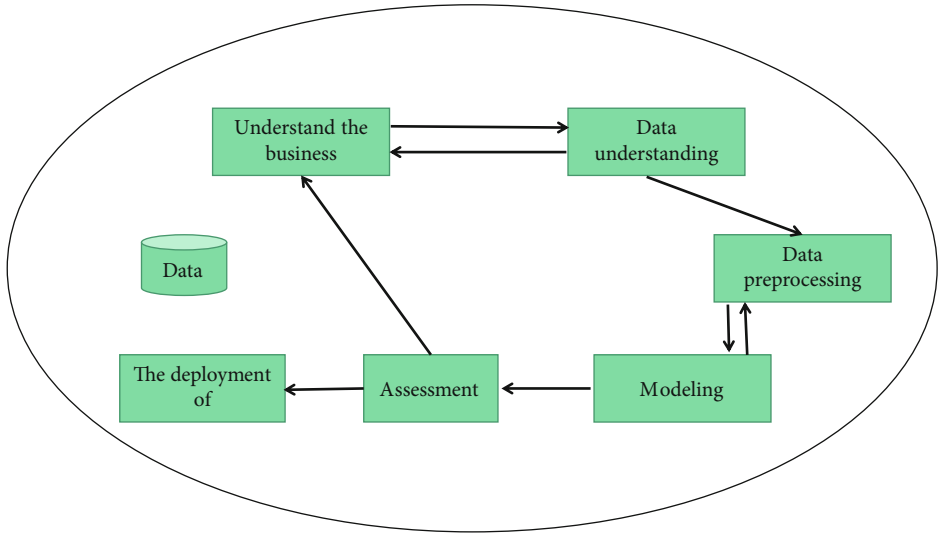

Figure 2: Data mining process.

entire data mining, as well as the effectiveness of the extracted information and knowledge; we can further subdivide data preparation into three stages: data integration, data selection, and data preprocessing [12].

(1) *Data Integration*. That is, data integration from different databases agrees to be stored

(2) *Data Preprocessing*. Preprocessing is obviously the preprocessing work before data mining, mainly carry out data form conversion and data reduction to suit the entire data mining process

3.1.2. Data Mining. Select a data mining algorithm (such as classification algorithm, association rule, regression, and clustering algorithm), mining the data prepared in the data preparation stage to obtain patterns that users are interested in.

3.1.3. Result Description and Interpretation. Mainly the patterns and rules that will be mined, analyze the mining patterns and rules according to the specific needs of users, extract the most useful and interesting information for users, and finally submit it to users through decision-making tools. Therefore, not only the presentation and interpretation of the results (visualization tools) is the main task of this step; the final information data needs to be filtered and processed [13]. If the user is not satisfied with the conclusion, the mining process needs to be repeated. The steps and criteria of the data mining process are summarized, as shown in Figure 2 below.

3.2. Distributed Storage Structure Model and Multilevel Integration of Data

3.2.1. Distributed Storage Structure Model of Target Data. To realize the fusion tracking and optimization identification of heterogeneous network multisource target data, firstly, a distributed storage structure model of heterogeneous network multisource target data is constructed; assuming that N_k $(k = 1, 2, \cdots, l)$ represents the number of multisource target data fusion tracking distribution sets in the kth heterogeneous network, a_i^k represents the heterogeneous network multisource target data, the activity of the ith node is in the kth layer in the data sampling, x_i^k is the data input at the multisource target data fusion node i of the kth layer heterogeneous network, and w_i^k represents the energy threshold at the ith node of the kth layer in the heterogeneous network, then the statistical analysis model of the sampling node of the heterogeneous network multisource target data can be obtained as $S = (\mu \sum_{i=1}^{n} a_i^k \times x_i^k) \times w_i^k$; among them, μ represents the connection weight of each node in the heterogeneous network. Assuming that the effective activation function of the heterogeneous network sampling data is f, analyze the amplitude of periodic oscillation of multivariate target data in heterogeneous networks, using the semantic ontology fusion method and the three-dimensional reconstruction of the multisource target data in the heterogeneous network; the fuzzy decision function of the distributed storage to obtain the target data is $F = \partial \times S/f$, where ∂ represents the ambiguity coefficient. There are several data layers at the input of the heterogeneous network, which is obtained in the normalized linear subspace; the multisource target data distribution function of heterogeneous network in the first layer is $D = \lambda \sum_{k=1}^{l} F \times N_k$, where λ represents the normalization coefficient [14]. Constructed from the above model, the optimal design of the distributed storage structure of the target data is realized.

3.2.2. Multilevel Fusion and Adaptive Mining of Data. In the above pair of heterogeneous networks, based on the design of the distributed storage structure model of the target data, let c_i denote the fuzzy closeness function between multisource target data sharing nodes in heterogeneous networks; extract the intracluster distribution information of multisource target data in heterogeneous networks; the incluster distribution model of the multisource target data is

obtained as $C = D \times c_i + (S + T)\eta$; among them, η represents a natural parameter, and T represents a sufficient statistic. On the basis of, using information fusion and fuzzy tomographic analysis methods for multisource target data in heterogeneous networks, information fusion, and adaptive scheduling, extract 3D visualization feature quantities of heterogeneous network multisource target data; then, the optimized within-cluster distribution function can be rewritten as $C' = [(a \times C)/y] \times g$, where a is the correlation coefficient of multilevel fusion of data, y is the number of symmetrical voxels in the three-dimensional regular data field, and g represents the adaptive optimization function. When C' has a finite stable solution in g, it means that the optimization process is convergent; at this time, the objective function in heterogeneous network tracking and identification is gC'; under the fixed perturbation step size, it is assumed that the fuzzy weighted value of the multisource target data fusion tracking and identification of the heterogeneous network is β; through the optimization of decision function, the feature optimal solution of multisource target data mining in heterogeneous network is obtained as follows:

$$J = \frac{\left(\beta C' - \varepsilon\right) \times g_c}{2}. \tag{1}$$

Among them, ε is the decision error. Based on the above analysis, build multilevel fusion and adaptive mining models of data, and by visual scheduling and automatic monitoring design of heterogeneous network multisource target data, the statistical feature extraction of heterogeneous network multisource target data is carried out.

3.3. Fusion Tracking of Multisource Target Data

3.3.1. Statistical Feature Analysis of Multisource Target Data. Based on the abovementioned distributed storage and fusion mining of multisource target data in heterogeneous networks, the author proposes a multisource target data fusion tracking method based on data mining in heterogeneous networks [15]. Using the phase space reconstruction method, a grid distribution structure model for fusion tracking of heterogeneous network multisource target data is constructed, and by visual scheduling and automatic monitoring of multisource target data in heterogeneous networks, the feature distribution dimension of the multisource target data obtained in heterogeneous networks is$m$; if the type attribute of multisource data in heterogeneous networks is r, then there is a maximum independent set for all nodes:

$$P_i = \{mrN_k | i = 1, 2, \cdots, k = 1, 2, \cdots, l\}. \tag{2}$$

Initialize the cluster center e for heterogeneous network multisource target data classification; then, the fuzzy membership function of multisource target data fusion tracking in heterogeneous network is as follows:

$$x = \prod_{i=1}^{n} (e_i)^k (1 - \rho) P_i. \tag{3}$$

Among them, e_i represents the fusion cluster center of heterogeneous network multisource target data, and ρ represents the prior probability density of multisource target data in heterogeneous networks; on this basis, the mean phase space reconstruction of multisource target data in heterogeneous networks is obtained as follows:

$$\bar{x} = \frac{\left(\sum_{i=1}^{n} |x|\right)}{k}. \tag{4}$$

According to the phase space reconstruction results of multisource data of heterogeneous networks, the data state characteristics are monitored, combined with statistical analysis methods; the variance of the multitarget data fusion is obtained as follows:

$$\sigma^2 = \frac{\left[\sum_{i=1}^{n} (x - \bar{x})^2\right]}{k}. \tag{5}$$

Assuming that the heterogeneous network multisource target data set contains N samples, for the limited data sample set X_N, the impulse response function of the 3D visual feature reconstruction is as follows:

$$I = \frac{\left(\sum_{I}^{N} X_N \times \sigma^2\right)}{f_0}. \tag{6}$$

Among them, f_0 represents the initial sampling frequency. On the basis of, the metric feature extraction method is used to perform benchmark feature matching of multisource target data in heterogeneous networks, design the dominant frequency feature extraction model of multisource target data in heterogeneous network, realize the statistical feature analysis of multisource target data, and obtain the statistical feature quantity as follows:

$$Q = I \times \left[\frac{(\varphi \times q - t)}{N}\right]. \tag{7}$$

Among them, q represents the feature attributes of multisource target data in heterogeneous networks, φ represents a limited data set, and t represents the time delay of data fusion tracking.

3.3.2. Data Feature Extraction and Fusion Tracking Output. For heterogeneous network multisource target data, the method used to extract adaptive feature information is information fusion, the information fusion method is used to extract adaptive feature information, the method of multilevel fusion and self-adaptive mining of multisource target data in heterogeneous network is fuzzy tomographic analysis method, and for heterogeneous network multisource target data, information fusion and fuzzy tomographic analysis methods are used to perform big data scheduling [16]; then, the rule itemset for quantitative evaluation of heterogeneous network multisource target data is as follows:

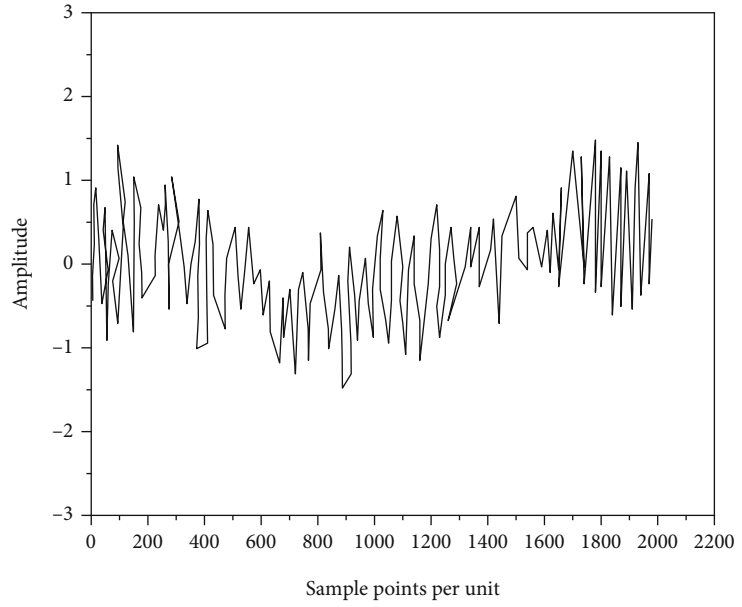

(a) Simulation result A

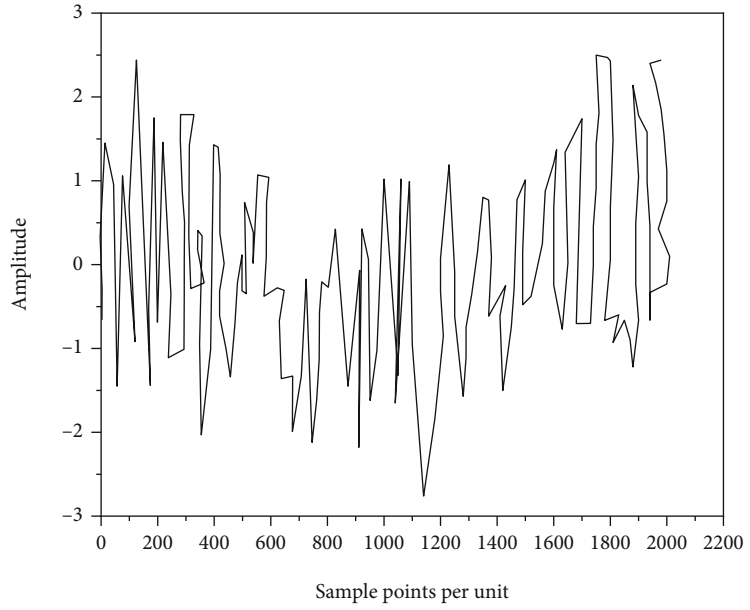

(b) Simulation result B

Figure 3: Amplitude distribution status of multisource target data in heterogeneous networks.

$$U = \frac{(\sum_{i=1}^{n} Q \times \delta)}{E_i}. \tag{8}$$

Among them, E_i represents the expected spectral output value of the ith node of the multisource target data output layer of the heterogeneous network, and δ represents the Kronecker function.

Assuming that z represents the measurement feature set of heterogeneous network multisource target data, analyze the statistical vector dimension of multisource target data in heterogeneous networks, and use the correction function to correct the state; the constraint function for the fusion tracking and identification of heterogeneous network multisource target data is obtained:

$$Y = \frac{(\tau \times z)}{U}. \tag{9}$$

Among them, τ represents the reliability factor of multisource target data sampling in heterogeneous network; it is a constant greater than 0 but less than 1. The output of the fusion of heterogeneous network multisource target data through the fuzzy C-means cluster analysis method is as follows:

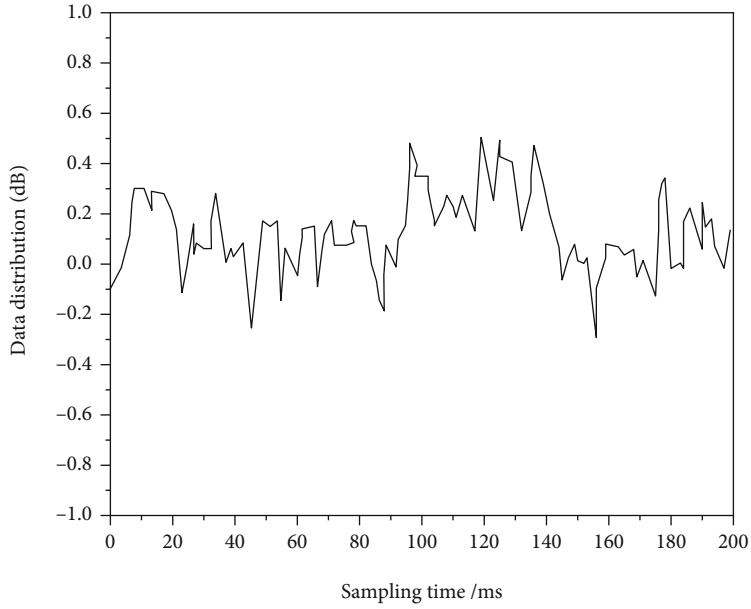

Figure 4: Experimental group.

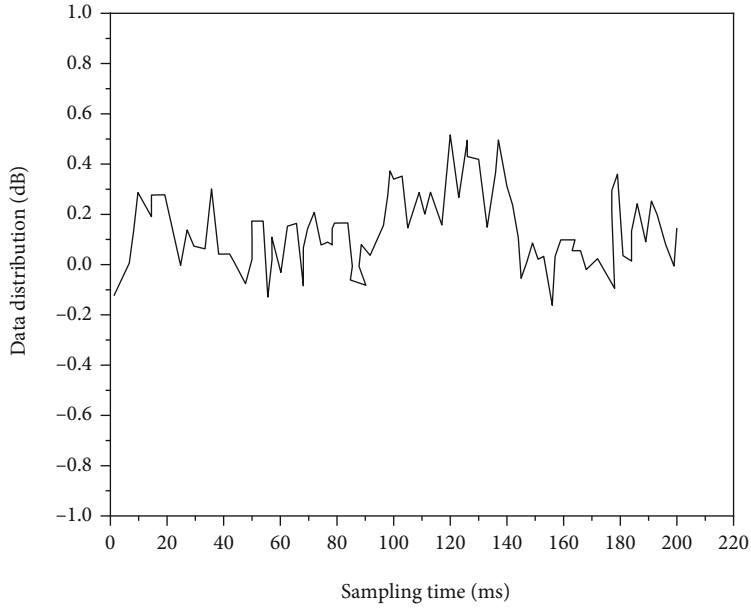

Figure 5: Control group 1.

$$T = \frac{(Q - U)}{\gamma \times Y}. \tag{10}$$

Among them, γ represents the fusion factor. Assuming that R represents the three-dimensional distribution attribute value of heterogeneous network multisource target data, through the above analysis, the optimal fusion tracking of multisource target data in heterogeneous networks is realized, and the output results are as follows:

$$M = \frac{(Y \times T - Q)v}{R}. \tag{11}$$

Among them, v represents the distance between data nodes. Based on the above analysis, the basis of extracting associated feature quantities of multisource target data in heterogeneous networks realizes data optimization mining and fusion tracking identification.

4. Simulation Experiments

In order to verify the reliability of the research method, taking the data fusion method of this study as the experimental group, the traditional method 1 was used as the control group 1, and the traditional method 2 was used as the control group 2. Design simulation experiments, and verify the

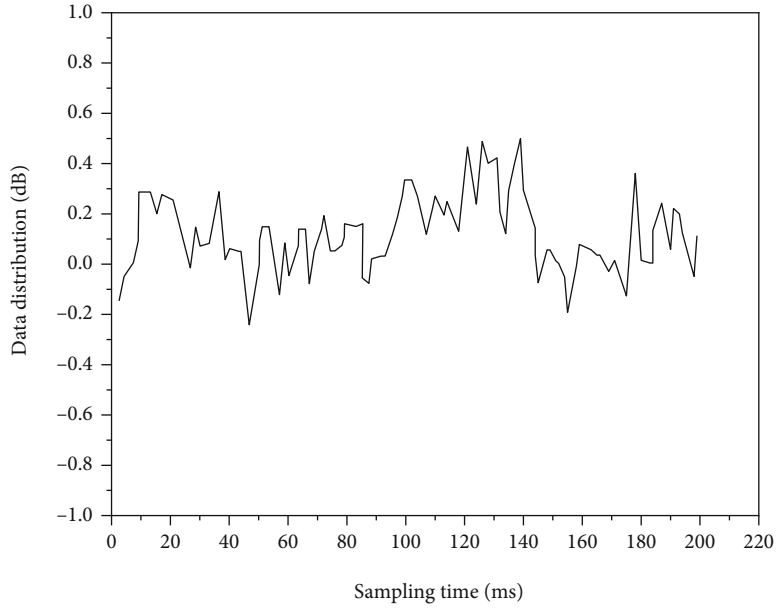

Figure 6: Control 2 groups.

Table 1: Mining error comparison of different methods/%.

Number of iterations	Test group	Control group 1	Control 2 groups
100	11.24	18.76	18.54
200	10.6	14.93	14.6
300	9.21	11.6	12.5
400	7.85	9.34	9.56
500	6.58	8.76	8.26
600	6.5	8.53	8.64
700	6.45	8.78	8.57
800	6.56	8.81	8.64
900	6.58	8.56	8.63
1000	6.45	8.86	8.52

fusion effect of different methods on multisource target data in heterogeneous networks.

4.1. Experiment Preparation. The experimental group simulated in the Matlab environment, set the number of iteration steps for heterogeneous network multisource target data fusion to 2000, and set the sampling interval to 1.0 s; at the same time, ensure that the length of the sampled data to 2000. Set the dimension is 4, reconstruct spatial structure of multisource target data in heterogeneous networks, and set the embedding delay to 15 ms; the sampling frequency of multisource data is 10 kHz. According to the above basic conditions, using the simulation test software, the experimental group conducted two heterogeneous networks in different periods; build a multisource target data amplitude distribution map, as shown in Figure 3 below.

The two sets of simulation results in Figure 2 are the initial input data for the experimental group. Using two control test groups, obtain the amplitude distribution status of multisource target data in heterogeneous networks [17, 18]. Three test groups were used, respectively, mining data features in the two test environments and performing data fusion based on the mining results. In this paper, in order to make the experiment full of accuracy and authenticity, between the beginning of the test, the computer and the test software are run for trial operation, and the experiment is started after there is no problem.

4.2. Data Fusion of Simple Heterogeneous Networks. The three groups of time-domain distribution states are similar to the simulation environment A in Figure 3; as the basic test conditions of the first stage, three test groups are used; mining multisource target data features in simple heterogeneous networks, the result is shown in Figures 4–6 below.

According to the curve in the figure, when faced with a relatively simple heterogeneous network test environment; although the characteristic data obtained by the three test groups are relatively similar [19], however, the temporal characteristics of the data mined by the two control groups are slightly weaker than the experimental group. Therefore, the data mining errors of the three test groups are further calculated. Table 1 shows the experimental results.

It can be seen from the test results in Table 1 that when the number of iterations exceeds 500, mining errors for the three test groups are gradually controlled within a stable range. For ease of comparison, when computing 600 to 100 iterations, there is average mining error of the three test groups; among them, the experimental group was 6.58%, and the control group was 8.76% and 8.62%, respectively. The mining error of the experimental group is 2.18% and 2.04% smaller than that of the two control groups [20], respectively.

4.3. Data Fusion of Complex Heterogeneous Networks. In the second stage of testing, the time domain distribution state

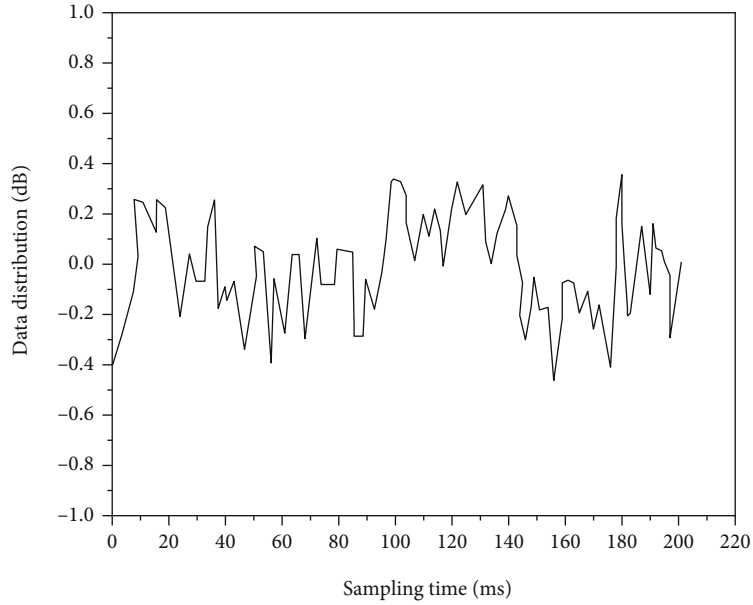

Figure 7: Control group 1.

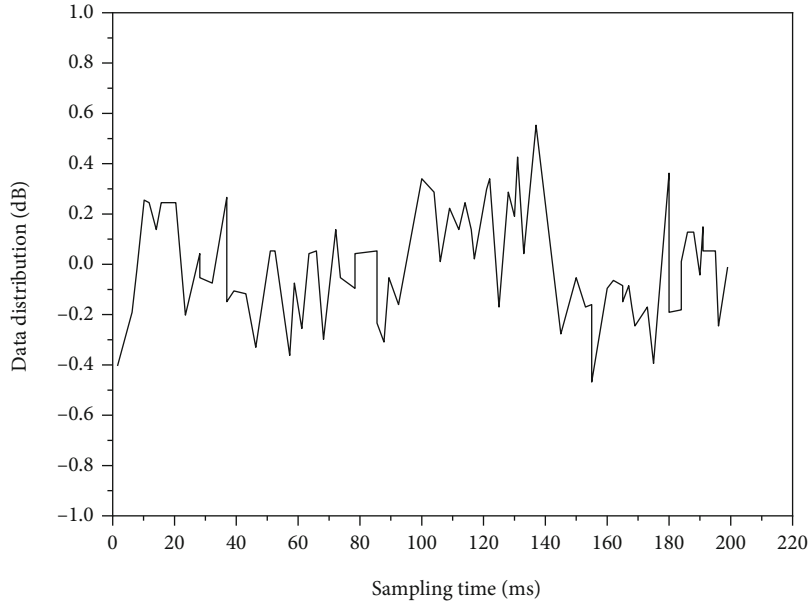

Figure 8: Control 2 groups.

similar to the simulation environment B in Figure 2 is used as the basic condition, using three test groups, mining complex heterogeneous networks, and the characteristics of multisource target data, and the results are shown in Figures 7 and 8 below.

According to the curve in the figure, due to the complex heterogeneous network environment, the volume of data is large, and there are many different types of data; therefore, it brings huge mining difficulty to data feature mining; therefore, the feature mining results of the two control groups do not match the data distribution characteristics of the respective simulation environment B. The data feature mining errors of different methods are further calculated. Table 2 shows the experimental results [21].

It can be seen from the test results in Table 2 that in the process of 600-1000 iterations, the mining errors of the three test groups gradually became stable, and the average mining error of the experimental group was 7.2%, and the average mining errors of the control group were 13.81% and 13.55%, respectively. In a complex test environment, the mining error of the experimental group was 6.61% lower than that of the control group 1; it was 6.35% lower than the control group 2. Based on the above two sets of test results, it can be seen that, whether in a simple test environment or in a complex environment, the proposed data fusion

Table 2: Mining error comparison of different methods/%.

Number of iterations	Test group	Control group 1	Control 2 groups
100	11.78	28.36	30.96
200	11.27	24.05	24.7
300	10.23	21.16	22.2
400	9.2	17.63	20.03
500	8.36	14.6	14.56
600	8.14	13.66	13.14
700	7.26	13.57	13.5
800	7.3	13.62	13.57
900	7.25	13.7	13.5
1000	7.15	13.79	13.53

method, with the help of time series mining technology, the obtained mining results are more representative of multisource target data and provide more realistic information for data fusion.

5. Conclusion

Based on the establishment of a heterogeneous network multisource target data fusion tracking model, combined with big data mining and information reconstruction methods, fusion detection and feature analysis of multisource target data in heterogeneous networks can be realized. The author proposes a multisource target data fusion tracking method based on data mining in heterogeneous networks. Build a distributed storage structure model of heterogeneous network multisource target data and statistical feature analysis of heterogeneous network multisource target data based on feature extraction results; for heterogeneous network multisource target data, the information fusion method is used to extract adaptive feature information, using the fuzzy tomographic analysis method, multilevel fusion, and adaptive mining of heterogeneous network multisource target data, extract the associated feature quantities of heterogeneous network multisource target data, and realize data optimization mining and fusion tracking and identification. From the experimental analysis, it can be seen that using this method for fusion tracking of heterogeneous network multisource target data has better adaptability; the information retrieval process has strong anti-interference ability and small control error and can be used to fuse and identify target data from multiple sources in the same network. However, affected by personal ability and research experience, there is no experimental demonstration of the data fusion results in this study, and only the data mining in the fusion process is simulated and tested; therefore, in future research, data fusion can also be used as an experimental test standard; the reliability of this research method is verified from more angles.

Data Availability

The data used to support the findings of this study are included within the article.

Conflicts of Interest

All of the authors do not have any possible conflicts of interest.

Acknowledgments

This work was supported by the Project of Science and Technology of Henan Province (No. 212102210428).

References

[1] G. Jiao and W. Li, "Neural network data mining clustering optimization algorithm," *IETE Journal of Research*, vol. 2, pp. 1–11, 2021.

[2] M. Naeem, H. M. Elattar, and M. Aboul-Dahab, "An optimized load balance solution for multi-homed host in heterogeneous wireless networks," *Sensors*, vol. 19, no. 12, p. 2773, 2019.

[3] L. Meng, C. Li, H. Zhang, and J. Dong, "Construction of community life circle database based on high-resolution remote sensing technology and multi-source data fusion," *European Journal of Remote Sensing*, vol. 3, pp. 1–16, 2020.

[4] F. Wang, Q. I. Huan, X. Zhou, and J. Wang, "Demonstration programming and optimization method of cooperative robot based on multi-source information fusion," *Jiqiren/Robot*, vol. 40, no. 4, pp. 551–559, 2018.

[5] J. Wan, J. Yang, S. Wang, D. Li, P. Li, and M. Xia, "Cross-network fusion and scheduling for heterogeneous networks in smart factory," *IEEE Transactions on Industrial Informatics*, vol. 16, no. 9, pp. 6059–6068, 2020.

[6] W. Liu, Q. Lü, Z. Cheng, G. Xing, and C. Chen, "Multi-element geochemical data mining: implications for block boundaries and deposit distributions in South China," *Ore Geology Reviews*, vol. 133, article 104063, 2021.

[7] L. Yi, S. Ji, L. Ren, R. Su, and Y. Liang, "A nonlinear feature fusion-based rating prediction algorithm in heterogeneous network," *IEEE Transactions on Computational Social Systems*, vol. 8, no. 3, pp. 728–736, 2021.

[8] Q. Li, Q. Xiong, S. Ji, M. Gao, Y. Yu, and C. Wu, "Multi-view heterogeneous fusion and embedding for categorical attributes on mixed data," *Soft Computing*, vol. 24, no. 14, pp. 10843–10863, 2020.

[9] Y. Liu, "Research on heterogeneous data fusion algorithm based on IoT," *Revista de la Facultad de Ingenieria*, vol. 32, no. 4, pp. 549–556, 2017.

[10] I. Alqerm and B. Shihada, "Sophisticated online learning scheme for green resource allocation in 5G heterogeneous cloud radio access networks," *IEEE Transactions on Mobile Computing*, vol. 17, no. 10, pp. 2423–2437, 2018.

[11] A. Ishaq, S. Sadiq, M. Umer, S. Ullah, and M. Nappi, "Improving the prediction of heart failure patients' survival using smote and effective data mining techniques. IEEE," *Access*, vol. 9, pp. 39707–39716, 2021.

[12] Y. Liu, D. Chen, A. Ma, Y. Zhong, and K. Xu, "Multiscale u-shaped CNN building instance extraction framework with edge constraint for high-spatial-resolution remote sensing imagery," *IEEE Transactions on Geoscience and Remote Sensing*, vol. 59, pp. 1–15, 2020.

[13] L. Zhang and Y.-C. Liang, "Deep reinforcement learning for multi-agent power control in heterogeneous networks," *IEEE*

Transactions on Wireless Communication, vol. 20, no. 4, pp. 2551–2564, 2020.

[14] S. Baloch and M. S. Muhammad, "An intelligent data mining-based fault detection and classification strategy for microgrid. IEEE," *Access*, vol. 9, pp. 22470–22479, 2021.

[15] Q. Liu, Q. Dou, L. Yu, and P. A. Heng, "MS-Net: multi-site network for improving prostate segmentation with heterogeneous MRI data," *IEEE Transactions on Medical Imaging*, vol. 39, no. 9, pp. 2713–2724, 2020.

[16] W. Chen, Z. Yin, and T. He, "Enabling global cooperation for heterogeneous networks via reliable concurrent cross technology communications," *IEEE Transactions on Mobile Computing*, vol. PP(99), pp. 1–1, 2021.

[17] F. Fang, G. Ye, H. Zhang, J. Cheng, and V. C. M. Leung, "Energy-efficient joint user association and power allocation in a heterogeneous network," *IEEE Transactions on Wireless Communications*, vol. 19, no. 11, pp. 7008–7020, 2020.

[18] K. Yang, H. Song, K. Zhang, and J. Fan, "Deeper Siamese network with multi-level feature fusion for real-time visual tracking," *Electronics Letters*, vol. 55, no. 13, pp. 742–745, 2019.

[19] S. Fu, G. Zhang, and T. Fujii, "A heuristic method-based parallel cooperative spectrum sensing in heterogeneous network," *Journal of Supercomputing*, vol. 75, no. 6, pp. 3249–3263, 2019.

[20] N. Zhao, Y. C. Liang, D. Niyato, Y. Pei, and Y. Jiang, "Deep reinforcement learning for user association and resource allocation in heterogeneous cellular networks," *IEEE Transactions on Wireless Communications*, vol. 18, no. 11, pp. 5141–5152, 2019.

[21] W. Yi, Y. Yuan, R. Hoseinnezhad, and L. Kong, "Resource scheduling for distributed multi-target tracking in netted colocated MIMO radar systems," *IEEE Transactions on Signal Processing*, vol. 68, pp. 1602–1617, 2020.

Hindawi
Wireless Communications and Mobile Computing
Volume 2022, Article ID 4927504, 10 pages
https://doi.org/10.1155/2022/4927504

Research Article

Computer Network Confidential Information Security Based on Big Data Clustering Algorithm

Weigang Liu

College of Information Engineering, Tianjin Modern Vocational Technology College, Tianjin 300350, China

Correspondence should be addressed to Weigang Liu; liuweigang1981@stu.wzu.edu.cn

Received 15 March 2022; Revised 21 April 2022; Accepted 28 April 2022; Published 9 June 2022

Academic Editor: Jun Ye

Attacks on network systems are becoming more and more common, the current state of increasingly sophisticated attack methods, the emergence of intrusion prevention technology is the inevitable result of the development of computer technology and network technology, and research on intrusion prevention has become a new focus of network security technology research in recent years. In order to ensure the security of computer network confidential information, the authors propose a semisupervised clustering intrusion detection algorithm. An overview of machine learning, followed by an explanation of the theory of cluster analysis, simulation experiments were carried out using the K-means algorithm and the semisupervised clustering algorithm proposed by the author, for 10,000 records, the K-means clustering algorithm and the semisupervised clustering algorithm described in this paper are used, respectively, and intrusion detection data tests were performed. At the same time, different K values were selected, three datasets were selected from "kddcup.newtestdata_10_percent_corrected," the test data were tested separately, and their average value was taken as the test result. From the simulation results, the detection rate of the semisupervised clustering algorithm is higher than that of the K-means clustering algorithm, and the false alarm rate and K-means algorithms have also been improved. Therefore, the author's semisupervised algorithm enhances the stability of the system, and the performance of the K-means algorithm is improved to a certain extent. When the value of K gradually increases, the false alarm rate also increases; however, when K is 20, the detection rate is maximized, from this, it can be known that when K is 20, its detection rate reaches 91.76%, and the false alarm rate is 8.54%. The detection rate of the author's algorithm is significantly higher than the other two algorithms, the false positive rate is slightly higher than K-means, and the false positive rate is lower than that of the other algorithm, proving the superior performance of our algorithm.

1. Introduction

With the continuous updating of computer Internet technology, it has gradually been applied in various fields, it has had a huge impact on people's lives and work, a large amount of data information has exploded, and it involves a lot of private information. Aerospace transportation, as an extremely important information industry in the development of modern society, it is related to classified information security and aerospace security and is also closely related to the stable development of social security. The spread of the Internet, so that everyone will be exposed to the Internet in their daily lives, personal information data security also has certain threats and risks. Therefore, strengthening the management and protection of computer network information security is a very important project [1]. In the process of designing and implementing computer network information security protection, Bayesian classification algorithm is one of the most common methods and has achieved significant research results, considering the growing maturity of big data clustering algorithm, the scope of application is also getting wider and wider, and more well-known technical achievements are gradually born [2]. At present, the research on computer network information security protection strategies is still in its infancy, especially the correlation between different target attributes, the

proportion of nonlinear relationship occupies more than half, if the conventional method is used, it is difficult to fully reflect the actual relationship, and in the process of analysis, there will also be contradictions, and disorders are likely to occur. In the process of computer network information transmission, because the network itself has certain security risks, this is also a relatively common information security risk, it is also affected by human factors, there will be more and more unsafe factors in the existence of information [3]. The most common network information security problems are as follows: the first is the vulnerability of TCP/IP, the second is the insecurity of the network structure, the third is the possibility of information being stolen, and the fourth is the weak awareness of safety management of relevant staff [4]. Computer network technology is inseparable from the TCP/IP protocol, TCP/IP is vulnerable, the main reason is that the protocol does not pay enough attention to computer network security issues, and the TCP/IP protocol reflects the openness of the network more. This also gives attackers an opportunity to take advantage of, attackers open up the environment through the network, find loopholes, and attack the network, resulting in various information security problems. The computer network system has security risks, mainly because the network system is composed of countless local area networks, this also makes the computer network very large, if there is a communication behavior, there may be a risk of being attacked, the attacker only needs to pass a host, can operate, steal information and data, and continue to carry out the next attack. Computer network information has great security risks and is easy to be stolen, the main reason is that in the computer network, a large amount of data information has not been encrypted, when users use the computer network, they also use some free software, there will be some security risks, and gives attackers an opportunity to exploit vulnerabilities to eavesdrop. During the operation of computer users, due to the lack of security awareness, there will also be greater security risks, although the current computer network also has certain security protection mechanisms and measures; however, users do not make full use of security protection mechanisms and measures [5]. For example, some users think that the firewall is very troublesome and affect their use of some software, so they choose to close the firewall, in the case of not obtaining the authentication of the firewall proxy server, and the PPP connection, as a result, the firewall is useless, and the potential security risks may break out at any time [6]. There are many factors that threaten the security of computer network information, among which, hacking is one of the most common factors, hackers are one of the biggest threats to modern computer network systems, if the network is attacked by hackers and the server is damaged, it cannot provide normal services for users, as a result, the network is paralyzed, resulting in very serious consequences. Intrusion prevention system combines the functions of intrusion detection and firewall, it can monitor network traffic, timely interruption, adjustment or isolation of intrusion behavior is an active and resourceful intrusion defense system [7]. Figure 1 shows the application deployment of intrusion prevention.

2. Literature Review

In recent years, with the improvement of hardware performance and the gradual improvement of medical networks, a large number of breast cancer diagnosis and treatment plans based on machine learning algorithms have been proposed, for example, Xiong et al. applied SVM classifier and Naive Bayes classifier to diagnose breast cancer data [8]. Kim et al. propose a breast cancer diagnosis scheme that mixes k-means clustering algorithm and SVM classifier. The scheme first uses the k-means clustering algorithm to identify the hidden patterns of benign and malignant breast cancer and set up an effective value to measure the clustering effect to determine the optimal number of clusters. Then, the similarity between the data and the hidden pattern is measured by the membership function, the dimensionality reduction of the data is realized, and finally, the breast cancer data is classified and diagnosed through the SVM classifier [9]. Al-Salhi et al. based on logistic regression algorithm and decision tree algorithm, analysis of prognostic factors for breast cancer [10]. Qian et al. proposed a safe outsourcing drug detection system based on DT-PKC encryption system, the system classification is completed by the SVM algorithm, and privacy protection is achieved by designing a secure multiparty protocol [11]. Yao et al. based on the fully homomorphic encryption algorithm, in the ciphertext domain, the minor allele frequencies and chi-square detection in genome-wide association analysis are calculated and support the calculation of Hamming distance and approximate edit distance for encrypted DNA sequences [12]. Meng et al. based on the BGV fully homomorphic encryption scheme, a secure mobile medical model using edge computing technology is proposed, provide health data diagnosis and analysis for members of the smart medical system, the calculation types are k-means clustering and fuzzy c-means clustering [13]. Monteith et al. proposed differential privacy protection technology, which is a strictly defined privacy protection model, it is resistant to all attacks based on background knowledge assumptions. The main principle is to achieve privacy protection by adding random noise to distort the original data, but at the same time, it does not affect the statistical properties of the original data [14]. Kirubakaran and Ilangkumaran proposed a fully dynamic fully homomorphic encryption scheme, and the scheme no longer limits the number of allowable parties [15]. Based on the BGV encryption scheme, Ge et al., a BGV-type multikey fully homomorphic scheme CZW is constructed, and the security of the scheme is based on the LWE problem on the ring. Compared with the GSW-type multikey fully homomorphic scheme, the CZW scheme has simpler ciphertext expansion, and the encryption method is no longer by bit encryption, but can encrypt ring elements. In addition, the scheme also supports technical acceleration such as batch processing, and the computational efficiency is higher than that of the GSW-type multikey fully homomorphic encryption scheme [16]. Based on the BCP encryption algorithm with double decryption mechanism, Cui et al., an outsourced secure multiparty computation framework is proposed. The scheme uses two noncollusion cloud servers,

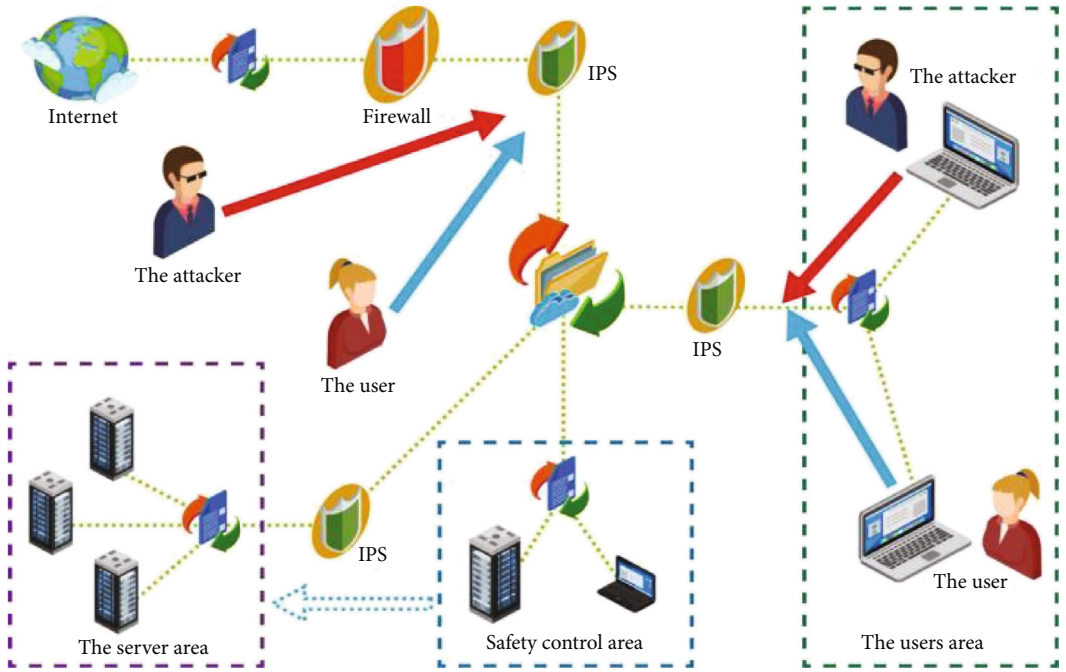

Figure 1: Application deployment of intrusion prevention.

one for storage and computing, a master private key that contains decryptable user data, realizes computing outsourcing by constructing a secure protocol [17]. This paper is an overview of machine learning, followed by an explanation of the theory of cluster analysis. Analyzing the author's intrusion detection method, and comparing it with several other common intrusion detection algorithms, for example, the correct can be established to improve the detection accuracy, the false alarm rate is reduced, and the robustness of the system is enhanced. In the author's algorithm, a small number of labeled samples provide correct guidance for the initial formation of normal and abnormal cloud models. The dynamic weighting method is used to solve the problem that high-level data is difficult to process, enable the data to learn from each other, and gradually form a relatively stable cloud model, and over-reliance on prior knowledge of the data is avoided. In contrast, the performance of the author's algorithm relative to the general clustering algorithm has greatly improved, for a certain extent, it solves some problems existing in the current intrusion detection.

3. Methods

3.1. Overview of Machine Learning. With the development of computers, machine learning has penetrated into many fields such as pattern recognition, data mining, and computer graphics. Machine learning is based on different classification basis, and there are different classification methods. According to whether the training sample data used in the training process has label information, machine learning can be divided into unsupervised learning, supervised learning, supervised learning, and semisupervised learning [18].

3.1.1. Unsupervised Learning. Unsupervised learning is a kind of unclassified data information for analysis and recognition, at the same time, cluster-related knowledge can be applied to unsupervised learning, in order to analyze the sample data and predict the category information of the sample. In unsupervised learning, a set of known samples:

$$X = (x_1, x_2, \cdots, x_n). \tag{1}$$

The sample is independent and identically distributed, thus, a research method for unsupervised learning is to define a $(n \times d)$ matrix whose rows represent samples:

$$X = \left(x_i^T\right)_{i\in[n]}^T. \tag{2}$$

The purpose of unsupervised learning is to discover the different structural information and laws contained in the matrix X.

Unsupervised learning does not pretrain on training samples, there is also no supervision information available, and the feature library of the samples cannot be established. If the classifier continues to accept a large number of edge test samples, it may affect the classification accuracy, resulting in misclassification [19].

3.1.2. Supervised Learning. Supervised learning is a traditional machine learning method, and it utilizes the prior knowledge provided by the system (such as the labeled class information of the sample, pairwise constraint information, and prior probability), learns the known training sample set, adjusts the parameters of the classifier, and establishes a sample learning model, then, the classification of unknown

samples is realized according to the sample model [20]. In supervised learning, the sample set X and the class label of the sample:

$$Y = (y_1, y_2, \cdots, y_n). \quad (3)$$

This is known, where y_i is the class label corresponding to sample x_i, and data pair (x_i, y_i) constitutes the training set of samples needed to construct the learner. Supervised learning, hoping to find the mapping relationship between x and y through the known training set, constructs the required learner accordingly.

Labeled data is often difficult to obtain in supervised learning, and it is necessary to establish a feature library in the training phase of supervised learning, and this will easily lead to the features of the new data may not match the features in the library, resulting in the possibility of misclassification.

3.1.3. Semisupervised Learning. Semisupervised learning is a method between unsupervised learning and supervised learning, the data set used in its learning process usually contains a small amount of labeled information, through these samples of identification information, constraints guide the learning of unknown samples [21].

In semisupervised learning, the entire dataset $X = (x_1, x_2, .., x_n)$ is divided into two parts: known labeled dataset $X = (x_1, x_2, .., x_l)$, corresponding labeled $Y = (y_1, y_2, .., y_l)$, and unknown labeled datasets:

$$X_u = (x_{l+1}, x_{l+2}, \cdots, x_{l+u}). \quad (4)$$

The main content to be studied in semisupervised learning, it is how to comprehensively utilize labeled samples and unlabeled samples.

According to different learning methods, common semisupervised learning algorithms can be classified into the following categories:

(1) *Generative Model Algorithm*. Such algorithms usually use generative models as learners, the probability of dividing unlabeled samples into each class is regarded as a set of missing parameters, then apply the EM (expectation—maximization; expectation maximization) algorithm, estimate feature labels and model parameters. This algorithm is a widely used method in the early days and can be regarded as clustering within the range of a small number of labeled samples

(2) *Based on the Graph Regularization Algorithm*. This kind of algorithm usually adopts the manifold assumption and generally builds a graph based on the training samples and the relationship between them, the connecting line in the figure represents the similarity between samples, then, define the objective function to be optimized, based on the smoothness of the graph as regularization, use the decision function to find the optimal model parameters

(3) *Cotraining Algorithms*. These methods use two or more classifiers and improve classification accuracy through collaboration between classifiers. The classifier trained each time marks the unlabeled samples and selects samples with higher confidence to add to each other's training sets, this is continuously updated until a certain condition is met, thereby, the classification interface is gradually updated

3.2. Cluster Analysis Theory

3.2.1. Definition of Cluster Analysis. A class or cluster is a collection of data objects, the data objects in the same cluster are similar to each other, unlike objects in other clusters. From a machine learning point of view, cluster analysis is a type of supervised learning [22]. Before performing cluster analysis on the data, we do not know how many categories we will eventually divide into, instead, it is clustered according to the similarity of information between the data; finally, the similarity between individuals of the same class is maximized, while the similarity between individuals of different classes is minimized.

3.2.2. Basic Steps of Clustering. The clustering methods adopted for different problems are also different, but they are all based on a specific process frame, as shown in Figure 2, broadly speaking, most clustering methods have four steps: feature selection or feature extraction, clustering algorithm design or selection, cluster confirmation, and result interpretation. It is also a process of transforming useless data into useful knowledge. In a narrow sense, clustering includes the design and selection of clustering algorithms, the process of clustering confirmation, and the interpretation of results.

3.2.3. Classification of Clustering Methods. (1) Partitioning method: this kind of method is easy to describe and simple to implement, and it is also the most studied clustering method, the division method requires a given number of clusters k to be divided into, when classifying, it is first necessary to obtain a set of k initial divisions, then adopt the method of iterative relocation, and improve the quality of partitioning by moving data objects from one cluster to another [23]. The process can be represented as a binary hierarchical tree, the leaf node represents a data object, the middle point indicates that the dataset is split into two distinct classes, or a class is merged from its two subclasses. Density-based methods break through this limitation, the main idea is to give a density threshold, as long as the point in the region is higher than the threshold, it is assigned to the cluster close to it, that is, the purpose of clustering is achieved by finding high-density regions divided by low-density. (2) Grid-based method (grid-based method): grid-based methods first quantify the object space and are divided into a certain number of cells, which are called grids, and the next clustering operation is performed in this quantized grid structure. (3) Model-based method: assuming that a given

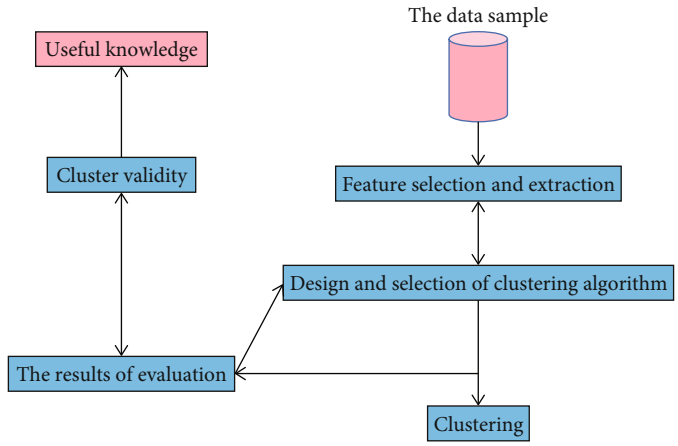

Figure 2: Clustering process diagram.

data distribution has underlying regularities, then, model-based methods try to find out this pattern, find some kind of mathematical model, and fit it to the given data.

3.3. K-Means Algorithm. The K-means algorithm is the most classic division method, K-means is a centroid-based technique, it takes k as a parameter and divides n objects into k clusters, in order to have a high similarity within the class, and the intraclass similarity is lower. The flow of the K-means algorithm is as follows.

Algorithm 1. Input: Parameter k, n data objects.
Output: k clusters.
Step:
(1) Select k points as the initial centroids
(2) repeat
(3) Assign n data objects to the nearest centroids to form k clusters
(4) Recalculate the centroid of each cluster
(5) until the centroid no longer changes.

The K-means algorithm has the advantages of simple use, fast convergence, and low memory overhead, at the same time, there are some shortcomings, such as the performance of the algorithm depends on the initialized k cluster prototypes, and the clustering performance is unstable, sensitive to noise outliers, etc.

3.4. Semisupervised Clustering Algorithm. Semisupervised clustering is a new clustering method, and it combines the characteristics of supervised learning and unsupervised learning, using a small amount of labeled data as supervision information improves the quality of clustering [24]. Depending on how supervised information is used, semisupervised clustering can be divided into three categories:

(1) Such methods use clustering to constrain the search process of clusters using supervisory information and guide the algorithm to obtain good clustering results. Typical algorithms include COP-K-means method, seed-K-means, and constrained-K-means

(2) *Distance-Based Semisupervised Clustering Method.* Such methods utilize identifying data, train a similarity metric that satisfies constraint information or categories, and then use distance-based clustering algorithm for clustering

(3) *Method Based on Constraint and Distance Fusion (Constraint and Distance-Based Semisupervised Clustering Method).* This type of method combines the above two methods to use, one of the typical algorithms is MPC-K-means algorithm

Semisupervised clustering algorithms have been widely used in practical fields, and these include biological information processing, image processing, text classification, and intrusion detection [25]. According to the needs of the subsequent intrusion detection algorithm, the semisupervised clustering algorithm process adopted by the author is as follows.

Algorithm 2. Input: Parameter k, labeled dataset S_l, unlabeled dataset S_u.
Output: k clusters
(1) Use the labeled data in S_l to determine L initial cluster centroids
(2) $\forall x \in S_u$ calculates the minimum distance from each cluster centroid, take the data point corresponding to the maximum value of the minimum distance, as the centroid of the next cluster, record it as the L+1 centroid
(3) $\forall x \in S_u$ calculates its distance from each cluster centroid, assign x to the cluster to which the centroid with the smallest distance belongs, and update the centroid of each cluster
If the cluster centroid is k, repeatedly assigning each data point in S_l and S_u to the cluster to which the cluster centroid with the smallest cluster distance belongs, recalculate the centroid of each cluster, otherwise turn to step (2);
(4) Cluster the k cluster centroids until the cluster centroids no longer change
(5) Output k clusters.

In the initial stage of the above algorithm, the initial cluster center is generated by using the label information of the

data, make the initial cluster center controllable, the robustness of the system is enhanced by the method of gradually generating cluster centers, and the convergence speed and accuracy of the clustering algorithm have been improved.

3.5. Cloud Model-Based Semisupervised Clustering Intrusion Detection Algorithm. Whether it is a K-means clustering algorithm or a semisupervised clustering algorithm, there is a problem of threshold division in the intrusion detection algorithm, the value of the threshold directly affects the detection result, and in practice, it cannot flexibly respond to intrusion situations. Furthermore, the application of general cloud model classifiers in intrusion detection, it is often implemented through an association rule generator, which is slow in processing, considering the properties of network data is not comprehensive, in practical applications, it cannot cope with the complex and changing network environment. Based on the above methods, the author combines the algorithm of semisupervised clustering and the characteristics of cloud model, this aspect does not require thresholding after the initial clustering, extract relevant data directly from a small amount of identification information, build a cloud model classifier, and use a dynamic weighting method in the classification process, and the flexible use of real-time detection data makes the weighting method more reasonable. After a certain data is classified, the data record and other data learn from each other, continuously adjust the cloud model, enhancing its classification ability, the classifier can adapt to the changing network environment.

3.5.1. Relative Proximity of Clouds. Cloud relative closeness is proposed on the basis of cloud model theory, it reflects the degree of similarity between clouds and fully express the randomness and ambiguity of evaluating language concepts, and it is in line with people's subjective feelings and has greater objectivity. Its specific definition is as follows.

Suppose there are two clouds $A1(Ex1, En1, He1)$ and $A2(Ex2, En2, He2)$ in the universe of discourse space U, define $D_{1,2} = |Ex1 - Ex2|$, then, $D_{1,2}$ reflects the relative closeness of the two clouds.

3.5.2. Weighted Intrusion Detection Algorithm. The reverse cloud generator obtains the digital features of the cloud from the real training set, form judgment rules, realize normal modeling, in practice, this method requires a large amount of training data and training time, the cloud digital eigenvalues obtained from the training data does not reflect the actual situation at the time of the invasion, and the calculation of attribute weights in the article is too subjective, at the same time, it is very difficult to determine the threshold value during detection.

The author first uses a semisupervised clustering algorithm to cluster the dataset, then, the results of the clustering are arranged in order of the size of the clusters, at the same time, the normal data clusters and abnormal data clusters are preliminarily screened out according to the tag information, use the data in the cluster to build a normal cloud model and an abnormal cloud model, with the improved 1D inverse cloud generator and X-condition cloud generator, build a cloud model classifier to classify the remaining data objects, at the same time, the classification adopts the method of continuously updating the cloud model and recalculating the weight of each attribute, in order to guide the classification of data. Since the relative closeness of the cloud has greater objectivity, the author refers to this concept for the setting of attribute weights, that is, assuming that the normal cloud is Al in intrusion detection, the abnormal cloud is A2, then, when building a cloud model for each dimension attribute, the size of $D_{1,2}$ reflects the degree of difference between normal clouds and abnormal clouds and the relative importance of this attribute in the classification process. Using this method to weight attributes is in line with people's cognition of the concept of things, the dynamic weighting method can make full use of the implicit information of the data itself, and the weighting method is more scientific.

The steps of the intrusion detection method based on semisupervised clustering are as follows.

Algorithm 3. Input: A dataset S containing nd-dimensional data, $S = S_l \cup S_u$ (labeled dataset S_l, unlabeled dataset S_u).

Output: The data type of data $x \in S_u$ (normal or abnormal).

(1) Use the semisupervised clustering algorithm in 4.4 to cluster the dataset S

(2) Arrange the clustering results in ascending order according to the size of the clusters

(3) Combined with the label information of the data, the initial normal clusters and abnormal clusters are screened out as C_n and C_a, respectively, the rest of the data is allocated into C_r

(4) For each dimension of data in C_n, the corresponding cloud digital eigenvalue $(Ex1_i, En1_i, He1_i), i = 1, \cdots, d$ is obtained by using the reverse cloud generator

(5) For each dimension of data in C_a, use the reverse cloud generator to obtain the corresponding cloud digital eigenvalue $(Ex2_i, En2_i, He2_i), i = 1, \cdots, d$

(6) Use formula (5) to calculatse the weight of each attribute

$$w_i = \frac{|Ex1_i - Ex2_i|}{\sum_{j=1}^{d} |Ex1_j - Ex2_j|}, \tag{5}$$

(7) Take a data object x from C_r in turn, according to the X-condition forward cloud generator using the formula, the abnormal and normal cloud classification models are calculated:

$$\mu_j = \sum_{i=1}^{d} w_i \cdot \exp\left[\frac{-(x - Exj_i)}{2 \cdot Enj_i}\right], j = 1, 2. \tag{6}$$

If $\mu_1 > \mu_2$ then x belongs to the normal class, assign it to C_n, after returning to step (4) to update the normal cloud model, go to step (6) to recalculate the weight of each attribute, otherwise, assign x to C_a and return to step (5) after updating the abnormal cloud model, then, go to step (6) to

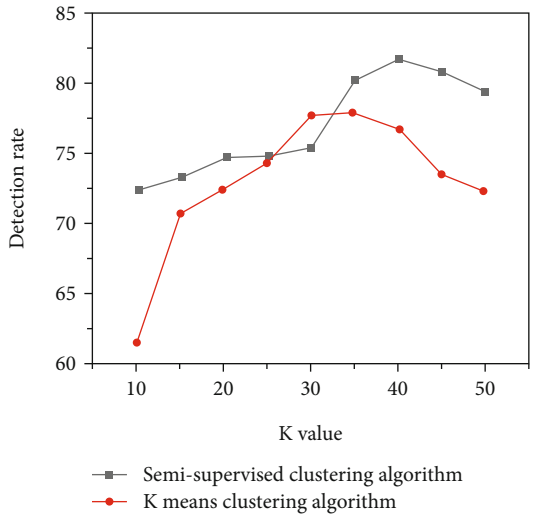

Figure 3: Comparison of detection rate detection results.

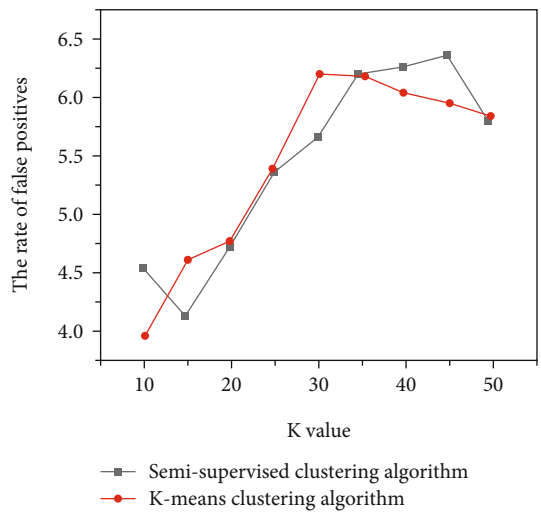

Figure 4: Comparison of false positive rate detection results.

recalculate the weight of each attribute until all data classification ends.

4. Results and Analysis

4.1. Semisupervised Clustering Algorithm Experimental Data Selection and Preprocessing. Since the original dataset is too large, we select some representative data for experiments, a subset U was selected for testing from "kddcup.newtestdata_10__percent_corrected," and selected 500 records as identification data records, 10000 records as test data, among them, 758 were DoS attacks, 15 were R2L attacks, 42 were U2R attacks, and 92 were probe attacks.

In the experiment, we use the experimental platform based on MATLAB, the KDDCUP99 dataset contains symbolic data attributes, which cannot be recognized by MATLAB; therefore, it is necessary to renumber the attribute value of the symbol type and use the natural number set to renumber the seven values, taking protocol_type as an example, tcp, udp, and icmp are replaced by natural numbers 1, 2, and 3, respectively. And so on, the original data will become a numeric type. There are two types of numerical variables, one is a continuous attribute characteristic variable, and the other is a discrete attribute characteristic variable. For continuous attribute feature variables, attribute characteristics of different attributes may have different metrics, if before experimenting, if the data is not preprocessed, there may be a problem of large numbers eating decimals, as a result, the attribute characteristics of some values are masked, thereby affecting the experimental results, therefore, in the process of data preprocessing, it is necessary to normalize and normalize attribute values.

4.1.1. Standardization.

$$x_{ij} = \frac{x_{ij} - m_j}{S_j}, \quad (i = 1, \cdots, n\,; j = 1, \cdots, r). \tag{7}$$

Among

$$m_j = \frac{1}{n}\sum_{i=1}^{n} x_{ij}, \qquad s_j = \sqrt{\frac{1}{n-1}\left(x_{ij} - m_j\right)^2}. \tag{8}$$

4.1.2. Normalization.

$$x_{ij}{}' = \frac{x_{ij} - \min\left(x_{ij}\right)}{\max\left(x_{ij}\right) - \min\left(x_{ij}\right)}. \tag{9}$$

Among $i = 1, \cdots, n\,; j = 1, \cdots, r$.

4.2. Simulation Experiment and Result Analysis. The experiments were run on a machine with CPU 2.2 GHz, 2.00 GB, Microsoft Windows XP, and adopt MATLAB7.8.0 to realize. In order to evaluate the performance of intrusion detection methods, the experiment adopts detection rate and false alarm rate as the metrics of algorithm performance. Its definition is as follows:

$$\text{Detection rate} = \frac{\text{number of detected attacks}}{\text{total number of attacks}}, \qquad \text{False positive rate} = \frac{\text{the number of normal samples that were falsely reported as intrusions}}{\text{the number of normal samples}}. \tag{10}$$

Table 1: Experimental test data table.

Test data	Quantity	DoS (%)	R2L (%)	U2R (%)	Probe (%)
Dataset 1	5844	3.56	0.87	0.55	1.18
Dataset 2	5836	3.72	0.87	0.46	1.18
Dataset 3	5737	3.78	0.89	0.45	1.29

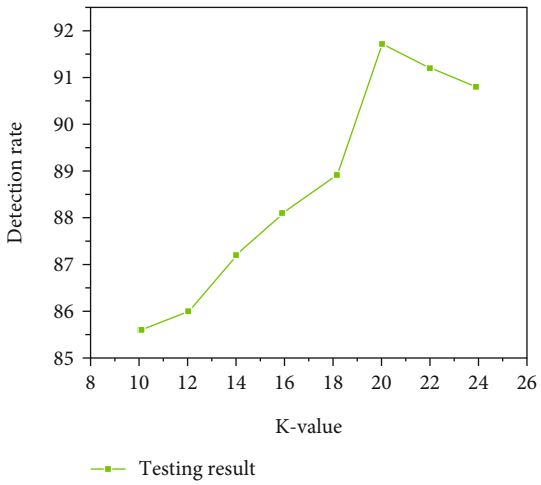

Figure 5: Detection rate under different K values.

For the above 10,000 records, the K-means clustering algorithm and the semisupervised clustering algorithm described by the author were used, respectively, intrusion detection data tests were performed, Figures 3 and 4 show that under different K values, average detection rate and false positive rate under the K-means clustering algorithm and the authors' semisupervised clustering algorithm.

By comparison, it can be seen that the detection rate of the author's semisupervised clustering algorithm is higher than that of the K-means clustering algorithm, and the false alarm rate and K-means algorithms have also been improved. Therefore, the author's semisupervised algorithm enhances the stability of the system, and the performance of the K-means algorithm is improved to a certain extent.

4.3. Experimental Data Selection of Semisupervised Clustering Intrusion Detection Algorithm. Experimental simulation of semisupervised clustering intrusion detection algorithm for cloud model, three sets of data sets were selected for testing from "kddcup.newtestdata_10_percent_corrected," at the same time, 500 pieces of data are selected as identification data records. The test data types and distributions are shown in Table 1.

Among them, the attacks of Do S are smurf and neptune; the attacks of R2L are guess passwd; U2R's attack is buffer_overflow, land module, perl, and rootkit; and probe's attack is port sweep.

4.4. Simulation Experiment and Result Analysis. Different K values were selected to test the above three sets of data, respectively, take their average as the detection result. Figures 5 and 6 show the detection results of the cloud

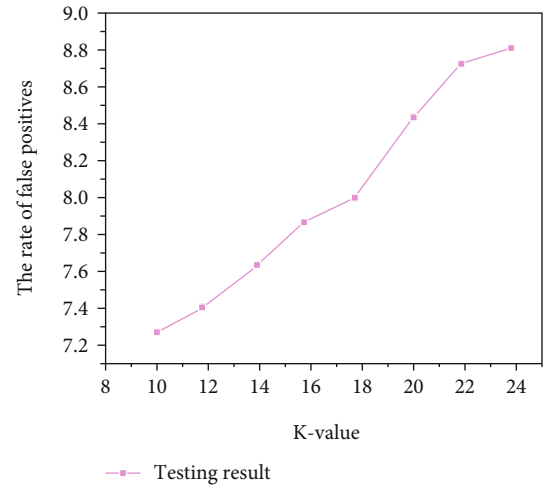

Figure 6: False alarm rate under different K values.

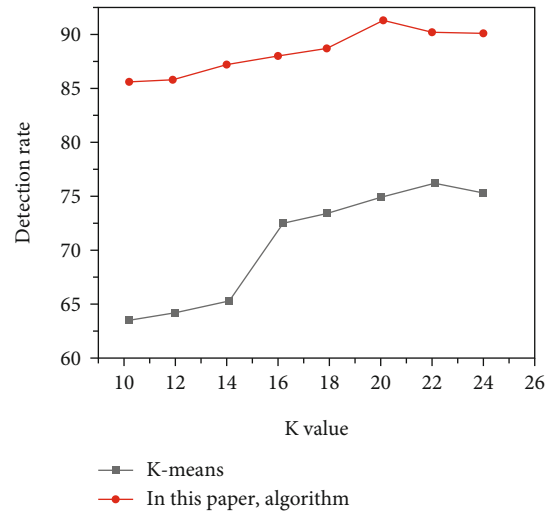

Figure 7: Comparison of detection rate results under different K values.

model semisupervised clustering algorithm under different K values.

From the experimental results in the figure, it can be seen that, when the value of K gradually increases, the false alarm rate also increases; however, when K is 20, the detection rate is maximized. From this, it can be known that when K is 20, the semisupervised clustering algorithm based on cloud model can obtain better intrusion detection effect, its detection rate reaches 91.76%, and the false alarm rate is 8.54%. In the cloud model-based semisupervised clustering algorithm, the detection rate and false alarm rate when K takes different values are compared with the K-means algorithm, as shown in Figures 7 and 8.

As can be seen from the above figure, in the case of different values of K, the author's algorithm is significantly higher than the K-means algorithm in terms of detection rate, the false positive rate is slightly higher than that of K-means, but this false positive rate is within an acceptable range.

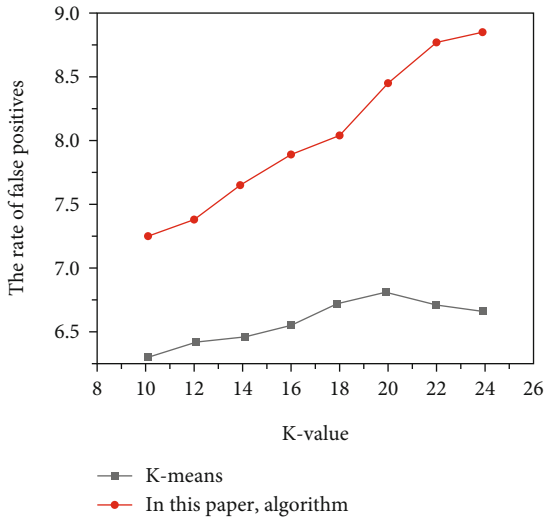

Figure 8: Comparison of false alarm rate results under different K values.

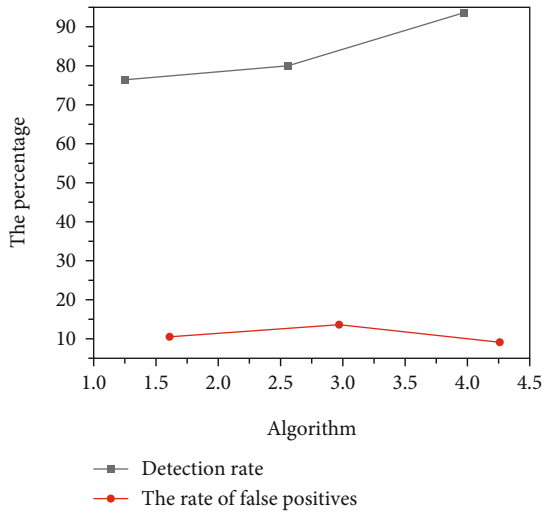

Figure 9: Comparison of test results.

The detection results of the cloud model-based semisupervised clustering algorithm, and the comparison results of the general clustering algorithm and the general cloud model classifier, are shown in Figure 9.

The above figure shows the comparison between the detection results of the author's algorithm and several other algorithms, by comparison, it can be found that the detection rate of the author's algorithm is significantly higher than the other two algorithms, and the false positive rate is slightly higher than that of K-means, the false positive rate is lower than that of the other algorithm, proving the superior performance of our algorithm.

5. Conclusion

The author proposes a research on computer network confidential information security based on big data clustering algorithm, intrusion detection data has the characteristics of high-dimensional attributes, currently, cloud model classifiers can only handle one-dimensional and two-dimensional data, and the traditional intrusion detection method based on semisupervised learning relies heavily on prior knowledge. In order to solve the above problems, the author proposes a semisupervised clustering intrusion detection algorithm based on cloud model, a new cloud model classifier is constructed, and make full use of a small number of labeled samples and unlabeled samples to guide the classification of data. For the semisupervised clustering intrusion detection algorithm proposed by the author, the simulation experiment of the intrusion detection method based on cloud model semisupervised clustering is done. Analyzing the author's intrusion detection method and comparing it with several other common intrusion detection algorithms, the results show that the method proposed by the author improves the performance of the intrusion detection system, the detection accuracy is improved, the false alarm rate is reduced, and the robustness of the system is enhanced. In the author's algorithm, since there are few labeled samples, it provides correct guidance for the initial formation of normal and abnormal cloud models. The dynamic weighting method is used to solve the problem that high-level data is difficult to process and enable the data to learn from each other and gradually form a relatively stable cloud model, and over-reliance on prior knowledge of the data is avoided. In contrast, compared with the general clustering algorithm, the author's algorithm has a great improvement in performance, to a certain extent, solve some problems existing in the current intrusion detection, however, there are still some problems, such as the false positive rate is still high, and it is sensitive to some data with special distribution and cannot obtain a good classification effect, in future research, further improvements to the algorithm are still needed.

Data Availability

The data used to support the findings of this study are available from the corresponding author upon request.

Conflicts of Interest

The author do not have any possible conflicts of interest.

References

[1] Y. Guo and S. Yan, "Research on hospital computer network topology based on complex network theory," *Basic & Clinical Pharmacology & Toxicology*, vol. 118, 1, pp. 114–114, 2016.

[2] Y. Chen, H. Zhang, L. Liu, X. Chen, and J. Xie, "Fuzzy risk analysis based on the ranking of generalized trapezoidal fuzzy numbers," *Applied Intelligence*, vol. 26, no. 1, pp. 1–11, 2007.

[3] Y. Lun, X. Zhang, and J. Q. Zhao, "Research on prediction method of anti viral polymer drug efficacy based on neural network algorithm," *Basic & Clinical Pharmacology & Toxicology*, vol. 119, no. 4, pp. 46–46, 2016.

[4] G. Wang, X. Tian, J. Geng, and B. Guo, "A knowledge accumulation approach based on bilayer social wiki network for computer-aided process innovation," *International Journal of Production Research*, vol. 53, no. 8, pp. 2365–2382, 2015.

[5] R. Sharma, V. Vashisht, and U. Singh, "Woatca: a secure and energy aware scheme based on whale optimisation in clustered wireless sensor networks," *IET Communications*, vol. 14, no. 8, pp. 1199–1208, 2020.

[6] Q. Ding, Y. Wu, and W. Liu, "Molecular mechanism of reproductive toxicity induced by Tripterygium wilfordii based on network pharmacology," *Medicine*, vol. 100, no. 27, article e26197, 2021.

[7] Y. J. Liang, C. Ren, H. Y. Wang, Y. B. Huang, and Z. T. Zheng, "Research on soil moisture inversion method based on ga-bp neural network model," *International Journal of Remote Sensing*, vol. 40, no. 5-6, pp. 2087–2103, 2019.

[8] W. Xiong, C. M. Cheung, P. Sander, and A. Joneja, "Rationalizing architectural surfaces based on clustering of joints," *IEEE transactions on visualization and computer graphics*, vol. 1, p. 1, 2021.

[9] D. H. Kim, K. H. Choi, K. J. Li, and Y. S. Lee, "Performance of vehicle speed estimation using wireless sensor networks: a region-based approach," *Journal of Supercomputing*, vol. 71, no. 6, pp. 2101–2120, 2015.

[10] A. A. L.-S. Ye and S. Lu, "Quantum image steganography and steganalysis based on lsqu-blocks image information concealing algorithm," *International Journal of Theoretical Physics*, vol. 55, no. 8, pp. 3722–3736, 2016.

[11] P. Qian, T. Shang, Y. Gao, and G. Ding, "Research on dynamic handover decision algorithm based on fuzzy logic control in mobile fso networks," *Photonic Network Communications*, vol. 41, no. 2, pp. 136–147, 2021.

[12] B. Yao, L. Wang, and S. Liu, "Research on ocean government data extraction and clustering based on xml document similarity technology," *Journal of coastal research*, vol. 98, no. sp1, p. 259, 2019.

[13] Y. Meng, Y. Chen, F. Zhu, and E. Tian, "The integration of marine biodiversity information resources based on big data technology," *Journal of coastal research*, vol. 103, no. sp1, p. 806, 2020.

[14] D. T. Monteith, P. A. Henrys, C. D. Evans, I. Malcolm, E. M. Shilland, and M. G. Pereira, "Spatial controls on dissolved organic carbon in upland waters inferred from a simple statistical model," *Biogeochemistry*, vol. 123, no. 3, pp. 363–377, 2015.

[15] B. Kirubakaran and M. Ilangkumaran, "Selection of optimum maintenance strategy based on fahp integrated with gra–topsis," *Annals of Operations Research*, vol. 245, no. 1-2, pp. 285–313, 2016.

[16] J. Ge and J. Liu, "Security assessment algorithm of navigation control system based on big data," *Journal of coastal research*, vol. 93, no. sp1, p. 1026, 2019.

[17] Z. Cui and J. Yang, "Research on ocean big data service technology in distributed network environment," *Journal of coastal research*, vol. 98, no. sp1, p. 141, 2019.

[18] W. Zhou and S. Yu, "Research on the communication method of mobile network shadow fading based on interference alignment algorithm," *Journal of Supeuting*, vol. 72, no. 7, pp. 2891–2909, 2016.

[19] J. S. Teh, A. Samsudin, and A. Akhavan, "Parallel chaotic hash function based on the shuffle-exchange network," *Nonlinear Dynamics*, vol. 81, no. 3, pp. 1067–1079, 2015.

[20] C. Lu, "Research on optimization of computer network quality of service based on improved red algorithm," *Revista de la Facultad de Ingenieria*, vol. 32, no. 4, pp. 321–328, 2017.

[21] T. Steiner, R. Verborgh, J. Gabarro, E. Mannens, and R. Walle, "Clustering media items stemming from multiple social networks," *Computer Journal*, vol. 58, no. 9, pp. 1861–1875, 2015.

[22] I. Hababeh, I. Khalil, and A. Khreishah, "Designing high performance web-based computing services to promote telemedicine database management system," *IEEE Transactions on Services Computing*, vol. 8, no. 1, pp. 47–64, 2015.

[23] Y. Duan, R. Yang, and S. Duan, "Overall layout and security measures of campus wireless local area networks," in *The International Conference on Cyber Security Intelligence and Analytics CSIA 2020: Cyber Security Intelligence and Analytics*, pp. 25–32, Springer, Cham, 2020.

[24] P. Xia, "Data security risk and preventive measures of virtual cloud server based on cloud computing," in *The International Conference on Cyber Security Intelligence and Analytics CSIA 2020: Cyber Security Intelligence and Analytics*, pp. 40–45, Springer, Cham, 2020.

[25] Z. Zheng, "Information security risk assessment based on cloud computing and bp neural network," in *The International Conference on Cyber Security Intelligence and Analytics CSIA 2020: Cyber Security Intelligence and Analytics*, pp. 85–91, Springer, Cham, 2020.

Hindawi
Wireless Communications and Mobile Computing
Volume 2022, Article ID 2468799, 13 pages
https://doi.org/10.1155/2022/2468799

Research Article

Digital Dissemination of Scene Art in Changbai Mountain Area of Visual Sensor Images

Xingru Wang,[1] Weili Wang,[2] and Weiliang Zhang[3]

[1]*Animation College, Jilin University of the Arts, Changchun, 130060 Jilin, China*
[2]*Jilin Radio and Television Center, Changchun, 130060 Jilin, China*
[3]*School of Visual Arts, Changchun Sci-Tech University, Changchun, 130060 Jilin, China*

Correspondence should be addressed to Weiliang Zhang; 100316@cstu.edu.cn

Received 28 March 2022; Revised 12 May 2022; Accepted 21 May 2022; Published 9 June 2022

Academic Editor: Jun Ye

With the booming development of the tourism industry, how to bring good benefits to the tourist attractions has become a topic worth pondering. In today's Internet age, digital communication has become a mainstream way of disseminating art and culture in tourist attractions. This paper takes Changbai Mountain as the research object and realizes the digital dissemination of scene art in Changbai Mountain based on visual sensor image technology. Digital communication not only changes the way of information dissemination but also profoundly affects people's life, work, and entertainment, changing the way people receive information and the way of thinking, and people have higher requirements for information. Therefore, on the one hand, the communication of Changbai Mountain tourism culture should develop with the development of the times. On the other hand, it should evolve with the evolution of information and constantly change its own form of expression and dissemination to meet the needs of the audience. Finally, the effectiveness of digital dissemination of scene art in Changbai Mountains is reflected through the tourism statistics. The results show that the total tourism revenue of Changbai Mountain in 2019 is the largest, which is 5.61 billion yuan.

1. Introduction

For a long time, as an artistic expression medium, film and television can present vivid, vivid, and timely audio-visual images, expand and extend people's horizons, and promote the dissemination of cultural information. Many tourist cities take the image advertisement of the tourist destination as the main form to display the characteristic culture of the tourist destination. Today, with the development of digital technology and computer technology, the means of film and television production have been greatly enriched. The digital image conveys the highly concentrated history and culture, local customs, and natural landscape of the tourist destination to the audience vividly and vividly through digital technology and artistic techniques. Through high-definition digital images, viewers can intuitively understand the rich cultural relics, folk customs, religious culture, literature, and art of the tourist destination and meet the needs of increasing knowledge, broadening their horizons and feeling happy.

The innovation of this paper lies in the new point of view, and the application of digital art in the tourism and cultural communication activities of Changbai Mountain will be the general trend. It believes that the reasonable use of digital art expressions and dissemination methods can effectively improve the attractiveness, influence, and dissemination of Changbai Mountain tourism culture and effectively expand the scope, breadth, and depth of Changbai Mountain tourism culture dissemination. In the future, digital art will surely become an important means of Changbai Mountain tourism culture dissemination with its diversified and vivid expression forms and efficient, convenient, and interactive communication methods. In addition, this research introduces visual sensor image technology to realize the digital dissemination of scene art in Changbai Mountain.

2. Related Work

Many scholars at home and abroad have provided a lot of references for research on visual sensor images, Changbai Mountain, scene art, and digital communication.

Tang et al. proposed to adjust the density of key tree species in the forest and cultivate large-diameter wood according to the competition among key tree species. Once the tree's DBH exceeds 20 cm, the growth of the tree is not affected by competition [1].

Sun et al. measured the leaf dark respiration of two dominant tree species (Korean pine and Tilia) in the broad-leaved Korean pine mixed forest in Changbai Mountain under light and dark conditions. They discussed the reasons for the differences in leaf dark respiration and light inhibition [2].

Huaiwei and Guo reviewed the experimental research progress on the conductivity of silicate melts. The Na + concentration and H2O concentration are the key factors to control the conductivity. Two applications include the low-velocity zone of the oceanic asthenosphere and the magma chamber below the Tianchi volcano in Changbai Mountain [3].

Rongqin et al. use the electrical constraint inversion method, which can improve the accuracy of inversion interpretation by using the constraints of electrical logging data in the inversion process, which is beneficial to obtain richer geoelectrical information. Taking the geothermal exploration in the Changbai Mountain area as an example, the measured CSAMT data is used as the resistivity model for inversion, and the electrical characteristics are constrained by the actual drilling data in this section [4].

Huo et al. studied the content and density of soil organic carbon (SOC) and unstable and stable SOC components in peat soils from wetlands, soybean fields, and rice fields around Xingkai Lake in Northeast China [5].

Lv et al. designed a label-free sensing strategy for OTA detection using aptamers, SYBR Gold, and exonuclease. In the presence of the target molecule (OTA), the concept of OTA-specific aptamers was transformed from random coils to antiparallel G-quadruplexes [6].

The data of these studies are not comprehensive, and the results of the studies are still open to question; so, they cannot be recognized by the public and thus cannot be popularized and applied.

3. Visual Sensor Images and Digital Dissemination of Scene Art in Changbai Mountains

3.1. Vision Sensor Image. The visual sensor selected in this experiment is AVT Guppy's CCD camera [7, 8]. AVT Guppy cameras are designed to be extremely compact and have an excellent IEEE 1394 interface. It includes 10 different types of cameras (each with available B/W and color) and a wide variety of sensors and bandwidths, providing the right solution for almost any application imaginable. Guppy is available in casing or panel version (on request) and therefore fits in the smallest of spaces. A selection of high-quality, sensitive sensors (CCD sensor CMOS) enables Guppy to provide excellent image quality and true-to-life colors. The other two interleaved versions (EIA, CCIR) also enable more conversion image processing from analog to digital. Based on its modularity and significant price/performance ratio, adoption of Guppy is an ideal approach in many applications to achieve digital transformation of image processing [9]. The picture of the CCD camera is shown in Figure 1.

In front of the CCD camera, an interference filter with a transmission wavelength of 650 nm and a transmittance greater than 80% and a multilayer antireflection UV protective lens of the L37 Super Pro brand are installed [10, 11]. This specification filter can effectively filter out a large amount of arc light, and at the same time, let the laser structured light pass as much as possible and increase the signal-to-noise ratio of the image. The main function of the multilayer antireflection UV protection lens of L37 Super Pro grade is to prevent the splash and smoke generated during the process from polluting the filter [12]. This experiment uses the NI PCI-8254R acquisition card [13, 14]. The NI PCI-8254R capture card is equipped with reconfigurable I/O (RIO), IEEE 1394a interface devices compatible. The NI 8254R is driven by NI Vision Acquisition software, which includes all drivers in the NI Vision product line. With NI Vision Acquisition software, applications can be launched quickly and easily without having to go at the register level. The NI 8254R includes TTL controls for inputs and outputs, with isolated inputs and outputs for connecting to external devices such as lighting controllers, proximity sensors, and quadrature encoders. Behind the digital I/O of the NI 8254R is an FPGA that is preconfigured for the most common machine vision tasks. However, if this factory configuration function does not meet your requirements, the user can configure the LabVIEW FPGA Module for use on the FPGA. The NI 8254R provides a convenient 44-pin D-subconnector on its front panel for digital I/O [15].

The general visual sensor working system model is shown in Figure 2 [16, 17].

3.2. Digital Dissemination of Scene Art in Changbai Mountains. Within the scope of Jilin Province, Changbai Mountain, as a landmark geographical form, has a high degree of recognition and has an important historical and social status and the protection of ecological resources [18]. Changbai Mountain starts from the Liaohe River in the west, the Yellow Sea in the south, the Songnen Plain in the north, and the Mudanjiang River Basin in the east. Changbai Mountain has rich ecosystems and diverse species. There are animals such as sika deer, Siberian tiger, and mink and 2,639 kinds of plant resources, including spruce, fir, Yuehua, Korean pine, and sand pine, among which there are more than 960 medicinal plants, such as ginseng [19, 20].

The characteristics of Changbai Mountain art are reflected in its unique national characteristics, regionality, and history, and it is an art derived from nature and humanities. In the course of thousands of years of development, it integrates humanistic spirit and material needs and

Figure 1: The CCD video camera.

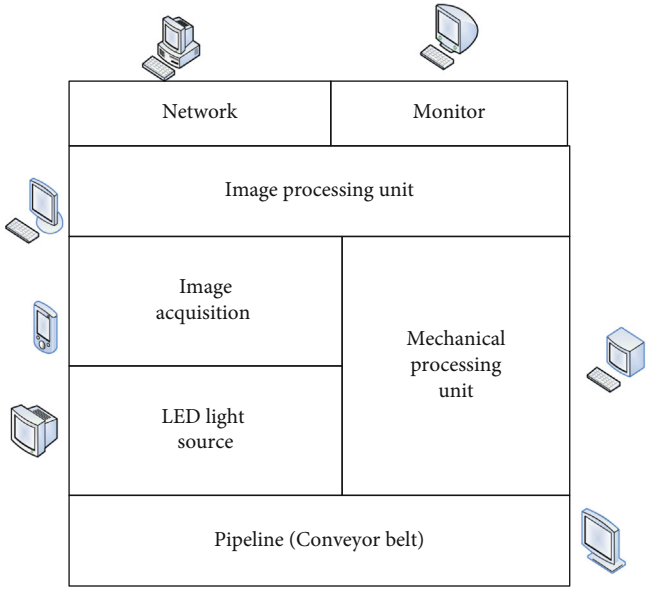

Figure 2: General visual sensor working system model.

Figure 3: Real scene of Changbai Mountain.

represents the spirit of "symbiosis and coexistence" of the Jilin people.

This is also the spirit of Changbai Mountain, the symbiosis, and coexistence of white mountain and black soil and the symbiosis and coexistence of water and fire. The real scene of Changbai Mountain is shown in Figure 3 [21].

The influence index system of tourist satisfaction in Changbai Mountain Scenic Spot is shown in Tables 1–3[22, 23].

Culture is the source of attraction for tourist landscapes. From the perspective of tourism resources, the landscapes, cultural relics, and other landscapes of the land of Shenzhou contain rich culture, and it is a treasure mine worthy of digging. No one will appreciate the beautiful tourism resources without publicity, and they will not be able to show their value [24]. With the rapid development of China's tourism industry, more and more tourist destinations are optimistic about the role of communication, and communication has become a key point in the development of tourism. The further development of tourism needs to rely on the mass and extensive dissemination of tourism information by the media. The weights of the influence indicators of tourist satisfaction in Changbai Mountain Scenic Spot are shown in Tables 4 and 5.

In the digital information society, digital communication affects the way of life and ideas of the modern public, and people have diverse needs for information acquisition and interaction. Visual and media-based communication

Table 1: Impact index system of tourist satisfaction in Changbai Mountain Scenic Area.

Order number	Influence elements	Quota
1	Scenic spot	Scenic spot characteristic A1
2		Ornamental value A2
3		Resource enrichment A3
4	Service facility	Facilities safety A4
5		Facility capacity A5
6		Facilities comfort level A6

Table 2: Impact index system of tourist satisfaction in Changbai Mountain Scenic Area.

Order number	Influence elements	Quota
7	Personnel service	Tour guide explanation service A7
8		Travel consulting services A8
9		Ticket staff service A9
10	Tourism traffic	Transportation convenience A10
11		Traffic safety A11
12		Traffic comfort level A12

Table 3: Impact index system of tourist satisfaction in Changbai Mountain Scenic Area.

Order number	Influence elements	Quota
13	Scenic area environment	Environmental health A13
14		Environmental protection A14
15		Environmental capacity: A15
16	Travel shopping	Shopping price A16
17		Shopping features the A17
18		Shopping quality A18

endows the tourist audience with more independent choices, provides the tourist audience with richer and more vivid and intuitive image information, and expands the scope and depth of the tourism culture of Changbai Mountain.

In modern society, it is necessary to communicate at the spiritual level through various means, and various forms of digital interaction invisibly promote the continuous extension and expansion of this new type of network communication system. Currently, in the era of rapid development of digital technology, we should pay attention to the fit of people's culture, feelings, and values, and we must break through the way of cultural cognition, the obstacles of emotional communication, and the direction of value concepts.

The ways in which digital is experienced is diverse, and the paths it presents are overwhelming. The development of digital technology in the art world is also multi-interactive, and the corresponding information obtained by the audience can be decomposed and expressed through digital technology. People, things, events, society, and nature will eventually be expressed in the form of sound, language, text, image, animation, etc. Massive and complex information storage is the advantage of digitalization, and it is an art for the audience to recognize and share this information.

In the traditional information transmission process, the audience's cognition of information is a flat, one-way source of information. Digital technology has changed this status quo. In the abstract digital information world, audiences can obtain multidimensional, multifaceted, multidirectional, and various forms of information content or abstractly explain and invent information. Familiar or unfamiliar events and objects or some other sources of information about events and objects themselves have been continuously processed and extended through various virtual abstract means such as network, program application, and digital technology. Information based on digitization will inevitably bring new cognition, new aesthetics, new thinking, new concepts, new experiences, and new perceptions. In addition, it can promote people to transform from practical behavior in the real society to a breakthrough in thinking in the virtual world, and the practical behavior built on the virtual world model gradually becomes a kind of trial and habit of people. Communication and exchange in the virtual world will become a new way of practice and information transmission.

All information should have the characteristics of cognition and sharing, as well as the characteristics of restoring events, feelings, and scenes. Digital art itself is a restoration and transmission of information, which can make it more convenient for the audience to send and transmit information, and realize the exchange of material, spiritual, and cultural information between audiences in different regions. All information will have a suitable artistic expression and characteristics, and these expressions and characteristics can be felt through the various sense organs of the audience. This feeling is a sublimation of art and superior to art.

Due to technical reasons, transmission methods, representational functions, and limitations of media forms, the information of digital art is different from other information content such as pure art, pure text, pure music, and pure video. Digital art is the integration of digital technology, art, and concept, and they will virtualize, sensualize, and abstract all information in our minds. Digital art is from the perspective of transmitting information through digital media, so as to examine the degree of influence of its information transmission. The greater and wider the influence of general information transmission, the easier it is for people to accept this digital art. For example, Weibo has the attributes of combining concept, art, and digitization, and it is a digital medium that absorbs massive information sources. It transmits information to the audience, and being recognized and shared by the audience is the ultimate goal of digital art. The information of digital art is a process in which

Table 4: Personnel service weight distribution table.

Personnel service	Facility distribution density	Ticket staff service	Guide explanation service	Weight
Facility distribution density	1	2.7672	3.2328	0.5923
Ticket staff service	0.3614	1	0.4476	0.1555
Guide explanation service	0.3093	2.2328	1	0.2522

Table 5: Table of weight distribution of service facilities.

Service facility	Security of facilities	Facilities hygiene	Facility capacity	Weight
Security of facilities	1	4.45	2.55	0.5872
Facilities hygiene	0.2247	1	0.2198	0.0959
Facility capacity	0.3922	4.55	1	0.3169

various divergent ideas are created and shared. It can also cross regions, narrow distances, break through various bottlenecks, and form innovative cultural exchanges and visual information of spiritual resonance.

In today's era of information superhighway, digital art has excellent artistic innovation and expansion. In the era of rapid progress of digital technology, in order to grasp the needs of the audience and complete the information transmission, it is necessary to use diversified, novel, and special information expression methods. The connotations and ideas contained in various digital forms of information in art cannot be reflected in traditional information transmission. It has better expansion space and development direction and combines virtual imagination with real appearance. In other words, digital art is a symbol of the information environment in the new era, it can be recognized and perceived, and it can also be innovatively and virtually exploited the advantages of the new world information environment. The audience can create and recreate digital art with the concept of thinking, form virtual abstract art information, and carry out infinite horizontal and vertical divergence of information transmission in the entire digital age.

Information transmission is the purpose of digital art, which invisibly forms a dynamic platform for communication and sharing. The message itself is real long before the audience wants to present their own thoughts and concepts. At the same time, only efficient, fast, profound, and accurate information can be quickly received and shared by the audience. However, in the process of information transmission and sharing, whether the audience's tolerance and feedback are good or bad, and whether directly related information can be transmitted and shared again, such complex and repeated sharing is a dynamic performance of information transmission.

There are many forms of expression and knowledge involved in digital art. In order to promote the information transmission of digital art efficiently, accurately, and quickly, it is necessary to consider the connection between digital art and information transmission. In this way, the familiarity and cognition of each individual in human, nature, and society will be promoted, and people will be familiar with and build material civilization and spiritual civilization.

In visual communication, audio-visual, graphics, and video are used to disseminate information, and the requirements for cultural level and reading ability are reduced. Visual communication presents the most intuitive and perceptual information content for tourist audiences, which can mobilize more sensory responses to perceive information. In the environment of digital media, with the development and progress of digital technology and communication technology, more diverse forms of visual expression and experience will inevitably emerge, which influence people's understanding and experience of Changbai Mountain tourism culture to varying degrees.

In an era of transition from text communication to visual communication, visual culture and visual communication have grown into a crucial part of Baishan tourism culture communication. The 21st century has entered an era of image competition, and the visual image of tourist destinations has become the dominant force in competition. It establishes a tourism visual image with a clear visual image and distinctive personality, which can give tourists a good impression and improve the cultural awareness, reputation, and influence of the tourist destination. Therefore, the role of the visual image of Changbai Mountain's tourism culture has also changed from "informing" to "persuading" and then to further influence the decision-making behavior of tourists and potential tourists. Therefore, we must pay attention to the visual communication design of Changbai Mountain tourism culture and improve the communication ability of Changbai Mountain tourism culture visual image information. Through the outgoing information, it can obtain the audience's approval, influence their attitude, and become interested in the tourist destination. Finally, after the perceptual knowledge, it can influence the audience's behavioral decision and attract them to travel to the tourist destination.

The emergence and development of mass media have profoundly affected the development of human society. With the help of the mass media, information on the earth can be disseminated synchronously. Space-time distance and difference are being eliminated by mass communication, and the concept of "global village" has become a reality. Mass communication has also made a fundamental change in the communication of Changbai Mountain tourism culture, and the communication form of Changbai Mountain

tourism culture has changed, showing new characteristics that are different from the past: there are more and more channels for disseminating Changbai Mountain tourism culture; the speed of disseminating Changbai Mountain tourism culture is getting faster and faster; the amount of Changbai Mountain tourism culture disseminated is increasing; the content of Changbai Mountain tourism culture disseminated is more and more abundant. Through the mass media, people have gained more convenience in carrying out tourism and cultural activities in Changbai Mountain, and their aesthetic ability to Changbai Mountain tourism culture has also been enhanced. The scope and depth of Changbai Mountain tourism culture have been greatly expanded.

In the information age, mass communication is an important channel for people to understand information. In Changbai Mountain's tourism and cultural communication activities, the basic function of digital media is to spread cultural information. It is responsible for informing and conveying tourism information such as recent new trends in the tourism industry, policies, and regulations, new changes in scenic spots, tourist routes, and cultural knowledge of tourist destinations. All forms of mass media can become the carrier of Changbai Mountain tourism culture. Among them, newspapers, magazines, books, and other flat paper media have the advantages of low cost, convenient storage, and repeatable reading. The content is specialized and has a certain depth, which can focus on the in-depth interpretation of the tourism culture of Changbai Mountain. The disadvantage is that the timeliness is poor, there are certain requirements for the audience's educational level, thus limiting the scope of the newspaper's dissemination of the audience; television, radio, and other film, and television media spread relatively fast, with many people, wide spread, and vivid content. It can act on the audience's audio-visual senses to produce a strong sense of authenticity and appeal and has a great impact on the audience's emotions. It is a popular communication method for tourism audiences; the Internet is the "fourth media" after newspapers, radio, and television. Network communication is a new trend in the dissemination of tourism culture in Changbai Mountain. Its rise and development have brought greater convenience and advantages to the dissemination of tourism culture in Changbai Mountain. Online media provide tourist audiences with timely and rich Changbai Mountain tourism cultural consultation, vivid Changbai Mountain tourism cultural content display, and humanized Changbai Mountain tourism cultural services, etc., to meet the needs of tourists for diversified access to information and interactive exchanges. The Internet has become the most important area for the dissemination of Changbai Mountain tourism culture. Various domestic and foreign tourism units and related enterprises and institutions have used the Internet to spread the Changbai Mountain tourism culture. Various types of Changbai Mountain tourism and cultural websites came into being and flourished, creating a new course of Changbai Mountain tourism culture communication and development.

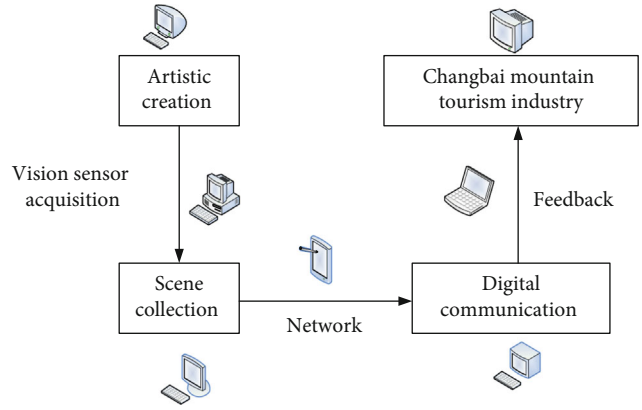

Figure 4: Changbai Mountain scene art digital communication framework.

The rise and development of digital art have penetrated into various media and various information service fields, and the communication activities of Changbai Mountain tourism culture are inevitably affected by it. From the perspective of communication, communication is the flow of information, and the communication of Changbai Mountain tourism culture is also the flow of cultural information. The following will use Laswell's famous "5W communication model," namely, communicator research, content research, media research, audience research, and effect research, to analyze the impact of digital art on Changbai Mountain's tourism culture, so as to have a clearer understanding and understanding of the transmission of Changbai Mountain tourism culture in the digital age. Figure 4 shows the digital communication framework of scene art in Changbai Mountain.

3.2.1. The Relationship between Transmission and Reception: From Single Passive to Active Interaction and Acceptance. The theory of reception aesthetics holds that literary works are not mere texts produced exclusively by writers. In the process of text interpretation, the interactive participation of readers occupies an extremely important position. It can be said that the reader not only appreciates the work but also participates in the creation of the work together with the writer, and the real value and life of the work lies in the endless interpretation of the reader. Reception aesthetics raises the status of the audience to a new height, emphasizes the audience's participation in the process of information decoding, and plays a very important role in the acceptance of the entire work.

Introducing the theory of reception aesthetics to the dissemination of Changbai Mountain tourism cultural information, readers are tourists, and literary works are the Changbai Mountain tourism cultural information or works provided by the media. The general expectations and requirements of the audience for the travel news works provided by the media are as follows: the content is true and accurate, fresh, and interesting, the form is novel and lively, and the image is vivid, that is, the pursuit of aesthetic artistry in the way of information presentation. The most important feature of digital art works is that they can conduct real-time

"interaction" and "communication" with the audience through the Internet, which greatly stimulates the enthusiasm of tourists. The dissemination of information in the 21st century is active information dissemination, which is more receptive and effective than traditional passive information reception. Digital art relies on digital technology to reemerge active communication. The audience can actively "pull" the required cultural information of Changbai Mountain from digital media, changing the one-way passive communication of traditional media. By attracting audiences to participate in the dissemination of Changbai Mountain tourism culture, it enhances the appeal and influence of Changbai Mountain tourism culture.

3.2.2. Forms of Dissemination: Multiple Forms of Dissemination Coexist. Digital art can strengthen the visual perception of Changbai Mountain tourism culture through the rational use of digital technology and creative art design. Through the use of dynamic visual modeling language, it sets off and renders the artistic atmosphere and artistic conception of Changbai Mountain tourism culture and meets people's new aesthetic needs. Human's audio-visual perception experience is rich, dynamic, and endlessly changeable. The dynamic communication method helps our audio-visual senses to better perceive the cultural information and connotation of Changbai Mountain tourism. If tourism communicators skillfully use the combination of words, sounds, pictures, and images in the process of communication, they will receive better communication effects. The comprehensive use of a variety of communication media helps to impress the recipients and enhance the communication power. Pictures, texts, images, sounds, animations, and other comprehensive media forms present a more realistic, vivid, and intuitive image of Changbai Mountain's tourism and cultural content. This can bring people an all-round and three-dimensional audio-visual experience, improve the audience's immersive sense of the scene, and make the cultural performance of Changbai Mountain more appealing and influential. This can also attract the audience to actively participate in the activities of Changbai Mountain tourism culture communication, so as to open up a new vision of Changbai Mountain tourism culture communication and realize the efficient interactive communication of Changbai Mountain tourism culture.

3.2.3. Communication Media: Integrated Communication of Multimedia

(1) From Single media to Multiple Media. When digital media was not yet popularized, the dissemination of Changbai Mountain tourism cultural information mainly relied on newspapers, books, radio, television, outdoor, etc. The dissemination of information capacity was small, and timeliness was low. This is because the traditional mass communication media is a single communication medium, its own communication characteristics, and the limitation of the communication medium. Due to the limitation of space and time in the communication activities, it can no longer meet the needs of Changbai Mountain tourism culture communication in the information age. With the development and application of digital technology, all information can be expressed in the form of digital combinations of "0" and "1." The unified digital form enables many single traditional media to form a multimedia integrated crossmedia communication platform-digital communication media. The tourism website gives full play to the integration effect of digital multimedia, collects, organizes, and typesets the Changbai Mountain tourism culture information on the mass media, provides the audience with rich and massive Changbai Mountain tourism culture information, and becomes the main way for the tourist audience to obtain the Changbai Mountain tourism culture. The tourist audience under the digital network can choose the tourist cultural information of Changbai Mountain that they need to the greatest extent and have more right to choose independently. However, no matter what kind of communication media has its own flaws and deficiencies, a single form of dissemination is also not conducive to the maximum dissemination of Changbai Mountain tourism cultural information. Therefore, various media should be comprehensively measured as a whole system in dissemination activities. As an integrated diversified media, digital media is the product of the combination of information technology and multimedia technology and has obvious advantages compared with traditional mass media. It has influenced the way of tourism culture in Changbai Mountain, which has played a great role in the dissemination of tourism culture in Changbai Mountain. Digital media integrates the functions of traditional media such as newspapers, radio, and television for information dissemination, forming a high-efficiency, high-capacity, and diversified dissemination method, breaking the boundaries of time and space, and giving tourists sufficient selectivity and autonomy. Therefore, digital technology and media technology have brought profound changes to the dissemination of social information. The communication of Changbai Mountain tourism culture should also adapt to the development of the times. It should not only be satisfied with the communication mode of a single media but should make full use of the comprehensive communication effect of digital multimedia. According to the content of Changbai Mountain tourism culture information and the characteristics of tourism audience, this paper understands the advantages and disadvantages of various media, optimizes the combination of media, and makes full use of the integrated communication advantages of the media to achieve the best communication of Changbai Mountain tourism culture.

(2) Continuation and Integration of Old and New Media. Some people may think that the new digital media will replace the old media, and the old media will withdraw from the stage of history. Facts have proved that the old media has not disappeared in the tourism and cultural communication activities of Changbai Mountain. Because travel audiences have the habit and preference of using certain media, different audience groups differ in choosing media to obtain travel information, and young groups with high income and high education use new online media more, while older groups

prefer traditional media such as newspapers and television. In the face of the rise of digital media, traditional media have also begun to use digital technology to realize the comprehensive digitalization of program content production and dissemination. It can be seen that both old and new media are constantly changing and blending. Both old and new communication media play a role in the field of Changbai Mountain tourism culture communication, and the digital communication method of Changbai Mountain tourism culture is the general trend. However, no matter what kind of media the Changbai Mountain tourism culture relies on, its dissemination method is based on the purpose of disseminating content and the needs of the audience and will only develop in a more humanized and interactive direction. The communication of Changbai Mountain tourism culture in the digital media environment should make full use of the technological advantages and artistic advantages of digital art to expand the breadth and depth of Changbai Mountain tourism culture communication.

3.2.4. Communication Effect: Multiple Reinforcement of Cognitive Psychology. The cognitive and psychological situation of the tourist audience is the basis and premise for the dissemination of Changbai Mountain tourism culture. Under the influence of digital art, the information dissemination method of Changbai Mountain tourism culture and the way tourists receive information have undergone new changes compared with traditional dissemination. The new forms of expression and communication will inevitably have an impact on the cognitive psychology of tourism audiences. The following will analyze the cognitive psychology of tourist audiences from three aspects: selective attention, selective understanding, and selective memory.

(1) Vivid and Interesting Forms Attract Selective Attention. Tourists hope to obtain fresh, interesting, novel, and lively Changbai Mountain tourism cultural information. Digital art relies on nonmaterial digital technology and comprehensively uses a combination of media such as text, sound, graphics, and images to provide tourism audiences with an all-round, multisensory interactive audio-visual experience. It is good at creating a vivid, relaxed, and lively immersive atmosphere, directly stimulating the sense organs of tourists and attracting the attention of tourists' visual perception. It also stimulates and satisfies its curiosity and desire for inquiry and pleasure, so as to better understand and memorize the content of Changbai Mountain tourism cultural information.

The one-way passive information dissemination method of traditional mass media has limited the time and space of information dissemination. Digital art relies on digital network media to spread Changbai Mountain's tourism culture, which has obvious advantages, allowing tourists to notice the information to the greatest extent, including information dissemination beyond the limitations of time and space, and tourists can access anytime, anywhere. At the same time, the mass, diversification, and personalization of information content can fully satisfy tourists' full autonomy and right of choice, and the interactive and participatory nature of dissemination forms creates a good dissemination environment, which can easily win the favor of tourists.

(2) Diversified Designs Help Selective Understanding. Understanding is a complex process and an important part of effective communication. The understanding of tourists is similar to a filter, and different tourist audiences can make different interpretations and conclusions about the cultural information or works of Changbai Mountain. The stimuli felt by tourists in this process are selected, organized, and transformed into their own comprehensible range. Due to differences in cultural background, age, gender, occupation, education, and interests of each audience, their understanding of Changbai Mountain tourism cultural information or works is also different.

The humanized digital technology and multidimensional design language of digital art have the characteristics of "media integration." It integrates visual, auditory, and tactile functions and can provide tourists with diversified, multisensory, all-round, and entertaining Changbai Mountain tourism cultural information services and create an immersive environment. Many exhibition halls, museums, and other places are dedicated to interactive multimedia displays, including interactive games, recognition interaction, video interaction, and other high-tech and experiential games, which combine the original plain graphics with creative interactive games. It integrates the display content and achieves a perfect integration, which helps the tourist audience to understand the information in the process of participating in the interactive game, so as to better realize the effective dissemination of Changbai Mountain tourism cultural information. For tourists, not only can they appreciate the external perceptual beauty composed of elements such as the shape, sound, color, and taste of natural landscapes but also the "inner beauty" of natural landscapes and cultural landscapes. The cultural connotation and symbolic meaning of "inner beauty" can expand one's own aesthetic experience and improve the aesthetic realm.

For the communicators of Changbai Mountain tourism culture, in addition to trying their best to express the external perceptual beauty of the natural landscape, they should also dig and display the cultural connotation contained in the natural landscape and improve the aesthetic value and cultural content of the natural landscape. For the communicators of Changbai Mountain tourism culture, in addition to trying their best to express the external perceptual beauty of the natural landscape, they should also dig and display the cultural connotation contained in the natural landscape and improve the aesthetic value and cultural content of the natural landscape. The charm of human landscape culture is more reflected in the historical and cultural values contained in the landscape. Only by understanding the era background of the human landscape and the historical meaning it contains can tourists better appreciate the human landscape and truly appreciate the unique aesthetic charm of the human landscape.

L_1	L_2	L_3
L_4	L_5	L_6
L_7	L_8	L_9

Figure 5: Definition of l in the domain of $3 * 3$.

4. Image Processing Algorithms

The definition of the Laplace operator of a two-dimensional function $\delta(\mu, \nu)$ is the second derivative as follows:

$$\nabla^2\delta = \frac{\partial^2\delta}{\partial\mu^2} + \frac{\partial^2\delta}{\partial\nu^2}. \tag{1}$$

For a 3×3 area, the following two forms are often used in practice:

$$\nabla^2\delta = 4l_5 - (l_2 + l_4 + l_6 + l_8), \tag{2}$$

$$\nabla^2\delta = 8l_5 - (l_1 + l_2 + l_3 + l_4 + l_6 + l_7 + l_8 + l_9). \tag{3}$$

In the formula, the definition of l is shown in Figure 5.

The commonly used template of Laplacian operator is shown in Figure 6.

Gaussian smoothing function is as follows:

$$\chi(\alpha) = -e^{-\mu^2+\nu^2/2\varepsilon^2}. \tag{4}$$

The corresponding Laplace operator of this function is as follows:

$$\nabla^2\chi(\alpha) = -\left[\frac{\mu^2 + \nu^2 - \varepsilon^2}{\varepsilon^4}\right]e^{-\mu^2+\nu^2/2\varepsilon^2}, \tag{5}$$

where ε is the standard deviation.

Threshold for cluster binarization is as follows:

$$\varphi_j = \frac{1}{2}(\phi_1 + \phi_2), \tag{6}$$

where ϕ_1 and ϕ_1 are the average gray values of all pixels in the two regions.

New threshold value is as follows:

$$\Delta\varphi_j = \left|\varphi_j - \varphi_{j-1}\right|s. \tag{7}$$

All pixels of the image are divided into two groups, and the probability of these two groups are as follows:

0	−1	0
−1	4	−1
0	−1	0

−1	−1	−1
−1	8	−1
−1	−1	−1

Figure 6: Convolution kernel of the Laplace implementing formula (2) and formula (3).

$$\begin{aligned}\gamma_0 &= \sum_{j=1}^{p}\frac{e_j}{E} = \gamma(p),\\ \gamma_1 &= \sum_{j=p+1}^{G}\frac{e_j}{E} = 1 - \gamma(p),\end{aligned} \tag{8}$$

where e_j is the pixel with gray level j, E is the number of pixels in the entire image, and $\gamma(p)$ is the sum of the frequencies of gray level j.

The overall average grayscale of the entire image is as follows:

$$\phi_\varphi = \phi(\varphi) = \sum_{j=1}^{G} jq_j, \tag{9}$$

where q_j is the frequency of occurrence of gray level j.

The respective average grayscale values of the two groups are as follows:

$$\begin{aligned}\phi_0 &= \sum_{j=1}^{p} jq_j.\\ \phi_0 &= \sum_{j=p+1}^{g} jq_j\end{aligned} \tag{10}$$

The variance between the two groups is as follows:

$$\kappa^2(p) = \gamma_0\left(\phi_0 - \phi_\varphi\right)^2 + \gamma_1\left(\phi_1 - \phi_\varphi\right)^2. \tag{11}$$

Open set ξ using struct ω is as follows:

$$\xi \circ \omega = (\xi - \omega) \oplus \omega. \tag{12}$$

Closing set ξ using struct element ω is as follows:

$$\xi\bullet\omega = (\xi \oplus \omega) - \omega. \tag{13}$$

The principle of least squares fitting a straight line is as follows:

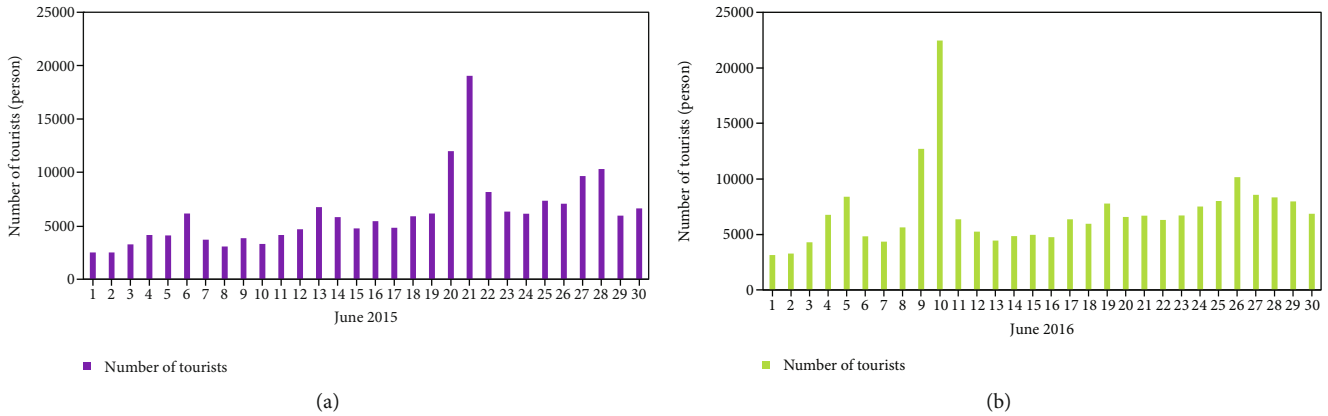

Figure 7: Tourists of Changbai Mountain from 2015 to June 2016.

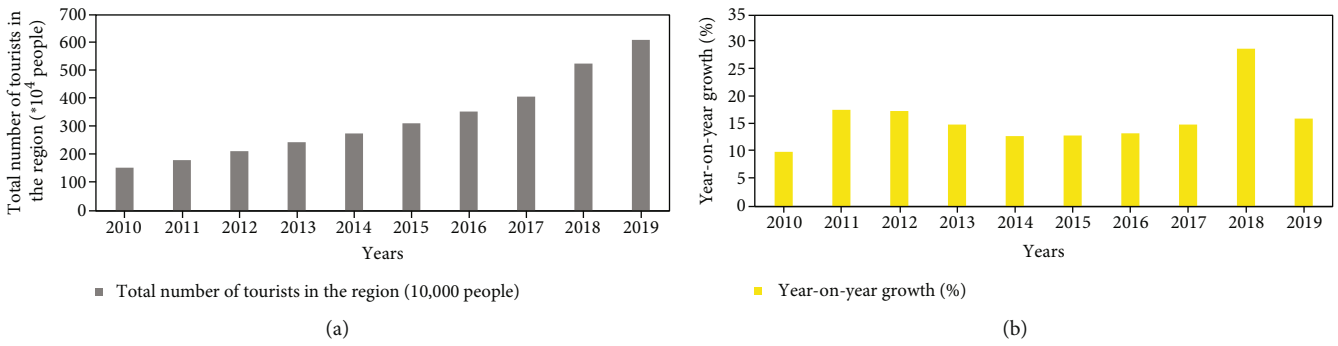

Figure 8: Statistical results of the total tourism number and year-on-year growth in Changbai Mountain from 2010 to 2019.

A series of data points are known:

$$D = \{(\mu_1, \nu_1), (\mu_2, \nu_2), \cdots, (\mu_s, \nu_s)\}. \tag{14}$$

Set the function prototype of the line to be fitted:

$$\nu = p\mu + \beta. \tag{15}$$

Minimize the sum of squared errors:

$$M(p, \beta) = \sum_{j=1}^{s} \left[\left(p\mu_j + \beta\right) - \nu_j\right]^2. \tag{16}$$

Find the parameters p and β by formula (16):

$$\begin{cases} \dfrac{\partial M}{\partial p} = \displaystyle\sum_{j=1}^{s} 2\left[\left(p\mu_j + \beta\right) - \nu_j\right]\mu_j = 0, \\ \dfrac{\partial M}{\partial \beta} = \displaystyle\sum_{j=1}^{s} 2\left[\left(p\mu_j + \beta\right) - \nu_j\right] = 0. \end{cases} \tag{17}$$

Linearity of the fitted line is as follows:

$$K = 1 - \frac{S}{T^2}, \tag{18}$$

where T is the distance range from the point to the line.

All lines passing through valid feature points in the image domain satisfy the equation:

$$\mu \cos \varpi + \nu \sin \varpi = \psi, \tag{19}$$

where ψ represents the distance from the line to the origin, ϖ represents the angle between the normal and the μ -axis, and (μ, ν) represents the coordinates of the pixel in the image domain.

The tourism situation of Changbai Mountain in June 2015 is shown in Figure 7(a). The tourism situation of Changbai Mountain in June 2016 is shown in Figure 7(b).

Figure 7 shows that in June 2016, Changbai Mountain Scenic Area received a total of 210,225 domestic and foreign tourists, a year-on-year increase of 14.4%. Among them, June 10 ushered in the day with the largest number of tourists in a single day, with 22,466 tourists. In addition, in the first half of 2016, Changbai Mountain Scenic Area received a total of 467,607 tourists, a year-on-year increase of 9.9%.

The statistical results of the total number of tourists and the year-on-year growth in Changbai Mountain from 2010 to 2019 are shown in Figure 8.

Figure 8 shows that from 2010 to 2019, the total number of tourists in Changbai Mountain increased year by year, and in 2018, the year-on-year increase was the largest, with a growth rate of 28.9%.

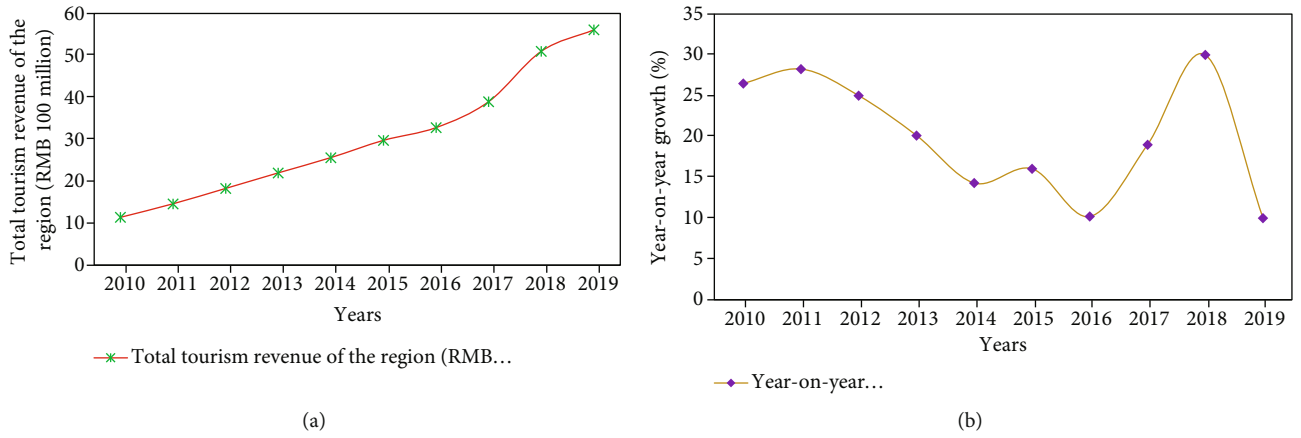

Figure 9: Statistical results of total tourism revenue and year-on-year growth in Changbai Mountain from 2010 to 2019.

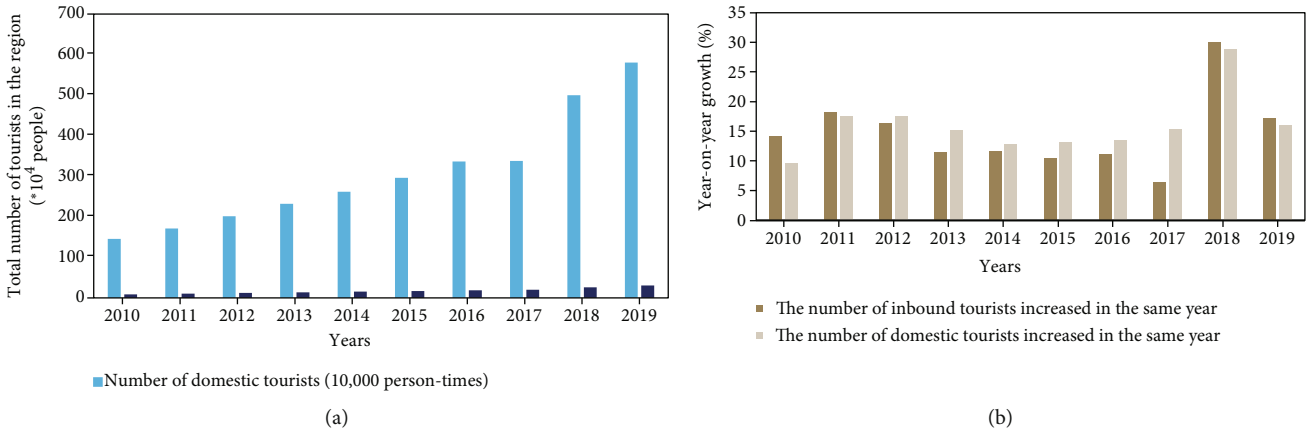

Figure 10: Statistical results of the number of domestic tourists, inbound tourists, and the corresponding year-on-year growth in Changbai Mountain from 2010 to 2019.

The statistical results of the total tourism revenue and year-on-year growth of Changbai Mountain from 2010 to 2019 are shown in Figure 9.

Figure 9 shows that although the total tourism revenue of Changbai Mountain in 2019 was the highest at RMB 5.61 billion, the year-on-year growth was the lowest, only 10%.

The statistical results of the number of domestic tourists and inbound tourists in Changbai Mountain from 2010 to 2019 and the corresponding year-on-year growth are shown in Figure 10.

Figure 10 shows that although the proportion of inbound tourists to the total number of tourists in Changbai Mountain is still low, it is still increasing year by year. The year-on-year growth in the period from 2012 to 2017 was greater than the year-on-year growth of domestic tourism, which shows that the digital communication of scene art in Changbai Mountain has played a very important role in tourism culture.

5. Discussion

The technical means and artistic design of digital art have penetrated into all aspects of Changbai Mountain tourism culture communication activities, not only the transmission, promotion, exhibition, and display of Changbai Mountain tourism culture information but also the digital collection of historical relics and monuments in Changbai Mountain tourism culture. As time goes by, more and more historical and cultural relics will be buried by time. It will be the general trend to use modern digital technology to record and preserve more permanent and complete historical and cultural information for human beings.

Secondly, digital art has a certain impact on the transmission of Changbai Mountain tourism culture, from the perspective of the relationship between transmission and reception. From single passive to active interactive acceptance, the autonomy and participation of tourism audiences in acquiring Changbai Mountain tourism cultural information have been improved. Compared with the passive reception of information in traditional mass communication, this makes the communication of Changbai Mountain tourism culture more accepting and conveying and can enhance the appeal and influence of Changbai Mountain tourism culture; from the perspective of communication form, the coexistence of multiple communication forms has been realized, bringing people all-round and multisensory audio-visual effects, which will help the tourist audience to better perceive

the information and connotation of Changbai Mountain tourism culture, thereby enhancing the communication effect of Changbai Mountain tourism culture; from the perspective of communication media, the integrated communication of multimedia forms a high-efficiency, high-capacity, and diversified communication method, which transcends the boundaries of time and space, gives tourism audiences full selectivity and autonomy, and promotes the scope of Changbai Mountain tourism culture communication; from the perspective of communication effect, the vivid and interesting forms of digital art can attract the selective attention of the audience, and the diversified design helps the audience to selectively understand and improve the perception and aesthetic ability of Changbai Mountain tourism culture. In addition, the comprehensive application of various means can deepen the audience's selective memory of Changbai Mountain tourism culture, which is conducive to the effective dissemination of Changbai Mountain tourism culture.

6. Conclusion

As an emerging art form, digital media art integrates the expression techniques and characteristics of traditional art and at the same time has unique artistic characteristics and dissemination advantages, which can more vividly display and disseminate the tourism culture of Changbai Mountain. In the development, utilization, and dissemination of Changbai Mountain tourism cultural resources in Changbai Mountain, the Changbai Mountain Changbai Mountain tourism culture communication under the digital media art mainly transmits information with audio-visual symbols. Before the information is delivered, the design must be made. The distinctive feature of digital media art is that computers are mainly used as creative tools or display means. With new changes in media attributes, Changbai Mountain tourism culture will inevitably show a new design language. Among them, the dematerialization and virtuality of design language are the development trend of Changbai Mountain tourism culture in the information age. At the same time, the new design language also brings time-sharing, immersive, and popular aesthetic characteristics, enriches the aesthetic information of the tourist audience, expands the aesthetic experience of the tourist audience, and improves the aesthetic realm. This different design language and aesthetic characteristics can inject fresh blood and vitality into cultural dissemination, which is helpful for the effective dissemination of Changbai Mountain tourism culture in Changbai Mountain.

Data Availability

The data that support the findings of this study are available from the corresponding author upon reasonable request.

Conflicts of Interest

The authors declare that they have no conflicts of interest.

Acknowledgments

This work was supported by the Scientific Research Project of Jilin Provincial Department of Education: "Research on the practical and innovative model of design higher education serving rural revitalization in Jilin Province" (JJKH20221326SK).

References

[1] Y. Tang, H. Chen, Y. W. Tong et al., "Competition of key tree species with selective cutting at different intensities in broadleaved-Korean pine mixed forest in the Changbai Mountain, China," *The Journal of Applied Ecology*, vol. 30, no. 5, pp. 1469–1478, 2019.

[2] J. W. Sun, F. Q. Yao, and Z. H. Zhang, "Differences of leaf dark respiration and light inhibition between saplings and mature trees of Pinus koraiensis and Tilia amurensis," *The Journal of Applied Ecology*, vol. 30, no. 5, pp. 1454–1468, 2019.

[3] N. I. Huaiwei and X. Guo, "Experimental investigation of electrical conductivity of silicate melts implications for melting in Earth's interior," *Journal of University of Science & Technology of China*, vol. 47, no. 2, pp. 155–162, 2017.

[4] H. E. Rongqin, Y. U. Qingshui, and L. I. Jing, "Research and application on CSAMT constraint inversion," *Global Geology*, vol. 22, no. 2, pp. 41–47, 2019.

[5] L. Huo, Y. Zou, and L. Xianguo, "Effect of wetland reclamation on soil organic carbon stability in peat mire soil around Xingkai Lake in Northeast China," *Chinese Geographical Science*, vol. 28, no. 2, pp. 325–336, 2018.

[6] L. Lv, D. Li, and R. Liu, "Label-free aptasensor for ochratoxin a detection using SYBR Gold as a probe," *Sensors & Actuators*, vol. 246, pp. 647–652, 2017.

[7] Q. Zhu, W. M. Zhou, X. Jia, L. Zhou, D. P. Yu, and L. M. Dai, "Ecological vulnerability assessment on Changbai Mountain National Nature Reserve and its surrounding areas, Northeast China," *The Journal of Applied Ecology*, vol. 30, no. 5, pp. 1633–1641, 2019.

[8] X. Y. Wang, S. L. Wang, Y. Tang et al., "Characteristics of non-structural carbohydrate reserves of three dominant tree species in broadleaved Korean pine forest in Changbai Mountain, China," *The Journal of Applied Ecology*, vol. 30, no. 5, pp. 1608–1614, 2019.

[9] P. H. Wang, Z. Chen, G. R. Yu, Q. F. Wang, Y. L. Jia, and S. J. Han, "Regulation effects of temperate broadleaved Korean pine forest on temperature and humidity in Changbai Mountain, China," *The Journal of Applied Ecology*, vol. 30, no. 5, pp. 1521–1528, 2019.

[10] X. W. Chen, H. Q. Wei, and L. F. Yang, "Petrological and mineralogical characteristics of Tianchi volcanoe, Changbai Mountain: Implications for crystallization differentiation and magma mixing," *Acta Geoscientica Sinica*, vol. 38, no. 2, pp. 177–192, 2017.

[11] Y. Wang, L. Guan, Z. Piao, Z. Wang, and Y. Kong, "Monitoring wildlife crossing structures along highways in Changbai Mountain, China," *Transportation Research Part D*, vol. 50, pp. 119–128, 2017.

[12] H. Y. Diao, A. Z. Wang, F. H. Yuan, X. Guan, H. Yin, and J. B. Wu, "Stable carbon isotopic characteristics of plant-litter-soil continuum along a successional gradient of broadleaved Korean pine forests in Changbai Mountain, China," *The Journal of Applied Ecology*, vol. 30, no. 5, pp. 1435–1444, 2019.

[13] T. Wu, "The ridge of Northeast:Changbai Mountain," *China's Foreign Trade*, vol. 571, no. 1, pp. 62–65, 2019.

[14] X. Y. Zhou, Z. J. Chen, S. C. Geng, J. H. Zhang, and S. J. Han, "Effects of nitrogen deposition on carbon and nitrogen contents in soil aggregates in temperate forests of Changbai Mountain, Northeast China," *The Journal of Applied Ecology*, vol. 30, no. 5, pp. 1543–1552, 2019.

[15] H. Jin, Y. Zhao, L. J. Liu et al., "Quantitative characteristics and population dynamics of the endangered plant Thuja koraiensis in Changbai Mountain, China," *The Journal of Applied Ecology*, vol. 30, no. 5, pp. 1563–1570, 2019.

[16] Y. G. Han, W. M. Zhou, L. Qi et al., "Tree radial growth-climate relationship in Changbai Mountain, Northeast China," *The Journal of Applied Ecology*, vol. 30, no. 5, pp. 1513–1520, 2019.

[17] S. Yan, C. Mu, and B. Wang, "Carbon storage of natural broad-leaved forested marsh wetland ecosystem in temperate Changbai Mountain of northeastern China," *Beijing Linye Daxue Xuebao/Journal of Beijing Forestry University*, vol. 40, no. 8, pp. 1–11, 2018.

[18] B. B. Chen, K. Wang, and R. Q. Ni, "Composition and spatial pattern of tree seedlings in a coniferous and broadleaved mixed forest in Changbai Mountain of northeastern China," *Journal of Beijing Forestry University*, vol. 40, no. 2, pp. 68–75, 2018.

[19] Y. Yao, N. Zhang, H. Cao, C. Zong, and M. Sun, "Induction and identification of polyploidy plants from superior individuals of wild Lonicera edulis Turcz. in Changbai Mountains," *Agricultural Biotechnology*, vol. 7, no. 4, pp. 25–28, 2018.

[20] P. Chen, X. Shan, and G. Hao, "Faults and karsts controlled geothermal genesis model of Xianrenqiao Hot Spring in Changbai Mountain," *Journal of Jilin University*, vol. 47, no. 4, pp. 1236–1246, 2017.

[21] X. Yin, L. Qiu, Y. Jiang, and Y. Wang, "Diversity and spatial-temporal distribution of soil macrofauna communities along elevation in the Changbai Mountain, China," *Environmental Entomology*, vol. 46, no. 3, pp. 454–459, 2017.

[22] Y. Li, S. Zhao, H. Pei et al., "Distribution of glycerol dialkyl glycerol tetraethers in surface soils along an altitudinal transect at cold and humid mountain Changbai: implications for the reconstruction of paleoaltimetry and paleoclimate," *Science China*, vol. 61, no. 7, pp. 925–939, 2018.

[23] W. W. Guo, X. J. Wang, X. G. Kang et al., "Structure and regeneration dynamics of three forest types at different succession stages of spruce – fir mixed forest in Changbai Mountain, northeastern China," *Journal of Mountain Science*, vol. 14, no. 9, pp. 1814–1826, 2017.

[24] S. L. Wang, Y. Zhao, and X. R. Gai, "Response of radial growth of Picea jezoensis var. Komarovii to climate factors along an altitudinal gradient on Changbai Mountain, Northeast China," *Chinese Journal of Ecology*, vol. 36, no. 11, pp. 3131–3137, 2017.

Hindawi
Wireless Communications and Mobile Computing
Volume 2022, Article ID 3822836, 12 pages
https://doi.org/10.1155/2022/3822836

Research Article

A Novel Vulnerable Code Clone Detector Based on Context Enhancement and Patch Validation

Junjun Guo, Haonan Li, Zhengyuan Wang, Li Zhang, and Changyuan Wang

School of Computer Science and Engineering, Xi'an Technological University, Xi'an, 710021 Shaanxi, China

Correspondence should be addressed to Junjun Guo; guojunjun@xatu.edu.cn

Received 12 March 2022; Revised 30 April 2022; Accepted 12 May 2022; Published 4 June 2022

Academic Editor: Jun Ye

With the rapid growth of open-source software, code cloning has become increasingly prevalent. If there are security vulnerabilities in a cloned code segment, those vulnerabilities may spread in the related software to potentially lead to security incidents. The existing methods of vulnerable code detection are performed on the condition that the source code is converted into an intermediate representation. However, these methods do not fully consider the rich semantic knowledge and patch information available for vulnerable codes, which can induce a high false positive rate (FPR). To address this problem, this paper proposes a vulnerable code clone detection method based on code fingerprints, named the Context-enhanced and Patch-validation-based Vulnerable code clone Detector (CPVDetector). A fingerprint database is built for functions, code snippets, and patches derived from preprocessed vulnerable source code. The target code to be detected is firstly transformed into function-level fingerprints. If clone detection fails at this coarse granularity, the detector is then applied at the finer line-level granularity. When fingerprint matching is successful between the target code and the vulnerable code segments, the detector will proceed to verify the context of vulnerable codes. Finally, CPVDetector can verify the fingerprints of patches corresponding to vulnerable codes to further reduce the FPR. Based on the generally accepted classification of code clones, CPVDetector can identify Type 1 and Type 2 vulnerable code clones at the coarse-grained level and offers significantly improved detection sensitivity for Type 3 and Type 4 code clones at the fine-grained level. Experimental results show that the proposed method can achieve high accuracy with a fast detection speed, and the FPR is as low as 2.35%, which is less than one-third of that of other existing methods. In view of its competitive performance and efficiency, CPVDetector can be applied in large-scale vulnerable code detection scenarios.

1. Introduction

The number of open-source software projects has increased rapidly in recent years [1, 2]. There were 170 million code repositories in GitHub [3] in 2020, of which 54.21 million were active code repositories, an increase of 36.4% compared to 2019. In the software development stage, programmers need to complete their tasks within a given time frame [4]. Therefore, copying and pasting of code often occur, either without any modifications or with only some simple modifications in the copied code segments, such as identifier replacement, sequence adjustment, or annotation modification. It is evident that such frequent copy-and-paste operations may be detrimental to software quality and maintenance [5–9]. The process of copying code snippets is called code cloning. Cloning vulnerable codes may cause the same vulnerabilities to be propagated in the development process, which can lead to security incidents [6].

Developers usually modify cloned code to meet software requirements by performing operations such as deleting unnecessary statements or adding some assertion statements for debugging. These operations may modify cloned vulnerable code, making vulnerability detection more difficult. Nevertheless, even if the structure of vulnerable code is modified, vulnerabilities may still exist in the cloned code segment [10, 11]. This kind of vulnerability is known as restructured clone vulnerability. Deckard, ReDeBug, and VUDDY can detect restructured clone vulnerabilities with extremely limited semantic information on the vulnerable code [12–15]. However, existing tools for restructured clone detection cannot

validate associated patch files, which results in a high false positive rate [16–20].

This paper proposes the Context-enhanced and Patch-validation-based Vulnerable code clone Detector (CPVDetector) as a tool for vulnerable code clone detection based on code fingerprints, which can effectively identify common types of code clones. The target code is detected at function-level and line-level granularity. A code fingerprint consists of a series of MD5 hash bits with a length of 32 that is simple and unique. In addition, the proposed method can leverage the context of vulnerable code snippets to reduce false positives caused by context-sensitive vulnerability. Through patch validation, CPVDetector can effectively locate patch codes in the target segments; thus, it can further reduce the false positive rate. Accordingly, CPVDetector can effectively identify vulnerabilities in practical software projects that cannot be detected by other state-of-the-art methods. More importantly, the proposed method can reduce the FPR to as low as 2.35% while improving the F-measure by approximately 30% when compared to existing methods.

The main contributions of this paper are as follows:

(1) We collect 983 vulnerabilities in common C/C++ open-source software projects from 2010 to 2020 and build a scalable fingerprint database for vulnerable code

(2) We propose a 2-level vulnerable code clone detection tool based on the source code fingerprints of functions and statements. To further reduce false positives, the context and patch information of vulnerable code is considered in line-level detection

(3) CPVDetector can detect four different types of vulnerable code clones. Compared to existing code clone detection methods, the proposed detection method can achieve the best balance in terms of accuracy and speed

The rest of this paper is organized as follows. Section 2 describes the classification of code clones and the existing code clone detection methods. Section 3 describes the collection and processing of vulnerability data and fingerprint generation. Section 4 presents how CPVDetector performs vulnerable code clone detection. In Section 5, we evaluate the proposed CPVDetector in comparison with other vulnerable code clone detection methods. Finally, Section 6 presents the conclusion and future work.

2. Background

2.1. Code Clone Classification. The original codes in cloned code segments are usually modified through operations such as variable renaming, redundant code insertion, annotation modification, data type modification, operator modification, statement order modification, code block order modification, and equivalent conversion of control structures [21, 22]. A set of widely accepted definitions for the classification of code clones is given as follows [5, 6]:

Type 1: exact clone. The code layout may be modified by modifying spaces and tabs, and the annotations may be edited; however, the code part is copied without any modifications.

Type 2: renamed clone. In addition to the modifications of Type 1, only the data types of variables and function return values are modified, or identifiers and variables are renamed.

Type 3: restructured clone. In addition to the modifications of Type 1 and Type 2, structural modification operations such as deletion, insertion, and rearrangement of statements are performed to generate restructured clones.

Type 4: semantic clone. In addition to the modifications of Type 1, Type 2, and Type 3, although the semantics of the code do not change, the syntax is adjusted.

2.2. Related Works. The existing code clone detection methods can be divided into five types: text-based, token-based, graph-based, abstract-syntax-tree-based, and metric-based methods.

(1) *Text-Based Methods*. Text-based methods convert source codes into sequences of lines or segments. To find a similar sequence, a given code segment is compared with other segments. To improve the detection accuracy, it is necessary to perform a series of preprocessing steps on the source code, such as standardization and normalization [23]. With granularity at the level of lines of code, ReDeBug leverages the sliding window method on the source code to detect files by means of a Bloom filter. ReDeBug can effectively detect Type 3 code clones, but it cannot effectively detect Type 1 or Type 2 code clones; as a result, a large number of clones of vulnerable code are missed. In addition, the false positive rate is high for methods based on line-level detection that do not consider code context or patch knowledge. With granularity at the level of functions, VUDDY can effectively detect clones of vulnerable code by detecting the fingerprint of the code for each function. However, VUDDY has difficulty detecting some common methods of code modification, such as code word order changes or additions and deletions of redundant code. Based on the sequences obtained via compilation and decompilation of Java source code, a tree-based clone detector has been proposed that can effectively recognize Type 1, Type 2, and Type 3 clones [24, 25]. Jadon proposed a technique for detecting Type 3 clones and quantifying their similarity [26]. This method can identify Type 3 clones for the C language by means of intermediate representation vectors and a support vector machine classifier

(2) *Token-Based Methods*. The source code is parsed into a token sequence that is easy to compute. Taking CCFinder [27] as an example, the similarity between two token sequences is calculated using a suffix tree algorithm. However, CCFinder has a rather high false positive rate because of its abstraction and filtering heuristics. SourcererCC can detect Type 3 code clones by using token package technology [28]. If the similarity between two functions exceeds a predetermined

threshold, then a clone is detected. However, if a statement is inserted into vulnerable code to make a simple modification, for example, adding an if statement, then SourcererCC will not be able to accurately detect the code clone. Moreover, Nishi and Damevski applied adaptive prefix filtering heuristics in a clone detection method [29] that could find Type 1, Type 2, and Type 3 clones. Wang et al. proposed CCAligner, which is a token-based clone detection tool [30] that uses C and Java files as data sets and can detect Type 1, Type 2, and Type 3 clones

(3) *Tree-Based Methods*. The source code is represented as an abstract syntax tree, in which nodes represent program entities and edges represent the connections between these entities. A heuristic tree search algorithm is used to identify clone pairs in similar subtrees. For example, Deckard constructs abstract syntax trees for files and then extracts feature vectors from the tree. After the feature vectors are clustered based on the Euclidean distance, vectors that are sufficiently close to each other in the Euclidean space are identified as code clones. This method based on a tree structure incurs a considerable time overhead because the subgraph isomorphism problem is an NP-complete problem. In addition, Deckard has a relatively high false positive rate, which indicates that cloning is not necessarily present in vulnerable codes with similar abstract syntax trees. Yang et al. proposed an automatic code clone detection method [31] that generates an abstract syntax tree with function-level units and uses the Smith–Waterman algorithm to calculate the score for each function

(4) *Graph-Based Methods*. In these methods, a program is converted into a graph such as a program dependence graph (PDG). These methods can achieve a higher level of abstraction of their code representations than other methods because they consider the semantic information of the source code. Crussell et al. proposed a detection tool based on the PDGs of C-language source code [32]. This tool uses the locality-sensitive hashing (LSH) algorithm to search for vectors that approximate nearest neighbors and the Min-Hash algorithm to calculate the similarity [33].

(5) *Metric-Based Methods*. Various metrics of the source code are calculated, such as the number of lines of code, the number of operators, and the cyclomatic complexity. Then, these metrics are compared to detect clone pairs that have the same metrics. Svajlenko and Roy summarized the concept of CloneWorks [34], which is a Type 3 clone detection tool that uses the IJaDataset and the Jaccard similarity measure for clone detection

The code clone detection methods introduced above all have relatively high detection capabilities for Type 1 code clones. Text-based or token-based methods are better for Type 2 code clone detection. Tree-based or metric-based methods are suitable for detecting Type 3 code clones. Graph-based methods can detect some Type 4 code clones, but graph generation and subsequent detection are time-consuming processes. Singh proposed a hybrid method based on code metrics and PDGs to convert Java source code into abstract syntax trees and PDGs [35], which can detect Type 1, Type 2, and Type 3 code clones. VulPecker uses a variety of source code representation methods and similarity calculations for code clone detection [36]. However, due to the poor efficiency of this method, it is not suitable for code clone detection for large open-source projects.

3. Vulnerability Fingerprint Database

A series of preprocessing steps is performed on obtained sample data of vulnerable source code, and fingerprints are generated in accordance with granularities at the code line and function levels. Thus, a fingerprint database for code clone detection is constructed.

3.1. Data Collection. Samples of vulnerable source code are obtained from open-source projects in GitHub, including the Linux kernel, FFmpeg, and OpenSSL. Corresponding patch information is obtained from the submission histories. Vulnerable code segments are extracted from the diff files in the patches. A diff file is composed of one or more code segments that are used as the characteristic fingerprint of the corresponding vulnerable code. In a diff file, there are code statements identified by special notations. Statements beginning with "+" are statements added by the patch, and statements beginning with "-" are statements deleted by the patch. Finally, the vulnerable functions, the vulnerable code segments, and the statements added and deleted by each vulnerability patch for vulnerable source codes are saved in a local file library for subsequent fingerprint generation and clone detection of vulnerable codes.

3.2. Preprocessing. The vulnerable code segments in a patch cannot completely represent the context of the vulnerable code. To better obtain the semantic information of vulnerable code, the vulnerable functions are converted into code flow graphs, and vulnerability patch code control statements with contextual information are notated for subsequent code clone detection. The Code2flow tool can convert vulnerable functions into flow graphs to determine and notate the control statements corresponding to patch codes [37]. Figure 1 shows an example of a simple vulnerable function and its generated flow diagram.

It is necessary to preprocess the source code before generating fingerprints. The first step of preprocessing the source code is to normalize the vulnerable source code by deleting annotations, spaces, tabs, and line breaks and converting all characters into lowercase letters to eliminate the influence of factors unrelated to syntax on the detection results. The steps of abstract replacement in the source code are as follows.

Step 1. Formal parameter replacement. Replace the formal parameters of functions in the code with FPARAM symbols.

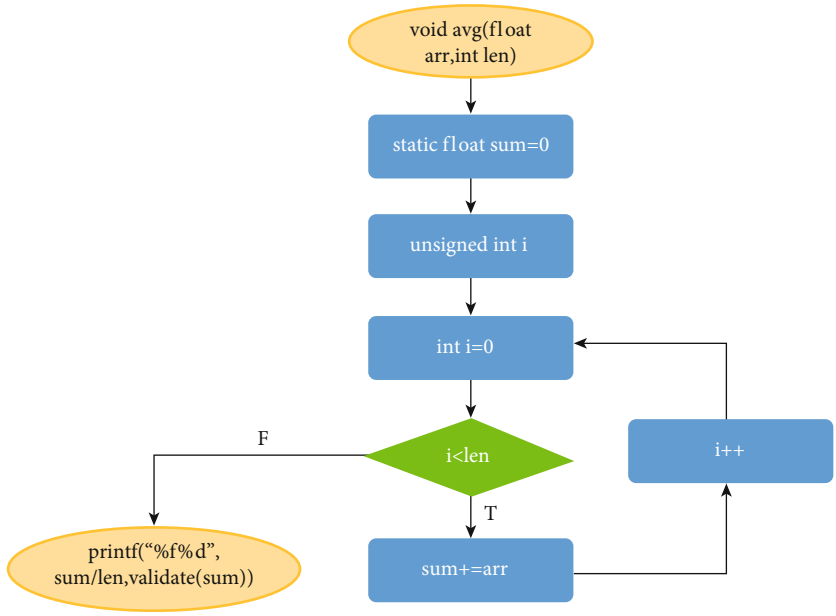

Figure 1: An instance of Code2flow for vulnerable function.

Step 2. Local variable replacement. Replace local variables in the code with LVAR symbols.

Step 3. Data type replacement. Replace the data types in the code with DTYPE symbols. These data types include C-language data types and custom data types. Modifiers such as unsigned will not be replaced because they have a significant impact on some vulnerabilities, such as integer overflow.

Step 4. Function replacement. Replace the function calls in the code with FUNCCALL symbols. Function calls are an important source of vulnerability.

Figure 2 shows the transformation of a vulnerable function before and after preprocessing. Figure 2(a) shows the vulnerable function code before preprocessing, and Figure 2(b) shows the vulnerable function code after preprocessing.

3.3. Granularity Selection. For Type 1 and Type 2 code clones, clone detection is performed on the preprocessed vulnerable code with function-level granularity, which takes less time than detection with line-of-code-level granularity. However, in the face of Type 3 and Type 4 code clones, it is difficult for detection with function-level granularity to succeed because it ignores the possible methods of internal modification of vulnerable functions, such as modification of the code statement sequence or the insertion of redundant code. Thus, to detect multiple types of clones, the proposed method combines line-level granularity and function-level granularity for detection. First, fingerprints of vulnerable codes are generated to detect Type 1 and Type 2 code clones with the vulnerable functions as the units for detection, and then, fingerprints are generated to detect Type 3 and Type 4 code clones with code lines as the units. If only the vulnerable code segments themselves are used to generate the fingerprints, contextual information may be omitted. Thus, the control statements corresponding to vulnerability patch codes are also selected for fingerprint generation. Finally, the added and deleted statements in each patch file are also used to generate fingerprints for subsequent patch verification.

Figure 3 shows the process of generating fingerprints of vulnerable code in detail. The preprocessed vulnerable source code is divided into a vulnerable function code set and a vulnerable line-level code set for the vulnerable code segments, the vulnerability patch codes, and the control statements corresponding to the vulnerability patch codes. Fingerprints of vulnerable functions are generated at the function level and stored in the fingerprint database. Then, fingerprints of the vulnerable code segments, vulnerability patch codes, and control statements corresponding to vulnerability patch codes in the vulnerable line-level code set are generated at the line-of-code level of granularity. The line-level code fingerprints are associated with the corresponding vulnerable function fingerprints to complete the construction of the whole fingerprint database.

3.4. Fingerprint Generation. In the process of detecting Type 1 and Type 2 code clones, a triple $t = (l, h, f)$ represents a vulnerable function fingerprint. Here, l represents the length of the vulnerable function, h is the Common Vulnerabilities and Exposures (CVE) identification number of the vulnerability corresponding to the vulnerable function, and f denotes the hash value of the vulnerable function fingerprint. Vulnerable function fingerprints of the same length are stored as one data set. Thus, CPVDetector can locate vulnerable function fingerprints based on the vulnerable function length and can quickly search for any associated CVE number that may exist in the target code to be detected. Table 1 presents the vulnerable function fingerprints of the vulnerabilities numbered CVE-2017-13012 and CVE-2015-1308, with a vulnerable function length of 143.

Step 1: Formal parameter replacement	DumpStyleGeneaology(nsIFrame* fparam, const char* fparam)
	nsFrame::ListTag(fparam, fparam);
	nsStyleContext* sc = aFrame->GetStyleContext();
	printf("%p", fparam);
	psc = sc->GetParent();
	sc = psc;
	printf("%p ", fparam);

Step 2: Local variable replacement.	DumpStyleGeneaology(nsIFrame* fparam, const char* fparam)
	nsFrame::ListTag(fparam, fparam);
	nsStyleContext* lvar = aFrame->GetStyleContext();
	printf("%p ", fparam);
	lvar = sc->GetParent();
	lvar = lvar;
	printf("%p ", fparam);

Step 3: Data type replacement.	DumpStyleGeneaology(dtype* fparam, const dtype* fparam)
	nsFrame::ListTag(fparam, fparam);
	dtype* lvar = aFrame->GetStyleContext();
	printf("%p ", fparam);
	lvar = sc->GetParent();
	lvar = lvar;
	printf("%p ", fparam);

Step 4: Function replacement.	DumpStyleGeneaology(dtype* fparam, const dtype* fparam)
	nsFrame::funccall(fparam, fparam);
	dtype* lvar = aFrame->funccall();
	funccall("%p ", fparam);
	lvar = sc->funccall();
	lvar = lvar;
	funccall("%p ", fparam);

Figure 2: Example of line-by-line abstract replacement.

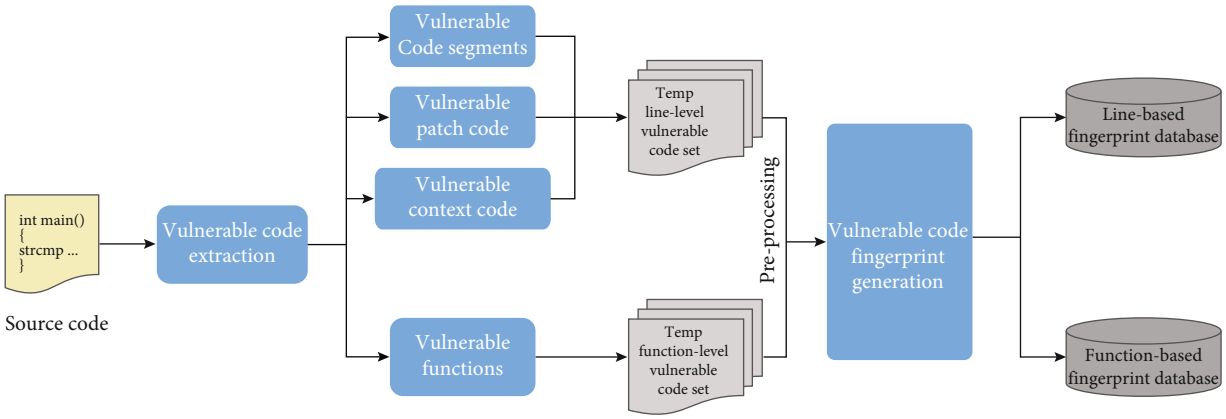

Figure 3: Construction of the fingerprint database.

The vulnerable line-level code fingerprints for Type 3 and Type 4 code clones can be divided into three types: (i) fingerprints of vulnerable code segments, generated by rows; (ii) fingerprints of the control statements corresponding to vulnerability patch codes, used to further verify the context of cloned code when detecting code clones; and (iii) fingerprints of vulnerability patch codes, including fingerprints of patch-deleted statements marked with "-" and fingerprints of patch-added statements marked with "+." The specific operations are as follows. Fingerprints of the vulnerable code segments in the vulnerable line-level code set are generated, followed by the fingerprints of the corresponding vulnerability patch code control statements and vulnerability patch codes at line-level granularity, and the above three

Table 1: Examples of vulnerable function fingerprints.

Vulnerable function length	CVE number of the vulnerability	Vulnerable function fingerprint
143	CVE-2017-13012	08345519ec358d8af82812efab5051f6
	CVE-2015-1308	78675ef39f395a7d95076b3354f0e48e

types of fingerprints are stored in a table space as the fingerprints of the vulnerable line-level codes. Finally, each vulnerable line-level code fingerprint is linked to the corresponding vulnerable function fingerprint to allow the corresponding vulnerability CVE number to be output in the results of code clone detection. Table 2 presents the preprocessed vulnerable code and vulnerable line-level code fingerprints of the vulnerable code segments, patch code control statements, and vulnerability patch code for CVE-2017-13012.

4. Code Clone Detection

CPVDetector first eliminates the influence of operations such as renaming in the target code on the clone detection results. Second, each function in the target code is converted into a fingerprint to detect Type 1 and Type 2 code clones. Once any matching vulnerable function fingerprint is discovered, detection is terminated, and the CVE number corresponding to the vulnerable function fingerprint will be output to end the detection process. If no corresponding vulnerable function fingerprint is discovered, the target code should be processed with lines of code as the units. Then, Type 3 and Type 4 code clones should be detected in the fingerprint database of vulnerable line-level codes, and the context of the vulnerable codes and any corresponding patches should be further verified in the process of detecting target line-level code clones. Finally, the detection results are output. The process of detecting code clones with CPVDetector is shown in Figure 4.

4.1. Function-Level Vulnerable Code Clone Detection. Vulnerable function fingerprints are employed to detect Type 1 and Type 2 code clones. In the detection process for the target code, the length of the vulnerable function is first used as an index to search for any vulnerable function of the same length. If any vulnerable function fingerprint with the same length is discovered, hash lookup will be used to match hash values with the given length, which may help reduce the search space and improve the detection efficiency. As a result, the CVE number corresponding to the vulnerable function fingerprint will be output. Fingerprints of vulnerable functions that may have been cloned can be quickly located with an average time complexity of $O(1)$ and a worst-case time complexity of $O(n)$.

4.2. Line-Level Vulnerable Code Clone Detection. Line-level clone detection is mainly used for the detection of Type 3 and Type 4 code clones. Detection based on the fingerprint of the vulnerable code segment is performed first. In general, there will be a vulnerability in target code that includes an entire vulnerable code segment. In other words, fingerprint detection for vulnerable code segments can be regarded as a problem of finding whether a given subsequence is present. Therefore, we introduce a greedy algorithm to handle this problem. The fingerprints in the vulnerable line-level code fingerprint database are used as the input to match against the target code. If a vulnerable code segment associated with a vulnerability is found, it can be judged that the target code may contain this vulnerability. Algorithm 1 describes the detection algorithm for vulnerable line-level code clones.

In Algorithm 1, T represents the set of line-level fingerprints of the target code, and F represents the set of line-level fingerprints of a given vulnerable code segment. t and f represent the MD5 fingerprints at the line-of-code level in T and F, respectively. The symbol $|\bullet|$ denotes the size of the set $\bullet$. If the size of T is smaller than the size of F, then the vulnerable code cannot appear as a subsequence in the destination code, which means that there is no successful match. After this conditional judgment, the corresponding vulnerable code fingerprints are matched in the destination code, and the number of matches is recorded by the counter j. When the value of the counter j is equal to the length of the vulnerable code fingerprint, this indicates that the complete sequence of the vulnerable code exists in the destination code, which means that the match is successful. As is clearly seen from Algorithm 1, the complexity of Algorithm 1 is $O(|T| \times |F|)$ in the worst case, depending on the number of lines in the target code and the number of fingerprints of the vulnerable code segment.

4.3. Vulnerability Context and Patch Validation. If the target code is matched only with the fingerprints of the vulnerable code segment, the following two problems may affect the detection result. (i) The context of the vulnerable code is difficult to completely express. When the context of the vulnerable code has changed, the detection method may fail to recognize it. (ii) Even if the vulnerable code segment in the target code has been patched, the detection method may still indicate that there is a vulnerability in the target code. To address these two problems, the proposed method verifies the vulnerability context of the target code. Because a vulnerability patch is designed to fix a specific vulnerability and the patch code can only work if it acts on the corresponding vulnerable code, the contextual relationship is the same for the patch code and the corresponding vulnerable code. Therefore, before patch verification, the contextual relationship is first verified to ensure that the contextual relationship of the vulnerable code has not changed and to guarantee that the patch code can be successfully applied to the corresponding vulnerable code. If the target code successfully passes the vulnerable code segment detection process, the previously introduced line-level vulnerable code clone detection algorithm will be used to verify the vulnerability context, and the target code and the fingerprints of corresponding

Table 2: Examples of vulnerable line-level code fingerprints.

Type	Preprocessed vulnerable code	Vulnerable line-level code fingerprint
Vulnerable code segments	*FPARAM+=8;* *FUNCCALL((FPARAM, "\n\t"));* *FPARAM=(const struct FPARAM *)LVAR;* *FPARAM=FPARAM;* *LVAR=FPARAM->FPARAM;* *FUNCCALL(FPARAM,LVAR,FUNCCALL(&FPARAM));* *FPARAM=FPARAM;*	*62e857215c2c8b10a1ebe99046b1b463* *04a27a8b584e00db088f18a16ddc1ac6* *c3250b774d4bd8bbeea848ae8e091777* *4830812a7240fa89419da5ef1e440566* *01689c59d66b453ae92f59560a0a430f* *d1f3dbd2ab6d7e6199391bb86d1d343a* *57e012af713ea16d25ed7bd54a216887*
Vulnerability patch code	*FUNCCALL(&FPARAM);* *FUNCCALL(&FPARAM->FPARAM);*	+90b650dba71b052ca2a85608a2447c1c -e58a03ee48a74c4d50af5bee1ba18d08
Vulnerability context code	*if(FPARAM>=1&&FUNCCALL(FPARAM))*	*8fddbc554a5ad97e8805a956a8ab5968*

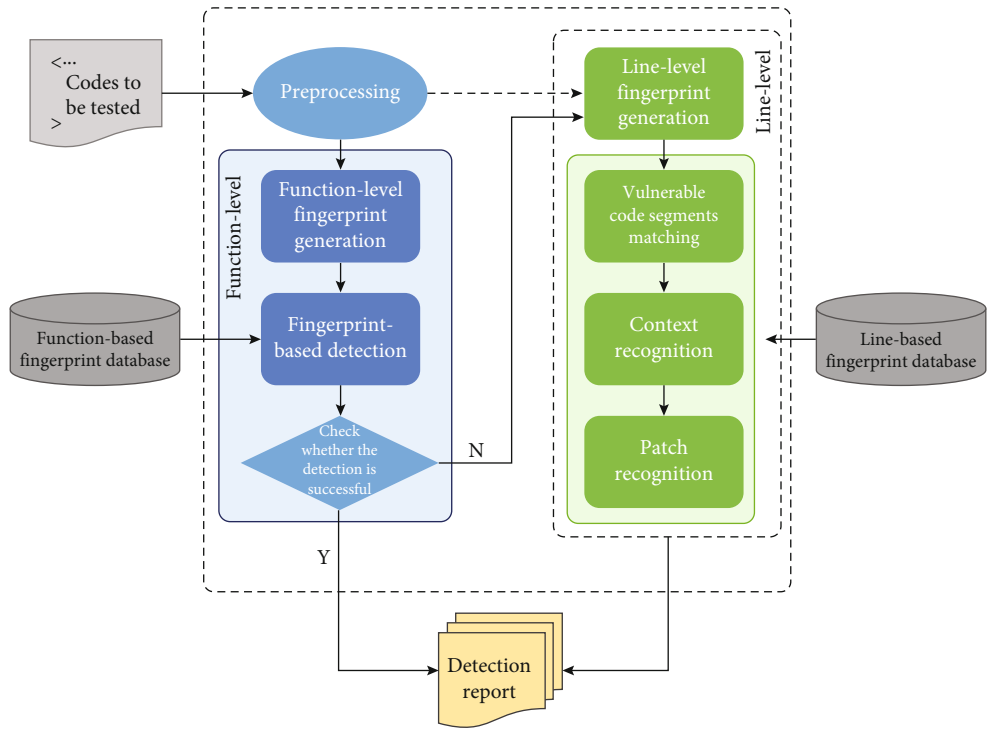

Figure 4: Framework of code clone detection in CPVDetector.

patch code control statements will jointly serve as the input to the detection algorithm.

To lower the false positive rate caused by the neglect of patch information, a method proposed in this paper uses the target code passing the context verification as the input for the vulnerable patch validation. This method is different from the previous detection method. The package of vulnerability patch codes can be divided into patch-added statements and patch-deleted statements. Based on this premise, for vulnerability patch validation, the fingerprints of statements identified by "-" as patch deletions in the patch code will firstly be detected in the target code. If these deleted patch code fingerprints are not detected, the fingerprints of statements identified by "+" as patch additions will be detected in the target code. If no fingerprints of the deleted statements are detected and the fingerprints of the added statements are detected in the target code, it is identified that the vulnerabilities in the code have been patched, and the false positives caused by patching are thus eliminated.

5. Experiment

To evaluate the effectiveness of the proposed method, it is compared with VUDDY, ReDeBug, and Deckard in this section. In the experiment, common C/C++ open-source software projects obtained from GitHub, such as the Linux kernel and FFmpeg, and their vulnerability information and patch files were obtained from the Common Weakness Enumeration (CWE) website to establish a complete vulnerability code fingerprint database. Moreover, many test cases for different vulnerabilities have been posted in the Software Assurance Reference Dataset (SARD) [38], including vulnerable

```
Input:T, F
Output:r
Initialize:r←False
1.if |T|<|F| then
2.      returnr
3.end if
4.for each t in T do
5.   j←0
6.   for each f in F do
7.      if t = f then
8.         goto 14
9.      end if
10.      j←j+1
11.      if j=|F| then
12.         returnr
13.      end if
14.   end for
15.end for
16. r←True
17.returnr
```

Algorithm 1: Line-level vulnerable code clone detection algorithm.

Table 3: Evaluation metrics.

Evaluate indicator	Formula
Precision	P = TP/(TP + FP)
Accuracy	A = (TP + TN)/(TP + FP + TN + FN)
False positive rate	FPR = FP/(FP + TN)
False negative rate	FNR = FN/(FN + TP)
F-measure	F-Measure = (2 ∗ P ∗ (1-FNR))/(P + (1-FNR))

Table 4: Experimental results of different methods on the test set.

Method	P (%)	A (%)	FPR (%)	FNR (%)	F-measure (%)
CPVDetector	96.47	92.94	2.35	10.09	93.07
VUDDY	94.11	75.29	7.06	56.47	59.52
ReDeBug	91.76	67.05	8.23	57.64	57.96
Deckard	57.65	50.59	47.05	55.29	50.36

cases, nonvulnerable cases, and patched cases, to build a set of test cases for experimentation.

5.1. Evaluation Indicators. To verify the effectiveness of each model, the precision (P), accuracy (A), false positive rate (FPR), false negative rate (FNR), and F-measure were used as the performance indicators in this study. In the expressions for these indicators, TP represents the number of samples correctly detected as vulnerabilities, FP is the number of samples incorrectly detected as vulnerabilities, TN represents the number of samples correctly detected as nonvulnerabilities, and FN is the number of samples incorrectly detected as nonvulnerabilities. The specific calculation formulas for the 5 abovementioned indicators are shown in Table 3.

5.2. Accuracy Evaluation. In the comparative test, the size of the ReDeBug sliding window was set to 4, and the length of the extracted code segment was set to 10. In Deckard, the minimal number of tokens required for clones was 30, the size of the sliding window was set to 2, and the similarity value was set to 0.95. The computer used to run the experiment was configured with an AMD Ryzen 5 3600 CPU, an Nvidia RTX 2060S 8 GB GPU, 16 GB of memory, and a 500 GB SSD.

The experimental results are shown in Table 4. Compared with the results of the other three methods, the F-measure of the proposed method is increased by at least 33%. Meanwhile, the proposed CPVDetector has higher precision and accuracy, indicating that more vulnerabilities can be detected without incurring more false positives. CPVDetector preserves the context information of vulnerable code, generates more accurate code fingerprints, and thus achieves a higher accuracy of detection. Furthermore, it is low for the FNR of CPVDetector, reaching approximately 10%, i.e., a quarter of that of the other methods, which suggests that false positives can be reduced by means of context and patch validation. VUDDY and ReDeBug use code fingerprinting to characterize code, but due to the choice of granularity, incomplete analysis of semantic information, and incomplete consideration of specific situations, they result in high FPRs and an inability to effectively deal with different types of code clones. Meanwhile, Deckard is an abstract-syntax-tree-based code clone detection method, and syntax tree generation and subtree finding are relatively inefficient processes. This results in low overall efficiency of the method, and the fact that detection is performed only on the basis of structural similarities can also lead to false positives due to the neglect of changes in internal details, which is also the reason for the relatively low detection precision and accuracy. An experimental analysis of different types of code cloning and the corresponding detection efficiency is as follow.

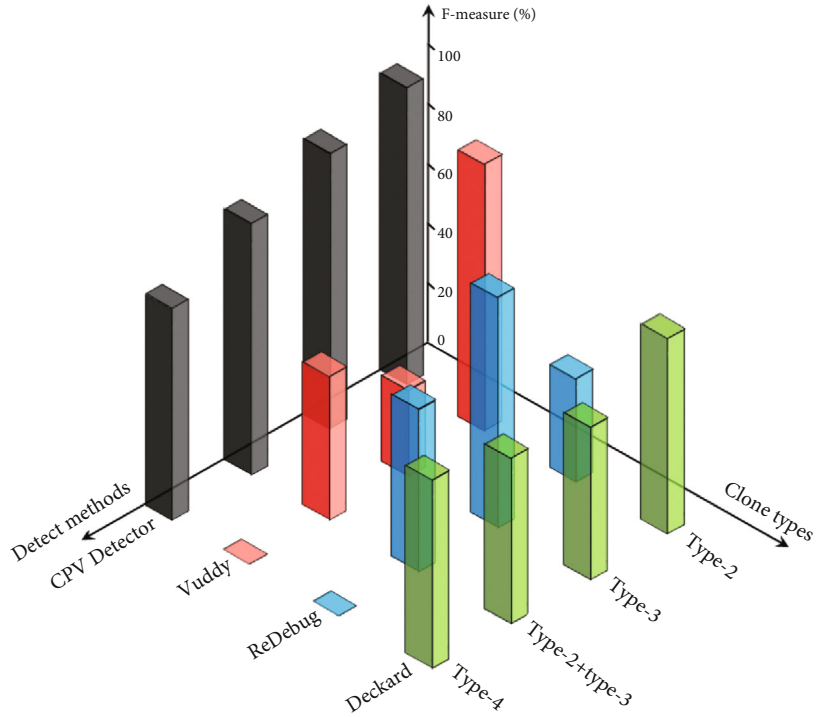

Figure 5: F-measure comparisons for different clone types and detection methods.

To study the detection effect of the proposed method for different types of code clones, the cases were divided into 4 test sets, i.e., Type 2 code clones, Type 3 code clones, mixed Type 2 and Type 3 code clones, and Type 4 code clones. CPVDetector, VUDDY, ReDeBug, and Deckard were all tested on each of these 4 test sets individually.

Figure 5 depicts the experimental results of the 4 methods for detecting different types of code clones. As shown in Figure 5, the F-measure of the method presented herein was increased by at least 7%, 19%, and 17% compared with the other three methods in terms of detecting Type 2, Type 3, and Type 4 code clones, respectively, and can effectively detect different types of code clones. VUDDY has good performance in detecting Type 2 code clones, but for Type 3, its F-measure was 13.6%, and it also could not detect Type 4 code clones. The F-measure of ReDeBug was only 27.3% in detecting Type 2 code clones, and it could not detect Type 4 code clones either. Although Deckard works for all different types of code clones, its F-measure for the detection of Type 2 code clones was only 52%. In summary, the experimental results of the other three types of detection methods were not ideal; accordingly, the main problems of VUDDY, ReDeBug, and Deckard are analyzed as follows. Because function-level granularity is used for detection in VUDDY, it cannot effectively detect clones in cases of insertion of redundant code or deletion of irrelevant code. Therefore, VUDDY does not have an ideal effect in detecting Type 3 and Type 4 code clones. For ReDeBug, it is difficult to detect cloned codes whose data types have been changed or whose variables and functions have been renamed, which leads to a serious problem of false negatives in the detection of Type 2 code clones. Deckard converts code into an abstract syntax tree and detects code clones by searching for similar subtrees; consequently, target code with subtrees similar to existing vulnerabilities and without actual code clones will be falsely determined as vulnerable one because of the lack of patch validation.

Table 5: Time overhead comparisons.

LoC	CPVDetector	VUDDY	ReDeBug	Deckard
1k	0.62	0.44	11.6	1.12
10k	1.45	0.81	27.6	3.63
50k	6.47	4.86	38.5	14.27
100k	17.63	10.34	42.92	34.67
200k	38.44	24.81	103.43	185.69
300k	65.12	47.43	195.24	332.42

For experiments to evaluate the detection efficiency of the proposed method, the test cases were divided into sets of different sizes, ranging from 1k LoC to 300k LoC. Table 4 lists the run times of the different methods on the test case sets of different sizes. As seen in Table 5, the proposed method shows significantly higher efficiency than ReDeBug and Deckard. In these experiments, Deckard required considerably more time as the data scale increased because this detection method is based on abstract syntax trees. VUDDY consumed less time than the other methods because it performs detection at the function level granularity; however, as a result, it cannot effectively detect Type 3 and Type 4 code clones, so a high FPR is generated. Compared with VUDDY, the proposed method

```
if (ndo->ndo_vflag >= 1 &&
    ICMP_ERRTYPE(dp->icmp_type)){
  bp += 8;
  ND_PRINT((ndo, "\n\t"));
  ip = (const struct ip *)bp;
  snapend_save = ndo->ndo_snapend;
  ip_print(ndo, bp, EXTRACT_16BITS
      (&ip->ip_len));
  ndo->ndo_snapend = snapend_save;
}
```

(a) Vulnerability source code of CVE-2017–13012

```
if (ndo->ndo_vflag >= 1 &&
    ICMP_ERRTYPE(dp->icmp_type)){
  bp += 8;
  ND_PRINT((ndo, "\n\t"));
  ip = (const struct ip*)bp;
  snapend_save = ndo->ndo_snapend;
  ND_TCHECK_16BITS(&ip->ip_len);
  ip_print(ndo, bp, EXTRACT_16BITS
    (&ip->ip_len));
  ndo->ndo_snapend = snapend_save;
}
```

(b) Patched code of CVE-2017–13012

```
if (ndo->ndo_vflag >= 1 &&
    ICMP_ERRTYPE(dp->icmp_type)){
  bp += 8;
  ND_PRINT((ndo, "\n\t"));
  ip = (const struct ip *)bp;
  ndo->ndo_snaplen = ndo->
  ndo_snapend - bp;
  snapend_save = ndo->ndo_snapend;
  ip_print(ndo, bp, EXTRACT_16BITS
      (&ip->ip_len));
  ndo->ndo_snapend = snapend_save;
}
```

(c) Test case of CVE-2017–13012

Figure 6: Three versions of the vulnerability CVE-2017-13012.

shows improved efficiency in detecting different types of code clones at the expense of a small increase in run time. In addition, the time overhead of CPVDetector exhibits roughly linear growth as the size of the test case set increases, indicating that it can be feasibly applied in large-scale code detection scenarios.

5.3. Case Analysis of Vulnerable Code Clone Detection. In this section, three specific cases are analyzed for vulnerable code clone detection. Taken the vulnerability CVE-2017-13012 as an example, the proposed method could successfully detect the vulnerability, whereas VUDDY, ReDeBug, and Deckard all failed. CVE-2017-13012, a high-risk vulnerability with a Common Vulnerability Scoring System (CVSS) risk score of 9.8, is generated when the ICMP parser in tcpdump suffers from buffer overreading. Figure 6 shows three versions of the vulnerability CVE-2017-13012. Figure 6(a) presents the original source code that led to this vulnerability. The calls of *ip_print* and *EXTRACT_16BITS (&ip->ip len)* lead to the occurrence of this vulnerability. Therefore, it is meaningful to check the value of *ip->ip_len* before using it. Figure 6(b) presents the patched code in which this vulnerability is corrected, with the addition of the call to the statement of *ND_TCHECK 16BITS(&ip->ip_len)*. A test case of the constructed test set is shown in Figure 6(c). It can be seen that the callee function is not present, which suggests that this code has not been repaired by the vulnerability patch and that consequently, the vulnerability may still exist. Moreover, the statement *ndo->ndo_snaplen=ndo->ndo_snapend-bp* has been added in Figure 6(c); this statement does not affect the vulnerable code because it cannot prevent buffer overreading caused by *ip_print* and *EXTRACT_16BITS (&ip->ip len)*.

Second, the vulnerability CVE-2018-18314 is a buffer overflow vulnerability that occurs via a crafted regular expression that triggers invalid write operations. Its patch fixes the vulnerability by adding multiple sets of conditional validations to the regcomp.c file. A sample code for a version of this vulnerability exists in the test set. Although this sample also adds conditional judgments to further validate the input regular expressions, there are individual conditional validation statements that are not added in the appropriate places, and their contextual relationships are broken, causing the patch code to fail to work. For example, an *if (UCHAR-AT(RExC_parse)! = ')')* statement needs to be added in the *S_handle_regex_sets* function, and *RExC_parse* needs to be updated with *switch* judgment rather than *if* statement. This vulnerability has a CVSS score of 9.8; it affects products such as MySQL, Oracle, and Solaris and requires patching to be completed as soon as possible.

Finally, the vulnerability CVE-2020-25643 was detected in the Linux kernel. With a CVSS value of 7.5, it is also a high-risk vulnerability. This vulnerability is generated when incorrect input verification in the *ppp_cp_parse_cr* function of the HDLC_PPP module of the Linux kernel causes memory corruption and read overflow, and it can lead to system denial of service or direct breakdown. This vulnerability was not patched in Fedora after it was repaired in the Linux kernel, and consequently, the risk still exists. In addition, there are vulnerabilities such as CVE-2016-9376, CVE-2018-13014, CVE-2018-10937, and CVE-2019-12981, which are not detected by the other three code clone detection methods, while the method proposed in this paper can effectively detect these vulnerabilities from source code by detecting them at different granularities.

6. Conclusion

This paper presents a vulnerable code clone detection tool, CPVDetector, based on code fingerprints with context and patch validation. Vulnerable code can be located via the corresponding diff file and is preprocessed to eliminate the impact of extraneous elements of the code and the renaming operation on detection. First, code clone detection is carried out at the function level for the target code. Then, context and patch validation of the vulnerable code is implemented in line-level code clone detection, which can obviously reduce the false

positive rate. CPVDetector can effectively detect vulnerable code clones of Type 1, Type 2, Type 3, and Type 4. Experimental results show that the proposed method achieves an accuracy of 92.94% and a precision of 96.47%, resulting in an improvement in the F-measure by at least 7% compared with other methods, and can discover vulnerable code clones that other methods cannot detect. In terms of time overhead, CPVDetector is close to VUDDY, but CPVDetector outperforms VUDDY in detection. Our future work is as follows. First, some abstraction methods can be combined with vulnerable code extraction to retain more semantic information in order to verify the contextual relationships. Second, the vulnerable code fingerprint database can be further complemented and enriched by considering vulnerable codes written in different languages to broaden the application scope of the method. Finally, machine learning or deep learning can be considered to improve the effectiveness of the detection approach.

Data Availability

No datasets available.

Conflicts of Interest

The authors declare that they have no conflicts of interest.

Acknowledgments

This work was partly supported by the National Nature Science Foundation of China (Grant No. 52072293), the Scientific Research Program Funded by the Shaanxi Provincial Education Department (Program No. 19JC021), the Science and Technology Project Funded by Xi'an City in Shaanxi Province of China (Program No. 2020KJRC0039), and the Science and Technology Project Funded by Weiyang District in Xi'an City, Shaanxi Province, China (Program No. 201922).

References

[1] W. Scacchi, "Understanding open source software evolution 181," *Software Evolution and Feedback: Theory and Practice*, vol. 181-205, 2006.

[2] X. Tan, M. Zhou, and B. Fitzgerald, "Scaling open source communities: an empirical study of the Linux kernel," in *2020IEEE/ACM 42nd International Conference on Software Engineering (ICSE)*, pp. 1222–1234, Seoul, Korea (South), 2020.

[3] "GitHub," https://github.com.

[4] N. Nurmuliani, D. Zowghi, and S. Powell, "Analysis of requirements volatility during software development life cycle," in *2004 Australian Software Engineering Conference. Proceedings*, pp. 28–37, Melbourne, VIC, Australia, 2004.

[5] S. Bellon, R. Koschke, G. Antoniol, J. Krinke, and E. Merlo, "Comparison and evaluation of clone detection tools," *IEEE Transactions on Software Engineering*, vol. 33, no. 9, pp. 577–591, 2007.

[6] C. K. Roy and J. R. Cordy, "A survey on software clone detection research," *Queen's School of Computing TR*, vol. 541, no. 115, pp. 64–68, 2007.

[7] D. Rattan, R. Bhatia, and M. Singh, "Software clone detection: a systematic review," *Information and Software Technology*, vol. 55, no. 7, pp. 1165–1199, 2013.

[8] G. Shobha, A. Rana, V. Kansal, and S. Tanwar, "Code clone detection—a systematic review," *Emerging Technologies in Data Mining and Information Security*, vol. 1300, 2021.

[9] Y. Wu, D. Zou, S. Dou et al., "SCDetector: software functional clone detection based on semantic tokens analysis," in *Proceedings of the 35th IEEE/ACM International Conference on Automated Software Engineering*, pp. 821–833, Australia, 2020.

[10] I. Keivanloo and J. Rilling, *Source Code Clone Search [M]// Code Clone Analysis*, Springer, Singapore, 2021.

[11] D. Y. Lee, U. Ko, I. Aitkazin, S. Park, H. S. Tak, and H. G. Cho, "A fast detecting method for clone functions using global alignment of token sequences," in *Proceedings of the 2020 12th International Conference on Machine Learning and Computing*, pp. 17–22, Shenzhen, China, 2020.

[12] L. Jiang, G. Misherghi, Z. Su, and S. Glondu, "Deckard: scalable and accurate tree-based detection of code clones," in *29th International Conference on Software Engineering (ICSE'07)*, pp. 96–105, Minneapolis, MN, USA, 2007.

[13] J. Jang, A. Agrawal, and D. Brumley, "ReDeBug: finding unpatched code clones in entire OS distributions," in *2012 IEEE symposium on security and privacy*, pp. 48–62, San Francisco, CA, USA, 2012.

[14] P. M. Caldeira, K. Sakamoto, H. Washizaki, Y. Fukazawa, and T. Shimada, "Improving syntactical clone detection methods through the use of an intermediate representation," in *2020 IEEE 14th international workshop on software clones (IWSC)*, pp. 8–14, London, ON, Canada, 2020.

[15] S. Kim, S. Woo, H. Lee, and H. Oh, "Vuddy: a scalable approach for vulnerable code clone discovery," in *2017 IEEE symposium on security and privacy (SP)*, pp. 595–614, San Jose, CA, USA, 2017.

[16] W. Jiang, B. Wu, Z. Jiang, and S. Yang, "Cloning vulnerability detection in driver layer of IoT devices," in *International Conference on Information and Communications Security*, pp. 89–104, Springer, Cham, 2020.

[17] F. Cheirdari and G. Karabatis, "Analyzing false positive source code vulnerabilities using static analysis tools," in *2018 IEEE International Conference on Big Data*, pp. 4782–4788, Seattle, WA, USA, 2018.

[18] S. Kim and H. Lee, "Software systems at risk: an empirical study of cloned vulnerabilities in practice," *Computers & Security*, vol. 77, pp. 720–736, 2018.

[19] X. S. Cybersecurity, "Dynamics: a foundation for the science of cybersecurity," in *Proactive and Dynamic Network Defense*, pp. 1–31, Springer, Cham, 2019.

[20] G. Lin, J. Zhang, W. Luo et al., "Cross-project transfer representation learning for vulnerable function discovery," *IEEE Transactions on Industrial Informatics*, vol. 14, no. 7, pp. 3289–3297, 2018.

[21] A. S. Bin-Habtoor and M. A. Zaher, "A survey on plagiarism detection systems," *International Journal of Computer Theory and Engineering*, vol. 4, no. 2, pp. 185–188, 2012.

[22] E. L. Jones, "Metrics based plagarism monitoring," *Journal of Computing Sciences in Colleges*, vol. 16, no. 4, pp. 253–261, 2001.

[23] D. Budgen and P. Brereton, "Performing systematic literature reviews in software engineering," in *Proceedings of the 28th*

international conference on Software engineering, pp. 1051-1052, Shanghai, China, 2006.

[24] C. Ragkhitwetsagul and J. Krinke, "Using compilation/decompilation to enhance clone detection," in *2017 IEEE 11th International Workshop on Software Clones (IWSC)*, vol. 1-7, Klagenfurt, Austria, 2017.

[25] C. K. Roy and J. R. Cordy, "NICAD: accurate detection of near-miss intentional clones using flexible pretty-printing and code normalization," in *2008 16th IEEE international conference on program comprehension*, pp. 172–181, Amsterdam, Netherlands, 2008.

[26] S. Jadon, "Code clones detection using machine learning technique: Support vector machine," in *2016 International Conference on Computing, Communication and Automation (ICCCA)*, p. 399, Greater Noida, India, 2016.

[27] T. Kamiya, S. Kusumoto, and K. Inoue, "CCFinder: a multilinguistic token-based code clone detection system for large scale source code," *IEEE Transactions on Software Engineering*, vol. 28, no. 7, pp. 654–670, 2002.

[28] H. Sajnani, V. Saini, J. Svajlenko, C. K. Roy, and C. V. Lopes, "SourcererCC: scaling code clone detection to big-code," in *Proceedings of the 38th International Conference on Software Engineering*, pp. 1157–1168, Austin, Texas, 2016.

[29] M. A. Nishi and K. Damevski, "Scalable code clone detection and search based on adaptive prefix filtering," *Journal of Systems and Software*, vol. 137, no. MAR., pp. 130–142, 2018.

[30] P. Wang, J. Svajlenko, Y. Wu, Y. Xu, and C. K. Roy, "CCAligner: a token based large-gap clone detector," in *Proceedings of the 40th International Conference on Software Engineering*, pp. 1066–1077, Gothenburg, Sweden, 2018.

[31] Y. Yang, Z. Ren, X. Chen, and H. Jiang, "Structural function based code clone detection using a new hybrid technique," in *2018 IEEE 42nd annual computer software and applications conference (COMPSAC)*, pp. 286–291, Tokyo, Japan, 2018.

[32] J. Crussell, C. Gibler, and H. Chen, "Andarwin: scalable detection of android application clones based on semantics," *IEEE Transactions on Mobile Computing*, vol. 14, no. 10, pp. 2007–2019, 2015.

[33] A. Andoni, P. Indyk, T. Laarhoven, I. Razenshteyn, and L. Schmidt, "Practical and optimal LSH for angular distance," 2015, https://arxiv.org/abs/1509.02897.

[34] J. Svajlenko and C. K. Roy, "Fast and flexible large-scale clone detection with CloneWorks," in *ICSE (Companion Volume)*, pp. 27–30, Buenos Aires, Argentina, 2017.

[35] G. Singh, "To enhance the code clone detection algorithm by using hybrid approach for detection of code clones," in *2017 International Conference on Intelligent Computing and Control Systems (ICICCS)*, pp. 192–198, Madurai, India, 2017.

[36] Z. Li, D. Zou, S. Xu, H. Jin, H. Qi, and J. Hu, "Vulpecker: an automated vulnerability detection system based on code similarity analysis," in *Proceedings of the 32nd Annual Conference on Computer Security Applications*, pp. 201–213, Los Angeles, California, USA, 2016.

[37] F. Ji, "A method of hierarchical reconfiguration of flow chart reversing from C source code," *Software Engineering and Applications*, vol. 7, no. 3, pp. 168–176, 2018.

[38] "SARD," https://samate.nist.gov/SARD/.

Hindawi
Wireless Communications and Mobile Computing
Volume 2022, Article ID 5441170, 13 pages
https://doi.org/10.1155/2022/5441170

Research Article

Artificial Intelligence-Based Sustainable Development of Smart Heritage Tourism

Dan Li, Pengju Du, and Haizhen He

College of International Education, Yulin University, Yulin, 719000 Shaanxi, China

Correspondence should be addressed to Dan Li; clairedan@yulinu.edu.cn

Received 24 March 2022; Revised 27 April 2022; Accepted 11 May 2022; Published 30 May 2022

Academic Editor: Jun Ye

World heritage is a kind of affirmation and high honor given by the international community to the important civilization, historical relics, or natural landscape of a country and nation. This paper studies and analyzes the sustainable development of heritage tourism boosted by smart tourism based on big data artificial intelligence. This paper first analyzes big data and then introduces the concept of smart tourism. Smart tourism is a new future-oriented tourism form that serves the public, enterprises, and governments. It uses the Internet of Things, cloud computing, next-generation communication network, high-performance information processing, intelligent data mining, and other technologies in tourism experience, industrial development, administrative management, and other applications, so that tourism physical resources and information resources have been highly systematically integrated and deeply developed and activated. And then, we analyze and discuss artificial intelligence algorithms. Artificial intelligence is a new technological science that is researched and developed on the basis of computer science as a simulation and extension of human intelligence activities. Finally, a comprehensive analysis is made on the tourism ecological footprint of natural heritage sites and the carrying capacity of tourism ecology in natural heritage sites. The experimental results of this paper show that the tourism development of this natural heritage site is in a sustainable state. The reasons are as follows: First, the average tourist ecological footprint of the place is 0.009466 hm^2, the average tourism ecological carrying capacity is 0.032861 hm^2, and there is an average ecological surplus of 0.02339 hm^2; secondly, the average tourist natural footprint is 18285.93 hm^2, the average tourism environmental carrying capacity is 40421.97 hm^2, and the average ecological surplus is 22136.04 hm^2. To sum up, it shows that its tourism development is in a state of sustainable development.

1. Introduction

Tourism, also known as the "smoke-free industry" and "sunrise industry," has gradually developed into one of the largest and most powerful industries in the world. However, the rapid development of tourism has also produced a certain impact while driving economic benefits. For example, the blind overexploitation of tourism resources has caused a series of problems such as ecological environment damage, extensive management of scenic spots, and idle tourism infrastructure. As the concept of "sustainable development" is deeply rooted in the hearts of the people, the concept of "sustainable tourism development" has been widely accepted by all sectors of society once it has been clearly put forward. The world heritage is a nonrenewable and scarce resource, which has comprehensive value in tourism value, scientific value, artistic value, and so on. It is necessary to protect the world heritage.

World natural heritage is a nonrenewable tourism resource. At this stage, the biggest threat facing China's world natural heritage is blindly dislocated, overloaded, and uncontrolled tourism development. There are many contradictions and close links between the development and protection of world natural heritage. A large number of theoretical discussions are difficult to effectively solve the contradiction and unified dialectical relationship between the protection and development of world natural heritage, and it is difficult to find an effective and reasonable path for symbiotic development. Therefore, it is necessary to select examples to systematically study the current situation

of China's world natural heritage tourism development. It is even more necessary to explore the development of world natural heritage with reasonable coexistence, fair distribution and sustainable development of protection, and development in the region, so as to permanently preserve and sustainably utilize natural heritage. This paper studies and analyzes the sustainable development of heritage tourism boosted by smart tourism based on big data artificial intelligence. It is aimed at providing theoretical support and practical guidance for the tourism development of World Heritage Sites in China and around the world.

The innovations of this paper are as follows: (1) Big data is firstly analyzed. Big data refers to a large number of resources that cannot be acquired, processed, and integrated by software within a reasonable time. (2) The smart tourism is introduced. Smart tourism is a brand new tourist operation method. It is based on new technologies such as the Internet of Things and cloud computing and is centered on the needs of tourists. After highly systematic integration and in-depth development and activation of the tourist information system, highly intelligent tourist information service, operation, and management are carried out. (3) The artificial intelligence algorithm is analyzed and discussed. Artificial intelligence is a new technological science that is researched and developed on the basis of computer science as a simulation and extension of human intelligence activities. (4) Finally, a comprehensive experiment is carried out to explore the tourism ecological footprint of natural heritage sites and the carrying capacity of tourism ecology of natural heritage sites.

2. Related Work

According to the research progress at home and abroad, different scholars also have a certain degree of cooperative research in the field of big data artificial intelligence and smart tourism boosting heritage tourism. Yu and Xu developed a tripartite framework for a holistic and structural understanding of the cultural heritage elements of a tourist destination based on its place in cultural heritage, tourism production, and tourism consumption. This research provided knowledge based on empirical cultural data and provided insights into cultural heritage tourism practice and research questions [1]. Using the legacy of Umm Qais as a case study, Alobiedat argued that tourism can fundamentally shape or reshape the intangible and tangible heritage of the communities in which tourist destinations are located. The findings showed that the local cultural and tangible heritage of Umm Qais was not resilient enough to absorb the changes brought about by tourism development [2]. Li et al. highlighted the opportunities and challenges of leveraging artificial intelligence to enable smart 5G networks and demonstrated the effectiveness of artificial intelligence in managing and coordinating cellular network resources. It is also envisaged that artificial intelligence-enabled 5G cellular networks will make the acclaimed ICT enabler a reality [3]. Caviglione et al. aimed to discover malware by secretly exchanging data by using two detection methods based on artificial intelligence tools such as neural networks and decision trees. To verify their effectiveness, seven covert channels had been implemented and tested on the measurement framework using Android devices. Experimental results demonstrate the feasibility and effectiveness of the method to detect hidden data exchanges between colluding applications [4]. To create a more convenient medical business and environment, Zhang et al. provided a patient-centric medical application and environmental business cyber physical system called Health CPS using technologies such as cloud and big data mining. The system is mainly composed of a unified and standardized information collection layer, an information management layer for distributed network storage and parallel computing, and an information service layer for data analysis. The results of this study show that cloud and big data analysis technologies can be used to improve the characteristics of medical systems, thereby enabling people to obtain various smart medical applications and consulting services [5]. Zhang et al. provided an overview of big data topics and a comprehensive survey of how cloud computing and its related technologies address the challenges posed by big data. Then, it analyzed the disadvantage of cloud computing when big data encounters the Internet of Things and introduced two promising computing paradigms, fog computing and transparent computing, to support big data services for the Internet of Things. Finally, some open challenges and future directions are summarized [6]. However, these scholars did not conduct research and analysis on the sustainable development of heritage tourism boosted by smart tourism based on big data artificial intelligence, but only discussed its significance unilaterally.

3. A Sustainable Development Method for Smart Tourism to Boost Heritage Tourism Based on Big Data Artificial Intelligence

3.1. Big Data. Big data is another revolution after mobile internet, Internet of Things, and cloud computing. It is a new opportunity arising from the contradiction between the rapidly developing information technology field and the increasing demand for information processing capabilities. For its concept, there are many different definitions and understandings [7]. Figure 1 shows the big data information processing system.

Big data, also known as massive data, refers to a large amount of resources that cannot be acquired, processed, and integrated by software in a reasonable time [8]. The acquisition, storage, big data analysis, and management capabilities of conventional database software simply cannot cope with such a large scale of data processing. The types and formats of data also go beyond traditional structured data. More and more predictions, decisions, and business behaviors in society are based on objective analysis of data [9]. Figure 2 shows the basic process of big data processing.

According to Gartner's definition, big data processing is a huge, changeable, and rapidly growing information system asset. Its decisiveness, insight, and optimal optimization power can only be exerted in the new processing mode [10].

The research on the characteristics of big data mainly focuses on the five dimensions of quantity, diversity, speed, value, and authenticity, which are called the 5V characteristics of big data [11].

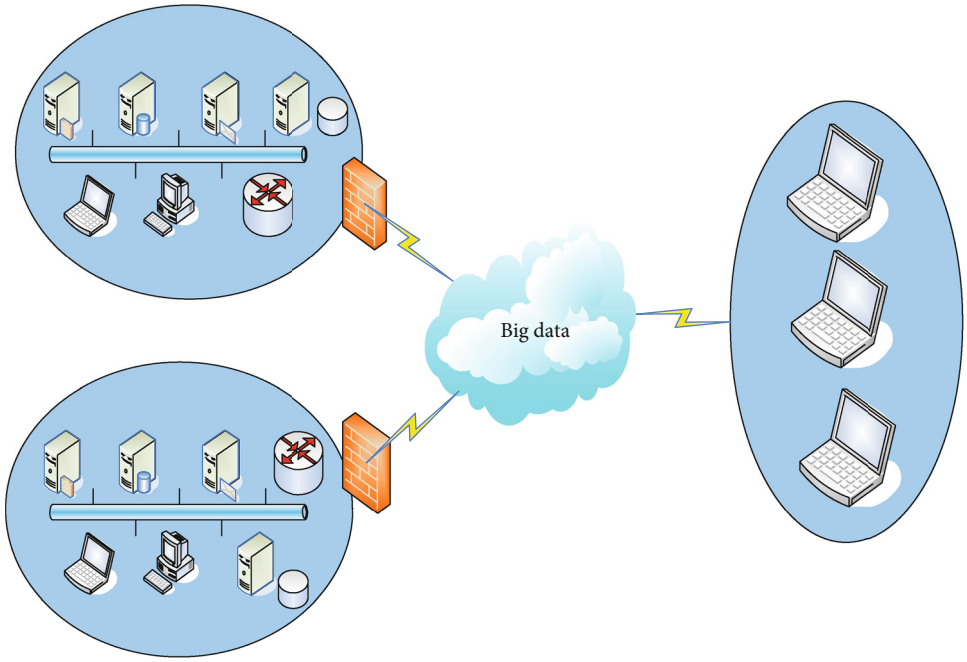

Figure 1: Big data information processing.

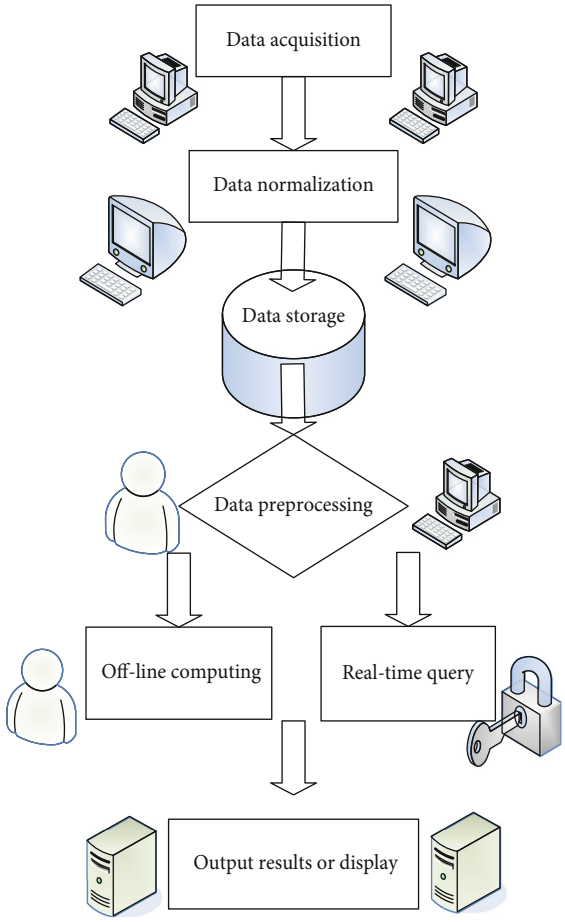

Figure 2: Basic process of big data processing.

3.1.1. Quantity. The scale of data is huge. As the cost of data acquisition, storage, and processing decreases, almost all electronic products and technologies become data sources [12].

3.1.2. Diversity. The diversity of data analysis types refers to a wide variety of modalities. Due to the widespread application of social media and smart devices, all kinds of information have been generated for enterprises, government departments, and communities. It not only has fully structured data types but also distributes a large number of semistructured and unstructured data analysis types such as text, pictures, and videos [13].

3.1.3. Speed. Global data usage will surge 44 times in 2020. The massive growth of data has resulted in rapid changes in data. In addition, the huge amount of data also puts forward higher requirements on the speed of data analysis and processing [14].

3.1.4. Value. Data has become a new type of asset, called "new oil." Whether data can be converted into value has also become a decisive factor for many companies to occupy the commanding heights of the market. However, the effective information hidden in the data is not proportional to the rapidly growing amount of data, which makes our task of mining value in the data more and more difficult [15].

3.1.5. Authenticity. Distorted data is prone to appear in the virtual network environment, and effective measures need to be taken to determine its authenticity. This is an inevitable need for the development of big data analysis. Only in this way can we truly restore and predict the true nature of things [16].

3.2. Smart Tourism. This paper believes that smart tourism is a tourist operation method based on new technologies such as the Internet of Things and cloud computing and centered on the needs of tourists [17]. It carries out highly intelligent tourist information service, operation and management through highly systematic integration, and in-depth development and activation of the tourist information system. The essence of smart travel is the in-depth integration of the new generation of information technology and the traditional tourism industry, which runs through the entire process of tourism activities, the entire process of tour operation, and the entire chain of tourism services. It enhances the strength of tourism enterprises with technological innovation, optimizes the experience of tourists, and enhances the level of the tourism industry. In this way, the intelligent management and operation of the tourism industry has been realized, and the traditional service industry has been upgraded to a modern service industry [18].

The fundamental value of intelligent tourism is to achieve a highly systematic integration and deep activation of the travel information system. Using new computer technology, large-scale collectible information data, high-performance data transmission network system, huge computing processing system, and core data center will be formed [19]. Big data analytics is blood. It will flow in the information network. Big data analysis of travel-related meals, accommodation, attractions, transportation, entertainment, etc., will serve as an important basis for tourists' life and government decision-making; network systems are like capillaries. The massive data information required for smart tourism will be transmitted and exchanged through this ubiquitous information network; the intelligent computing processing system is like the human brain, which will process various information data and issue various command instructions; the core data center, like the heart, has become an important cornerstone to support smart tourism. The smart tourism constructed based on the above elements has the characteristics of people-oriented, comprehensive sensing, full integration, and self-innovation [20]. Figure 3 features of smart tourism.

3.3. Artificial Intelligence Algorithms

(1) Artificial intelligence

A new generation of artificial intelligence is found, sometimes called mechanical intelligence. It is a new scientific theory of information technology that is researched and developed on the basis of traditional computer technology to imitate and expand the scope of human intelligence activities. It integrates the theoretical knowledge of mathematics, logic, financial control theory, simulation, information management theory, linguistics, industrial automation, engineering psychology, medicine, and philosophy. Artificial intelligence technology mainly has four important branches and application areas, mainly computer teaching, data analysis and discovery, model identification, and intelligent computing. At present, many software use artificial intelligence technology, including logical derivation, mathematical optimization, and retrieval. However, calculations based on probability theory, bionics, economics, and cognitive psychology are still under discussion.

(2) Machine learning

Machine learning is an interdisciplinary course that includes statistics, probability theory, approximation theory research, convex analysis, and computational complexity theory. And machine learning has different concepts due to its wide range of use: It belongs to a branch of artificial intelligence, which can use experience to learn to optimize the characteristics of specific calculations; it is a study of computer algorithms that can be improved by themselves by using practical experience; it is a performance criterion that can be automatically analyzed to obtain rules by using statistics or past practical experience to optimize computer programs. Machine learning mainly includes the following types: The training set of supervised learning requires features and objectives. These targets are marked by others. However, for the training method set of unsupervised learning, others cannot be labeled. Algorithms that are in the middle of supervised learning and unsupervised learning are usually semi-supervised learning. Reinforcement learning assesses whether the feedback after an action is positive or negative. At present, machine learning technology has been applied to many application fields such as data analysis and mining, natural language information processing, and detection of credit card fraud.

(3) Deep learning

Deep learning is a subcategory of machine learning, which refers to an artificial neural network algorithm created by the structure and function of the human brain. The core of deep learning is to have fast enough computer performance and utilize huge amounts of data to train large neural networks. Deep learning is not only scalable but also has the ability to automatically extract features from raw data (called feature learning). The main purpose of deep learning is to learn feature hierarchies using higher-level features formed by combining lower-level features. The self-learning function at the abstract level in deep learning can make the system no longer rely entirely on manually set features but learn to feed the input results directly to the output. The advantage of deep learning is to replace manually acquired features with unsupervised or semisupervised feature learning and efficient hierarchical feature extraction algorithms. Up to now, it has been proved that there are many frameworks of deep learning methods, which are widely used in computer image vision, human natural language information processing, speech recognition, voice recognition, and other fields, and have achieved good results.

(4) Logistic regression model

The logistic regression model is a classic discriminative method for solving classification problems. The binomial logistic regression model is represented by the conditional probability distribution $R(B|a)$, where the value range of

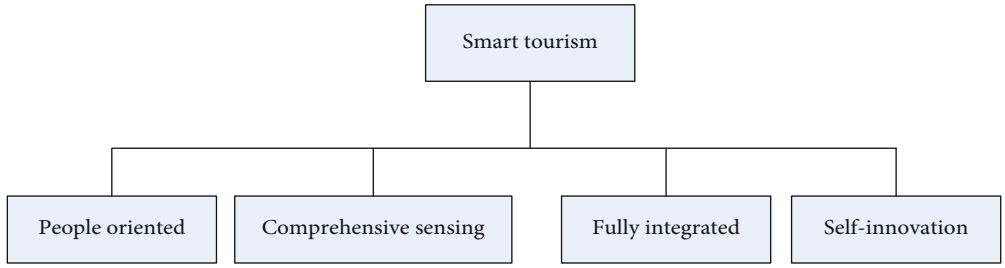

Figure 3: Characteristics of smart tourism.

the random variable B is 1 or 0. A value of 1 indicates a positive sample, and a value of 0 indicates a negative sample. Then, the binomial logistic regression model is

$$R(B=1|a)=\frac{\exp\left(U\cdot a\right)}{1+\exp\left(U\cdot a\right)}, \tag{1}$$

$$R(B=0|a)=\frac{1}{1+\exp\left(U\cdot a\right)}. \tag{2}$$

Here, $a\in T^{p+1}, a=\left(a^{(1)},a^{(2)},\cdots,a^{(p)},1\right)^{S}$ represents the input; $B\in\{0,1\}$ represents the output; $U\in T^{p+1}, U=\left(u^{(1)},u^{(2)},\cdots,u^{(p)},1\right)^{S}$ is the parameter, called the weight vector; and c is the bias.

The parameters of the model are estimated below. Supposing there are P samples, each sample i consists of the independent variable a_i and the corresponding dependent variable b_i. Among them, when $b_i=1$, it represents a positive sample, and when $b_i=0$, it represents a negative sample. Assuming that b_i is independent and obeys Bernoulli distribution, that is,

$$R(B=1|a)=\pi(a), \tag{3}$$

$$R(B=0|a)=1-\pi(a). \tag{4}$$

Then, the likelihood function is

$$\prod_{i=1}^{P}\left[\pi(a_i)\right]^{b_i}\left[1-\pi(a_i)\right]^{1-b_i}. \tag{5}$$

After sorting out the above formula, the log-likelihood function formula can be obtained as

$$K(U)=\sum_{i=1}^{P}\left[b_i(U\cdot a_i)-\log\left(1+\exp\left(U\cdot a_i\right)\right)\right]. \tag{6}$$

Using the maximum likelihood estimation method to find the extreme value of the above formula, the estimated value of U can be solved.

Assuming that the value range of random variable B is $\{1,2,\cdots,H\}$, the multinomial logistic regression model is

$$R(B=h|a)=\frac{\exp\left(U_h\cdot a\right)}{1+\sum_{h=1}^{H-1}\exp(U_h\cdot a)}, k=1,2,\cdots,H-1, \tag{7}$$

$$R(B=H|a)=\frac{1}{1+\sum_{h=1}^{H-1}\exp(U_h\cdot a)}. \tag{8}$$

Here,

$$a\in T^{p+1}, U_h\in T^{p+1}. \tag{9}$$

Parameter estimation for multinomial logistic regression models works in the same way as for binomial logistic regression models.

Logistic regression models are simple classifier algorithms with some salient features. First of all, the form of the logistic regression model is relatively simple. By observing the coefficients trained by the simulation, we can clearly see the relationship between the corresponding independent variable and the dependent variable. At the same time, the result R can also be regarded as the probability coefficient of classification, which makes it easier to understand its connotation. Secondly, compared with complex models such as support vector machines and random forests, the logistic regression model has higher training efficiency and can achieve higher modeling efficiency under similar effects. Finally, whether it is a discrete variable or a continuous variable, logistic regression models can be used concurrently and require no additional transformation and processing.

(5) Multilayer perceptron

The multilayer perceptron (MLP) pattern is an artificial neural network pattern. It maps multiple input datasets to a single dataset. Its network structure includes the input layer, hidden layer, and output layer. Figure 4 shows the multilayer perceptron algorithm model. MLP is a typical deep learning model. It can solve more complex problems. Compared with machine learning models, MLP has many characteristics.

(6) Decision tree

The decision tree model is a supervised learning algorithm with a relatively simple theory, which provides decision-making basis through a tree structure. The learning process of decision tree generally includes three parts: feature selection, generating decision tree, and pruning, among which feature selection is the most important part. A

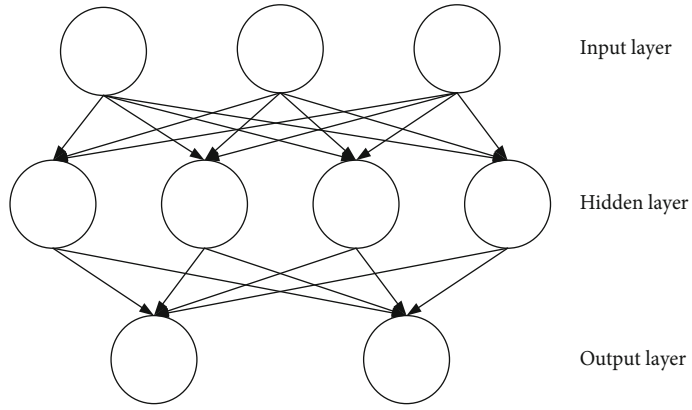

Figure 4: Multilayer perceptron algorithm.

common way of selecting features is based on information theory.

First, the concept of entropy is introduced. Assuming that the possible values of random variable a are $a_1, a_2, \cdots, a_p$, the value probability is

$$R(A = a_i) = r_i, i = 1, 2, \cdots, p. \tag{10}$$

So, the entropy of random variable a is

$$L(A) = -\sum_{i=1}^{p} r_i \log_2 r_i. \tag{11}$$

For the sample set T, the random variable A is the category of the sample, that is, if the sample has S categories, the probability of each category is $|V_s|/|T|$, where $|V_s|$ is the number of samples of the category, and $|T|$ is the total number of samples.

The information entropy of the sample set T is

$$L(T) = -\sum_{s=1}^{S} \frac{|V_s|}{|T|} \log \frac{|V_s|}{|T|}, \tag{12}$$

$$\varphi_n^c = \sum \left(\varphi_n^0 U_{mk}^3\right) g_m^{'}(\cdot). \tag{13}$$

It is one of the commonly used metrics to measure the purity of the sample set T. The smaller $L(T)$, the higher the purity of T.

3.3.1. Information Gain. Assuming that the value range of attribute D is $\{d_1, d_2, \cdots, d_p\}$, when a certain attribute D is used to divide the sample set T, the formula for its information gain is

$$f(T, D) = L(T) - \sum_{i=1}^{p} \frac{|T_i|}{|T|} L(T_i). \tag{14}$$

Here $|T_i|$ is the number of samples with a value of d_i on attribute D. Generally, the larger the value of $f(T, D)$, the greater the improvement in purity obtained by dividing by attribute D.

3.3.2. Information Gain Rate. The formula for the information gain rate is

$$f_U(T, D) = \frac{f(T, D)}{L_D(T)}. \tag{15}$$

Here,

$$L_D(T) = -\sum_{i=1}^{p} \frac{|T_i|}{|T|} \log_2 \frac{|T_i|}{|T|}. \tag{16}$$

3.3.3. Gini Index. The Gini index of the sample set T is

$$\text{Gini}(T) = 1 - \sum_{s=1}^{S} \left(\frac{|V_s|}{|T|}\right)^2. \tag{17}$$

The smaller the value of $\text{Gini}(T)$, the higher the purity of the sample set T is.

The Gini index based on property D is

$$\text{Gini}(T, D) = \sum_{i=1}^{p} \frac{|T_i|}{|T|} \text{Gini}(T_i). \tag{18}$$

Here,

$$\text{Gini}(T_i) = 1 - \sum_{s=1}^{S} \left(\frac{|V_s|}{|T_i|}\right)^2, i = 1, 2, \cdots, p. \tag{19}$$

(6)Random forest

The random forest model is a very well-known algorithm in ensemble learning theory. It uses decision tree as a basic learner, establishes Bagging ensemble calculation, and introduces random feature selection in the training of decision tree. The specific process is shown in Figure 5.

The random forest model has significant advantages over a single decision tree. It has the ability to process big data and evaluate the importance of each variable when making class decisions. It is easy to implement and has low computational overhead, and the model training speed is fast.

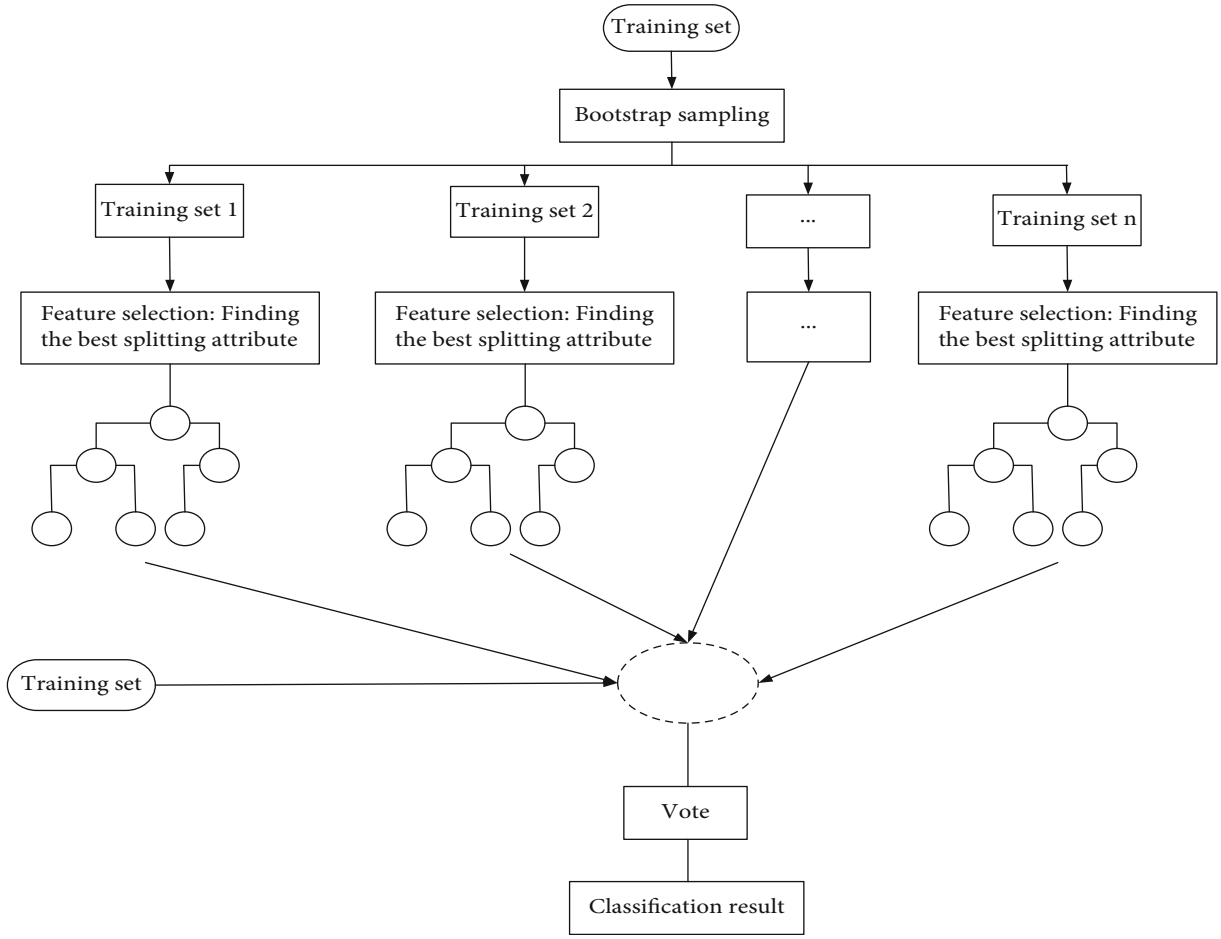

Figure 5: Random forest algorithm.

4. Experiment Results of Research on Sustainable Development of Heritage Tourism Boosted by Smart Tourism Based on Big Data Artificial Intelligence

In 2015, a scenic spot was rated as a world natural heritage as a symbol, and the real heritage tourism of the scenic spot officially began. From 2015 to 2020, Wulong's tourism reception volume and total tourism revenue are shown in Tables 1 and 2. It can be seen from the table that after the place was rated as a World Heritage Site, the number of tourists increased rapidly. The number of tourist receptions has increased from 1,639,700 in 2015 to 16,110,100 in 2020, a growth rate of 881.1%; the total tourism revenue has increased from 166.49 million in 2015 to 8,100.69 million in 2020, an increase of nearly 50 times. It can be seen that the brand effect of world heritage sites has a direct driving effect on tourism development.

4.1. Comprehensive Analysis of Tourism Ecological Footprint of Natural Heritage Sites. The tourism ecological footprint simulation is based on the statistics of the number of ecological footprints and the ecological carrying capacity, and the difference between the tourism ecological footprint of a certain place and the national tourism ecological carrying capacity is used to represent the impact of tourism development on the natural environment, so as to evaluate the impact of tourism development on the natural environment and the sustainable development of local tourism. This paper will conduct a comprehensive study on the tourism ecological footprint, tourism ecological carrying capacity, tourism ecological deficit or surplus of a natural heritage site in the time range of 2015-2020,in order to explore the status quo of the sustainable development of tourism in this natural heritage site, and put forward relevant opinions and suggestions on the sustainable development mode and existing problems of tourism.

Based on the analysis results of the tourism ecological footprint sub-models of a natural heritage site from 2015 to 2020, the development law of the overall tourism ecological footprint of the study area during the study period was sorted out and analyzed.

By summarizing and sorting them, the changes in the tourism ecological footprint of Wulong World Natural Heritage Site and the per capita tourism ecological footprint from 2015 to 2020 are shown in Figure 6, as well as the change trend of the proportion of tourism ecological footprint accounts, as shown in Figure 7.

Table 1: Tourism reception in 2015-2017.

Years	Number of tourist reception (10,000 person-times)	Total tourism revenue (ten thousand yuan)
Year 2015	163.97	16649
Year 2016	219.96	22939
Year 2017	470.01	231201

Table 2: Tourism reception in 2018-2020.

Years	Number of tourist reception (10,000 person-times)	Total tourism revenue (ten thousand yuan)
Year 2018	1020.01	500201
Year 2019	1331.02	657198
Year 2020	1611.01	810069

According to the statistical results, a comprehensive analysis of the development trend of tourism ecological footprint of a natural heritage site from 2015 to 2020 was carried out.

(1) The per capita ecological footprint of tourism in this natural heritage site shows an overall increasing trend. Mainly because tourists tend to choose comfortable and convenient (comparatively speaking, usually with a higher ecological footprint per unit) travel mode and consumption behavior pattern. Compared with the growth of the total tourism ecological footprint, the growth rate of the per capita ecological footprint of tourism in this natural heritage site is relatively small and the growth is relatively gentle

(2) The ecological footprint of tourism and catering and the ecological footprint of tourism transportation account for the majority of China's tourism ecological footprint. Among them, the ecological footprint of tourism and catering occupies the largest proportion, followed by the ecological footprint of tourism transportation, and then, the ecological footprint of tourism waste occupies a larger proportion and shows a trend of increasing year by year, and the remaining four categories account for a small proportion

4.2. Comprehensive Analysis of Tourism Ecological Carrying Capacity of Natural Heritage Sites. After consulting the data, it is found that the county's forest land covers an area of 73.5%, and the average forest coverage rate is as high as 59.3%. The research area of this paper is a mountainous scenic spot, and the forest coverage rate of the heritage scenic spot is more than 80%. Therefore, all the ecologically productive land in the research area of our institute can be regarded as forest land. The following will calculate the ecological carrying capacity of tourists and per capita tourism ecological carrying capacity of the natural heritage site in turn from 2015 to 2020. The specific calculation results are shown in Tables 3 and 4.

Based on the above calculation results, a comprehensive analysis of the change trend of the tourism ecological carrying capacity of the natural heritage site from 2015 to 2020 is carried out.

(1) The tourism ecological carrying capacity of the natural heritage site will remain basically unchanged from 2015 to 2020. Because of the strong protection of the core area and buffer zone of the World Heritage Site, the land use status has not changed much in recent years. Therefore, this paper assumes that the area of ecologically productive land within the study area remains unchanged and is all forest land. Although in fact the ecological carrying capacity within the research scope will change to a certain extent, the assumption of this paper is reasonable considering the integrity and subjectivity of the research

(2) From 2015 to 2020, the per capita tourism ecological carrying capacity of this natural heritage site showed a significant downward trend, and the decline was very large, reaching 81.9%. The main reason is that during the study period, the total value of tourism and ecological carrying capacity remained unchanged, while the number of tourists received within the study area increased rapidly, resulting in a significant decline in per capita tourism ecological carrying capacity

4.3. Comprehensive Analysis of Ecological Deficit or Surplus of Natural Heritage Sites. According to the above calculation results, by comparing the tourism ecological footprint of the natural heritage site with the tourism ecological carrying capacity from 2015 to 2020, it can be concluded that the tourism ecological deficit (or surplus) of the Wulong World Natural Heritage Site. By comparing the per capita ecological footprint of the natural heritage site with the per capita ecological carrying capacity of the natural heritage site from 2015 to 2020, it can be concluded that the per capita ecological deficit (or surplus) of the Wulong World Natural Heritage site. Among them, the tourist ecological footprint of the world natural heritage site does not exceed the ecological carrying capacity of tourists, which is expressed as the ecological surplus of tourists, as shown in Figure 8; the per capita tourist ecological footprint of the world natural heritage site also does not exceed the global average ecological carrying capacity of tourists. It is mainly reflected in the ecological surplus of tourists per capita, as shown in Figure 9.

Based on the above numerical calculations, a comprehensive analysis was made on the tourism ecological surplus of this natural heritage site from 2015 to 2020.

(1) During the period 2015-2020, the natural heritage site showed an ecological surplus, and the results

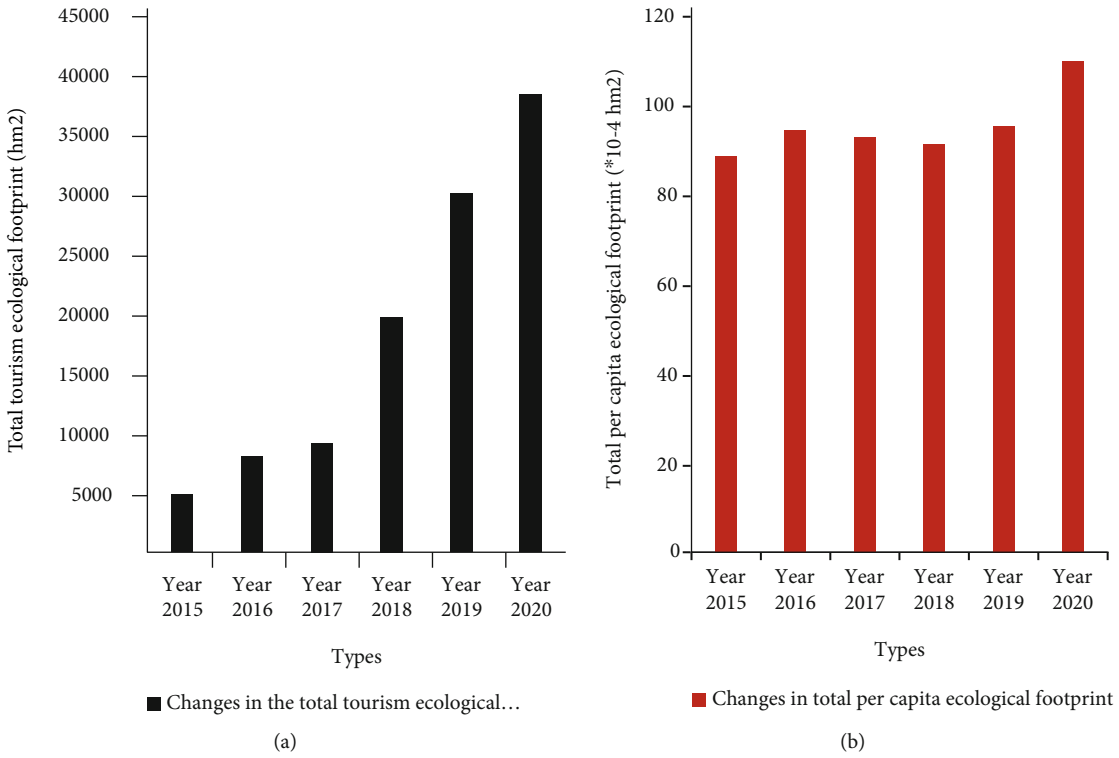

Figure 6: Changes in tourism ecological footprint of natural heritage sites and changes in per capita ecological footprint.

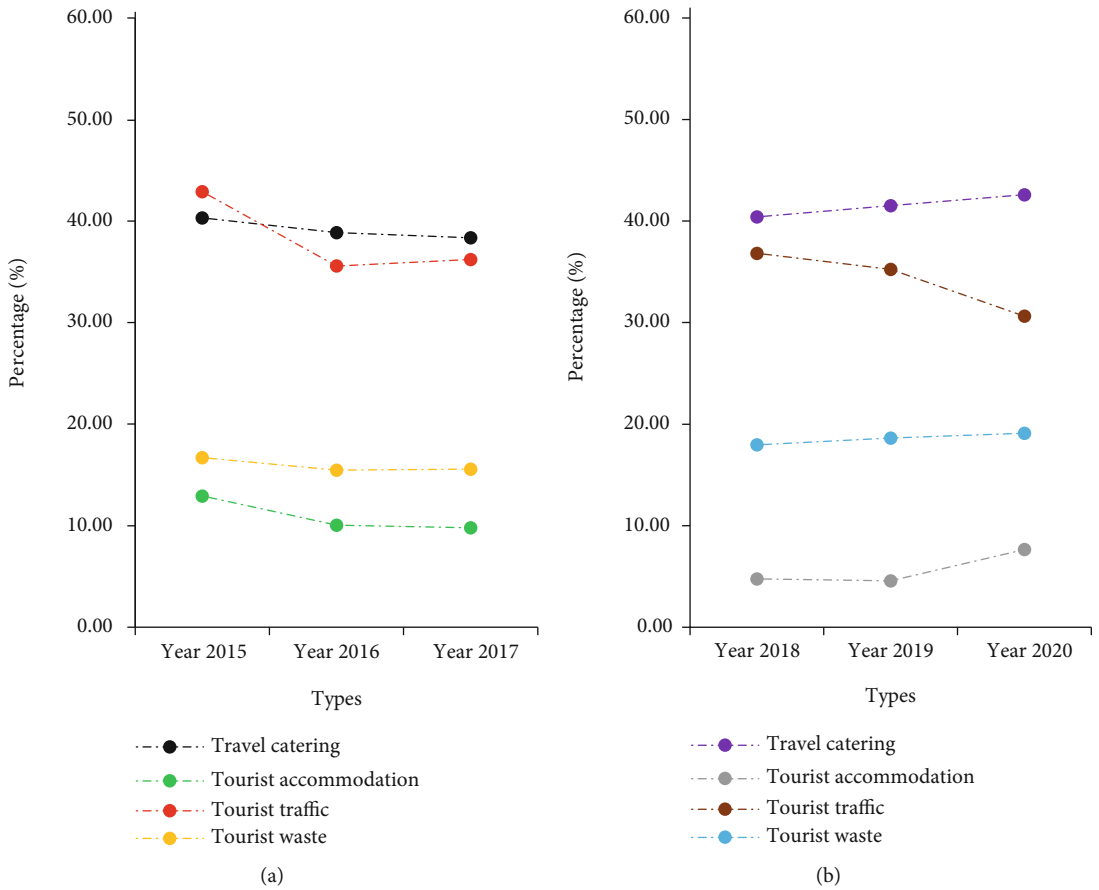

Figure 7: Trends in the composition of the ecological footprint of tourism in natural heritage sites.

Table 3: Summary of tourism ecological carrying capacity of natural heritage sites in 2015-2017.

	Regional area (hm^2)	Land type	Equilibrium factor	Yield factor	Ecological carrying capacity (hm^2)	Biodiversity conservation	Ecological carrying capacity per capita ($*10^{-4}hm^2$)
Year 2015	38000	Woodland	1.0	0.9	40419.76	5509.99	654.79
Year 2016	38000	Woodland	1.0	0.9	40419.76	5509.99	476.97
Year 2017	38000	Woodland	1.0	0.9	40419.76	5509.99	407.79

Table 4: Summary of tourism ecological carrying capacity of natural heritage sites in 2018-2020.

	Regional area (hm^2)	Land type	Equilibrium factor	Yield factor	Ecological carrying capacity (hm^2)	Biodiversity conservation	Ecological carrying capacity per capita ($*10^{-4}hm^2$)
Year 2018	38000	Woodland	1.0	0.9	40419.76	5509.99	187.01
Year 2019	38000	Woodland	1.0	0.9	40419.76	5509.99	127.97
Year 2020	38000	Woodland	1.0	0.9	40419.76	5509.99	116.02

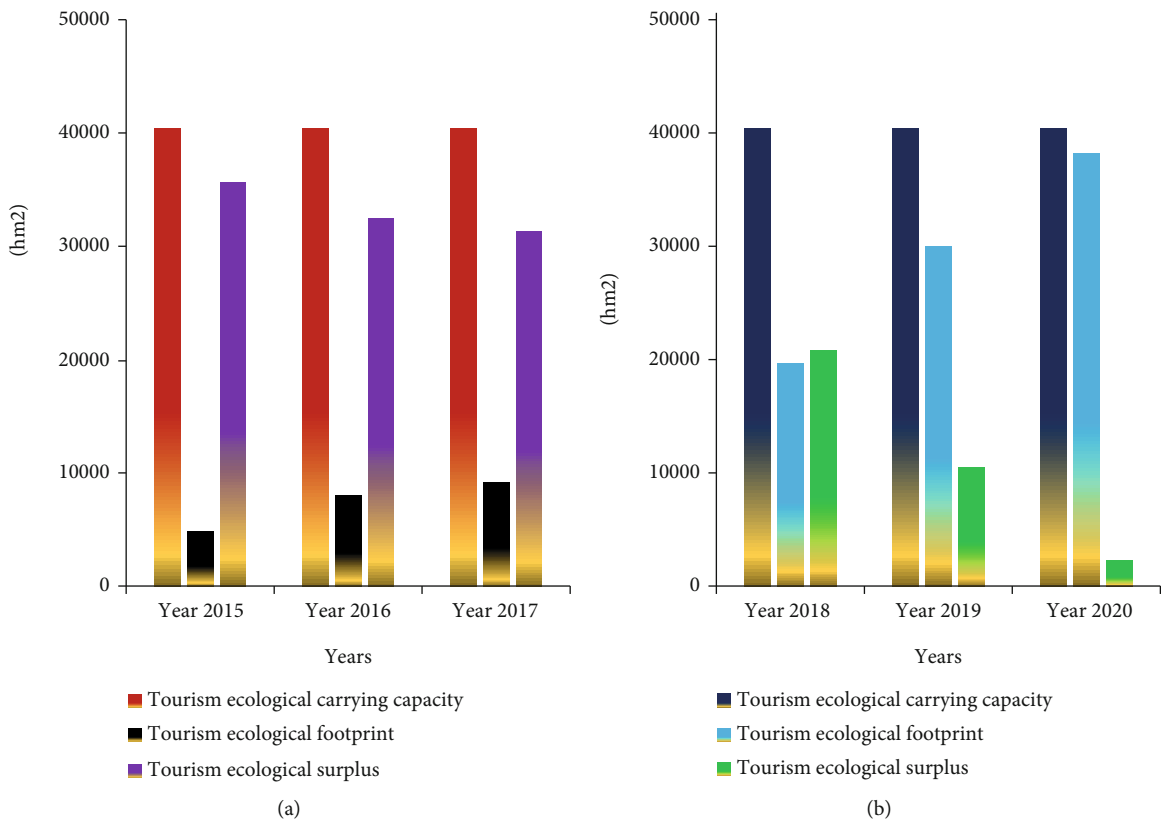

Figure 8: Summary of tourism ecological surplus in natural heritage sites from 2015 to 2020.

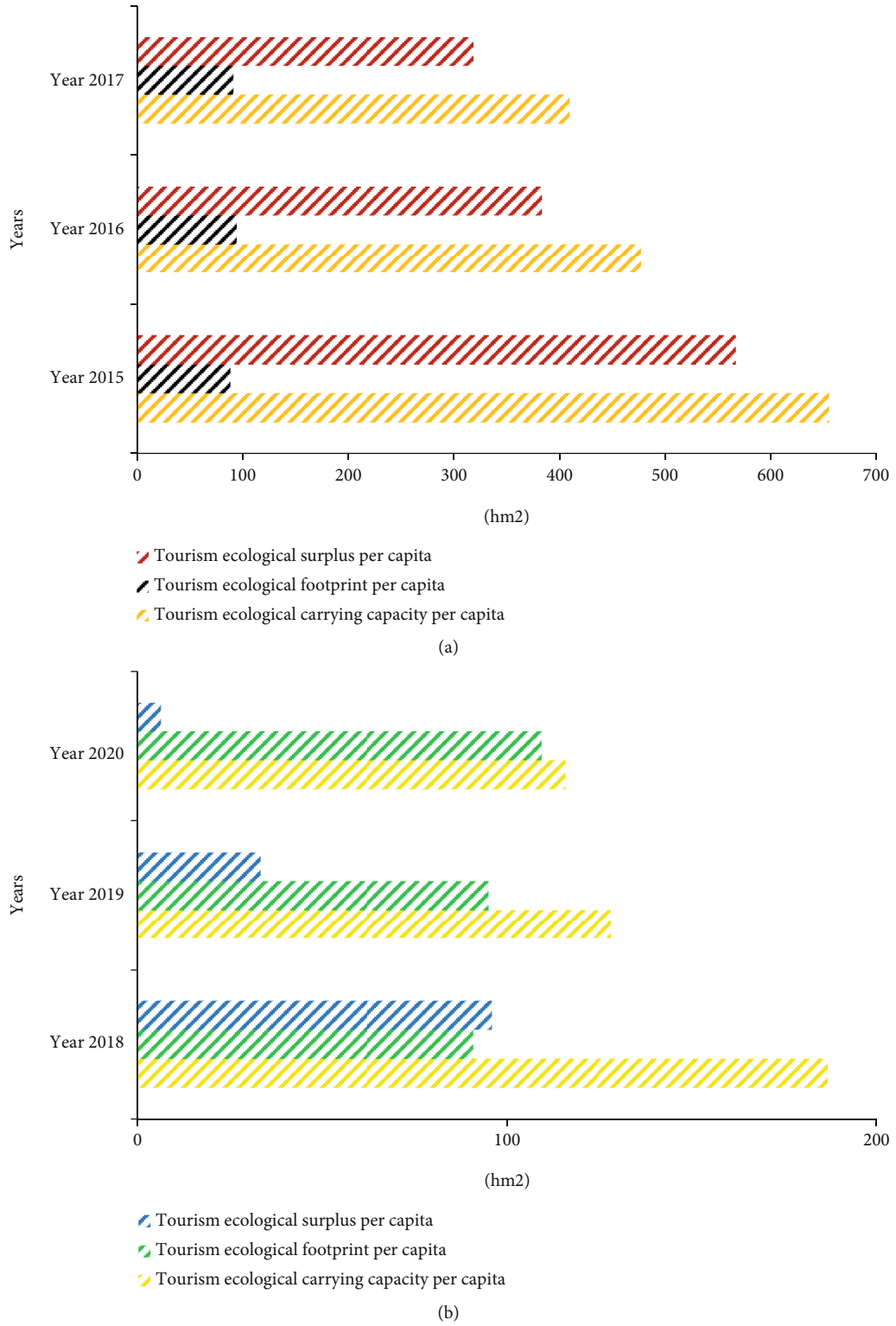

Figure 9: Summary of per capita tourism ecological surplus in natural heritage sites from 2015 to 2020.

show that its development is in a continuous trend. At the same time, the average travel ecological construction affordability is 40421.97 hm^2, the average travel ecological construction footprint is 18285.93 hm^2, and the average value is 22136.04 hm^2 of ecological construction profit. The average per capita travel ecological construction affordability is 0.032861 hm^2, and the average per capita travel ecological footprint is 0.009466 hm^2, both with 0.02339 hm^2 of ecological construction profit

(2) From 2015 to 2020, the tourism ecological surplus and per capita ecological surplus of this natural heritage site showed a rapid downward trend. Among them, the tourism ecological surplus decreased by 93.75%, and the per capita ecological surplus decreased by 98.88%. The main reason is that during the study period, the ecological carrying capacity is basically unchanged, while the rapid increase in tourism reception and the change in tourists' consumption behavior have resulted in a large increase in the ecological footprint of tourism. As a result, the tourism ecological surplus and the per capita tourism ecological surplus have dropped significantly

5. Discussion

The development of smart tourism meets the needs of urban informatization development. On the basis of urban modernization, the functions of the city have been further extended and sublimated through a new generation of information technology. The development of smart tourism involves the comprehensive operation of various systems. While applying smart technology to tourist attractions and related services, the scope of application should be expanded in a timely manner, and the mode of economic development should be changed adaptively, promoting the development of informatization in urban public services, social management, etc. Let urban people focus on using intelligence to discover new problems and solve them, so as to form stronger innovation and development capabilities, enhance the city's soft power, change the city's image, and improve people's quality of life. At the same time, the intelligent scenic spot customer service system also focuses on the formation of a new type of intelligent tourism service technology through the construction of innovative information service methods. These methods include not only the horizontal development of expanding the scope of scenic spot information consulting services but also the vertical in-depth experience and expansion of tourists through in-depth exploration of scenic spot information consulting service resources. On the one hand, the intelligent scenic spot customer service system strives to implement effective, safe, reliable, multifaceted, and personalized information consulting services for tourists at home and abroad. On the other hand, it pays more attention to the benefits in the process of pushing the information service process, so that the development of tourist attractions and tourism services has a healthier development direction. The construction of intelligent scenic spots will attach great importance to the construction of scenic resources and environmental management and monitoring systems. Through unified information technology facilities, big data infrastructure and information public service facilities, various resources, and environmental protection information systems will be seamlessly integrated. In order to achieve the comprehensive automation of various resources and environments, it can provide information consulting services for scenic resources and environments, as well as the comprehensive decision-making process of scenic spots, thereby promoting the sustainable development of scenic spots.

6. Conclusions

The value orientation of sustainable tourism development should focus on coordinating the balance between human society and nature. When considering the relationship between man and human society, the relationship between man and other living things should be considered at the same time. We respect life to maintain the vitality and diversity of organisms, protecting the life system, and keeping the sustainable use of renewable resources at a minimum. The sustainable development of heritage tourism calls for new values. And new values will drive people to embark on the road of sustainable development of heritage tourism. The idea of sustainable development of heritage tourism provides a new opportunity for the development of heritage tourism. At the same time, it also provides a new value concept for the rational development and utilization of tourism resources in heritage sites. It has obvious guiding significance for forming a new social relationship between man and nature, and cultivating people's ecological responsibility and ecological ethics for their offspring. This paper adopts the tourism ecological footprint model to study the sustainable development of tourism in world natural heritage sites. For the sake of research integrity and subjectivity, some research variables are assumed and ignored. Although such processing methods have little impact on the final results of the study, there are still some deviations from the actual results. This paper will optimize it in the follow-up research.

Data Availability

The data that support the findings of this study are available from the corresponding author upon reasonable request.

Conflicts of Interest

The authors declare that they have no conflicts of interest.

References

[1] X. Yu and H. Xu, "Cultural heritage elements in tourism: a tier structure from a tripartite analytical framework," *Journal of Destination Marketing and Management*, vol. 13, no. 1, pp. 39–50, 2019.

[2] A. A. Alobiedat, "Heritage transformation and the sociocultural impact of tourism in Umm Qais," *Journal of Tourism and Cultural Change*, vol. 16, no. 1, pp. 22–40, 2018.

[3] R. Li, Z. Zhao, X. Zhou et al., "Intelligent 5G: when cellular networks meet artificial intelligence," *IEEE Wireless Communications*, vol. 24, no. 5, pp. 175–183, 2017.

[4] L. Caviglione, M. Gaggero, J. F. Lalande, W. Mazurczyk, and M. Urbański, "Seeing the unseen: revealing mobile malware hidden communications via energy consumption and artificial intelligence," *IEEE Transactions on Information Forensics & Security*, vol. 11, no. 4, pp. 799–810, 2016.

[5] Y. Zhang, M. Qiu, C. W. Tsai, M. M. Hassan, and A. Alamri, "Health-CPS: healthcare cyber-physical system assisted by cloud and big data," *IEEE Systems Journal*, vol. 11, no. 1, pp. 88–95, 2017.

[6] Y. Zhang, J. Ren, J. Liu, C. Xu, H. Guo, and Y. Liu, "A survey on emerging computing paradigms for big data," *Chinese Journal of Electronics*, vol. 26, no. 1, pp. 1–12, 2017.

[7] R. C. Carlos, C. E. Kahn, and S. Halabi, "Data science: big data, machine learning, and artificial intelligence," *Journal of the American College of Radiology*, vol. 15, no. 3, pp. 497-498, 2018.

[8] A. L. Kotsenas, P. Balthazar, D. Andrews, J. R. Geis, and T. S. Cook, "Rethinking patient consent in the era of artificial intelligence and big data," *Journal of the American College of Radiology*, vol. 18, no. 1, pp. 180–184, 2021.

[9] A. Nayarisseri, R. Khandelwal, P. Tanwar et al., "Artificial intelligence, big data and machine learning approaches in precision medicine & drug discovery," *Current Drug Targets*, vol. 22, no. 6, pp. 631–655, 2021.

[10] J. Skinner, "Heritage that hurts: tourists in the memoryscapes of September 11," *Journal of Tourism and Cultural Change*, vol. 15, no. 1, pp. 101–103, 2017.

[11] S. Price and P. A. Flach, "Computational support for academic peer review," *Communications of the ACM*, vol. 60, no. 3, pp. 70–79, 2017.

[12] P. Glauner, J. A. Meira, P. Valtchev, R. State, and F. Bettinger, "The challenge of non-technical loss detection using artificial intelligence: a survey," *International Journal of Computational Intelligence Systems*, vol. 10, no. 1, pp. 760–775, 2017.

[13] J. H. Thrall, X. Li, Q. Li et al., "Artificial intelligence and machine learning in radiology: opportunities, challenges, pitfalls, and criteria for success," *Journal of the American College of Radiology*, vol. 15, no. 3, pp. 504–508, 2018.

[14] C. Cath, S. Wachter, B. Mittelstadt, M. Taddeo, and L. Floridi, "Artificial intelligence and the 'good society': the US, EU, and UK approach," *Science and Engineering Ethics*, vol. 24, no. 7625, pp. 1–24, 2017.

[15] M. Hutson, "Artificial intelligence faces reproducibility crisis," *Science*, vol. 359, no. 6377, pp. 725-726, 2018.

[16] J. Lemley, S. Bazrafkan, and P. Corcoran, "Deep learning for consumer devices and services: pushing the limits for machine learning, artificial intelligence, and computer vision," *IEEE Consumer Electronics Magazine*, vol. 6, no. 2, pp. 48–56, 2017.

[17] R. Chatila, K. Firth-Butterflied, J. C. Havens, and K. Karachalios, "The IEEE global initiative for ethical considerations in artificial intelligence and autonomous systems [standards]," *IEEE Robotics & Automation Magazine*, vol. 24, no. 1, pp. 110–110, 2017.

[18] F. Wang, "Artificial intelligence in research," *Science*, vol. 357, no. 6346, pp. 28–30, 2017.

[19] J. Bryson and A. Winfield, "Standardizing ethical design for artificial intelligence and autonomous systems," *Computer*, vol. 50, no. 5, pp. 116–119, 2017.

[20] E. Burton, J. Goldsmith, S. Koenig, B. Kuipers, N. Mattei, and T. Walsh, "Ethical considerations in artificial intelligence courses," *AI Magazine*, vol. 38, no. 2, pp. 22–34, 2017.

Hindawi
Wireless Communications and Mobile Computing
Volume 2022, Article ID 7452638, 11 pages
https://doi.org/10.1155/2022/7452638

Research Article

The Implementation of Multiobjective Flexible Workshop Scheduling Based on Genetic Simulated Annealing-Inspired Clustering Algorithm

Ming Huang,[1] Fei Wang,[2,3] and Si Wu[4]

[1]*College of Software, Dalian Jiaotong University, Dalian, 116028 Liaoning, China*
[2]*College of Mechanical Engineering, Dalian Jiaotong University, Dalian, 116028 Liaoning, China*
[3]*Department of Basics, Dalian University of Science and Technology, Dalian, 116052 Liaoning, China*
[4]*College of Foreign Languages, Dalian University of Science and Technology, Dalian, 116052 Liaoning, China*

Correspondence should be addressed to Si Wu; wusi@dlust.edu.cn

Received 18 March 2022; Revised 23 April 2022; Accepted 6 May 2022; Published 20 May 2022

Academic Editor: Jun Ye

Multiobjective flexible workshop scheduling is an important subject to improve resource utilization and production efficiency and enhance the competitiveness of enterprises. As the situation of resource constraints becomes more and more severe, the problem of companies rationally allocating limited resources in production is becoming more and more serious. Today, the manufacturing industry widely adopts advanced manufacturing modes such as computer-integrated manufacturing and intelligent manufacturing, but in these semi-intelligent manufacturing modes with a high degree of uncertainty and a high degree of personnel dependence, it is difficult to adapt to the work of large-scale production. Therefore, suitable clustering algorithms are urgently needed to help solve these problems, and this paper selects a clustering algorithm based on the genetic simulation annealing algorithm. This article is aimed at studying the problem of efficiency improvement in the production process of large-scale manufacturing and at finding a stronger and more effective production mode for the manufacturing industry. Firstly, this paper introduces the basic principles of simulated annealing genetic algorithm and regularized clustering algorithm. These algorithms have excellent performance in searching for global optimal solutions. They can be constantly tested and computed to keep the calculation results close to the global optimal solution. In this paper, the K-means clustering algorithm is used to select the shortest completion time to represent the clustering target. According to the minimum distance principle, the machine, workpiece, and other objects are input into the clustering of the algorithm, and the K-means algorithm will send out the sorting plan. Therefore, a multiobjective flexible job shop scheduling model based on genetic simulated annealing algorithm and clustering algorithm is established. Then, by using hypothetical production data to simulate the operation of the workshop, the scheduling model was applied to conduct a deduction and empirical comparative study. The experimental results showed that the model shortened the completion time of the workpiece by 4.4% and increased the average load rate of the machine by 10%.

1. Introduction

Simulated annealing algorithm, genetic algorithm, and clustering algorithm have been applied in the fields of grouping technology, job division and scheduling, equipment layout, vehicle routing, etc., and the application scope of various algorithms is continuously expanding. In recent years, the domestic market environment has undergone earth-shaking changes, and market trends are often the direction of change that the manufacturing industry needs to adapt. Changes in the market structure directly lead to changes in the production structure. This is mainly because the corresponding supply and demand relationship has changed. With the continuous advancement of information

technology applications, people's ability to obtain information has been greatly improved, the people's cognitive abilities have continued to improve, and their living standards have continued to improve. With their full understanding of the market, the individual needs of the people will play a production-oriented role, leading to the diversification of product demand in the market. In the market competition of economic globalization and multilayered demand, enterprises are under increasing pressure to survive, and production methods tend to be diversified and small batches of customized production routes. How to enhance the core competitiveness of enterprises is a long-term and severe challenge faced by many enterprises.

With the rapid development of information technology and the rapid development of Internet of Things technology, the combination of Internet of Things technology and logistics technology has created many new opportunities for the manufacturing industry and also presented many challenges. Extract valuable information from a large amount of rapidly generated production data, thereby promoting the development of logistics data big data mining, providing decision support for logistics managers, and optimizing the structure of the logistics industry. This study found that the improved genetic simulation-based clustering algorithm is helpful to solve the multiobjective flexible workshop scheduling problem. Therefore, this paper has some practical significance for the related clustering algorithm based on the improved genetic simulation-based annealing algorithm. The case empirical evidence presented in this paper provides theoretical and practical references for promoting the reform of the manufacturing workshop.

Many scholars have conducted research on the use of advanced algorithms to improve the efficiency of workshop scheduling. Aiming at the problem of the lack of conformational design and weight training algorithms in neural network applications, Zhang et al. proposed a backpropagation neural network learning algorithm combined with simulated annealing genetic algorithm. The simulated annealing mechanism is built into the genetic algorithm to optimize the neural network at the same time. For the conformation and network weight design and optimization, this algorithm increases the amount of network weight calculation, thereby greatly increasing the loss, only suitable for laboratory research; it is difficult to apply in practical work [1]. Cen et al. proposed the genetic simulated annealing algorithm, which is an algorithm that combines genetic algorithm and simulated annealing algorithm, which is used in soil slope operations to quickly and accurately locate the critical slip surface of the soil slope to calculate the safety factor. They believe that compared with the golden section method based on the finite element calculation of the same stress field, the genetic simulated annealing algorithm is more accurate and efficient in searching for the critical slip surface of the slope of the earth-rock dam. The measurement is not in place [2]. Reddy et al. adopt a new method based on the hybrid technology of genetic algorithm and simulated annealing. This method is called the clustering algorithm concept of additive and split hierarchical clustering. They described a method by classifying the unit into various clusters which is a new method to solve the unit combination problem. Its purpose is to save fuel costs, reduce overall operating costs, and easily meet the minimum upper and lower constraints through the proper use of generator sets. However, the premise of this algorithm is that the generator set will never shut down. There is no failure, once an unexpected situation occurs. It will cause the algorithm to crash [3]. Aiming at the problem of high energy consumption of the spectral clustering algorithm in the construction of similarity matrix and feature decomposition of the overall data set, Wang et al. proposed a clustering algorithm based on grid division and decision graph to reduce the amount of calculation and improve the efficiency of clustering. In addition, they also added a decision graph method to quickly identify the clustering center and improve the stability of the algorithm. Numerical experiments show that the algorithm can effectively improve the efficiency of the spectral clustering algorithm. However, many scholars do not need any prior knowledge of the algorithm. Will this behavior cause the machine to learn every time it runs, resulting in repeated labor [4]. Aiming at the problem that the positioning system of the ship automatic identification system cannot find the ship navigation characteristics in real time, Li et al. propose an adaptive time interval clustering algorithm based on density grid. The algorithm can cluster the adaptive time interval according to the size of the real-time ship trajectory data. In order to efficiently and real-time discover the information of ship hot spots, the areas discovered by clustering algorithm are generally marine transportation hubs and existing hot issues, and their support for decision-making is very limited [5]. Wu et al. proposed a clustering algorithm based on adaptive multiresolution map, which can not only improve the efficiency of the calculation process but also obtain stable propagation results. Their research results have been applied to log facies analysis and improved the old method. The in-depth analysis of multidimensional logging curves based on the clustering of multiresolution graphs is very time-consuming and highly dependent on initial parameters. However, the research only focuses on the field of logging facies, and the research results can only be applied to this reference application in other fields [6]. Liu et al. have studied a model called flexible workshop. From the perspective of practical application, they use energy-sensitive production scheduling technology to minimize energy consumption. In order to deal with large-scale problems and further improve its energy efficiency, they designed another one. A special genetic algorithm makes the operation sequence of the model work change within certain constraints. The experimental numerical results show that the flexible workshop proposed by them has good effectiveness and efficiency, but the research optimizes energy efficiency, and there are few studies on machine efficiency and personnel efficiency [7]. In view of the unsustainable use of machines in the workshop, the preventive maintenance and transportation process of machines are considered. Wang et al. put forward the problem of flexible job shop scheduling considering the preventive maintenance activities and the transportation process and established numbers of ways to reduce the total energy consumption. The target flexible job shop scheduling

model has less human demand, which is not in line with the actual situation, and more consideration should be given to the configuration of functional personnel [8].

The research innovation of this paper is mainly reflected in the improvement and practical application of the genetic simulated annealing algorithm. The main innovations are as follows: use the Metropolis criterion of the simulated annealing algorithm to improve the genetic algorithm selection operator, enhance the genetic algorithm while maintaining the good performance of the genetic algorithm selection scheme, and then, make the performance of the clustering algorithm based on the genetic simulation annealing algorithm better played in the application process. This paper uses genetic simulated annealing algorithm to solve the optimal scheduling problem of workshop production.

2. Multiobjective Flexible Workshop Scheduling Model Establishment Method

2.1. The Basic Principles of Simulated Annealing Genetic Algorithm. Scholars such as Metropolis proposed the simulated annealing algorithm in 1953. The algorithm is inspired by the similarities between many combinatorial optimization problems in mathematics and the solid-state cooling annealing process in physics. The proposed algorithm is a stochastic optimization algorithm based on Monte Carlo iterative solutions, which combines both SA and GA algorithms with good probabilistic optimization capability. Combining the probability jump ability of the algorithm, the solution of the objective function is randomly searched in the executable solution space of the problem. This iterative process gradually continues to find the global optimal solution of the problem and decides whether to accept the new solution according to the Metropolis criterion [9]. The purpose of designing the simulated annealing algorithm is to achieve the optimal value of the objective function. During the annealing process, the probability of accepting the optimized solution should be greater than the probability of accepting the degraded solution. As the temperature drops, it is more likely to accept the optimized solution. Close to zero, the probability of accepting the degraded solution also approaches zero [10]. Among them, the Metropolis criterion is the core theory of the simulated annealing algorithm. The criterion is defined according to the above theory, and the expression is

$$f(\Delta n, x) = \begin{cases} 1 & \Delta n \le 0, \\ e^{-\Delta n/x} & \Delta n > 0. \end{cases} \tag{1}$$

In the formula, $f(x)$ represents the acceptance probability of the current new solution; Δn represents the difference of the objective function corresponding to the current new solution and the previous solution; and x represents the temperature control parameter during the iteration of the simulated annealing algorithm [11]. The Metropolis acceptance standard allows the algorithm to accept degraded solutions with a certain probability and prevents the algorithm from falling into a local optimum. A larger value of x is more likely to accept a degraded solution, but as the iteration progresses, x gradually decreases and approaches 0 [12]. The simulated annealing algorithm is different from the random algorithm that accepts all new solutions and the local search characteristics of the local search algorithm, which makes the algorithm have better global search capabilities and greater probability to obtain the best global solution [13].

The value of the fitness function is the only criterion for evaluating individual interests in the combination. The design of the fitness function is usually related to the objective function in question. In flexible workshop production scheduling problems, the fitness function is often related to the production time of the workshop. In the fastest scheduling problem, the scheduling goal is the shortest time at the end of the entire production process. At this time, the fitness function is generally designed as the reciprocal of the total scheduling processing time as the fitness function [14]. Assuming that there are n machines processing x workpieces, the processing completion time of the machine m_n to the workpiece g_x is $y(g_x, m_n)$. Since the processing time of the workpiece g_x on the machine tool m_n is $t(g_x, m_n)$ and the scheduling plan of the workpiece is $\{g_1, g_2, \cdots, g_x\}$, the time model until the completion of all workpieces is as follows:

$$\begin{gathered} y(g_x, 1) = t(g_1, m_1), \\ y(g_1, m_n) = y(g_1, m_{n-1}) + t(g_1, m_n), \\ y(g_x, 1) = y(g_{x-1}, 1) + t(g_x, m_1), \\ y(g_x, m_n) = \mathrm{MAX}\{y(g_{x-1}, m_n); y(g_x, m_{n-1})\} + t(g_x, m_n), \\ y_{\max} = y(g_x, n). \end{gathered} \tag{2}$$

$x = 2, 3 \cdots, +\infty$ and $n = 2, 3 \cdots, +\infty$. In this scheduling problem, the fitness function is $f(y) = 1/y_{\max}$.

The coding methods currently used in genetic algorithms mainly include binary coding, decimal coding, and real number coding [15]. The orderly coding list (chromosome) of the process completion time is expressed as *[y1 y2 y3]*; the workpiece chromosome is expressed as *[g1 g2 g3]*; the machine is expressed as *[m1 m2 m3]*; thus, the machine list corresponding to this chromosome is *[y1m1 y2m2 y3m3]*. Accordingly, the processing sequence scheduling scheme of each workpiece on the machine is shown in Figure 1.

According to the design criteria of the fitness function of the genetic algorithm, the following conditions are mainly considered in the design of the fitness function: first, make the fitness function monotonic, continuous, and nonnegative, so that the optimization algorithm can find the maximum value. The goodness-of-fit value should reflect the strength of the solution, which is usually difficult to implement [16]. The function design should be as simple as possible to reduce the calculation time and improve the calculation efficiency. The design should improve the robustness of the fitness function as much as possible. The goal of this research is to find the minimum value of the time

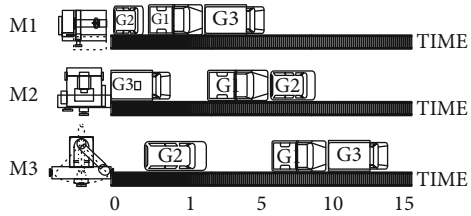

Figure 1: A feasible scheduling scheme based on process coding.

required to complete the workpiece, so it is assumed that the fitness function is

$$f(x) = \exp\{(ab) \cdot E(x)\}^{-1}, \tag{3}$$

where $f(x)$ represents the energy value of the individual, x represents the fitness of the individual chromosome, and a and b are variable parameters. The values are selected according to the duration of the algorithm and various actual environments to facilitate the annealing operation and the population. Adjusted in the diversity, there is greater flexibility [17].

Suppose G is the population size, g is the current population generation, and g_i is the maximum genetic generation. First, save the two individuals with the smallest and the largest fitness in the current population in the result set. When $g \le g_i/2$, randomly select $2g$ individuals from the current population for screening, arrange them in the order of the strength of individual fitness, and save the selection in the result set. The number of outstanding individuals is g. The probability of individual fitness value is selected in a proportional manner, and the fitness of individual i is obtained as S_i; then, the probability p_i of the individual being selected is

$$p_i = \frac{S_i}{\sum_{i\in[1,g]}^{G} S_i}. \tag{4}$$

This paper combines simulated annealing algorithm and genetic algorithm; combining genetic simulated annealing algorithm and simulated annealing algorithm can effectively avoid the premature phenomenon of traditional genetic algorithm, and at the same time, according to the specific situation, the fitness function and genetic code can be designed to make the algorithm more effective. Accelerate convergence [18]. Figure 2 shows a specific method that combines genetic algorithm and simulated annealing algorithm to obtain the global optimal solution.

The specific algorithm process is as follows: initialize algorithm control parameters, such as initial annealing temperature, temperature cooling rate, end iteration threshold, maximum iteration limit, and result probability [19]. Random initialization generates executable determinants and initial data sets for each set of executable solutions. Calculate the fitness value; perform genetic operations in the initial data set, such as selective crossmutation; apply the fitness function to new individuals to calculate the fitness value; and select new individuals using simulated annealing algorithm [20], design the maximum number of loop iterations [21]. Determine whether the current temperature is lower than the end temperature. If it is lower than the end temperature, the algorithm ends and returns to the global optimal solution. If not, the temperature attenuation operation is cycled [22].

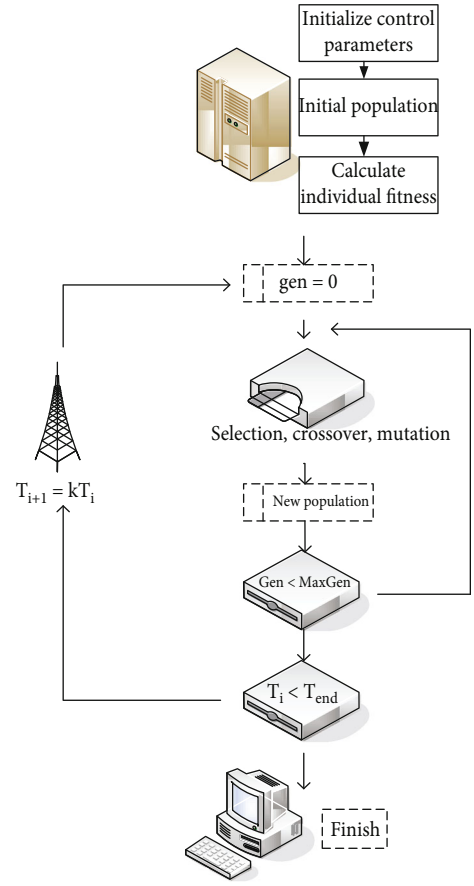

Figure 2: Genetic simulated annealing algorithm solution flow chart.

2.2. Regularized Clustering Algorithm. Everitt proposed the definition of clustering in 1974. Clustering is the process of dividing a collection of physical objects into multiple classes consisting of similar objects. The purpose of clustering is to divide a sample data set that has not been split into clusters and divide it into different clusters according to their unique similarities, so that the sample data with similar characteristics can be clustered into a single cluster, and determine that the interclass spacing of the sample data is greater than the intraclass spacing. Measuring similarity is a method used to measure the similarity between sample data. When measuring similarity, it is necessary to combine the components of the vector being measured, but there is no unified method to combine them. It should be decided according to the actual situation [23]. Therefore, various distance measurement formulas have appeared.

The method of Euclidean distance is to set *X1X2* as two n -dimensional model samples. It is necessary to note that the physical quantity of each feature vector and the unit of the

physical quantity must be consistent in the corresponding dimension. The Euclidean distance measure is to measure the similarity of unit-consistent physical quantities. This is the use of Euclidean distance as a measure of similarity. The Euclidean distance formula is as follows:

$$D(X_1, X_2) = (X_1 - X_2)^T (X_1 - X_2) = (X_1 - X_2)^2 + \cdots + (X_n - X_{n-1})^2. \tag{5}$$

The accuracy of the Euclidean distance algorithm will significantly improve with the number of iterations of the model sample, which manifested by the concentration of the population distribution [24]. Figure 3 shows the distribution of the population in the search space during the iteration.

Overall, there are five poles in the figure, and the size of the poles gradually decreases [25]. When $(X_1 - X_2)^T = 1$, it can be seen that the population is more evenly distributed in the search space. As the number of iterations increases or decreases, the population gradually gathers towards the peak point. When $(X_1 - X_2)^T = 10$, the population gathers near the five peak points. Therefore, the Euclidean distance method is helpful for the clustering algorithm to search for multipeak extreme values and develop them in detail. The reason is that the Euclidean distance uses neighborhood information for local search. Once the neighborhood range of the peak point is determined, the algorithm will search for a better solution in the neighborhood and only find a better solution to replace the current solution [26]. Therefore, it is possible to always save nearby peak points in the iterative process and gradually reduce the neighborhood.

The Mahalanobis distance assumes two n-dimensional vectors X and Y, and its square expression is

$$D^2 = (\mathrm{X} - Y)^T C^{-1} (X - Y). \tag{6}$$

In the Mahalanobis distance equation, X represents the pattern vector, Y represents the average vector, and C represents the population covariance matrix [27]. The overall covariance matrix of each type of sample is expressed as

$$C = E\left\{(X - Y)(X - Y)^T\right\} = E\begin{Bmatrix} (x1 - y1) \\ \vdots \\ (xn - yn) \end{Bmatrix} [(x1 - y1) \cdots (xm - yn)]. \tag{7}$$

The advantage of Mahalanobis distance is that it can eliminate the correlation effect between model samples [28]. When $C = 1$, the distance can be regarded as Euclidean distance.

Set X1X2 as two n-dimensional pattern sample vectors; the formula is

$$D_m(X_i, X_j) = \left[\sum_{k=1}^{n} x_{ik} - x_{jk}^{\ m}\right]^{1m}. \tag{8}$$

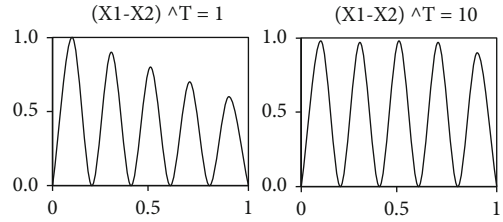

Figure 3: The distribution of the search space of the population with the evaluation times of the function.

Among them, the kth component of i and j is represented by X_{ik} and X_{jk}. When m is not equal to 1, $D_1(X_i, X_j) = \sum_{k=1}^{n} x_{ik} - x_{jk}^{\ 1}$. When m is equal to 1, this distance represents the Minnesota distance.

The Hamming distance method is to set X_i and X_j as two n-dimensional binary sample vectors, and the formula is as follows, where X_{ik} and X_{jk} represent the kth component of i and j, respectively:

$$D_m(X_i, X_j) = \frac{1}{2}\left(n - \sum_{k=1}^{n} x_{ik} \cdot x_{jk}\right). \tag{9}$$

The Tanimoto measure is applicable to the case of binary features from 0 to 1, and the specific formula is as follows:

$$S(x_i, x_j) = \frac{X_i^T X_j}{X_i^T X_i + X_j^T X_j - X_i^T X_j} = \frac{x_i, x_j \text{ feature number in common}}{x_i, x_j \text{ total number of features}}. \tag{10}$$

The K-means clustering algorithm believes that the closer the distance between samples, the higher the similarity, and each cluster is composed of samples with similar distances [29]. The algorithm uses Euclidean distance to measure the similarity, the clustering criterion uses the square error sum function, and the reference function of the K-means clustering algorithm for the jth cluster is expressed as follows:

$$Y_y = \sum_{i=1}^{N_y} \left\|X_i - Z_y\right\|^2, \quad X_i \in S_y. \tag{11}$$

This equation solves the clustering problem by solving the extreme value optimization problem of the reference function. The clustering criterion is used to measure the difference or similarity function between the model sample data sets $\{S_j, j = 1, 2 \cdots, n\}$. Z_y represents the average value of the yth class of samples, which is the cluster center of the class; N_y represents the number of samples in S_y, and S_y represents the yth cluster. The algorithm has all Q modes:

$$Y_y = \sum_{y=1}^{Q} \sum_{i=1}^{N_y} \left\|X_i - Z_y\right\|^2, \quad X_i \in S_y. \tag{12}$$

Among them, Z_y represents the cluster center; N_y represents the number of samples in S_y, and S_y represents the yth cluster set (domain).

This paper uses the K-means clustering algorithm to randomly select n objects to represent the initial cluster center of each cluster: $Y1, Y2, \cdots, Yn$, and divide the remaining objects into the minimum distance between the clusters of the n cluster centers according to the principle. The formula is as follows:

$$Y_y(n) = \min\{X - Y_i(n), i = 1, 2 \cdots n\}, \quad X_i \in S_y(n). \tag{13}$$

Calculate the mean value of each cluster center again:

$$Y_y(n+1) = \frac{1}{N}\sum_{x \in S_y(n)} X, \quad y \in [1, n]. \tag{14}$$

Among them, N_y is the number of samples in the yth category. If $Y_y(n+1) \neq Y_y(n), y \in [1, n]$, then repeat formula (13) for an iterative loop until $Y_y(n+1) = Y_y(n), y \in [1, n]$, the algorithm converges, and stop the iterative loop [30]. In the double crescent data set experiment, two clustered data points were represented by two colors. In the two cases, multiple experiments were carried out, and the single-cluster data y was 60 and 120, respectively. Figure 4 is a schematic diagram of the original data point clustering results of the K-means clustering algorithm.

2.3. Flexible Workshop Production Scheduling Model. According to the method of describing uncertainty, there are three corresponding flexible scheduling modeling methods. One is to analyze and summarize the probability distribution of uncertain parameters and use random variables to describe uncertain parameters for analysis and modeling. Determine the parameters, and establish a production scheduling model; the third is to use fuzzy numbers to represent uncertain parameters, that is, parameter fuzzy scheduling model.

(1) The random distribution describes the scheduling model with uncertain parameters

$$\min_{j,x,l} \quad E\{f(j,x,l,\theta)\}$$
$$\text{s.t.} \quad \left\{\begin{array}{l} g(j,x,l,\theta) \geq 0 \\ h(j,x,l,\theta) = 0 \\ j \in J, x \in X, l \in L, \theta \in \theta \end{array}\right\}, \tag{15}$$

where j is the decision coefficient representing the time required for product production and machine utilization; X is the decision variable representing the processing time, processing times, and quantity; and the objective function $f()$ represents the discrete variables in the production process, θ. The objective function $f()$ contains the shortest completion time, manufacturing cost, and customer satisfaction. The ultimate goal of scheduling is the expected value of the objective function, so the uncertain parameters in the model were represented by random variables

(2) Scheduling model for interval description of uncertain factors

$$\min_{j,x,l} \quad \tilde{f}\left(j,x,l,\tilde{\theta}\right)$$
$$\text{s.t.} \quad \left\{\begin{array}{l} \tilde{g}\left(j,x,l,\tilde{\theta}\right) \geq 0 \\ \tilde{h}\left(j,x,l,\tilde{\theta}\right) = 0 \\ j \in J, x \in X, l \in L, \tilde{\theta} \in \theta \end{array}\right. \tag{16}$$

If the distribution probability of the uncertain parameter is difficult to obtain, the interval of the uncertain parameter can obtained or the range of the uncertain parameter is relatively small; the interval $\theta \in [\theta_i \min, \theta_i \max]$ is used to obtain the uncertain parameter and establish the schedule interval planning model.

(3) Scheduling model of fuzzy parameters

$$\min_{j,x,l} \quad E\left\{\tilde{f}\left(j,x,l,\tilde{\theta}\right)\right\}$$
$$\text{s.t.} \quad \left\{\begin{array}{l} \tilde{g}\left(j,x,l,\tilde{\theta}\right) \geq 0 \\ \tilde{h}\left(j,x,l,\tilde{\theta}\right) = 0 \\ j \in J, x \in X, l \in L, \tilde{\theta} \in \theta \end{array}\right. \tag{17}$$

There are many uncertain parameters in the manufacturing process, and the probability distribution and interval range cannot obtained. Only the probability distribution of these uncertain parameters can be obtained. There are multiple distribution intervals and different distribution probabilities. Then, fuzzy numbers can be used to express uncertainty. Parameterize, establish, and solve the fuzzy scheduling model.

In order to verify the performance of the four algorithms mentioned above, this article uses these algorithms to simulate the shortest completion time of processes, machines, and workpieces in typical workshop scheduling. After comparing the calculation results, a comparison chart is obtained. It can be seen that the simulated annealing algorithm not only has fast convergence speed but also has good quality. It not only overcomes the premature phenomenon of genetic algorithms but also avoids the shortcomings of slow maturity of improved algorithms. Figure 5 shows the comparison of the convergence speed of each algorithm.

3. Workshop Production Scheduling Case Experiment and Analysis

3.1. Multiobjective of Flexible Workshop. The K-means algorithm optimizes the processing sequence and maximizes the

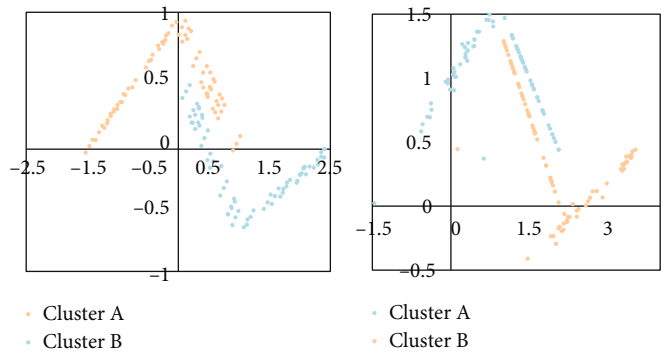

Figure 4: Clustering results of double crescent synthetic data.

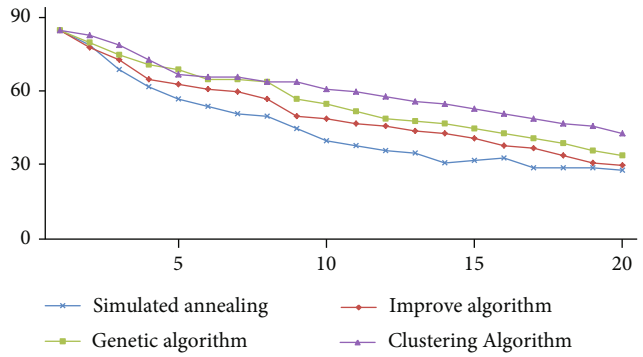

Figure 5: Comparison of algorithm convergence curves.

Table 1: Product processing schedule.

Product name	Processing time	Product name	Processing time
1	32	11	14
2	22	12	30
3	25	13	24
4	24	14	17
5	16	15	20
6	18	16	21
7	13	17	20
8	24	18	25
9	24	19	31
10	13	20	30

Table 2: Processing scheduling and corresponding processing schedule.

Machine number	Corresponding product serial number	Total machine processing time
1	3, 7, 9	62
2	10, 13, 18	62
3	11, 17, 20	64
4	4, 5, 8	64
5	6, 12, 14	65
6	2, 15, 16	63
7	1, 19	63

processing performance index. Flexible workshop production scheduling needs to determine all job statuses such as each machine and process constraints. The constraints are the processing time of each process and the processing sequence constraints of each job on each machine, processing start time, or completion time. Job shop scheduling is related to many factors, including equipment operating efficiency and employee work ability. As a multiobjective combinatorial optimization problem, predecessors proposed 27 scheduling schemes for shop scheduling. These goals can be divided into two categories: time-based goals and resource-based goals. The main characteristics of time-based goals are quick response to demand goals and satisfaction of customer needs, which are mainly reflected in the control of the completion time. It is uneconomical to complete too early and too late. If it is too early, accumulation time will be generated. It consumes storage space and deteriorates product liquidity. If it is too slow, it will not be able to meet customer needs. Improving resource utilization is also an important consideration in system research. The resource-based goal is to be able to use as few resources as possible to complete tasks and achieve better cost utilization. Taking cost as an evaluation value, it is not difficult to find today's society for energy conservation and higher requirements for emission reduction.

In actual production, many engineering problems are multiobjective optimization problems. In terms of workshop production scheduling, different departments of the enterprise also have different goals for scheduling decision-making. For example, the equipment department wants to maximize the utilization of machines and reduce the failure rate, the manufacturing department wants to increase the productivity of the workshop, and the sales department wants to hand over the goods as soon as possible to better meet customer needs. Therefore, when determining the production schedule of an enterprise, it is necessary to make a reasonable compromise between the interests of multiple parties.

3.2. Flexible Workshop Scheduling Model. The simulated annealing genetic algorithm has a strong global search

Table 3: Processing schedule for each calculation.

Calculation times	Minimum time	Calculation times	Minimum time
1	63	6	65
2	64	7	65
3	62	8	62
4	63	9	62
5	63	10	61
Average minimum processing time			63

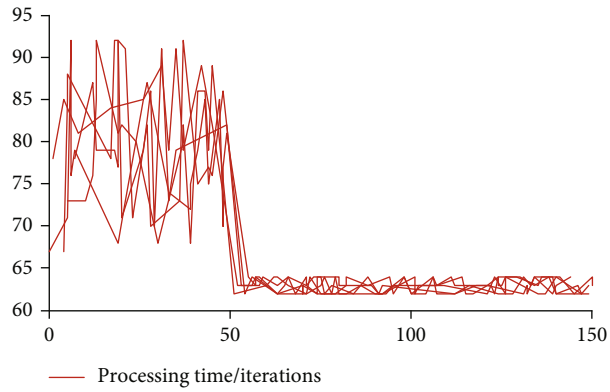

Figure 6: Graph of the results of 10 consecutive calculations.

function, so it is used by many researchers to solve other combinatorial optimization problems, including production scheduling problems. In order to observe the effect of applying simulated annealing algorithm in production scheduling problem, a simple scheduling case model is established here. The case is explained below: given seven machines with the same function, a total of 20 products must be produced. The production plan will be solved to minimize the total production time. The processing time of each product is shown in Table 1.

For the above cases, the simulated annealing genetic algorithm is applied to solve the problem. The designed scheduling system consists of six parts: system management, algorithm management, data entry, and output management. Among them, the scheduling algorithm management module can be used for algorithm selection, comparison, and configuration. Data import or input and scheduling process modules are the core of the entire system. The scheduling progress can be viewed in real time, and the output results can be output or formatted as needed. Then, carry on the simulation calculation to the above-mentioned problem; one of the results is shown in Table 2.

The shortest total processing time in the above table is 62. As a result of the solution, the processing time on each machine is balanced. In order to verify the stability of the algorithm, this paper uses the K-means clustering algorithm to solve the above problem 10 times, and the shortest processing time obtained is shown in Table 3.

It can be concluded from the above table that the algorithm is stable and the error generated is small. During 10 consecutive iterations of the K-means clustering algorithm, the corresponding results fluctuate as shown in Figure 6.

It can be observed that the simulation calculation results of the algorithm fluctuate greatly in the early stage and gradually fluctuate in the later stage. This is also in line with the characteristics of the algorithm, indicating that the algorithm is more stable in applications with simple scheduling problems.

In order to fully verify the performance and effectiveness of the genetic simulated annealing algorithm proposed in this paper, here is a simulation of a more complex situation.

That is, add different workpieces and processes to simulate a more real workshop situation, assuming that the relevant parameter data is shown in Table 4.

Table 4: Process and processing schedule.

Workpiece		Working procedure				
		1	2	3	4	5
Machine	W1	M5	M4	M3	M2	M1
	W2	M1	M2	M3	M4	M5
	W3	M4	M3	M2	M1	M5
	W4	M3	M4	M5	M1	M2
	W5	M2	M3	M4	M5	M1
Working procedure		Workpiece				
		M1	M2	M3	M4	M5
Processing time	1	1	2	2	2	8
	2	7	10	5	6	3
	3	5	8	5	3	10
	4	8	4	1	10	8
	5	10	3	2	5	9

Table 5: The machine's optimal processing sequence table.

	Workpiece					
Machine	M1	W2	W3	W4	W1	W5
	M2	W5	W3	W2	W1	W4
	M3	W4	W3	W5	W1	W2
	M4	W3	W4	W5	W1	W2
	M5	W1	W4	W5	W3	W2

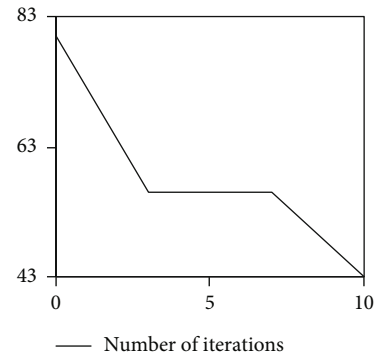

Figure 7: Curve graph of processing time and number of iterations.

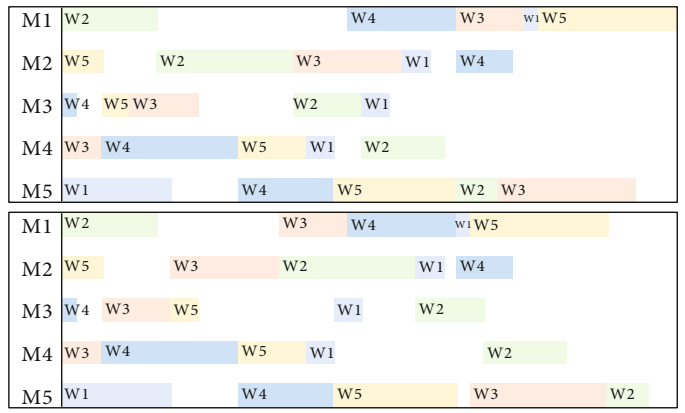

Figure 8: Workshop scheduling plan before and after optimization.

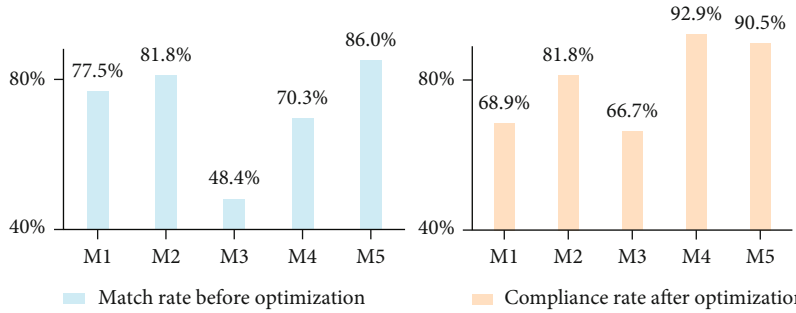

Figure 9: Machine load rate before and after optimization.

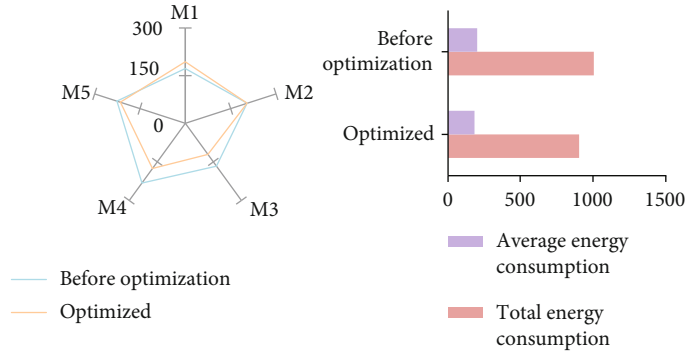

Figure 10: Comparison of energy consumption of each group of machines (kW·h).

In view of the above situation, this paper sets the initial parameter values according to the annealing algorithm and sets the machine procedures and processing time into a matrix arrangement. The optimal processing sequence obtained after applying the genetic simulated annealing algorithm proposed in this paper is recorded in Table 5.

It is calculated that the shortest processing time is 43, which has reached the optimal solution of the problem. Figure 7 is a graph showing the relationship between the processing time of the algorithm and the number of iterations.

3.3. Empirical Comparison of Production Scheduling. Based on the hypothetical production conditions in Table 4, randomly select a flexible workshop scheduling plan with an iteration number of 5, and then, take a plan with an iteration number of 10, which is, respectively, defined as before and after optimization, and make their Gantt. The plan is shown in Figure 8.

According to the data in Figure 8 and then according to the scheduling Gantt chart, the maximum processing completion time is observed. It is easy to find that the completion time before optimization is 45, and the optimization is 43. The production time efficiency is increased by 4.4%, because the system scheduling goal should be to make the machine load factor as high as possible to improve machine utilization even if the idle time of the machine is as short as possible; set the load rate = 1 − idle time/total start − up time. The

comparison of the machine load rate calculated according to the Gantt chart is shown in Figure 9.

It can be observed that the optimized machine load rate is more averaged, the extreme value is higher, and the fluctuation is smaller. The average load rate before optimization is 72.8%, and that after optimization is 80.1%, and the machine load rate is significantly improved.

Then, calculate the power of each machine before and after the optimization, and get Figure 10.

Under the premise of the same workload, the optimized machine's startup time is shortened, and the energy consumption is also significantly reduced.

4. Discussion

This article has completed two aspects of method introduction and experiment, but limited by the author's level, some research is basic, and some algorithms proposed there need to be further improved. The following is the work that this paper thinks can be further improved: This paper studies the K-means clustering algorithm for multiobjective flexible job shop scheduling problem, but there are more and more nonnumerical data in practical work. According to the specific methods and design methods, developing an efficient and improved K-means big data clustering method to study these nonnumerical data is a very promising work. This paper mainly uses the hypothetical production data to simulate the operation of the workshop and trains a large number of logistics data to accelerate. How to improve the accuracy needs further research, such as using workpiece handover time, error-driven method to optimize the results, and the random storage of correctly classified data. This paper uses a simple model, a logistics data cloud computing scheduling research model considering only virtual machine. However, real-world cloud computing scheduling algorithms need to consider various aspects such as memory and maximum completion time. In this complex situation, how to comprehensively consider these resources to achieve this scheduling model and the ability to be applied to actual cloud computing task scheduling needs further research.

5. Conclusions

Relying on the K-means algorithm, this paper fully considers the multiple goals of workshop production, proposes a flexible workshop scheduling model, and conducts an empirical comparison study. Based on some production data assumed in the previous article, the two preoptimization and postoptimization models are deduced. As a result, the model proposed in this paper shortens the production time by 4.4%, increases the average load rate of the machine by 10%, and improves the efficiency of the machine. However, the study in this paper also has some shortcomings in some aspects; for example, the experimental method is not innovative enough, and the whole experimental process is still somewhat complicated. It is hoped that improvements can be made in future research to contribute more to improving the machine efficiency in the production workshop.

Data Availability

Data sharing is not applicable to this article as no new data were created or analyzed in this study.

Conflicts of Interest

The authors state that this article has no conflict of interest.

References

[1] D. Zhang, W. Li, X. Wu, and X. Lv, "Application of simulated annealing genetic algorithm optimized back propagation(BP) neural network in fault diagnosis," *International Journal of Modeling Simulation & Scientific Computing*, vol. 10, no. 4, pp. 1950024–1950049, 2019.

[2] W. Cen, J. Luo, J. Yu, and M. Shamin Rahman, "Slope stability analysis using genetic simulated annealing algorithm in conjunction with finite element method," *KSCE Journal of Civil Engineering*, vol. 24, no. 1, pp. 30–37, 2020.

[3] G. V. Reddy, V. Ganesh, and C. Srinivasarao, "Cost reduction in clustering based unit commitment employing hybrid genetic-simulated annealing technique," *Journal of Electrical Engineering & Technology*, vol. 14, no. 1, pp. 27–35, 2019.

[4] L. Wang, S. Ding, Y. Wang, and L. Ding, "A robust spectral clustering algorithm based on grid-partition and decision-graph," *International Journal of Machine Learning and Cybernetics*, vol. 12, no. 5, pp. 1243–1254, 2021.

[5] J. Li, H. Jiao, J. Wang, Z. Liu, and J. Wu, "Online real-time trajectory analysis based on adaptive time interval clustering algorithm," *Big Data Mining and Analytics*, vol. 3, no. 2, pp. 131–142, 2020.

[6] H. Wu, C. Wang, Z. Feng, Y. Yuan, H. F. Wang, and B. S. Xu, "Adaptive multi-resolution graph-based clustering algorithm for electrofacies analysis," *Applied Geophysics*, vol. 17, no. 1, pp. 13–25, 2020.

[7] N. Liu, Y. F. Zhang, and W. F. Lu, "Improving energy efficiency in discrete parts manufacturing system using an ultra-flexible job shop scheduling algorithm," *International Journal of Precision Engineering and Manufacturing-Green Technology*, vol. 6, no. 2, pp. 349–365, 2019.

[8] H. Wang, B. Sheng, Q. Lu et al., "A novel multi-objective optimization algorithm for the integrated scheduling of flexible job shops considering preventive maintenance activities and transportation processes," *Soft Computing*, vol. 25, no. 4, pp. 2863–2889, 2021.

[9] A. Y. Prasad and B. Rayanki, "A generic algorithmic protocol approaches to improve network life time and energy efficient using combined genetic algorithm with simulated annealing in MANET," *International journal of intelligent unmanned systems*, vol. 8, no. 1, pp. 23–42, 2020.

[10] Y. Zhu, L. Zhou, and H. Xu, "Application of improved genetic algorithm in ultrasonic location of transformer partial discharge," *Neural Computing and Applications*, vol. 32, no. 6, pp. 1755–1764, 2020.

[11] M. F. Shirjini, S. Farzi, and A. Nikanjam, "MDPCluster: a swarm-based community detection algorithm in large-scale graphs," *Computing*, vol. 102, no. 4, pp. 893–922, 2020.

[12] X. Dong and Y. Cai, "A novel genetic algorithm for large scale colored balanced traveling salesman problem," *Future Generation Computer Systems*, vol. 95, no. JUN., pp. 727–742, 2019.

[13] Y. J. Yoo, "Hyperparameter optimization of deep neural network using univariate dynamic encoding algorithm for searches," *Knowledge-Based Systems*, vol. 178, no. AUG.15, pp. 74–83, 2019.

[14] M. Liu, B. Liu, C. Zhang, and W. Sun, "Spectral Nonlinearly Embedded Clustering Algorithm," *Mathematical Problems in Engineering*, vol. 2016, Article ID 9264561, 9 pages, 2016.

[15] S. Rhim, C. Kim, and Y. Choi, "Coupled GA-SA optimization algorithm and application for compressive curved damper springs of automotive lockup clutches," *International Journal of Automotive Technology*, vol. 21, no. 3, pp. 641–647, 2020.

[16] X. Qin, J. Li, W. Hu, and J. Yang, "Machine learning K-means clustering algorithm for interpolative separable density fitting to accelerate hybrid functional calculations with numerical atomic orbitals," *The Journal of Physical Chemistry A*, vol. 124, no. 48, pp. 10066–10074, 2020.

[17] C. Tang, "A clustering algorithm based on nonuniform partition for WSNs," *Open Physics*, vol. 18, no. 1, pp. 1154–1160, 2020.

[18] Y. Wang, X. Liu, and L. Xiang, "GA-based membrane evolutionary algorithm for ensemble clustering," *Computational Intelligence and Neuroscience*, vol. 2017, Article ID 4367342, 11 pages, 2017.

[19] C. Shi, B. Wei, S. Wei, W. Wang, H. Liu, and J. Liu, "A quantitative discriminant method of elbow point for the optimal number of clusters in clustering algorithm," *EURASIP Journal on Wireless Communications and Networking*, vol. 2021, no. 31, pp. 1–16, 2021.

[20] Y. Peng, B. Li, X. Mao, C. Li, H. Liu, and F. Peng, "Partition of the workspace for machine tool based on position-dependent modal energy distribution and clustering algorithm," *International Journal of Advanced Manufacturing Technology*, vol. 108, no. 3, pp. 943–955, 2020.

[21] S. Loganathan and J. Arumugam, "Energy centroid clustering algorithm to enhance the network lifetime of wireless sensor networks," *Multidimensional Systems and Signal Processing*, vol. 31, no. 3, pp. 829–856, 2020.

[22] V. N. Kuchuganov, A. V. Kuchuganov, and D. R. Kasimov, "Clustering algorithm for a set of machine parts on the basis of engineering drawings," *Programming and Computer Software*, vol. 46, no. 1, pp. 25–34, 2020.

[23] A. Hamdi, N. Monmarché, M. Slimane, and A. M. Alimi, "Fuzzy rules for ant based clustering algorithm," *Advances in Fuzzy Systems*, vol. 2016, Article ID 8198915, 16 pages, 2016.

[24] S. Samji and H. Cattermole, "Promoting less-than-full-time (LTFT) training in your local trust: a workshop in conjunction with your champion of flexible training," *Future healthcare journal*, vol. 6, Suppl 2, pp. 12-13, 2019.

[25] M. Ramezani Mayiami, M. Hajimirsadeghi, K. Skretting, X. Dong, R. S. Blum, and H. V. Poor, "Bayesian topology learning and noise removal from network data," *Discover Internet of Things*, vol. 1, no. 1, p. 11, 2021.

[26] F. Mosquera, P. Smet, and G. V. Berghe, "Flexible home care scheduling," *Omega*, vol. 83, pp. 80–95, 2019.

[27] J. L. Andrade-Pineda, D. Canca, P. L. Gonzalez-R, and M. Calle, "Scheduling a dual-resource flexible job shop with makespan and due date-related criteria," *Annals of Operations Research*, vol. 291, no. 1-2, pp. 5–35, 2020.

[28] A. E. Ezugwu, A. K. Shukla, M. B. Agbaje, O. N. Oyelade, A. José-García, and J. O. Agushaka, "Automatic clustering algorithms: a systematic review and bibliometric analysis of relevant literature," *Neural Computing and Applications*, vol. 33, no. 11, pp. 6247–6306, 2021.

[29] B. Moore, P. Chair, J. Real, and W. Chair, "Summary of the 19th International Real-Time Ada Workshop," *Ada Letters*, vol. 38, no. 1, pp. 9–13, 2018.

[30] S. Bock, "Finding optimal tour schedules on transportation paths under extended time window constraints," *Journal of Scheduling*, vol. 19, no. 5, pp. 527–546, 2016.

Hindawi
Wireless Communications and Mobile Computing
Volume 2022, Article ID 5438290, 11 pages
https://doi.org/10.1155/2022/5438290

Research Article

Site Selection Optimization of Reverse Logistics Network for Waste Tires

Qiang Wang,[1] Rong Li,[2] Li Jiang,[1] Liufen Chen,[1] Yunlong Wang,[1] and Guotian Wang[1]

[1]*School of Automotive and Transportation Engineering, Heilongjiang Institute of Technology, Harbin, 150050 Heilongjiang, China*
[2]*School of Business, Huaihua College, Huaihua, 418008 Hunan, China*

Correspondence should be addressed to Rong Li; lirong@hhtc.edu.cn

Received 19 February 2022; Revised 11 April 2022; Accepted 18 April 2022; Published 20 May 2022

Academic Editor: Jun Ye

In order to solve the problem of reverse recycling of waste tires in Heilongjiang Province, this paper chooses the third party as the core to construct a reverse logistics network system of waste tires based on the current situation of reverse logistics of waste tires. The reverse recycling area of waste tires in Heilongjiang Province is divided into five areas (the first area is Harbin; the second area contains Qiqihar, Daqing, and Suihua; the third area contains Yichun, Hegang, Jiamusi, and Shuangyashan; Qitaihe, Jixi, and Mudanjiang form the fourth area; and the fifth area contains Daxinganling and Heihe). The analytic hierarchy process (AHP) is employed to analyze the influence factors of site selection of reverse logistics network and obtain the total weight of each evaluation factor. The weights of economic conditions, the number of waste tires, traffic conditions, development planning and policy, and geographical conditions are obtained as 0.3547, 0.2256, 0.1690, 0.1644, and 0.0863, respectively. The economic conditions and the number of waste tires with high weights are vital factors for selecting a reverse logistics network for waste tires. The linear mixed-integer programming method (LINGO) is utilized for site selection. Harbin, Qiqihar, Daqing, Mudanjiang, Jiamusi, and Suihua are chosen for the recovery center's site selection, while Daqing, Mudanjiang, and Suihua are chosen as the site selection of remanufacturing enterprise.

1. Introduction

China is not only a tire manufacturing and consumption country but also a country lacking in rubber resources. The annual consumption of rubber globally accounts for about 30% of the total rubber consumption, while the rubber products industry requires 80% of natural rubber and 30% of synthetic rubber depending on imports. The contradiction between supply and demand is very prominent [1]. Scientific recycling of waste tires and reusing and harmlessly treating them can protect the ecological environment, save rubber resources, reduce energy consumption, and develop a circular economy. As a national strategic emerging industry, the comprehensive utilization of waste tires provides significant social benefits in the circular economy development. According to the industry specification conditions for comprehensive utilization of waste tires released by the Ministry of Industry and Information Technology in 2020 [2], the total production of auto tires in China in 2019 is 650 million, and the domestic consumption is 380 million, while the market holding of motor tires reaches 1.7 billion. In recent years, waste tire production in China has grown significantly. In 2020, the amount of produced waste tires was about 350 million, and the equivalent weight exceeded 10 million tons. The disposal of waste tires has attracted much attention. Improper disposal of waste tires leads to environmental impact, safety risks, and a waste of resources. After years of development, China's waste tire comprehensive utilization industry has initially formed four business segments: used tire retreading, waste tire production of recycled rubber, waste tire production of rubber powder, and waste tire (rubber) thermal pyrolysis [1]. The industrial system of comprehensive utilization of waste tires with Chinese characteristics has been initially established, and the industrial chain of comprehensive utilization of waste tires has been formed [1]. However, due to the lack of specific logistics system management methods and effective management measures from generation, recovery, transportation, storage to

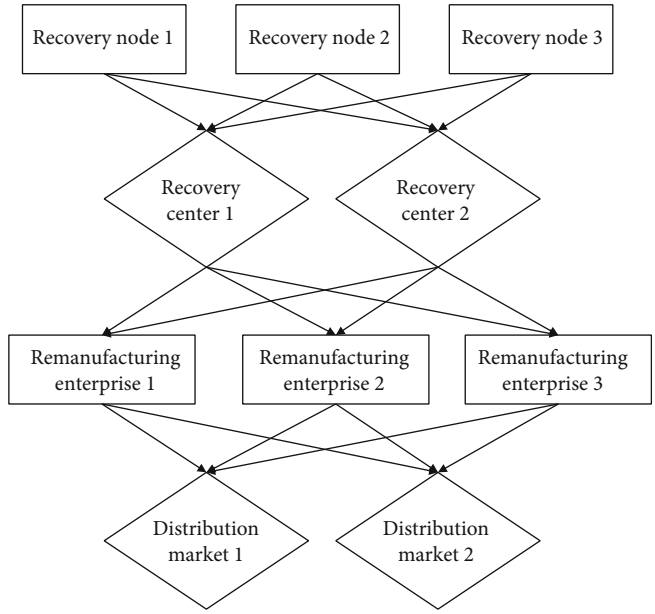

Figure 1: The reverse logistics network system of waste tires in Heilongjiang Province.

disposal, the current reverse logistics network system of waste tires in China is not standardized.

Meanwhile, few studies have been performed on the network site selection of the reverse logistics for waste tires. Various works have been performed in foreign countries on the construction and site selection of reverse logistics network systems, and high achievements have been obtained in both theory and practice [3–5]. Although the corresponding research was recently performed in China, scholars achieved specific results in this area. The existing research mainly focused on the single period and single objective levels in certain environment and multiperiod and multiobjective levels in uncertain environment. Different reverse logistics network systems and models have been studied and established to satisfy different requirements and constraints. After constructing the mathematical model, LINGO, neural network, genetic algorithm, grid algorithm, and other methods can be utilized to solve the model. Analytic hierarchy process (AHP), the center of gravity method, integer or mixed-integer programming method, Baumol-Wolfe method, antipodean method, fuzzy theory analysis, and other methods have been adopted for site selection [6–8].

Given the existing research at home and abroad, it can be found that the construction and site selection of a waste tire reverse logistics network system can be complex and should be studied further. With improving the living standards, car ownership in Heilongjiang Province and the number of waste tires gradually increase. However, the research on reverse logistics of waste tires in Heilongjiang Province is still in its infancy, and there is no perfect reverse logistics system of waste tires. In recent years, the Government of Heilongjiang Province has encouraged the development of green circular economy systems. As the primary source of recycled rubber, the reverse recycling of waste tires has been concerned by the government. The effective reuse of waste tires is the key field to achieve the goal of "carbon peak and carbon neutralization." With the concept of sustainable development and circular economy becoming more and more popular, people pay more and more attention to the activities of reverse logistics. The establishment of waste tire reverse logistics system can effectively recycle and reuse waste tire rubber, which not only saves a lot of rubber resources, but also effectively controls the harm to the environment. The recycling of waste tires, as an effective way of recycling and harmless disposal of these "solid wastes," is of great significance for the development of circular economy, saving rubber resources, reducing energy consumption, protecting the ecological environment, reducing and gradually eliminating "black pollution," and promoting the green and sustainable development of the rubber industry, and achieving my country's "carbon peak" and "carbon neutrality."

2. Construction of the Reverse Logistics Network System of Waste Tires in Heilongjiang Province

Waste tire reverse logistics refers to a series of activities that meet the development requirements of circular economy, recycle the tires that cannot meet the actual use requirements and scrap tires, classify, treat, disassemble and remanufacture the recycled waste tires, and maximize the potential value of waste tires. Agricultural vehicles, private cars, public vehicles, trucks, and engineering vehicles are the primary sources of waste tires in Heilongjiang Province. Most existing waste tire recycling in Heilongjiang Province are agricultural machinery sales points, vehicle maintenance shops, large passenger transport companies, and waste (renewable resources) recycling centers. Most existing reprocessing enterprises are small waste tire processing plants or remanufacturing enterprises, including other renewable resources reprocessing. The existing

reverse logistics recycling mode of waste tires in Heilongjiang Province includes recycling waste tires by mobile recycling personnel, agricultural machinery sales points, vehicle maintenance shops, large passenger transportation companies, and waste (renewable resources) recycling centers. The recycling of waste tires will be sold according to the requirements of the waste tire remanufacturing enterprises. Since waste tires' existing reverse logistics system is not mature and perfect, it cannot guarantee a high waste tire recovery rate. The site selection of remanufacturing enterprises is not reasonable and normative, and most of them are located in densely populated areas, which will cause significant cost consumption.

According to the development goals of "China tire recycling industry" fourteenth five-year development plan, by 2025, laws and regulations, policies, standards, technologies, suitable information statistical service system, and a standardized waste tire recycling system should be established to achieve the comprehensive utilization of waste tires in China [1]. Therefore, in combination with the actual geographical environment and the current economic development situation in Heilongjiang Province, the reverse logistics network system of waste tires in Heilongjiang Province is established based on the recycling mode with the third party as the core (see Figure 1). Under the reverse logistics network mode of waste tires with the third party as the core, the waste tires are recycled by the third-party enterprise, and the manufacturer does not directly participate and has a high recycling level and professional level. This mode can reduce the operation risk and management cost borne by the manufacturer. Figure 1 shows that the reverse logistics network system of waste tires in Heilongjiang Province consists of four levels: recovery node, recovery center, remanufacturing enterprise, and distribution market. The first level is the recovery node established by consumers as the main body. The addition of the recovery node ensures the maximum recovery of waste tires and improves their recovery rate. The second level is the recycling center, which collects the waste tires recovered by each recycling node for primary classification and processing. The third level is the remanufacturing enterprise, which aims to process and reproduce recycled tires. The fourth level is the distribution market, which gathers all kinds of remanufactured products to realize trading, recycling, and achieving economic benefits.

3. Analysis of Factors Affecting the Site Selection of Reverse Logistics Network

AHP is employed to analyze factors influencing the site selection of the reverse logistics network in Heilongjiang Province. According to the administrative planning of Heilongjiang Province, the reverse recycling area of waste tires is divided into five areas. The first area is Harbin; the second area contains Qiqihar, Daqing, and Suihua; the third area contains Yichun, Hegang, Jiamusi, and Shuangyashan; the fourth area includes Qitaihe, Jixi, and Mudanjiang; and the fifth area includes Daxinganling and Heihe. Traffic conditions, geographical conditions, economic conditions, the number of waste tires, and development planning and policy are selected as the evaluation factors.

3.1. Analytic Hierarchy Process (AHP). The AHP steps are as follows: (1) determining the aims; (2) determining the hierarchy according to the goal; (3) constructing the comparative judgment matrix to determine the priority relationship; and (4) testing the hierarchy order and consistency [9, 10].

(1) The eigenvectors $\bar{w} = (\overline{w_1}, \overline{w_2}, \cdots, \overline{w_n})^T$ are obtained by normalizing and summing the judged columns as

$$\overline{w_i} = \sum_{j=1}^{n} \frac{a_{ij}}{\sum a_{ij}}, \tag{1}$$

where a_{ij} stands for the ratio of the importance of element i to element j.

(2) The eigenvectors are normalized to obtain the elements of the weight vector $w = (w_1, w_2, \cdots, w_n)^T$ as

$$w_i = \frac{\overline{w_i}}{\sum \overline{w_i}}. \tag{2}$$

(3) The maximum eigenvalue is calculated as

$$\lambda_{\max} = \sum_{i=1}^{n} \frac{(Aw)_i}{nw_i}, \tag{3}$$

where $(Aw)_i$ represents the ith element of the vector Aw

(4) The consistency test index CI and the consistency ratio index CR are calculated as

$$\begin{aligned} \mathrm{CI} &= \frac{\lambda_{\max} - n}{n-1}, \\ \mathrm{CR} &= \frac{\mathrm{CI}}{\mathrm{RI}}. \end{aligned} \tag{4}$$

If CR < 0.1, the consistency of the judgment matrix is acceptable; otherwise, the matrix should be modified.

(5) Hierarchical total sorting and consistency test are performed.

(a) The criterion-level and subcriteria-level weight vectors are obtained according to the single order sorting as

$w^{(k-1)} = (w_1{}^{(k-1)}, w_2{}^{(k-1)}, \cdots, w_n{}^{(k-1)})^T$; $w_j{}^k = (w_{1j}{}^{(k)}, w_{2j}{}^{(k)}, \cdots, w_{nj}{}^{(k)})^T$.

Accordingly, the total weights of the subcriterion layer to criterion layer can be calculated as

$$w_i^{(k)} = \sum_{j=1}^{m} P_{ij}^{(k)} w_i^{(k)}. \tag{5}$$

(b) Calculate the $CI^{(k-1)}$ and $RI^{(k-1)}$ of the subcriteria level, and then, perform the consistency check of the criterion level:

$$\begin{aligned} CI^{(k)} &= \left(CI_1{}^{(k)}, CI_2{}^{(k)}, \cdots, CI_m{}^{(k)}\right) w^{(k-1)}, \\ RI^{(k)} &= \left(RI_1{}^{(k)}, RI_2{}^{(k)}, \cdots, RI_m{}^{(k)}\right) w^{(k-1)}, \\ CR^{(k)} &= \frac{CI^{(k)}}{RI^{(k)}}, \end{aligned} \tag{6}$$

where $CR^{(k)} < 0.1$ is considered that the overall consistency of the judgment matrix meets the requirements.

(6) Analyze the sorting result and make the corresponding decision.

3.2. Constructing a Hierarchical Structure Model. Figure 2 shows the hierarchical structural model of site selection of the reverse logistics network for waste tires, in which the target layer (A) is the analysis of the reverse logistics network site selection. The middle layer (B) includes the first, second, third, fourth, and fifth areas. The bottom layer (C) consists of five evaluation factors: traffic conditions, geographical conditions, economic conditions, the number of waste tires, and development plans and policies [11].

3.3. Construction of Judgment Matrices. The judgment matrix of the first layer (denoted by A) describes the judgment matrix relative to the highest level.

$$A = \begin{bmatrix} 1 & 1 & 3 & 4 & 6 \\ 1 & 1 & 2 & 3 & 4 \\ 1/3 & 1/2 & 1 & 1 & 3 \\ 1/4 & 1/3 & 1 & 1 & 2 \\ 1/6 & 1/4 & 1/3 & 1/2 & 1 \end{bmatrix}. \tag{7}$$

The five secondary judgment matrices relative to the middle layer, denoted by B_i (i=1,2,3,4,5), are given in the following.

Comparison results of the influencing factor indices in the first area:

$$B_1 = \begin{bmatrix} 1 & 3 & 1/3 & 2 & 1 \\ 1/3 & 1 & 1/5 & 1/3 & 1/3 \\ 3 & 5 & 1 & 2 & 1 \\ 1/2 & 3 & 1/2 & 1 & 1/4 \\ 1 & 3 & 1 & 4 & 1 \end{bmatrix}. \tag{8}$$

Comparison results of the influencing factor indices in the second area:

$$B_2 = \begin{bmatrix} 1 & 3 & 1/3 & 1/2 & 2 \\ 1/3 & 1 & 1/2 & 1/3 & 1/2 \\ 3 & 2 & 1 & 2 & 4 \\ 2 & 3 & 1/2 & 1 & 3 \\ 1/2 & 2 & 1/4 & 1/3 & 1 \end{bmatrix}. \tag{9}$$

Comparison results of the influencing factor indices in the third area:

$$B_3 = \begin{bmatrix} 1 & 2 & 1/3 & 1/2 & 2 \\ 1/2 & 1 & 1/2 & 1/3 & 3 \\ 3 & 2 & 1 & 2 & 3 \\ 2 & 3 & 1/2 & 1 & 4 \\ 1/2 & 1/3 & 1/3 & 1/4 & 1 \end{bmatrix}. \tag{10}$$

Comparison results of the influencing factor indices in the fourth area:

$$B_4 = \begin{bmatrix} 1 & 2 & 1/5 & 1/3 & 2 \\ 1/2 & 1 & 1/3 & 1/5 & 1 \\ 5 & 3 & 1 & 2 & 3 \\ 3 & 5 & 1/2 & 1 & 3 \\ 1/2 & 1 & 1/3 & 1/3 & 1 \end{bmatrix}. \tag{11}$$

Comparison results of the influencing factor indices in the fifth area:

$$B_5 = \begin{bmatrix} 1 & 1/3 & 1/3 & 1/5 & 2 \\ 3 & 1 & 1/2 & 1/3 & 1 \\ 3 & 2 & 1 & 1 & 3 \\ 5 & 3 & 1 & 1 & 5 \\ 1/2 & 1 & 1/3 & 1/5 & 1 \end{bmatrix}. \tag{12}$$

3.4. Calculation of the Weight of Each Evaluation Factor. The

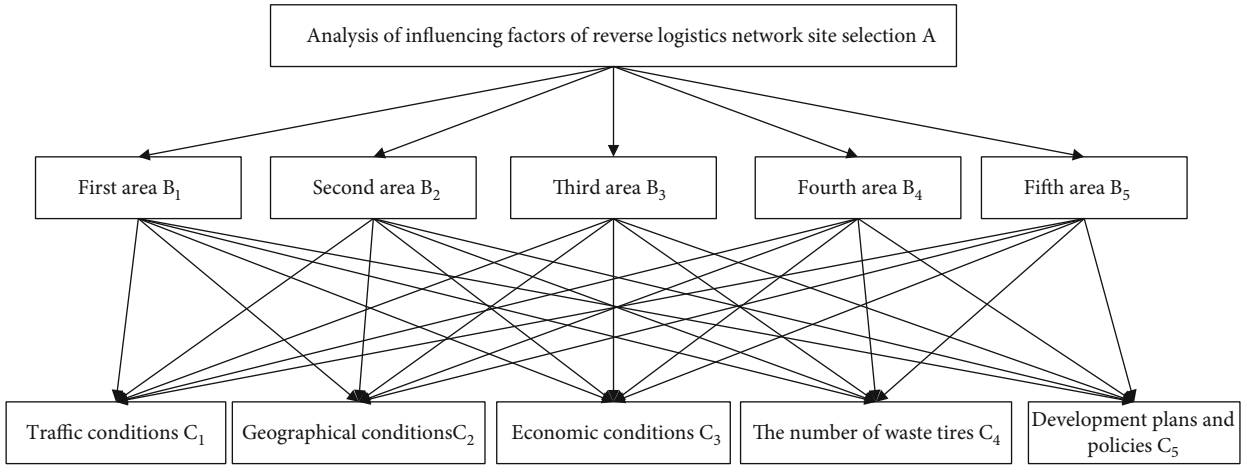

Figure 2: Hierarchical structural model.

Yaahp software is employed to calculate each matrix's weight coefficients and maximum eigenvalues [12, 13].

The weight coefficient can be calculated through the judgment matrix A. Among all areas, the first area has the highest weight (0.3806), followed by the second area (0.3055), the third area (0.1409), the fourth area (0.1131), and the fifth area with the lowest weight (0.0599).

The judgment matrix B_1 that corresponds to each influencing factor index of the first area can calculate the weight coefficient. The weight of economic conditions is the highest (0.3371), followed by development planning and policies (0.2806), traffic conditions (0.1961), the number of waste tires (0.1222), and geographical conditions (0.0640).

The judgment matrix B_2 that corresponds to each influencing factor index of the second area is employed to obtain the weight coefficient. The weight of economic conditions is the highest (0.3728), followed by the number of waste tires (0.2668), traffic conditions (0.1719), development planning and policies (0.1046), and geographical conditions (0.0839).

The judgment matrix B_3 that corresponds to each influencing factor index of the third area is employed to calculate the weight coefficient. The weight of economic conditions is the highest (0.3533), followed by the number of waste tires (0.2836), traffic conditions (0.1591), geographical conditions (0.1307), and development planning and policies (0.1046).

The judgment matrix B_4 that corresponds to each influencing factor index of the fourth area is adopted to determine the weight coefficient. The weight of economic conditions is the highest (0.3994), followed by the number of waste tires (0.3027), traffic conditions (0.1247), development planning and policies (0.0911), and geographical conditions (0.0822).

The judgment matrix B_5 that corresponds to all influencing factor indices of the fifth area is utilized to determine the weight coefficient. The weight of the number of waste tires is the highest (0.3908), followed by economic conditions (0.2938), geographical conditions (0.1435), traffic conditions (0.0884), and development planning and policies (0.0835).

Table 1: Maximum eigenvalues of each matrix.

	A	B_1	B_2	B_3	B_4	B_5
λ_{max}	5.0562	5.2614	5.2858	5.2591	5.2285	5.2511

Table 2: Consistency indices (RI).

n	1	2	3	4	5	6	7
RI	0	0	0.58	0.90	1.12	1.24	1.32

Table 3: The number of waste tires in Heilongjiang Province.

City	Number of waste tires ($\times 10^4$)	Recovery amount of waste tires ($\times 10^4$)	Recovery amount of waste tires (tons)
Harbin	800	160	13300
Qiqihar	180	36	3000
Daqing	210	42	3500
Mudanjiang	200	40	3330
Jiamusi	140	28	2330
Suihua	150	30	2500
Jixi	60	12	1000
Shuangyashan	40	8	660
Yichuan	50	10	830
Qitaihe	30	6	500
Hegang	28	5.6	470
Daxinganling	50	10	830
Heihe	45	9	750

The maximum eigenvalue for each matrix (λ_{max}) is presented in Table 1, and the corresponding consistency indices (RI) are given in Table 2.

Table 4: Distance between recovery nodes (km).

City	A	B	C	D	E	F	G	H	I	J	K	L	M
A	0	—	—	—	—	—	—	—	—	—	—	—	—
B	305.2	0	—	—	—	—	—	—	—	—	—	—	—
C	153.1	159	0	—	—	—	—	—	—	—	—	—	—
D	334.6	649.5	494.4	0	—	—	—	—	—	—	—	—	—
E	384.8	670.1	517.8	339.6	0	—	—	—	—	—	—	—	—
F	151.1	403.2	248.2	452.9	470.1	0	—	—	—	—	—	—	—
G	487.4	775.6	620.5	172.8	206.6	572.8	0	—	—	—	—	—	—
H	457.7	746.2	591.1	415.8	85.3	543.4	280.6	0	—	—	—	—	—
I	323.3	475.5	456.8	661.6	204.5	212.6	407.1	285.4	0	—	—	—	—
G	430.5	719	564	225.4	150.6	516.3	90.2	225.4	352.5	0	—	—	—
K	443.2	625.2	582.1	404.7	66.8	362.4	269.5	147.7	152	213.8	0	—	—
L	706.3	430.7	559.7	1050.9	776.4	578.3	1173.7	857.2	573.9	1118	723.6	0	—
M	573.4	493	622	384.8	681.8	483.7	1028.6	762.6	479.3	972.9	629	337.9	0

According to Equations (2)–(5), the consistency ratio index (CR) for each matrix can be calculated as

$$\begin{aligned} \mathrm{CR}^{(\mathrm{A})} &= 0.0125 < 0.1; \\ \mathrm{CR}^{(B_1)} &= 0.0584 < 0.1; \\ \mathrm{CR}^{(B_2)} &= 0.0638 < 0.1; \\ \mathrm{CR}^{(B_3)} &= 0.0578 < 0.1; \\ \mathrm{CR}^{(B_4)} &= 0.0510 < 0.1; \\ CR^{(B_5)} &= 0.0560 < 0.1. \end{aligned} \tag{13}$$

It can be concluded from the above values that all the areas passed the consistency test and all the judgment matrices meet the requirements. The weights of traffic conditions, geographical conditions, economic conditions, the number of waste tires, and development planning and policy are 0.1690, 0.0863, 0.3547, 0.2256, and 0.1164, respectively. Among them, economic conditions and the number of waste tires have the highest weights. Thus, these two factors are vital in selecting the reverse logistics network site for waste tires. The area's economic conditions directly affect the development level of the automobile industry, infrastructure, and logistics. Choosing areas with better economic conditions as the site selection of each facility can ensure the continuity of the reverse logistics system of waste tires and enhance the system's practical use value. Choosing an area with many waste tires as the site selection of each facility point can help the facility point to give full play to its functions and reduce transportation costs.

4. Construction of the Reverse Logistics Network Model of Waste Tires

4.1. Model Assumption. This paper employs the linear mixed-integer programming method (LINGO) for mathematical modeling and obtains each facility's optimal location, quantity, and flow rate under the objective of an ideal state and minimum cost. Before establishing the model, the following assumptions should be considered: (1) The capacity of the recovery node is infinite and can work stably and continuously; (2) the investment cost, unit operating cost, and transportation cost of each facility are fixed values and are not related to the period; (3) each recycling node can recycle all the waste tires in the corresponding area, while the waste tires are not overstocked; (4) all the facilities and the work among them in the reverse logistics network system of waste tires are in ideal mode; that is, waste tires are fully utilized without any loss; and (5) the reverse logistics network system of waste tires can operate effectively for a long time [14].

4.2. Model Construction. The reverse logistics network of waste tires contains many factors influencing the site selection. Considering all of these factors makes the model highly complex and challenging to solve. Thus, this paper only considers fixed cost, transportation cost, and treatment cost [15]. The model's relevant parameters and decision variables are defined as follows:

4.2.1. Symbol Definition. a_i represents the ith recovery node, and A stands for the collection of all recovery nodes; b_j represents the jth recovery center, and B stands for the collection of all recovery centers; and $c_k$represents the kth remanufacturing enterprise, and C stands for the collection of all remanufacturing enterprise.

4.2.2. Parameters. $D_{ABa_i}^{b_j}$ represents the transportation distance from the ith recovery node to the jth recovery center. $D_{BCb_j}^{c_k}$ represents the transportation distance from the ith recovery center to the jth remanufacturing enterprise.

E, F, G represent the costs. The unit transportation cost from the ith recovery node to the jth recovery center is represented by $E_{ABa_i}^{b_j}$. $E_{BCb_j}^{c_k}$ describes the unit transportation cost from the jth recovery center to the kth remanufacturing enterprise. F_{Aa_i} stands for the fixed cost of the ith recovery

node. F_{Bb_j} represents the fixed cost of the jth recovery center. The fixed cost of the kth remanufacturing enterprise is denoted by F_{Cc_k}. G_{Aa_i} describes the unit operating cost of the ith recovery node. G_{Bb_j} represents the unit operating cost of the jth recovery center. G_{Cc_k} stands for the unit operating cost of the kth remanufacturing enterprise.

H_{Aa_i} represents the maximum inventory of waste tires at the ith recovery node (infinite inventory is assumed in this paper). H_{Bb_j} describes the maximum disposal capacity of waste tires in the jth recovery center. The maximum disposal capacity of waste tires in the kth remanufacturing enterprise is denoted by H_{Cc_k}. P_{Aai} stands for the recovery amount of waste tire of the ith recovery node.

4.2.3. Decision Variable. $P_{AB}{}_{a_i}^{b_j}$ represents the transportation volume from the ith recovery node to the jth recovery center. $P_{BC}{}_{b_j}^{c_k}$ stands for the transportation volume from the j th recovery center to the kth remanufacturing enterprise.

If a_i is selected as the recovery node, Y_{Aa_i} is 1; otherwise, it is 0. If b_j is selected as the recovery center, Y_{Bb_j} is 1; otherwise, it is 0. If c_k is equal to the remanufacturing enterprise, Y_{Cc_k} is 1; otherwise, it is 0, $Y_{Aa_i}, Y_{Bb_j}, Y_{Cc_k} \in Y$.

The objective function is constructed as:

$$\begin{aligned}\operatorname{Min} Z = &\sum_{a_i}\left(F_{Aa_i}Y_{Aa_i}\right) + \sum_{b_j}\left(F_{Bb_j}Y_{Bb_j}\right) + \sum_{c_k}\left(F_{Cc_k}Y_{Cc_k}\right)\\ &+ \sum_{a_i}\sum_{b_j}\left(D_{AB}{}_{a_i}^{b_j}E_{AB}{}_{a_i}^{b_j}P_{AB}{}_{a_i}^{b_j}\right) + \sum_{b_j}\sum_{c_k}\left(D_{AB}{}_{a_i}^{b_j}E_{BC}{}_{b_j}^{c_k}P_{BC}{}_{b_j}^{c_k}\right)\\ &+ \sum_{a_i}\left(G_{Aa_i}P_{Aai}Y_{Aa_i}\right) + \sum_{b_j}\left(G_{Bb_j}P_{AB}{}_{a_i}^{b_j}Y_{Bb_j}\right)\\ &+ \sum_{c_k}\left(G_{Cc_k}P_{BC}{}_{b_j}^{c_k}Y_{Cc_k}\right),\end{aligned} \tag{14}$$

where Z represents the total cost of the reverse logistics network of waste tires. $\sum_{a_i}(F_{Aa_i}Y_{Aa_i})$ describes the fixed cost of recovery nodes; $\sum_{b_j}(F_{Bb_j}Y_{Bb_j})$ stands for the fixed cost of recovery centers; the fixed cost of remanufacturing enterprise is represented by $\sum_{c_k}(F_{Cc_k}Y_{Cc_k})$; $\sum_{a_i}\sum_{b_j}(D_{AB}{}_{a_i}^{b_j}E_{AB}{}_{a_i}^{b_j}P_{AB}{}_{a_i}^{b_j})$ denotes the transportation cost of the recovery node to the recovery center; $\sum_{b_j}\sum_{c_k}(D_{AB}{}_{a_i}^{b_j}E_{BC}{}_{b_j}^{c_k}P_{BC}{}_{b_j}^{c_k})$ describes the transportation cost from the recovery center to the remanufacturing enterprise; and $\sum_{a_i}(G_{Aa_i}P_{Aai}Y_{Aa_i})$, $\sum_{b_j}(G_{Bb_j}P_{AB}{}_{a_i}^{b_j}Y_{Bb_j})$, and $\sum_{c_k}(G_{Cc_k}P_{BC}{}_{b_j}^{c_k}Y_{Cc_k})$ stand for the operating costs of recovery nodes, the recovery center, and the remanufacturing enterprise, respectively.

4.3. The Constraints. The mathematical model should meet constraints to ensure the applicability of the construction system [16].

$$\begin{cases}\sum_{a_i}P_{Aa_i} = \sum_{a_i}\sum_{b_j}P_{AB}{}_{a_i}^{b_j}\\ \sum_{a_i}\sum_{b_j}P_{AB}{}_{a_i}^{b_j} = \sum_{b_j}\sum_{c_k}P_{BC}{}_{b_j}^{c_k}\\ P_{Aa_i} \le H_{Aa_i}Y_{Aa_i}\\ \sum_{a_i}P_{AB}{}_{a_i}^{b_j} \le H_{Bb_j}Y_{Bb_j}\\ \sum_{b_j}P_{BC}{}_{b_j}^{c_k} \le H_{Cc_k}Y_{Cc_k}\\ P_{Aa_i} \le P_{Aa_i}Y_{Aa_i}\\ \sum_{a_i}P_{AB}{}_{a_i}^{b_j} \le \sum_{a_i}P_{AB}{}_{a_i}^{b_j}Y_{Bb_j}\\ \sum_{b_j}P_{BC}{}_{b_j}^{c_k} \le \sum_{b_j}P_{BC}{}_{b_j}^{c_k}Y_{Cc_k}\\ a_i \in A\\ b_j \in B\\ c_k \in C\\ i \in N^*\\ j \in N^*\\ k \in N^*\\ Y \in 1, 0\end{cases}, \tag{15}$$

where $\sum_{a_i}P_{Aa_i} = \sum_{a_i}\sum_{b_j}P_{AB}{}_{a_i}^{b_j}$ indicates that the shipment amount should be equal to the recovery node's recovery amount. $\sum_{a_i}\sum_{b_j}P_{AB}{}_{a_i}^{b_j} = \sum_{b_j}\sum_{c_k}P_{BC}{}_{b_j}^{c_k}$ reflects that the shipment amount should be equal to the recovery center's recovery amount. $P_{Aa_i} \le H_{Aa_i}Y_{Aa_i}$ indicates that the recovery amount should be less than or equal to the maximum inventory amount of each recovery node. $\sum_{a_i}P_{AB}{}_{a_i}^{b_j} \le H_{Bb_j}Y_{Bb_j}$ reflects that the recovery amount should be less than or equal to the maximum inventory amount of each recovery center. $\sum_{b_j}P_{BC}{}_{b_j}^{c_k} \le H_{Cc_k}Y_{Cc_k}$ indicates that the recovery amount of each remanufacturing enterprise should be less than or equal to the maximum processing capacity. $P_{Aa_i} \le P_{Aa_i}Y_{Aa_i}$, $\sum_{a_i}P_{AB}{}_{a_i}^{b_j} \le \sum_{a_i}P_{AB}{}_{a_i}^{b_j}Y_{Bb_j}$, and $\sum_{b_j}P_{BC}{}_{b_j}^{c_k} \le \sum_{b_j}P_{BC}{}_{b_j}^{c_k}Y_{Cc_k}$ indicate that the transportation will occur if and only if each facility point is selected.

4.4. The Number of Waste Tires at Each Recycling Node. According to the 2020 Statistical Yearbook of Heilongjiang Province and each city, the number of tires in each city in Heilongjiang Province is integrated, as presented in Table 3.

Since the distance calculated by the distance formula between two points cannot represent the actual

Table 5: Site selection decision of recovery center.

City	Harbin	Qiqihar	Daqing	Mudanjiang	Jiamusi	Suihua	Jixi	Shuangyashna	Yichuan	Qitaihe	Hegang	Daxinganling	Heihe
Selected or not	1	1	1	1	1	1	0	0	0	0	0	0	0

Table 6: Site selection decision of remanufacturing enterprise.

City	Harbin	Qiqihar	Daqing	Mudanjiang	Jiamusi	Suihua	Jixi	Shuangyashna	Yichuan	Qitaihe	Hegang	Daxinganling	Heihe
Selected or not	0	0	1	1	0	1	0	0	0	0	0	0	0

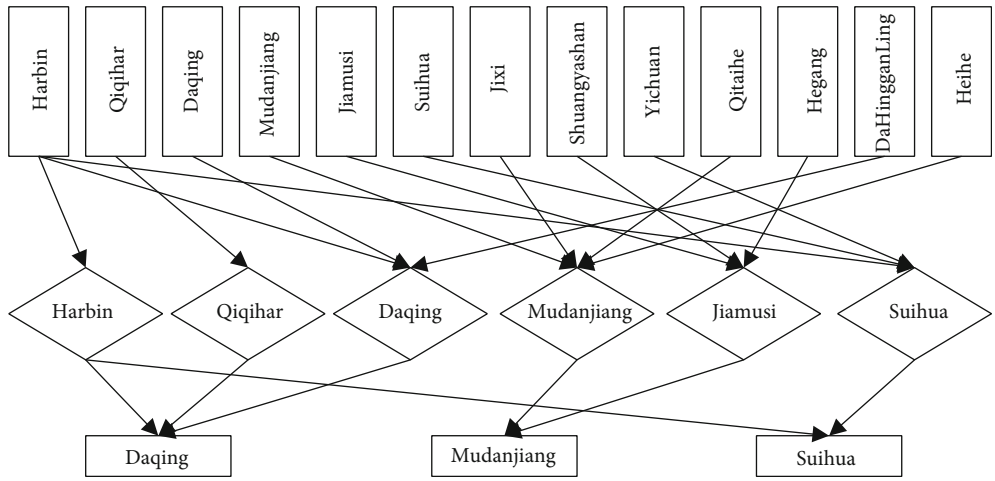

Figure 3: Reverse logistics network diagram of waste tires in Heilongjiang Province.

Table 7: Transport flow between facilities points (tons).

Proposed facilities	site	The area to be recovered and the amount of transportation
recovery center	Harbin	Harbin (6800)
	Qiqihar	Qiqihar (3000), DaHingganLing (560)
	Daqing	Harbin (3030), Daqing (3500), DaHingganLing (270)
	Mudanjiang	Mudanjiang (3330), Jixi (1000), Qitaihe (500), Heihe (750)
	Jiamusi	Jiamusi (2330), Shuangyashan (660), Hegang (470)
	Suihua	Harbin (3470), Suihua (2500), Yichuan (830)
Remanufacturing enterprise	Daqing	Harbin (1600), Qiqihar (3560), Daqing (6800)
	Mudanjiang	Mudanjiang (5580), Jiamusi (3460)
	Suihua	Harbin (5200), Suihua (6800)

transportation distance of goods, the distance query tool is utilized to query the distance between two cities considering the comprehensive judgment of aviation, waterway, highway, and railway data (Harbin, Qiqihar, Daqing, Mudanjiang, Jiamusi, Suihua, Jixi, Shuangyashan, Yichun, Qitaihe, Hegang, Daxinganling, and Heihe are denoted by A, B, C, D, E, F, G, H, I, J, K, L, and M, respectively). Consider that the service life of the reverse logistics network system of waste tires is long at each facility point. Thus, it can be drawn from market research and relevant literature that the construction specifications of each facility point have the same initial construction. Besides, the construction sites of each facility point are all industrial lands, and the construction cost gap is ignored. In this paper, each facility point's annual fixed cost and unit operating cost is assumed to be the same. The annual fixed cost of the recovery center is 1 million yuan, the operating cost is 120 yuan/ton, and the disposal amount is 6,800 tons. The annual fixed cost of remanufacturing enterprises is 15 million yuan, the operating cost is 300 yuan/ton, and the disposal amount is 12,000 tons. Based on the consulting China's Internet of materials and market research, the average freight per kilometer for a waste tire is 1.8 yuan/ton from the recovery node to the recovery center and 1.5 yuan/ton from the recovery center to the remanufacturing enterprise.

4.5. Model Solution. Since the proposed model involves a large amount of data and requires a large amount of calculation, highly targeted software is required to solve it. As a kind of simulation software with strong optimization capability, LINGO can be utilized to solve linear and nonlinear programming problems. LINGO can simulate and solve the location model. After iterative calculations, the optimal value (lowest cost) is obtained as 73 million yuan. Table 5 and Table 6 show the site selections for each facility point.

The site selections of the recovery center include Harbin, Qiqihar, Daqing, Mudanjiang, Jiamusi, and Suihua. In contrast, the site selections of remanufacturing enterprises include Daqing, Mudanjiang, and Suihua. Figure 3 shows the reverse logistics network diagram of waste tires in Heilongjiang Province obtained from the LINGO solution results. Based on the traffic distribution results, the transport traffic distribution among each facility point is sorted out, as presented in Table 7.

5. Conclusion

This paper mainly studies the site selection of the reverse logistics network system for waste tires in Heilongjiang Province. The main conclusions of this paper are given as follows:

(1) The reverse logistics network system of waste tires is constructed with the third party as the core by analyzing the reverse logistics of waste tires in Heilongjiang Province. This system comprises four parts: recovery node, recovery center, remanufacturing enterprise, and distribution market.

(2) The AHP is employed to analyze the influence factors of site selection of reverse logistics network for waste tires in Heilongjiang Province. Economic conditions, the number of waste tires, traffic conditions, development planning and policy, and geographical conditions were selected as the evaluation factors, and their corresponding weights were obtained as 0.3547, 0.2256, 0.1690, 0.1644, and 0.0863, respectively. The above results provide a reference for site selection of the reverse logistics network for waste tires in Heilongjiang Province.

(3) The linear mixed-integer programming method is utilized to select the reverse logistics network site for waste tires in Heilongjiang Province. Finally, the recovery center locations were Harbin, Qiqihar, Daqing, Mudanjiang, Jiamusi, and Suihua. Moreover, Daqing, Mudanjiang, and Suihua were chosen as the remanufacturing enterprise sites.

The established reverse logistics network system is suitable for a variety of recyclable goods. Due to the strong applicability and flexibility of the site selection model, it can be applied to various logistics systems. The solution method employed in the site selection model can be applied to numerous models. Because it is difficult to collect data, some data are replaced in the process of site selection, and the site selection may not be very accurate. In the future, the research on site selection methods will be further strengthened, the relevant data collection will be more comprehensive and complete, and the site selection of this study will be more practical and authentic.

Data Availability

No data were used to support this study.

Conflicts of Interest

There is no potential conflict of interest in this study

Acknowledgments

This study was supported by the Humanities and Social Science Research Youth Fund Project of Ministry of Education (21YJCZH163); the Basic Scientific Research Business Expenses in Provincial Universities (2021GJ10); and the Provincial Leading Talent Echelon Cultivation Project of Heilongjiang Institute of Technology (2020LJ04). This work was supported by the Education Planning Key Project of Hunan Province (project number: XJK21AJG002).

References

[1] China Tire Recycling Association, *The "14th five-year plan" development plan of China's tire recycling industry. Comprehensive utilization of tire resources in China*, vol. 4, pp. 9–18, 2021.

[2] Ministry of Industry and Information Technology, "Industry standard conditions for comprehensive utilization of used tires released," *Rubber Technology*, vol. 18, no. 7, pp. 416-417, 2020.

[3] E. Bottani, G. Vignali, D. Mosna, and R. Montanari, "Economic and environmental assessment of different reverse logistics scenarios for food waste recovery," *Sustainable Production and Consumption*, vol. 20, pp. 289–303, 2019.

[4] B. Wang and H. H. Li, "Multi-objective optimization model of waste tire recycling network," *E3S Web of Conferences*, vol. 214, pp. 03052–03055, 2020.

[5] J. Oyola-Cervantes and R. Amaya-Mier, "Reverse logistics network design for large off-the-road scrap tires from mining sites with a single shredding resource scheduling application," *Waste Management*, vol. 100, pp. 219–229, 2019.

[6] L. D. Fagundes, E. S. Amorim, and R. da Silva Lima, "Action research in reverse logistics for end-of-life tire recycling," *Systemic Practice and Action Research*, vol. 30, no. 5, pp. 553–568, 2017.

[7] P. Ali, "Integrated forward and reverse supply chain: a tire case study," *Waste Management*, vol. 60, pp. 460–470, 2017.

[8] D. Dhouib, "An extension of MACBETH method for a fuzzy environment to analyze alternatives in reverse logistics for automobile tire wastes," *Omega*, vol. 42, no. 1, pp. 25–32, 2014.

[9] J. Lina, *Research and application analysis of packaging waste Recycling based on reverse logistics network*, Xi'an University of Technology, Xi'an, 2020.

[10] J. Zhou and Y. Shao, "Rational selection of rail transit emergency site using complex network topology and genetic algorithm," *Scientific Programming*, vol. 2022, Article ID 6420806, 8 pages, 2022.

[11] M. Jianlong and J. Jingqiu, "Research on urban solid waste reverse logistics and saving environmental governance cost: based on multi-cycle and multi-objective dynamic site selection analysis," *Price Theory and Practice*, vol. 7, pp. 77–80, 2020.

[12] S. Xinxin, "Research on site selection of recovery point of reverse logistics," *Guangxi Quality Supervision Guide Periodical*, vol. 6, p. 175, 2019.

[13] Y. Li and L. Zhang, "The nested site selection model for water treatment plants based on the optimization of water supply radius," *Abstract and Applied Analysis*, vol. 2014, Article ID 529062, 9 pages, 2014.

[14] Z. Xianghong, C. Sijie, and C. Pengfei, "Multi-cycle and multi-objective site selection planning of remanufacturing reverse logistics network under self-recovery mode," *Systems Engineering*, vol. 36, no. 9, pp. 146–153, 2018.

[15] Q. Peili and W. Na, "Study on the location path of the third party distribution of reverse logistics," *Computer Engineering and Applications*, vol. 53, no. 10, pp. 55–60, 2017.

[16] Z. Wei, *Remanufacturing reverse logistics recovery and network optimization design*, Tianjin University of Science and Technology, Tianjin, 2016.

Hindawi
Wireless Communications and Mobile Computing
Volume 2022, Article ID 5606316, 13 pages
https://doi.org/10.1155/2022/5606316

Research Article

Risk Management of Investment Projects Based on Artificial Neural Network

Limei Deng[1] **and Ying Chang**[2]

[1]*The School of Accounting, Changchun University of Finance and Economics, Changchun, 130122 Jilin, China*
[2]*The School of International Economics and Trade, Changchun University of Finance and Economics, Changchun, 130122 Jilin, China*

Correspondence should be addressed to Ying Chang; changying@ccufe.edu.cn

Received 15 March 2022; Revised 18 April 2022; Accepted 25 April 2022; Published 9 May 2022

Academic Editor: Jun Ye

The benefit evaluation of investment projects is the key to the whole investment activities. This paper mainly describes the risk management of investment projects using an artificial neural network. It generally adopts the index system of project risk through modern scientific measurement methods, to evaluate whether the investment project of artificial neural network is feasible or not. It establishes a benefit evaluation model based on an artificial neural network, from the analysis and consideration of 4 groups of experiments, comparing four sets of data: BP network convergence rate, artificial neural network identification efficiency, enterprise risk, artificial neural network output, and error; it is concluded that the relative risk is reduced by about 20% after using the artificial neural network. This also verifies the feasibility of artificial neural networks in the application of raw materials.

1. Introduction

The artificial neural network has better learning ability and can also perform some complex programs at the same time. This contribution to our computing is large, so increasing scholars are interested in investing in this related project. Artificial neural networks are used in various fields. In this regard, there are many researches on investment projects of artificial neural networks, and the risks of these projects also have research directions.

A human neural network is an essential research subject for modern science and technology. It is also a major direction for the subsequent scientific and technological progress of mankind. It plays an indispensable role in human life, medical care, and related work and has a certain guiding role in investment projects in this area.

This paper makes a comparison between the common traditional network convergence rate and the generalized network convergence rate combined with an artificial neural network. The artificial neural network is covered by the traditional BP network convergence rate. It not only retains its original characteristics but also adds the characteristics of artificial neural networks. This problem can be idealized between enterprises, such as corporate finance, asset management, power risk management, corporate environment, production technology, and other issues, and it can also balance enterprise income and expenditure.

2. Related Work

Alanis presents an extension to the basic usage results of the recurrent neural network training algorithm of the Kalman filter and presents a predictive application for electrical energy. And it describes the one-step ahead prediction and n-step idea on European power system data and whether the proposed method is practical and applicable [1].

Isik and Inalli obtained data from the Meteorological Directorate General (MGM) and modeled it with an artificial neural network and an adaptive network-based fuzzy inference system. MATLAB software is used in thermal systems for modeling and prediction of forward-looking data with high sensitivity. It can also be used to verify whether the results of the proposed method are satisfactory [2].

Hodo et al. introduce threat analysis for the Internet of Things and use artificial neural networks (ANNs) to counter these threats. Then evaluate its ability to prevent distributed denial of service (DDoS/DoS) attacks. The ANN program was validated on a simulated IoT network. The experimental results show that the accuracy rate is 99.4%, which can successfully detect various DDoS/DoS attacks [3].

Ascione et al. combine EnergyPlus and MATLAB. Genetic algorithms allow the selection of recommended retrofit package optimization procedures by minimizing energy consumption and thermal discomfort. The algorithm uses an artificial neural network to predict the building performance and conducts large-scale uncertainty and sensitivity analysis to support the generation of the network. The latter has been tested against data provided by the current literature with very good results [4].

Hussain et al. discuss the use of machine learning methods for error prediction and parameter optimization. A combination of a genetic algorithm and an artificial neural network hybrid model is used to optimize the parameter set to minimize the shape error [5].

Tarawneh developed an artificial neural network (ANN) model to predict 60 values of CPT data. The model inputs are static probe tip resistance, effective vertical stress, and static probe casing friction. Artificial neural networks are good tools for predicting 60 values from CPT data with acceptable accuracy [6].

Ivanov et al. conducted an experimental comparison of various functional neural networks for visas and built a signature database for implementing computational experiments. It has been demonstrated that, to a certain extent, an increase in the dimension of decision rules reduces the probability of signature verification errors, while an increase in the number of neurons in the network reduces the number of errors [7].

3. Investment Project Risk Management Method

3.1. Current Situation of Artificial Neural Networks at Home and Abroad. In the 1980s, due to the rapid recovery of artificial neural network technology in the world, a research upsurge has gradually emerged in China. In October 1989, the World Symposium on Neural Network Theory and Application was held at Peking University, and in November 1989, the first academic conference was also started. On February 8, 1990, the University Association organized a grand meeting together. In subsequent conferences held at Peking University, many scholars contributed hundreds of related articles. This action opens a new chapter in the scientific research of artificial neural networks and other technologies in China. With the accumulation and accumulation of time, in the related theoretical research, the martial arts field has gradually achieved relatively pertinent results. A key focus of the modern machine learning field is the neural network. Its concept was first proposed in the 1950s. After the 1990s, it was slowly unveiled by humans. And with the passage of time, people gradually become proficient in its application, mostly in medicine. However, artificial neural networks also have their advantages and disadvantages. Its advantage is that it does not require people to keep looking at the details of what is inside and does not have to pay full attention. This reduces the burden on researchers to a certain extent. Artificial neural networks are simple and can be retrained all time to deal with differently classified data. It can also be perfectly used to deal with its learning problems. The following are its disadvantage: it needs to obtain a large amount of data, and it is difficult to obtain these data. The details of the artificial neural network are mainly the weights after the activation function, and its meaning is still very useful. However, with the current concept of human beings, there is no way to understand it, nor how to explain it. The artificial neural network also needs to be trained repeatedly, in case of coincidence, usually reducing the dimension of the content as much as possible. The artificial neural network is shown in Figure 1.

The following is the structure of the artificial neural network as shown in Figure 1.

Among them, $1, 2, 3, \cdots, N$ is the input value of the neural network. $A1, A2, A3, \cdots,$ An is the way weight from the input node to the internal node. σ is the activation point. The activation point of each function is the function diagram on the right in Figure 1.

It can also be called a sigmoid function, and the meaning expression can be expressed as follows:

$$F(a) = \frac{1}{1 + \exp(-a)}. \tag{1}$$

3.2. The Basic Mechanism and Principle of Artificial Neural Network. This is where neurons must be introduced. As a concept in biology, it is also the most basic structural unit. Neurons are mainly composed of dendritic cell bodies and axons. Each synergy performs a transmission process on the information. Among them, dendrites are used as a kind of signal processing. The collected information is processed by the collection and then by the cell body. The axon here is to transmit the information processed by the cell body to the next neuron and carry out the transmission processing of the information. Therefore, after being inspired by the principle of neurons, scientists have proposed a basic structural pattern in artificial neural networks. In the model, both of them also play the role of an information transmission process, which is similar in purpose. In this multidimensional input model, neurons are responsible for docking activation functions. After processing the docking, the resulting information is passed to the next neuron [8]. After getting information from the outside world, it becomes a basic neuron. After the activation function is processed, its information can be

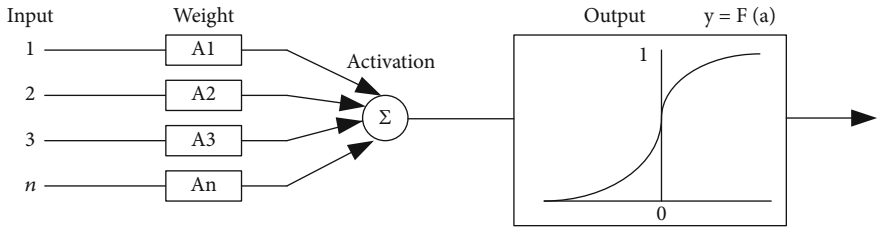

Figure 1: Artificial neural networks.

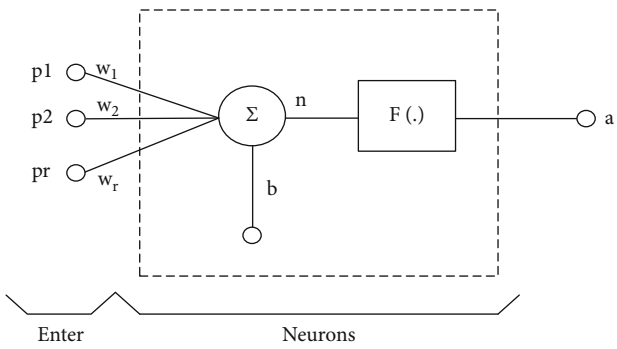

Figure 2: Single neuron model.

transmitted. To better process information and reduce the loss of information, there will be a "wrench to prevent deviation" when information is transmitted, which is also defined as a threshold. This reduces information errors, the threshold acts as a switch in the artificial neural network, and the activation function is a key to turn on the neural network in the neural network. The input value and the threshold make a judgment, and if the judgment is within the threshold range, it can pass the threshold; before entering, the activation step becomes part of the activation function.

The r neurons under the input node $1, 2, 3 \cdots$ are shown in Figure 2. $1, 2, \cdots, n$ are the weights. b is the threshold. Enter a product of the vector i-p and the weight i plus the total value of the bias b to get a new information input. This gives the following formula:

$$A = (w * p + b) = f(w_i * p_i + b). \tag{2}$$

b is used as an integral part of the activation function. The selection of the b value will play a decisive role in the performance of the network. Its center of gravity is the activation function. It plays an essential and decisive role in the quality of the network. And its value selection is also essential. There are three types of activation functions that are generally used.

(i) Threshold activation function: threshold activation function is a special kind of function. Its application is to convert the input information between 0 and 1. Among them, the function $f(\cdot)$ is a step function. The mathematical expression of the threshold activation function is

$$A = f(w * p + b) = \begin{cases} 1, & w * p + b < 0, \\ 0, & w * p + b \geq 0. \end{cases} \tag{3}$$

(ii) Linear activation function: the output of a linear activation function is the weighted input plus the bias. Then the formula can be obtained as

$$A = f(w * p + b) = w * p + b. \tag{4}$$

The linear activation function is shown in Figure 3.

(iii) S-shaped activation function: the role of the sigmoid activation function is to directly convert the values before information processing between 0 and 1. The image of a sigmoid activation function resembles an "S." It is generally used in logarithmic functions, and its logarithmic activation function formula is

$$f = \frac{1}{1 + \exp(-n)}. \tag{5}$$

The formula for the hyperbolic tangent activation function is

$$f = \frac{1 - \exp(-2n)}{1 + \exp(-2n)}. \tag{6}$$

The hyperbolic tangent activation function is shown in Figure 4.

The advantage of the sigmoid activation function is that it can amplify the nonlinearity and can have gain. It can also convert the information obtained from the outside into a curve, which is represented by the slope of the line segment. Scientists and scholars can make the most of this feature. Its gain area is mainly reflected in the docking of some small signals, the gain of large signals, and the processing of amplifying signals, so that both large and small signals can be well gain. The linearity or nonlinearity of a neural network is usually related to the activation function. The selection of

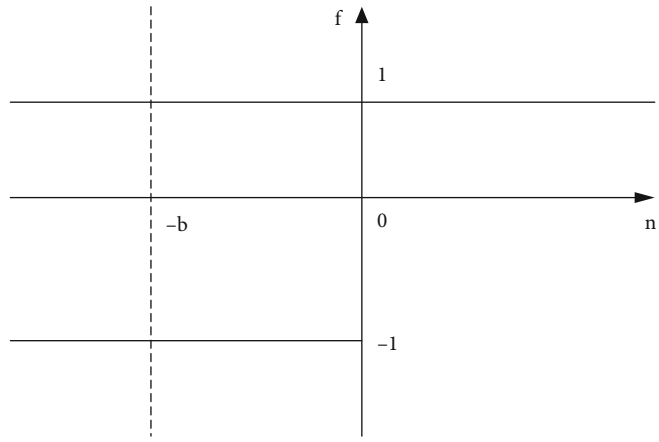

Figure 3: Linear activation function.

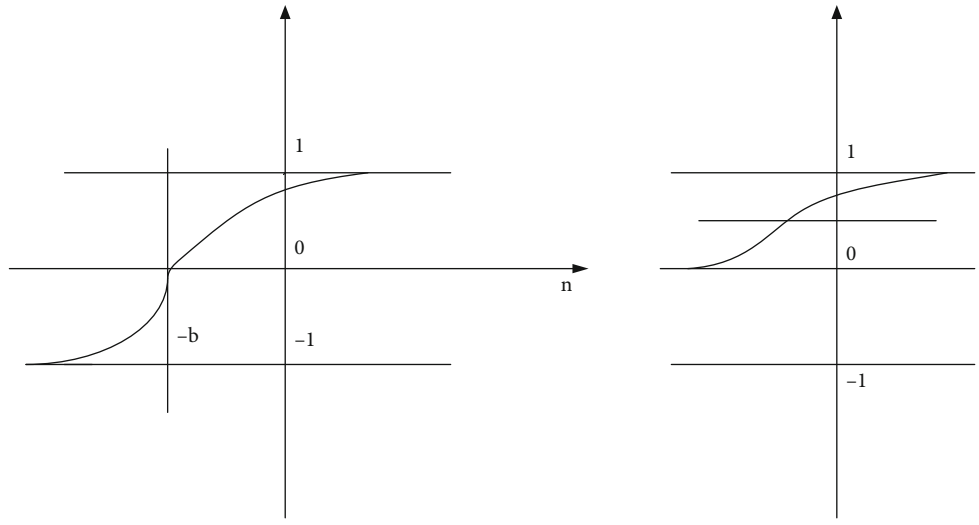

Figure 4: Hyperbolic tangent activation function.

the structure of the artificial neural network is crucial to the subsequent output.

The above is mainly to give a brief introduction to artificial neural networks. It mainly talks about the transmission of some signals, the advantages, and disadvantages. It also explains the required activation function, as well as its basic unit information and the inspiration points for scholars. This is also a hot topic right now. For scholars, because this is the key to subsequent people's progress, how to unlock this key is crucial. This algorithm of artificial neural network has gradually become the most representative algorithm, and it has also become a routine algorithm for researchers.

3.3. The Main Application and Structure and Calculation of Artificial Neural Network. Artificial neural networks are still widely used in contemporary applications. It is multilayered, and there are many types, such as BP, convolution, and recursion. It is also called a multilayer feedforward neural network because of the variety of docking, as shown in Figure 5. The nonlinear matching generalization of artificial neural network can be used in seismic survey, traditional circuit matching, local area network, dynamic image matching, etc. It has practical applications in nonlinear matching generalization, and it has back-propagation algorithm training, which can reduce the error between data.

In the form of the BP neural network model, it has another name called backpropagation algorithm. Its network structure is not single; it is a multilayer group. In its essence, it extends downwards and improves on it, and has a contrasting error in weight. It also has certain advantages in the application, and the specific performance can make the output data more detailed, thereby reducing errors. However, there are still some imperfections. When encountering some complex problems, its limitations are revealed, and sometimes, there is no way to get the desired answer for the optimal solution. Because of this situation, some scholars have combined traditional models to form their own unique set of methods, also called AdaBoost-BP model, as shown in

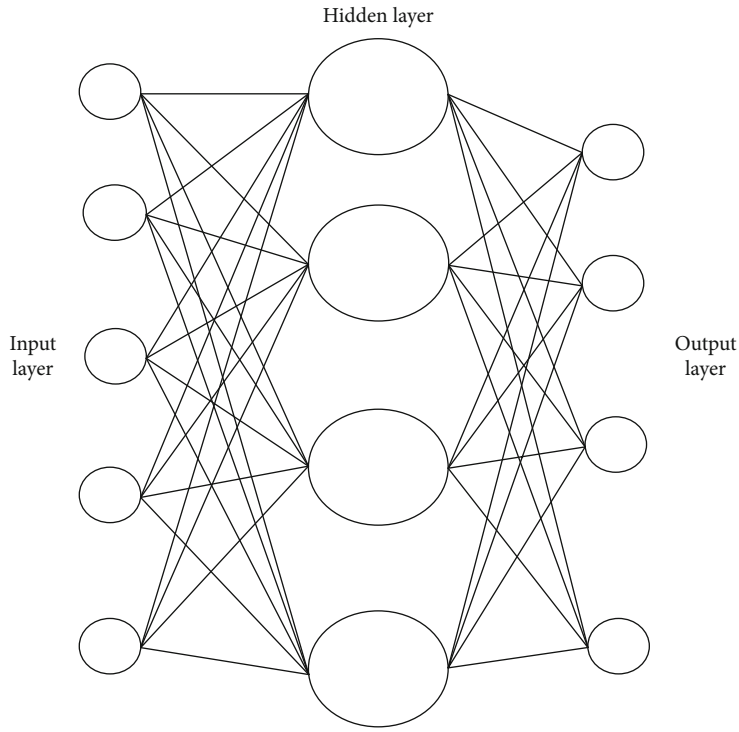

Figure 5: Structure diagram of artificial neural network.

Figure 6. The AdaBoost-BP model can be used to calculate its weight and error rate, and the calculated weight can be used as the next weight parameter, which can be used for iterative calculation using this method to calculate. In terms of short-term sales, the mean error has been reduced to 18.89%, which is much lower than the previous error value. The previous error value can reach 53%, which is already a big breakthrough. However, in some cases where the sample span is relatively large, there will still be large deviations, and only the sample data within 5 days can more intuitively see the expected sale changes.

On this flow chart, the general situation is that there is no best answer. In this case, scholars can only slowly adjust the expected value of the experiment by changing some data, to achieve the desired weight and threshold. After a series of data changes, the required weight and threshold can be achieved by changing the mean of the input value and the size of the threshold. Slowly on a set of changed data, the expected value of the peaks and valleys can be made [9]. Because of the problems encountered before, relevant scholars gradually use some better calculation methods. On the basis of the previous optimization, optimizing the activation function to make the error slowly can also improve the running speed and efficiency of the computer. In the simulation experiments, the generalized BP network can get the result faster than the traditional original BP network. For the corresponding problems, with a momentum of learning rates of 0.5 and 0.7, 6,000 iterations in the traditional mode and the iterations through 6 hidden units are only a quarter of the time required. Through experimental comparative observation, several possible configurations are considered. When the two are used together in experiments, their performance values greatly meet people's expectations, and the convergence rate is almost 100% [10]. This is also a breakthrough in the experiment. There is a lot of room for improvement in terms of data, and the convergence rate is increased by about 20%, as shown in the comparison of Figures 7 and 8. This has been a lot of progress than expected [11]. Based on the dynamics of inertial impulses, the scientific community has discovered that it can be used to influence the rate of learning. In this regard, subsequent improvements can also greatly optimize its operation. The unexpected discovery is that it can also be used to affect the threshold, which is an unexpected and pleasant surprise. In this way, the useless iterations generated in the network learning process are removed, and the number of iterations is reduced, thereby improving the algorithm. These later are also used in the fuzzy diagnosis of steam condensing equipment [12]. It can also be optimized by the optimization algorithm. When working with the BP network, the project of the enterprise can also be estimated, and the identification of the efficiency of the enterprise is very high, as shown in Figures 9 and 10; the resolution accuracy is also better [13]. Some scientists combine back propagation algorithm with optimization algorithm and find that it can solve some enterprise problems well [14]. It can help enterprises make financial estimates, standardize employee information, and control and adjust the power of enterprises. There are also some power grid companies that combine BP and other algorithms to perform a predictive analysis on some financial aspects of the company. On the basis of the neural network, it can also be more in line with a company's income

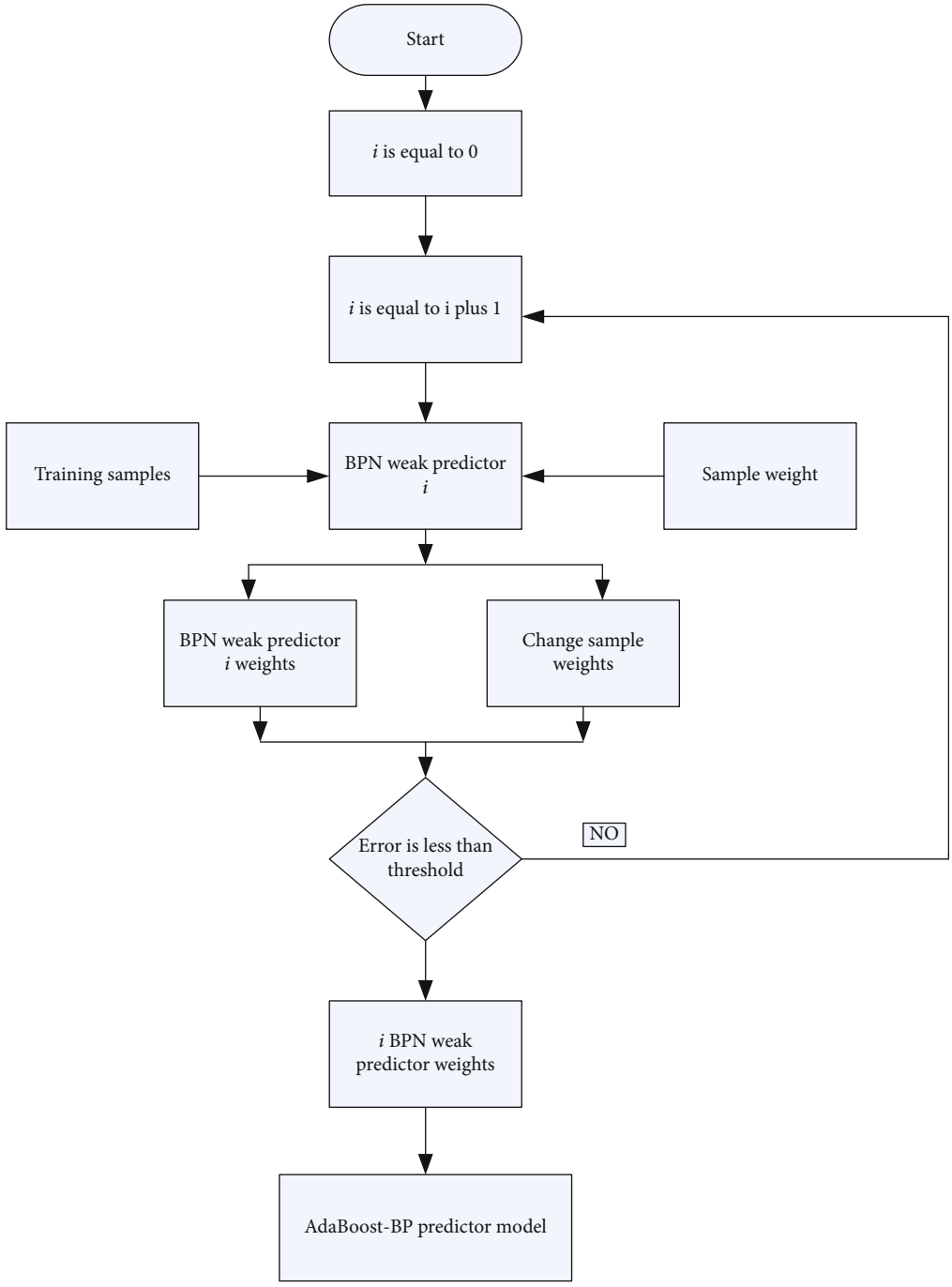

Figure 6: AdaBoost network model flow chart.

and expenses. It can predict the balance of income and expenditure and financial benefits within a certain range and can also deal with problems between enterprises more ideally.

3.3.1. The Role of Neural Network Learning Algorithms. It can be applied to natural language processing, image recognition, speech recognition, and other fields.

(1) Error Correction Learning. Let $x_k(z)$ be the real input value of the neuron at this moment when $y(z)$ and $c_k(z)$ be a deviation signal $f_k(z)$ of the control sample at the output; the general formula of the deviation signal can be obtained as

$$f_k(z) = c_k(z) - x_k(z). \tag{7}$$

The purpose of the error is mainly to make the obtained value $x_k(z)$ as close as possible to the expected one. In the case of guaranteeing a single variable, such an error value will be reduced as much as possible. This is also a problem of finding its optimal solution. Use Q to represent the error

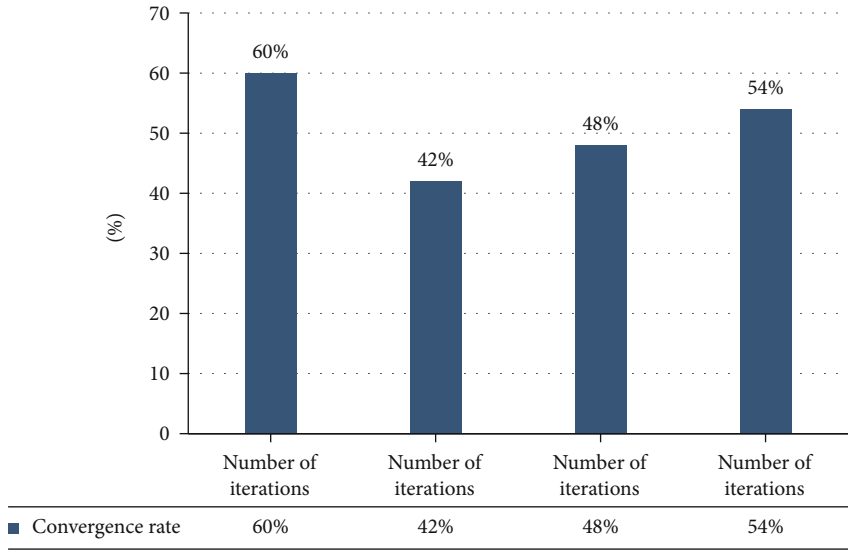

Figure 7: Convergence rate of traditional BP network.

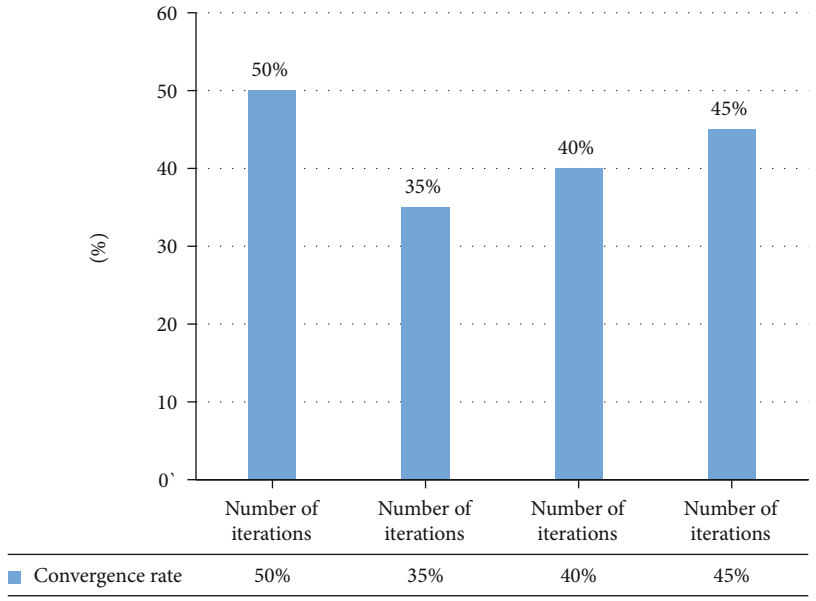

Figure 8: Generalized BP network convergence rate.

value of the optimal solution; then its formula can be as follows:

$$Q = \left(E \frac{1}{2} \sum_{k} f_k^2(n) \right). \tag{8}$$

Among them, E is an operation method to find the expected value. What it needs to have is a smooth, step-descent-like method. When expressed in error Q, some digital information must be connected. The overall method uses Q together to represent the instantaneous value$Q$at time$n$at time; then its formula can be obtained:

$$\varepsilon(n) = \frac{1}{2} \sum_{k} f_k^2(n). \tag{9}$$

Find $\varepsilon(n)$ with the minimum value of weight W; according to the above method, we can get

$$\varepsilon(n) = \frac{1}{2} \sum_{k} f_k^2(n). \tag{10}$$

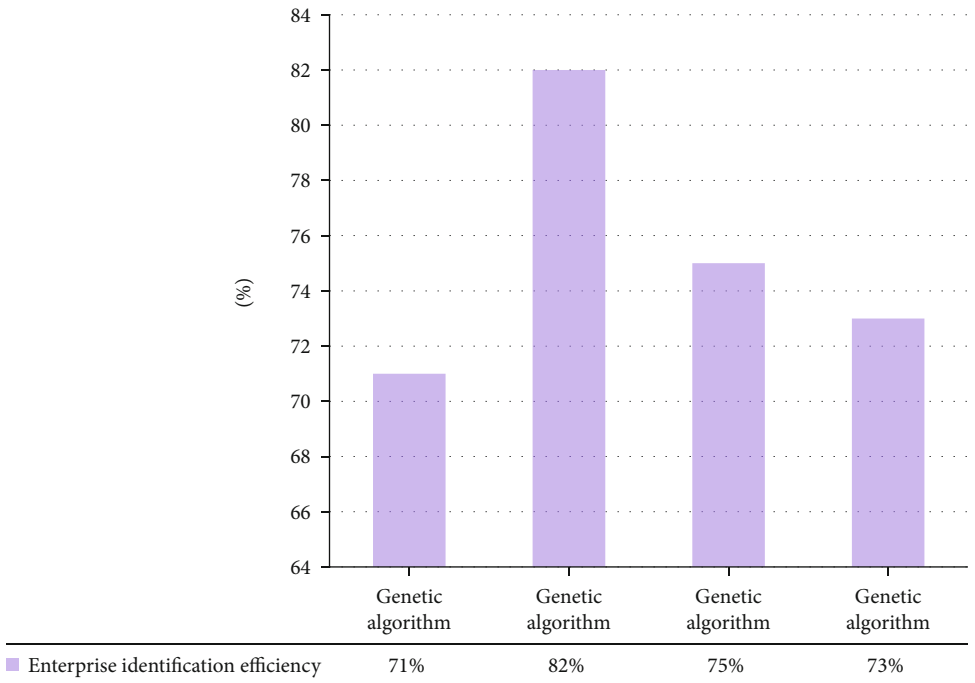

Figure 9: The identification efficiency of enterprises after the genetic algorithm is connected to the artificial neural network.

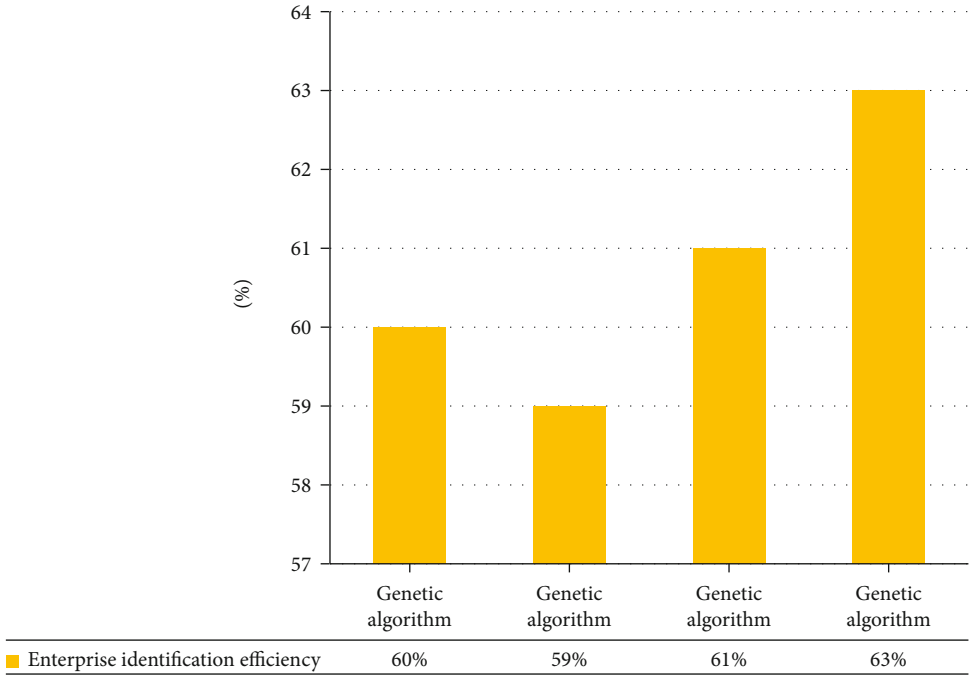

Figure 10: Identification efficiency of enterprises based on genetic algorithm.

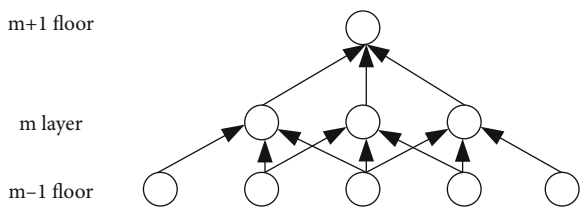

Figure 11: Schematic diagram of sparsely connection.

Among them, η is designed for learning step size, which can also be said to be a rule to find the best data through multiple error signals.

$$\nabla w_{kj}(n) = \eta f_k(n) x_j(n). \tag{11}$$

(2) Learning. Neuropsychologists judged according to this rule that "the activation and inhibition states will appear

at both ends of the neuron's activation." The response increases when activated and decreases when inhibited. Its formula can be

$$\nabla w_{kj}(n) = Ff_k(n)x_j(n). \tag{12}$$

Among them, $f_k(n)x_j(n)$ is the state of the neurons on both sides, and one of the most commonly used cases is

$$\nabla w_{kj}(n) = \eta x_k(n)x_j(n). \tag{13}$$

∇w, x_k, and x_j have a certain proportional relationship, which also becomes a relevant learning rule. Convolutional neural networks (CNN) can be regarded as a relatively common structural model in instrument learning. These are generally reflected in image classification and recognition, semantic segmentation, and translation, and the effect is still good. There are four traditional CNN structures: fully connected layer, output layer, convolutional layer, and pooling layer. CNN's achievements in images are still very good, and it is not much less in practical applications. Especially in identification, under its calculation, the instrument can more accurately identify the information of the picture and text and then record it. The resulting output vector is approximately equal to 0.434, the optimal interval for working together. Scholars combined the previous convolutional neural network CNN application with VGG16 and then applied it to face recognition and discarded the previously collected information and then combined the previous CNN to obtain a new model. Compared with the previous ICA algorithm, CNN has achieved significant improvement and image accuracy and recognition rate [15, 16]. Some scholars will apply CNN to fault-type problems, monitor the processed signals, and classify them autonomously. Through the intelligent diagnosis of the convolutional neural network CNN, the previous signal is processed to obtain a two-dimensional data image, thereby eliminating the influence of experience and the characteristics of the information. Experiments conducted in the experiments verify the effectiveness of the method, and based on the experiments, it can also be better used in the variation of workload [17]. Some other scholars apply this technique to the deformation module crack detector. In the last layer, it is transformed into a similar intelligent learning machine, which can achieve a pass rate of 97% in actual person recognition. And it will not conflict with other methods; on the contrary, there are some advantages. The sparse connection method of convolutional structure in the BP neural network is shown in Figure 11.

Suppose the bottom layer is the input layer. In the BP neural network, the neuron nodes in the middle layer are connected to all neuron nodes in the lowest layer. However, in the convolutional neural network, the connection method is different, but the neuron node in the middle layer is connected with its three similar nodes. This reduces the parameter size [18].

Table 1: Scoring criteria for individual indicators.

Risk	High risk	Higher risk	General risk	Lower risk	Low risk
Score value	<0.2	0.2-0.4	0.4-0.6	0.6-0.8	>0.8
Environmental risk	—	0.38	—	—	—
Technical risk	—	—	0.51		—
Production risk	—	—	0.48	—	—
Market risk	—	0.32	—	—	—
Financial risk	—	—	0.53	—	—
Manage risk	—	0.36	—	—	—

(3) Applications of Artificial Neural Networks.

(1) Face recognition: it is mainly based on information theory, operation and maintenance imitate the brain's thinking method and process information. Compared with the previous pass-through algorithm, although it has shortcomings in empirical characteristics, its characteristic is that it can process high-dimensional data [19].

(2) Smart city: in the era of innovation and convenience, people are committed to the control and management of resource efficiency. This is mainly used to improve the quality of life of urban residents. In the process of real plan implementation, this can process a lot of data information [20], such as urban street lights, online monitoring, enterprise risk assessment, and medicine. The neural network mainly analyzes, filters, and disseminates data to realize graphics and video.

(3) Risk assessment and forecasting: due to the limitations of traditional computing methods, the processing of data cannot reach the expected value of human beings, so it will be gradually applied in this estimation and other aspects. Because the previous information processing is incomplete, there are no rules, and the data is not obvious, then the future price and risk are processed in economics, and there must be a scientific basis [21]. The population can be modeled and analyzed according to the distribution and income of people, and a relatively stable and convergent scheme can be obtained.

(4) Traditional medical data storage: because in terms of traditional medical data, the storage requirements are relatively high, but artificial neural networks can solve this problem very well. It can analyze and classify case models, which greatly facilitates medical workers, improves the ability to organize data, and more intuitively shows that biological signals can be effectively restored. This facilitates expert medical judgment.

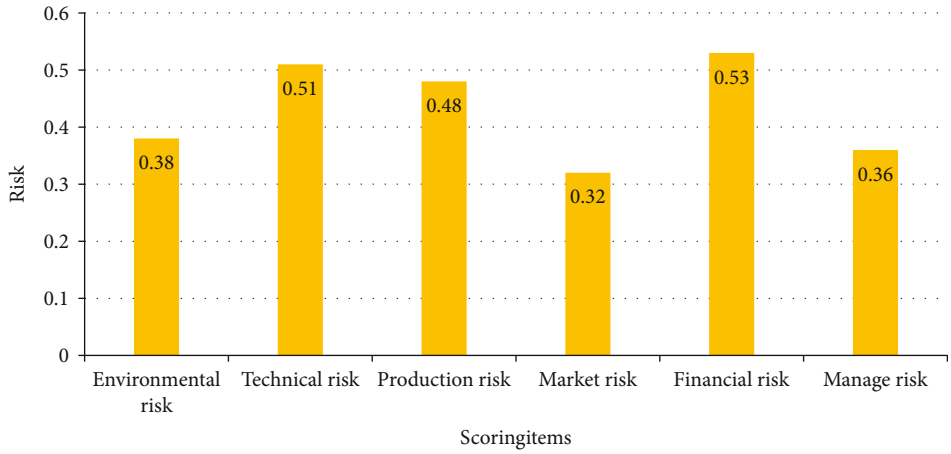

Figure 12: Various risk scores.

Table 2: Risk item score assessment.

Evaluation sample	Environmental risk	Technical risk	Production risk	Market risk	Financial risk	Manage risk	Evaluation value
1	0.82	0.61	0.86	0.83	0.75	0.82	0.8001
2	0.94	0.41	0.49	0.95	0.55	0.94	0.7100
3	0.88	0.47	0.50	0.88	0.62	0.65	0.5687

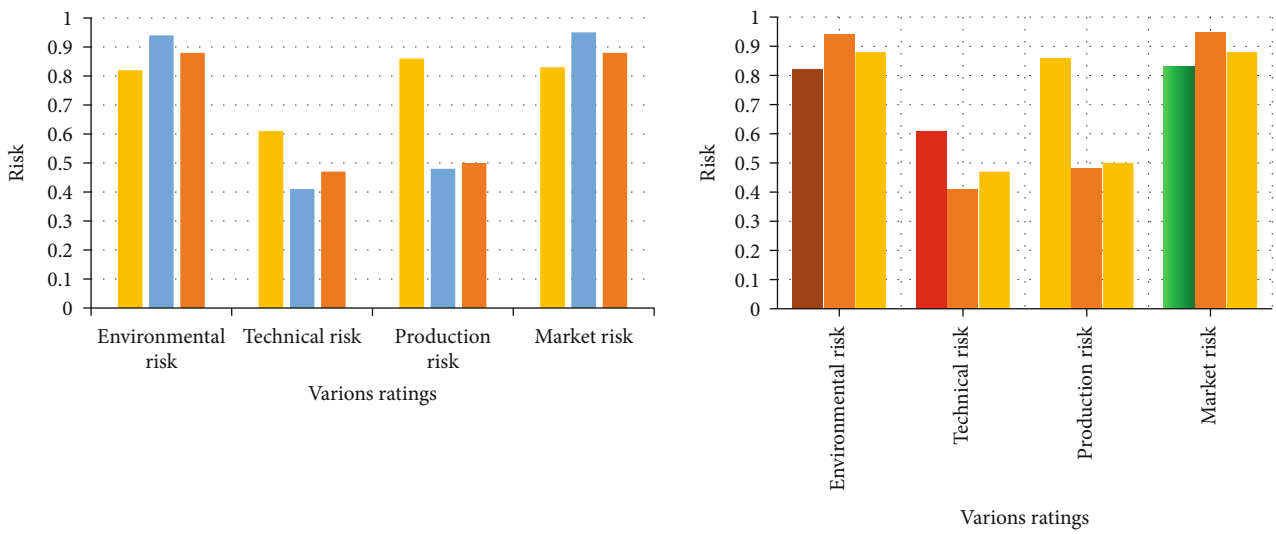

Figure 13: Enterprise risk comparison chart.

4. Experimental Analysis of Venture Capital Projects Based on Artificial Neural Network

The following is mainly to compare the risks between the enterprise market, finance, and management and investment risks and the output errors of artificial neural networks. It is a project evaluation model. It is mainly through a lot of intensive training and data sorting and analysis and then through the integration of the obtained data, to make a reasonable judgment on the project. In the absence of human subjective factors, the evaluation project is judged through experience and technology to ensure its accuracy and numerical idealization of risks. An evaluation index in the evaluation is quite important. The information contained in it should be more and not repeated, and the selection of indicators needs to be accurate, and it can have a variety of selectivities. In this way, the risk assessment of the evaluation project will be more reasonable and the value will not be obtained blindly. Because the evaluation is a single project, the overall impact will be relatively large. What the enterprise needs is an overall assessment, so it needs to use a variety of methods to ensure the consequences of risk

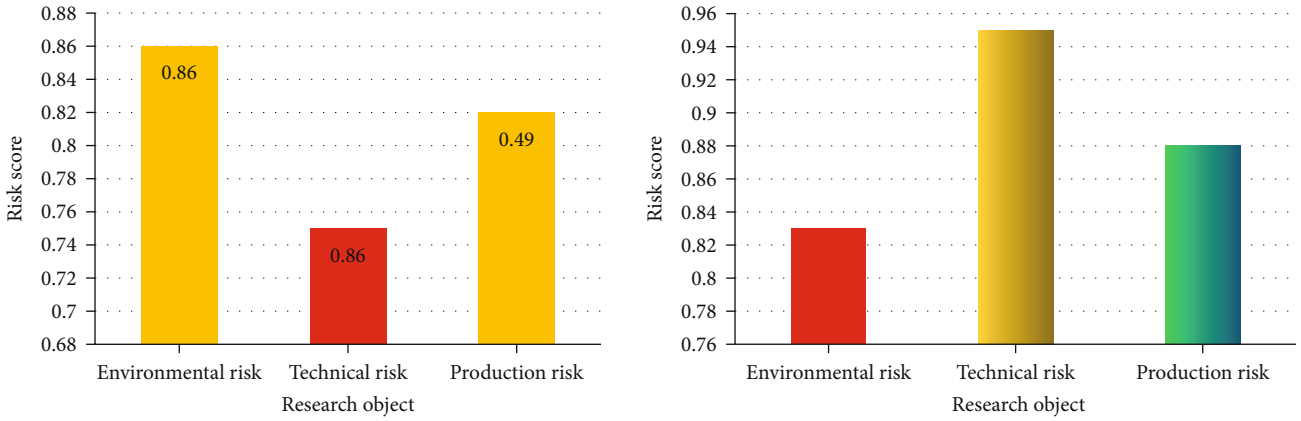

Figure 14: Investment risk comparison chart.

Table 3: Ship risk assessment model output values of neural network.

Ship	Actual value at risk	Conventional neural network		Improve neural networks	
		Output value	Error	Output value	Error
1	0.37	0.3669	-0.031	0.3722	0.022
2	0.43	0.4329	0.029	0.4281	-0.019
3	0.31	0.3122	0.022	0.3121	0.021
4	0.39	0.3846	-0.054	0.3864	-0.036
5	0.58	0.5861	0.061	0.5779	-0.021
6	0.44	0.4436	0.036	0.4417	-0.017
7	0.49	0.4858	-0.042	0.4926	0.026

events, as well as the acceptable worst results. Then there are different ways of dealing with the risks. Therefore on how to strengthen the rationality and scientificity of evaluation, this system and method becomes more important. Taking into account the actual situation of our country and for the convenience of research, six risk evaluation indicators are used to analyze the risk of the project. In actual use, it can be adjusted and increased or decreased appropriately according to the specific situation. This does not affect the application of this model. The six indicators are technology, production, market, environment, financial risk, and management risk. Each type of risk can also be classified in more detail. Such an evaluation is also unreasonable, and its influence on the weights is also varied and inaccurate. Each item should state its risk level assessment. Summarize the scoring results of each risk index, and obtain the average value. The resulting risk score value will also be more accurate. For the convenience of application, the score is controlled between 0 and 1. According to the evaluation level, the risk level can be divided into five levels: low, low, medium, high, and high. The scoring standard of a single index is shown in Table 1, and each risk score is shown in Figure 12, where less than 0.2 is high risk, between 0.2 and 0.4 is medium to high risk, 0.4 to 0.6 is medium risk, 0.6 to 0.8 is medium low risk, and greater than 0.8 is low risk.

The following 2 companies have overall risk assessment based on artificial neural network as shown in Table 2.

In the environment and technology, production risk comparison is shown in Figure 13.

The comparison of risks in market, finance, and management is shown in Figure 14.

There is also a set of model values for ship risk assessment, and a comparison of the two is shown in Table 3. The error is equal to the output value minus the input value. If it is a positive number, it means that the risk assessment of the ship is correct and there is a risk. If it is a negative number, it means that the risk of the ship can be ignored, which proves that there is no risk.

After the comparison, the comparison between the conventional artificial neural network and the improved artificial neural network can be found. In the evaluation of ship risk, it can be seen that the error after improvement will be lower, and this is also better for the safety of the ship. The risk of the ship will also be lower and more in line with the forecast results of the ship.

5. Discussion

5.1. Codevelopment of Artificial Neural Networks and Simulation Algorithms in Other Fields. Nowadays, many technologies are slowly being combined, which is also the trend of the times. An artificial neural network is no exception, and it is also a contemporary direction. There are many similar ones. Among them, there are chaotic neural network theory, quantum science, and quantum neural network generated by combination, and there are other simulations with contacts in related fields. It can help to have a better collaboration when contacting experimental neural networks, as well as better robustness to optimize its performance, and it is also slowly improving and optimized in related majors.

5.2. Cooperative Development of Artificial Neural Networks and Edge Computing. In the development of contemporary technology, artificial neural networks and edge computing also have a certain connection. After all, it is the focus of the Internet of Things. It will receive various information and need to process local data. The processing of these is

the edge server, which can be equipped with a network system and can better analyze the information processing and connect the output signal.

5.3. Development Status of Artificial Neural Network in Artificial Intelligence Core. The chip structure that simulates the network neural model of the human brain on the market is currently a new type of chip programming architecture. This architecture can more realistically simulate a perception, behavior, and thinking of the brain. However, this technology is relatively difficult and requires a lot of time investment. For example, some chip strategies include Qualcomm and Intel. However, most of them are the brain synapses of high-defense humans.

6. Conclusions

Artificial neural networks are currently a focus of research, and their significance is obvious to humans. It can greatly facilitate human life, and it is also a key for us to further develop and research new technologies. This article starts from the fundamental point and explores the origin, development, history, essence, structure, and use of artificial neural networks one by one. Although the current scientific research results cannot open this door, I have always believed that this door will eventually open in the near future, bringing us convenience and moving forward. It is a new world we have not explored yet that humanity has been waiting for.

Data Availability

The data underlying the results presented in the study are available within the manuscript.

Conflicts of Interest

The authors declare that they have no conflicts of interest.

Acknowledgments

This work was supported by the Social Science Fund of Jilin Province in 2021 (No. 2021B84); the Scientific Research Project of the Education Department of Jilin Province in 2021 (Nos. JJKH20211394SK and JJKH20211396SK).

References

[1] A. Y. Alanis, "Electricity prices forecasting using artificial neural networks," *IEEE Latin America Transactions*, vol. 16, no. 1, pp. 105–111, 2018.

[2] E. Isik and M. Inalli, "Artificial neural networks and adaptive neuro-fuzzy inference systems approaches to forecast the meteorological data for HVAC: the case of cities for Turkey," *Energy*, vol. 154, no. JUL.1, pp. 7–16, 2018.

[3] E. Hodo, X. Bellekens, and A. Hamilton, "Threat analysis of IoT networks using artificial neural network intrusion detection system," *Tetrahedron Letters*, vol. 42, no. 39, pp. 6865–6867, 2017.

[4] F. Ascione, N. Bianco, and C. De Stasio, "CASA, cost-optimal analysis by multi-objective optimisation and artificial neural networks: a new framework for the robust assessment of cost-optimal energy retrofit, feasible for any building," *Energy & Buildings*, vol. 146, no. Jul., pp. 200–219, 2017.

[5] S. F. Hussain, G. Hussain, and N. Rahman, "Artificial neural network modelling and optimization of elastic and an-elastic spring back in polymer parts produced through ISF," *The International Journal of Advanced Manufacturing Technology*, vol. 118, no. 7-8, pp. 2163–2176, 2022.

[6] B. Tarawneh, "Predicting standard penetration test *N*-value from cone penetration test data using artificial neural networks," *Geoence Frontiers*, vol. 8, no. 1, pp. 199–204, 2017.

[7] A. I. Ivanov, P. S. Lozhnikov, and A. E. Sulavko, "Evaluation of signature verification reliability based on artificial neural networks, Bayesian multivariate functional and quadratic forms," *Computer Optics*, vol. 41, no. 5, pp. 765–774, 2017.

[8] S. Diffo, W. Lemotio, and C. M. Adiang, "Contribution of the artificial neural network (ANN) method to the interpolation of the Bouguer gravity anomalies in the region of Lom-Pangar (East-Cameroon)," *Geomechanics and Geophysics for Geo-Energy and Geo-Resources*, vol. 8, no. 1, pp. 1–15, 2022.

[9] M. Hojati, E. Mansouri, and H. Moradzadeh, "Stirling engine parameters prediction to control its rotation speed using artificial neural network," *Journal of the Brazilian Society of Mechanical Sciences and Engineering*, vol. 44, no. 2, pp. 1–9, 2022.

[10] R. Lahmyed, M. E. Ansari, and Z. Kerkaou, "Automatic road sign detection and recognition based on neural network," *Soft Computing*, vol. 26, no. 4, pp. 1743–1764, 2022.

[11] Y. Rumiantsev and F. Romaniuk, "An artificial neural network developed in MATLAB-Simulink for reconstruction a distorted secondary current waveform. Part 2," *ENERGETIKA Proceedings of CIS higher education institutions and power engineering associations*, vol. 65, no. 1, pp. 5–21, 2022.

[12] P. V. Chandrika, K. S. Srinivasan, and G. Taylor, "Predicting stock market movements using artificial neural networks," *Universal Journal of Accounting and Finance*, vol. 9, no. 3, pp. 405–410, 2021.

[13] D. Liu, X. Jiang, L. Meng, and Y. E. E. Ge, "Minimizing investment risk of integrated rail and transit-oriented-development projects over years in a linear monocentric city," *Discrete Dynamics in Nature and Society*, vol. 2016, Article ID 1840673, 8 pages, 2016.

[14] G. Toa, B. Atalay, and M. D. Toksari, "COVID-19 prevalence forecasting using autoregressive integrated moving average (ARIMA) and artificial neural networks (ANN): case of Turkey," *Journal of Infection and Public Health*, vol. 14, no. 7, pp. 811–816, 2021.

[15] L. C. Nunes, P. R. Pinheiro, M. C. D. Pinheiro, M. S. Filho, and R. E. C. Nunes, "Toward a novel method to support decision-making process in health and behavioral factors analysis for the composition of IT projects teams," *Neural Computing and Applications*, vol. 32, no. 15, pp. 11019–11040, 2020.

[16] Y. Liu, T.-H. Yi, and C.-Q. Wang, "Investment decision support for engineering projects based on risk correlation analysis," *Mathematical Problems in Engineering*, vol. 2012, Article ID 242187, 14 pages, 2012.

[17] N. Hong, X. Wang, and Z. Xu, "Probabilistic reliable linguistic term sets applied to investment project selection with the gained and lost dominance score method," *International Journal of Machine Learning and Cybernetics*, vol. 12, no. 8, pp. 2163–2183, 2021.

[18] Y. Zhao, H. Li, S. Wan et al., "Knowledge-aided convolutional neural network for small organ segmentation," *IEEE Journal of Biomedical and Health Informatics*, vol. 23, no. 4, pp. 1363–1373, 2019.

[19] X. Zheng, G. Zhu, N. Metawa, and Q. Zhou, "Machine learning based customer meta-combination brand equity analysis for marketing behavior evaluation," *Information Processing and Management*, vol. 59, no. 1, article 102800, 2022.

[20] O. S. Kotsyuba, "Estimating the payback period of an investment project in the framework of a fuzzy set statement of the problem," *Business Inform*, vol. 10, no. 513, pp. 173–179, 2020.

[21] J. A. Nikolova and L. V. Skopina, "Options method for oil exploitation investment project efficiency evaluation under risk conditions," *Interexpo GEO-Siberia*, vol. 3, no. 1, pp. 159–167, 2020.

Hindawi
Wireless Communications and Mobile Computing
Volume 2022, Article ID 2396645, 11 pages
https://doi.org/10.1155/2022/2396645

Research Article

Basic Theory and Practice Teaching Method Based on the Cerebellar Model Articulation Controller Learning Algorithm

Meng Huang, Shuai Liu, Yahao Zhang, Kewei Cui, and Yana Wen

School of Information Engineering, Institute of Disaster Prevention, Sanhe, 065201 Hebei, China

Correspondence should be addressed to Meng Huang; huangmeng@cidp.edu.cn

Received 18 February 2022; Revised 11 April 2022; Accepted 19 April 2022; Published 9 May 2022

Academic Editor: Jun Ye

With the continuous in-depth development of science and technology in my country, the field of artificial intelligence has also made considerable progress. For example, the comprehensiveness and operability of technology have been enhanced. Artificial intelligence, as a comprehensive and intersecting research field in the fields of computer science, information science, and mathematics, has also made a certain contribution to the progress of international students in colleges and universities. This article is aimed at studying the problems based on basic theories and time teaching methods, mainly through a comprehensive data analysis of artificial intelligence technology and fusion differential evolution algorithm, and then improving the learning ability of students and comprehensive quality. This paper proposes a swarm intelligence algorithm, K-means clustering algorithm, and vector machine algorithm and summarizes the process and application fields of the swarm intelligence algorithm. In addition, the CMAC learning algorithm is proposed, which shows that robots under the background of industrial intelligence and machine learning can organize themselves to form groups to perform complex tasks. The experimental results of this paper show that the communication range is between 0 and 1, which can enable more robots to communicate in order to improve the individual's social learning opportunities, thereby enhancing the individual's learning ability to improve the performance of learning behavior and improving the efficiency of practical teaching and research, making the efficiency reach 0.9.

1. Introduction

1.1. Background. In English teaching, frontline teachers are often troubled by the following problems:

(1) The polarization of students' comprehensive ability to use English is serious. With the increase in the content of learning and the deepening of the difficulty, the gap between the students' comprehensive ability to use English has become increasingly obvious, and the phenomenon of polarization has become serious

(2) Class time is limited, it is impossible to test students' mastery in full coverage in class, and it is impossible to mobilize students to actively participate in learning and discussion with high frequency

(3) Students are not good at listening and not good at cooperating and communicating, or cooperating and communicating are only limited to imitating example sentences or dialogues. They will not learn actively, actively explore, cooperate, and communicate, let alone creative learning

(4) Cooperative learning is only effective in the classroom. After class, the cooperation is terminated after the completion of specific learning tasks, and there is no continuity

(5) The evaluation model is relatively simple, mainly based on the one-way evaluation of the individual students by the teacher, there are few student evaluations, and it is more difficult to achieve instant evaluation and multiple evaluations

How to solve this series of problems has always plagued frontline teachers. Sato Xue believes, "The classroom is quietly changing. The desks and chairs are arranged in rows facing the blackboard and the podium. The teacher uses the

textbook as the center and uses the blackboard and chalk to explain. The teacher asks the students and answers—this is the scenery of the classroom that we are accustomed to. This kind of classroom scenery is entering museums in Europe and the United States." It can be seen that the traditional teacher "Yiyantang" teaching is no longer acceptable to Teachers must make changes and do everything possible to return the classroom to the real master: the learner. Teachers should strive to make classrooms enjoyable for students to learn and teachers to enjoy teaching and build classrooms into a learning community. However, in the process of building a learning community, we should also focus on understanding individual differences.

1.2. Significance. The development of service learning has been quite mature, and the implementation from system to management has reached the level of regularization and institutionalization. Based on a comprehensive understanding of the concept of service learning in many aspects, this research discussed the theoretical basis and functional characteristics of service learning and introduced the guarantee mechanism and organization related to service learning and the implementation process of service learning. The research of this paper takes the service-learning American university as the case study object, and the purpose is to experience the various links and details of service-learning, explore the role of various factors in the implementation and development of service learning, and have the opportunity to update our country. The content of practical teaching in higher education promotes the development of citizen participation in education. The implementation and application of service learning in American colleges and universities provide students with more opportunities for growth, which can enable college students to deeply experience and feel contemporary social development, cultivate college students' sense of social mission and national responsibility, and can study the service learning of American colleges and universities. It is conducive to exerting the functions of universities and affecting the related development of higher education in our country. Service learning is conducive to promoting the cultivation of critical thinking, so that students possess the spirit of questioning questions and have a deeper grasp of theories. Therefore, through the research on artificial intelligence learning in colleges and universities, reflecting on the status quo of the social practice education of Chinese college students, and trying to critically learn from the ideas and practices of artificial intelligence learning and learning in colleges and universities, it is conducive to solving the problems existing in the development of the social practice activities of college students in our country, so as to further strengthen the basic theoretical research of the social practice system of college students.

1.3. Related Work. In recent years, with the rapid development of big data and other technologies, artificial intelligence and machine learning algorithms have made great contributions to education. Jia and Zhang and Ramezani Mayiami et al. analyzed the application status of artificial intelligence technology in university psychology and pedagogy teaching mode and put forward a research on university psychology and pedagogy teaching mode based on artificial intelligence technology. This article conducted a survey and analysis of 290 teachers and students, and their recognition of artificial intelligence technology reached more than 90%. And after the application of artificial intelligence to psychology teaching, the satisfactory learning environment, learning methods, and learning effects were compared and analyzed, and the results were discussed and analyzed [1, 2]. Guo and Sun proposed that teaching effects need to be combined with artificial intelligence systems. In order to change the traditional teaching mode and improve the classroom detection effect, based on the open Internet of Things and cloud computing technology, the college classroom real-time monitoring system has been constructed, and a number of new improvement measures and algorithms have been proposed to provide automatic identity positioning in large scenes. The application provides a theoretical and technical basis. Field scenes are obtained through field image data collection and field data processing, and then the regional scenes are combined with field measured data to verify accuracy and trends and obtain student morphological characteristics [3]. In general, their analysis is in place. The only drawback is that the research process is not rigorous enough, which leads to differences in research results. Although these studies are related to artificial intelligence and machine learning algorithms, their research processes are complex and difficult to operate.

1.4. Innovation. The innovation of this article is as follows: (1) the first is the innovation of the method, which is mainly reflected in the new method that combines artificial intelligence and machine learning algorithms when conducting research in this paper; (2) the innovation of viewpoints, firstly elaborating and sorting out the connotation, characteristics and functions, and theoretical basis of service learning; secondly, further grasping the implementation situation of service learning from the operating mechanism and organization management of service learning and in-depth study of its service-learning practice inquiry; and finally, combined with the specific practice of service learning, sum up successful experience and put forward localization suggestions suitable for my country's higher education teaching reform; and (3) innovation in project practice. In recent years, with the rapid development of big data and other technologies, artificial intelligence has ushered in a turning point in its development. Artificial intelligence will become the world's most critical technology in the next two decades. Artificial intelligence can make human life better and more convenient.

2. Particle Swarm Optimization Algorithm

2.1. Theoretical Source of Service Learning in Universities

2.1.1. The Difference between Service Learning and Traditional Courses. As an experiential learning, service learning has many differences from traditional classrooms. We can use Table 1 to reflect the differences between traditional courses and service learning in several aspects.

Table 1: The difference between service learning and traditional courses.

	Traditional course	Service-learning process
Location	Classroom	Classroom and community
Teachers	Teacher	Teachers, supervisors, community mentors, learners, and peers
Ready to work	Designated readings, selected courses	Designated readings plus optional readings; selected courses Personal traits; access to service locations
Study	Writing, examination, understanding, short-term	Writing, examination, cognition, experience, short term, and long term
Evaluation	Teachers	Teachers, community supervision, and self-evaluation

The teaching and learning characteristics of traditional courses and service learning are also completely different. When implementing teaching activities in traditional courses, more attention is paid to theoretical teaching in the classroom. The teaching method is mainly based on teacher lectures, and the form is relatively rigid. Under the guidance of this teaching mode, students have a single way of thinking, thinking in a unitary thinking orientation, and there are many teachers. The teaching method of deductive reasoning is used to impart book knowledge. In terms of course evaluation, the teacher only makes the evaluation during the course or after the course. Generally speaking, it is a traditional negative learning method, while service learning pays more attention to practical teaching. With community service as the main form of learning, teachers and supervisors interact with academics in the form of training, so that students can learn by doing. This learning method reflects the characteristics of flexibility. Therefore, students can think in diversified ways. Orientation to divergent thinking and inductive methods are used to impart knowledge in the teaching process. In terms of course evaluation, service learning [4] can conduct current evaluation and reflection at any time during the course of the course.

2.1.2. Cooper's Empirical Learning Theory. Cooper proposed the ELM experience learning model theory in 1984 (see Figure 1). We can discover Cooper's experience learning. The model theory can be applied to almost all theories about service learning. Cooper believes that learners circulate in energy. The process of spiraling up the learning ability of learners is very similar to this ancient Chinese philosophy. This too Cheng started with specific experience, conducted continuous reflection and observation, formed abstract concepts [5] of specific problems and proposed solutions, and finally carried out practice and summary, as shown in Figure 2:

2.2. Theoretical Overview of Swarm Intelligence Algorithm

2.2.1. Bat Algorithm (BA). The bat algorithm is one of the closest algorithms to particle swarm optimization. In 2010, Dr. Yang from the University of Cambridge studied the bat algorithm, a new type of swarm intelligence optimization algorithm, by simulating the echolocation behavior of bats. Echolocation refers to animals such as bats that establish their cognition of the surrounding environment by echoing the sound they emit. Similar to all population-based stochastic optimization algorithms [3], the solution in each optimization problem is a bat in the search space, and the positions of all bats represent the fitness value of the problem. Each bat acts as a basic individual of the algorithm, and the entire group gradually changes from disorder to order in the problem-solving space by approaching the food; then the optimal solution is obtained. Every bat has to constantly adjust its own frequency, loudness, and pulse.

The firing rate [6] is to follow the bat with the highest fitness value to search in the solution space. In BA, bats fly to a new position by adjusting their speed, and the change of speed is obtained by obtaining the global optimal information. The updated formula of the speed V_t^b and position of bat t at time X_t^b is

$$f_b = f_{\min} + (f_{\max} - f_{\min})\beta, \tag{1}$$

$$v_t^{b+1} = v_t^b + \left(x_t^b - x_*\right) f_b, \tag{2}$$

$$x_t^{b+1} = x_t^b + v_t^{b+1}. \tag{3}$$

Through the above introduction to the bat algorithm, we can see the algorithm flow chart 2 as follows:

The gray wolf algorithm simulates the strict hierarchy of the gray wolf leadership, shaping four different roles, from low to high, namely α, β, δ, and ω. At the same time, α, β, and δ will also change each other's levels due to age and other issues. ω is the follower at the bottom, and the task is to balance the internal relations of the population. These four roles follow the strict social ruling class of gray wolves. In addition, group hunting is a very important group activity among gray wolves, including encircling prey, hunting, attacking, and searching. These activities are all considered in the GWO algorithm. Due to the mandatory and strict social ruling class [7], most members act as followers (ω) of the ruling class (α, β, and δ). The ruling class occupies the top three positions based on their performance. In GWO, the characters α, β, and δ will automatically change based on their current positions in each iteration. Social learning is adopted in GWO, and the position X_n^y of gray wolf t in the i-th iteration is updated to

$$x_b^{t+1} = \sum_1 \in (\alpha \times \beta \times \delta) xn/3, \tag{4}$$

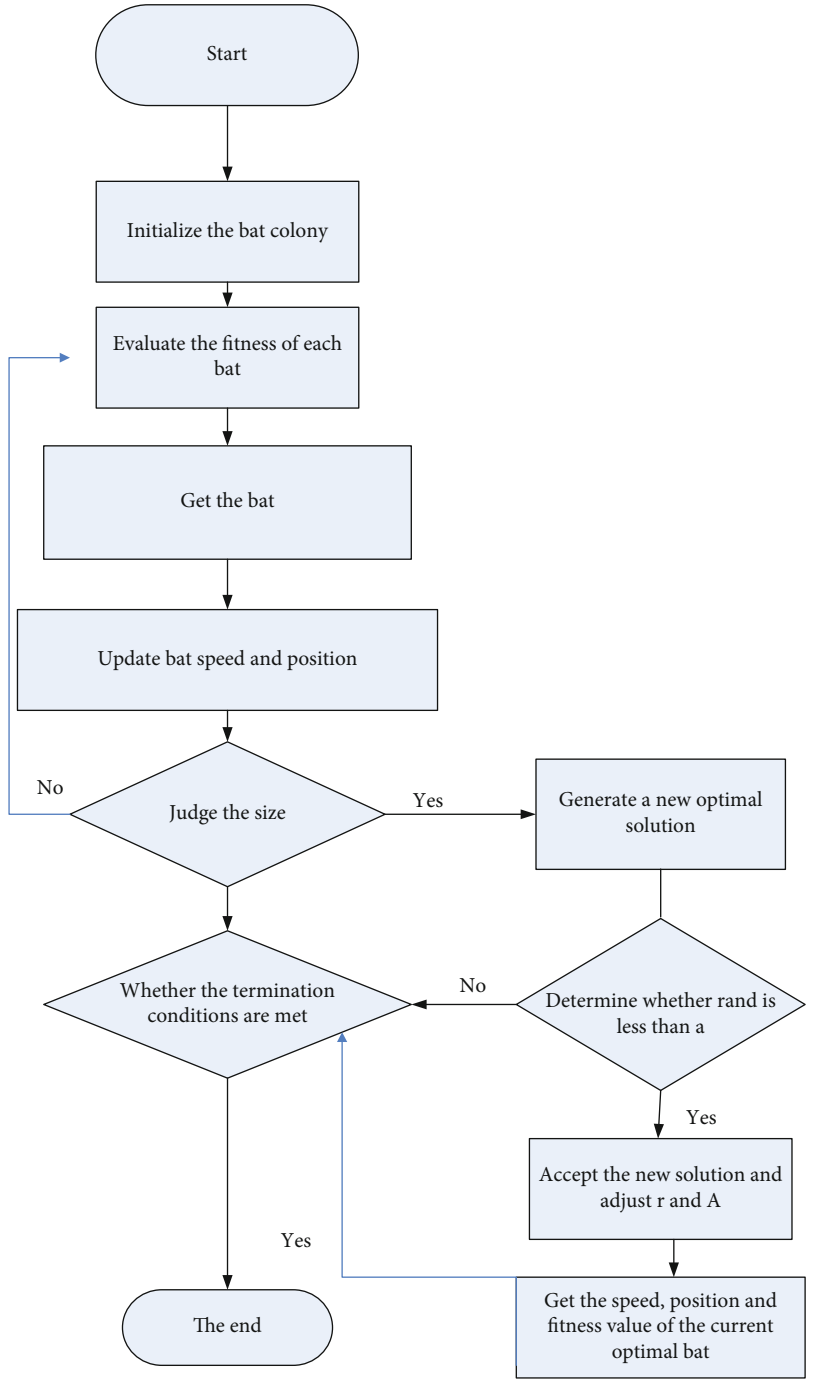

Figure 1: Flow chart of the BA algorithm.

$$x_u^{b+1} = x_u^b - (2 \times \alpha \times r_2 - \alpha) \times \left| 2 \times r_4 \times x_t^b - x_t^b \right|, u \in \{\alpha, \beta, \delta, \eta\}. \tag{5}$$

2.2.2. K-Means Clustering Algorithm. The clustering algorithm belongs to unsupervised learning [8], which mainly uses the learning of unlabeled samples to expose the inherent properties and laws of the data and provide a basis for further data analysis.

For sample set $C = (x_1, x_2, \cdots, x_m)$ and the cluster center set $D = (D_1, D_2, \cdots, D_m)$, obtained by the K-means algorithm after clustering, the minimized square error function can be expressed as follows:

$$E = \sum_{r=1}^{D} 7 \sum_{x \in C_i} \|x - u^q\|_3^3. \tag{6}$$

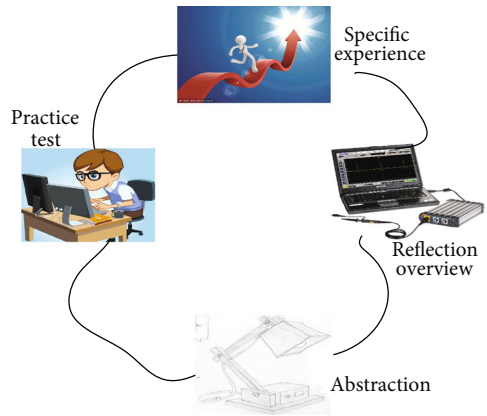

Figure 2: Cooper's ELM experience learning model cycle diagram.

2.2.3. Vector Machine Algorithm. For the training set $G = \{(x_1y_1), (x_2y_2), \cdots, (x_ky_k)\}, y_k = \{-1,+1\}$, the division result obtained in this way is the most robust and the best generalization performance. The above divided hyperplane can be expressed by the following linear equation:

$$j^A x + h = 0. \tag{7}$$

The basic formula of a support vector machine is

$$\min_{sd} \frac{1}{2}\|A\|^2. \tag{8}$$

When $D = (D_1, D_2, \cdots, D_m)$ is linear and inseparable for a given training sample set, there may not be a partitioning hyperplane that meets the requirements in the feature space of the sample. Let $\phi(x)$ denote the feature vector after mapping x, so

$$\text{s.t.} y_u\left(W^R X_Q + B\right) \geq 1, i = 1, 2, \cdots, m. \tag{9}$$

Given the training sample set $D = (D_1, D_2, \cdots, D_m)$, the loss function is as follows:

$$F(D, c\,; g, h) = \frac{1}{2}\|h_e(e) - i\|^2. \tag{10}$$

For data containing m samples, the overall cost function is

$$D(Q, c) = \left[\frac{1}{f}\sum_{i=1}^{p} W(E, b\,; x, y)\right] + \frac{\lambda}{4}\sum_{i=1}^{n_q-1}\sum_{i=1}^{g}\sum_{i=1}^{h_m+2}\left(D_{ji}^s\right)^2. \tag{11}$$

2.3. Countermeasures to Strengthen the Cultivation of the Subject Consciousness of Foreign Students in Colleges and Universities

2.3.1. Shaping the Independent Personality of International Students. Subjective consciousness requires people to have an independent personality and independent spirit. Independent personality manifests itself as not being dependent on others, not deliberately catering to others, not being able to obey others blindly, neglecting oneself, and losing dignity.

2.3.2. Cultivate the Innovative Consciousness of International Students. As the youngest and most energetic group of intellectuals, international students are more confident, are more self-reliant, are more enthusiastic about transforming the world, and have a stronger knowledge structure [9], have rational concepts, and have judgment and decision-making capabilities, whether they are both in life and in learning have demonstrated the innovative talents of female college students.

2.3.3. Reshape the Social Characteristics of International Students. The school is a student, a member of the society, and the initiative of the society in the society. It exerts its subjective initiative and assumes the responsibility to itself and the mission to the society. Instead of asking for it blindly from the society, you have to become the master of the society, and you have to pay and contribute to the society, so that you can truly find the value of life.

3. Comparative Research on Swarm Intelligence Algorithms

3.1. Experimental Data Based on the Improved CMAC Learning Algorithm. In order to verify the effectiveness of this learning algorithm and compare it with the conventional CMAC learning algorithm, we set up a comparison experiment here. One is the robot learning system based on the artificial emotion-based CMAC network learning algorithm, and the other is based on the conventional CMAC network algorithm. In the robot learning system [10], both algorithms have carried out 10 simulation experiments, and each test runs up to 100 times. This is done to ensure the generality and reliability of the resulting data. The learning speed of the robot is an important indicator of the learning algorithm. The faster the learning speed, the better it can adapt to changes in the environment and have better adaptability. Figure 3 shows the robot learning curve for the final comparison experiment.

It can be seen from Figure 3 that in this experiment with the drug, the changes in the number of runs and the number of survivals fluctuated greatly, and the changes between the two were basically consistent. The improved genetic algorithm [11] is applied to the simulation experiment, and for comparison, the traditional genetic algorithm is also applied to the experiment, a set of comparison experiments are performed, and the other basic parameters are the same. Finally, the corresponding simulation results are shown in Figures 4 and 5.

It can be seen from Figure 4 that the improved genetic algorithm has a strong learning performance. It can reach the goal of 5,000 survival times after it has evolved to about 23 generations, indicating that this improvement based on artificial emotion [12] is very effective. In addition, Figure 5 shows that the improved genetic algorithm has a higher optimal fitness value than the traditional genetic algorithm, and the speed of reaching the optimal fitness value is also faster. In other words, the learning speed is faster, the final learning effect is better, and the ability to adapt to the environment is stronger.

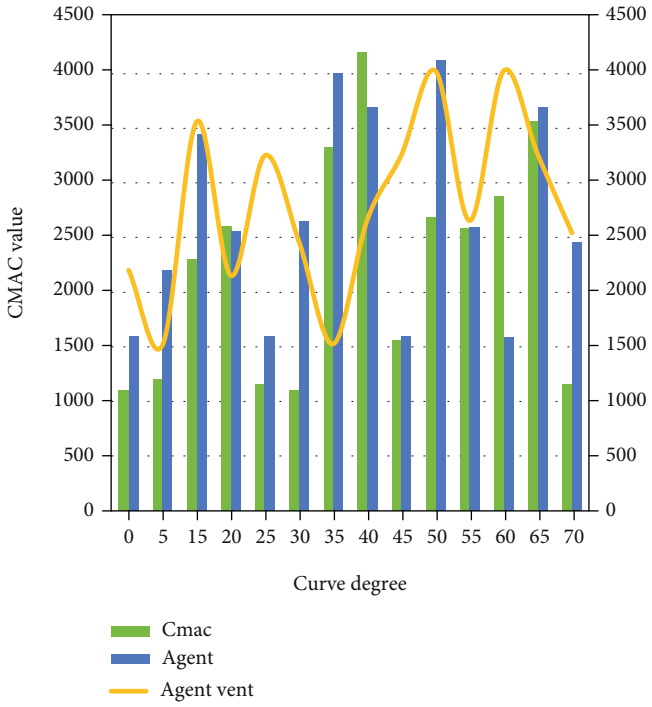

Figure 3: The number of trial runs of the agent—the number of survival curves.

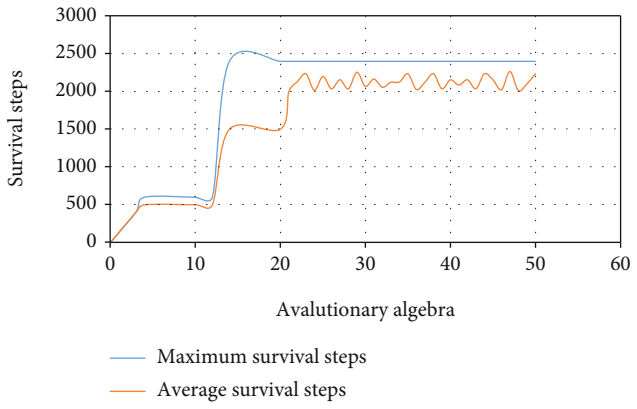

Figure 4: The number of survival steps of the improved genetic algorithm.

3.2. Construction of the Experimental Model. Firstly, according to the control principle of the two-wheeled robot, the required electrical system is divided into four parts: detection system [13], control system, power supply system, and execution system. The electrical system structure diagram is shown in Figure 6. Among them, the detection system is composed of the MTI attitude detection module to detect the robot attitude information; the control system receives and processes the signals provided by the detection system, sends instructions in real time, controls the robot to complete the corresponding actions, and finally calculates the output through the control algorithm [14], sent to the execution system; the power system is composed of a lithium battery, a power distribution board, and a switch, powered by

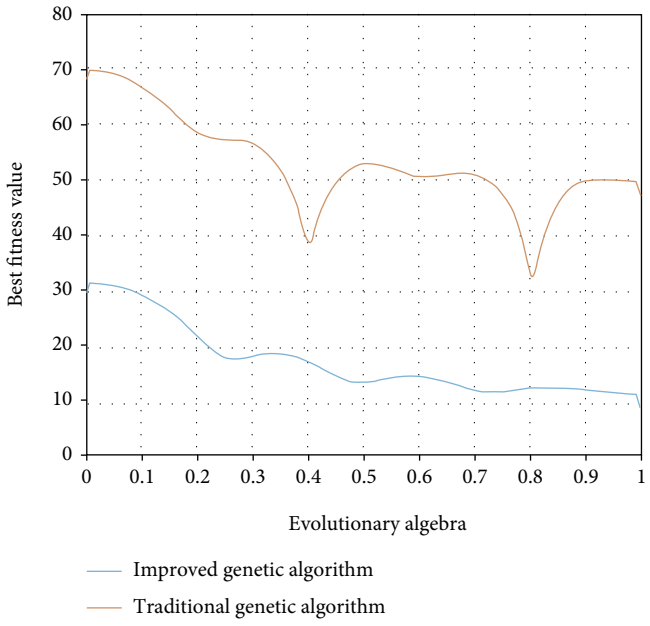

Figure 5: Convergence curves of the best fitness values of the two algorithms.

the lithium battery, the detection system and the control system obtain the required voltage through the power distribution board; the execution system drives the received command signal through the left and right wheel motors. The wheel rotates to realize the movement of the robot, as shown in Figure 6.

Mechanism modeling is to establish a mathematical model of the system according to the physical and chemical laws of the system's internal operation mechanism, material, and energy conservation [15]. The general steps are as follows:

(1) Determine the input and output according to the working principle of the system and its role in the control system

(2) Write down basic equations based on the relationship between the conservation of materials and energy

(3) Eliminate intermediate variables

(4) Obtain system dynamic model

(5) For a weakly nonlinear system, in order to simplify the model, it can be linearized at the operating point to obtain an approximate linearized model of the system

3.3. Simulation Experiment Data. The experiment selects standard test functions BTM1, BMT3, and BTMZ2 to evaluate the performance of the algorithm. They have different characteristics, such as nonconvexity and discontinuity, and can be used to test the optimization capabilities of different aspects of the algorithm [16]. The first two are the two-objective minimum problem, and BTMZ2 is the three-objective minimum problem. The definitions of these test functions are as follows:

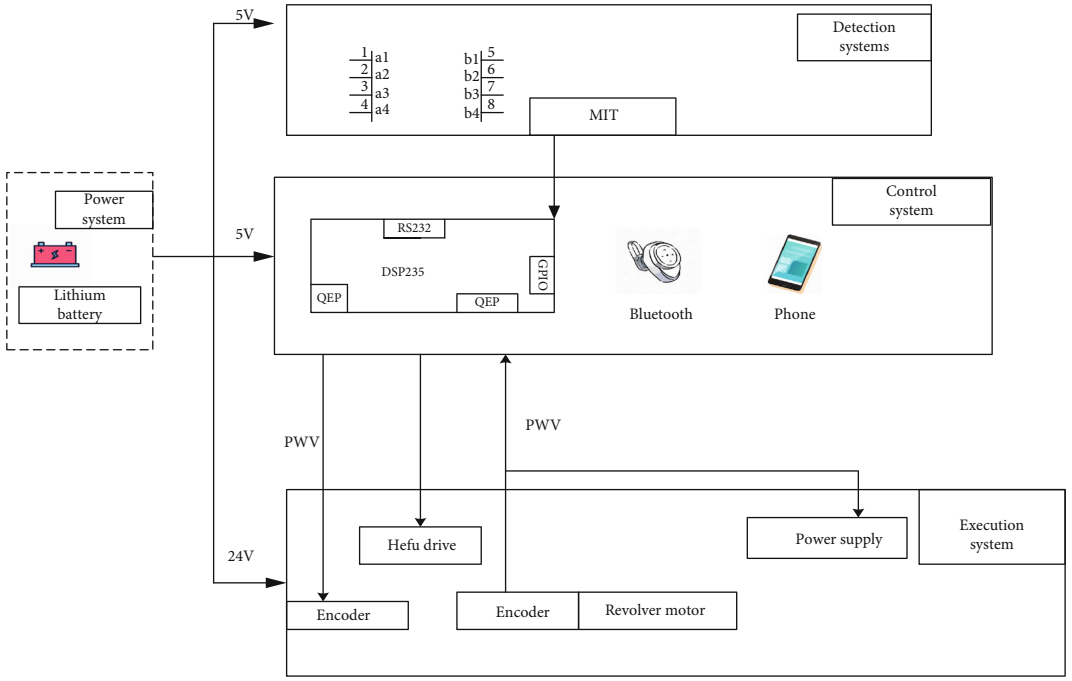

Figure 6: Two-wheeled robot electrical system structure diagram.

$$\begin{cases} \min\{f_2 = x_i\} \\ \min\{f_2 = g \times h\} \end{cases}, g = 2 + 9 \times \sum_{i=3}^{f} \frac{x_q}{j-1}, h = 1 - \sqrt{\frac{f_2}{g}}, \tag{12}$$

$$\begin{cases} \min\{f_2 = x_i\} \\ \min\{f_2 = g \times h\} \end{cases}, g = 2 + 9 \times \sum_{i=3}^{f} \frac{x_q}{j-1}, h = 1 - \sqrt{\frac{f_2}{g}} - \sqrt{\frac{f_2}{g}} - \left(\frac{f_1}{g}\right) \sin(10\pi f_1). \tag{13}$$

When $x_i = 0, i = 2, \cdots, m$, it corresponds to the true Pareto optimal frontier of the above two test functions: the most optimal frontier of ZDT1.

The optimal front is a convex front, and the optimal front that meets the two goals of $f_2 = 1 - \sqrt{f_1}$ ZDT3 is 5 segments of the discontinuous convex front.

$$\begin{aligned} \min f_1 &= \left\{(2+d)\cos\left(\frac{\pi x_2}{2}\right)\cos\frac{\pi x_2}{2}\right\} \\ \min f_2 &= \left\{(2+d)\cos\left(\frac{\pi x_2}{2}\right)\sin\frac{\pi x_2}{2}\right\} \\ \min f_3 &= \left\{(2+d)\sin\frac{\pi x_1}{2}\right\}. \end{aligned} \tag{14}$$

4. Results and Analysis

4.1. The Overall Analysis of the Distribution of Intelligence Characteristics of Foreign Students in Colleges and Universities. The student's "multiple intelligence questionnaire" is designed based on the questionnaire intelligence checklist compiled by Gardner [17] and the multiple intelligence questionnaire compiled by the United States Department of Education in Kentucky, combined with the cognitive level of the students. This intelligence questionnaire is designed. It focuses on the description and supplementary explanation of the seven intelligences with high learning relevance. The four descriptions in each part correspond to a kind of intelligence, namely verbal intelligence, spatial intelligence, body-motor intelligence, natural observation intelligence, interpersonal intelligence, introspective intelligence, and logical-mathematical intelligence; the data obtained from the survey is used to roughly analyze the distribution of individual students and the overall intelligence of the class and the intelligence development status, as a basis for determining the superior intelligence and intelligence differences of the class students, and at the same time for personalized teaching activities that provide guidance to a certain extent to help teachers develop reasonable strategies for teaching students in accordance with their aptitude [18]. According to the statistical data of the student's multiple intelligence survey summary table, the intelligence distribution statistics chart is drawn to visually display the intelligence distribution status of the students in the experimental class. The construction of geographic mental maps is related to multiple intelligences, and the development of geographic capabilities is mostly manifested as an extension of spatial intelligence. First, determine the distribution of intelligence for a specific student. Taking four students as an example, the students have outstanding performance in natural observation intelligence, spatial intelligence, and self-observation intelligence, as shown in Figure 7.

The students' self-cognitive intelligence, natural observation intelligence, and spatial intelligence development levels are higher, and the development level of sports intelligence is the lowest, followed by language intelligence and interpersonal intelligence, as shown in Figure 8.

Comprehensive analysis shows that the students in the experimental class are in the transitional stage from specific calculations to formal calculations [19], as Piaget said. Thinking mainly in images, logical thinking skills have

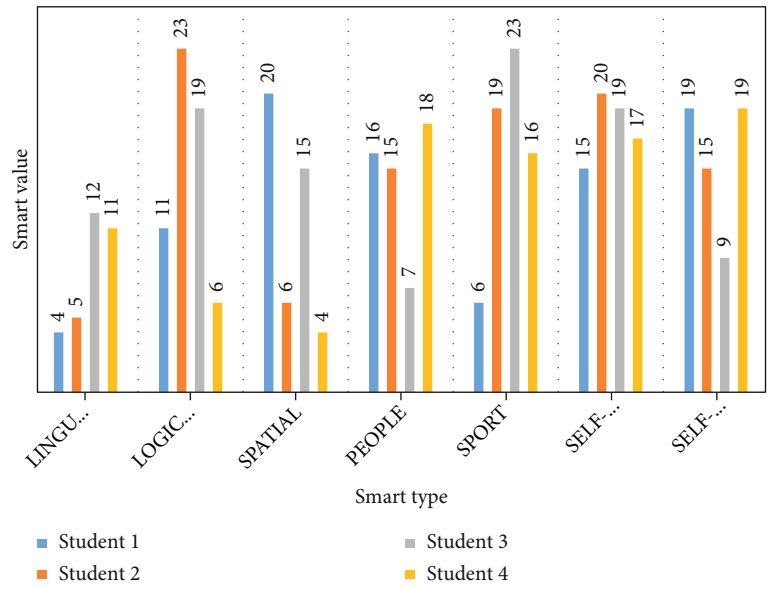

Figure 7: Intelligent distribution performance of the first four students in the experiment.

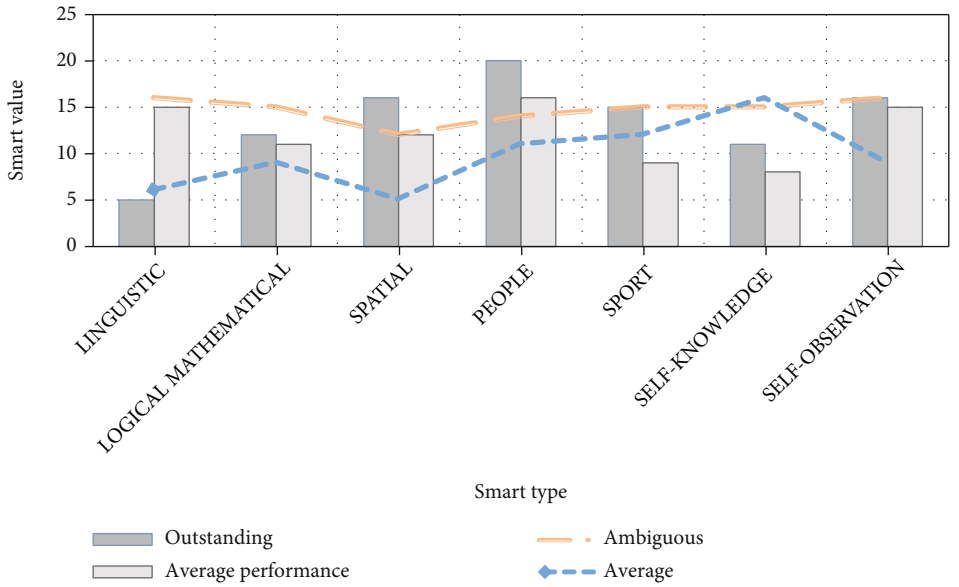

Figure 8: Overall intelligence distribution performance before the experiment.

developed to a certain extent, and they begin to have relatively strong self-introspection. And self-development awareness is generally concerned about the interaction with classmates and partners, but the perception of space is low. I have had a preliminary understanding of physical geographic phenomena, but there are relatively few direct or indirect perceptual understandings and a lack of active observation and thinking of various physical geographic phenomena in daily life, and students have great differences in the extension of knowledge. After the experiment, the number of students with outstanding overall spatial intelligence in the class rose from 13 to 21, while the average grade for these students dropped from 15 to 9. The number of fuzzy performance was significantly reduced, and the overall average level of spatial intelligence in the class improved, as shown in Table 2.

It can be seen from the above statistical chart that the total number of students in the experimental class who performed outstandingly in spatial intelligence after the experiment has increased by 7 people. The spatial intelligence of 14 people has improved significantly. The spatial intelligence of the students in the control class basically did not change after a semester of study. The experiment shows that the geography teaching strategy adopted from [20] obviously promotes the development of the overall spatial intelligence of the students in the experimental class. After the experiment, Wang's overall intelligence related to geography was measured, and it was

Table 2: Spatial intelligence performance before and after the experimental class and the control class.

Class	Spatial intelligence	Outstanding	Average performance	Ambiguous
Experimental class	Front side	13	14	6
	Back side	19	12	3
Control class	Front side	13	19	3
	Back side	14	19	2

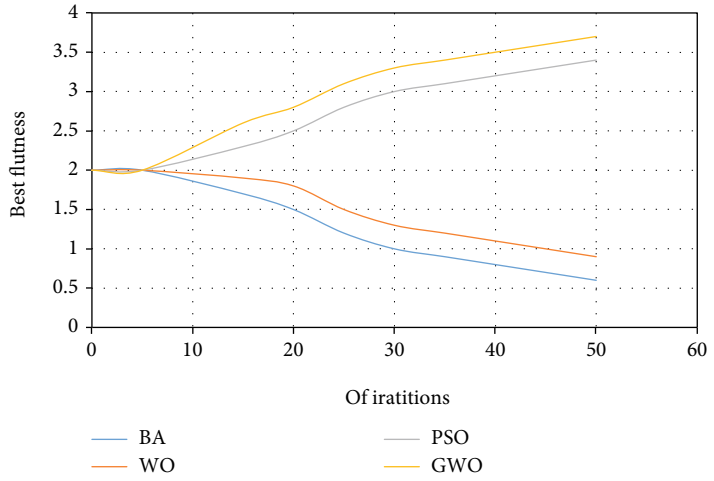

Figure 9: Convergence curves of BA, WO, PSO, and GWO.

found that in addition to the obvious improvement in spatial intelligence, his natural observation intelligence, language intelligence, logical-mathematical intelligence, interpersonal intelligence, self-cognition intelligence, and sports intelligence all correspond. The natural observational intelligence, in which Wang showed the most outstanding performance, has been maintained at a higher scoring position.

4.2. Experimental Results. Since the data obtained from the experiment in this paper is relatively large, it is necessary to review the purpose of the experiment and establish a learning community in order to extract the most useful data from the experimental results for analysis. The analysis of this experiment is divided into two parts:

(1) Adaptability analysis of swarm intelligence algorithm [21]. That is, the overall analysis of the results of the three swarm intelligence algorithms is carried out, and from a macro perspective, which algorithm has a better performance as a whole is compared. Including the general stable settings in the first subsection, by comparing the optimization results of the three algorithms and the optimization process as a whole to grasp the pros and cons of the three swarm intelligence algorithms. And in the second subsection, under different CR and NR combinations, a more detailed comparison of the different pros and cons shown by the three swarm intelligence algorithms

(2) Comparative analysis of swarm intelligence algorithms. That is to say, for each algorithm, we compare the learning performance of the algorithm in robot group obstacle avoidance under different parameter settings. Including the analysis of the changes in the performance results of each algorithm under different settings of CR in the third subsection. And in the fourth subsection, under different settings of NR, analyze the changes in the performance results of each algorithm. In addition, in order to avoid subjective assumptions and make the data analysis of experimental results more convincing and effective, we not only include box-plot analysis in each part of the detailed comparative analysis but also add t-test. The t-test is to infer the probability of the difference based on the t-distribution theory and then compare the two features that have significant differences [22]. In order to have a better understanding of the t-test results, we explain the test standards and test results of the t-test as follows (where A and B, respectively, represent the two test arrays in the t-test, and the symbols of the test results of A and B). The order of presentation is A first, then B

(1) When the p value in the t-test result is <0.05, we use the ">>" symbol to indicate that A is significantly better than B in this comparison

(2) When the p value in the t-test result is between 0.05 and 0.9, we use the ">" symbol to indicate that A is

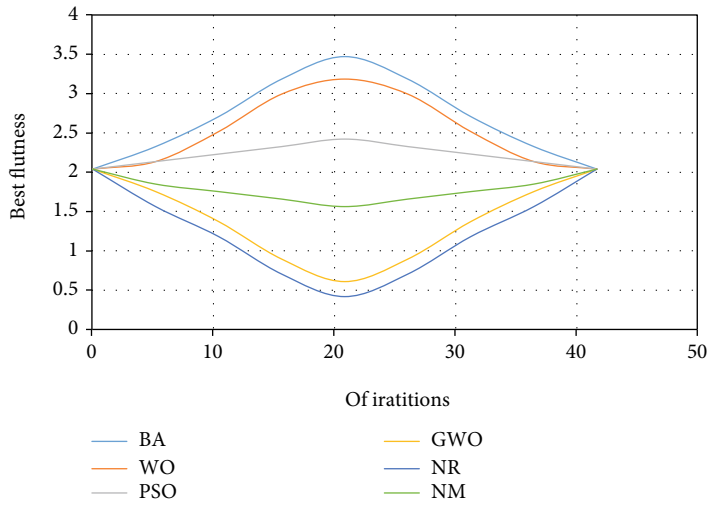

Figure 10: Convergence curves of BA, WO, PSO, GWO, NR, and NM.

Table 3: t-test results of each algorithm under varying CR.

Algorithm	NR	#1	#2	#3
BA	4	1.5 (>, >)	1.6 (>, >)	0.9
BA	15	0.3 (=, >)	0.4 (=, >)	0.9
WO	16	1.5 (>>, >>)	1.7 (>>, >>)	0.38
WO	12	1.5 (>, >>)	1.8 (>, >>)	0.2
PSO	5	1.5 (>, >>)	1.9 (>, >>)	0.3
PSO	12	0.3 (>, >)	0.2(>, >)	0.5
GWO	16	0.3 (>, >)	0.9 (>, >)	0.5
GWO	12	1.5 (>, >)	1.3 (>, >)	0.65

only better than B in this experiment, but it is not prominent

(3) When the p value > 0.90 in the t-test result, we use the "=" symbol to indicate that the performance between A and B is similar, and there is no difference

(4) In the t-test list, the two symbols in the "#1" column represent the comparison results of the t-test between A and B, and the symbols in the "#2" column represent the comparison results of the t-test between B and C.. (We assume that A, B, and C represent the experimental results of the three experimental groups, respectively, and the t-test is performed in two groups)

Next, we analyze and compare the optimization process. In order to avoid the influence of contingency on the analysis of the results, we arrange the optimal solutions of 30 experiments of each algorithm [23] in order from largest to smallest, select the 15th experiment, and compare the experimental process. That is, the 50 iterations of the optimization process of each population intelligence algorithm are compared, and the results are shown in the curves in Figures 9 and 10.

Similarly, in order to avoid the impact of subjective assumptions on the reliability of experimental data, we perform t-test on the experimental data of each algorithm under three different robot communication ranges. The t -test statistical analysis results are shown in Table 3.

Through the above analysis and comparison of the experimental data, we can make a summary of the analysis of the experimental results:

(1) For the GWO algorithm, the larger the NR, the better the performance of GWO

(2) When the communication range becomes larger, the performance of GWO is significantly improved. This is also because the iterative optimization of the GWO algorithm only relies on social learning capabilities. A larger communication range [24] can enable more robots to communicate to improve individual social learning opportunities, thereby enhancing individual learning capabilities to improve learning behavioral performance. It can be seen that the differences between the different algorithms are still quite obvious

5. Conclusions

This paper combines artificial intelligence and machine learning algorithms to conduct research on basic theoretical and practical teaching methods. After the study, we can clarify that the teaching of computers and artificial intelligence and the study of foreign students in colleges and universities have become an inevitable trend. In addition, the pressure of future employment competition will make the practice link more and more important in the whole teaching activities. How to set the content of practice teaching reasonably and effectively improve the students' comprehensive application ability of the knowledge is a problem that we must face and solve. The artificial intelligence teaching proposed in this article has been tried out for one year in the practical teaching process. The reliability of the key fusion differential evolution algorithm has also been studied, and the basic theory and practical teaching methods after the algorithm have also been improved to varying degrees. Although the workload of teachers has increased to a certain extent, the

feedback from students is very good. Therefore, we will share our experience with everyone and look forward to making progress together. However, the research in this paper also has some deficiencies, for example, the research method is still not innovative enough. We hope to get more suggestions and suggestions for improvement.

Data Availability

No data were used to support this study.

Conflicts of Interest

There is no potential conflict of interest in this study.

Acknowledgments

This work was supported by the Special Fund of Fundamental Scientific Research Business Expense for Higher School of Central Government (No. ZY20180124).

References

[1] S. Jia and X. Zhang, "Teaching mode of psychology and pedagogy in colleges and universities based on artificial intelligence technology," *Journal of Physics: Conference Series*, vol. 1852, no. 3, article 032033, 2021.

[2] M. Ramezani Mayiami, M. Hajimirsadeghi, K. Skretting, X. Dong, R. S. Blum, and H. V. Poor, "Bayesian topology learning and noise removal from network data," *Discover Internet of Things*, vol. 1, no. 1, p. 11, 2021.

[3] J. Guo and C. Sun, "Real-time monitoring of physical education classroom in colleges and universities based on open IoT and cloud computing," *Journal of Intelligent Fuzzy Systems*, vol. 40, no. 4, pp. 7397–7409, 2021.

[4] L. Li, "Application of BIM technology in practical teaching of engineering management specialty," *E3S Web of Conferences*, vol. 253, article 01031, 2021.

[5] G. Zhu, G. Zhu, and J. Zhang, "Computer simulation of ideological and political teaching under big data of complexity," *Complexity*, vol. 2021, Article ID 9941592, 13 pages, 2021.

[6] C. Zeng, "Application of large-scale cognitive social networks based on cooperative transmission mechanisms in exploration of flipped classroom teaching strategy," *Complexity*, vol. 2021, no. 11, Article ID 8988165, 11 pages, 2021.

[7] W. Li, "Multimedia teaching of college musical education based on deep learning," *Mobile Information Systems*, vol. 2021, no. 2, Article ID 5545470, 10 pages, 2021.

[8] G. Li, "Optimization and simulation of virtual experiment system of human sports science based on VR," *Complexity*, vol. 2021, Article ID 3872881, 10 pages, 2021.

[9] V. Sadkovyi, O. Mietielov, O. Tarasenko, and M. Goroneskul, "Features of teaching technical, physical and mathematical disciplines by means of distance learning in guarantine conditions," *New Collegium*, vol. 3, no. 101, pp. 46–53, 2020.

[10] E. J. Cook, L. Crane, S. Kinash et al., "Australian postgraduate student experiences and anticipated employability: a national study from the students' perspective," *Journal of Teaching and Learning for Graduate Employability*, vol. 12, no. 2, pp. 148–168, 2021.

[11] D. Babik, R. Singh, X. Zhao, and E. W. Ford, "What you think and what I think: studying intersubjectivity in knowledge artifacts evaluation," *Information Systems Frontiers*, vol. 19, no. 1, pp. 31–56, 2017.

[12] Z. Zhen, "Investigation and analysis of the status quo of the practical teaching ability of English normal students in the Higher Vocational College in China [J]," *English Language Teaching*, vol. 10, no. 11, p. 15, 2017.

[13] J. Lemley, S. Bazrafkan, and P. Corcoran, "Deep learning for consumer devices and services: pushing the limits for machine learning, artificial intelligence, and computer vision," *IEEE Consumer Electronics Magazine*, vol. 6, no. 2, pp. 48–56, 2017.

[14] S. Michie, J. Thomas, M. Johnston et al., "The human behaviour-change project: harnessing the power of artificial intelligence and machine learning for evidence synthesis and interpretation," *Implementation Science*, vol. 12, no. 1, p. 121, 2017.

[15] R. Allen and D. Masters, "Artificial intelligence: the right to protection from discrimination caused by algorithms, machine learning and automated decision-making," *ERA-Forum*, vol. 20, no. 4, pp. 585–598, 2020.

[16] F. Ng, R. Jiang, and J. Chow, "Predicting radiation treatment planning evaluation parameter using artificial intelligence and machine learning," *IOP Sci Notes*, vol. 1, no. 1, article 014003, 2020.

[17] U. Ferizi, H. Besser, P. Hysi et al., "Artificial intelligence applied to osteoporosis: a performance comparison of machine learning algorithms in predicting fragility fractures from MRI data," *Journal of Magnetic Resonance Imaging*, vol. 49, no. 4, pp. 1029–1038, 2019.

[18] A. Hassanat, "Greedy algorithms for approximating the diameter of machine learning datasets in multidimensional Euclidean space: experimental results," *ADCAIJ: Advances in Distributed Computing and Artificial Intelligence Journal*, vol. 7, no. 3, pp. 15–30, 2018.

[19] N. Jia and Z. Madina, "An association rule-based multiresource mining method for MOOC teaching," *Computational and Mathematical Methods in Medicine*, vol. 2022, Article ID 6503402, 7 pages, 2022.

[20] X. Zheng, "Reform of university english teaching and examination based on stratified teaching method and mobile computing," *Wireless Communications and Mobile Computing*, vol. 2022, Article ID 1518799, 13 pages, 2022.

[21] Y. Kumar, "Artificial intelligence-based learning techniques for diabetes prediction: challenges and systematic review," *SN Computer Science*, vol. 1, no. 6, 2020.

[22] P. Radanliev, D. De Roure, K. Page et al., "Design of a dynamic and self-adapting system, supported with artificial intelligence, machine learning and real-time intelligence for predictive cyber risk analytics in extreme environments–cyber risk in the colonisation of Mars," *Safety in Extreme Environments*, vol. 2, no. 3, pp. 219–230, 2020.

[23] L. Xia, "Learning and decision-making from rank data," *Synthesis Lectures on Artificial Intelligence and Machine Learning*, vol. 13, no. 1, pp. 1–159, 2019.

[24] S. L. Goldenberg, G. Nir, and S. E. Salcudean, "A new era: artificial intelligence and machine learning in prostate cancer," *Nature Reviews Urology*, vol. 16, no. 7, pp. 391–403, 2019.

Hindawi
Wireless Communications and Mobile Computing
Volume 2022, Article ID 1013714, 7 pages
https://doi.org/10.1155/2022/1013714

Research Article

RBF-Based 3D Visual Detection Method for Chinese Martial Art Wrong Movements

Xi Wang,[1] Yi-Hsiang Pan,[1] Zongbai Li,[2] and Bing Li[3]

[1]*Graduate Institute of Physical Education, National Taiwan Sport University, Tao Yuan, 333325 Taipei, China*
[2]*College of History and Culture, Hunan Normal University, Changsha, 410081 Hunan, China*
[3]*College of art, Design, & Physical Education, Chosun University, Gwangju 61452, Republic of Korea*

Correspondence should be addressed to Bing Li; libingwushu@poers.edu.pl

Received 6 March 2022; Revised 6 April 2022; Accepted 15 April 2022; Published 30 April 2022

Academic Editor: Jun Ye

The accuracy of action detection is limited by the extracted action, and there are problems of high processing complexity and low efficiency. Therefore, a three-dimensional visual detection method of martial art wrong action based on RBF is proposed. After noise reduction and weighting processing of martial art action video images, a martial art action 3D visual transformation model is established. According to the 3D visual model, C3D features are used to represent martial art actions. The video is segmented using sparse coding to determine the detection range. RBF neural network model is established, and the combination of the above 3D visual model and network parameters is obtained by sample training to detect martial art wrong actions. The test method of the experimental results shows the detection of the research under the condition of different degrees of precision, an average of at least 5%, and the method of detection of high efficiency and stability.

1. Introduction

Martial art is an ancient science in China's traditional sports, with attack action as the main content, routines, and combat as the main movement form, paying attention to the internal and external repairing of traditional ethnic sports [1]. As an excellent national traditional culture in China, Chinese martial art has formed its own unique expression and development means in the process of development and derivation for thousands of years. At present, the teaching of Chinese martial art at home and abroad mostly stays in the traditional way of face-to-face teaching or practitioners only follow video learning [2]. On the one hand, the inheritors of Chinese martial art are scarce, and it is difficult for people to get access to authentic face-to-face teaching; on the other hand, there are problems such as poor intuition and low efficiency in learning skillful movements only by following videos, and practitioners are very likely to do wrong movements and cause muscle damage. Therefore, an effective human movement posture detection method can play a role in correcting wrong movements for athletes' regular training. Action detection is widely used in industrial production, daily safety behavior monitoring, social operation management, and other work areas, and scholars at home and abroad have made some research results. Ohl and Rolfs use causality in the human visual system to adapt to show the causal relationship linked between action directions. It is used as a key low-level feature of visual events to detect motion direction [3]. Reference [4] combines perceptual learning and statistical learning to improve information acquired through experience and achieve action detection by statistical cooccurrence between environmental features. Reference [5] uses the frame difference method to subtract the background to achieve effective detection of the slightest motion. Reference [6] uses the YOLOv4 deep-learning motion target detection algorithm to achieve localization and recognition of motion targets. Real-time image detection of pictures, videos, and cameras is achieved by identifying and tagging the location and type of objects contained in the image, which improves the accuracy and speed of detection. NagiReddy et al. proposed a novel background

modeling mechanism using a bias illumination field fuzzy C-means algorithm to separate nonstationary pixels from stationary ones by background subtraction. Feature extraction under the condition of noise and illumination changes is completed by using the fuzzy C-means method of biased lighting field, and the detection accuracy is improved through clustering [7]. The above methods can achieve high-quality motion detection in different environments, but the overall detection performance of the method is degraded due to the strong coherence of martial art actions and the influence of the accuracy of extracting wrong action features when wrong actions occur.

The neural network can simulate some systems that cannot be described by mathematical models, and it has strong learning and adaptability, but it also has obvious nonlinear characteristics. The radial basis function (RBF) neural network belongs to the forward neural network; this kind of network to the structure of the multilayer forward network control is similar, and it is a kind of forward neural network with three layers structure [8]. The transformation function of neurons in the hidden layer refers to the radial basis function and is aimed at the center of radial symmetry and nonlinear function with an attenuation trend [9]. In order to better detect the wrong movements of Wushu, in future research, we should conduct in-depth research on the martial art movements with rapid changes in the movement connection, so as to improve the detection accuracy of the detection method. On the basis of the above analysis, this paper will study the three-dimensional visual detection method of martial art wrong action based on RBF, combined with the advantages of the RBF neural network, combined with the three-dimensional visual model to realize martial art wrong action detection and test the comprehensive performance of this method.

2. Research on RBF-Based 3D Visual Detection Method for Martial Art Error Movements

2.1. Martial Art Action Video Image Processing

2.1.1. Video Image Preprocessing. The video image collection of Chinese martial art action is mainly completed by a high-resolution color camera. The image with a continuous signal taken in photogrammetry is the analog image, and its two-dimensional function is represented by $p(x, y)$. Any (x, y) in the image can be used as the two-dimensional coordinate point here. In the intake of the original image, there will be noise interference before certain processing, in the filtering process, and will lose part of the details of the picture, so in the process of noise; at the same time, we need to do our best to ensure the quality of the original picture. In this study, the commonly used mean filter and median filter are used to process Chinese martial art action video images to make the images smooth [10].

In the actual mean filtering, a filtering template is also set based on a point pixel (x, y), which is composed of the remaining surrounding pixels except for this pixel. The average value can be calculated by using the pixels in this template to replace the value of this point pixel (x_i, y_i). The gray value $h(x, y)$ corresponding to this point in the digital image can be obtained. In this way, the pixel value of each position in the original image can be replaced by the mean value solved by the filter template, which is the basic principle in the application of mean filtering. The formula is as follows [11]:

$$h(x, y) = \frac{1}{n}\sum_{i=1}^{n} p_i(x_i, y_i). \tag{1}$$

In the above formula, n is the total number of pixels in the filtering template after the target pixels.

Median filtering was adopted while on noise suppression to eliminate the nonlinear smoothing technique, which uses the principle of order statistics, based on the different pixels to build a template. The selected pixel values in the template, sorted somewhere in the middle of pixel values to replace the target pixel gray value, thus reduce the image noise pixel gray value. In practical operation, the neighborhood around the target pixel is required to conduct size-sorting statistics of some columns according to gray value, and the median of the two-dimensional sequence is filtered, which is expressed as follows [12]:

$$h'(x, y) = Med\{h(x - q, y - w), (q, w) \in M\}. \tag{2}$$

In the above formula, M is defined as a two-dimensional template. The function Med is used to get the median of the entire two-dimensional sequence; $h'(x, y)$ represents the gray value of the image after processing, and $h(x, y)$ represents the gray value of the image after the previous step of mean filtering.

Using the method of spatial domain and frequency domain method, the two methods are used to describe the image-enhancement processing. In the spatial domain method, the gray value of each image point is directly processed to ensure the enhancement effect of the image. Specifically, taking a target pixel and its adjacent pixels as a whole, the pixels excluding the target pixel can be set as a template, so that the original gray value can be represented by the average value solved by the filtering template. The processing of spatial domain method is as follows [13]:

$$H(x, y) = H_T\left[h'(x, y)\right]. \tag{3}$$

In the above formula, H_T is a spatial operation with respect to h'; $H(x, y)$ is the Chinese martial art action video image after enhanced processing; $h'(x, y)$ is the Chinese martial art action video image after smooth noise reduction.

2.1.2. The 3D Visual Transformation Model of Chinese Martial Art Action Is Established. The difference between Chinese martial art action and the human body's routine action is that Chinese martial art action has certain obvious changes in three-dimensional space, and the detection of Chinese martial art wrong action also needs to be discriminated from the perspective of three-dimensional

space. Therefore, combined with the collection of Chinese martial art movements, this paper will establish a three-dimensional visual transformation model of Chinese martial art movements. The 3D visual data of Chinese martial art movement is accomplished by using the 3D visual collector of line structured light. Based on the principle of optical triangulation, the optical projector projects the structured light onto the surface of the human body, and the camera captures the information of the light strip, so as to obtain the two-dimensional distorted image of the light strip. The degree to which the strip varies depends on the position of the light plane relative to the camera and the surface shape of the object. Since the brightness of the strip is obviously different from that of the unilluminated region, the two-dimensional coordinates of the strip in the camera image can be obtained by using a specific image processing method. The mathematical model of line structured light sensor is used to establish the mapping between the image plane coordinate system and world coordinate system. According to this model, the coordinates of points on the strip can be calculated according to the pixel coordinates of the image. The camera model, the basic imaging model, often referred to as the basic pinhole model, is given by a central projection transformation from three-dimensional space to plane. The relation diagram of the Chinese martial art action acquisition object in the coordinate system of the online structured light image collector is shown in Figure 1 [14, 15].

If the coordinate of the Chinese martial art movement acquisition object is $R = (x_s, y_s, z_s)$ in the spatial coordinate system, and the equation $\alpha x_s + \beta y_s + \gamma z_s + \theta = 0$ of the spatial plane where the imaging object is located in the collector coordinate system is known, then the spatial linear equation between the collector imaging spot center and the measured object is as follows:

$$\frac{x_s}{x_s - X_s} = \frac{y_s}{y_s - Y_s} = \frac{z_s}{z_s - Z_s}. \tag{4}$$

In the above formula, (X_s, Y_s, Z_s) is the coordinate position of the measured object on the collector imaging plane. By putting the equation of the space plane of the imaging object in the collector coordinate system into formula (3), the three-dimensional space coordinates of any point on the light plane in the camera coordinate system can be worked out, and the three-dimensional visual transformation model $H'(x, y, z) = \text{new}(X_s, Y_s, Z_s)$ of martial art action can be established.

2.2. Generate Chinese Martial Art Error Action Fragments to Be Detected. In this paper, C3D features are used for video motion representation, and C3D features show excellent performance in motion recognition tasks. C3D features are generated by a 3D-CNN deep network. Compared with traditional features, C3D features can better represent the characteristics of action videos in time and space. Compared with 2D-CNN, 3D-CNN can better extract timing features of videos, which is very suitable for motion detection tasks. The C3D network consists of 8 convolution layers, 5 maximum pooling layers, 2 full connection layers, and one softening output layer. All the convolution layers use $3 \times 3 \times 3$ 3D convolution cores, the first pooling layer uses $1 \times 2 \times 2$ pooling cores, and the other pooling layers use $2 \times 2 \times 2$ pooling cores [16, 17].

After feature extraction in the C3D network, the visual dictionary needs to be established when sparse coding is used to generate action fragments to be detected. The establishment of the visual dictionary is based on the sample video set. For each video sample, the run-time space point of the interest detection algorithm is used to extract 3D HOG features at each detected point of interest location to obtain a feature vector. The feature vector cannot be directly used as a visual word due to its high dimension and large variance, so it needs to be quantitatively processed. Moreover, as the feature quantity of the whole sample set is very large, the calculation is usually carried out on its subset [18]. All feature vectors extracted from all video sets are taken as a set, and a subset is obtained by random sampling. The clustering algorithm is performed on the subset to obtain K categories. The center of each category is computed as the visual words of that category, which constitute the dictionary of visual features on this data set.

The traditional sparse coding method of multiple dictionaries is used, and the basic sparse dictionary learning method is used to learn each dictionary. T represents the feature of the action fragment used to train the dictionary, and ZD represents the dictionary to be learned. Dictionary learning for each category uses the following formula [19, 20]:

$$(ZD, B) = \arg\min_{ZD,B} \frac{1}{b} |T - ZDB|^2 + \lambda B_t^2, \tag{5}$$

where B is the sparse representation coefficient and λ is the length of the sparse window. The learning process of a dictionary is the same as that of using a dictionary. In each iteration, the dictionary is updated by the fixed coefficient matrix first, then the coefficient matrix is updated by the fixed dictionary, and the result of minimizing formula (5) is finally obtained. Each dictionary learned was used to encode the candidate fragments. Formula (6) was used to calculate the reconstruction error of each dictionary, and the corresponding fragment score of each dictionary was calculated using the normalized formula. At this point, each candidate fragment has different scores from each category dictionary, and the final score of the candidate fragment can be obtained by calculating these scores [21].

$$B_m = \arg\min_{b_m} \frac{1}{b_m} |U_m - ZDB|^2 + \lambda B_t^2. \tag{6}$$

According to the above-obtained clip scores, the video clips that may contain wrong moves are selected using the correlation coefficient coding between Chinese martial art moves. After selecting the video clips that may contain wrong moves, the Chinese martial art move features in the images are extracted by combining the Chinese martial art

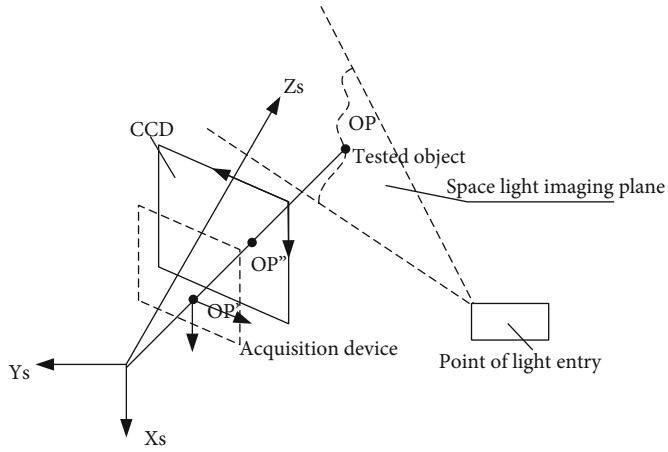

Figure 1: Coordinate diagram of the three-dimensional visual-spatial relationship of the detected object.

move 3D visual transformation model, and the Chinese martial art wrong moves are detected using RBF.

2.3. The RBF Model Is Used to Detect the Wrong Action of Chinese Martial Art. Since there are differences in the initial position relative to the camera and the body orientation when people perform actions, this has a significant impact on the description of human posture and action recognition. Therefore, it is necessary to first regularize the coordinated system so that the initial position and orientation of the human skeleton after coordinated transformation are the same. Since the set of 3D trajectories of all skeletal joint points contains the full information of the complete action, the original action data can be reconstructed from three projections, i.e., by a 2D sequence of motion units. 2D human joint point detection is performed using a cascade pyramid network (CPN) to determine the relative position between the human joint points corresponding to each frame of the Chinese martial art action in the video. Use the k-means clustering algorithm to extract the Chinese martial art movements and the Chinese martial art action characteristics, and use the convolution network fusion [22].

In the feature fusion structure, multiple video segments are fed into the network structure at the same time, but in this paper, only the same network model is used, and these segments fed into the network at the same time will share all the parameters of the convolutional layer and some of the parameters of the fully connected layer in the network. More specifically, for a given video, the video will be segmented for the first time into multiple nonoverlapping video segments of the same duration, and then a sequence of images will be obtained in each video segment using a certain sampling strategy [23]. In the proposed framework, the extracted image sequences will be fed into the 3D convolutional neural network, and each image sequence will be given a corresponding spatiotemporal feature. These features will be merged in the training phase and the resulting features will be considered the spatiotemporal features of the whole video and will be used in the subsequent optimization process. In this way, during the whole learning process, the target of optimization becomes the loss of the whole video, rather than the loss of a video segment or slice [24].

After extracting and fusing the Chinese martial art action features from the video clip, an RBF neural network model is built to detect the wrong Chinese martial art action. The radial basis function often used in RBF neural networks is a Gaussian function, from which the activation function involved in the RBF neural network can be represented by the following equation [25].

$$R_{bf}\left(x_r - c_g\right) = \exp\left(-\frac{1}{2\sigma^2}\left\|x_r - c_g\right\|^2\right), \tag{7}$$

where $\|x_r - c_g\|$ is a Euclidean norm, c_g represents the center of the Gaussian function, and σ is the variance of the Gaussian. Thus, the relationship between processing output O_i and input I_j of the RBF neural network is as follows:

$$O_i = \sum_{i=1}^{n} Q_{ij} R_{bf}\left(x_r - c_g\right)_{I_j}. \tag{8}$$

Based on the above analysis, this paper designs a stereo matching reconstruction model including four input nodes and three output nodes in the constructed RBF network model. The input nodes take the pixel values of the standard martial art action video image and the action video image to be detected in turn, and the output node is the three-dimensional coordinates of the corresponding points. The RBF network is trained with the training sample set, and the network parameters that minimize the output error are selected as the parameters of the final detection model. Input the processed standard Wushu action video image into the RBF network model, and the processed output result vector is the Wushu action detection result. Compare it with the standard Wushu action to find out whether there are wrong Wushu actions. Above, the research of three-dimensional visual detection of Chinese martial art wrong movements is realized by using radial basis function neural network technology.

Table 1: Comparison of average detection accuracy and time consumption between processing algorithm and model.

Data set	YOLOv algorithm		Fuzzy C-means algorithm		RBF neural network	
	Accuracy, %	Time consumed, ms	Accuracy, %	Time consumed, ms	Accuracy, %	Time consumed, ms
KTH	97.6	151.5	97.4	149.8	98.8	102.3
UCF101	96.5	232.6	95.7	241.7	98.0	137.8
HMDB51	96.9	298.1	93.2	301.5	97.6	151.4
Kinetics	95.7	364.3	90.3	344.3	97.1	156.9

3. Experimental Study

In order to verify the feasibility of the above theoretical design and the performance of the proposed detection method, experimental research on the detection method will be conducted in this section. According to the final experimental data analysis, the comprehensive performance and practical application of the proposed motion detection method are evaluated.

3.1. Experiment Content. In this experiment, various experimental standards were calibrated for a single user test environment for subsequent threshold settings. In the experiment, all experimental factors were consistent except for experimental control variables. The motion detection method based on the YOLOv algorithm in reference [6] and the motion detection method based on the fuzzy C-means algorithm in reference [7] are selected as comparison method 1 and comparison method 2, respectively. The two comparison methods were applied to the same experimental background and comprehensively compared with the 3D vision detection method based on RBF proposed in this paper. In order to verify the stability of this method, this experiment simulates the method test in different background environments and selects several subjects to test the method in the simple background and complex background, respectively.

3.2. Experimental Data and Preparation. Considering that martial art actions include kicking, hitting, falling, holding, falling, hitting, splitting, stabbing, and other actions, this paper uses KTH, UCF101, HMDB51, and dynamics data sets as the test data sets of algorithm performance in the experiment. The above four data sets contain different movements similar to Wushu movements. Among them, the contents of the KTH data set are simple six types of actions completed by 25 adults in four different scenes, including walking, jogging, running, boxing, hand waiting, and hand clipping, with a total of 2391 video samples. The fixed camera and single background used for image acquisition in this data set are not close to the objective and real scene performance. Part of the data set UCF101 comes from various sports samples collected by BBC/ESPN radio and television channels, and part comes from video samples downloaded from the Internet. The video website with the most sources is YouTube. UCF101 contains 13320 video samples, which are divided into 101 categories in total. Most of the data samples in the HMDB51 data set are collected from movies, which are more difficult to understand than videos in natural scenes. The data set has 6849 samples and 51 categories, and each category contains at least 101 data samples. The kinetics data set comes from YouTube and contains 400 kinds of actions, with a total of about 300000 videos. Professional practitioners in the martial art industry are invited to make a demonstration video and compare the video data as the detection standard sample of action detection methods. Using the known data set with parameters as above, the YOLOv algorithm, fuzzy C-means algorithm, and RBF neural network used in the three methods are tested.

3.3. Experimental Results. Table 1 shows the processing algorithms and models for the application of the detection method on the selection of test data set processing, and different data sets with corresponding processing compare the average detection accuracy and time.

Analyzing the data in Table 1, when processing the KTH data set, the detection accuracy of the three algorithm models is basically the same. With the increase in the complexity of samples in the data set, the accuracy of the three algorithms decreases, and the processing time increases rapidly. Among them, the processing accuracy of the RBF neural network for the four data sets is higher than 97%, and the processing time is 156.9 ms, which is far less than the other two algorithms, indicating that the performance of this algorithm is relatively better.

In order to further verify the effectiveness of the proposed method, the average accuracy of martial art error action detection under the use of the three methods is compared under the simple background and complex background. The results are shown in Figures 2 and 3. The simple background refers to the background of martial art error action, which is a single background, has low noise, and has stable illumination, and the complex background refers to the background with many interference factors, the background with more noise and unclear light and dark lines.

By comparing and analyzing the figures in Figures 2 and 3, it can be seen that in a simple scene, the detection accuracy of the three detection methods has little difference. The main reason is that the simple background is a single background, has low noise, and has stable illumination, which has little impact on the extraction action of the three methods. In complex scenes, the complexity of the scene gradually increases with the scene number, the interference factors such as background and noise in the scene increase resulting in the gradual decline of the detection accuracy of the three methods, and the decline of the detection accuracy

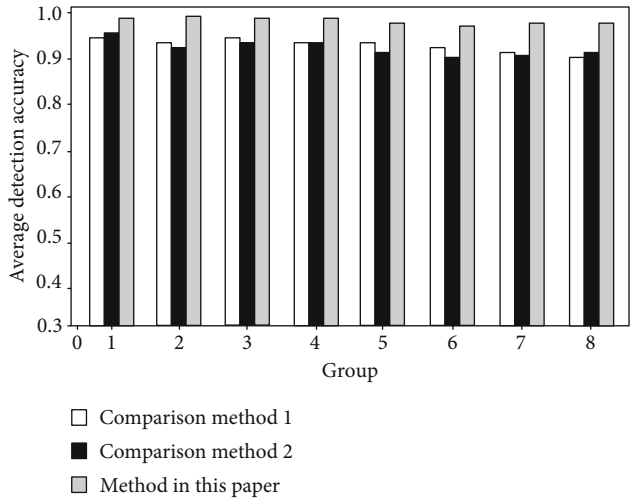

Figure 2: Comparison of detection accuracy in simple scenes.

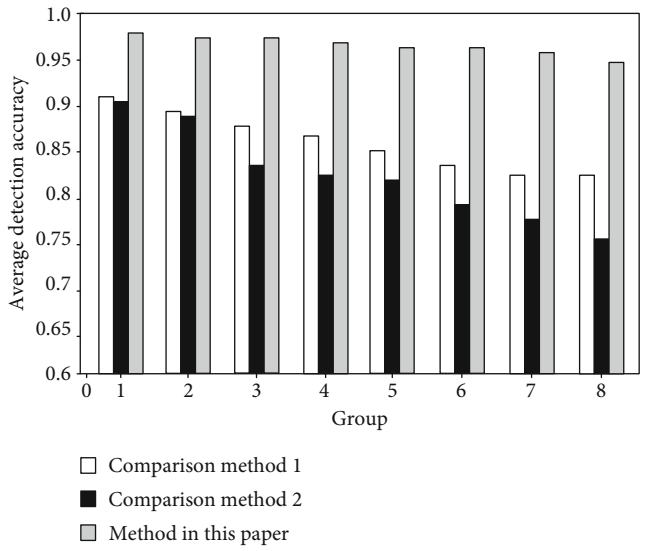

Figure 3: Comparison of detection accuracy in complex scenes.

of the comparison method is the largest. Based on the above analysis, in simple and complex detection scenarios, the detection accuracy of this method is higher than that of the two comparison methods. On average, the detection accuracy of this method is improved by at least 5%. Therefore, the detection efficiency of this method is higher, and the detection is less affected by the background environment. The stability of this detection method is good.

Summarizing the above test data, it can be seen that the three-dimensional visual detection method of martial art wrong action based on RBF proposed in this paper has high detection accuracy and sensitivity, and the application stability of the method is good, which is suitable for different action detection conditions. The comprehensive performance of this method is significantly improved and has higher practical application value and application effect. This method meets the research expectation.

4. Conclusion

With the continuous maturity of video image processing technology, the use of a computer to process images to detect martial art movements is gradually applied. However, in order to solve the problems of low detection accuracy, slow detection speed, and slow detection response, this paper proposes a three-dimensional visual detection method of martial art wrong action based on RBF. Using the characteristics of radial basis function neural network, this method realizes the accurate detection of martial art wrong actions. Experiments show that the proposed three-dimensional vision detection method has high precision, high efficiency, and good stability and can be used to effectively detect martial art wrong movements.

Data Availability

The data used to support the findings of this study are available from the corresponding author upon request.

Conflicts of Interest

The authors declare that they have no conflicts of interest.

References

[1] M. Xu, J. Yiran, X. He, Y. Juntong, and Y. Gao, "Dynamic analysis of the complex motion of three-section cudgel in Wushu sports," *Applied Sciences*, vol. 11, no. 21, pp. 10407–10407, 2021.

[2] L. Wenbo and D. Guobin, "The inheritance and dissemination of Wushu culture in the global era," *The International Journal of the History of Sport*, vol. 38, no. 7, pp. 768–778, 2021.

[3] S. Ohl and M. Rolfs, "Causality detection in the visual system is tuned to motion direction," *Journal of Vision*, vol. 21, no. 9, pp. 1946–1946, 2021.

[4] A. Phillips, G. Erlikhman, and P. J. Kellman, "On the relationship between perceptual learning and statistical learning: evidence from coherent motion detection," *Journal of Vision*, vol. 21, no. 9, pp. 2871–2871, 2021.

[5] N. Pooja, B. S. Bhaskar, J. Aman, and C. Sarika, "Motion detection of webcam using frame differencing method," *Research Journal of Engineering and Technology*, vol. 12, no. 2, pp. 32–38, 2021.

[6] H. Yu and W. Chen, "Motion target detection and recognition based on YOLOv4 algorithm," *Journal of Physics: Conference Series*, vol. 2025, no. 1, article 012053, 2021.

[7] K. S. NagiReddy, T. Suresh, A. Prasanth, T. Muthumanickam, and K. Mohanram, "An effective motion object detection using adaptive background modeling mechanism in video surveillance system," *Journal of Intelligent & Fuzzy Systems*, vol. 41, no. 1, pp. 1777–1789, 2021.

[8] S. Nabil, A. Ahmed, J. I. Muhammad, M. Muhammad, and O. Pablo, "Multi-sensor fusion for underwater vehicle localization by augmentation of RBF neural network and error-state Kalman filter," *Sensors*, vol. 21, no. 4, pp. 1149–1149, 2021.

[9] I. Anantraj, B. Umarani, B. P. Kumar, B. R. Palaniyappan, and R. Ravishankar, "Feature space replica and locomote dimensional detection using Gaussian RBF," *Journal of Critical Reviews*, vol. 7, no. 4, pp. 1019–1024, 2020.

[10] K. B. Gyu, "Digital signal, image and video processing for emerging multimedia technology," *Electronics*, vol. 9, no. 12, pp. 2012–2012, 2020.

[11] S. Takeda, M. Isogai, S. Shimizu, and H. Kimata, "Local Riesz pyramid for faster phase-based video magnification," *IEICE Transactions on Information and Systems*, vol. E103.D, no. 10, pp. 2036–2046, 2020.

[12] P. Shamsolmoali, M. Emre Celebi, and R. Wang, "Advances in deep learning for real-time image and video reconstruction and processing," *Journal of Real-Time Image Processing*, vol. 17, no. 6, pp. 1883-1884, 2020.

[13] A. Khandual, T. Grover, Y. Luximon, N. Rout, and R. Nayak, "Instrumentation and objective evaluation of flammability of textiles by video image processing," *The Journal of The Textile Institute*, vol. 111, no. 8, pp. 1176–1183, 2020.

[14] L. Santeri, N. Longchuan, H. Lionel, N. Jouni, and M. Jouni, "Autonomous robotic rock breaking using a real-time 3D visual perception system," *Journal of Field Robotics*, vol. 38, no. 7, pp. 980–1006, 2021.

[15] M. Kyritsis, S. R. Gulliver, and E. Feredoes, "Visual search fixation strategies in a 3D image set: an eye-tracking study," *Interacting with Computers*, vol. 32, no. 3, pp. 246–256, 2020.

[16] K. Kanagaraj and G. G. Priya, "A new 3D convolutional neural network (3D-CNN) framework for multimedia event detection," *Signal, Image and Video Processing*, vol. 15, no. 4, pp. 779–787, 2021.

[17] R. Alfaifi and A. M. Artoli, "Human action prediction with 3D-CNN," *SN Computer Science*, vol. 1, no. 5, pp. 689–704, 2020.

[18] D. Wang, "Simulation research on safety detection of pattern rope jumping motion based on large data background," *Connection Science*, vol. 33, no. 4, pp. 1047–1059, 2021.

[19] M. Marc, D. Glen, D. Jesse et al., "Motion sensor-based detection of outlier days supporting continuous health assessment for single older adults," *Sensors*, vol. 21, no. 18, pp. 6080–6080, 2021.

[20] Z. Jing, W. Wang, Z. Yang, and Z. Jiwen, "Robust high precision multi-frame motion detection for PMLSMs' mover based on local upsampling moving least square method," *Mechanical Systems and Signal Processing*, vol. 159, no. 6, article 107803, 2021.

[21] I. Lorato, S. Stuijk, M. Meftah et al., "Automatic separation of respiratory flow from motion in thermal videos for infant apnea detection," *Sensors*, vol. 21, no. 18, pp. 6306–6306, 2021.

[22] H. K. Azeem, P. Alain, L. Marcus, S. Didier, and A. M. Zeshan, "CasTabDetectoRS: cascade network for table detection in document images with recursive feature pyramid and switchable atrous convolution," *Journal of Imaging*, vol. 7, no. 10, pp. 214–214, 2021.

[23] C. Beltran-Perez, H.-L. Wei, and A. Rubio-Solis, "Generalized multiscale RBF networks and the DCT for breast cancer detection," *International Journal of Automation and Computing*, vol. 17, no. 1, pp. 55–70, 2020.

[24] K. Z. Ahmad, K. Laiq, A. Saghir, M. Sidra, J. Muhammad, and K. Qudrat, "RBF neural network based backstepping terminal sliding mode MPPT control technique for PV system," *PLoS One*, vol. 16, no. 4, pp. e0249705–e0249705, 2021.

[25] A. D. Izzat, P. Dimitrios, A. A. Kakei et al., "Adaptive robust controller design-based RBF neural network for aerial robot arm model," *Electronics*, vol. 10, no. 7, pp. 831–831, 2021.